

# Talanta

The International Journal of Pure and Applied Analytical Chemistry

---

## Aims & Scope

**Talanta** provides a forum for the publication of original research papers, preliminary communications, and reviews in all branches of pure and applied analytical chemistry. Analytical data should be submitted only if they are clearly related to new analytical measurements. Original research papers on fundamental studies and novel sensor and instrumentation development are especially encouraged. Novel or improved applications in areas such as clinical chemistry, environmental analysis, geochemistry, and materials science and engineering are welcome. Methods should be validated by comparison with a standard method or analysis of a certified reference material, and relevant literature should be cited. Since classical spectrophotometric measurements and applications, solvent extraction, titrimetry, chemometrics, etc. are well established, studies in such areas should demonstrate a unique and substantial advantage over presently known systems. New reagents or systems should demonstrate clear advantage, and their presentation should be comprehensive rather than generating a series of similar papers for several analytes. Modifications of reagents should demonstrate significant improvements. Solvent extraction methods in particular, but others as well, should focus on the use of non-hazardous material substitutes and the minimization of waste generation. But obvious application of known chemistries or methods to established techniques are discouraged. Application of classical analytical approaches to relatively sample matrices having no major interferences, such as pharmaceutical preparations or reconstituted samples, are discouraged unless considerable improvements over other methods in the literature are demonstrated. Papers dealing with analytical data such as stability constants,  $pK_a$  values, etc. should be published in more specific journals, unless novel analytical methodology is demonstrated, or important analytical data are provided which could be useful in the development of analytical procedures.

## Editors-in-Chief

**Professor G.D. Christian**, University of Washington, Department of Chemistry, 36 Bagely Hall, P.O. Box 351700, Seattle, WA 98195-1700, U.S.A.

**Professor J.-M. Kauffmann**, Université Libre de Bruxelles, Institut de Pharmacie, Campus de la Plaine, C.P. 205/6, Boulevard du Triomphe, B-1050 Bruxelles, Belgium

## Associate Editors

**Professor J.-H. Wang**, Research Center for Analytical Sciences, Northeastern University, Box 332, Shenyang 110004, China

**Professor J.L. Burguera**, Los Andes University, IVAIQUIM, Faculty of Sciences, P.O. Box 542, 5101-A Mérida, Venezuela.

## Assistant Editors

**Dr R.E. Synovec**, Department of Chemistry, University of Washington, Box 351700, Seattle, WA 98195-1700, U.S.A.

**Professor J.-C. Vire**, Université Libre de Bruxelles, Institut de Pharmacie, Campus de la Plaine, C.P. 205/6, Boulevard du Triomphe, B-1050 Bruxelles, Belgium

## Talanta

R. Apak (Istanbul, Turkey)  
E. Bakker (Auburn, AL, U.S.A.)  
D. Barceló (Barcelona, Spain)  
B. Birch (Luton, UK)  
K. S. Booksh (Tempe, AZ, U.S.A.)  
J.-L. Capelo-Martinez (Caparica, Portugal)  
Z. Cai (Kowloon, Hong Kong)  
O. Chailapakul (Thailand)  
S. Cosnier (Grenoble, France)  
D. Diamond (Dublin, Ireland)  
W. Frenzel (Berlin, Germany)  
A.G. Gonzales (Seville, Spain)  
P. de B. Harrington (OH, U.S.A.)

A. Ho (Hsin-chu, Taiwan)  
P. Hubert (Liège, Belgium)  
J. Kalivas (Pocatella, ID, U.S.A.)  
B. Karlberg (Stockholm, Sweden)  
J.-M. Lin (Beijing, China)  
Y. Lin (Richland, WA, U.S.A.)  
M.D. Luque de Caastro (Cordoba, Spain)  
I.D. McKelvie (Victoria, Australia)  
S. Motomizu (Okayama, Japan)  
J.-M. Pingarron (Madrid, Spain)  
E. Pretsch (Zürich, Switzerland)  
W. Schuhmann (Bochum, Germany)  
M. Shamsipur (Kermanshah, Iran)

M. Silva (Porto Alegre, Brazil)  
P. Solich (Hradec Králové, Czech Republic)  
K. Suzuki (Yokohama, Japan)  
D.G. Themelis (Thessaloniki, Greece)  
D.L. Tsalev (Sofia, Bulgaria)  
B. Walczak (Katowice, Poland)  
J. Wang (Tempe, AZ, U.S.A.)  
J.D. Winefordner (Gainesville, U.S.A.)  
Xiu-Ping Yan (Tianjin, China)  
E.A.G. Zagatto (Piracicaba, SP, Brazil)  
X. Zhang (China)



# Application of continuous wavelet transformation to the simultaneous kinetic determination of binary mixtures

Abbas Afkhami\*, Maryam Abbasi-Tarighat

Faculty of Chemistry, Bu-Ali Sina University, Hamadan 65174, Iran

## ARTICLE INFO

### Article history:

Received 17 September 2008

Received in revised form

24 November 2008

Accepted 24 November 2008

Available online 30 November 2008

### Keywords:

Wavelet transformation

Kinetic profiles

Simultaneous spectrophotometric determination

Binary mixtures

## ABSTRACT

Wavelet transformation of kinetic profiles as a new and simple method was developed for the simultaneous determination of binary mixtures without prior separation steps. The mathematical explanation of the procedure is illustrated. Daubechies (db), symlet (sym) and discrete meyer wavelet (meyr) from the family of wavelet transforms were selected and applied under the optimal conditions for the resolution of binary mixtures. A model data as well as experimental data were tested. The results from the experimental data relating to the simultaneous spectrophotometric determination of phosphate and silicate based on the formation of phospho- and silico-molybdenum blue complexes in the presence of ascorbic acid, and also simultaneous determination of  $\text{Co}^{2+}$  and  $\text{Ni}^{2+}$  based on their complexation reactions with 1-(2-pyridylazo)-2-naphthol (PAN) in micellar media at pH 6.0 were presented as real models. The proposed method was validated by simultaneous determination of phosphate and silicate in detergent and tap water and also  $\text{Co}^{2+}$  and  $\text{Ni}^{2+}$  in tap water samples.

© 2008 Elsevier B.V. All rights reserved.

## 1. Introduction

Kinetic methods of chemical analysis differ in a fundamental way from the equilibrium, or thermodynamic methods. These methods are powerful tools for multi-component analysis as they permit the sensitive and selective determination within no sample pre-treatment in many cases. Kinetic methods have been widely used for the simultaneous determination of multi-component mixtures as the results of the incorporations of computerized data acquisition systems and the development of powerful mathematical treatments for processing the recorded information [1]. Kinetic methods based on difference in reaction rates are effective way for simultaneous determination of mixtures especially in cases where the analytes react with a common reagent and create similar or identical spectra that cannot be resolved by equilibrium-based methods [2–5].

Kinetic methods have made a great improvement by using the chemometric procedures. Principal component regression (PCR) and partial least squares regression (PLS) are well-known multivariate calibration procedures widely used in recent years for the simultaneous determination of analytes in mixtures by means of kinetic-spectrophotometric procedures [6–9]. Also the chemometric methods based on artificial neural networks (ANN) [10,11] and

factor analysis [12,13] have found increasing applications for multi-component kinetic determinations.

We proposed mean centering of ratio kinetic profiles as a simple and efficient method to the resolving of binary and ternary mixtures without prior separation steps [14–16]. The method has been successfully applied to the simultaneous analysis of binary mixtures of cobalt and nickel based on the kinetic profiles of their complexation reactions with 1-(2-pyridylazo)-2-naphthol (PAN) in micellar media [14], and simultaneous determination of iodate and bromate based on the difference in the rate of their reaction with iodide ion [15]. In another work, we examined the applicability of the mean centering of ratio kinetic profiles to the analysis of ternary mixtures [16]. Ternary mixtures of hydrazine, phenylhydrazine and acetylhydrazine were resolved based on their condensation reactions with *p*-(dimethylamino)benzaldehyde and *p*-nitrobenzaldehyde in micellar sodium dodecyl sulfate media.

Few reports have been published on the application of wavelet transforms for simultaneous determination of chemical species. Recently, the use of combination of CWT and zero-crossing has firstly formulated by Dinç and Baleanu [17–19] for the quantitative resolution of two component mixtures. The simultaneous use of the CWT and zero-crossing technique was applied to the resolution of various binary mixtures [20–24]. Also Dinç et al. used the ratio spectra-CWT with zero-crossing technique for the multi-component spectral analysis of ternary mixtures of three active compounds with overlapping spectral [25–28].

\* Corresponding author. Fax: +98 811 8272404.

E-mail address: [afkhami@basu.ac.ir](mailto:afkhami@basu.ac.ir) (A. Afkhami).

Recently, we applied continuous wavelet transformation for the simultaneous determination of metal ions in different mixtures [29] and determination of enantiomeric ratios [30].

In this study, application of wavelet transformation to the resolution of kinetic profiles of binary systems and the simultaneous determination of binary mixtures by kinetic methods was studied. To the best of our knowledge, this is the first report on the application of CWT to the simultaneous determination of binary mixtures by kinetic methods.

## 2. Theory

### 2.1. First order and pseudo-first order reactions

Consider the analytes A and B react with a reagent R to give the absorbing specie, P



Then it could be written as

$$-\frac{dA}{dt} = k_A[A] \quad (3)$$

$$-\frac{dB}{dt} = k_B[B] \quad (4)$$

If two rates correspond to first order kinetics with respect to each of components of the mixture then the concentration of the sum of the product at time  $t$  is given by

$$\frac{dP}{dt} = k_A[A] + k_B[B] \quad (5)$$

$$[P]_t = ([A]_0 - [A]_t) + ([B]_0 - [B]_t) \\ = [A]_0[1 - \exp(-k_A t)] + [B]_0[1 - \exp(-k_B t)] \quad (6)$$

where,  $k_A$ ,  $k_B$  and  $[A]_0$ ,  $[B]_0$ ,  $[A]_t$  and  $[B]_t$  are the rate constants, initial concentration and concentrations of A and B at time  $t$ , respectively.

The product P can be monitored by recording its absorbance as a function of time at a fixed wavelength. It has been assumed that the reactions involved both processes to follow first or pseudo-first order kinetics with respect to the analyte concentrations. If the reaction follows with changing amounts of product formed, then, in the absence of interactions between the kinetics of both analytes, the total amount of absorbance at any time  $t$ ,  $A_{T,t}$ , will be given by:

$$A_{T,t} = (C_{PA,t} + C_{PB,t})E_P \quad (7)$$

where  $C_{PA,t}$  and  $C_{PB,t}$  are the concentration of the products of the analytes A and B at time  $t$ , respectively, and  $E_P$  is the molar absorptivity of product in the Beer–Lambert law in spectrophotometric measurements.

$$\text{Or } A_{T,t} = \sum_i E_i C_i^0 \quad (8)$$

where  $C^0$  is the initial concentration of the  $i$  to be quantified for first-order reaction and  $E_{i,t} = \varepsilon_i [1 - \exp(-kt)]$ . The variation of the absorbance as a function of time at a given wavelength can be used to construct a 'kinetic profile',  $A_{t1}, A_{t2}, \dots, A_{tn}$  at times  $t_1, t_2, \dots, t_n$ .

### 2.2. Rate law for second order reaction

Consider a typical analytical reaction in which A and B react with the reagent R to give a single absorbing specie P, according to the following scheme:



If the reaction occurs in a single elementary step, the rate is proportional to the concentration of each reactants and the rate law is

$$\frac{dP}{dt} = \frac{-dA}{dt} = \frac{-dB}{dt} = k_2(C_A^0 - C_P)(C_B^0 - C_P) \quad (11)$$

The reaction is first order in each of the reactants. By integration from Eq. (1):

$$\frac{1}{C_A^0 - C_B^0} \ln \left( \frac{C_B^0(C_A^0 - C_P)}{C_A^0(C_B^0 - C_P)} \right) = k_2 t \quad (12)$$

where  $k_2$ ,  $C_A^0$ ,  $C_B^0$ ,  $C_A$  and  $C_B$  are the rate constant, initial concentration for A, B and concentration for A and B at time  $t$ . If reaction contains only species A:

$$-\frac{dA}{dt} = k_2 C_A^2 \quad (13)$$

$$\frac{dP}{dt} = k_2(C_A^0 - C_A)^2 \quad (14)$$

Integration of Eq. (12) gives

$$\frac{1}{C_A} = \frac{1}{C_A^0} + k_2 t \quad (15)$$

$$C_{P,t} = C_A^0 - C_A = C_A^0 \left( 1 - \frac{1}{C_0 + k_2 t} \right) \quad (16)$$

If the reaction follows by monitoring the product P by spectrophotometry, then the total amount of absorbance will be given by

$$A_T = C_{P,t} E_P \quad (17)$$

where  $C_{P,t}$  is the concentration of product at time  $t$  and  $E_P$  is the molar absorptivity of product in the Beer–Lambert law in spectrophotometric determinations.

### 2.3. Continuous wavelet transformation

Wavelet theory is based on analyzing signals to their components by using a set of basis functions. One important characteristic of the wavelet basis functions is that they relate to each other by simple scaling and translation. The original wavelet function, known as mother wavelet, which is generally designed based on some desired characteristics associated to that function, is used to generate all basis functions. For the purpose of multi-resolution formulation, there is also a need for a second function, known as scaling function, to allow analysis of the function to finite number of components. The subspace of scale  $a$  or frequency band is generated by the functions

$$\psi_{(a,b)}(t) = \frac{1}{\sqrt{a}} \psi \left( \frac{t-b}{a} \right) \quad (18)$$

where  $a$  is positive and defines the scale and  $b$  is any real number and defines the shift. The original signal can be reconstructed by suitable integration over all the resulting frequency components after projection of given signal on a continuous family of frequency bands. For binary mixtures of A and B by transformation of calibration set of two analytes, the calibration functions of them will be obtained. Prediction of concentration of each analyte in binary mixture was estimated by measuring CWT-signal calibration equations at zero-crosses. In this study daubechies (db), symlet8 (sym8) and discrete meyer (dmey) were used as mother wavelets.

## 3. Validation of the method with model data

In order to evaluate the performance of the method for the analysis of binary mixtures, simulated kinetic spectrophotometric

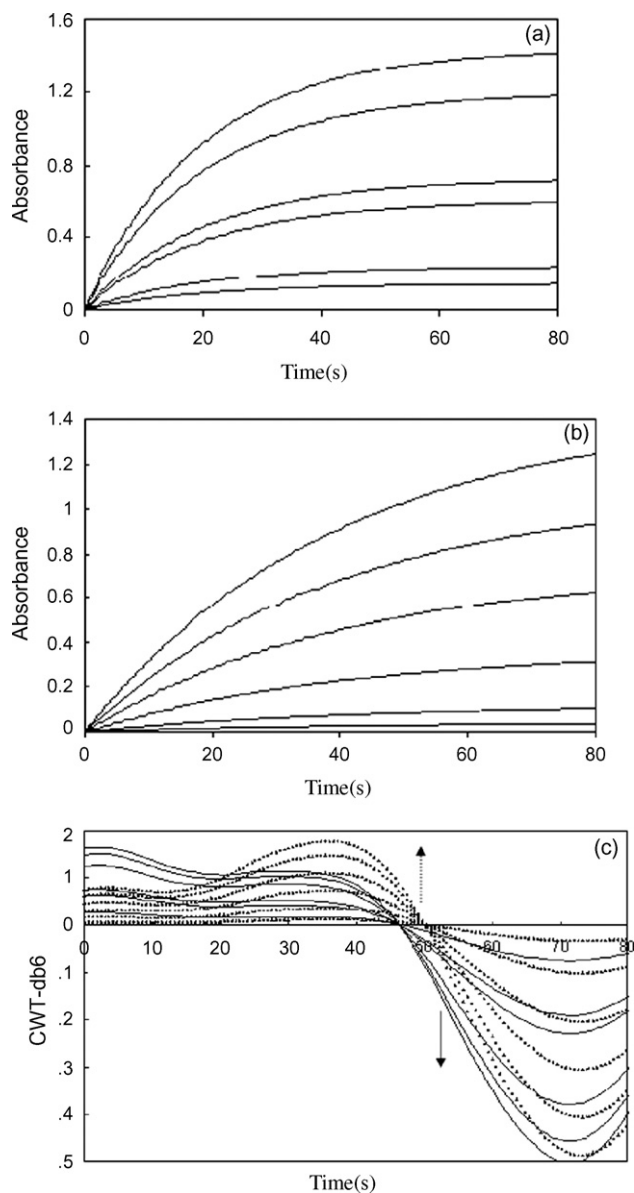


**Fig. 1.** The model kinetic profiles of randomly selected mixtures of the (a) A 0.05, 0.2, 0.5, 0.6, 1.0 and 1.2 and (b) B 0.1, 0.3, 0.4, 0.6, 0.9 and 1.2, and (c) the CWT-db6 spectra were obtained by transformation of mixtures of A and B with rate constant ratio of 2.

profiles for first order reactions was created. As Fig. 1a and b shows, kinetic profiles for first order reactions in the linear dynamic range in the range 0–80.4 s were created by considering different rate constant ratios. The kinetic profiles for different concentrations of A and B were created as calibration sets (e.g. Fig. 1a and b for rate constant ratio of 2) and transformed with mother wavelet db6 to obtain the CWT signals (Fig. 1c for kinetic ratio of 2). The optimum value of scaling factor was determined as 100. Calibration graphs were obtained by measuring the CWT signals at 47.4 and 46.2 s, corresponding to the zero-crosses of two analytes. The calibration graphs and their statistical results are shown in Table 1. The influence of analyte concentration ratio by using a data set in A/B ratios 1:2, 1:3, 2:1, 6:1 and 1:1 at different rate constant ratios was studied. As Table 2 shows relative error % values for components A and B at different rate constant ratios are acceptable. As the results show, analysis of data with db as mother wavelet was possible, but by changing the rate constant ratios not only scaling values but also

type of mother wavelet should be changed. Therefore, in order to obtain the best values for concentrations or lower values for SEP% or relative error %, two parameters should be selected carefully. The first parameter is the type of mother wavelet and the second one is the scaling value.

Also the proposed method was validated using dmey and sym8 with optimized scaling values (Table 1). By obtaining the calibration graphs, the concentrations of A and B in the synthetic mixtures were determined by these mother wavelets. The relative standard error of prediction (SEP%) was calculated as

$$\text{SEP\%} = \sqrt{\frac{\sum_{i=1}^n (\hat{y}_i - y_i)^2}{n}} \quad (19)$$

where  $n$  is the number of the samples,  $y_i$  is the real value and  $\hat{y}_i$  is the predicted value. The SEP% values of prediction of proposed mother wavelets with different kinetic ratios are presented in Table 1. Analysis of data with dmey and sym8 was performed at different rate constant ratios only by changing the scaling values. The results show that the proposed method can be applied to first or pseudo-first order reactions with different rate constant ratios.

The proposed method was also validated using second order reaction rate simulated data. Different kinetic rate constant ratios were tested. The analysis was performed as described for the first order reactions. The SEP% values of found concentrations were calculated (Table 3). The SEP% values for different kinetic constant ratios show that the proposed method can be applied for simultaneous determination in binary mixtures too. Comparison of SEP% values for first order and second order data shows that the proposed method can be applied for second order reaction as well as for first order reactions with good predictions.

## 4. Experimental

### 4.1. Reagent and standard solutions

All solutions were prepared with analytical grade reagents and used without any purification. Stock solutions of  $\text{Co}^{2+}$  and  $\text{Ni}^{2+}$  ( $1000 \text{ mg L}^{-1}$ ) were prepared by dissolving  $\text{CoCl}_2$  and  $\text{NiCl}_2 \cdot 6\text{H}_2\text{O}$  (Fluka) in water. A  $5.0 \times 10^{-3} \text{ mol L}^{-1}$  1-(2-pyridylazo)-2-naphthol solution was prepared by dissolving appropriate amount of PAN in 100 mL ethanol. Triton X-100 (TX-100) stock solution (10%, v/v) was prepared by dissolving 15 mL of concentrate solution (Merck) in hot distilled water. A buffer solution of pH 6.0 was prepared from  $\text{KH}_2\text{PO}_4$  and  $\text{Na}_2\text{HPO}_4$ . A stock solution of phosphate ( $1000 \text{ mg L}^{-1}$ ) was prepared by dissolving potassium dihydrogen phosphate (Merck) in water. A stock solution of silicate was prepared by appropriate dilution of sodium silicate solution (Merck) with water. A sodium molybdate solution ( $0.11 \text{ mol L}^{-1}$ ) was prepared by dissolving appropriate amount of  $(\text{NH}_4)_6\text{Mo}_7\text{O}_{24} \cdot 2\text{H}_2\text{O}$  in  $0.4 \text{ mol L}^{-1}$  nitric acid. Ascorbic acid,  $0.050 \text{ mol L}^{-1}$ , was prepared by dissolving appropriate amount of ascorbic acid (Merck) in 100.0 mL of distilled water. The detergent was brought from local markets.

### 4.2. Apparatus and data processing

Kinetic profiles were obtained using a T80 UV/VIS PG instruments Ltd. double beam spectrophotometer using 1-cm quartz cells at room temperature. Wavelet transformation was performed using Wavelet-Toolbox for MATLAB 7.1 and CWT coefficients were transferred to Microsoft Excel 2003 for further analysis.

**Table 1**  
Statistical results of calibration graphs obtained in zero-cross points for first order reaction at different rate constant ratios with different mother wavelets.

Mother wavelet	$k_A/k_B$	Time/s		Regression equation		$r^2$		Scaling value	SEP/%	
		A	B	A	B	A	B		A	B
sym8	1.2	22.8	19.8	$A = 0.276C_A + 0.00$	$A = -0.227C_B + 0.00$	1	1	100	6.40	0.01
sym8	1.5	22.2	19.8	$A = 0.276C_A + 0.00$	$A = -0.227C_B - 0.00$	1	1	100	1.77	0.01
sym8	1.8	27.6	19.8	$A = 0.793C_A + 0.00$	$A = -0.570C_B - 0.00$	1	1	100	0.62	0.00
sym8	2.0	28.8	19.8	$A = 0.811C_A + 0.00$	$A = -0.620C_B + 0.00$	1	1	100	1.03	0.00
sym8	5.0	34.2	19.8	$A = 1.25C_A + 0.00$	$A = -0.594C_B + 0.00$	1	1	120	0.51	0.01
sym8	8.0	30.0	19.8	$A = 1.91C_A + 0.00$	$A = -0.558C_B + 0.00$	1	1	120	0.23	0.00
sym8	12.0	30.0	19.8	$A = 1.91C_A + 0.00$	$A = -0.416C_B + 0.00$	1	1	120	0.86	0.02
sym8	16.0	30.6	19.8	$A = 2.03C_A + 0.00$	$A = -0.330C_B + 0.00$	1	1	100	0.17	0.02
sym8	25.0	30.6	19.8	$A = 2.03C_A + 0.00$	$A = -0.219C_B + 0.00$	1	1	120	0.17	0.23
sym8	40.0	30.0	19.8	$A = 1.91C_A + 0.00$	$A = -0.146C_B - 0.00$	1	1	120	0.78	0.23
sym8	80.0	30.0	19.8	$A = 1.91C_A + 0.00$	$A = -0.192C_B - 0.00$	1	1	120	0.45	0.70
dmey	1.2	30.6	28.8	$A = 0.191C_A + 0.00$	$A = -0.224C_B + 0.00$	1	1	120	2.59	0.24
dmey	1.5	33.0	29.4	$A = 0.458C_A + 0.00$	$A = -0.454C_B + 0.00$	1	1	120	0.148	0.12
dmey	1.8	28.8	25.2	$A = 0.811C_A + 0.00$	$A = -0.617C_B + 0.00$	1	1	140	0.70	0.09
dmey	2.0	35.4	28.8	$A = 0.733C_A + 0.00$	$A = -0.72C_B + 0.00$	1	1	140	1.19	0.08
dmey	5.0	33.0	25.2	$A = 1.66C_A + 0.00$	$A = 0.691C_B + 0.00$	1	1	140	0.24	1.03
dmey	8.0	28.8	21.6	$A = 2.32C_A + 0.00$	$A = -0.551C_B + 0.00$	1	1	140	0.24	0.05
dmey	12	29.4	21.6	$A = 2.02C_A + 0.00$	$A = -0.413C_B + 0.00$	1	1	140	0.43	0.76
dmey	16	27.6	19.8	$A = 2.02C_A + 0.00$	$A = -0.32C_B + 0.00$	1	1	140	0.34	1.73
dmey	25	27.6	19.8	$A = 2.07C_A + 0.00$	$A = -0.218C_B + 0.00$	1	1	140	0.08	7.65
dmey	40	40.2	30	$A = 1.30C_A + 0.00$	$A = -0.130C_B + 0.00$	1	1	140	0.31	14.0
db6	1.2	47.4	46.2	$A = 0.749C_A + 0.00$	$A = 0.749C_B + 0.00$	1	1	120	9.79	1.29
db6	1.5	47.4	46.2	$A = 0.749C_A + 0.00$	$A = 0.162C_B + 0.00$	1	1	120	1.35	0.87
db6	1.8	49.8	46.2	$A = -0.759C_A + 0.00$	$A = 0.556C_B + 0.00$	1	1	120	0.67	0.48
db6	2.0	50.4	46.2	$A = 0.618C_A + 0.00$	$A = -0.556C_B + 0.00$	1	1	120	0.52	0.42
db8	5.0	25.2	16.8	$A = 1.97C_A + 0.00$	$A = -0.764C_B + 0.00$	1	1	100	0.94	0.34
db8	8.0	29.4	20.4	$A = -1.55C_A + 0.00$	$A = 0.540C_B + 0.00$	1	1	100	0.94	0.34
db8	12	30.0	20.4	$A = -1.66C_A + 0.00$	$A = 0.404C_B + 0.00$	1	1	100	0.23	0.08
db8	16	30.0	20.4	$A = -1.66C_A + 0.00$	$A = 0.322C_B + 0.00$	1	1	100	0.44	0.08
db8	25	30.0	20.4	$A = -1.66C_A + 0.00$	$A = 0.325C_B + 0.00$	1	1	120	0.23	0.21
db8	40	30.6	20.4	$A = -1.78C_A + 0.00$	$A = 0.428C_B + 0.00$	1	1	120	0.43	5.49
db8	80	31.2	20.4	$A = -1.88C_A + 0.00$	$A = 0.074C_B + 0.00$	1	1	120	0.19	0.42

**Table 2**  
Relative errors for the determination of the analytes A and B with CWT-db at different concentration ratios and at different rate constant ratios.

Mother wavelet	$k_A/k_B$	A:B ratio									
		1:2		1:3		2:1		1:1		6:1	
		A	B	A	B	A	B	A	B	A	B
db6	1.2	5.12	1.65	9.96	1.10	6.62	0.20	-3.31	3.30	4.16	4.25
db6	1.5	3.68	(1.11)	5.53	(0.74)	3.68	(1.11)	1.83	(2.20)	0.41	1.28
db6	0.8	1.32	0.611	4.20	0.411	1.32	0.61	(1.55)	1.21	0.06	0.02
db6	2.0	0.00	0.53	0.70	0.35	2.04	0.53	0.314	1.08	0.04	0.25
db8	5.0	1.02	(0.14)	0.26	(0.63)	1.83	0.14	(0.21)	1.33	(0.18)	0.26
db8	8.0	(0.01)	(0.14)	(0.02)	(0.63)	(0.01)	(0.14)	(0.01)	1.33	0.09	0.36
db8	12	(0.63)	0.09	(0.95)	0.07	0.06	0.09	(0.31)	0.18	0.14	0.96
db8	16	1.18	0.09	1.78	0.05	1.18	0.09	0.59	0.20	0.01	1.36
db8	25	(0.63)	0.27	(0.95)	0.19	(0.63)	0.27	(0.31)	0.52	0.01	1.22
db8	40	0.18	0.27	0.27	0.19	0.18	0.27	0.09	0.52	0.15	1.26
db8	80	0.52	0.54	0.28	0.38	0.52	0.54	0.26	1.02	0.01	1.92

**Table 3**  
Statistical results of calibration graphs obtained in zero-cross points for second order reaction by proposed method at different rate constant ratios with different mother wavelets.

Mother wavelet	$k_A/k_B$	Time/s		Regression equation		$r$		R.S.E.%	
		A	B	A	B	A	B	A	B
Sym8	2	10	12	$A = 0.521C_A - 0.170$	$A = -0.139C_B + 0.00$	0.9885	0.9924	2.3	1.2
	5	18	10	$A = 0.365C_A - 0.170$	$A = -0.120C_B + 0.00$	0.9885	0.9909	2.9	1.2
	8	18	10	$A = -0.263C_A - 0.052$	$A = 0.999C_A - 0.2735$	0.9945	0.9938	3.8	1.4
	10	18	10	$A = -0.263C_A - 0.051$	$A = 0.999C_A - 0.2735$	0.9945	0.9983	3.8	1.4
dmey	2	18	14	$A = 0.521C_A - 0.170$	$A = -0.120C_B + 0.00$	0.9988	0.9908	0.80	1.7
	5	18	14	$A = 0.521C_A - 0.17$	$A = -0.130C_B + 0.00$	0.9908	0.9985	0.29	1.6
	8	18	14	$A = 0.503C_A - 0.260$	$A = -0.197C_B + 0.03$	0.9952	0.9974	0.92	1.7
	10	18	10	$A = 0.521C_A - 0.170$	$A = -0.111C_B + 0.02$	0.9988	0.9956	0.30	1.0
db8	2	24	20	$A = 0.492C_A + 0.160$	$A = 0.237C_A - 0.022$	0.9998	0.9917	0.02	0.20
	5	26	20	$A = -0.492C_A + 0.160$	$A = 0.2374C_A - 0.022$	0.9918	0.9989	0.10	0.24
	8	26	20	$A = -0.539C_A + 0.180$	$A = 0.237C_A - 0.022$	0.9991	0.9989	0.15	0.92
	10	26	20	$A = -0.534C_A + 0.180$	$A = 0.237C_A - 0.022$	0.9991	0.9989	0.15	2.6

### 4.3. Kinetic measurements

#### 4.3.1. Simultaneous determination of silicate and phosphate

A 0.8-mL ascorbic acid reagent was accurately pipetted into a 5.0-mL volumetric flask containing an appropriate amount of orthophosphate or silicate sample or their mixture. The solution was mixed and diluted to the mark with doubly distilled water. Then 2 mL of this solution was transferred into a cleaned cell in sample holder. Then 0.5 mL of the molybdate solution was added and the solution was mixed immediately using a capillary and kinetic profiles were recorded at 820 nm. The time between the addition of the molybdate reagent and the start of kinetic measurements was controlled to less than 5 s. The kinetic measurements continued for a period of 10 min with the intervals of 2-s by measuring the increase in absorbance at 820 nm.

#### 4.3.2. Simultaneous determination of cobalt and nickel by PAN

A 1.0-mL of pH 6.0 phosphate buffer solution was transferred into a 5.0 mL volumetric flask containing an appropriate amount of  $\text{Ni}^{2+}$  or  $\text{Co}^{2+}$  or their mixture and 0.1 mL TX-100 solution. The solution was mixed and diluted to the mark with doubly distilled water. Then 2.0 mL of this solution was transferred into a cleaned cell in sample holder. Then 0.5 mL of  $5 \times 10^{-3} \text{ mol L}^{-1}$  of PAN solution was added and the solution was mixed immediately and kinetic measurements were begun. The kinetic measurement continued for a period of 10 min with the intervals of 2-s by measuring the increase in absorbance at 568 nm.

### 4.4. Simultaneous determination of phosphate and silicate in detergents

Detergent formulation samples were prepared according to the procedure reported previously [31]. One gram of powder was weighed and dissolved in about 150 mL of hot water by vigorous stirring for about 5 min. The solution was then diluted with water to 250 mL. A 20-mL of the diluted solution was transferred into a 500-mL beaker, and 30 mL of water and 50 mL of dilute nitric acid was added to the solution. The solution was cooled rapidly and then a few drops of phenolphthalein indicator was added. To neutralize the solution, drop wise concentrated NaOH was added and then diluted to 250 mL with water. Four milliliters of this sample was subjected to the using procedure.

## 5. Results and discussion

### 5.1. Preliminary study of the system

#### 5.1.1. Study of polyhetromolybdenum blue complexes

The widely used methods for orthophosphate and silicate determination by spectrophotometry are based on the formation of

a stable phosphomolybdenum blue and silicomolybdenum blue complexes. These complexes have significant spectral overlap [32]. Therefore, simultaneous determination of these ions with classical spectrophotometric methods is impossible. A kinetic spectrophotometric procedure for simultaneous determination of phosphate and silicate is suggested. The reaction between molybdate with phosphate and silicate was carried out under pseudo-first order conditions at room temperature. The kinetic profiles of the complexation reactions of phosphate and silicate with molybdenum blue in the presence of ascorbic acid (at 820 nm) are presented in Fig. 2a. As Fig. 2a shows the kinetic profiles for the reactions of the equimolar concentration of silicate and phosphate are not exactly the same. Therefore, the system can be used to the simultaneous kinetic determination of these elements.

#### 5.1.2. Study of colored complexes of PAN

The spectra of the PAN and the colored complexes with  $\text{Co}^{2+}$  and  $\text{Ni}^{2+}$  overlap with each other; in the other words, they cannot be resolved by classical methods [33]. A  $1.0 \times 10^{-3} \text{ mol L}^{-1}$  PAN (at least 24-fold excess over maximum concentration of metal ions) was applied to obtain a pseudo-first order reaction with respect to each analyte concentration. The kinetic profiles of the complexation reactions of  $\text{Co}^{2+}$  and  $\text{Ni}^{2+}$  with PAN in micellar media (at 568 nm) are presented in Fig. 2b. The reaction rate of  $\text{Co}^{2+}$  and  $\text{Ni}^{2+}$  with PAN are different and as Fig. 2b shows the kinetic profiles of the complexation reactions of  $\text{Co}^{2+}$  and  $\text{Ni}^{2+}$  can be used to their simultaneous determinations.

### 5.2. Optimization of the reaction conditions

The optimum working conditions for the simultaneous determination of  $\text{Co}^{2+}$  and  $\text{Ni}^{2+}$  were obtained as:  $2.0 \times 10^{-4} \text{ mol L}^{-1}$  PAN, 3% (v/v) TX-100 and 1 mL of pH 6.0 phosphate buffer solution. For simultaneous determination of phosphate and silicate the optimum working conditions were obtained as  $2.2 \times 10^{-3} \text{ mol L}^{-1}$  molybdate and  $8 \times 10^{-2} \text{ mol L}^{-1}$  ascorbic acid.

### 5.3. Spectral characteristics and selection of appropriate mother wavelets

A set of sample solutions with different concentrations of ions was prepared and measurements were carried out under the optimum conditions described in Section 5.2 for each system. The calibration curves were linear in the ranges  $0.04\text{--}2.6 \text{ mg L}^{-1}$ ,  $0.05\text{--}2.5 \text{ mg L}^{-1}$  for  $\text{Ni}^{2+}$  and  $\text{Co}^{2+}$ , respectively. The equations of the calibration curves were as:  $A = 2.2 \times 10^{-2}C + 1.6 \times 10^{-2}$ ,  $r^2 = 0.9984$  and  $A = 1.98 \times 10^{-1}C + 90. \times 10^{-3}$ ,  $r^2 = 0.9985$  for  $\text{Ni}^{2+}$  and  $\text{Co}^{2+}$  at 34 s after initialization of the reactions, respectively. The calibration curves were linear in the ranges  $0.2\text{--}6.5 \text{ mg L}^{-1}$ ,  $0.1\text{--}4.0 \text{ mg L}^{-1}$

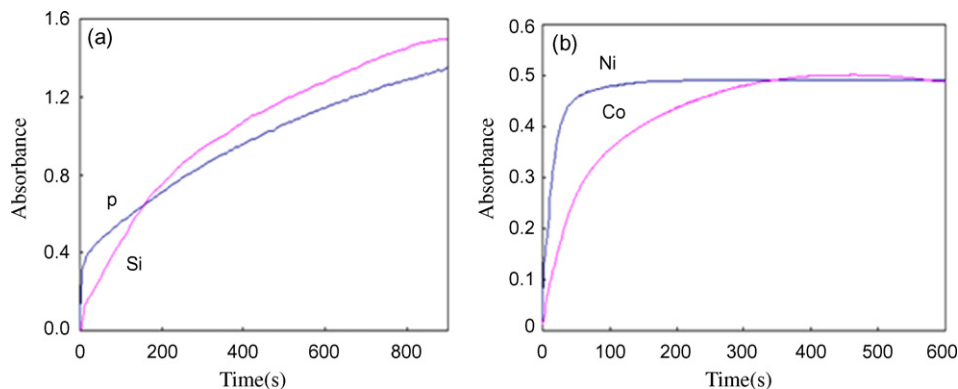
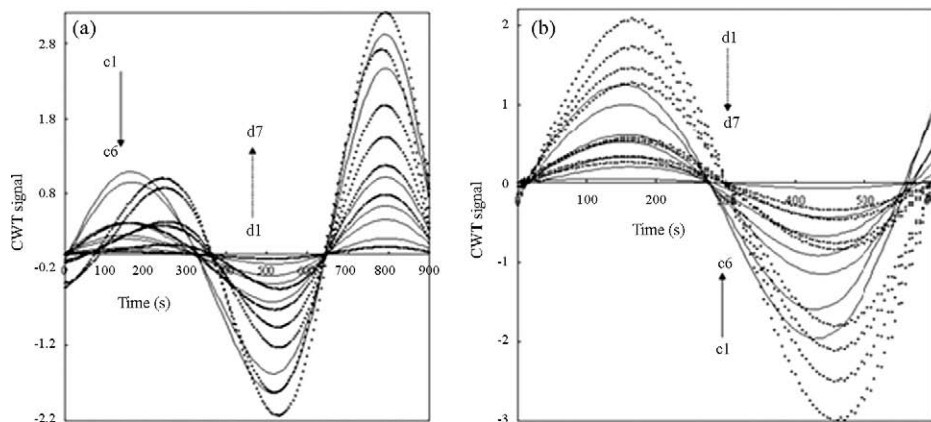


Fig. 2. The absorption kinetic profiles of the standard solutions of (a) phosphate and silicate ( $1.0 \times 10^{-4} \text{ mol L}^{-1}$  of each) at 820 nm and (b)  $\text{Co}^{2+}$  and  $\text{Ni}^{2+}$  ( $1.7 \times 10^{-5} \text{ mg L}^{-1}$ ) at 568 nm at optimum conditions.

**Table 4**

Statistical results of calibration graphs obtained in zero-cross points of phosphate and silicate by proposed method.

Mother wavelet	Anion	Time/s	Linear range/mg L <sup>-1</sup>	Regression equation	r <sup>2</sup>	LOD/mg L <sup>-1</sup>	LOQ/mg L <sup>-1</sup>
dmey	Phosphate	330	0.2–6.5	$A = 0.299C_p + 0.004$	0.9974	0.010	0.033
sym8	Phosphate	305	0.2–6.5	$A = 0.596C_p + 0.003$	0.9988	0.005	0.016
dmey	Silicate	370	0.1–4.0	$A = 0.104C_{si} - 0.005$	0.9959	0.028	0.096
sym8	Silicate	280	0.1–4.0	$A = -0.125C_{si} - 0.006$	0.9984	0.023	0.080

**Fig. 3.** (a) CWT-dmey and (b) CWT-sym8 signals of silicate (c1) 0.1 mg L<sup>-1</sup>, (c2) 0.8 mg L<sup>-1</sup>, (c3) 1.5 mg L<sup>-1</sup>, (c4) 1.8 mg L<sup>-1</sup>, (c5) 3.5 mg L<sup>-1</sup>, (c6) 4.0 mg L<sup>-1</sup> and phosphate (d1) 0.2 mg L<sup>-1</sup>, (d2) 0.80 mg L<sup>-1</sup>, (d3) 1.0 mg L<sup>-1</sup>, (d4) 2.0 mg L<sup>-1</sup>, (d5) 2.5 mg L<sup>-1</sup>, (d6) 4.2 mg L<sup>-1</sup> and (d7) 5.0 mg L<sup>-1</sup>.**Table 5**

Mean recoveries and relative standard deviations for the simultaneous determination of phosphate and silicate in various synthetic mixtures by the proposed method.

Mother wavelet	Anion <sup>a</sup>	
	Phosphate	Silicate
dmey	102 ± 2	107 ± 3
Sym8	97 ± 1	105 ± 4

<sup>a</sup> Average of three determinations ± standard deviation.

for phosphate and silicate, respectively. Typical equations of the calibration curves were as follows:  $A = 1.3 \times 10^{-2}C + 2.2 \times 10^{-2}$ ,  $r^2 = 0.9998$  and  $A = 1.76 \times 10^{-1}C + 1.1 \times 10^{-2}$ ,  $r^2 = 0.9985$  for phosphate and silicate at 200 s, respectively.

Various wavelet families were tested to find the optimal signal processing for obtaining desirable calibration graphs and reliable determination. The value of scaling factor for determination of phosphate and silicate in their binary mixture was optimized for different mother wavelets. As Fig. 2a shows the kinetic profiles for the complexation reactions of phosphate and silicate can be used for simultaneous determination of ions with CWT successfully. The graphs of CWT for calibration sets of phosphate and silicate were obtained by dmey with scaling value ( $a$ ) of 100 (Fig. 3a). Calibration graphs of phosphate and silicate with dmey ( $a = 100$ ) were obtained by measuring the CWT signals at 330 and 370 s correspond to zero-crosses of silicate and phosphate, respectively, for determination of phosphate and silicate. The calibration graphs and the statistical results are shown in Table 4. Concentration of phosphate and silicate in synthetic binary mixtures was estimated with calibration equations at zero-crosses. Also transformation

of calibration spectra of phosphate and silicate were performed by sym8 with optimum scaling value ( $a = 105$ ) (Fig. 3b). Transformation of their binary mixtures were also performed by sym8 ( $a = 105$ ). The amplitudes of CWT signals at times correspond to zero-crosses of phosphate and silicate was created the calibration graphs for phosphate and silicate, respectively. The estimated recoveries for phosphate and silicate which obtained by proposed mother wavelets are given in Table 5.

The graphs of CWT for calibration sets of Ni<sup>2+</sup> and Co<sup>2+</sup> were obtained by dmey with scaling value ( $a$ ) of 80. Calibration graphs of Ni<sup>2+</sup> and Co<sup>2+</sup> dmey ( $a = 80$ ) were obtained by measuring the CWT signals at 112 and 86 s correspond to zero-crosses of Ni<sup>2+</sup> and Co<sup>2+</sup>, respectively. The calibration graphs and the statistical results are shown in Table 6. For the prediction of concentration of Ni<sup>2+</sup> and Co<sup>2+</sup> in synthetic mixtures binary mixtures were estimated by CWT-dmey calibration equations at zero-crosses. Linear regression analysis and the statistical results are shown in Table 6. The estimated recoveries of Ni<sup>2+</sup> and Co<sup>2+</sup> which obtained by proposed mother wavelet are given in Table 6. Also transformation of calibration spectra of Ni<sup>2+</sup> and Co<sup>2+</sup> were performed by db5 with optimum scaling value ( $a = 100$ ) (Fig. 3b). Transformation of their binary mixtures were also performed by db5 ( $a = 100$ ). The amplitude of CWT signals at times corresponds to zero-crosses of Ni<sup>2+</sup> and Co<sup>2+</sup>, were created the calibration graphs for Ni<sup>2+</sup> and Co<sup>2+</sup>, respectively. By using the calibration equations, Ni<sup>2+</sup> and Co<sup>2+</sup> were determined in binary synthetic mixtures with proposed mother wavelets. Mean recoveries and the relative standard deviations were calculated and their results were given in Table 7.

The limit of detection (LOD) and limit of quantitation (LOQ) [34] of the method were calculated and are given in Tables 4 and 6. The obtained results show that proposed method based on using differ-

**Table 6**Statistical results of calibration graphs obtained in zero-cross points of Co<sup>2+</sup> and Ni<sup>2+</sup> by proposed method.

Mother wavelet	Cation	Time/s	Linear range/mg L <sup>-1</sup>	Regression equation	r <sup>2</sup>	LOD/mg L <sup>-1</sup>	LOQ/mg L <sup>-1</sup>
dmey	Co <sup>2+</sup>	84	0.05–3.00	$A = 0.22C_{Co} + 0.13$	0.9878	0.014	0.05
db5	Co <sup>2+</sup>	86	0.05–3.00	$A = 0.22C_{Co} + 0.13$	0.9988	0.014	0.05
dmey	Ni <sup>2+</sup>	112	0.04–2.60	$A = -0.26C_{Ni} - 0.12$	0.9842	0.011	0.04
db5	Ni <sup>2+</sup>	112	0.04–2.60	$A = -0.22C_{Ni} - 0.20$	0.9968	0.014	0.05

**Table 7**

Mean recoveries and relative standard deviations for the simultaneous determination of  $\text{Co}^{2+}$  and  $\text{Ni}^{2+}$  in synthetic mixtures by the proposed method.

Mother wavelet	Anion <sup>a</sup>	
	$\text{Co}^{2+}$	$\text{Ni}^{2+}$
dmey	96 ± 5	95 ± 5
db5	95 ± 6	100 ± 3

<sup>a</sup> Average of three determinations ± standard deviation.

ent mother wavelets is suitable for simultaneous determination of desirable elements in binary mixtures.

In the present study, we tried to examine the applicability of CWT-zero-crossing method as a new and easy method for analysis of kinetic profiles. PLS can be also used to resolve of spectral overlapping, but the error of prediction results will be increased by increasing the correlation of components.

In order to validate the proposed method, the experimental data were also analyzed using partial least squares (PLS-1) algorithm. PLS-1 factors were optimized. To select the number of factors in the PLS-1 algorithm a cross-validation method leaving out one sample at a time, was employed [35]. For finding the smallest number of factors, the *F*-statistic test was used. Relative standard errors (R.S.E.) were obtained using the following equation:

$$\text{R.S.E. (\%)} = \left( \frac{\sum_{i=1}^N (\hat{C}_{ij} - C_{ij})^2}{\sum_{j=1}^N (C_{ij})^2} \right)^{1/2} \times 100 \quad (20)$$

The R.S.E.% was calculated as  $3.7 \pm 0.0$  ( $n=4$ ),  $4.6 \pm 0.0$  ( $n=4$ ),  $6.1 \pm 0.5$  ( $n=3$ ) and  $5.3 \pm 0.0$  for phosphate, silicate,  $\text{Co}^{2+}$  and  $\text{Ni}^{2+}$ , respectively. Number of factors was determined as 4 for silicate and phosphate and 3 for  $\text{Co}^{2+}$  and  $\text{Ni}^{2+}$ . The concentrations were predicted and the mean recoveries were calculated as  $98 \pm 0$  ( $n=4$ ),  $106 \pm 0$  ( $n=4$ ),  $102 \pm 6$  ( $n=3$ ) and  $97 \pm 5$  ( $n=3$ ) for phosphate, silicate,  $\text{Co}^{2+}$  and  $\text{Ni}^{2+}$ , respectively. The results obtained by the proposed method were compared with those obtained by PLS method using student's *t*-test. The results are given in Table 8. As the results show the calculated *t*-values for phosphate and silicate and for  $\text{Co}^{2+}$  by CWT-db5 are less than the tabulated values. This indicates that the values obtained by the proposed method and PLS method do not differ. The calculated *t*-values for  $\text{Co}^{2+}$  by CWT-dmey and  $\text{Ni}^{2+}$  are higher than the tabulated values for  $P=0.05$  but are less than those for  $P=0.02$  (*t* is 3.75 and 3.14 for 4 and 6 degrees of freedom for  $P=0.02$ ). This indicates that the results obtained by proposed and PLS methods do differ at 5% level but do not differ at 2% level.

The results show that CWT-zero-crossing method is a good calibration method for the kinetic determination of phosphate and silicate or  $\text{Co}^{2+}$  and  $\text{Ni}^{2+}$ . The method is easy to understand and apply, without any complex algorithm. It is also a time saving method. The results show it is applicable for the analysis of kinetic data even when the correlation is high.

**Table 8**

Comparison of the results obtained for the determination of phosphate, silicate,  $\text{Co}^{2+}$  and  $\text{Ni}^{2+}$  by proposed method with those obtained by PLS method using *t*-test.

Analyte	$t_{\text{calculated}}$		$t_{\text{critical}} (P=0.95)$
	dmey	db5	
Phosphate	2.46	2.68	2.78 <sup>a</sup>
Silicate	2.46	2.68	2.78 <sup>a</sup>
$\text{Co}^{2+}$	2.68	2.40	2.45 <sup>b</sup>
$\text{Ni}^{2+}$	2.92	2.87	2.45 <sup>b</sup>

<sup>a</sup> For 6 degrees of freedom.

<sup>b</sup> For 4 degrees of freedom.

**Table 9**

Effect of foreign ions on the simultaneous determination of phosphate and silicate ( $2 \text{ mg L}^{-1}$  each of phosphate and silicate) and  $\text{Co}^{2+}$  and  $\text{Ni}^{2+}$  ( $2 \text{ mg L}^{-1}$  each of  $\text{Co}^{2+}$  and  $\text{Ni}^{2+}$ ).

Foreign ion	Tolerance limit/ $\text{mg L}^{-1}$	
	Phosphate or silicate	$\text{Co}^{2+}$ or $\text{Ni}^{2+}$
$\text{Na}^+$ , $\text{K}^+$	1000	1000
$\text{Mg}^{2+}$ , $\text{Al}^{3+}$	500	500
$\text{Cu}^{2+}$ , $\text{Pb}^{2+}$	500	80
$\text{F}^-$ , $\text{SO}_4^{2-}$	1000	1000
$\text{NO}_3^-$	1000	1000
$\text{SCN}^-$	500	>600
$\text{AsO}_4^{3-}$	2	1000

#### 5.4. Study of interferences

The effects of foreign species on the simultaneous determination of  $\text{Ni}^{2+}$  and  $\text{Co}^{2+}$ , and also simultaneous determination of phosphate and silicate in their binary mixtures were investigated by measuring the kinetic profiles of the solutions containing  $2.0 \text{ mg L}^{-1}$  of each cation or anion in the presence of various amounts of other ions. The tolerance limit was taken as the amount of added ions causing less than 5% relative error in the determination of ions. Table 9 summarizes the maximum tolerances of cations and anions.

#### 5.5. Applications

Result for the analysis of synthetic mixtures by the proposed method (Table 4) showed satisfactory results for the simultaneous determination of phosphate and silicate. The method was tested by its application to the simultaneous determination of phosphate and silicate in a detergent formulation. The mean values for three determinations were obtained as  $3.4 \pm 0.6$  and  $3.8 \pm 0.3 \text{ mg L}^{-1}$  with CWT-dmey and CWT-sym8, respectively, for silicate and  $4.5 \pm 0.2$  and  $5.8 \pm 0.4 \text{ mg L}^{-1}$  for phosphate. The results obtained by standard method are  $5.6 \pm 0.0$  and  $4.0 \pm 0.0 \text{ mg L}^{-1}$  for phosphate and silicate, respectively [36].

Also phosphate and silicate was determined in tap water. The mean value of three determinations for phosphate and silicate was calculated as  $5.9 \pm 2.6$  and  $2.1 \pm 1.5 \text{ mg L}^{-1}$  with CWT-dmey and  $6.5 \pm 2.4$  and  $2.7 \pm 1.7 \text{ mg L}^{-1}$ , respectively. The results obtained by standard method are  $6.2 \pm 1.1$  and  $2.2 \pm 0.0$  for phosphate and silicate, respectively [36].

The proposed method was also validated by determination of  $\text{Co}^{2+}$  and  $\text{Ni}^{2+}$  in tap water. The tested water samples was found to be free from  $\text{Co}^{2+}$  and  $\text{Ni}^{2+}$  and so synthetic samples were prepared by adding known amounts of  $\text{Co}^{2+}$  and  $\text{Ni}^{2+}$  to the water samples. The recoveries were  $105 \pm 4$  and  $98 \pm 4$  for  $\text{Co}^{2+}$  and  $\text{Ni}^{2+}$ , respectively, as obtained by CWT-dmey and were  $967 \pm 3$  and  $96 \pm 2$  as obtained by CWT-db5.

## 6. Conclusion

A simple, sensitive, precise, and easy to understand and use method for resolving kinetic profiles of binary mixtures for first order, pseudo-first order and second order reactions was introduced. The method does not decrease S/N ratio and does not need to use any separation steps. The main advantage of the proposed method is its applicability for resolving kinetic profiles for the mixtures with kinetic ratios less than 2. High amplitude of WT graphs at zero-crosses improves slope of CWT calibration graphs and the sensitivity of the determinations.



## Acknowledgements

The authors acknowledge the Bu-Ali Sina University Research Council and Center of Excellence in Development of Chemical Methods (CEDCM) for support of this work.

## References

- [1] M. Bahram, A. Afkhami, J. Iran. Chem. Soc. 5 (2008) 352.
- [2] A. Afkhami, A.R. Zarei, Talanta 53 (2001) 815.
- [3] A. Afkhami, T. Madrakian, A.R. Zarei, Anal. Sci. 17 (2001) 1199.
- [4] A. Afkhami, A.R. Zarei, Talanta 60 (2003) 63.
- [5] E. Furusjo, L.G. Danielson, Anal. Chim. Acta 373 (1998) 83.
- [6] B.G.M. Vandeginste, D.L. Massart, L.M.C. Buydens, S. De Jong, P.J. Lewi, J. Smeyers-Verbeke, Handbook of Chemometrics and Qualimetrics, Elsevier, Amsterdam, 1998.
- [7] G. López-Cueto, J. Lizarreta, M. Ostra, C. Ubide, Talanta 58 (2002) 569.
- [8] Y. Ni, Y. Wang, S. Kokot, Food Chem. 109 (2008) 431.
- [9] A. Afkhami, N. Sarlak, A.R. Zarei, Talanta 71 (2007) 893.
- [10] M. Chamsaz, A. Safavi, J. Fadaee, Anal. Chim. Acta 603 (2007) 140.
- [11] Y. Ni, Y. Wang, S. Kokot, Spectrochim. Acta A 70 (2008) 1049.
- [12] Z.L. Zhu, W. Li, J. Xia, Anal. Chim. Acta 527 (2004) 203.
- [13] M.A. Nicholson, J.F. Aust, K.S. Booksh, W.C. Bell, M.L. Myrick, Vib. Spectrosc. 24 (2000) 157.
- [14] A. Afkhami, M. Bahram, Anal. Chim. Acta 526 (2004) 211.
- [15] A. Afkhami, T. Madrakian, M. Bahram, J. Hazard. Mater. 123 (2005) 250.
- [16] A. Afkhami, M. Bahram, Talanta 68 (2006) 1148.
- [17] E. Dinç, D. Baleanu, Talanta 59 (2003) 707.
- [18] E. Dinç, D. Baleanu, J. Pharm. Biomed. Anal. 31 (2003) 969.
- [19] E. Dinç, D. Baleanu, J. AOAC Int. 87 (2004) 360.
- [20] E. Dinç, M. Kanbur, D. Baleanu, Spectrochim. Acta A 68 (2007) 225.
- [21] E. Dinç, D. Baleanu, J. Braz. Chem. Soc. 18 (2007) 962.
- [22] E. Dinç, S. Kaya, T. Doganay, D. Baleanu, J. Pharm. Biomed. Anal. 44 (2007) 991.
- [23] E. Dinç, A. Ozdamir, D. Baleanu, J. Pharm. Biomed. Anal. 37 (2005) 569.
- [24] E. Dinç, D. Baleanu, O. Ustundag, H.Y. Aboul-Enein, Pharmazie 59 (2004) 618.
- [25] E. Dinç, D. Baleanu, J. AOAC Int. 87 (2004) 834.
- [26] E. Dinç, D. Baleanu, A. Tas, Rev. Chim. (Bucharest) 57 (2006) 626.
- [27] E. Dinç, M. Kanbure, D. Baleanu, Pharmazi 60 (2005) 892.
- [28] E. Dinç, A. Özdemir, D. Baleanu, Talanta 65 (2005) 36.
- [29] A. Afkhami, T. Madrakian, M. Abbasi-Tarighat, Food Chem. 109 (2008) 660.
- [30] A. Afkhami, M. Abbasi-Tarighat, M. Bahram, Talanta 75 (2008) 91.
- [31] A. Youssef El-Sayed, Y.Z. Hussein, M.A. Mohammed, Analyst 126 (2001) 1810.
- [32] A. Afkhami, M. Abbasi-Tarighat, Anal. Sci. 24 (2008) 779.
- [33] A. Afkhami, M. Bahram, Microchim. Acta 155 (2006) 403.
- [34] J.C. Miller, J.N. Miller, Statistics and Chemometrics for Analytical Chemistry, Pearson Education, Great Britain, Prentice Hall, 2000.
- [35] H. Abdollahi, Anal. Chim. Acta 442 (2001) 327.
- [36] American Public Health Association, Standard Methods for the Examination of Water and Wastewater, 19th ed., Water Environment Federation, American Water Works Association, 1995.



## Chiral separation of $\beta$ -adrenergic blockers on CelluCoat column by HPLC

Imran Ali<sup>a</sup>, Vinay D. Gaitonde<sup>b</sup>, Hassan Y. Aboul-Enein<sup>c,\*</sup>, Afzal Hussain<sup>a</sup>

<sup>a</sup> Department of Chemistry, Jamia Millia Islamia (Central University), New Delhi 110025, India

<sup>b</sup> Prochrome India, A/2, Varsha Milan, Sahar Road, Andheri East, Mumbai 400999, India

<sup>c</sup> Pharmaceutical and Medicinal Chemistry Department, Pharmaceutical and Drug Industries Research Division, National Research Centre, Dokki, Cairo 12311, Egypt

### ARTICLE INFO

#### Article history:

Received 22 September 2008

Received in revised form

25 November 2008

Accepted 26 November 2008

Available online 6 December 2008

#### Keywords:

$\beta$ -adrenergic blockers

Chiral separation

CelluCoat column

Supra-molecular mechanism

### ABSTRACT

The chiral separation of 10  $\beta$ -adrenergic blockers (acebutalol, alprenolol, bufuralol, bisoprolol, celiprolol, carazolol, indenolol, metoprolol, oxprenolol and propranolol) was achieved on CelluCoat column (250 mm  $\times$  4.6 mm, 5  $\mu$ m particle size). The mobile phases used were (90:10:0.2, v/v/v) and (95:5:0.2, v/v/v) combinations of *n*-heptane–ethanol–diethylamine, respectively. The flow rates were 0.5, 1.0 and 2.0 mL min<sup>-1</sup> with detection at 225 nm. The capacity (*k*), selectivity ( $\alpha$ ) and resolution (*R*<sub>s</sub>) factors were 0.44–12.91, 1.12–2.19 and 1.00–9.50, respectively. The proposed supra-molecular models indicated that the chiral resolution were governed by  $\pi$ – $\pi$  interactions, hydrogen bondings and steric effect.

© 2008 Elsevier B.V. All rights reserved.

## 1. Introduction

US FDA, European Committee for Proprietary Medicinal Products and other drugs regulatory agencies have restricted the marketing of racemic drugs [1,2] since usually the desired pharmacological activity resides in one enantiomer while the other enantiomer may be toxic, less active and possesses undesirable side effects [3]. Therefore, dosage concentration of a racemic drug is an illusion to the patients as normally 50% drugs is active while the other 50% is inactive or toxic [4,5]. Therefore, some pharmaceutical companies are manufacturing pure enantiomeric drugs using enantiomeric separations techniques. Chiral separation by high performance liquid chromatography (HPLC) has become a powerful tool in the development of chiral drugs. There are numerous commercially available chiral selectors that are used for the resolution of racemic drugs including  $\beta$ -blockers [2,6–8]. Recently, Kromasil introduced a polysaccharide based column named CelluCoat. It is similar to Chiralcel OD-H and has *tris*-3,5-(dimethylphenylcarbamate) cellulose as chiral selector, which is effective, efficient and inexpensive.

Globally,  $\beta$ -adrenergic blockers are used as the drugs of choice in the treatment of hypertension, angina pectoris, cardiac arrhythmias and glaucoma; as millions people are suffering from these disease [9]. Generally, *S*-(–)-enantiomers are pharmacologically effective showing about 50–500-fold higher activities [10–14]. Higher activ-

ities of *S*-(–)-enantiomers are due to their higher receptor affinities because of better stereospecific fitting, which are responsible for a high stereospecific hepatic oxidation [15–20]. Besides, *R*-(+)-propranolol is also used for the treatment of hyperthyroidism (by inhibiting the conversion of thyroxine to triiodothyroxine) and under such situation racemic propranolol mixture can not be administered as it may cause serious side effects to the patients due the prominent adrenergic effect of *S*-(–)-propranolol [21]. Recently, it has been reported that a long term use of these medications may cause the hypertensive patients to be diabetic [6,22,23]. This represents another serious concern to health. In view of these facts, the current prescription of racemic  $\beta$ -adrenergic blockers is not safe from the clinical, medical and health point of views. Therefore, attempts have been made to separate *S*-(–)- and *R*-(+)-enantiomers of  $\beta$ -adrenergic blockers (Fig. 1) by chiral HPLC on CelluCoat column. The results of these findings are presented and discussed herein.

## 2. Experimental

### 2.1. Chemicals and reagents

*n*-Heptane, ethanol, methanol and diethyl amine were of HPLC grade and obtained from E. Merck, India. The other reagents were of AR grade and purchased from E. Merck, India. Ten  $\beta$ -adrenergic blockers (acebutalol, alprenolol, bisoprolol, bufuralol, carazolol, celiprolol, indenolol, metoprolol, oxprenolol and propranolol) were purchased from Sigma Chemical Co., USA. Some  $\beta$ -blockers were extracted from commercial tablets. pH was recorded using a pH

\* Corresponding author. Fax: +20 2 33370931.

E-mail address: [enein@gawab.com](mailto:enein@gawab.com) (H.Y. Aboul-Enein).

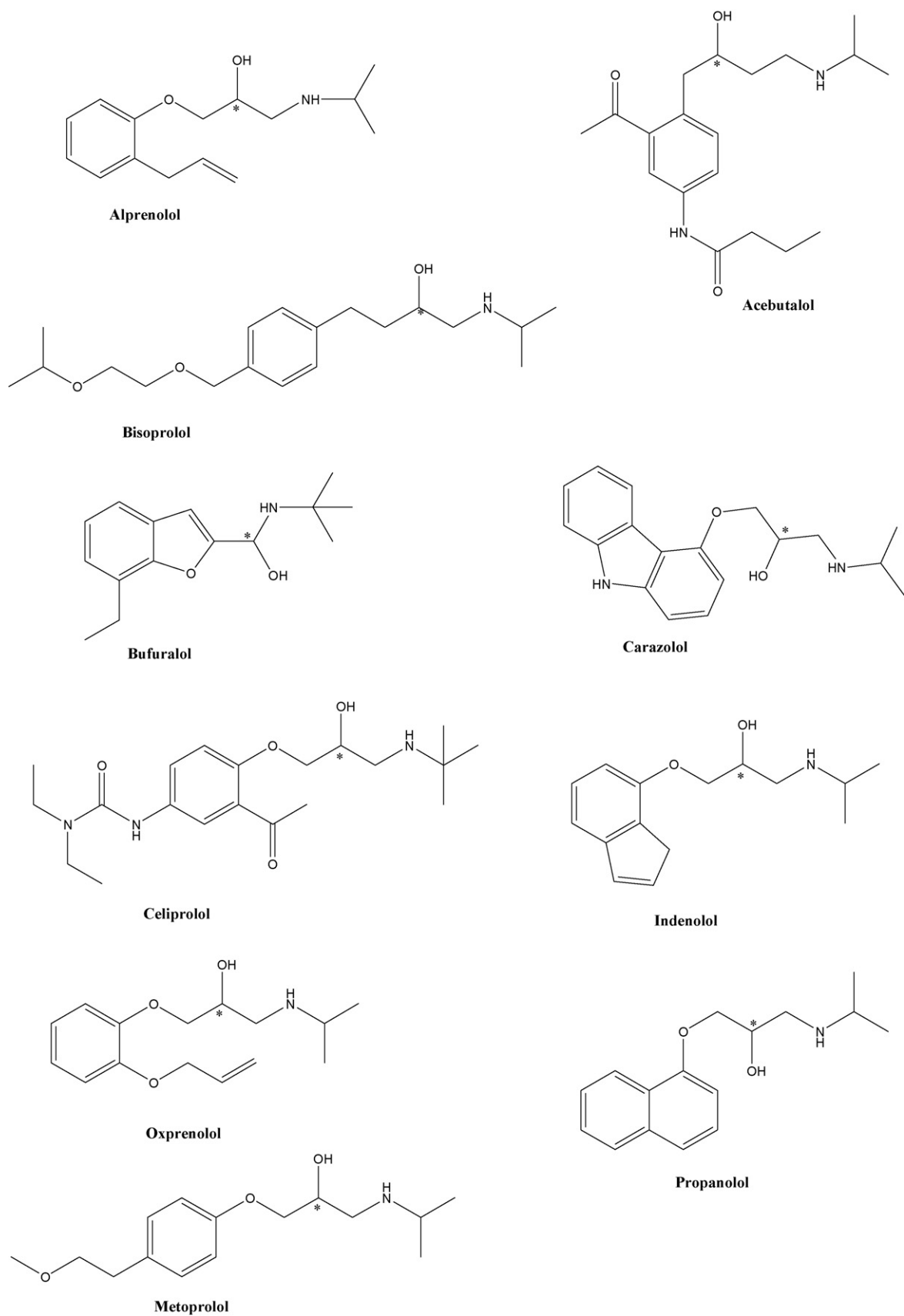


Fig. 1. The chemical structures of  $\beta$ -blockers.

**Table 1**  
Chiral HPLC experimental conditions for  $\beta$ -blockers.

Sl. no.	$\beta$ -blockers	Flow rates ( $\text{mL min}^{-1}$ )	Mobile phases
1.	Acebutalol	1.0	<i>n</i> -Heptane:ethanol:diethylamine (90:10:0.2, v/v/v)
2.	Alprenolol	1.0	<i>n</i> -Heptane:ethanol:diethylamine (90:10:0.2, v/v/v)
3.	Bufuralol	0.5	<i>n</i> -Heptane:ethanol:diethylamine (95:05:0.2, v/v/v)
4.	Bisoprolol	1.0	<i>n</i> -Heptane:ethanol:diethylamine (90:10:0.2, v/v/v)
5.	Celiprolol	1.0	<i>n</i> -Heptane:ethanol:diethylamine (90:10:0.2, v/v/v)
6.	Carazolol	2.0	<i>n</i> -Heptane:ethanol:diethylamine (90:10:0.2, v/v/v)
7.	Indenolol	1.0	<i>n</i> -Heptane:ethanol:diethylamine (90:10:0.2, v/v/v)
8.	Metoprolol	1.0	<i>n</i> -Heptane:ethanol:diethylamine (90:10:0.2, v/v/v)
9.	Oxprenolol	1.0	<i>n</i> -Heptane:ethanol:diethylamine (90:10:0.2, v/v/v)
10.	Propranolol	1.0	<i>n</i> -Heptane:ethanol:diethylamine (90:10:0.2, v/v/v)

Concentration:  $0.1 \text{ mg mL}^{-1}$ . Column: CelluCoat (250 mm  $\times$  4.6 mm,  $5.0 \mu\text{m}$  particle size).

meter (model 611, Orion Research Inc., USA). Purified water was prepared using a Millipore Milli-Q (Bedford, MA, USA) water purification system

## 2.2. Extraction of $\beta$ -blockers from commercial tablets

The extraction of some  $\beta$ -blockers in commercial tablets (10–50 mg) was carried out using methanol. Five tablets of individual  $\beta$ -blocker were weighed and grinded to a fine powder and extracted with 50 mL methanol for 15 min using sonicator at  $40^\circ\text{C}$ . Methanol was decanted and the residue was again extracted twice with methanol. The combined methanol extracts were combined and was filtered through  $0.22 \mu\text{m}$  membrane and evaporated to 20 mL under reduced pressure. The crystallization of  $\beta$ -blockers was carried out and the crystals were separated and washed with diethyl ether and dried in air. The product purity was confirmed by melting points and spectral analysis. These products were used for enantiomeric resolution by HPLC.

## 2.3. HPLC analysis

All HPLC experiments were carried out on an HPLC system of ECOM (Czech Republic) consisting of solvent delivery pump (model Alpha 10), manual injector, absorbance detector (Sapphire 600 UV-vis), chromatography I/F module data integrator (Indtech. Instrument, India) and Winchrome software. The chiral column used was CelluCoat (250 mm  $\times$  4.6 mm,  $5.0 \mu\text{m}$  silica particle size); a gift from Kromasil, Sweden. Samples ( $5.0 \mu\text{L}$ ) were injected manually by Hamilton syringe of  $50 \mu\text{L}$ . The stock solutions ( $0.1 \text{ mg mL}^{-1}$ ) of the racemic  $\beta$ -blockers were prepared in methanol. The mobile phases used in this study were different combinations of *n*-heptane–ethanol–diethylamine, which were used at various flow rates (Table 1). The mobile phases were filtered and degassed on-line daily for 2 min only; before use. The separations were carried out at  $27 \pm 1^\circ\text{C}$  temperature with detection at 225 nm. The chromatographic parameters such as capacity ( $k$ ), selectivity ( $\alpha$ ) and resolution ( $R_s$ ) factors were calculated. The limits of detection (LOD) were determined as per standard procedure [24].

## 3. Results and discussion

The chromatographic parameters are calculated and given in Table 2. The values of selectivity and resolution for all the racemates were greater than one indicating a good separation. The values of retention, separation and resolution factors ranged from 0.44–12.91, 1.12–2.19 and 1.00–9.50, respectively. The peaks were sharp for most of the  $\beta$ -blockers. The chromatograms of the resolution of oxprenolol ( $R_s = 9.50$ ) and bisoprolol enantiomers ( $R_s = 1.00$ ) on CelluCoat column are shown in Figs. 2 and 3, respectively. Most of the  $\beta$ -adrenergic blockers used in this study were separated using *n*-heptane–ethanol–diethylamine (90:10:0.2, v/v/v) [1]

**Table 2**

The capacity ( $k$ ), selectivity ( $\alpha$ ) and resolution ( $R_s$ ) factors for chiral separation of  $\beta$ -blockers on CelluCoat column.

Sl. no.	$\beta$ -blockers	$k_1$	$k_2$	$\alpha$	$R_s$
1.	Acebutalol	3.22	3.63	1.12	1.10
2.	Alprenolol	0.46	0.79	1.71	3.60
3.	Bufuralol	2.43	2.70	1.11	1.04
4.	Bisoprolol	1.00	1.21	1.21	1.00
5.	Celiprolol	2.51	3.62	1.44	3.73
6.	Carazolol	5.52	6.25	1.12	1.06
7.	Indenolol	0.83	2.83	3.37	4.70
8.	Metoprolol	0.82	1.05	1.27	1.30
9.	Oxprenolol	1.31	2.88	2.19	9.50
10.	Propranolol	2.00	2.90	1.40	3.05

Chromatographic conditions: column: CelluCoat (250 mm  $\times$  4.6 mm,  $5.0 \mu\text{m}$  silica particle size), detection: UV, 225 nm, sample volume:  $5.0 \mu\text{L}$  of  $0.1 \text{ mg mL}^{-1}$  concentration and temperature:  $27 \pm 1^\circ\text{C}$ .

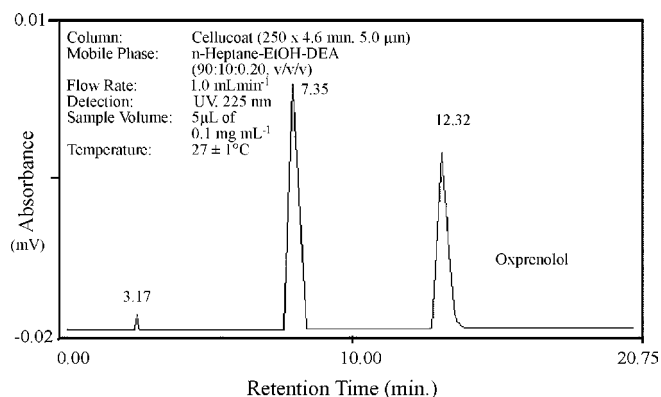


Fig. 2. Chromatograms of the chiral resolution of oxprenolol on CelluCoat column.

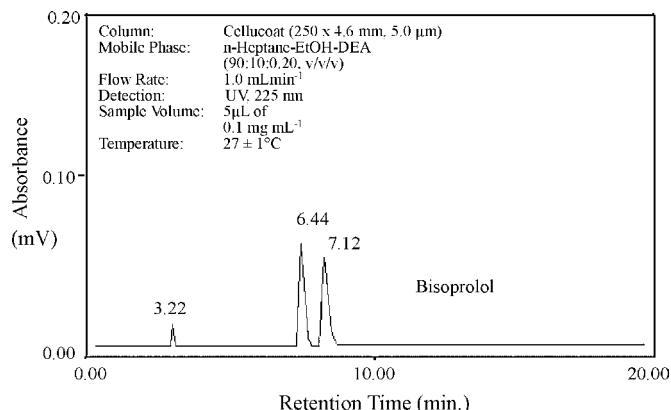


Fig. 3. Chromatograms of the chiral resolution of bisoprolol on CelluCoat column.

as mobile phase with the exception of bufurolol, which resolved using *n*-heptane–ethanol–diethylamine (95:05:0.2, v/v/v) [II] as mobile phase. The polarity of mobile phase [I] is slightly higher in comparison to mobile phase [II]. This may be due to the pronounced steric effect (in the presence of mobile phase [II]) which could be in the vicinity of chiral centre of bufurolol; resulting in poor chiral discrimination of the enantiomers on the reported CSP. All  $\beta$ -adrenergic blockers were separated using  $1.0 \text{ mL min}^{-1}$  flow rate except bufurolol and carazolol, which were resolved by using 0.5 and  $2.0 \text{ mL min}^{-1}$  flow rates, respectively. It may be due to weak and strong bindings of bufurolol and carazolol enantiomers on CeluCoat column, respectively. Furthermore, the maximum ( $R_s = 9.50$ ) and minimum ( $R_s = 1.00$ ) resolution achieved was of oxprenolol and bisoprolol at  $1.0 \text{ mL min}^{-1}$  flow rate, respectively. It is due to higher enantio-selective bondings of oxprenolol enantiomers in comparison to the bondings in bisoprolol enantiomers.

The effect of diethylamine (DEA) was also investigated on chiral resolution as shown in Fig. 4. This Figure indicates that there was an incomplete resolution with 0.1% DEA (for analytes 1–4 and 6) while it was complete with 0.2 and 0.3, respectively. Furthermore, it is evident from this figure that the values of resolution are high at 0.2% in comparison to 0.3%; indicating 0.2% as the best concentration of DEA. These facts suggest that the chiral resolutions of  $\beta$ -blockers under the reported HPLC conditions are highly sensitive to the DEA concentration in the mobile phase. Moreover, the detection limits ( $\mu\text{g mL}^{-1}$ ) were also poor at 0.3% DEA than 0.2% thereby making 0.2% as the optimum concentration used. Similarly, the polarity of the mobile phase was also varied using 5–10 mL of ethanol. As a result of exhaustive experimentation the chromatographic conditions were varied and optimized, the optimized chromatographic conditions are reported herein. These results can be explained on the basis of the chiral recognition mechanisms as described by Okamoto and Yashima [25] and Aboul-Enein and Ali [2]. Basically, cellulose has fair defined grooves providing the chiral surface to the enantiomers. The retention of enantiomers is controlled by  $\pi$ – $\pi$  interactions, hydrogen bondings, dipole induced dipole interactions and steric effects. It may be concluded that  $\beta$ -blockers having strong bondings such as carazolol could resolved with 10 mL ethanol in mobile phase (high polarity) and high flow rate ( $2.0 \text{ mL min}^{-1}$ ).

It is not practical to describe bondings in all 10 racemates reported in this study. However, bondings and chiral recognition mechanisms in two  $\beta$ -adrenergic blockers viz. oxprenolol ( $R_s = 9.50$ ) and bisoprolol ( $R_s = 1.00$ ) are presented herein. These drugs are relatively less polar and containing both hydroxyl and amine groups located close to their chiral centers. The most impor-

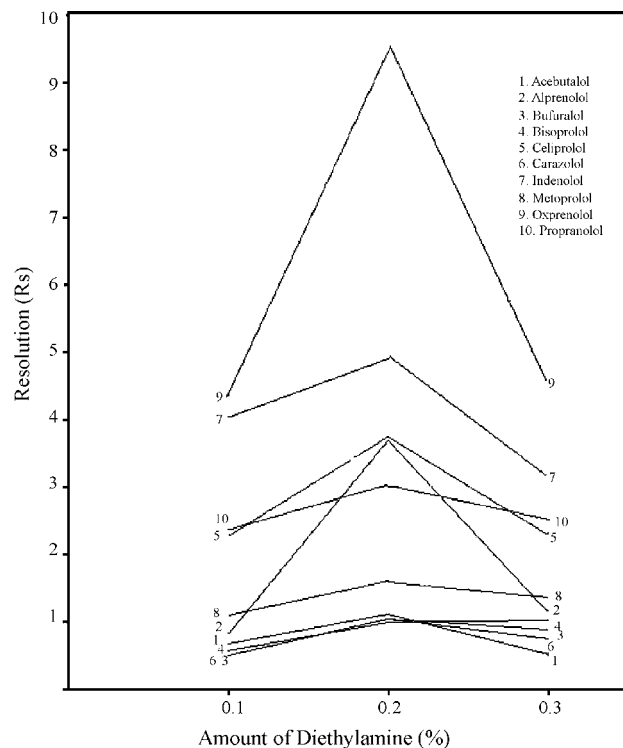


Fig. 4. Effect of diethylamine on the chiral resolution of  $\beta$ -blockers.

tant interactions are  $\pi$ – $\pi$ , hydrogen bonding, van der Waals forces, dipole induced dipole attractions and steric effects [2]. The supra-molecular models of chiral bondings in oxprenolol and bisoprolol are shown in Figs. 5 and 6, respectively. High values of selectivity and resolution of oxprenolol indicate a quite good magnitude of bondings between oxprenolol enantiomers and chiral selector [*tris*-(3,5-dimethylphenyl)carbamate]. Fig. 5 indicates the possibilities of four  $\pi$ – $\pi$  interactions and four hydrogen bondings. On the other hand, Fig. 6 shows only two  $\pi$ – $\pi$  interactions due to steric effect generated by alkyl ester chain; along with four hydrogen bondings. The best resolution of oxprenolol indicates that the chiral resolution of these  $\beta$ -blockers; under the reported experimental conditions; is controlled by  $\pi$ – $\pi$  interactions. However, hydrogen bondings and steric effects also play significant roles in chiral recognition mechanism. These facts are also supported by a model of the enantiomeric recognition mechanism involving helical arrangement of carbamate moieties of several polysaccharide based CSPs [25].

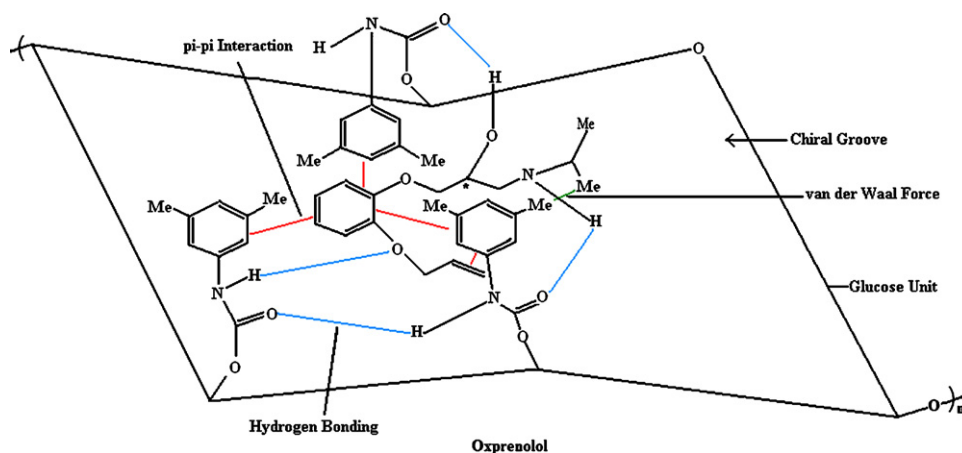


Fig. 5. The representation of supra-molecular bondings of oxprenolol in chiral groove of *tris*-(3,5-dimethylphenyl) carbamate cellulose unit. \* denotes the chiral centre on oxprenolol.

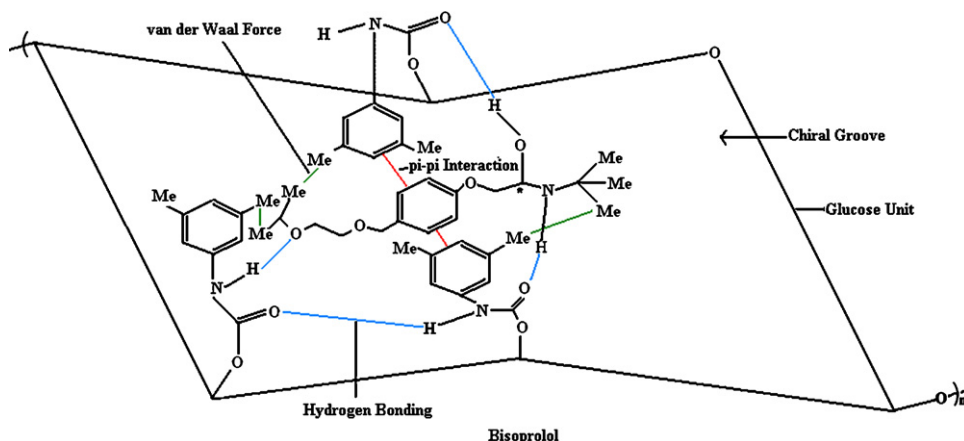


Fig. 6. The representation of supra-molecular bindings of bisoprolol in chiral groove of *tris*-(3,5-dimethylphenyl) carbamate cellulose unit. \* denotes the chiral centre on bisoprolol.

#### 4. Method validation

The validation of the developed method was ascertained by carrying out five sets ( $n=5$ ) of the chromatographic procedures under the identical experimental conditions. The developed method was applied to resolve the enantiomers of  $\beta$ -blockers in some commercially available tablets. The regression analysis was carried out using Microsoft Excel program. The standard deviation (SD) and correlation coefficients ( $R$ ) of chromatographic experiments in commercial tablets were  $\pm 0.05$  and  $0.9999$ , respectively while the confidence levels ranged from 99.5 to 99.8. Low detection limits for these  $\beta$ -blockers ranged from 3.0 to 297.0  $\mu\text{g mL}^{-1}$ . The application of the developed chiral HPLC methods is shown in Fig. 7 depicting enantiomeric resolution of propranolol in commercial tablets.

#### 5. Comparison of CelluCoat with other polysaccharide CSPs

Recently, we have published a review article on the chiral resolution of  $\beta$ -blockers using liquid chromatography including the enantiomeric separation using several polysaccharide based SCPs [8]. Attempts have been made to compare the results of chiral resolution of  $\beta$ -blockers on CelluCoat column with those on other polysaccharide based CSPs. It is not possible to compare point by point but, in general, we observed a complimentary nature of CelluCoat column with other polysaccharide chiral columns. The effect of DEA was almost similar on CelluCoat and other polysaccharide chiral columns for  $\beta$ -blockers. Furthermore, as per our experimental observation some advantages of this column include effective, efficient, fast, inexpensive enantiomeric separations. It has also been

noticed that no pressure limit, quick regeneration after using acidic and basic mobile phase additives and mechanical and chemical stabilities of this column are other working advantages.

#### 6. Conclusion

The reported results describe a successful enantiomeric resolution of 10  $\beta$ -adrenergic blockers on a single chiral column (CelluCoat). All  $\beta$ -blockers are base line resolved with sharp peaks. CelluCoat chiral column is an ideal for enantiomeric resolution of these drugs due to good resolution along with cost friendly and time saving nature. Moreover, the reported HPLC method is simple, fast and reproducible and can be used for the enantiomeric resolution of  $\beta$ -blockers in biological fluids and also on a semi-preparative scale for further pharmacological investigations of the individual enantiomers. The proposed supra-molecular models indicate that the chiral resolution is governed by  $\pi$ - $\pi$  interactions, hydrogen bondings and steric effect. The reported HPLC method was applied for monitoring chiral ratios of some  $\beta$ -blockers in the commercially available tablets and the results obtained were found reliable, selective and reproducible.

#### References

- [1] FDA policy statement for the development of new stereoisomeric drugs, Publication Date: 05/01/1992.
- [2] H.Y. Aboul-Enein, I. Ali, Chiral Separation by Liquid Chromatography and Related Technologies, Marcel Dekker Inc., New York, USA, 2003.
- [3] D. Stevenson, I.D. Wilson, Chiral Separations, Plenum Press, New York, USA, 1988.
- [4] S. Allenmark, Chromatographic Enantioseparation: Methods and Applications, Ellis Horwood Ltd., New York, USA, 1991.
- [5] D.T. Eurich, J.M. Gamble, S.H. Simpson, J.A. Johnson, Diabetes Care 31 (2008) 2136.
- [6] K. Balmer, P.O. Lagerström, B.A. Persson, G. Schill, J. Chromatogr. A 592 (1992) 331.
- [7] H. Navratilova, R. Opatrilova, Z. Kriz, J. Koca, Chirality 16 (2004) 139.
- [8] I. Ali, A. Hussain, H.Y. Aboul-Enein, G. Bazylak, Curr. Drug Discovery Technol. 4 (2007) 255.
- [9] E.H. Meyers, E. Jawetz, A.A. Goldheim, Review of Medical Pharmacology, Lange Medical Publication, Los Altos, USA, 1980.
- [10] T. Walle, U.K. Walle, M.J. Wilson, T.C. Fagan, T.E. Gaffney, Br. J. Clin. Pharmacol. 18 (1984) 741.
- [11] M.G. Schmid, O. Gecse, Z. Szabo, F. Kilar, G. Gubitza, I. Ali, H.Y. Aboul-Enein, J. Liq. Chromatogr. Related Technol. 24 (2001) 2493.
- [12] E.J. Lee, K.M. William, Clin. Pharmacokinet. 18 (1990) 339.
- [13] W.L. Nelson, T.R. Burke, Res. Commun. Chem. Pathol. Pharmacol. 21 (1978) 77.
- [14] A.M. Barrett, V.A. Cullum, J. Pharmacol. 20 (1968) 911.
- [15] J.C. Danilewicz, J.K. Kamp, J. Med. Chem. 16 (1973) 168.
- [16] A.K. Sing, E.R.M. Kedor-Hackmann, M.I.R.M. Santoro, J. AOAC Int. 8 (2001) 1724.
- [17] A.M. Krstulovic, M.H. Fouchet, J.T. Burke, G. Gillet, A. Durand, J. Chromatogr. A 452 (1988) 477.

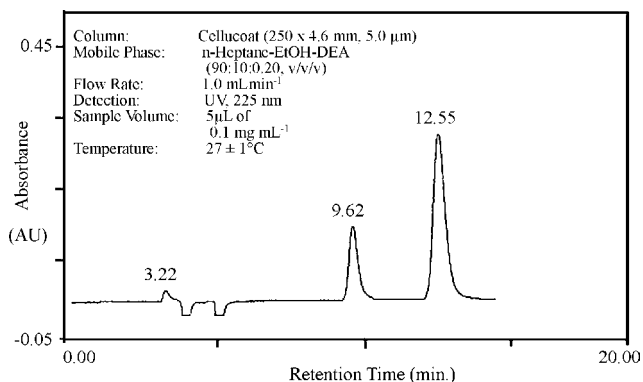


Fig. 7. The enantiomeric resolution of propranolol in commercial tablets on CelluCoat column.

- [18] H.L. Zhang, J.T. Stewart, M. Ujheliyi, *J. Chromatogr. B* 668 (1995) 309.
- [19] A.B. Jeppsson, U. Johansson, B. Waldeck, *Acta Pharmacol. Toxicol.* 54 (1984) 285.
- [20] B. Silber, N.H.G. Holford, S. Regelman, *J. Pharm. Sci.* 71 (1982) 699.
- [21] O. Eber, W. Buchinger, W. Lindner, P. Lind, M. Rath, G. Klima, W. Langsteger, P. Költringer, *Clin. Endocrinol. (Oxf.)* 32 (1990) 363.
- [22] C.V. Ram, *Am. J. Cardiol.* 102 (2008) 242.
- [23] S. Belknap, *Evid. Based Med.* 13 (2008) 50.
- [24] The United State Pharmacopeia, 24th ed., United States Pharmacopeial Convention Rockville, MD, 2000, p. 2150.
- [25] Y. Okamoto, E. Yashima, *Angew. Chem. Int.* 37 (1998), 1020.



# An inhibition type amperometric biosensor based on tyrosinase enzyme for fluoride determination

Engin Asav, Emine Yorganci, Erol Akyilmaz\*

Department of Biochemistry, Faculty of Science, Ege University, 35100 Bornova-Izmir/Turkey

## ARTICLE INFO

### Article history:

Received 3 July 2008

Received in revised form

26 November 2008

Accepted 2 December 2008

Available online 11 December 2008

### Keywords:

Fluoride

Biosensor

Catechol

Tyrosinase

Fluoride determination

Enzyme electrode

## ABSTRACT

In this study, a new biosensor based on the inhibition of tyrosinase for the determination of fluoride is described. To construct the biosensor tyrosinase was immobilized by using gelatine and cross-linking agent glutaraldehyde on a Clark type dissolved oxygen (DO) probe covered with a teflon membrane which is sensitive for oxygen. The phosphate buffer (50 mM, pH 7.0) at 30 °C were established as providing the optimum working conditions. The method is based on the measurement of the decreasing of dissolved oxygen level of the interval surface that related to fluoride concentration added into reaction medium in the presence of catechol. Inhibitor effect of fluoride results in decrease in dissolved oxygen concentration. The biosensor response depends linearly on fluoride concentration between 1.0 and 20 μM with a response time of 3 min.

In the characterization studies of the biosensor some parameters such as reproducibility, substrate specificity and storage stability were carried out. From the experiments, the average value ( $\bar{x}$ ), Standard deviation (S.D) and coefficient of variation (C.V %) were found as 10.5 μM, ± 0.57 μM, 5.43%, respectively for 10 μM fluoride standard.

© 2008 Elsevier B.V. All rights reserved.

## 1. Introduction

Tyrosinase is found in almost all organisms and catalyses several essential biological reactions. It initiates the synthesis of melanin and is responsible for pigmentation of skin and hair, browning of fruit and wound healing in plants and arthropods [1]. Tyrosinase is a binuclear copper containing metalloprotein that oxidizes monophenols and *o*-diphenols into their corresponding *o*-quinones, at the expense of oxygen reduction to water. The conversion of monophenols by tyrosinase proceeds in two consecutive steps, i.e. in the first step monophenol is hydroxylated to its corresponding *o*-diphenol (hydroxylase activity), which in a second step is oxidized to its corresponding *o*-quinone, whereby the enzyme is oxidized by molecular oxygen back to its native form (the enzyme's catecholase activity) [2]. This enzyme which produced from mushrooms has an isoelectric point of 4.5 and carries a negative charge at pH >4.5 in aqueous solution [3]. Tyrosinase tightly inhibits by copper chelators (competitive with respect to oxygen) like tropolon, benzhydroxamic, salicylhydroxamic acid. In addition halide anions such as fluoride, chloride, iodide and bromide play a role in the inhibition of tyrosinase. The fluoride and chloride inhibitions appear competitive, whereas iodide and bromide inhibit through an apparent non-competitive mechanism. The order of strength of inhibition

is I > F > Cl > Br with apparent inhibition constants of 3.8 mM, 11 mM, 0.16 M, and 0.23 M, respectively [4–10].

Sodium fluoride is an ionic compound with the formula NaF. This colourless solid is the main source of the fluoride ion in diverse applications. Fluoride salts are used widely to enhance the strength of teeth by the formation of fluoroapatite, a naturally occurring component of tooth enamel. Toothpaste often contains sodium fluoride to prevent cavities. Sodium fluoride is also used as an antibiotic, as rat poison, and in ceramics. Sodium fluoride strongly reduces tyrosinase activity like acid and cyanide and also inhibition of sodium fluoride is highly depending on pH [11–13].

Biosensors, one of newer areas in analytical chemistry, have simple analysis methods, reproducibility, non-expensive, sensitivity and short response time. Fluoride can be accurately detected by using fluorescence systems [14], immunoassay methods [15], potentiometric chemical sensors [16], colorimetric methods [17–18], spectrophotometry [19], ion chromatography [20], high-performance liquid chromatography [21], optical sensors [22] and gas chromatography [23]. Although all these methods are currently available for fluoride detection, some of them present complicated and time-consuming protocols and also they required expensive equipment and advanced technical support especially to comment on the problems about the results and equipments.

In this study we have developed a tyrosinase biosensor for the detection of fluoride by using its inhibitory effect on the activity of tyrosinase. This effect was monitored amperometrically by

\* Corresponding author. Fax: +90 232 3438624.

E-mail address: [erol.akyilmaz@ege.edu.tr](mailto:erol.akyilmaz@ege.edu.tr) (E. Akyilmaz).



using Clark type dissolved oxygen electrode that is combined YSI oxygenmeter.

## 2. Experimental

### 2.1. Chemicals

Tyrosinase (E.C 1.14.18.1) from mushroom (*Agaricus bisporus*) and calf skin gelatine (225 bloom), glutaraldehyde (25%), sodium fluoride, catechol and all other chemicals were purchased from Sigma Chemical Co. (USA). All solutions used in experiments were prepared just before their use.

### 2.2. Apparatus

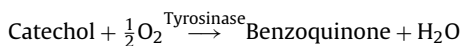
In the study, a YSI Model 58 digital dissolved oxygen (DO) oxygenmeter, YSI 5739 Model DO probes (with YSI 5740 model cable)(YSI Co., Yellow Springs, USA), high sensitive teflon membranes (0.0005 in. thick) for oxygen and Nuve Thermostat (Ankara, TR) were used for constant temperature in the experiments.

### 2.3. Preparation of the biosensors

First DO probe was covered with standard teflon membrane by using an O-ring and then teflon membrane which is selective for oxygen was pre-treatment with 0.5% SDS (sodiumdodecylsulfate) in phosphate buffer (50 mM, pH 7.5) to reduce the tension on the membrane surface, thus microbial contamination was prevented. After that, tyrosinase (69U), and gelatine (5 mg) were mixed in 300  $\mu$ l of phosphate buffer (pH 7.0; 50 mM) for a few minutes. The mixture was dissolved at 38 °C. 200  $\mu$ l of the solution was spread over the DO probe membrane surface and allowed to dry at 4 °C for 25 min and then the enzyme was cross-linked with glutaraldehyde solution (2.5%) in phosphate buffer (50 mM, pH 7.5) for 4 min. Excess of glutaraldehyde was eliminated by washing phosphate buffer and double distilled water.

### 2.4. Principle of the measurement

The principle of the measurement is based on the determination of decreasing oxygen level by the activity of tyrosinase and the detection of changes in consumed oxygen level related to concentration of fluoride added into the reaction medium.



At the beginning, when there is no fluoride in the reaction medium, consumed oxygen level obtained from the enzymatic reaction is measured as ( $\text{DO}_I$ ). After that, fluoride is injected into the reaction medium together with catechol and decrease in the consumed oxygen level is determined as ( $\text{DO}_{II}$ ). Difference between two measurements ( $\text{DO}_I - \text{DO}_{II} = \text{DO}_{III}$ ) is related to concentration of fluoride added into the reaction medium. By using this inhibition based biosensor we detected the both substrate (catechol) and inhibitor (fluoride) of enzyme.

All the measurements were carried out at 35 °C by using thermostatic reaction cells and oxygen saturated phosphate buffer (50 mM, pH 7.0).

## 3. Results and discussion

### 3.1. Detection of the inhibition effect of fluoride on the activity of tyrosinase

For the detection of the inhibition effect of fluoride on the activity of tyrosinase biosensor some experiments were made. In

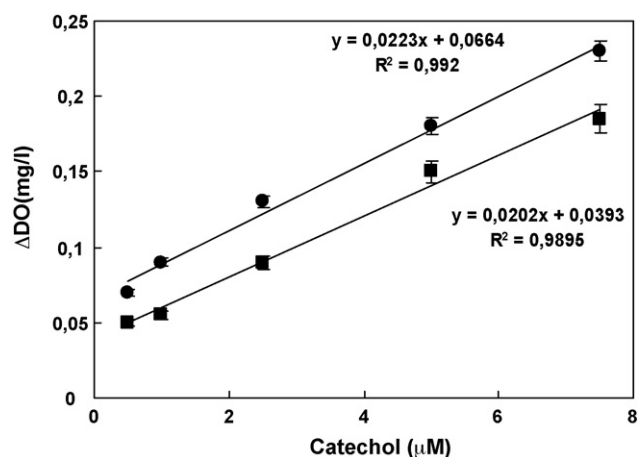


**Fig. 1.** The inhibition effect of sodium fluoride on the biosensor response (phosphate buffer; pH 7.0, 50 mM at 30 °C). (●) without fluoride; (■) with fluoride. The activity of tyrosinase, the concentration of fluoride, the percentage of glutaraldehyde and gelatine amount were kept constant at 40.7 U/cm<sup>2</sup>, 10  $\mu$ M, 2.5%, and 4.21 mg/cm<sup>2</sup>, respectively.

experiments first, the biosensor was used for obtaining a standard curve for catechol detection by using catechol standards between 0.5  $\mu$ M and 7.5  $\mu$ M concentration in the absence of fluoride. In the second step, by using the same catechol standards, that all of them containing 10.0  $\mu$ M fluoride, a new standard curve was obtained. From the second standard curve, we investigated that fluoride competitively decreased the biosensor responses. Fig. 1 shows this obvious effect on the tyrosinase enzyme.

### 3.2. Optimization of the immobilization parameters

#### 3.2.1. Effect of enzyme activity on the biosensor response

To determine the effect of enzyme activity on the biosensor response, different amounts of tyrosinase were studied. For this purpose, we prepared three different biosensors that contained 20.35 U/cm<sup>2</sup>, 40.7 U/cm<sup>2</sup> and 81.4 U/cm<sup>2</sup> activity of tyrosinase, and all of them immobilized with gelatine (5 mg) and glutaraldehyde (2.5%) as cross-linking agent. Results obtained from the experiments were shown in Fig. 2. The best useful curve was obtained by the biosensor which was prepared to 40.7 U/cm<sup>2</sup> activity of

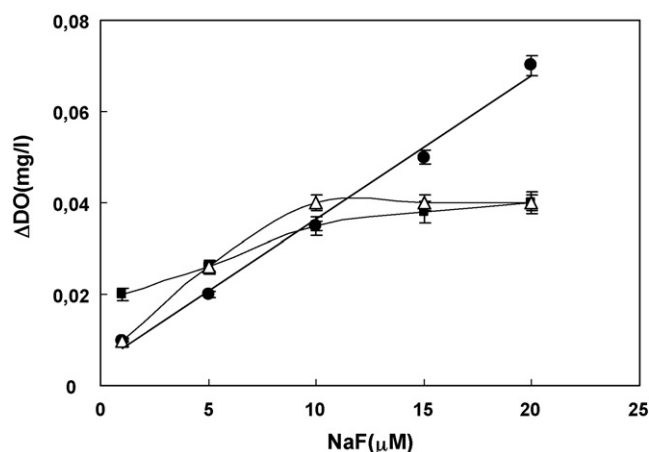


**Fig. 2.** The effect of tyrosinase activity on the biosensor response. The activity of tyrosinase: (Δ-Δ) 20.35 U/cm<sup>2</sup>, (●) 40.7 U/cm<sup>2</sup>, (■) 81.4 U/cm<sup>2</sup>. Phosphate buffer; pH 7.0, 50 mM; T=30 °C; the concentration of catechol, the amount of gelatine and the percentage of glutaraldehyde were kept constant at 2.5  $\mu$ M, 4.21 mg/cm<sup>2</sup>, 2.5%, respectively.

tyrosinase. Response of this biosensor was higher and correlated linearly at fluoride concentration between 1  $\mu\text{M}$  and 20  $\mu\text{M}$ . By using the other biosensors containing 20.35 U/cm<sup>2</sup> and 81.4 U/cm<sup>2</sup> tyrosinase activity, narrow linear regions that were correlated linearly at fluoride concentration between 1  $\mu\text{M}$  and 10  $\mu\text{M}$  were obtained. As a result, the best responses and linear range were obtained by the biosensor prepared to 40.7 U/cm<sup>2</sup> activity of tyrosinase.

### 3.2.2. Effect of gelatine amounts on the biosensor response

To determine the effect of gelatine amounts on the biosensor response different amounts of gelatine were used. For this purpose the biosensors containing 2.10 mg/cm<sup>2</sup>, 4.21 mg/cm<sup>2</sup>, and 8.42 mg/cm<sup>2</sup> gelatine, were prepared and used. All biosensors had 40.7 U/cm<sup>2</sup> tyrosinase activity and all of them were cross-linked by glutaraldehyde (2.5%). According to results obtained from experiments it can be said that fluoride was correlated linearly with a range between 1  $\mu\text{M}$  and 20  $\mu\text{M}$  concentrations by the biosensor prepared to 4.21 mg/cm<sup>2</sup> gelatine.

On decreasing the amount of gelatine from 4.21 mg/cm<sup>2</sup> to 2.10 mg/cm<sup>2</sup> showed a swerve on the curve and also decreases on biosensor responses. The most important reason of this effect was the escape of enzyme from the bioactive layer, due to insufficient tightness of the enzyme immobilization. When we used 8.42 mg/cm<sup>2</sup> gelatine in the biosensor preparation, the biosensor responses were very low and in addition we obtained a linear standard graph for the fluoride concentration only between 5  $\mu\text{M}$  and 15  $\mu\text{M}$ . Because, increasing of gelatine leads to thicker diffusion barriers in between the bioactive layer and the electrode surface. Thicker diffusion barrier hinders the effective working of the enzyme and also diffusion of substrate and inhibitor from the bioactive layer to interval surface. These experiments showed that optimal biosensor responses were achieved by the biosensor which contained 4.21 mg/cm<sup>2</sup> gelatine.

### 3.2.3. Effect of the percentage of glutaraldehyde on the biosensor response

In this part of the optimization studies, different percentages of glutaraldehyde were used in the biosensor preparation for the determination of the effect of the glutaraldehyde on the biosensor response. For this purpose first three biosensors containing 40.7 U/cm<sup>2</sup> activity of tyrosinase and 4.21 mg/cm<sup>2</sup> gelatine were prepared, and then the biosensors prepared were treated with 1.25%, 2.50%, and 5.0% glutaraldehyde solutions for cross-linking. When we used 1.25% concentration of glutaraldehyde in the biosensor preparation we detect a linear region that is between 1  $\mu\text{M}$  and 10  $\mu\text{M}$  concentrations of fluoride. In this concentration range the biosensor's responses higher than the other biosensor's responses which obtained by preparing 2.5% and 5.0% glutaraldehyde. Nevertheless, response obtained for 1  $\mu\text{M}$  NaF was nearly the same, the response obtained for 10  $\mu\text{M}$ . In this case, the linear region obtained was nearly horizontal and not useful for quantitative analysis. Lower concentrations of glutaraldehyde were not sufficient enough to allow adequate cross-linking of the enzyme and gelatine molecules. So, the most useful and better responses were obtained by using the biosensor prepared to 2.5% glutaraldehyde. From experiments it is obvious that fluoride was detected with a linear range between 1  $\mu\text{M}$  and 20  $\mu\text{M}$  concentrations by the biosensor which was prepared to 2.5%.

When we considered about this findings it is clear that an increase in the percentage of glutaraldehyde from 2.5% to 5.0% brought about an explicit decrease in biosensor responses. The most important reason of this effect was the formation of stricter cross-links. Hence catechol, the substrate molecule, could not be approached easily and converted into the product.

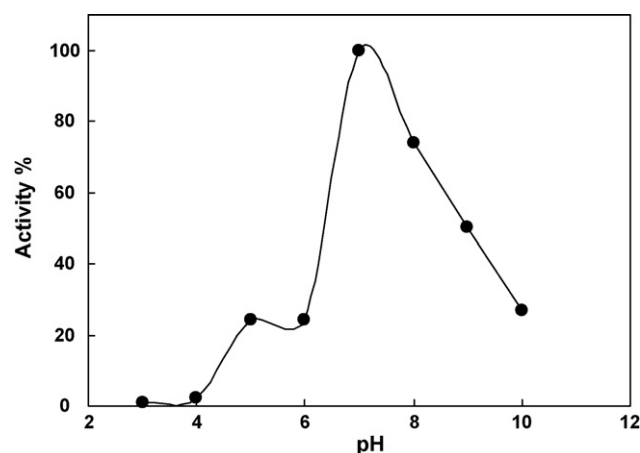


**Fig. 3.** The effect of pH on the biosensor response acetate buffer (3.0–4.0), citrate buffer (5.0–6.0), phosphate buffer (7.0–8.0) and glycine buffer (9.0–10.0) 50 mM, 30 °C. The activity of tyrosinase, the concentration of catechol and fluoride, the percentage of glutaraldehyde and amount of gelatine were kept constant at 40.7 U/cm<sup>2</sup>, 2.5  $\mu\text{M}$ , 10  $\mu\text{M}$  and 4.21 mg/cm<sup>2</sup>, respectively.

### 3.3. Optimization of working conditions

#### 3.3.1. Effect of temperature on the biosensor response

To determine the effect of temperature on the biosensor response is very important due to nature of biocomponent and also obtain the best biosensor responses. Experiments were carried out between 15 °C and 40 °C. From results, it can be said that the highest biosensor responses were obtained at 30 °C for biosensor. At upper and lower temperature than 30 °C decreases in the biosensor responses were observed.

#### 3.3.2. Effect of pH on the biosensor response

The experiments were carried out at different buffer systems for the determination of the effect of pH value on the biosensor response. For this purpose 50 mM concentrations of acetate (pH 3.0–4.0), citrate (pH 5.0–6.0), phosphate (pH 7.0–8.0) and glycine (pH 9.0–10.0) buffers were prepared and used. Results obtained from experiments were shown in Fig. 3. According to findings, optimum pH value was achieved as 7.0. There was no response in the biosensor at pH 3.0 and pH 4.0 values. If we consider the optimum pH value (pH 7.0) of the enzyme it can be said that the most important factor in this result is the instability of the enzyme at pH values lower than ca. 5. In addition, from the literature Tepper et al. [5] were discussed that acidic form of the enzyme is capable for binding of fluoride.

### 3.4. Analytical characteristics of the biosensor

#### 3.4.1. Linear range of the biosensor

After optimizations of the biosensor, experiments were carried out to achieve a calibration curve for fluoride at optimal conditions. From results it can be said that the biosensor responses correlated linearly at sodium fluoride concentration between 1.0  $\mu\text{M}$  and 20  $\mu\text{M}$ . From the experiments a linear regression equation was obtained for ( $y = 0.0031x + 0.005$ ) with  $R^2 = 0.9934$ , where  $y$  represents  $\Delta\text{DO}$  (mg/l) and  $x$  represents concentration of NaF ( $\mu\text{M}$ ).

#### 3.4.2. Reproducibility

For determination of the reproducibility of the biosensor experiments were also carried out at 10  $\mu\text{M}$  sodium fluoride and 2.5  $\mu\text{M}$  catechol concentration ( $n = 8$ ). From experiments, the average value ( $\bar{x}$ ), standard deviation (S.D) and coefficient of variation (CV %) were calculated as 10.5  $\mu\text{M}$ ,  $\pm 0.57 \mu\text{M}$  and 5.43% respectively.

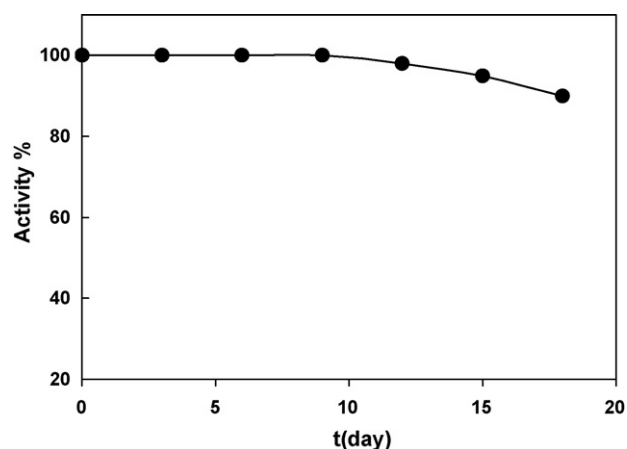


**Fig. 4.** Storage stability. (Phosphate buffer; pH 7.0, 50 mM at 30 °C) The activity of tyrosinase, the concentration of catechol and fluoride, the percentage of glutaraldehyde and amount of gelatine were kept constant at 40.7 U/cm<sup>2</sup>, 2.5 μM, 10 μM, 2.5% and 4.21 mg/cm<sup>2</sup>, respectively.

#### 3.4.3. Storage stability

To observe storage stability of the biosensor a newly prepared biosensor was stored at +4 °C. Measurements were carried out in every third day along 18 days. The biosensor was used only for this experiment. Results obtained from experiments were shown in Fig. 4. Although 18 days were passed, there was only 10% loss in the activity and also responses of the biosensor for fluoride.

## 4. Conclusions

Inhibition based biosensors have been used very efficiently especially in environmental analysis. The principle of operation of these biosensors is based on the interaction that occurs between specific chemical and biological agents “inhibitors”, present in the sample, and the biocatalyst such as an enzyme, a polyenzymatic sequence and/or even a whole tissue immobilized on the biosensor

itself. The response of the biosensor is therefore proportional to the reduction rate of the enzymatic reaction which takes place at the sensor’s interface.

This work demonstrates that the biosensor which is based on inhibition of fluoride has good analytical properties such as fast response (3 min), long-time stability and a good detection range and it is suitable for routine analysis of catechol and sodium fluoride at the same time. As a result, all of these advantages suggested that sodium fluoride can be detected easily, accurately and rapidly.

## References

- [1] H. Decker, T. Schweikardt, D. Nillius, U. Salzbrunn, E. Jaenicke, F. Tuzcek, *Gene* 398 (2007) 183.
- [2] Y.D. Tanimoto, L.F. Ferreira, *Anal. Chim. Acta* 596 (2007) 210.
- [3] C. Védrine, S. Fabiano, C.T. Minh, *Talanta* 59 (2003) 535.
- [4] A. Rescigno, F. Sollai, B. Pisu, A. Rinaldi, E. Sanjust, *J. Enzyme Inhib. Med. Chem.* 17 (2002) 207.
- [5] A.W.J.W. Tepper, L. Bubacco, G.W. Canters, *J. Biol. Chem.* 277 (2002) 30436.
- [6] R. Peñafiel, J.D. Galindo, F. Solano, E. Pedreño, J.L. Iborra, J.A. Lozano, *Biochim. Biophys. Acta* 788 (1984) 327.
- [7] J.H. Martinez, F. Solano, R. Peñafiel, J.D. Galindo, J.L. Iborra, J.A. Lozano, *Comp. Biochem. Physiol. B* 83 (1986) 633.
- [8] J.H. Martinez, F. Solano, J.C. García-Borrón, J.L. Iborra, J.A. Lozano, *Biochem. Int.* 11 (1985) 729.
- [9] K. Streffer, H. Kaatz, C.G. Bauer, A. Makower, T. Schulmeister, F.W. Scheller, M.G. Peter, U. Wollenberger, *Anal. Chim. Acta* 362 (1998) 81.
- [10] A.W.J.W. Tepper, L. Bubacco, G.W. Canters, *J. Biol. Chem.* 279 (2004) 13434.
- [11] G.M. Whitford, *J. Dent. Res.* 66 (1987) 1056.
- [12] M.S. McDonagh, P.F. Whiting, P.M. Wilson, A.J. Sutton, I. Chestnutt, J. Cooper, K. Misso, M. Bradley, E. Treasure, J. Kleijnen, *Br. Med. J.* 321 (2000) 855.
- [13] Z. Laufer, R.P. Beckett, F.V. Minibayeva, *Ann. Bot.* 98 (2006) 1035.
- [14] S. Chakraborty, M.A. Tarr, *Can. J. Chem.* 85 (2007) 153.
- [15] M.A. Sagot, F. Heutte, P.Y. Renard, F. Dollé, P. Pradelles, E. Ezan, *Anal. Chem.* 76 (2004) 4286.
- [16] S. Tokalioglu, S. Kartal, U. Sahin, *Turk. J. Chem.* 28 (2004) 203.
- [17] X. Gao, H. Zheng, G. Shang, J.G. Xu, *Talanta* 73 (2007) 770.
- [18] X.F. Shang, H. Lin, H.K. Lin, *J. Fluor. Chem.* 128 (2007) 530.
- [19] H.B. Li, X.R. Xu, *Talanta* 48 (1999) 57.
- [20] S. Thangavel, K. Dash, S.M. Dhavile, S.C. Chaurasia, T. Mukherjee, *J. Chromatogr. A* 1074 (2005) 229.
- [21] X.R. Xu, H.B. Li, J.D. Gu, K.J. Paeng, *Chromatographia* 59 (2004) 745.
- [22] H.S.M. Abd-Rabboh, M.E. Meyerhof, *Talanta* 72 (2007) 1129.
- [23] G. Wejnerowska, A. Karczmarek, J. Gaca, *J. Chromatogr. A* 1150 (2007) 173.



# A fast screening method for the presence of atrazine and other triazines in water using flow injection with chemiluminescent detection

David J. Beale<sup>a,c</sup>, Nichola A. Porter<sup>a,c,\*</sup>, Felicity A. Roddick<sup>b,c</sup>

<sup>a</sup> School of Applied Sciences (Applied Chemistry), RMIT University, GPO Box 2476V, Melbourne 3001, Australia

<sup>b</sup> School of Civil, Environmental and Chemical Engineering, RMIT University, GPO Box 2476V, Melbourne 3001, Australia

<sup>c</sup> Cooperative Research Centre for Water Quality and Treatment, Private Mail Bag 3, Salisbury, South Australia 5108, Australia

## ARTICLE INFO

### Article history:

Received 20 August 2008

Received in revised form 17 November 2008

Accepted 17 November 2008

Available online 30 November 2008

### Keywords:

Pesticides

Atrazine

Chemiluminescence

Flow injection analysis

Natural organic matter

Solid phase extraction (SPE)

## ABSTRACT

Atrazine is a triazine herbicide which contains two secondary aliphatic amine groups. Previous studies have shown that aliphatic amines react with tris(2,2'-bipyridyl)ruthenium(III) to produce chemiluminescence. This paper describes the application of tris(2,2'-bipyridyl)ruthenium(III) to the detection of atrazine and related triazine herbicides in water by flow injection chemiluminescence analysis. The optimised experimental conditions were determined to be: sample and carrier flow rates of 4.6 mL min<sup>-1</sup>, sample at pH 9 buffered with 50 mM borax, and reagent concentration of 1 mM tris(2,2'-bipyridyl)ruthenium(III) in 20 mM H<sub>2</sub>SO<sub>4</sub> (pH 1). Under these conditions, the logarithm of the chemiluminescence intensity versus concentration was linear in the range of 2.15–2150 μg L<sup>-1</sup> for samples in MilliQ water, and the limit of detection of atrazine in water was determined to be 1.3 ± 0.1 μg L<sup>-1</sup>. Validation of the method was performed using direct injection HPLC. The presence of natural organic matter (NOM) significantly increased the chemiluminescence, masking the signal generated by atrazine. Isolating the target analyte via solid phase extraction (SPE) prior to analysis removed this interference and concentrated the samples, resulting in a greatly improved sensitivity with a detection limit of 14 ± 2 ng L<sup>-1</sup>.

© 2008 Elsevier B.V. All rights reserved.

## 1. Introduction

The manufacture of pesticides is a multi-billion dollar industry. The United States alone has an annual market of over USD 10 billion per annum, while Australia spends approximately one tenth of that amount [1]. If pesticides were not used, it is estimated that one third of the world's food crops would be destroyed by pests either during growth, harvesting, or storage. Losses would be even higher in developing countries [1].

Pesticide contamination has been a widely publicised topic over the past 30 years and will continue to be a problem in the future. Already we are observing large scale pesticide contamination within Australia, in particular from triazine herbicides such as atrazine, simazine and hexazinone. In 1992, atrazine was recorded at concentrations as high as 53 mg L<sup>-1</sup> in northern Tasmania [2]. In 1996, atrazine and hexazinone were recorded throughout a northern Queensland groundwater system at concentrations up to 1.4 μg L<sup>-1</sup> [2] and in 2000, they were found along with simazine at levels up to 0.6 μg L<sup>-1</sup> within the South Australian groundwater system [2]. More recently in 2004, an aerial pesticide sprayer crashed

in northern Tasmania releasing its load of atrazine, simazine, and alphacypermethrin (a pyrethroid insecticide) into the environment. This resulted in 90% mortality at a nearby oyster farm as well as an observed increase in health complaints in the local community [3]. Despite these incidents, water catchments are not monitored on a continuous basis for these contaminants. While the reported results for atrazine in the Melbourne catchments are below 0.1 μg L<sup>-1</sup>, which is well below the Australian safe drinking water guidelines of 40 μg L<sup>-1</sup> [4], aquatic organisms have been shown to be very sensitive. An example of this was recently reported where atrazine at 0.1 μg L<sup>-1</sup> was shown to be detrimental to amphibians [5].

The routine analysis of water for pesticide residues is generally time consuming and expensive. A thorough monitoring program requires the analysis of hundreds of samples, most of which have pesticide residues below detectable limits. Hence there is a need for a continuous, user friendly, sensitive screening method which is capable of performing rapid analyses to detect pollution events of the type described above. This initial screening will reduce the time wasted in analysing hundreds of pesticide-free samples by conventional methods. This goal is becoming more attainable as screening methods are being developed based on fluorescence, immunoenzymatic and chemiluminescence flow injection techniques.

Pesticide analysis using flow injection techniques was first reported by Méndez et al. in 1988 [6]. Analysis of triazines by flow injection was not applied until 1996 when Martinez et al. coupled an on-line liquid–liquid extraction manifold for the enrichment of

\* Corresponding author at: School of Applied Sciences (Applied Chemistry), RMIT University, GPO Box 2476V, Melbourne 3001, Australia. Tel.: +61 3 9925 1787; fax: +61 3 9639 1321.

E-mail address: [nichola.porter@rmit.edu.au](mailto:nichola.porter@rmit.edu.au) (N.A. Porter).

triazines in surface waters with spectrophotometric detection. They used a 10 min pre-concentration step to achieve a detection limit for atrazine of  $5 \mu\text{g L}^{-1}$  [7]. Galeano Diaz et al. incorporated solid phase extraction for the rapid pre-concentration (under 5 min) of naptalam with fluorescence detection, reaching a detection limit of  $0.03 \mu\text{g L}^{-1}$  [8], while Coly and Aaron [9], and Maniasso et al. [10] used photochemically induced fluorescence for the detection of sulfonylurea herbicides ( $0.1 \mu\text{g L}^{-1}$ ) and fenvalerate ( $17 \mu\text{g L}^{-1}$ ) respectively. In 2001, Vilchez et al. used the same detection method for imidacloprid ( $0.3 \mu\text{g L}^{-1}$ ) [11], and Icardo et al. also used it for the detection of sulfonamides ( $30 \mu\text{g L}^{-1}$ ) [12].

Many researchers have utilized the inhibitory effects of pesticides on acetyl cholinesterase or other enzymes to develop biosensors for their determination [13–20]. While these methods are sensitive (e.g., detection of atrazine as low as  $0.03 \mu\text{g L}^{-1}$ ; 2,4-D at  $0.2 \mu\text{g L}^{-1}$ ; TNT at  $0.1 \mu\text{g L}^{-1}$ ; and diuron at  $0.2 \mu\text{g L}^{-1}$ ) enzymatic methods are time consuming, expensive to develop, have a limited lifespan, and need to be operated under temperature controlled laboratory conditions.

More recently, chemiluminescence has gained in popularity [21]; it is a cheaper alternative to immunoenzymatic flow injection methods, requires less method development and less stringent operating conditions. Chemiluminescence has been successfully applied to the determination of carbaryl using a variety of chemiluminescent reagents; the detection limits obtained were  $4.9 \mu\text{g L}^{-1}$  with luminol [22],  $29 \mu\text{g L}^{-1}$  with cerium(IV) [23],  $5 \mu\text{g L}^{-1}$  with peroxyoxalate [24,25], and  $12 \mu\text{g L}^{-1}$  using photo-generated tris(2,2'-bipyridyl)ruthenium(III) [26]. Wang et al. applied luminol chemiluminescence to the determination of dichlorvos ( $8 \mu\text{g L}^{-1}$ ) [27], and Adcock et al. used tris(2,2'-bipyridyl)ruthenium(III) for glyphosate determination in commercial formulations [28].

As demonstrated by Adcock et al. [28], Perez-Ruiz et al. [26] and Costin et al. [29,30], tris(2,2'-bipyridyl)ruthenium(III) chemiluminesces with aliphatic amines at 610 nm. This paper further explores the application of tris(2,2'-bipyridyl)ruthenium(III) chemiluminescence to the determination of atrazine (which contains two secondary aliphatic amines) in natural waters.

## 2. Experimental

### 2.1. Dissolved organic carbon (DOC)

After filtration ( $0.45 \mu\text{m}$  hydrophilic membrane (Durapore PVDF)) dissolved organic carbon (DOC) was determined using a Sievers 820 TOC analyser.

### 2.2. Direct injection HPLC—sample validation method

High performance liquid chromatography (HPLC) direct injection was carried out according to the method of Perkins et al. [31] with a Waters HPLC pump (M-6000A, Waters Associates Inc., USA.) operated isocratically with a water–acetonitrile–methanol (60:25:15, v/v/v) mobile phase at a flow rate of  $1.5 \text{ mL min}^{-1}$ . Aqueous samples were injected ( $500 \mu\text{L}$ ) via a Waters HPLC injection valve fitted with a  $500 \mu\text{L}$  loop using a 2 mL glass barrel syringe. The injected sample passed through a C8,  $5 \mu\text{m}$   $250 \text{ mm} \times 4.6 \text{ mm}$  column (Model 831815 Spherisorb, Phase Separation, USA). The HPLC system was connected to a UV–vis detector (SPD-10AV, Shimadzu, Japan) set at 220 nm coupled to a chart recorder (Model 3395, Hewlett Packard, USA).

### 2.3. FIA instrumentation

Sample and carrier streams were propelled using a peristaltic pump (Ismatec, Switzerland) through bridged PVC tubing ( $1.85 \text{ mm}$  i.d.; Global FIA, USA). All other tubing was PTFE ( $0.5 \text{ mm}$  i.d.; Global

FIA, USA). The chemiluminescent reagent was injected into the carrier stream via a six-port injection valve (Rheodyne, USA). The reagent and sample streams merged at a T-piece positioned 20 mm from a coiled PTFE ( $0.5 \text{ mm}$  i.d.) flow cell. The flow cell was mounted flush against the window of a red sensitive photomultiplier tube (PMT) (Hamamatsu H5784-20, Japan) which was powered by a stable power supply (built in-house, RMIT, Australia). Output from the PMT was monitored using a chart recorder. The arrangement is shown in Fig. 1.

### 2.4. Solution preparation

A stock solution of atrazine ( $9.8 \text{ g L}^{-1}$ ) (Sigma–Aldrich) was prepared in 10 mL acetonitrile and sonicated for an hour. Working standard solutions of atrazine were prepared daily in MilliQ water. Stock solutions were stored at  $4^\circ\text{C}$  in the dark when not in use.

Atrazine metabolites (hydroxyatrazine, deethylatrazine, deisopropylatrazine) and the pesticides (simazine and hexazinone) were obtained from Orica.

### 2.5. Tris(2,2'-bipyridyl)ruthenium(III)

Tris(2,2'-bipyridyl)ruthenium(II) was synthesised according to the method described by Broomhead and Young [32], and 1 mM solutions were freshly prepared in 20 mM sulfuric acid (LR). Lead dioxide ( $0.1 \text{ g}$ ) (Sigma–Aldrich) was added to 100 mL tris(2,2'-bipyridyl)ruthenium(II) in 20 mM sulfuric acid to oxidise the ruthenium complex prior to filtration ( $0.45 \mu\text{m}$  syringe filter) and injection ( $100 \mu\text{L}$ ) into a MilliQ water carrier stream pumped at  $4.6 \text{ mL min}^{-1}$ . The second stream carried atrazine ( $50 \text{ mM}$  borax, pH 9) pumped at  $4.6 \text{ mL min}^{-1}$  (Fig. 1).

### 2.6. Interference species

All materials added were of analytical grade or higher. Fulvic acid and sodium humate (80% purity) from brown coal in North Eastern Victoria were sourced from Omnia Pty. Ltd., Australia. Humic acid sodium salt was obtained from Aldrich, USA TG. The humic and fulvic standards were freshly prepared weekly in MilliQ water. Stock solutions of  $\text{Al}^{3+}$ ,  $\text{Cu}^{2+}$ ,  $\text{Fe}^{3+}$  and  $\text{Fe}^{2+}$  ( $1000 \text{ mg L}^{-1}$ ) were prepared in 2% nitric acid and kept in high density polyethylene bottles. These were diluted to  $100 \text{ mg L}^{-1}$  and adjusted to pH 7 with NaOH prior to analysis. All solutions were stored at  $4^\circ\text{C}$  in the dark when not in use. All other cations and anions were prepared daily at  $100 \text{ mg L}^{-1}$  in MilliQ water.

### 2.7. Membrane filtration

The microfiltration/ultrafiltration (MF/UF) rig incorporated a stirred-cell (Amicon 8050, membrane area  $13.4 \text{ cm}^2$ ) connected to a feed reservoir, and operated at a transmembrane pressure of 70 kPa (MF) and 110 kPa (UF) regulated using nitrogen gas, and stirrer

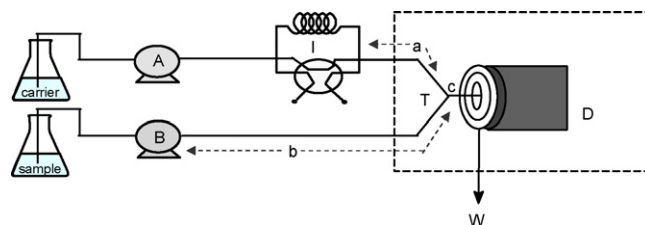


**Fig. 1.** FIA schematic for tris(2,2'-bipyridyl)ruthenium(III) chemiluminescence for atrazine determination. (A) MilliQ water carrier stream peristaltic pump ( $4.6 \text{ mL min}^{-1}$ ). (B) Sample stream peristaltic pump ( $4.6 \text{ mL min}^{-1}$ ). (I) Injection valve ( $100 \mu\text{L}$  1 mM tris(2,2'-bipyridyl)ruthenium(III) reagent). (T) T-piece. (D) PMT. (W) Waste. Tubing lengths: (a) 11 cm, (b) 20 cm and (c) 2 cm.

speed of 430 rpm. All experiments were conducted at room temperature (22 °C). Hydrophilic polyvinylidene fluoride MF membranes (Durapore GVWP, 0.22 µm, Millipore) and hydrophilic polyethersulphone UF membranes (100 kDa MWCO, Millipore) were used for filtration tests.

### 2.8. Solid phase extraction (SPE)

SPE cartridges (0.5 mg Bond Elut C18) were pre-conditioned with 5 mL methanol followed by 5 mL MilliQ water (Millipore MilliQ Water System) prior to sample introduction (1 L aliquot, filtered 0.45 µm hydrophilic membrane) at 2–4 mL min<sup>-1</sup>. The SPE cartridges were then washed with two 5 mL aliquots of MilliQ water prior to analyte elution (2 mL min<sup>-1</sup>) with a 4 mL and two 3 mL methanol aliquots (final eluent volume 10.0 mL).

## 3. Results and discussion

### 3.1. Optimisation of experimental parameters

Experiments were constructed in Minitab 14 (statistical software, Minitab Inc., USA) to optimise carrier flow rate, sample flow rate, sample pH, reagent pH and reagent concentration. These experiments were designed using an inbuilt optimisation function within Minitab; the main batch of experiments consisted of 96 runs which included 16 centre points and a random combination of the chosen variables containing the maximum and minimum parameter settings. Upon completion, the optimisation was fine tuned within Minitab to determine the most suitable optimisation parameters for analysis of the pesticides. Detailed below are the outcomes of the design and subsequent values for each parameter chosen.

### 3.2. Effect of flow rate

Flow rate is a very important FIA chemiluminescence parameter. The ideal flow rate will deliver the sample plug to the detector at the point of maximum chemiluminescence and minimal sample dispersion. The effect of flow rate on the chemiluminescence reaction between atrazine and tris(2,2'-bipyridyl)ruthenium(III) was investigated over 1.0–8.0 mL min<sup>-1</sup>. The highest chemiluminescence signal generated from atrazine and the lowest blank signal (overall highest signal to blank ratio (SBR)) was recorded at 4.6 mL min<sup>-1</sup> (RSD 0.1%, *n* = 5; 100 µg L<sup>-1</sup> atrazine). Flow rates ± 1.0 mL min<sup>-1</sup> resulted in a decreased SBR (>15%) and RSD (>0.5%).

### 3.3. Effect of pH

The pH of tris(2,2'-bipyridyl)ruthenium(III) was investigated over the range of 1–4. Reagent pH greater than pH 4 was not studied since at that pH and above tris(2,2'-bipyridyl)ruthenium(III) is reduced instantly upon filtration from lead dioxide back to the inactive tris(2,2'-bipyridyl)ruthenium(II). It was found that pH 1 was optimal, giving more reproducible results than pH 2 and above. Due to the acidic nature of the chemiluminescence reagent, and its reactivity with protonated aliphatic amines, an investigation of analyte pH over the range of 1–13 was carried out with freshly prepared buffer solutions: 0.2 M potassium chloride and 0.2 M hydrochloric acid (HCl) (pH 1–2), 0.1 M potassium hydrogen phthalate and 0.1 M HCl (pH 2–5), 0.1 M potassium dihydrogen phosphate and 0.1 M sodium hydroxide (NaOH) (pH 6–8), 0.25 M sodium borate (borax) and 0.1 M HCl/0.1 M NaOH (pH 8–10), 0.1 M sodium carbonate/0.1 M sodium phosphate and 0.1 M NaOH (pH 11–12), and potassium chloride and 0.2 M NaOH (pH 13). When the sample pH was below 7 no chemiluminescence was generated by the target analyte. Above pH

**Table 1**

Summary of analytical and statistical parameters achieved for the determination of atrazine by flow injection chemiluminescence (*n* = 4).

Statistical figures of merit	
Intercept	-0.0944
Slope	0.1515
Linear dynamic range (µg L <sup>-1</sup> )	2.15–2150
Limit of detection (LOD) <sup>a</sup> (µg L <sup>-1</sup> )	1.3
Limit of quantification (LOQ) <sup>b</sup> (µg L <sup>-1</sup> )	3.1
Practical method detection limit (MDL) <sup>c</sup> (µg L <sup>-1</sup> )	2.0
Standard deviation of the slope	0.003
Standard deviation of the intercept	0.01
Standard deviation of the regression	0.03
Correlation coefficient	0.9795

<sup>a</sup> Limit of detection calculated using 3 × SD of the blank (*n* = 36) [33].

<sup>b</sup> Limit of quantification calculated using 10 × SD of the blank (*n* = 36) [33].

<sup>c</sup> Practical method detection limit calculated using 0.01 µg L<sup>-1</sup> atrazine (*n* = 8), the standard deviation was calculated and multiplied by the one-sided *t* distribution [33].

7, the SBR for the reaction significantly increased, reaching maximum chemiluminescence at pH 9 (borax buffer) before tailing off at pH 13, due to an increase in the blank signal.

The effect of the borax buffer strength was investigated at 25, 50 and 100 mM. On increasing the concentration of borax from 25 to 50 mM the chemiluminescence intensity increased 5.6%, but there was no significant effect on chemiluminescence at the higher borax concentration. All subsequent analyses were conducted at pH 9 buffered with 50 mM borax.

### 3.4. Effect of tris(2,2'-bipyridyl)ruthenium(III) concentration

The effect of tris(2,2'-bipyridyl)ruthenium(III) concentration was investigated over the range of 1–5 mM. The highest SBR recorded for the reaction with atrazine (50 µg L<sup>-1</sup> in 50 mM borax buffer pH 9) was when the reagent was 2 mM (SBR 23.6); there was a 50% reduction in SBR when the reagent was 3 mM (SBR 11.4). The optimal concentration was determined to be 1 mM (SBR 22.8). Although the SBR was reduced by 4% from the maximum, the overall cost efficiency is greater since only half the amount of reagent is consumed. All subsequent analyses were performed using 1 mM tris(2,2'-bipyridyl)ruthenium(III).

### 3.5. Determination of the limit of detection

Atrazine solutions over the concentration range 2.15 µg L<sup>-1</sup> to 10.5 mg L<sup>-1</sup> were prepared in 50 mM borax pH 9 and analysed using the optimised conditions. The analytical and statistical parameters obtained for the determination of atrazine by flow injection chemiluminescence are summarised in Table 1.

MilliQ water spiked with increasing amounts of atrazine (30.0, 50.0 and 100.0 µg L<sup>-1</sup>) was analysed using the flow injection method and the results were confirmed using direct HPLC. Table 2 reports observed concentrations and recovery for both analytical methods. The recoveries for both methods were excellent, with

**Table 2**

Recovery for MilliQ water samples spiked with atrazine using the flow injection chemiluminescence and direct injection HPLC methods (*n* = 4).

Analytical method	[Atr] spike (µg L <sup>-1</sup> )	[Atr] observed ± 2SD (µg L <sup>-1</sup> )	Recovery (%)
Flow injection	30.0	32.1 ± 0.1	107
	50.0	51.8 ± 0.3	104
	100.0	102.6 ± 0.3	103
HPLC direct injection	30.0	29 ± 4	97
	50.0	48 ± 2	96
	100.0	99 ± 3	99

**Table 3**

Summary of characteristics of natural water samples analysed by flow injection chemiluminescence analysis for atrazine using tris(2,2'-bipyridyl)ruthenium(III). DOC (dissolved organic carbon).

Sample identification tag	Water source	DOC (mg L <sup>-1</sup> )	Location in Victoria	Activity
1	Ground water	3.1	South East	Cattle farm
2	Creek (seasonal)	4.5	South East	Livestock
3	River (metropolitan)	6.5	Central	Metropolitan
4	Catchment	10.7	South West	Agriculture
5	Decommissioned catchment	11.1	East	None
6	Catchment	11.7	South West	Agriculture

the FI-chemiluminescence method giving slightly higher recoveries than the HPLC method.

### 3.6. Method validation

Natural water samples contain natural organic matter (NOM) originating from decaying plant and animal litter. It is a very complex mixture of compounds containing a wide variety of functional groups, including amines and hydroxyl groups. Since amine groups are known to cause a chemiluminescent response with tris(2,2'-bipyridyl)ruthenium(III), it was anticipated that NOM would cause interference with the detection of atrazine. To test the effect of the presence of NOM on the detection of atrazine, six water samples collected throughout Victoria, Australia, in 2006 (Table 3) were spiked with 10 µg L<sup>-1</sup> atrazine and adjusted to pH 9 (50 mM borax) prior to testing.

The signal from the chemiluminescence emitted in natural water samples was significantly greater than for the control sample (10 µg L<sup>-1</sup> atrazine in MilliQ water pH 9, SBR 8.20), masking the signal generated from reaction of atrazine with 1 mM tris(2,2'-bipyridyl)ruthenium (III) (Fig. 2). It was originally thought that by spiking the natural water sample with a large dose of atrazine that either the emitted signal would be larger than the natural water blank, or a significant change in the peak profile might occur as a result of a difference in the kinetics of the production of chemiluminescence. However, close inspection showed no changes in the peak characteristics and the interfering signal completely dominated the signal from atrazine.

To confirm the identity of the interference, a 1 L aliquot of each of the natural water samples was filtered first through a microfiltration membrane (0.22 µm) and then through an ultrafiltration membrane (100 kDa). Microfiltration did not remove the interference but ultrafiltration did. This showed that the interfering molecules or colloidal particles were less than 0.22 µm but greater than 100 kDa. Attenuated Total Reflectance Fourier Transform Infrared (ATR-FTIR) spectra of the fouled ultrafiltration membrane showed the presence of amine and hydroxyl functional groups. The spectra provided strong evidence that the cause of the

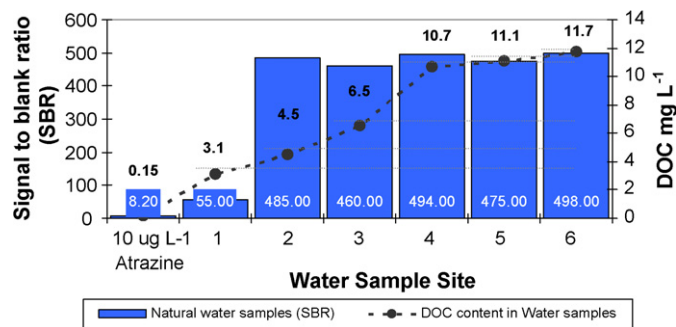


**Fig. 2.** Chemiluminescence response from six natural samples spiked with 10 µg L<sup>-1</sup> atrazine and buffered with 50 mM borax to pH 9. The figure also shows the dissolved organic carbon content (DOC). The signal generated for all six natural waters far exceeds the signal generated from a 10 µg L<sup>-1</sup> standard solution.

interference was due to NOM with distinctive peaks present at 1500–1650 cm<sup>-1</sup> (amine bend); 1200–1500 cm<sup>-1</sup> (hydroxyl bend) and 950–1300 cm<sup>-1</sup> (amine stretch).

### 3.7. Influence of interfering species

The influence of the concentration of a selection of cations, anions, natural organic matter fractions (based on the concentrations likely to be found in natural waters) and selected amine-containing molecules on the analysis of atrazine was ascertained (Table 4).

There was no significant interference from the metal cations or anions with the exception of Fe<sup>3+</sup> and Fe<sup>2+</sup> (2 mg L<sup>-1</sup> and 40 mg L<sup>-1</sup> respectively, which are above Australian Drinking Water Guidelines (ADWG, 2004)) for the flow injection system described. The NOM fractions (above 5 mg L<sup>-1</sup> for humic acid and humate and at 2 mg L<sup>-1</sup> for fulvic acid) and the amino acids tryptophan and tyrosine above 5 mg L<sup>-1</sup> produced a positive response, while sample pH above 9 or an ammonia concentration greater than 0.2 mg L<sup>-1</sup>, increased the blank signal significantly.

### 3.8. Removal of NOM

The interference caused by NOM in natural samples in the determination of atrazine was overcome through solid phase extraction

**Table 4**

Influence of interfering species on the analysis of atrazine by flow injection chemiluminescence, and the subsequent increase/decrease in SBR (number of replicates, n = 4).

Species	FIA <sup>A</sup> (mg L <sup>-1</sup> )	ADWG <sup>B</sup> (mg L <sup>-1</sup> )	ΔSBR
Ni <sup>2+</sup>	100 <sup>a</sup>	–	<1%
Ca <sup>2+</sup>	100 <sup>a</sup>	200	<1%
Zn <sup>2+</sup>	80	3	<1%
Mg <sup>2+</sup>	60	0.1	<1%
Cu <sup>2+</sup>	80	1	<1%
Cl <sup>-</sup>	100 <sup>a</sup>	250	<1%
K <sup>+</sup>	100 <sup>a</sup>	–	<1%
CO <sub>3</sub> <sup>2-</sup>	100 <sup>a</sup>	200	<1%
HCO <sub>3</sub> <sup>-</sup>	100 <sup>a</sup>	200	<1%
Na <sup>2+</sup>	80	180	<1%
Al <sup>3+</sup>	100 <sup>a</sup>	0.2	<1%
Fe <sup>2+</sup>	40	0.3	10%
Fe <sup>3+</sup>	2	0.3	12%
Fulvic acid <sup>c</sup>	2	–	15%
Humic acid <sup>d</sup>	5	–	13%
Humate <sup>c</sup>	5	–	12%
Tryptophan	25	–	8%
Tyrosine	5	–	11%
Nitrate	100	50	<1%
Nitrite	100	3	<1%
Ammonia	0.2	0.5	25%
pH <sup>e</sup>	7–10	6.5–8.5	Exponential

<sup>A</sup> Minimum concentration that caused an increase/decrease in chemiluminescence response (SBR).

<sup>a</sup> Maximum concentration tested.

<sup>b</sup> Australian Drinking Water Guidelines (2004) minimum recommended guideline value for physical and chemical characteristics.

<sup>c</sup> Brown coal origin, North East Victoria.

<sup>d</sup> Technical grade standard.

<sup>e</sup> pH adjustments made with the addition of 2 M HCl and 2 M NaOH.

**Table 5**  
Validation of the proposed flow injection method using direct injection HPLC for comparison. Samples analysed were atrazine spiked MilliQ and natural water samples ( $n = 3$ ).

Sample	Atrazine $0.5 \mu\text{g L}^{-1}$ ( $n = 3$ )		Atrazine $10 \mu\text{g L}^{-1}$ ( $n = 3$ )	
	FIA Recovery % (RSD%)	HPLC Recovery % (RSD%)	FIA Recovery % (RSD%)	HPLC Recovery % (RSD%)
MilliQ	97.5 (0.3)	99.1 (0.5)	99.3 (0.3)	98.6 (0.2)
1	91.6 (3.8)	99.1 (0.6)	83.9 (3.6)	101.5 (0.5)
2	94.9 (0.7)	94.3 (1.4)	88.9 (3.5)	95.5 (0.5)
3	86.6 (1.1)	88.9 (1.5)	85.7 (0.5)	89.7 (4.3)
4	89.5 (5.2)	87.6 (2.8)	92.9 (1.0)	96.5 (0.7)
5	87.8 (6.1)	90.0 (2.1)	96.4 (0.5)	96.7 (1.4)
6	114.9 (6.2)	94.8 (2.4)	106.8 (6.0)	93.5 (1.2)
Statistical comparison—method validation				
$t$ -test (6)		0.39		-0.74
$P$ two tailed		0.71		0.48

(SPE). It is well documented that C18 SPE can be used to capture atrazine from natural waters with recoveries as high as 95%, depending on the nature and retention of the natural organic matter [34]. The six natural water samples and a MilliQ water sample (1 L,  $n = 9$ ) were filtered (0.45  $\mu\text{m}$  nylon filter, Millipore), spiked with  $0.5 \mu\text{g L}^{-1}$  ( $n = 3$ ) or  $10 \mu\text{g L}^{-1}$  ( $n = 3$ ) atrazine and passed through an SPE cartridge. A paired  $t$ -test was performed to determine if there was a significant difference between the HPLC and FIA methods in the analysis of the above samples. The results reported in Table 5 show that there was no significant difference at the 95% confidence level.

The addition of the SPE step removed the interference from NOM (since it was not retained on the cartridge), and concentrated the sample, greatly enhancing sensitivity. The detection limit was reduced to  $14 \text{ ng L}^{-1}$  and the recoveries were very similar to those for HPLC.

HPLC analysis of the natural water sample extracts revealed that the apparent large recovery observed for the flow injection method for natural water 6 was due to the presence of an unknown compound which caused a chemiluminescent reaction with tris(2,2'-bipyridyl)ruthenium(III). On identifying chemicals used within the sample location, it was found that the sample was contaminated with hexazinone, a triazinone herbicide.

### 3.9. Atrazine degradation products and other pesticides

Atrazine is degraded both biologically and photochemically in aqueous environments, with the rate of degradation being

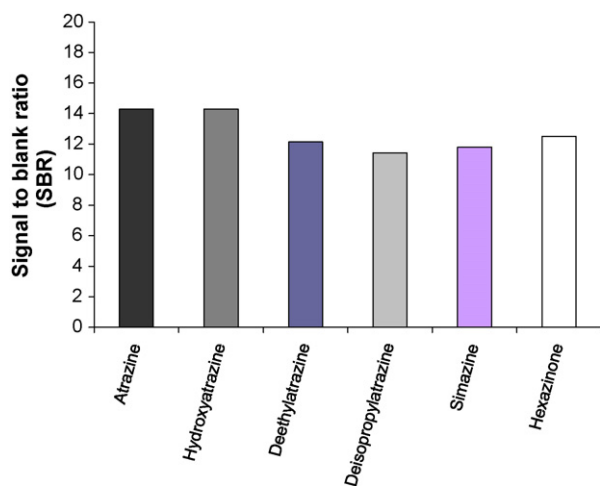


**Fig. 3.** Chemiluminescent response for a range of triazine pesticides (simazine and hexazinone) and atrazine metabolites (hydroxyatrazine, deethylatrazine and deisopropylatrazine) at a concentration of  $20 \mu\text{g L}^{-1}$  in MilliQ water with 50 mM borax (pH 9) with 1 mM tris(2,2'-bipyridyl)ruthenium(III) reagent.

dependent upon numerous variables [5]. In the described flow injection method, it was expected that the degradation products of atrazine would give a chemiluminescent signal similar to the response by hexazinone observed in sample 6 since the metabolites of atrazine also contain secondary and primary aliphatic amines.

A chemiluminescent response was generated when atrazine metabolites and other triazine pesticides were used in the described system, and although the chemiluminescent intensities were slightly weaker (Fig. 3), the ability of the system to detect triazines and their metabolites was demonstrated. The SBRs shown (ranging from 11 to 14) for triazine pesticides (simazine and hexazinone) and atrazine metabolites (hydroxyatrazine, deethylatrazine and deisopropylatrazine) were produced using a concentration of  $20 \mu\text{g L}^{-1}$  in MilliQ water with 50 mM borax (pH 9).

## 4. Conclusions

Atrazine was detected by flow injection chemiluminescence using tris(2,2'-bipyridyl)ruthenium(III) chemiluminescence with a limit of detection of  $1.3 \pm 0.1 \mu\text{g L}^{-1}$  in MilliQ water without pre-concentration. Validation of the method was performed by direct injection HPLC, with a good correspondence between the methods.

However, in natural waters the presence of NOM causes a significant positive chemiluminescent response which masks the response from the atrazine. The functional groups responsible for the interference were identified by ATR-IR as amines and hydroxyl groups present in the natural water. The interference from NOM was removed by SPE (10.0 mL concentrated sample from a 1 L extraction using sample SPE C18 extraction) as the NOM is not retained on the SPE cartridge. This also significantly improved the detection limit for atrazine in natural water samples to  $14 \pm 2 \text{ ng L}^{-1}$  with no significant difference at the 95% confidence level between the results obtained between the FI-chemiluminescence and HPLC methods. When cations and anions were present at levels common in natural waters, only  $\text{Fe}^{3+}$  and  $\text{Fe}^{2+}$  (which were at above the ADWG levels) caused interference.

It was shown that similar compounds, such as the atrazine metabolites and other triazine pesticides, produced a chemiluminescent signal with tris(2,2'-bipyridyl)ruthenium(III). As a consequence, the described system will be very useful as a quick, very sensitive screening method for atrazine and related triazines in natural waters.

## Acknowledgement

This research was funded by the Cooperative Research Centre for Water Quality and Treatment, Australia.



## References

- [1] G.W. Ware, *The Pesticide Book*, 5th ed., W.H. Freeman, San Francisco, 2000.
- [2] J.C. Radcliff, *Pesticide Use in Australia*, Australian Academy of Technological Sciences and Engineering, Melbourne, 2002.
- [3] G. Davis, N. Rushworth, *Tasmania: Name your Poison*, in Sunday, September 26th, 2004, Nine Network: Australia.
- [4] ADWG, National Health and Medical Research Council/Australian Water Resources Council 2004: *Guidelines for Drinking Water Quality in Australia* (2004).
- [5] T. Hayes, *From Silent Spring to Silent Night: Endocrine disruption, amphibian declines, and environmental justice*, Rachel Carson Memorial Lecture, Pesticide News, 70, December 2005.
- [6] J.H. Méndez, R.C. Martínez, F.B. Dominguez, J.I. Jiménez, *Analytica Chimica Acta* 209 (1988) 205–212.
- [7] R.C. Martínez, E.R. Gonzalo, M.P. Santiago Toribio, J.H. Méndez, *Analytica Chimica Acta* 321 (1996) 147–155.
- [8] T. Galeano Díaz, M.I. Acedo Valenzuela, F. Salinas, *Analytica Chimica Acta* 384 (2) (1999) 185–191.
- [9] A. Coly, J. Aaron, *Analytica Chimica Acta* 392 (1999) 255–264.
- [10] N. Maniasso, E.A.G. Zagatto, S. Reis, J.L.M. Santos, J.L.F.C. Lima, *Laboratory Automation and Information Management* 34 (2) (1999) 143–148.
- [11] J.L. Vilchez, M.C. Valencia, A. Navalón, B. Molinero-Morales, L.F. Capitan-Vallvey, *Analytica Chimica Acta* 439 (2) (2001) 299–305.
- [12] M.C. Icardo, J.V.G. Mateo, M.F. Lozano, J.M. Calatayud, *Analytica Chimica Acta* 499 (1–2) (2003) 57–69.
- [13] I.M. Ciumasu, P.M. Kramer, C.M. Weber, G. Kolb, D. Tiemann, S. Windisch, I. Frese, A.A. Ketrup, *Biosensors Bioelectronics* 21 (2) (2005) 354–364.
- [14] S.R. Jain, E. Borowska, R. Davidsson, M. Tudorache, E. Pontén, J. Emnéus, *Biosensors Bioelectronics* 19 (8) (2004) 795–803.
- [15] S. Jin, Z. Xu, J. Chen, X. Liang, Y. Wu, X. Qian, *Analytica Chimica Acta* 523 (1) (2004) 117–123.
- [16] C.A. Marquette, L.J. Blum, *Talanta* 51 (2) (2000) 395–401.
- [17] C.A. Marquette, L.J. Blum, *Sensors and Actuators B: Chemical* 51 (1–3) (1998) 100–106.
- [18] R. Shi, K. Stein, *Analytica Chimica Acta* 324 (1) (1996) 21–27.
- [19] M. Wortberg, C. Middendorf, A. Katerkamp, T. Rump, J. Krause, K. Cammann, *Analytica Chimica Acta* 289 (1994) 177–186.
- [20] R.D. Schmid, R. Kindervater, W. Kunnecke, *Analytica Chimica Acta ACACAM* 234 (1990) 113–117.
- [21] L. Gámiz-Gracia, A.M. García-Campaña, J.J. Soto-Chinchilla, J.F. Huertas-Pérez, A. González-Casado, *TrAC Trends in Analytical Chemistry* 24 (11) (2005) 927–942.
- [22] J.F. Huertas-Pérez, A.M. García-Campaña, L. Gámiz-Gracia, A. González-Casado, M.d.O. Iruela, *Analytica Chimica Acta* 524 (1–2) (2004) 161–166.
- [23] J.A.M. Pulgarín, A.A. Molina, P.F. López, *Talanta* 68 (3) (2006) 586–593.
- [24] J.J. Soto-Chinchilla, L. Gámiz-Gracia, A.M. García-Campaña, L. Cuadros-Rodríguez, *Analytica Chimica Acta* 541 (1–2) (2005) 111–116.
- [25] J.J. Soto-Chinchilla, A.M. García-Campaña, L. Gámiz-Gracia, L. Cuadros-Rodríguez, J.L.M. Vidal, *Analytica Chimica Acta* 524 (1–2) (2004) 235–240.
- [26] T. Pérez-Ruiz, C.M. Lozano, V. Tomás, J. Martín, *Analytica Chimica Acta* 476 (1) (2003) 141–148.
- [27] J. Wang, C. Zhang, H. Wang, F. Yang, X. Zhang, *Talanta* 54 (6) (2001) 1185–1193.
- [28] J.L. Adcock, N.W. Barnett, R.D. Gerardi, C.E. Lenehan, S.W. Lewis, *Talanta* 64 (2) (2004) 534–537.
- [29] J.W. Costin, N.W. Barnett, S.W. Lewis, *Talanta* 64 (4) (2004) 894–898.
- [30] J.W. Costin, N.W. Barnett, S.W. Lewis, D.J. McGillivray, *Analytica Chimica Acta* 499 (1–2) (2003) 47–56.
- [31] B.L. Perkins, R.J. Bushway, L.E. Katz, *Journal of AOAC International* 82 (6) (1999) 1505–1508.
- [32] J.A. Broomhead, C.G. Young, *Inorganic Syntheses* 28 (1) (1990) 338–340.
- [33] G.L. Long, J.D. Winefordner, *Analytical Chemistry* 55 (7) (1983) 713A–724A.
- [34] N.J.K. Simpson, in: N.J.K. Simpson (Ed.), *Solid-Phase Extraction: Principles, Techniques and Applications*, 1, CRC Press, Harbor City, California, USA, 2000, p. 536.



# Determination of vanadium by reaction cell inductively coupled plasma mass spectrometry

A.J. Bednar\*

U.S. Army Engineer Research and Development Center, Environmental Laboratory, 3909 Halls Ferry Rd., Vicksburg, MS 39180, United States

## ARTICLE INFO

### Article history:

Received 24 October 2008

Received in revised form

24 November 2008

Accepted 25 November 2008

Available online 3 December 2008

### Keywords:

Vanadium

Chloride and sulfur interference

Reaction cell

ICP-MS

## ABSTRACT

Recent advances in inductively coupled plasma mass spectrometry (ICP-MS) have included the addition of interference reduction technologies, such as collision and reaction cells, to improve its detection capability for certain elements that suffer from polyatomic interferences. The principle behind reaction cell (RC)-ICP-MS is to remove a particular polyatomic interference by dissociation or formation of a different polyatomic species that no longer interferes with the analyte of interest. However, some interferences cannot be removed by commonly reported reaction gases, such as hydrogen, oxygen, or methane, necessitating using more reactive and hazardous gases, such as ammonia. The current study investigates oxygen as a reaction gas in RC-ICP-MS to specifically react with vanadium analyte ions, rather than the interferents, to produce a polyatomic analyte species and thereby provide a way to analyze for vanadium in complex environmental matrices. The technique has been tested on a series of river water, tap water, and synthetic laboratory samples, and shown to be successful in vanadium analyses in high chloride and sulfate matrices. The zinc isobaric interference on the new vanadium oxide analyte at  $m/z$  67 is also investigated, and can be corrected by using a standard mathematical correction equation. The results of this study further increase the utility of RC-ICP-MS analytical techniques for complex environmental matrices.

Published by Elsevier B.V.

## 1. Introduction

In recent years, inductively coupled plasma mass spectrometry (ICP-MS) has become the premier method for elemental analysis due to its  $\mu\text{g L}^{-1}$  to sub- $\mu\text{g L}^{-1}$  sensitivity and simultaneous detection capabilities, compared to other techniques, such as graphite furnace atomic absorption spectroscopy (GF-AAS). However, ICP-MS does have limitations, which limits its ultimate applicability to all types of samples matrices. Much of this limitation is due to polyatomic interferences caused by concomitant matrix components and the argon plasma gas [1,2]. Some atmospheric-based polyatomic interferences make determination of certain elements almost impossible by ICP-MS, such as  $^{16}\text{O}_2$  on  $^{32}\text{S}$ , while severely hindering detection of others. Chloride-based interferences, for example, are a common problem for many environmentally relevant analytes, including arsenic, selenium, chromium, and vanadium [3–6]. The various polyatomic species that chloride forms in the plasma with oxygen and argon force the use of alternative isotopes, mathematical correction equations, high resolution instruments, or GF-AAS to measure these analytes at low levels in many environmental samples [6,7].

New interference reduction technologies in ICP-MS, specifically reaction or collision cells, have opened new possibilities for analyte determination by ICP-MS. Inclusion of a reaction or collision cell prior to the quadrupole mass analyzer has been shown to effectively reduce or remove these matrix-caused polyatomic interferences, greatly increasing the utility of ICP-MS [4,7–9]. However, alternative isotopes are not always available, as in the case of monoisotopic arsenic. Furthermore, for elements such as chromium and selenium, multiple isotopes are already employed, because all available isotopes have some type of potential interference [4,8,9]. Vanadium, similar to arsenic, is essentially monoisotopic for the purposes of ICP-MS analysis because of the low abundance of the  $^{50}\text{V}$  isotope. The primary isotope,  $^{51}\text{V}$ , is 99.75% abundant, but its determination is hindered in many matrices by  $^{35}\text{Cl}^{16}\text{O}$  and  $^{34}\text{S}^{16}\text{O}^{1}\text{H}$  polyatomic species [1,5]. The minor isotope,  $^{50}\text{V}$  (0.25%), has direct interferences from isotopes of titanium and chromium and various polyatomic species, which limit its utility. One accepted RC-ICP-MS method for vanadium determination uses ammonia as the reaction gas to remove the chloride-based interference [5,10]. However, the use of less troublesome and toxic alternative gases would be advantageous if they are equally effective.

The RC-ICP-MS method reported in the current work uses oxygen as a reaction gas, not to remove the  $^{35}\text{Cl}^{16}\text{O}$  and  $^{34}\text{S}^{16}\text{O}^{1}\text{H}$  interferences on  $^{51}\text{V}$ , but rather to specifically form the  $^{67}(\text{VO})$  polyatomic species [ $^{51}\text{V}^{16}\text{O}$ ] to move it away from the polyatomic interferences, in a similar manner to arsenic determination by

\* Tel.: +1 601 634 3652.

E-mail address: [Anthony.J.Bednar@erdc.usace.army.mil](mailto:Anthony.J.Bednar@erdc.usace.army.mil).

$^{91}\text{(AsO)}$  [10,11]. The  $^{67}\text{(VO)}$  species is then used to quantitatively determine vanadium in complex environmental samples containing high levels of chloride and sulfate. The isobaric interference on  $^{67}\text{(VO)}$  from  $^{67}\text{Zn}$  is corrected by monitoring  $^{68}\text{Zn}$  and applying a mathematical correction equation.

The method has been tested on laboratory spike samples, tap water, and river water collected during dredging activities. The dredged river water samples were of interest due to an oil barge sinking accident south of New Orleans, Louisiana during the summer of 2008. Vanadium can be a constituent in certain oil products, and therefore may indicate oil contamination [12,13]. These matrices were used to test the reliability, robustness, and versatility of the method, and elucidate the benefits of this application of RC-ICP-MS on real-world samples.

## 2. Experimental

### 2.1. Reagents

All chemicals used were of analytical grade or higher purity and used without further purification. The deionized water used had a resistivity of 18.3 M $\Omega$  cm. Single element (vanadium and zinc) and mixed analyte standards for vanadium, zinc, and chromium determination by standard and RC mode ICP-MS and matrix spiking were purchased from SPEX CertiPrep (Metuchen, NJ) and PlasmaCal (Champlain, NY). An external quality control standard (P136-500) was purchased from Environmental Resource Associates (ERA, Golden, CO). Standards were diluted to appropriate concentrations using 1% nitric acid.

### 2.2. Sample collection and preparation

All samples were processed through a 0.45  $\mu\text{m}$  pore-size syringe filter to obtain classically defined 'dissolved' constituents and to prevent clogging of the ICP-MS nebulizer. The samples were diluted 1:10 with 1% nitric acid prior to analysis; triplicate samples were diluted and analyzed for all experiments. River water was obtained from the Mississippi River near Head of Passes, south of Venice, Louisiana, during maintenance dredging operations, and stored in 4 L glass bottles at 4 °C until use. The municipal tap water sample was collected from our laboratory located in Vicksburg, MS, and used immediately after collection.

### 2.3. Instrumentation

All analyses were performed using a PerkinElmer (Wellesley, MA) Elan<sup>®</sup> DRC<sup>®</sup> II ICP-MS equipped with a Burgener Research (Mississauga, Ontario, Canada) MiraMist nebulizer (following modifications of EPA Method 6020) [14]. Details of the ICP-MS instrumental conditions are listed in Table 1. Ultrapure oxygen (Nordan Smith, Vicksburg, MS) was used in the dynamic reaction cell at 0.8 mL min<sup>-1</sup> to create the VO polyatomic species used for vanadium quantitation. Method detection and reporting limits

**Table 1**  
Operating conditions and parameters for the RC-ICP-MS system.

RC-ICP-MS	
PerkinElmer Sciex Elan <sup>®</sup> DRC <sup>®</sup> II	
MiraMist nebulizer argon flow rate	0.85 L min <sup>-1</sup>
Plasma RF power	1.250 W
Sample flush, read delay, and rinse time	18, 20, 40 s
Primary and secondary internal standards	$^{103}\text{Rh}$ , $^{159}\text{Tb}$ , and $^{175}\text{(TbO)}$
Instrument dwell time (per isotope)	50 ms
Analytes monitored in standard mode	$^{51}\text{V}$ , $^{66}\text{Zn}$ , $^{68}\text{Zn}$ , $^{52}\text{Cr}$ , $^{53}\text{Cr}$
Analytes monitored in reaction cell mode	$^{67}\text{(VO)}$ and $^{68}\text{Zn}$
Reaction cell gas and flow rate	Ultrapure oxygen, 0.8 mL min <sup>-1</sup>
Rp <sub>q</sub> reaction cell parameter	0.65

were determined from 8 replicate analyses of a 0.1  $\mu\text{g L}^{-1}$  standard solution in standard and DRC mode. The method detection limit (0.02  $\mu\text{g L}^{-1}$ ) was then calculated as three times the standard deviation of these replicate analyses, with the reporting limit (0.2  $\mu\text{g L}^{-1}$ ) calculated as 10 times the detection limit.

### 2.4. Calibration

All analytes were quantified using linear calibration functions established from the analysis of a blank and a series of three standard solutions (0, 1, 10, and 100  $\mu\text{g L}^{-1}$ ) with typical correlation coefficients ( $R^2$ ) greater than 0.9999 for all analytes. The linear dynamic range extends to at least 1000  $\mu\text{g L}^{-1}$  when using the dual-detector mode in standard ICP-MS. However, in DRC mode, some analyte signal suppression is observed, and therefore 1000  $\mu\text{g L}^{-1}$  is still within the pulse counting mode range.

Instrument calibration was checked periodically with standards containing the analytes of interest at 50  $\mu\text{g L}^{-1}$  and always produced results within  $\pm 10\%$  of the nominal value; blank samples analyzed immediately after the calibration verification standards were always less than the detection limit. Rhodium and terbium were added on-line using a mixing-T prior to the nebulizer as internal standards to correct for instrumental drift. Rhodium ( $m/z$  103) was used for all corrections, yet  $^{159}\text{Tb}$  and  $^{175}\text{(TbO)}$  were also monitored for secondary confirmation.

## 3. Results and discussion

### 3.1. Analysis by standard mode ICP-MS

Quality control and independent source calibration check standards were analyzed with each analytical batch prior to any test matrix samples to verify instrument accuracy. An independent source check standard containing vanadium, zinc, and chromium at 40  $\mu\text{g L}^{-1}$  each, yielded concentrations of 40.2, 36.7, 40.3, and 39.3  $\mu\text{g L}^{-1}$  for  $^{51}\text{V}$ ,  $^{66}\text{Zn}$ ,  $^{52}\text{Cr}$ , and  $^{53}\text{Cr}$ , respectively. The external quality control sample (ERA Standard P136-500 diluted 1:2000 into the ICP-MS calibration range) containing 36, 78, and 26  $\mu\text{g L}^{-1}$  of vanadium, zinc, and chromium, respectively, yielded concentrations of 36.0, 79.9, 25.6, and 25.1  $\mu\text{g L}^{-1}$ , respectively, for  $^{51}\text{V}$ ,  $^{66}\text{Zn}$ ,  $^{52}\text{Cr}$ , and  $^{53}\text{Cr}$ , respectively. Finally, to verify the low level accuracy of the instrument, a 0.5  $\mu\text{g L}^{-1}$  standard was analyzed, and yielded concentrations of 0.48, 0.53, 0.50, and 0.29  $\mu\text{g L}^{-1}$  for  $^{51}\text{V}$ ,  $^{66}\text{Zn}$ ,  $^{52}\text{Cr}$ , and  $^{53}\text{Cr}$ , respectively. The minor  $^{53}\text{Cr}$  isotope (9.5% abundant) yields slightly low values at the 0.5  $\mu\text{g L}^{-1}$  level, yet all other analytes show acceptable recovery at this level.

The deionized water sample, tap water, and five river water samples were analyzed in triplicate for vanadium, zinc, and chromium by standard mode ICP-MS, with the results listed in Table 2. Chromium data are included as a representative example of the potential error chloride-based interferences can produce in such matrices. The  $^{53}\text{Cr}$  results in the five river water samples are significantly higher than the  $^{52}\text{Cr}$  values, primarily due to the  $^{37}\text{Cl}^{16}\text{O}$  polyatomic interference [1,4]. Furthermore, the discrepancy between the two chromium isotope results increases as the chloride concentrations in the samples increase. Therefore, the vanadium values listed in Table 2 determined using  $^{51}\text{V}$  are likely erroneously high due to chloride and sulfur-based polyatomic interferences [1,5].

The results of a matrix spike experiment are given in Table 3. For this study, the test matrices were spiked with 10  $\mu\text{g L}^{-1}$  vanadium, 500  $\mu\text{g L}^{-1}$  zinc, and 10  $\mu\text{g L}^{-1}$  vanadium + 500  $\mu\text{g L}^{-1}$  zinc. The vanadium-only spike experiment yielded recoveries above 120% for river water samples 09 and 13, and over 115% for samples 07 and 24, whereas recoveries in the DI water, tap water, and river water 20

**Table 2**

Average concentrations and standard deviations of triplicate analyses of metal analytes ( $\mu\text{g L}^{-1}$ ) determined by standard mode ICP-MS. Concentrations of chloride and sulfate matrix constituents ( $\text{mg L}^{-1}$ ) determined by ion chromatography. The discrepancy between the two chromium isotopes suggests the vanadium results are also affected by chloride-based interferences. Less than values are below the reporting limit.

Analyte measured Sample matrix	Chloride ( $\text{mg L}^{-1}$ )	Sulfate ( $\text{mg L}^{-1}$ )	$^{51}\text{V}^{\text{a}}$ ( $\mu\text{g L}^{-1}$ )	$^{66}\text{Zn}$ ( $\mu\text{g L}^{-1}$ )	$^{52}\text{Cr}$ ( $\mu\text{g L}^{-1}$ )	$^{53}\text{Cr}^{\text{b}}$ ( $\mu\text{g L}^{-1}$ )
DI water	<0.02	<0.02	<0.2	<0.2	<0.2	<0.2
Tap water	7.0	3.1	<2.0	$5.5 \pm 1.91$	<2.0	<2.0
River water 07	16,000	1100	$124 \pm 6.05$	$13.7 \pm 1.45$	$4.4 \pm 0.35$	$417 \pm 17.9$
River water 09	15,700	1000	$129 \pm 1.21$	$13.5 \pm 1.27$	$5.8 \pm 0.84$	$432 \pm 4.16$
River water 13	11,600	1000	$97.3 \pm 1.80$	$12.0 \pm 0.55$	$4.5 \pm 0.06$	$330 \pm 1.00$
River water 20	840	270	$8.2 \pm 1.59$	$9.5 \pm 9.41$	<2.0	$25.4 \pm 5.00$
River water 24	7700	670	$60.7 \pm 0.81$	$18.2 \pm 1.16$	$3.4 \pm 0.40$	$205 \pm 4.58$

<sup>a</sup> Potential interferences include  $^{35}\text{Cl}^{16}\text{O}$  and  $^{34}\text{S}^{16}\text{O}^1\text{H}$ .

<sup>b</sup> Potential interferences include  $^{37}\text{Cl}^{16}\text{O}$ .

samples were within  $\pm 10\%$  of the nominal spike value. Additionally, the presence of  $500 \mu\text{g L}^{-1}$  zinc did not adversely affect the recovery of  $10 \mu\text{g L}^{-1}$  vanadium, due to the element specific nature of ICP-MS. Vanadium recoveries in the vanadium + zinc spiked experiments were all within  $\pm 10\%$  of the nominal value, as were the zinc recoveries in the zinc-only spiked experiment. The spike recovery results shown in Table 3 would not normally suggest a matrix interference on vanadium, however, in light of the chromium discrepancies in Table 2, it is likely an interference is present, and therefore requires RC-ICP-MS analysis to confirm the vanadium concentrations.

### 3.2. Analysis by RC-ICP-MS with multi-element standard

All test matrix samples previously analyzed by standard mode ICP-MS were reanalyzed for vanadium by RC-ICP-MS using oxygen as a reaction gas. For the reanalysis by RC-ICP-MS, the instrument was calibrated using the same multi-element standard, containing V, Zn, Cr, and other common heavy metals (Spex CertiPrep Instrument Calibration Standard 2), used in the standard mode ICP-MS analysis described above. The analyte  $^{67}\text{VO}$  was used for detection, however, the method quantified vanadium using this species with and without a correction equation for  $^{67}\text{Zn}$  [ $\text{CPS } ^{67}\text{VO} = \text{CPS at } m/z 67 - 0.2181 \times \text{CPS at } m/z 68$ ]. Quantitation of vanadium by measuring  $m/z 83$  ( $^{51}\text{V}^{16}\text{O}_2$ ) was also investigated to eliminate the  $^{67}\text{Zn}$  isotope interference problem, however, insufficient amounts of  $^{83}\text{VO}_2$  are produced under the instrumental conditions tested to provide acceptable method performance and therefore was not investigated further.

The same suite of calibration check and quality control standards were analyzed by RC-ICP-MS as with the standard mode ICP-MS method. The  $0.5 \mu\text{g L}^{-1}$  vanadium standard yielded  $0.56 \mu\text{g L}^{-1}$  for both the zinc-corrected and uncorrected  $^{67}\text{VO}$  analytes. The  $40 \mu\text{g L}^{-1}$  independent source check standard yielded 40.2 and  $40.0 \mu\text{g L}^{-1}$  for the zinc-corrected and uncorrected analytes, whereas, the external quality control sample containing  $36 \mu\text{g L}^{-1}$  vanadium yielded concentrations of 36.2 and  $38.1 \mu\text{g L}^{-1}$  for the zinc-corrected and uncorrected analytes, respectively.

The vanadium concentrations and spike recovery values for the test matrices are shown in Table 4. The first two columns in Table 4 list the measured vanadium concentrations in the test matrices using the  $^{67}\text{VO}$  species with and without the  $^{67}\text{Zn}$  correction equation. The comparison to the vanadium values using  $^{51}\text{V}$  from Table 2 now clearly demonstrates the erroneously high vanadium concentrations determined by standard mode ICP-MS due to polyatomic interferences. The highest vanadium concentration observed by RC-ICP-MS was  $3.6 \mu\text{g L}^{-1}$  in river water 24, compared to  $61 \mu\text{g L}^{-1}$  by standard mode ICP-MS. Other samples with higher chloride concentrations show even larger discrepancies (e.g. river waters 07, 09, and 13). River water 20 had the lowest chloride concentration ( $840 \text{ mg L}^{-1}$ ), and the smallest discrepancy between standard and reaction cell mode ICP-MS results. Furthermore, these low  $\mu\text{g L}^{-1}$  vanadium concentrations are in line with values reported by others [12]. The tap water matrix vanadium concentrations by standard and RC modes were in agreement at less than  $2 \mu\text{g L}^{-1}$ , suggesting that negligible interferences were present in this sample at the 1:10 dilution used for analysis.

There is some difference between the zinc-corrected and -uncorrected vanadium concentrations listed in Table 4, suggesting that the small amount of zinc naturally present in the samples can lead to slightly elevated vanadium concentrations determined by uncorrected  $^{67}\text{VO}$ . When larger amounts of zinc are present (e.g. the  $500 \mu\text{g L}^{-1}$  spike experiments), the effect is more pronounced, and yields apparent vanadium concentrations of 279–368  $\mu\text{g L}^{-1}$  in the matrices tested. However, if the zinc correction equation is applied, erroneously high vanadium concentrations are not observed, yet low  $\mu\text{g L}^{-1}$  levels of vanadium may be obscured in high zinc matrices by the correction equation.

This underestimation of vanadium when using the correction equation in high zinc matrices is likely due to using  $^{68}\text{Zn}$  as the correction isotope, which itself is subject to several polyatomic interferences (e.g.  $^{34}\text{S}_2$ ,  $^{36}\text{Ar}^{32}\text{S}$ ,  $^1\text{H}^{35}\text{Cl}^{16}\text{O}_2$ ,  $^{40}\text{Ca}^{14}\text{N}_2$ , etc.) [1]. Generally,  $^{66}\text{Zn}$  is the preferred isotope for analysis, and any isotopic correction that may be needed, however, due to the isobaric interference of  $^{50}\text{V}^{16}\text{O}$  on  $^{66}\text{Zn}$ ,  $^{68}\text{Zn}$  was used for the current work. The test conditions used represent a worst case scenario, in which

**Table 3**

Average analyte recoveries and standard deviations for triplicate matrix spike experiments using standard mode ICP-MS.

Analyte measured Sample matrix	10 $\mu\text{g L}^{-1}$ V spike recovery (%)	500 $\mu\text{g L}^{-1}$ Zn spike recovery (%)	10 $\mu\text{g L}^{-1}$ V + 500 $\mu\text{g L}^{-1}$ Zn spike recovery (%)	
	$^{51}\text{V}$ (%)	$^{66}\text{Zn}$ (%)	$^{51}\text{V}$ (%)	$^{66}\text{Zn}$ (%)
DI water	$97.1 \pm 3.0$	$102 \pm 0.3$	$99.0 \pm 4.7$	$99.5 \pm 0.1$
Tap water	$96.7 \pm 1.8$	$102 \pm 1.7$	$92.4 \pm 2.7$	$98.4 \pm 0.7$
River water 07	$119 \pm 3.7$	$93.4 \pm 0.6$	$104 \pm 2.3$	$90.2 \pm 1.5$
River water 09	$124 \pm 3.0$	$95.1 \pm 1.4$	$104 \pm 2.3$	$91.0 \pm 0.8$
River water 13	$123 \pm 5.5$	$97.9 \pm 4.0$	$108 \pm 1.8$	$92.2 \pm 0.4$
River water 20	$101 \pm 2.8$	$105 \pm 4.5$	$95.3 \pm 2.7$	$99.6 \pm 1.4$
River water 24	$117 \pm 2.9$	$96.4 \pm 2.9$	$100 \pm 0.7$	$89.7 \pm 0.9$

Samples were spiked with  $10 \mu\text{g L}^{-1}$  V or  $500 \mu\text{g L}^{-1}$  Zn or both. Less than values are below the reporting limit.

**Table 4**  
Average vanadium concentrations and standard deviation in the test matrices determined by RC-ICP-MS using  $^{67}\text{VO}$  uncorrected and  $^{67}\text{VO}$ -C corrected for the  $^{67}\text{Zn}$  interference. The instrument was calibrated using a multi-element standard that contained vanadium and zinc. The average matrix spike recoveries and standard deviations for vanadium are also given for the samples spiked with vanadium, zinc, and vanadium + zinc.

	V concentration ( $\mu\text{g L}^{-1}$ ) by RC-ICP-MS		V spike recovery (%) in 10 $\mu\text{g L}^{-1}$ V spiked sample		Apparent V concentration ( $\mu\text{g L}^{-1}$ ) in 500 $\mu\text{g L}^{-1}$ Zn spiked sample		V spike recovery (%) in 10 $\mu\text{g L}^{-1}$ V + 500 $\mu\text{g L}^{-1}$ Zn spiked sample	
	$^{67}\text{VO}$	$^{67}\text{VO}$ -C	$^{67}\text{VO}$	$^{67}\text{VO}$ -C	$^{67}\text{VO}$	$^{67}\text{VO}$ -C	$^{67}\text{VO}$	$^{67}\text{VO}$ -C
DI water	<0.2	<0.2	90.4 ± 2.0	105 ± 2.2	360 ± 4.0	-0.32 ± 0.16	448 ± 5.2	103 ± 3.9
Tap water	1.5 <sup>a</sup>	1.1 <sup>a</sup>	87.3 ± 2.7	101 ± 3.2	368 ± 17	-2.1 ± 1.39	438 ± 2.8	99.8 ± 2.3
River water 07	3.3 ± 0.18	2.3 ± 0.14	98.9 ± 2.3	115 ± 2.6	279 ± 3.6	<2.0	367 ± 2.5	109 ± 1.2
River water 09	3.4 ± 0.05	2.7 ± 0.09	99.6 ± 3.2	116 ± 3.6	281 ± 4.6	<2.0	365 ± 4.8	109 ± 2.6
River water 13	3.1 ± 0.11	2.0 ± 0.14	101 ± 5.6	117 ± 6.3	297 ± 13	-2.8 ± 1.31	381 ± 3.2	111 ± 2.9
River water 20	1.9 <sup>a</sup>	1.1 <sup>a</sup>	93.2 ± 6.0	108 ± 6.6	366 ± 17	-2.8 ± 1.79	433 ± 4.5	100 ± 1.5
River water 24	3.6 ± 0.06	1.8 <sup>a</sup>	100 ± 4.0	116 ± 4.6	311 ± 10	-2.7 ± 0.55	383 ± 1.6	105 ± 0.6

<sup>a</sup> Estimated value, below detection limit of 2.0  $\mu\text{g L}^{-1}$  with dilution factor.

**Table 5**  
Average vanadium concentrations and standard deviation in the test matrices determined by RC-ICP-MS using  $^{67}\text{VO}$  uncorrected and  $^{67}\text{VO}$ -C corrected for the  $^{67}\text{Zn}$  interference. The instrument was calibrated using a single element vanadium standard rather than a multi-element standard (Table 4). The average matrix spike recoveries and standard deviations for vanadium are also given for the samples spiked with vanadium, zinc, and vanadium + zinc.

	V concentration ( $\mu\text{g L}^{-1}$ ) by RC-ICP-MS		V spike recovery (%) in 10 $\mu\text{g L}^{-1}$ V spiked sample		Apparent V concentration ( $\mu\text{g L}^{-1}$ ) in 500 $\mu\text{g L}^{-1}$ Zn spiked sample		V spike recovery (%) in 10 $\mu\text{g L}^{-1}$ V + 500 $\mu\text{g L}^{-1}$ Zn spiked sample	
	$^{67}\text{VO}$	$^{67}\text{VO}$ -C	$^{67}\text{VO}$	$^{67}\text{VO}$ -C	$^{67}\text{VO}$	$^{67}\text{VO}$ -C	$^{67}\text{VO}$	$^{67}\text{VO}$ -C
DI water	<0.2	<0.2	102 ± 2.4	102 ± 2.4	405 ± 1.0	-0.3 ± 0.12	504 ± 5.0	100 ± 4.0
Tap water	1.8 <sup>a</sup>	1.1 <sup>a</sup>	100 ± 2.4	100 ± 3.4	418 ± 17	<2.0	492 ± 8.0	93.8 ± 3.3
River water 07	3.7 ± 0.13	2.2 ± 0.11	106 ± 2.9	106 ± 2.8	310 ± 5.3	<2.0	367 ± 4.9	103 ± 1.8
River water 09	3.8 ± 0.15	2.7 ± 0.05	107 ± 3.8	107 ± 3.8	307 ± 4.9	<2.0	404 ± 0.9	102 ± 0.9
River water 13	3.5 ± 0.10	2.0 ± 0.07	110 ± 4.7	110 ± 4.6	330 ± 12	-2.8 ± 1.35	401 ± 2.7	105 ± 1.8
River water 20	2.5 ± 0.75	1.4 <sup>a</sup>	105 ± 7.6	105 ± 7.1	413 ± 13	-2.8 ± 0.71	420 ± 2.0	97.6 ± 1.6
River water 24	4.2 ± 0.02	1.9 <sup>a</sup>	109 ± 4.8	109 ± 4.9	349 ± 11	-2.6 ± 0.92	432 ± 3.5	104 ± 1.3

<sup>a</sup> Estimated value, below detection limit of 2.0  $\mu\text{g L}^{-1}$  with dilution factor.

the zinc interferent is present at two orders of magnitude higher concentration than the native vanadium concentration (500  $\mu\text{g L}^{-1}$  vs.  $\sim 3 \mu\text{g L}^{-1}$ ). The spike recovery data for 10  $\mu\text{g L}^{-1}$  vanadium, with or without the zinc correction, shows acceptable performance of the methods. Furthermore, the data in Table 4 demonstrate that a 10  $\mu\text{g L}^{-1}$  vanadium spike in the presence of 500  $\mu\text{g L}^{-1}$  zinc can be successfully recovered using the zinc corrected  $^{67}\text{VO}$  species ( $\pm 10\%$  of nominal spike amount).

### 3.3. Analysis by RC-ICP-MS with single element standard

The final analysis performed used a single element vanadium standard to calibrate the RC-ICP-MS, such that no zinc was present during initial instrument calibration. The same suite of check and quality control standards were again analyzed by RC-ICP-MS, now with the single analyte calibration. The 0.5  $\mu\text{g L}^{-1}$  vanadium standard yielded 0.55 and 0.64  $\mu\text{g L}^{-1}$  for the zinc-corrected and uncorrected  $^{67}\text{VO}$  analytes, respectively. The 40  $\mu\text{g L}^{-1}$  independent source check standard yielded 39.4 and 45.5  $\mu\text{g L}^{-1}$  for the zinc-corrected and uncorrected analytes, whereas, the external quality control sample containing 36  $\mu\text{g L}^{-1}$  vanadium yielded concentrations of 35.8 and 43.8  $\mu\text{g L}^{-1}$  for the zinc-corrected and uncorrected analytes, respectively. The results from these three multi-element check standards suggest that the zinc correction is necessary to achieve acceptable method performance in clean standard matrices if zinc is present.

Vanadium concentrations listed in Table 5 show agreement with the results in Table 4. The zinc-corrected vanadium concentrations are again slightly lower than the uncorrected values, but both single and multi-element calibration RC-ICP-MS methods yield lower vanadium concentrations than the standard mode ICP-MS analysis (Table 2).

When the test matrices were spiked with 10  $\mu\text{g L}^{-1}$  vanadium, both zinc-corrected and uncorrected  $^{67}\text{VO}$  analyses gave acceptable spike recoveries in all matrices tested ( $\pm 10\%$  of nominal values). However, when the samples were spiked with 500  $\mu\text{g L}^{-1}$

zinc, the uncorrected  $^{67}\text{VO}$  analyte yielded apparent vanadium concentrations of 307–418  $\mu\text{g L}^{-1}$ . The zinc-corrected vanadium concentrations in 500  $\mu\text{g L}^{-1}$  zinc spiked experiment were below the detection limit, again suggesting that for low  $\mu\text{g L}^{-1}$  vanadium concentrations in high zinc matrices, the interferences on  $^{68}\text{Zn}$  can result in overcorrection. For samples spiked with 10  $\mu\text{g L}^{-1}$  vanadium and 500  $\mu\text{g L}^{-1}$  zinc, only the zinc-corrected  $^{67}\text{VO}$  species yielded acceptable vanadium recoveries ( $\pm 7\%$  of the nominal value).

## 4. Conclusions

A quantitative RC-ICP-MS method is described for the determination of vanadium in high chloride and sulfate natural water matrices. The technique focuses on specifically creating a polyatomic species for vanadium quantitation that is removed from the primary  $^{35}\text{Cl}^{16}\text{O}$  and  $^{34}\text{S}^{16}\text{O}^{1}\text{H}$  interferences on  $^{51}\text{V}$ . The quantitation of vanadium by  $^{67}\text{VO}$  can potentially be affected by zinc in the sample matrix ( $^{67}\text{Zn} = 4.1\%$  abundance), however, this can be corrected by monitoring  $^{68}\text{Zn}$  and applying an appropriate mathematical correction. The technique allows an alternative determination of vanadium in complex natural matrices by RC-ICP-MS compared to gases that react with the chloride or sulfur-based interferents. There are some method limitations with determination of low  $\mu\text{g L}^{-1}$  vanadium concentrations in sample matrices that have zinc present at orders of magnitude higher concentrations. The overcorrection is primarily due to matrix interferences on  $^{68}\text{Zn}$  used for correction of  $^{67}\text{Zn}$  on  $^{67}\text{VO}$ . All analytical methods contain inherent limitations, however, the use of nonstandard isotopes, polyatomic species, and instrumental conditions, provides a means to determine difficult metal analytes in complex environmental matrices.

## Acknowledgments

The use of trade, product, or firm names in this report is for descriptive purposes only and does not imply endorsement by the U.S. Government. The tests described and the resulting data

presented herein were obtained from research conducted under the Dredging Operations Technical Support Program of the United States Army Corps of Engineers by the USAERDC and in support of the New Orleans US Army Engineer District. Permission was granted by the Chief of Engineers to publish this information. The findings of this report are not to be construed as an official Department of the Army position unless so designated by other authorized documents. The author also thanks Frances Hill and Chris Griggs of the USACE for their editorial comments, and Robert Kirgan and Jeff Corbino of the USACE, and Charolett Hayes of SpecPro, Inc. for technical and sampling assistance.

## References

- [1] T.W. May, R.H. Wiedmeyer, *Atom. Spectrosc.* 19 (1998) 150.
- [2] S.H. Tan, G. Horlick, *Appl. Spectrosc.* 40 (1986) 445.
- [3] R.E. Wolf, K.R. Neubauer, Perkin Elmer Application Note, 2002, Determination of arsenic in chloride matrices, D-6357A.
- [4] A.J. Bednar, R.A. Kirgan, W.T. Jones, *Anal. Chim. Acta* 632 (2009) 27.
- [5] D.E. Nixon, J. Butz, S.J. Eckdahl, M.F. Burritt, K.R. Neubauer, Perkin Elmer Application Note, 2003, Determination of vanadium in serum and urine using the Elan DRC ICP-MS, 006456A.
- [6] C.-F. Wang, C.Y. Chang, C.J. Chin, L.C. Men, *Anal. Chim. Acta* 2–3 (1999) 299.
- [7] P.J. Parsons, F. Barbosa, *Spectrochim. Acta* 62 (2007) 992.
- [8] Z. Chen, M. Megharaj, R. Naidu, *Talanta* 73 (2007) 948.
- [9] K. Jitmanee, N. Teshima, T. Sakai, K. Grudpan, *Talanta* 73 (2007) 352.
- [10] C.C. Chery, K. De Cremer, R. Cornelius, F. Vanhaecke, L. Moens, *J. Anal. Atom. Spectrosc.* 18 (2003) 1113.
- [11] R.W. Reuter, L. Davidowski, K. Neubauer, J. Di Bussolo, Perkin Elmer Application Note, Speciation of five arsenic compounds in urine by HPLC–ICP-MS.
- [12] A.M. Shiller, L. Mao, *Chem. Geol.* (2000) 13–22.
- [13] See for example: HESS MSDS No. 9907, No. 6 Fuel Oil.
- [14] U.S. Environmental Protection Agency. SW-846 Methods for the Analysis of Hazardous Waste, ICP-MS Method 6020A, 2007.



## Development of a flow system for the determination of cadmium in fuel alcohol using vermicompost as biosorbent and flame atomic absorption spectrometry

Joyce Nunes Bianchin<sup>a</sup>, Edmar Martendal<sup>a</sup>, Renata Mior<sup>a</sup>, Vanessa Nunes Alves<sup>b</sup>, Cleide Sandra Tavares Araújo<sup>b</sup>, Nívia Maria Melo Coelho<sup>b</sup>, Eduardo Carasek<sup>a,\*</sup>

<sup>a</sup> Departamento de Química, Universidade Federal de Santa Catarina, Florianópolis 88040900, SC, Brazil

<sup>b</sup> Instituto de Química, Universidade Federal de Uberlândia, Av. João Naves de Ávila 2121, CEP 38400-902, Uberlândia, Brazil

### ARTICLE INFO

#### Article history:

Received 16 October 2008

Received in revised form

13 November 2008

Accepted 14 November 2008

Available online 21 November 2008

#### Keywords:

Cadmium

Fuel alcohol

Vermicompost

Solid-phase extraction

On-line preconcentration

Full factorial design

### ABSTRACT

In this study a method for the determination of cadmium in fuel alcohol using solid-phase extraction with a flow injection analysis system and detection by flame atomic absorption spectrometry was developed. The sorbent material used was a vermicompost commonly used as a garden fertilizer. The chemical and flow variables of the on-line preconcentration system were optimized by means of a full factorial design. The selected factors were: sorbent mass, sample pH, buffer concentration and sample flow rate. The optimum extraction conditions were obtained using sample pH in the range of 7.3–8.3 buffered with tris(hydroxymethyl)aminomethane at 50 mmol L<sup>-1</sup>, a sample flow rate of 4.5 mL min<sup>-1</sup> and 160 mg of sorbent mass. With the optimized conditions, the preconcentration factor, limit of detection and sample throughput were estimated as 32 (for preconcentration of 10 mL sample), 1.7 µg L<sup>-1</sup> and 20 samples per hour, respectively. The analytical curve was linear from 5 up to at least 50 µg L<sup>-1</sup>, with a correlation coefficient of 0.998 and a relative standard deviation of 2.4% (35 µg L<sup>-1</sup>, *n* = 7). The developed method was successfully applied to spiked fuel alcohol, and accuracy was assessed through recovery tests, with recovery ranging from 94% to 100%.

© 2008 Elsevier B.V. All rights reserved.

### 1. Introduction

The contamination of soil and water resources with environmentally harmful chemicals represents a problem of great concern not only in relation to the biota in the receiving environment, but also to humans. The continuing growth in industrialization and urbanization has led to the natural environment being exposed to ever increasing levels of toxic elements, such as heavy metals [1].

Sugar cane, as with other plants, can absorb enzymes and essential elements as part of their metabolism. However, non-essential or toxic elements, such as cadmium, can also be sorbed by plants, as they have similar characteristics as the essential elements [1].

In Brazil, with the aim of reducing expenditure on oil importation, the National Program of Alcohol (*Programa Nacional do Alcool, Proálcool*) was created on 14 November 1975, under Resolution No. 79.953, aiming to stimulate the production of ethanol using sugar cane as the raw material.

Thus, the development of analytical methods for the determination of trace metals in fuel alcohol began to gain attention, and

remains important due to ethanol increasingly being used as a replacement for fossil fuels [2–6].

The presence of metal ions in fuel alcohol is undesirable, as it may induce the corrosion of some vehicle components and lead to low fuel performance due to oxidative decomposition, as well as generate environmental pollution [7].

Flame atomic absorption spectrometry is a commonly employed technique for elemental determination in several kinds of samples, offering the advantages of excellent precision, selectivity and low cost. However, there are some problems inherent to its sensitivity, such as interference when dealing with complex samples. Thus, in cases where the target analyte is present in a low concentration and/or in a complex sample, separation and preconcentration methods are necessary for the analysis to be performed successfully [7,8].

Of the existing preconcentration techniques, solid-phase extraction (SPE) is one of the most powerful tools, as it provides matrix separation and high preconcentration of the analyte, reducing matrix effects and detection limits considerably. Solid-phase extraction becomes even more attractive when coupled on-line with the detection instrument and with the use of a high sorption capacity sorbent, such as a vermicompost.

Vermicomposting involves the degradation, biological stabilization and neutralization of organic matter through its ingestion

\* Corresponding author. Fax: +55 48 3721 6850.

E-mail address: [carasek@qmc.ufsc.br](mailto:carasek@qmc.ufsc.br) (E. Carasek).

**Table 1**  
Operating parameters employed in Cd(II) determination by F AAS.

Parameters	
Wavelength (nm)	228.8
Lamp current (mA)	4
Burner height (mm)	17
Acetylene flow rate (L min <sup>-1</sup> )	1
Air flow rate (L min <sup>-1</sup> )	10
Aspiration flow rate (mL min <sup>-1</sup> )	5

by earthworms, *Eisenia foetida* being the species most often used. The product of this process is called vermicompost [9]. The humic substances present in the vermicompost are considered excellent sorbents for a great variety of metal ions [10], and their use as cation exchangers is an interesting alternative to the use of commercial sorbents, mainly due to their high sorption capacity and facility of obtainment. Pereira et al. [11] characterized vermicompost samples from different regions of Brazil, and studied their cation exchange behavior in water samples, reporting satisfactory results. Vermicompost has also proved to be an excellent alternative for removing metal ions, such as cadmium, zinc, lead and copper, from aqueous laboratory effluents [12].

Our research groups have been applying chemometric tools, such as factorial design and response surface methodologies, to the optimization of factors influencing extraction conditions, both for the development of methods employing gas chromatography [13–15] and for elemental determination [16–18]. The rapid and effective optimization and the capacity to evaluate the interaction between variables in the system under study are important advantages of the multivariate methods compared to univariate approaches. Chemometric tools have been successfully applied for the optimization of factors influencing the preconcentration of lead and iron by F AAS [19,20].

Thus, in this study, the suitability of vermicompost as a sorbent for the preconcentration of cadmium in a complex sample, that is, fuel alcohol, is demonstrated. A full factorial experimental design was used for optimization of the main variables affecting the preconcentration. The vermicompost was obtained from the vermicomposting of material commonly used as a garden fertilizer and the solid-phase preconcentration system was coupled on-line with the flame atomic absorption spectrometer.

## 2. Experimental

### 2.1. Instrumentation

A Varian SpectrAA 50 (Victoria, Australia) flame atomic absorption spectrometer, equipped with a Hitachi cadmium hollow cathode lamp (HLA-4S) and a deuterium lamp as a background corrector, was used for the detection of cadmium. The operational parameters of the spectrometer are shown in Table 1. An Ismatec-IPC (Zurich, Switzerland) peristaltic pump equipped with eight channels and Tygon® tubes was used to pump the working and sample solutions in the elution and preconcentration steps. A 320 Mettler Toledo pH meter (Schwerzenbach, Switzerland) was used to set the pH of the samples to the desired value.

### 2.2. Reagents and solutions

All working solutions were prepared with ultra pure water obtained from a Milli-Q® (Bedford, MA, USA) water purification system. All reagents were analytical grade. The working solution employed in this study consisted of a hydroalcoholic solution containing 80% (v/v) of fuel alcohol and 20% (v/v) of water with an appropriate buffer. All laboratory glassware was washed with a neutral detergent, then kept overnight in a 10% (v/v) nitric acid aqueous

solution, followed by ultrasonification for 1 h, and finally rinsing with deionized water.

Working solutions were prepared daily through dilution of a 2000 mg L<sup>-1</sup> stock solution of cadmium.

The nitric acid solution used as the eluent was prepared through dilution in water of concentrated nitric acid obtained from Merck (Darmstadt, Germany).

The vermicompost sample was purchased in a supermarket (Minas Gerais, Brazil) as gardening humus. The sample was dried at 110 °C for 24 h, followed by sieving through a 32-mesh sieve.

### 2.3. On-line preconcentration system

The vermicompost was placed in a column which was coupled to the FIA system. The analysis module is composed of a peristaltic pump, four three-way solenoid valves and a Teflon® minicolumn filled with a variable mass of the sorbent, coupled on-line with the flame absorption spectrometer as described in a previous report [16]. The minicolumn, with dimensions of 55 mm length and 3 mm inner diameter, was filled with a small amount of glass wool at its extremity to avoid loss of the sorbent material. The minicolumn was used for approximately 150 sorption/desorption cycles without loss of efficiency.

## 3. Results and discussion

### 3.1. Optimization

The optimization of the on-line preconcentration system was performed with a multivariate approach, using a full factorial design including four replicate center points, totalizing 20 experiments. The factors selected were: sorbent mass, sample pH, buffer concentration and sample flow rate. Eluent type, eluent concentration and eluent flow rate were fixed as a nitric acid aqueous solution at 1.0 and 5 mL min<sup>-1</sup>, respectively. These were selected based on preliminary studies, which took into account the absence of a carry-over effect, the background signal and the shape of the transient signal obtained.

In Table 2, the response for each experiment of the factorial design is shown. The response was taken as integrated absorbance, and the sample volume preconcentrated was 10 mL spiked at 50 µg Cd L<sup>-1</sup>.

From the results presented in Table 2, a Pareto chart was constructed (Fig. 1). An effect was considered significant when it was above the standard error at the 95% confidence level ( $p > 0.05$ ), which is denoted by the vertical line on the graph.

According to the Pareto chart, only the effect of sample pH (−9.17) was significant in the interval studied, with pH 7.3 leading to better results than pH 9.3. The sample pH plays a very important role in the adsorption process. To optimize the interaction between the metal ion and the sorbent, the sorbent surface should be highly negative (pH higher than the isoelectric point of the sorbent), and the metal ion at a pH where the most abundant specie is M<sup>n+</sup>, that is, a low pH. Since these conditions cannot be achieved simultaneously, a compromise pH value must be found. The interaction between sample pH and buffer concentration (denoted as 2/3) indicates that a lower pH and higher buffer concentration also lead to a high response (see Fig. 1). Hence, 50 mmol L<sup>-1</sup> was selected as the buffer concentration for the method. The sample flow rate is not significant in the range studied and was fixed for the method at the center point, 4.5 mL min<sup>-1</sup>. The sample flow rate influences the time for which the metal ion and sorbent interact and, thus, the adsorption time. If the adsorption kinetics is slow, a low sample flow rate will be required. If the adsorption kinetics is fast, a higher flow rate can be employed, improving sample throughput. The sorbent mass used to prepare the minicolumn



**Table 2**

Preconcentration conditions of Cd(II) and analytical response for the study of multivariate optimization using SPE with vermicompost column and detection by F AAS.

Run	Sorbent mass	Sample pH	Buffer (mol L <sup>-1</sup> )	Sample flow rate (mL min <sup>-1</sup> )	Integrated absorbance
1	80	7.3	0.010	6	0.8478
2	80	7.3	0.010	3	0.8391
3	80	7.3	0.050	6	0.9017
4	80	7.3	0.050	3	0.8046
5	80	9.3	0.010	6	0.7741
6	80	9.3	0.010	3	0.7275
7	80	9.3	0.050	6	0.7315
8	80	9.3	0.050	3	0.7132
9	160	7.3	0.010	6	0.8692
10	160	7.3	0.010	3	0.8581
11	160	7.3	0.050	6	0.9063
12	160	7.3	0.050	3	0.9055
13	160	9.3	0.010	6	0.7890
14	160	9.3	0.010	3	0.7650
15	160	9.3	0.050	6	0.7423
16	160	9.3	0.050	3	0.7312
17	120	8.3	0.030	4.5	0.7813
18	120	8.3	0.030	4.5	0.8181
19	120	8.3	0.030	4.5	0.7555
20	120	8.3	0.030	4.5	0.8132

was not significant, indicating that 80 mg is enough to retain completely the analyte from a 10 mL sample. However, based on the positive signal of the effect of sorbent mass, 160 mg was used for the method since no change was observed in the dynamic flow on increasing the amount of vermicompost. The curvature parameter is not significant, indicating that the response is roughly linear between the minimum and maximum levels selected for each variable.

Thus, from the results of the first step of the optimization, a final optimization was performed considering the sample pH. In order to evaluate whether the type of buffer influences the sorption process, two types of buffer were evaluated for each sample pH. The results are shown in Fig. 2, where it can be observed that there is no difference in the response when working in the pH range of 7.3–8.3 using tris or phosphate buffers.

### 3.2. Analytical features

With the optimized conditions, the method was evaluated through the main analytical features shown in Table 3. The detection limit was calculated as three times the standard deviation of 10 independent measurements of a blank sample divided by the slope

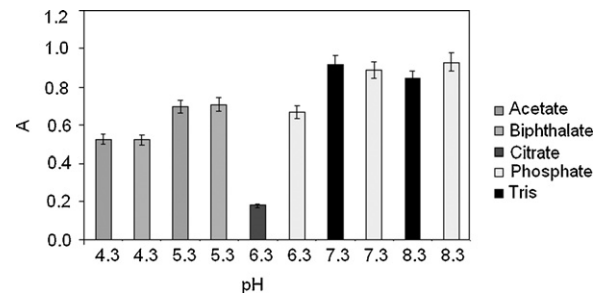


**Fig. 2.** Final optimization involving two types of buffer for each sample pH. Buffer concentration: 50 mmol L<sup>-1</sup>; sample flow rate: 4.5 mL min<sup>-1</sup>; sorbent mass: 160 mg; eluent concentration: 1.0 mol L<sup>-1</sup> nitric acid; eluent flow rate: 5 mL min<sup>-1</sup>.

of the calibration function. The detection limit obtained is comparable to others cited in the literature using solid-phase extraction as the sample preparation method and fuel alcohol as the sample. A satisfactory correlation was obtained ( $R=0.998$ ) between the analytical signal predicted by the linear function and the analytical signal experimentally observed in the linear range studied (5–50  $\mu\text{g L}^{-1}$ ).

The repeatability of the proposed method was assessed by performing seven consecutive extractions at a concentration level of 35  $\mu\text{g L}^{-1}$ , and expressing the result in terms of the relative standard deviation. A value of 2.4% was obtained, demonstrating an excellent repeatability.

### 3.3. Application of the method and recovery tests

The proposed method was applied to four fuel alcohol samples obtained at four different gas stations. In all samples the analyte concentration was below the limit of detection of the method. Thus, in order to assess whether analyte recovery could change from sample to sample due to matrix effects, all the samples were spiked at concentration levels from 0 up to 50  $\mu\text{g L}^{-1}$ , and analytical curves

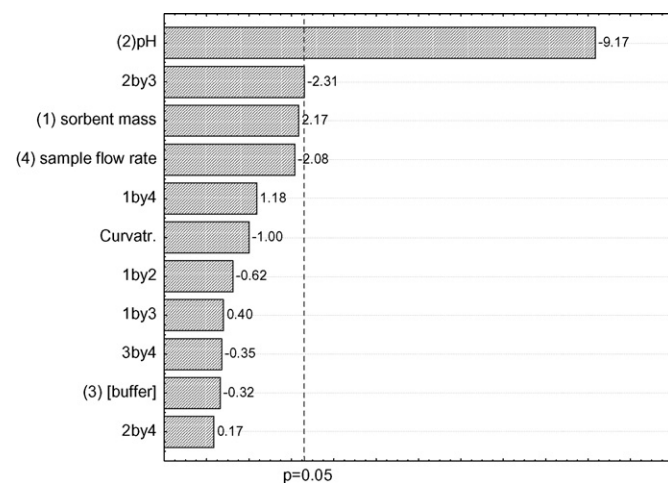


**Fig. 1.** Pareto chart obtained from the optimization study of the variables, with their significance, for the preconcentration of Cd(II) using vermicompost as the sorbent and F AAS. The experimental conditions for the study of factorial optimization are shown in Table 2.

**Table 3**

Analytical features for the determination of cadmium in fuel alcohol through the proposed method.

Linear range <sup>a</sup> ( $\mu\text{g L}^{-1}$ )	5–50
Correlation coefficient (R)	0.998
R.S.D.% (35.0 $\mu\text{g L}^{-1}$ , $n=7$ )	2.4
Limit of detection ( $\mu\text{g L}^{-1}$ )	1.7

<sup>a</sup> Linear range studied.

**Table 4**  
Relative recovery for the four samples submitted to the proposed method.

	Recovery (%)	R.S.D. (%)
Sample 1	100.0	0.5
Sample 2	94.4	2.6
Sample 3	96.7	5.3
Sample 4	97.3	4.8

were constructed in order to compare the slopes. The results are shown in Table 4, where it can be seen that there is no difference in the recovery values for the four samples, indicating that the analyte is quantitatively retained in all the samples evaluated. In order to further verify the accuracy of the proposed method, the results obtained for the vermicompost as a sorbent were compared with a method previously published by our research group [7], which is based on the sorption of cadmium from fuel alcohol on  $\text{SiO}_2\text{-Nb}_2\text{O}_5$ . As expected, the difference between the results obtained using the two methods was not statistically significant at the 95% confidence level, confirming the reliability of the proposed method.

#### 4. Conclusions

Vermicompost used as a sorbent in an on-line preconcentration system was shown to be stable and efficient in the preconcentration of cadmium from a complex sample, in this case fuel alcohol. The method presented a satisfactory detection limit as well as good accuracy. Since vermicompost as a sorbent could be applied to other samples and metal ions, it represents an excellent alternative

for cation exchange, due to its facility of operation and obtainment.

#### Acknowledgment

The authors thank CNPq for financial support.

#### References

- [1] M.L. Sereno, R.S. Almeida, D.S. Nishimura, A.V.O. Figueira, J. Plant Physiol. 164 (2007) 1499.
- [2] N.R. Stradiotto, M.F. Oliveira, A.A. Saczk, L.L. Okumura, Eclet. Quím. 27 (2002) 153.
- [3] M.F. Bergamini, S.I. Vital, A.L. Santos, N.R. Stradiotto, Eclet. Quím. 31 (2006) 45.
- [4] L.S.G.I. Teixeira, J.F. Brasileiro, M. Borges Jr., P.W.L. Cordeiro, S.A.N. Rocha, A.C.S. Costa, Quím. Nova 29 (2006) 741.
- [5] T.D. Saint'Pierre, V.L.A. Frescura, A.J. Curtius, Talanta 68 (2006) 957.
- [6] T.D. Saint'Pierre, T.A. Maranhão, V.L.A. Frescura, A.J. Curtius, Spectrochim. Acta 60 (2005) 605.
- [7] E.L. Silva, D. Budziak, E. Carasek, Anal. Lett. 37 (2004) 1.
- [8] H.F. Maltez, E. Carasek, Talanta 65 (2005) 537.
- [9] E.T.G. Cavaleiro, J.P. Soares, J.A. Souza, Quím. Nova 27 (2004) 5.
- [10] C.P. Jordão, J.L. Pereira, C.R. Bellato, Quím. Nova 24 (2001) 18.
- [11] M.G. Pereira, M.A.Z. Arruda, Chem. Soc. 14 (2003) 39.
- [12] G.D. Matos, M.A.Z. Arruda, Process Biochem. 39 (2003) 81.
- [13] D. Budziak, E. Martendal, E. Carasek, J. Chromatogr. A 1198 (2008) 54.
- [14] D. Budziak, E. Martendal, E. Carasek, J. Chromatogr. A 1187 (2008) 34.
- [15] E. Martendal, D. Budziak, E. Carasek, J. Chromatogr. A 1148 (2007) 131.
- [16] J.S. Carletto, K. Roux, H.M. Maltez, E. Martendal, E. Carasek, J. Hazard. Mater. 1579 (2008) 88.
- [17] T.A. Maranhão, E. Martendal, D.L.G. Borges, E. Carasek, B. Welz, A.J. Curtius, Spectrochim. Acta 62 (2007) 1019.
- [18] R.L. Dutra, H.F. Maltez, E. Carasek, Talanta 699 (2006) 488.
- [19] M. Soylak, I. Narin, M.A. Bezerra, S.L.C. Ferreira, Talanta 65 (2005) 895.
- [20] S. Saracoglu, M. Soylak, D.S.K. Peker, L. Elçi, W.N.L. dos Santos, V.A. Lemos, S.L.C. Ferreira, Anal. Chim. Acta 575 (2006) 133.



# The spatial effect of near-infrared spectroscopy and its application to the study of supramolecular chemistry

Chen-Bo Cai, Qing-Juan Han, Li-Juan Tang, Lu Xu, Hai-Long Wu, Jian-Hui Jiang, Ru-Qin Yu\*

State Key Laboratory of Chemo/Biosensing and Chemometrics, College of Chemistry and Chemical Engineering, Hunan University, Changsha 410082, PR China

## ARTICLE INFO

### Article history:

Received 17 July 2008

Received in revised form

16 November 2008

Accepted 17 November 2008

Available online 25 November 2008

### Keywords:

Near-infrared spectroscopy (NIR)

The first overtone

The second overtone

Spatial effect

Molecular sieve

Supramolecular structure

## ABSTRACT

An unlooked-for experimental observation that in near-infrared spectroscopy (NIR) the absorption peak of the second overtone of aniline adsorbed by 13X molecular sieve nearly disappeared led us investigate a fundamental question: the behavior of NIR when the outside space surrounding a molecule is too small to allow the molecule to vibrate freely. Through NIR of various organic compounds adsorbed by different porous inorganic materials like 13X molecular sieve, silica gel and active aluminium oxide, and NIR of supramolecular cyanuric acid-melamine, we can reasonably confirm a theoretical inference that in the micro-environment above, all intensities of NIR absorbance decrease, and the second overtone decreases more than the first overtone does. Furthermore, one distinct feature of NIR, higher sensitivity to the size of micro-environmental space as compared with mid-infrared (MIR), and its potential application to the study of supramolecular structure are outlined by our experiments.

© 2008 Elsevier B.V. All rights reserved.

## 1. Introduction

Our research was initiated from an unlooked-for experimental observation that the absorption peak of the second overtone of aniline's C–H stretching vibrations nearly disappeared when the gas of aniline was adsorbed by 13X molecular sieve (a common kind of zeolite). Naturally, it made us ask: whether the molecular sieve decreases the intensity of the second overtone, since we all know that NIR, in essence, results from the vibration of molecules, and that molecular sieve, unlike other porous inorganic materials such as silica gel or active aluminium oxide, probably supplies tiny and uniform crystal cavities to restrain vibrations of aniline molecules within the cavities.

How tiny does the space become in order to restrict the molecular vibration? According to a highly simplified quantum model, in which the stretching vibration is depicted as a harmonic oscillator of two atoms, the Schrödinger equation of the system is

$$\left[ -\frac{\hbar^2}{8\pi^2\mu} \frac{d^2}{dq^2} + \frac{1}{2}kq^2 \right] \psi = E\psi, \quad k = 4\pi^2\mu\gamma^2, \quad \mu = \frac{m_1m_2}{m_1 + m_2}$$

Here,  $\psi$  is the wave functions,  $k$  the force constant,  $q$  the amplitudes of the harmonic oscillator, and  $\gamma$  is the frequency of baseband transition, while  $m_1$  and  $m_2$  are the mass of the two atoms respectively.

On the assumption that the baseband transition of C–H stretching vibration is  $3000 \text{ cm}^{-1}$ , the solution of the Schrödinger equation could be obtained, which indicates that the most probable amplitudes of C–H stretching vibrations are 0 pm at the ground state, 10 pm, 17 pm and 23 pm at the first, second, and third excited state, respectively. As for N–H and O–H stretching vibrations, answers are roughly the same to the question posed above. Of course, this simplified model cannot quantitatively provide an exact answer. Nevertheless, it suggests the approximate range of space in which the stretching vibration of molecule might be restrained, and the conclusion that in that confined space, the strength of NIR's second overtone (corresponding to the third excited state) decreases more than that of its first overtone (corresponding to the second excited state) does. These will help us to design following experiments for explaining the unexpected phenomenon above and confirming the theoretical conclusion, into which nearly no effect has been put experimentally, saying nothing of thoroughly investigating it as far as we know.

## 2. Experimental

### 2.1. Materials

Active aluminium oxide (average pore diameter: 10–15 nm), silica gel (average pore diameter: 8–10 nm), barium sulfate, 13X molecular sieve, aniline, methylbenzene, ethanol, carbon tetrachloride, melamine, cyanuric acid. All organic compounds were

\* Corresponding author.

E-mail address: [rquy@hnu.cn](mailto:rquy@hnu.cn) (R.-Q. Yu).

analytical reagents. Before using, the inorganic materials (including active aluminium oxide, silica gel, barium sulfate, 13X molecular sieve), melamine and cyamuric acid were all dehydrated as possible.

## 2.2. Near-infrared instrument and measurement

All NIR measurements were implemented with a FT-IR/NIR spectrometer (Nexus 870, Nicolet) furnished with an indium gallium arsenide (InGaAs) detector. The optical fiber probe (Smart Near-IR FiberPort Accessory) was also used. All spectra were collected under the same conditions, i.e., resolution:  $4\text{ cm}^{-1}$ ; number of scans: 32; range of scans:  $4000\text{--}10,000\text{ cm}^{-1}$ ; granularity of inorganic materials:  $<0.1\text{ mm}$ . All the collected spectra are difference spectra, namely, subtracting their reference spectra from sample spectra to obtain “pure” spectral effect of the organic compound.

## 2.3. Experimental setup

In the paper, NIR of two kinds of objects were recorded; one was adsorbate–adsorbent system, and the other was the mechanical mixture of several substances. Scheme 1 shows the experimental setup for recording the NIR of adsorbent–adsorbate systems [1]. Pure nitrogen gas was introduced through valves 1 and 2. Part of the  $\text{N}_2$  flowed through gas reservoir 1 and 2, which contained one kind of liquid organic compound or water. After coming out of the gas reservoir 2, the  $\text{N}_2$  was already saturated by the vapor of the organic compound or water, and then mixed with another part of  $\text{N}_2$  in a mixer that had a stirrer to improve blending. Later the mixture gas was ushered into a rectangular quartz-cell (40 mm in length, 10 mm in width and 2 mm in thickness), where the gas penetrated through one kind of inorganic material (adsorbent) and was adsorbed by the adsorbent. At the same time, the NIRDRS (NIR Diffuse Reflection Spectra) of the inorganic material that contained the organic compound or water was continuously recorded by the NIR spectrometer via the optical fiber probe.

As for the mixture of several substances, its NIRDRS was collected in the same rectangular quartz-cell but unnecessary to introduce any gas.

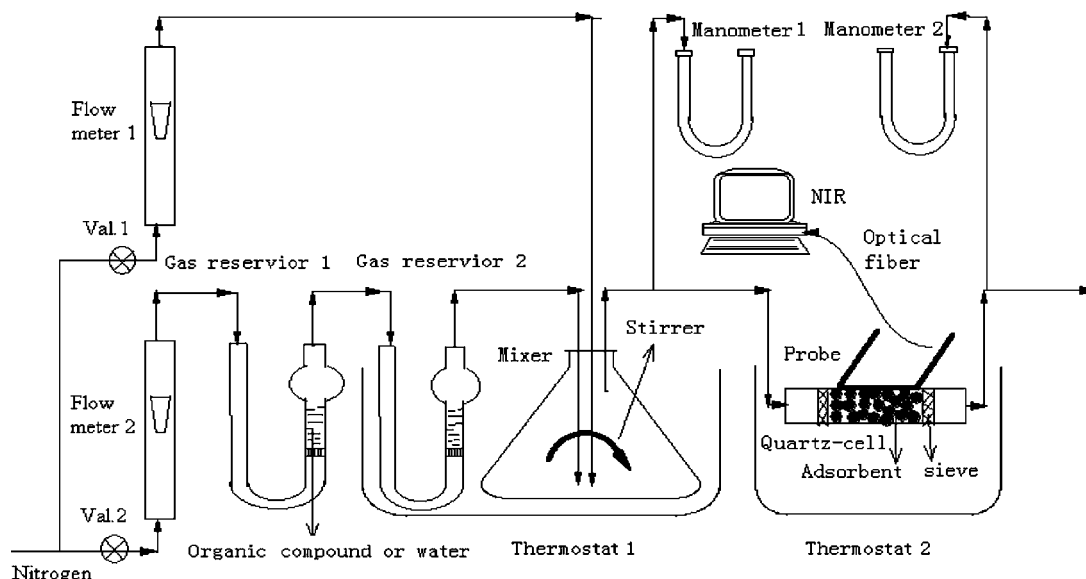
## 3. Results and discussion

### 3.1. NIR of organic compounds adsorbed by porous inorganic materials

In fact, the actual situation in 13X molecular sieve is not as simple as we might suppose in the introduction section. The crystal pore diameter of 13X molecular sieve is slightly less than  $1000\text{ pm}$ , and the diameter of its major crystal cavity is about  $1180\text{ pm}$ . Therefore, a molecule, which moves through the crystal pore and finally is adsorbed in the major crystal cavity, has a free space of more than  $180\text{ pm}$  ( $1180 - 1000 = 180\text{ pm}$ ), a space enough for the molecule to vibrate freely even at its third excited state according to the theoretical answers of the introduction section. In order to reduce the space of cavities, the 13X was partially adsorbed by water molecules (about 5%) before the adsorption of organic compounds, because water was hardly replaced by the organic compounds, and, like molecular sieve, scarcely absorbed NIR radiation in wavebands of C–H stretching vibrations. In fact, we discovered later that owing to its strong hydrophilicity almost all 13X normally preserved in a glass desiccator usually adsorbed some water, and it was just the case of the unlooked-for phenomenon observed.

With the setup shown in Scheme 1, the silica gel, active aluminium oxide or 13X molecular sieve (adsorbent) was filled in the rectangular quartz-cell (of course, the adsorbent could neither be compressed so tightly that the gas penetrated it difficultly, nor so loosely that large part of the adsorbent did not contact the gas at all). Water or one kind of organic compound was introduced respectively as gas phase to avoid un-negligible amount of them being left on the surface of the adsorbent rather than being adsorbed in the cavities of the adsorbent. The gas entered the cell from the entrance, penetrated through the adsorbent, and at last came out of the cell from the exit, when the adsorbent was continuously monitored by a non-invasive NIR spectrometer via an optical fiber probe.

NIRDRS of aniline adsorbed by active aluminium oxide, silica gel, and 13X containing about 5% water are shown in Fig. 1. For comparison, the NIRDRS of the mixture of aniline and  $\text{BaSO}_4$  was also recorded and shown in the figure. Barium sulfate was a usual and nonporous reference for NIRDRS, which does not affect the vibrations of aniline. It is worth noting that although all spectra shown in the paper are raw ones without any preprocessing treatment



Scheme 1. Experimental setup.

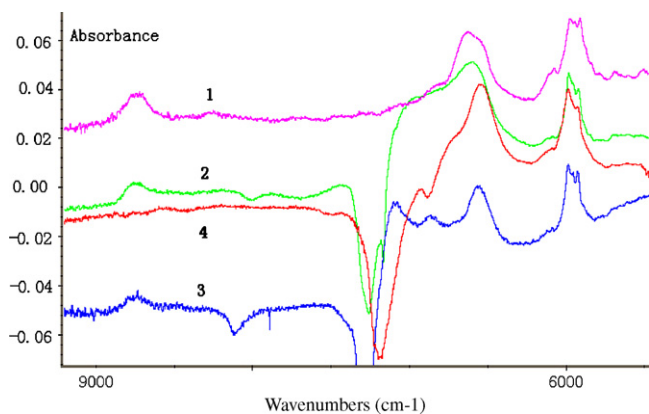


**Fig. 1.** Raw NIRDRS of aniline adsorbed or mixed by different inorganic materials. Spectrum 1: mixed with barium sulfate; spectrum 2: adsorbed by active aluminium oxide; spectrum 3: adsorbed by silica gel; spectrum 4: adsorbed by 13X molecular sieve (containing about 5% water).

in order to give an intuitional view, all intensities of absorption peaks were compared after their baselines were corrected with linear method by using OMNIC 5.2a (the accessory software of Nexus 870 FT-IR/NIR spectrometer).

In Fig. 1, the intensities of the first overtone (about  $5800\text{--}6200\text{ cm}^{-1}$ ) of all C–H stretching vibrations are nearly equal, while their second overtones ( $8500\text{--}9000\text{ cm}^{-1}$ ) are different, and the second overtone of aniline adsorbed by 13X vanishes roughly. This is comprehensible: other materials provide larger spaces for adsorbed or mixed aniline to vibrate at its third excited state than the 13X. Similar experimental results were obtained with methylbenzene, whose molecular size is almost the same as aniline (Fig. 2).

Figs. 1 and 2 also indicate that the stretching vibration of C–H is not obviously affected by the interaction between the adsorbate and the adsorbent or the interaction between the adsorbate and water (in fact, it is unreasonable to assume that the C, H or C–H in aniline or methylbenzene has obvious interaction with strong polar bonds of these inorganic adsorbents or water), since all absorption peaks of the first overtone have roughly the same wavelength and spectral profile. In other words, the difference in the second overtones mainly results from the distinction of adsorbents' pore structure.

In addition, we also recorded NIRDRS of ethanol adsorbed or mixed by 13X molecular sieve, silica gel, active aluminium oxide or barium sulfate with the same experimental method. From Fig. 3, it seems that the experimental result is completely different from

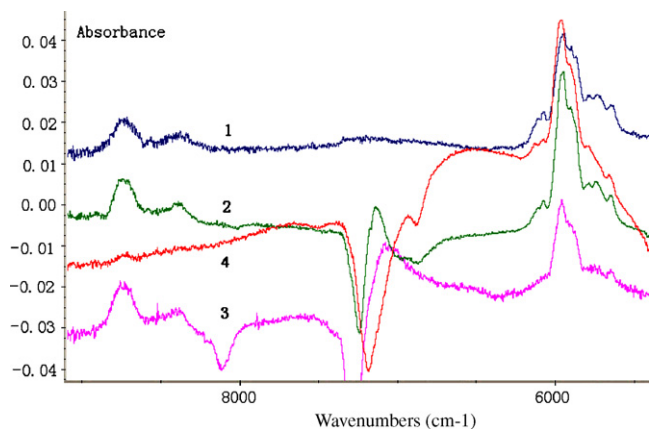


**Fig. 2.** Raw NIRDRS of methylbenzene adsorbed or mixed by different inorganic materials. Spectrum 1: mixed with barium sulfate; spectrum 2: adsorbed by active aluminium oxide; spectrum 3: adsorbed by silica gel; spectrum 4: adsorbed by 13X molecular sieve (containing about 5% water).

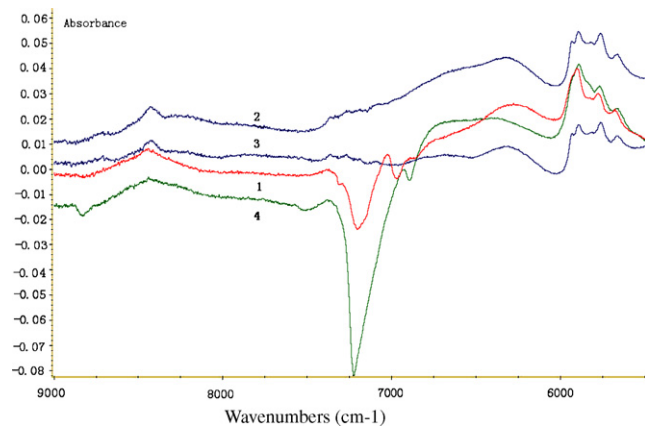


**Fig. 3.** Raw NIRDRS of ethanol adsorbed or mixed by different inorganic materials. Spectrum 1: adsorbed by 13X molecular sieve (containing about 5% water); spectrum 2: mixed with barium sulfate; spectrum 3: adsorbed by silica gel; spectrum 4: adsorbed by active aluminium oxide.

aniline or methylbenzene. Here, not only the NIRDRS of ethanol adsorbed by 13X molecular sieve did not vanish, but equal strengths of the first overtone resulted in nearly equal strengths of the second overtone whether the inorganic material was active aluminium oxide, silica gel, barium sulfate or 13X molecular sieve. However, this result is consistent rather than incompatible with the result of aniline or methylbenzene, because the molecular size of ethanol is much smaller than that of aniline or methylbenzene, and consequently needs a smaller space for vibrating freely.

In spite of the positive evidence described above, we still cannot definitely conclude that in a constrained space, the strength of the second overtone decreases more than that of the first overtone does, because the difference in their second overtones may be attributed to the difference in inorganic adsorbents' optical characteristics (for example, its diffuse reflectivity), though this influence is commonly relatively insignificant. So we designed another experiment to further confirm the mentioned conclusion. In this crucial experiment, the NIRDRS of aniline were recorded in an identical chemical and optical environment except that in one case aniline was adsorbed in the major crystal cavities of 13X molecular sieve so that the vibration was restrained, while in another case the aniline was left on the surface of the 13X molecular sieve so that the vibration was not affected by a constrained space. In order to make aniline not enter 13X's crystal cavities, the molecular sieve was filled with  $\text{CCl}_4$  in advance. We selected carbon tetrachloride since it is non-polar and NIR-transparent compound. For comparison, NIRDRS of aniline adsorbed by 13X molecular sieve nearly without water (calcined at  $300\text{ }^\circ\text{C}$ , then encapsulated in the rectangular quartz-cell at once for adsorption and NIR detection), and aniline mixed with 13X molecular sieve containing about 20% water, are also shown in Fig. 4.

Comparing spectrum 4 (the aniline adsorbed in the 13X's major crystal cavities) with spectrum 1 (water and carbon tetrachloride had filled the major crystal cavities of molecular sieve so that the aniline stayed on the 13X's surface) in Fig. 4, the effect of constrained space is clearly demonstrated, for the second overtone of the spectrum 4 vanishes at all, whereas the strengths of their first overtones are nearly equal. The difference in the second overtones between spectra 4 and 3 can be explained by the same mechanism rationally, for a large amount of water in 13X's cavities could prevent aniline from entering cavities rather than merely decrease the space of cavities. But, as for spectrum 2, there is a different situation: the 13X nearly without water has larger crystal cavities than those of the 13X containing about 5% water, and accordingly, the third excited state of C–H stretching vibration within the former is less restricted

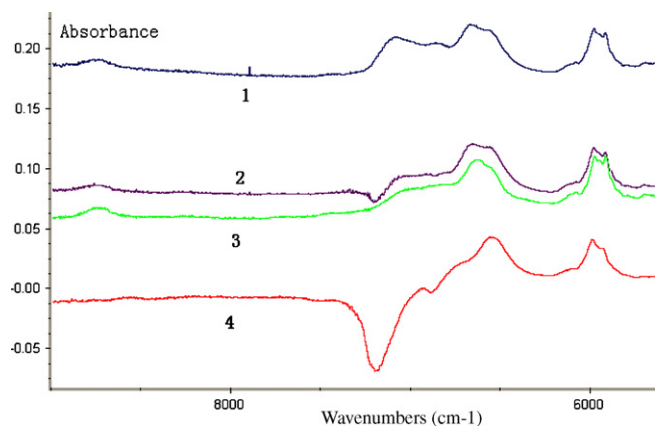


**Fig. 4.** Raw NIRDRS of aniline adsorbed or mixed by 13X molecular sieve. Spectrum 1: mixed by 13X containing about 5% water and 10% carbon tetrachloride; spectrum 2: adsorbed by 13X nearly without water; spectrum 3: mixed by 13X containing about 20% water; spectrum 4: adsorbed by 13X containing about 5% water.

than that within the latter. Similar experiments were performed with methylbenzene, and the results are the same as those of aniline (spectra not shown).

Similar to Figs. 1 and 2, the fact that in Fig. 4 all absorption peaks of the first overtone of C–H stretching vibration have roughly the same wavelength and spectral profile indicates that the difference in the second overtones can only be attributed to the change of pore structure in 13X molecular sieve rather than the difference in the interaction between the aniline and 13X molecular sieve or water.

### 3.2. NIR of MCA (1:1 supramolecule formed by melamine and cyanuric acid)

From experimental results above, one would assume that a confined space smaller than the crystal cavity of 13X should be required if the first overtone is restricted obviously as well. In an ordinary hydrogen bond, O–H...O, the bond length of H...O at the ground state is about 167 pm, a distance smaller than 260 pm (the sum of O and H's van der Waals atomic radius) or 180 pm (the distance at which the repulsive force between O and H's electronic clouds becomes significant). Therefore, within this cramped space,

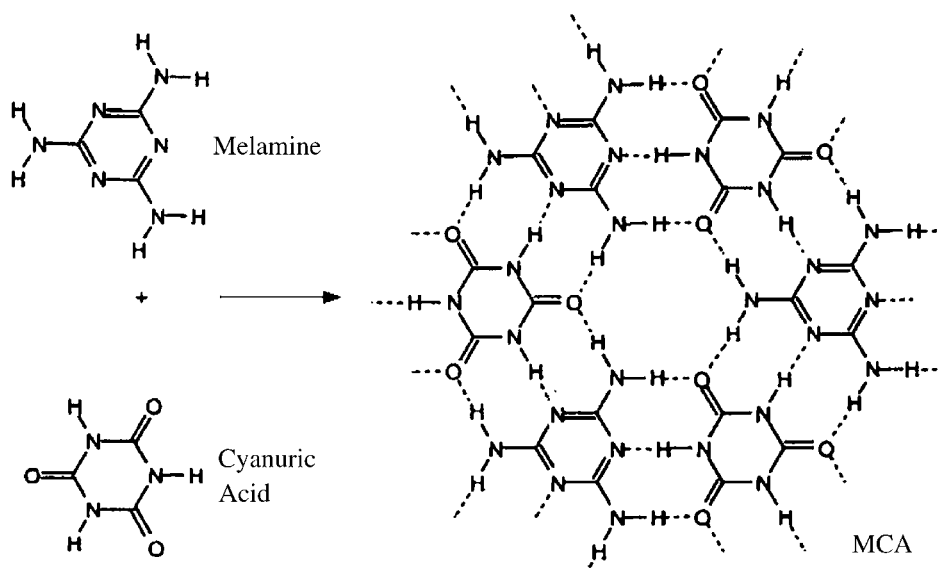
distance change of H...O due to stretching vibration of O–H is relatively so great that the repulsive force within H...O may inhibit the O–H stretching vibration as well, especially at its second and third excited state. One can expect similar cases taking place in other hydrogen bonds like O–H...N, N–H...O, or N–H...N.

As shown in Scheme 2, MCA is a supramolecular self-assembly formed through hydrogen bonding [2,3]. In MCA, all bonds of N–H form hydrogen bonds of N–H...O or N–H...N, and consequently a significant reduction of NIR absorbance of all N–H stretching vibrations can be predicted. Furthermore, in this system the explanation of NIR spectra become simplified, for there is not any bonds of C–H in melamine, cyanuric acid, nor MCA, at all.

MCA was prepared according to the process described in Ref. [4]. Besides the amount of melamine, cyanuric acid or MCA, three other factors (i.e., thickness, granularity and packing density) influence the NIRDRS. We solved them with following strategies respectively: the granularity of all samples is less than 0.1 mm; NIRDRS were recorded in the same rectangular quartz-cell (namely, the thickness was 2 mm for all experiments); and all samples were compressed into the same length in the same rectangular quartz-cell. In this way, the NIRDRS of MCA, and a mechanical mixture of melamine and cyanuric acid are shown in Fig. 5. Moreover, in order to eliminate or diminish the influence of diffuse reflectivity upon NIR absorbance, we also recorded NIRDRS of the mixture of MCA and BaSO<sub>4</sub> as well as the mixture of melamine, cyanuric acid and BaSO<sub>4</sub>, since it is well known that BaSO<sub>4</sub> has a high diffuse reflectivity and the interaction between it and organic compounds is negligible. In Fig. 5, references of spectrum 1–4 were barium sulfate; and those of spectrum 5 and 6 were standard background of the FiberPort Accessory, which was supplied by producer of the spectrometer.

Comparing spectra 1, 3 and 5 with 2, 4 and 6 of Fig. 5, respectively, one can clearly conclude that the hydrogen bonds between melamine and cyanuric acid in supramolecular MCA not only shift the absorption peaks of N–H stretching vibration to longer wavebands, but also greatly decrease intensities of the first overtone (about 6000–7000 cm<sup>-1</sup>) as well as the second overtone (about 9700–10,100 cm<sup>-1</sup>) of N–H stretching vibration.

The results of these experiments also indicate a potential application of the NIR methodology to the study of supramolecular phenomenon, which is very important in chemistry and biochemistry. In supramolecule, the space among its component molecules is so tiny that the reduction of NIR absorbance would become



**Scheme 2.** Structure of MCA.

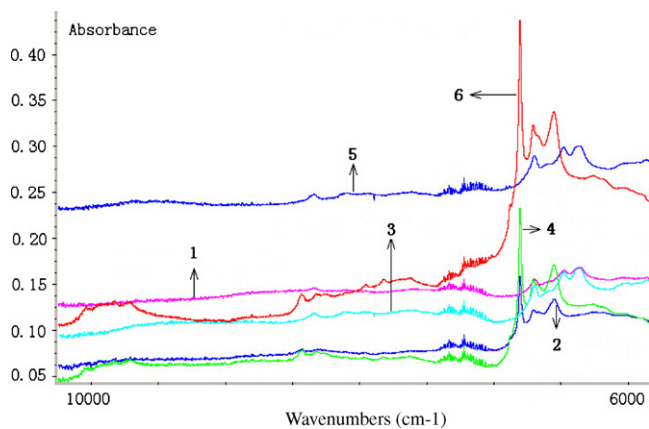


**Fig. 5.** Raw NIRDRS of MCA, and the mechanical mixture of melamine and cyanuric acid. Spectrum 1: 7.843 mmol (about 2 g) MCA + 10 g barium sulfate; spectrum 2: 7.843 mmol (about 1 g) melamine + 7.843 mmol (about 1 g) cyanuric acid + 10 g barium sulfate; spectrum 3: 7.843 mmol MCA + 2 g barium sulfate; spectrum 4: 7.843 mmol melamine + 7.843 mmol cyanuric acid + 2 g barium sulfate; spectrum 5: MCA; spectrum 6: 7.843 mmol melamine + 7.843 mmol cyanuric acid.

obvious, whereas until recently this tiny space or distance can be measured only by diffraction methods, and merely for crystals that is very difficult to obtain in many cases. Therefore, the space information obtained by the experiments described in this report, aided

by other NIR information like wavelength of the absorption peak, might be valuable for the study of supramolecular structure.

#### 4. Conclusion

It has been shown experimentally that the strength of NIR absorbance would decrease if the outside space is too small to allow the molecule to vibrate freely, and the strength of the second overtone decreases more than that of the first overtone does. We named this phenomenon as the spatial effect of NIR. Moreover, unlike the common usefulness of NIR developed so far, from our research, one innovative application of NIR could be found in the fact that NIR is more sensitive to the size of micro-environment space than MIR, which mainly corresponds to the first excited state of vibrations. And an example of the innovative application of NIR spatial effect to a supramolecule is implemented in the paper, too. Of course, the research of the paper is qualitative and preliminary, and a quantitative model for NIR spatial effect is indispensable to developing its application to measuring tiny distance or space.

#### References

- [1] C.B. Cai, Q.J. Han, L.J. Tang, Y. Zhang, R.Q. Yu, *Ind. Eng. Chem. Res.* 47 (2008) 6835.
- [2] C.T. Seto, G.M. Whitesides, *J. Am. Chem. Soc.* 112 (1990) 6409.
- [3] Y. Wang, B. Wei, Q. Wang, *J. Crystallogr. Spectrosc. Res.* 20 (1990) 79.
- [4] M. Kazuo, K. Hironobu, Y. Koichiso, N. Junichi, *Jap. Kokai Tokkyo Koho* 79 (55) (1979) 588.



# Chitosan modified ordered mesoporous silica as micro-column packing materials for on-line flow injection-inductively coupled plasma optical emission spectrometry determination of trace heavy metals in environmental water samples

Dahui Chen, Bin Hu\*, Chaozhang Huang

Department of Chemistry, Wuhan University, Wuhan 430072, China

## ARTICLE INFO

### Article history:

Received 8 July 2008

Received in revised form

28 November 2008

Accepted 29 November 2008

Available online 6 December 2008

### Keywords:

Ordered mesoporous silica

SPE

Trace heavy metals

Chitosan

ICP-OES

## ABSTRACT

A novel adsorbent of chitosan chemically modified ordered mesoporous silica was synthesized and employed as a solid phase extraction (SPE) material for flow injection (FI) micro-column preconcentration on-line coupled with inductively coupled plasma optical emission spectrometry (ICP-OES) determination of trace heavy metals V, Cu, Pb, Cd and Hg in environmental water samples. The factors affecting separation and preconcentration of target heavy metals such as pH, sample flow rate and volume, eluent concentration and volume, interfering ions were investigated. Under the optimized experimental conditions, an enrichment factor of 20 and sampling frequency of 10 h<sup>-1</sup> were obtained. The detection limits of the method for V, Cu, Pb, Cd and Hg were 0.33, 0.30, 0.96, 0.05 and 0.93 ng mL<sup>-1</sup>, and the relative standard deviations (RSDs) were 2.8%, 6.7%, 1.8%, 4.0% and 5.3% (*n* = 7, *C* = 10 ng mL<sup>-1</sup>), respectively. The adsorption capacities of chitosan modified ordered mesoporous silica for V, Cu, Pb, Cd, and Hg were found to be 16.3, 21.7, 22.9, 12.2 and 13.5 mg g<sup>-1</sup>, respectively. In order to validate the developed method, a certified reference material of GSBZ50009-88 environmental water sample was analyzed and the determined values were in good agreement with the certified values. The proposed method has also been applied to the determination of trace heavy metals in natural water samples with satisfactory results.

© 2008 Elsevier B.V. All rights reserved.

## 1. Introduction

Recently, heavy metals pollution in natural water has been receiving tremendous attention. The toxic heavy metals such as Pb, Cd, Hg are insignificant elements in human body and are capable of causing ecological risk to aquatic organisms. The toxic heavy metals could also gradually accumulate in human body through food chain and cause damage to human health [1,2]. In view of the above facts, accurate determination of heavy metals has become increasingly necessary to solve the problems connected with environmental water pollution.

In recent years, a number of promising techniques for the determination of heavy metal including atomic absorption spectrometry (AAS) [3,4], inductively coupled plasma optical emission spectrometry/mass spectrometry (ICP-OES/MS) [5,6], electrochemical analysis [7], neutron activation analysis (NAA) [8] have been reported. Among these techniques, ICP-OES has gained strong recognition in heavy metals analysis due to the following advan-

tages: multi-element analysis capability, wide linear range and low detection limits [9]. However, direct determination of heavy metals by the modern techniques is often difficult due to the complexity of sample matrix and the low concentrations of heavy metals. Therefore, separation/preconcentration of trace heavy metals prior to their analysis is often required. Nowadays, various separation/preconcentration techniques for metal ions such as, liquid liquid extraction (LLE) [10], cloud point extraction (CPE) [11,12], coprecipitation [13], ions exchange [14] and solid phase extraction (SPE) [15,16] have been developed. Of all these methods, SPE was widely used for trace metals analysis in various samples. Compared with traditional extraction techniques, SPE is simple, fast, inexpensive, less polluting to the environment and can easily be automated [15,16].

It is evident that the coupling of flow injection on-line solid phase extraction techniques to ICP-OES is a very efficient technique for the determination of heavy metals in natural water. This combination not only provides an improvement in detection limits and reduces the interference from matrix, but also significantly improves the analytical performance of the methods. In comparison with their off-line batch counterparts, these systems have a number of significant advantages for trace determination, such as higher efficiency, lower consumption of sample and reagent,

\* Corresponding author. Tel.: +86 27 68752162; fax: +86 27 68754067.

E-mail address: [binhu@whu.edu.cn](mailto:binhu@whu.edu.cn) (B. Hu).



improved precision, possibility of working in a closed system with a significant reduction of airborne contamination, and increased sampling frequency [17–19]. On-line column preconcentration systems coupled with ICP-OES are based on retention of the analytes in micro-column packed with adsorbent that determines the sensitivity and the selectivity of the analytical method. Therefore, new adsorbent is explored and searched actively in SPE technique. More recently, nanometer-sized materials [20,21], mesoporous materials [22], ion imprinted materials [23,24], biomaterials [25], C<sub>60</sub>–C<sub>70</sub> and their derivatives [26–28] have been extensively explored for this purpose.

In 90s of 20th century, mesoporous material was quickly developed and attracted much attention in various scientific areas of physics, chemistry and material science. Because of its good performance, such as large surface area, well-defined pore size, excellent mechanical resistance, none swelling, excellent chemical stability and well modified surface properties, ordered mesoporous silica has become an ideal supporting material of adsorbent in SPE, and modified mesoporous silica has been successfully used for the preconcentration and separation of trace elements recently [29–31]. Jamali et al. [29] employed thiophene-2-carbaldehyde modified mesoporous silica as sorbent for the separation and preconcentration of Pd(II) in water samples. Peñez-Quintanilla et al. [30] synthesized 2-mercaptopyrimidine modified mesoporous silica and found that it was an effective adsorbent for Cd(II). Evangelista et al. [31] employed 2-mercaptothiazoline modified mesoporous silica as an extractant for the removal of mercury from water solution.

Chitosan (CTS), obtained by deacetylation of chitin, is a natural polysaccharide. It is the most abundant polysaccharide after cellulose on the earth. Chitosan can form stable chelating compounds with many transition metal ions through the hydroxyl and amino groups. Hence, it can selectively adsorb some metal ions and has been successfully used in wastewater treatment [1,32]. Because of its solubility in acidic conditions, unsatisfaction mechanical property and swelling, chitosan cannot be employed as a SPE material. However, chitosan can react with silica through the –NH<sub>2</sub> functional group found on its surface, and could be employed as modifier for mesoporous silica. Fujiwara et al. [33] have studied the adsorption properties of Pt(IV), Pd(II), Au(III) on L-lysine modified chitosan resin. Li et al. [34] synthesized silica-supported porous sorbent by organic–inorganic hybridization combined with chitosan and polyethylene glycol imprinting for Cu(II) removal in wastewater treatment. Hakim et al. [35] synthesized chitosan resin derivatized with serine diacetic acid moiety and employed it as an adsorbent for preconcentration of trace heavy metals and rare earth elements. Oshita et al. [36] prepared cross-linked chitosan and used it to preconcentrate precious metal of Pd, Pt and Au as well as remove Hg in concentrated hydrochloric acid.

In this work, chitosan modified ordered mesoporous silica was synthesized and used as a packing material for flow injection micro-column separation and preconcentration on-line coupled with ICP-OES determination of trace heavy metals in environmental water samples. The factors affecting the on-line micro-column separation/preconcentration of target analytes were systematically studied. The developed method was validated by analysis of the target heavy metals in the certified reference material of GSBZ50009–88 environmental water and real natural waters.

## 2. Experimental

### 2.1. Apparatus

Intrepid XSP Radial ICP-OES (Thermo, Waltham, MA, USA) with a concentric model nebulizer and a cinnabar model spray chamber was used for the determination of target metals. The optimum

**Table 1**

Operation parameters of Intrepid XSP Radial ICP-OES.

RF generator power (W)	1150
Frequency of RF generator (MHz)	27.12
Coolant gas flow rate (L min <sup>-1</sup> )	14
Auxiliary gas flow rate (L min <sup>-1</sup> )	0.5
Carrier gas flow rate (L min <sup>-1</sup> )	0.6
Max integration times (s)	15
Analytical wavelength (nm)	
Cd	228.802
Cu	224.700
Pb	220.353
V	214.009
Hg	184.950

operation conditions and the wavelengths of the emission lines used were summarized in Table 1. The pH values were controlled with a Mettler Toledo 320-S pH meter (Mettler Toledo Instruments Co. Ltd., Shanghai, China) supplied with a combined electrode. An IFIS-C flow injection system (Ruimai Tech. Co. Ltd., Xi'an, China) and a self made PTFE micro-column (20 mm × 4.0 mm i.d.) packed with chitosan modified ordered mesoporous silica was used for on-line separation/preconcentration. FT-IR spectra (4000–400 cm<sup>-1</sup>) in KBr was recorded using a NEXUS 870 FT-IR (Thermo, Madison, USA), and a transmission electron microscope (JEM-2010, JEOL, Japan) and an auto N<sub>2</sub> adsorption instrument (GEMINI 2360, Micrometrics, USA) were both used for the characterization of the prepared mesoporous materials. An X2-6-13 muffle furnace (YingshanYahua Instrument Factory, Hubei, China) was used to achieve the desired temperature.

### 2.2. Standard solution and reagents

The stock standard solutions (1000 g L<sup>-1</sup>) of V, Cu, Pb, Cd and Hg were prepared by dissolving appropriate amounts of NH<sub>4</sub>VO<sub>3</sub>, CuSO<sub>4</sub>·5H<sub>2</sub>O, Pb(NO<sub>3</sub>)<sub>2</sub>, Cd(NO<sub>3</sub>)<sub>2</sub>·4H<sub>2</sub>O and HgCl<sub>2</sub> (The First Reagent Factory, Shanghai, China) in high purity water, respectively. Working solutions were prepared daily by appropriate dilutions of their stock solutions. Chitosan was purchased from Yuhuan Shell Biological Agents Factories, Zhejiang, China. 3-Aminopropyl trimethoxysilane (APTMS) and tetraethyl orthosilicate (TEOS) were obtained from Wuhan University Chemical Factory, Wuhan, China.

All reagents used, including cetyltrimethylammonium bromide (CTAB) (Acros Organics, USA) and 1,3,5-trimethylbenzene (TMB) (The First Reagent Factory, Shanghai, China) were of analytical grade. High purity deionized water (18.2 MΩ cm) obtained from a Labconco system (Labconco Co., Kansas City, MO, USA) was used throughout this work. All containers were treated with 10% HNO<sub>3</sub> for at least 24 h, rinsed with high purity deionized water, and dried at room temperature before usage.

### 2.3. Synthesis procedure

#### 2.3.1. Synthesis of ordered mesoporous silica and aminopropyl modified ordered mesoporous silica

Ordered mesoporous silica was prepared according to the reported method [37]. Briefly, 1.8 g CTAB was placed in a PTFE vessel, and dissolved with 100 mL of 2 mol L<sup>-1</sup> HCl with stirring, then 8.2 mL TEOS and 2.4 mL TMB were added dropwisely with vigorous stirring. After vigorous stirring at room temperature for 1.5 h, the gel was aged at 80 °C in vacuum for 8 h. The products were filtered, washed and dried. The synthesized samples were calcined at 540 °C for 6 h.

Preparation of aminopropyl modified ordered mesoporous silica was performed as follows: 10 g of ordered mesoporous silica was added to the round bottom flask containing with 100 mL of

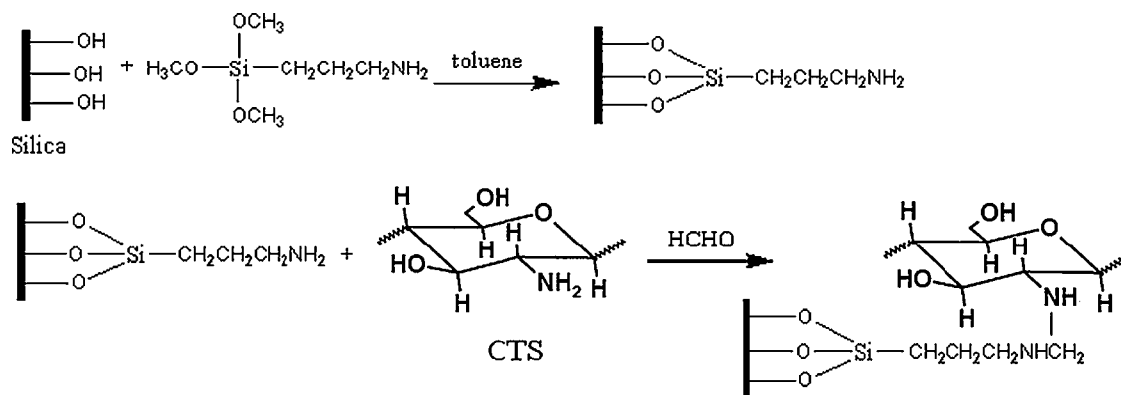


Fig. 1. Scheme for the preparation of chitosan modified ordered mesoporous silica.

4 mol L<sup>-1</sup> HNO<sub>3</sub>, and refluxed for 6 h at 60 °C by magnetic stirring, then filtered after cooling and washed with high purity deionized water and ethanol for several times and dried in vacuum. Subsequently, 5 g of activated ordered mesoporous silica was immersed into 50 mL of toluene with 10 mL APTMS inside 250 mL three-neck round bottom flask. Finally, the mixture was refluxed for 12 h under dry nitrogen atmosphere. The solid was filtered, washed with toluene, ethanol and acetone sequentially, and later it was dried in vacuum at 80 °C for 12 h.

### 2.3.2. Synthesis of chitosan modified ordered mesoporous silica

3 g of chitosan was placed in a 250-mL three-neck flask, and dissolved with 100 mL 2% acetic acid under stirring, then 10 mL 37% formaldehyde solution was added dropwisely. After refluxed for 1 h, the mixture was decompressed distillation to remove water, acetic acid and unreacted formaldehyde, then 30 mL of methanol and 6 g of aminopropyl modified ordered mesoporous silica were added. After reaction at 90 °C for 30 min, the product was washed by methanol and ethanol. Then it was dried at 60 °C for 12 h and stored in brown bottle. The schematic representation of the reaction is shown in Fig. 1.

### 2.4. Preparation of micro-column

50 mg of chitosan modified ordered mesoporous silica was packed into self made PTFE micro-column (20 mm × 4.0 mm i.d.), plugged with a small portion of glass wool at both ends, then connected to a peristaltic pump. Before use, methanol and high purity deionized water were passed through the column in sequence in order to clean it. Then, the column was conditioned to the desired pH with 0.1 mol L<sup>-1</sup> NH<sub>4</sub>Cl/NH<sub>3</sub>·H<sub>2</sub>O buffer solution.

### 2.5. Sample preparation

Lake and river water samples were obtained from Wenzhou, China. After collection, they were filtered through a 0.45-μm membrane filter (Tianjing Jinteng Instrument Factory, Tianjin, China). The samples were adjusted to pH 6.5 with 0.01 mol L<sup>-1</sup> HCl and NH<sub>3</sub>·H<sub>2</sub>O and immediately analyzed.

Certified reference material of GSBZ50009-88 (Institute for Environmental Reference Materials, Ministry of Environmental Protection of China, Beijing, China) environmental water sample was adjusted to pH 6.5 with 0.01 mol L<sup>-1</sup> HCl and NH<sub>3</sub>·H<sub>2</sub>O and immediately analyzed.

### 2.6. General procedure

The operation sequence of the FI on-line micro-column preconcentration and determination is shown in Fig. 2. In preconcentration

step (a), pump P1 was activated, so that the sample was drawn through the column; the effluent from the column was flowing to waste. And in elution step (b), pump P2 was activated while the injection valve turned to the elution position to propel eluent through the column reversely for eluting the analyte retained on the column. In this instance, the continuous impact on the sorbent could be avoided. Then, the eluting solution was introduced into the ICP-OES for determination. NH<sub>4</sub>Cl/NH<sub>3</sub>·H<sub>2</sub>O buffer solution was chosen as the blank solution and the blank values were determined. The determined values for V, Cu, Pb, Cd, Hg were obtained after subtracting the blank values.

## 3. Results and discussion

### 3.1. Characterization of ordered mesoporous silica and chitosan modified ordered mesoporous silica

A TEM pattern of ordered mesoporous silica is presented in Fig. 3, and the ordered array of mesoporous was clearly observed on

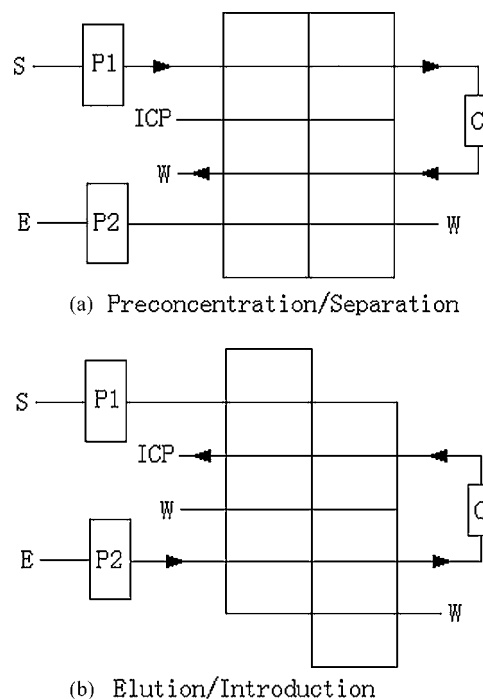


Fig. 2. FI manifold and operation for on-line preconcentration/separation and ICP-OES determination. (a) Preconcentration/separation step, (b) elution/introduction step. For details see text. S, sample; E, elution; W, waste; C, micro-column packed with modified ordered mesoporous silica; P1, P2, peristaltic pumps; ICP, ICP torch.

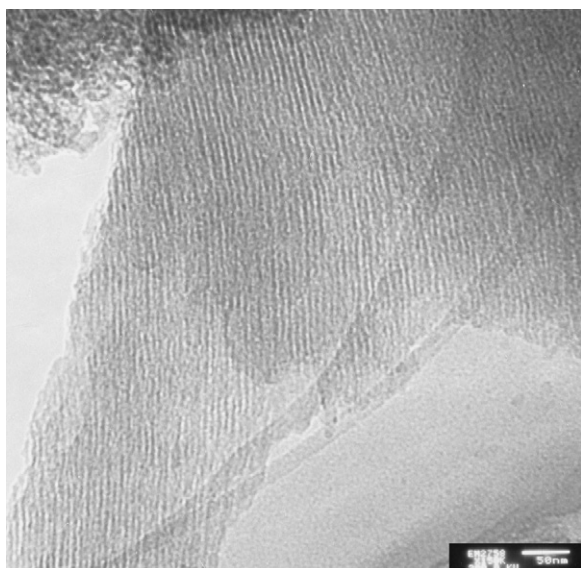


Fig. 3. Characterization of ordered mesoporous silica powders by TEM.

the surface of the prepared ordered mesoporous silica. The results obtained by the auto  $N_2$  adsorption instrument show that the BET surface area of ordered mesoporous silica is  $827 \text{ m}^2/\text{g}$  and the average pore size was 6 nm.

To ascertain the grafting of chitosan onto the surface of ordered mesoporous silica, FT-IR spectroscopy was employed to characterize chitosan modified ordered mesoporous silica. It could be seen from Fig. 4 that the spectral bands at  $1472.75$ ,  $1045.17$ ,  $915.38$  and  $781.76 \text{ cm}^{-1}$  are the vibrational frequencies of  $-\text{NH}-$ ,  $\text{Si}-\text{O}-\text{Si}$ ,  $\text{Si}-\text{O}-\text{H}$  and  $\text{Si}-\text{O}$ , respectively, which indicates the successful immobilization of chitosan on the surface of ordered mesoporous silica.

### 3.2. Effect of pH

pH value plays a great role in the SPE procedure. An appropriate pH value can not only improve the adsorption efficiency, but also depress the matrix interference. The adsorption behavior of the target analytes with a concentration of  $0.05 \mu\text{g mL}^{-1}$  each metal on chitosan modified ordered mesoporous silica was studied, and the experimental results are shown in Fig. 5. It could be seen that the studied ions were poorly adsorbed at  $\text{pH} < 4$ , the adsorption per-

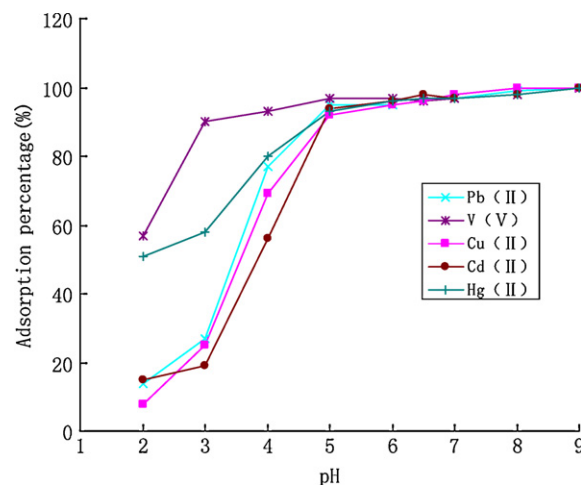


Fig. 5. Effect of pH on the adsorption percentage of V, Cu, Pb, Cd and Hg. Concentration of V, Cu, Pb, Cd and Hg:  $50 \mu\text{g L}^{-1}$ .

centages of the analytes were increased with the increase of pH, and a quantitative adsorption ( $>90\%$ ) for all the studied metals could be obtained in the pH range of 5–9. For Cu, Pb, Cd and Hg, the adsorption mechanism could be attributed to the chelation of the amino group in the chitosan with the studied metal ions. In the acidic condition, the amino group was protonated (with positive charge), the chelation between amino group and the studied metal ions became weak, which resulted in a weak adsorption capability of sorbent towards the studied metal ions, while the chelation became stronger and stronger with the increase of pH, thus, the chelating capability of chitosan with target metal ions was increased with the increase of pH. As for V(V), it existed as anion when the pH value was higher than 3. In the pH range of 1–9, the  $-\text{NH}_2$  of chitosan was partially protonated (with positive charge), thus anion V(V) could be retained on the surface of sorbent by electrostatic effect. Hence, pH 6.5 was selected as the optimum pH for all subsequent studies.

### 3.3. Effect of eluent concentration

It is clear in Fig. 5 that the adsorption percentages of the metal ions were decreased sharply with the decrease in pH value. Based on that, various concentrations of HCl were studied for desorption of the retained analytes from the micro-column. The experimental results showed that  $1.0 \text{ mol L}^{-1}$  HCl was sufficient for quantitative

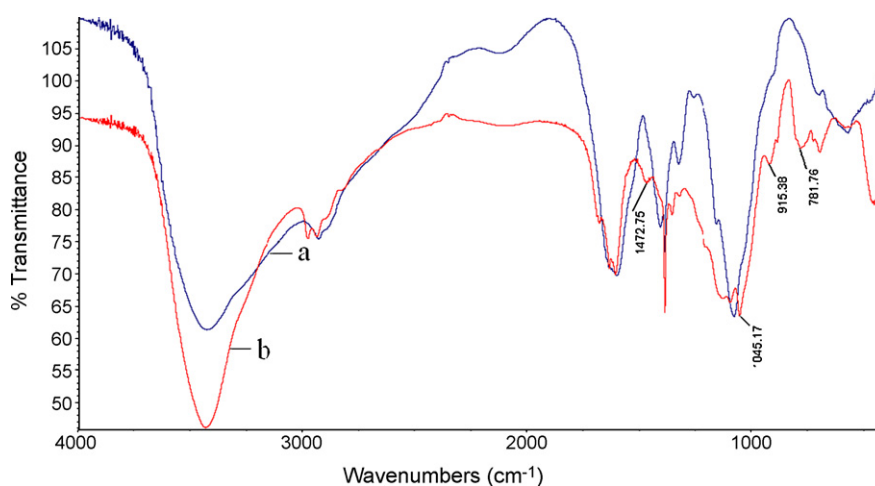


Fig. 4. The FT-IR spectra of chitosan (a) and chitosan modified ordered mesoporous silica (b).

**Table 2**

Comparison of adsorption capacity with some literatures.

Elements	Sorbent	Adsorption capacities (mg g <sup>-1</sup> )	Ref.
V, Cu, Pb, Cd, Hg	Chitosan modified ordered mesoporous silica	16.3, 21.7, 22.9, 12.2, 13.5	This method
Cu, Pb, Cd	APDC-loaded-XAD-4	11.1, 9.5, 10.2	[39]
V, Cu, Cd	Mesoporous TiO <sub>2</sub>	13.1, 8.1, 8.1	[9]
V, Cu, Cd	High surface area ZrO <sub>2</sub>	<5, <5, <5	[40]
V, Cu, Pb, Cd	Nanometer-sized alumina	11.7, 13.3, 17.7, 17.5	[20]

elution. Hence, 1.0 mol L<sup>-1</sup> HCl was selected as eluent for subsequent experiments.

### 3.4. Effect of eluent volume and eluent flow rate

The effect of eluent volume on desorption of analytes was studied with eluent volume varying from 0.2 to 1 mL. It was found that 0.3 mL of 1 mol L<sup>-1</sup> HCl was sufficient to recover the target analytes quantitatively. Therefore, 0.3 mL of eluent was selected for subsequent experiments. The effect of eluent flow rate varying from 0.4 to 2.0 mL min<sup>-1</sup> on the recovery of the studied analytes was also investigated by keeping the eluent at 0.3 mL of 1 mol L<sup>-1</sup> HCl. The results showed that the analytes could be recovered quantitatively at flow rate range of 0.4–2.0 mL min<sup>-1</sup>. To enhance the analytical speed, an eluent flow rate of 2.0 mL min<sup>-1</sup> was chosen in this work.

### 3.5. Effect of sample flow rate and sample volume

The effect of sample flow rate on the recovery of analytes was examined by passing the sample solution through the micro-column. It was found that all the metal ions (V, Cu, Pb, Cd, and Hg) could be recovered quantitatively (>90%) in the whole tested flow rate range of 0.4–2.0 mL min<sup>-1</sup>. It means that the adsorption kinetics of the chitosan modified ordered mesoporous silica is very excellent to the studied ions. For further experiments, a sample flow rate of 2.0 mL min<sup>-1</sup> was employed.

In order to obtain a higher enrichment factor, a larger sample volume is required. The effect of the sample volume on the recoveries of the target metal ions was investigated by passing 10, 20, 30 and 50 mL of sample solutions containing 0.05 µg of each metal through the micro-column under the optimum conditions. Quantitative recoveries of the target analytes were obtained when the sample volume was less than 30 mL. Under this circumstance, an enrichment factor of 100 could be achieved. To trade off the enrichment factor and analytical speed, a sample volume of 6 mL and an eluent volume of 0.3 mL were used, so that an enrichment factor of 20 and a sampling frequency of 10 h<sup>-1</sup> were obtained in this work.

### 3.6. Adsorption capacity and regeneration

Adsorption capacity is an important factor to evaluate the sorbent, because it determines how much chitosan modified ordered mesoporous silica is required for quantitative adsorption of the target analytes in a given solution. The adsorption capacity of the

**Table 3**

Tolerance limits for coexisting ions.

Coexisting	Tolerance limit of ions (mg L <sup>-1</sup> )
Na <sup>+</sup> , K <sup>+</sup>	1000
Ca <sup>2+</sup> , Mg <sup>2+</sup>	100
Al <sup>3+</sup>	50
Fe <sup>3+</sup>	20
Zn <sup>2+</sup>	5
NO <sub>3</sub> <sup>-</sup> , SO <sub>4</sub> <sup>2-</sup>	5000
Cl <sup>-</sup>	500

chitosan modified ordered mesoporous silica was studied, and the method used was adopted from that recommended by Maquieira et al. [38]. The adsorption capacities of the chitosan modified ordered mesoporous silica for V, Cu, Pb, Cd, and Hg were 16.3, 21.7, 22.9, 12.2 and 13.5 mg g<sup>-1</sup>, respectively. For comparison, the adsorption capacity data of chitosan modified ordered mesoporous silica and other methods reported in the literatures [9,20,39,40] were listed in Table 2. As could be seen, the adsorption capacity of modified ordered mesoporous silica is significantly higher than most of the reported adsorbents.

Regeneration is one of the key factors in evaluating the performance of the adsorption materials. The regenerability and stability of the micro-column was investigated. The experimental results indicated that the chitosan modified ordered mesoporous silica is stable in operation process, enabling more than 40 loading and elution cycles without decrease in the recoveries of the studied target analytes.

### 3.7. Effects of coexisting ions

The effects of common coexisting ions on the adsorption of studied metal ions in modified ordered mesoporous silica were investigated. For this purpose, a mixture solutions containing 0.05 µg mL<sup>-1</sup> of V, Cu, Pb, Cd and Hg and the added interfering ions were treated according to the recommended procedure. The tolerance of the coexisting ions, defined as the largest amount making the recovery of the studied elements less than 90% are given in Table 3. As could be seen, the presence of the coexisting ions studied has no obvious effect on the determination of the target analytes. The results also show the tolerance limits of the coexisting ions are much higher than their concentrations found in the natural water [41], indicating that the proposed method could be applied for the determination of target analytes in the natural water.

**Table 4**

Comparison of detection limits with some literatures.

Elements	LOD (ng mL <sup>-1</sup> )	Analysis method	Preconcentration technique	Sorbent	Ref.
Cd, Cu, Pb, Hg, V	0.05, 0.30, 0.96, 0.93, 0.33	ICP-OES	SPE	Chitosan modified ordered mesoporous silica	This method
Cd, Cu, Pb	0.7, 1.0, 1.7	ICP-OES	SPE	APDC-loaded-XAD-4	[39]
Cd, Cu	0.36, 0.12	ICP-OES	SPE	Mesoporous TiO <sub>2</sub>	[9]
Cd, Pb	1.0, 2.0	ICP-OES	SPE	Cationic resin (AG50W-X8)	[42]

**Table 5**  
Analytical results of Cu, Pb, Cd, Hg and V in certified reference material of GSBZ50009-88 environmental water (mean  $\pm$  s.d.,  $n = 3$ ).

Sample	Elements	Certified ( $\mu\text{g mL}^{-1}$ )	Found ( $\mu\text{g mL}^{-1}$ )
GSBZ50009-88	Cu	1.49 $\pm$ 0.04	1.57 $\pm$ 0.10
	Cd	0.105 $\pm$ 0.004	0.107 $\pm$ 0.02
	Pb	1.21 $\pm$ 0.05	1.21 $\pm$ 0.02
	V	–	nd <sup>a</sup>
	Hg	–	nd <sup>a</sup>

<sup>a</sup> Not detected.

### 3.8. Analytical performance

According to the definition of IUPAC, the detection limits ( $3\sigma$ ) of this method for V, Cu, Pb, Cd and Hg with an enrichment factor of 20 were 0.33, 0.30, 0.96, 0.05 and 0.93  $\text{ng mL}^{-1}$ , respectively, and relative standard deviations (RSDs) were 2.8%, 6.7%, 1.8%, 4.0% and 5.3% ( $n = 7$ ,  $C = 10 \text{ ng mL}^{-1}$ ), respectively. Compared with other SPE-ICP-OES methods with different adsorbent as shown in Table 4, the detection limits of this method were comparable with that obtained by other established methods.

### 3.9. Sample analysis

In order to validate the proposed method, a certified reference material of GSBZ50009-88 environmental water sample was analyzed, and the analytical results were given in Table 5. As could be seen, the determined values were in good agreement with the certified values. The proposed method was also applied to the determination of the target analytes in natural water samples, and the analytical results along with the recoveries for the spiked samples were given in Table 6. It could be seen that the recoveries for the spiked samples were between 92% and 105%.

**Table 6**  
Analytical results of Cd, Cu, Hg, Pb and V in natural water (mean  $\pm$  s.d.,  $n = 3$ ).

Sample	Elements	Added ( $\text{ng mL}^{-1}$ )	Found ( $\text{ng mL}^{-1}$ )	Recovery (%)
Oujiang River	Cd	0	1.90 $\pm$ 0.014	92.6
		5	6.39 $\pm$ 0.65	
	Cu	0	6.23 $\pm$ 0.34	98.8
		5	11.09 $\pm$ 0.11	
	Hg	0	6.35 $\pm$ 0.12	102.6
		5	11.64 $\pm$ 0.67	
	Pb	0	4.38 $\pm$ 0.37	95.1
		5	8.92 $\pm$ 0.53	
	V	0	2.51 $\pm$ 0.18	99.3
		5	7.46 $\pm$ 0.14	
Jiushan Lake	Cd	0	nd <sup>a</sup>	98.2
		5	4.91 $\pm$ 0.11	
	Cu	0	4.00 $\pm$ 0.02	103.2
		5	9.28 $\pm$ 0.36	
	Hg	0	5.37 $\pm$ 0.28	96.7
		5	10.03 $\pm$ 0.31	
	Pb	0	nd <sup>a</sup>	105.8
		5	5.29 $\pm$ 0.52	
	V	0	1.76 $\pm$ 0.15	98.5
		5	6.66 $\pm$ 0.06	
Wenruitang River	Cd	0	nd <sup>a</sup>	97.0
		5	4.85 $\pm$ 0.12	
	Cu	0	14.50 $\pm$ 0.63	105.4
		5	20.55 $\pm$ 0.69	
	Hg	0	7.46 $\pm$ 0.34	97.0
		5	12.08 $\pm$ 0.06	
	Pb	0	10.94 $\pm$ 0.43	93.2
		5	14.82 $\pm$ 0.20	
	V	0	1.72 $\pm$ 0.13	97.2
		5	6.53 $\pm$ 0.44	

<sup>a</sup> Not detected.

## 4. Conclusion

A novel adsorbent of chitosan modified ordered mesoporous silica was synthesized and used as a packing material for on-line flow injection micro-column separation/preconcentration coupled with ICP-OES determination of trace heavy metals in environmental water samples. The advantages of the proposed method can be summarized as follows: (1) the separation conditions are mild and pH of 6.5 is similar to that of natural water, (2) high efficiency, the sample frequency is about 10 samples per hour, (3) high sensitivity, the detection limits were between 0.05 and 0.96  $\text{ng mL}^{-1}$ , which was equal or slightly superior to the detection limits reported in the literatures [9,39,42], (4) high adsorption capacity, the adsorption capacity of modified ordered mesoporous silica is significantly higher than most of the reported adsorbents [9,20,39,40]. The proposed method is simple, fast, sensitive, selective, and can be applied to the determination of trace heavy metals in environmental water samples.

## Acknowledgements

Financial supports from the Science Fund for Creative Research Groups of NSFC (No. 20621502) and MOE of China (NCET-04-0658) are gratefully acknowledged.

## References

- [1] G. Crini, Prog. Polym. Sci. 30 (2005) 38.
- [2] N. Coen, C. Mothersill, M. Kadhim, E.G. Wright, J. Pathol. 195 (2001) 293.
- [3] K. Ndung'u, S. Hibdon, A.R. Flegal, Talanta 64 (2004) 258.
- [4] K.W. Jackson, Anal. Chem. 72 (2000) 159.
- [5] Z.H. Wang, X.P. Yan, Z.P. Wang, Z.P. Zhang, L.W. Liu, J. Am. Soc. Mass. Spectrom. 17 (2006) 1258.
- [6] P.S. Fedotov, E. Wennrich, S.R. Yu, B.Y. Spivakov, Analyst 131 (2006) 509.
- [7] V. Beni, V.I. Ogurtsov, N.V. Bakunin, D.W.M. Arrigan, M. Hill, Anal. Chim. Acta 552 (2005) 190.
- [8] S. Ayrault, L. Galsomies, G. Amblard, M.D. Sciarretta, P. Bonhomme, A. Gaudry, Int. J. Environ. Anal. Chem. 82 (2002) 463.
- [9] C.Z. Huang, Z.C. Jiang, B. Hu, Talanta 73 (2007) 274.
- [10] S. Igarashi, A. Takahashi, Y. Ueki, H. Yamaguchi, Analyst 125 (2000) 797.
- [11] Y.J. Li, B. Hu, Spectrochim. Acta Part B 62 (2007) 1153.
- [12] J.C.A. Wuilloud, R.G. Wuilloud, M.F. Silva, R.A. Olsina, L.D. Martinez, Spectrochim. Acta Part B 57 (2002) 365.
- [13] K. Inagaki, A. Takatsu, A. Uchiyumi, A. Nakama, K. Okamoto, J. Anal. At. Spectrom. 16 (2001) 1370.
- [14] E. Pehlivan, T. Altun, J. Hazard. Mater. 140 (2007) 299.
- [15] X.L. Pu, Z.C. Jiang, B. Hu, H.B. Wang, J. Anal. At. Spectrom. 19 (2004) 984.
- [16] S. Dadfarnia, A. Mohammed, H. Shabani, F. Tamaddon, M. Rezaei, I. Salen, Anal. Chim. Acta 539 (2005) 69.
- [17] R.G. Wuilloud, J.A. Salonia, R.A. Olsina, L.D. Martinez, Spectrochim. Acta Part B 55 (2000) 671.
- [18] V.L. Dressler, D. Pozebon, A.J. Curtius, Spectrochim. Acta Part B 53 (1998) 1527.
- [19] H. Karami, M.F. Mousavi, Y. Yamini, M. Shamsipur, Anal. Chim. Acta 509 (2004) 89.
- [20] J. Yin, Z. Jiang, G. Chang, B. Hu, Anal. Chim. Acta 540 (2005) 333.
- [21] X.L. Pu, B. Hu, Z.C. Jiang, C.Z. Huang, Analyst 130 (2005) 1175.
- [22] C.Z. Huang, B. Hu, Z.C. Jiang, Spectrochim. Acta Part B 62 (2007) 545.
- [23] G.Z. Fang, J. Tan, X.P. Yan, Sep. Sci. Technol. 40 (2005) 1597.
- [24] N. Zhang, J.S. Suleiman, M. He, B. Hu, Talanta 75 (2008) 536.
- [25] M. Soyulak, M. Tuzen, D. Mendil, I. Turkecul, Talanta 70 (2006) 1129.
- [26] J. Muñoz, M. Gallego, M. Valcárcel, J. Chromatogr. A 1055 (2004) 185.
- [27] M.G. Pereira, E.R. Pereira-Filho, H. Berndt, M.A.Z. Arruda, Spectrochim. Acta Part B 59 (2004) 515.
- [28] B.A. Lesniewska, I. Godlewska, Z.B. Godlewska, Spectrochim. Acta Part B 60 (2005) 377.
- [29] M.R. Jamali, Y. Assadi, F. Shemirani, M. Salavati-Niasari, Talanta 71 (2007) 1524.
- [30] D. Peirez-Quintanilla, I. Hierro, M. Fajardo, I. Sierra, J. Mater. Chem. 16 (2006) 1757.
- [31] S.M. Evangelista, E. DeOliveira, G.R. Castro, L.F. Zara, A.G.S. Prado, Surf. Sci. 601 (2007) 2194.
- [32] V. Boddu, K. Abburi, J.L. Talbott, E.D. Smith, Environ. Sci. Technol. 37 (2003) 4449.
- [33] K. Fujiwara, A. Ramesh, T. Maki, H. Hasegawa, K. Ueda, J. Hazard. Mater. 146 (2007) 39.
- [34] F. Li, P. Du, W. Chen, S.S. Zhang, Anal. Chim. Acta 585 (2007) 211.
- [35] L. Hakim, A. Sabarudin, M. Oshima, S. Motomizu, Anal. Chim. Acta 588 (2007) 73.
- [36] K. Oshita, M. Oshima, Y. Gao, K.-H. Lee, S. Motomizu, Anal. Sci. 18 (2002) 1121.

- [37] G. Tian, W. Chen, L. Chen, J. Zhou, J. Guo, J. Wuhan Univ. Technol. -Mater. Sci. Edit. 20 (2005) 1600.
- [38] A. Maquieira, H.A.M. Elmahadi, R. Puchades, Anal. Chem. 66 (1994) 3632.
- [39] A. Ramesh, K.R. Mohan, K. Seshiah, Talanta 57 (2002) 243.
- [40] E. Vassileva, N. Furuta, Fresen. J. Anal. Chem. 370 (2001) 52.
- [41] K. Wang, B.H. Xu, R.H. Tang, X.M. Luo, China Metrology, Publishing House, 1989, p. 5.
- [42] C.E.S. Miranda, B.F. Reis, N. Baccan, A.P. Packer, M.F. Giné, Anal. Chim. Acta 453 (2002) 30.



# Quantification of testosterone and epitestosterone in biological samples by capillary electrophoresis with immunoaffinity extraction

Hong-Xu Chen, Qin-Pei Deng, Li-Wei Zhang, Xin-Xiang Zhang\*

Beijing National Laboratory for Molecular Sciences, BNLMs, Key Laboratory of Bioorganic Chemistry and Molecular Engineering of Ministry of Education, Institute of Analytical Chemistry, College of Chemistry, Peking University, Beijing 100871, China

## ARTICLE INFO

### Article history:

Received 20 July 2008

Received in revised form

25 November 2008

Accepted 26 November 2008

Available online 14 December 2008

### Keywords:

Epitestosterone

Testosterone

Immunoaffinity column

Capillary electrophoresis

## ABSTRACT

Testosterone is one of the most common doping drugs abused by athletes. Therefore, it is necessary to develop a sensitive and simple method to monitor testosterone and its epimer epitestosterone. An off-line immunoaffinity extraction followed by capillary electrophoresis for simultaneous determination of testosterone and epitestosterone has been described in this paper. Anti-epitestosterone monoclonal antibody which is specific to both testosterone and epitestosterone had been prepared and immobilized on a Sepharose 4B stationary phase. The immunoaffinity column was used for sample cleanup, extraction and preconcentration. After elution and reconstitution, testosterone and epitestosterone in the sample were separated and quantified by micellar electrokinetic chromatography (MEKC) using the borate buffer (200 mM borate, pH 8.7) containing 40 mM sodium cholate as a chiral selector. The immunoaffinity column was evaluated in different parameters such as the retention mechanism, selectivity, binding capacity, elution protocol, and reusability. The separation of these two compounds by MEKC was also optimized. Limit of detection for testosterone and epitestosterone were 5 and 23 ng mL<sup>-1</sup>, respectively. It was satisfactory to apply this method to analyze testosterone and epitestosterone in spiked urine sample with the recoveries from 78% to 109%.

© 2008 Elsevier B.V. All rights reserved.

## 1. Introduction

Testosterone (17 $\beta$ -hydroxyandrost-4-en-3-one, T) is an endogenous androgen with both anabolic and androgenic effects in human body. It plays important roles in male sexual differentiation, accelerates protein synthesis and improves human physical performance. Testosterone and its synthetic derivatives have been widely doped by athletes since 1950s [1]. Epitestosterone (17 $\alpha$ -hydroxyandrost-4-en-3-one, E) is the 17 $\alpha$  epimer of testosterone. The structures of these two compounds are shown in Fig. 1. The normal levels of testosterone and epitestosterone in healthy male urine are both 30–60 ng mL<sup>-1</sup> [2]. The ratio of the two compounds (T/E) is remarkably stable in males [3]. The administration of testosterone will increase the ratio of T/E and the threshold for doping control has been set as 4 [4]. Thus, epitestosterone has been applied illegally to mask testosterone intake. The cut-off level of epitestosterone in urine had to be set as 200 ng mL<sup>-1</sup> by International Olympic Committee in 1992.

Different kinds of techniques have been developed in the monitoring of testosterone and its relative compounds such as

chromatographic methods including GC–MS [5] and HPLC–MS [6]; and immuno-based methods including radioimmunoassay [7], enzyme-linked immunosorbent assay (ELISA) [8], and immunosensor [9]. Capillary electrophoresis (CE) has also been used recently [10–12]. Normally, enzymatic hydrolysis is needed for most detection since the conjugation with glucuronic acid and sulfate is a common route of metabolism for steroids [13]. Analysis of the conjugated forms has also been reported [14]. Different kinds of pretreatment processes such as liquid–liquid extraction, solid phase extraction, and supercritical fluid extraction have to be applied before the chromatographic separation. On the other side, cross-reactivities in immunoassay will cause the false positive results. Thus alternative approaches should be developed to simplify the pretreatment and enhance the selectivity. Immunocapture is one of the specific extraction techniques and a group of immunological similar compounds can be trapped and then separated by chromatographic procedure. Off-line and on-line combinations of immunoaffinity column (IAC) with HPLC and GC have been reported [15]. The specificity of immunoassay and the separation ability of chromatography make this approach attractive.

CE is a powerful separation technique with the advantages of low sample and reagent consumption, high efficiency and speed. It has been used in the detection of a broad range of analytes from cell to small molecule. The neutral compounds can be separated efficiently by MEKC mode. The sensitive detectors such as laser

\* Corresponding author at: College of Chemistry, Peking University, Beijing 100871, China. Tel.: +86 10 6275 4680; fax: +86 10 6275 1708.

E-mail address: [zxx@pku.edu.cn](mailto:zxx@pku.edu.cn) (X.-X. Zhang).

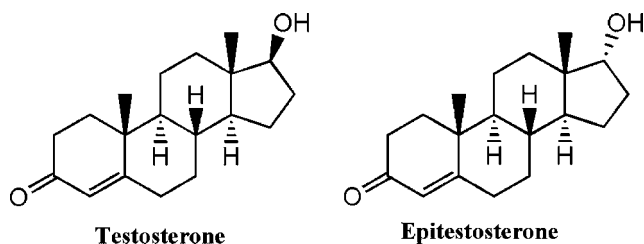


Fig. 1. Structures of testosterone and epitestosterone.

induced fluorescence can be used to improve the sensitivity of CE. However, preconcentration is required in order to achieve lower limit of detection (LOD) for those analytes without fluorescence or are unsuitable to be labeled. IAC can be one of the off-line concentrator as well as an extractor. The specific preconcentration can be obtained firstly by percolating a large volume of the sample onto the affinity column and washing any unbounded or non-specifically adsorbed interferences, and then eluting the specifically captured compounds, followed by volatilizing and reconstituting the eluate into a small volume for the following separation. This off-line combination of IAC and MEKC has been used in the detection of heroin metabolites, steroids and natural estrogens [16–18] in our group. Amudsen et al. also described the use of an IAC–MEKC system, both off-line and on-line, for the detection of testosterone in urine samples [2].

It is important to develop a method that can quantify testosterone and epitestosterone simultaneously since the concentrations of them are the key indicators for monitoring testosterone doping. Anti-epitestosterone monoclonal antibody was prepared and used in an immunoaffinity column to extract testosterone and epitestosterone selectively in this paper. The eluate from IAC was concentrated and then separated by MEKC. This has been the first time to detect these two steroids simultaneously with high selectivity by IAC–MEKC. Spiked urine samples were also assayed. Results showed that the presented method was simple, practical, and reliable in simultaneous quantification of testosterone and epitestosterone.

## 2. Experimental

### 2.1. Apparatus

ELISA was carried out on GENios microplate reader (TECAN Co., Austria). Experiments on affinity column were performed at 4 °C in a chromatography refrigerator (Beijing Freezing Equipment Factory). Capillary electrophoresis experiments were performed on MDQ CE system equipped with a PDA detector (Beckman Coulter Instrument, Fullerton, CA, USA). Other related instruments used in the experiments included GS-15R multi-purpose refrigerate centrifuge (Beckman, Fullerton, CA, USA), Cary 1E UV–vis spectrophotometer (Varian Instruments, USA) and IP-41 CO<sub>2</sub> incubator (Yamato, Japan).

### 2.2. Material and reagents

Testosterone, 17-methyltestosterone and carboxymethoxyamine hemihydrochloride were purchased from Acros (NJ, USA). Nandrolone was purchased from Yumei Biological Health-Care Co. Ltd. (Hangzhou, China). Epitestosterone, estrone, estradiol, estriol, N-hydroxysuccinimide (NHS), 1-ethyl-3-(3-dimethylaminopropyl)-carbodiimide-HCl (EDC), bovine serum albumin (BSA), sodium cholate, polyethylene glycol 1500, HAT medium, Freund's complete adjuvant and Freund's incomplete adjuvant were purchased from Sigma (St. Louis, MO, USA). Cocaine hydrochloride

was from National Institute for the Control of Pharmaceutical and Biological Products (Beijing, China). The artificial antigen, E and BSA conjugation at C<sub>3</sub> (E-3-BSA), was synthesized by conjugating E with BSA. The monoclonal antibody was prepared and purified from ascites collected from immunized Balb/c mice (Monoclonal Laboratories, College of Life Science, Peking University, China). Fetal bovine serum, Dulbecco's modified Eagle's medium and normal saline solution used in the preparation of monoclonal antibody were from Sijiqing Company (Hangzhou, China), Invitrogen (Carlsbad, CA) and Siyao Co. Ltd. (Shijiazhuang, China) respectively. Horseradish peroxidase (HRP)-conjugated goat anti-mouse IgG was obtained from Huamei Biochemicals (Beijing, China). CNBr-activated Sepharose 4B was purchased from Pharmacia Biotech (Uppsala, Sweden). Methanol was from Beijing Chemicals (Beijing, China). All other chemicals were of analytical-reagent grade. Female urine sample were provided by a healthy volunteer (25 years old without pregnancy), and stored at –20 °C at dark for one day.

In ELISA, phosphate buffered saline (PBS, 0.01 M, pH 7.4) was prepared. Sodium carbonate–sodium bicarbonate solution (50 mM, pH 9.6) was used as coating buffer. Blocking buffer was made by dissolving 1 g of glutin in 100 mL of PBS, and washing buffer (PBST) consisted of 500 μL of Tween-20 and 1 L of PBS. The substrate solution was prepared before use by mixing phosphate buffer (0.1 M, pH 6.0), 3,3',5,5'-tetramethylbenzidine (TMB) (6 mg mL<sup>-1</sup> in DMSO) and H<sub>2</sub>O<sub>2</sub> (30%) at a volume ratio of 1000:10:1.5.

4 mg mL<sup>-1</sup> of stock solutions of epitestosterone, testosterone and their analogs were prepared in methanol and stored at –20 °C. The working solutions were made by diluting the stock solutions with PBS serially.

### 2.3. Anti-epitestosterone monoclonal antibody

#### 2.3.1. Synthesis of artificial antigen

E-3-hapten was designed and prepared as follows: The mixture of 0.2 g of epitestosterone, 0.2 g of carboxymethoxyamine hemihydrochloride and 4 mL of 5% sodium hydroxide in 40 mL of ethanol was stirred by heating to reflux for 10 h. The solvent was removed under reduced pressure, and the residue was dissolved in 3 mL of water and washed with 5 mL of diethyl ether for three times. The water layer was neutralized by adding 5 mL of 1 M HCl until white solid precipitated, and then extracted with 10 mL of diethyl ether for three times. The organic layer was collected and filtered after drying over anhydrous MgSO<sub>4</sub>, and the filtrate was concentrated. On standing, 0.15 g of E-3-hapten was obtained as a yellow solid by crystallization (yield = 60%, IR: –COOH, 3000–3300 cm<sup>-1</sup>, ESI-MS: [M+H]<sup>+</sup> m/z 362). According to similar method previously reported [19], E-3-hapten was covalently attached to BSA as an immunogen for antibody producing and coating antigen for ELISA. The synthesis procedure of E-3-BSA was shown in Fig. 2. The molar ratio of E-3-hapten, NHS, EDC and BSA was 40:50:50:1. After dialyzed exhaustively against PBS and deionized water to remove the unbound hapten and residual solvent, the artificial antigen was lyophilized to white powder and stored at –20 °C before use.

#### 2.3.2. Production of the monoclonal antibody

E-3-BSA was dissolved in 500 μL of normal saline solution and emulsified with 500 μL of Freund's complete adjuvant. Each of Five Balb/c mice was injected intraperitoneally with 70 μg of antigen. Two weekly booster injections were given with a similar dosage of antigen emulsified with an equal volume of Freund's incomplete adjuvant after 3 and 5 weeks. One week after final booster, serum was taken and tested to be positive. Spleen cells from immunized mice were fused with Sp2/0 myeloma cells at a ratio of 10:1 in the presence of 50% polyethylene glycol 1500. Fused cells were cultured in HAT medium (100 μM sodium hypoxanthine, 0.4 μM aminopterin, and 16 μM thymidine in Dulbecco's modi-



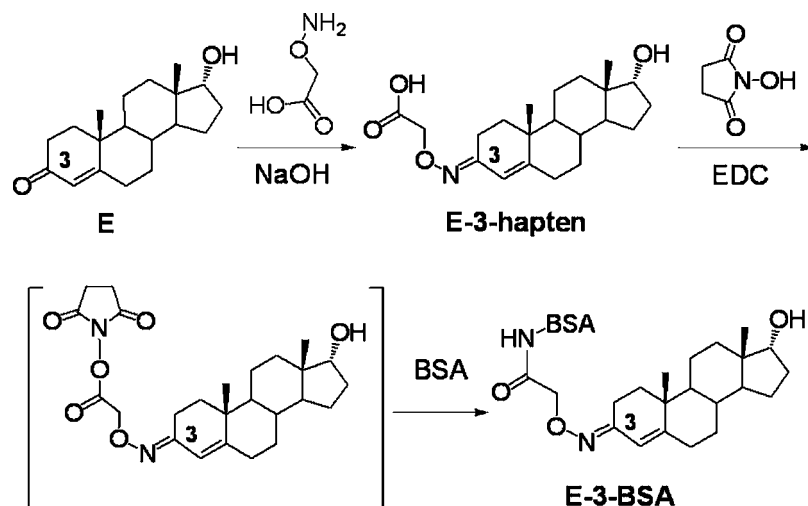


Fig. 2. Synthesis of E-3-BSA.

fied Eagle's medium supplemented with 20% fetal bovine serum) at 37 °C in CO<sub>2</sub> incubator, until all nonfused Sp2/0 cells were eliminated. The hybridoma cells were selected by indirect ELISA with continuously high positivity. Hybridomas chosen were cloned by the limited dilution method, and final hybridoma cells which developed monoclonal antibody against epitestosterone were expanded and transferred into liquid nitrogen for long-time storage. Positive hybridoma cells (10<sup>6</sup> cells per capita) were injected into Balb/c mice pre-injected with paraffin intraperitoneally to produce the monoclonal antibodies. The ascites were collected 7 days later and stored at –20 °C.

Monoclonal antibody was purified based on caprylic acid-saturated ammonium sulfate method [19]. Suspension emulsion of 297 μL of caprylic acid and 1.5 mL of acetate buffer was gently added to 3 mL of ascites and 4.5 mL of acetate buffer (0.06 M, pH 4.8). The formed solution was slowly stirred for 30 min and then centrifuged at 13000 rpm for 30 min at room temperature. The precipitate was discarded and the supernatant was adjusted to pH 7.4 with 1.0 M NaOH. Saturated ammonium sulfate (pH adjusted to 7.4) of the same volume was added dropwise under stirring. The obtained solution stood for 2 h and then was centrifuged at 13000 rpm for 3 min at 4 °C. The supernatant was discarded and the precipitate was dissolved in 1 mL of PBS. The solution was dialyzed against PBS for 24 h, aliquoted and then stored at –20 °C. The concentration of purified antibody was determined by UV method using the Lowry–Kalckar formula:  $C_{\text{Protein}} (\text{mg mL}^{-1}) = 1.45A_{280} - 0.74 A_{260}$ , where  $A_{280}$  and  $A_{260}$  represent the ultraviolet absorbance at 280 and 260 nm, respectively.

### 2.3.3. Titer and affinity constant for purified antibody

The optimized concentration of coating antigen and the titer of purified antibody were determined by ELISA based on a chessboard method [18]. A 96-well microtiter plate was coated with 100 μL of coating buffer containing E-3-BSA at an optimized concentration for 16 h at 4 °C. Then the wells were washed with PBST for three times and blocked with 1% glutin in PBS for 2 h at 37 °C. After washed for three times with PBST, 100 μL of 10-fold serially diluted purified antibodies were added to each well and incubated for 1 h at 37 °C. After the same washing procedure, 100 μL of 5000-fold diluted HRP-labeled goat anti-mouse IgG was added and incubated for 1 h at 37 °C. Then the wells were washed with PBST for three times and deionized water twice. 100 μL of substrate solution containing TMB, H<sub>2</sub>O<sub>2</sub> and phosphate buffer was added and subsequently placed in dark to react for 15 min. The enzyme reaction was stopped with 50 μL of 2 M H<sub>2</sub>SO<sub>4</sub> and the absorption was read by the GENios

at 450 nm. The affinity constant was measured at different concentrations of coating antigen (125, 250, 500 and 1000 ng mL<sup>-1</sup>). Other steps were the same as above.

### 2.3.4. Cross-reactivities of monoclonal antibody with epitestosterone analogs

The specificity of the obtained monoclonal antibody was investigated by testing its cross-reactivities with several epitestosterone analogs (testosterone, nandrolone, 17-methyltestosterone, estrone, estradiol and estriol) by competitive ELISA. The microtiter plate was coated with 100 μL of E-3-BSA at an optimized concentration. 50 μL of the competitive compounds were then added at different concentrations together with 50 μL of the 10<sup>4</sup>-fold diluted purified antibody. Other steps were the same as described in Section 2.3.3.

### 2.4. Preparation of immunoaffinity column

0.33 g of CNBr-activated Sepharose 4B was swelled and washed with 1 mM HCl, and then added to 5 mL of coupling buffer (0.1 M NaHCO<sub>3</sub>, 0.5 M NaCl, pH 8.3) containing 11 mg of the monoclonal antibody. The coupling reaction was performed in a rotated vessel for 3 h at 20 °C. After the slurry was poured into a glass column with 0.7 cm i.d., the excess ligand was washed out with coupling buffer. The remaining active groups were blocked with Tris–HCl buffer (0.1 M, pH 8.0) for 2 h. The gel was then washed for three times by repeating the cycles of 5 mL of NaAc–HAc buffer (0.1 M, pH 4.0) followed by 5 mL of Tris–HCl buffer (0.1 M, pH 8.0). Both of the buffers contained 0.5 M NaCl. Finally, the column was equilibrated with PBS. Another two columns with anti-morphine polyclonal antibody and without any antibodies, which were taken as controls, were prepared by similar procedure.

### 2.5. Procedure of immunoaffinity extraction

**Loading samples:** 3 mL of samples with different concentrations of the analytes were loaded into the IAC continuously. **Washing:** The column was washed with 5 mL of PBS and 1 mL of deionized water in order to wash out the unbounded or weakly bounded analytes. **Eluting:** 1 mL of 80% methanol in water was used to elute captured analytes at room temperature. **Preconcentration:** Methanol in collected eluate was volatilized under vacuum dry oven (0.08 MPa, 60 °C) and the final analyte was dissolved in 30 μL of borate/sodium cholate buffer (200/40 mM, pH 8.7) and analyzed by MEKC. **Regeneration:** IAC was regenerated by 5 mL of PBS. The flow velocity throughout the experiments was set to be 15 mL h<sup>-1</sup>

by controlling the valve at the end of the glass column. The IAC procedures were carried out at 4 °C in chromatography refrigerator in order to keep the activity of antibody.

## 2.6. MEKC separation

A fused-silica capillary (32 cm × 50 μm i.d., 20 cm effective length) (Ruifeng Inc., Hebei, China) was used in the separation. Capillary electrophoresis conditions were set as follows: applied voltage, 15 kV (80 μA); sample injection, 0.5 psi for 10 s; capillary temperature, 15 °C. Signals at 254 nm were collected for quantification.

The capillary was conditioned daily by sequentially rinsing (positive pressure, 20 psi) with 1 M NaOH for 10 min, deionized water for 10 min and running buffer for 5 min. Between consecutive analyses, the capillary was only rinsed with running buffer for 2 min.

The running buffer was borate buffer (200 mM, pH 8.7) containing 40 mM sodium cholate. All the solutions were filtered through 0.22 μm membrane and degassed by ultrasonication before use.

## 3. Results and discussion

### 3.1. Anti-epitestosterone monoclonal antibody

The hapten–protein conjugate was first introduced by Landsteiner to induce immune responses against non-immunogenic compound since immune system cannot recognize relatively small molecules [20]. In our work, epitestosterone was linked to BSA to increase its immunogenicity. The conjugation product or so-called artificial antigen was confirmed by UV and MS. The UV absorbance spectra of E-3-hapten, BSA, and E-3-BSA conjugate were recorded from 200 to 400 nm (Supporting Information Fig. 1). All absorbance values of E-3-BSA conjugate between 230 and 280 nm were higher than those of BSA, which were contributed by the hapten. The conjugation ratio ( $n$ ) of E-3-hapten and BSA was calculated as 26 via the following formula, where MW of E-3-BSA and BSA were measured to be 75390 and 66451 by MALDI-TOF-MS (Supporting Information Fig. 2).

$$n = \frac{MW_{E-3BSA} - MW_{BSA}}{MW_{E-3-hapten}}$$

Monoclonal antibodies are generally made by cloning cells containing a particular antibody gene to produce a population of identical cells derived from a single cell. The cloning cells were obtained by the fusion of spleen cells of an immunized mouse and myeloma cells. Two hybridoma cell lines that stably secreted epitestosterone monoclonal antibodies were obtained: 3D7 belonged to IgG2a and 1E5 belonged to IgG1. The hybridoma cell lines were verified by chromosome analysis. The average chromosomes were 90–92. Both antibodies showed similar cross-reactivities. However, the titer of 3D7 was a little higher. Thus 3D7 was used for following immunoassay. The concentration of purified monoclonal antibody was 8.6 mg mL<sup>-1</sup> by UV measurement. With an optimized coating antigen concentration (15 μg mL<sup>-1</sup> of E-3-BSA), titer of purified antibody was found to be 1:10<sup>5.2</sup> (antibody dilution corresponding to 50% of the maximum absorption). Affinity constant ( $K_{aff}$ ) which represents the binding stability of antigen–antibody complex was determined by ELISA based on the law of Mass Action [21]. The affinity constant of anti-epitestosterone monoclonal antibody and E-3-BSA was 9.3 × 10<sup>9</sup> M<sup>-1</sup>, which was high enough for immunoassay. The cross-reactivities of monoclonal antibody with epitestosterone analogs were determined by ELISA and calculated according to 50% displacement method [22]. As shown in Fig. 3A, the cross-

reactivities with all analogs were lower than 1%, indicating the excellent specificity of this anti-epitestosterone monoclonal antibody.

### 3.2. Evaluation of immunoaffinity column

The absolute amount of anti-epitestosterone monoclonal antibody immobilized in 0.33 g of CNBr-Sepharose 4B was 11.0 mg (33 mg g<sup>-1</sup>) which was determined by measuring the concentrations of antibody before and after the coupling reaction. The final gel volume of the affinity column (dead volume) was about 1 mL.

In order to investigate whether epitestosterone can be retained on the immunoaffinity column, breakthrough curves from three different columns were compared. Column 1 contained 11 mg of anti-epitestosterone antibodies, while the other two control columns contained the same amount of anti-morphine antibodies (column 2) and only pure Sepharose 4B matrix (column 3), respectively. An epitestosterone standard solution (5 μg mL<sup>-1</sup> in PBS) was loaded onto each column and the eluate was collected in each 470 μL fraction. The concentrations of epitestosterone in the eluate were determined by UV method. The breakthrough curves obtained in columns 2 and 3 were similar. In both cases, epitestosterone was already detected in the first fraction after discarding the dead volume of 1 mL. In contrast, epitestosterone was strongly retained in column 1. The breakthrough of epitestosterone was not observed until 3.7 mL (Fig. 3B). These results demonstrated that the retention of epitestosterone in the immunoaffinity column was specific.

Selective extraction was the primary objective of immunoaffinity assay. However due to the cross-reactivities of antibody, other analytes with a similar structure to hapten may also be captured. Here, the retentions of several analogs on affinity column were investigated by front analysis method. The breakthrough volume in Fig. 3C reflected the extent of cross-reactivities. The analogs with stronger cross-activity will show larger breakthrough volume. Targets or analytes (5 μg mL<sup>-1</sup> in PBS for each) were loaded onto the immunoaffinity column. The eluate was collected in each 470 μL fraction and determined by UV method. With the same loading concentration, epitestosterone showed the largest breakthrough volume of 3.7 mL, while the control analyte (cocaine hydrochloride) with a completely different structure, and epitestosterone analogs (estrone, estradiol, estriol, nandrolone, and 17-methyltestosterone) gave nearly no retention. Breakthrough volumes of all of them were less than 1.0 mL. There was some retention of testosterone on the affinity column (breakthrough volume of 3.2 mL) even though anti-epitestosterone antibody showed no cross-reactivities with testosterone in ELISA. This could be due that the excess antibodies on the column increased the capacity to closely related analytes. When immunoaffinity extraction was followed by a separation technique such as chromatography and capillary electrophoresis, the cross-reactivities of antibody turned out to be a positive feature. A group of related drugs may be extracted, preconcentrated and separated simultaneously [23]. Thus testosterone and epitestosterone can be co-extracted by this anti-epitestosterone antibodies immobilized affinity column and separated by capillary electrophoresis.

Binding capacity is defined as the maximal amount of antigen captured by immobilized antibodies. It is very important not to overload the capacity in quantitative analysis. The theoretical binding capacity was calculated according to the amount of immobilized antibody. Because the antibodies immobilized on the column was 11.0 mg and each antibody has two antigen binding sites, the binding capacity of the affinity column of epitestosterone was estimated to be 38.4 μg. The experimental binding capacity was measured by overloading epitestosterone with different concentrations and volumes and then testing the amount of captured antigen, which were

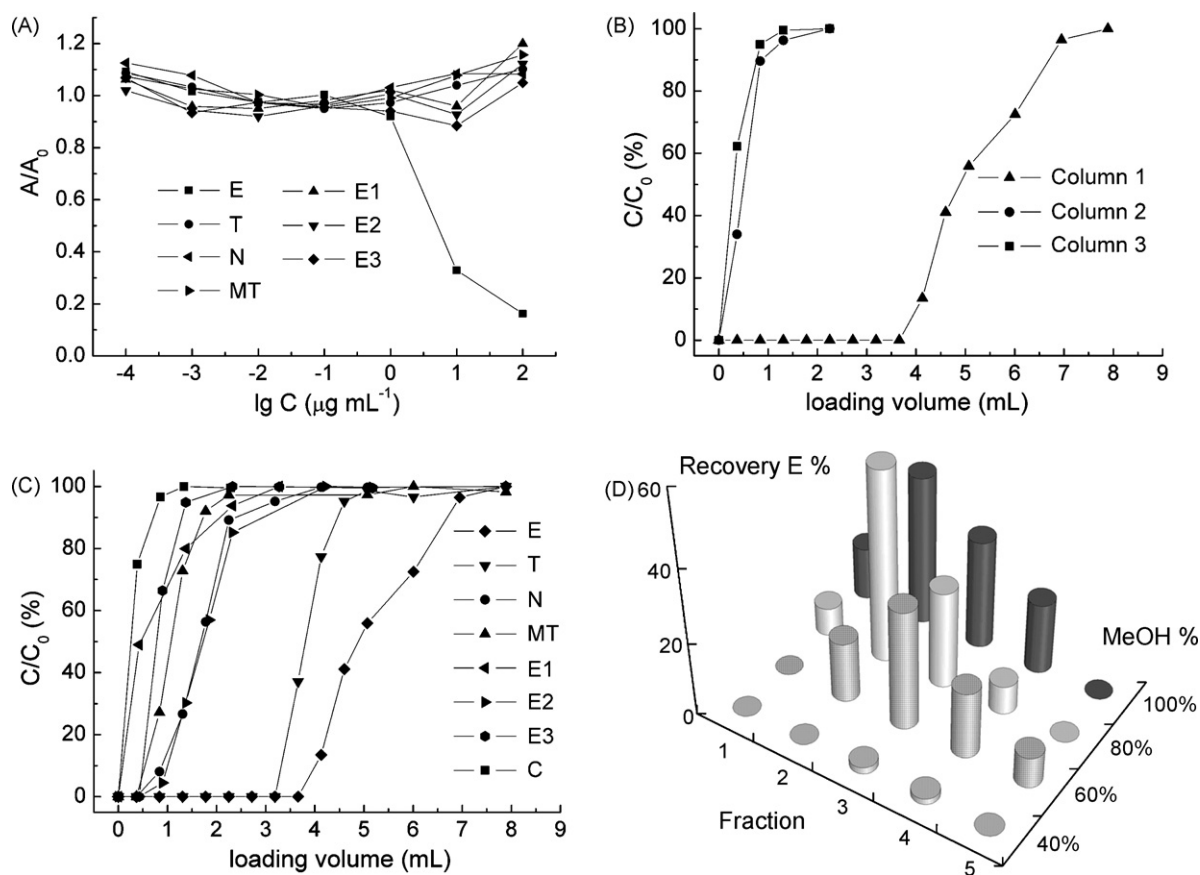


**Fig. 3.** (A) Cross-reactivities of anti-epitestosterone monoclonal antibody with epitestosterone analogs by ELISA method. Testosterone (T), nandrolone (N), 17-methyltestosterone (MT), estrone (E1), estradiol (E2), and estriol (E3). The microtiter plates were coated with  $100 \mu\text{L}$  of  $15 \mu\text{g mL}^{-1}$  E-3-BSA. The concentrations of analytes were 100, 10, 1, 0.1, 0.01, 0.001, and  $0.0001 \mu\text{g mL}^{-1}$ , respectively. (B) Breakthrough curves of epitestosterone ( $5 \mu\text{g mL}^{-1}$ ) in different columns. Column 1: Sepharose 4B coupled with anti-epitestosterone antibody; column 2: Sepharose 4B coupled with anti-morphine antibody; column 3: Sepharose 4B without antibody. (C) Breakthrough curves of several analytes obtained in affinity column immobilized with anti-epitestosterone monoclonal antibody. Sample concentration was  $5 \mu\text{g mL}^{-1}$  for each analyte. (D) Elution profile of epitestosterone with different percentages of methanol.

between 19.6 and  $21.3 \mu\text{g}$  (Supporting Information 3). It was reasonable that the experimental binding capacity was lower than the theoretical one, which also happened in other supporting materials [24]. The theoretical binding capacity was estimated based on the hypothesis that the antibody activity was fully retained and active sites accessibility was complete when estimating the theoretical binding capacity. However the random orientated antibody and the steric hindrances may prevent the antigen from access to complementary-determining-regions, resulting in the relatively lower experimental binding capacity.

### 3.3. Eluting conditions

The antigen-antibody complex was formed via electrostatic forces, hydrogen bonds and van der Waals forces. The complex had to be disrupted by effective elution solvent to dissociate the analyte without adversely affecting the immobilized antibodies. Low pH solvent and water-organic modifier mixture were generally used. Although the change of pH avoided damaging immobilized antibodies, large volume of solution was required for complete dissociation. Thus the low pH solvent was not suitable for off-line procedure. High percentage of an organic solvent was chosen to dissociate captured small molecules efficiently in our experiment. The volatility of organic solvent made off-line preconcentration easier. The actual methanol concentration needed was dependent on the affinity of immobilized antibody. In order to make a compromise between complete elution and minimal damage to antibody,

different percentages of methanol in water (40%, 60%, 80%, 100%) were investigated with  $200 \mu\text{L}$  as an elution fraction. After the loading of epitestosterone ( $5 \mu\text{g mL}^{-1}$ ), each of the elution fraction was detected by UV. The elution results were shown in Fig. 3D. No target compounds were eluted when the percentage of methanol was less than 50% and the recovery of these compounds increased with the increase of methanol. Finally, 80% methanol (in water, v/v) was chosen as the suitable elution solvent, with the recovery of 93.4%. No damage to antibody was observed because of its short exposing time to organic solvent.

### 3.4. MEKC separation

It is difficult to separate testosterone and epitestosterone in typical CE mode because those two compounds are diastereomers and neutral under CE conditions. MEKC which is very suitable for the separation of neutral analytes with the aid of micelles [25]. Testosterone and epitestosterone can be separated easily by adding 40 mM chiral ionic surfactant (sodium cholate) into 200 mM borate buffer. CE conditions such as temperature and applied voltage were optimized. Capillary temperature was studied in the range of  $15\text{--}25 \text{ }^\circ\text{C}$ . Results showed that the best separation efficiency was obtained at  $15 \text{ }^\circ\text{C}$ . As for the applied voltage,  $15 \text{ kV}$  ( $469 \text{ V cm}^{-1}$ ) was applied in 32 cm capillary considering the effect of current and Joule heat. Testosterone and epitestosterone can be baseline separated within 7 min under the optimized conditions. RSDs ( $n=5$ ) for migration times and peak heights were 0.12%, 3.0% (T) and 0.04%, 2.8% (E), respectively.

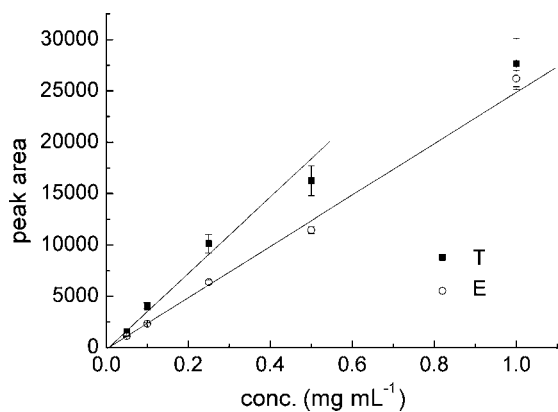


Fig. 4. Calibration curves of standard E and T samples by IAC-MEKC method.

### 3.5. Evaluation of off-line IAC-MEKC method

Series of standard samples with the same concentration of testosterone and epitestosterone (0.05, 0.1, 0.25, 0.5, 1.0  $\mu\text{g mL}^{-1}$ ) were analyzed by IAC extraction and MEKC separation (Fig. 4). The average RSD of testosterone and epitestosterone for three repetitions was 9% and 3%, respectively. Calibration curves of the peak area (A) versus concentration (c) for testosterone and epitestosterone were as follows:

$$T: A = 3.22 \times 10^4 \times c + 752 \quad (r^2 = 0.978)$$

$$E: A = 2.61 \times 10^4 \times c - 432 \quad (r^2 = 0.996)$$

LOD of testosterone and epitestosterone were 5 and 23  $\text{ng mL}^{-1}$  ( $S/N=3$ ), and their linear ranges were 17–500 and 21–1000  $\text{ng mL}^{-1}$ , respectively. This relatively low LOD was achieved due to the preconcentration after elution. Since the abnormal levels of testosterone and epitestosterone in urine are above 200  $\text{ng mL}^{-1}$ , both LODs and linear ranges can meet the requirement of testosterone doping detection. 3 mL of sample was loaded onto the IAC and the eluate was reconstituted in 30  $\mu\text{L}$  CE separation buffer, thus the theoretic preconcentration factor of IAC should be 100. The immobilized antibody showed excellent stability, with the column capacity of IAC keeping constant even after 119 runs during 3 months.

### 3.6. Application in spiked urine samples

The normal values of testosterone and epitestosterone in healthy female urine are very low (less than 0.6  $\text{ng mL}^{-1}$ ) [26]. Furthermore, most of them in urine exists in conjugated forms and cannot be detected without enzyme hydrolysis. Thus such urine can be used as blank urine sample. Fig. 5a showed the MEKC separation of blank urine sample without IAC pretreatment. There were many unknown peaks from complicated urine sample, which would interfere with the analysis of target compounds. On the contrary, after pretreatment by IAC, nothing was retained (Fig. 5b). This result proved that the IAC was specific to testosterone and epitestosterone. The interferences from complex matrix can be eliminated.

The spiked urine samples were obtained by diluting the testosterone and epitestosterone stock solutions with the blank urine. Concentrations of T and E in the spiked urine samples above and below the normal level (500 and 100  $\text{ng mL}^{-1}$ ) were investigated. Samples were analyzed by the developed procedure. Electropherogram in Fig. 5c showed that testosterone and epitestosterone were clearly identified. Analysis data including recoveries were shown in Table 1. Satisfactory recoveries (78–109%) of these urine samples

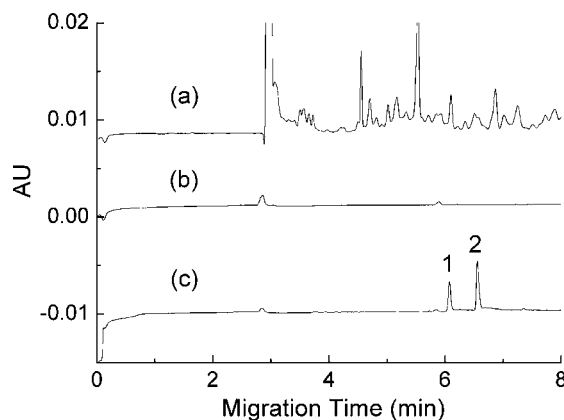


Fig. 5. Electropherograms of blank and spiked urine samples. (a) Blank urine sample without pretreatment by IAC; (b) blank urine sample with pretreatment by IAC; (c) spiked urine sample (500  $\text{ng mL}^{-1}$  testosterone, and 500  $\text{ng mL}^{-1}$  epitestosterone) with pretreatment by IAC. Peak 1: epitestosterone; peak 2: testosterone. CE conditions: running buffer,  $\text{H}_3\text{BO}_3/\text{Na}_2\text{B}_4\text{O}_7$  (200/50 mM) containing sodium cholate (40 mM), pH 8.7; applied potential, 15 kV; temperature, 15.0  $^\circ\text{C}$ ; injection, 0.5 psi for 10 s; detector, UV at 254 nm.

Table 1

Quantification of testosterone and epitestosterone in spiked urine samples.

Sample	Spiked sample ( $\text{ng mL}^{-1}$ )	Detected sample ( $\text{ng mL}^{-1}$ )	Recovery (%)	RSD (% $n=3$ )
T	100	76 $\pm$ 8	78	9
	500	547 $\pm$ 33	109	6
E	100	81 $\pm$ 2	80	3
	500	443 $\pm$ 23	89	5

indicated that this IAC-MEKC method was promising to be applied in practical detection.

## 4. Conclusions

A simultaneous determination of testosterone and epitestosterone in urine samples was achieved by an off-line IAC-MEKC procedure. Samples could be cleaned up and preconcentrated by IAC, and targets were separated by MEKC. After more than 100 cycles during 3 months, the IAC still worked well without any decrease of the efficiency, which proved its good durability and reusability. Since the concentration and ratio of testosterone and epitestosterone are the key indicators to determine the abusing of testosterone, the simultaneous detection of them with high selectivity was of great significance. This developed approach will be a potential complement to the current methods.

## Acknowledgements

This work was supported by National Natural Science Foundation of China (No. 90713013) and the National Scientific Support Project 2006BAF07B03 (MOST, China).

## Appendix A. Supplementary data

Supplementary data associated with this article can be found, in the online version, at doi:10.1016/j.talanta.2008.11.048.

## References

- [1] L. Rivier, CHIMIA 56 (2002) 84.
- [2] L.K. Amundsen, J.T.K. Nevanen, K. Takkinen, S. Rovio, H. Sirén, Electrophoresis 28 (2007) 3232.
- [3] G.J. Trout, R. Kazlauskas, Chem. Soc. Rev. 33 (2004) 1.

- [4] The 2005 Prohibited List Published by the World Anti-Doping Agency.
- [5] M. Becchi, R. Aguilera, Y. Farizon, M.M. Flament, H. Casabianca, P. James, *Rapid Commun. Mass Spectrom.* 8 (1994) 304.
- [6] R. Navajas, C. Imaz, D. Carreras, M. García, M. Pérez, C. Rodríguez, A.F. Rodríguez, R. Cortés, *J. Chromatogr. B* 673 (1995) 159.
- [7] S. Boschi, R. Deiasio, P. Mesini, G.F. Bolelli, R. Sciajno, R. Pasquali, M. Capelli, *Clin. Chim. Acta* 231 (1994) 107.
- [8] L.T. DiBenedetto, T. Dimitrakopoulos, R.M. Davy, P.J. Iles, *Anal. Lett.* 29 (1996) 2125.
- [9] G. Conneely, M. Aherne, H. Lu, G.G. Guilbault, *Anal. Chim. Acta* 583 (2007) 153.
- [10] L.K. Amundsen, J.T. Kokkonen, S. Rovio, H. Sirén, *J. Chromatogr. A* 1040 (2004) 123.
- [11] L.K. Amundsen, H. Sirén, *J. Chromatogr. A* 1131 (2006) 267.
- [12] H.X. Chen, X.X. Zhang, *Electrophoresis* 29 (2008) 3406.
- [13] W. Schänzer, *Clin. Chem.* 42 (1996) 1001.
- [14] K.A. Bean, J.D. Henion, *J. Chromatogr. B* 690 (1997) 65.
- [15] N. Delaunay, V. Pichon, M.-C. Hennion, *J. Chromatogr. B* 745 (2000) 15.
- [16] X.-H. Qi, J.-Q. Mi, X.-X. Zhang, W.-B. Chang, *Anal. Chim. Acta* 551 (2005) 115.
- [17] X.-H. Qi, L.-W. Zhang, X.X. Zhang, *Electrophoresis* 29 (2008) 3398.
- [18] P. Su, X.-X. Zhang, W.-B. Chang, *J. Chromatogr. B* 816 (2005) 7.
- [19] M.-P. Zhao, Y.-Z. Li, Z.-Q. Guo, X.-X. Zhang, W.-B. Chang, *Talanta* 57 (2002) 1205.
- [20] K. Landsteiner, *Specificity of Serological Reactions*, Charles C Thomas Publisher, Springfield, IL, 1936.
- [21] J.D. Beatty, B.G. Beatty, W.G. Vlahos, *J. Immunol. Methods* 100 (1987) 173.
- [22] J.J. Pratt, *Clin. Chem.* 24 (1978) 1869.
- [23] M.-C. Hennion, V. Pichon, *J. Chromatogr. A* 1000 (2003) 29.
- [24] J. Dallüge, T. Hankemeier, R.J.J. Vreuls, U.A.Th. Brinkman, *J. Chromatogr. A* 830 (1999) 377.
- [25] S. Terabe, K. Otsuka, K. Ichikawa, A. Tsuchiya, T. Ando, *Anal. Chem.* 56 (1984) 111.
- [26] F.C.W. Wu, *Clin. Chem.* 43 (1997) 1289.



## Inert matrix and Na<sub>4</sub>EDTA improve the supercritical fluid extraction efficiency of fluoroquinolones for HPLC determination in pig tissues

Jeong-Heui Choi<sup>a</sup>, M.I.R. Mamun<sup>a,b</sup>, A.M. Abd El-Aty<sup>c,d,\*\*</sup>, Kyung Tae Kim<sup>a</sup>, Hong-Bum Koh<sup>e</sup>, Ho-Chul Shin<sup>c</sup>, Jin-Suk Kim<sup>c</sup>, Kang Bong Lee<sup>f</sup>, Jae-Han Shim<sup>a,\*</sup>

<sup>a</sup> Natural Products Chemistry Laboratory, Division of Applied Bioscience and Biotechnology, College of Agriculture and Life Science, Chonnam National University, 300 Yongbong-dong, Buk-gu, Gwangju 500-757, Republic of Korea

<sup>b</sup> Department of Chemistry, University of Dhaka, Dhaka 1000, Bangladesh

<sup>c</sup> Department of Veterinary Pharmacology and Toxicology, College of Veterinary Medicine, Konkuk University, 1 Hwayang-dong, Kwangjin-gu, Seoul, Republic of Korea

<sup>d</sup> Department of Pharmacology, Faculty of Veterinary Medicine, Cairo University, 12211 Giza, Egypt

<sup>e</sup> Department of Veterinary Medicine, College of Veterinary Medicine, Chonnam National University, 300 Yongbong-dong, Buk-gu, Gwangju 500-757, Republic of Korea

<sup>f</sup> Division of Food and Risk Standardization, Korea Food and Drug Administration, Seoul 122-704, Republic of Korea

### ARTICLE INFO

#### Article history:

Received 16 September 2008

Received in revised form 17 November 2008

Accepted 17 November 2008

Available online 25 November 2008

#### Keywords:

Fluoroquinolones

Supercritical fluid extraction

Na<sub>4</sub>EDTA

Inert matrix

Pig tissues

### ABSTRACT

A supercritical fluid extraction method combined with high-performance liquid chromatography-fluorescence detection was developed for the determination of enrofloxacin, danofloxacin, and ciprofloxacin in pig muscle, lung, and kidney samples. The optimal SFE conditions were 80 °C, 300 kg/cm<sup>2</sup>, 30% methanol for 40 min as a dynamic extraction time, in addition to 0.2 g Na<sub>4</sub>EDTA and 7.0 g sea sand in the extraction vessel. The use of Na<sub>4</sub>EDTA and sea sand on SFE extraction resulted in improvement of the recoveries of ciprofloxacin, a polar and hydrophilic compound, as well as enrofloxacin and danofloxacin. Overall, the recoveries ranged from 86.7 to 113.1% using the Na<sub>4</sub>EDTA/sea sand-assisted SFE extraction method. The Na<sub>4</sub>EDTA/sea sand-assisted SFE-HPLC-FLD validated method was successfully carried out in pig tissues, and proved to be specific, sensitive, reliable, and accurate. The method was also applied satisfactorily for accurate quantitative residue analysis in incurred pig tissues.

© 2008 Elsevier B.V. All rights reserved.

### 1. Introduction

Veterinary drugs are currently being used on a large scale in food-producing animal husbandry practices. The majority of these drugs are administered either by injection or orally in the form of feed additives or via drinking water for pigs, broiler and laying chickens, beef cattle, dairy cows, and fish in order to prevent or treat bacterial infections, as well as to increase the animal mass [1]. There are 17 classes of antibiotics currently available for human use; some of these antibiotics are also being used in animal feeds. Fluoroquinolones (FQs) are currently being considered as the last resort antibiotics [2].

The FQs are one of the major classes of antibiotics being used in livestock industries because they have a broad spectrum of activity

against both Gram-positive and Gram-negative bacteria [3]. These antibiotics have received great attention due to the potentials for both oral and parenteral routes of administration, good tolerability for handling, excellent diffusion throughout tissues, strong activity against Gram-negative bacteria, fewer side effects, and long half-lives. In particular, the ease of their oral administration has justified their widespread adoption in animal industries [4–7]. The widespread administration and extensive use and misuse of the FQs can be a cause of a potential risk, as drug residues may remain in edible tissues [8]. The presence of drug residues in livestock products gives rise to public health concerns (related to toxic effects, development of resistant strains of bacteria, allergic hypersensitivity reactions, etc.) as well as environmental and industrial (cheese or yoghurt production, etc.) problems [9,10].

Maximum residue limits (MRLs) of veterinary medicines and their residual analyses in foodstuffs of animal origin have been continuously assessed and established not only to determine admissible use, but also to produce and serve safe livestock products to consumers. Among the FQs, enrofloxacin (ENRO) and danofloxacin (DANO) are often used to treat respiratory, urinary tract, and enteric bacterial infections in cattle, swine, chicken, and turkey, as well as diseases in aquacultured fish [11,12]. The safety

\* Corresponding author. Tel.: +82 62 530 2135; fax: +82 62 530 0219.

\*\* Corresponding author at: Department of Veterinary Pharmacology and Toxicology, College of Veterinary Medicine, Konkuk University, 1 Hwayang-dong, Kwangjin-gu, Seoul, Republic of Korea. Tel.: +82 2 450 3769; fax: +82 2 450 3037.

E-mail addresses: [abdlaty44@hotmail.com](mailto:abdlaty44@hotmail.com) (A.M.A. El-Aty), [jhshim@jnu.ac.kr](mailto:jhshim@jnu.ac.kr) (J.-H. Shim).

use guidelines in animals and MRL of ENRO and DANO in meat have been established by the Korea Food and Drug Administration (KFDA). The MRL values in pig tissues such as muscle, liver, fat, and kidney are in the range of 100–300  $\mu\text{g}/\text{kg}$  for enrofloxacin (the sum of enrofloxacin and ciprofloxacin (CIP) as the main metabolite), and in the range of 50–200  $\mu\text{g}/\text{kg}$  for danofloxacin.

Determination of the FQs in body fluids and animal tissues has been carried out using various analytical methods. Most extraction methods have utilized traditional liquid extraction methods with organic solvents or mixtures of organic liquids and acidic or basic liquids; in some of these techniques, extraction is followed by solid-phase extraction cleanup [4,8,9,13–16]. Matrix solid phase dispersion (MSPD) with bulk  $\text{C}_{18}$  [17], a form of diphasic dialysis using cellulose dialysis tubing [18], and the accelerated solvent extraction method [19] were developed as new extraction procedures. Detection methods have generally taken advantage of high-performance liquid chromatography (HPLC) equipped with an ultraviolet [4,8,20], fluorescence [9,13–16,21], or photodiode array detector [22,23]. Other techniques such as immunoaffinity chromatography [24,25] and capillary electrophoresis with a diode array detector or laser-induced fluorescence detector [6,26] have also been used. Recently, LC coupled with mass spectrometry (MS) or electrospray tandem mass spectrometry (MS/MS) detection has been reported for confirmation of the FQ identities in biological [10,27–30] and environmental samples [31,32].

Another extraction method is supercritical fluid extraction (SFE) using supercritical carbon dioxide, which has a comparatively low critical temperature (31.1  $^{\circ}\text{C}$ ) and pressure (75.3  $\text{kg}/\text{cm}^2$ ). Supercritical  $\text{CO}_2$  is the most widely used of these methods, and is able to easily extract nonpolar or slightly polar compounds, but not polar molecules because of the properties of supercritical  $\text{CO}_2$  [33,34]. However, the range of solvation power of supercritical  $\text{CO}_2$  is conveniently varied by changing the temperature or the pressure of the fluid and/or modification of the fluid with a polar solvent such as water, methanol, ethanol, or acetonitrile [35,36]. The control of the various parameters allows the extraction of compounds with a wide range of polarities. The use of SFE has been introduced as an alternative conventional liquid solvent extraction method. The SFE method has been applied for the extraction of phytochemicals [36–39] and the analysis of pesticides [40–42], antibiotics [43,44], PCBs [45], and PAHs [46,47] from various samples. SFE is more economical, environmentally acceptable, and simpler than traditional

solvent extraction methods. Determination of the FQs in chicken breast muscles and eggs by a combination of SFE and HPLC has been reported by the author's laboratory [44,48]. This paper describes an extraction and cleanup procedure for ENRO, DANO, and CIP in pig muscles, lungs, and kidneys using SFE with EDTA tetra-sodium salt and inert matrix, followed by centrifugation and determination by HPLC-FLD. After that, the residual concentrations of ENRO, DANO, and CIP were determined simultaneously at set intervals from pig tissues that were treated through oral or intramuscular administration. To the best of our knowledge, this article is the first to report the excellent efficiency of SFE for the determination of FQs in animal tissues.

## 2. Experimental

### 2.1. Chemicals and materials

Reference standards of enrofloxacin (ENRO) and danofloxacin (DANO) of certified purity were purchased from Riedel-de Haën (Sigma–Aldrich GmbH, Seelze, Germany). A standard of ciprofloxacin (CIP) was kindly supplied by Jaijledang (Seoul, Republic of Korea). Their chemical structures are shown in Fig. 1. Sodium sulfate monobasic, phosphoric acid, (ethylenedinitrilo)-tetraacetic acid tetra-sodium salt ( $\text{Na}_4\text{EDTA}$ ), ammonium sulfate, and hyflo super cel medium were bought from Sigma (Missouri, USA). Sea sand (15–20 mesh) was obtained from Junsei Chemicals Co. Ltd. (Tokyo, Japan). All organic solvents used throughout the study were of HPLC grade, and were obtained from Merck (Darmstadt, Germany). All other chemicals were of analytical grade, unless otherwise stated.

### 2.2. Supercritical fluid extraction system

Jasco Model PU980 dual pumps (Tokyo, Japan) were used for supercritical fluid extraction. One pump was for pure liquid  $\text{CO}_2$  changed from gas by circulating antifreezing liquid in the cooling jacket connected to a RBC-10 Refrig. Bath Circulator (Jeio Tech, Seoul, Republic of Korea), and the other was for methanol. Both pumps were connected to a 10-mL stainless SFE vessel (10 mm i.d.  $\times$  15 cm length) to make liquid  $\text{CO}_2$  into supercritical  $\text{CO}_2$ , which was placed in a column oven chamber (Jasco Model CO-965)

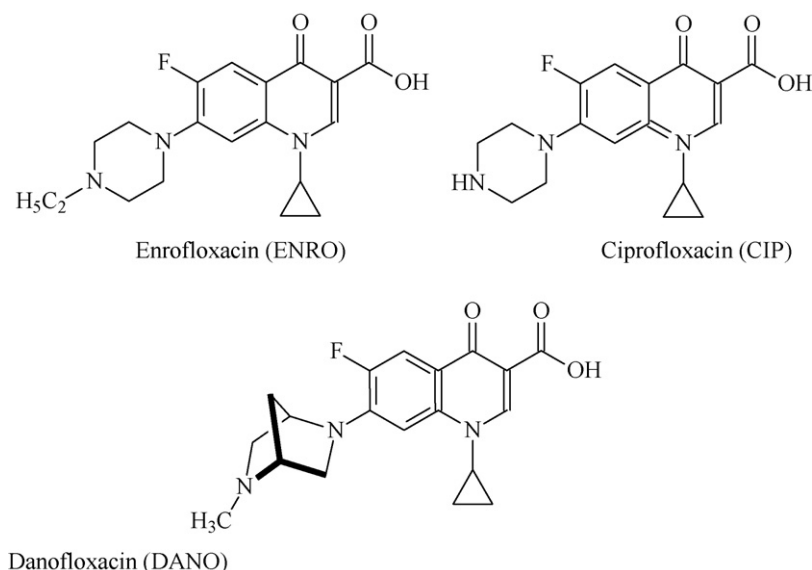


Fig. 1. Chemical structures of fluoroquinolones.

directly connected to the same SFE extraction vessel noted previously. This was then connected to an SFE pressure regulator. The pressure of supercritical fluid and sample elution were controlled by a Jasco Model 880-81 pressure regulator.

### 2.3. High-performance liquid chromatography

The HPLC system consisted of a Shimadzu (Japan) Model SCL-10A VP system controller, model LC-6 AD dual pumps, a CTO-20A column oven, a spectrofluorometric detector (RF-10 A), and a Shimadzu provided CLASS VP computing program. Analytical separation of the antibiotics from the pig tissues was achieved on a 250 mm × 4.6 mm i.d., 5 μm, pre-packed Apollo C<sub>18</sub> column (Alltech, Illinois, USA), protected by a 4.6 mm × 7.5 mm, 5 μm, Apollo C<sub>18</sub> guard column, and eluted by a mobile phase consisting of a 82:18 (v/v) mixture of phosphate buffer (pH 3.0) and acetonitrile, respectively. The concentration of phosphate buffer was 0.04 M, prepared by dissolving 4.8 g of sodium sulfate monobasic (≥99%) in 1 L of deionized water. The pH of this liquid was then adjusted to 3.0 by the addition of 50% phosphoric acid. Chromatographic separation in the column was carried out at ambient temperature, 40 °C, and the flow rate of the mobile phase was 1 mL/min. The FQs were simultaneously detected at an excitation wavelength of 278 nm and an emission wavelength of 450 nm.

### 2.4. Preparation of stock and working solution

The stock solutions of the three FQs were prepared by dissolving 10 mg of each standard in 100 mL of methanol to reach a final concentration of 100 μg/mL. The working solutions for the HPLC injections were prepared by serial dilution of stock solution with a mixture of 0.04 M phosphate buffer and acetonitrile (8: 2, v/v) at five different levels. The standard and working solutions were stored at –24 °C in amber bottles.

### 2.5. Sample collection

#### 2.5.1. Blank pig tissues

Six-week-old pigs with no history of FQ treatment were bought from the Corporate Society for Pig Farmers (Gokseong, Republic of Korea), and were acclimated to experimental conditions with antibiotic-free feed and water for 7 days at the animal house of the College of Veterinary Medicine, Chonnam National University, Gwangju, Republic of Korea. The animals were kept in groups in separate rooms, where the temperature was maintained at 25 ± 2 °C. The average body weight was 56 kg. After acclimatization, all pigs were killed, and muscle, lung and kidney were collected. Individual tissues were chopped, mixed, and stored at –24 °C until analysis.

#### 2.5.2. Incurred pig tissues

Seven-week-old pigs were treated with both ENRO and DANO. ENRO (Enril Capsule, a.i. 50 g/kg, CTCbio Co., Hwaseongsi, Republic of Korea) and DANO (Advocin, a.i. 25 mg/mL, Brazil, Laboratório Pfizer Ltd.) were administered orally with feed (Pig solution I, Cargill Incorporated, Republic of Korea) at a dose of 5.0 and 1.25 mg of active ingredient per kg body weight for 7 and 3 consecutive days, respectively. The doses were recommended by the Korea Food and Drug Administration (KFDA). Animals were treated with DANO for 3 days starting at day 5 (the fifth day from the beginning of ENRO treatment). The treated pigs were killed at days 1, 2, 3, 5, and 7 after final administration of the drugs, and muscle, lung, and kidney tissues were collected. All samples were packed separately and kept at a temperature of –24 °C as soon as possible.

### 2.6. Supercritical fluid extraction and cleanup

Just before the analysis, 2 g of muscle, lung, and kidney samples were thawed, homogenized, cooled to –70 °C and lyophilized overnight (154.98 kg/cm<sup>2</sup>) by means of a freeze-dry system (model SFDSM12, Samwon, Busan, Korea) equipped with vacuum pump (Samwon, Busan, Republic of Korea). Seven grams of sea sand and 0.2 g of Na<sub>4</sub>EDTA were put into the extraction vessel, and the dried samples were transferred and extracted by supercritical CO<sub>2</sub> modified under optimal extraction conditions. The extract was then evaporated using a vacuum rotary evaporator at a bath temperature not exceeding 50 °C, and the residue was dissolved in 10 mL of 0.04 M phosphate buffer (pH 1.5)–acetonitrile (8:2, v/v). The aliquot was transferred into a microcentrifuge tube, to which 0.02 g ammonium sulfate and 0.02 g hyflo super cel medium were added. The mixture was then vortexed for at least 1 min, and was then kept in the freezer at –24 °C for 20 min. After centrifugation at 5000 rpm for 5 min, the supernatant was filtered through a membrane filter (PTFE, 0.20 μm) and injected for HPLC.

### 2.7. Method validation

#### 2.7.1. Specificity

The validation parameters were carried out according to KFSA guidelines for analytical assay procedures [51]. Specificity was assessed by analyzing the standards of analytes, drug-free blank pig tissues, and blank tissues spiked with analytes. All of the peaks presenting retention times exactly the same as their corresponding standards were investigated using a fluorescence detector. The spiked blank tissues were prepared at concentrations of 0.05, 0.02, and 0.1 mg/kg for ENRO, DANO, and CIP, respectively. The drug-free blank and spiked samples were extracted by SFE as described above.

#### 2.7.2. Sensitivity

To elucidate the sensitivity of the experimental method, the limit of detection (LOD) and limit of quantification (LOQ) were determined through the detection of analytes in blank samples. The standard working solutions were added to blank pig muscle, lung, and kidney samples, and were then extracted under the optimal SFE extraction conditions described previously. The LOD and LOQ were calculated by the ratios of signal-to-noise of the analytes.

#### 2.7.3. Linearity

In order to construct standard calibration curves for linearity and quantitation of the drugs in treated samples, stock solutions of ENRO and CIP were serially diluted to obtain five different concentrations of 0.005, 0.01, 0.02, 0.05, and 0.1 μg/mL, whereas the stock solution of DANO was diluted to obtain concentrations of 0.001, 0.002, 0.005, 0.01, and 0.03 μg/mL. The calibration curves were obtained by plotting the peak area vs. the concentrations of the working solutions.

#### 2.7.4. Accuracy and precision

The accuracy and precision of the developed method were evaluated by intra- and inter-day repeatability. Intra- and inter-day accuracy and precision were determined using fortified pig muscle, lung, and kidney samples with ENRO, DANO, and CIP at three concentrations (0.05, 0.1, and 0.5 mg/kg), which were extracted under the optimal SFE extraction conditions. Intra- and inter-day assays were performed in six replicates for single run and in triplicate for three different runs, respectively. Since the SFE system used in this study was able to extract and analyze nine samples a day, it took 6 days for the intra-day assay ( $n = 54$ ) and 9 days for the inter-day assay ( $n = 81$ , one set of 3 days) for all pig tissues.



**Table 1**

Extraction efficiencies of ENRO, DANO, and CIP from fortified pig muscle, lung, and kidney samples on dynamic SFE extraction times.

FQ	Tissue	10 min	20 min	30 min	40 min	50 min	60 min
ENRO	Muscle	76.8 <sup>a</sup> ± 1.6 <sup>b</sup>	17.7 ± 0.3	5.3 ± 1.2	0.1 ± 0.2	0.1 ± 0.1	T <sup>c</sup>
	Lung	78.8 ± 2.0	19.0 ± 4.3	2.0 ± 2.5	0.3 ± 0.4	T	T
	Kidney	73.5 ± 2.6	19.6 ± 3.3	6.2 ± 0.6	0.6 ± 0.3	T	T
DANO	Muscle	63.5 ± 0.9	25.6 ± 4.7	9.3 ± 4.1	2.0 ± 3.5	T	T
	Lung	63.1 ± 1.0	30.4 ± 9.5	5.7 ± 1.1	0.7 ± 0.6	T	T
	Kidney	65.9 ± 6.9	25.1 ± 3.8	7.3 ± 5.6	1.7 ± 0.5	T	T
CIP	Muscle	52.2 ± 2.2	27.3 ± 7.6	6.3 ± 3.0	5.3 ± 7.6	8.1 ± 6.4	0.8 ± 1.4
	Lung	70.5 ± 2.7	27.5 ± 2.7	2.0 ± 1.4	T	T	T
	Kidney	72.7 ± 2.5	15.9 ± 7.4	11.5 ± 6.0	T	T	T

<sup>a</sup> Percentage of area to sum.<sup>b</sup> Standard deviation of triplicate.<sup>c</sup> Trace.

### 3. Results and discussion

#### 3.1. Supercritical fluid extraction

Biological samples such as eggs, milk, and animal tissues are difficult matrices in which to perform veterinary drug analysis because they have the potential to form emulsions and foams with extraction solvent. Protein in biological matrices is a potential binder with drugs. These features result in poor extraction and isolation of the FQs [14,50,52]. The current study aimed to use an SFE extraction method to overcome these experimental problems. To achieve optimal extraction conditions for SFE, individual variables such as extraction temperature, SFE system pressure, the modifier ratio, and extraction time were considered. Lyophilized blank pig muscle, lung, and kidney samples were spiked with mixtures of standard working solution of ENRO, DANO, or CIP at individual concentrations of 0.2, 0.1, and 0.2 mg/kg, individually, and were then oven-dried at 50 °C for 10 min to remove solvent and protect against the loss of analytes by lyophilization. The temporary conditions for SFE extraction were 30% methanol (as a modifier), 80 °C oven temperature, 300 kg/cm<sup>2</sup> system pressure, and 3 mL/min flow rate. The obtained results of various experimental parameters that had been tested on different tissues are presented in Tables 1 and 2 and Fig. 2.

##### 3.1.1. Effects of extraction time

The effects of dynamic extraction times for the analytes were investigated while other parameters were fixed at 80 °C, 300 kg/cm<sup>2</sup>, and 30% methanol. The extracts were collected every 10 min for 60 min of the total extraction time after reaching a pressure of 300 kg/cm<sup>2</sup>. The results were described as a percentage of each peak area to the sum of the peak area detected each 10 min for 60 min, and are shown in Table 1. The results revealed that after

40 min there were no residuals of ENRO and DANO. A further study for static extraction time was not necessary because the FQs were eluted at an early point in the dynamic extraction time. Although slight detection of CIP occurred at 50 and 60 min, an extraction time longer than 40 min is undesirable for extraction efficiency. Therefore, a dynamic time of 40 min was chosen for the FQs from pig tissues in subsequent extractions.

##### 3.1.2. Extraction temperature

We studied the effect of temperature on the extraction efficiency of the FQs by varying oven temperature from 40 to 80 °C at increments of 20 °C, while the other conditions were the same as the temporary conditions. The extraction efficiency of the FQs was improved by increasing the temperature in most of the sets of parameters shown in Table 2. The recoveries of ENRO and DANO varied from 89.1 to 100.1% at 80 °C in pig tissues. In the case of ENRO, the recoveries remained constant at both 60 and 80 °C, which indicated that the extractability of modified supercritical CO<sub>2</sub> for ENRO is sufficient at an oven temperature of 60 °C at 300 kg/cm<sup>2</sup> pressure. These trends demonstrate that the increasing temperature enhances the vapor pressure of the analytes and desorption of the analytes from the matrix, although it lowers the fluid density. Increasing the extraction temperature can provide more of the energy that is required for the process of desorption [53]. Additionally, the vaporization of the molecule affecting extraction efficiency may be influenced by high temperature [54]. It was noted that the enhancement of desorption and the volatility of the analytes from the matrix, rather than the decrease in solvent density, may become dominant with increasing temperature [43]. However, overall recoveries of CIP were below 70% through the three types of samples. It was decided that the temperature of SFE should be fixed at 80 °C for the FQs in pig tissues.

##### 3.1.3. Extraction pressure

To evaluate the effect of pressure on the SFE efficiency of the FQs, extractions were performed at pressures of 250, 280, and 300 kg/cm<sup>2</sup> for 40 min, at a fixed oven temperature of 80 °C. As can be seen in Table 2, ENRO recoveries increased with increasing pressure. These results led to a rise in solubility of supercritical fluid owing to the enhancement of fluid density correspondence with increasing pressure. However, recoveries of CIP were still constant despite the increasing pressure, and DANO recovery was maximized at 280 kg/cm<sup>2</sup>. The pressure was set at 300 kg/cm<sup>2</sup> as an optimal extraction pressure for simultaneous determination of the FQs in pig tissues.

##### 3.1.4. Extraction modifier

Supercritical CO<sub>2</sub> is considered to be a nonpolar solvent like hexane. This character of supercritical CO<sub>2</sub> is adequate for efficient extraction of nonpolar compounds, but is not capable of functioning

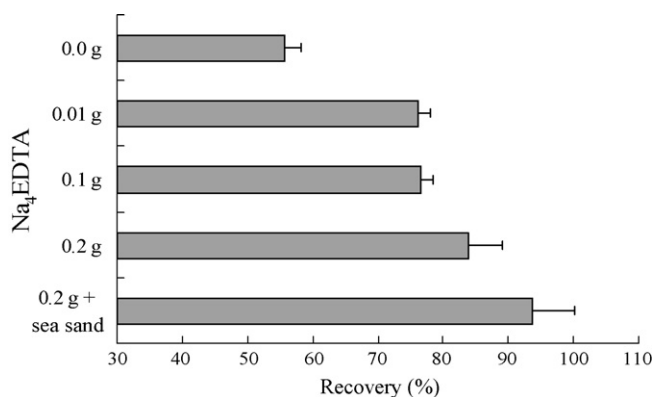


**Fig. 2.** Extraction profile of CIP from fortified pig muscle at 80 °C, 300 kg/cm<sup>2</sup>, using 30% methanol-modified supercritical CO<sub>2</sub> flowed with 3 mL/min for 40 min.

**Table 2**  
Effects of temperature, pressure, and modifier ratio on the SFE of ENRO, DANO, and CIP from fortified pig muscle, lung, and kidney samples.

Compound	Tissue	Recovery <sup>a</sup> (%)		
		Temperature (300 kg/cm <sup>2</sup> , 30% methanol, 3 mL/min)		
		40 °C	60 °C	80 °C
ENRO	Muscle	66.6 ± 3.6	92.8 ± 5.5	98.3 ± 2.7
	Lung	86.4 ± 12.9	102.9 ± 7.0	100.1 ± 6.9
	Kidney	81.9 ± 17.3	103.3 ± 2.7	89.6 ± 2.5
DANO	Muscle	70.0 ± 8.7	75.0 ± 10.8	97.1 ± 15.6
	Lung	37.6 ± 4.5	59.2 ± 6.6	96.7 ± 24.5
	Kidney	36.2 ± 3.2	79.5 ± 10.3	99.2 ± 12.2
CIP	Muscle	34.8 ± 2.9	42.1 ± 4.8	63.6 ± 8.9
	Lung	38.6 ± 0.2	58.6 ± 3.6	59.5 ± 0.1
	Kidney	27.7 ± 4.1	42.9 ± 3.3	67.6 ± 19.1
		Pressure (80 °C, 30% methanol, 3 mL/min)		
		250 kg/cm <sup>2</sup>	280 kg/cm <sup>2</sup>	300 kg/cm <sup>2</sup>
ENRO	Muscle	78.3 ± 3.6	83.7 ± 17.9	94.0 ± 3.5
	Lung	94.1 ± 7.2	94.6 ± 4.7	99.4 ± 7.8
	Kidney	71.9 ± 0.4	85.3 ± 3.0	92.8 ± 4.9
DANO	Muscle	70.6 ± 20.4	90.8 ± 2.4	61.6 ± 2.0
	Lung	93.6 ± 9.9	103.7 ± 4.9	80.8 ± 16.0
	Kidney	83.3 ± 3.7	99.2 ± 11.5	73.8 ± 10.7
CIP	Muscle	64.6 ± 1.5	45.1 ± 13.8	68.3 ± 3.9
	Lung	68.2 ± 4.0	65.3 ± 4.7	55.7 ± 2.6
	Kidney	68.1 ± 4.3	53.2 ± 5.1	55.5 ± 11.0
		Methanol ratio (80 °C, 300 kg/cm <sup>2</sup> , 3 mL/min)		
		10%	20%	30%
ENRO	Muscle	63.2 ± 0.4	94.6 ± 0.9	94.8 ± 2.1
	Lung	75.0 ± 7.5	88.6 ± 7.1	98.1 ± 2.1
	Kidney	69.2 ± 1.8	90.2 ± 0.8	92.2 ± 6.5
DANO	Muscle	49.3 ± 9.9	62.6 ± 17.6	103.2 ± 0.8
	Lung	32.7 ± 0.5	83.8 ± 8.4	95.4 ± 8.5
	Kidney	24.5 ± 1.7	66.2 ± 3.2	96.4 ± 12.9
		20%	30%	40%
CIP	Muscle	38.0 ± 5.8	56.4 ± 19.1	59.0 ± 1.4
	Lung	40.8 ± 15.9	54.3 ± 0.2	55.4 ± 2.5
	Kidney	36.7 ± 8.1	54.6 ± 1.7	59.6 ± 10.1

<sup>a</sup> Mean recovery and standard deviation of duplicate determinations.

as an extraction solvent to extract polar materials [49]. It is necessary to add a modifier, usually methanol or ethanol, to enhance the solubility of the analyte into supercritical CO<sub>2</sub> by increasing the polarity of the fluid. The modifier can also help increase the extraction efficiency by displacing the analytes from the sample matrix or by disrupting the analyte–matrix complex [55,56]. Table 2 shows that the extraction efficiency increased when more methanol was added into the extraction vessel. The ENRO and DANO recoveries ranged from 92.2 to 103.2% in all samples with the use of 30% methanol. However, the recoveries of CIP were lower than 70% even with 40% methanol.

### 3.1.5. Effects of Na<sub>4</sub>EDTA and sea sand

Table 2 shows that the recoveries of CIP were still quite limited in spite of any increase in parameters. These results can be explained by the *n*-octanol/water partition coefficient (*K*<sub>ow</sub>) value and polarity of the FQs. The *K*<sub>ow</sub> value of CIP ranges from 0.036 to 0.165 between pH 5 and pH 9, which means that CIP is more a hydrophilic and polar compound than ENRO and DANO, which have *K*<sub>ow</sub> values of 0.4–3.1 and 0.14–0.39, respectively [57,58]. In terms of their chemical structures, all of the analytes have a quinoline carboxylic acid as a main chemical frame, a cyclopropyl group at N-1, and a 1-piperazinyl group at C-7. CIP has only a 1-piperazinyl group, but the others have

the piperazinyl group bonded with hydrocarbons. Therefore, CIP is more polar than ENRO and DANO. Similar observations were also reported in our previous studies [44,50]. Therefore, it was predicted that modification of supercritical CO<sub>2</sub> with methanol is not sufficient to extract CIP from pig tissues. Meanwhile, the use of water as

**Table 3**

The limit of detection (LOD) and limit of quantification (LOQ) of ENRO, DANO, and CIP in pig muscle, lung, and kidney by SFE extraction coupled with HPLC-FLD.

Fluoroquinolone	ENRO	DANO	CIP
LOD (mg/kg)			
All tissues	0.01	0.002	0.015
LOQ (mg/kg)			
All tissues	0.025	0.005	0.05
MRL <sup>a</sup> (mg/kg)			
Muscle	0.1	0.1	– <sup>b</sup>
Kidney	0.3	0.2	
Liver	0.2	0.05	
Fat	0.1	0.1	

<sup>a</sup> MRLs of veterinary drugs in food, 11-1470000-000532-01, KFSA, 2004.

<sup>b</sup> MRL of ciprofloxacin is not established as a major metabolite of enrofloxacin. The MRL of enrofloxacin is a sum of enrofloxacin and ciprofloxacin.

a modifier was not allowed because SFE extraction is affected by ice generated in the SFE system used in this study. Therefore, Na<sub>4</sub>EDTA was added into the extraction vessel to improve the extraction efficiency of CIP. Alcantara-Licudine et al. and Guo et al. used Na<sub>4</sub>EDTA as a modifier or mixed with a sample to increase the extraction efficiency of phloxine B or acidic pesticides. Their recoveries were remarkably increased by the use of Na<sub>4</sub>EDTA, as demonstrated by its chelating effect [33,34].

Pig muscle samples were representatively used to prove the effect of Na<sub>4</sub>EDTA on SFE extraction of CIP, since muscle is denser than the other sample types. Na<sub>4</sub>EDTA was added into the extraction vessel at 0.01, 0.1, and 0.2 g of sample weight. The recovery was dramatically increased to 83.9% by the addition of 0.2 g Na<sub>4</sub>EDTA to the sample, although the recovery was moderate (74.9–78.0%) in samples to which 0.01 and 0.1 g Na<sub>4</sub>EDTA were added (Fig. 2). An important observation was that the recovery was enhanced to 93.8% following the addition of 7 g of sea sand to samples with 0.2 g Na<sub>4</sub>EDTA, compared to samples to which only 0.2 g Na<sub>4</sub>EDTA was added. This result was achieved by the relative enhancement of the density of modified supercritical CO<sub>2</sub> according to the reduction of the empty space in the extraction vessel filled by sea sand. The improved solvating power of that fluid can dissolve the analytes directly, and Na<sub>4</sub>EDTA increases the extraction efficiency. The

elevated pressure supplies energy to analytes for desorption [47]. Additionally, the chelating effect of Na<sub>4</sub>EDTA in disturbing or displacing the analyte from the matrix was increased.

Therefore, the optimal extraction conditions of SFE to extract ENRO, DANO, and CIP from pig muscle, lung, and kidney samples were 40 min, 80 °C, 300 kg/cm<sup>2</sup>, 30% modifier, 0.2 g Na<sub>4</sub>EDTA, and 7 g sea sand.

### 3.2. Method validation

#### 3.2.1. Specificity

Specificity is the ability of a method to distinguish between the analyte of interest and other substances that may be present in a test sample. The interference of endogenous compounds was assessed by extracting a blank sample using a previously developed method. Figs. 3–5 show the representative FQ standards chromatogram and chromatograms of blank, spiked blank samples, and incurred samples extracted using SFE. There were no interference peaks at the retention times of the tested analytes. The retention times of the tested drugs at the spiked samples matched with those of the standard solutions, and indicated good separation between the FQs on the HPLC system. These data suggest that our method can detect ENRO, DANO, and CIP simultaneously and selectively in pig tissues.

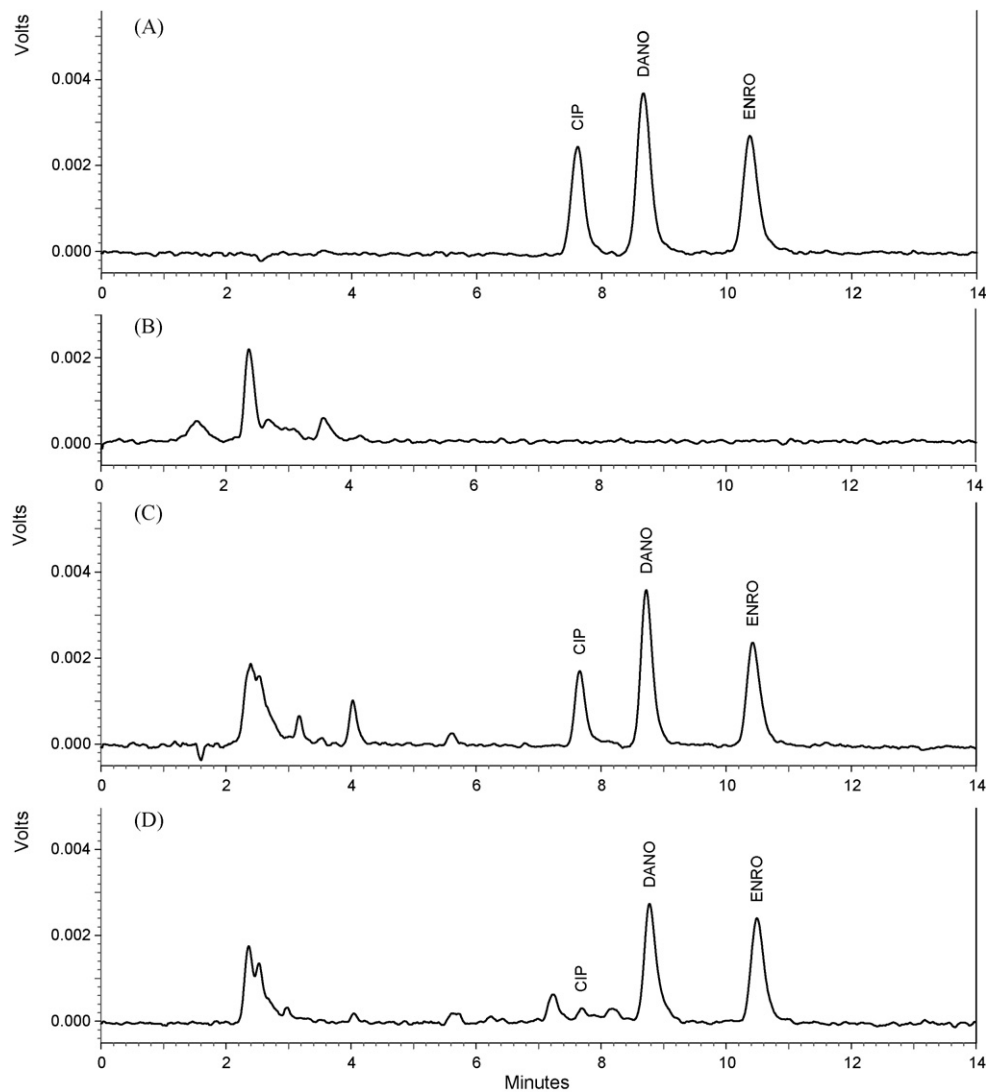


**Fig. 3.** Chromatograms of (A) a standard mixture of the selected fluoroquinolones; (B) muscle blank sample; (C) muscle spiked sample at 50 µg/kg (ENRO), 20 µg/kg (DANO), and 100 µg/kg (CIP) and (D) incurred muscle sample at 2 days after final treatment.

### 3.2.2. Sensitivity

The limit of detection (LOD) and limit of quantification (LOQ) for each analyte were calculated on the basis of the noise that was produced by injecting blank test samples into the detection instrument. The LOD was determined as the fortified sample concentration that produces a peak height with three times the level of sample noise of the blank, and the LOQ was calculated as the fortified sample concentration that produces a peak height with ten times the signal-to-noise ratio. The LOQ is the lowest concentration of the analyte that can be determined with acceptable precision and accuracy. The LODs for ENRO, DANO, and CIP in all pig tissues were found to be 0.01, 0.002 and 0.015 mg/kg, respectively. The LOQs of ENRO, DANO, and CIP in all tissues were 0.025, 0.005, 0.05 mg/kg, respectively. The LOQ value of DANO and the sum of ENRO and CIP were lower than the MRL values for the FQs (Table 3). The LOD and LOQ values observed in this study justified that the introduction of SFE extraction and HPLC-FLD detection is possible for determination of the FQ residues in pig muscle, lung, and kidney tissues.

### 3.2.3. Linearity

The standard calibration curve of each of the FQs was obtained by measuring the peak areas of the HPLC chromatograms of

the standard working mixture solutions. The linearity of the method was assessed by calibration in the concentration range of 0.005–0.1  $\mu\text{g/mL}$  for ENRO and CIP, whereas the range of concentration for DANO was 0.001–0.02  $\mu\text{g/mL}$ . The calibration parameters for the three drugs are shown in Table 4. The correlation coefficient ( $r^2$ ) values from 0.9967 to 0.9990 observed in this study indicated a good linearity between the FQ concentrations and peak areas. When the calibration curves were prepared using the standard working mixture solutions, we found that the standards on the curve were well dispersed.

### 3.2.4. Accuracy and precision

Accuracy and precision experiments for ENRO, DANO, and CIP were carried out to assess the application of this method for the investigation of residue analysis. The intra- and inter-day accuracy and precision of the assay were determined by analyses using fortified samples at three concentrations (0.05, 0.1, and 0.5 mg/kg). These concentrations were compared to the MRLs of the drugs in pig tissues. The percentage recoveries for accuracy were determined by comparing the peak areas of blank samples spiked with different amounts of analyte, with the peak areas of the same standards prepared in solvent. The precision of a method is usually expressed as a relative standard deviation (R.S.D.). The results for the accuracy

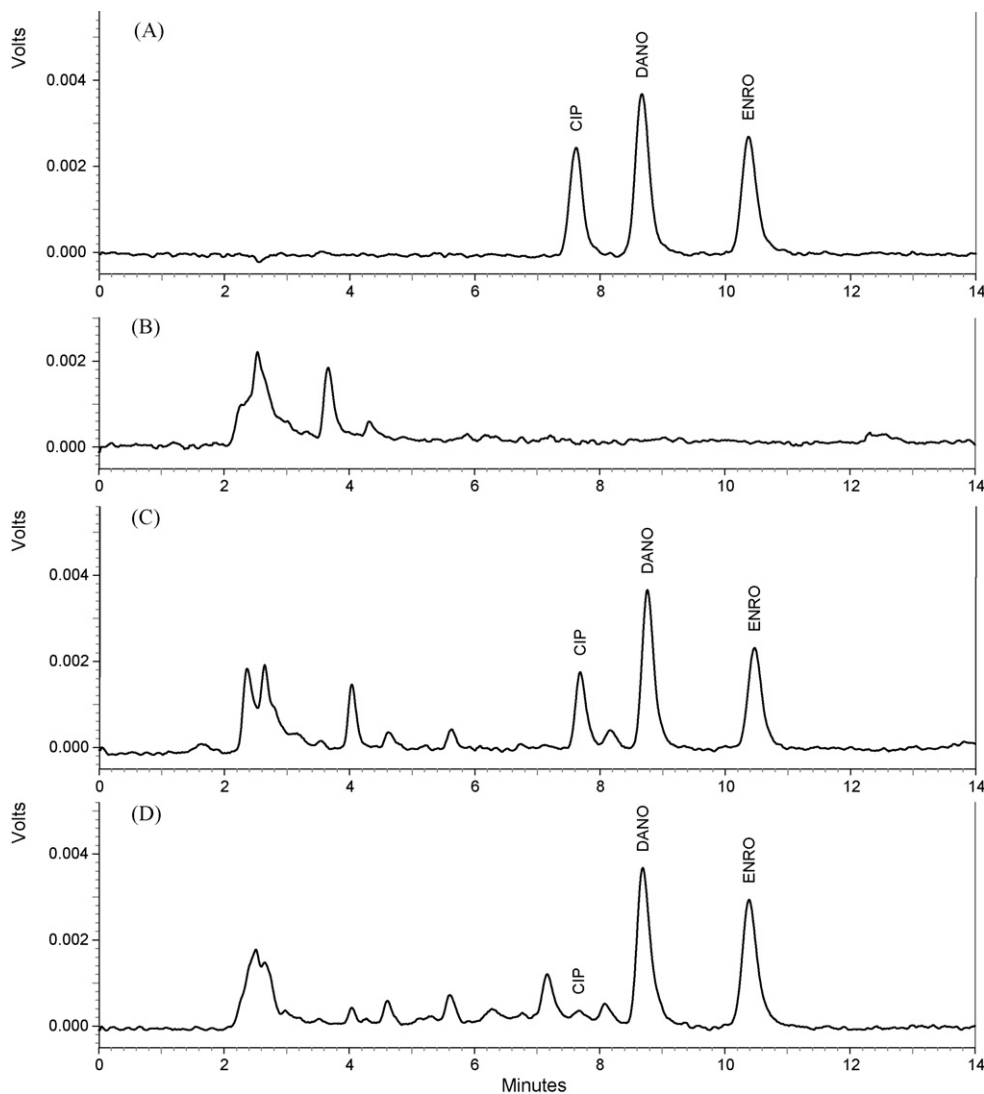


**Fig. 4.** Chromatograms of (A) a standard mixture of the selected fluoroquinolones; (B) lung blank sample; (C) lung spiked sample at 50  $\mu\text{g/kg}$  (ENRO), 20  $\mu\text{g/kg}$  (DANO), and 100  $\mu\text{g/kg}$  (CIP) and (D) incurred lung sample at 2 days after final treatment.

**Table 4**  
Linearity of ENRO, DANO, and CIP by HPLC with fluorescence detection.

Compound	Linear range ( $\mu\text{g/mL}$ )	No. of points	Regression and correlation		
			Slope	Intercept	Correlation coefficient
Enrofloxacin	0.005–0.1	5	51.545	–1.0754	0.9982
Danofloxacin	0.001–0.02		257.01	–1.8048	0.9990
Ciprofloxacin	0.005–0.1		27.924	+1.1372	0.9967

and precision of the FQs are shown in Table 5. Excellent recoveries and R.S.D. were observed for analytes at all fortification levels and tissues. The overall mean accuracy and precision of the intra-day assay for the FQs ranged from 88.4 to 115.8% and from 1.7 to 9.5%, respectively. The inter-day accuracy for the FQs varied from 86.7 to 113.1%, and the precision ranged from 1.8 to 11.2%. Excellent recoveries of CIP resulted from the use of  $\text{Na}_4\text{EDTA}$  and sea sand. Obviously, the method is quite reliable, reproducible, and accurate for ENRO, DANO, and CIP.

### 3.3. Quantitation of the FQs in incurred samples

The method validation results indicated that the developed method could successfully extract ENRO, DANO, and CIP from for-

tified pig muscle, lung, and kidney samples. In addition to fortified samples, the SFE extraction method was applied to incurred pig tissues in order to determine its reliability in performing routine residue analysis of the FQs in biological samples. Each commercial product was treated with ENRO and DANO at the dose recommended by the KFDA. The extraction of analytes from incurred pig samples was accomplished under optimized SFE conditions. Quantitation was achieved using a calibration curve. The results were examined by time course determination of the FQs in pig tissues (Table 6). As ENRO was metabolized to CIP, ENRO represents the total concentration by summing up the residual amount of CIP along with it. The residual concentration of ENRO and DANO was maximal at day 1 in all tissues, and the highest residual level was recorded in kidney tissue. The residual concentrations were sharply decreased

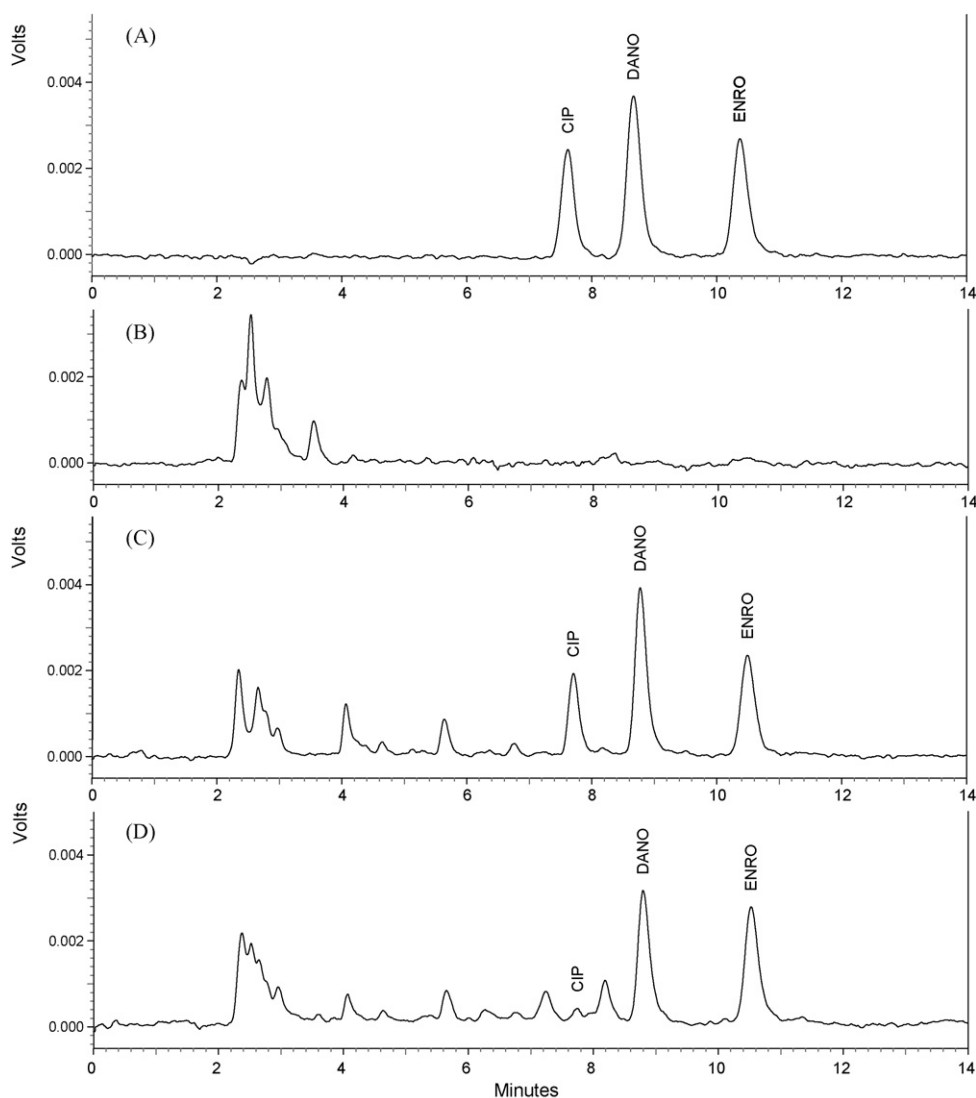


**Fig. 5.** Chromatograms of (A) a standard mixture of the selected fluoroquinolones; (B) kidney blank sample; (C) kidney spiked sample at 50  $\mu\text{g/kg}$  (ENRO), 20  $\mu\text{g/kg}$  (DANO), and 100  $\mu\text{g/kg}$  (CIP) and (D) incurred kidney sample at 2 days after final treatment.

**Table 5**  
Intra-day and inter-day accuracy and precision of ENRO, DANO, and CIP in pig tissues.

FQs	Concentration (mg/kg)	Accuracy (%)			Precision (R.S.D., %)		
		Muscle	Lung	Kidney	Muscle	Lung	Kidney
Intra-day accuracy and precision (n = 54)							
ENRO	0.05	100.0	94.1	92.9	3.5	5.1	4.7
	0.1	96.9	93.3	97.2	9.5	7.4	8.0
	0.5	97.6	99.0	92.5	1.7	7.2	1.9
DANO	0.05	98.1	95.1	98.2	3.1	5.6	3.9
	0.1	108.4	98.2	94.9	6.5	2.2	6.1
	0.5	115.8	91.7	94.1	2.1	7.7	4.5
CIP	0.05	91.9	95.7	94.0	2.7	6.6	5.9
	0.1	95.1	89.7	89.9	2.5	3.4	5.1
	0.5	91.7	88.4	91.4	4.3	2.6	6.3
Inter-day accuracy and precision (n = 81)							
ENRO	0.05	98.7	91.3	96.4	4.5	6.6	7.2
	0.1	102.5	93.0	93.1	11.2	6.8	9.6
	0.5	97.4	95.5	94.8	1.8	8.3	4.0
DANO	0.05	96.6	98.1	95.4	4.2	6.3	6.1
	0.1	107.6	97.1	91.4	11.0	2.5	8.2
	0.5	113.1	93.3	91.4	4.3	6.6	5.9
CIP	0.05	91.7	91.5	92.0	2.2	11.2	7.1
	0.1	93.8	92.2	93.5	4.4	6.0	8.2
	0.5	88.8	86.7	90.5	6.1	3.7	5.5

**Table 6**  
Time course residues ( $\mu\text{g}/\text{kg}$ ) of ENRO and DANO in pig muscle, lung, and kidney.

FQs	Tissue	1 day	2 days	3 days	5 days	7 days
ENRO <sup>a</sup>	Muscle	694.3 $\pm$ 51.6	94.5 $\pm$ 3.1	155.7 $\pm$ 12.4	21.6 $\pm$ 3.0	T <sup>b</sup>
	Lung	705.2 $\pm$ 10.9	110.7 $\pm$ 1.3	81.7 $\pm$ 7.3	20.8 $\pm$ 3.1	T
	Kidney	1198.7 $\pm$ 235.4	105.9 $\pm$ 1.6	107.5 $\pm$ 14.0	34.7 $\pm$ 3.0	52.3 $\pm$ 7.9
DANO	Muscle	69.9 $\pm$ 4.3	16.1 $\pm$ 4.4	24.6 $\pm$ 1.1	T	T
	Lung	75.0 $\pm$ 1.3	23.0 $\pm$ 1.5	26.7 $\pm$ 2.5	6.5 $\pm$ 0.9	T
	Kidney	135.1 $\pm$ 12.6	19.8 $\pm$ 0.4	28.4 $\pm$ 2.0	6.0 $\pm$ 0.4	5.6 $\pm$ 0.2

<sup>a</sup> Total residue of enrofloxacin calculated as follows:  $A = B + C \times (\text{MW of ENRO}/\text{MW of CIP})$  where  $A$  = total residual concentration of ENRO,  $B$  = residual concentration of ENRO and  $C$  = residual concentration of CIP.

<sup>b</sup> Trace.

at day 2, although the concentrations at day 3 were a slightly higher, possibly due to mishandling of samples. However, the residue of ENRO was found to be below the MRL values fixed by KFDA at day 5, and that of DANO was found to be below the MRL values fixed by KFDA at day 2 in all tissues. The time to reach a level lower than the LOQ for ENRO was 5 days in muscle and lung tissue, and 7 days in kidney tissue. That day of DANO was 5 days in muscle tissue, 7 days in lung tissue, and after 7 days in kidney tissue. In terms of the distribution of antibiotic agents, the difference in residues was caused by different degrees of intestinal absorption and elimination between tissues. Consequently, our developed method could be considered as an appropriate method to perform reliable determination of the FQs in incurred animal samples at levels lower than MRL values.

#### 4. Conclusion

Thus far, the study of supercritical fluid extraction for fluoroquinolones has only been carried out by our laboratory. This study is the first to report successful extraction using supercritical fluid extraction for ciprofloxacin in biological samples. A  $\text{Na}_4\text{EDTA}$ /sea sand-assisted SFE procedure was developed for the extraction of polar and nonpolar fluoroquinolone antibiotics. Excellent separation of enrofloxacin, danofloxacin, and ciprofloxacin in pig tissues was achieved by HPLC-FLD. The optimized method with enrofloxacin, danofloxacin, and ciprofloxacin was successfully applied to extract the analytes, with recoveries ranging from 86.7 to

113.1% (from inter-day assay data) in pig tissues. The recoveries of polar ciprofloxacin were remarkably increased, to 88.8–93.8% (from inter-day assay data), when  $\text{Na}_4\text{EDTA}$  and sea sand were added. The method reported here is selective, sensitive, reliable, and accurate, as shown by method validation results. A combination of  $\text{Na}_4\text{EDTA}$  and sea sand in SFE is also valuable for quantitative residue analysis to assess the risk of the presence of polar to nonpolar compounds in animal tissues. However, considerable optimization is needed before this procedure can be used for general application.

#### Acknowledgements

We are grateful to the Agricultural R&D Promotion Center, Ministry for Food, Agriculture, Forestry and Fisheries (grant No. 204152-3) for its financial support of this work. The authors are also thankful to Agricultural Science and Technology, Chonnam National University, for providing partial support for the study.

#### References

- [1] Antibiotics in Farm Animals, CIWF (Compassion in World Farming) Factsheet, 2004 (<http://www.ciwf.org.uk/publications/index2.html>).
- [2] T. Garcia, US Authority Reviews Use of Animal Antibiotics, Elsevier Science Channel, 1999.
- [3] D.F. King, R. Malone, S.H. Lilley, Am. Fam. Phys. 61 (2002) 2741.
- [4] D.H. Wright, V.K. Herman, F.N. Konstantinides, J.C. Rotschafer, J. Chromatogr. B 709 (1998) 97.
- [5] A. Marzo, L.D. Bo, J. Chromatogr. A 812 (1998) 17.
- [6] M. Hernández, F. Borrull, M. Calull, J. Chromatogr. B 742 (2000) 255.

- [7] D. Gendrel, M. Chalumeau, F. Moulin, J. Raymond, *Lancet Infect. Dis.* 3 (2003) 537.
- [8] N. Gorla, E. Chiostri, L. Ugnia, A. Weyers, N. Giacomelli, R. Davicino, H.G. Ovando, *Int. J. Antimicrob. Agents* 8 (1997) 253.
- [9] M.K. Hassouan, O. Ballesteros, J. Taoufiki, J.L. Vilchez, M. Cabrera-Aguilera, A. Navalón, *J. Chromatogr. B* 852 (2007) 625.
- [10] D.A. Volmer, B. Mansoori, S.J. Locke, *Anal. Chem.* 69 (1997) 4143.
- [11] M. Hernández, C. Aguilar, F. Borrull, M. Calull, *J. Chromatogr. B* 772 (2002) 163.
- [12] P.J. Ihrke, M.G. Papich, T.C. Demanuelle, *Vet. Dermatol.* 10 (1999) 193.
- [13] M. Horie, K. Saito, N. Nose, H. Nakazawa, *J. Chromatogr. B* 653 (1) (1994) 69.
- [14] A. Posyniak, J. Zmudzki, S. Semeniuk, J. Niedzielska, R. Ellis, *Biomed. Chromatogr.* 13 (1999) 279.
- [15] J.C. Yorke, P. Froc, *J. Chromatogr. A* 882 (2000) 63.
- [16] G.J. Krol, G.W. Beck, T. Benham, *J. Pharm. Biomed. Anal.* 14 (1995) 181.
- [17] S.L. Boulaire, J.C. Bauduret, F. Andre, *J. Agric. Food Chem.* 45 (1997) 2134.
- [18] M. Lolo, S. Pedreira, C. Fente, B.I. Vazquez, C.M. Franco, A. Cepeda, *Anal. Chim. Acta* 480 (2003) 123.
- [19] E.M. Golet, A. Strehler, A.C. Alder, W. Giger, *Anal. Chem.* 74 (2002) 5455.
- [20] J. Manceau, M. Gicquel, M. Laurentie, P. Sanders, *J. Chromatogr. B* 726 (1999) 175.
- [21] R.J. Maxwell, E. Cohen, D.J. Donoghue, *J. Agric. Food Chem.* 47 (1999) 1563.
- [22] A.L. Cinquina, P. Roberti, L. Giannetti, F. Longo, R. Draisci, A. Fagiolo, N.R. Brizioli, *J. Chromatogr. A* 987 (2003) 221.
- [23] P.G. Gigosos, P.R. Revesado, O. Cadahía, C.A. Fente, B.I. Vazquez, C.M. Franco, A. Cepeda, *J. Chromatogr. A* 871 (2000) 31.
- [24] C.K. Holtzappple, S.A. Buckley, L.H. Stanker, *J. Agric. Food Chem.* 47 (1999) 2963.
- [25] J.A. Hernández-Arteseros, J. Barbosa, R. Compano, M.D. Prat, *J. Chromatogr. A* 945 (2002) 1.
- [26] K.H. Bannefeld, H. Stass, G. Blaschke, *J. Chromatogr. B* 692 (1997) 453.
- [27] R. Hindle, C.K. Meng, *The Analysis of Fluoroquinolones in Beef Kidney Using HPLC Electrospray Mass Spectrometry*, Agilent Technologies Inc., 2004.
- [28] M.J. Schneider, D.J. Donoghue, *Anal. Chim. Acta* 483 (2003) 39.
- [29] B. Toussaint, M. Chedin, G. Bordin, A.R. Rodriguez, *J. Chromatogr. A* 1088 (2005) 32.
- [30] G.V. Vyncht, A. Jànosi, G. Bordin, B. Toussaint, G. Maghuin-Rogister, E.D. Pauw, A.R. Rodriguez, *J. Chromatogr. A* 952 (2002) 121.
- [31] H.-B. Lee, T.E. Peart, M. Lewina Svoboda, *J. Chromatogr. A* 1139 (2007) 45.
- [32] J.E. Renew, C.H. Huang, *J. Chromatogr. A* 1042 (2004) 113.
- [33] F. Guo, Q.X. Li, J.P. Alcantara-Licudine, *Anal. Chem.* 71 (1999) 1309.
- [34] J.P. Alcantara-Licudine, M.K. Kawate, Q.X. Li, *J. Agric. Food Chem.* 45 (1997) 766.
- [35] T. Yarita, A. Nomura, Y. Horimoto, S. Gonda, *J. Chromatogr. A* 750 (1996) 175.
- [36] C.D. Bevan, P.S. Marshall, *Nat. Prod. Rep.* (1994) 451.
- [37] C. Doneanu, G. Anitescu, *J. Supercrit. Fluids* 12 (1998) 59.
- [38] M.D.A. Saldaña, C. Zetzl, R.S. Mohamed, G. Brunner, *J. Supercrit. Fluids* 22 (2002) 119.
- [39] W.-J. Kim, J.-D. Kim, J. Kim, S.-G. Oh, Y.-W. Lee, *J. Food Eng.* 89 (2008) 303.
- [40] J.W. King, M.L. Hopper, R.G. Luchtefeld, S.L. Taylor, W.L. Orton, *J. AOAC Int.* 76 (1993) 857.
- [41] S.J. Lehotay, *J. Chromatogr. A* 785 (1997) 289.
- [42] Y. Ono, T. Yamagami, T. Nishina, T. Tobino, *Anal. Sci.* 22 (2006) 1473.
- [43] M.T. Combs, M. Gandee, M. Ashraf-Khorassani, L.T. Taylor, *Anal. Chim. Acta* 341 (1997) 285.
- [44] J.Y. Shen, M.R. Kim, C.J. Lee, I.S. Kim, K.B. Lee, J.H. Shim, *Anal. Chim. Acta* 513 (2004) 451.
- [45] K.S. Nam, S. Kapila, A.F. Yanders, R.K. Puri, *Chemosphere* 20 (1990) 873.
- [46] Y. Yang, A. Gharaibeh, S.B. Hawthorne, D.J. Miller, *Anal. Chem.* 67 (1995) 641.
- [47] J.J. Langenfeld, S.B. Hawthorne, D.J. Miller, J. Pawliszyn, *Anal. Chem.* 65 (1993) 338.
- [48] J.H. Choi, A.E. Abd El-Aty, J.Y. Shen, M.R. Kim, J.H. Shim, *Berliner Münchener Tierärztl Wochenschr.* 119 (2006) 456.
- [49] J.H. Shim, J.Y. Shen, M.R. Kim, C.J. Lee, I.S. Kim, *J. Agric. Food Chem.* 51 (2003) 7528.
- [50] J.H. Shim, M.H. Lee, M.R. Kim, C.J. Lee, I.S. Kim, *Biosci. Biotechnol. Biochem.* 67 (2003) 1342.
- [51] Guideline for analytical method validation of medicines, Drug Evaluation Department, Pharmaceutical Safety Bureau, Korean Food & Drug Administration (KFDA), November 2004.
- [52] M.M.L. Aerts, A.C. Hogenboom, U.A.Th. Brinkman, *J. Chromatogr. B* 667 (1995) 1.
- [53] S.B. Hawthorne, D.J. Miller, *Anal. Chem.* 66 (1994) 4005.
- [54] Y. Yamini, M. Asghari-Khiavi, N. Bahramifar, *Talanta* 58 (2002) 1003.
- [55] J.W. Pensabene, W. Fiddler, *J. AOAC Int.* 82 (1999) 1334.
- [56] V. Arancibia, M. Valderrama, P. Rodriguez, F. Hurtado, R. Segura, *J. Sep. Sci.* 26 (2003) 1710.
- [57] G.G. Gagliano, F.T. McNamara, Study Title: Environmental Assessment for Enrofloxacin, BAYTRIL® 3.23% Concentrate Antimicrobial Solution, Guideline 21 CFR Part 25 (1996) (<http://www.fda.gov/cvm/FOI/140-828EA.pdf>).
- [58] Environmental Assessment: Danofloxacin 18% Injectable Solution for the Treatment of Respiratory Disease in Cattle (2002) (<http://www.fda.gov/cvm/FOI/141-207EA.pdf>).



# Ion-imprinted polymethacrylic microbeads as new sorbent for preconcentration and speciation of mercury

Ivanka Dakova\*, Irina Karadjova, Ventsislava Georgieva, George Georgiev

Department of Chemistry, Sofia University, Sofia, Bulgaria

## ARTICLE INFO

### Article history:

Received 17 April 2008

Received in revised form

30 November 2008

Accepted 2 December 2008

Available online 7 December 2008

### Keywords:

Solid phase extraction

Ion-imprinted polymer

Hg

Inorganic mercury

Cold vapor atomic absorption spectrometry

## ABSTRACT

Metal ion-imprinted polymer particles have been prepared by copolymerization of methacrylic acid as monomer, trimethylolpropane trimethacrylate as cross-linking agent and 2,2'-azobisisobutyronitrile as initiator, in the presence of Hg(II)-1-(2-thiazolylazo)-2-naphthol complex. The separation and preconcentration characteristics of the Hg-ion-imprinted microbeads for inorganic mercury have been investigated by batch procedure. The optimal pH value for the quantitative sorption is 7. The adsorbed inorganic mercury is easily eluted by 2 mL 4 M HNO<sub>3</sub>. The adsorption capacity of the newly synthesized Hg ion-imprinted microbeads is 32.0 μmol g<sup>-1</sup> for dry copolymer. The selectivity of the copolymer toward inorganic mercury (Hg(II)) ion is confirmed through the comparison of the competitive adsorptions of Cd(II), Co(II), Cu(II), Ni(II), Pb(II), Zn(II) and high values of the selectivity and distribution coefficients have been calculated. Experiments performed for selective determination of inorganic mercury in mineral and sea waters showed that the interfering matrix does not influence the extraction efficiency of Hg ion-imprinted microbeads. The detection limit for inorganic mercury is 0.006 μg L<sup>-1</sup> (3σ), determined by cold vapor atomic adsorption spectrometry. The relative standard deviation varied in the range 5–9% at 0.02–1 μg L<sup>-1</sup> Hg levels. The new Hg-ion-imprinted microbeads have been tested and applied for the speciation of Hg in river and mineral waters: inorganic mercury has been determined selectively in nondigested sample, while total mercury e.g. sum of inorganic and methylmercury, has been determined in digested sample.

© 2008 Elsevier B.V. All rights reserved.

## 1. Introduction

Due to the high toxicity and accumulative character of mercury, the determination of trace amounts of this element in environmental samples is an actual analytical task. For mercury in natural waters, the main species to be identified and determined, are inorganic mercury (Hg(II)) and methylmercury (CH<sub>3</sub>Hg(I)). Recent reports estimate a total mercury concentration in natural waters ranging from 0.2 to 100 ng L<sup>-1</sup> [1], while methylmercury levels are much lower (ca. 0.05 ng L<sup>-1</sup>) [2]. Highly sensitive methods are required for direct determination of such extremely low levels and most frequently accurate and reliable results for Hg-species content in natural waters have been achieved after suitable separation and preconcentration step. A great variety of analytical procedures for Hg(II) preconcentration and separation, based mainly on liquid–liquid extraction [3–5], coprecipitation [6,7], and solid phase extraction (SPE) [8–16] have been proposed. The SPE procedures as separation and preconcentration methods exhibit numerous advantages such as flexibility, high preconcentration factors, high retention capacity, speed and simplicity, possibilities for field sam-

pling, ease of automation [17]. However, it should be noted that the extraction efficiency and selectivity of this technique is strongly dependent on the sorbent material used. Therefore, the development of new adsorbents with high affinity and specific recognition for Hg(II) or CH<sub>3</sub>Hg(I) ion is of great interest.

During the last years ion-imprinted polymers (IIPs), as selective sorbents for a particular chemical form of the given element, have received much attention. The high selectivity of IIPs can be explained by the polymer memory effect toward the metal ion interaction with a specific ligand, coordination geometry, metal ion coordination number, charge and size [18]. Numerous studies on IIPs and their application for selective preconcentration and separation of metal ions have been reported lately [19–28] including Hg(II)-imprinted ones [29–32]. Due to the high toxicity and accumulative character of the mercury species the synthesis of sorbents for mercury preconcentrative separation in water samples is of special interest.

In the present paper we report the synthesis of polymer microbeads using methacrylic acid (MAA) as a monomer, trimethylolpropane trimethacrylate (TMPTM) as a cross-linking agent, and 1-(2-thiazolylazo)-2-naphthol (TAN) as a specific ligand for Hg(II). The extraction characteristics of the non-imprinted (blank P(B)), treated with TAN alone (control P(TAN)), and imprinted with Hg(II)-TAN complex (P(TAN-Hg)) polymer microbeads have been

\* Corresponding author. Tel.: +3592 81 61 244.

E-mail address: [i.dakova@chem.uni-sofia.bg](mailto:i.dakova@chem.uni-sofia.bg) (I. Dakova).



compared. The sorption and desorption characteristics have been investigated using batch procedures. The Hg(II) selectivity versus other interfering metal ions (Cd(II), Co(II), Cu(II), Ni(II), Pb(II), Zn(II)) and methylmercury (CH<sub>3</sub>Hg(I)) has been studied. A method for the application of Hg ion-imprinted (P(TAN-Hg)) polymer microbeads for the determination of Hg(II) and CH<sub>3</sub>Hg(I) in water samples has been developed. The analytical procedure is carried out in two steps: (1) selective determination of Hg(II) in nondigested water sample; (2) determination of total Hg e.g. sum of Hg(II) and CH<sub>3</sub>Hg(I) in digested water sample. The content of methylmercury is defined as the difference between these two measurements.

## 2. Experimental

### 2.1. Reagents

All reagents used were of analytical reagent grade. The stock standard solutions for Cd(II), Cu(II), Co(II), Ni(II), Pb(II) and Zn(II) (1000 µg mL<sup>-1</sup>) were Titrisol, Merck (Darmstadt, Germany), in 2% HNO<sub>3</sub>. Stock standard solutions for Hg were: Hg(II), stock standard solution for AAS, Trace CEPT TM, 998 µg mL<sup>-1</sup> in 2 M HNO<sub>3</sub>, Sigma–Aldrich (USA); 200 µg mL<sup>-1</sup> methylmercury chloride (CH<sub>3</sub>HgCl) prepared by dissolving of methylmercury(I) chloride PESTANAL<sup>®</sup>, analytical standard, Sigma–Aldrich in bidistilled water. The working standard solutions were prepared weekly and kept refrigerated at 4 °C.

pH was adjusted with the following buffer solutions: monopotassium citrate/HCl for pH 3, CH<sub>3</sub>COONa/CH<sub>3</sub>COOH for pH 4 and 5; KH<sub>2</sub>PO<sub>4</sub>/NaOH for pH 6, 7 and 8; H<sub>3</sub>BO<sub>3</sub>/KCl/NaOH for pH 9. MAA, TMPTM, 2,2'-azobisisobutyronitrile (AIBN), (Merck, Darmstadt, Germany), TAN (Fluka A.G., Buchs, Switzerland) and acetonitrile (ACN) (Labskan, Dublin, Ireland) were used without further purification. Bidistilled water was used in all experiments.

### 2.2. Apparatus

Flame atomic absorption spectrometric (FAAS) measurements were carried out on a Perkin Elmer Zeeman 1100 B spectrometer (Uberlingen, Germany) with an air/acetylene flame. The instrumental parameters were optimized in order to obtain maximum signal-to-noise ratio. Continuous flow (CF) cold vapor atomic absorption spectrometric (CV AAS) measurements were carried out on a Varian AA 240 atomic absorption spectrometer, equipped with a continuous flow VGA-77 vapor generation accessory and externally heated quartz tube atomizer controlled with an ETC-60 electrothermal temperature controller. Sample solutions were introduced via both sample channel and acid channel at flow rates of 7 mL min<sup>-1</sup> and 1 mL min<sup>-1</sup>, while reductant solution was introduced via reductant channel at a flow rate of 1 mL min<sup>-1</sup>. Instrumental parameters for VGA-77 were presented in Table 1.

- A microprocessor pH meter (Hanna Instruments, Portugal) was used for pH measurements.
- A scanning electron microscope (SEM, JEOL JSM-5500, Tokyo, Japan) was used for the determination of the microbead shape and size.

**Table 1**  
Optimal instrumental parameters for VGA-77.

Measurement mode	Integration
Band pass	0.5 nm
Quartz tube temperature	Room temperature for Hg(II); 850 °C for CH <sub>3</sub> Hg(I)
Delay time	45 s
Read time	3 s
Reductant	0.04% NaBH <sub>4</sub> for Hg(II); 1% NaBH <sub>4</sub> for CH <sub>3</sub> Hg(I)
Sample + acid flow rate	7.8 mL min <sup>-1</sup>

- Conventional IR-spectra were measured on a Bomem Michelson 100 FTIR spectrometer within 4000–400 cm<sup>-1</sup>, 2 cm<sup>-1</sup> at resolution, 200 scans.

### 2.3. Preparation of sorbents

The imprinted polymer materials were synthesized as described earlier [33,34]. As a template species (0.024 mmol) the complexes of (Hg(II)) with TAN or TAN only were used (Fig. 1). Polymer microbeads were prepared via dispersion polymerization using ACN (5 mL) as solvent, AIBN (3.45 mg) as initiator, MAA (0.116 mmol) as monomer and TMPTM (0.186 mmol) as cross-linking agent at T=60 °C for 24 h. Non-imprinted (blank) polymer (P(B)) was synthesized in the same way as described above, in the absence of template.

Hg(II) was eluted from the prepared polymer networks by stirring with 10 mL 4 mol L<sup>-1</sup> HNO<sub>3</sub> for 2 h. Then polymer microbeads were dried in a vacuum oven at 60 °C. The yields were 88.6% for P(TAN-Hg), 86.5% for P(TAN) and 85.7% for P(B).

### 2.4. Static adsorption test

A portion of the solution containing 0.1 µg Hg(II) was diluted to a 10 mL total volume and pH was adjusted with buffer solution to the desired value. Polymer microbeads of ca. 25 mg were added to this solution and stirred for 15 min with a magnetic stirrer. The sample was centrifuged (3000 rpm), the supernatant was removed and the polymer gel was washed twice with bidistilled water. The Hg(II) was eluted from the sorbents with 2 mL 4 mol L<sup>-1</sup> HNO<sub>3</sub>. The eluate was transferred in 10 mL volumetric flask and diluted up to the mark with bidistilled water. Hg(II) content in the eluate was determined by CV AAS. CV AAS was also used for the determination of Hg(II) in the collected supernatant and washing liquids.

### 2.5. Selectivity experiments

A 20 mL solutions containing 0.1 µg Hg(II), 0.1 µg CH<sub>3</sub>Hg(I) and 20 µg Cd(II), Cu(II), Co(II), Ni(II), Pb(II), Zn(II) were stirred with ca. 25 mg P(TAN-Hg), P(TAN) or P(B) at pH 7 for 15 min with a magnetic stirrer. The solutions were centrifuged (3000 rpm), sorbent microbeads washed twice with bidistilled water and elution performed with 2 mL 4 mol L<sup>-1</sup> HNO<sub>3</sub>. The concentration of Hg(II) and CH<sub>3</sub>Hg(I) in the supernatant and eluate solutions was determined by CV/HG AAS respectively. The concentration of metal ions in the supernatant and eluate solutions was measured by a FAAS.

### 2.6. Extraction efficiency and selectivity characteristics

The extraction efficiency (E) of Hg(II) ions is

$$E\% = \left[ \frac{A_i - A_{\text{eff}}}{A_i} \right] 100, \quad (1)$$

where A<sub>eff</sub> (µg) is the cation amount in the effluente solution after extraction by P(X) (X = TAN-Hg, TAN, B) from a solution with a total cation amount A<sub>i</sub> (µg).

The distribution ratio (D) is defined as

$$D = \frac{A_i - A_{\text{eff}}}{A_{\text{eff}}} \quad (2)$$

The selectivity coefficient (S<sub>Hg/Me</sub>) is

$$S_{\text{Hg/Me}} = \frac{D_{\text{Hg}}}{D_{\text{Me}}} \quad (3)$$

where D<sub>Hg</sub> and D<sub>Me</sub> are the distribution ratios for Hg(II) and Cd(II), Co(II), Cu(II), Ni(II), Pb(II), Zn(II) and CH<sub>3</sub>Hg(I), respectively.

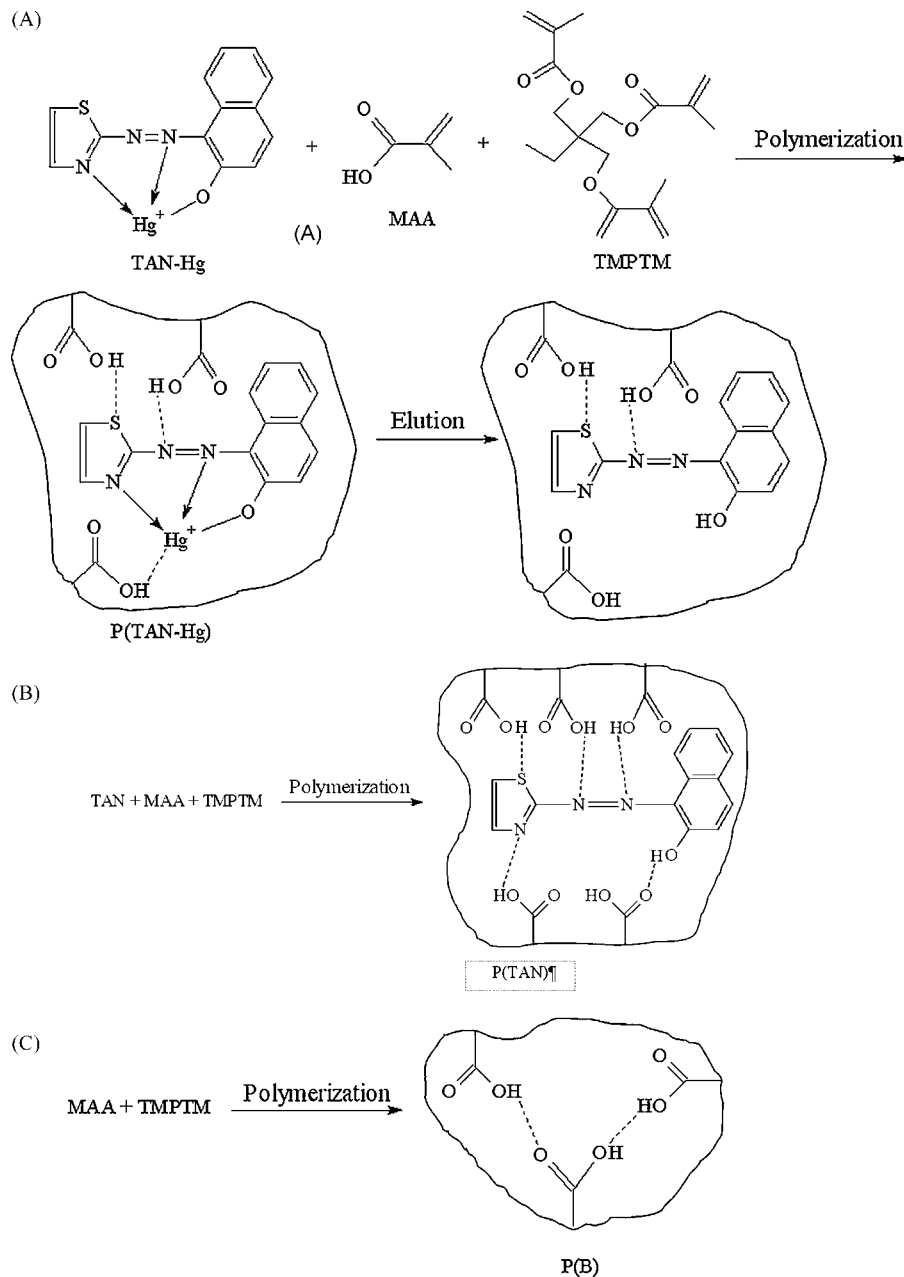


**Fig. 1.** Schemes of the Hg(II)-IIP preparation. (A) IIP prepared with TAN-Hg(II) complex as a template ( $P(\text{TAN-Hg})$ ). (B) polymer gel prepared with TAN as a template ( $P(\text{TAN})$ ). (C) Non-imprinted polymer  $P(\text{B})$ .

The ratio  $\rho(E)_{P(\text{TAN-Hg})/P(X)}$  is defined as

$$\rho(E)_{P(\text{TAN-Hg})/P(X)} = \frac{E_{P(\text{TAN-Hg})}}{E_{P(X)}} \quad (4)$$

where  $E_{P(\text{TAN-Hg})}$  and  $E_{P(X)}$  are the extraction efficiencies of Hg(II) for the SPE with  $P(\text{TAN-Hg})$  and  $P(X)$  ( $X = \text{TAN}, \text{B}$ ), respectively

The ratio  $\rho(D)_{P(\text{TAN-Hg})/P(X)}$  is defined as

$$\rho(D)_{P(\text{TAN-Hg})/P(X)} = \frac{D_{P(\text{TAN-Hg})}}{D_{P(X)}}, \quad (5)$$

where  $D_{P(\text{TAN-Hg})}$  and  $D_{P(X)}$  are the distribution ratios of Hg(II) for the SPE with  $P(\text{TAN-Hg})$  and  $P(X)$  ( $X = \text{TAN}, \text{B}$ ), respectively.

The binding capacity of the Hg(II) ion-imprinted microbeads is defined as the amount of the adsorbed Hg(II) ions per gram of the sorbent.

### 2.7. Analytical procedure for Hg(II) and $\text{CH}_3\text{Hg(I)}$ determination in mineral and sea waters

Water (mineral, sea) sample ca. 100 mL was stirred with 100 mg  $P(\text{TAN-Hg})$  for 15 min. After centrifugation (3000 rpm) the supernatant was removed and polymer was washed twice with bidistilled water, finally Hg(II) was eluted with 2 mL  $4 \text{ mol L}^{-1}$   $\text{HNO}_3$ . The eluate was transferred in 10 mL volumetric flask and diluted up to the mark with bidistilled water. Hg(II) was measured by CV AAS under optimal instrumental parameters. In parallel same water (mineral, sea) sample ca. 100 mL was MW digested according to EPA (in order to transform  $\text{CH}_3\text{Hg(I)}$  into Hg(II)) and than prepared according to the already described analytical protocol. In this case the sum Hg(II)+ $\text{CH}_3\text{Hg(I)}$  was determined by CV AAS. Finally,  $\text{CH}_3\text{Hg(I)}$  content in the analyzed water sample was defined as a difference between two measured values.

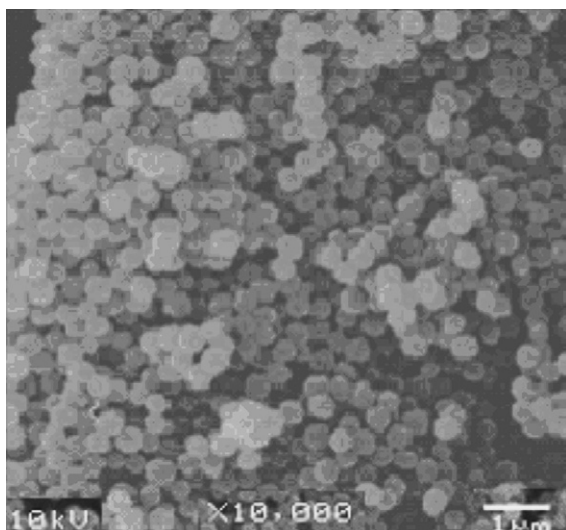


Fig. 2. Scanning electron micrograph of Hg ion-imprinted microbeads at a  $\times 10000$  magnification.

### 3. Results and discussion

#### 3.1. Characterization studies

Scanning electron micrograph of the Hg ion-imprinted polymer microbeads is shown in Fig. 2. Analogous micrographs are obtained for  $P(\text{TAN})$  and  $P(\text{B})$ . In all cases the obtained microparticles are in the shape of microspheres. Their mean diameters, determined from the micrographs, are 210 nm for the  $P(\text{B})$  and 320 nm for the  $P(\text{TAN})$  and  $P(\text{TAN-Hg})$ , respectively.

The surface area (BET method) is:  $34 \text{ m}^2 \text{ g}^{-1}$  for  $P(\text{TAN-Hg})$ ,  $9 \text{ m}^2 \text{ g}^{-1}$  for  $P(\text{TAN})$  and  $80 \text{ m}^2 \text{ g}^{-1}$  for  $P(\text{B})$ . The results obtained demonstrate the adsorption of TAN and TAN-Hg in the polymer microbeads pores, the most considerable for TAN. Fig. 3 shows the FTIR spectra of ligand TAN and polymers:  $P(\text{TAN-Hg})$ ,  $P(\text{TAN})$  and  $P(\text{B})$ , respectively. The strong and broad absorption band observed at  $3670\text{--}3200 \text{ cm}^{-1}$  is due to  $-\text{OH}$  stretching of  $-\text{COOH}$  group in polymer matrix ( $P(\text{B})$ ,  $P(\text{TAN})$ ,  $P(\text{TAN-Hg})$ ) and of phenolic  $-\text{OH}$  group in TAN,  $P(\text{TAN})$  and  $P(\text{TAN-Hg})$ . In addition absorption band at  $1720 \text{ cm}^{-1}$  due to  $\text{C}=\text{O}$  stretching of carboxylic acid ( $P(\text{B})$ ,  $P(\text{TAN})$ ,  $P(\text{TAN-Hg})$ ). The low intensive bands about  $1612 \text{ cm}^{-1}$ , eventually

assigned to the stretching vibrations of double bonds ( $\nu_{\text{N}=\text{N}}$ ), is low frequency shifted about  $8 \text{ cm}^{-1}$ , assuming a coordination of TAN through the N-atom from the fragment. On the other side, the observed low frequency shifting at the  $\nu_{\text{C}-\text{O}(\text{H})}$  stretching vibration of the phenol fragment, about  $13 \text{ cm}^{-1}$  is a direct assignment for the coordination of the O-atom also, thus forming a stable six-membered ring with the metal ion. In addition the observed splitting of the out-of-plane vibration of the naphtholic fragment ( $755 \text{ cm}^{-1}$  in the ligand) is usually observed, when the heteroatom direct joined with the system participate in the coordination processes [35,36]. The observed shifting of the  $\nu_{\text{C}=\text{N}}$  IR band about  $4 \text{ cm}^{-1}$  and increasing of its intensity could be related to a hydrogen bond of the  $\text{N} \cdots \text{H}$  type (Fig. 1).

#### 3.2. Influence of pH on the sorption of Hg(II) with imprinted and non-imprinted polymer microbeads

Three synthesized microbeads: blank  $P(\text{B})$ , control  $P(\text{TAN})$  and Hg ion-imprinted were tested for Hg(II) sorption from aqueous solution at various pH (3–9) in batch experiments using the procedure described in 2.4. The results obtained for the influence of pH on the Hg(II) extraction efficiency ( $E$ ) are presented in Fig. 4. It can be seen that  $E$  values registered, when  $P(\text{TAN-Hg})$  was used as a sorbent, are well above those for  $P(\text{TAN})$  and  $P(\text{B})$ . This result is confirmed by the values of the ratios between the extraction efficiencies and the distribution coefficients at pH 7:  $\rho(E)_{P(\text{TAN-Hg})/P(\text{TAN})} = 2.51$ ,  $\rho(E)_{P(\text{TAN-Hg})/P(\text{B})} = 1.31$  and  $\rho(D)_{P(\text{TAN-Hg})/P(\text{TAN})} = 70$ ,  $\rho(D)_{P(\text{TAN-Hg})/P(\text{B})} = 16.3$ . These large differences in the values obtained confirm the advantages of the Hg ion-imprinted polymer microbeads over the control, treated only with TAN ( $P(\text{TAN})$ ) and the blank  $P(\text{B})$  microbeads for the separation and preconcentration of Hg(II) ions.

The values of  $E$  show that the polymer with incorporated TAN molecules is not so effective as those imprinted with the TAN-Hg complex (Fig. 4) though the TAN adsorption is higher than TAN-Hg complex as it follows from the mentioned BET results. Most probably, the value of  $\rho(E,D)_{P(\text{TAN-Hg})/P(\text{TAN})}$  higher than 1 is due to the quite different configurations of the TAN molecules immobilized in Hg ion-imprinted  $P(\text{TAN-Hg})$  and control  $P(\text{TAN})$  microbeads. In the first case, the TAN molecule configuration in  $P(\text{TAN-Hg})$  exhibits maximum activity for Hg(II) complex formation because the configuration is completely the same as in the complex. In the control microbeads ( $P(\text{TAN})$ ), the fraction of the active TAN molecules is less than one because some of the gel-immobilized TAN molecules

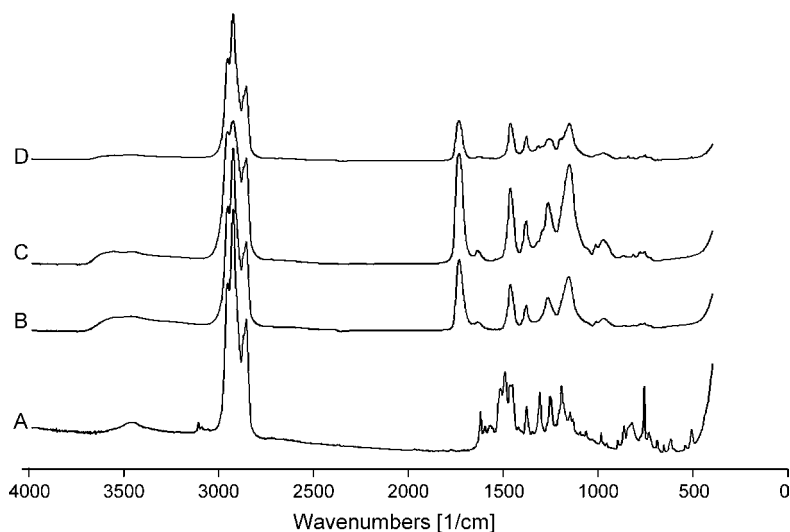
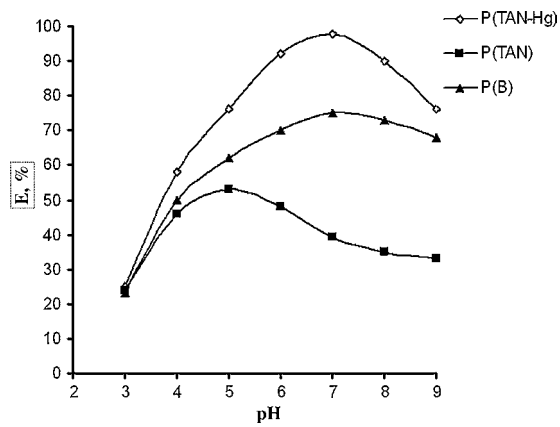


Fig. 3. FTIR spectra: (A) TAN; (B)  $P(\text{B})$ ; (C)  $P(\text{TAN})$ ; (D)  $P(\text{TAN-Hg})$ .



**Fig. 4.** pH-dependence of the extraction efficiencies of Hg(II) ions with P(TAN-Hg), P(TAN) and P(B). (25 mg polymer gel, 0.1  $\mu\text{g}$  Hg(II)).

are blocked for the formation of the TAN-Hg complex (see Fig. 1). The reason for the inequality between P(TAN-Hg) and P(B) (Fig. 4) is, however, quite different. Evidently, if P(B) is used for Hg(II) sorption, the specific interaction between TAN and Hg(II) does not take place, thus explaining low extraction efficiency observed.

The ratios  $\rho(E)_{P(\text{TAN-Hg})/P(\text{B})}$  and  $\rho(D)_{P(\text{TAN-Hg})/P(\text{B})}$  show maximum values in the pH range from 6 to 7, but extraction efficiency reaches it's highest value at pH 7 (Fig. 4). Therefore, pH 7 was selected for our further investigations. Comparison of the extraction efficiencies (Fig. 4) of the tested polymer microbeads shows that at higher pH values (7–9) the  $E$  values decrease for P(TAN-Hg) and P(B), while for P(TAN) – this decrease is at pH 5–9. This could be related to the precipitation of the metal hydroxide and its quick decomposition to oxide.

### 3.3. Adsorption isotherm of Hg(II) on P(TAN-Hg)

The sorption capacity of P(TAN-Hg) for Hg(II) was determined by batch method. The Hg ion-imprinted microbeads (25 mg) were saturated with metal ion (0.02–0.14  $\mu\text{mol L}^{-1}$ ) under optimum conditions and the total metal sorbed was measured with FAAS after eluting from the resin by  $\text{HNO}_3$ . As can be seen in Fig. 5, the amount of Hg(II) adsorbed per unit mass of P(TAN-Hg) was increased with the initial concentration of Hg(II) and reach the plateau values, determining the adsorption capacity values. The average maximum adsorption capacity was 32.0  $\mu\text{mol g}^{-1}$ . By the same procedure, the determined capacities of P(TAN) and P(B) were 9.8  $\mu\text{mol g}^{-1}$  and 13.2  $\mu\text{mol g}^{-1}$ , respectively.

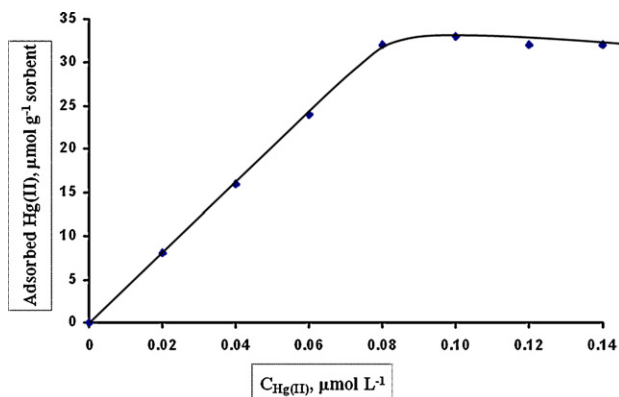


**Fig. 5.** Adsorption isotherm ( $T=20^\circ\text{C}$ ) of Hg(II) ions on P(TAN-Hg) (25 mg P(TAN-Hg), pH 7, 2 mL 4 mol  $\text{L}^{-1}$   $\text{HNO}_3$ ).

**Table 2**

Recovery (%) for Hg(II) from P(TAN-Hg) using different eluents (25 mg P(TAN-Hg); 1  $\mu\text{g mL}^{-1}$  Hg(II); 2 mL eluent solution).

Eluent	Recovery (%)
2 mol $\text{L}^{-1}$ HCl	68 $\pm$ 5
4 mol $\text{L}^{-1}$ HCl	80 $\pm$ 4
2 mol $\text{L}^{-1}$ HCl + 5% thiourea	>99
2 mol $\text{L}^{-1}$ $\text{HNO}_3$	72 $\pm$ 4
4 mol $\text{L}^{-1}$ $\text{HNO}_3$	>99

### 3.4. Selection of the eluent and its concentration

The choice of the suitable eluent is important for the analytical performance of the solid phase extraction procedure. In order to elute mercury adsorbed on the P(TAN-Hg), different eluents at different concentration levels were tested (Table 2). Among the acids employed as eluents, HCl has been reported to have an enhanced performance due to its complexing abilities with mercury. However in the present study the quantitative elution of Hg(II) could not be achieved even with 4 mol  $\text{L}^{-1}$  HCl. Frequently, thiourea as a complexing agent was added to HCl for fast elution of Hg. Experiments performed showed quantitative elution but with relatively high blank levels which makes this eluent not feasible for the determination of extremely low levels of Hg in water samples. Fast and quantitative elution was achieved also with 4 mol  $\text{L}^{-1}$   $\text{HNO}_3$ . In order to ensure enough volume for CF CVAAS measurements, after dilution, this eluent proved very suitable as reaction media for Hg determination.

The effect of the eluent volume (1–5 mL 4 mol  $\text{L}^{-1}$   $\text{HNO}_3$ ) on the Hg(II) desorption was evaluated as well. The full extraction of the Hg(II) ions was reached when the adsorbed Hg(II) was eluted with 2 mL 4 mol  $\text{L}^{-1}$   $\text{HNO}_3$  (for 20 min).

### 3.5. Hg(II) sorption and desorption kinetics

The kinetics of the Hg(II) sorption and desorption were investigated in a batch system with 25 mg of the P(TAN-Hg) particles for 5–40 min. Time dependence of the sorption of Hg(II) onto the P(TAN-Hg) particles was determined at pH 7 and results are plotted in Fig. 6. As seen, high sorption rates are observed at the beginning, and then a plateau values are gradually attained within 15 min. The loading half time ( $t_{1/2}$ ), defined as the time required for reaching 50% of the sorbent total loading capacity, was determined from the curve. The value obtained for loading half time is 3 min. The fast sorption time is most probably a result of the high complexation rate (i.e. high affinity) between tested ion and TAN of the polymer microbeads and the geometric shape affinity between Hg(II) ions and Hg(II) cavities in the P(TAN-Hg) structure.

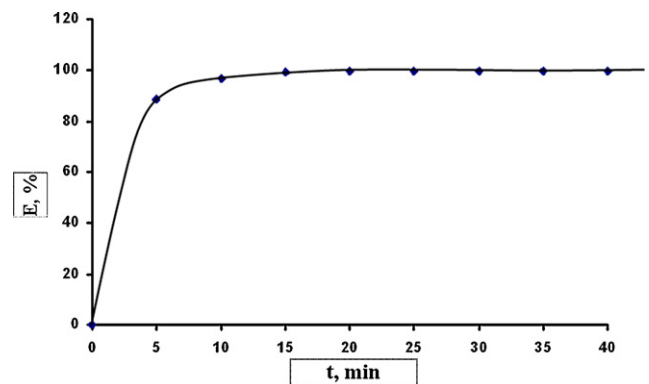


**Fig. 6.** Kinetic of Hg(II) sorption on P(TAN-Hg) (25 mg of P(TAN-Hg), pH 7, 1  $\mu\text{g mL}^{-1}$  Hg(II), 2 mL 4 mol  $\text{L}^{-1}$   $\text{HNO}_3$ ).

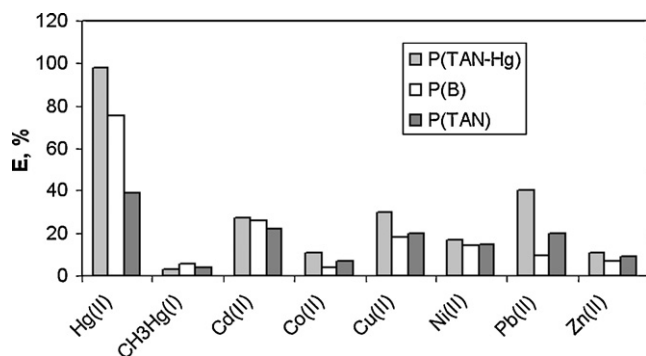


**Fig. 7.** Extraction efficiencies of template and competitive ions upon SPE with *P*(TAN-Hg), *P*(TAN) and *P*(B) (25 mg sorbent; pH 7; 2 mL 4 mol L<sup>-1</sup> HNO<sub>3</sub> as eluent).

It is well known that removal of the template from the polymeric matrix leaves cavities of complementary size, shape and chemical functionality to the templates [18]. The monodisperse microsphere form of the *P*(TAN-Hg) contributes also to the fast sorption kinetic established. The adsorbed Hg(II) ions were desorbed by treatment with 4 mol L<sup>-1</sup> HNO<sub>3</sub> under continuous stirring. The Hg(II) ions could be quantitatively eluted for 20 min. Using the same procedure, the similar results for time dependence of sorption and desorption of Hg(II) onto the *P*(B) and *P*(TAN) were obtained.

### 3.6. Competitive adsorption

In order to prove the selectivity of *P*(TAN-Hg), a competitive adsorption of Cd(II), Co(II), Cu(II), Ni(II), Pb(II), Zn(II) and CH<sub>3</sub>Hg(I) from their model mixture was investigated as well. The extraction efficiency of cations, achieved by using *P*(TAN-Hg), *P*(TAN) and *P*(B), are given in Fig. 7. Although these ions have the same charge, similar chemical properties and ionic radii, significant differences in their extraction characteristic *E* (Fig. 7) were observed. Similar differences are also observed for the distribution ratio (*D*). The extraction efficiencies of Hg(II) with *P*(TAN-Hg) are much higher than those of Cd(II), Co(II), Cu(II), Ni(II), Pb(II), Zn(II) and CH<sub>3</sub>Hg(I). The greatest difference is established between extraction efficiencies of Hg(II) and CH<sub>3</sub>Hg(I) (97.5% and <3%, respectively). The large size of CH<sub>3</sub>Hg(I) probably hinders the ion diffusion and the ions can not reach the functional groups. The result is very low extraction efficiency of *P*(TAN-Hg) toward CH<sub>3</sub>Hg(I). The selectivity coefficients (calculated by Eq. (3)) are the highest for CH<sub>3</sub>Hg(I) – 1633 (Table 3). These results unambiguously confirm the very good selectivity of *P*(TAN-Hg) toward the target (imprinted Hg(II)) ions. The lowest extraction efficiency and relatively low selectivity coefficients were found for *P*(TAN) most probably due to very low fraction of the TAN molecules in the active for a Hg(II) coordination state during the imprinting. The higher values observed for *P*(B) could be explained with more available for complex for-

**Table 3**

Distribution (*D*) and selectivity coefficients (*S*<sub>Hg/Me</sub>) of *P*(TAN-Hg), *P*(TAN) and *P*(B) for Hg(II).

Me ion	<i>P</i> (TAN-g)		<i>P</i> (B)		<i>P</i> (TAN)	
	<i>D</i>	<i>S</i> <sub>Hg/Me</sub>	<i>D</i>	<i>S</i> <sub>Hg/Me</sub>	<i>D</i>	<i>S</i> <sub>Hg/Me</sub>
Hg(II)	49	–	2.33	–	0.64	–
CH <sub>3</sub> Hg(I)	0.03	1633	0.15	15.5	0.04	16
Cu(II)	0.43	113.9	0.22	10.6	0.28	2.3
Ni(II)	0.21	233.3	0.16	14.6	0.07	9.1
Co(II)	0.13	376.9	0.04	58.3	0.33	1.9
Pb(II)	0.67	73.1	0.11	21.2	0.18	3.6
Cd(II)	0.37	132.4	0.35	6.7	0.25	2.6
Zn(II)	0.11	445.5	0.07	33.3	0.10	6.4

mation free carboxylic groups and higher active surface of this sorbent.

### 3.7. Analytical figures of merit

The accuracy and precision of the proposed analytical procedure has been checked by added found method. Sea water samples and mineral water samples ca. 200 mL were spiked with Hg(II) and CH<sub>3</sub>Hg(I) at different ratios and analyzed as described. Results obtained are presented in Table 4.

The detection limit achieved for Hg(II) determination (calculated as three times standard deviation of the blank, 100 mL water sample) is 0.006 μg L<sup>-1</sup> and the determination limit is 0.02 μg L<sup>-1</sup>. The relative standard deviation varied in the range 5–9% for Hg(II) and CH<sub>3</sub>Hg(I) levels at 0.02–1 μg L<sup>-1</sup>. Several sea water samples from the Black sea were analyzed according to the proposed procedure: Hg(II) content determined in some samples was in the range 0.03–0.05 μg L<sup>-1</sup>, CH<sub>3</sub>Hg(I) was below the limit of detection for all of them. Neither Hg(II) nor CH<sub>3</sub>Hg(I) were found in mineral waters above the presented determination limits.

## 4. Conclusions

In the present paper, we report the preparation of Hg ion-imprinted microbeads by cross-linking dispersion copolymerization of methacrylic acid and trimethylolpropane trimethacrylate in acetonitrile. Its possible application as adsorbent for the selective separation and preconcentration of Hg(II) and the subsequent determination by CV AAS in water samples has been studied. The method proposed exhibits a series of advantages: the procedure for the trace Hg(II) preconcentration and determination is simple, reproducible and less susceptible to contamination; the analytical procedure is performed in one vessel – extremely convenient in routine analytical practice. The limit of detection is lower than those given in refs. [29–32]. The sorption time and enrichment factors of the present Hg(II)-IIP are comparable with other Hg-imprinted polymers [29–32]; the sorption capacity of this new sorbent is better than the one, reported by Andac et al. [31], but it is lower

**Table 4**  
Added/found method for Hg(II) and CH<sub>3</sub>Hg(I) determination in sea and mineral water (25 mg *P*(TAN-Hg), pH 7, water samples 200 mL, elution with 2 mL 4M HNO<sub>3</sub>, three parallel determinations).

Sample	Added	Found Hg(II) (μg L <sup>-1</sup> )	Found CH <sub>3</sub> Hg(I) (μg L <sup>-1</sup> )
Sea water	0.1 μg L <sup>-1</sup> Hg(II) and 0.1 μg L <sup>-1</sup> CH <sub>3</sub> Hg(I)	0.11 ± 0.01	0.09 ± 0.01
Sea water	0.1 μg L <sup>-1</sup> Hg(II) and 0.05 μg L <sup>-1</sup> CH <sub>3</sub> Hg(I)	0.09 ± 0.01	0.06 ± 0.01
Sea water	0.1 μg L <sup>-1</sup> Hg(II) and 0.02 μg L <sup>-1</sup> CH <sub>3</sub> Hg(I)	0.12 ± 0.01	0.03 ± 0.01
Mineral water (Bankia)	0.1 μg L <sup>-1</sup> Hg(II) and 0.05 μg L <sup>-1</sup> CH <sub>3</sub> Hg(I)	0.09 ± 0.01	0.04 ± 0.01

than those reported by Liu et al. [29], Fan [30] and Wu et al. [32]. The most important characteristic of the Hg(II)-imprinted copolymer is its excellent selectivity towards Hg(II) over Cd(II), Co(II), Cu(II), Ni(II), Pb(II), Zn(II) and CH<sub>3</sub>Hg(I). The application of Hg ion-imprinted polymer microbeads for the determination of inorganic and methylmercury in mineral and sea water is demonstrated.

### Acknowledgements

The authors gratefully acknowledge the financial support provided by the University of Sofia Scientific Foundation (Grant 032/2007) and the Joint Research Project IB7320-110933/1 within the framework of the SCOPES Program of Swiss National Science Foundation.

### References

- [1] D. Cossa, J. Sanjuan, J. Cloud, P.B. Stockwell, W.T. Toms, *J. Anal. Spectrom.* 10 (1995) 287.
- [2] M. Horvat, L. Liang, N.S. Bloom, *Anal. Chim. Acta* 282 (1993) 153.
- [3] G. Xin, Z. Chuguang, J. Zexiang, T. Zhiyong, *Microchim. Acta* 148 (2004) 221.
- [4] N. Biçak, S. Sungur, M. Gazi, N. Tan, *Sep. Sci. Technol.* 38 (2003) 201.
- [5] I. Karadjova, S. Arpadjan, J. Cvetković, T. Stafilov, *Microchim. Acta* 147 (2004) 39.
- [6] D. Leyva, J. Esteívez, A. Montero, I. Pupo, *X-Ray Spectrom.* 36 (2007) 355.
- [7] M. Vircavs, A. Peine, V. Rone, D. Vircava, *Analyst* 117 (1992) 1013.
- [8] M.V. Balarama Krishna, D. Karunasagar, S.V. Rao, J. Arunachalam, *Talanta* 68 (2005) 329.
- [9] E.M. Soliman, M.B. Saleh, S.A. Ahmed, *Talanta* 69 (2006) 55.
- [10] Y. Zhai, X. Chang, Y. Cui, N. Lian, S. Lai, H. Zhen, Q. He, *Microchim. Acta* 154 (2006) 253.
- [11] J.C.A. de Wuilloud, R.G. Wuilloud, R.A. Olsina, L.D. Martinez, *J. Anal. At. Spectrom.* 17 (2002) 389.
- [12] T. Duan, X. Song, J. Xu, P. Guo, H. Chen, H. Li, *Spectrochim. Acta Part B* 61 (2006) 1069.
- [13] B.C. Mondal, A.K. Das, *Anal. Chim. Acta* 477 (2003) 73.
- [14] J. Chwastowska, A. Rogowska, E. Sterlinska, J. Dudek, *Talanta* 49 (1999) 837.
- [15] S.R. Segade, J.F. Tyson, *Talanta* 71 (2007) 1696.
- [16] A. Krata, K. Pyrzynska, E. Bulska, *Anal. Bioanal. Chem.* 377 (2003) 735.
- [17] T. Prasada Rao, R. Kala, S. Daniel, *Anal. Chim. Acta* 578 (2006) 105.
- [18] G. Wulff, *Angew. Chem., Int. Ed. Engl.* 34 (1995) 1812.
- [19] P. Metilda, K. Prasad, R. Kala, J.M. Gladis, T. Prasada Rao, G.R.K. Naidu, *Anal. Chim. Acta* 582 (2007) 147.
- [20] S. Daniel, P.E.J. Babu, T. Prasada Rao, *Talanta* 65 (2005) 441.
- [21] E. Birlik, A. Ersöz, A. Denizli, R. Say, *Anal. Chim. Acta* 565 (2006) 145.
- [22] A. Ersöz, R. Say, A. Denizli, *Anal. Chim. Acta* 502 (2004) 91.
- [23] Y. Liu, X. Chang, S. Wang, Y. Guo, B. Din, S. Meng, *Anal. Chim. Acta* 519 (2004) 173.
- [24] X. Chang, N. Jiang, H. Zheng, Q. He, Z. Hu, Y. Zhai, Y. Cui, *Talanta* 71 (2007) 38.
- [25] D. Zhang, W.Y. Wang, Y.Q. Fan, J. Li, H.P. Han, *Microchim. Acta* 157 (2007) 7.
- [26] J. Pan, S. Wang, R. Zhang, *Int. J. Environ. Anal. Chem.* 86 (2006) 855.
- [27] J. Zhao, B. Han, Y. Zhang, D. Wang, *Anal. Chim. Acta* 603 (2007) 87.
- [28] M. Khajeh, Y. Yamini, E. Ghasemi, J. Fasihi, M. Shamsipur, *Anal. Chim. Acta* 581 (2007) 208.
- [29] Y. Liu, X. Chang, D. Yang, Y. Guo, S. Mehg, *Anal. Chim. Acta* 538 (2005) 85.
- [30] Z. Fan, *Talanta* 70 (2006) 1164.
- [31] M. Andac, S. Miel, S. Senel, R. Say, A. Ersoz, A. Denizli, *Int. J. Biol. Macromol.* 40 (2007) 159.
- [32] G. Wu, Z. Wang, J. Wang, C. He, *Anal. Chim. Acta* 582 (2007) 304.
- [33] L. Ye, P.A.G. Cormack, K. Mosbach, *Anal. Chim. Acta* 435 (2001) 187.
- [34] I. Dakova, I. Karadjova, I. Ivanov, V. Georgieva, B. Evtimova, G. Georgiev, *Anal. Chim. Acta* 584 (2007) 196.
- [35] B.B. Ivanova, H. Mayer-Figge, *J. Coord. Chem.* 58 (2005) 653.
- [36] B.B. Koleva, E.N. Trendafilova, M.G. Arnaudov, W.S. Sheldrick, H. Mayer-Figge, *Trans Met. Chem.* 31 (2006) 866.



## Short communication

## HPLC analysis of organic acids using a novel stationary phase

A. Rodríguez-Bernaldo de Quirós\*, M.A. Lage-Yusty, J. López-Hernández

Analytical Chemistry, Nutrition and Bromatology Department, Pharmacy Faculty, Campus Sur s/n, University of Santiago de Compostela, 15782 Santiago de Compostela (La Coruña), Spain

## ARTICLE INFO

## Article history:

Received 1 September 2008

Received in revised form 3 November 2008

Accepted 14 November 2008

Available online 21 November 2008

## Keywords:

Organic acids

Stationary phase

Liquid chromatography

Mass spectrometry

## ABSTRACT

In the present work, a high performance liquid chromatographic method with UV detection for the separation of six organic acids including, tartaric, malic, acetic, lactic, citric and succinic is described.

The separation was performed on a novel stationary phase TEKNOKROMA, Tr-010065 Mediterranea sea<sub>18</sub> (15 cm × 0.4 cm, i.d. 3 μm) and using water with a 0.1% (v/v) of formic acid as mobile phase. The advantages of this packing over a conventional octadecylsilane (ODS2) column are reported.

The method was validated with respect to linearity, limits of detection and repeatabilities within day and between days and satisfactory results were obtained.

The proposed method was applied for the determination of these compounds in commercially available white wines. The samples were injected directly without previous treatment. LC–MS was used as a confirmatory technique.

© 2008 Elsevier B.V. All rights reserved.

## 1. Introduction

The analysis of organic acids in different food items such as fruit juices, vegetables, dairy products, coffee and wine is of great interest for food industry since these compounds are responsible of sensory properties and may also influence their stability [1–5].

Regarding the analytical techniques, simple rapid and reliable methods are required for control purposes.

Gas chromatography with flame ionization detector has been used to determine carboxylic acids in citric fruits [6] however this procedure presents a disadvantage, a derivatization step is necessary for non-volatile acids. Liquid chromatography with different separation mechanism including ion-exchange [4,7–9], ion-exclusion [7,10–12] and reversed phase [3,7,13,14] has been widely employed in different matrix. Nowadays capillary zone electrophoresis (CZE) with photodiode array detection appears as a promising analytical tool to determine these compounds in short time [15]. In complex samples mass spectrometry coupled to capillary electrophoresis or liquid chromatography constitutes a powerful technique due to its high sensitivity and selectivity [16–19].

In chromatography, the selection of the stationary phase is essential in order to achieve a suitable separation. In the present work a new reversed packing based on perfectly spherical par-

ticles of ultra pure silica and suitable for a wide pH range and aqueous mobile phases was used to analyse six organic acids including, tartaric, malic, lactic, acetic, citric and succinic. A comparison with a conventional octadecylsilane (ODS2) column in what concerns to system suitability parameters such as number of theoretical plates, and peaks width, and sensitivity is reported. The proposed method was validated in terms of linearity, limits of detection and repeatabilities within day and between days. In the second part of the work the method was applied to analyse white wine samples. LC–MS was used as a confirmatory technique.

## 2. Experimental

## 2.1. Chemicals and standard solutions

All chemicals were of analytical grade. Formic acid (98–100%) was from Riedel-de Haën (Seelze, Germany) and meta-phosphoric acid was purchased from Sigma (St. Louis, MO, USA). Ultrapure water was obtained from a Milli-Q water purification system (Millipore, Bedford, MA, USA).

Organic acid standards were obtained as follows: citric acid (≥99.5%) and DL-lactic acid (~90%) were from Fluka BioChemika (Steinheim, Germany), malic acid (95–100%), succinic acid (99%) and DL-tartaric acid (99%) were from Sigma–Aldrich (St. Louis, MO, USA) and acetic acid (99–100%) was from Riedel-de Haën (Seelze, Germany).

Stock standard solutions were dissolved in mobile phase, Milli-Q water (0.1% formic acid), and stored at 4 °C in the dark.

\* Corresponding author. Tel.: +34 981 598450; fax: +34 981 594912.  
E-mail address: [ana.rodriquez.bernaldo@usc.es](mailto:ana.rodriquez.bernaldo@usc.es) (A.R.-B. de Quirós).

**Table 1**  
System suitability parameters and limits of detection of both stationary phases.

Compound	Teknokroma ODS2 5 $\mu\text{m}$ column			Mediterranea sea <sub>18</sub> 3 $\mu\text{m}$ column		
	Width <sup>a</sup>	Plates <sup>b</sup>	LoD <sup>c</sup>	Width <sup>a</sup>	Plates <sup>b</sup>	LoD <sup>c</sup>
Tartaric	0.20 $\pm$ 0.04	2281.7	0.50	0.21 $\pm$ 0.009	1679.11	0.10
Malic	0.24 $\pm$ 0.13	2738.7	0.70	0.15 $\pm$ 0.005	5224.7	0.10
Lactic	0.38 $\pm$ 0.09	1324	1.00	0.16 $\pm$ 0.005	6500.2	0.10
Acetic	0.21 $\pm$ 0.01	4738.8	1.00	0.16 $\pm$ 0.007	7180.1	0.10
Citric	0.37 $\pm$ 0.02	2335.1	0.70	0.23 $\pm$ 0.007	10729.9	0.50
Succinic	0.41 $\pm$ 0.01	2644.6	1.00	0.25 $\pm$ 0.004	10300.3	0.30

<sup>a</sup> Peak-width (mean of 10 injections).

<sup>b</sup> Plates (mean of 10 injections).

<sup>c</sup> mg/L.

## 2.2. Sampling

Commercial available white wines from Galicia (NW Spain) and from the same vintage (2006) were analysed. The samples were filtered through a 50  $\mu\text{m}$  PTFE membrane filter (Advantec MFS, INC, CA, USA) and directly injected into the chromatograph without previous treatment. The analyses were performed in triplicate.

## 2.3. Equipment and analytical conditions

### 2.3.1. HPLC–UV

The HPLC system (Hewlett-Packard, CA, USA) consisted of an HP1100 quaternary pump, an HP1100 degassing device, a 20  $\mu\text{L}$  injection loop (Rheodyne, Cotati, CA, USA) an HP1100 UV-detector set at 215 nm. The HPLC was controlled by a personal computer running HP ChemStation software.

Operating conditions were as follows: the chromatographic separation was performed on a TEKNOKROMA, Tr-010065 Mediterranean sea<sub>18</sub> (15 cm  $\times$  0.4 cm, i.d. 3  $\mu\text{m}$ ) and a TEKNOKROMA, Tr-015605 TRACER EXTRASIL Octadecylsilane (ODS2) (25 cm  $\times$  0.4 cm, i.d. 5  $\mu\text{m}$ ). The characteristics of the stationary phases regarding particle size ( $\mu\text{m}$ ); total carbon content (%); surface area ( $\text{m}^2/\text{g}$ ); and average pore diameter ( $\text{\AA}$ ) are: 5  $\mu\text{m}$ ; 12%; 200  $\text{m}^2/\text{g}$ ; and 80  $\text{\AA}$  for octadecylsilane (ODS2) column and 3  $\mu\text{m}$ ; 17%; 450  $\text{m}^2/\text{g}$  and 80  $\text{\AA}$  for Mediterranean sea<sub>18</sub>, respectively.

The mobile phase consisted of ultra-pure Milli-Q water containing 0.1% formic acid. The flow rate was set at 0.5  $\text{mL min}^{-1}$  and the injection volume was 20  $\mu\text{L}$ . The analysis was performed at room temperature.

### 2.3.2. HPLC–MS: confirmation analysis

A high performance liquid chromatograph 1100 Agilent coupled to a Microtof-Bruker spectrometer was used for organic acids identification. MS data were acquired in the negative ion electrospray ionization (ESI) mode. The operating conditions for ESI were: capillary voltage 4500 V and fragmentor voltage 70 V. The column and mobile phase were the same as in the HPLC–UV analysis.

## 2.4. Identification and quantification

Identification of organic acids was made by comparison of their retention times with those of pure standards solutions. Moreover, citric acid, lactic acid, malic acid, succinic acid and tartaric acid were also confirmed by liquid chromatography mass spectrometry. Quantification was performed on the basis of linear calibration plots of peak area against concentration. Calibration lines were constructed based on five concentration levels of standard solutions.

## 3. Results and discussion

Preliminary experiments were carried out in order to optimize the chromatographic conditions. Acidic mobile phases are common used in the analysis of carboxylic acids. Phosphoric acid is the typical eluent when a LC–UV system is employed, however this acid is not suitable for ESI since could damage the surface of the interface [17,19]. More volatile acids are required.

Formic acid was selected because of their appropriate properties. On the one hand is compatible with ESI and on the other hand help to maintain a low pH. Two different proportions were tested (0.1 and 0.5% formic acid), the best separation was obtained with 0.1%, this is in agreement with a previous study conducted by Gamoh et al. [17].

Another essential step in the development of a chromatographic method is the selection of the stationary phase. In this study a conventional Tracer Extrasil Octadecylsilane (ODS2) and a novel Mediterranean sea<sub>18</sub> were tested.

The novel chromatographic support is based on perfectly spherical particles of extremely pure silica; with a very low metal content, additionally this packing is prepared to work with aqueous mobile phases in a wide pH range [20]. These characteristics make of this column an excellent alternative to the conventional octadecylsilane (ODS2) for the analysis of the organic acids.

Both columns were compared concerning the sensitivity and system suitability parameters such as the number of the theoretical plates and the width of the peaks.

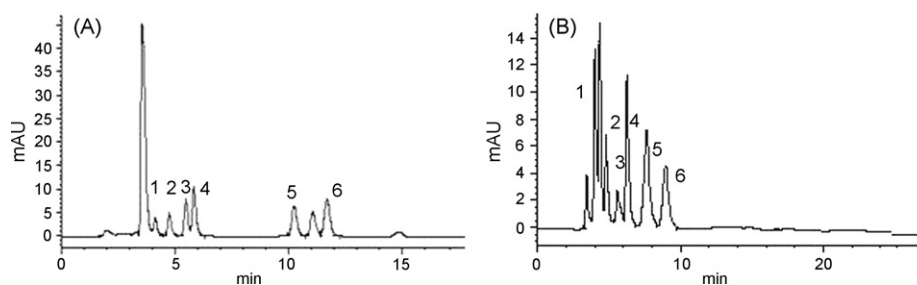


**Fig. 1.** Chromatograms of a standard solution performed on a Mediterranean sea<sub>18</sub> (A) and on an octadecylsilane (ODS2) (B) columns using Milli-Q water containing 0.1% formic acid as mobile phase and at a flow rate of 0.5  $\text{mL min}^{-1}$ . Peaks: (1) tartaric; (2) malic; (3) acetic; (4) lactic; (5) citric; (6) succinic.



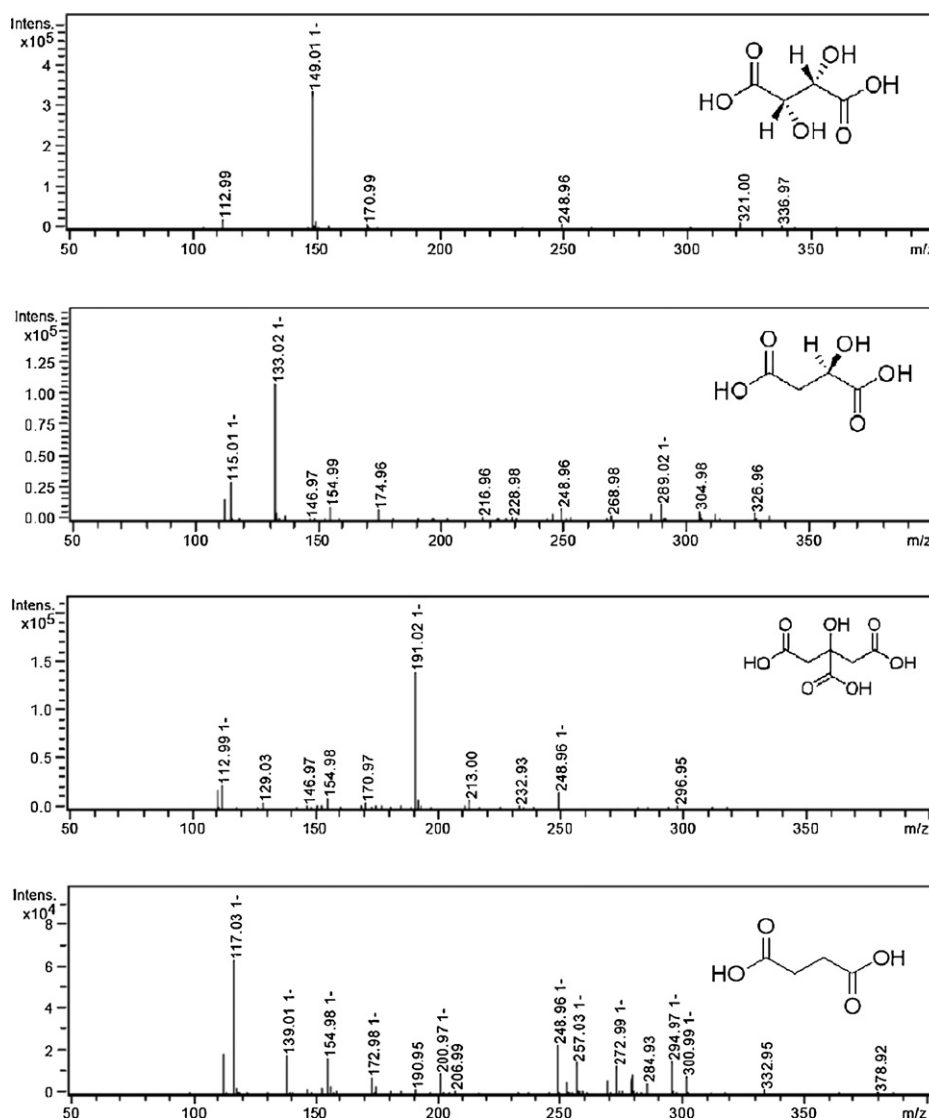


Fig. 2. ESI-MS spectra: tartaric, malic, citric, succinic.

As can be seen from the data of Table 1 the use of the Mediterranean sea<sub>18</sub> column lead to better performance and sensitivity as compared to the conventional octadecylsilane (ODS2) column, therefore this stationary phase was used for further assays.

Chromatograms performed on a Mediterranean sea<sub>18</sub> and on an octadecylsilane (ODS2) columns are presented in Fig. 1.

The proposed analytical method was validated with regard to linearity, limits of detection and repeatabilities within day and between days. The linearity of the method was tested by using a series of organic acids standard solutions of known concentration. The calibration curves were constructed using five concentration levels and they were fitted to a linear equation. Each point of the calibration curve is the average of three peak–area measurements. Table 2 shows the linear equation, the range of linearity and the determination coefficients of the carboxylic acids studied. The method showed good linearity, determination coefficients were in all cases greater than 0.995.

The detection limits (defined as a signal three times the high of the noise level) determined in accordance with the Analytical Chemical Subcommittee guidelines [21] are presented in Table 1. Lower limits of detection were obtained when using Mediterranean sea<sub>18</sub> column.

The intra- and inter-day repeatabilities were determined by analyzing six replicates of the standards at three different concentration levels, expressed as the percentage of R.S.D. (%R.S.D. ( $n=6$ )), in the same day and in different days, respectively. All analytes except acetic and malic acids presented a repeatability within day, expressed as the %R.S.D. ( $n=6$ ) lower than 1%; in what concerns to the repeatabilities between days the values obtained were lower than 3% except for acetic acid (Table 3).

Organic acids were identified by comparing their retention times with the standards and confirmed by LC–MS. Characteristic masses ( $m/z$ ) were 149, 133, 191, 117 and 89 for tartaric, malic, citric, suc-

Table 2  
Equations of calibration curves.

Analyte	Range of linearity <sup>a</sup>	Equation	R <sup>2</sup>
Tartaric	1–200	$y = 3.100X(\pm 0.005) - 0.7211(\pm 0.518)$	0.999992
Malic	5–200	$y = 1.7506X(\pm 0.07) - 7.0561(\pm 6.97)$	0.995
Lactic	1–200	$y = 1.067X(\pm 0.001) + 0.0490(\pm 0.10)$	0.999997
Acetic	5–200	$y = 6.6606X(\pm 0.04) - 1.4363(\pm 3.77)$	0.99990
Citric	5–200	$y = 3.1589X(\pm 0.01) - 3.1478(\pm 1.958)$	0.99994
Succinic	1–200	$y = 1.467X(\pm 0.0008) - 0.0390(\pm 0.08)$	0.9999991

<sup>a</sup> mg/L.

**Table 3**  
Repeatability within day and between days (%R.S.D. ( $n=6$ )) at three concentrations levels.

No.	Compound	Concentration (ppm)	Intra-day %R.S.D. ( $n=6$ )	Inter-day %R.S.D. ( $n=6$ )
1	Tartaric	0.50	0.5	0.7
		10	0.2	0.2
		100	0.4	1.3
2	Malic	0.50	0.8	0.9
		10	1	1
		100	0.5	2
3	Acetic	0.50	1	1
		10	0.9	3
		100	0.4	1.5
4	Lactic	0.50	0.3	0.4
		10	0.4	0.5
		100	0.4	1.2
5	Citric	0.50	0.4	0.5
		10	0.4	0.7
		100	0.2	1.6
6	Succinic	0.50	0.4	0.5
		10	0.6	1.3
		100	0.2	0.2

**Table 4**  
Content of organic acids in samples analysed.

Organic acid	Sample 1	Sample 2	Sample 3
Tartaric	191	193.7	198
Malic	147.6	157.7	147.5
Acetic	68.2	67.5	69.8
Lactic	57.1	57.6	57.7
Citric	149	155.5	147.8
Succinic	36.7	37.9	36.9

cinic and lactic respectively. They correspond to the deprotonated molecular ion  $[M-H]^-$ . Acetic acid could not be identified with the LC-MS system available because it is not suitable to analyse low weight molecules. The ESI-MS spectra corresponding to the tartaric, malic, citric and succinic acid are illustrated in Fig. 2.

Once the chromatographic conditions were established and just to test the new column with real samples the proposed method was applied to the determination of organic acids in three different commercial available white wines from the same origin; the

analysis were performed directly without previous treatment. The amounts of organic acids found are presented in Table 4.

#### 4. Conclusions

The new stationary phase could be an excellent alternative to the conventional octadecylsilane (ODS2) columns to analyse organic acids in different matrix. This novel packing showed an extraordinary sensitivity and a suitable performance.

#### Acknowledgement

A. Rodríguez-Bernaldo de Quirós is grateful to Xunta de Galicia for the award of a grant Parga Pondal.

#### References

- [1] L.M.L. Nollet, Food Analysis by HPLC, Marcel Dekker, Inc., Basel, 2000.
- [2] C.I. Rodrigues, L. Marta, R. Maia, M. Miranda, M. Ribeirinho, C. Máguas, J. Food Compos. Anal. 20 (2007) 440.
- [3] G. Shui, L.P. Leong, J. Chromatogr. A 977 (2002) 89.
- [4] A. de Villiers, F. Lynen, A. Crouch, P. Sandra, Chromatographia 59 (2004) 403.
- [5] A. Kotani, Y. Miyaguchi, E. Tomita, K. Takamura, F. Kusu, J. Agric. Food Chem. 52 (2004) 52.
- [6] F. Silva, V. Ferraz, Food Chem. 88 (2004) 609.
- [7] M.Y. Ding, H. Koizumi, Y. Suzuki, Anal. Sci. 11 (1995) 239.
- [8] M. Castellari, A. Versari, U. Spinabelli, S. Galassi, A. Amati, J. Liq. Chrom. Rel. Technol. 23 (2000) 2047.
- [9] A. Edelmann, J. Diewok, J. Rodriguez Baena, B. Lendl, Anal. Bioanal. Chem. 376 (2003) 92.
- [10] M.I.H. Helaleha, K. Tanakaa, H. Taodaa, W. Hub, K. Hasebeb, P.R. Haddad, J. Chromatogr. A 956 (2002) 201.
- [11] Y. Soyer, N. Koca, F. Karadeniz, J. Food Compos. Anal. 16 (2003) 629.
- [12] M.J. Nozal, J.L. Bernal, J.C. Diego, L.A. Gómez, M. Higes, J. Liq. Chrom. Rel. Technol. 26 (2003) 1231.
- [13] N. Dinkci, A.S. Akalin, S. Gönc, G. Ünal, Chromatographia 66 (2007) S45.
- [14] T. Pérez-Ruiz, C. Martínez-Lozano, V. Tomás, J. Martín, J. Chromatogr. A 1026 (2004) 57.
- [15] A. Santalad, P. Teerapornchaisit, R. Burakham, S. Srijaranai, LWT 40 (2007) 1741.
- [16] S.K. Johnson, L.L. Houk, J. Feng, D.C. Johnson, R.S. Houk, Anal. Chim. Acta 341 (1997) 205.
- [17] K. Gamoh, H. Saitoh, H. Wada, Rapid Commun. Mass Spectrom. 17 (2003) 685.
- [18] C.W. Klampfl, Electrophoresis 28 (2007) 3362.
- [19] Z. Chen, X. Jin, Q. Wang, Y. Lin, L. Gan, C. Tang, J. Sep. Sci. 30 (2007) 2440.
- [20] Teknokroma Home Page <http://www.teknokroma.es/mediterranea/>.
- [21] American Chemical Society (ACS), Subcommittee of Environmental Analytical Chemistry, Anal. Chem. 52 (1980) 2242.



# Simultaneous determination of Cd and Fe in grain products using direct solid sampling and high-resolution continuum source electrothermal atomic absorption spectrometry

Lisia M.G. dos Santos<sup>a,b</sup>, Rennan G.O. Araujo<sup>a</sup>, Bernhard Welz<sup>a,\*</sup>, Silvana do C. Jacob<sup>b</sup>, Maria Goreti R. Vale<sup>c</sup>, Helmut Becker-Ross<sup>d</sup>

<sup>a</sup> Departamento de Química, Universidade Federal de Santa Catarina, 88040-900 Florianópolis-SC, Brazil

<sup>b</sup> Instituto Nacional de Controle de Qualidade em Saúde–INCQS–Fiocruz, Av. Brazil, 4365, 21040-900 Rio de Janeiro–RJ, Brazil

<sup>c</sup> Instituto de Química, Universidade Federal do Rio Grande do Sul, Porto Alegre–RS, Brazil

<sup>d</sup> ISAS - Institute for Analytical Sciences, Department of Interface Spectroscopy, Berlin, Germany

## ARTICLE INFO

### Article history:

Received 17 October 2008

Received in revised form 2 December 2008

Accepted 3 December 2008

Available online 11 December 2008

### Keywords:

Grain products

Simultaneous determination of Cd and Fe

High-resolution continuum source AAS

Electrothermal atomization

Direct solid sample analysis

## ABSTRACT

Cadmium and iron are antagonistic elements in the sense that they produce different effects in the human body. Both elements have to be determined routinely in grain products, cadmium because of its toxicity, and iron because all grain products, according to Brazilian law, have to contain a minimum of 42 mg kg<sup>-1</sup> Fe to combat anemia. A routine screening method has been developed for the quasi simultaneous determination of cadmium and iron using high-resolution continuum source electrothermal atomic absorption spectrometry and direct solid sampling. The primary absorption line at 228.802 nm has been used for Cd, and an adjacent secondary line at 228.726 nm for the determination of Fe. Various chemical modifiers have been investigated, and a mixture of tungsten and iridium, applied as a permanent modifier, showed the best performance; it stabilized Cd up to a pyrolysis temperature of 700 °C and did not over-stabilize Fe. Two atomization temperatures were used sequentially, 1700 °C for Cd and 2600 °C for Fe, because of their significantly different volatilities. The characteristic masses obtained were 0.9 pg for Cd and 1.2 ng for Fe. The limits of detection (3σ, n = 10) were 0.6 μg kg<sup>-1</sup> for Cd and 0.5 mg kg<sup>-1</sup> for Fe. The relative standard deviation ranged from 3 to 7% for Cd and from 4 to 13% for Fe, which is satisfactory for the purpose. The accuracy of the method was confirmed by the analysis of three certified reference materials; the results were in agreement with the certified values at a 95% confidence interval. The Cd content in the investigated grain products was between 0.9 and 10.5 μg kg<sup>-1</sup>, but most of them did not contain the required minimum amount of iron.

© 2008 Elsevier B.V. All rights reserved.

## 1. Introduction

The chemical analysis of human food is a topic of interest for consumers and health professionals. Because of this, significant research has been carried out in order to aware government authorities about the need of controlling and supervising the quality of food [1–3]. Cadmium and iron are very important elements for two completely different reasons. Cadmium is an extremely toxic element even at low concentration; it was classified as carcinogenic of group 1 [4], by the International Agency for Research on Cancer (IARC), and set at the 7th position in the list of the most aggressive substances to health and to the environment by the Program for Answers, Reparations and Environmental Responsibilities (Cercla)

of the ATSDR-EPA [5]. The *Codex Alimentarius* limits the concentration of Cd in food to a maximum of 0.2 mg kg<sup>-1</sup> [6], and Brazilian legislation sets an upper limit of 1.0 mg kg<sup>-1</sup> [7]. Iron, in contrast, is an essential element, and iron deficiency in food may cause diseases, such as anemia. Many researchers, and also the World Health Organization, are therefore recommending fortification of food, mainly of grain products, with iron as one of the best options to combat iron deficiency. Brazilian legislation, for example, requires a minimum content of 42 mg kg<sup>-1</sup> Fe in all kind of grain products in order to combat anemia in the country [8].

Usually, food samples are analyzed after they were brought into solution by traditional techniques, such as dry ashing or wet digestion [9]. For the subsequent determination of trace elements these techniques present some limitations associated with (a) the applied temperature, (b) the form in which the analyte is present in the sample, (c) the chemical environment in the ashing/digestion stage, and (d) the dilution that is inevitably associated with any digestion, which obviously affects the limits of detection that can be attained.

\* Corresponding author. Fax: +55 48 3721 6850.

E-mail address: [Welz@qmc.ufsc.br](mailto:Welz@qmc.ufsc.br) (B. Welz).

Contamination and/or losses by volatilization are among the most frequent sources of systematic errors and affect directly the accuracy of analytical results [10]. An alternative to minimize these problems is the direct analysis of solid samples, which presents a number of advantages such as high detection power, high speed of analysis, minimum risk of contamination and loss of the analyte(s), and the absence of toxic and/or corrosive chemicals [11]. The only disadvantage of this technique is the higher imprecision due to the natural heterogeneity of solid samples [12–14].

High-resolution continuum source absorption spectrometry (HR-CS AAS), which has been investigated as an alternative to line source AAS (LS AAS) since the 1960s [15] has finally become feasible in the 1990s [16,17] and became commercially available a few years ago. The technique and the instrumental concept have been fully described by Welz et al. [15]. The major features of this technique are the use of a single radiation source for all analytes and wavelengths, the visibility of the spectral environment around the analytical line at high resolution, and its unsurpassed background correction capabilities that make it ideally suited for the direct analysis of complex samples. Particularly for the direct analysis of solid samples, HR-CS AAS has demonstrated its superiority over conventional LS AAS [11].

Although the currently available spectrometers for HR-CS AAS are not designed for simultaneous multi-element determination, it is possible to determine more than one element at a time if the absorption line of a second (or third) element appears within the spectral interval that reaches the CCD array detector, which is between about 0.4 and 2 nm, depending on the wavelength range. This second line, almost inevitably, is a less sensitive analytical line, and, although there are ways to increase or reduce sensitivity in HR-CS AAS [18], the sensitivity ratio between the two lines has to be in accordance with the analytical task. Additional problems for the simultaneous determination of more than one element in ET AAS are the selection of compromise pyrolysis and atomization temperatures and to choose a chemical modifier that is equally suited for both elements. Usually it is considered difficult to determine elements of significantly different volatility simultaneously with this technique.

The goal of the present work has been to investigate the possibility of a simultaneous determination of Cd and Fe in grain products using direct solid sampling (SS) analysis in order to establish a fast routine screening procedure for food analysis. There is an iron absorption line at 228.726 nm close to the main resonance line of cadmium at 228.802 nm, i.e., it is available for simultaneous determination. The sensitivity of the secondary iron line is also some two orders of magnitude lower than that of the primary resonance line, which roughly corresponds to the difference in concentration between the two elements in food samples. The major challenge, hence, has been to develop a temperature program and to find a modifier that is compatible with the significantly different volatility of the two analytes.

## 2. Experimental

### 2.1. Instrumentation

All experiments were carried out using a prototype high-resolution continuum source atomic absorption spectrometer, based on a Model AAS 6 Vario (Analytik Jena, Jena, Germany), from which all optical components have been removed and replaced by a spectrometer built at ISAS (Berlin, Germany). This spectrometer consists of a high-intensity xenon short-arc lamp operating in a hot-spot mode, a high-resolution double monochromator and a CCD array detector. The double monochromator consists of a pre-dispersing prism monochromator and a high-resolution echelle

**Table 1**

Temperature program for the simultaneous determination of cadmium and iron in food samples by SS-HR-CS AAS using W–Ir as the permanent modifier.

Stage	Temperature (°C)	Ramp (°C s <sup>-1</sup> )	Hold time (s)	Ar flow rate (L min <sup>-1</sup> )
Drying	90	10	10	2.0
Drying	130	5	5	2.0
Pyrolysis	700	50	15	2.0
Auto Zero*	700	100	1	0
Atomization*	1700	2000	3	0
Atomization*	2600	3000	12	0
Cleaning	2600	1000	3	2.0

\* Signal registration in these stages

grating monochromator, both in Littrow mounting, resulting in a resolution of  $\lambda/\Delta\lambda \approx 140,000$ , corresponding to a resolution per pixel of  $\sim 2$  pm at the cadmium line. The system is controlled by a Pentium III personal computer (100 MHz), running a data acquisition program developed at ISAS Berlin. Details of this equipment have been described in previous publications of our group [19,20]. The primary resonance line for Cd at 228.802 nm, and the adjacent secondary line for Fe at 228.726 nm were used for the simultaneous determination of the two elements. The atomic absorption for both elements was measured using peak volume selected absorbance (PVSA) [18] using three pixels ( $A_{\Sigma 3, \text{int}}$ ), corresponding to a spectral interval of  $\sim 6.0$  pm, as these conditions resulted in the best signal-to-noise (S/N) ratio.

The transversely heated graphite tube atomizer system supplied by Analytik Jena together with the Model AAS 6 Vario was used throughout. All experiments were carried out using pyrolytically coated solid sampling (SS) graphite tubes without dosing hole (Analytik Jena Part No. 407-A81.303) and SS platforms (Analytik Jena Part No. 407-152.023). The samples were weighed directly onto the SS platforms using an M2P microbalance (Sartorius, Göttingen, Germany) and inserted into the graphite tube using a pre-adjusted pair of tweezers, which is part of the SSA 5 manual solid sampling accessory (Analytik Jena). For the measurement of solid samples the PVSA was normalized for a sample mass of 1 mg, as it is impossible (and unnecessary) to weigh and introduce always the same sample mass into the graphite furnace. Aqueous standards and modifier solutions were injected manually onto the SS platform using micropipettes with disposable tips. Argon (99.996%, White Martins, São Paulo, Brazil) was used as purge and protective gas throughout. The optimized graphite furnace temperature program used for the simultaneous determination of Cd and Fe is shown in Table 1. Obviously, the solid samples analyzed in this work would not need any drying stage; nevertheless, the same temperature program has been used for aqueous standards and for the solid samples in this work for simplicity reason.

A vibration ball mill Model MM 200 (Retsch, Düsseldorf, Germany) with agate balls has been used to grind the bread and biscuit samples.

### 2.2. Standard solutions, modifiers and samples

A standard solution containing 1000 mg L<sup>-1</sup> Cd was prepared from a Spex standard (Spex, Eddison, NJ, USA) and a 1000 mg L<sup>-1</sup> Fe solution was prepared from a Titrisol concentrate (Merck). The calibration solutions were prepared daily through serial dilutions of the stock solution with the addition of 0.5% (v/v) nitric acid. De-ionized water from a Milli-Q system (Millipore, Bedford, MA, USA) with a resistivity of 18 M $\Omega$  cm was used throughout. The following atomic absorption standard solutions were used for the permanent modifiers: 1000 mg L<sup>-1</sup> Ir and 1000 mg L<sup>-1</sup> W (both from Fluka, Buchs, Switzerland). In order to coat the platform surface with a permanent modifier, ten aliquots of 40  $\mu$ L each of the modifier solu-

**Table 2**

Temperature program for the thermal deposition of the permanent modifier on the SS graphite platform; the gas flow was 2 L min<sup>-1</sup> in all stages.

Stage	Temperature (°C)	Ramp (°C s <sup>-1</sup> )	Hold time (s)
1	130	30	20
2	400	30	20
3	1000	100	10
4	2000	100	5

tion were injected onto the platform, and the temperature program shown in Table 2 was executed after each injection, resulting in a total mass of 400 µg of modifier on the SS platform. In order to coat the platform with the W–Ir mixed permanent modifier, five aliquots of 40 µL of the W modifier solution were applied first, each one followed by the temperature program shown in Table 2, then five aliquots of 40 µL of the Ir modifier solution were applied, also followed by the same temperature program, resulting in a coating with 200 µg each of W and Ir.

The following certified reference materials (CRM) have been used in this work: NIST SRM 1567a wheat flour, NIST SRM 1573a tomato leaves (National Institute for Standards and Technology, Gaithersburg, MD, USA) and BCR No. 191 brown bread (Community Bureau of Reference, Brussels, Belgium).

One wheat flour, one corn flour, two samples of French bread and two samples of biscuits have been collected from local supermarkets in Florianópolis, SC, for this investigation. The samples were dried in a stove at 70 °C for a period of 48 h; then they were ground in a vibration ball mill with agate balls for 30 min with a frequency of 30 s<sup>-1</sup>; the samples have not been sieved, as a very fine powder has been obtained after the treatment in the mill.

### 3. Results and discussion

#### 3.1. Method development

The currently available spectrometers for HR-CS AAS are not designed for simultaneous multi-element determination. Nevertheless, it is possible to determine more than one element at a time if the absorption line of a second element is located within the spectral interval that reaches the detector. In the case of Cd this interval corresponds to about ±0.2 nm at both sides of the analytical line. This is of only minor interest in flame AAS, where fast sequential determination of several analytes under optimized conditions is obviously the better choice [21]. In ET AAS, in contrast, where fast sequential determination is not feasible because of the transient nature of the absorbance signals, simultaneous determination of more than one analyte is of great interest, as it reduces analysis time proportionally. However, several requirements have to be met in order to make this approach feasible, and conditions have to be optimized, as any simultaneous determination implies compromises.

The first requirement is that the sensitivity ratio between the elements to be determined at the available analytical lines corresponds roughly to the concentration ratio of the analytes in the samples to be analyzed. Although HR-CS ET AAS offers various possibilities to increase or decrease sensitivity by choosing appropriate pixels for measurement [18], particularly the option to increase sensitivity is limited. Fortunately this condition was fulfilled in the present case, as the iron line at 228.725 nm is about two orders of magnitude less sensitive than the primary resonance line at 248.327 nm, and about three orders of magnitude less sensitive than cadmium at the 228.802-nm line, as shown in Fig. 1. This corresponds in a first approximation to the situation in grain products, where the concentration of cadmium is typically 3–4 orders of magnitude lower than that of iron.

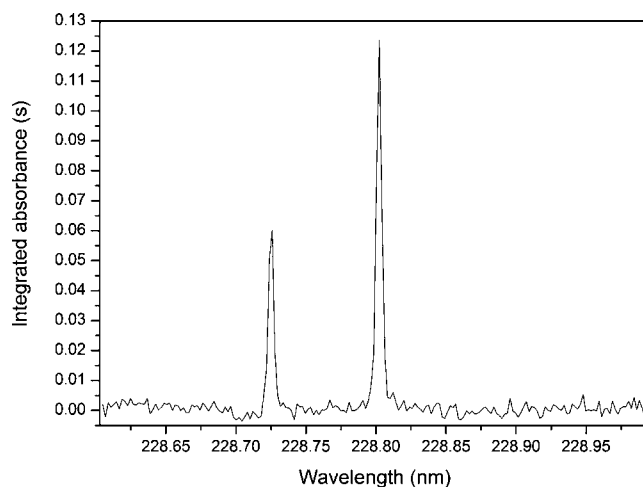


**Fig. 1.** Integrated absorbance spectrum in the vicinity of the cadmium resonance line at 228.802 nm using an aqueous standard containing 50 µg Cd and 30 ng Fe; pyrolysis temperature: 700 °C; atomization temperature: 1700 °C for Cd and 2600 °C for Fe; W–Ir mixed permanent modifier.

Another problem in the present case is the significantly different volatility of cadmium and iron, which requires careful optimization of the compromise conditions. It is obvious that the most volatile element determines the maximum pyrolysis temperature, and the most refractory element determines the atomization temperature. An additional problem is the selection of a suitable modifier, as it is well known that cadmium requires a chemical modifier, as otherwise it is lost already at pyrolysis temperatures above 300 °C, at least from aqueous solution. Iron, on the other hand, does not need a modifier, and it might be ‘over-stabilized’ by the use of a modifier, i.e., become even more difficult to atomize.

Only permanent chemical modifiers have been considered in this work, as the goal has been the development of a fast routine procedure, and injecting manually a modifier solution on top of each solid sample would have complicated the procedure considerably. Iridium and tungsten alone and a combined tungsten and iridium (W–Ir) permanent modifier have been investigated in this work. The pyrolysis and atomization temperatures have been optimized using a univariate approach, as for a given modifier, temperature is the only variable that determines the measured signal. Multivariate approaches have been used occasionally to determine optimum pyrolysis and atomization temperatures; however, the result might be falsified by artifacts and suggest less-than-optimum temperatures. In addition, valuable details might be overlooked that appear in ‘conventional’ univariate pyrolysis and atomization curves.

Two reference materials (BCR No. 191, brown bread and NIST SRM 1573a, tomato leaves) and aqueous standard solutions have been used for the development and optimization of the method, but only the results obtained for the brown bread CRM will be shown. The curves for the tomato leaves CRM have been very similar, and the behavior of the aqueous standards will be discussed where necessary.

The pyrolysis and atomization curves for Cd in the brown bread CRM without modifier and with the three permanent modifiers (Ir, W and W–Ir) are shown in Fig. 2a and b. In contrast to aqueous standards, where Cd without a modifier is lost at pyrolysis temperatures above 300 °C, no significant losses have been observed from the CRM up to about 600 °C. Above this temperature Cd was lost rapidly, and neither Ir alone nor W alone used as permanent modifier could prevent these losses, although some stabilizing effect has been observed. The W–Ir mixed permanent modifier stabilized Cd up to a pyrolysis temperature of 700 °C, which was sufficient to

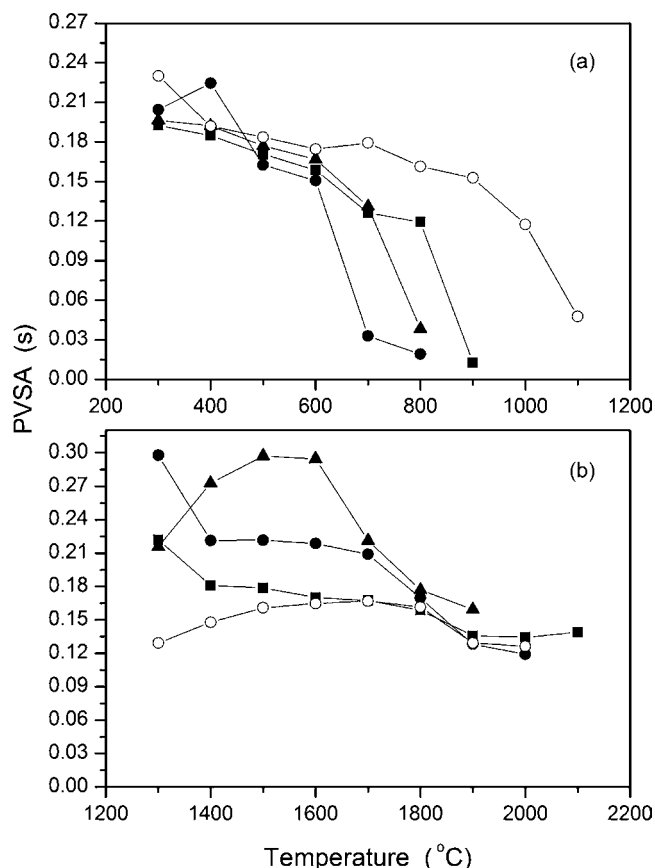


**Fig. 2.** Pyrolysis and atomization curves for Cd in CRM BCR 191 brown bread; -●- without modifier; -▲- W permanent modifier; -■- Ir permanent modifier; -○- W-Ir permanent modifier; a - pyrolysis curves; atomization temperature of 1600 °C without modifier and 1800 °C with permanent modifier; b - atomization curves; pyrolysis temperature of 500 °C without modifier and 700 °C with permanent modifier.

efficiently remove the bulk of the matrix. The atomization curve for Cd without a modifier shows the typical behavior for a volatile element, i.e., a maximum, in this case around 1500–1600 °C, followed by a decrease in sensitivity; this is due to the increasing diffusion velocity at higher temperatures, which results in a shorter residence time of the atoms in the absorption volume. The atomization curves with the permanent modifiers exhibit lower sensitivity up to about 1700 °C, which indicates an incomplete release of Cd at these temperatures due to the stabilizing power of the modifiers. Above this temperature the sensitivity becomes very similar to that without modifier, indicating a complete release of the analyte from the modifier and the same diffusion losses with further increasing temperature.

Fig. 3 shows the absorbance signal for Cd and the background for the brown bread CRM without and with correction for continuous background using the W-Ir mixed permanent modifier, a pyrolysis temperature of 700 °C and an atomization temperature of 1700 °C. It is obvious that the background can be corrected without any problems, resulting in a very smooth atomization signal for Cd.

The pyrolysis and atomization curves for Fe in the brown bread CRM are shown in Fig. 4a and b. Iron exhibits very high thermal stability up to at least 1500 °C even without a modifier, which is typical for this element. The explanation for the lower sensitivity obtained with the W-Ir mixed permanent modifier can be obtained from the atomization curves in Fig. 4b. When the atomization curves without modifier and with the W-Ir mixed modifier are compared, the similarity with the corresponding atomization curves for Cd becomes obvious. Although Fe is a much less volatile element, the

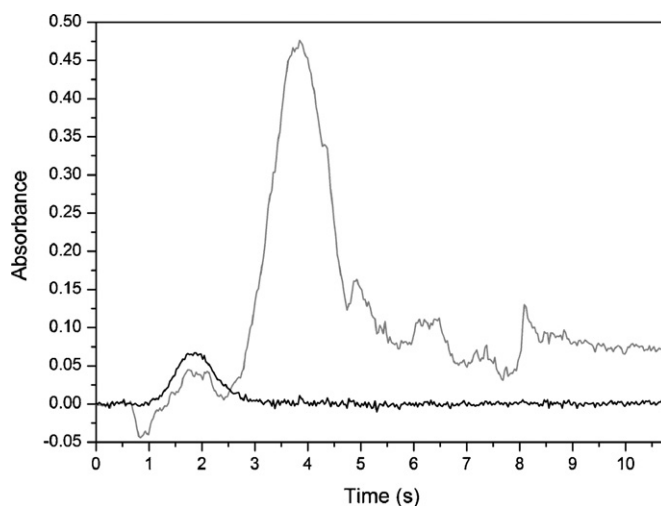


**Fig. 3.** Absorbance signals measured for BCR 191 brown bread CRM at the center pixel at 228.802 nm using the Ir-W permanent modifier, using a pyrolysis temperature of 700 °C and an atomization temperature of 1700 °C; gray line: without background correction; black line: with correction for continuous background absorption.

curve without modifier also exhibits a maximum at 2000 °C and a decreasing sensitivity for higher atomization temperatures. In the presence of the W-Ir mixed modifier complete release of Fe is only achieved at 2500 °C, where the atomization curve coincides with

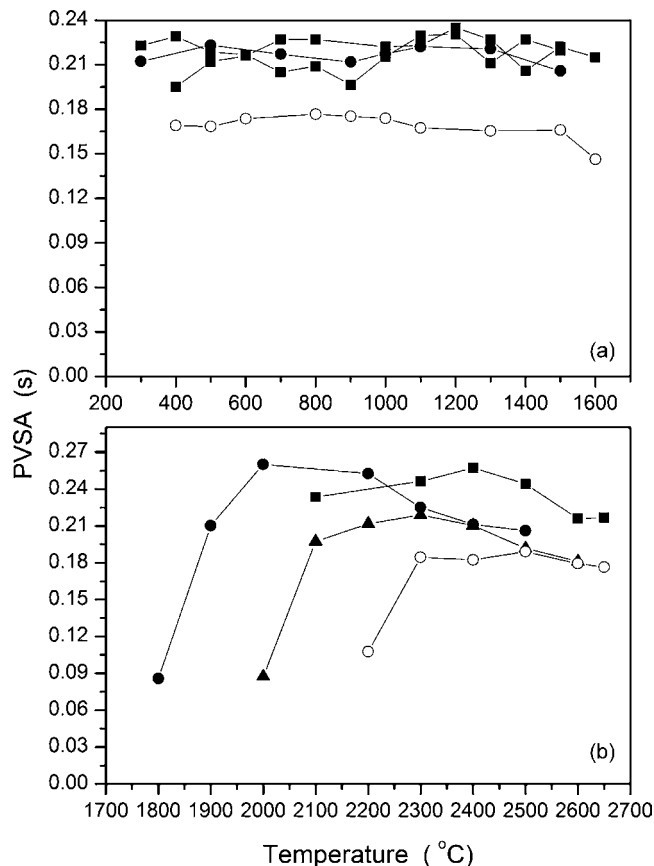


**Fig. 4.** Pyrolysis and atomization curves for Fe in CRM BCR 191 brown bread; -●- without modifier; -▲- W permanent modifier; -■- Ir permanent modifier; -○- W-Ir permanent modifier; a - pyrolysis curves; atomization temperature of 2500 °C without modifier and 2600 °C with permanent modifier; b - atomization curves; pyrolysis temperature of 500 °C without modifier and 700 °C with permanent modifier.

**Table 3**

Figures of merit for the simultaneous determination of Cd and Fe by SS-HR-CS ET AAS at 228.802 nm and 228.726 nm, respectively, using the temperature program in Table 1.

Parameter	Analyte	
	Cd	Fe
Analytical range	3–70 pg/0.3–7 $\mu\text{g L}^{-1}$	2.6–40 ng/0.26–4 $\text{mg L}^{-1}$
Analytical curve, aqueous standards	$A_{\Sigma 3, \text{int}} = 0.0051 m_{\text{Cd}} + 0.0098$	$A_{\Sigma 3, \text{int}} = 0.0037 m_{\text{Fe}} + 0.0091$
Analytical curve using CRM	$A_{\Sigma 3, \text{int}} = 0.0051 m_{\text{Cd}} + 0.0033$	$A_{\Sigma 3, \text{int}} = 0.0037 m_{\text{Fe}} + 0.0022$
R	0.9981	0.9992
LOD <sup>a</sup>	0.9 pg/0.6 $\mu\text{g kg}^{-1}$	0.8 ng/0.5 $\text{mg kg}^{-1}$
LOQ <sup>a</sup>	3.0 pg/2.0 $\mu\text{g kg}^{-1}$	2.6 ng/1.7 $\text{mg kg}^{-1}$
$m_0$	0.9 pg	1.2 ng

<sup>a</sup> Based on 1.5 mg of sample mass

that without a modifier. The apparently slightly higher sensitivity obtained with W and Ir alone is actually an artifact; both modifiers are 'over-stabilizing' iron, resulting in a poorly defined, very broad atomization signal that is very difficult to integrate.

According to these results it becomes apparent that the W–Ir mixed modifier gives best results for both analytes, although Fe obviously would not need any modifier at all. It also became apparent that the bulk of the matrix could be removed at a pyrolysis temperature of 700 °C in the presence of this modifier. However, it also became obvious that no common atomization temperature could be used for the two analytes without impairing significantly the performance for Cd. For this reason, two atomization temperatures were used sequentially, 1700 °C for Cd and 2600 °C for Fe, according to the program shown in Table 1. The atomization signals obtained for the two analytes for an aqueous standard and for the brown bread CRM are shown in Fig. 5a and b. Although the determination of the two elements is not strictly 'simultaneous', we prefer to use this term in order to distinguish the procedure used in this work from 'fast sequential' procedures that include a change of wavelength and of other experimental parameters, as it is common practice in HR-CS AAS with flame atomization [21].

### 3.2. Calibration and figures of merit

Several calibration approaches were proposed in the literature to compensate for potential matrix effects in direct SS-ET AAS, such as calibration against solid standards (usually CRM) with a matrix composition and analyte concentration similar to that of the sample to be analyzed, and the 'generalized analyte addition method', a three-dimensional calibration technique [22]. The latter has been applied by only a limited number of authors due to its complexity, whereas the former is routine in other solid sampling techniques, such as arc and spark emission and X-ray fluorescence. The major problem associated with the use of solid CRM for calibration, besides the high cost of these materials, is that the uncertainty of the certified value adds to the uncertainty of the calibration and hence of the final analytical result. However, if the literature about SS-ET AAS of the last 15–20 years is consulted, the vast majority of determinations have actually been carried out using aqueous standards for calibration [12], which is mostly due to the uncompromising use of the stabilized temperature platform furnace (STPF) concept [23]. Besides the classical components, which include atomization from a L'vov platform, integration over the peak area and the use of a chemical modifier, the introduction of transversely heated, spatially isothermal atomizers had a significant contribution to freedom from interferences. The weak link in LS AAS has always been the background correction, a problem that has been finally solved with the introduction of HR-CS ET AAS, which also reflects in the publications about direct SS using aqueous standards for calibration [11]. Calibration against aqueous standards and against a solid CRM has been compared in this work, and the slopes of the calibration curves have been found to be very similar, as shown in Table 3. The appearance times and peak shapes are

also very similar for the two analytes in aqueous solution and for direct SS analysis, as has been shown in Fig. 5a and b. The aqueous standard in Fig. 5a corresponds to a mass of 50 pg Cd and 30 ng Fe, and the PVSA values were 0.262 and 0.124 s, respectively; in Fig. 5b 1.022 mg of CRM BCR 191 was introduced into the graphite atomizer, corresponding to 29 pg Cd and 42 ng Fe, and the PVSA values were 0.147 and 0.160 s, respectively. This is another indication for a very similar atomization behavior and the absence of matrix effects.

Table 3 also shows the other figures of merit for the simultaneous determination of Cd and Fe in grain products by SS-HR-CS ET AAS. The linearity assessment was based on the methodology described by Souza and Junqueira [24]. Three calibration curves were prepared on different days, with concentration levels of 1, 3, 5 and 7  $\mu\text{g L}^{-1}$  Cd (corresponding to 10, 30, 50, 70 pg Cd), and 1, 2, 3 and 4  $\text{mg L}^{-1}$  Fe (corresponding to 10, 20, 30 and 40 ng Fe).

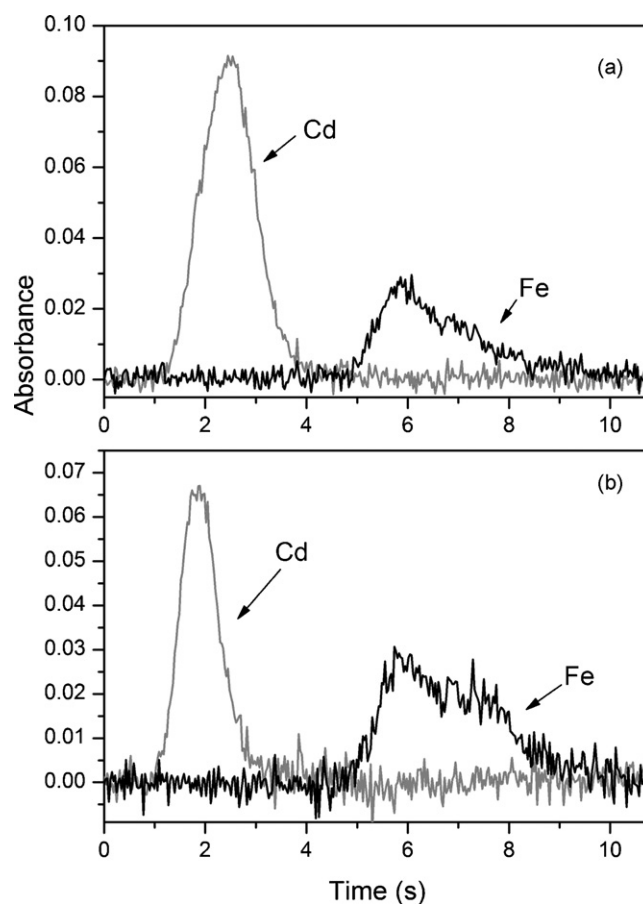


**Fig. 5.** Superimposed absorbance signals for Cd (gray line) and Fe (black line) after automatic correction for continuous background absorption; pyrolysis temperature: 700 °C; atomization temperature: 1700 °C for Cd and 2600 °C for Fe; a – aqueous standard; b – BCR 191 brown bread CRM.

**Table 4**  
Results obtained for the determination of cadmium and iron in CRM by SS-HR-CS ET AAS using aqueous calibration standards and NIST SRM 1567a for solid calibration and Ir–W as a permanent modifier.

CRM	Analyte	Certified/mg kg <sup>-1</sup>	Found/mg kg <sup>-1</sup>	
			Aqueous calibration	Solid calibration
BCR 191	Cd	0.028 ± 0.002	0.025 ± 0.002	0.026 ± 0.002
NIST 1573a		1.52 ± 0.04	1.4 ± 0.1	1.4 ± 0.1
NIST 1567a		0.026 ± 0.002	0.023 ± 0.001	Used for calibration
BCR 191	Fe	40.7 ± 2.4	37.8 ± 6.3	43.4 ± 7.4
NIST 1573a		367 ± 7	342 ± 19	400 ± 21
NIST 1567a		14.1 ± 0.5	15.2 ± 1.5	Used for calibration

The linearity was tested by examining a plot of residuals produced by linear regression of the response on the concentration in an appropriate calibration set. The statistic test (Ryan-Joine, Levene, Durbin-Watson) has been carried out by comparing the lack-of-fit variance with that due to pure error, which confirmed the linearity of the calibration curves for Cd and Fe [25–27].

In this work precision is expressed as relative standard deviation (%RSD) of five replicate measurements of a CRM. Although five replicates might appear insufficient to obtain a reliable RSD, it has been found that the values do not improve significantly in SS-ET AAS when a greater number of replicates are used. The RSD values were between 3 and 7% for Cd and between 4 and 13% for Fe. The significantly higher RSD for the latter element could be due to the omnipresence of this element in the environment, i.e., due to some contamination; however, as no systematic bias has been observed, it is more likely due to the inhomogeneous distribution of iron in the investigated CRM.

The accuracy of the method has been evaluated by analyzing three CRM of different composition, demonstrating the wide applicability of the method [28], using both aqueous standards and a solid CRM for calibration. The results, shown in Table 4 confirm that there is no significant difference between both calibration techniques, based on a Student's *t*-test at a confidence level of 95% [26].

The limit of detection (LOD) was calculated according to the 'zero mass response' [22,28,29] as three times the standard deviation of the signal obtained for 10 repetitive "atomizations" of an empty SS platform, only containing the modifier. The LOD was 0.6 µg kg<sup>-1</sup> for Cd and 0.5 mg kg<sup>-1</sup> for Fe. The limit of quantification (LOQ), defined as ten times the standard deviation, was 2.0 µg kg<sup>-1</sup> for Cd and 1.3 mg kg<sup>-1</sup> for Fe.

The characteristic mass for Cd found in this work was 0.9 pg, which is in agreement with literature data; the characteristic mass found for Fe was 1.2 ng, and no values could be found in the literature for this line for comparison. The high sensitivity of the method can be attributed mainly to the absence of any dilution for the SS procedure.

### 3.3. Analysis of real samples

The simultaneous determination of Cd and Fe was also used to evaluate the concentration of these elements in a few selected local grain products, wheat flour, corn flour, bread and biscuits. The concentrations of Cd and Fe found in these products, using aqueous standards for calibration, are shown in Table 5. The values for cadmium were in the range between 0.9 µg kg<sup>-1</sup>, a value close to the LOD, and 10.5 µg kg<sup>-1</sup> values that are well below those established by the *Codex Alimentarius* (0.2 mg kg<sup>-1</sup>) and the Brazilian National Health Surveillance Agency–ANVISA (1.0 mg kg<sup>-1</sup>) [7]. For Iron, the values ranged from 15.7 mg kg<sup>-1</sup> to 72.7 mg kg<sup>-1</sup>. Considering Brazilian legislation [8], which requires enriching any grain product with Fe to at least a concentration of 42 mg kg<sup>-1</sup>, the levels of Fe in the wheat and corn flour samples, with values below 20 mg kg<sup>-1</sup>,

**Table 5**  
Results of the simultaneous determination of cadmium and iron in different grain products collected in local supermarkets of Florianópolis, Brazil, using SS-HR-CS ET AAS and calibration against aqueous standards; all values are average and standard deviation of *n* = 5 determinations.

Sample	Found concentration	
	Cd/µg kg <sup>-1</sup>	Fe/mg kg <sup>-1</sup>
Wheat flour	5.9 ± 0.6	15.7 ± 4.7
Corn flour	0.9 ± 0.3	19.8 ± 2.7
French bread A	10.5 ± 0.3	37.2 ± 2.0
French bread B	6.2 ± 0.7	34.0 ± 2.7
Biscuit A	3.5 ± 0.9	72.7 ± 17.3
Biscuit B	7.5 ± 0.6	60.8 ± 0.6

and in the bread samples, with values below 42 mg kg<sup>-1</sup>, were lower than the minimum amount required. Only the biscuit samples had iron levels above the minimum amount required by law.

The wheat and corn flour and the bread samples did not exhibit any molecular absorption except for the continuous background absorption shown in Fig. 3. For the biscuit samples, in contrast, a structured molecular absorption appeared together with the atomization of Fe, as is shown in Fig. 6. This spectrum has been identified as being due to the sulfur monoxide SO; it could be removed by least-squares background correction [30] using a reference spectrum established with an aqueous solution of (NH<sub>4</sub>)<sub>2</sub>SO<sub>4</sub>. However, this correction was actually found to be unnecessary, as none of the

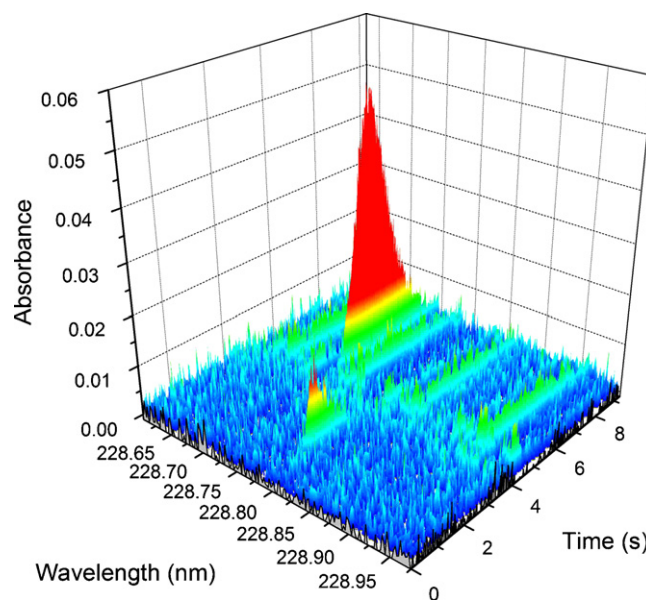


**Fig. 6.** Absorbance over time and wavelength for a biscuit sample in the vicinity of Cd resonance line at 228.802 nm; pyrolysis temperature: 700 °C; atomization temperature: 1700 °C for Cd and 2600 °C for Fe.



molecular absorption 'lines' was overlapping with the iron line, so that no interference could be observed.

#### 4. Conclusion

This work has shown that it is possible to determine more than one analyte simultaneously (or quasi simultaneously) using HR-CS ET AAS if their absorption lines are within the spectral interval that reaches the CCD array detector. This is obviously a situation that might not be found for a great number of cases, but besides for iron, which has more than 600 absorption lines, cobalt, chromium and nickel, which all have more than 200 absorption lines, are other candidates, the lines of which might be found in the vicinity of other analytes. The other condition that has to be fulfilled is that the sensitivity ratio between the analytical lines combines with the concentration ratio of the analytes in the samples to be analyzed. This condition has been fulfilled in the present application, but it might as well be similar for a large number of other biological materials, so that the proposed procedure might be extended to other samples. The present work has also shown that a significantly different volatility of the analytes is not a barrier that would make their simultaneous determination impossible in HR-CS ET AAS, which is an important aspect, considering future equipment that might offer truly simultaneous multi-element ET AAS. Last not least, the present work has demonstrated one more time that HR-CS AAS is ideally suited for interference-free direct SS-ET AAS, and that aqueous standards can be used for calibration. And it has been shown one more time that permanent chemical modifiers can be used successfully for direct SS ET AAS.

#### Acknowledgement

The authors are grateful to Conselho Nacional de Desenvolvimento Científico e Tecnológico (CNPq) and Coordenação de Aperfeiçoamento de Pessoal de Nível Superior (CAPES). R.G.O.A., B.W. and M.G.R.V. have research scholarships from CNPq and L.M.G.S. has a scholarship from CAPES. The authors are also grateful to Analytik Jena AG for the donation of the HR-CS AAS prototype.

#### References

- [1] A.G. Renwick, S.M. Barlow, I. Hertz-Picciotto, A.R. Boobis, E. Dybing, L. Elder, G. Eisenbrand, J.B. Greig, J. Kleiner, J. Lambe, D.J.G. Muller, M.R. Smith, A. Tritscher, S. Tuijtelaars, P.A. van den Brandt, R. Walker, R. Kroes, *Food Chem. Toxicol.* 41 (2003) 1211.
- [2] O. Muñoz, J.M. Bastias, M. Araya, A. Morales, C. Orellana, R. Rebolledo, D. Velez, *Food Chem. Toxicol.* 43 (2005) 1647.
- [3] B. Welz, D.L.G. Borges, U. Heitmann, in: S. Caroli (Ed.), *The Determination of Chemical Elements in Food: Applications for Atomic and Mass Spectrometry*, Wiley-Interscience, Hoboken, NJ, USA, 2007, p. 81.
- [4] Agency for Toxic Substances and Disease Registry. Top 20 Hazardous Substances from the CERCLA Priority List of Hazardous Substances for 2005. <http://www.atsdr.cdc.gov/>.
- [5] E. Vassileva, H. Baeten, M. Hoenig, *Fresenius J. Anal. Chem.* 369 (2001) 491.
- [6] World Health Organization. Safety evaluation of certain food additives and contaminants. WHO food additives Series: 59. Geneva: IPCS-International Programme on Chemical Safety, 2008 <http://www.codexalimentarius.net>.
- [7] BRASIL. Decreto nº 55871, de 26 de março do 1965. Modifica o Decreto nº 50040, de 24 de Janeiro de 1961, referente a normas reguladoras do emprego de aditivos para alimento, alterado pelo Decreto nº 691 de 13 de Abril de 1962. Diário Oficial [da] República Federativa do Brasil, Poder Executivo, Brasília, DF, 09 abr. 1965.
- [8] BRASIL. Resolução - RDC nº 344, de 13 de dezembro de 2002. Aprova o Regulamento Técnico para a Fortificação das Farinhas de Trigo e das Farinhas de Milho com Ferro e Ácido Fólico, constante do anexo desta Resolução. Diário Oficial [da] República Federativa do Brasil, Poder Executivo, Brasília, DF, 18 dez. 2002.
- [9] M.G.A. Korn, E.S. da Boa Morte, D.C.M.B. dos Santos, J.T. Castro, J.T.P. Barbosa, A.P. Teixeira, A.P. Fernandes, B. Welz, W.P.C. dos Santos, E.B.G.N. dos Santos, M. Korn, *Appl. Spectrosc. Rev.* 43 (2008) 67.
- [10] C.S. Noumura, C.S. da Silva, P.V. Oliveira, *Quim. Nova* 31 (2008) 104.
- [11] B. Welz, M.G. Vale, D.L.G. Borges, U. Heitmann, *Anal. Bioanal. Chem.* 389 (2007) 2085.
- [12] M.G. Vale, N. Oleszczuk, W.N.L. dos Santos, *Appl. Spectrosc. Rev.* 41 (2006) 377.
- [13] A.F. da Silva, D.L.G. Borges, F.G. Lepri, B. Welz, A.J. Curtius, U. Heitmann, *Anal. Bioanal. Chem.* 382 (2005) 1835.
- [14] B. Welz, *Anal. Bioanal. Chem.* 381 (2005) 69.
- [15] B. Welz, H. Becker-Ross, S. Florek, U. Heitmann, *High-resolution Continuum Source AAS—The Better Way to do Atomic Absorption Spectrometry*, Wiley-VCH, Weinheim, 2005.
- [16] U. Heitmann, M. Schutz, H. Becker-Ross, S. Florek, *Spectrochim. Acta Part B* 51 (1996) 1095.
- [17] J.M. Harnly, *J. Anal. At. Spectrom.* 14 (1999) 137.
- [18] U. Heitmann, B. Welz, D.L.G. Borges, F.G. Lepri, *Spectrochim. Acta Part B* 62 (2007) 1222.
- [19] M.G.R. Vale, I.C.F. Damin, A. Klassen, M.M. Silva, B. Welz, A.F. Silva, F.G. Lepri, D.L.G. Borges, U. Heitmann, *Microchem. J.* 77 (2004) 131.
- [20] A.F. Silva, D.L.G. Borges, B. Welz, M.G.R. Vale, M.M. Silva, A. Klassen, U. Heitmann, *Spectrochim. Acta Part B* 59 (2004) 841.
- [21] J.L. Raposo Júnior, S.R. de Oliveira, N.M. Caldas, J.A. Gomes Neto, *Anal. Chim. Acta* 627 (2008) 198.
- [22] U. Kurfürst, in: U. Kurfürst (Ed.), *Solid Sample Analysis—Direct And Slurry Sampling Using GF AAS and ETV-ICP*, Springer, Berlin, Heidelberg, New York, 1998, p. 21.
- [23] W. Slavin, D.C. Manning, G.R. Carnrick, *At. Spectrosc.* 2 (1981) 137.
- [24] S.V.C. Souza, J.A. Lima, J.C. Teodoro, R.G. Junqueira, *Ciênc. Tecnol. Aliment.* 274 (2007) 823.
- [25] J.C. Miller, J.N. Miller, *Statistics for Analytical Chemistry*, 2nd ed., Ellis Harwood Limited, England, 1998.
- [26] D.L.G. Borges, A.J. Curtis, B. Welz, U. Heitmann, *Revista Analytica* 18 (2005) 58.
- [27] B. Welz, M. Sperling, *Atomic Absorption Spectrometry*, Wiley-VCH, Weinheim, 1999.
- [28] INMETRO. DOQ-CGCRE-008-revisão 01: orientação sobre validação de métodos de ensaios químicos. Março 2003.
- [29] S.V.C. Souza, R.G. Junqueira, *Anal. Chem. Acta* 552 (2005) 25.
- [30] D.L.G. Borges, A.F. da Silva, B. Welz, A.J. Curtis, U. Heitmann, *J. Anal. At. Spectrom.* 21 (2006) 763.



## Electrical and humidity characterization of m-NA doped Au/PVA nanocomposites

Madhavi V. Fuke<sup>a,\*</sup>, P.V. Adhyapak<sup>b</sup>, U.P. Mulik<sup>b</sup>, D.P. Amalnerkar<sup>b</sup>, R.C. Aiyer<sup>a</sup>

<sup>a</sup> Center for Sensor Studies, Department of Physics, University of Pune, Pune 411007, India

<sup>b</sup> Centre for Materials for Electronics Technology, Panchavati, off Pashan Road, Pune 411008, India

### ARTICLE INFO

#### Article history:

Received 18 October 2008

Received in revised form 5 December 2008

Accepted 5 December 2008

Available online 13 December 2008

#### Keywords:

Relative humidity

m-NA/Au/PVA nanocomposite

Electrical properties

### ABSTRACT

The Meta-Nitroaniline (m-NA) doped (by varying weight percentage (wt. %)) gold/polyvinyl alcohol (Au/PVA) nanocomposites were synthesized using gold salt and hydrazine hydrate (HH) by in situ process. The composite was coated on ceramic rods having two end electrodes by drop casting method for studying their electrical behavior at different relative humidity (RH) levels, ranging from 4 to 95% RH at room temperature. The optimized wt. % was used to prepare coatings of various thicknesses (20–40  $\mu\text{m}$ ) of the films. As the humidity decreases, the resistance increases. The low humidity sensing characteristic can be tailored by varying wt. % of m-NA and thicknesses of the nanocomposite films. The resistive-humidity sensor shows two regions of sensitivity having highest sensitivity for lower RH. The sensor response and recovery time is about 6–10 s and 52 s respectively. The dynamic range of variation of the resistance allows a promising use of the films as a humidity sensor. The material was characterized by X-ray diffraction (XRD) and impedance spectroscopy at 60% RH.

© 2008 Elsevier B.V. All rights reserved.

### 1. Introduction

Nowadays humidity measurement and control has gained importance in many areas such as weather prediction, agriculture, industrial, process control, household electric appliances, medical field and research. The advancement in science and technology led greater emphasis on the measurement and control of humidity. Therefore the advanced research on humidity sensitive materials is going on by using various polymers, including polymer electrolytes, conjugated polymers, etc. [1–3]. Different criteria are used for measuring sensitivity to humidity and gases like changes in mechanical, optical and electrical properties [4]. Different humidity sensors are popularly studied that are mainly based on the two properties, i.e. electrical and optical. The sensors based on the electrical properties such as impedance, resistance or capacitance are best suited to modern automatic control systems. Electrical detection is the most commonly used and is based on the change in resistance or capacitance of the sensor on exposure to water vapor and gases [5]. Chilled mirror optical method, infrared hygrometers, aspirated psychomotor, etc., are some of the techniques used for the measurement of relative humidity. The electrical measurement techniques are useful and convenient due to the easy signal processing capability and flexibility for miniaturization [6–10].

Nanosized devices are constructed by using nanoparticles because of their high surface to volume ratio and special physical and chemical properties resulting from the reduced sizes [11]. A humidity sensor based on nanostructured materials such as carbon nanotubes [12,13], metal oxide nanoparticles [14] and Nano-Wire (NW) films [15,16] are explored to promote sensitivity, selectivity, chemical and thermal stability. Metallic nanoparticles such as gold, silver, etc. are more efficient for several applications. Gold nanoparticles are synthesized by chemical reduction method with capping agents like alkanethiol [17] alkylamine molecules [18]. They are embedded in polymers, e.g. polyvinyl pyrrolidone (PVP) and polyvinyl alcohol (PVA) [19,20] for their use in several applications. For opto-electronic and electronic applications, the controlled particle size and uniform distribution of nanoparticles within the polymer are essential. The embedded or encapsulated nano-particles within a polymer are useful for gas or humidity sensing. Generally polymer plays two roles: (1) it acts as a surface capping agent and (2) provides matrix to disperse nanoparticles. In addition, casting of film becomes easier and the particle size can be controlled well within the desired regime [1]. m-NA is studied for Nonlinear Optics (NLO) by Adhyapak et al. [21]. Similarly, gold nano-particles with specific size and shape are NLO active [22,23].

In the present work, the humidity sensing characteristics based on the m-NA/Au/PVA composite in the form of thin film on a cylindrical alumina rod having two end electrodes were investigated for their electrical behavior as a function of relative humidity at room temperature. It is observed that these resistors are humidity

\* Corresponding author. Tel.: +91 20 2569 2678; fax: +91 20 2569 1684.

E-mail address: [mfuke@physics.unipune.ernet.in](mailto:mfuke@physics.unipune.ernet.in) (M.V. Fuke).

sensitive; their working range can be tailored by varying the m-NA wt. % (55–100% RH) and the thickness of the films (4–95% RH).

## 2. Experimentation

All chemicals used were of AR grade. Gold chloride solution (0.01 M) of 10 mL (to maintain the final Au (0) concentration of about 2 wt. % of PVA) was added to a viscous solution of 1 g of PVA and was dissolved in 25 mL water. The reaction mixture was stirred at room temperature. A separate solution of a diluted hydrazine hydrate was prepared in water. 20  $\mu$ L of it was added by a micro syringe in the above reaction mixture. Then by injecting the methanolic solution of m-NA (0.01 M) dropwise with syringe in 25 mL of above prepared solution (to get 0–4.14 wt. % of m-NA) and stirring the reaction mixture for 1 h, m-NA doped Au/PVA nanocomposites were formed. m-NA/Au/PVA nanocomposite was characterized by X-ray diffraction, Uv–visible spectroscopy, photoluminescence, scanning electron microscopy and transmission electron microscopy [24].

The films of m-NA/Au/PVA nanocomposite were prepared by drop coating (2  $\mu$ L of solution by a micropipette) the solution on the ceramic rods, which were used as resistors. A simple chemical method was used to test the prepared films for their sensitivity towards humidity. Closed humidity system for testing the humidity responses of the films was fabricated as shown in Fig. 1. It consists of a closed glass chamber (volume: 6 L), with a neck for inserting a sample under test and a probe of the standard Vaisala humidity meter (humidity range: 0–100% RH with an accuracy of 1–5% RH for different humidity ranges). The chamber was kept on an aluminum plate and was sealed from outside by modeling clay to make the system air tight. The relative humidity was created inside the chamber by passing water vapors and simultaneously monitoring the humidity to get 100% RH at room temperature (25–30 °C) as measured by the standard Vaisala humidity meter. After achieving 100% RH flow of water vapors was stopped. The 100% RH was kept for 5 min. The chamber was gently lifted and the saturated vapors were wiped by tissue papers and the chamber was kept at its original position. Humidity was decreased by putting dehumidifying materials like phosphorous pentoxide ( $P_2O_5$ ), calcium carbonate, silica gel, etc. in an appropriate amount in a pettry dish. While humidifying and dehumidifying the chamber, the 2–5 °C change in the temperature was observed. The change in relative humidity is related to the change in the resistance of the sample.

The samples were kept in the chamber and were exposed to the highest humidity and related output in the form of resistance

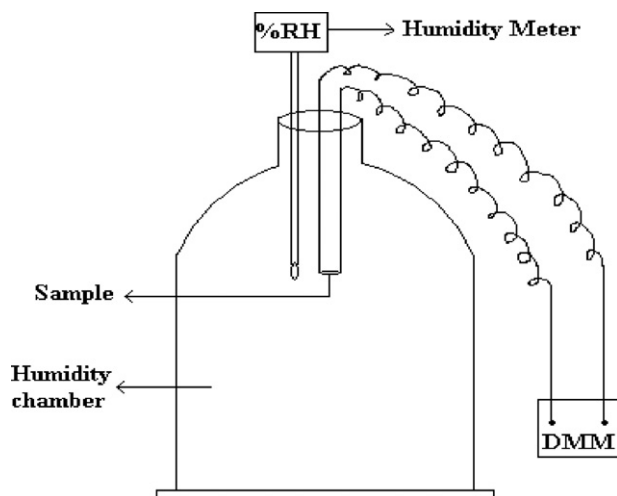


Fig. 1. Experimental set up for the measurement of relative humidity.

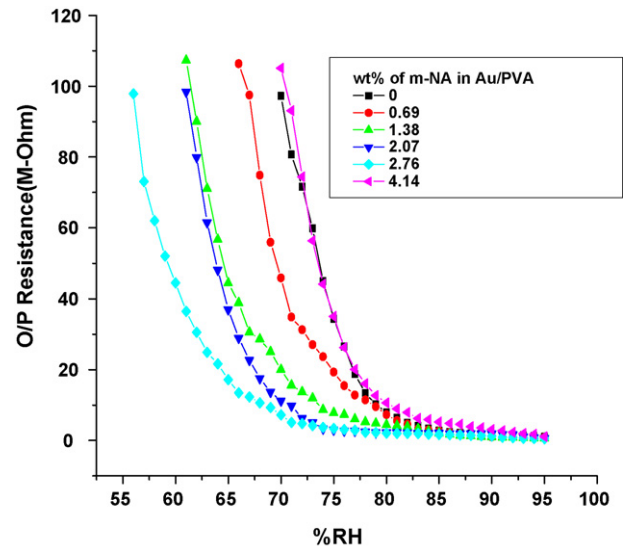


Fig. 2. Variation of resistance with respect to the relative humidity for different wt. % (0, 0.69, 1.38, 2.07, 2.76, 4.14) of m-NA in Au/PVA nanocomposite.

was measured by Digital Multimeter (DMM) (Agilent U1241A) as given in Fig. 1. Putting dehumidifying material (Thomas Baker's  $P_2O_5$  LR grade) in the chamber, relative humidity was decreased to the lowest value and related resistance was noted. Output is plotted with respect to the relative humidity. The sensitivity is defined as change in electrical resistance per unit change in relative humidity [25]. The samples of Au/PVA nanocomposite with variable wt. % of m-NA were checked for humidity and the wt. % of m-NA doping was optimized. This optimized concentration was further used to optimize the film thickness. The thicknesses of the films were varied by changing the number of coats of m-NA/Au/PVA nanocomposite. Proper care was taken to have uniform coating. The thicknesses of the films were measured by using micrometer screw gauge (L.C. = 0.01 mm).

The maximum difference in the output of the two cycles at any particular RH was measured as the hysteresis. It was measured for increasing and decreasing cycle of humidity. To study the reliability and repeatability of the sensor, 5 cycles were performed on a sample of the sensor.

Response time was measured for direct transition from ambient air (i.e.  $\approx$ 55% RH) to higher % RH (i.e. 95% RH). Recovery time was measured after exposing the sensor directly to the ambient air from 95% RH by removing the sample from the test chamber, till the sensor regains the original output value.

## 3. Results and discussions

The output (O/P) resistance versus % RH is plotted (Fig. 2) for m-NA/Au/PVA nanocomposite films (20  $\mu$ m thickness) of different wt. % of m-NA. All the samples are showing response to humidity with some threshold values of RH. All the experiments were carried out at room temperature (25–30 °C).

For zero wt. % m-NA lowest humidity sensed was 70% RH while the limit of sensing goes on increasing towards the lower humidity with increase in wt. % of m-NA up to 55% RH for 2.76 wt. % of m-NA. Thus the sensor can sense minimum 55% RH for 2.76 wt. % of m-NA. Further increase in wt. % of m-NA (4.14 wt. %) decreases the humidity sensing range up to 70% RH.

Change in humidity sensing range is explained on the basis of XRD (Fig. 3). XRD shows two prominent peaks. The peak at  $2\theta$  of about  $20^\circ$  is due to m-NA/PVA and it is little bit shifted against its original value of about  $18^\circ$  [26] and the peak at  $2\theta$  of about  $39^\circ$

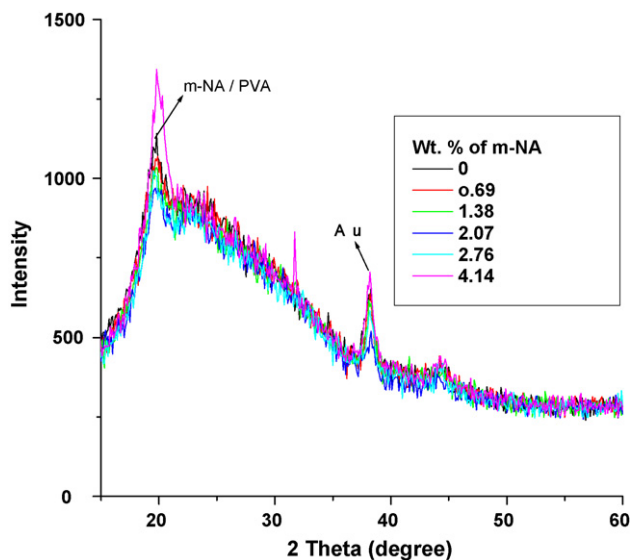


Fig. 3. XRD spectra of variable wt. % of m-NA doped Au/PVA nanocomposite.

presenting the (1 1 1) Bragg's reflection of fcc crystal structure of gold (ASTM data) is present in all the XRD patterns.

Peak intensity decreases gradually from 0 to 2.76 wt. % of m-NA. This is because of more number of protonic sites created by m-NA for adsorbing water molecules. At m-NA of 4.14 by wt. %; there is a sudden increase in peak intensity which happens because of increase in crystallinity. Due to crystallisation particle size increases which supports the increase in resistivity.

Output resistance versus wt. % of m-NA is plotted at constant humidity (70% RH) as shown in Fig. 4. From Fig. 4 it is clear that at a constant humidity with the increase in wt. % of m-NA there is a decrease in the resistivity of m-NA/Au/PVA nanocomposite films up to 2.76 wt. % of m-NA. Further addition of m-NA increases the resistivity due to crystallization of m-NA in the nanocomposite.

On the basis of the composition of the nanocomposites, an explanation to the change in sensing behavior is proposed as follows.

In m-NA/Au/PVA nanocomposite, insulating PVA is acting as a host or matrix having very high resistance (60 M $\Omega$ ) value at higher

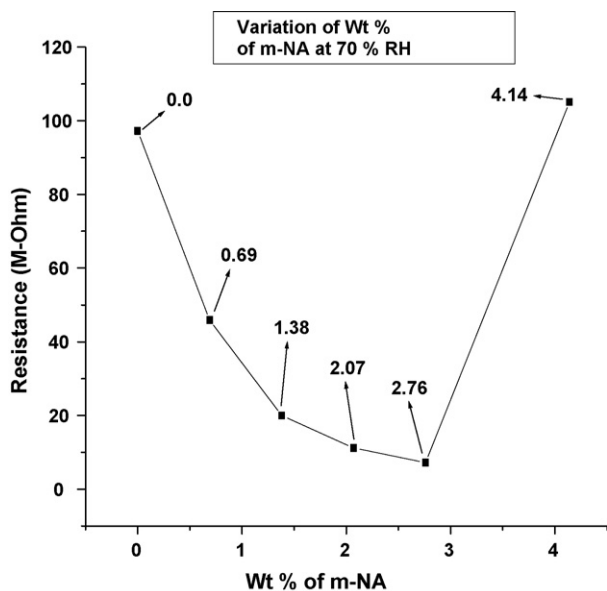
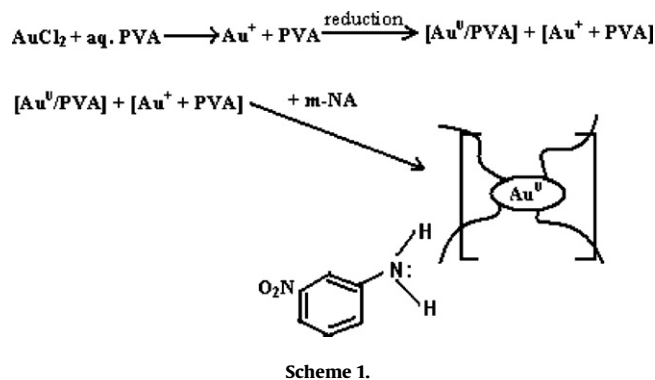


Fig. 4. Variation of wt. % of m-NA in Au/PVA nanocomposite with respect to output resistance at 70% RH.



humidity (95% RH). For 1% RH decrease, the resistance of PVA goes beyond measurable limit.

The next constituent of given nanocomposite, i.e. gold (Au) which is a metallic nanoparticle enhances the humidity sensing [27–29]. As Au nanoparticles are added into PVA the color of the solution changes. Thus there is red-shift in the absorption spectra of the nanocomposite [24,30]. Dispersion of Au nanoparticles in the host decreases the resistivity of the composite up to 1 M $\Omega$  at 95% RH. This is because when water molecule adsorbs on the film surface, Au<sup>+</sup> ions get loosely attached with OH<sup>-</sup> ions and H<sup>+</sup> is free for conduction (Scheme 1).

As m-NA is doped in the Au/PVA nanocomposite the humidity response increases gradually. Doping of m-NA gives the lone pair of electrons on the nitrogen from the amine which is a functional group of m-NA, which offers some sort of binding with vacant *d*-orbitals of Au<sup>0</sup> as shown below [21].

Au<sup>0</sup> ions are loosely attached to the nitrogen by weak Van der Waals' forces of attraction. Hence more numbers of H<sup>+</sup> ions are free for conduction decreasing resistivity for the m-NA/Au/PVA nanocomposite.

Humidity sensing mechanism is explained on the basis of protonic conduction. Water is highly polar as it has lone-pair of electrons and thus, it is a good donor [31] of H<sup>+</sup> and electrons, which is useful in proton conduction mechanism. Proton is the dominant carrier responsible for the electrical conductivity in bulk water. On the basis of adsorption and capillary condensation of water, protons are produced. For ionic sensing materials, if the humidity increases, the conductivity increases and the dielectric constant increases [32,33]. When water molecule is adsorbed on film surface, it splits to produce protons as shown by the following equation.



More numbers of protons (H<sup>+</sup>) are produced when the sensing material is exposed to more humidity in the testing system. In the first stage of H<sup>+</sup> ions production no proton can move because for the first monolayer water molecule is chemically adsorbed on an activated site to form an adsorption complex, which subsequently transfers to surface hydroxyl groups. Next water molecule is bonded with two neighboring hydroxyl groups through hydrogen bonding. Thus there is a restriction on the top water molecule layer condensed due to the two-hydrogen bonding.

In the second step, water continues to condense on the surface which forms an extra, somewhat un-ordered layer of adsorbed water on the top of the first physically adsorbed water layer. These extra layers vanish the ordering from the initial surface and more and more protons become free to move inside the condensed water (Grotthuss mechanism). Fig. 5 illustrates the tunnelling of protons from one water molecule to the next via hydrogen bonding which universally exists in liquid-phase of water.

The m-NA/Au/PVA nanocomposite based humidity sensor is showing sensitivity over the humidity range of 95–55% RH. There

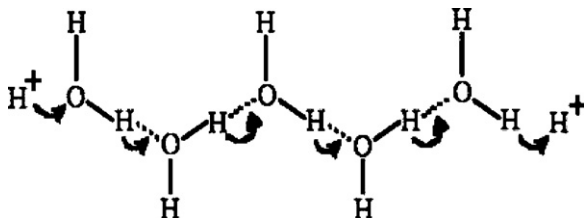


Fig. 5. Brief illustration of the Grotthuss mechanism.

**Table 1**  
Regionwise sensitivity of m-NA/Au/PVA nanocomposite films for several of wt. % of m-NA.

wt. % of m-NA in Au/PVA nanocomposite	Sensitivity (MΩ/%RH)	
	Region I (95–80% RH)	Region II (Below 80%RH)
0	0.373	9.877
0.69	0.359	7.069
1.38	0.258	4.827
2.07	0.101	4.422
2.76	0.113	3.188
4.14	0.549	10.56

are two sensitivity regions for all sensors shown in Fig. 2. The resistance increases from  $10^3$  to  $10^6$  Ω when RH is decreased from 95 to 55% at room temperature. The lower humidity region is more sensitive as compared to higher humidity region as the results given in Table 1.

The process affects electrical properties. The film effectively consists of grain and grain boundaries. When the monolayer of water molecules get adsorbed effective potential barrier between the boundaries goes on decreasing increasing the surface conductivity of the film. As more and more water molecules get condensed on the walls of the capillaries (boundaries), the resistance of the grain starts coming in parallel increasing its conductivity almost exponentially. Therefore at higher humidity the effective change in resistance is small. Though this change in resistance is relatively small compared to low humidity, the sensor offers higher sensitivity than reported earlier by Ansari et al. [34], the resistive humidity sensor.

To enhance the humidity sensing range thickness of the film is playing vital role. The graph (Fig. 6) is plotted between relative humidity and resistance of the sensor for variable thicknesses (20 μm, 27 μm, 32 μm and 40 μm) of the films of m-NA/Au/PVA nanocomposite.

Increase in thicknesses of the films increases the depth of pores forming bigger channels for conducting protons. This happens because, as the wt. % of m-NA increases in the nanocomposite, depth of pore sites increases for adsorption of water molecules which increases the humidity sensing range and sensitivity. Thus the 40 μm thickness film shows maximum range, i.e. 4–95% RH. The results for different thicknesses are tabulated in Table 2.

For m-NA/Au/PVA humidity sensor, surface area is fixed with almost same number of pore sites. When the samples are exposed to humidity, water molecules adsorb on the film surface (physisorp-

**Table 2**  
Humidity ranges and sensitivity for various thicknesses.

Thickness of m-NA/Au/PVA composite film (μm)	Sensitivity (MΩ/%RH)	
	Region I	Region II
20	0.104 (95–70% RH)	3.878 (70–55% RH)
27	0.182 (95–66% RH)	5.376 (65–42% RH)
32	0.190 (95–50% RH)	6.029 (50–34% RH)
40	0.201 (95–10% RH)	16.95 (10–4% RH)

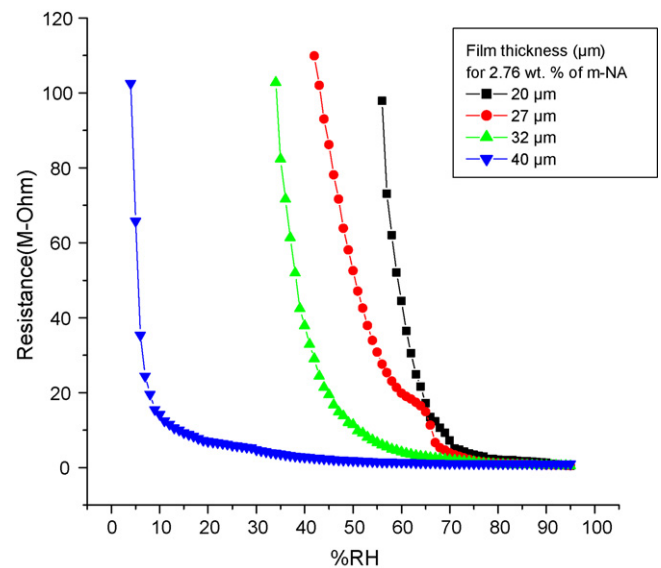


Fig. 6. Variation of resistance with respect to % RH for different thicknesses of the films of 2.76% m-NA/Au/PVA nanocomposite.

tion) and condensed into pores available in the film thus capillary condensation takes place as shown in Fig. 7. At low humidity (Fig. 7(a)), when adsorption starts on the film surface, a layer of hydroxyl groups is formed by dissociative mechanism. In the middle range (Fig. 7(b)) monolayer of water molecules will be adsorbed along sites available on the thickness of the film giving rise to better conductivity. At a higher RH (Fig. 7(c)) multilayer adsorption of water takes place due to which it penetrates deeply inside the film. The adsorbed water molecules form channels for conduction of protons which in turn sense humidity by shorting the grains effectively reducing the resistance. To understand humidity sensing mechanism in brief equivalent circuit for humidity sensing system is drawn as shown in Fig. 8. m-NA/Au/PVA nanocomposite is having some voids/channels separated by grains.  $R_1$  is surface resistance at the interface of air and grain and  $R$  is the resistance along the thickness of the film. The pores are represented by capacitance  $C$ . It is assumed that the pores are of uniform size.

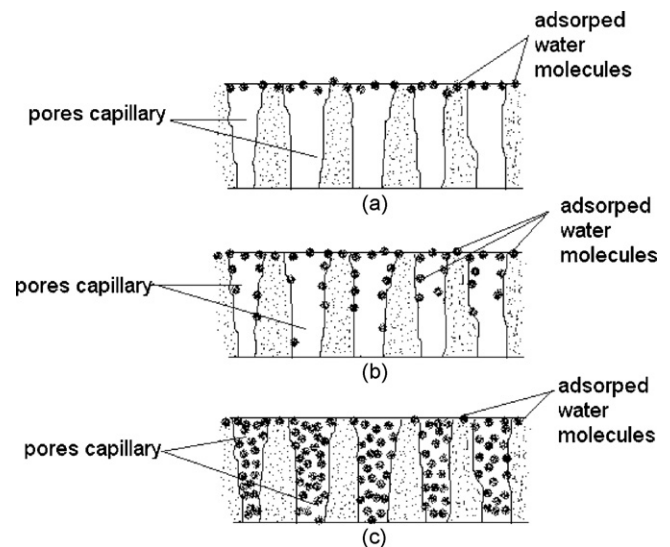


Fig. 7. The adsorption phenomena of water molecules on film (a) at lower humidity (surface adsorption); (b) at intermediate humidity (adsorption on capillary walls); (c) at higher humidity (full capillary condensation).

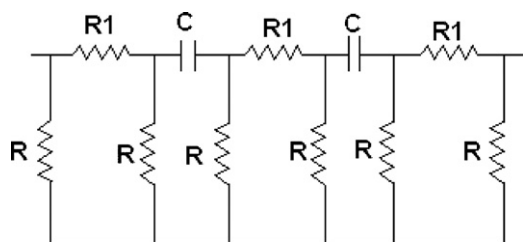


Fig. 8. Equivalent circuit for humidity sensing system.

When the film is exposed to humidity, surface resistance decreases very fast and capacitance  $C$  increases because of higher dielectric constant of water. The change in resistance is due to occupied surface sites. When pores started filling with moisture the boundary resistance decreases up to 95% RH. In this region as the resistances  $R$  are joined in parallel, there is a slow decrease in resistance. Thus for higher humidity, resistance decreases with increasing the conductivity of the sensor and vice versa.

### 3.1. Impedance spectroscopy

The impedance spectroscopy of m-NA/Au/PVA nanocomposite thin films was done at room humidity (60%) by using LCR meter (Hioki 3532-50 LCR HiTESTER) to support the aforementioned results.

The complex impedance ( $Z = Z' + jZ''$ ) are plotted to get Nyquist (Cole–Cole) plots. Fig. 9 shows the  $\text{Re } Z (Z')$  Vs  $\text{Im } Z (Z'')$  plots of the m-NA/Au/PVA films. As the wt. % of m-NA increases the inclined semicircle obtained in Cole–Cole plots shifts down towards X-axis indicating increase in the conductivity up to m-NA of 2.76 wt.%. For 4.14 wt. % of m-NA the plot is suddenly shifting upward indicating the increase in resistance because of crystallization of nanocomposite. This is complimentary to the results shown in Fig. 2. The sample with zero wt. % m-NA shows the highest resistance. This also supports our statement that m-NA is a source sites for water molecules to produce  $\text{H}^+$ .

One semicircle at higher frequencies on the plot is due to kinetically controlled charge transfer and a spur at lower frequencies is because of mass transfer [35,36]. In impedance spectra, frequency decreases from left to right for each spectrum. The semicircles

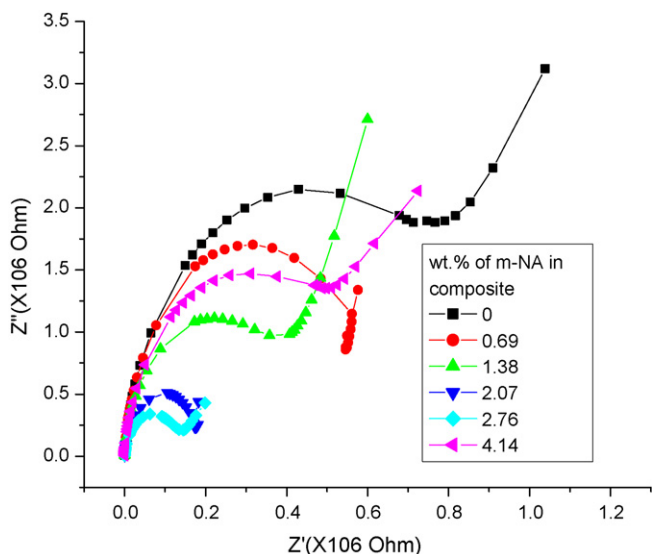


Fig. 9. Cole-Cole plot of m-NA/Au/PVA nanocomposite samples for different wt. % of m-NA at room humidity.

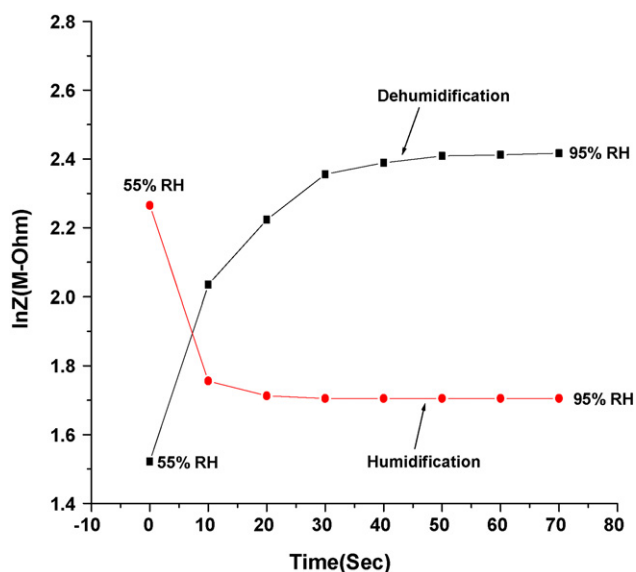


Fig. 10. Response and Recovery properties of m-NA/Au/PVA nanocomposite based humidity sensor at 25 °C.

obtained at higher frequencies (Fig. 9) are resulted as a finite amount of screening, exerted by the hopping charges or dipoles, which cannot follow the rapid changes of polarization. On the other hand, the spur obtained at lower frequencies is because of polarization. Thus at a higher frequencies, sensor shows better conductivity than that of lower frequencies.

The sensor is having about 2% hysteresis which is nothing but result of adsorption and desorption process which indicates that the desorption rate of water molecules in the m-NA doped Au/PVA film is slower than the adsorption one.

The response time of m-NA/Au/PVA composite films was measured by changing the humidity from 95% to 55% RH and recovery time by varying humidity from 55 to 95% RH. Thus adsorption and desorption time of the electrical characteristic is 6–10 and 52 s which is response and recovery time (Fig. 10) of the sensor respectively.

To study the repeatability and reproducibility of the m-NA doped Au/PVA nanocomposite based humidity sensor, five succes-

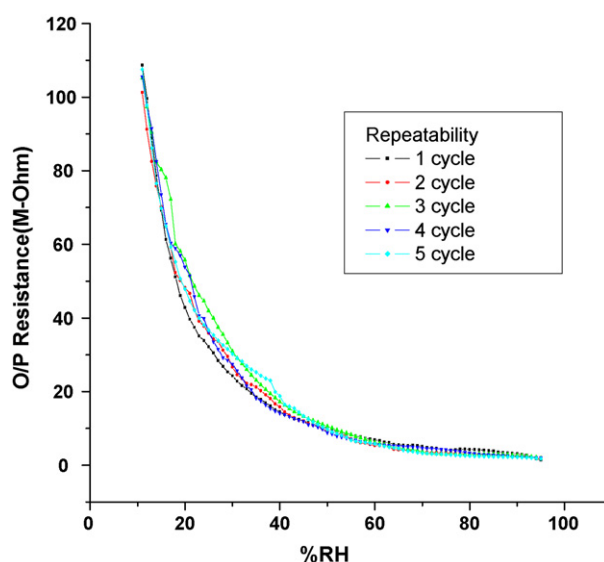


Fig. 11. Repeatability result for 2.76 wt. % of m-NA in Au/PVA nanocomposite.

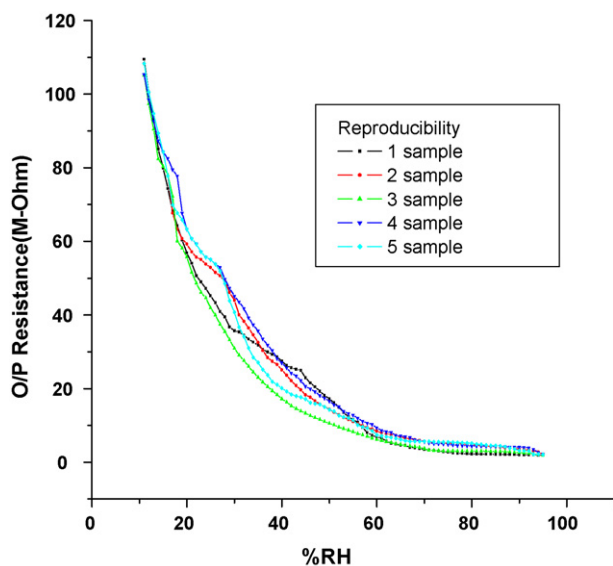


Fig. 12. Reproducibility result for 2.76 wt. % of m-NA in Au/PVA nanocomposite.

sive cycles for 95–10% RH was carried out for each. The response of the sensor has been shown in Figs. 11 and 12. From figures it can be seen that the m-NA/Au/PVA films possesses a quite good repeatability and reproducibility.

#### 4. Conclusions

m-NA/Au/PVA nanocomposite based humidity sensors were prepared by varying weight percentage of m-NA in Au/PVA composite. m-NA/Au/PVA nanocomposite shows changes in resistance by the amount of three orders of magnitudes in response to 4–95% relative humidity (RH) change in the measuring chamber. Thus m-NA/Au/PVA can be used for fabricating humidity-sensing elements. The sensor shows good repeatability, low hysteresis and quite good reproducibility at room temperature.

#### Acknowledgements

One of the authors, Madhavi Fuke would like to acknowledge Center for Sensor Studies, University of Pune, for their financial support.

#### References

- [1] B.R. Mayer, Mater. Sci. Eng. C6 (1998) 155.
- [2] R. Jin, Y.W. Cao, A. Mirkin, K.L. Kelly, G.C. Schatz, J.G. Zhang, Science 294 (2001) 1901.
- [3] J.R. Gould, J.R. Lenhard, A.A. Muentner, S.A. Godleski, S. Farid, J. Am. Chem. Soc. 122 (2000) 11934.
- [4] M. Viviani, M.T. Buscaglia, V. Buscaglia, M. Leoni, P. Nanni, J. Euro. Ceram. Soc. 21 (2001) 1981–1984.
- [5] Komilla Suri, S. Annapoorni, A.K. Sarkar, R.P. Tandon, Sens. Actuators B 81 (2002) 277–282.
- [6] T. Nitta, in: T. Seiyama (Ed.), Development and Application of Ceramic Humidity Sensors, Chemical Sensor Technology, vol. 1, Elsevier, Amsterdam, Kodansha, Tokyo, 1998, pp. 55–78.
- [7] S. Yang, J. Wu, J. Mater. Sci. 26 (1991) 631–636.
- [8] L. Wu, C. Wu, J. Her, J. Mater. Sci. 26 (1991) 3874–3878.
- [9] K. Camman, U. Lemke, A. Rohen, J. Sander, H. Wilken, B. Winter, Angew. Chem. Int. Edn. Engl. 30 (1991) 516–539.
- [10] N. Yamazoe, Y. Shimizu, Sens. Actuators B 10 (1986) 379–539.
- [11] Qin Kuang, Changshi Lao, Zhong Lin Wang, Zhaoxiong Xie, Lansun Zheng, J. Am. Chem. Soc. 129 (2007) 6070–6071.
- [12] X.J. Huang, Y.F. Sun, L.C. Wang, F.L. Meng, J.H. Liu, Nanotechnology 15 (2004) 1284.
- [13] J.T.W. Yeow, J.P.M. She, Nanotechnology 17 (2006) 5441.
- [14] M.M. Ahmad, S.A. Makhlof, K.M.S. Khalil, J. Appl. Phys. 100 (2006) 094323.
- [15] Y.S. Zhang, K. Yu, D.S. Jiang, Z.Q. Zhu, H.R. Geng, L.Q. Luo, Appl. Surf. Sci. 242 (2005) 212.
- [16] R.J. Wu, Y.L. Sun, C.C. Lin, H.W. Chen, M. Chavali, Sens. Actuators B 115 (2006) 198.
- [17] J. Fink, C.J. Kiely, D. Bethell, D.J. Schiffrin, Chem. Mater. 10 (1998) 922.
- [18] D.V. Leff, L. Brandt, J.R. Heath, Langmuir 12 (1996) 472.
- [19] G. Carotenuto, L. Nicolais, J. Mater. Chem. 13 (2003) 1038.
- [20] P.K. Khanna, R. Gokhale, V.V.V.S. Subbarao, A.K. Viswanath, B.K. Das, C.V.V. Satyanarayana, Mater. Chem. Phys. 92 (2005) 229.
- [21] P.V. Adhyapak, P.K. Khanna, J.W. Dadge, R.C. Aiyer, J. Nanosci. Nanotechnol. 6 (2006) 2141.
- [22] J. Sasai, K. Hirao, J. Appl. Phys. 89 (2001) 4548.
- [23] S. Qu, H. Li, T. Peng, Y. Gao, J. Qiu, C. Zhu, Mater. Lett. 58 (2004) 1427.
- [24] P.V. Adhyapak, Narendra Singh, Anu Vijayan, R.C. Aiyer, P.K. Khanna, Mater. Lett. 61 (2007) 3456–3461.
- [25] Z.A. Ansari, R.N. Karekar, R.C. Aiyer, Thin Solid Films 305 (1997) 330–335.
- [26] Y.S. Negi, P.V. Adhyapak, S.R. Damkale, R.K. Goyal, M. Islam, R.C. Aiyer, Mater. Lett. 58 (2004) 3929.
- [27] Pengfei Pang, Zongduan Guo, Qingyun Cai, Talanta 65 (2005) 1343–1348.
- [28] Zhi-meimei Qi, Itaru Honma, Haoshen Zhou, Opt. Lett. 3112 (2006) 1854–1856.
- [29] Yi-Lu Sun, Yi-Zhen Chen, Ren-Jang Wu, Murthy Chavali, Yu-Ching Huang, Pi-Guey Su, Chu-Chieh Lin, Sens. Actuators B 126 (2007) 441–446.
- [30] Shawn M. Dirk, Stephen W. Howell, B. Katherine Price, Hongyou Fan, Cody Washburn, David R. Wheeler, James M. Tour, Joshua Whiting, R. Joseph Simonson, J. Nanomater., in press.
- [31] V.E. Henrich, P.A. Cox, The Surface Science of Metal Oxides, Cambridge University Press, Cambridge, 1996.
- [32] F. Ansbacher, A.C. Jason, Nature 24 (1953) 177.
- [33] J.M. Thorp, Trans. Faraday Soc. 55 (1959) 442.
- [34] S.G. Ansari, Z.A. Ansari, M.R. Kadam, R.N. Karekar, R.C. Aiyer, Sens. Actuators B 21 (3) (1994) 159–163.
- [35] Seema Agarwal, G.L. Sharma, Sens. Actuators B 85 (2002) 205–211.
- [36] Y.C. Yeh, T.Y. Tseng, J. Mater. Sci. 24 (1989) 2739–2745.



## Comparative studies of ONNO-based ligands as ionophores for palladium ion-selective membrane sensors

Vinod K. Gupta\*, Rajendra N. Goyal, Ram A. Sharma

Department of Chemistry, Indian Institute of Technology Roorkee, Roorkee 247 667, India

### ARTICLE INFO

#### Article history:

Received 25 September 2008

Received in revised form

26 November 2008

Accepted 27 November 2008

Available online 3 December 2008

#### Keywords:

Ion-selective electrode

Palladium ion

Schiff base

Poly(vinyl chloride) membranes

### ABSTRACT

Palladium sensors based on two neutral ionophores, *N,N'*-bis(acetylacetonate) cyclohexanediamine (**L**<sub>1</sub>) and *N,N'*-bis(*o*-hydroxyacetophenone)-1,2-cyclohexanediamine (**L**<sub>2</sub>) for quantification of palladium ions are described. Effect of various plasticizers (*o*-NPOE, DBP, DEP, DOP, TBP, and CN) and anion excluder, sodium tetra phenyl borate (NaTPB) has been studied. The best performance is obtained with a membrane composition of PVC:*o*-NPOE:ionophore (**L**<sub>1</sub>):NaTPB of 150:300:5:5 (% w/w). The sensor exhibits significantly enhanced selectivity towards palladium ion over the concentration range  $1.0 \times 10^{-8}$  to  $1.0 \times 10^{-1}$  M with a lower detection limit of  $4.0 \times 10^{-9}$  M and a Nernstian compliance ( $29.1 \pm 0.3$  mV decade<sup>-1</sup> of activity) within pH range 2.0–6.0 and fast response time of 10 s. Influence of the membrane composition and possible interfering ions has also been investigated on the response properties of the electrode. Fast and stable response, good reproducibility and long-term stability of the sensor are demonstrated. The sensor has been found to work satisfactorily in partially non-aqueous media up to 20% (v/v) content of methanol, ethanol and acetonitrile and could be used for a period of 4 months. Selectivity coefficients determined with fixed interference method (FIM) indicate high selectivity for palladium. The proposed electrode shows fairly good discrimination of palladium from other cations. The application of prepared sensor has been demonstrated in determination of palladium ions in spiked water sample.

© 2008 Elsevier B.V. All rights reserved.

### 1. Introduction

Palladium is a rare and lustrous silvery-white metal, owing to its chemical erosion resistance nature and alloying ability [1,2]. Palladium alloys are used in dental, medicinal devices and in jewellery manufacture. Palladium is found in many electronics items including computers, mobile phones, multilayer ceramic capacitors, component plating, low-voltage electrical contacts and SED/OLED/LCD television. It plays key role in the technology used in fuel cell, which combines hydrogen and oxygen to produce electricity, heat and water. The finely divided palladium forms a good catalyst and is used to speed up hydrogenation and dehydrogenation reactions as well as in petroleum cracking. A number of methods have been used for the determination of palladium, such as inductively coupled plasma, atomic absorption spectrometer, glow discharge mass spectrometer, adsorptive cathodic stripping voltammetry and electrothermal atomic absorption spectrometer either with or without separation and pre-concentration step. Palladium is widely determined spectrometrically after pre-concentration by extraction, adsorption or reversed phase high-performance liquid chromatography. In spite of the fact that these methods provide accurate

results, they are not very convenient for analysis of large number of environmental samples because of the requirement of sample pre-treatment and sufficient infrastructure backup.

In recent years, a number of sensors for transition metal ions have been reported by our group and other researchers. Potentiometric detection based on ion-selective electrode is a simplest method, offers several advantages such as fast and easy preparation procedures, simple instrumentation, relatively fast response time, wide concentration range, reasonable selectivity, low cost and may also be suitable for online analysis. In view of such advantages, a number of Pd<sup>2+</sup> selective sensors have been reported using PVC membrane and coated wire-electrode [3,4]. These sensors have a limited use for determination of palladium ions due to their poor detection limit and narrow concentration range. The aim of present work is the development of selective and sensitive palladium ion-selective electrode. For this purpose cyclohexane based substituted Schiff base ionophores *N,N'*-bis(acetyl acetone) cyclohexanediamine (Fig. 1a, **L**<sub>1</sub>) and *N,N'*-bis(*o*-hydroxyacetophenone)-1,2-cyclohexanediamine (Fig. 1b, **L**<sub>2</sub>) have been synthesized and explored as a sensing materials to prepare palladium selective electrode. In the screening of response to two ionophores, it is found that **L**<sub>1</sub> is quite suitable for making a palladium(II) ion-selective electrode. The formation constant study shows that **L**<sub>1</sub> forms strong complex with palladium ( $\log K_f = 9.8$ ) as compared to **L**<sub>2</sub> ( $\log K_f = 6.8$ ) and relatively weaker complex with many metals as

\* Corresponding author. Fax: +91 1332273560.

E-mail addresses: [vinodfcy@iitr.ernet.in](mailto:vinodfcy@iitr.ernet.in), [vinodfcy@gmail.com](mailto:vinodfcy@gmail.com) (V.K. Gupta).



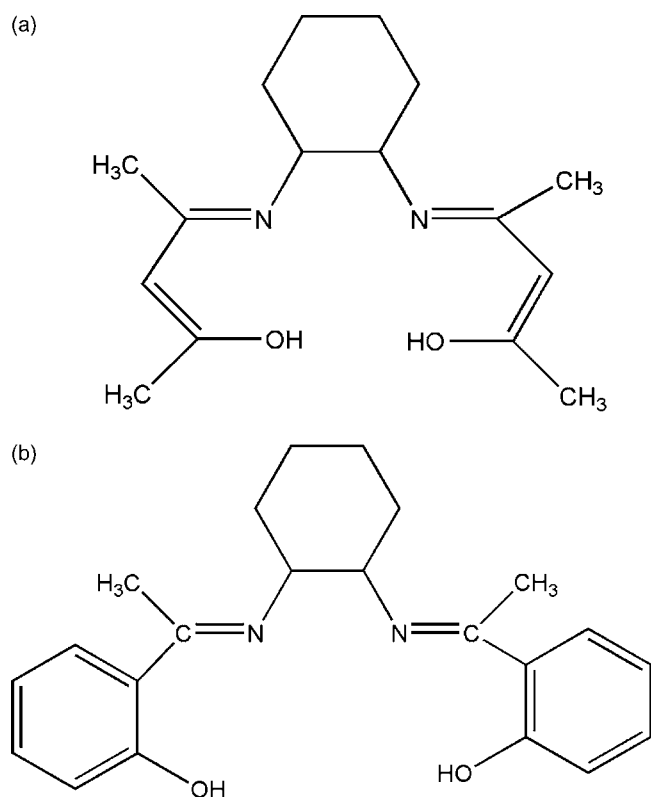


**Fig. 1.** (a) Structure of ionophore *N,N'*-bis(acetylacetonate) cyclohexanediimine (**L<sub>1</sub>**). (b) Structure of ionophore *N,N'*-bis(*o*-hydroxy acetophenone)-1,2-cyclohexanediimine (**L<sub>2</sub>**).

reported in Table 1. Thus it is reasonable to state that membrane of **L<sub>1</sub>** will act as more selective sensor for Pd<sup>2+</sup> in comparison to **L<sub>2</sub>**. The PVC-based membranes of **L<sub>1</sub>** and **L<sub>2</sub>** as ionophores have been prepared and investigated for Pd<sup>2+</sup>. The comparative results obtained using two ionophores are analyzed and discussed in this paper.

## 2. Experiment

### 2.1. Reagent and solution

Acetylacetonate, 1,2-cyclohexanediamine and *o*-hydroxyacetophenone were purchased from Aldrich and used as received.

**Table 1**  
Formation constants of Schiff base–metal complexes.

Metal ions	Formation constants (log β <sub>L<sub>n</sub></sub> ) <sup>a</sup>	
	Schiff base ( <b>L<sub>1</sub></b> )	Schiff base ( <b>L<sub>2</sub></b> )
Pt <sup>2+</sup>	7.2	6.1
Mn <sup>2+</sup>	6.8	5.4
Co <sup>2+</sup>	6.5	4.7
Pb <sup>2+</sup>	6.1	4.9
Cu <sup>2+</sup>	6.0	5.2
Hg <sup>2+</sup>	5.6	4.7
Ni <sup>2+</sup>	6.4	5.2
Zn <sup>2+</sup>	5.7	5.0
Sn <sup>2+</sup>	4.8	4.0
Ca <sup>2+</sup>	6.5	5.8
Ba <sup>2+</sup>	7.4	4.8
Mg <sup>2+</sup>	6.1	5.3
Fe <sup>3+</sup>	5.8	3.8
Al <sup>3+</sup>	5.2	3.5
Na <sup>+</sup>	4.1	2.9
K <sup>+</sup>	4.5	3.1
Pd <sup>2+</sup>	9.8	6.8

<sup>a</sup> n = 5, RSD% < 1.2.

Analytical-grade *o*-nitrophenyloctylether (*o*-NPOE), sodium triphenyl borate and high molecular weight polyvinyl chloride (PVC) were purchased from Fluka and used as received. Chloronaphthalene (CN) and Tri-*n*-butyl phosphate (TBP) were obtained from Highmedia laboratories (Mumbai, MH, India); dioctylphthalate (DOP), di-*n*-butylphthalate (DBP) and dibutyl butylphosphonate (DBBP) were obtained from SD-Fine Chem. Limited (Mumbai, MH, India). Palladium dichloride (Merck) was used without further purification. Doubly distilled water was used for the preparation of metal salts solutions of different concentrations by diluting stock solution (0.1 M).

### 2.2. Synthesis of ionophore

#### 2.2.1. Synthesis of *N,N'*-bis(acetylacetonate) cyclohexanediimine (**L<sub>1</sub>**)

The ionophore [*N,N'*-bis(acetylacetonate) cyclohexanediimine] was synthesized as previously described [5], by refluxing 0.1 mol of acetyl acetone and 0.05 mol of 1,2-cyclohexanediamine for 30 min, and cooling the reaction mixture. The compound was separated as a colorless powder and recrystallized twice from ethanol. The compound was stable at room temperature. Anal. Calc. for [C<sub>16</sub>H<sub>26</sub>N<sub>2</sub>O<sub>2</sub>]: C, 69.03; H, 9.41; N, 10.06; O, 11.49 (%). Found: C, 69.07; H, 9.35; N, 10.05; O, 11.50 (%). The <sup>1</sup>H NMR (CDCl<sub>3</sub>) exhibited signals at: δ<sub>H</sub> 1.0–1.7 (s, 12H, CH<sub>3</sub>), 1.2–1.6 (m, 8H, CH<sub>2</sub>), 3.1 (t, 2H, CH), 5.2 (s, 2H, C=CH–), 15.14 (s, 2H, OH).

#### 2.2.2. Synthesis of *N,N'*-bis(*o*-hydroxyacetophenone)-1,2-cyclohexanediimine (**L<sub>2</sub>**)

The ionophore [*N,N'*-bis(*o*-hydroxyacetophenone)-1,2-cyclohexanediimine] was synthesized as previously described [6], by refluxing 0.1 mol of *o*-hydroxyacetophenone and 0.05 mol of 1,2-cyclohexanediamine for 30 min, and cooling the reaction mixture. The compound was separated as a yellow powder and recrystallized twice from ethanol. The compound was stable at room temperature. Anal. Calc. for [C<sub>22</sub>H<sub>26</sub>N<sub>2</sub>O<sub>2</sub>]: C, 75.40; H, 7.48; N, 7.99 (%). Found: C, 75.35; H, 7.25; N, 7.90 (%). The <sup>1</sup>H NMR (CDCl<sub>3</sub>) exhibited signals at: δ<sub>H</sub> 1.90–1.50 (m, 8H, CH<sub>2</sub>CH<sub>2</sub>), 3.07 (s, 6H, CH<sub>3</sub>), 3.90 (dd, 2H, CH), 7.37–6.70 (m, 8H, Ar–H), 16.50 (s, 2H, OH).

### 2.3. Fabrication of PVC membranes and sandwich PVC membranes

The general procedure to prepare PVC-based membranes were to mix thoroughly an appropriate amounts of ionophores (**L<sub>1</sub>** and **L<sub>2</sub>**), cation excluder (NaTBP), plasticizers (CN, DOP, DBP, DBBP, TBP and *o*-NOPE) and PVC in THF (10 ml). After complete mixing of all components, the homogeneous mixture was obtained and the resulting mixture was concentrated by evaporation of THF up to 4 mL. Now the oily viscous mixture was obtained and poured into polyacrylate rings placed on a smooth glass plate and it was covered by glass plate. The solution was then allowed to evaporate for 24 h at room temperature. Transparent membranes of about ~0.5 mm thickness were obtained, which were then cut to sized and glued to one end of a 1.5 cm diameter Pyrex glass tube with araldite. The molar ratio of membrane components, contact time and concentration of equilibrating solution were optimized so that the potential recorded were reproducible and stable within the standard deviation. The membrane that gave best performance and reproducible result was selected for detailed studies.

The sandwich membrane was prepared by pressing two individual membranes (ordinarily one without ionophore and one with the same components and an additional ionophore) together immediately after blotting them individually dry with tissue paper. The obtained sandwich membrane was visibly checked for air bubbles before mounting on electrode body with the ionophore-containing

**Table 2**  
Optimization of membrane composition of palladium sensors.

Sensor no.	Composition (mg, w/w)				Slope (mV decade <sup>-1</sup> of activity)	Linear working range (M)	Detection limit (M)	Response time (s)	Lifetime (months)
	Ionophore	NATBP	Plasticizer	PVC					
1	L <sub>1</sub> , 5	5	300, CN	150	25.1 ± 0.3	1.0 × 10 <sup>-6</sup> to 1.0 × 10 <sup>-1</sup>	3.1 × 10 <sup>-7</sup>	30	2
2	L <sub>1</sub> , 5	5	300, DBP	150	27.2 ± 0.3	5.6 × 10 <sup>-7</sup> to 1.0 × 10 <sup>-1</sup>	1.3 × 10 <sup>-7</sup>	25	2.5
3	L <sub>1</sub> , 5	5	300, TBP	150	28.1 ± 0.2	1.0 × 10 <sup>-7</sup> to 1.0 × 10 <sup>-1</sup>	3.9 × 10 <sup>-8</sup>	15	3.5
4	L <sub>1</sub> , 3	5	300, DBBP	150	30.0 ± 0.2	5.0 × 10 <sup>-7</sup> to 1.0 × 10 <sup>-1</sup>	1.0 × 10 <sup>-7</sup>	20	3.0
5	L <sub>1</sub> , 5	5	300, DOP	150	32.3 ± 0.1	1.0 × 10 <sup>-6</sup> to 1.0 × 10 <sup>-1</sup>	1.7 × 10 <sup>-7</sup>	23	3.5
6	L <sub>1</sub> , 5	5	300, <i>o</i> -NPOE	150	29.1 ± 0.3	1.0 × 10 <sup>-8</sup> to 1.0 × 10 <sup>-1</sup>	4.0 × 10 <sup>-9</sup>	10	4
7	L <sub>2</sub> , 5	5	300, CN	150	27.0 ± 0.4	1.0 × 10 <sup>-5</sup> to 1.0 × 10 <sup>-1</sup>	2.8 × 10 <sup>-6</sup>	32	2.7
8	L <sub>2</sub> , 5	5	300, DBP	150	26.4 ± 0.1	5.6 × 10 <sup>-6</sup> to 1.0 × 10 <sup>-1</sup>	5.4 × 10 <sup>-7</sup>	26	2.3
9	L <sub>2</sub> , 5	5	300, TBP	150	29.2 ± 0.2	1.0 × 10 <sup>-6</sup> to 1.0 × 10 <sup>-1</sup>	1.7 × 10 <sup>-7</sup>	18	3.2
10	L <sub>2</sub> , 5	5	300, DBBP	150	30.0 ± 0.3	5.6 × 10 <sup>-6</sup> to 1.0 × 10 <sup>-1</sup>	3.9 × 10 <sup>-7</sup>	20	2.8
11	L <sub>2</sub> , 5	5	300, DOP	150	31.1 ± 0.2	1.0 × 10 <sup>-6</sup> to 1.0 × 10 <sup>-1</sup>	5.7 × 10 <sup>-7</sup>	23	3.0
12	L <sub>2</sub> , 5	5	300, <i>o</i> -NPOE	150	29.3 ± 0.1	1.0 × 10 <sup>-7</sup> to 1.0 × 10 <sup>-1</sup>	5.6 × 10 <sup>-8</sup>	14	3.8

segment facing the sample solution. The combined segmented membrane was then rapidly mounted on to the electrode body for further equilibration and potential measurements.

#### 2.4. Equilibration of membranes and potential measurements

The membranes were equilibrated for 2 days in 1.0 × 10<sup>-1</sup> M PdCl<sub>2</sub> solution. The potential were measured by varying the concentration of PdCl<sub>2</sub> in test solution in the range of 1.0 × 10<sup>-10</sup> to 1.0 × 10<sup>-1</sup> M. The standard PdCl<sub>2</sub> solutions were obtained by the gradual dilution of 0.1 M PdCl<sub>2</sub> stock solution. The best result was obtained when the inner electrolyte was 0.1 M PdCl<sub>2</sub> + 5.0 × 10<sup>-1</sup> Na<sub>2</sub>EDTA M [7–8]. This may be due to the decreasing zero-current ion fluxes from the membrane into the sample. The potential measurement was carried out at room temperature using the saturated calomel electrodes (SCE) as reference electrode with the following assembly:

SCE | test solution | PVC membrane | 0.1 M PdCl<sub>2</sub> M + 5.0 × 10<sup>-1</sup> Na<sub>2</sub> EDTA M | SCE

### 3. Results and discussion

#### 3.1. Optimization of membrane composition

The composition of PVC membrane affected the selectivity, linearity and sensitivity of the ionophore and it was optimized by varying the ratio of ionophore, plasticizer and additive used [9–11]. The potentials of membrane of two Schiff bases L<sub>1</sub> and L<sub>2</sub> are investigated as a function of palladium ion concentration and the best result are presented in Table 2. It was observed that the membranes incorporating the ingredients with composition: ionophores (L<sub>1</sub> or L<sub>2</sub>): NaTBP: Plasticizer: PVC as (mg, w/w) of 5:5:300:150, displayed the linear potential response and best performance for palladium ions. This indicates from composition of membrane a synergism between lipophilicity and polarity, where best results for detection limit was obtained when these properties reach an intermediate value.

#### 3.2. Effect of plasticizer

The nature of plasticizer improves the sensitivity and stability of sensors. For a plasticizer to be very adequate for its use in the polymeric membrane ion-selective electrode, it should gather certain properties and characteristics such as having lipophilicity, high molecular weight, low vapor pressure and high capacity to dissolve the substrate and other additives present in the polymeric membrane [12]. We have tested several membranes of varying compositions and different plasticizers CN, DOP, DBP, DBBP, TBP and *o*-NPOE in PVC matrix and some of the best results obtained are shown in Figs. 2 and 3. It is clear from Table 2 and

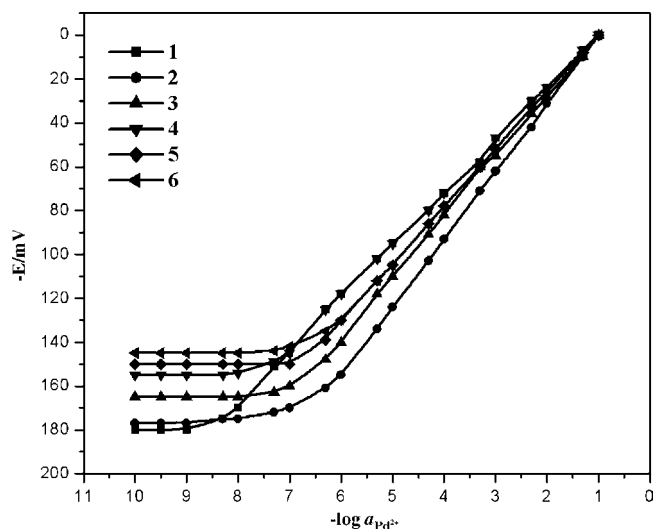


**Fig. 2.** Variation of membrane potential with activity of Pd<sup>2+</sup> ions, of PVC-based membranes of L<sub>1</sub> with plasticizers (1) *o*-NPOE, (2) DBP, (3) DBBP, (4) DOP, (5) TBP and (6) CN.

Figs. 2 and 3 that the best results were obtained with the sensors prepared by using *o*-NPOE as plasticizer. The values of detection limit obtained, with respect to ionophore L<sub>1</sub> and different plasticizers has the following order: *o*-NPOE (4.0 × 10<sup>-9</sup> M) > TBP

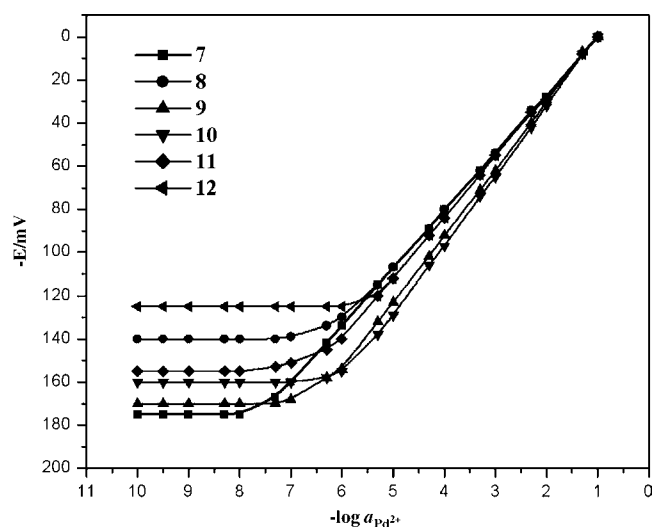


**Fig. 3.** Variation of membrane potential with activity of Pd<sup>2+</sup> ions, of PVC-based membranes of L<sub>2</sub> with plasticizers (7) *o*-NPOE, (8) DBP, (9) DBBP, (10) DOP, (11) TBP and (12) CN.

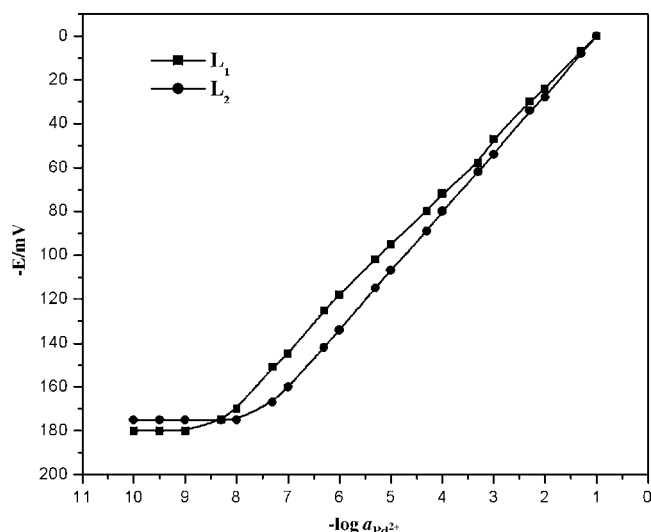


Fig. 4. Calibration plot of the palladium ion-electrode with ionophore  $L_1$  and  $L_2$ .

$(3.9 \times 10^{-8} \text{ M}) > \text{DBBP} (1.0 \times 10^{-7} \text{ M}) > \text{DBP} (1.3 \times 10^{-7} \text{ M}) > \text{DOP} (1.7 \times 10^{-7} \text{ M}) > \text{CN} (3.1 \times 10^{-7} \text{ M})$  and ionophore  $L_2$  and different plasticizers has the following order:  $o\text{-NPOE} (5.6 \times 10^{-8} \text{ M}) > \text{TBP} (1.7 \times 10^{-7} \text{ M}) > \text{DBBP} (3.9 \times 10^{-7} \text{ M}) > \text{DBP} (5.4 \times 10^{-7} \text{ M}) > \text{DOP} (5.7 \times 10^{-7} \text{ M}) > \text{CN} (2.8 \times 10^{-6} \text{ M})$ . Hence, the results show that as the value of dielectric constant of plasticizers decreases, the detection limit of sensors also decreases. The values of detection limit for DOP and DBP are approximately same.

### 3.3. Working concentration range and slope

The result presented in Table 2 and Fig. 4, indicate that the best electrode (no. 6) based on  $L_1$  exhibits nice Nernstian slope ( $29.1 \pm 0.3 \text{ mV decade}^{-1}$  of activity) over a wide concentration range of  $1.0 \times 10^{-8}$  to  $1.0 \times 10^{-1} \text{ M}$  with detection limit  $4.0 \times 10^{-9} \text{ M}$  while electrode (no. 12) based on  $L_2$  exhibits a Nernstian slope ( $29.3 \pm 0.1 \text{ mV decade}^{-1}$  of activity) and concentration range  $1.0 \times 10^{-7}$  to  $1.0 \times 10^{-1} \text{ M}$  with limit of detection  $5.6 \times 10^{-8} \text{ M}$ . The values of slopes correspond to those expected by Nernst for divalent cation. The most sensible values of slope and working concentration range correspond to sensors constructed by using  $o\text{-NPOE}$ . This indicates the solvent medium of  $o\text{-NPOE}$  is probably providing the best complexation environment between palladium ions and their respective carriers.

### 3.4. Lifetime of proposed sensor

The high lipophilicity of ionophore and plasticizer ensure stable potentials and longer lifetime [13] for the membrane. Among all the membranes prepared, the lifetime of membrane sensor based on  $o\text{-NPOE}$  and  $L_1$  (no. 6) found to be 4, and 3.8 months for sensor based on  $o\text{-NPOE}$  and  $L_2$  (sensor no. 12). As shown in Table 2, not all the prepared sensors have a long lifetime, when compared with the time of experiment. The best values were obtained for  $o\text{-NPOE}$  and TBP, since they have grater polarity. During this period, changes in potential were within the standard deviation ( $\pm 0.2 \text{ mV}$ ). However, it is important to emphasize that the membrane were stored in a  $0.1 \text{ M Pd}^{2+}$  solution when not in use.

### 3.5. Effect of pH change and non-aqueous solvent

The pH effect on the potential response was investigated over the pH range 1.5–8.0 for  $1.0 \times 10^{-3}$  and  $1.0 \times 10^{-4} \text{ M Pd}^{2+}$  solution (Fig. 5). The working range was calculated by varying the pH of the

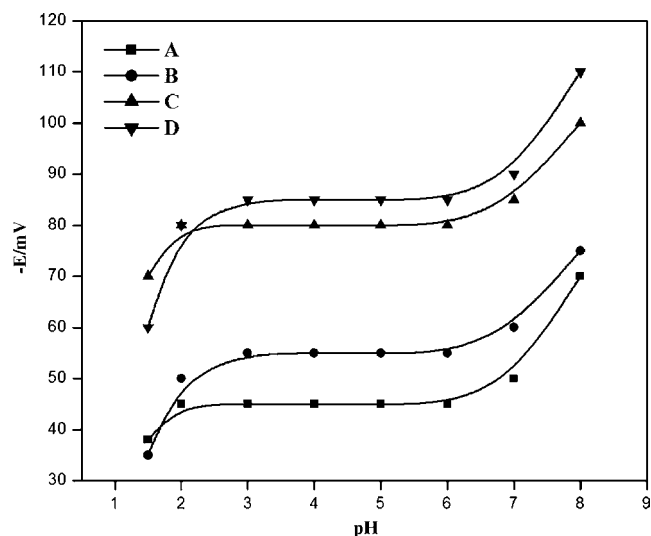


Fig. 5. Effect of pH on cell potential of sensor no. 6 (A)  $1.0 \times 10^{-3} \text{ M}$ , (C)  $1.0 \times 10^{-4} \text{ M}$  and sensor no. 12 at (B)  $1.0 \times 10^{-3} \text{ M}$ , (D)  $1.0 \times 10^{-4} \text{ M Pd}^{2+}$  solutions.

test solution with nitric acid or sodium hydroxide. As can see from Fig. 5, the potential is independent of the pH range 2.0–6.0 and 2.5–6.0 for sensor nos. 6 and 12, based on  $L_1$  and  $L_2$ , respectively. Therefore, the same was taken as the working range of the sensors assemblies. The change in potential at higher pH values may be due to hydrolysis of the  $\text{Pd}^{2+}$  ion, while at lower pH the values  $\text{H}^+$  ion interfering in the charge transport of membrane.

The performance of the sensor no. 6 was further assessed in partial non-aqueous media, i.e. methanol–water, ethanol–water and acetonitrile–water mixture. The results obtained are compiled in Table 3 and show that up to 20% non-aqueous content no significant change occurs in the slope and working concentration of the sensor is significantly reduced, and thus the sensor can only be utilized in mixtures containing up to 20% non-aqueous content.

### 3.6. Dynamic response time behavior of the proposed electrode

Dynamic response time is an important factor for palladium sensitive sensor. In this study, the practical response time has been recorded (for sensor no. 6) by changing solutions with different palladium ion concentrations. The measurement sequence was from the lower ( $1.0 \times 10^{-6} \text{ M}$ ) to the higher ( $1.0 \times 10^{-3} \text{ M}$ ) concentration.

Table 3

Performance of sensor no. 6 in partially non-aqueous medium.

Non-aqueous content (% v/v)	Working concentration range (M)	Slope ( $\text{mV decade}^{-1}$ activity)
0	$1.0 \times 10^{-8}$ to $1.0 \times 10^{-1}$	$29.3 \pm 0.1$
Methanol		
10	$1.0 \times 10^{-8}$ to $1.0 \times 10^{-1}$	$29.3 \pm 0.1$
20	$1.0 \times 10^{-8}$ to $1.0 \times 10^{-1}$	$29.1 \pm 0.2$
30	$4.2 \times 10^{-7}$ to $1.0 \times 10^{-1}$	$27.1 \pm 0.3$
35	$1.5 \times 10^{-7}$ to $1.0 \times 10^{-1}$	$25.1 \pm 0.3$
Ethanol		
10	$1.0 \times 10^{-8}$ to $1.0 \times 10^{-1}$	$29.3 \pm 0.1$
20	$6.1 \times 10^{-8}$ to $1.0 \times 10^{-1}$	$29.3 \pm 0.1$
30	$3.8 \times 10^{-7}$ to $1.0 \times 10^{-1}$	$27.6 \pm 0.4$
35	$5.2 \times 10^{-6}$ to $1.0 \times 10^{-1}$	$24.6 \pm 0.3$
Acetonitrile		
10	$1.0 \times 10^{-8}$ to $1.0 \times 10^{-1}$	$29.3 \pm 0.1$
20	$5.3 \times 10^{-8}$ to $1.0 \times 10^{-1}$	$29.3 \pm 0.1$
30	$5.3 \times 10^{-7}$ to $1.0 \times 10^{-1}$	$28.3 \pm 0.2$
35	$5.3 \times 10^{-7}$ to $1.0 \times 10^{-1}$	$25.3 \pm 0.1$

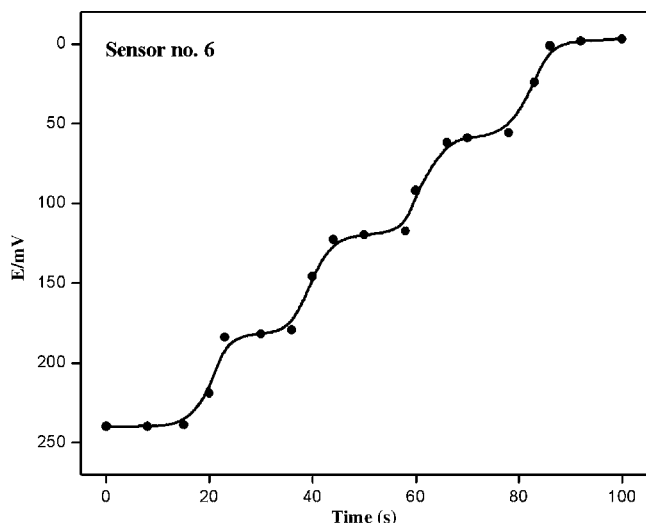


Fig. 6. Dynamic response of the membrane sensor (no. 6) based on  $N,N'$ -bis(acetylacetonate) cyclohexanediimine ( $L_1$ ).

The actual potential versus time traces is shown in Fig. 6. As it is seen, the electrode reached the equilibrium response in a very short time of about 10 s. To evaluate the reversibility of the electrode, a similar procedure in the opposite direction was adopted. The measurements have been performed in the sequence of high-to-low from ( $1.0 \times 10^{-4}$  to  $1.0 \times 10^{-5}$  M) sample concentrations. The results showed that, the potentiometric response of the electrodes was reversible; although the time needed to reach equilibrium values (40 s) were longer than that of low-to high sample concentrations.

### 3.7. Determination of binding constants

The binding constant of the ion–ionophore complex within the membrane phase is a very important parameter that dictates the practical selectivity of the sensor. In this method, two membrane segments are fused together, with only one containing the ionophore, to give a concentration-polarized sandwich membrane. A membrane potential measurement of this transient condition reveals the ion activity ratio at both interfaces, which translates into the apparent binding constants of the ion–ionophore complex [14]. In this method complex formation constants obtained by neglecting

Table 4

Selectivity coefficient values ( $-\log K_{Pd^{2+}, B}^{Pot}$ ) of sensor nos. 6 and 12 of the membranes of  $L_1$  and  $L_2$ , respectively.

Interfering ions (B)	Selectivity coefficients [ $-\log K_{Pd^{2+}, B}^{Pot}$ ] <sup>a</sup> by FIM method	
	Sensor no. 6	Sensor no. 12
Mn <sup>2+</sup>	3.50	3.10
Co <sup>2+</sup>	3.45	3.12
Pb <sup>2+</sup>	2.80	2.50
Cu <sup>2+</sup>	2.60	2.30
Hg <sup>2+</sup>	2.78	2.47
Ni <sup>2+</sup>	2.40	2.00
Zn <sup>2+</sup>	2.41	2.22
Sn <sup>2+</sup>	4.20	3.80
Ca <sup>2+</sup>	4.30	3.90
Ba <sup>2+</sup>	2.62	2.30
Mg <sup>2+</sup>	2.25	2.00
Fe <sup>3+</sup>	3.15	2.95
Al <sup>3+</sup>	3.10	2.30
Na <sup>+</sup>	2.30	2.28
K <sup>+</sup>	2.80	2.50
Pt <sup>2+</sup>	3.0	2.60

<sup>a</sup>  $n = 5$ , RSD% < 1.5.

Table 5  
Comparison of the potentiometric parameters of the proposed palladium sensor (sensor no 6) with the literature reported palladium selective sensor.

Ref. no.	Ionophore name	Linear range (M)	Slope (mV decade <sup>-1</sup> of activity)	pH range	Selectivity coefficients ( $-\log K_{Pd^{2+}, B}^{Pot}$ )	Response time (s)
Proposed sensor	$N,N'$ -Bis(acetylacetonate) cyclohexanediimine ( $L_1$ )	$1.0 \times 10^{-8}$ to $1.0 \times 10^{-1}$	$29.1 \pm 0.3$	2.0–6.0	Pt <sup>2+</sup> (3.0), Mn <sup>2+</sup> (3.50), Co <sup>2+</sup> (3.45), Pb <sup>2+</sup> (2.80), Cu <sup>2+</sup> (2.60), Hg <sup>2+</sup> (2.78), Ni <sup>2+</sup> (2.40), Zn <sup>2+</sup> (2.41), Sn <sup>2+</sup> (4.20), Ca <sup>2+</sup> (4.30), Ba <sup>2+</sup> (2.62), Fe <sup>3+</sup> (3.15), Al <sup>3+</sup> (3.10), Na <sup>+</sup> (2.30), K <sup>+</sup> (3.0)	10
[3]	Hexadecylpyridiniumtetrabromopalladate	$1.0 \times 10^{-8}$ to $1.0 \times 10^{-3}$	$29.8 \pm 0.8$	3.0–8.0	Pt <sup>2+</sup> (1.6), Mn <sup>2+</sup> (3.0), Co <sup>2+</sup> (3.4), Pb <sup>2+</sup> (2.65), Cu <sup>2+</sup> (2.48), Hg <sup>2+</sup> (2.6), Ni <sup>2+</sup> (2.3), Zn <sup>2+</sup> (2.48), Sn <sup>2+</sup> (4.30), Ca <sup>2+</sup> (4.6), Ba <sup>2+</sup> (2.6), Fe <sup>3+</sup> (3.6), Al <sup>3+</sup> (3.6), NO <sub>3</sub> <sup>-</sup> (2.6), ClO <sub>4</sub> <sup>-</sup> (3.0), CN <sup>-</sup> (2.0), SCN <sup>-</sup> (2.20), SO <sub>4</sub> <sup>2-</sup> (2.65)	30

**Table 6**  
Determination of palladium in spiked water samples using proposed sensor no. 6.

Sample	Added ( $\mu\text{g L}^{-1}$ )	Found by proposed sensor ( $\mu\text{g L}^{-1}$ )	Found by AAS ( $\mu\text{g L}^{-1}$ )	Recovery <sup>a</sup> $\pm$ S.D. (%)
Roorkee City	8	8.05	8.86	100 $\pm$ 0.2
	100	101.05	99.52	99.9 $\pm$ 0.1
	400	402.0	400.32	100 $\pm$ 0.1

<sup>a</sup>  $n = 5$ , RSD% < 1.2.

ion pairing. As reported, the membrane potential  $E_M$  is determined by subtracting the cell potential for a membrane without ionophore from that for the sandwich membrane. The formation constant is then calculated from the following equation:

$$\beta_{IL_n} = \left( L_T - \frac{nR_T}{Z_I} \right)^{-n} \exp \left( \frac{E_M Z_I F}{RT} \right) \quad (2)$$

where  $L_T$  is the total concentration of ionophore in the membrane segment,  $R_T$  is the concentration of lipophilic ionic site additives,  $n$  is the ion–ionophore complex stoichiometry, and  $R$ ,  $T$  and  $F$  are the gas constant, the absolute temperature, and the Faraday constant. The ion  $I$  carries a charge of  $Z_I$ . The determined formation constants ( $\log \beta_{IL_n}$ ) for the examined different complexes were recorded in Table 1. The elapsed time between sandwich fusion and exposure to electrolyte was typically <1 min. The potential was recorded as the mean of the last minute of a 5 min measurement period in the appropriate salt solution. The potential of such sandwich membranes remains free of diffusion-induced potential drifts for about 20 min. Standard deviations were obtained based on the measurements of sets of at least three replicate membrane disks that were made from the same parent membrane. A careful analysis of the data in Table 1 reveals that palladium ion has significant cation-binding characteristics.

### 3.8. Potentiometric selectivity

The Potentiometric selectivity of PVC sensors is one of the most characteristic parameter that determines the efficacy of sensor. Thus, the selectivity studies were carried out only for sensors nos. 6 and 12 which exhibit the best performance in terms of working concentration range, slope, response time and lifetime. Different methods of selectivity determination have been found in literature. In present study, the selectivity coefficient ( $K_{Pd^{2+},B}^{Pot}$ ) has been evaluated using modified form of fixed interference method [15] at  $1.0 \times 10^{-2}$  M concentration of interfering ions as per IUPAC recommendation. In this method, the electromotive force (emf) was measured for solutions of constant activity of the interfering ion,  $a_B$  and varying activity of the primary ion,  $a_A$  in a cell comprising an ion-selective electrode and a reference electrode (ISE cell). The emf values obtained are plotted versus the logarithm of the activity of the primary ion. The intersection of the extrapolated linear portions of the plot indicates the value of  $a_A$  that is to be used to calculate  $K_{Pd^{2+},B}^{Pot}$  from the following equations:

$$K_{A,B}^{pot} = \frac{a_A}{(a_B)^{Z_A/Z_B}}$$

where both  $Z_A$  and  $Z_B$  have the positive charges of both ions.

It is seen from Table 4 and Fig. 7 that the selectivity coefficients determined are much smaller than 1.0. Thus, both electrodes are substantially selective to  $Pd^{2+}$  ions over the all interfering ions studied and listed in Table 4. Thus, it is clear from the values of selectivity coefficients that it is possible to determine  $Pd^{2+}$  in the presence of interfering ions at a concentration level smaller or slightly higher than the  $pd^{2+}$  concentration. Of the two sensors, the selectivity of the sensor no. 6 was found to be better (Table 5) and it has been seen that the selectivity of proposed sen-

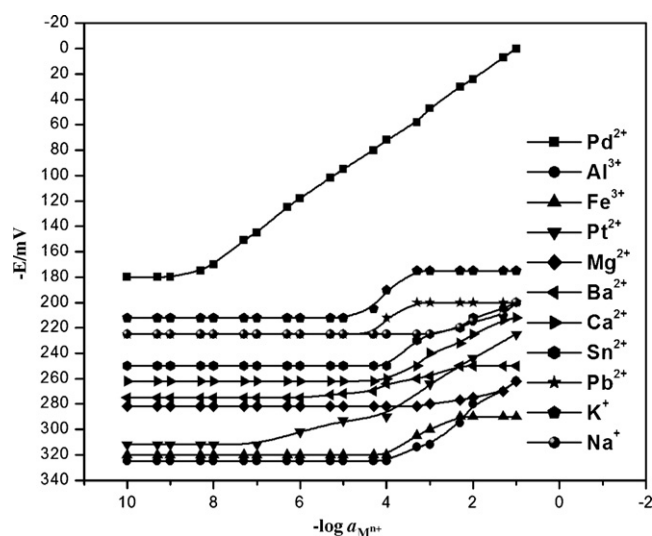


**Fig. 7.** Potential response calibration curves of ion-selective membrane sensor (no. 6) for various metal ions.

sor towards palladium is better for most of the cations as compared to reported sensor and thus it is superior. As sensor no. 6 is better than sensor no. 12 and to other reported on palladium (Table 5) in terms of wider concentration range, high selectivity and Nernstian compliance.

### 3.9. Analytical application

Using ion-selective sensor is very convenient for the analysis of sample with difficult matrices, such as urine, river water and industrial wastewater. The membrane sensor was successfully used in the potentiometric determination of palladium in spiked water samples. The samples were prepared by addition of 8, 100 and 400  $\mu\text{g}$  palladium per liter in tap water of Roorkee city and analysis was done after adjustment pH 4. The data presented in Table 6, shows that the results obtained by sensor are comparable with atomic absorption spectrometer and recovery is 99.9–100.

## 4. Conclusion

The developments of PVC-based membranes of two ionophores  $L_1$  and  $L_2$  have been studied. They are selective sensors for  $Pd^{2+}$  ions. The sensor (no. 6) based on  $N,N'$ -bi(acetylaceton) cyclohexanediimine ( $L_1$ ), having membrane composition PVC: *o*-NPOE:ionophore ( $L_1$ ):NaTPB ratio (% w/w) of 150:300:5:5 get the best performance. It respond linearly over a wider linear working concentration range  $1.0 \times 10^{-8}$  to  $1.0 \times 10^{-1}$  M, Nernstian slope of  $29.1 \pm 0.3$  mV decade<sup>-1</sup> of activity, lower detection limit  $4.0 \times 10^{-9}$  M and fast response time <10 s. The electrode was found to perform satisfactory over the pH range 2.0–6.0 and the presence of 20% non-aqueous content. Comparison of this electrode and reported electrode in Table 4 was shown that sensor no. 6 is superior in terms of wider concentration range, lower detection limit and

fast response time. However, the electrode based on ionophore **L**<sub>2</sub> is selective for palladium ion but they show narrow concentration rangel and higher detection limit.

### Acknowledgement

One of the authors Ram Avatar Sharma is thankful to Ministry of Human Resource Development (MHRD), New Delhi, India, for financial support.

### References

- [1] W.P. Griffith, *Platinum Met. Rev.* 47 (4) (2003) 175.
- [2] W.H. Wollaston, *Philos. Trans. R. Soc. London, Ser. A* 94 (1804) 419.
- [3] M. Aghamohammadi, N. Alizadeh, *Anal. Chim. Acta* 480 (2003) 299.
- [4] K. Vytras, J. Kolous, B. Simickova, J. Cerna, I. Silena, *Anal. Chim. Acta* 209 (1988) 357.
- [5] P.J. McCarthy, R.J. Hovey, K. Ueno, A.E. Martell, *J. Am. Chem. Soc.* 77 (1955) 5820.
- [6] W.T. Gao, Z. Zheng, *Molecules* 7 (2002) 511.
- [7] T. Solkalski, A. Ceresa, M. Fibbiali, R. Zwickl, E. Bakker, E. Pretsch, *Anal. Chem.* 71 (1999) 1210.
- [8] T. Sokalski, A. Ceresa, T. Zwickl, E. Pretsch, *J. Am. Chem. Soc.* 119 (1997) 1134.
- [9] D. Siswanta, K. Nagatska, H. Yamada, K. Kumakura, H. Hisamoto, Y. Shichi, K. Toshima, K. Suzuki, *Anal. Chem.* 68 (1996) 4166.
- [10] N. Tavakkoli, M. Shamsipur, *Anal. Lett.* 29 (1996) 2269.
- [11] M. Javanbakht, M.R. Ganjali, H. Sharghi, M. Shamsipur, *Electroanalysis* 11 (1999) 81.
- [12] R. Eugster, T. Rosatzin, B. Rusterholz, B. Aebersold, U. Pedrazza, D. Ruegg, A. Schmid, U.E. Spinger, W. Simon, *Anal. Chim. Acta* 289 (1994) 1.
- [13] M. Telting-Diaz, E. Bakker, *Anal. Chem.* 73 (2001) 5582.
- [14] M. Yanming, E. Bakker, *Anal. Chem.* 71 (1999) 5279.
- [15] Y. Umezawa, P. Buhlmann, K. Umezawa, K. Tohda, S. Amemiya, *Pure Appl. Chem.* 72 (2000) 1851.



## $\beta$ -Sonogel-Carbon electrodes: A new alternative for the electrochemical determination of catecholamines

Nissrin Izaoumen<sup>a</sup>, Laura M. Cubillana-Aguilera<sup>b</sup>, Ignacio Naranjo-Rodríguez<sup>b</sup>,  
José L. Hidalgo-Hidalgo de Cisneros<sup>b,\*</sup>, Dounia Bouchta<sup>a</sup>,  
Khalid R. Temsamani<sup>a</sup>, José M. Palacios-Santander<sup>b</sup>

<sup>a</sup> University Abdelmalek Essaâdi, Department of Chemistry, Faculty of Sciences of Tétouan. Equipe de Recherche Electrochimie et Systèmes Interfaciaux (ERESI). M'Hannech II, B.P. 2121, 93002-Tétouan, Morocco

<sup>b</sup> Departamento de Química Analítica, Facultad de Ciencias, Universidad de Cádiz, Apdo.40, 11510 Puerto Real, Cadiz, Spain

### ARTICLE INFO

#### Article history:

Received 22 July 2008

Received in revised form

18 November 2008

Accepted 20 November 2008

Available online 27 November 2008

#### Keywords:

$\beta$ -Cyclodextrin

Catecholamines

Sonogel-Carbon electrodes

Adsorptive differential pulse voltammetry

Cyclic voltammetry

Neurotransmitters

### ABSTRACT

In this work, a new alternative for the electrochemical determination of catecholamines based on  $\beta$ -cyclodextrin-Sonogel-Carbon electrodes is reported. The incorporation of  $\beta$ -CD and graphite in the preparation of the Sonogel-Carbon material leads to a modification of the electrode surface properties which causes a significant increase in the oxidation peak current of biomolecules such as dopamine, L-epinephrine, D,L-norepinephrine and catechol. This phenomenon might be attributed to the formation of an inclusion complex between  $\beta$ -CD and the catecholamines. The amount of  $\beta$ -CD necessary to form the Sonogel electrode was studied and optimization of electrochemical parameters, perm selectivity and mechanical stability of the sensor are discussed. Scanning electron microscopy and electrochemical impedance spectroscopy measurements were employed to characterize the electrical parameters and the structural properties of the new electrode surface, respectively. Cyclic voltammetry (CV) and Adsorptive differential pulse voltammetry (AdDPV) measurements were also used to explore the electrochemical behaviour of the electrode versus the quoted catecholamines. The  $\beta$ -CD-Sonogel-Carbon electrode offers fast and linear responses towards dopamine, norepinephrine, epinephrine and catechol, with good and low detection limits: 0.164, 0.294, 0.699 and 0.059  $\mu\text{mol L}^{-1}$ , respectively.

© 2008 Elsevier B.V. All rights reserved.

### 1. Introduction

In literature, there are many papers reporting the manufacture process and analytical applications involving Sonogels. The Sonogel-Carbon materials were patented and described first by Hidalgo-Hidalgo de Cisneros et al. [1,2]. The fabrication procedure of Sonogel-Carbon materials is based on the use of sonocatalysis. Sonocatalysis consists of applying high-energy ultrasound directly to the precursors. In this way, ultrasonic cavitation is achieved, promoting hydrolysis with acidic water in the absence of any additional solvent. As a consequence of this, the time necessary to get a unique phase is reduced drastically, with regard to the classical sol-gel processes [3,4]. The mixture of Sonogel with spectroscopic grade graphite leads to the Sonogel-Carbon electrodes, which possesses especially favourable electrochemical properties.

Moreover, a good deal of modifiers has been included in this type of electrodes: polyethylenglycol (PEG), C-18, thioureas, hydro-

talchyte, polythiophene [5–14], or has been used to recover their surface: glutaraldehyde, alumine, PEG, nafion, and several enzymes, such as tyrosinase, laccase, peroxydase and acetylcholinesterase [15–18], in order to test their electrochemical and structural behaviour. In this paper, we have agglutinated  $\beta$ -cyclodextrins into the matrix of the Sonogel-Carbon electrodes.

Cyclodextrins (CDs) are cyclic oligomers composed of six, seven or eight glucopyranose units ( $\alpha$ ,  $\beta$  or  $\gamma$ -cyclodextrins, respectively), linked by  $\alpha(1-4)$  bonds [19]. They are widely studied in aqueous media as examples of host molecular receptors owing to their high affinity for hydrophobic molecules [20]. It is well known that CDs form inclusion complexes with a great variety of analytes having a diameter of 5–8 Å [21,22]. The ability to build inclusion complexes has been widely used in pharmaceuticals [23], as well as in analysis of organic and inorganic materials [24]. Current methods for the determination of these inclusion complexes include UV/vis spectrophotometry [25], IR spectroscopy [26], spectrofluorimetry [27], and electrochemical methods. Considerable attention has been paid to the electrochemical studies of inclusion complexes between cyclodextrins and electroactive species. Electrochemical techniques such as cyclic voltammetry [28], polarography [29,30],

\* Corresponding author. Tel.: +34 956 015355; fax: +34 956 016460.

E-mail address: [jluis.hidalgo@uca.es](mailto:jluis.hidalgo@uca.es) (J.L.H.-H. de Cisneros).

and pH determination [31], are particularly useful in the study of guest molecules lacking of a chromophore group for spectrophotometric measurement, but able to develop electroactivity.

Cyclodextrins, spread on an electrode surface, have proved to be effective and selective binding agents to form inclusion complexes with various compounds fulfilling structural requirements of the CDs cavity. This is important for electrochemical and electroanalytical applications [32].

As far as we know, the use of CDs to modify Sonogel-Carbon electrodes is a totally new challenge in the field of the chemically modified electrodes. The employment of  $\beta$ -cyclodextrin in electroanalysis is very frequent; particularly, it is used as modifier in carbon paste electrodes [33–36]. There is also a review about immobilization of cyclodextrins, their complexation abilities and analytical applications [32]. In this paper, we have carried out the incorporation of the monomeric form of  $\beta$ -CD into the electrode, instead of on its surface; in this way, no polymerization process was required.

In order to explore these possibilities further, in this paper we propose a new alternative, based on  $\beta$ -cyclodextrin-Sonogel-Carbon electrodes, for the electrochemical determination of several neurotransmitters belonging to catecholamines: catechol, dopamine (DA), norepinephrine (NE), and epinephrine (EN). The study was performed using two electroanalytical techniques: cyclic voltammetry (CV), and adsorptive differential pulse voltammetry (AdDPV). The objective was focused on the capability of the  $\beta$ -cyclodextrin-Sonogel-Carbon electrodes to detect better this neurotransmitters and thus to develop an original electroanalytical method for the determination of these substances. The optimization of all the analytical conditions are described and close attention is paid to the interferences due to ascorbic and uric acid, and some anions.

## 2. Experimental

### 2.1. Reagents and materials

Methyltrimethoxysilane (MTMOS) was from Merck (Darmstadt, Germany) and hydrochloric acid was from Panreac (Barcelona, Spain).

$\beta$ -Cyclodextrin (>99%) was obtained from Fluka (Switzerland). L-ascorbic acid (99%) was purchased from Sigma (Barcelona, Spain). L-dopamine, D,L-norepinephrine, epinephrine and catechol were all purchased from Aldrich (Milwaukee, USA) and used as received. Potassium phosphate dibasic-anhydrous and potassium phosphate monobasic used to obtain the phosphate buffer solution (PBS,  $0.1 \text{ mol l}^{-1}$ , about pH 7) were also purchased from Fluka. All reagents were of analytical grade or higher and used as received without further purification.

Graphite powder (spectroscopic grade RBW) was from SGL Carbon (Ringsdorf, Germany). Nanopure water was obtained by passing twice-distilled water through a Milli-Q system (18 M $\Omega$  cm, Millipore, Bedford, MA).

Glassy capillary tubes, i.d. 1.15 mm, were used as the bodies for the composite electrodes.

### 2.2. Instrumentation

The experimental work was realized in the Faculties of Sciences of Cadiz (Spain) and Tetouan (Morocco).

The electrochemical measurements were performed in two equipments, depending on the electrochemical technique employed. On one hand, the AdDPV and CV measurements were performed with an AutoLab PGSTAT20 (Ecochemie, Utrecht, The Netherlands) potentiostat/galvanostat interfaced with a personal

computer, using the AutoLab software GPES for waveform generation, data acquisition and elaboration. The experiments were carried out in a single-compartment three-electrode cell, at room temperature ( $25 \pm 1$  °C). The counter electrode was a platinum wire, and a silver/silver chloride/3 M KCl electrode was used as the reference. The composite-filled glass capillary tubes were used as the working electrode.

On the other hand, the electrochemical impedance spectroscopy (EIS) measurements were performed with a Voltalab<sup>®</sup> 10, type PGZ 100, from Radiometer (Villeurbanne, France). The impedance spectra were recorded using the same three-electrode cell setup described above. The initial frequency used was 100 kHz and the final frequency was 10 mHz, with an AC amplitude of 10 mV. A potential of 0 V was chosen in order to insure the stability of the films on the electrodes during the experiments.

The synthesis of the Sonogel-Carbon materials was carried out sonicating with a high power ultrasonic generator, SONICATOR 3000, from MISONIX (MISONIX, Inc. Farmingdale, NY, USA) (equipped with a 13 mm titanium tip), that provides a maximum power of 600 W.

Scanning electron microscopy (SEM) studies were carried out on a QUANTA 200 (FEI Company, Hillsboro, Oregon, USA) operating at 20 keV and equipped with a microanalyzer (EDAX) to perform energy dispersive spectroscopy (EDS).

### 2.3. Electrode preparation procedure

To prepare the Sonogel-Carbon materials modified with  $\beta$ -cyclodextrin, the following steps were carried out. On one hand, a mixture of 500  $\mu\text{l}$  of MTMOS and 100  $\mu\text{l}$  of 0.2 M HCl was insonated for 5 s, obtaining the Sonosol. On the other hand, different amounts of  $\beta$ -cyclodextrin and graphite powder (until 1 g) were homogenized, in order to obtain different percentages of modification. Afterwards, this mixture was added and adequately dispersed into the Sonosol, resulting in the  $\beta$ -cyclodextrin-Sonosol-Carbon. After several minutes, the resulting material acquires enough consistency to filled the capillary tubes, giving place to the  $\beta$ -cyclodextrin-Sonogel-Carbon electrodes. 24 h later, the surface of the electrodes could be polished and a copper wire inserted as the electrical contact into the electrodes, being ready to be used.

The electrochemical measurements were carried out using a phosphate buffer solution as the supporting electrolyte. The optimal instrumental parameters for AdDPV scans were as follows: potential range from +0.1 to +0.8 V; accumulation potential: 0.4 V; accumulation time: 120 s; modulation time: 0.06 s; interval time: 0.6 s; scan rate:  $10 \text{ mV s}^{-1}$ ; pulse amplitude: 100 mV. The optimal instrumental parameters for CV sweeps were as follows: range from 0 to +1 V; scan rate:  $50 \text{ mV s}^{-1}$ . Measurements were carried out under N<sub>2</sub> atmosphere when required.

## 3. Results and discussion

The preparation mode of the Sonogel Carbon electrodes is different from the one usually used with other solid electrodes and similar to the one used in carbon paste electrodes.

Comparing with carbon paste electrodes, the preparation of Sonogel-Carbon electrodes, although easy and fast, is a bit less easy. Nevertheless Sonogel-Carbon electrodes have several advantages versus carbon paste electrodes: the robustness against the presence of organic solvents is bigger; the amounts of reagents required to prepare an electrode are lesser; the regeneration of the surface is easy and allows that the same Sonogel-Carbon electrode is utilized for many times (a longer life time), with respect to carbon paste electrodes that are usually used only once. These advantages are complemented with their good reproducibility.



### 3.1. Influence of $\beta$ -cyclodextrin in the responses of the Sonogel-Carbon electrodes

Different percentages of  $\beta$ -cyclodextrin ( $\beta$ -CD) were added into the Sonosol matrix in order to study the influence of the modifier proportion in the  $\beta$ -CD-Sonogel-Carbon electrodes. The modification percentages tested were: 2.5%, 5% and 7%, w/w  $\beta$ -cyclodextrin:graphite. The AdDPV responses of the modified electrodes were compared with an unmodified Sonogel-Carbon electrode. The analyte employed was catechol ( $5 \times 10^{-4}$  M in the electrochemical cell).

The results obtained showed that the unmodified Sonogel-Carbon electrode had a poor and low response with respect to the modified electrodes. The presence of  $\beta$ -CD in the composite caused a spectacular increase in the response. The maximum response was for 5% of  $\beta$ -CD modification. For higher proportions, the current peak values were lower, the signal loosing resolution.

Furthermore, the increase up to 7%  $\beta$ -CD presented gelification troubles, affecting the structure of the basis material and, subsequently, the mechanical and electrochemical behaviour. This circumstance could explain the loss of signal resolution. The gelification troubles depend on the nature of the modifier and its modification percentage included in the graphite powder, as it has previously been reported [11].

From the previous discussion, the 5% modification of  $\beta$ -CD into the Sonogel-Carbon electrodes was kept as optimal for the subsequent experiments.

### 3.2. Influence of the supporting electrolyte

Several types of 0.1 M supporting electrolytes were also tested: phosphate buffer solution (PBS),  $H_2SO_4$ , KCl and Britton–Robinson, at different pH values depending on the chemical nature of the reagents used. The AdDPV responses of the modified electrodes versus catechol ( $5 \times 10^{-4}$  M) were compared using the different buffers. The results obtained were very similar in all cases; nevertheless, the PBS was chosen due to the following reasons: (1) it is very easy to manipulate their components and to prepare it, since the initial pH value of the solution is always approximately 7; (2) this pH value is the most appropriate to analyze biological samples as neurotransmitters, so there is no need to modify the pH of the buffer; (3) the use of buffers at very acid or basic pH values may deteriorate the analytes or the composite electrodes.

### 3.3. Influence of pulse amplitude, accumulation time and accumulation potential

Different values of pulse amplitude, accumulation time and accumulation potential were tested in order to determine their influence on the peak intensity values when analyzing the neurotransmitters: L-dopamine (DA), D,L-norepinephrine (NE), epinephrine (EN) and catechol (CA),  $5 \times 10^{-4}$  M in all cases. The electrochemical technique employed was AdDPV.

The effect of varying pulse amplitude and its influence on the peak height was studied. This electrochemical parameter ranged from 75 to 200 mV, the maximum having been found at 100 mV.

On one hand, the accumulation time ranged from 40 to 400 s. The peak intensity increased with the accumulation time, as Fig. 1 shows. However, the greatest increment occurs up to 80 s, after which a very slight increase is observed. For future analyses, 120 s were considered the optimum value of accumulation time, since saturation was observed for higher values.

On the other hand, the accumulation potential ranged from 0V to 500 mV. The maximum peak intensity value was found at 400 mV.

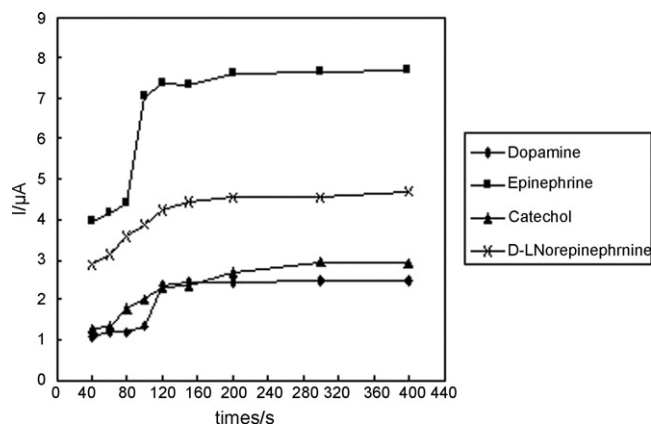


Fig. 1. Effect of the accumulation time on the peak height for  $5 \times 10^{-4}$  M of epinephrine, dopamine, D,L-norepinephrine and catechol in PBS buffer at pH 7.4 using a 5%  $\beta$ -CD-Sonogel-Carbon electrode.

Consequently, for successive experiments the optimal values reported here were utilized.

### 3.4. Studies of repeatability, reproducibility and stability

The repeatability was established carrying out six consecutive determinations of the different catecholamines in order to determine the peak intensity values in AdDPV measurements. The electrochemical parameters used were the optimized ones previously. The concentration of the analytes was  $4 \times 10^{-5}$  M. The relative standard deviations for DA, EN and NE were 1.8%, 0.9% and 3.9%, respectively. These results showed that the 5%  $\beta$ -CD-Sonogel-Carbon electrode has good repeatability.

In order to study both the reproducibility and the stability, a 5%  $\beta$ -CD-Sonogel-Carbon electrode was used, measuring daily  $4 \times 10^{-5}$  M solutions of DA. After the measurements, the electrode was stored at the lab environment. A relative standard deviation of 2.7% was obtained after 30 days of consecutive measurements.

### 3.5. Study of the electrochemical behaviour of neurotransmitters by cyclic voltammetry

Fig. 2 shows the cyclic voltammograms of 5 mM DA, EN and NE, measured at an unmodified Sonogel-Carbon electrode (a) and at a 5%  $\beta$ -CD-Sonogel-Carbon electrode (b). As it can be seen there are clear differences between the responses obtained from the two types of electrodes. No peak is observed with the unmodified electrode; nevertheless, the presence of the  $\beta$ -cyclodextrin in the structure of the electrodes causes the appearance of the redox activity of the neurotransmitters tested.

The results reported here for DA, EN and NE are better than those obtained by some of us using other type of electrodes [37]. The electrochemical peak parameters are summarized in Table 1. From these data, it can be concluded that, under these conditions, the 5%  $\beta$ -CD-Sonogel-Carbon electrode shows the following electrochemical kinetics: reversible or quasi-reversible behaviours with  $\Delta E_p$  of 346, 374, and 432 mV for DA, NE and EN, respectively.

Excepting for the borderline case of NE, the currents ratio of the oxidation and the reduction peaks is less than 1; this means that these compounds do not undergo complex reactions and they are stable at the modified electrode.

### 3.6. Influence of scan rate on the electrochemical responses

The scan rate has great influence on the peak current of cyclic voltammograms. In this paper, the effect of varying the scan rate for

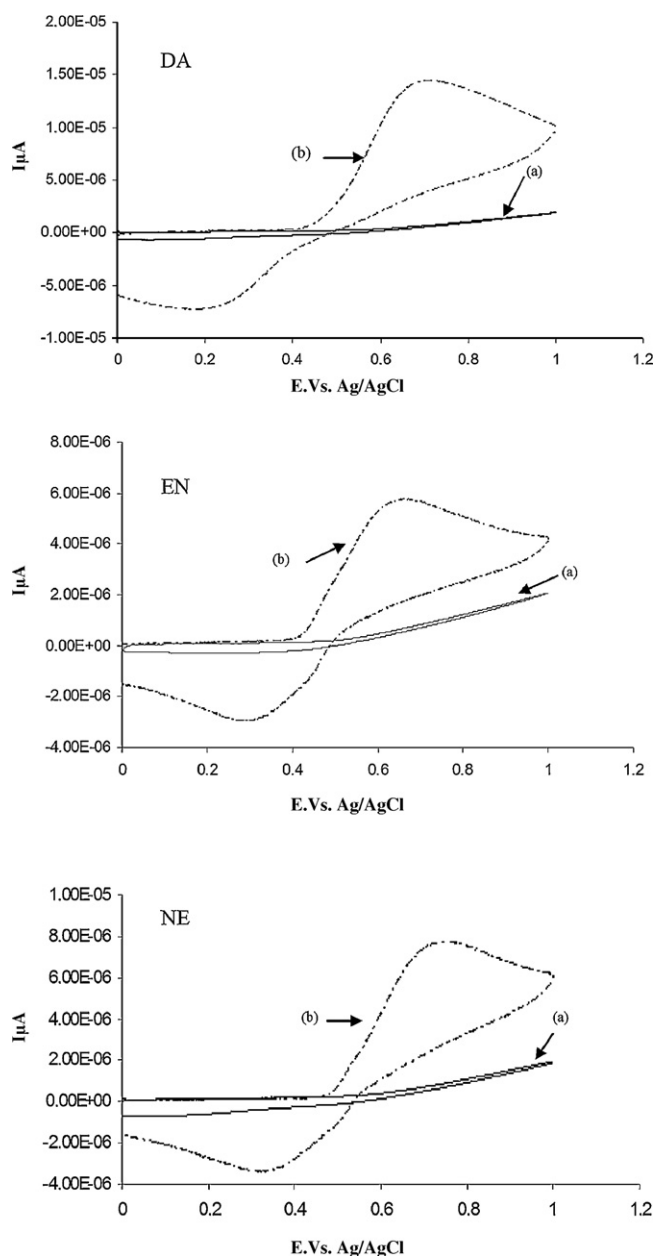


**Fig. 2.** Cyclic voltammograms for 5 mM of D,L-norepinephrine (1), epinephrine (2), and dopamine (3) at: (a) an unmodified Sonogel-Carbon electrode, and (b) a 5%  $\beta$ -CD-Sonogel-Carbon electrode; scan rate = 50  $\text{mV s}^{-1}$ ; PBS buffer at pH 7.4.

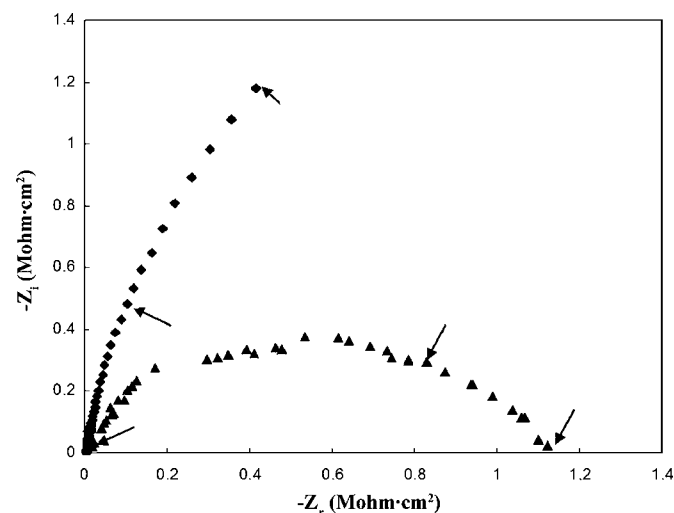


**Fig. 3.** Nyquist plots for impedance data obtained at 0 V for unmodified Sonogel-Carbon electrodes (▲) and 5%  $\beta$ -CD-Sonogel-Carbon electrodes (◆). Frequency range: 100 kHz–10 mHz.

the determination of the neurotransmitters selected was studied in the optimized conditions described above. The anodic peak currents  $I_{pa}$  obtained with a 5%  $\beta$ -CD-Sonogel-Carbon electrode had a linear dependence with respect to the square root of the scan rate ( $\nu^{1/2}$ ) in the range from 5 to 200  $\text{mV s}^{-1}$ . The correlation coefficients ( $R^2$ ) were 0.9997, 0.9997, and 0.9975 for DA, NE, and EN, respectively. The linear regression equations obtained were  $I_{pa}(\text{DA}) = 0.3764 + 0.4121 \times \nu^{1/2}$ ;  $I_{pa}(\text{NE}) = -0.7293 + 0.3873 \times \nu^{1/2}$ ; and  $I_{pa}(\text{EN}) = -0.0724 + 0.1211 \times \nu^{1/2}$ , where the units are  $I_{pa}(\mu\text{A})$  and  $\nu^{1/2} (\text{mV s}^{-1})^{1/2}$ . Our results indicate that the electron transfer reaction is diffusion controlled in the case of the neurotransmitters studied.

### 3.7. Electrochemical impedance spectroscopy (EIS) studies

Electrochemical impedance spectroscopy (EIS) is an effective method to explore the interfacial properties of modified electrodes [38]. It is based on the perturbation of a system at equilibrium by a small AC potential amplitude wave from 5 to 10 mV. The interaction of an analyte with the electrode surface is indicated by a shift in the impedance or a change in capacitance of the bulk electrode [39–41]. In our case, the impedance experiments were performed in order to characterize the electrode/electrolyte interface. Fig. 3 shows EIS spectra of an unmodified Sonogel-Carbon electrode (▲) and a 5%  $\beta$ -CD-Sonogel-Carbon electrode (◆) in 0.1 M  $\text{H}_2\text{SO}_4$ , recorded at 0 V versus a saturated calomel electrode (SCE). The frequency range and the AC potential amplitude have been previously described in the Section 2.

**Table 1**

Electrochemical peak parameters obtained from the cyclic voltammograms for dopamine, epinephrine, and D,L-norepinephrine. Scan rate: 50  $\text{mV s}^{-1}$ .

	Dopamine	Epinephrine	D,L-Norepinephrine
$E_{pa} (\text{V})^a$	0.674	0.755	0.663
$E_{pc} (\text{V})^a$	0.328	0.323	0.289
$I_{pa} (\text{A})^b$	$1.060 \times 10^{-06}$	$1.502 \times 10^{-06}$	$1.511 \times 10^{-06}$
$I_{pc} (\text{A})^b$	$-1.276 \times 10^{-06}$	$-1.871 \times 10^{-06}$	$-1.463 \times 10^{-06}$
$\Delta E (\text{V})^c$	0.346	0.432	0.374
$I_{pa}/I_{pc} (\text{A})$	0.832	0.804	1.034
$E_p - E_p/2(\text{V, oxidation})$	0.074	0.077	0.076
$E_p - E_p/2(\text{V, reduction})$	-0.087	-0.099	-0.091

<sup>a</sup>  $E_{pa}$  and  $E_{pc}$  are the oxidation and reduction potential peaks.

<sup>b</sup>  $I_{pa}$  and  $I_{pc}$  are current intensity of oxidation and reduction peaks.

<sup>c</sup>  $\Delta E (\text{V})$ : is the difference between oxidation and reduction potential (or the peak separations for the molecules at 5%  $\beta$ -CD-Sonogel-Carbon electrode). Scan rate = 50  $\text{mV s}^{-1}$ ; buffer = PBS at pH 7; concentration of the analytes = 5 mM.

**Table 2**

Electrical parameters calculated from the impedance spectra in 0.1 M of H<sub>2</sub>SO<sub>4</sub> for an unmodified-Sonogel-Carbon electrode and a 5% β-CD-Sonogel-Carbon electrode.

	$R_e$ ( $\Omega$ cm <sup>2</sup> )	$R_{ct}$ (M $\Omega$ cm)	$C_{dl}$ (nF cm <sup>2</sup> )
Sonogel-Carbon	4.909	5.537	177
5% β-CD-Sonogel-Carbon	5.012	1.006	287.3

$R_e$  = electrolyte resistance;  $R_{ct}$  = charge transfer resistance;  $C_{dl}$  the double layer capacitance at the electrode/electrolyte interface.

The EIS spectra are characterized by a perfect semicircle corresponding to the charge transfer process at the electrode surface with a correlation of 0.999 for the two complexes plot. The presence of cyclodextrin in the Sonogel-Carbon electrode seems to influence the interfacial impedance values. Electrical parameters were calculated using a Voltmaster<sup>®</sup> 4.0 software. Fitting results are presented in Table 2.  $R_e$  is the electrolyte resistance,  $R_{ct}$  is the charge transfer resistance, and  $C_{dl}$  is the double layer capacitance at the electrode/electrolyte interface.

On one hand and from these data, we can notice a decrease in the charge transfer resistance value for the 5% β-CD-Sonogel-Carbon system with respect to the unmodified Sonogel-Carbon system. On the other hand, the higher value calculated for the electrical double layer,  $C_{dl}$ , was observed at the 5% β-CD-Sonogel-Carbon/electrolyte interface. This result could be probably attributed to an increase in the electrode surface area [42]. This change in the capacitance suggested that cyclodextrin was successfully incorporated into the Sonogel-Carbon electrode. The reproducibility of the measurements from several 5% β-CD-Sonogel-Carbon electrodes was good and this could be explained by an exhaustive control of the experimental conditions of the electrodes preparation.

### 3.8. Interference studies

In order to explore possible analytical applications of the sensors described in this paper, the effect of ascorbic acid (AA), which causes severe interference, and several inorganic ions, was studied during the determination of the neurotransmitters selected.

In the literature, it has been already reported the catalytic effect of DA on the AA oxidation at the surface of different types of electrodes [43,44]. In these papers, the strong AA interference on the electrochemical determination of DA and other catecholamines is confirmed.

With the aim of investigating this issue, we have carried out a careful study of this catalytic effect employing a 5% β-CD-Sonogel-Carbon electrode in solutions containing DA (analyte of reference) and AA; AdDPV was the electrochemical technique employed. On one hand, Fig. 4a shows that the peak height of DA remained constant when the concentration of AA in the mixture was varied from 0 to  $8 \times 10^{-4}$  M, while peak height of ascorbic acid increased linearly with concentration. On the other hand, when varying the concentration of DA from 0 to  $2 \times 10^{-7}$  M instead of AA, the peak height of ascorbic acid remained constant (Fig. 4b). These results demonstrate that there is no homogeneous catalytic coupling between AA and DA at the 5% β-CD-Sonogel-Carbon electrode. Moreover, although the peaks of ascorbic acid and dopamine are partially overlapped, it seems that the modified electrode has the ability to resolve the system allowing the determination of DA even in the presence of high amounts of ascorbic acid (250-fold higher).

To achieve this purpose, we have adopted as a criterion to evaluate the peak height of DA taking the distance between the maximum of the peak and the tangent to the baseline of the DA peak with no interferents [45]. The linear relation between these heights and the concentration of DA can be verified with the following equation and correlation coefficient:  $I_p$  (nA) =  $0.0264 \times C_{DA}$  ( $\mu$ M) + 0.1318;  $r^2 = 0.9954$ .

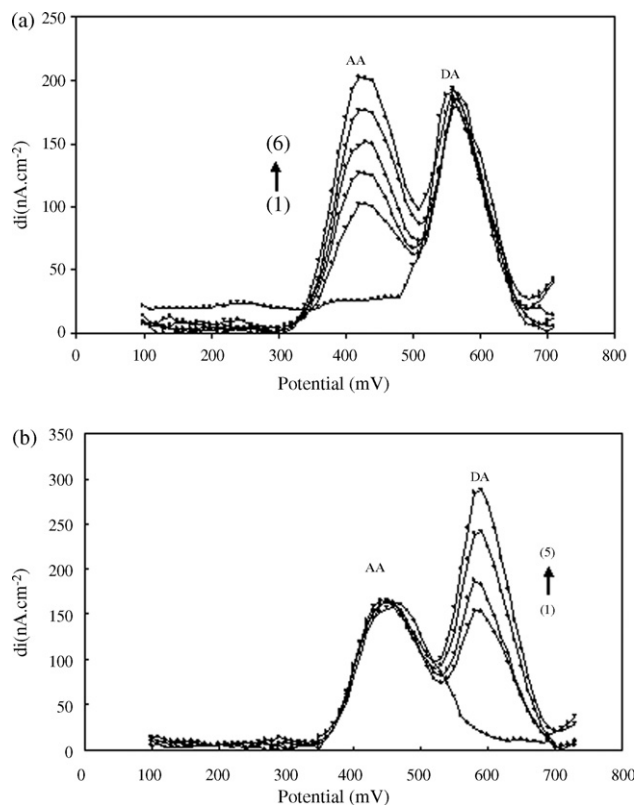


**Fig. 4.** AdDPV voltammograms corresponding to the interference studies when dopamine (DA) is determined in the presence of ascorbic acid (AA) at a 5% β-CD-Sonogel-Carbon electrode. (a) Concentration of DA is constant ( $2 \times 10^{-7}$  M), and concentration of AA is varied: (1) 0 M; (2)  $3 \times 10^{-4}$  M; (3)  $4 \times 10^{-4}$  M; (4)  $5 \times 10^{-4}$  M; (5)  $6 \times 10^{-4}$  M; (6)  $8 \times 10^{-4}$  M. (b) Concentration of AA is constant ( $10^{-4}$  M), and concentration of DA is varied: (1) 0 M; (2)  $1 \times 10^{-7}$  M; (3)  $2 \times 10^{-7}$  M; (4)  $4 \times 10^{-7}$  M; (5)  $6 \times 10^{-7}$  M.

Our modified electrode is also able to allow the selective determinations of other catecholamines in the presence of ascorbic acid and in the presence of uric acid as well, which has a similar behaviour to AA.

With respect to the interference studies using inorganic ions, the concentration of all the neurotransmitters chosen was kept at  $1 \times 10^{-5}$  M. After the measurements, no significant interference was obtained from the following species: K<sub>2</sub>SO<sub>4</sub> (150), KCl (400), KBr (400), where the values in parentheses are the interferent/analyte concentration ratios.

### 3.9. Analytical applications to the determination of neurotransmitters

The quantitative determination of dopamine (DA), norepinephrine (NE) and epinephrine (EN) at the 5% β-CD-Sonogel-Carbon electrode was performed using adsorptive differential pulse voltammetry. In our case, the oxidation peaks, obtained by this voltammetric technique, for these neurotransmitters, were taken as the analytical signal.

Under the optimal experimental conditions obtained above, linear relationships between the concentrations and peak currents for DA, EN, and NE were obtained. The linear regression equations were: DA,  $I$  ( $\mu$ A) =  $-0.0438 + 0.276 \times C$  ( $\mu$ M); EN,  $I$  ( $\mu$ A) =  $0.2279 + 0.0119 \times C$  ( $\mu$ M); NE,  $I$  ( $\mu$ A) =  $0.0039 + 0.002 \times C$  ( $\mu$ M). The  $r^2$  correlation coefficients were 0.9939, 0.9989 and 0.9992, respectively. The detection limit was considered as the concentration whose intensity value equals the blank intensity plus three times the standard deviation of the blank; for the determi-

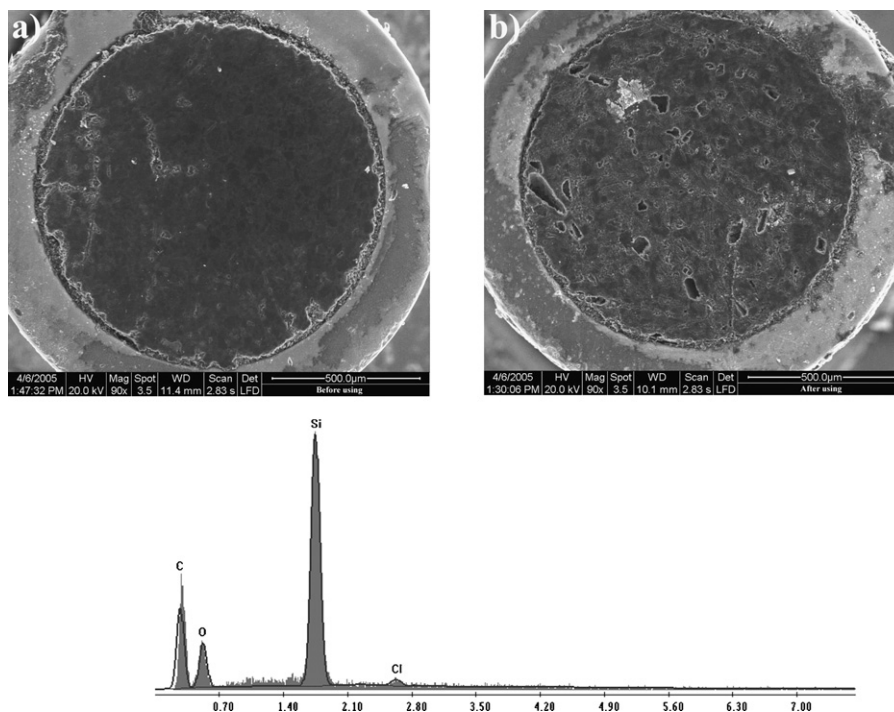


**Fig. 5.** Micrographs corresponding to the 5%  $\beta$ -CD-Sonogel-Carbon electrode polished: (a) before using, and (b) after using. The EDS spectrum corresponding to both micrographs is also included.

nation limit 10 times the standard deviation of the blank was used [46]. The detection limits were  $0.164 \mu\text{M}$  for DA,  $0.294 \mu\text{M}$  for NE, and  $0.699 \mu\text{M}$  for EN. The latest LOD (Epinephrine) was much lower than the one obtained recently using a conducting polymer glassy carbon modified electrode [37]. These LODs are good enough to be exploited for the detection of these neurotransmitters in pharmaceutical products and/or biological fluids. The determination limits were  $0.546 \mu\text{M}$  for DA,  $0.980 \mu\text{M}$  for NE and  $2.328 \mu\text{M}$  for EN.

The determination of catechol was also studied. A linear relationship between the anodic peak current and the concentration of catechol, ranging from  $2 \times 10^{-7}$  to  $2.2 \times 10^{-5}$  M, was obtained with a linear regression equation  $I (\mu\text{A}) = 0.1467 + 0.2356 \times C (\mu\text{M})$ , and  $r^2 = 0.9992$ . The LOD:  $0.059 \mu\text{M}$ , was lower than the value obtained in the literature with a polymer glassy carbon electrode [37]. The determination limit for this compound was  $0.197 \mu\text{M}$ .

### 3.10. Scanning electron microscopy (SEM) studies

Six different samples were studied: 2.5%  $\beta$ -CD-Sonogel-Carbon electrode polished and not used, 2.5%  $\beta$ -CD-Sonogel-Carbon electrode polished and used, 5%  $\beta$ -CD-Sonogel-Carbon electrode polished and not used, 5%  $\beta$ -CD-Sonogel-Carbon electrode polished and used, 7%  $\beta$ -CD-Sonogel-Carbon electrode polished and not used, 7%  $\beta$ -CD-Sonogel-Carbon electrode polished and used. For each sample, the SEM and EDS studies were performed on the same equipment and at the same time.

Since SEM studies were carried out at low vacuum, it was not necessary a previous step of coating the samples with gold. The micrographs were always taken at 20 kV.

In all used electrodes, it can be observed the presence of certain type of erosion, in the form of a marked widening of the separation material/capillary tubes, detected in their surface. The fact of using an electrode on measurements in aqueous solution increases highly the quoted separation, as well as the appearance of holes and fissures in their surface. When comparing the erosion suffered by

the three different electrodes, it can be concluded that 2.5%  $\beta$ -CD modified samples had a greater separation material/capillary tubes due to erosion, while the other two types of materials: 5% and 7%  $\beta$ -CD modified samples, present a minor separation. The greatest quantity of fissures and holes was presented by 2.5%  $\beta$ -CD modified samples, although electrodes with 7% of modification had quite a lot of them as well.

This fact could be used to corroborate the worst electrochemical results obtained with 2.5% and 7%  $\beta$ -CD modified materials, and the better electrochemical results for 5%  $\beta$ -CD modified material. This material presented smaller erosion and less number of fissures and holes, as well as better mechanical behaviour.

As an example to illustrate the surface of the materials studied, Fig. 5 shows two micrographs corresponding to a 5%  $\beta$ -CD-Sonogel-Carbon electrode polished: (a) before using and (b) after using. With regard to the data obtained by means of EDS, Fig. 5 also gives the composition for the materials studied. Furthermore, from all the spectra collected, it can be concluded that no differences were observed in the composition of the materials that denote the influence of the quantity of  $\beta$ -cyclodextrin.

## 4. Conclusions

In this paper, a new alternative for the electrochemical determination of catecholamines has been reported. Our choice is based on the use of  $\beta$ -cyclodextrin-Sonogel-Carbon electrodes. Besides, this is the first time that this electroanalytical performance has been carried out with this type of formulation:  $\beta$ -cyclodextrin included in Sonogel-Carbon matrices.

The modification percentage of  $\beta$ -cyclodextrin, the supporting electrolyte and the pH, as well as the electrochemical parameters were optimized in order to obtain the best responses for the electrodes. The results showed that  $\beta$ -cyclodextrin incorporated in Sonogel-Carbon electrodes gives better responses towards catecholamine molecules than unmodified Sonogel-Carbon electrodes. This is probably due to the formation of inclusion complexes between catecholamines and the  $\beta$ -CD. When comparing the cyclic

voltammetry responses with those obtained at modified glassy carbon electrodes, the results were also improved. This type of electrodes also showed excellent reproducibility, repeatability and stability. The good electroanalytical and structural properties of this type of electrodes have been corroborated by EIS and SEM studies.

Furthermore, the negligible effect of ascorbic and uric acids on the measurements together with the very encouraging LODs obtained for the different catecholamines make the new electrodes very stable and allow easy operation life time during more than 4 weeks. This life time of the electrode can be explained too by a weak leaching of the cyclodextrin in the solution. Our preparation method is sensitive enough to be applied to single tablet assay which may open new horizons for their use in the medical and biochemical analysis field.

### Acknowledgements

This paper was possible owing to the Moroccan Ministry of Higher Education through the program PROTARSII: P21/96 and the funds given by Junta de Andalucía.

### References

- [1] M.M. Cordero-Rando, J.L. Hidalgo-Hidalgo de Cisneros, E. Blanco, I. Naranjo-Rodríguez, *Anal. Chem.* 74 (10) (2002) 2423.
- [2] J.L. Hidalgo-Hidalgo de Cisneros, M.M. Cordero-Rando, I. Naranjo-Rodríguez, E. Blanco-Ollero, L. Esquivias-Fedriani, Spain Patent P200100556, 2001.
- [3] Z. Ji, A.R. Guadalupe, *Electroanalysis* 11 (3) (1999) 167.
- [4] M.M. Collinson, A.R. Howells, *Anal. Chem.* 72 (21) (2000) 702A.
- [5] M.M. Cordero-Rando, Development and characterization of Sonogel-Carbon materials as a base for electrochemical sensors, Doctoral Thesis, University of Cadiz, Spain, 2001.
- [6] J.M. Palacios-Santander, Application of chemometric techniques to resolve overlapped electrochemical sensors, Doctoral Thesis, University of Cadiz, Spain, 2003.
- [7] M.M. Cordero-Rando, I. Naranjo-Rodríguez, J.M. Palacios-Santander, L.M. Cubillana-Aguilera, J.L. Hidalgo-Hidalgo de Cisneros, *Electroanalysis* 17 (9) (2005) 806.
- [8] B. Ballarin, M. Gazzano, J.L. Hidalgo-Hidalgo de Cisneros, D. Tonelli, R. Seeber, *Anal. Bioanal. Chem.* 374 (2002) 891.
- [9] J.M. Palacios-Santander, L.M. Cubillana-Aguilera, M. Cocchi, A. Ulrici, I. Naranjo-Rodríguez, R. Seeber, J.L. Hidalgo-Hidalgo de Cisneros, *Chemom. Intell. Lab. Syst.* 91 (2008) 110.
- [10] L.M. Cubillana-Aguilera, J.M. Palacios-Santander, I. Naranjo-Rodríguez, J.L. Hidalgo-Hidalgo de Cisneros, *J. Sol-Gel Sci. Technol.* 40 (2006) 55.
- [11] L.M. Cubillana-Aguilera, J.M. Palacios-Santander, O.L. Estévez-Hernández, I. Naranjo-Rodríguez, J.L. Hidalgo-Hidalgo de Cisneros, *J. Sol-Gel Sci. Technol.*, Submitted for publication.
- [12] B. Ballarin, M.M. Cordero-Rando, E. Blanco, J.L. Hidalgo-Hidalgo de Cisneros, R. Seeber, D. Tonelli, *Collect. Czech. Chem. C.* 68 (8) (2003) 1420.
- [13] B. Ballarin, C. Zanardi, L. Schenetti, R. Seeber, J.L. Hidalgo-Hidalgo de Cisneros, *Synthetic Met.* 139 (1) (2003) 29.
- [14] H. Zejli, P. Sharrock, J.L. Hidalgo-Hidalgo, I. Naranjo-Rodríguez, K.R. Temsamani, *Talanta* 68 (2005) 79.
- [15] M. El Kaoutit, I. Naranjo-Rodríguez, K.R. Temsamani, M. Domínguez de la Vega, J.L. Hidalgo-Hidalgo de Cisneros, *J. Agric. Food. Chem.* 55 (20) (2007) 8011.
- [16] M. El Kaoutit, I. Naranjo-Rodríguez, K.R. Temsamani, J.L. Hidalgo-Hidalgo de Cisneros, *Biosens. Bioelectron.* 22 (2007) 2958.
- [17] H. Zejli, J.L. Hidalgo-Hidalgo de Cisneros, I. Naranjo-Rodríguez, B. Liu, K.R. Temsamani, J.L. Marty, *Anal. Chim. Acta* 612 (2) (2008) 198.
- [18] H. Zejli, J.L. Hidalgo-Hidalgo de Cisneros, I. Naranjo-Rodríguez, B. Liu, K.R. Temsamani, J.L. Marty, *Talanta* 77 (1) (2008) 217.
- [19] M.L. Bender, M. Komiyama, *Cyclodextrin Chemistry*, Springer-Verlag, Berlin, 1997.
- [20] H.J. Schneider, F. Hacket, V. Rudiger, *Chem. Rev.* 98 (5) (1998) 1755.
- [21] J. Szejtli, *Cyclodextrin and their Inclusion Complexes*, in: Akademiai Kiado (Ed.), Budapest, Hungary, 1982, p. 296.
- [22] P.M. Bersier, B. Klingert, *Electroanalysis* 3 (6) (1991) 443.
- [23] G. Puglisi, N.A. Santagati, R. Pingnatello, C. Ventura, F.A. Bottino, S. Mangiafico, G. Mazzone, *Drug Dev. Ind. Pharm.* 16 (3) (1990) 395.
- [24] D.L. Van Der Jagt, F.L. Killian, M.L. Bender, *J. Am. Chem. Soc.* 92 (4) (1970) 1016.
- [25] L.M. de León-Rodríguez, D.A. Basuil-Tobias, *Anal. Chim. Acta* 543 (1–2) (2005) 282.
- [26] H.Y. Wang, J. Han, X.G. Feng, Y.L. Pang, *Spectrochim. Acta A* 65A (1) (2006) 100.
- [27] O. Jules, S. Scypinsky, L.J.C. Love, *Anal. Chim. Acta* 169 (1985) 355.
- [28] A.I. Gopalan, K.P. Lee, K.M. Manesh, P. Santhosh, J.H. Kim, *J. Mol. Catal. A Chem.* 256 (1–2) (2006) 335.
- [29] C. Yañez, L.J. Nuñez-Vergara, J.A. Squella, *Electroanalysis* 15 (22) (2003) 1771.
- [30] E. Norkus, G. Grincienė, R. Vaitkus, *Carbohydr. Res.* 337 (18) (2002) 1657.
- [31] R.I. Gelb, L.M. Scharz, C.T. Murray, D.A. Laufer, *J. Am. Chem. Soc.* 100 (11) (1978) 3553.
- [32] A. Ferancová, J. Labuda, *Fresenius J. Anal. Chem.* 370 (1) (2001) 1.
- [33] A. Ferrancová, E. Korgova, J. Labuda, J. Zima, J. Barek, *Electroanalysis* 14 (23) (2002) 1668.
- [34] G. Roa, M.T. Ramírez Silva, M.M. Romero Romo, L. Galicia, *Application of Analytical Chemistry in Environmental Research*, Research Signpost, Trivandrum, INDE, 2005, pp. 57–66.
- [35] S. Tingry, C. Innocent, S. Touil, A. Deratani, P. Seta, *Mater. Sci. Eng. C* 26 (2006) 222.
- [36] T. Madhusudanda Reddy, K. Balaji, S. Jayarama Reddy, *J. Anal. Chem.* 62 (2) (2007) 168.
- [37] N. Izaoumen, D. Bouchta, H. Zejli, M. El Kaoutit, A.M. Stalcup, K.R. Temsamani, *Talanta* 66 (1) (2005) 111.
- [38] X. Ren, P.G. Pickup, *J. Electroanal. Chem.* 420 (1–2) (1997) 251.
- [39] L. Montelius, J.O. Tegenfeldt, T.G. Ling, *J. Vac. Sci. Technol. A* 13 (3) (1995) 1755.
- [40] P. Van Gerwen, W. Laureyn, W. Laureys, H. Huyberechts, M. Op De Beeck, K. Baert, J. Suls, W. Sansen, P. Jacobs, L. Hermans, R. Mertens, *Sens. Actuators B.* 49 (1–2) (1998) 73.
- [41] E. Souteyrand, C. Chen, J.P. Cloarec, X. Nesme, P. Simonet, I. Navarro, J.R. Martin, *Appl. Biochem. Biotechnol.* 89 (2–3) (2000) 195.
- [42] P. Zoltowski, *J. Electroanal. Chem.* 443 (1) (1998) 149.
- [43] M.A. Dayton, A.G. Ewing, R.M. Wightman, *Anal. Chem.* 52 (14) (1980) 2392.
- [44] M. Ferreira, L.R. Dinelli, K. Wohnrath, A.A. Batista, O.N. Oliveira, *Thin Solid Films* 446 (2) (2004) 301.
- [45] *Instructions Manual of AutoLab® General Purpose Electrochemical System (GPES)*, Ed. Eco Chemie B.V., Utrecht, The Netherlands.
- [46] J.C. Miller, J.N. Miller, *Estadística para Química Analítica*, Addison-Wesley Iberoamericana, Wilmington, 1993, pp. 96–98.



# Molecularly imprinted solid-phase extraction for the selective determination of 17 $\beta$ -estradiol in fishery samples with high performance liquid chromatography

Tianhe Jiang<sup>a</sup>, Lixia Zhao<sup>b,\*</sup>, Baolin Chu<sup>a</sup>, Qinzhong Feng<sup>b</sup>, Wei Yan<sup>b</sup>, Jin-Ming Lin<sup>c,\*</sup>

<sup>a</sup> State Key Laboratory of Chemical Resource Engineering, Beijing University of Chemical Technology, Beijing 100029, China

<sup>b</sup> State Key Laboratory of Environmental Chemistry and Ecotoxicology, Research Center for Eco-Environmental Sciences, Chinese Academy of Sciences, P.O. Box 2871, Beijing 100085, China

<sup>c</sup> Department of Chemistry, Tsinghua University, Beijing 100084, China

## ARTICLE INFO

### Article history:

Received 10 September 2008

Received in revised form

24 November 2008

Accepted 24 November 2008

Available online 9 December 2008

### Keywords:

17 $\beta$ -Estradiol

Molecularly imprinted polymer

Solid-phase extraction

High performance liquid chromatography

## ABSTRACT

A molecularly imprinted polymer (MIP) has been synthesized by a thermo-polymerization method using methacrylic acid (MAA) as functional monomer, ethylene glycol dimethacrylate (EGDMA) as cross-linker, acetonitrile as porogenic solvent, and 17 $\beta$ -estradiol as template. The MIP showed obvious affinity for 17 $\beta$ -estradiol in acetonitrile solution, which was confirmed by absorption experiments. After optimization of molecularly imprinted solid-phase extraction (MISPE) conditions, three structurally related estrogenic compounds (17 $\beta$ -estradiol, estriol, and diethylstilbestrol) were used to evaluate the selectivity of the MIP cartridges. The MIP cartridges exhibited highly selectivity for E<sub>2</sub>, the recoveries were 84.8  $\pm$  6.53% for MIPs and 19.1  $\pm$  1.93% for non-imprinted polymer (NIP) cartridges. The detection and quantification limits correspond to 0.023 and 0.076 mg L<sup>-1</sup>. Furthermore, the MISPE methods were used to selectively extract E<sub>2</sub> from fish and prawn tissue prior to HPLC analysis. This MISPE-HPLC procedure could eliminate all matrix interference simultaneously and had good recoveries (78.3–84.5%).

© 2008 Elsevier B.V. All rights reserved.

## 1. Introduction

Endogenous estrogens have been linked to the possible development of breast cancers and other diseases [1]. 17 $\beta$ -Estradiol (E<sub>2</sub>; 1,3,5(10)-estratriene-3,17 $\beta$ -diol), the most active estrogen, has been used in animal fattening for its anabolic effects [2]. Some authors reported that concentration as low as ng L<sup>-1</sup> level of E<sub>2</sub> induces vitellogenin production in male trout [3], and E<sub>2</sub> also had been found in many aquatic environments [4]. Chronic exposure of humans to E<sub>2</sub> through food chain can cause drastic problem, therefore, the detection of E<sub>2</sub> in fishery products is urgent to ensure public health.

Currently, many methods have been described for the effectively monitoring and detecting endogenous estrogens in animal tissues. These methods can be generally divided into two groups. The first group is immunological methods [5–7], which are highly selective due to the antibody-antigen specificity interaction, but their applications in the real samples are limited to some extent due to the instability of natural antibodies. Second, chromatographic methods including LC–MS [8], HPLC [9,10], GC–MS [11],

which combined with sample pretreatment methods such as solid-phase extraction (SPE), liquid–liquid extraction (LLE), accelerated solvent extraction (ASE), supercritical fluid extraction (SFE), etc., are most commonly used technique for detecting endogenous estrogens. In which, solid-phase extraction (SPE) is routinely used for preconcentration and clean-up in the analysis of biological and environmental samples due to the advantages of simplicity, rapidness and little consumption of organic solvents. Despite these attractive features, the classical SPE sorbents (C<sub>8</sub>, C<sub>18</sub>, etc.) retain analytes by non-selective hydrophobic reaction which lead to a partial coextraction of interfering substances and further purification procedure is still required to remove coextractant [12,13]. Therefore, new sorbents such as immunosorbents and molecular imprinting polymers (MIPs) were increasingly developed to meet the need of high selectivity.

MIPs are synthetic polymers with specific binding sites complementary size, shape, and functional groups to the template molecule, involving a retention mechanism based on molecular recognition. The advantages that MIPs hold over natural antibodies, including stability, ease of preparation, low cost, and reusability have led to their wide application in chromatography [14], catalysis [15], chemical sensors [16], and solid-phase extraction (SPE) [17,18]. Among these applications, molecularly imprinted solid-phase extraction (MISPE) is a very desirable technique for the selective extraction or the clean-up of target analytes from various complex matrices, for example, the extraction of pollutants from

\* Corresponding author. Fax: +86 10 62841953.

\*\* Corresponding author.

E-mail addresses: [zlx@rcees.ac.cn](mailto:zlx@rcees.ac.cn) (L. Zhao), [jmlin@mail.tsinghua.edu.cn](mailto:jmlin@mail.tsinghua.edu.cn) (J.-M. Lin).

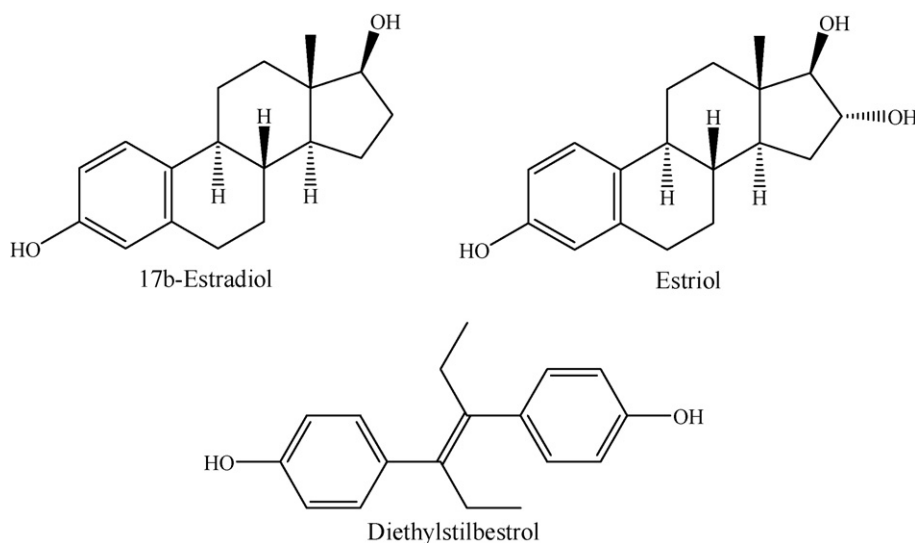


Fig. 1. Chemical structures of 17β-estradiol, estriol and diethylstilbestrol.

soil or river water and various drugs from plasma or food [19–21]. However, the use of MISPE in fishery tissue samples has not been reported previously. The novel extraction method with MIPs was desired to eliminate the tissue matrix interferences, to have cleaner extracts than the traditional SPE method, which resulting in a more selective and reliable analytical protocol.

The aim of this study was to synthesize non-covalent molecularly imprinted polymers using  $E_2$  as template molecule, methacrylic acid (MAA) as functional monomer and ethylene glycol dimethacrylate (EGDMA) as a cross-linker. Then, a MISPE method based on the imprinted polymer was developed to selectively extract  $E_2$  from fish and prawn tissue samples.

## 2. Experimental

### 2.1. Materials

17β-Estradiol, estriol, and diethylstilbestrol were purchased from Wako (Osaka, Japan). The structures of these estrogens were shown in Fig. 1. EDGMA and 2,2'-azobis(2-methylpropionitrile) (AIBN) were purchased from Acros (NJ, USA), and purified prior to use as follows: EDGMA was washed consecutively with 10% NaOH, water and then brine. After drying over  $MgSO_4$ , it was distilled under reduced pressure; AIBN was recrystallized from methanol. MAA was purchased from Alfa Aesar (USA) and distilled under reduced pressure. Acetonitrile, methanol were all of HPLC grade and from Fisher Scientific (USA). Water was deionized ultrapure water ( $18.3 M\Omega cm^{-1}$ , EasyPure LF Barnstead, USA). All other reagents used in the experiment were of analytical grade. Stock solutions of 17β-estradiol were prepared with acetonitrile. Tilapia and prawn were purchased from local market.

### 2.2. Instrumentation

HPLC analysis was performed using a Shimadzu HPLC system containing a SCL-10Avp system controller, a RF-10AXL fluorescence detector, a DEU-12A degasser, a SIL-10AP auto injector and a CTO-10AS column oven (Shimadzu, Japan). Excitation and emission wavelengths were set at 280 and 310 nm, respectively. The analytical column was packed with ODS C18 stationary phase (VP-ODS, 150 mm × 4.6-mm-i.d., particle size 5 μm, pore size 12 nm, pore volume 1.25 cm<sup>3</sup>/g, specific surface area 410 m<sup>2</sup>/g, Shimadzu). The column thermostat was set at 40 °C. The mobile

phase was water–methanol (30:70, v/v), and its flow rate was set at 1.0 mL min<sup>-1</sup>. Scanning electron micrograph of the MIPs was obtained with an S-4700 SEM (Hitachi, Japan) at 30 kV. UV analyses of  $E_2$  were carried out using a UV–vis recording spectrophotometer (Shimadzu, Japan). Fluorescence analyses of  $E_2$  were performed using a Fluorescence spectrophotometer (F-2500, Hitachi, Japan). Adsorption/desorption analyses were carried out using a nitrogen surface area analyzer (ASAP 2000, Micromeritics, USA).

### 2.3. Preparation of molecularly imprinted polymers

The MIPs for  $E_2$  were prepared using a method described by Ye et al. [22] with little modification: by dissolving  $E_2$  (0.272 g, 1 mmol), MAA (0.517 g, 6 mmol), EDGMA (5.930 g, 30 mmol), and initiator AIBN (0.062 g, 0.381 mmol) in 8 mL of acetonitrile in a 40 mL thick-walled glass tube. The prepolymerization mixture was sparged with nitrogen for 5 min to remove oxygen, and then polymerized at 60 °C in a water bath for 24 h. Thereafter, the MIPs monolith was crushed, ground and sieved through 30–45 μm sieves, and the remaining fines were removed by sedimentation in acetone. The MIPs particles obtained were washed with methanol:acetic acid (9:1, v/v) to remove the template molecules. Then, the particles were dried at 55 °C in oven for 12 h.

As a control, non-imprinted polymers were synthesized simultaneously under the same procedure in the absence of template molecule.

### 2.4. Binding experiments

To evaluate the binding capacity of the MIPs obtained, static adsorption test and dynamic adsorption test were carried out in acetonitrile solutions. 20 mg of polymer particles were added in 10-mL flask containing 3.0 mL  $E_2$  solutions of various concentrations (0.09–0.73 mmol L<sup>-1</sup>). After shaken in a water bath for 12 h at room temperature, the samples were centrifuged, filtered. The free concentration of  $E_2$  after the adsorption was recorded by UV spectrometry at 280.0 nm. The adsorption quantity ( $B$ ) was calculated by subtracting the free concentrations from the initial concentrations. Meanwhile, the maximum binding capacity ( $B_{max}$ ) and dissociation constant ( $K_D$ ) were estimated by processing with the Scatchard equation  $B/C_{free} = (B_{max} - B)K_D$  (where  $B$  is the amount of  $E_2$  bound to polymer at equilibrium,  $C_{free}$  is the concentration of free target).

### 2.5. Molecularly imprinted solid-phase extraction procedures

300 mg of dry imprinted and non-imprinted polymer particles were packed into 3.0 mL hollow SPE cartridges (Besep, USA) with two glass-wool frits at each end. The cartridges were washed with methanol (3 mL) and conditioned with acetonitrile (3 mL) before use.

2 mL  $E_2$  solution was loaded onto MISPE and NISPE cartridges, respectively. After loading, vacuum was applied to the cartridges for 10 min in order to remove the residual solvent. The cartridges were washed with 3.0 mL of acetonitrile/water mixture (4/6, v/v) to eliminate molecules retained by non-specific adsorption by the polymer. Eluting step was then performed using 3.0 mL of methanol/acetic acid (99/1, v/v) mixture solution. Finally, the elution fractions were dried under a gentle nitrogen stream. The residue was reconstituted with methanol to final volume of 0.5 mL for subsequent HPLC analysis.

Following the optimized MISPE procedure for  $E_2$ , estriol ( $E_3$ ) and diethylstilbestrol (DES) were selected to evaluate the selectivity of the MISPE cartridges. Each assay was repeated six times.

### 2.6. Molecularly imprinted solid-phase extraction and determination of fish and prawn sample extracts

In this experiment, the tissue samples were wrung, and stored at  $-18^\circ\text{C}$  before analysis. The Tilapia and prawn samples were spiked with two concentration levels of  $E_2$  at 0.01 and  $0.1\text{ mg g}^{-1}$ .

5 g of spiked samples were homogenized in 20 mL of acetonitrile, and were ultrasonicated for 30 min at room temperature. The homogenates were centrifuged twice at 10,000 rpm (CR22GII, himac, HITACHI, Japan) for 10 min at  $4^\circ\text{C}$ . After blowing down with nitrogen, the residue was reconstituted with 4 mL acetonitrile. 2 mL of these solutions were loaded on the cartridges. Washing step was performed with  $2 \times 3\text{ mL}$  of acetonitrile/water mixture (4/6, v/v) solution. Finally, the columns were eluted with 3.0 mL of methanol/acetic acid mixture (99/1, v/v). Experiments were repeated six times.

## 3. Results and discussion

### 3.1. Preparation and characteristic of the molecularly imprinted polymers

Since MIPs have a stronger load capacity and a larger population of micropores by thermal initiation [23], a thermo-polymerization procedure was employed at  $60^\circ\text{C}$  for 24 h. MAA was chosen as functional monomers and EGDMA was used as cross-linker in the synthesis of  $E_2$  imprinted polymers. Generally, the affinity and imprinting effect of MIPs toward its template molecule were affected by the molar ratios between template and monomer in the synthesis of molecularly imprinted polymers [24]. Therefore, three molar ratios between template and monomer of 1:4, 1:6 and 1:8 were tested in our experiment, while the molar ratio of monomer to cross-linker was selected at 1:5 to ensure the formation of defined recognition sites with polymers [25]. The results revealed that the MIPs with the molar ratios between template and monomer of 1:6 showed best specific affinity and low non-specific affinity. Since the low molar ratios induced less binding sites in polymers due to the fewer of template–monomer mixture, but high molar ratios produced high non-specific affinity. Theoretically, the accuracy of the assembly between the template and the monomer was related to the characteristics of the porogen solvent in non-covalent approach [26]. Thus, acetonitrile, the less polar porogen, which can eliminate interferences with hydrogen bonds and electrostatic interactions, was employed in polymerization. The porogen volume was also

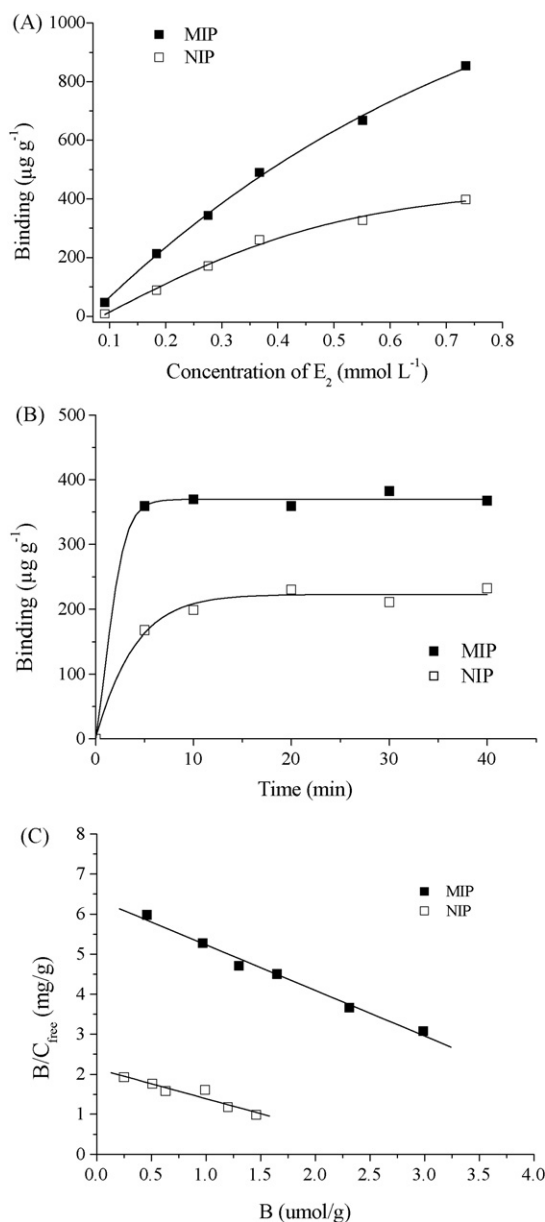


**Fig. 2.** (A) Binding isotherm of MIPs and NIPs for  $E_2$  in acetonitrile. (B) Time profiles of  $E_2$  (0.28 mM) binding by  $6.7\text{ ng mL}^{-1}$  polymer in acetonitrile. (C) Scatchard plot of MIP and NIP.

one of the most important factors influencing both the solubility of template–monomer mixture and the morphology of polymers. The large volume of porogen led to higher surface area and pore size, while small volume resulted in a low mechanical intensity. Thus, different proportions of template to porogen volume ( $\text{mol/mL}$ ) of 1:6, 1:8 and 1:10 were studied, and the optimum proportion was confirmed at 1:8 ( $\text{mol/mL}$ ).

After MIP synthesis, the imprinting effect was initially evaluated by performing binding experiments in which fixed amounts of imprinted and non-imprinted polymers were incubated with different concentrations of  $E_2$  in acetonitrile. The static adsorption data (Fig. 2A) showed the binding capacity of imprinted polymer increased with the increasing of the initial concentration of  $E_2$ , and displayed a higher affinity for template molecule than non-imprinted polymer. This high affinity of imprinted polymers was also demonstrated by dynamic adsorption tests (Fig. 2B) in which the imprinted polymer always adsorbed larger amount of  $E_2$  than that of non-imprinted polymer. From the



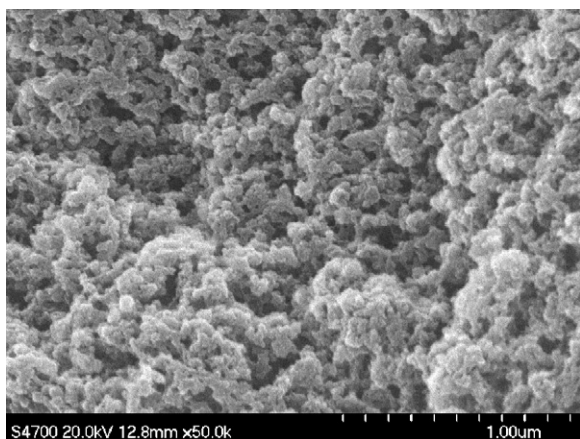


Fig. 3. Scanning electron microscopy of the MIP.

Scatchard plot (Fig. 2C), the  $B_{\max}$  values were calculated to be 5.59 and 2.86  $\mu\text{mol g}^{-1}$  for imprinted and non-imprinted polymer, respectively. The dissociation constant  $K_D$  was 0.86  $\mu\text{mol L}^{-1}$  was calculated from the Scatchard slope. Since specific surface area and pore volume strongly influenced the efficiency of adsorption, these parameters should be evaluated. The specific surface areas, pore volumes and pore size from nitrogen adsorption experiments were 55.28  $\text{m}^2/\text{g}$ , 0.33  $\text{cm}^3/\text{g}$  and 23.24 nm for imprinted polymer, 53.26  $\text{m}^2/\text{g}$ , 0.28  $\text{cm}^3/\text{g}$  and 14.70 nm for non-imprinted polymer, respectively. The similar surface area, pore volumes and pore size of imprinted and non-imprinted polymers suggested that the affinity of the imprinted polymer was due to specific binding sites. The microscopic characteristic of the imprinted polymer was shown in Fig. 3, and a porous surface could be clearly observed. All these characteristics indicated that the imprinted polymer was a potential sorbents for selective enrichment and separation, detection of  $E_2$  from sample matrix.

### 3.2. Optimization of the MISPE procedures

In order to evaluate the imprinting effect and applicability of the MIPs for separation and determination of trace  $E_2$  by HPLC, a general procedure for a generic SPE (conditioning, loading, washing, eluting) were optimized to achieve good sensitivity and precision of this method.

Different loading solvents such as acetonitrile, acetone, methanol, methylene chloride, chloroform, acetonitrile/water (9:1 and 7:3, v/v) and loading volume (1, 2, 3, and 4, mL) were investigated. The best results were obtained when (2 mL) acetonitrile was employed, which all the loaded  $E_2$  was retained by MIP cartridges. This might be because that acetonitrile as the porogen solvent in polymerization, could influence the degree of polymer chain solvation and adjusted the solvation of microenvironment of the binding sites similar with in the developing polymer [27]. Methylene chloride could entirely load  $E_2$  onto MIP cartridge, however, the specific interaction between the template molecule and the MIPs was disrupted. The polar and contained water-containing media also had a direct disruption for the recognition ability of the MIPs, which led to a significant loss in loading step for both MIP and NIP cartridges. Thus, acetonitrile (2 mL) was selected as the loading solvent.

The washing step was the most crucial procedure to maximize the specific interactions between the analytes and binding sites, and to simultaneously decrease non-specific interactions to discard matrix components in the polymer [28]. Thus, acetonitrile/water (1/9, 2/8, 3/7, 4/6, and 5/5, v/v) were investigated in washing step. The results were showed in Fig. 4 washing with 3 mL of acetonitrile/water (3/7, v/v) mixture solvent had no obviously effect on the

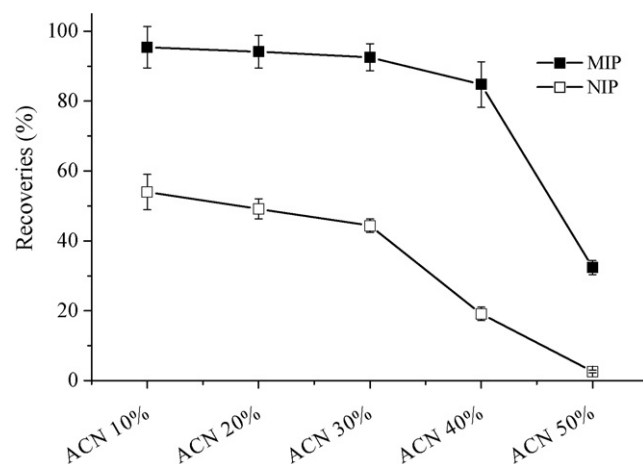


Fig. 4. Effect of acetonitrile in washing step to SPE cartridges.

retention of  $E_2$  on both MIP and NIP cartridges. With the increase of acetonitrile in the washing solutions (4/6, v/v), the recovery of  $E_2$  in NIP cartridge was decreased rapidly to 16.7%, while the recovery of  $E_2$  by the MIP cartridges was not reduced (83.7%). Meanwhile, increasing of the washing volume with 2 × 3 mL of acetonitrile/water (4/6, v/v) just had a light effect on MIP, thus confirming the presence of specific interactions taking place in the binding sites. However, the higher portion of acetonitrile in mixture solvent (5/5, v/v) led to a large decrease of  $E_2$  retention both on the MIP and NIP cartridges due to the disruption of specific interactions between the analytes and binding sites.

The optimized elution solvent was obtained by employing 3 mL of methanol containing 1% (v/v) of acetic acid which eluted  $E_2$  from MIP and NIP cartridges absolutely.

### 3.3. Selectivity of the MISPE cartridges

In order to estimate the selectivity of  $E_2$  MIP cartridges, several estrogen compounds with similar structure and characteristics such as  $E_3$  and DES were selected. The molecular structures were shown in Fig. 1.  $E_3$ , holding the same carbon skeleton with  $E_2$ , had an hydroxyl group in position 17 and a phenol hydroxyl group in position 3 but exceeded an hydroxyl group in position 18. DES had two phenol hydroxyl groups, and the carbon skeleton was different from  $E_2$  and  $E_3$ .

The previously described MISPE procedure was applied to these estrogen compounds on MIP and NIP cartridges. The results were showed in Fig. 5. A quantitative extraction and excellent selectivity were obtained for  $E_2$ . The recovery in MIP cartridges was  $84.8 \pm 6.53\%$ , which was significantly higher than that of NIP cartridges ( $19.1 \pm 1.93\%$ ). The better efficiency and selectivity of the MIP for  $E_2$  compared with that of NIP was further demonstrated when this compound was used in the presence of  $E_3$  and DES. The recovery of  $E_3$  in MIP cartridges was  $72.1 \pm 1.20\%$ , which was a bit less than that of  $E_2$ , because the hydroxyl group in position 18 could bring steric hindrance with the hydroxyl group in position 17 suspected to preferentially bind to the functional monomer in the specific binding sites [29]. However, the significant difference between the recovery of MIP and NIP ( $28.0 \pm 6.28\%$ ) demonstrated the specific interaction also happened in a certain extent. On the contrary, DES recovery obtained for the MIP cartridges was low ( $31.7 \pm 5.90\%$ ). The main reason might be the two phenol hydroxyl groups of DES display weak acidity [30], and might be not appropriate to interaction with MAA (the functional monomer of the polymer) by hydrogen bonding. Meanwhile, the different structure as in particular with  $E_2$  also was the crucial factor for the low recovery.

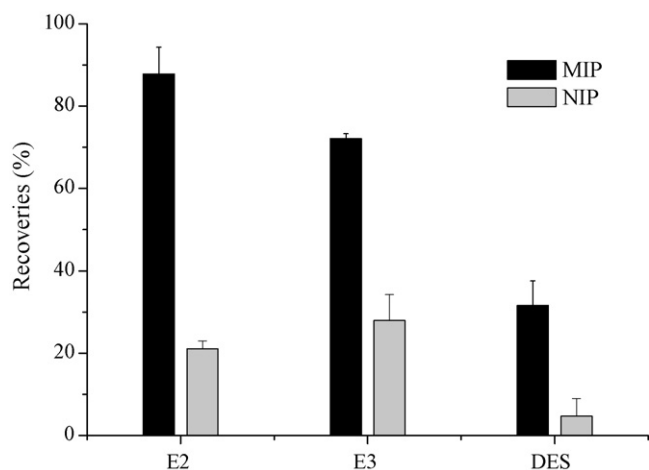


Fig. 5. Recoveries of E<sub>2</sub>, E<sub>3</sub>, and DES on MIP and NIP cartridges.

### 3.4. Molecularly imprinted solid-phase extraction and determination of E<sub>2</sub> in fish and prawn samples

In this experiment, acetonitrile which had good ability for precipitating protein, lower solubility of lipids than other solvents and could penetrate meat after homogenization was selected to extract E<sub>2</sub> from fish and prawn tissues. After

ultrasonication, centrifugation, dryness and reconstitution, the obtained solution was analyzed by HPLC (Fig. 6A.1. and B.1.). Despite most amounts of matrices was removed by centrifugation at 10,000 rpm for 10 min, this kind of matrices even containing small amounts protein and lipids may deteriorate the analytical results seriously and harm the column.

Therefore, a satisfactory clean-up of the matrix was obtained by loading the extraction solution to MIP cartridges and washing with 2 × 3 mL of acetonitrile/water (4/6, v/v) solution. The results obtained after HPLC analysis of the elution fractions are presented in Fig. 6A and B. Chromatograms obtained for spiked samples without MISPE (1), blank and spiked samples purified by MISPE (2–4), revealed that the samples were significantly cleaner after the MISPE had been applied. Table 1 showed the average recoveries of E<sub>2</sub> were 78.3–84.5% and 10.9–16.9% for MIP cartridges and NIP cartridges, respectively. The comparison of the MISPE elution fractions with the non-imprinted solid-phase extraction and the direct analysis of the spiked fish and prawn demonstrated the high efficiency and selectivity of the MISPE cartridges. The LOD (S/N = 3) and LOQ (S/N = 10) correspond to 0.023 and 0.076 mg L<sup>-1</sup>. The linear range was established between 0.01 and 2.0 mg L<sup>-1</sup> with a correlation coefficient (R<sup>2</sup>) of 0.9997. The intraday precisions of the relative peak areas were below 3.0% and interday precisions below 6.5%.

The MISPE protocol was also applied to water samples (tap and river water). The high molecular recognition ability of imprinted polymer was not exhibited because the hydrophobic character

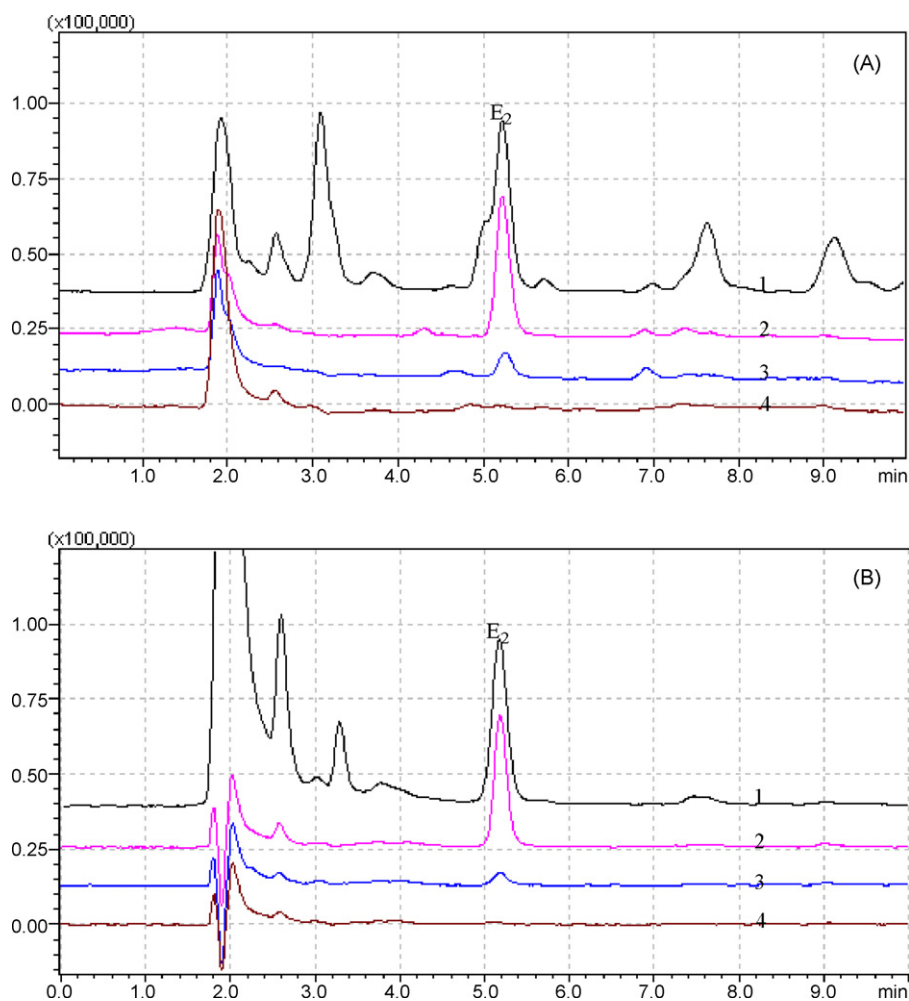


Fig. 6. Chromatograms of spiked fish (A) and prawn (B) samples using MISPE: (1) samples extract in acetonitrile; (2) extracted sample spiked with 0.01 mg g<sup>-1</sup> purified on MIP cartridges; (3) extracted sample spiked with 0.01 mg g<sup>-1</sup> purified on NIP cartridges; (4) blank samples purified on MIP cartridges.

**Table 1**Recoveries and RSD of E<sub>2</sub> after SPE of spiked fish and prawn samples.

Samples	Adding (mg g <sup>-1</sup> )		Found (mg g <sup>-1</sup> )		Recoveries (%)		RSD (%) n = 6	
	MIP	NIP	MIP	NIP	MIP	NIP	MIP	NIP
Fish	0.01	0.01	0.00845	0.00169	84.5	16.9	10.7	14.8
	0.1	0.1	0.0800	0.0147	80.0	14.7	5.79	10.2
Prawn	0.01	0.01	0.00818	0.00109	82.8	10.9	2.26	16.5
	0.1	0.1	0.0783	0.0150	78.3	15.0	3.33	11.9

**Table 2**

Compared the methods used before to the one this article described.

Pretreatment methods	Analytical system	Samples	Selective	Ref.
MISPE	HPLC/fluorescence	Fishery tissue	Yes	This article
GF/C filters prior to solid-phase extraction (SPE) using C18 as sorbent	LC/MS/MS	Wastewater	No	[31]
On-line SPE using cigarette filter as sorbent	HPLC/UV	River water, well water, lake water	No	[32]
SPE using C18 as sorbent	HPLC/fluorescence	Human urine	No	[33]
Liquid-liquid extraction	HPLC/electrochemical detection	Plasma	No	[34]

of the polymer badly destroyed the molecular identification of imprinted sites. Thus, a kind of water-compatible molecularly imprinted polymer should be studied to substitute this hydrophobic imprinted polymer for selective extraction of estrogen in water system.

#### 4. Conclusions

This study demonstrated the potential of a 17 $\beta$ -estradiol imprinted polymer which was synthesized by bulk thermal polymerization for the separation and preconcentration of 17 $\beta$ -estradiol in acetonitrile. It has been proved that the polymer has a good selectivity for imprinted molecule by both functional groups and dimensional structure of specific binding site. Furthermore, the MIP polymer as adsorbents in SPE was successfully applied for extraction of 17 $\beta$ -estradiol from fishery tissue matrix followed by HPLC with FL detection. Some methods have been used for the determination of 17 $\beta$ -estradiol summarized in Table 2. Each method has its advantages and limitations including of selectivity and interference of matrix, and has to add further purification procedure to remove coextractant. Comparing with these methods, the method developed by this article was sufficiently accurate and precise to be used for 17 $\beta$ -estradiol analysis in fishery tissue samples, and performed better characteristics such as selectivity and cleanliness of the extracts. Future research should focus on preparing water-compatible molecularly imprinted polymer for detection of hydrophobic compounds in water system.

#### Acknowledgements

This work was supported by the National Natural Science Foundation of China (Grant Nos. 20437020, 20575073 and 20621703) and the Major Research Program of the Chinese Academy of Sciences (KZCX3-SW-432).

#### References

[1] M. Clemons, P. Goss, N. Engl, J. Med. 344 (2001) 276.

- [2] H. Noppe, B. Le Bizec, K. Verheyden, H.F. De Brabander, Anal. Chim. Acta 611 (2008) 1.
- [3] L.X. Zhao, J.M. Lin, Z.J. Li, X.T. Ying, Anal. Chim. Acta 558 (2006) 290.
- [4] T. Tanaka, H. Takeda, F. Ueki, K. Obata, H. Tajima, H. Takeyama, Y. Goda, S. Fujimoto, T. Matsunaga, J. Biotechnol. 108 (2004) 153.
- [5] T. de Boer, D. Otjens, A. Muntendam, E. Meulman, M. van Oostijnen, K. Ensing, J. Pharmaceut. Biomed. 34 (2004) 671.
- [6] J.Q. Zhang, B.Y. Su, W.Q. Cai, Brain Res. 997 (2004) 89.
- [7] C. Bennetau-Pelissero, B. Arnal-Schnebelen, V. Lamothe, P. Sauvart, J.L. Sagne, M.A. Verbruggen, J. Mathey, O. Lavialle, Food Chem. 82 (2003) 645.
- [8] P. Tong, Y. Kasuga, C.S. Khoo, J. Food Compos. Anal. 19 (2006) 150.
- [9] Q.W. Xiao, Y.Q. Li, H.X. Ouyang, P.Y. Xu, D.S. Wu, J. Chromatogr. B 830 (2006) 322.
- [10] J.A. Russell, R.K. Malcolm, K. Campbell, A.D. Woolfson, J. Chromatogr. B 744 (2000) 157.
- [11] D. Arroyo, M.C. Ortiz, L.A. Sarabia, J. Chromatogr. A 1157 (2007) 358.
- [12] J.J. Seo, H.Y. Kim, B.C. Chung, J.K. Hong, J. Chromatogr. A 1067 (2005) 303.
- [13] Z. Long, L. Hong, J. Jie, Chin. J. Anal. Chem. 35 (2007) 983.
- [14] H. Khan, T. Khan, J.K. Park, Sep. Purif. Technol. 62 (2008) 363.
- [15] A. Visnjevski, E. Yilmaz, O. Brüggemann, Appl. Catal. A-Gen. 260 (2004) 169.
- [16] R. Thoelen, R. Vansweevelt, J. Duchateau, F. Horemansa, J. D'Haen, L. Lutsen, D. Vanderzande, M. Ameloot, M. vandeVen, T.J. Cleij, P. Wagner, Biosens. Bioelectron. 23 (2008) 913.
- [17] F. Puoci, G. Cirillo, M. Curcio, F. Iemma, U.G. Spizzirri, N. Picci, Anal. Chim. Acta 593 (2007) 164.
- [18] S.L. Moullec, A. Bégos, V. Pichon, B. Bellier, J. Chromatogr. A 1108 (2006) 7.
- [19] A. Beltran, E. Caro, R.M. Marcé, P.A.G. Cormack, D.C. Sherrington, F. Borrull, Anal. Chim. Acta 597 (2007) 6.
- [20] B. Boyd, H. Björk, J. Billing, O. Shimelis, S. Axelsson, M. Leonora, E. Yilmaz, J. Chromatogr. A 1174 (2007) 63.
- [21] B. Claude, P. Morin, M. Lafosse, A.S. Belmont, K. Haupt, Talanta 75 (2008) 344.
- [22] L. Ye, R. Weiss, K. Mosbach, Macromolecules 33 (2000) 8239.
- [23] B. Sellergrén (Ed.), Man-made Mimics of Antibodies and Their Applications in Analytical Chemistry, Elsevier, Amsterdam, 2001, p. 40.
- [24] S.L. Moullec, A. Bégos, V. Pichon, B. Bellier, J. Chromatogr. B 850 (2007) 24.
- [25] S.T. Wei, A. Molinelli, B. Mizzaikoff, Biosens. Bioelectron. 21 (2006) 1943.
- [26] B. Boyd, H. Björk, J. Billing, O. Shimelis, S. Axelsson, M. Leonora, E. Yilmaz, J. Chromatogr. A 1152 (2007) 41.
- [27] D. Spivak, M.A. Gilmore, K.J. Shea, J. Am. Chem. Soc. 119 (1997) 4388.
- [28] C.Y. He, Y.Y. Long, J.L. Pan, K.A. Li, F. Liu, J. Biochem. Biophys. Methods 70 (2007) 133.
- [29] A. Rachkov, S. McNiven, A. El'skaya, K. Yano, I. Karube, Anal. Chim. Acta 405 (2000) 23.
- [30] L. Ye, Y.H. Yu, K. Mosbach, Analyst 126 (2001) 760.
- [31] Y.K.K. Koh, T.Y. Chiu, A. Boobis, E. Cartmell, J.N. Lester, M.D. Scrimshaw, J. Chromatogr. A 1173 (2007) 81.
- [32] S. Wang, W. Huang, G.Z. Fang, J.X. He, Y. Zhang, Anal. Chim. Acta 606 (2008) 194.
- [33] L.S. Mao, C.J. Sun, H. Zhang, Y.X. Li, D.S. Wu, Anal. Chim. Acta 522 (2004) 241.
- [34] H. Yamada, K. Yoshizawa, T. Hayase, J. Chromatogr. B 775 (2002) 209.



# Effect of UV irradiation on detection of cocaine hydrochloride and crack vapors by IMIS and API-MS methods

Yuri N. Kolomiets\*, Viktor V. Pervukhin

Nikolaev Institute of Inorganic Chemistry of SB RAS, Acad. Lavrentieva ave. 3, 630090 Novosibirsk, Russia

## ARTICLE INFO

### Article history:

Received 4 May 2008

Received in revised form 2 December 2008

Accepted 2 December 2008

Available online 11 December 2008

### Keywords:

Cocaine hydrochloride

Crack

Photolysis

Ion mobility increment spectrometry

API-MS

## ABSTRACT

Detection of drug vapors and volatile products of their decomposition is an important, and sometimes the only way to determine the presence of illegal drug traces at the surface of mail items, documents, hands and banknotes. This paper gives the results of experimental studies on the effect of UV irradiation on the sensitivity of a vapor phase detection of cocaine of different origin by a technology of ion mobility increment spectrometry (IMIS). It is shown that the influence of UV irradiation on the surface of cocaine hydrochloride and crack increases the amplitude of IMIS signals by about eight times. We analyzed ions emerged by photolysis of tested cocaine samples using mass-spectrometry with atmospheric pressure ionization (API-MS). The assumption is made about structural formula of volatile products of photolysis of crack and cocaine hydrochloride. By the results of API-MS and IMIS studies on photolysis of cocaine samples it is assumed that compound  $C_{10}H_{15}NO_3$  with a molecular weight of 197 amu and ecgonidine methyl ester with a molecular weight of 181 amu are responsible for the increase of an amplitude of IMIS signals upon UV irradiation of samples of crack and cocaine hydrochloride.

© 2008 Elsevier B.V. All rights reserved.

## 1. Introduction

There are a lot of tasks for which detection of drug vapors in a gas phase above an object is necessary. Forensic science and customs services encounter with such problems upon detection of concealed drugs, drug traces at the surface of mail items, documents, hands and banknotes. Methods using atmospheric pressure ionization followed by ion separation by mobility parameters are widely used for detection of drug vapors in a gas phase.

An ion mobility spectrometry method (IMS) first submitted by Cohen and Karasek [1], is now advanced for fast detection of concealed illicit substances (drugs, explosives) as well as for the evidence for the presence of concealed drug or explosive traces at the surface of suspicious or confiscated objects [2,3]. The most complete review of the IMS applications is given by Eiceman and Karpas [4].

One of the latest selective ionization methods for analyzing impurities in a gas phase is ion mobility increment spectrometry (IMIS) [5,6]. Ion nonlinear drift spectrometer [7], high-field asymmetric waveform ion mobility spectrometer (FAIMS) [8], field ion spectrometer (FIS) [9], radio-frequency-based ion-mobility analyzer [10], differential mobility spectrometer (DMS) [11] are used as a synonym for the IMIS.

Unlike the IMS where ions are separated in a longitudinal electrical field by their mobility coefficients, ion separation in the IMIS is based on the difference of ion mobility coefficient in strong and weak electric fields (effect of nonlinear ion mobility in a strong electric field [12]). Dispersion electric fields in the IMIS are formed by periodic asymmetric voltage  $U(t)$  satisfying the following condition:

$$\frac{1}{T} \int_t^{t+T} U(t) dt \equiv \langle U(t) \rangle = 0$$

$$\frac{1}{T} \int_t^{t+T} U^{2m+1}(t) dt \equiv \langle U(t)^{2m+1} \rangle \neq 0 \quad (1)$$

where broken brackets mean time averaging, and  $m \geq 1$  is an integer.

Ions executing fast oscillatory motions with period,  $T$ , drift across a carrier-gas flow along field lines with velocity,  $V_i$ , characteristic for each type of  $i$  ions. Transverse drift is compensated by a dc electric field created by compensation voltage,  $U_{ci}$ . Ions for which  $V_i = 0$ , are detected in the IMIS, the other one recombine at the electrodes. A signal registered by the IMIS is the compensation voltage dependence of the ion current ( $I(U_c)$ , drift spectrum). Thus, a measure of ion separation is compensation voltage,  $U_c$ , proportional to ion's parameter of nonlinear mobility.

As compared with the IMS, the IMIS technology offers advantages in sensitivity and resolution. First, while in the IMS ions injection is of a pulse nature, ions are continuously introduced into the IMIS, thus ensuring higher sensitivity. Second, the parameter of nonlinear ion mobility for the ions with a molecular weight

\* Corresponding author. Fax: +7 383 330 94 89.

E-mail address: [ykolom@che.nsk.su](mailto:ykolom@che.nsk.su) (Y.N. Kolomiets).

>100 amu is more specific than mobility coefficient, providing the advantage in ion separation by the IMIS.

The main problem of drug detection in a gas phase is a low saturated vapor pressure of these compounds. Actually, saturated cocaine vapor pressure (the most volatile drug) above its solid phase at room temperature is  $2.3 \times 10^{-12}$  g/cm<sup>3</sup> and above cocaine hydrochloride (the most widespread form of illegitimate and commercial cocaine) is  $5.6 \times 10^{-13}$  g/cm<sup>3</sup> [13]. Therefore, efficient sampling techniques are required to detect the compounds of interest.

One of the often-used techniques involves drug detection by the compound microparticles or by dust particles with drug molecules adsorbed on them. One takes drug samples from an object surface with special cloths, or cuts a test piece from an object surface sometimes. Cloths containing microparticles are placed into a heated injection device, and drug molecule desorb into analytical path of a gas analyzer. Such a technique along with a high sensitivity gives a high background level. Another way is to detect drugs by the products of their decomposition, or by attached foreign materials. Neudorfl et al. [14] suggested to detect cocaine concealed in marine containers by ecgonidine methyl ester (EDME), the product of cocaine thermal decomposition. The authors considered EDME as a possible compound for cocaine detection in a gaseous phase, since the saturated vapor pressure of EDME exceeds that of cocaine vapor by 5 orders of magnitude. We think photochemical decomposition of cocaine to be a possible way to increase sensitivity of its detection. We have no information about the papers on using the effect of UV irradiation to the purpose, but benzene ring and carbonyl group present in structural formula of cocaine suggest that cocaine can easily decompose under the action of UV yielding high-volatile decomposition products, by which it will be easy to detect cocaine in a gas phase above an object.

The present paper deals with experimental study on a gas phase above cocaine irradiated with UV to enhance sensitivity of cocaine detection with ion mobility increment spectrometry. At the same time using a method of mass-spectrometry with atmospheric pressure ionization (API-MS) one defines ions that appear upon cocaine photolysis and are responsible for the increase of the IMIS sensitivity.

## 2. Experimental

### 2.1. Instrumentation

To analyze sample vapor phase by the ion mobility increment spectrometry we used an experimental IMIS device developed by the Nikolaev Institute of Inorganic Chemistry of SB RAS, Novosibirsk, RUSSIA.

An experimental IMIS device (Fig. 1) contains ionization chamber 1 ( $\beta$ -source <sup>63</sup>Ni, temperature,  $t = 20 \pm 1$  °C); ion separation chamber 2 that is formed by two coaxial cylindrical electrodes with diameters  $d_1 = 0.5$  cm and  $d_2 = 0.94$  cm, 4 cm in length; ion collector 3; electrometric amplifier (width of baseline noise,  $5 \times 10^{-15}$  A) 4; asymmetric waveform dispersion voltage generator 5, compensation voltage generator 6. Flow of air–vapor mixture,  $Q_s = 50$  cm<sup>3</sup>/s, transports ions from the ionization chamber into the separation one, and further to the collector.

The asymmetric waveform dispersion voltage generator generated dispersion voltage  $U_d(t) = U_d \times f(t)$  that met conditions (1) with the following parameters:

voltage form  $f(t)$  described by equations

$$f(t) = \sin\left(\frac{\pi \cdot (t - mT)/t - (2\tau/\pi T)}{(1 - 2\tau/\pi T)}\right) \quad \text{with } mT \leq t \leq (mT + \tau),$$

$$f(t) = -\frac{(2\tau/\pi T)}{(1 - 2\tau/\pi T)} \quad \text{with } (mT + \tau) \leq t \leq (m + 1)T$$
(2)

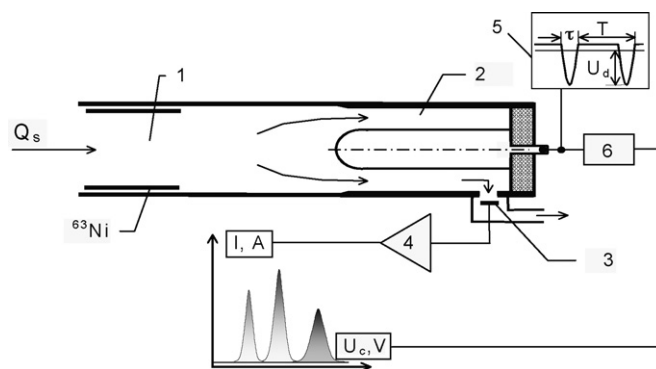


Fig. 1. Circuit diagram of IMIS device. (1) Ionization chamber; (2) ion separation chamber; (3) ion collector; (4) electrometer; (5) dispersion voltage generator; (6) compensation voltage generator;  $Q_s$ , flow of air–vapor mixture.

where  $m \geq 0$  is an integer. Voltage form (2) is shown graphically in rectangle 5. Voltage amplitude is  $U_d = -3600$  V; period is  $T = 14$   $\mu$ s; pulse duration is  $\tau = 4$   $\mu$ s. The limits of measurement error are:  $\delta U_c = \pm 2\%$  for compensation voltage;  $\delta U_d = \pm 10\%$  for asymmetric dispersion voltage amplitude;  $\delta t = \pm 5\%$  for pulse duration and oscillation period.

For chromatographic identification of the registered IMIS signals we used an EKHIO-M chromatograph of Multichrom Ltd., Novosibirsk, Russia (multicapillary column 220 mm in length; SE-30 stationary phase; ionization detector (ID) with  $\beta$ -source <sup>63</sup>Ni;

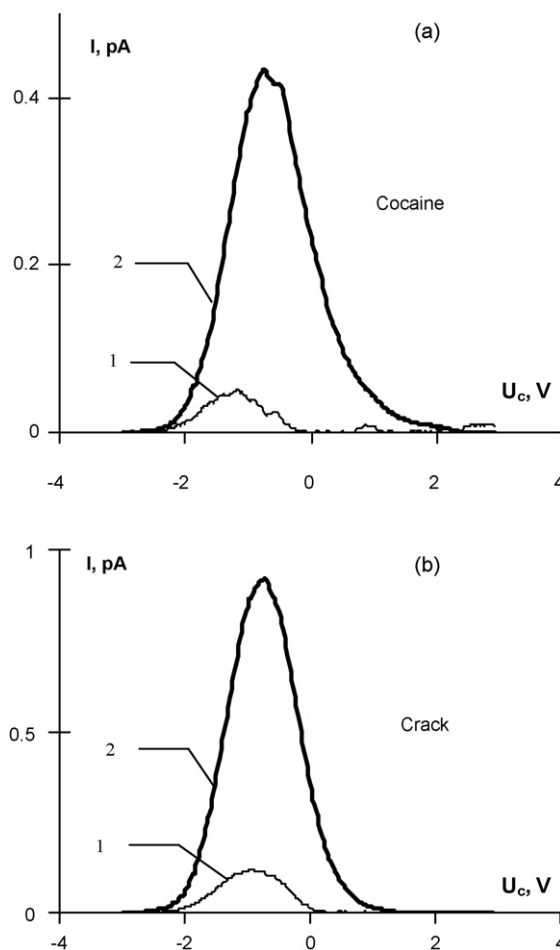


Fig. 2. Drift spectra of cocaine (a) and crack (b) vapors. Effect of ultraviolet irradiation (UV): (1) without UV, (2) with UV. Time of UV sample irradiation, 50–60 s.

**Table 1**  
Mass-spectrum peaks registered upon photolysis of cocaine hydrochloride and crack samples. The time of UV sample irradiation is 200 s.

M+1	Cocaine		Crack		Assumed structural formula
	Relative intensity <sup>a</sup> (without UV)	Relative intensity <sup>a</sup> (with UV)	Relative intensity <sup>a</sup> (without UV)	Relative intensity <sup>a</sup> (with UV)	
124	-	-	-	2.5	$\begin{array}{c} \text{C}_8\text{H}_{13}\text{N (Tropidine)} \\ \text{CH}_2 - \text{CH} - \text{CH} \\   \quad   \quad    \\   \quad \text{N-CH}_3 \quad \text{CH} \\   \quad   \\ \text{CH}_2 - \text{CH} - \text{CH}_2 \end{array}$
142	-	2.4	-	-	$\begin{array}{c} \text{C}_8\text{H}_{15}\text{NO (Tropanol)} \\ \text{CH}_2 - \text{CH} - \text{CH}_2 \\   \quad   \quad   \\   \quad \text{N-CH}_3 \quad \text{CH} - \text{OH} \\   \quad   \\ \text{CH}_2 - \text{CH} - \text{CH}_2 \end{array}$
150	-	-	2.8	2.5	$\begin{array}{c} \text{C}_{10}\text{H}_{15}\text{N} \\ \text{CH}_2 - \text{CH} - \text{C} - \text{CH} = \text{CH}_2 \\   \quad   \quad    \\   \quad \text{N-CH}_3 \quad \text{CH} \\   \quad   \\ \text{CH}_2 - \text{CH} - \text{CH}_2 \end{array}$
182	-	-	2.1	6.2	$\begin{array}{c} \text{C}_{10}\text{H}_{15}\text{NO}_2 \text{ (EDME)} \\ \text{CH}_2 - \text{CH} - \text{C} - \text{C} - \text{O} - \text{CH}_3 \\   \quad   \quad    \quad    \\   \quad \text{N-CH}_3 \quad \text{CH} \quad \text{O} \\   \quad   \\ \text{CH}_2 - \text{CH} - \text{CH}_2 \end{array}$
198	-	2.2	-	15	$\begin{array}{c} \text{C}_{10}\text{H}_{15}\text{NO}_3 \\ \text{CH}_2 - \text{CH} - \text{CH} - \text{C} - \text{O} - \text{CH}_3 \\   \quad   \quad   \quad    \\   \quad \text{N-CH}_3 \quad \text{C} = \text{O} \quad \text{O} \\   \quad   \\ \text{CH}_2 - \text{CH} - \text{CH}_2 \end{array}$
200	-	4.3	-	-	$\begin{array}{c} \text{C}_{10}\text{H}_{17}\text{NO}_3 \text{ (EME)} \\ \text{CH}_2 - \text{CH} - \text{CH} - \text{C} - \text{O} - \text{CH}_3 \\   \quad   \quad   \quad    \\   \quad \text{N-CH}_3 \quad \text{CH} - \text{OH} \quad \text{O} \\   \quad   \\ \text{CH}_2 - \text{CH} - \text{CH}_2 \end{array}$
260	-	-	-	5.8	$\begin{array}{c} \text{C}_{16}\text{H}_{21}\text{NO}_2 \\ \text{CH}_2 - \text{CH} - \text{CH} - \text{CH}_3 \\   \quad   \quad   \quad   \\   \quad \text{N-CH}_3 \quad \text{CH} - \text{O} - \text{C} - \text{C}_6\text{H}_5 \\   \quad   \quad    \\ \text{CH}_2 - \text{CH} - \text{CH}_2 \quad \text{O} \end{array}$

<sup>a</sup> From here on relative intensity =  $I/(3\text{Noise})$ , where  $I$ -peak amplitude,  $3\text{Noise}$ -threefold value of noise signal measured within a given mass range. Precision of relative intensity measurements-30% by 5 spectra. EDME-ecgonidine methyl ester, EME-ecgonine methyl ester.

flow rate through the column, 50 mL/min; column temperature, 175 °C; carrier-gas, purified air). As a standard we used cocaine solution in methanol (with a concentration of  $10^{-3}$  g/mL) of All-tech" (cat. No. 018003). An injected sample volume was 1  $\mu$ L. The ID output was fed directly into the analytical channel of the IMIS.

For API-MS studies we used a mass-spectrometer produced at the Nikolaev Institute of Inorganic Chemistry of SB RAS, Novosibirsk, RUSSIA on a basis of a monopole MX-7304A mass-analyzer (Electron production association, Sumy, Ukraine), which was described earlier [15]. Briefly, a vacuum system of the mass-spectrometer is a three-stage system of differential pumping.

During the first stage pumped down to 500 Pa with a backing pump with a rate of 5 L/s, ions transported into an inlet focus at a skimmer opening 0.3 mm in diameter and run into the second stage of differential pumping. The second staged is pumped down to  $10^{-1}$  Pa with a turbomolecular pump with a rate of 100 L/s. During this stage ions focus on the entrance aperture of the mass-analyzer. The monopole MX-7304A mass-analyzer is at the third stage of differential pumping with a vacuum of  $10^{-4}$  Pa. A minimum ion concentration registered at the device inlet is  $10^7$  cm<sup>-3</sup>. The analyzer resolution for a mass range of 10–350 amu is 1 M. To ionize a gas sample we use a 10 mCurie <sup>63</sup>Ni beta source.

For sample ionization we used a DRK-120 mercury-quartz lamp (LOMO PLC, St-Petersburg, Russia) (wavelength,  $\lambda = 360\text{--}440\text{ nm}$ ; power,  $W=280$ ). With a quartz lens we focused lamp beam at the sample to a spot of size  $20\text{ mm} \times 40\text{ mm}$  (IMIS) and  $10\text{ mm} \times 20\text{ mm}$ .

To control the heating of test samples during UV irradiation, we measured near-surface temperature using a Cu-Constantan thermocouple. We submerged one thermocouple junction in the sample to a depth of 1 mm and kept another one at  $0^\circ\text{C}$ . Precision of temperature measurement was  $\pm 1^\circ\text{C}$ . To determine the effect UV irradiation on sample heating, we recorded the IMIS and API-MS signals with no UV irradiation, in which case we heated the samples with an IR heater to the same temperature as upon UV irradiation.

## 2.2. Chemicals

The Research Institute of Special Techniques and Communication (Novosibirsk, Russia) provided samples of rock cocaine hydrochloride (hereafter cocaine) and crack in amounts of 96.2 and 8.8 ng, respectively. With a VG 7070 HS chromat-mass-spectrometer we tested the purity of cocaine hydrochloride samples; the main component content was 98%. We took crack samples, criminal objects that were of importance upon contraband detection, for comparison with pure cocaine samples. We did not study the crack sample composition on purpose. During experiments we used untreated powdered samples. We inserted samples tested with the IMIS into an open quartz weighing bottle, and samples tested with the API-MS we placed upon a body paper. We performed vapor sampling under laboratory atmosphere with a flow rate of 50 mL/s. Upon sampling we positioned an inlet of the gas analyzer (IMIS, API-MS)  $\sim 1\text{ cm}$  in diameter above an surface of sample examined at a distance of 10 mm.

## 3. Results and discussion

Drift spectra of cocaine and crack vapors and the effect of UV irradiation upon them are shown in Fig. 2. With no UV irradiation the peaks of cocaine samples (a thin line; peak amplitude, 0.05 pA; Fig. 2a) and crack samples (a thin line; peak amplitude, 0.12 pA; Fig. 2b) were registered at compensation voltage  $U_c = -1.2\text{ V}$  and  $U_c = 0.95\text{ V}$ , respectively. The action of UV irradiation on samples during 50–60 s results in considerable increase of peak amplitude (by eight times) (Fig. 2a and b, heavy line). The peak of cocaine increases to  $I = 0.43\text{ pA}$  ( $U_c = -0.67\text{ V}$ ), and the peak of crack grows to  $I = 0.92\text{ pA}$  ( $U_c = -0.76\text{ V}$ ). It is marked therewith that the value of compensation voltage shifts to zero and a slight peak asymmetry appears. It is most evident in cocaine (compensation voltage changes from  $U_c = -1.2$  to  $U_c = -0.67\text{ V}$ ). It should be mentioned that during the experiments with the IMIS UV irradiation for 50–60 s causes the sample surface to heat just by  $2\text{--}3^\circ\text{C}$ . As it is clear from the experiment, such a sample heating by  $3^\circ\text{C}$  without UV irradiation using an IR heater does not produce sensible changes in drift spectra reordered.

To determine whether the IMIS signals registered from crack and cocaine samples with no UV irradiation belonged to cocaine base, we identified peaks 1(a) and 1(b) with an ETKO-M chromatograph. We obtained a one-to-one correspondence between the peak of crack and cocaine hydrochloride detected by the IMIS and chromatographically separated cocaine fraction of an "Alltech" standard. Thus, one can state that in the absence of UV irradiation the IMIS detects from cocaine and crack samples the vapors of cocaine itself. It is very important for crack samples, which are criminal objects containing foreign compounds

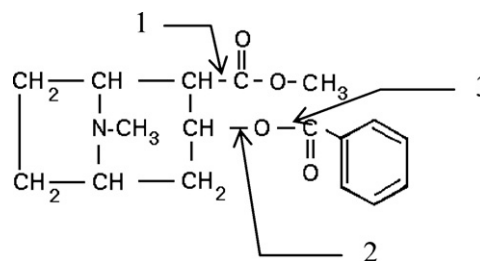


Fig. 3. Structural formula of cocaine. 1, 2, 3-chemical bonds broken at photolysis.

The compensation voltage shift and peak asymmetry (Fig. 2, curves 2a and b) can be caused by the emission of several compounds from the samples upon UV irradiation, which are not separated by the given IMIS experimentally. Ions registered possess a very low nonlinear ion mobility coefficient as indicated by low values of compensation voltage,  $U_c$  (from  $-0.67$  to  $-1.2\text{ V}$ ). Besides, halfwidth of peaks ( $\Delta U_c^{0.5} \sim 1.3\text{ V}$ ) compares well with  $U_c$  value. Under these conditions it is almost impossible to separate ions detected. To determine which ions are responsible for the signal increase upon UV irradiation of the samples, we conducted experiments on detection of cocaine and crack in a vapor phase with the API-MS simultaneously with the experiments using the IMIS.

Because of a very low MS sensitivity (as compared with the IMIS), we placed the samples tested on the body paper immediately under a sampling tube of the MS at a distance of 10 mm and not into the quartz weighing bottle. In the experiments with the MS the maximum time of UV irradiation was 50 min. The sample temperature after 5 min of UV irradiation became constant; therewith the sample heating did not exceed  $25\text{--}30^\circ\text{C}$ . Similar heating without UV irradiation using the IR heater did not give rise to signals in the MS-spectra.

Table 1 gives molecular weights registered in a vapor phase of cocaine and crack samples upon photolysis and assumed structural formulas. By the structural formulas of the compounds given in the table it is possible to assume that the main mechanisms of the photolytic reactions in cocaine hydrochloride and crack samples are similar to those of ketone photolysis and are linked with the presence of carbonyl groups in a cocaine molecule [16]. It is assumed that upon the action of UV irradiation substituting groups separate from tropan nucleus of a cocaine molecule along the bonds indicated by 1, 2 and 3 in Fig. 3. This results in volatile photolysis products given in Table 1, which are detected by the API-MS and IMIS.

There is a difference in the photolysis of cocaine hydrochloride and crack. The action of UV irradiation upon cocaine hydrochloride tends to break bonds 1 and 3 (Fig. 3). As a result emission of 3 compounds from the sample surface is observed. These

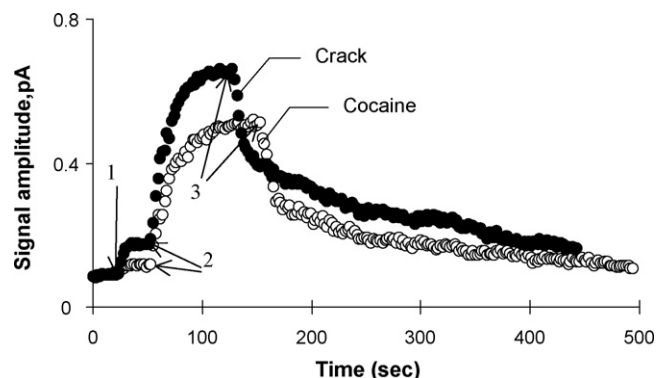
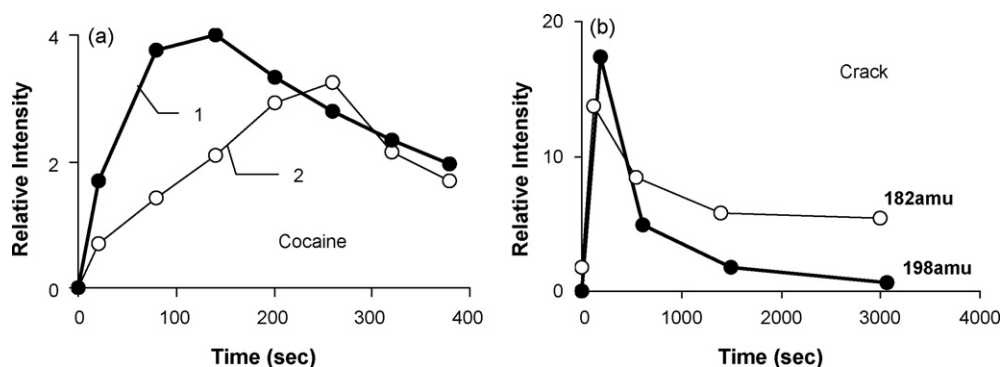


Fig. 4. Amplitudes of IMIS signals from crack and cocaine samples versus the time of UV irradiation. (1) Sample injection, (2) onset of UV irradiation, (3) termination of UV irradiation.



**Fig. 5.** Amplitudes of API-MS signals from cocaine and crack samples versus the time of UV irradiation. (a) Cocaine sample; amplitude of a peak with a molecular weight of  $M+1 = 198$  amu; area of UV irradiation focusing: (1)  $1\text{--}100\text{ mm}^2$ , (2)  $200\text{ mm}^2$ ; (b) crack sample.

compounds are: tropanol ( $\text{C}_8\text{H}_{15}\text{NO}$ , molecular weight, 141 amu); compound  $\text{C}_{10}\text{H}_{15}\text{NO}_3$  (molecular weight, 197 amu); ecgonine methyl ester ( $\text{C}_{10}\text{H}_{17}\text{NO}_3$ , molecular weight, 199 amu). Upon UV irradiation of crack bonds 1, 2 and 3 break and 5 compounds emit from its surface. These are: tropidine ( $\text{C}_8\text{H}_{13}\text{N}$ , molecular weight, 123 amu); compound  $\text{C}_{10}\text{H}_{15}\text{N}$  (molecular weight, 149 amu); ecgonidine methyl ester ( $\text{C}_{10}\text{H}_{15}\text{NO}_2$ , molecular weight, 181 amu); compound  $\text{C}_{10}\text{H}_{15}\text{NO}_3$  (molecular weight, 197 amu); compound  $\text{C}_{16}\text{H}_{21}\text{NO}_2$  (molecular weight, 259 amu).

Of all the compounds detected the two one that arouse interest are: compound  $\text{C}_{10}\text{H}_{15}\text{NO}_3$ , molecular weight, 197 amu and ecgonidine methyl ester (EDME). We think these compounds to be responsible for considerable increase of the signals in the IMIS spectrum upon UV irradiation (Fig. 2). Indeed, the proximity of compensation voltage values for crack and cocaine samples ( $U_c = -0.67\text{ V}$  for cocaine and  $U_c = -0.76\text{ V}$  for crack) allows one to assume that only one compound contributes to the increase of their signals upon UV irradiation. It is  $\text{C}_{10}\text{H}_{15}\text{NO}_3$  that we have detected both in crack and cocaine hydrochloride samples upon UV irradiation. Just as in the IMIS spectra (Fig. 2, curves 2a and b) the signal intensity of compound  $\text{C}_{10}\text{H}_{15}\text{NO}_3$  from the crack sample is much higher than that of signals from cocaine (Table 1). As for EDME, it should be mentioned that it is a product of thermal cocaine decomposition as well as a possible compound by which cocaine in a vapor phase can be detected. The production of EDME upon photochemical reaction of crack suggests that the mechanisms of photolysis and thermolysis of cocaine in crack samples are similar.

The time dependence of recorded spectra is a distinguishing feature of photochemical processes. Figs. 4 and 5 give the curves of the amplitude of MS and IMIS signals versus time. During the experiments performed with the IMIS we set compensation voltage to a value corresponding to a peak maximum and determined the time dependence of the IMIS signal. During the experiments with the MS we chose a narrow interval including molecular weights of 182 and 198 amu, and registered the variation of peak amplitudes with time.

Very early in the action of UV irradiation the crack and cocaine samples behave in a similar way: a sharp increase of their signals is observed in the IMIS and MS spectra (Figs. 4 and 5). From the estimation of the data obtained it is evident that the first 10 s of UV irradiation of the cocaine and crack samples result in a signal increase by a factor of 2–3. For crack, the increase of MS signals is observed both for a molecular weight of 182 and 198 amu (Fig. 5b). Following the termination of UV irradiation (3 on Fig. 4), at the decrement curve of the IMIS signals one can see portions of a relatively fast and slow change, which are likely to be responsible for different photochemical processes in samples tested. At the end of 500 s the IMIS signal falls to its initial value. The MS signal amplitudes of cocaine and crack samples reach their maximum within

100–200 s following the onset of UV irradiation (Fig. 5a and b). The rate of their increase grows with radiation intensity. Thus, a two times decrease in the area of UV irradiation focusing (from 200 to  $100\text{ mm}^2$ ) results in a twofold decrease of the time for the MS signal of cocaine to reach a maximum (Fig. 5a, curves 1 and 2). Long-term action of UV irradiation upon tested samples (more than 300 s) tends to decrease MS signals. Such a behavior can be explained by the fact that the products of photolysis conceal a free sample surface, and the rate of compound emission during photochemical reaction is thereby reduced. This is supported by the fact that after UV irradiation at the surface of crack and cocaine samples tested one can find traces tinged with yellow. One should point to the difference in the time dependence of the amplitudes of MS signals corresponding to molecular weights of 182 and 198 amu upon long-term irradiation of the crack samples. After 25 min of UV irradiation the peak amplitude of molecular weight 182 becomes constant, the intensity of molecular weight 198 after 50 min of UV irradiation goes down to zero. To find out what is responsible for this, is the subject of further studies on the processes of crack and cocaine photolysis. By the results of experiments with IR heating of the samples tested one may conclude that variations in sample temperature during UV irradiation thereof do not considerably affect the results obtained.

#### 4. Conclusion

The present paper shows that the action of UV irradiation upon crack and cocaine samples gives a eight times increase in sensitivity of a vapor phase detection of these compounds by the IMIS technology. From the results of mass-spectrometric studies with atmospheric pressure ionization one can assume that compound  $\text{C}_{10}\text{H}_{15}\text{NO}_3$  with a molecular weight of 197 amu, and ecgonidine methyl ester (EDME) produced upon UV irradiation contribute significantly to the increase of IMIS signals upon photolysis of crack and cocaine. Despite of the fact that crack is a raw substance containing impurities, the results of our studies show that it is possible to detect cocaine in crack samples of different origin by a vapor phase upon UV irradiation of the samples. The result obtained is of great practical importance in the light of the use of the IMIS device by forensic science and customs services for detection of cocaine traces at the surface of mail items, documents, hands and banknotes

#### Acknowledgements

The present work was performed with a financial support of RFBR Project # 07-08-00143-a, Russia.

#### References

- [1] M.J. Cohen, F.W. Karasek, J. Chromatogr. Sci. 8 (1970) 330.



- [2] C.-W. Su, K. Babcock, S. Rigdon, *IJIMS* 1 (1) (1998) 15–27.
- [3] Th. Keller, et al., *IJIMS* 2 (1) (1999) 22–34.
- [4] G.A. Eiceman, Z. Karpas, *Ion Mobility Spectrometry*, CRC Press, Boca Raton, FL, 1994.
- [5] M.P. Gorshkov, USSR Inventors Certificate No. 966583 (1982).
- [6] I.A. Buryakov, E.V. Krylov, E.G. Nazarov, U.K. Rasulev, *Int. J. Mass Spectrom. Ion Process.* 128 (1993) 143.
- [7] I.A. Buryakov, Y.N. Kolomiets, B.V. Luppu, *J. Anal. Chem.* 56 (2001) 336.
- [8] R. Guevremont, *J. Chromatogr. A* 1058 (2004) 3–19.
- [9] B.L. Carnahan, A.S. Tarassov, US Patent 5,420,424 (1995).
- [10] G.A. Eiceman, B. Tadjikov, E. Krylov, E.G. Nazarov, R.A. Miller, J. Westbrook, P. Funk, *J. Chromatogr. A* 917 (2001) 205.
- [11] C.A. Veasey, C.L.P. Thomas, *Analyst* 129 (2004) 198.
- [12] E.A. Mason, E.W. McDaniel, *Transport Properties of Ions in Gas*, John Wiley & Sons, New York, 1988, p. 160.
- [13] A.B. Dindal, M.V. Buchanan, R.A. Jenkins, C.K. Bayne, *Analyst* 125 (2000) 1393–1396.
- [14] P. Neudorfl, M. Hupe, P. Pilon, A.H. Lawrence, *Anal. Chem.* 69 (1997) 4283–4285.
- [15] V.V. Pervukhin, R.R. Ibragimov, V.M. Moralev, *Instrum. Exp. Technol.* 40 (1997) 700.
- [16] J.G. Calvert, J.N. Pitts, *Photochemistry*, John Wiley & Sons, New York, 1966.



## Quantitative analysis of human serum leptin using a nanoarray protein chip based on single-molecule sandwich immunoassay

Seungah Lee<sup>a</sup>, Shinae Lee<sup>b</sup>, Young-Ho Ko<sup>b</sup>, Hyungil Jung<sup>c</sup>, Jung Dong Kim<sup>c</sup>, Joon Myong Song<sup>d</sup>, Jaebum Choo<sup>e</sup>, Seong Kug Eo<sup>f</sup>, Seong Ho Kang<sup>a,\*</sup>

<sup>a</sup> Department of Chemistry and Research Institute of Physics and Chemistry (RINPAC), Chonbuk National University, 664-14, 1-Ga, Duckjin-Dong, Duckjin-Gu, Jeonju 561-756, South Korea

<sup>b</sup> Department of Physical Education, Chonbuk National University, Jeonju 561-756, South Korea

<sup>c</sup> Department of Biotechnology, Yonsei University, Seoul 120-749, South Korea

<sup>d</sup> Research Institute of Pharmaceutical Sciences and College of Pharmacy, Seoul National University, Seoul 151-742, South Korea

<sup>e</sup> Department of Applied Chemistry, Hanyang University, Ansan 426-791, South Korea

<sup>f</sup> Laboratory of Microbiology, College of Veterinary Medicine, Chonbuk National University, Jeonju 561-756, South Korea

### ARTICLE INFO

#### Article history:

Received 20 October 2008

Received in revised form 6 December 2008

Accepted 8 December 2008

Available online 24 December 2008

#### Keywords:

Human leptin

Nanoarray protein chip

Single-molecule sandwich immunoassay

Total internal reflection fluorescence microscopy (TIRFM)

### ABSTRACT

We report a method for the quantitative analysis of human serum leptin, which is a protein hormone associated with obesity, using a nanoarray protein chip based on a single-molecule sandwich immunoassay. The nanoarray patterning of a biotin-probe with a spot diameter of 150 nm on a self-assembled monolayer functionalized by MPTMS on a glass substrate was successfully accomplished using atomic force microscopy (AFM)-based dip-pen nanolithography (DPN). Unlabeled leptin protein molecules in human serum were detected based on the sandwich fluorescence immunoassay by total internal reflection fluorescence microscopy (TIRFM). The linear regression equation for leptin in the range of 100 zM–400 aM was determined to be  $y = 456.35x + 80,382$  ( $R = 0.9901$ ). The accuracy and sensitivity of the chip assay were clinically validated by comparing the leptin level in adult serum obtained by this method with those measured using the enzyme-linked immunosorbent assay (ELISA) performed with the same leptin standards and serum samples. In contrast to conventional ELISA techniques, the proposed chip methodology exhibited the advantages of ultra-sensitivity, a smaller sample volume and faster analysis time.

© 2009 Elsevier B.V. All rights reserved.

### 1. Introduction

Leptin is a protein hormone associated with obesity, appetite regulation, energy expenditure, and reproduction in animals and humans. Noticeably higher leptin levels have been observed in obese humans than in non-obese humans [1–3]. Leptin is thought to contribute to body weight regulation by controlling food intake and energy expenditure at the hypothalamic level [4]. It has been suggested that abnormalities in its level increase the propensity to obesity. In addition to its role in metabolic disorders and obesity, leptin also has an important regulatory effect on bodily hormonal [5,6] and gonadal [7] functions. So far, the capillary electrophoresis [8–10], immunofunctional assay [11], enzyme-linked immunosorbent assay (ELISA) [12,13], radioimmunoassay [14–18] and Western blotting [19–21] techniques have been conventionally used to determine human leptin. Although they are reliable, these methods are relatively expensive and are restricted to the determination of single target specificity.

The possible application of microarray biochips to the analysis of various cytokines, including leptin, in serum samples, was demonstrated by Du et al. [22]. The ability to fabricate highly robust microarrays in which a thousand samples are immobilized enables the generation of massive amounts of biologically relevant data using low sample quantities. Recently, nanoarray technology has been suggested as a means of overcoming the problems of microarray technology, such as the relatively large sample volumes and long incubation times that are required, and the high limits of detection (LOD). A new generation nanoarray biochip has also been described which is capable of supporting high-throughput and multiplexed ELISA. Despite its advantages, the nanoarray assay is not able to achieve the femtomolar (fM,  $\times 10^{-15}$  M) LOD of ELISA, which limits its applications in immunoassays [23,24]. However, the detection of proteins in the zeptomolar concentration range (zM,  $\times 10^{-21}$  M) has recently been demonstrated using a mass spectrometer or gold nanoparticles conjugated with antibodies [25,26]. Proteins in the zM concentration range exhibit almost no detectable, nonspecific binding to the passivated portions of nanoarrays, even when they are present in the form of complex mixtures, and therefore provide the opportunity to study a variety of surface-mediated, biological recognition processes.

\* Corresponding author. Tel.: +82 63 270 3421; fax: +82 63 270 3408.  
E-mail address: [shkang@chonbuk.ac.kr](mailto:shkang@chonbuk.ac.kr) (S.H. Kang).

This paper reports the development of a nanoarray protein chip for the quantitative analysis of human leptin in serum at the zM–aM concentration level. The leptin protein nanoarrays formed via atomic force microscopy (AFM)-based dip-pen nanolithography (DPN) were detected using a total internal reflection fluorescence microscopy (TIRFM) system at the single-molecule level based on a single-molecule sandwich fluorescence immunoassay. Leptin protein molecules at the 100 zM concentration level in human serum were detected on the nanoarray protein chip without any non-specific binding of protein molecules. The nanoarray protein chip assay was further clinically validated by comparing the leptin level in adults obtained by this method with that measured using the conventional ELISA performed with the same leptin standards and serum samples.

## 2. Experimental

### 2.1. Chemical and reagents

(3-Mercaptopropyl)trimethoxysilane (MPTMS), streptavidin, biotinylated protein G (BPG) and Tween-20 were obtained from Sigma–Aldrich (St. Louis, MO). mPEG–maleimide (5K), used as a blocking solution, was purchased from IDB (ID Biochem Inc., Seoul, Korea), streptavidin–Alexa Fluor® 488 from Molecular Probes (Eugene, OR, USA), and Ez-Link® maleimide–PEO<sub>2</sub>–biotin from Dojindo (Dojindo Laboratories, Japan). Rabbit polyclonal antibody to human leptin (Abcam, Cambridge, UK) was used as the first antibody on the nanoarray protein chip. All samples were diluted with a 1× phosphate buffered saline (PBS; 137 mM NaCl, 2.7 mM KCl, 4.3 mM Na<sub>2</sub>HPO<sub>4</sub>, 1.4 mM KH<sub>2</sub>PO<sub>4</sub>, and pH 7.4) buffer solution. All buffer solutions were prepared with ultra-pure water (>18 MΩ) and filtered through a 0.2-μm membrane filter (nylon membrane filter, Whatman International Ltd., Maidstone, England) and photo-bleached overnight using a UV–B lamp (G15TE, 280–315 nm, Philips, The Netherlands). A human leptin ELISA kit (cat. no. EZHL-80SK) was purchased commercially from Millipore Co. (Charles, MO, USA).

### 2.2. Preparation of human serum samples

Blood samples were obtained from five healthy humans with a body mass index (BMI) range of 19.1–30.5 kg/m<sup>2</sup>. The serum samples were isolated from the blood by centrifuging at 2000 rpm for 15 min at 2 °C and stored at –20 °C prior to the experiment. The concentrations of human leptin in the serum samples were quantified using the conventional sandwich ELISA and the nanoarray protein chip.

### 2.3. Nano-patterning on the MPTMS-coated cover glass

The following, two-step silanization procedures were performed for the fabrication of the nano-pattern [27]. Briefly, a Corning glass cover slip (No. 1, 22 mm<sup>2</sup>) was silanized by evaporating 2 μL of neat liquid MPTMS onto it at 120 °C for 30 min and then gently washing with deionized water. After drying in nitrogen, the resulting, MPTMS-coated substrate was arrayed with maleimide–PEO<sub>2</sub>–biotin (1 mg/mL) at room temperature by DPN. The DPN nano-pattern was produced using an evaporation method [28]. Briefly, 2 μL of MPTMS was evaporated onto the substrate using a clean AFM tip (silicon nitride cantilever, force constant (*k*) of 42 N/m) with a radius of curvature of ≤10 nm at 120 °C for 30 min and then further coated with DPN ink for 10 min in maleimide–PEO<sub>2</sub>–biotin (1 mg/mL) containing 0.05% Tween-20 in 1× PBS, and blow-dried with nitrogen. The DPN experiments were performed using a Bio-AFM (atomic force microscope, NanoScope IIIa controller) from Digital Instruments. The relative humidity was

adjusted to 60% by purging with nitrogen gas that had been bubbled through water in a large glove box. All DPN experiments were performed in tapping mode at room temperature.

### 2.4. Nanoarray protein chip assay of human leptin

The MPTMS-coated cover glasses were nano-patterned with biotin molecules using the DPN technique. mPEG–maleimide (5K) (1 mg/mL in 1× PBS), which is resistant to nonspecific adsorption, was incubated on the biotin nano-pattern chip for 10 min, because the maleimide groups of mPEG–maleimide (5K) react efficiently and specifically with free sulfhydryl groups at pH 6.5–7.5 to form stable thioether bonds. Streptavidin (33.4 nM) was incubated with the biotin nano-pattern chip for 10 min. The streptavidin-bound biotin chip was allowed to react for 1 h with 50 μL of 2 μg/mL BPG to facilitate the binding of the antibody Fc regions, after which it was reacted for 1 h with 50 μL of rabbit polyclonal antibody to human leptin (150 kDa; 13.3 nM). The chip was incubated again for 1 h with various concentrations of standard leptin antigens (100 zM–7.8 pM) or human serum samples and then for 1 h with 50 μL of human leptin detection antibody (i.e., the biotinylated mouse anti-human leptin antibody in the ELISA kit). Finally, streptavidin–Alexa Fluor® 488 was reacted leptin antigens for 10 min to obtain the TIRFM images. The chip was washed by dipping it in 100 mL of 1× PBS-T for 2 min at each step, and washed for 2 min with PBS before image acquisition. All reactions were carried out under agitation at 25 °C.

### 2.5. Laboratory-built TIRFM system

The basic experimental set-up of the lab-built, prism-type, TIRFM system (Fig. 1) used to quantitatively analyze the human leptin on the nanoarray protein chip was similar to that described in previous reports [29,30]. Briefly, an argon ion laser (model 532-LAP-431-220; Melles Griot, Irvin, CA; output 40 mW at 488 nm) was used as the excitation source. TIRFM was performed using an upright Olympus BX51 microscope (Olympus Optical Co. Ltd., Shinjuku-ku, Tokyo) with an Olympus 100x UPLFL objective lens (oil type, 1.3 N.A., W.D. 0.1 mm). The objective lens was matched to the nanoarray chip with an immersion oil (ImmersoI™ 518F, Zeiss, *n* = 1.518). A CCD camera (QuantEM 512SC, Photometrics, Tucson, AZ) was used as a detector with an exposure time of 100 ms. A filter cube with a 488-nm notch filter (Korea Electro Optics, Korea) and a 530-nm band-pass filter (FWHM 20 nm, Olympus Optical Co. Ltd., Shinjuku-ku, Tokyo) was installed between the CCD camera and the objective lens. After the completion of all reactions, the nanoarray

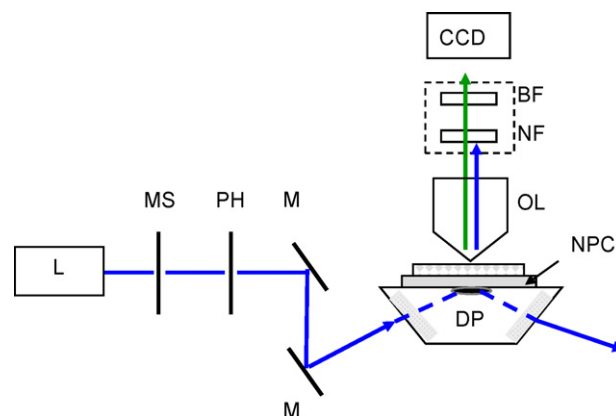


**Fig. 1.** Schematic diagram of the TIRFM system used for the quantitative analysis of human leptin. The dotted box indicates the filter cube with NF and BF. The following acronyms are used: L, laser; MS, mechanical shutter; PH, pinhole; M, mirror; DP, dove prism; NPC, nanoarray protein chip; OL, objective lens; NF, notch filter; BF, band-pass filter.

protein chip was placed on an all-side polished dove prism. The laser beam was then directed through the prism toward the protein chip/media interface at an incidence angle ( $\theta_i$ ) slightly greater than  $72^\circ$ . In order to reduce the photobleaching, a Uniblitz mechanical shutter (Model LS3Z2, Vincent Associates, Rochester, NY) was used to block the laser beam when the camera was switched off. All images were acquired and analyzed with MetaMorph 7.0 software (Universal Imaging Co., Downing Town, PA).

## 2.6. ELISA of human leptin

The sandwich ELISA was conducted according to the protocol of the human leptin ELISA kit [31]. Human leptin standards (1.95–780 pM) and 25  $\mu$ L/well human serum samples were added to 75  $\mu$ L/well of assay buffer (0.05 M PBS, pH 7.4, containing 0.025 M EDTA, 0.08% sodium azide, 1% BSA and 0.05% Triton X-100). After the completion of all reactions, stop solution was added, and the absorbance at 430 nm was measured with a SpectraCount™ ELISA reader (Packard Instrument Co., Downers Grove, IL, USA).

## 2.7. AFM measurement

The height of the surface topology of the first antibody/BPG/streptavidin/biotin layer on the chip was obtained using an AFM (NanoScope microscope, Digital Instruments) equipped with a type-J scanner (scan size, 100  $\mu$ m) and operating in tapping mode for air imaging. The resonance frequency of the silicon tips (Olympus Co. Ltd., Japan) was 300 kHz. These 150–160  $\mu$ m short cantilevers had a nominal force constant ( $k$ ) of 42 N/m and a tip with a radius curvature of  $\leq 10$  nm. The AFM images were obtained by means of NanoScope software.

## 3. Results and discussion

### 3.1. Functionalized MPTMS-coated glass surface for nanoarray leptin chip

The direct deposition of the functional protein in the nanodomains demonstrated the viability of the nanoarray leptin protein chip (Fig. 2A). To construct oriented streptavidin layers, the MPTMS-coated glass surface consisting of thiol-terminated silane was patterned ( $4 \times 4$  dot) with biotin as the maleimide group of maleimide-PEO<sub>2</sub>-biotin by DPN. The diameter of the spots of maleimide-PEO<sub>2</sub>-biotin, which have a theoretical height of 2.91 nm, was measured to be 150 nm by AFM (upper figure of Fig. 2B). Streptavidin (height of 5 nm) [32] was uniformly oriented through the reaction for 10 min at 25 °C. To immobilize the polyclonal leptin antibody, the other side of the oriented streptavidin chip was reacted with BPG. The epitope binding site of the antibody was immobilized on the protein G, because protein G facilitates the binding of the antibody Fc regions. To test whether the leptin antibody proteins deposited in the nanoarrays retain their biological activity and the accessibility of the antigen–antibody binding sites, we measured the height of the first antibody/BPG with streptavidin on the biotin-patterned chip after reacting the first antibody for 1 h (bottom at Fig. 2B). The height of protein G is theoretically 1.35 nm [33] and the first antibody is a Y-shaped molecule with approximate dimensions of 8.5 nm in height, 14.5 nm in width and 4 nm in thickness [34]. The measured height of the first antibody/BPG interacting with streptavidin on the biotin-patterned chip was approximately  $19.9 \pm 1.5$  nm ( $n=3$ ), which differed from the theoretical height of 17.8 nm by about 2.1 nm. This result indicated that the use of the MPTMS-coated, glass nanoarray, protein chips functionalized with streptavidin and protein G decreased the steric effect and nonspecific binding, as well as the binding of the first antibody.

### 3.2. Single-molecule sandwich fluorescence immunoassay on nanoarray leptin chip

In the nanoarray leptin protein chip based on the single-molecule sandwich fluorescence immunoassay, the fluorescence intensity of the array spot was proportional to the antigen concentration (Fig. 3). With increasing standard leptin concentration, the spot size and number of relative fluorescence units (RFUs) increased. However, when the leptin concentration exceeded 400 aM, the number of RFUs no longer increased due to its dependence on the number of leptin molecules at the first antibody concentration (13.3 nM) on the nanoarray chip. After the reaction of BPG with the first antibody on the nanoarray protein chip for 1 h, the chip was incubated again for 1 h with various human serum samples and standard leptin antigens. At concentrations of leptin above 800 zM, the optimum incubation time between the antigen and antibody was 1 h. However, at a leptin concentration of 100 zM, the incubation time required to attain a sufficient binding probability of individual leptin molecules to the antibody molecules was extended to 4 h, because the theoretical molecular number of leptin is only 3 at the ultra-low concentration of 100 zM. This result demonstrated the potential application of single-molecule, sandwich-type, antibody nanoarrays for the detection of individual protein molecule markers at the single-molecule level.

### 3.3. Quantification of human leptin protein using the nanoarray chip

The leptin standards in the human leptin ELISA kit of Linc Research (cat. no. EZHL-80SK) were used as human leptin standards. The leptin was serially diluted with  $1 \times$  PBS buffer solution to determine the linear range and define the LOD. A representative calibration curve based on the plot of the spot fluorescence intensity against the human leptin standard in the range of concentrations of 100 zM–7.8 pM using the nanoarray protein chip and TIRFM is shown in Fig. 4A. The linear range was 100 zM–400 aM (correlation coefficient,  $R=0.9901$ ) in the assay of the nanoarray protein chip (Fig. 4B). The spot intensity values were calculated after background subtractions. The LOD of the leptin protein was 100 zM in the nanoarray leptin protein chip assay.

### 3.4. Comparison of ELISA and nanoarray protein chip

We used the linear ranges to compare the nanoarray leptin protein chip with a commercially available ELISA kit having a linear range of 1.95 pM–0.78 nM ( $R=0.9968$ ). The LOD of the ELISA was 1.95 pM. The features of the two methods for the quantitative analysis of human serum leptin (ELISA and nanoarray leptin protein chip assay) are shown in Table 1. The lowest LOD was obtained using the assay of the nanoarray protein chip based on the single-molecule sandwich fluorescence immunoassay at a leptin concentration of 100 zM, which was about  $1.95 \times 10^5$ -fold lower than the LOD of 1.95 pM achieved using the conventional ELISA assay technique. The minimum sample volume required by ELISA was 100  $\mu$ L, compared to 20  $\mu$ L for the nanoarray protein chip, although a 50  $\mu$ L sample was used at the zeptomolar concentration level due to the scarcity of leptin molecules (i.e., 3 and 24 molecules at 100 and 800 zM, respectively, in Fig. 3). The nanoarray leptin protein chip method exhibited the advantages of a shorter reaction time, smaller required sample volume and excellent sensitivity (Table 1).

### 3.5. Clinical applications of nanoarray leptin protein chip

We used ELISA and the nanoarray leptin protein chip to make single measurements on five different serum samples obtained from five healthy females. For the quantitative analysis of leptin, the

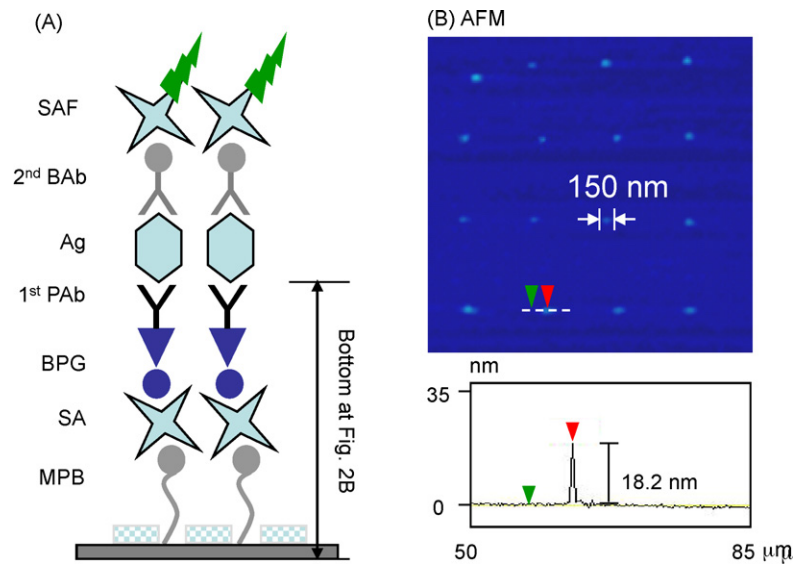


**Fig. 2.** (A) Schematic diagram of the antibody–antigen reactions on the nanoarray protein chip based on the single-molecule sandwich immunoassay, and (B) AFM tapping mode images of a  $4 \times 4$  nanoarray (150 nm) of dots patterned by DPN (upper figure) and height profile of first antibody/BPG with streptavidin on biotin-patterned chip (lower figure). The red and green arrows indicate the reacted spot on the chip surface. The following acronyms are used: MPB, maleimide- $\text{PEO}_2$ -biotin; SA, streptavidin; BPG, biotinylated protein G; 1st PAb, first polyclonal antibody; Ag, antigen; 2nd BAb, second biotinylated antibody; SAF, streptavidin-Alexa 488.

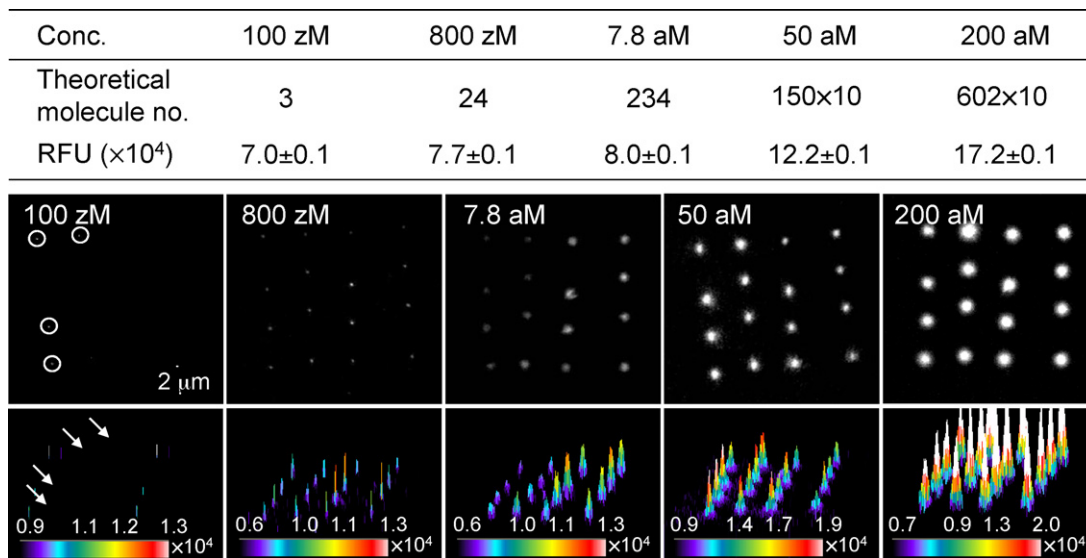


**Fig. 3.** Spot fluorescence intensity produced by serially diluted, human standard leptins in the linear range of the calibration standard curve. Serially diluted, human standard leptins were exposed to 13.3 nM first polyclonal antibodies. The determined spot fluorescence intensities were corrected by background subtraction ( $n=5$ ). RFU = relative fluorescence unit.

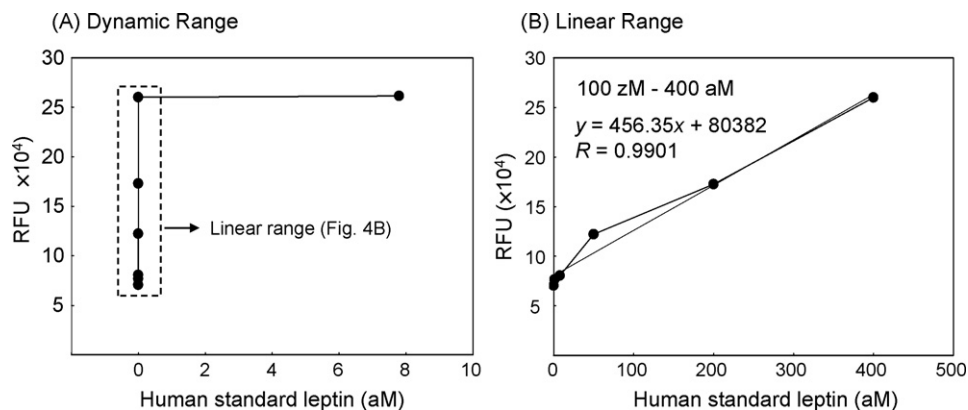


**Fig. 4.** Calibration curve of (A) dynamic range and (B) linear range on the nanoarray protein chip for human standard leptin using TIRFM. Serially diluted, human standard leptins were exposed to 13.3 nM first polyclonal antibodies. The other conditions used were the same as those shown in Fig. 3. RFU = relative fluorescence unit.

**Table 1**  
Comparison of the two methods for the quantitative analysis of human serum leptin.

	Reaction time	Sample vol.	LOD <sup>a</sup>	Linear range <sup>b</sup>	R <sup>c</sup>
ELISA	3.5 h	100 $\mu$ L	1.95 pM	1.95–780 pM <sup>d</sup>	0.9968
Nanoarray chip	2.5 h	50 $\mu$ L	100 zM	100 zM–400 aM	0.9901

<sup>a</sup> LOD: limit of detection.

<sup>b</sup> The linear range of the method is the human leptin concentration range over which the response is proportional to concentration.

<sup>c</sup> R: correlation coefficient.

<sup>d</sup> The linear range of ELISA was decided on the ELISA kit [31].

**Table 2**  
Paired *t*-test for comparing individual differences of human serum leptin by the methods of ELISA and nanoarray leptin protein chip.

Serum samples	Age	BMI <sup>a</sup> (kg/m <sup>2</sup> )	ELISA (pM)	Nanoarray chip (pM)	Difference
1	39	19.1	16.4	17.3	–0.9
2	46	23.9	77.0	82.1	–5.1
3	43	22.7	127.3	122.5	4.8
4	36	21.6	212.9	211.7	1.2
5	34	26.6	417.0	401.5	15.5

Mean = 3.1; std. dev. = 7.8;  $t_{\text{calculated}} = 0.8$ .

<sup>a</sup> BMI (kg/m<sup>2</sup>) = the body mass index.

linear range of human leptin was used with the leptin standards in the human leptin ELISA kit, which has a response proportional to the concentration. The leptin level in the human serum was quantified by two methods (ELISA vs. nanoarray leptin protein chip assay), and the significance of any difference ( $d_i$ ) between the methods was determined using the paired Student's *t*-test. The "Difference" column in Table 2 presents the difference ( $d_i$ ) between the two results for each serum sample. The calculated mean ( $\bar{d}$ ) and standard deviation ( $S_d$ ) of the 5 differences were 3.1 and 7.8, respectively. The value of  $t_{\text{calculated}}$  was calculated to be 0.8 according to the following formula:

$$t_{\text{calculated}} = \left( \frac{|\bar{d}|}{S_d} \right) (n)_{1/2} = 0.8$$

where  $|\bar{d}|$  is the absolute value of the mean difference.

The difference between the two assay methods was not significantly different at the 95% confidence level. These results showed that the signal response on the nanoarray chip was proportional to the concentration, which may produce correct values in the ultra-low concentration range. These study results support the feasibility of using the nanoarray leptin protein chip for the detection and quantification of leptin proteins in human serum at ultra-low concentration levels (i.e., aM–zM).

#### 4. Conclusions

We successfully developed a single-molecule sandwich-type nanoarray chip for the analysis and quantification of leptin, which is a protein hormone associated with obesity. Leptin protein molecules at concentrations of the order of 100 zM ( $\times 10^{-21}$  M) in human serum were detected on the nanoarray protein chip without any nonspecific binding of protein molecules. We compared the LOD and quantification of our nanoarray protein chip with that of a commercial ELISA kit. The nanoarray leptin protein chip exhibited an ultra-low LOD of 100 zM, which was  $1.95 \times 10^7$ -fold lower than that of the ELISA used. The high accuracy and sensitivity of the nanoarray leptin protein chip could facilitate its use in the quantification of other marker proteins of cytokines in serum samples.

#### Acknowledgments

The authors thank KBSI for supporting the AFM experiments. This work was supported by a grant from the Korea Science & Engineering Foundation (R01-2007-000-20238-0).

#### References

- [1] R.V. Considine, M.K. Sinha, M.L. Heiman, A. Kriauciunas, T.W. Stephens, M.R. Noyce, J.P. Ohannessian, C.C. Marco, L.J. Mckee, T.L. Bauer, J.F. Caro, N. Engl. J. Med. 334 (1996) 292.
- [2] M. Rosicka, M. Krsek, M. Matoulek, Z. Jarkovska, J. Marek, V. Justova, Z. Lacinova, Physiol. Res. 52 (2003) 61.
- [3] M. Orel, R. Lichnovska, S. Gwozdziwiczova, N. Zlamalova, I. Klementa, A. Merkunova, J. Hrebicek, Physiol. Res. 53 (2004) 501.
- [4] M. Wauters, R.V. Considine, L.F.V. Gaal, Eur. J. Endocrinol. 143 (2000) 293.
- [5] E. Carro, R. Senaris, R.V. Considine, F.F. Casanueva, C. Dieguez, Endocrinology 138 (1997) 2203.
- [6] M. Shimabukuro, K. Koyama, G. Chen, M.T. Wang, F. Trieu, Y. Lee, C.B. Newgard, R.H. Unger, Proc. Natl. Acad. Sci. U.S.A. 94 (1997) 4637.
- [7] R.V. Garcia-Mayor, M.A. Andrade, M. Rios, M. Lage, C. Dieguez, F.F. Casanueva, J. Clin. Endocrinol. Metab. 82 (1997) 2849.
- [8] M.P. Richards, C.M. Ashwell, J.P. McMurtry, Electrophoresis 21 (2000) 792.
- [9] M.P. Richards, C.M. Ashwell, J.P. McMurtry, J. Chromatogr. A 853 (1999) 321.
- [10] A.N. Blackburn, R.R. Holloway, Proceedings of the 60th Southwest Regional Meeting of the American Chemical Society, September 29–October 4, Fort Worth, TX, United States, 2004 (abstracts).
- [11] J. Kratzsch, A. Berthold, A. Lammert, W. Reuter, E. Keller, W. Kiess, Horm. Res. 57 (2002) 127.
- [12] www.lincoresearch.com.
- [13] A. Theriault, T. Agdinaoay, N.B. Ladao, H. Chang, A. Grandinetti, Clin. Lab. Sci. 14 (2001) 6.
- [14] Y. Shi, G.T. Yan, J. Lin, Regul. Pept. 133 (2006) 27.
- [15] D. Modan-Moses, H. Kanety, O. Dagan, C. Pariente, R. Ben-Abraham, L. Freedman, T. Prince, I. Shimon, Z. Barzilay, G. Paret, J. Cardiothorac. Vasc. Anesth. 15 (2001) 740.
- [16] T. Laml, B.W. Hartmann, O. Preyer, E. Ruecklinger, G. Soeregi, P. Wagenbichler, Gynecol. Endocrinol. 14 (2000) 442.
- [17] U. Leonhardt, U. Ritzel, G. Schafer, W. Becker, G. Ramadori, J. Endocrinol. 157 (1998) 75.
- [18] M.C. Henson, V.D. Castracane, J.S. O'Neil, T. Gimpel, K.F. Swan, A.E. Green, W. Shi, J. Clin. Endocrinol. Metab. 84 (1999) 2543.
- [19] M.G. Li, G.L. Ding, X.J. Chen, X.P. Lu, L.J. Dong, M.Y. Dong, X.F. Yang, X.E. Lu, H.F. Huang, J. Clin. Endocrinol. Metab. 92 (2007) 4771.
- [20] C.R. Cederroth, M. Vinciguerra, A. Gjinovci, F. Kühne, M. Klein, M. Cederroth, D. Caille, M. Suter, D. Neumann, R.W. James, D.R. Doerge, T. Wallimann, P. Meda, M. Foti, F. Rohner-Jeanrenaud, J.D. Vassalli, S. Nef, Diabetes 57 (2008) 1176.
- [21] J.E. Brown, S.J. Dunmore, Diabetes Metab. Res. Rev. 23 (2007) 497.
- [22] W. Du, Z. Xu, X. Ma, L. Song, E.M. Schneider, J. Biotechnol. 106 (2003) 87–100.
- [23] J. Henry, A. Anand, M. Chowdhury, G. Cotei, R. Moreira, T. Good, Anal. Biochem. 334 (2004) 1.
- [24] S. Wang, C. Zhang, J. Wang, Y. Zhang, Anal. Chim. Acta 546 (2005) 161.
- [25] Y. Shen, N. Tolić, C. Masselon, L. Pasa-Tolić, D.G. 2nd Camp, M.S. Lipton, G.A. Anderson, R.D. Smith, Anal. Bioanal. Chem. 378 (2004) 1037.
- [26] S.-Y. Hou, H.-K. Chen, H.-C. Cheng, C.-Y. Huang, Anal. Chem. 79 (2007) 980.
- [27] H. Jung, R. Kulkarni, C.P. Collier, J. Am. Chem. Soc. 125 (2003) 12096.
- [28] H. Jung, C.K. Dalal, S. Kuntz, R. Shah, C.P. Collier, Nano Lett. 4 (2004) 2171.
- [29] S. Lee, J.S. Choi, S.H. Kang, J. Nanosci. Nanotechnol. 7 (2007) 3689.
- [30] S.H. Kang, Y.-J. Kim, E.S. Yeung, Anal. Bioanal. Chem. 387 (2007) 2663.
- [31] http://www.abcam.com.
- [32] A.S. Anderson, A.M. Dattelbaum, G.A. Montano, D.N. Price, J.G. Schmidt, J.S. Martinez, W.K. Grace, K.M. Grace, B.I. Swanson, Langmuir 24 (2008) 2240.
- [33] J.M. Lee, H.K. Park, Y. Jung, J.K. Kim, S.O. Jung, B.H. Chung, Anal. Chem. 79 (2007) 2680.
- [34] M.E. Browning-Kelley, K. Wadu-Mesthrige, V. Hari, G.Y. Liu, Langmuir 13 (1997) 343.



# Lead(II) ion-selective electrode based on polyaminoanthraquinone particles with intrinsic conductivity

Xin-Gui Li<sup>a,b,\*</sup>, Xiao-Li Ma<sup>a</sup>, Mei-Rong Huang<sup>a,b,\*</sup>

<sup>a</sup> Institute of Materials Chemistry, Key Laboratory of Advanced Civil Engineering Materials of the Ministry of Education, College of Materials Science and Engineering, Tongji University, 1239 Si-Ping Road, Shanghai 200092, China

<sup>b</sup> Key Laboratory of Molecular Engineering of Polymers of the Ministry of Education, Fudan University, Shanghai 200433, China

## ARTICLE INFO

### Article history:

Received 2 August 2008

Received in revised form

27 November 2008

Accepted 29 November 2008

Available online 6 December 2008

### Keywords:

Polyaminoanthraquinone

Lead(II) ion-selective electrode

Conducting polymer

Lead(II) ionophore

Performance optimization

Membrane electrode

## ABSTRACT

A new polyvinylchloride membrane electrode was facily prepared by using polyaminoanthraquinone (PAAQ) microparticles with an intrinsically electrical conductivity as a lead(II) ionophore. It is found that the electrode performance will significantly be improved with adding 1 wt% PAAQ microparticles and decreasing the membrane thickness. A 90  $\mu\text{m}$ -thick membrane electrode consisting of PAAQ(salt):polyvinyl chloride:dioctylphthalate:sodium tetraphenylborate of 1:33:66:1 (wt) but without any traditional lead(II) ionophore achieved the optimal performance and exhibited a good Nernstian response for Pb(II) ions over a wide concentration range from  $2.5 \times 10^{-6}$  to 0.1 M with a slope of 28.9 mV/decade and a detection limit down to 776 nM. A reasonably short response time of 12 s was revealed together with a long lifetime over a period of around 4 months in a wide pH range between 2.8 and 5.2. A fixed interference method indicated that the electrode has an excellent selectivity for lead(II) ion over alkali, alkaline earth and other heavy metal ions. The proposed electrode has been also found to be a powerful indicator electrode for potentiometric titration of Pb(II) ions with EDTA. The electrode can be used to accurately monitor the Pb(II) pollution in environmental waters.

© 2009 Published by Elsevier B.V.

## 1. Introduction

Lead(II)-ISE is of great significance because the lead is ubiquitous in the environment and extremely hazardous to human health. A large number of lead(II)-ISEs reported are mainly based on polymeric membrane containing ionophores [1–6]. The key part of these electrodes is a highly sensing ionophore having strong affinity for a particular metal ion but giving low or even no response to others. Enormous efforts have been made to design and synthesize suitable materials that are highly selective to lead(II) ions. Macrocyclic crown ethers [2–4], calixarenes [5–7], and Schiff base [8,9], have been widely investigated for this purpose. Other ligands such as porphyrin [10,11], pyridinecarboximide [12], piroxicam [13], tetra-benzyl pyrophosphate [14], capric acid [15], phenyl disulfide [16], dithiodibenzoic acid [17], and quinaldic acid derivatives [18] are also served for the fabrication of the lead(II)-ISEs. In spite of availability of various lead(II)-ISEs, the narrow working concentration

range, high detection limit, slow response rate and especially poor selectivity over interfering ions have restricted their widespread application. In particular, the ionophores studied are almost all the lipophilic compounds that easily leak out from matrix. Only one report on the polymer as ionophores with good anti-leaking ability and then long lifetime was found [19]. However, the response time is long because of its intrinsically high membrane resistance. Therefore, it is of great challenge and significance to further search a new ionophore that possesses an intrinsically low membrane resistance and therefore high sensitivity and selectivity to lead(II) ions so as to develop lead(II)-ISEs with excellent detection performance including quick responsibility and long duration.

In recent years, it is found that the conducting polymers especially some polymers from aromatic diamines have a unique ability to form stable complexes with some heavy metal ions such as Pb(II), Hg(II) and Ag(I) ions [20–26]. Polyphenylenediamine synthesized in our laboratory was found to possess a strong capability to adsorb lead ions through complexation between  $\text{Pb}^{2+}$  ions and  $-\text{NH}-/\text{N}$ -groups in the macromolecular chains [23]. Concerning these properties, attempts have been made to employ these polymers to extract and sense heavy metal ions. Carbon paste electrode modified with poly(1,8-diaminonaphthalene) was successfully used to determine lead(II) ions in a concentration range from 0.2 to 10  $\mu\text{M}$  [21]. The detection process was complicated due to an indispensable combination of ion pre-enrichment and anodic-stripping

\* Corresponding authors at: Institute of Materials Chemistry, Key Laboratory of Advanced Civil Engineering Materials of the Ministry of Education, College of Materials Science and Engineering, Tongji University, 1239 Si-Ping Road, Shanghai 200092, China. Fax: +86 21 65980524.

E-mail addresses: [adamxgli@yahoo.com](mailto:adamxgli@yahoo.com) (X.-G. Li), [meironghuang@gmail.com](mailto:meironghuang@gmail.com) (M.-R. Huang).

voltammogram, accompanying with a quite narrow work concentration range. Nevertheless, these results have indicated the possibility of some aromatic conducting polymers with strong affinity to lead(II) ions to act as ionophores in lead(II)–ISEs. Unfortunately, no relevant reports have been found up to now.

A novel multifunctional polyaminoanthraquinone (PAAQ) was successfully synthesized through a chemically oxidative polymerization [26]. PAAQ exhibits a strong adsorbability to lead ions owing to its strong complexibility with lead ion through N and O coordination centers in the polymer chains. It seems that the PAAQ could be a potential ionophore for construction of a new membrane sensor for lead ions. The ingredient and thickness of the membrane were optimized to provide unique  $Pb^{2+}$ –ISE that could result in reproducible, noiseless and stable potentials. The excellent performance of the electrode containing PAAQ as the sensing ionophore to lead(II) ions in the determination of lead(II) ions has been elaborated for the first time.

## 2. Experimental

### 2.1. Reagents

1-Aminoanthraquinone (AAQ), ammonium persulfate ( $(NH_4)_2S_2O_8$ ),  $HClO_4$  (70%), acetonitrile, high molecular weight polyvinyl chloride (PVC), dioctylphthalate (DOP), sodium tetraphenyl borate (NaTPB), tetrahydrofuran (THF) and lead nitrate of analytical reagent grade were commercially obtained and used as received. 0.1 M  $Pb(NO_3)_2$  stock solution was prepared by dissolving lead nitrate in distilled deionized water and standardized whenever necessary. The working solutions of different concentrations were confected by gradually diluting the stock solutions.

### 2.2. Synthesis of fine PAAQ microparticles as ionophore

PAAQ particles used as ionophore were simply prepared by a chemically oxidative polymerization of the AAQ monomer [26]. A typical procedure for the preparation of PAAQ particles is as follows: AAQ monomer (446 mg, 2 mmol) and  $HClO_4$  (11.8 M, 0.17 mL) were added into acetonitrile (40 mL) in a 100 mL glass flask in a water bath at 20 °C and the mixture was then stirred vigorously for 30 min.  $(NH_4)_2S_2O_8$  (456 mg, 2 mmol) was dissolved separately in deionized water of 0.75 mL to prepare an oxidant solution. The oxidant solution was then added dropwise into the monomer solution at a rate of one drop (around 60  $\mu$ L) every 3 s. The reaction mixture was stirred continuously for 24 h at 20 °C. After reaction, the resulting polymer particles as precipitates were isolated from the reaction mixture by filtration and washed with ethanol to remove the residual oxidant, remaining monomers and soluble oligomers. The PAAQ particles were left to dry in ambient air at 50 °C for 3 days. The bluish black PAAQ particles obtained have nominal macromolecular structural formula in Scheme 1 and bulk electrical conductivity of  $5.0 \times 10^{-5}$  S/cm at 15 °C.

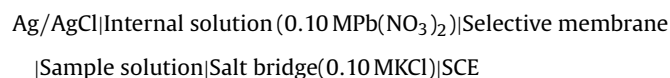
### 2.3. Electrode fabrication

To prepare a selective membrane, an appropriate amount of PAAQ particles were dispersed in 5 mL THF by an intermittently ultrasonic treatment. Proper amounts of PVC, DOP and NaTPB were gradually added into the PAAQ dispersion and subsequently stirred for 10 min to ensure a uniform mix. The mixture obtained thus was poured on a smooth plate glass and then allowed to evaporate for 24 h at room temperature. The translucent elastic membranes with different compositions and thicknesses were obtained after the evaporation of THF. The thickness of the membrane was measured by a roller type thickness gauge with the minimum scale of

10  $\mu$ m. A circular membrane of 16 mm diameter was carefully cut out and glued to one end of plastic tube that would be filled with 0.10 M  $Pb(NO_3)_2$  solution as internal reference solution. The prepared electrodes were conditioned in a 0.01 M  $Pb(NO_3)_2$  solution for 12 h and finally washed by distilled deionized water until stable potentials were reached before using.

### 2.4. Potential measurement

All potentiometric measurements were performed by a PHS-3C digital pH meter (Shanghai Kangyi Instruments Factory, China). A double-junction saturated calomel electrode (SCE) was used as the external reference electrode with the outer junction containing 0.10 M KCl and inner reference containing saturated KCl. The representative electrochemical cell for the electromotive force (EMF) measurement is as follows:

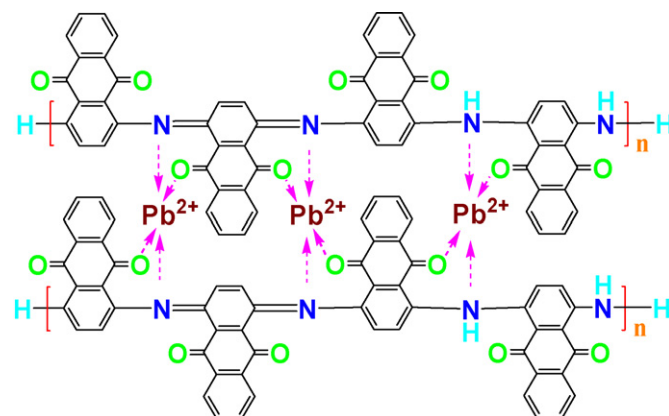


The performance of the electrodes was examined by measuring the EMFs of the  $Pb^{2+}$  solutions in a concentration range of  $10^{-8}$  to  $10^{-1}$  M. The pH values were adjusted by  $HNO_3$  and NaOH when considering the applicable pH range of the electrode. The response time of the electrode was determined based on the potentials at different times for various concentrations of  $Pb(NO_3)_2$  solution until the EMFs value kept constant in 5 min.

## 3. Results and discussion

### 3.1. Doping state of PAAQ microparticles

For the PAAQ ionophore of  $Pb^{2+}$  in this study, it is certain that the N and O atoms could be soft coordination centers to complex  $Pb^{2+}$  ions. Besides, the as-prepared PAAQ salt particles contain a certain amount of doped anions just like  $ClO_4^-$  and  $SO_4^{2-}$ , which come from the  $HClO_4$  and reducing products of  $(NH_4)_2S_2O_8$  used for the polymerization. Both of them could be removed from the polymer chains through dedoping process in ammonia, accompanying with the significant decline of conductivity. The reversible conversion between salt and base states of the PAAQ chains is a unique nature of aromatic conducting polymers [20–23]. Concerning this, the electrodes based on PAAQ salt and base particles have been constructed separately to study the effect of doping state on the response performance to  $Pb^{2+}$  ions. It is apparently observed from Fig. 1 that the PAAQ salt particles-based electrode performs better response properties in all aspects, especially broader working concentration range



**Scheme 1.** The macromolecular structural formula of PAAQ polymer together with the exchange mechanism involved in producing potential signal.



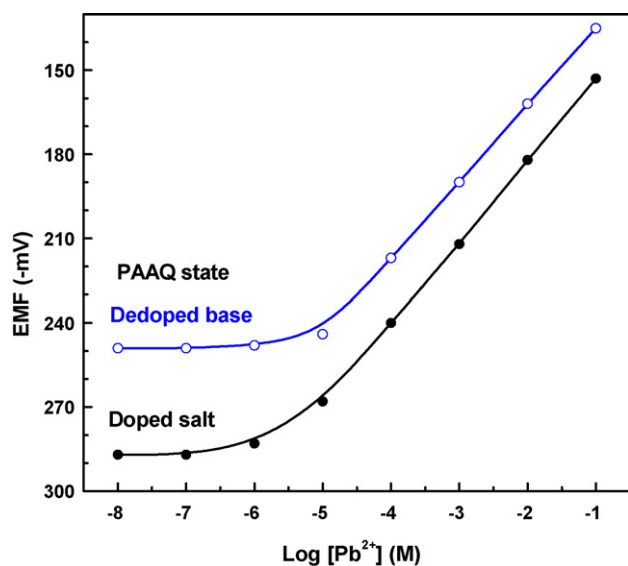


Fig. 1. Potentiometric responses of  $\text{Pb}^{2+}$  selective electrodes based on PAAQ microparticles at two doping states of salt and base at PAAQ:PVC:DOP:NaTPB of 1:33:66:1 and membrane thickness of 160  $\mu\text{m}$ .

from  $4.0 \times 10^{-6}$  to 0.1 M, higher slope (28.1 mV/decade), lower detection limit ( $1.86 \times 10^{-6}$  M), and shorter response time (14 s) than the PAAQ base particles-based electrode (working concentration range:  $1.0 \times 10^{-5}$  to 0.1 M; slope: 27.3 mV/decade; detection limit:  $6.67 \times 10^{-5}$  M; response time: 17 s). It should be noted that the possibility of forming  $\text{PbSO}_4$  precipitate during detection process has been ruled out because possibly maximal  $\text{SO}_4^{2-}$  and  $\text{Pb}^{2+}$  concentrations are  $10^{-11}$  M and 0.1 M, respectively, and the product of  $\text{SO}_4^{2-}$  and  $\text{Pb}^{2+}$  concentrations would be  $10^{-12}$  that is much lower than the solubility product constant of  $\text{PbSO}_4$  ( $1.6 \times 10^{-8}$ ). The residual  $\text{SO}_4^{2-}$  and  $\text{ClO}_4^-$  ions existing along the PAAQ salt chains as the counter-anions are loose associated with protonated  $=\text{NH}^+$  sites on the macromolecular chains, forming a negatively charged layer around PAAQ chains. The static attraction of the negatively charged layer to  $\text{Pb}^{2+}$  ions, as well as complexation between N/O sites and  $\text{Pb}^{2+}$ , could hold the  $\text{Pb}^{2+}$  ions within the membrane and therefore suppress the zero-current flux of the primary ions from membrane into sample solution of low  $\text{Pb}^{2+}$  concentration, which is considered as one important factor restricting the detection limit [27–29], ultimately leading to a low detection limit and broad linear range. On the other hand, the presence of  $\text{SO}_4^{2-}$  and  $\text{ClO}_4^-$  in the PAAQ salts would prevent the extraction of anions and then the primary ions from the inner reference solution, i.e., the  $\text{Pb}^{2+}$  in the inner reference solution would not be extracted into the membrane phase. As we know, the absence of primary ion flux is necessary to achieve low detection limit. Generally, the primary ions always tend to transit from bulk membrane into the sample solution at a low  $\text{Pb}^{2+}$  concentration, leading to a local higher concentration than the sensing concentration. Consequently, true concentration of sample solution could not be satisfactorily detected. Vigorous agitation could improve the homogeneity of the local concentration to some extent. Additionally, much higher electrical conductivity of PAAQ(salt) ( $5.0 \times 10^{-5}$  S/cm) than PAAQ(base) ( $3.7 \times 10^{-8}$  S/cm) would remarkably enhance the sensitivity of electrode as well, contributing to a nearer Nernstian slope and quicker response.

Fig. 2 shows the FTIR spectra of the ionophores of PAAQ base and salt before and after the exposure of PAAQ in 0.001 M  $\text{Pb}(\text{NO}_3)_2$  solution for 1 h. The peaks at 3440, 1640 and 1270  $\text{cm}^{-1}$  due to the N–H, C=O and C–N, respectively, become weaker after contacting  $\text{Pb}^{2+}$  ions, indicating an interaction between N–H/C=O groups and  $\text{Pb}^{2+}$  ions, i.e., complexation between the  $\text{Pb}^{2+}$  ions and the

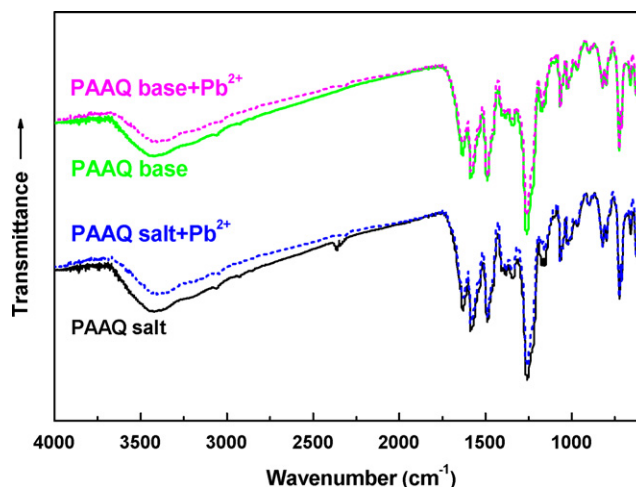


Fig. 2. FTIR spectra of PAAQ ionophores (base and salt) before and after the exposure of PAAQ in the 0.001 M  $\text{Pb}(\text{NO}_3)_2$  solution for 1 h.

PAAQ. Furthermore, the PAAQ salt– $\text{Pb}^{2+}$  complex illustrates weaker N–H absorbance at 3440  $\text{cm}^{-1}$  than the PAAQ base– $\text{Pb}^{2+}$  complex, suggesting stronger interaction between the PAAQ salt and  $\text{Pb}^{2+}$  ions. Therefore, the as-prepared PAAQ salt particles with stronger response to  $\text{Pb}^{2+}$  ions are selected as lead(II) ionophore in the following study.

### 3.2. PAAQ microparticle content

It is well known that the sensitivity and selectivity of ISEs depend significantly on the nature of ionophore and the membrane composition. Thus the loading content of ionophore should be optimized to produce the best performance of the proposed electrode. The complexation function of ionophore with  $\text{Pb}^{2+}$  cannot be visualized sufficiently at low ionophore content. On the contrary, high ionophore content is unfavorable to the transportation of ions in membrane and may even cause pinholes in membrane, leading to a deterioration of performance ultimately. To study the effect of ionophore content, three electrodes loading different amounts of PAAQ ionophore were prepared and their potential responses are shown in Fig. 3 and Table 1. Interestingly, PAAQ:PVC:DOP:NaTPB

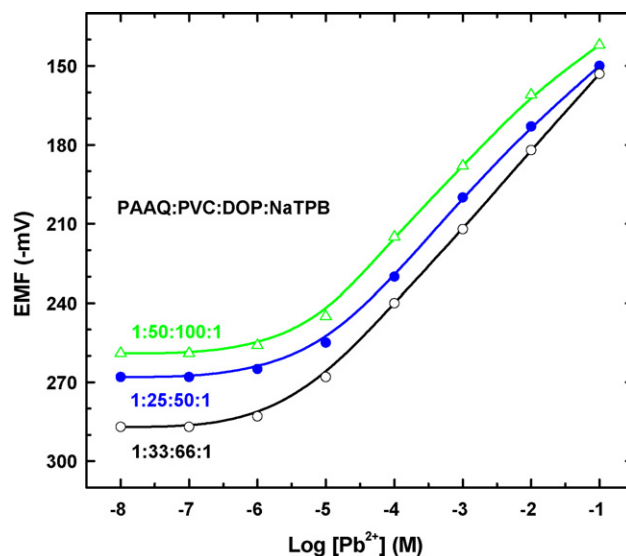


Fig. 3. Potentiometric responses of the Pb(II) ISEs based on different contents of PAAQ in a 160  $\mu\text{m}$ -thick matrix membrane.

**Table 1**  
Composition and performance characteristics of Pb(II) ISEs in Fig. 3.

PAAQ:PVC:DOP:NaTPB (weight ratio)	Working concentration range (M)	Working linear equation	Slope (mV/decade)	Detection limit (M)	Response time (s)
1:25:50:1	$1.0 \times 10^{-5}$ to 0.1	$E = -129.6 + 26.7 \log[\text{Pb}^{2+}]$	26.7	$3.29 \times 10^{-6}$	16
1:33:66:1	$4.0 \times 10^{-6}$ to 0.1	$E = -126.1 + 28.1 \log[\text{Pb}^{2+}]$	28.1	$1.86 \times 10^{-6}$	14
1:50:100:1	$1.0 \times 10^{-5}$ to 0.024	$E = -112.6 + 27.9 \log[\text{Pb}^{2+}]$	27.9	$2.92 \times 10^{-6}$	17

of 1:33:66:1 (wt) exhibits the best performance involving the widest working concentration range from  $4.0 \times 10^{-6}$  to 0.1 M with the largest Nernstian slope of 28.1 mV/decade, the lowest detection limit of  $1.86 \times 10^{-6}$  M, and the shortest response time of 14 s. This great improvement of electrode performance should originate from the presence of PAAQ ionophore. In fact, the PAAQ:PVC:DOP:NaTPB (0:33:66:1) membrane with the thickness of 160  $\mu\text{m}$  has much lower potential stability and lower conductivity ( $2.13 \times 10^{-8}$  S/cm) than the PAAQ:PVC:DOP:NaTPB (1:33:66:1) membrane ( $1.35 \times 10^{-7}$  S/cm). The PAAQ-free electrode might not be suitable to detect potential response. It is reported that the addition of only a small amount of conducting polymers could significantly enhance the electrical and other properties of matrix polymers [24,25]. Excellent performance has also been realized at a high ionophore content for some PVC membrane ISEs based on hexathia-18-crown-6-tetraone ionophore:PVC of 1:6(wt) [2] and *N,N'*-dimethylcyanodiazia-18-crown-6 ionophore:PVC of 1:5(wt) [4]. However, the optimal weight ratio of PAAQ ionophore and PVC is 1:33 for most electrodes involving the PAAQ-based electrode in this study. Much less PAAQ particles are required to produce the best performance of the ISEs, i.e., PAAQ might be more efficient ionophore than hexathia-18-crown-6-tetraone and *N,N'*-dimethylcyanodiazia-18-crown-6.

### 3.3. Nature of plasticizer

The plasticizer is considered to play an important role in optimizing the performance of ISEs through influencing the dielectric constant of the membrane phase [5–7]. Four plasticizers of different polarity were used to study the effect of plasticizer on the selective response of the  $\text{Pb}^{2+}$ -ISEs based on PAAQ. As shown in Fig. 4, the ISE with DOP as plasticizer obviously performs a higher Nernstian response slope of 28.1 mV/decade over a wider range from

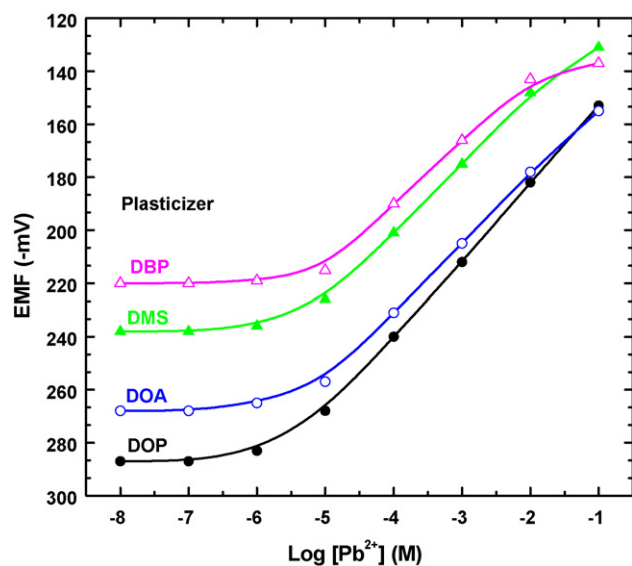


**Fig. 4.** Potentiometric responses of Pb(II) ISEs based on PAAQ microparticles with different plasticizers at PAAQ:PVC:plasticizer:NaTPB of 1:33:66:1 and membrane thickness of 160  $\mu\text{m}$ .

$4.0 \times 10^{-6}$  to 0.1 M. The ISEs based on the other three plasticizers only give a diminished response slope ( $<27$  mV/decade) over narrow working concentration range. Therefore, DOP was proved to be the most effective plasticizer in preparing the proposed  $\text{Pb}^{2+}$ -ISEs based on PAAQ.

### 3.4. Lipophilic anion additive content

The presence of lipophilic anion additive in cation-selective membrane electrodes can not only reduce the ohmic resistance and anion interference but also improve the sensitivity and selectivity [11]. The potential responses of the  $\text{Pb}^{2+}$ -ISEs containing lipophilic anion additive (NaTPB) were investigated to examine the effect of additive content. It can be seen from Fig. 5 that the potential response of the  $\text{Pb}^{2+}$ -ISE without NaTPB gives the weakest sensitivity with a diminished slope of 25.3 mV/decade over a narrow linear range from  $10^{-5}$  to  $10^{-2}$  M. The sensitivity can be greatly improved by the addition of NaTPB. The  $\text{Pb}^{2+}$ -ISE with PAAQ:NaTPB of 1:1 (wt) displays the best response characteristics with a higher Nernstian response slope of 28.1 mV/decade over a wider linear range of  $4.0 \times 10^{-6}$  to 0.1 M and a lower detection limit of  $1.86 \times 10^{-6}$  M. Higher content of additive (PAAQ:NaTPB = 1:1.5) is also unfavorable for the improvement of sensitivity. More additive may deteriorate the mechanical property of membrane and the lifetime of electrode. Therefore, the optimal lipophilic additive content is 100 wt% relative to the ionophore.

### 3.5. Thickness of the membrane containing PAAQ microparticles

Three electrodes with different membrane thicknesses but the same membrane composition of PAAQ:PVC:DOP:NaTPB = 1:33:66:1 were fabricated to examine the effect of membrane thickness. As shown in Fig. 6 and Table 2, a significant improvement is achieved in the response characteristics of electrodes including linear range,

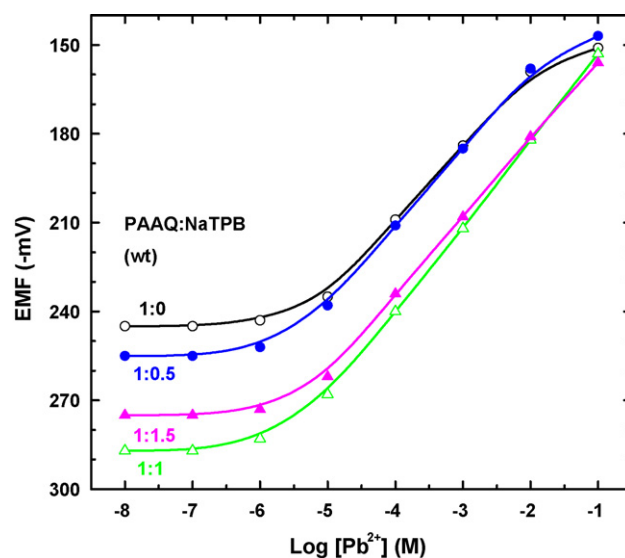


**Fig. 5.** Potentiometric responses of Pb(II) ISEs based on PAAQ microparticles with different NaTPB contents at PAAQ:PVC:DOP of 1:33:66 and membrane thickness of 160  $\mu\text{m}$ .

**Table 2**  
Performance characteristics of Pb(II) ISEs in Fig. 6.

Membrane thickness ( $\mu\text{m}$ )	Working concentration range (M)	Working linear equation	Slope (mV/decade)	Detection limit (M)	Response time (s)
220	$1.0 \times 10^{-5}$ to 0.1	$E = -120.5 + 28.7 \log[\text{Pb}^{2+}]$	28.7	$4.47 \times 10^{-6}$	15
160	$4.0 \times 10^{-6}$ to 0.1	$E = -126.1 + 28.1 \log[\text{Pb}^{2+}]$	28.1	$1.86 \times 10^{-6}$	14
90	$2.5 \times 10^{-6}$ to 0.1	$E = -132.5 + 28.9 \log[\text{Pb}^{2+}]$	28.9	$7.76 \times 10^{-7}$	12

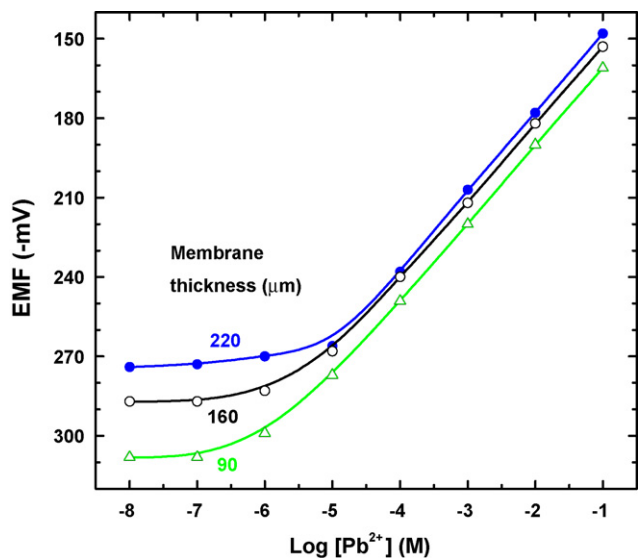


**Fig. 6.** Potentiometric responses of the Pb(II) ISEs based on different membrane thicknesses at PAAQ:PVC:DOP:NaTPB of 1:33:66:1 (wt).

detection limit, slope and response time with decreasing the membrane thickness. At the smallest membrane thickness of 0.09 mm, the electrode exhibits an almost Nernstian slope of 28.9 mV/decade and a widest working concentration range from  $2.5 \times 10^{-6}$  to 0.1 M, which has been broadened nearly by four times compared with that at the thickness of 0.22 mm. The electrode also possesses the lowest detection limit of  $7.76 \times 10^{-7}$  M and the shortest response time of 12 s. It seems that the optimal PAAQ membrane exhibits comparable or even better performance than 10 representative lead(II)-ISEs with PVC matrix in Table 3.

It is reported that the membrane thickness of the PVC-based  $\text{Pb}^{2+}$  ISEs is mostly between 0.2 and 0.5 mm [1,10,11,27,28]. The sensing unit supported by a highly porous polymeric layer in these electrodes is practically liquid state comprising a lipophilic organic ionophore dissolved in oil phase such as DOP. The detection limits of these electrodes commonly keep at the order of  $10^{-6}$  or  $10^{-7}$  M,

beyond which the potential response would deviate from the Nernstian equation, because a zero-current flux of the primary ions from the membrane into sample solutions would result in ion activity of the primary ions maintaining as high as  $10^{-6}$  or  $10^{-7}$  M in the local domain near the membrane surface at the sample side. The flux of primary ions is generated by a transmembrane concentration gradient which occurs when the concentrations of the sample and inner solutions are not the same. The detection limit could be improved through reducing the transmembrane concentration gradient by adjusting the concentration of the inner solution to the value of sample solution, decreasing the total ion concentration, or increasing the thickness of the membrane [29]. However, the result here is reverse to the above-mentioned circumstance. The potential response characteristics of the proposed electrodes can be enhanced by decreasing the thickness of the membrane. This may be relevant to the existing state of the ionophore. The fine PAAQ particle ionophore that is insoluble in DOP oil phase, disperses uniformly in the PVC membrane as the solid state. The transporting rate of lead(II) ions in solid phase is much slower and more arduous than that in liquid phase. Hence the flux of lead(II) ions is not encouraged in solid membrane. Nevertheless, the response is still very fast due to the relatively thin membrane, as discussed below. Considering the remarkable decrease of membrane strength, it is not suggested to further reduce the membrane thickness. All further detailed studies were carried out on the electrode with the composition of PAAQ:PVC:DOP:NaTPB (1:33:66:1) and the membrane thickness of 0.09 mm.

Another result which disagrees with the theory that increasing membrane thickness might improve the detection limit was also reported in the investigation on the electrode based on diphenylmethyl-*N*-phenylhydroxamic acid ionophore [30]. Among three styrene/acrylonitrile copolymer membranes with different thicknesses of 0.14, 0.21, and 0.45 mm, the 0.21 mm-thick membrane demonstrates the lowest detection limit.

### 3.6. Effect of pH

The dependence of the potentiometric response of the proposed ISE on the pH value of the  $\text{Pb}^{2+}$  solution was tested at three  $\text{Pb}^{2+}$

**Table 3**  
Comparison of performance characteristics of the proposed electrode with the PVC membrane lead(II) ISEs reported in literature.

Ionophore	Working concentration range (M)	Slope (mV/decade)	Detection limit (M)	Response time (s)	Lifetime (month)	Refs.
<i>N,N'</i> -Dibenzyl-1,4,10,13-tetraoxa-7,16-diazacyclooctadecane	$8.2 \times 10^{-6}$ to 0.1	30.0	$8.2 \times 10^{-6}$	10	3	[1]
Hexathia-18-crown-6-tetraone	$1.0 \times 10^{-6}$ to 0.008	29.0	$8.0 \times 10^{-7}$	40	2	[2]
2'-Methoxyethoxyl	$5.0 \times 10^{-5}$ to 0.5	28.9	$1.0 \times 10^{-6}$	30	3	[3]
<i>sym</i> -dibenzo-16-crown-5-ether	$1.0 \times 10^{-6}$ to 0.1	29.4	$8.0 \times 10^{-7}$	20	1	[6]
Tetrakis( <i>p</i> -carboxyphenyl)azo]-8-tetrahydroxy calix[4]arene	$1.0 \times 10^{-6}$ to 0.1	29.4	$8.0 \times 10^{-7}$	20	1	[6]
Meso-tetrakis(2-hydroxy-1-naphthyl) porphyrin	$3.2 \times 10^{-5}$ to 0.1	29.2	$3.5 \times 10^{-6}$	10	3	[11]
Chiral 2,6-bis-pyridinecarboximide	$3.5 \times 10^{-6}$ to 0.01	27.9	$2.2 \times 10^{-6}$	25	0.5	[12]
Piroxicam	$1.0 \times 10^{-5}$ to 0.1	30.0	$4.0 \times 10^{-6}$	45	3	[13]
Tetrabenzyl pyrophosphate	$1.0 \times 10^{-5}$ to 0.01	28.7	$3.0 \times 10^{-6}$	10	0.7	[14]
Capric acid	$1.0 \times 10^{-5}$ to 0.01	29.0	$6.0 \times 10^{-6}$	15	3	[15]
Phenyl disulfide	$2.0 \times 10^{-6}$ to 0.01	29.3	$1.2 \times 10^{-6}$	45	1.7	[16]
Solid PAAQ particles	$2.5 \times 10^{-6}$ to 0.1	28.9	$7.8 \times 10^{-7}$	12	4	This study

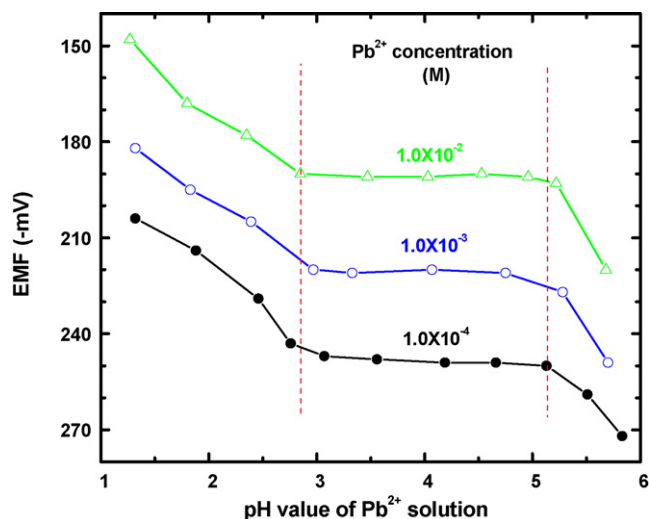


Fig. 7. The pH dependence of the PAAQ:PVC:DOP:NaTPB (1:33:66:1) membrane electrode with the thickness of 90  $\mu\text{m}$  on the potentiometric response under three constant concentrations of lead ion.

concentrations ( $1.0 \times 10^{-2}$ ,  $1.0 \times 10^{-3}$  and  $1.0 \times 10^{-4}$  M) over the pH range between 1 and 6. It is seen from Fig. 7 that the potential response remains almost constant over the pH range from 2.8 to 5.2, beyond which a gradual change in potential can be observed. As a result, this range can be taken as the working pH range of the proposed electrode. The declined potential at higher pH values may be ascribed to the formation of some hydroxy complexes of  $\text{Pb}^{2+}$  such as  $\text{Pb}(\text{OH})^+$  and  $\text{Pb}(\text{OH})_2$ , leading to a decreased  $\text{Pb}^{2+}$  concentration, while at lower pH, the abundant  $\text{H}^+$  ions can protonate the N atoms of PAAQ and even cause the decomplexation of  $\text{Pb}^{2+}$ -PAAQ complex. The  $\text{H}^+$  ions itself can make interference to the electrode response simultaneously. Both of them could result in the rise of the potential.

The wide working pH range of the proposed electrode is comparable to the reported  $\text{Pb}^{2+}$ -ISEs based on the following ionophores: *N,N'*-dibenzyl-1,4,10,13-tetraoxa-7,16-diazacyclooctadecane [1], hexathia-18-crown-6-tetraone [2], phosphorylated calyx[4]arene [31], and 5,11-dibromo-25,27-dipropoxycalix[4]arene [32]. The lower limit of the working pH range is expected to be further improved in case that the binding ability of  $\text{Pb}^{2+}$  onto PAAQ chains is strengthened. The electrode based on 2,12-dimethyl-7,17-diphenyltetrapyrzole with strong complex capability shows wider working pH range of 1.6–6.0, whereas the electrode based on 5,11-dibromo-25,27-dipropoxycalix[4]arene with a relatively weaker complex capability has narrower pH range of 2.3–6.0 [32].

### 3.7. Response and lifetime of the electrode

The response time of the PAAQ ISE was determined by measuring the time required to achieve a steady potential in  $\text{Pb}^{2+}$  solution with three concentrations of  $1.0 \times 10^{-2}$ ,  $1.0 \times 10^{-3}$  and  $1.0 \times 10^{-4}$  M. It is found from Fig. 8 that the response time is 12 s, approaching to the fastest response of  $\text{Pb}^{2+}$ -ISEs based on *N,N'*-dibenzyl-1,4,10,13-tetraoxa-7,16-diazacyclooctadecane [1] and *N,N'*-bis(salicylidene)-2,6-pyridinediamine [33] as ionophores. This fast response is relevant to the fast kinetic process of complexation between  $\text{Pb}^{2+}$  and PAAQ ionophore in the doped state. On the other hand, the fine particles of the PAAQ salts, together with their higher intrinsic conductivity ( $5.0 \times 10^{-5}$  S/cm), may promote the formation of a uniform, thin, and highly conducting composite membrane. All of these features are beneficial to the transition of charges in membrane, resulting in the fast response of the electrode. There was no difference for the potential responses for each

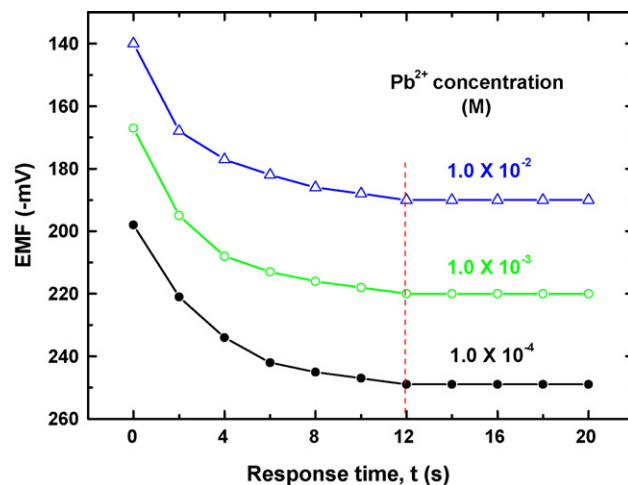


Fig. 8. Response time profile of the  $\text{Pb}(\text{II})$  ISE based on PAAQ:PVC:DOP:NaTPB (1:33:66:1) membrane with the thickness of 90  $\mu\text{m}$ .

concentration recorded from high concentration to low concentration and from low concentration to high concentration, indicating that the ISE has an excellent reversibility. The standard deviations of ten replicate potential measurements of 1 mM and 0.1 mM sample solutions were 0.58 and 0.65 mV, respectively, indicating the good reproducibility of the prepared ISE. It is also observed that the electrode could be satisfactorily used over a period of 4 months without any significant loss of the performance characteristics such as working concentration range, slope and response time. Unlike the ordinary ionophore, PAAQ salts existing as fine solid particles do not leak from the matrix while contacting with aqueous solution, ensuring a reasonably long lifetime of the proposed electrode.

### 3.8. Electrode selectivity

The selectivity is one of the most important characteristics for selective electrodes, because it determines the feasibility and utility of the electrodes in real sample analysis. The potentiometric selectivity coefficient  $K_{\text{Pb}^{2+},B}^{\text{POT}}$  has been served to reflect the relative response of the membrane selective electrode for the primary ion over other interfering ions present in solution and can be used to predict response functions in mixed samples. It can be determined mainly through three different methods including separate solution, fixed interference and matched potential methods. The fixed interference method is preferable since it more closely mimics a practical application of the ISE. In the present study, the fixed interference method was employed to assess the selectivity of the fabricated  $\text{Pb}^{2+}$  ISE over other commonly interfering ions. The selectivity coefficients were calculated through the equation:

$$K_{\text{Pb}^{2+},B}^{\text{POT}} = a_{\text{Pb}^{2+}}(\text{DL}) / (a_B)^{2/z}$$

where  $\alpha_{\text{Pb}^{2+}}(\text{DL})$  is the detection limit of  $\text{Pb}^{2+}$  ion,  $\alpha_B$  the activity of the interfering ion, and  $z$  the charge of the interfering ion [34]. It is noteworthy that the selectivity coefficients for all diverse cations listed in Table 4 are in the order of  $10^{-2}$  or  $10^{-3}$ , indicating that the proposed electrode is highly selective over all the interfering ions studied. The interferences of alkali metal ions ( $\text{Na}^+$  and  $\text{K}^+$ ) and alkaline-earth metal ions ( $\text{Ba}^{2+}$  and  $\text{Ca}^{2+}$ ) are almost negligible with the selectivity coefficients in the order of  $10^{-3}$ . Some heavy metal ions and noble metal ions ( $\text{Cu}^{2+}$ ,  $\text{Hg}^{2+}$ ,  $\text{Au}^{3+}$  and  $\text{Ag}^+$ ) might cause a weak interference, which may arise from the complex capability of PAAQ to some transition metal ions. It is discovered that aromatic amine polymers can complex  $\text{Hg}^{2+}$  and  $\text{Ag}^+$  ions as well as  $\text{Pb}^{2+}$  ions through the  $-\text{NH}_2$  and  $-\text{NH}-$  groups in the chains [22–25].

**Table 4**  
Potentiometric selectivity coefficients of the PAAQ salt particles-based  $\text{Pb}^{2+}$ -ISE obtained by the fixed interference method at an interfering ion concentration of  $1.0 \times 10^{-3}$  M.

Interfering ions	Selectivity coefficient $K_{\text{Pb}^{2+}, B}^{\text{POT}}$
$\text{Hg}^{2+}$	$8.51 \times 10^{-2}$
$\text{Ag}^+$	$6.97 \times 10^{-2}$
$\text{Cu}^{2+}$	$5.82 \times 10^{-2}$
$\text{Au}^{3+}$	$4.68 \times 10^{-2}$
$\text{NH}_4^+$	$7.59 \times 10^{-3}$
$\text{Na}^+$	$7.18 \times 10^{-3}$
$\text{K}^+$	$4.27 \times 10^{-3}$
$\text{Ba}^{2+}$	$3.55 \times 10^{-3}$
$\text{Ca}^{2+}$	$3.09 \times 10^{-3}$

Nevertheless, with the selectivity coefficients in the order of  $10^{-2}$ , these metal ions could not make an obvious disturbance to the determination of  $\text{Pb}^{2+}$  ions. Even so, it should be noted that much more severe interference from  $\text{Ag}^+$ ,  $\text{Cu}^{2+}$ ,  $\text{Hg}^{2+}$  and some other cations was always found in other  $\text{Pb}^{2+}$  ISEs [9,11,14,27,31].

### 3.9. Application of the electrode

The analytical application of the electrode was investigated as an indicator electrode for the potentiometric estimation of  $1.0 \times 10^{-3}$  M  $\text{Pb}^{2+}$  solution by titrating with two EDTA concentrations of  $1.0 \times 10^{-3}$  M and  $1.0 \times 10^{-2}$  M. The titration plots presented in Fig. 9 do not show a standard sigmoid curve, probably due to some interference caused by  $\text{Na}^+$  ions from disodium EDTA salt. When  $\text{Pb}^{2+}$  solution was titrated by EDTA, the  $\text{Pb}^{2+}$  concentration decreased, accompanying by an increased concentration of  $\text{Na}^+$  ions from EDTA with the titration proceeding. In the later period, the amount of  $\text{Na}^+$  ions can greatly surpass the amount of  $\text{Pb}^{2+}$  ions, causing interference to the potential. Similar titration plots were observed when the ISEs based on *N,N'*-dibenzyl-1,4,10,13-tetraoxa-7,16-diazacyclooctadecane [1], 4-*t*-butylcalix[4]arene [35], and 4-*t*-butylcalix[6]arene [36] were served as indicator electrodes. The stoichiometry of  $\text{Pb}^{2+}$ -EDTA complex can be judged from the sharp break point in Fig. 9. It must be appreciated that the potentiometric titration of  $\text{Pb}^{2+}$  also performs well when the EDTA concentration is in the same order of  $\text{Pb}^{2+}$ . Under this circumstance, the error of reading of volume of EDTA solution used could be diminished

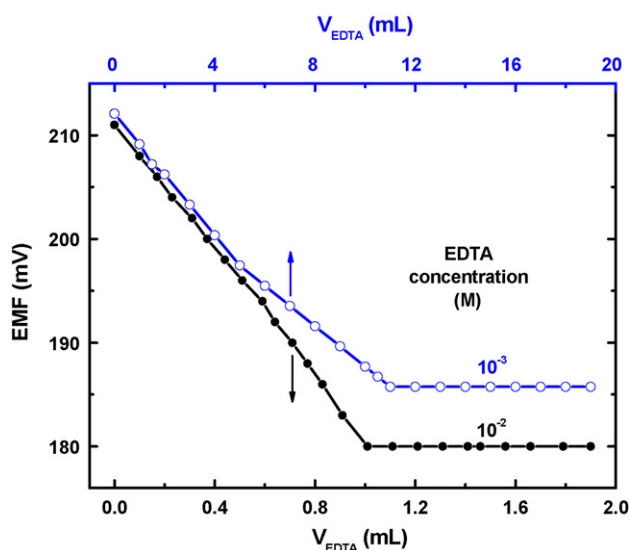


**Fig. 9.** Potentiometric titration plots of  $1.0 \times 10^{-3}$  M  $\text{Pb}(\text{NO}_3)_2$  solution of 10 mL with  $1.0 \times 10^{-2}$  M and  $1.0 \times 10^{-3}$  M EDTA, respectively by the ISE based on PAAQ:PVC:DOP:NaTPB (1:33:66:1) membrane with the thickness of 90  $\mu\text{m}$ .

**Table 5**  
Recovery studies of the PAAQ-based  $\text{Pb}^{2+}$ -ISE on the detection of lead(II) in tap and rain waters.

Water sample	Added $\text{Pb}^{2+}$ ( $\mu\text{M}$ )	Detected $\text{Pb}^{2+}$ ( $\mu\text{M}$ )	Recovery (%)
Tap water 1	50	48.9	97.8
Tap water 2	200	205	102.5
Rain water 1	50	51.5	103.0
Rain water 2	200	195	97.5

to some extent as compared to the titration just consuming ca. 1 mL titrant of much higher EDTA concentration than the  $\text{Pb}^{2+}$  concentration [30–36]. Obviously, the prepared electrode in this study shows the practical applicability as an indicator electrode in the potentiometric titration to  $\text{Pb}^{2+}$  solutions.

Since no  $\text{Pb}^{2+}$  traces in tap water and rainwater samples were detected by the prepared  $\text{Pb}^{2+}$ -ISE based on PAAQ, the electrode was applied to detect  $\text{Pb}^{2+}$  concentration in the water samples by standard addition method. To prepare the tap water samples, the collected tap water was first boiled for about 5 min to remove  $\text{Cl}_2$ . The pH values of the tap water and rainwater samples were both adjusted to around 4.5 by  $\text{HNO}_3$ . The five-replicate detection and recovery results are presented in Table 5. It can be seen that the  $\text{Pb}^{2+}$ -ISE performs satisfactorily with the reasonable recovery, indicating the feasibility of the electrode in the detection of  $\text{Pb}^{2+}$  concentration in the environmental water like tap and rainwaters.

## 4. Conclusions

The fine particles of aromatic PAAQ in PVC membrane well perform as a novel  $\text{Pb}^{2+}$  sensing ionophore with strong sensitivity and high selectivity because of their intrinsic electroconductivity and strong affinity towards  $\text{Pb}^{2+}$  ions. The  $\text{Pb}^{2+}$  ISEs based on the particles rather than traditional ionophores are high-performance ISEs with wide working range from  $2.5 \times 10^{-6}$  to  $1.0 \times 10^{-1}$  M, low detection limit down to  $7.76 \times 10^{-7}$  M, and long lifetime. The response time of shorter than 12 s has approached to the fastest response rate of the existing electrodes. 1% PAAQ particles-containing ISE demonstrates much better performance than the particles-free ISE. In particular, the proposed electrode shows an excellent selectivity for  $\text{Pb}^{2+}$  over alkali, alkaline earth, and heavy metal ions. And the PAAQ ionophore is easily available since the PAAQ particles can be facilely and productively synthesized through chemically oxidative polymerization of aminoanthraquinone. Thus the prepared electrode with a good combination of excellent performance, and long lifetime as well as low cost has a promising application in the determination of  $\text{Pb}^{2+}$  ions. The electrode can be used to accurately monitor the  $\text{Pb}(\text{II})$  pollution in environmental waters just like tap and rain waters. The results in this report have indicated the great potential of other aromatic conducting polymers with strong ability to chelate heavy metal ions to act as new ionophores in ISEs and thus the relevant research should be highly encouraged.

## Acknowledgements

The project is supported by the National Natural Science Foundation of China (20774065) and the Foundation of Key Laboratory of Molecular Engineering of Polymers, Fudan University, China.

## References

- [1] V.K. Gupta, A.K. Jain, P. Kumar, Sens. Actuators B 120 (2006) 259.
- [2] M. Shamsipur, M.R. Ganjali, A. Røihollahi, Anal. Sci. 17 (2001) 935.
- [3] C.C. Su, M.C. Chang, L.K. Liu, Anal. Chim. Acta 432 (2001) 261.
- [4] M.R. Ganjali, M. Hosseini, F. Basiripour, M. Javanbakht, O.R. Hashemi, M.F. Rastegar, M. Shamsipur, G.W. Buchanan, Anal. Chim. Acta 464 (2002) 181.
- [5] F. Cadogan, P. Kane, M.A. McKervey, D. Diamond, Anal. Chem. 71 (1999) 5544.
- [6] J.Q. Lu, R. Chen, X.W. He, J. Electroanal. Chem. 528 (2002) 33.

- [7] L.X. Chen, J. Zhang, W.F. Zhao, X.W. He, Y. Liu, J. Electroanal. Chem. 589 (2006) 106.
- [8] H. Kim, H.K. Lee, A.Y. Choi, S. Jeon, Bull. Korean Chem. Soc. 28 (2007) 538.
- [9] Z. Pilehvari, M.R. Yafitian, S. Rayati, M. Parinejad, Anal. Chim. 97 (2007) 747.
- [10] W.J. Zhang, C.Y. Li, X.B. Zhang, Z. Jin, Anal. Lett. 40 (2007) 1023.
- [11] H.K. Lee, K. Song, H.R. Seo, Y.K. Choi, S. Jeon, Sens. Actuators B 99 (2004) 323.
- [12] S.S.M. Hassan, M.H.A. Ghalia, A.G.E. Amr, A.H.K. Mohameda, Talanta 60 (2003) 81.
- [13] S. Sadeghi, G.R. Dashti, M. Shamsipur, Sens. Actuators B 81 (2002) 223.
- [14] D.F. Xu, T. Katsu, Talanta 51 (2000) 365.
- [15] M.F. Mousavi, M.B. Barzegar, S. Sahari, Sens. Actuators B 73 (2001) 199.
- [16] A. Abbaspour, B. Khajeh, Anal. Sci. 18 (2002) 987.
- [17] M.B. Gholivand, A. Mohammadi, Chem. Anal. (Warsaw) 48 (2003) 305.
- [18] M. Casado, S. Daunert, M. Valiente, Electroanalysis 13 (2001) 54.
- [19] M.R. Ganjali, A. Rouhollahi, A.R. Mardan, M. Hamzeloo, A. Mogimi, M. Shamsipur, Microchem. J. 60 (1998) 122.
- [20] X.G. Li, M.R. Huang, W. Duan, Y.L. Yang, Chem. Rev. 102 (2002) 2925.
- [21] S. Majid, M.E. Rhazi, A. Amine, A. Curulli, G. Palleschi, Microchim. Acta 143 (2003) 195.
- [22] X.G. Li, R. Liu, M.R. Huang, Chem. Mater. 17 (2005) 5411.
- [23] M.R. Huang, Q.Y. Peng, X.G. Li, Chem. Eur. J. 12 (2006) 4341.
- [24] Q.F. Lü, M.R. Huang, X.G. Li, Chem. Eur. J. 13 (2007) 6009.
- [25] X.G. Li, H. Li, M.R. Huang, Chem. Eur. J. 13 (2007) 8884.
- [26] X.G. Li, H. Li, M.R. Huang, China Patent CN1810852, 2008.
- [27] M.F. Mousavi, S. Sahari, N. Alizadeh, M. Shamsipur, Anal. Chim. Acta 414 (2000) 189.
- [28] A. Rouhollahi, M.R. Ganjali, M. Shamsipur, Talanta 46 (1998) 1341.
- [29] Z. Szigeti, T. Vigassy, E. Bakker, E. Pretsch, Electroanalysis 18 (2006) 1254.
- [30] K.C. Gupta, M.J. D'Arc, IEEE Sens. J. 1 (2001) 275.
- [31] M.R. Yafitian, S. Rayati, D. Emadi, D. Matt, Anal. Sci. 22 (2006) 1075.
- [32] A.K. Jain, V.K. Gupta, L.P. Singh, J.R. Raison, Electrochim. Acta 51 (2006) 2547.
- [33] T. Jeong, H.K. Lee, D.C. Jeong, S. Jeon, Talanta 65 (2005) 543.
- [34] E. Bakker, E. Pretsch, P. Bühlmann, Anal. Chem. 72 (2000) 1127.
- [35] V.K. Gupta, R. Mangla, S. Agarwal, Electroanalysis 14 (2002) 1127.
- [36] V.S. Bhat, V.S. Ijeri, A.K. Srivastava, Sens. Actuators B 99 (2004) 98.



## Evaluation of ferricyanide effects on microorganisms with multi-methods

Chang Liu<sup>a,b</sup>, Ting Sun<sup>a</sup>, Yueming Zhai<sup>b</sup>, Shaojun Dong<sup>b,\*</sup>

<sup>a</sup> College of Sciences, Northeastern University, Shen Yang 110004, PR China

<sup>b</sup> State Key Laboratory of Electroanalytical Chemistry, Changchun Institute of Applied Chemistry, Chinese Academy of Sciences, Changchun 130022, PR China

### ARTICLE INFO

#### Article history:

Received 21 July 2008

Received in revised form

27 November 2008

Accepted 10 December 2008

Available online 25 December 2008

#### Keywords:

Toxicity

Ferricyanide

*Escherichia coli* DH 5  $\alpha$

Viability

### ABSTRACT

In this study, we report the effects of ferricyanide on organisms based on the changes in physiological state and morphology of *Escherichia coli* (*E. coli*) DH 5  $\alpha$  after being pretreated by ferricyanide. The impact on bacterial cell growth and viable rate of exposure to different concentrations of ferricyanide was determined, and the morphology change of *E. coli* was studied by atomic force microscopy (AFM). Finally, recovery test was used to evaluate the recovery ability of injured cells. The results showed that the effects on growth and morphology of *E. coli* were negligible when the concentration of ferricyanide was below 25.0 mM. While the results showed 50.8% inhibition of growth in the presence of 50.0 mM ferricyanide for 3 h, 89.6% viability was detected by flow cytometry (FCM) assay. AFM images proved that compact patches appeared on the bacterial surface and protected the bacterial viability. Furthermore, the results revealed that deterioration of bacterial surface closely related to the incubation time from 0.5 to 3 h at 100.0 mM ferricyanide. In the recovery test, microbial cell population and dissolved oxygen individually decreased 36.7% and 28.3% with 25.0 mM ferricyanide. These results clearly demonstrated that ferricyanide indeed affected viability of cells than morphology damaged, and the effects of toxin on bacteria were not reversible.

© 2008 Elsevier B.V. All rights reserved.

### 1. Introduction

Ferricyanide is frequently used for the mediated bioreactions since redox-mediated microbial processes have been known for nearly 100 years [1]. Scheme 1 illustrates the principle of the catalytic reaction by a bacterial cell. Up to now the ferricyanide-mediated (FM) technique has gained its great significance in the environmental monitoring and examination of microorganisms [2–8], because ferricyanide can stably remain electrochemical activity and greatly increase the rate of electron transfer to the electrode.

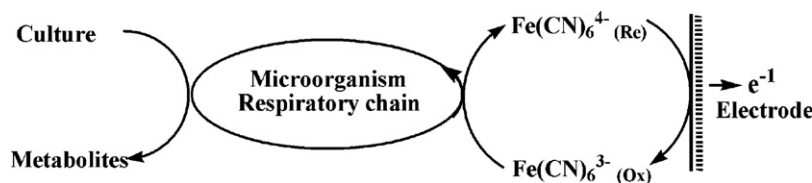
Although FM technique has been widely accepted in scientific research [9–16], its detrimental effects on coupled microorganisms are not neglected. It should be noted that ferricyanide ion itself usually is considered nearly nontoxic. Its toxicity is caused by ‘free’ cyanide anions that can block the electronic transfer and disrupt the respiratory chain when it is irradiated by UV light [17,18]. Furthermore, Pablo and co-workers discovered ferricyanide was more dissociated in the biological condition [18]. It means that ferricyanide could produce unexpected effects on biocatalytic reaction and disrupt electron transfer to itself, even directly result in death of organisms (referring to Scheme 1). However, a summary of effects of ferricyanide published by National Toxicology Program (NTP, USA

in 2005) stated that suitable concentrations of ferricyanide stimulated the growth of human melanoma cells (MM96 wild type) and also induced DNA synthesis and cell replication in serum starved PC12 cells. Obviously, these results are very inconsistent and further basic investigations are needed.

The use of bacteria in studying the effects of toxin or antibiotic on the organisms is well established, and microorganism growth or changes of respiration under given condition formed the basis for biological viability test [19–22]. In addition, the evidence of toxicity on bacteria can be obtained through atomic force microscopy (AFM), which directly observes the morphological alterations of cells before and after exposure to toxin [7,23]. Flow cytometry (FCM) combining with fluorescent probe is also used as an alternative to rapid assessment of bacterial viability [24,25]. The quantitative information on the presence and viability of microorganisms is valuable for sensitive risk assessment regarding toxicity or disease transmission. In these studies, *Escherichia coli* (*E. coli*) has been widely employed in the analysis of mechanisms or toxicity due to its excellent properties, such as easy culture and disposal, sensitivity to growth condition, and well characterized respiratory pathway, etc. [1,20].

In contrast to the wide applications of ferricyanide, there are very few data on its effects on coupled organisms. Therefore we tried to take an all-round estimation on the toxicity of ferricyanide when the iron-cyanide complexes were used in microbial processes. In this paper, the results of growth inhibition were compared to FCM method with particular reference to variation in cell surface

\* Corresponding author. Tel.: +86 431 85262101; fax: +86 431 85689711.  
E-mail address: [dongsj@ciac.jl.cn](mailto:dongsj@ciac.jl.cn) (S. Dong).



**Scheme 1.** Principle of the metabolism of microorganisms.

properties. There was direct and novel investigation of ferricyanide toxicity on bacteria. At last, recovery potential was assessed after *E. coli* were separated from ferricyanide solutions, and the results showed that the negative effects of ferricyanide on *E. coli* were not reversible.

Our studies have shown some unique feature in this area. First, besides conventional method such as inhibition of growth, the combination of AFM and FCM for toxicity investigation was employed, which has not been reported before, and the merit and difference from these methods were compared and discussed in detail. Second, AFM was used to clearly characterize the damages of bacterial surface, which was reliable and successfully explained why *E. coli* remained its viability in high concentration of ferricyanide. Third, the recovery test was further applied to study regeneration after pretreatment with ferricyanide.

## 2. Experimental

### 2.1. Reagents

All chemicals used in this study were of analytical reagents and all solutions were prepared with deionized water, unless otherwise stated. Peptone and yeast extract were from OXOID Ltd. Sodium chloride and  $K_3[Fe(CN)_6]$  were obtained from Sinophar Chemical Reagent Beijing Co., Ltd. Propidium iodide (PI) was purchased from Fluka. Stock solution of  $K_3[Fe(CN)_6]$  was freshly prepared before use. The Luria Bertani (LB,  $10\text{ g L}^{-1}$  tryptone,  $5\text{ g L}^{-1}$  yeast extract, and  $10\text{ g L}^{-1}$  NaCl) broth was adjusted to the desired pH with  $2\text{ mol L}^{-1}$  HCl and sterilized in high-pressure steam at  $120^\circ\text{C}$  for 20 min. The BOD<sup>198</sup> standard GGA solution ( $150\text{ mg L}^{-1}$  glucose and  $150\text{ mg L}^{-1}$  glutamic acid) was prepared according to APHA standard methods (APHA, 1997) [26].

### 2.2. Microorganism preparation

*E. coli* DH 5  $\alpha$  was maintained on nutrient agar plates at  $4^\circ\text{C}$ . Stock cultures were refreshed at intervals of 1 week to preserve the test strain. Bacterial cultures were grown overnight (within 12 h) at  $37^\circ\text{C}$  in LB substrate on a shaking incubation (220 rpm). 400  $\mu\text{L}$  overnight cultures were used to inoculate 50 mL LB media in 250 mL Erlenmeyer flask. *E. coli* grew to its mid-log phase after 4–5 h. Each fresh culture (50 mL, two multiple concentration) was inoculated with 2.5 mL *E. coli*. Then different volumes of ferricyanide solution were added into the cultures with final concentrations of 100.0, 50.0, 25.0, 12.5 and 6.25 mM. The final volume of cell suspensions were 100 mL by adding deionized water. The cell suspensions with ferricyanide shaken at 220 rpm were incubated for 1–6 h at  $37^\circ\text{C}$  under aerobic condition. The control samples were prepared as the same way but without ferricyanide.

### 2.3. Determination of bacterial optical density

Each 0.5 mL sample of 1 h interval from each culture was centrifuged at 10,000 rpm for 10 min and washed three times with 1.0 mL sterile deionized water (SDW). The supernatant was removed, and *E. coli* was resuspended in SDW. The optical den-

sity at 600 nm was recorded to monitor the cell growth. Growth curves were generated using a Cary 500 Scan UV–vis–NIR Spectrophotometer.

### 2.4. Determination of viability by FCM

Cell suspensions with and without ferricyanide were withdrawn from cultures, and washed three times. Thereafter, *E. coli* was incubated with  $50\text{ }\mu\text{g L}^{-1}$  PI at  $37^\circ\text{C}$  for 20 min. Samples were analyzed on a FACScan flow cytometer (BD Biosciences, San Jose, CA) equipped with a 15 mW air-cooled 488 nm argon ion laser for excitation of PI. At least 10,000 cells were analyzed for each sample.

### 2.5. Morphology studies

*E. coli* was incubated in 0, 25, 50 and 100 mM ferricyanide for 3 h, or in 100 mM ferricyanide for durations of 0.5, 1 and 2 h at  $37^\circ\text{C}$ . Then each sample was drawn out and washed with SDW for three times. The samples were placed on freshly treated cover slides and allowed to dry for  $\sim 30$  min. All images were obtained from a tapping mode atomic force microscope (AFM, SPI3800N-Spa 400, Seiko Instrument). A rectangular Si cantilever/tip with a spring constant of 17 N/m and a resonance frequency of  $\sim 150$  kHz were used. The scan speed was set at 0.7 Hz and final resolution was 256 by 256 pixels. Each scan resulted in a topography image and a phase image simultaneously. The height scale of cell was depicted as shades of gray, with bright area being nearer to the tip in topography images. The elasticity scale of cell was given as shades of gray, and whiter area showed more elastic in phase image [27].

### 2.6. Recovery studies

*E. coli* pretreated with ferricyanide for 3 h was chosen for the recovery study. Three hours were enough to induce cell deterioration but it is not enough to totally destroy by the toxicity of ferricyanide. The cell suspensions were centrifuged at 10,000 rpm for 10 min and washed three times with SDW. *E. coli* was resuspended in SDW and the ultimate concentration of cells was adjusted to an absorbance value of 1.5 at 600 nm. 1 mL cell suspension was added in 300 mL BOD bottles and standard GGA solution was used as new culture medium. The process was operated according to the BOD standard method. Initial dissolved oxygen (DO) was determined by dissolved oxygen analyzer (Orion 862A, Thermo Electron Corporation) as soon as filling BOD bottles with culture, and the final DO in the sample was determined after 16 h incubation. Counts of colony-forming units (cfu) which indicate the ability of cells to propagate under given conditions were executed by microscope directly.

## 3. Results and discussions

### 3.1. Growth rate and viability

Fig. 1 showed the growth curve for *E. coli* exposed to different concentrations of ferricyanide. Complete growth inhibition was observed when the cells were exposed to 100.0 mM ferricyanide.



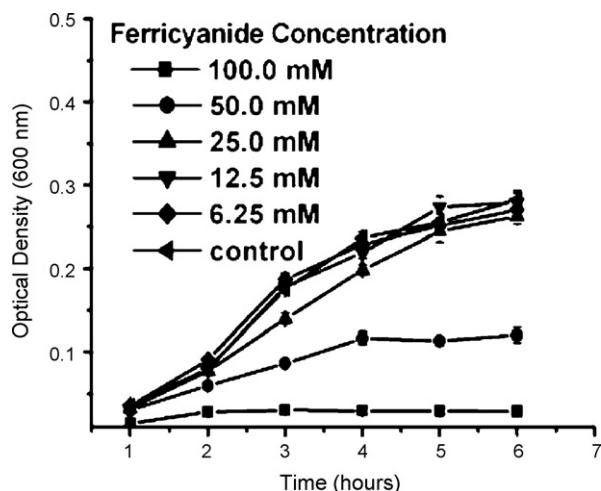


Fig. 1. Growth curve of *E. coli* DH 5  $\alpha$  at different concentrations of ferricyanide. The data are the mean  $\pm$  S.D. from triplicate experiments.

At 50.0 mM, ferricyanide showed 50.8% growth inhibition on *E. coli* after 3 h incubation, followed by stationary phase after 4 h. Negligible effects of ferricyanide for inhibition were obtained with concentration of 12.5 and 6.25 mM.

Although growth-based method is widely accepted, it inevitably shows a significant underestimation of viable cells, because a fraction of the cell population is often viable but nonculturable under the specific conditions [20]. Therefore, FCM combining with fluorescent dye (PI) was employed to further evaluate the viability of *E. coli*. Fluorescent dye PI can readily cross membranes that have been destroyed (dead cells), and after intercalating into GC-rich segments of DNA, cause 'dead' cells to fluoresce a bright red [28]. The advantage of this technology is the capacity for simultaneously measuring several parameters, based on light scattering and fluorescence, on thousands of individual cell within a few minutes [29]. Results were shown in Fig. 2. As expected, much lower toxicity was detected by FCM compared with test of growth inhibition. *E. coli* remained  $\sim$ 86% viability even the cells were pretreated with 100.0 mM ferricyanide, and negligible effects on the viability of cells were observed in ferricyanide at 25.0 mM concentration.

The similar trend was observed between growth inhibition test and viability test though high ferricyanide concentration showed some differences. One possible explanation was that high concentration of ferricyanide preferably induced nonculturable state of cells not completely losing their viability. Furthermore, the cells

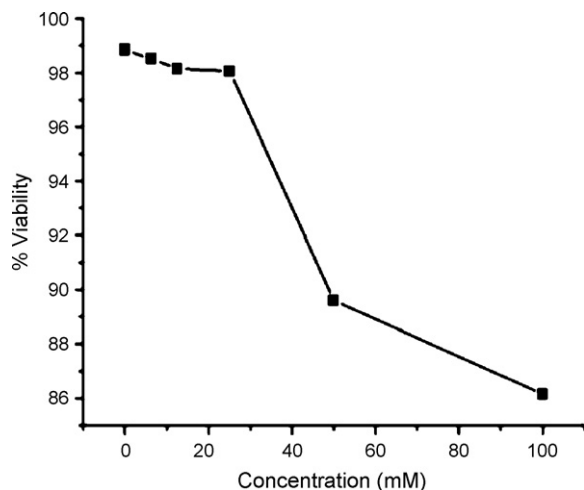


Fig. 2. Effect of different concentrations of ferricyanide on bacterial viability.

pretreated with low concentration of ferricyanide remained intact membranes and prevented the penetration of PI.

### 3.2. Characterization of damages induced by ferricyanide on *E. coli* envelopes

AFM provides the possibility of nanoscale visualization and characterization of the cells in situ, which makes it a powerful and very useful technique for the investigation of damages on outer membrane of Gram-negative bacteria. The sample-preparation process of AFM is simpler, which effectively reduces artifacts on samples in comparison with other nanoscale determination [30]. Here, we used AFM to study the effects of different concentration of ferricyanide on membrane of *E. coli*. Normal bacterial images (Fig. 3a and b) showed that untreated cells had a typical *E. coli* rod-shape and the surface was relatively smooth. The encircled areas showed a new fissiparous bacterial cell. Unfortunately, none of the bacteria was still attached with pili, owing to the centrifuging treatment.

No particular changes were observed when the cells were incubated in solution containing 25.0 mM ferricyanide for 3 h (Fig. 3c and d). Accordingly, AFM showed that with the addition of 50.0 mM of ferricyanide, the bacteria had surface morphology changes (Fig. 3e and f). We found that some obscure patches and formation of collapse (encircled area) appeared on the bacterial surface. We believe that the patches were the possible overexpression of biocomponents by stimulation of ferricyanide, and they could fall off the bacterial surface, which then led to the appearance of a concave part. This phenomenon was also observed by Yang and co-workers who proposed that these condensed patches could prevent the toxin to pass into the cell membrane [7].

Ferricyanide at concentration of 100.0 mM could cause obvious damages to *E. coli* envelope. A type of damages observed in the test was shown in Fig. 3g and h. The cell wall disappeared and led to the lysis of the bacteria. All bacterial surfaces seemed very rough and a small amount of cytoplasm remained. However, we also observed that the survived cells that remained intact cytoplasmic membrane, and only convex patches were obviously shown on the envelope (encircled area in Fig. 3g and h). The second type of damage in the experiments with 100.0 mM ferricyanide was shown in Fig. 3i and j. Flattened empty cells with rough surfaces were observed, and this meant that most of the intracellular content discharged. The phenomenon can be considered as a further step in the damage which follows the damage shown in Fig. 3g and h.

As we observed above, with the increasing concentration of ferricyanide, there were significant changes in bacterial surface. In order to farther investigate the toxic principle of ferricyanide on the bacteria, *E. coli* grown in 100.0 mM ferricyanide at different incubation times were detected. Fig. 4a and b showed that 30 min pretreatment of 100.0 mM ferricyanide did not obviously affect bacterial morphology. When the bacteria were treated with ferricyanide at 60 min, deteriorations of bacterial both ends were found (Fig. 4c and d). More damages were observed at 120 min incubation time, and *E. coli* showed incomplete morphology (Fig. 4e and f). All results of AFM revealed that the damages of the bacterial morphology were proportional to the ferricyanide concentration and incubation time.

### 3.3. Recovery test after exposure

We also investigated the recovery ability of *E. coli* after the cells had been exposed to different concentrations of ferricyanide for 3 h (Fig. 5). In comparison to the control experiment, growth rate of cells pre-exposed to 100.0 mM and 50.0 mM ferricyanide individually decreased to 8.2% and 24.5% after being transferred into uncontaminated medium to incubate for 16 h. Furthermore, the growth rate decreased to 36.7% and 59.2% when the ferricyanide

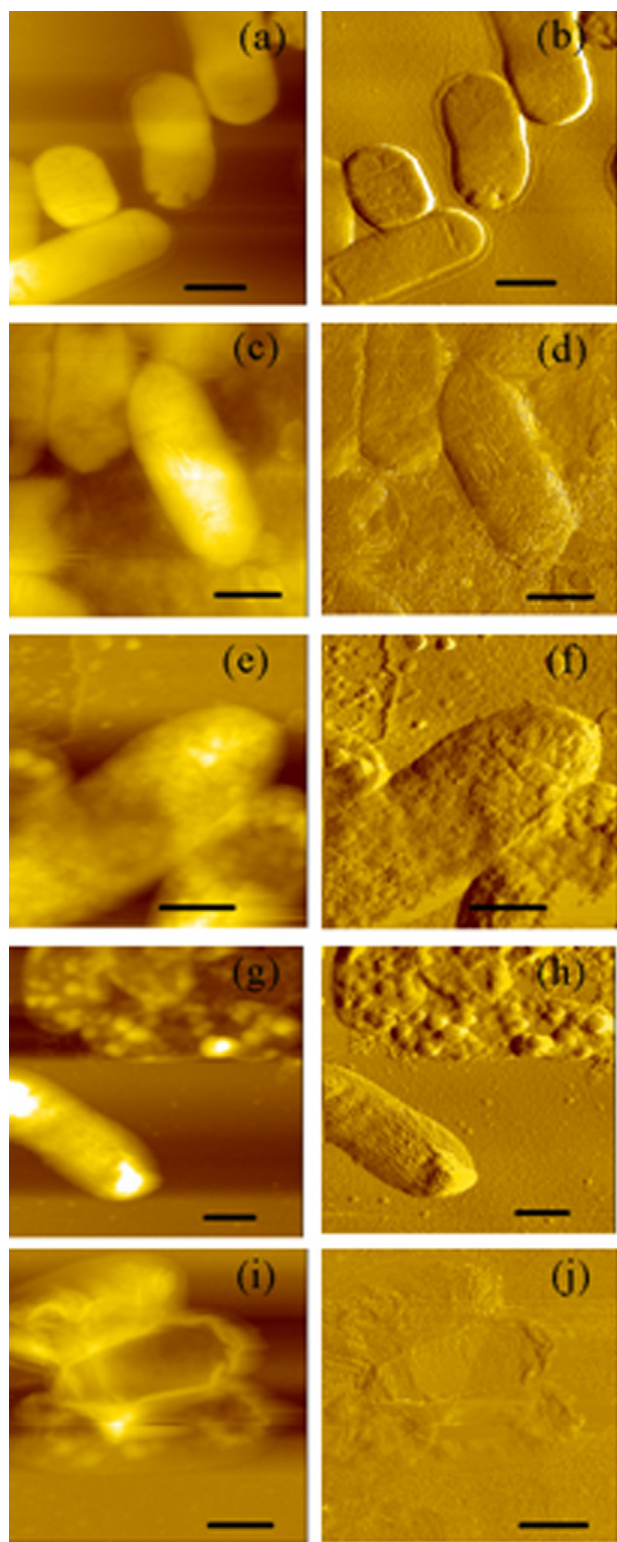


**Fig. 3.** AFM images of *E. coli* treated with different conditions of ferricyanide for 3 h. (a, b) 0 mM, control; (c, d) 25 mM; (e, f) 50 mM; (g–j) 100 mM. (a), (c), (e), (g), (i) are topography, (b), (d), (f), (h), (j) are their phase images, respectively. Scale bar of all images are 1  $\mu\text{m}$ .

concentrations were 25.0 and 12.5 mM, respectively. The recovery test exhibited obvious growth inhibition with ferricyanide of low concentration (i.e. 12.5, 25.0 mM), with overall effects greater than growth inhibition test. However, the reasons for greater effects of recovery were not clear, and further in-depth investigations are

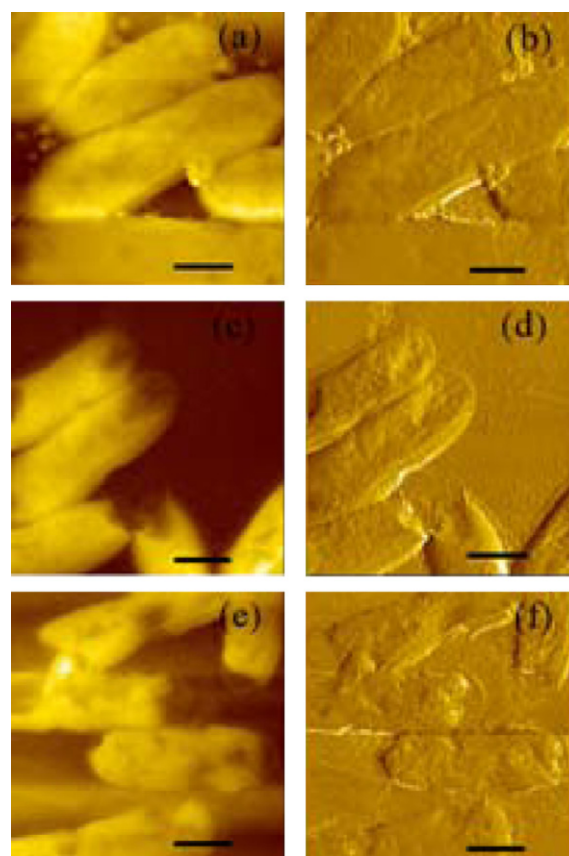


**Fig. 4.** AFM images of *E. coli* incubated with 100.0 mM ferricyanide at different time. (a), (c) and (e) individually show topography of *E. coli* that were pretreated 30, 60, 120 min in 100.0 mM ferricyanide solution, and (b), (d), (f) are their corresponding phase images. Scale bar of all images are 1  $\mu\text{m}$ .

needed to clarify the primary principles of ferricyanide on the different toxic tests.

The changes of respiration activity increased significantly from 0.45 to 3.27  $\text{mg L}^{-1}$  when ferricyanide concentration decreased from 100.0 to 25.0 mM. The weak difference of respiration activity induced by 25.0 and 12.5 mM ferricyanide was only 0.22  $\text{mg L}^{-1}$ . A negligible effect was observed at 6.25 mM ferricyanide. We believe that free  $\text{CN}^-$  is responsible for the bacterial deterioration because

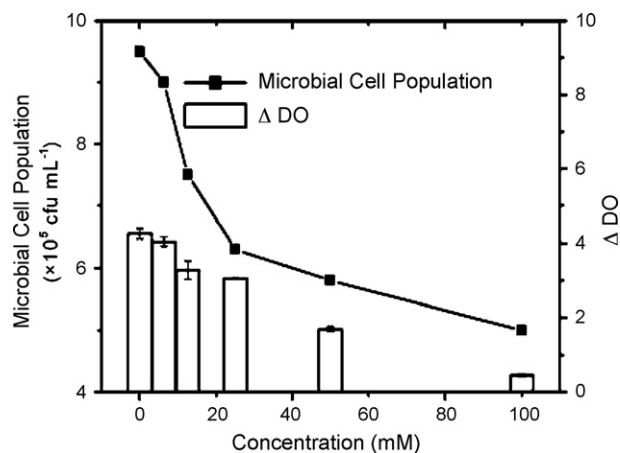


**Fig. 5.** Recovery of *E. coli* after a 3 h exposure to the different concentrations of ferricyanide. Afterwards bacteria were transferred to uncontaminated medium, and growth and changes of DO were respectively recorded for 16 h. The data of  $\Delta \text{DO}$  are the mean  $\pm$  S.D. from duplicated or triplicate experiments.

cyanide is extremely toxic to the activity of enzymes correlated with respiration.

#### 4. Conclusions

In this work, we tried to combine novel techniques of FCM and AFM for the toxic measurement, by which toxicity of ferricyanide on bacterial visibility and morphology were rapidly and directly fed back. Recovery test further proved that the toxicity of ferricyanide on bacteria was not reversible. The results showed that negligible effects were observed with concentrations below 12.5 mM ferricyanide, where 50.0 mM ferricyanide exhibited 50.8% growth inhibition at 3 h. Growth of cells was completely inhibited by 100.0 mM ferricyanide; however, *E. coli* remained ~86% viability based on the FCM. Furthermore, AFM images clearly revealed that the compact patches were induced on the bacterial surface under the stimulation of at least 50.0 mM ferricyanide, and the changes of bacterial morphology depended on concentration and incubation time with ferricyanide. In the recovery test, 50.0 mM ferricyanide showed 60.0% and 75.5% inhibitions on respiration and growth, respectively, and the effects were obviously greater than using other tests. As shown results indicated that the cells might keep in nonculturable state at high concentration of ferricyanide, and the effects of ferricyanide could be prevented by changes of morphology.

In any case, these systematic investigations can substantially contribute to the understanding of toxic principle of ferricyanide, and nanoscale studies of morphology will benefit our insight into the ferricyanide resistance of *E. coli*. Moreover, a large numbers of study provide significantly valuable reference in further research.

#### Acknowledgements

This project was supported by the State Plan for High-Tech Research and Development (2007AA061501), the National Natural Science Foundation of China (No. 20820102037).

#### References

- [1] K. Morris, H. Zhao, R. John, Aust. J. Chem. 58 (2005) 237.
- [2] G. Ramsay, A.P.F. Turner, Anal. Chim. Acta 208 (1998) 1.
- [3] T. Ding, R.D. Schmid, Anal. Chim. Acta 234 (1990) 247.
- [4] O.N. Oktyabrsky, G.V. Smirnova, E.V. Kuznetsova, Bioelectrochem. Bioenerg. 32 (1993) 267.
- [5] T. Kalab, P. Skladal, Electroanalysis 6 (1994) 1004.
- [6] T. Ikeda, T. Kurosaki, K. Takayama, K. Kano, Anal. Chem. 68 (1996) 192.
- [7] C. Yang, Y. Cheng, X. Ma, Y. Zhu, H.Y. Holman, C. Wang, Z. Lin, Langmuir 23 (2007) 4480.
- [8] K. Catterall, H. Zhao, N. Pasco, R. John, Anal. Chem. 75 (2003) 2584.
- [9] N. Yoshida, K. Yano, T. Morita, S.J. McNiven, H. Nakamura, I. Karube, Analyst 125 (2000) 2280.
- [10] K. Baronian, C. Jeffries, J. Hay, N. Pasco, Appl. Microbiol. Biotechnol. 53 (2000) 613.
- [11] K. Catterall, K. Morris, C. Gladman, H. Zhao, N. Pasco, R. John, Talanta 22 (2001) 1187.
- [12] N. Yoshida, J. Hoashi, T. Morita, S.J. McNiven, H. Nakamura, I. Karube, Biotechnology 88 (2001) 269.
- [13] K. Morris, K. Catterall, H. Zhao, N. Pasco, R. John, Anal. Chim. Acta 442 (2001) 129.
- [14] K. Baronian, C. Jeffries, J. Webber, J. Hay, N. Pasco, Biosens. Bioelectron. 20 (2004) 524.
- [15] J. Zhao, Z. Yang, M. Wang, Y. Lu, Z. Yang, J. Agric. Food Chem. 52 (2004) 7246.
- [16] K. Suzuki, H. Ishikuro, S. Kinoshita, R. Koizumi, S. Okuma, M. Gotoh, H. Nakamura, I. Karube, Talanta 72 (2007) 210.
- [17] W.S. Rader, L. Solujic, L. Hendrix, J.H. Nelson, E.B. Mollósavijevic, Environ. Sci. Technol. 27 (1993) 1875.
- [18] F. Pablo, R.T. Buckney, R.P. Lim, Bull. Environ. Contam. Toxicol. 58 (1997) 93.
- [19] M. Wang, Z. Yang, Z. Wang, H. Wang, Z. Yang, J. Zhao, Anal. Chim. Acta 597 (2007) 67.
- [20] P. Ertl, E. Robello, F. Battaglini, S.R. Mikkelsen, Anal. Chem. 72 (2000) 4957.
- [21] E. Fulladosa, J.C. Murat, J.C. Bollinger, I. Villaescusa, Sci. Total Environ. 377 (2007) 207.
- [22] A. Jain, B.S.J. Winkel, K.J. Brewer, J. Inorg. Biochem. 101 (2007) 1525.
- [23] L. Yang, W. Tan, X. He, R. Jin, J. Li, H. Li, K. Wang, Anal. Chem. 78 (2006) 7341.
- [24] D. Lloyd, M.T.E. Suller, Cytometry 35 (1999) 235.
- [25] C. Connell, A. Rutter, B. Hill, M. Suller, D. Lloyd, J. Appl. Microbiol. 90 (2001) 706.
- [26] Standard Methods for the Examination of Water and Wastewater, 19th edn., American Public Health Association, 1995.
- [27] M. Meincken, D.L. Holroyd, M. Rautenbach, Antimicrob. Agents Chemother. 49 (2005) 4085.
- [28] M.C. Flickinger, K.L. Swope, Biotechnol. Bioeng. 52 (1996) 340.
- [29] L.G. Chitarra, R.W. Bulk, Eur. J. Plant Pathol. 109 (2003) 407.
- [30] B. Li, D. Pant, J.S. Zheng, Y.J. Cheng, X.Y. Ma, F. Huang, Z. Lin, Langmuir 24 (2008) 9630.



# Determination of 7-aminoflunitrazepam in urine by dispersive liquid–liquid microextraction with liquid chromatography–electrospray–tandem mass spectrometry

Mahaveer B. Melwanki, Wei-Shan Chen, Hsin-Yu Bai, Tzuen-Yeuan Lin, Ming-Ren Fuh\*

Department of Chemistry, Soochow University, Taipei, Taiwan

## ARTICLE INFO

### Article history:

Received 22 September 2008

Received in revised form 10 December 2008

Accepted 10 December 2008

Available online 24 December 2008

### Keywords:

Dispersive liquid–liquid microextraction

7-Aminoflunitrazepam

Liquid chromatography–electrospray–

tandem mass spectrometry

Urine sample

## ABSTRACT

Dispersive liquid–liquid microextraction (DLLME) and liquid chromatography–electrospray–tandem mass spectrometry (LC–ES–MS/MS) procedure was presented for the extraction and determination of 7-aminoflunitrazepam (7-aminoFM2), a biomarker of the hypnotic flunitrazepam (FM2) in urine sample. The method was based on the formation of tiny droplets of an organic extractant in the sample solution using water-immiscible organic solvent [dichloromethane (DCM), an extractant] dissolved in water-miscible organic dispersive solvent [isopropyl alcohol (IPA)]. First, 7-aminoFM2 from basified urine sample was extracted into the dispersed DCM droplets. The extracting organic phase was separated by centrifuging and the sedimented phase was transferred into a 300  $\mu$ l vial insert and evaporated to dryness. The residue was reconstituted in 30  $\mu$ l mobile phase (20:80, acetonitrile:water). An aliquot of 20  $\mu$ l as injected into LC–ES–MS/MS. Various parameters affecting the extraction efficiency (type and volume of extraction and dispersive solvent, effect of alkali and salt) were evaluated. Under optimum conditions, precision, linearity (correlation coefficient,  $r^2 = 0.988$  over the concentration range of 0.05–2.5 ng/ml), detection limit (0.025 ng/ml) and enrichment factor (20) had been obtained. To our knowledge, DLLME was applied to urine sample for the first time.

© 2009 Elsevier B.V. All rights reserved.

## 1. Introduction

Flunitrazepam (FM2), a fluorinated derivative of 1,4-benzodiazepine is a highly potent hypnotic drug with powerful sedative, anxiolytic, amnesic and skeletal muscle relaxant properties commonly prescribed for the treatment of insomnia [1]. FM2 is known to induce anterograde amnesia; individuals are unable to remember certain events that they experienced while under the influence of the drug. This effect is particularly dangerous when abused to aid in the commission of sexual assault and FM2 is abused sometimes as a “date-rape” drug [2]. In addition, the abuse of FM2 has been connected to stealing from sedated victims making drug-assisted robbery [3]. Criminals sometimes use FM2 before committing robbery as it has a calming and anti-emotive effect that allows the criminal to perform the robbery without becoming anxious. Due to the therapeutically effectiveness at low dose and rigorous biotransformation, FM2 is seldom detected in urine sample [4,5]. The major urinary metabolite, 7-aminoflunitrazepam (7-aminoFM2), is commonly used to inspect the usage of FM2.

Thus, there is a need to develop an analytical technique for the determination of FM2 and 7-aminoFM2 in urine. Some analytical procedures have been reported including immunoassay [6], liquid chromatography–ultraviolet (LC–UV) [7], micellar electrokinetic chromatography [8] and gas chromatography–mass spectrometry (GC–MS) [9]. The lack of selectivity and sensitivity associated with immunoassay and LC based methods limit their application. GC–MS provides spectral information as well as excellent sensitivity; however, it required derivatization step prior to analysis. To address the limitations associated with the reported procedures, we have reported an online solid phase extraction cleanup prior to LC–electrospray–tandem mass spectrometry (ES–MS/MS) [10]. The detection limit for 7-aminoFM2 is reported to be 1  $\mu$ g/l and the method is suitable only for clinical applications where the concentration of FM2 is in sufficient doses and the urine sample is collected in time. However, when the drug is abused for sexual assault or robbery and if there is a time delay in suspecting the probable abuse, the method needs to achieve still lower detection limits.

Dispersive liquid–liquid microextraction (DLLME) developed by Rezaee et al. [11] is based on the formation of tiny droplets of the extractant in the sample solution using water-immiscible organic solvent (extractant) dissolved in a water-miscible organic dispersive solvent. Extraction of the analytes from aqueous sample into the dispersed organic droplets takes place. The extracting organic

\* Corresponding author. Tel.: +886 2 28819471x6821; fax: +886 2 28812685.  
E-mail address: [msfuh@mail.scu.edu.tw](mailto:msfuh@mail.scu.edu.tw) (M.-R. Fuh).

phase was separated by centrifuging and the sedimented phase was injected into GC. The technique has been applied for the analysis of polycyclic aromatic hydrocarbons [11], organophosphorus flame retardants and plasticizers [12], volatile phenols [13], organophosphorous pesticides [14], chlorobenzenes [15], chlorophenols [16], triazine herbicides [17], trihalomethanes [18], anilines [19], butyl and phenyltin compounds [20], and phthalate esters [21]. For the analytes which are incompatible with GC, the water-immiscible organic extract obtained after DLLME cannot be injected directly for reverse phase-liquid chromatography (RP-LC). Hence, evaporation of the organic extract to dryness and reconstitution of analytes into a suitable solvent prior to LC was required. This approach was used for the analysis of antioxidants by Farajzadeh et al. [22]. Herein, after extracting the analytes into the organic solvent by DLLME, the organic phase was transferred to another test tube with a conical bottom using a 100  $\mu$ l LC syringe and evaporated on a water bath. Subsequently, the residue was re-dissolved in a 50  $\mu$ l methanol and injected into LC.

In the present investigation, the concept of Farajzadeh et al. [22] has been used with modifications to assist high-throughput analysis. Here, the sedimented organic phase was transferred into a 300  $\mu$ l vial insert attached with polymeric feet. The organic phase was evaporated to dryness in a concentrator (operates under low pressure thus enhancing fast evaporation step) instead of an earlier reported water bath usage [22]. The residue was reconstituted in 30  $\mu$ l mobile phase. The vial insert with polymeric feet was placed in a 2 ml sample vial and positioned in a sample tray. An aliquot of 20  $\mu$ l was injected into LC–electrospray–tandem mass spectrometry (LC–ES–MS/MS) using an auto-injector. To our knowledge, DLLME was applied to urine sample for the first time.

## 2. Experimental

### 2.1. Materials and reagents

A 10 mg/l stock solution of 7-aminoFM2 (Cerilliant Corp., Austin, TX, USA) was prepared in methanol. Standard working solution was prepared everyday by spiking the stock solution to the urine sample. De-ionized water was from Milli-Q plus water purification system (Millipore, Bedford, MA, USA). Acetonitrile (ACN), dichloromethane (DCM), acetone, methanol, isopropyl alcohol (IPA) and tetrahydrofuran (THF) were obtained from Mallinckrodt [Mallinckrodt Baker, Inc., NJ, USA]. Sodium chloride (NaCl) [Riedel-de Haen (Sigma–Aldrich Laborchemikalien, Seelze)], tetrachloroethylene (TCE) [Sigma–Aldrich, Steinheim, Germany] and chlorobenzene (CB) [Aldrich Chemical Co. Inc., WI, USA] were used in the present study. All reagents and solvents used were analytical or LC grade unless otherwise mentioned. Drug free urine samples collected from healthy adults were used for the study.

### 2.2. Instrumentation

An HP1100 LC system (Hewlett–Packard Co., Palo Alto, CA, USA) consisting of a quaternary pump with an online degasser and an auto-injector was used for the study. Mass spectrometric detection was performed using an Agilent series LC/MSD trap SL instrument equipped with an ES ionization source that was operated in the positive mode with the spray voltage set at  $-3.5$  kV. The capillary exit voltage was 180 V. Agilent 1100 series LC/MSD Trap software (version 4.0) was utilized for system control, data acquisition and data analysis. Heated nitrogen gas (350  $^{\circ}$ C, 8 l/min) was used to evaporate solvent from the ES chamber, and compressed nitrogen gas (40 psi) was used for nebulization. Multiple reaction monitoring (MRM) was employed for quantitative measurement. The isolation width for precursor ion was 2. The settings for the MRM

were:  $m/z$  284  $\rightarrow$  264, 163 and 135. MS/MS data acquisition was performed under the following conditions: normal scan speed,  $m/z$  range 100–350, ion charge control target 30,000 and maximum accumulation time 300 ms.

A symmetry Shield RP18 [50  $\times$  2.1 mm, 3.5  $\mu$ m] (Waters, Ireland) column was used for separation of 7-aminoFM2. Mobile phase was a mixture of 20% ACN and 80% water at a flow rate of 0.2 ml/min. A model 2420 Kubota (Tokyo, Japan) centrifuging machine and miVac DUO centrifugal concentrator (Genevac Ltd., Ipswich, UK) operating at low pressure was used for the evaporation of extraction solvent (compared with an evaporation time carried out at atmospheric pressure). Test tubes with conical bottom were used for extraction process. Vial insert (Agilent, USA; 300  $\mu$ l with polymer feet) and syringe [1 ml (Gas tight #1001) and 100  $\mu$ l (Gas tight #1710); Hamilton Co., Reno, Nevada, USA] were also used.

### 2.3. Extraction process

Urine sample spiked with 7-aminoFM2 was basified using ammonia (overall concentration: 0.2 M) and added NaCl (5% overall). The precipitate formed was separated by centrifuging (3500 rpm, 10 min). An aliquot of 5 ml of the clear supernatant urine sample was placed in an 8 ml test tube. IPA (500  $\mu$ l) containing DCM (250  $\mu$ l) [total 750  $\mu$ l] was injected rapidly into the sample using a 1 ml syringe. The mixture was gently shaken. A cloudy solution was formed. The phases were separated by centrifuging (4000 rpm, 10 min). Herein, the dispersed fine droplets are sedimented at the bottom of the conical test tube. The sedimented DCM phase was transferred to a 300  $\mu$ l vial insert using a 100  $\mu$ l syringe. The organic phase was evaporated to dryness in the concentrator (20 min). The residue was reconstituted in 30  $\mu$ l of the mobile phase and a 20  $\mu$ l aliquot was injected into LC–ES–MS/MS using an auto-injector.

## 3. Results and discussion

### 3.1. Suitability of the auto-injector

The suitability of the auto-injector is studied by performing two sets of experiments. First, a 30  $\mu$ l of 7-aminoFM2 (25  $\mu$ g/ml) was taken into each of a series of (ten numbers) vial inserts fitted with polymeric feet. Each of the vial inserts was placed in a separate 2 ml sample vial and was positioned in a sample tray. A 20  $\mu$ l aliquot was injected into the LC–ES–MS/MS. Secondly, 1.5 ml of the sample (25  $\mu$ g/ml 7-aminoFM2) was taken into each of a series of 2 ml sample vial. An aliquot of 20  $\mu$ l was injected. It was observed that, there is no appreciable difference in the peak areas measured in these two experiments. Thus, it was concluded that the auto-injector could be used to inject an aliquot of 20  $\mu$ l from 30  $\mu$ l of the sample taken in the vial insert.

### 3.2. Selection of organic extractant and dispersive solvent

The selection of an appropriate organic extractant is of high importance in DLLME process. It is based on a few criterion *viz.* the solvent should be immiscible in urine, should have higher density than that of urine and have high extraction capability for 7-aminoFM2. However, the chromatographic behavior of the extractant is of less importance unlike the GC based techniques [11–22]. This is because the extractant is evaporated to dryness prior to reconstituting the residue in the mobile phase before injecting into LC. Based on these criterions, CB, DCM and TCE were selected for the study. Similarly, the criterion in the selection of a dispersive solvent is that, the solvent should form a cloudy state when injected with the organic extractant into urine, in addition to having solubility in the organic extracting solvent and urine. Considering these issues into account, ACN, acetone, methanol, THF

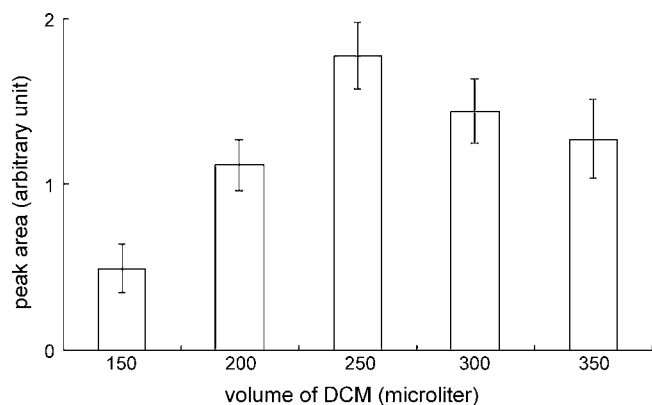


**Fig. 1.** Effect of volume of DCM on extraction efficiency. Experimental conditions: sample volume, 5 ml (in 0.1 M ammonia); dispersive solvent, IPA (500 μl); 7-aminoFM2 concentration spiked, 1 ng/ml.

and IPA were tested for their efficiency. Due to a limited number of organic extractants, all combinations of CB, DCM and TCE as extractants with acetone, ACN, methanol, THF and IPA as dispersive solvent, were tried. Forty microliter of extractant was used in case of TCE and CB, dissolved in 0.5 ml of each of the dispersive solvent. However, in the case of DCM, it was noted that no phase separation was observed when the amount of DCM was lower than 120 μl. This is probably due to the higher solubility of DCM in the matrix. Thus 150 μl of DCM was used for studying its extraction efficiency. Further experiments were conducted with DCM as an extractant and IPA as dispersive solvent, as the combination gave the highest extraction efficiency.

### 3.3. Impact of volume of organic extractant

To study the effect of extraction solvent volume, solutions containing increasing volumes (150–350 μl) of DCM dissolved in a fixed volume of IPA (500 μl) were subjected to DLLME by injecting the total amount using a 1 ml syringe. The results are presented in Fig. 1. It is clear from the figure that the extraction efficiency was increased with increase in volume of DCM till 250 μl followed by a decrease in extraction efficiency. In addition, the volumes of sedimented DCM drop and the enrichment factors at various volumes of organic extractant were summarized in Table 1. At higher volume of extracting organic solvent, the ratio between the dispersive solvent and the extracting organic solvent decreased that probably lowered the number of droplets formed thereby decreasing the efficiency of extraction. Based on these observations, a volume of 250 μl was used for further experiments.

### 3.4. Impact of volume of dispersive solvent

Volume of the dispersive solvent is one of the important factors to be considered. At lower volumes of the disperser, tiny droplet formation may not be effective thereby lowering the extraction efficiency. At higher volumes of the dispersive solvent, the solubility of 7-aminoFM2 in urine increases; thus, lowering the partition of 7-aminoFM2 into DCM leading to a decrease in efficiency. Considering these facts into account, a fixed amount of the organic

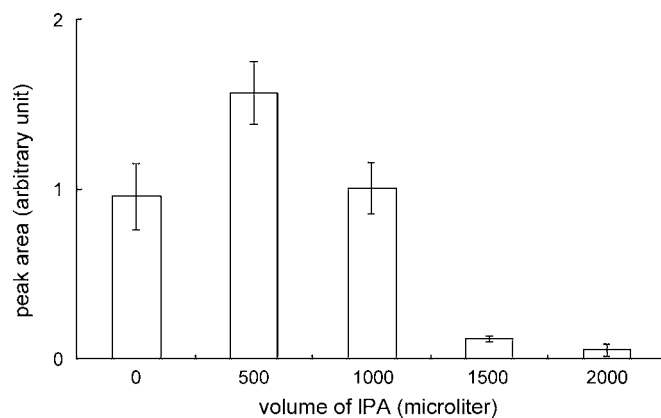


**Fig. 2.** Effect of volume of IPA on extraction efficiency. Experimental conditions: sample volume, 5 ml (in 0.1 M ammonia); organic extractant, 250 μl DCM; 7-aminoFM2 concentration spiked, 1 ng/ml.

extractant (250 μl DCM) was dissolved in an increasing volume of the disperser ranging from 0 to 2000 μl at an interval of 500 μl and injected the total volume into the sample for extraction. A graphical representation of efficiency versus volume of IPA is shown in Fig. 2. It was observed that the extraction efficiency increased with increase in IPA till 500 μl followed by a decrease in efficiency with increase in IPA volume. The decrease is probably due to the increase in the solubility of 7-aminoFM2 in the sample. Based on these results, 500 μl IPA was used for further experiments.

### 3.5. Impact of alkalinity

When extractions were performed using urine sample without the addition of a base, the extraction efficiency was very low. This could be attributed to the fact that, 7-aminoFM2 is slightly basic and needs to be basified to keep it in a molecular form, thus facilitating the partition of 7-aminoFM2 into DCM droplets. For this, NaOH was used to basify the urine sample. However, no phase separation was observed. When ammonia was used to basify the urine sample, phase separation as well as an increase in extraction efficiency was noted. The effect of concentration of ammonia (0.01–1 M) was examined and the results are shown in Fig. 3. A gradual increase in extraction efficiency was observed with increase in ammonia concentration up to 0.2 M. However, further increase in ammonia concentration led to a decrease in the volume of the organic phase thereby lowering extraction efficiency. A concentration of 0.2 M ammonia was used for further experiments.

### 3.6. Impact of salt

To evaluate the possibility of salting out effect, extraction efficiency was studied with increase in sodium chloride (NaCl) concentration over the concentration range of 0–30% (w/v). As shown in Fig. 4, there was an increase in extraction efficiency with an increase in salt concentration up to 5% and then a diminishment in efficiency. Additionally, phases were not separated above 20% NaCl. An initial increase and then a decrease in extraction efficiency with increase in concentration of NaCl can be explained by

**Table 1**  
Volume of sedimented DCM drop and enrichment at various IPA and DCM.

Vol. of IPA (μl)	500	500	500	500	500
Vol. of DCM (μl)	150	200	250	300	350
Vol. of sedimented DCM drop (μl)	38.6 ± 2.3	70.4 ± 3.8	99.0 ± 4.2	134.6 ± 6.5	154.3 ± 5.5
Enrichment factor <sup>a</sup>	5.5	12.5	20.0	16.2	14.3

<sup>a</sup> Enrichment factor, calculated as the ratio between the peak area on the chromatogram after and before the extraction.

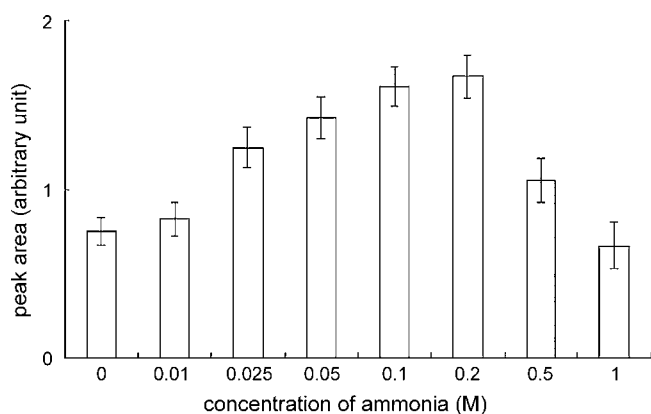


**Fig. 3.** Effect of concentration of ammonia on extraction efficiency. Experimental conditions: sample volume, 5 ml; organic extractant, 250  $\mu$ l DCM; dispersive solvent, IPA (500  $\mu$ l); 7-aminoFM2 concentration spiked, 1 ng/ml.

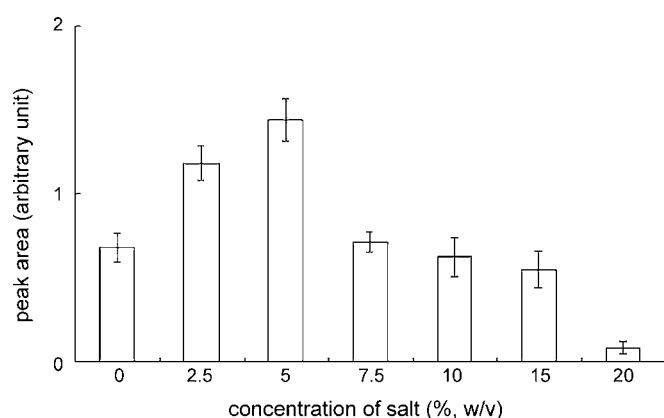


**Fig. 4.** Effect of salt concentration on extraction efficiency. Experimental conditions: sample volume, 5 ml (in 0.2 M ammonia); organic extractant, 250  $\mu$ l DCM; dispersive solvent, IPA (500  $\mu$ l); 7-aminoFM2 concentration spiked, 1 ng/ml.

two simultaneously occurring processes as described by Lord et al. [23]. Initially, extraction efficiency was increased due to salting out, whereby water molecules form hydration spheres around the ionic salt molecules that reduce the concentration of water available to dissolve the analyte molecules; thereby driving the additional analytes into the organic droplets. In competition with this process, polar molecules may participate in electrostatic interaction with the salt ions in solution. As a result, it reduces their ability to move into the extraction phase and decrease the extraction efficiency. Based on these observations, an overall salt concentration of 5% (w/v) was used for further studies.

### 3.7. Quantitative aspects

Repeatability, linearity, correlation coefficient and detection limit were investigated under the chosen experimental conditions

**Table 2**  
Performance of the method.

Parameter	Value
Linearity (ng/ml)	0.05–2.5
$r^2$	0.988
Relative standard deviation	
0.1 ng/ml	8.6%
2.0 ng/ml	6.3%
Method detection limit (ng/ml)	0.025

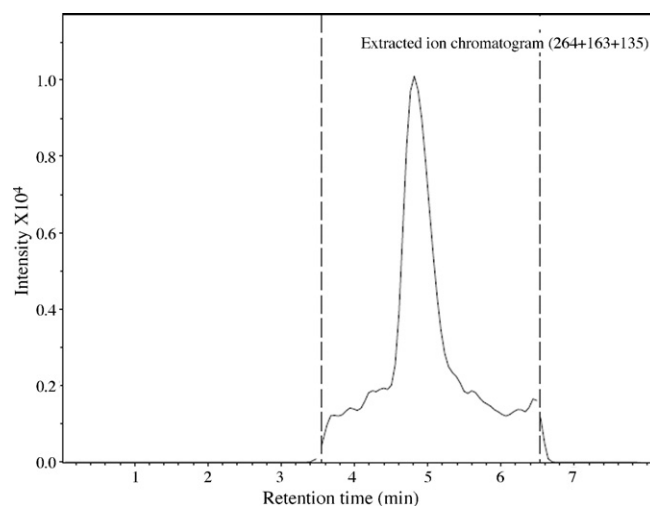


**Fig. 5.** Extracted ion chromatogram of the extract of the spiked urine sample. Experimental conditions: sample volume, 5 ml (in 0.2 M ammonia & 5% NaCl); organic extractant, 250  $\mu$ l DCM; dispersive solvent, IPA (500  $\mu$ l); 7-aminoFM2 concentration spiked, 0.1 ng/ml.

and summarized in Table 2. It was observed that, the relative standard deviation values were below 8.6% indicating a good precision of the method. It exhibited good correlation coefficient ( $r^2 = 0.988$ ) for the concentration range of 0.05–2.5 ng/ml. Acceptable accuracy, 92.3–103.7%, was determined. Method detection limit, calculated as three times the standard deviation of seven replicate runs was determined to be 0.025 ng/ml.

### 3.8. Application of the technique

To demonstrate the potentiality of the technique, the procedure was applied for the analysis of various urine samples. Each of the samples was basified using ammonia so that the overall concentration is 0.2 M in ammonia and was made 5% in NaCl concentration. The precipitate was filtered off and a 5 ml of an aliquot of the clear supernatant urine sample solution was placed in a test tube and extracted using the general procedure. The extract was injected into LC–ES–MS/MS. No target compound was found in any of the tested urine samples. Then the sample was spiked with low concentrations of 7-aminoFM2 (0.1 ng/ml) and extracted, and injected in the usual manner. A representative extracted ion chromatogram of the extract of one of 7-aminoFM2 spiked urine samples is shown in Fig. 5.

### 3.9. Comparison of the technique with other methods

A comparison of the technique in terms of detection limit, specificity and reaction conditions involved to carryout the extraction with other methods is provided in Table 3.

**Table 3**  
Comparison of the present technique with reported methods.

Parameter	Value/and remark	
	Reported method	Present method
Detection limit (ng/ml)	5.6 <sup>a</sup> ; 1 <sup>b,c</sup> ; 5 <sup>c</sup>	0.025
Specificity	Not specific <sup>c</sup>	Specific
Reaction require	Derivatization <sup>b,c</sup>	No derivatization

<sup>a</sup> Reference [1].

<sup>b</sup> Reference [6].

<sup>c</sup> Reference [24].

#### 4. Summary

A newly developed DLLME and LC–ES-MS/MS method was presented for the extraction and analysis of 7-aminoFM2 in urine sample. DCM as an organic extractant and IPA as a dispersive solvent were utilized for DLLME. The extracting organic phase was separated, evaporated to dryness and then reconstituted in mobile phase prior to LC–ES-MS/MS determination. The enrichment factor for the extraction process is about 20. Good linearity (0.05–2.5 ng/ml) and detection limit of this method, 0.025 ng/ml, were obtained. In this study, DLLME was successfully applied to urine sample analysis.

#### Acknowledgement

This work was supported by the National Science Council of Taiwan.

#### References

- [1] W. Wichstrom, R. Amrein, P. Haefelfinger, D. Hartmann, *Eur. J. Clin. Pharm.* 17 (1980) 189.
- [2] M.A. ElSohly, S. Feng, S.J. Salamone, R. Wu, *J. Anal. Toxicol.* 21 (1997) 335.
- [3] M. Kollroser, C. Schober, *J. Pharm. Biomed. Anal.* 28 (2002) 1173.
- [4] I.M. McIntyre, M.L. Syrjanen, K. Crump, S. Horomidis, A.W. Peace, O.H. Drummer, *J. Anal. Toxicol.* 17 (1993) 202.
- [5] O.H. Drummer, M.L. Syrjanen, S.M. Cordner, *Am. J. Med. Pathol.* 14 (1993) 238.
- [6] W. Huang, D.E. Moody, *J. Anal. Toxicol.* 19 (1995) 179.
- [7] V.F. Samandiou, A.P. Pechlivanidou, I.N. Papadoyannis, *J. Sep. Sci.* 30 (2007) 679.
- [8] C.-W. Huang, H.-P. Jen, R.-D. Wang, Y.-Z. Hsieh, *J. Chromatogr. A* 1110 (2006) 240.
- [9] D. Borrey, E. Meyer, W. Lambert, S. Van Calenbergh, C. Van Peteghem, A.P. De Leenheer, *J. Chromatogr. A* 910 (2001) 105.
- [10] M.-R. Fuh, S.-W. Lin, L.-L. Chen, T.-Y. Lin, *Talanta* 72 (2007) 1329.
- [11] M. Rezaee, Y. Assadi, M.R. Milani Hosseini, E. Aghaee, F. Ahmadi, S. Berijani, *J. Chromatogr. A* 1116 (2006) 1.
- [12] M. Garcia-Lopez, I. Rodrigues, R. Cela, *J. Chromatogr. A* 1166 (2007) 9.
- [13] L. Farina, E. Boido, F. Carrau, E. Dellacassa, *J. Chromatogr. A* 1157 (2007) 46.
- [14] S. Berijani, Y. Assadi, M. Anbia, M.R. Milani Hosseini, E. Aghaee, *J. Chromatogr. A* 1123 (2006) 1.
- [15] R. Rahnema Kozani, Y. Assadi, F. Shemirani, M.R. Milani Hosseini, M.R. Jamali, *Talanta* 72 (2007) 387.
- [16] N. Fattahi, Y. Assadi, M.R. Milani Hosseini, E.Z. Jahromi, *J. Chromatogr. A* 1157 (2007) 23.
- [17] D. Nagaraju, S.-D. Huang, *J. Chromatogr. A* 1161 (2007) 89.
- [18] R. Rahnema Kozani, Y. Assadi, F. Shemirani, M.R. Milani Hosseini, M.R. Jamali, *Chromatographia* 66 (2007) 81.
- [19] J.-S. Chiang, S.-D. Huang, *Talanta* 75 (2008) 70.
- [20] A.P. Birjandi, A. Bidari, F. Rezaei, M.R.M. Hosseini, Y. Assadi, *J. Chromatogr. A* 1193 (2008) 19.
- [21] H. Farahani, P. Norouzi, R. Dinarvand, M.R. Ganjali, *J. Chromatogr. A* 1172 (2007) 105.
- [22] M.A. Farajzadeh, M. Bahram, J.A. Jonsson, *Anal. Chim. Acta* 591 (2007) 69.
- [23] H. Lord, J. Pawliszyn, *J. Chromatogr. A* 902 (2000) 17.
- [24] J. Hackett, A.A. Elian, *Forensic Sci. Intl.* 157 (2006) 156.





# Enantioseparation of binaphthol and its monoderivatives by cyclodextrin-modified capillary zone electrophoresis: A mathematical approach

N. Mofaddel<sup>a</sup>, H. Krajian<sup>a,1</sup>, D. Villemin<sup>b</sup>, P.L. Desbène<sup>a,\*</sup>

<sup>a</sup> L.A.S.O.C. – IRCOF et IFRMP, Université de Rouen, 55 rue Saint Germain, 27000 Evreux, France

<sup>b</sup> Laboratoire de Chimie Moléculaire – Thioorganique, UMR 6507, ENSICAEN, Université de Caen, bd du Maréchal Juin, 14050 Caen, France

## ARTICLE INFO

### Article history:

Received 25 July 2008

Received in revised form 4 December 2008

Accepted 11 December 2008

Available online 24 December 2008

### Keywords:

Binaphthol derivatives

Mathematical approach

Apparent complexation constant

Enantioseparation

CD-CZE

## ABSTRACT

A simple model for the separation of atropisomers of binaphthol and its monoderivatives by means of cyclodextrin-modified capillary zone electrophoresis (CD-CZE) was used to describe the migration behavior of poly charged enantiomers in a chiral separation system. This mathematical approach allowed for the determination of the optimal cyclodextrin concentrations for the enantioseparation of binaphthols by taking into account the influence of the formed complex mobilities. Moreover, using this theoretical approach, the reversal of the enantiomers' migration order as a function of cyclodextrin concentration was predicted. The apparent complexation constants between the cyclodextrins and the binaphthol and its monoderivatives could be calculated using a non-linear curve fitting method and three linear plotting methods (*x*-reciprocal, *y*-reciprocal and double reciprocal). Good agreements between the theoretical and experimental cyclodextrin concentrations were obtained.

© 2008 Elsevier B.V. All rights reserved.

## 1. Introduction

Chiral separation by means of capillary electrophoresis (CE) has been proven to be an effective technique in recent years. The major advantages of CE are simplicity, high efficiency, versatility, rapid analysis, high resolution, small sample volume and low operating costs. Enantioseparation can be achieved in CE using chiral selectors, which discriminate between enantiomers by an enantioselective complexation between the enantiomers of the analyte and the chiral selector to differentiate based on the effective electrophoretic mobility of the enantiomers. Numerous chiral selectors are currently available and can be used for enantioseparation, such as cyclodextrins (CDs), chiral crown ethers, proteins, chiral surfactants, macrocyclic antibiotics, ligand-exchange complexes and polysaccharides [1]. Among them, the cyclodextrins are the most widely used chiral selectors [2].

The mechanism of the separation is fairly well understood. Several groups have developed mathematical models as theoretical approaches to evaluate the influence of the experimental variables and to describe the migration behavior of the analytes in the chiral separation systems.

Most models assume a 1:1 complexation between the enantiomers and the chiral selector. The analyte and the chiral selector can be neutral, anionic, cationic or zwitterionic.

Wren and Rowe [3–6] developed mobility difference models, and Sängler-Van de Griend et al. [7] proposed a model based on one analyte having two or more complexation sites for the selector and able to form multiple complexes. In a series of papers, Vigh and co-workers [8–10] introduced multiple equilibrium-based mobility models, including the effects of competing binding equilibria of the dissociated and non-dissociated analytes. They also developed the chiral charged resolving agent migration model (CHARM) [11]. Zhu et al. [12], Surapaneni et al. [13] and Lelièvre et al. [14] developed mathematical models for chiral separation systems using two chiral selectors.

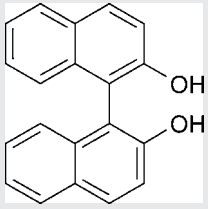
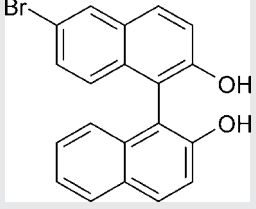
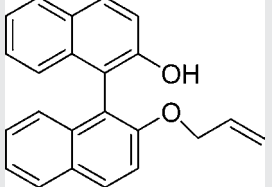
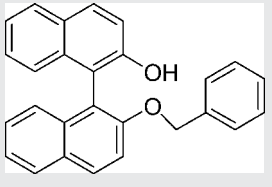
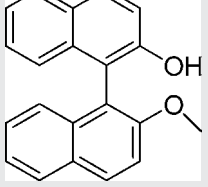
The atropisomers of 1,1'-binaphthyl-2,2'-diol (or Binol) are among the most widely used ligands for the asymmetric catalytic reactions, and serve as chiral hosts in the enantiomeric separation of racemic mixtures of "guest" compounds or as chiral reagents during optical purity studies of the enantiomers in <sup>1</sup>H NMR. Furthermore, they have also been used in enantiomeric mixture tests for evaluating new or developed chiral separation systems [15]. For these reasons, the enantioseparation of Binol by CE has been the subject of several studies. In a previous paper [16], we studied the enantiomeric separation of Binol and its monoderivatives by means of CD-CZE. First, we determined the acidity constants of Binols. Second, the nature of the CDs and the optimal conditions of the separation were reported. Additionally, working in a very basic

\* Corresponding author. Tel.: +33 2 32 29 15 40; fax: +33 2 32 29 15 35.

E-mail address: [paul-louis.desbene@univ-rouen.fr](mailto:paul-louis.desbene@univ-rouen.fr) (P.L. Desbène).

<sup>1</sup> Current address: Department of Chemistry, Atomic Energy Commission of Syria, P.O. Box 6091, Damascus, Syria.

**Table 1**  
Structures of the studied Binol and its derivatives.

Name	Abbreviation	Structure
1,1'-Binaphthalen-2,2'-diol	Binol	
6-Bromo-1-(2-hydroxynaphthalen-1-yl)naphthalen-2-ol	BN2	
1-(2-(Allyloxy)naphthalen-1-yl)naphthalen-2-ol	BN3	
1-(2-(Benzyloxy)naphthalen-1-yl)naphthalen-2-ol	BN4	
1-(2-Methoxynaphthalen-1-yl)naphthalen-2-ol	BN5	

medium (pH 11.5) was also clarified. Moreover, we observed two different types of inversion in the elution order of the two atropisomers of Binol: one as a function of the pH with  $\gamma$ -CD (pH range: 10–11.5) and the other as a function of the  $\gamma$ -CD concentration at pH 10.8.

In this paper, we adapted a simple model to describe the enantioseparation of Binol and its derivatives by means of CD-CZE. The reversal of the enantiomer migration order as a function of the cyclodextrin concentration was achieved using this model. Moreover, a mathematical approach was developed to determine the optimal cyclodextrin concentrations. These were compared to the experimental optimal concentrations to validate the theoretical model. Finally, the apparent complexation constants between binaphthols and the CDs were determined using four different plotting methods.

## 2. Experimental

### 2.1. Instrumentation

Capillary electrophoretic experiments were performed using a P/ACE MDQ capillary electrophoresis system (Beckman Coulter,

Fullerton, CA, USA) equipped with a photodiode array detector (PDA; 190–600 nm). An uncoated fused silica capillary (Thermo Electron SA, Courtaboeuf, France), 40.2 cm long (30 cm to the detector), and with a 50  $\mu$ m ID was used. The capillaries were thermostated at  $20.0 \pm 0.1$  °C. Samples were pressure-injected at 0.5 psi (34 mbar) for 3 s at the inlet side of the capillary (anode). Electrophoretic runs were performed with 10 kV potential. The UV detection was cathodic ( $\lambda = 214$  nm). The electropherograms were recorded and integrated by an IBM personal computer with 32 Karat software (Version 4.0, Beckman Coulter). The pH of the electrolyte solutions was measured using a Cyberscan pH510 pH meter (Bioblock Scientific, Illkirch, France).

The experimental data were fit with the CurveExpert program (Version 1.38, Daniel G. Hyams, Hixson, TN, USA) for the non-linear curve fitting method and with SigmaPlot 8.0 (Version 8.02, Systat Software Inc., San Jose, USA) for the linear plotting methods.

### 2.2. Chemicals and reagents

The racemate and the R enantiomer of Binol (1,1'-binaphthyl-2,2'-diol or 1,1'-binaphthalen-2,2'-diol) were provided by

Sigma–Aldrich (Sigma–Aldrich France, Saint-Quentin-Fallavier, France). Binol derivatives studied in this work (see Table 1) were synthesized as described previously [16]. Native  $\alpha$ -CD was purchased from Sigma–Aldrich,  $\beta$ -CD (98%) from Interchim (Montluçon, France) and  $\gamma$ -CD (98%) from Acros Organics (Acros Organics France, Noisy-le-Grand, France). 2-Hydroxypropyl- $\alpha$ -,  $\beta$ - and  $\gamma$ -CDs (HP-x-CDs) (d.s.  $\approx$  0.6) were obtained from Fluka Chemie (Sigma–Aldrich–Fluka France, L'Isle d'Abeau, Chesne, France), and heptakis-2,3,6-tri-O-methyl- $\beta$ -cyclodextrin (TM- $\beta$ -CD) was purchased from Sigma–Aldrich. Disodium hydrogenphosphate, trisodium phosphate, sodium hydroxide (+98% purity), and absolute ethanol (98.8%). were obtained from Sigma–Aldrich.

### 2.3. Electrolyte and sample preparation

All running electrolytes were prepared using ultrapure water produced with a Milli-Q-System water purification apparatus (Millipore France, Montigny-le-Brotonneux, France). The solutions were sonicated just before use for 10 min with a Branson 2510 sonication apparatus (Branson, Danbury, USA). For the enantioseparations and the apparent complexation constant determinations, a phosphate electrolyte ( $\text{Na}_2\text{HPO}_4$ – $\text{Na}_3\text{PO}_4$ ) with an ionic strength of 80 mM was used with cyclodextrin concentrations ranging from 0 to 20 mM or 25 mM. All samples were prepared in ethanol at a concentration of  $1 \times 10^{-4}$  M.

In order to determine the enantiomeric migration order, the racemic sample was spiked with the R enantiomer. New uncoated capillaries were activated by performing the following washing process: water for 2 min, 1 M NaOH for 30 min and water for 10 min. The capillary was conditioned for 15 min with the electrolyte before running and for 2 min between each run.

## 3. Results and discussion

### 3.1. Theory

In our previous work [16], we reported a reversal of the elution order of the two atropisomers of Binol as a function of the pH with  $\gamma$ -CD (pH range: 10–11.5). The R enantiomer of Binol migrated first at pH 10, and the second elution occurred at pH 11.5. We proposed two hypotheses for the origin of this inversion.

The first hypothesis involved the progressive ionization of  $\gamma$ -CD ( $\text{p}K_a$  of  $\gamma$ -CD is equal to 12.08) [17]. At pH 10,  $\gamma$ -CD is neutral and therefore is carried by the cathodic electroosmotic flow. Consequently, the enantiomer with the higher affinity for the hydrophobic cavity of the CD migrates firstly (R enantiomer of Binol), since the two enantiomers migrate towards the anode at this pH ( $\text{p}K_{a1}$  Binol = 9.04 and  $\text{p}K_{a2}$  Binol = 10.90). However, at pH 11.5, the  $\gamma$ -CD is slightly ionized (charge  $\ll -1/2$ ). Thus, under such conditions, it presents an electrophoretic mobility slightly diametrically opposed to that of the electroosmotic flow, and consequently slows down the migration of the enantiomer with the greatest affinity, i.e., the R enantiomer.

The second hypothesis was based upon the conclusions of the works of Vigh and co-workers [8–10], who modeled the enantiomeric separation of chiral weak acids and bases in CE. They showed that based on

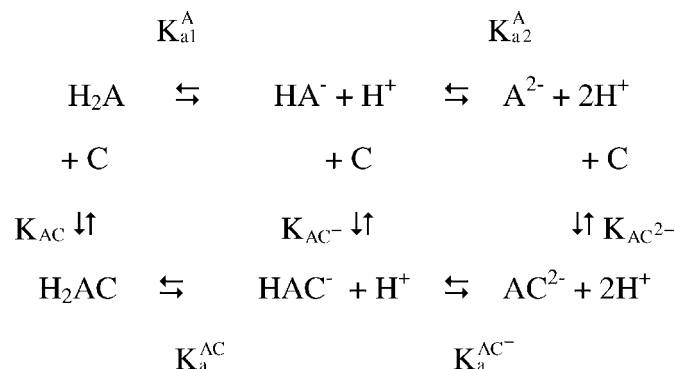
- the electrophoretic mobilities of the dissociated analytes/CD complexes ( $\mu_{\text{RCD}}^-$  and  $\mu_{\text{SCD}}^-$ ),
- the complex formation constants of the analytes in the dissociated and non-dissociated forms with the CD ( $K_{\text{RCD}}^-$ ,  $K_{\text{SCD}}^-$  and  $K_{\text{HRCD}}$ ,  $K_{\text{HSCD}}$ ),

- there are three kinds of separation. One works as a function of the pH, one based on the CD concentration, and one is systematically neutral. The three kinds are:
  - desionoselective separation or Type I ( $\mu_{\text{RCD}}^- = \mu_{\text{SCD}}^-$ ,  $K_{\text{RCD}}^- = K_{\text{SCD}}^-$  and  $K_{\text{HRCD}} \neq K_{\text{HSCD}}$ ),
  - ionoselective separation or Type II ( $\mu_{\text{RCD}}^- \neq \mu_{\text{SCD}}^-$ ,  $K_{\text{RCD}}^- \neq K_{\text{SCD}}^-$  and  $K_{\text{HRCD}} = K_{\text{HSCD}}$ ),
  - duoselective separation or Type III ( $\mu_{\text{RCD}}^- \neq \mu_{\text{SCD}}^-$ ,  $K_{\text{RCD}}^- \neq K_{\text{SCD}}^-$  and  $K_{\text{HRCD}} = K_{\text{HSCD}}$ ).

The last two allow for, if so desired, the reversal of the migration order of the enantiomers as a function of the electrolyte composition (pH, CD concentration).

Therefore, the origin of the reversal migration order of the Binol enantiomers as a function of the pH in presence of  $\gamma$ -CD is more likely to act according to the behavior of Type II or III than in the progressive ionization of  $\gamma$ -CD. In fact, the last option is unlikely even at pH 11.5, because the absolute value of its electrophoretic mobility is likely small in comparison to the electroosmotic flow.

However, the case of binaphthol and BN2 proves to be more complicated because they are diacids. Thus, all of the equilibria reported below that are based on acid–base equilibrium must be taken into account.



where  $K_{a1}^A$  and  $K_{a2}^A$  are the first and the second acidity constants of the diacid  $\text{H}_2\text{A}$  (or A);  $K_a^{AC}$  and  $K_a^{AC^-}$  are the acidity constants of the formed complexes  $\text{H}_2\text{AC}$  and  $\text{HAC}^-$ , respectively; and  $K_{AC}$ ,  $K_{AC^-}$  and  $K_{AC^{2-}}$  are the complexation formation constants of  $\text{H}_2\text{A}$  in its non-ionized, ionized and doubly ionized forms, respectively.

Not all of the data necessary to model the electrophoretic behavior of the enantiomers as a function of the pH and the cyclodextrin concentration was accessible experimentally. Thus, we decided to simplify the model by using an apparent equilibrium and apparent constants, as proposed by Lelièvre and Gareil [18], in the case of the monoacids, as an alternative approach to that of Vigh and co-workers [8–10].

If A' and AC' represent the analyte and the complex, respectively, in their ionized and non-ionized forms, then [A'] is the total concentration of the analyte and its related species, and [AC'] is the total concentration of the complex and its related species, so that

$$[A'] = [A] + [A^-] + [A^{2-}], \quad [AC'] = [\text{H}_2\text{AC}] + [\text{HAC}^-] + [\text{AC}^{2-}] \quad (1)$$

Then, as in the case of monoacids [18], the whole system can be described by an apparent equilibrium and an apparent equilibrium constant  $K'$ :

$$A' + C \rightleftharpoons AC', \quad K = \frac{[AC']}{[A'][C]} \quad (2)$$

with

$$\begin{aligned}
 K' &= K_{AC} \frac{[H^+]^2 + [H^+]K_a^{AC} + K_a^{AC}K_a^{AC-}}{[H^+]^2 + [H^+]K_{a1}^A + K_{a1}^AK_{a2}^A} \\
 &= K_{AC} \frac{K_{a1}^AK_{a2}^A}{K_a^{AC}} \frac{[H^+]^2 + [H^+]K_a^{AC} + K_a^{AC}K_a^{AC-}}{[H^+]^2 + [H^+]K_{a1}^A + K_{a1}^AK_{a2}^A} \\
 &= K_{AC} \frac{K_{a1}^AK_{a2}^A}{K_a^{AC}K_a^{AC-}} \frac{[H^+]^2 + [H^+]K_a^{AC} + K_a^{AC}K_a^{AC-}}{[H^+]^2 + [H^+]K_{a1}^A + K_{a1}^AK_{a2}^A} \quad (3)
 \end{aligned}$$

If all of equilibriums are fast, then  $\mu_A$ , the mobility of  $H_2A$  (or A), is a linear combination of its mobility in the free solution ( $\mu_A$ ) and its mobility when it is totally complexed ( $\mu_C$ ):

$$\begin{aligned}
 \mu_A &= \frac{[A']}{[A'] + [AC']} \mu_f + \frac{[AC']}{[A'] + [AC']} \mu_C \\
 \mu_f &= \frac{[H^+]^2}{[H^+]^2 + [H^+]K_{a1}^A + K_{a1}^AK_{a2}^A} \mu_A \\
 &+ \frac{[H^+]K_{a1}^A}{[H^+]^2 + [H^+]K_{a1}^A + K_{a1}^AK_{a2}^A} \mu_{A^-} \\
 &+ \frac{K_{a1}^AK_{a2}^A}{[H^+]^2 + [H^+]K_{a1}^A + K_{a1}^AK_{a2}^A} \mu_{A^{2-}} \quad (4) \\
 \mu_C &= \frac{[H^+]^2}{[H^+]^2 + [H^+]K_a^{AC} + K_a^{AC}K_a^{AC-}} \mu_{AC} \\
 &+ \frac{[H^+]K_a^{AC}}{[H^+]^2 + [H^+]K_a^{AC} + K_a^{AC}K_a^{AC-}} \mu_{AC^-} \\
 &+ \frac{K_a^{AC}K_a^{AC-}}{[H^+]^2 + [H^+]K_a^{AC} + K_a^{AC}K_a^{AC-}} \mu_{AC^{2-}}
 \end{aligned}$$

where  $\mu_{A^-}$ ,  $\mu_{A^{2-}}$ ,  $\mu_{AC}$ ,  $\mu_{AC^-}$  and  $\mu_{AC^{2-}}$  are the absolute mobilities of  $HA^-$ ,  $A^{2-}$ ,  $H_2AC$ ,  $HAC^-$  and  $AC^{2-}$ , respectively.

The first term in the equation that defines  $\mu_f$  is systematically null, because the acid compounds present a null electrophoretic mobility in ion suppression.

Therefore, the mobility of  $H_2A$  (or A) can be expressed as a function of the apparent equilibrium constant and the ligand concentration, which is the same equation in the case of a monoacid, but with a different constant:

$$\mu_A = \frac{1}{1 + K'[C]} \mu_f + \frac{K'[C]}{1 + K'[C]} \mu_C \quad (5)$$

If A is a racemic mixture, then the mobility of each enantiomer (S or R) can be described using:

$$\mu_S = \frac{\mu_f + \mu_{SC}K'_S[C]}{1 + K'_S[C]}, \quad \mu_R = \frac{\mu_f + \mu_{RC}K'_R[C]}{1 + K'_R[C]} \quad (6)$$

where  $\mu_S$  and  $\mu_R$  are the mobility of the S and R enantiomers, respectively;  $\mu_f$  is the mobility of the free enantiomer;  $\mu_{SC}$  and  $\mu_{RC}$  are the mobilities of the complexed S and R enantiomers, respectively;  $K'_S$  and  $K'_R$  are the apparent complexation constants between the S and R enantiomers, respectively, and the ligand; and [C] is the ligand concentration.

As a result, similar equations are obtained for both the monoacid and diacid, but with different apparent complexation constants. Moreover, the mobilities of the complexed S and R enantiomers are slightly different from each other due to the difference in their acidity constants, as can be observed from Eq. (4).

For the determination of the apparent complexation constant, Eq. (6) can be used. Additionally, linear plotting (Eqs. (7)–(9)) can be obtained from these equations, which have been used in CE for the determination of binding constants. In fact, these

linear plotting equations are analogous to those that have been employed for spectroscopy, chromatography and calorimetry techniques. These three linear plotting equations are known as double reciprocals (Eq. (7)) with  $K'$  = intercept/slope, y-reciprocal (Eq. (8)) with  $K'$  = slope/intercept, and x-reciprocal (Eq. (9)) with  $K'$  = –slope:

$$\frac{1}{\mu_i - \mu_f} = \frac{1}{(\mu_C - \mu_f)K'} \frac{1}{[C]} + \frac{1}{\mu_C - \mu_f} \quad (7)$$

$$\frac{[C]}{\mu_i - \mu_f} = \frac{1}{\mu_C - \mu_f} [C] + \frac{1}{(\mu_C - \mu_f)K'} \quad (8)$$

$$\frac{\mu_i - \mu_f}{[C]} = -K'(\mu_i - \mu_f) + K'(\mu_C - \mu_f) \quad (9)$$

Armstrong et al. [19] compared these different equations for the estimation of the binding constants by CE for both achiral and chiral analytes. Bellini et al. [20] determined the apparent association constants of four model drugs with  $\beta$ -CD by CE and compared the results obtained by these three linear plotting methods. The great advantage of the non-linear curve fitting method (Eq. (6)) is the determination of  $\mu_f$  and  $\mu_C$  by fitting the experimental data to the equations, so we can compare  $\mu_f$  and its experimentally determined value when no chiral selector is present. Moreover, we do not need to measure  $\mu_C$  experimentally in order to determine the binding constant. In fact,  $\mu_C$  often cannot be accurately measured or even is impossible to be determined due to experimental limitations such as ligand solubility [21] or capillary wall binding by the ligand [22]. The non-linear curve fitting methods avoid these problems and disadvantages. Similarly, the linear methods (Eqs. (7)–(9)) are advantageous for systems where the mobility of the analyte–ligand complex is not known and cannot be adequately measured with a marker or at saturating concentrations of the ligand.

These four plotting methods were used to estimate the apparent complexation constants of binaphthols and cyclodextrins at pH 11.5. The advantage of working at this pH for the enantioseparation of Binols was previously reported [16].

The mobilities of the analytes were systematically corrected for the electrolytes' viscosity changes due to the varied CD concentration. Thus, the electrophoretic mobilities were multiplied by the ratio between the currents obtained with and without CD in the solution [23].

The  $pK_a$  of cyclodextrins is about (12.08–12.3) [24], thus the cyclodextrin can begin to be dissociated at pH 11.5 and could exist in ionized form. However, the ionization percentage is almost poor  $\approx 15\%$ , and as a first approximation, we hypothesized that this percentage does not influence the determination of the apparent complexation constant or complex mobility. This hypothesis was validated by the comparison between the calculated mobility of free Binol in the case of the various studied CDs using Eq. (6) and the experimental values measured without CD (see Table 2). In fact, a good agreement is observed between the experimental and calculated values, and therefore, at pH 11.5, the dissociation of CD was effectively considered to be negligible and not influencing the calculation.

As a result, the proposed model could be used for estimating the apparent complexation constants between binaphthols and cyclodextrins at pH 11.5.

### 3.2. Apparent complexation constants and complex mobilities

As was illustrated above with a mathematical approach, in the case of binaphthol, the mobilities of the S- and R-complexed enantiomers are different from each other. Fig. 1a reports the theoretical evolution of the electrophoretic mobilities as a function of the  $\gamma$ -CD concentration for the R and S enantiomers of Binol. Table 3 contains the apparent complexation constants between these two

**Table 2**

Comparison between the experimental and calculated values of free Binol mobility in the case of various experimentations realized during the enantioseparation of Binol by means of various cyclodextrins at pH 11.5.

	$\mu_{\text{free,exp}} (\times 10^{-8} \text{ m}^2 \text{ V}^{-1} \text{ s}^{-1})$	Binol (S, R)	$\mu_{\text{free,cal}} (\times 10^{-8} \text{ m}^2 \text{ V}^{-1} \text{ s}^{-1})$
$\alpha$ -CD	-2.00	S	-2.00
		R	-2.01
$\beta$ -CD	-2.00	S	-2.02
		R	-2.02
$\gamma$ -CD	-2.01	S	-2.01
		R	-2.02
HP- $\alpha$ -CD	-2.03	S	-2.02
		R	-2.02
HP- $\beta$ -CD	-2.09	S	-2.10
		R	-2.11
HP- $\gamma$ -CD	-2.13	S	-2.12
		R	-2.13
TM- $\beta$ -CD	-2.12	S	-2.13
		R	-2.13

$\mu_{\text{free,exp}}$ : experimental value and  $\mu_{\text{free,cal}}$ : calculated value using (Eq. (6)).

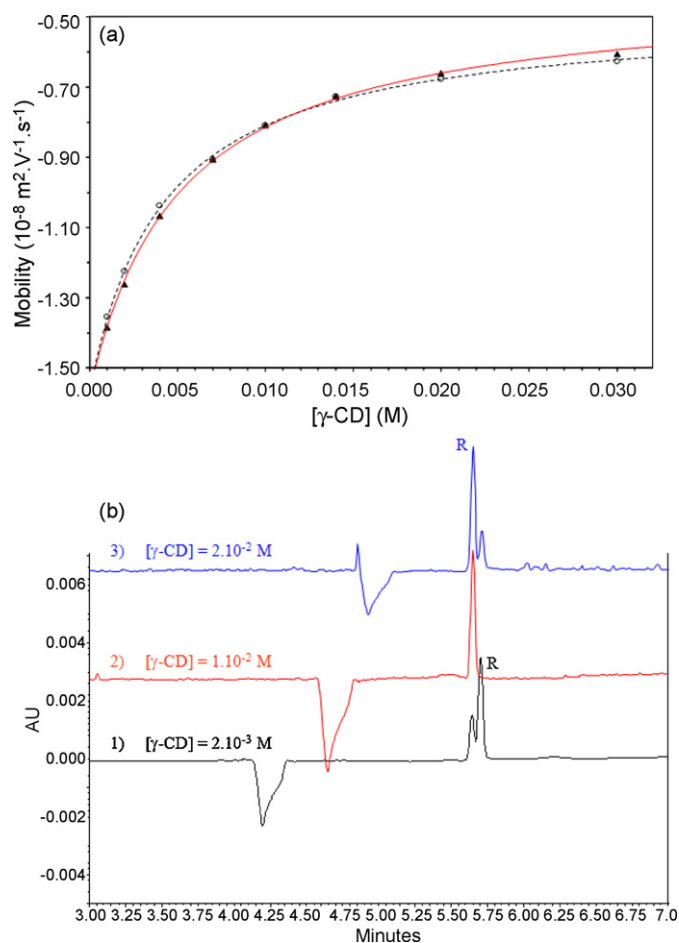


**Fig. 1.** (a) Variations of the electrophoretic mobility of Binol enantiomers as a function of  $\gamma$ -CD concentration. Curves identification: ( $\blacktriangle$ ) experimental points and continuous line for R-Binol; ( $\circ$ ) experimental points and dashed line for S-Binol. (b) Enantioseparation of Binol enantiomers with different concentrations of  $\gamma$ -CD. Experimental conditions: uncoated silica capillary (30 (40.2) cm  $\times$  50  $\mu\text{m}$  ID); hydrodynamic injection: 3 s at 0.5 psi;  $T = 20^\circ \text{C}$ ;  $\lambda = 214 \text{ nm}$ ; voltage: 10 kV; electrolyte:  $\text{Na}_2\text{HPO}_4/\text{Na}_3\text{PO}_4$ ; pH 10.8; ionic strength:  $8 \times 10^{-2} \text{ M}$ ; [ $\gamma$ -CD]: variable; sample: Binol racemate spiked with the R enantiomer.

**Table 3**

The apparent complexation constants, and the complex mobilities  $\mu_{\text{SC}}$ ,  $\mu_{\text{RC}}$  between the S, R enantiomers of Binol and  $\gamma$ -CD at pH 10.8.

$K'_S (\text{M}^{-1})$	235
$\mu_{\text{SC}} (\times 10^{-8} \text{ m}^2 \text{ V}^{-1} \text{ s}^{-1})$	-0.49
$R^2$	0.9996
$K'_R (\text{M}^{-1})$	194
$\mu_{\text{RC}} (10^{-8} \text{ m}^2 \text{ V}^{-1} \text{ s}^{-1})$	-0.43
$R^2$	0.9996

enantiomers and  $\gamma$ -CD and the complex mobilities deduced from the theoretical approach and the correlation coefficients.

It should be noted that these correlation coefficients are good. Through examination of Table 3, we find that the apparent complexation constants between the two enantiomers and  $\gamma$ -CD are different ( $235 \text{ M}^{-1}$  for the S enantiomer against only  $194 \text{ M}^{-1}$  in the case of the R enantiomer), and the electrophoretic mobilities of the formed complexes are also slightly different. In addition, the absolute values of the electrophoretic mobilities of the S-Binol/ $\gamma$ -CD complex are higher than that of the R-Binol/ $\gamma$ -CD complex. In fact, the electrophoretic mobilities of these two complexes, as they are deduced from the theoretical treatment, are equal to  $-0.49 \times 10^{-8}$  and  $-0.43 \times 10^{-8} \text{ m}^2 \text{ V}^{-1} \text{ s}^{-1}$ , respectively. This difference in the apparent complexation constants for the Binol enantiomers as well as the difference in the mobilities of the Binol/ $\gamma$ -CD complexes ( $K'_S > K'_R$  and  $\mu_{\text{SC}} > \mu_{\text{RC}}$ ) rationalize the inversion observed experimentally and shown in Fig. 1b.

The apparent complexation constants calculated between the two Binol enantiomers and  $\gamma$ -CD ( $K'_S = 235 \text{ M}^{-1}$  and  $K'_R = 194 \text{ M}^{-1}$ ) are similar to those reported by Zerbinati and Trotta [25] for the same enantiomers and the same cyclodextrin ( $272 \text{ M}^{-1}$  for the S enantiomer and  $246 \text{ M}^{-1}$  for the R enantiomer). In fact, the constants that we deduced have the same magnitude reported by these authors, and the interactions of the S enantiomer with the hydrophobic cavity of  $\gamma$ -CD are more favorable in the two cases. On the other hand, the  $K'_S/K'_R$  ratio, and thus the thermodynamic selectivity, is higher in our case than in the study of Zerbinati and Trotta (1.22 versus 1.11). However, the approach used by these authors is critical since they deduced their different values by applying the model of Wren and Rowe [3–6], meaning without taking into account the incomplete dissociation of binaphthol.

Table 4 shows some examples of the complex mobility of various binaphthol (S,R)/CD couples calculated using Eq. (6) and for which no inversion in the enantiomer migration order was observed as a function of the cyclodextrin concentration.

Such an observation could be attributed to an insufficient difference of the electrophoretic mobilities of the S- and R-formed complexes together with the magnitudes of the apparent com-

**Table 4**

Calculated mobilities of the formed complexes in the case of various BN/CD couples at pH 11.5 using Eq. (6).

Binols	CD	$\mu_{\text{c,cal}} (\times 10^{-8} \text{ m}^2 \text{ V}^{-1} \text{ s}^{-1})$
Binol (S)	$\alpha$ -CD	-0.37
Binol (R)		-0.39
BN2 (1)	HP- $\gamma$ -CD	-0.45
BN2 (2)		-0.44
BN3 (1)	$\gamma$ -CD	-0.38
BN3 (2)		-0.34
BN4 (1)	HP- $\alpha$ -CD	-0.46
BN4 (2)		-0.43
BN5 (1)	$\beta$ -CD	-0.34
BN5 (2)		-0.32

(1) and (2) corresponding to the first and second peaks of BN racemates.

**Table 5**

Apparent complexation constants of different binaphthols and cyclodextrins calculated at pH 11.5 by the four plotting methods: (X) *x*-reciprocal, (Y) *y*-reciprocal, (XY) double reciprocal and (XYZ) non-linear (*K'* in M<sup>-1</sup>).

	Binol		BN2 (S/R)		BN3 (S/R)		BN4		BN5	
	S	R	1	2	1	2	1	2	1	2
<b>α-CD</b>										
<i>K'</i> (X)	27	18	33		34		32	23	22	15
<i>K'</i> (Y)	27	20	33		34		31	23	22	15
<i>K'</i> (XY)	29	20	30		34		34	25	22	15
<i>K'</i> (XYZ)	25	23	32		25		23	15	22	20
	Binol		BN2		BN3		BN4		BN5	
	S	R	1	2	1	2	1	2	1	2
<b>β-CD</b>										
<i>K'</i> (X)	125	83	454	289	116	41	154	105	95	32
<i>K'</i> (Y)	129	85	447	299	114	41	155	106	92	33
<i>K'</i> (XY)	113	73	445	274	123	39	158	105	106	32
<i>K'</i> (XYZ)	150	106	450	319	90	48	145	108	75	41
	Binol		BN2 (S/R)		BN3		BN4		BN5	
	S	R	1	2	1	2	1	2	1	2
<b>γ-CD</b>										
<i>K'</i> (X)	118	75	639	564	171	145	145	97	63	39
<i>K'</i> (Y)	118	76	639	559	173	142	160	107	65	41
<i>K'</i> (XY)	121	75	652	581	178	154	134	89	60	36
<i>K'</i> (XYZ)	117	81	628	554	167	135	170	122	74	49
	Binol		BN2 (S/R)		BN3		BN4		BN5	
	S	R	1	2	1	2	1	2	1	2
<b>HP-α-CD</b>										
<i>K'</i> (X)	60	29	21		91	53	95	72	56	23
<i>K'</i> (Y)	60	29	21		91	53	93	69	55	23
<i>K'</i> (XY)	62	29	24		93	56	106	83	57	25
<i>K'</i> (XYZ)	56	25	17		86	57	79	49	51	21
	Binol		BN2 (S/R)		BN3		BN4		BN5	
	S	R	1	2	1	2	1	2	1	2
<b>HP-β-CD</b>										
<i>K'</i> (X)	264	159	344		195	125	443	268	219	113
<i>K'</i> (Y)	268	160	335		183	118	457	270	208	109
<i>K'</i> (XY)	263	160	340		204	135	439	266	234	128
<i>K'</i> (XYZ)	279	164	362		197	117	460	272	212	109
	Binol		BN2		BN3		BN4		BN5	
	S	R	1	2	1	2	1	2	1	2
<b>HP-γ-CD</b>										
<i>K'</i> (X)	91	52	607	476	109	90	122	71	34	14
<i>K'</i> (Y)	95	53	644	470	115	94	125	73	35	15
<i>K'</i> (XY)	93	51	598	473	103	84	124	72	34	14
<i>K'</i> (XYZ)	96	57	655	483	121	96	137	81	36	15
	Binol		BN2		BN3		BN4		BN5	
	S	R	1	2	1	2	1	2	1	2
<b>TM-β-CD</b>										
<i>K'</i> (X)	125	51	38	24	59	42	155	71	95	49
<i>K'</i> (Y)	128	51	40	24	60	42	158	70	94	48
<i>K'</i> (XY)	120	50	34	24	54	43	156	77	90	48
<i>K'</i> (XYZ)	135	55	51	17	65	38	163	66	92	44

plexation constants between the two enantiomers and the CD. In fact, the reported values of  $\Delta\mu_C$  in Table 4 are at most equal to  $0.04 \times 10^{-8} \text{ m}^2 \text{ V}^{-1} \text{ s}^{-1}$ , which must be closer to the calculated  $\Delta\mu_C$  value in the case of Binol and  $\gamma$ -CD ( $0.06 \times 10^{-8} \text{ m}^2 \text{ V}^{-1} \text{ s}^{-1}$ ). These results remain insufficient for such an inversion to be observed in the range of the experimentally explored concentration.

Table 5 shows the apparent complexation constant calculated for the various studied binaphthol/CD couples by the four plotting

methods (*x*-reciprocal, *y*-reciprocal, double reciprocal and non-linear).

A good linearization with all of the three plotting methods was observed with an average correlation coefficient of 0.997. Strong correlation coefficients were also observed for the non-linear method (average of 0.9991). As a result, a satisfactory agreement between the four methods was observed for all considered BN/CD couples.

In comparing the affinity between the different cyclodextrins and the binaphthols, with regard to the studied CDs, HP-β-CD has the highest affinity for the binaphthols, while α-CD has the lowest one. Moreover, we found that the derivative CDs have relatively stronger affinities for the binaphthols than the corresponding native ones, except for  $\gamma$ -CD, which globally developed stronger interactions than its homologue HP- $\gamma$ -CD derivative.

Finally, in the case of the Binol with the  $\gamma$ -CD, the effect of increasing the electrolyte pH by 0.7 units led to a decrease in the affinity of the two enantiomers for the hydrophobic cavity of the cyclodextrin, as we could expect, since the ionization degree is reinforced for the two partners.

### 3.3. Determination of ( $\Delta\mu_{S,Rmax}$ ) and the optimal concentration of cyclodextrin

The mobility difference between a pair of S and R enantiomers ( $\Delta\mu_{S,R}$ ) can be described from Eq. (6) in its most general form as

$$\Delta\mu_{S,R} = \frac{\mu_f + \mu_{RC}K'_R[C]}{1 + K'_R[C]} - \frac{\mu_f + \mu_{SC}K'_S[C]}{1 + K'_S[C]} \quad (10)$$

so ( $\Delta\mu_{S,R}$ ) depends not only on the apparent complexation constants of both of the S and R enantiomers with the chiral selector, but also on the electrophoretic mobility of each complex formed between the S and R enantiomers with the chiral selector and on the concentration of the chiral selector. Therefore, the optimal chiral selector concentration, which leads to a maximum electrophoretic

**Table 6**

Comparison between the theoretical optimal concentration of the cyclodextrin [ $C_{opt}cal$ ] calculated from (Eq. (12)) and the experimental optimal concentration of the cyclodextrin determined experimentally [ $C_{opt}exp$ ] at pH = 11.5 for various binaphthols and cyclodextrins (concentration in mM).

	Binol	BN2	BN3	BN4	BN5
<b>α-CD</b>					
[ $C_{opt}cal$ ]	56.2	–	–	25	26.3
[ $C_{opt}exp$ ]	20	–	–	20	20
<b>β-CD</b>					
[ $C_{opt}cal$ ]	3.9	1.4	6.7	5.2	12.6
[ $C_{opt}exp$ ]	10	1.2	8	4	10
<b>γ-CD</b>					
[ $C_{opt}cal$ ]	5	1.5	4.4	4.5	7.3
[ $C_{opt}exp$ ]	6	2	7.5	4	7
<b>HP-α-CD</b>					
[ $C_{opt}cal$ ]	14.8	–	9.3	14.6	17.4
[ $C_{opt}exp$ ]	15	–	10	10	15
<b>HP-β-CD</b>					
[ $C_{opt}cal$ ]	4.2	–	5.2	2.8	5.2
[ $C_{opt}exp$ ]	4.4	–	10	3.3	6
<b>HP-γ-CD</b>					
[ $C_{opt}cal$ ]	9.8	1.6	7.5	7.3	10.8
[ $C_{opt}exp$ ]	8	2	7.5	7.5	8
<b>TM-β-CD</b>					
[ $C_{opt}cal$ ]	9.9	30	13.6	8.3	9.7
[ $C_{opt}exp$ ]	10	25	15	7.5	10

mobility ( $\Delta\mu_{S,R\max}$ ) difference, can be achieved when

$$\frac{\partial\Delta\mu_{S,R}}{\partial C} = 0 \quad (11)$$

Wren and Rowe [3,4] simplified the determination of  $[C_{\text{opt}}]$  by assuming that  $\mu_{SC} = \mu_{RC} = \mu_C$ , and then  $[C^{\text{opt}}] = 1/\sqrt{K_S K_R}$ . In the case of the Binols and as it was illustrated above,  $\mu_{SC} \neq \mu_{RC}$ , so Wren–Rowe's model is not valid; therefore, a direct resolution of Eq. (11) must be used, which leads to a classic polynomial equation in the form of

$$a[C]^2 + b[C] + c \quad \text{with} \quad [C^{\text{opt}}] = \frac{-b + \sqrt{\Delta}}{2a} \quad (12)$$

where  $\Delta = b^2 - 4ac$ ,  $a = K'_S K'_R [K'_S(\mu_{RC} - \mu_f) - K'_R(\mu_{SC} - \mu_f)]$ ,  $b = 2K'_S K'_R(\mu_{RC} - \mu_{SC})$  and  $c = K'_R(\mu_{RC} - \mu_f) - K'_S(\mu_{SC} - \mu_f)$ .

Table 6 shows the comparison between the optimal concentration of the cyclodextrin  $[C_{\text{opt}}]_{\text{cal}}$  calculated with Eq. (12) and the optimal concentration of the cyclodextrin  $[C_{\text{opt}}]_{\text{exp}}$  determined experimentally by plotting ( $\Delta\mu_{S,R\text{exp}}$ ) as a function of the cyclodextrin concentration (0–20 or 25 mM).

We found a good agreement between the two concentrations. Moreover, by eliminating the  $[C_{\text{opt}}]_{\text{cal}}$  value corresponding to Bin1 and  $\alpha$ -CD outside of the studied concentration range, we obtained a 94% correlation between  $[C_{\text{opt}}]_{\text{cal}}$  and  $[C_{\text{opt}}]_{\text{exp}}$ .

As a result, the proposed model is perfectly adapted to describe the electrophoretic behavior of the enantioseparation of binaphthols by CD-CZE and to support the formed hypothesis that the weak electrophoretic mobilities of the various studied cyclodextrins could be negligible.

#### 4. Conclusion

With regard to these results, we conclude that the proposed theoretical model is well-suited to describe the electrophoretic behavior of the binaphthols in CD-CZE under the studied conditions (pH range from 10.8 to 11.5) and, consequently, to model the enantioseparation of binaphthols by means of CD-CZE.

The optimal cyclodextrin concentrations for the enantioseparation of binaphthols determined by this model are in strong agreement with the values deduced from experimental data. Moreover, the electrophoretic mobilities of the complexes formed

between the binaphthols and the various studied cyclodextrins played a significant role in the enantioseparation. This model can be applied to

- determine the optimal concentration of the chiral selector for the weak monoacid and diacid analytes, and
- the reversal of the enantiomer migration order as a function of the chiral selector concentration, using the apparent complexation constants and the complex mobilities.

#### Acknowledgements

This research was supported by the Scientific National Research Center (CNRS), ACI "Nouvelles technologies et capteurs". Dr H. Krajjian would like to thank the Atomic Energy Commission of Syria for the doctoral fellowship.

#### References

- [1] G. Gübitz, M.G. Schmid, *J. Chromatogr. A* 792 (1997) 179.
- [2] S. Fanali, *J. Chromatogr. A* 875 (2000) 89.
- [3] S.A.C. Wren, R.C. Rowe, *J. Chromatogr.* 603 (1992) 235.
- [4] S.A.C. Wren, R.C. Rowe, *J. Chromatogr.* 635 (1993) 113.
- [5] S.A.C. Wren, *J. Chromatogr.* 636 (1993) 57.
- [6] S.A.C. Wren, *Electrophoresis* 16 (1995) 2127.
- [7] C.E. Sanger-Van de Griend, K. Groningsson, T. Arvidsson, *J. Chromatogr. A* 782 (1997) 271.
- [8] Y.Y. Rawjee, D.U. Staerk, G. Vigh, *J. Chromatogr.* 635 (1993) 291.
- [9] Y.Y. Rawjee, R.L. Williams, G. Vigh, *J. Chromatogr. A* 652 (1993) 233.
- [10] Y.Y. Rawjee, R.L. Williams, G. Vigh, *J. Chromatogr. A* 680 (1994) 599.
- [11] B.A. Williams, G. Vigh, *J. Chromatogr. A* 777 (1997) 295.
- [12] X. Zhu, Y. Ding, B. Lin, A. Jakob, B. Koppenhoefer, *J. Chromatogr. A* 888 (2000) 241.
- [13] S. Surapaneni, K. Ruterbories, T. Lindstrom, *J. Chromatogr. A* 761 (1997) 249.
- [14] F. Lelievre, P. Gareil, Y. Bahaddi, H. Galons, *Anal. Chem.* 69 (1997) 393.
- [15] J.M. Brunel, *Chem. Rev.* 105 (2005) 857.
- [16] N. Mofaddel, H. Krajjian, D. Villemin, P.L. Desbene, *J. Chromatogr. A* 1211 (2008) 142.
- [17] S. Li, W.C. Purdy, *Chem. Rev.* 92 (1992) 1457.
- [18] F. Lelievre, P. Gareil, *Anal. Chem.* 69 (1997) 385.
- [19] K.L. Rundlett, D.W. Armstrong, *J. Chromatogr. A* 721 (1996) 173.
- [20] M.S. Bellini, Z. Deyl, G. Manetto, M. Kohlickova, *J. Chromatogr. A* 924 (2001) 483.
- [21] A. Shibukawa, D.K. Lloyd, I.W. Wainer, *Chromatographia* 35 (1993) 419.
- [22] K.L. Rundlett, D.W. Armstrong, *Anal. Chem.* 67 (1995) 2088.
- [23] R. Vespalec, P. Boek, *J. Chromatogr. A* 875 (2000) 431.
- [24] B. Chankvetadze, *Capillary Electrophoresis in Chiral Analysis*, Wiley, Chichester, 1997, p. 428 (Ch. 12).
- [25] O. Zerbinati, F. Trotta, *Electrophoresis* 22 (2001) 3578.



## Testing of the Region of Murcia soils by near infrared diffuse reflectance spectroscopy and chemometrics

Javier Moros<sup>a</sup>, María José Martínez-Sánchez<sup>b</sup>, Carmen Pérez-Sirvent<sup>b</sup>, Salvador Garrigues<sup>a</sup>, Miguel de la Guardia<sup>a,\*</sup>

<sup>a</sup> Department of Analytical Chemistry, University of Valencia, 50 Dr. Moliner Street, 46100 Burjassot, Valencia, Spain

<sup>b</sup> Department of Agricultural Chemistry, Geology and Pedology, Faculty of Chemistry, University of Murcia, E-30071 Murcia, Spain

### ARTICLE INFO

#### Article history:

Received 1 September 2008

Received in revised form

18 November 2008

Accepted 20 November 2008

Available online 3 December 2008

#### Keywords:

Partial least squares

Near infrared

Diffuse reflectance

Soils

Hierarchical cluster analysis

### ABSTRACT

A partial least squares near infrared (PLS-NIR) method has been developed for the determination of several physicochemical parameters in soils from different locations of the Region of Murcia. The method was based on the proper chemometric treatment of diffuse reflectance spectra of soil samples. Reflectance spectra were scanned from samples stored in glass vials in the NIR region between 800 and 2600 nm, averaging 36 scans per spectrum at a resolution of 8 cm<sup>-1</sup>. Models were built using reference data of 39 samples selected from a dendrogram obtained after hierarchical cluster analysis of NIR spectra of soils and prediction parameters were established from a validation set of 109 additional samples of the same area not considered to build the model. Organic matter, CaCO<sub>3</sub>, pH, electrical conductivity (EC), together with several trace metals as Cr, Co, Ni, Cu, Zn, As, Se, Cd and Tl, were employed as characteristic parameters of the soils under study, and found results evidenced that PLS-NIR provides a valuable tool for screening purposes providing residual predictive deviations which ranged from 0.9 to 1.5 as a function of the considered parameter.

© 2008 Elsevier B.V. All rights reserved.

### 1. Introduction

Soils are multi-functional media with a fundamental role in the environment. Soils are porous matrices, in which air, water and biota occur together and forming an essential part of the landscape, preserving the memories of our past and being themselves a relevant part of our cultural heritage [1].

Unfortunately, soil resources are being irreversibly lost and degraded at an unprecedented rate as a result of increasing and often conflicting demands coming from nearly all economic sectors, including agriculture, industry, construction, tourism and transport. This is the particular case of the Region of Murcia (South-East Spain) with an important agricultural activity for centuries and where the early detection and possible remediation of desertification processes is a main concern.

Resilience and capability of soils to filter and absorb contaminants imply that damages cannot be perceived till an advanced stage, being thus an important reason for the monitoring of soils. Nowadays, after many years of misuse, the signs and the impacts of human activities can be clearly evidenced and responses both, corrective and preventive are required, looking

to avoid the transference of soil damage to future generations [2].

Soil testing is the series of analysis of a soil sample made to determine nutrient content, composition and other characteristics, including contaminants. This analysis can provide useful information in the context of sustainable development in order to protect the soil against multiple hazards, among them contamination, particularly that from human actions [3].

The terms soil quality and soil health are often interchangeably used to describe the ability of soil to support several activities as crop growth without becoming degraded or otherwise harming the environment [4]. Soil quality can be evaluated from some particular biological, chemical and physical properties, which are defined with specific units of measure, being also possible to evaluate the aforementioned properties against some common standards or analyzed for improvements over time [5].

Organic matter is an essential fraction of the soil composed of anything that was once alive, which includes plant and animal remains in various stages of decomposition, cells and tissues of soil organisms, and other organic substances [6]. The importance of soil organic matter is due to its impact on other biological, chemical and physical indicators of soil quality [7]. Soil pH is a measure of the acidity or alkalinity of the soil, depends on the rock from which the soil was formed (parent material) and climate, vegetation, topography and time that acted on it [8]. In short, it is a master

\* Corresponding author. Tel.: +34 96 354 4838; fax: +34 96 354 4838.

E-mail address: [miguel.delaguardia@uv.es](mailto:miguel.delaguardia@uv.es) (M. de la Guardia).



**Table 1**

State-of-the-art of published works related to the characterization of soil and sediment samples using NIR spectroscopy.

Sample	Determined properties <sup>a</sup>	Chemometric technique	Spectral range (nm)	Total number of samples	Concentration ranges	Validation procedure	Prediction figures of merit	Ref.
Freshwater sediment	Zn, Cu, Ni and Cd	Partial Least Squares Regression (PLS)	1100–2500	169	Cd 0.011–2.49 µg/g Cu 1–48 µg/g Ni 2–27 µg/g Zn 10–65 µg/g	Odd-numbered spectra as calibration set and even-numbered spectra as prediction set	Cd RPD = 1.74 Cu RPD = 3.35 Ni RPD = 2.96 Zn RPD = 3.80	[20]
Soils from different locations across Uruguay	Cu	Modified PLS (MPLS)	400–2500 (Vis-NIR)	332	Cu 0.6–31.3 µg/g	Cross-validation	RPD = 2	[21]
Soil from a metal mining region	Zn, Cd, Cu and Ni	PLS	400–2500 2500–25000 (MIR)	70	Cd 1–36 µg/g Cu 1–78 µg/g Ni 1–78 µg/g Zn 1–4800 µg/g	Cross-validation	Cd <sup>b</sup> NRMSE = 0.92 Cu NRMSE = 0.49 Ni NRMSE = 0.29 Zn NRMSE = 0.84	[22]
Polluted soils	As, Cu and Zn	MPLS	400–2500	100	As 16.3–225.4 µg/g Cu 19.4–483.8 µg/g Zn 70.5–2112.3 µg/g	70 samples for calibration and 30 for an external validation	As RPD = 2.25 Cu RPD = 1.59 Zn RPD = 1.96	[23]
Forest soil organic horizons	Zn	MPLS	400–2500	74	40–4601 µg/g	Group cross-validation	RPD = 1.1	[24]
Soils	Ni, Cr, Co and Cd	PLS	400–2500	–	–	–	–	[25]
Soils	–	PLS	400–2500	200	–	Cross-validation	–	[26]
Soils	pH and organic matter	Classification and regression trees	400–2460	273	Organic matter 0–82% pH 3.33–7.21 units	Calibration using 67% of the data; validation performed using the remaining data (33%)	Organic matter RPD = 5.89 pH RPD = 2.39	[27]
Soils	–	MPLS	400–2500	127–175	–	–	–	[28]
Lake sediments	pH	PLS	400–2500	52	4.6–8.4	Internal cross-validation	pH RMSEP = 0.4	[29]
Soil from all regions of Denmark	–	PLS	400–2500	32–471	–	Cross-validation	–	[30]
Agricultural soils	–	PLS	350–2500	122	–	Calibration using 3/4 of the data; validation performed using the remaining data 1/4	–	[31]
Soils from four major land resource areas	pH, Cu and Zn	PCR	1300–2500	Cu n = 761 Zn n = 762 pH (H <sub>2</sub> O) n = 743 pH (CaCl <sub>2</sub> ) n = 743	Cu 0.3–130.6 µg/g Zn 0.1–373.3 µg/g pH (H <sub>2</sub> O) 3.9–8.5 units pH (CaCl <sub>2</sub> ) 3.5–8.0 units	Cross-validation	Cu RPD = 0.92 Zn RPD = 1.07 pH (H <sub>2</sub> O) RPD = 1.43 pH (CaCl <sub>2</sub> ) RPD = 1.47	[32]
Soils	Organic matter and pH	PCA-PLS	350–2500	165	Organic matter 1.05–1.65% pH 6.42–7.05 units	135 samples for calibration and 30 samples for validation	Organic matter RMSEP = 0.13% pH RMSEP = 0.09 units	[33]
Soils	Organic matter	PLS	400–2500	125	1.06–1.65%	95 samples for calibration and 30 samples for prediction	RMSEP = 0.13%	[34]
Soils	pH, electrical conductivity (EC)	PCR	250–2500	161	–	–	–	[35]
Soils	–	PLS	NIR	108	–	Randomly 30% samples for validation and the rest for calibration	–	[36]
Soils	Organic matter	Radial basis function networks (RBFN)	1000–2500	200	0.40–4.88%	140 samples for calibration and 60 samples for validation	RMSEP = 0.25%	[37]
Sediments	pH, As, Cd and Cr	PLS	833–2976	81	pH 7.41–8.48 units As 15.0–43.3 µg/g Cd 0.13–0.97 µg/g Cr 41.5–365 µg/g	31 samples for calibration and 50 samples for validation	pH RPD = 1.46 As RPD = 1.4 Cd RPD = 1.3 Cr RPD = 1.6	[38]

<sup>a</sup> Only physicochemical properties evaluated, in the cited reference, which are in concordance with those evaluated in the present study are reported.<sup>b</sup> NRMSE means ratio between normalized root mean squared deviation and mean content of each parameter.

variable that together with organic matter controls the speciation and bioavailability of metals [9].

Toxic metals, which are among the most widespread pollutants of the biosphere, are also an important soil quality parameters [9] due to their persistence and because soils with elevated levels of toxic metals exhibit negative effects on human health.

Calcium carbonate (also known as lime) is also an important parameter for measuring in soils as it dominates the problems related to agricultural land use. Calcium carbonate accumulation is a major influence in semiarid soil development as it accumulates over time in soils and systematic morphological changes occur affecting the way water infiltrates the soil profile [10].

The electrical conductivity (EC) evidences the ability of soil to conduct electrical current. EC estimates the soil salinity or the total amount of dissolved ions in the water and is the most useful and easily obtained spatial property of soil that influences crop productivity. The EC value can be considered a combination of physical and chemical properties of soils [11].

The soil quality assessment requires the analysis of many parameters in a great number of samples; but no official quantitative methods to determine soil quality are available at the present time. This absence of methodologies to evaluate soil health is in part associated with a lack of understanding of the soil ecological processes in sustaining plant growth and environmental quality [12]. So it implies the use of different conventional methods, generally based on the use of selective electrodes for pH [13], electrical resistivity, electromagnetic induction or coulter-based sensors for EC [14] measurements, loss-of-ignition and gravimetric methods for organic matter [15] gasometric and volumetric methods for calcium carbonate [16,17] as well as methods commonly involving wet digestion of solid samples in hot concentrated acids followed by inductively coupled plasma (ICP) or atomic absorption spectrometry (AAS) for trace metal determination [18,19].

In general, all the aforementioned methods are expensive, tedious, complex and highly time-consuming. For this reason a fast, cheap and accurate alternative is always welcoming. In contrast, near infrared (NIR) spectroscopy combined with the appropriate mathematical treatment can provide unique tools for the direct and simultaneous determination of many parameters in solid samples based on the treatment of well characterized samples and the deep evaluation of the prediction capabilities of built models.

On considering all the aforementioned advantages, there are several references in the literature related to the determination of soil parameters using fast non-destructive procedures.

After a bibliographic search, focused on applications of reflectance measurements to determine quality indicators of soils [21–28,30–37] or sediments [20,29,38] NIR measurements (see Table 1), it can be appreciated that for the determination of some biological, chemical and physical parameters it has been used the region compressed between 400 and 2500 nm, which belongs to visible plus near-infrared regions, combined with several multivariate approaches, such as partial least squares (PLS) [20,22,25,26,29–31,33,34,36,38], modified partial least squares (MPLS) [21,23,24,28], classification and regression trees [27], principal component regression (PCR) [32,35] and radial basis function networks (RBFN) [37].

However, one of the main drawbacks in the revised literature concerning this kind of studies is the wide employment of cross-validation strategy for evaluating obtained results. This procedure not permits to ascertain whether predicted values from the model are likely to accurately predict responses on future samples or samples not used to develop the model as it uses for prediction the same data used for fitting the model.

Through the present work, the development of a fast, accurate and reagent free analytical method useful for testing soils

from the Region of Murcia employing diffuse reflectance NIR spectroscopy measurements and multivariate calibration has been persecuted.

## 2. Experimental

### 2.1. Apparatus and reagents

A Fourier transform near infrared (FT-NIR) spectrometer Bruker model Multipurpose Analyzer (MPA) equipped with an integrating sphere, used as measurement accessory, and controlled by OPUS® for Windows® software from Bruker GmbH (Bremen, Germany), was employed for diffuse reflectance near infrared spectra acquisition.

For instrumental and measurement control, as well as for spectra acquisition and data manipulation and treatment, it was employed the OPUS program (Version 4.2) from Bruker. PLS calibration models were also established using the aforementioned program.

For locating the soil sampling points a Global Positioning System (GPS) *GeoExplorer*® 3, a Handheld GPS mapping and GIS (Geographic Information System) data collection/maintenance system, was used.

### 2.2. Site description, soil sampling and reference procedures

The field chosen for this study is located across Murcia region (South-East Spain) (Fig. 1). A total number of 148 soil samples, collected from 18 different locations were used for the present study.

Soil samples were taken with a spade from the surface to a depth of 10 cm. The samples were transported to the laboratory on the same day, where they were dried (35 °C) and sieved (2 mm) before analysis of physicochemical parameters, such as organic matter, CaCO<sub>3</sub>, pH, electric conductivity and trace metal content. Before the NIR analysis, the dried and sieved samples were ground with mortar and pestle.

Soils were grinded using a mixer mill model MM 200 from RETSCH GmbH (Haan, Germany) and split in fractions through a sieving test to separate the fraction with particle size lower than 45 µm and stored in plastic containers. Both, chemistries and diffuse reflectance NIR spectra scanning were directly done on this last fraction.

To obtain the reference data of samples the following methods were used.

Organic matter was determined by sulfochromic oxidation [38], according to the NF X 31-109 standard [39], while CaCO<sub>3</sub> content of soil samples was determined by volumetric method using a Bernard calcimeter previously calibrated against Na<sub>2</sub>CO<sub>3</sub> [40] being found a variability range from 0.04% to 6.93% (w/w) and from 3.3% to 75.2% (w/w), respectively.

Physical parameters like pH (H<sub>2</sub>O) and pH (KCl) (pH at a specified soil KCl ratio) ranged from 7.60 to 8.63 and between 6.7 and 8.2, respectively; as well as electric conductivity (EC), which varied from 0.04 to 23 dS/m, were also experimentally measured in the soil samples.

The pH was determined in a 1:5 suspension of soil in Milli-Q quality water and in a 1 M KCl solution [41] using a Crison GLP21 pH meter. Electrical conductivity (EC) (dS m<sup>-1</sup> at 25 °C) was measured using a Crison GLP31 meter in the extracts obtained by filtering the 1:5 suspensions through a 0.45 µm cellulose acetate disk filter.

Trace element data concentrations were experimentally determined in soil samples, by using reference procedures based on electrothermal atomic absorption spectrometry. Soil samples used in the present study contain from 5 to 197 µg g<sup>-1</sup> Cr, between 2 and 28 µg g<sup>-1</sup> Co, between 4 and 74 µg g<sup>-1</sup> Ni, from 2 to 93 µg g<sup>-1</sup> Cu, from 10 to 188 µg g<sup>-1</sup> Zn, between 0.3 and 64 µg g<sup>-1</sup> As, between

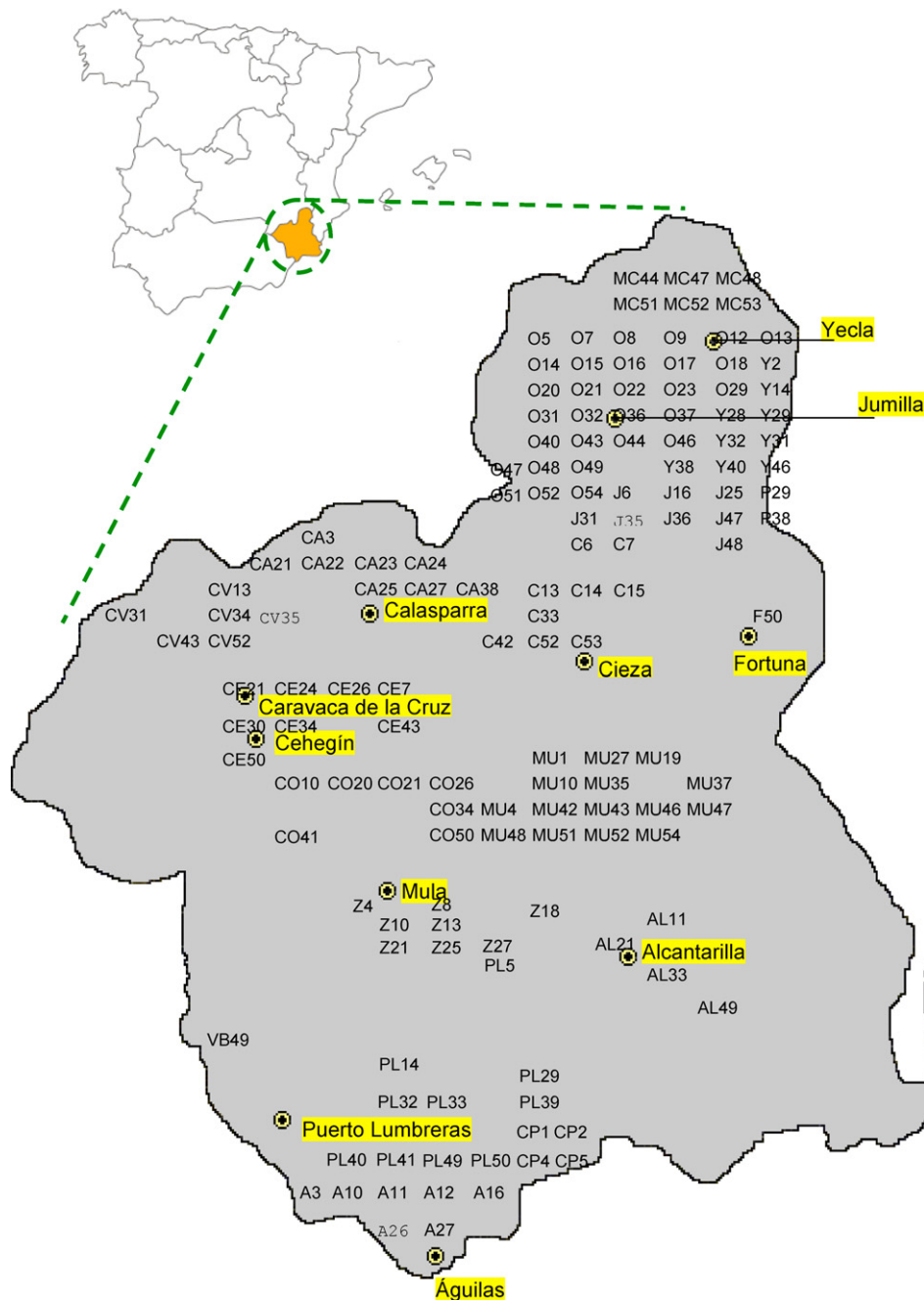


Fig. 1. Sampling soil locations in the Region of Murcia.

0.003 and  $0.8 \mu\text{g g}^{-1}$  Se, between 0.016 and  $0.8 \mu\text{g g}^{-1}$  Cd and between 0.10 and  $1.3 \mu\text{g g}^{-1}$  Tl, ranging from high concentrations in the part of the region with an important industrial activity, to natural background levels.

### 2.3. Diffuse reflectance NIR spectroscopy analysis

Samples were located in the same temperature controlled room where the spectrometer was placed before to carry out their analysis.

Diffuse reflectance near infrared spectra for each sample were obtained in Kubelka–Munk units, by triplicate, directly from the samples inside wheat on polyethylene terephthalate (PET) liquid scintillation glass vials (21 mm  $\times$  59 mm) of 20 ml volume used as measurement cell. Taking into consideration previously reported

works made on estuarine sediment samples [42,43], sample spectra were scanned from 800 to 2600 nm ( $12,500\text{--}3846 \text{ cm}^{-1}$ ) by averaging 36 scans per spectrum using a nominal resolution of  $8 \text{ cm}^{-1}$ , as instrumental conditions, which take a measurement time of 16.8 s per spectrum.

The background spectrum was acquired from the integrating sphere under the same instrumental conditions than those employed for soil sample measurement.

### 2.4. Chemometric data treatment

To evaluate possible classes among soil samples under study, hierarchical cluster analysis of their diffuse reflectance NIR spectra was made using OPUS program (Version 4.2) from Bruker. As already stated in previous works [43,44] similar criteria, as those

already used for other types of samples, were employed through this work.

We selected a dendrogram classification using Euclidean distance to compute the similarity between all pairs of samples to be clustered with Ward linkage as algorithm for hierarchical clustering upon considering the frequency range between 850 and 2550 nm on the vector normalized spectral data. Vector normalization algorithm normalizes a spectrum by first calculating the average intensity value and subsequent subtraction of this value from the spectrum. Then the sum of the squared intensities is calculated and the spectrum is divided by the square root of this sum.

From the dendrographic distribution, based on the diffuse reflectance NIR spectra of soil samples, both, calibration and validation, data sets were established. The appropriate PLS models were built using the best wavelength range, pre-processing method, and appropriate number of factors for physical (pHs and EC) and chemical (organic matter, CaCO<sub>3</sub> and trace metals) characterization of soils from a calibration set of analyzed samples and applied for the prediction of the previously cited parameters in a validation set of samples but different than those used for calibration.

For building the best PLS regression models, different spectral windows were tested. An approach similar than synergy interval PLS (siPLS) method [45], which splits the data set into a chosen number of intervals (continuous sections) and calculates all possible PLS models, was used in order to select the optimum spectral region/s. For this purpose, the spectral range compressed between 1000 and 2600 nm, was split into 10 equally large regions and successively combinations of them were calculated. The optimization procedure starts with one frequency range block and successively adds further blocks up to 10 to find the best combination, always looking for the lowest root mean square error of prediction (RMSEP).

The optimum number of PLS factors was selected from the minimum of the resulting graph of predicted residual error sum of squares (PRESS).

The main purpose was to estimate the average deviation of the model from the reference data and the actual possibilities to use NIR spectra of soils for screening of physical and chemical characteristics of soils.

Several figures of merit related to the model's fit, such as, the root mean square error of calibration (RMSEC), the root mean square error of cross-validation (RMSECV) and the coefficient of regression ( $r$ ) were calculated in order to test the model coherency.

Predictive power was evaluated through the use of the RMSEP. Moreover, prediction accuracy was established by using the quality coefficient (QC) [46,47], which gives an indication of the percentage error to be expected for the estimated parameters in samples not used for calibration, and was calculated using Eq. (1):

$$QC (\%) = \sqrt{\frac{\sum_{i=1}^n (\bar{x}_{\text{calc}} - x_{\text{ref}}/x_{\text{ref}})^2}{(n-1)}} \times 100 \quad (1)$$

where  $\bar{x}_{\text{calc}}$  is the mean value obtained from the triplicate analysis by NIR spectroscopy for a selected parameter,  $x_{\text{ref}}$  is the parameter value obtained using the reference procedure and  $n$  is the number of total objects (no triplicates).

An additional quality indicator, as the residual predictive deviation (RPD), was also used to evaluate the predictive ability of the PLS models by introducing the variability range of each considered parameter [48]. For robust NIR calibration models low error of estimation (RMSEP) as compared with the spread in composition of that property in the validation population must be achieved. The increase of the value of RPD means an improvement of the power of the model to predict accurately the considered property.

In spite that several data treatment were carried out for obtaining the best prediction capabilities of the corresponding models,

only the most significant information is presented through this paper.

## 2.5. Cluster analysis

Cluster analysis refers to different algorithms and segmentation methods used to identify groups of observations, within a data set, sharing common characteristics.

Hierarchical clustering is a general approach to *cluster analysis*, in which objects are analyzed to look for their similarities. Calculations start with any a priori notion of group characteristics and make the grouping of objects through a repeated calculation of the distance measures between objects.

The two main categories of methods for cluster grouping are *agglomerative* and *divisive* methods. In agglomerative methods each observation is considered as a separate cluster and then combined with other observations inside a cluster by considering similarity measurements. In contrast to that divisive methods start considering all the observations grouped in a single cluster and splitting it into smaller clusters through the consideration of dissimilarity measurements.

The outcome of hierarchical cluster analysis is represented graphically as a *dendrogram*, established using a characteristic distance, used to describe the union between samples, which is related to how similar the numerical properties of sample are (For our purpose, diffuse reflectance near infrared spectra).

In the present study, a divisive method based on the Euclidean normal and Ward linkage method was used.

It must be noticed that through this study replicate spectra obtained for each sample were considered separately for evaluating the dissimilarity for the same sample (as a consequence of the instrumental noise) and as a guide for the appropriate cut-off value selection for establishing the correct number of groups of samples. Additionally, for this purpose, a target sample located in different vials and measured in different days, was also used.

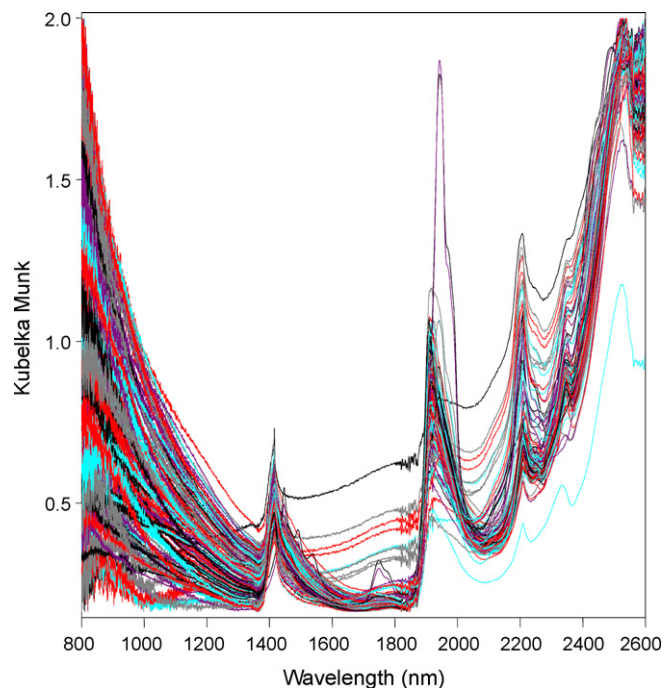


**Fig. 2.** Diffuse reflectance NIR spectra of different soil samples from the Region of Murcia. Instrumental conditions: 8 cm<sup>-1</sup> nominal resolution and 36 cumulated scans per spectrum. *Note:* All spectra were maximized on the y-axis in order to clearly show the spectral differences between them.

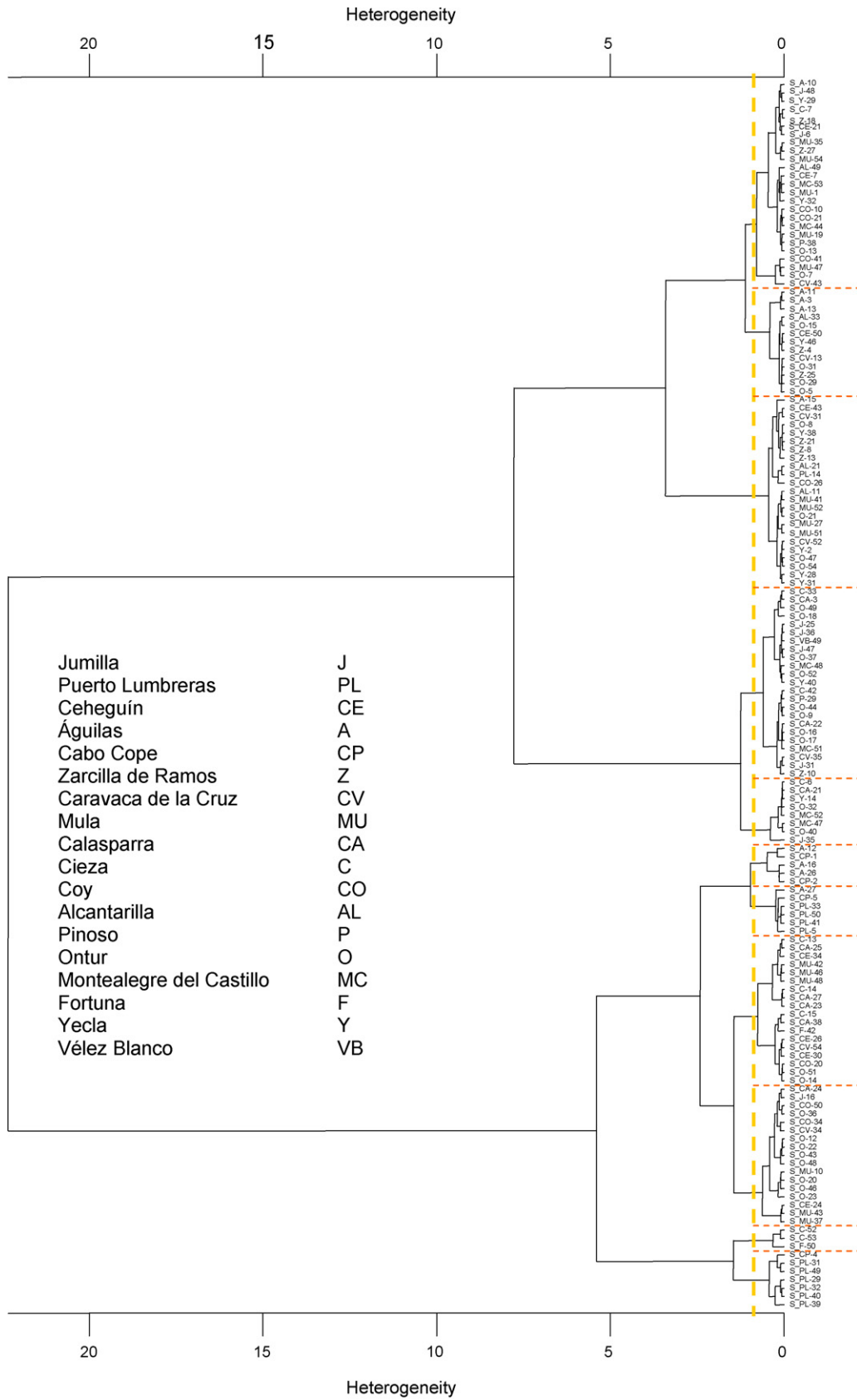


**Fig. 3.** Dendrographic classification of soil samples obtained using the Euclidean distance to compute the similarity between all pairs of samples to be clustered with Ward linkage as algorithm for hierarchical clustering upon considering the frequency range between 850 and 2550 nm on the vector normalized spectral data. For details about cluster group composition see data in Table 2. Samples were labeled using an abbreviation of the sampling location (see Fig. 1) joint to a numerical identification.

### 3. Results and discussion

#### 3.1. Soils diffuse reflectance near infrared NIR spectra

Soil samples tested in the present study provided characteristic NIR spectra in the region compressed between 800 and 2600 nm ( $12,500\text{--}3846\text{ cm}^{-1}$ ) as it can be seen in Fig. 2.

In general, the major part of soil spectra evidence three major absorption peaks (around 1400, 1900, and 2200 nm) across the near-infrared region.

As it has been stated in previous works [49,50], reflectance characteristics of soils are related to chemical groups present in the organic matter, among them chlorophyll, oil, cellulose, pectin, starch, lignin, and humic acids, which are spectrally active groups in the near infrared (400–2500 nm) region.

Prominent absorption bands exhibited in the near-infrared region around 1414 nm could be related to C–H combination or O–H (water) first overtone. The most intense band located at 1914 nm could be associated to the either O–H stretch first overtone or C=O stretch second overtone (in this latter case associated to the presence of inorganic carbonate fraction).

The absorption band at 2208 nm could correspond to C–H stretch/C=O stretch combination.

Around 2350 nm it is possible to identify an absorption band which could be assigned to the absorption of  $\text{CH}_2$  (cellulose) bend second overtone.

A no well defined band, near to the extreme region of spectra (2530 nm) can be also observed and associated to the asymmetric C–N–C stretch first overtone.

Additionally, some soil samples exhibit other relevant absorption bands located at 1444 nm (C–H combination, O–H stretch first overtone or carbonate stretch third overtone assignment), 1490 nm (N–H stretch first overtone, O–H stretch first overtone, symmetric N–H stretch first overtone or N–H stretch first overtone), 1538 nm (O–H stretch first overtone), 1748 nm (S–H stretch first overtone), 1780 nm (C–H stretch first overtone or C–H stretch/HOH deformation combination), 1942 nm (O–H bend second overtone) or 1989 nm (N–H stretch/N–H bend combination).

#### 3.2. Diffuse reflectance NIR spectra treatment

In order to achieve the best correlation between physical and chemical properties of soil samples and their corresponding NIR spectra, PLS regression models were built based on the use of opportune correction algorithms, such as the use of first order derivative spectra, multiplicative scattering correction or vector normalization on the selected spectral range.

First derivative spectra emphasize steep edges of a peak as well as pronounced, but small features over a broad background. The main drawback on using this method for spectral pre-treatment lies to the fact that spectral noise is also enhanced.

Vector normalization, generally employed to compensate the different samples sizes, implies the normalization of a spectrum calculating the average intensity and then subtracting this value from the spectrum. After that the sum of the squared intensities is calculated and the spectrum divided by the square root of this sum.

Other method often used for spectra pre-treatment in diffuse reflectance sampling mode, is Multiplicative Scatter Correction (MSC), which performs a linear transformation of each spectrum to match the average spectrum of the whole set.

#### 3.3. Cluster classification of soil samples from their NIR spectra

In order to check similarities among samples considered, a clustering method was applied previously to multivariate data

treatment. This task must be considered an important step to carry out the adequate selection of a representative calibration set according to the variability of samples under study, thus improving the prediction capabilities of the model.

Dendrographic classification of samples under study is shown in Fig. 3 and, as it can be seen, from this figure, 11 different types of samples could be identified for a cut-off value of 1.

After dendrogram observation it is possible to state that main groups of formed clusters (from left to right) are directly correlated with the intensity of the NIR spectra of soils being samples with high diffuse reflectance level grouped together.

It is clear that trace metal do not show specific absorption features in the NIR region, but it was detected a slight correlation between cluster structure and some trace metals due to their possible association with hydroxides, sulfides, carbonates, or oxides that are detectable [51]; or through their adsorption to clays that absorb in this wavelength range [52].

On the other hand, as diffuse reflectance intensity seems to be mainly related with the carbon, hydrogen and nitrogen composition, and in general, soil reflectance decreases on decreasing the organic matter content [50], clusters could basically relate with the content of these chemical parameters.

Mean and standard deviation values of soil physicochemical parameters (organic matter,  $\text{CaCO}_3$ , pH, EC and trace metals) under study are detailed in Table 2, for the 11 clusters obtained, ordered from the top to the bottom of Fig. 3.

As stated sample indicators no strict correlation, between the different identified clusters and collected samples from sampling locations, was found.

#### 3.4. Selection of the calibration and validation sets

One of the most important tasks in multivariate NIR analysis is building a good calibration model, being the number and nature of samples used for calibration main critical factors when multivariate analysis is used. Furthermore, the validity of the model must be tested, usually in a correct way by splitting sample data set into two independent sets; one for calibration and the other for validation.

The calibration can be used to predict future unknowns, assuming that they are in the same sample population as those used in the calibration set.

For this reason, dendrogram of Fig. 3 was considered as a useful tool to do both, the proper selection of the calibration and validation data sets, and the confirmation of the nature of unknown samples.

The criterion used to choose the calibration set was based on the selection of at least one sample from each cluster. In the case of clusters containing several samples, the round square root value of the total number of samples included in the cluster was selected for calibration while the remaining samples were integrated in the validation set. Samples were always randomly selected from each cluster.

Based on the aforementioned considerations, we built the calibration models using 39 samples. Predictive capabilities and analytical features of models were established using 109 samples. As shown in Table 3, the average data and data dispersion of all parameters evaluated are very similar for both considered sets.

#### 3.5. Determination of quality indicators from soils

Spectral range and number of factors employed to build PLS calibration models were optimized for each one of the parameters considered in order to avoid under-fitting and over-fitting as well as to avoid the consideration of uninformative variables. Tables 4 and 5 summarize the main figures of merit of the best found models for the considered parameters through this study.

**Table 2**  
 Characteristics of soil samples from different parts of the Region of Murcia (South-East Spain) classified into clusters after dendrographic treatment of NIR data.

Cluster index	Number of samples	Organic matter (% w/w)		CaCO <sub>3</sub> (% w/w)		pH (H <sub>2</sub> O)		pH (KCl)		Electric conductivity (dS/m)		Samples								
		Mean	±s	Mean	±s	Mean	±s	Mean	±s	Mean	±s									
1	25	1.2	0.7	42	18	8.1	0.3	7.5	0.3	1.5	1.4	A-10, J-48, Y-29, C-7, Z-18, CE-21, J-6, Mu-35, Z-27, Mu-54, AL-49, CE-7, MC-53, Mu-1, Y-32, CO-10, CO-21, MC-44, Mu-19, P-38, O-13, CO-41, Mu-47, O-7, CV-43								
2	13	2.1	1.7	35	18	8.09	0.18	7.45	0.18	3	4	A-11, A-3, A-13, AL-33, O-15, CE-50, Y-46, Z-4, CV-13, O-31, Z-25, O-29, O-5								
3	23	1.4	1.0	44	16	8.17	0.15	7.47	0.16	1.4	1.2	A-15, CE-43, CV-31, O-8, Y-38, Z-21, Z-8, Z-13, AL-21, PL-14, CO-26, AL-11, Mu-41, Mu-52, O-21, Mu-27, Mu-51, CV-52, Y-2, O-47, O-54, Y-28, Y-31								
4	23	2	2	39	12	8.1	0.3	7.53	0.19	0.9	1.0	C-33, CA-3, O-49, O-18, J-25, J-36, VB-49, J-47, O-37, MC-48, O-52, Y-40, C-42, P-29, O-44, O-9, CA-22, O-16, O-17, MC-51, CV-35, J-31, Z-10								
5	8	1.7	0.8	39	19	8.25	0.17	7.7	0.2	0.48	0.18	C-6, CA-21, Y-14, O-32, MC-52, MC-47, O-40, J-35								
6	5	1.0	0.5	15	8	8.18	0.16	7.68	0.08	4	3	A-12, CP-1, A-16, A-26, CP-2								
7	6	0.9	1.2	20	17	8.08	0.18	7.73	0.16	6	9	A-27, CP-5, PL-33, PL-50, PL-41, PL-5								
8	18	1.0	0.7	57	9	8.2	0.2	7.5	0.2	2	3	C-13, CA-25, CE-34, Mu-42, Mu-46, Mu-48, C-14, CA-27, CA-23, C-15, CA-38, F-42, CE-26, CV-54, CE-30, CO-20, O-51, O-14								
9	17	0.9	0.9	49	11	8.2	0.3	7.6	0.2	1.1	1.0	CA-24, J-16, CO-50, O-36, CO-34, CV-34, O-12, O-22, O-43, O-48, Mu-10, O-20, O-46, O-23, CE-24, Mu-43, Mu-37								
10	3	2.0	1.5	24	21	7.9	0.2	7.60	0.10	4	3	C-52, C-53, F-50								
11	7	0.8	1.2	9	4	8.0	0.2	7.64	0.17	5	4	CP-4, PL-31, PL-49, PL-29, PL-32, PL-40, PL-39								
Cluster index	Number of samples	[Cr]		[Co]		[Ni]		[Cu]		[Zn]		[As]		[Se]		[Cd]		[Ti]		Samples
		Mean	±s	Mean	±s	Mean	±s	Mean	±s	Mean	±s	Mean	±s	Mean	±s	Mean	±s	Mean	±s	
1	25	39	20	13	19	23	13	19	12	99	34	8	6	0.34	0.10	0.31	0.16	0.38	0.18	A-10, J-48, Y-29, C-7, Z-18, CE-21, J-6, Mu-35, Z-27, Mu-54, AL-49, CE-7, MC-53, Mu-1, Y-32, CO-10, CO-21, MC-44, Mu-19, P-38, O-13, CO-41, Mu-47, O-7, CV-43
2	13	50	31	12	8	25	16	23	14	107	69	11	9	0.27	0.09	0.3	0.2	0.50	0.19	A-11, A-3, A-13, AL-33, O-15, CE-50, Y-46, Z-4, CV-13, O-31, Z-25, O-29, O-5
3	23	43	30	11	6	25	16	21	15	105	44	7	3	0.28	0.10	0.3	0.3	0.39	0.17	A-15, CE-43, CV-31, O-8, Y-38, Z-21, Z-8, Z-13, AL-21, PL-14, CO-26, AL-11, Mu-41, Mu-52, O-21, Mu-27, Mu-51, CV-52, Y-2, O-47, O-54, Y-28, Y-31
4	23	35	21	8	4	20	13	26	43	99	56	5	2	0.31	0.14	0.40	0.19	0.43	0.16	C-33, CA-3, O-49, O-18, J-25, J-36, VB-49, J-47, O-37, MC-48, O-52, Y-40, C-42, P-29, O-44, O-9, CA-22, O-16, O-17, MC-51, CV-35, J-31, Z-10

Table 2 (Continued)

Cluster index	Number of samples	[Cr]		[Co]		[Ni]		[Cu]		[Zn]		[As]		[Se]		[Cd]		[Tl]		Samples
		Mean	±s	Mean	±s	Mean	±s	Mean	±s	Mean	±s	Mean	±s	Mean	±s	Mean	±s	Mean	±s	
5	8	39	30	8	4	21	9	18	6	120	51	7	2	0.30	0.12	0.45	0.17	0.43	0.18	C-6, CA-21, Y-14, O-32, MC-52, MC-47, O-40, J-35
6	5	87	19	17.8	1.9	46	8	56	8	130	53	39	16	0.31	0.11	0.385	0.018	0.8	0.2	A-12, CP-1, A-16, A-26, CP-2
7	6	122	42	22	5	57	9	56	22	145	29	20	10	0.30	0.06	0.16	0.11	0.86	0.12	A-27, CP-5, PL-33, PL-50, PL-41, PL-5
8	18	46	25	14	13	33	20	44	51	111	45	7	2	0.32	0.11	0.3	0.2	0.35	0.19	C-13, CA-25, CE-34, Mu-42, Mu-46, Mu-48, C-14, CA-27, CA-23, C-15, CA-38, F-42, CE-26, CV-54, CE-30, CO-20, O-51, O-14
9	17	30	18	7	5	19	14	29	48	89	45	6	2	0.30	0.11	0.5	0.2	0.44	0.14	CA-24, J-16, CO-50, O-36, CO-34, CV-34, O-12, O-22, O-43, O-48, Mu-10, O-20, O-46, O-23, CE-24, Mu-43, Mu-37
10	3	25	19	14	9	20	13	25	16	162	145	3.6	0.5	0.27	0.06	0.4	0.3	0.15	0.04	C-52, C-53, F-50
11	7	110	22	21	4	55	10	47	6	134	39	16	14	0.31	0.11	0.17	0.09	1.0	0.2	CP-4, PL-31, PL-49, PL-29, PL-32, PL-40, PL-39

Note: ±s refers to the standard deviation of the mean. See Fig. 1 for additional information on the sampling sites. All trace metal concentration values are expressed in  $\mu\text{g g}^{-1}$ .

### 3.5.1. Chemical and physical indicators determination

The main characteristics of models and results obtained for organic matter and  $\text{CaCO}_3$  contents, pH and EC determination are detailed in Table 4.

As it can be seen, from 1 to 3 combined optimal spectral regions were selected for the determination of each different physicochemical parameter under study. The number of PLS factors ranged from 2 to 6. It must be also noticed differences on optimal spectral region, pre-processing method and number of PLS factors used for the determination of the same parameter, pH, but based on a different measurement criterion with coincident results in both situations.

The best RPD value, 1.5, was achieved for  $\text{CaCO}_3$  determination while for all the rest of parameters RPD values around 1 were obtained.

The QC parameter obtained for pH prediction was 3% but increased till 40% for  $\text{CaCO}_3$  and it was 80% for organic matter and 166% for EC, thus indicating a poor predictive capability for the last two parameters. This fact and the RMSEP values found (which varied from 0.19 to 11) indicate that some of the aforementioned parameters may not be accurately predicted using NIR spectroscopy. However, it is clear that prediction results are of a great value for screening purposes, especially in long term studies focused on the same area.

Table 3

Descriptive statistics of calibration and validation data sets used for PLS-NIR analysis of soil samples from different parts of the Region of Murcia.

Set	Number of samples	Trace metals ( $\mu\text{g g}^{-1}$ )																	
		[Cr]		[Co]		[Ni]		[Cu]		[Zn]		[As]		[Se]		[Cd]		[Tl]	
		Mean	±s	Mean	±s	Mean	±s	Mean	±s	Mean	±s	Mean	±s	Mean	±s	Mean	±s	Mean	±s
Calibration	39	56	40	12	6	29	17	29	18	110	52	11	13	0.32	0.12	0.32	0.16	0.5	0.3
Validation	109	44	30	10	7	26	17	24	17	102	41	8	7	0.30	0.10	0.4	0.2	0.5	0.2
Set	Number of samples	Other parameters																	
		Organic matter (% w/w)				$\text{CaCO}_3$ (% w/w)		pH ( $\text{H}_2\text{O}$ )		pH (KCl)		EC (dS/m)							
		Mean	±s	Mean	±s	Mean	±s	Mean	±s	Mean	±s	Mean	±s						
Calibration	39	1.7	1.2	35	20	8.1	0.2	7.6	0.2	2	3								
Validation	109	1.3	1.3	42	17	8.1	0.2	7.5	0.2	2	3								

Table 4

Summary for the analytical figures of merit obtained through the use of PLS-NIR models for the determination of physicochemical parameters of soil samples from the Region of Murcia.

Parameter	Wavenumber range (nm)	Spectral treatment	PLS factors	r	RMSEC	RMSEP	QC (%)	RPD
Organic matter (% w/w)	1658–1886/2185–2374	MSC + FD	5	0.71	0.8	1.1	80	1.1
$\text{CaCO}_3$ (% w/w)	1336–1405/1480–1886/2185–2374	MSC + FD	2	0.83	11	11	40	1.5
pH ( $\text{H}_2\text{O}$ )	1404–1659	None	6	0.69	0.16	0.2	3	0.9
pH (KCl)	1369–1553	MSC + FD	2	0.54	0.18	0.19	3	1.0
EC (dS/m)	1011–1107/1224–1370/1552–1794	Vector normalization	4	0.87	1.2	3	166	1.1

Note: QC is the quality coefficient. RPD is the residual predictive deviation. For additional details see the text.



**Table 5**

Summary for the analytical figures of merit obtained through the use of PLS-NIR models for the determination of several trace metals in soil samples from the Region of Murcia.

Trace metal	Wavenumber range (nm)	Spectral treatment	PLS factors	<i>r</i>	RMSEC ( $\mu\text{g g}^{-1}$ )	RMSEP ( $\mu\text{g g}^{-1}$ )	QC (%)	RPD
Cr	1011–1553/2122–2598	MSC + FD	2	0.78	25	21	70	1.4
Co	1106–1224/1368–1552/1792–2598	MSC + FD	4	0.86	3	5	64	1.4
Ni	1368–1552/1792–2122	MSC + FD	5	0.91	7	13	175	1.3
Cu	1368–2598	MSC + FD	1	0.68	13	16	69	1.1
Zn	1224–1553	MSC + FD	2	0.73	40	30	37	1.1
As	1224–1370/1552–1794	MSC + FD	1	0.90	5	6	55	1.3
Se	1224–1370/1552–2123	MSC + FD	3	0.58	0.09	0.10	33	1.0
Cd	1107–1225/1369–2123	MSC + FD	2	0.50	0.14	0.20	64	1.0
Tl	930–1107/1224–1553/1793–2598	MSC + FD	2	0.68	0.19	0.17	41	1.2

Note: The meaning of the parameters is the same than that indicated in Table 4.

As compared with previous studies made by NIR on soil analysis it can be seen that organic matter can be predicted with a RMSEP of 1.1 higher than that found before [27,33,37] but pH was predicted with a RMSEP of 0.19–0.2 of the same order than that obtained before [34] and lower than values obtained for lake sediments [29].

On the other hand, the RPD values of 1.5 and 1.1 found for  $\text{CaCO}_3$  and EC prediction, respectively, provide encouraging precedents for the prediction of these parameters.

### 3.5.2. Trace metals determination

Through the use of the aforementioned calibration and validation data sets, NIR data previously obtained for soil samples were modeled by PLS to predict the total concentration of trace metals as Cr, Co, Ni, Cu, Zn, As, Se, Cd and Tl.

The best prediction capabilities obtained for the elements under study are summarized in Table 5.

Significant differences can be appreciated on considering the optimal spectral region as well as the number of PLS factors for the different models built. For the considered metals from 1 to 3 combined optimal regions as well as an optimum number of extracted factors varying from 1 to 5 can be achieved.

It must be also noticed that best results for all metals considered were achieved on using Multiplicative Scattering Correction (MSC) on the first derivative (FD) spectra.

Values ranging from 0.10 to 30  $\mu\text{g g}^{-1}$  were obtained for RMSEP parameter, which provided RPD values compressed between 0.9 and 1.4, thus indicating an appropriate residual predictive deviation for screening purposes at least for As, Co and Cr and relatively bad results for Ni. On the contrary, bad prediction results for the rest of metals can probably link to the presence of high proportions of them as inorganic forms without a remarkable influence in the NIR spectra.

On comparing results found in this study with previously reported it can be seen that an RPD value of 1.1 found for Cu and Zn compares well with those obtained for Cu [20–23,32] which ranged from 0.92 in soils to 3.35 in sediments and those for Zn [20,22–24,32] which ranged from 1.07 in soils to 3.80 for sediments.

On the contrary, reported results found for Ni, Cd, Cr and As in soils and sediments were better than those obtained in the present study, probably due to the wide range in concentration used for evaluating the aforementioned parameters in precedent studies.

## 4. Conclusions

This study confirms the possibilities offered by NIR spectroscopy for testing the main parameters of soils. In fact, the information obtained from the NIR spectra of chemically untreated soil samples can be used for screening of both, physical and chemical parameters, with drastic reductions on reagent consume and time analysis thus offering a sustainable alternative to the classical methods employed in soil analysis [53]. However, it is clear that NIR spec-

troscopy data process requires the use of an appropriate calibration based on previously characterized sample, and thus, the main applicability of this kind of measurements is related to long term studies focussed on the evolution of an ecosystem or on the screening of some of the reported data in samples with a nature comparable with that of those used to build the corresponding calibration.

It is also noticeable that prediction capabilities for  $\text{CaCO}_3$ , EC, or for metals like Co, Se and Tl determined from NIR spectra are reported for first time in this study.

## Acknowledgement

Authors acknowledge the financial support of the Ministerio de Educación y Ciencia (Project CTQ2005-05604-FEDER and AGL2007-64567).

## References

- [1] European Environment Agency (EEA). homepage//http://glossary.eea.europa.eu/EEAGlossary/S/soil.
- [2] European Environment Agency, Down to Earth: Soil Degradation and Sustainable Development in Europe: A Challenge for the 21st Century. Environmental Issue Series No. 16, EEA, Copenhagen, Belgium, 2000.
- [3] J. Benton Jones Jr., Soil Analysis: Handbook of Reference Methods, CRC, 1999.
- [4] D.F. Acton, L.J. Gregorich, The Health of our Soils: Toward Sustainable Agriculture in Canada, Agric. Agri-food Can., CDR Unit, 960 Carling Ave., Ottawa, Ont. K1A 0C6, 1995.
- [5] D. de la Rosa, Land Degrad. Dev. 16 (2005) 551.
- [6] C. Gardi, M. Tomaselli, V. Parisi, A. Petraglia, C. Santini, Eur. J. Soil Biol. 38 (2002) 103.
- [7] D.W. Reeves, Soil Tillage Res. 43 (1997) 131.
- [8] L.A. Schipper, G.P. Sparling, Soil Sci. Soc. Am. J. 64 (2000) 300.
- [9] A. Kabata-Pendias, Trace Elements in Soils and Plants, second ed., CRC, Ann Arbor, MI, 1992.
- [10] C.A. Seybold, R.B. Grossman, F.J. Pierce, Commun. Soil Sci. Plant Anal. 34 (2003) 765.
- [11] D.L. Corwin, S.M. Lesch, Agron. J. 95 (2003) 455.
- [12] J. Hatfield, B. Stewart, Soil Biology: Effects on Soil Quality (Advances in Soil Science), CRC Press, Boca Raton, FL, 1994.
- [13] ISO 10390:2005. Soil quality—determination of pH.
- [14] O. Šařec, P. Šařec, V. Prošek, Res. Agric. Eng. 48 (2002) 131.
- [15] M. Miyazawa, M.A. Pavan, E.L. de Oliveira, M. Ionashiro, A.K. Silva, Braz. Arch. Biol. Technol. 43 (2000) 475.
- [16] American Society for Testing and Materials. D4373-96 standard test method for calcium carbonate content of soils.
- [17] ISO 10693:1995. Soil quality – determination of carbonate content – volumetric method.
- [18] ISO 11047:1998. Soil quality – determination of cadmium, chromium, cobalt, copper, lead, manganese, nickel and zinc – flame and electrothermal atomic absorption spectrometric methods.
- [19] ISO/FDIS 22036. Soil quality – determination of trace elements in extracts of soil by inductively coupled plasma – atomic emission spectrometry (ICP-AES).
- [20] D.F. Malley, P.C. Williams, Environ. Sci. Technol. 31 (1997) 3461.
- [21] D. Cozzolino, A. Morón, J. Agric. Sci. 140 (2003) 65.
- [22] G. Siebielec, G.W. McCarty, T.I. Stuczynski, J.B. Reeves III, J. Environ. Qual. 33 (2004) 2056.
- [23] R. Font, M. del Río, M. Simón, J. Aguilar, A. de Haro, Fresen. Environ. Bull. 13 (2004) 1309.
- [24] M. Chodak, M. Niklińska, F. Beese, Biol. Fertil. Soils 44 (2007) 171.
- [25] Y. Wu, J. Chen, J. Ji, P. Gong, Q. Liao, Q. Tian, H. Ma, Soil Sci. Soc. Am. J. 71 (2007) 918.
- [26] A. Morón, D. Cozzolino, Commun. Soil Sci. Plant Anal. 38 (2007) 1965.

- [27] M.J. Cohen, J.P. Prenger, W.F. DeBusk, *J. Environ. Qual.* 34 (2005) 1422.
- [28] B. Butkutė, A. Slepėtienė, *Chemija* 15 (2004) 12.
- [29] M.B. Nilsson, E. Dåbakk, T. Korsman, I. Marrenberg, *Environ. Sci. Technol.* 30 (1996) 2586.
- [30] L.K. Sørensen, S. Dalsgaard, *Soil Sci. Soc. Am. J.* 69 (2005) 159.
- [31] A. Stevens, B. van Wesemael, G. Vandenschrick, S. Touré, B. Tychon, *Soil Sci. Soc. Am. J.* 70 (2006) 844.
- [32] C.W. Change, D.A. Laird, M.J. Mausbach, C.R. Hurburgh Jr., *Soil Sci. Soc. Am. J.* 65 (2001) 480.
- [33] Y. He, H. Song, *SPIE Int. Soc. Opt. Eng.* (2006), doi:10.1117/2.1200604.0164.
- [34] Y. He, H. Song, A. García Pereira, A. Hernández Gómez, *J. Zhejiang Univ. SCI.* 11 (2005) 1081.
- [35] K. Islam, B. Singh, Alex McBratney, *Aust. J. Soil Res.* 41 (2003) 1101.
- [36] C.W. Change, D.A. Laird, *Soil Sci.* 167 (2002) 110.
- [37] P.H. Fidêncio, R.J. Poppi, J.C. de Andrade, *Anal. Chim. Acta* 453 (2002) 125.
- [38] D.W. Nelson, L.E. Sommers, Total Carbon, Organic Carbon, and Organic Matter. *Methods of Soil Analysis, Part 2*, American Society of Agronomy and Soil Science Society of America, Madison, WI, 1982, pp. 539–580.
- [39] Norme française. NF X 31-109, 1069. Qualité des sols. Méthodes chimiques. Détermination du carbone organique par oxydation sulfochromique. AFNOR. p. 7.
- [40] G. Muller, M. Gatsner, *Chem. Anal. Neues Jahrbuch für Mineral-Monatshefte* 10 (1971) 466.
- [41] M. Peech, *Methods of Soil Analysis*, American Society of Agronomy, Madison, WI, 1965.
- [42] J. Moros, M.C. Barciela-Alonso, P. Pazos-Capeáns, P. Bermejo-Barrera, E. Peña-Vázquez, S. Garrigues, M. de la Guardia, *Anal. Chim. Acta* 624 (2008) 113.
- [43] J. Moros, P. Herbelo-Hermelo, A. Moreda-Piñeiro, P. Bermejo-Barrera, S. Garrigues, M. de la Guardia, *Anal. Bioanal. Chem. Anal* 392 (2008) 541.
- [44] J. Moros, F.A. Iñón, S. Garrigues, M. de la Guardia, *Anal. Chim. Acta* 538 (2005) 181.
- [45] L. Nørgaard, A. Saudland, J. Wagner, J.P. Nielsen, L. Munck, S.B. Engelsen, *Appl. Spectrosc.* 54 (2000) 413.
- [46] D.L. Massart, B.G.M. Vandeginste, L.M.C. Buydens, S. de Jong, P.J. Lewi, J. Verbeke, *Handbook of Chemometrics and Qualimetrics (Part A and B)*, Elsevier Science B.V., Amsterdam, 1997.
- [47] J. Moros, F.A. Iñón, M. Khanmohammadi, S. Garrigues, M. de la Guardia, *Anal. Bioanal. Chem.* 385 (2006) 708.
- [48] T. Fearn, in: J.M. Chalmers, P.R. Griffiths (Eds.), *Handbook of Vibrational Spectroscopy (vol. 3) Discriminant analysis*, Wiley, Chichester, 2002, p. 2086.
- [49] E. Ben-Dor, Y. Inbar, Y. Chen, *Remote Sens. Environ.* 61 (1997) 1.
- [50] L. Kooistra, J. Wanders, G.F. Epema, R.S.E.W. Leuven, R. Wehrens, L.M.C. Buydens, *Anal. Chim. Acta* 484 (2003) 189.
- [51] G.R. Hunt, J.W. Salisbury, *Model. Geol.* 283 (1970) 1.
- [52] V.P. Krischenko, S.G. Samokhvalov, L.G. Formina, G.A. Novikova, in: I. Murray, I.A. Cowe (Eds.), *Making Light Work: Advances in Near Infrared Spectroscopy*, VCH, Weinheim, New York, Basel, Cambridge, 1992, p. 239.
- [53] S. Armenta, S. Garrigues, M. de la Guardia, *TrAC Trend Anal. Chem.* 27 (2008) 497.



# Simultaneous kinetic spectrophotometric analysis of five synthetic food colorants with the aid of chemometrics

Yongnian Ni<sup>a,b,\*</sup>, Yong Wang<sup>b</sup>, Serge Kokot<sup>c</sup>

<sup>a</sup> State Key Laboratory of Food Science and Technology, Nanchang University, Nanchang, Jiangxi 330047, China

<sup>b</sup> Department of Chemistry, Nanchang University, Nanchang, Jiangxi 330047, China

<sup>c</sup> Inorganic Materials Research Program, School of Physical and Chemical Sciences, Queensland University of Technology, Brisbane, Queensland 4001, Australia

## ARTICLE INFO

### Article history:

Received 29 August 2008

Received in revised form

21 November 2008

Accepted 24 November 2008

Available online 3 December 2008

### Keywords:

Kinetic analysis

Spectrophotometry

Synthetic food colorants

Chemometrics

Foodstuffs

Prussian blue

## ABSTRACT

This paper describes a simple and sensitive kinetic spectrophotometric method for the simultaneous determination of Amaranth, Ponceau 4R, Sunset Yellow, Tartrazine and Brilliant Blue in mixtures with the aid of chemometrics. The method involved two coupled reactions, viz. the reduction of iron(III) by the analytes to iron(II) in sodium acetate/hydrochloric acid solution (pH 1.71) and the chromogenic reaction between iron(II) and hexacyanoferrate(III) ions to yield a Prussian blue peak at 760 nm. The spectral data were recorded over the 500–1000 nm wavelength range every 2 s for 600 s. The kinetic data were collected at 760 nm and 600 s, and linear calibration models were satisfactorily constructed for each of the dyes with detection limits in the range of 0.04–0.50 mg L<sup>-1</sup>. Multivariate calibration models for kinetic data were established and verified for methods such as the Iterative target transform factor analysis (ITTTA), principal component regression (PCR), partial least squares (PLS), and principal component-radial basis function-artificial neural network (PC-RBF-ANN) with and without wavelet packet transform (WPT) pre-treatment. The PC-RBF-ANN with WPT calibration performed somewhat better than others on the basis of the %RPE<sub>T</sub> (~9) and %Recovery parameters (~108), although the effect of the WPT pre-treatment was marginal (~0.5% RPE<sub>T</sub>). The proposed method was applied for the simultaneous determination of the five colorants in foodstuff samples, and the results were comparable with those from a reference HPLC method.

© 2008 Elsevier B.V. All rights reserved.

## 1. Introduction

Food dyes may be natural or synthetic, and they have been widely used to optimize food color, because freshness, ripeness, and flavour are all associated with the color of food [1]. However, the synthetic colorants may be toxic, especially if consumed in large amounts. Thus, each synthetic food colorant has been evaluated by the Food and Agricultural Organization (FAO) and World Health Organization (WHO) [2], and there is an increasing need to monitor the levels of such dyes in various products.

Amaranth, Ponceau 4R, Sunset Yellow, Tartrazine and Brilliant Blue are water-soluble synthetic colorants, widely used as additives in the food industry (chemical structures: Table 1). A number of methods have been available for their analysis individually or simultaneously in mixtures. These are generally based on high performance liquid chromatography (HPLC) techniques [3–7], which

are often adequate for analysis of colorants in mixtures. However, there are some potential drawbacks, such as the usage of toxic solvents, the need for complex sample pre-treatments, and the resulting waste products [8]. Thus, analytical methods from alternative techniques are always useful, especially if the methods are simple, cheap and comparatively fast. Spectrophotometry is a well known analytical technique, and direct spectrophotometric methods have been proposed for the simultaneous determination of binary/ternary/quaternary colorant mixtures [9–12].

In the present paper, we investigate an indirect kinetic spectrophotometric method of analysis for the simultaneous determination of the five colorants. This method is based on a sensitive chromogenic reaction of the dye analytes, and the interpretation of the results by chemometrics. The advantages of kinetic methods have been pointed out elsewhere [13,14]. In theory, the common kinetic modelling involving proportional equations and the logarithmic extrapolation based on well defined reaction mechanisms, does provide high levels of discrimination of the analyte components. However, such models are often complex to apply because they need well-defined orders of reaction and rate constants, which are often unavailable [15]. Commonly, only a small fraction of the kinetic data collected has been used, which led to poor analyti-

\* Corresponding author at: Department of Chemistry, Nanchang University, Nanchang, Jiangxi 330047, China. Tel.: +86 791 3969500; fax: +86 791 3969500.

E-mail address: [ynni@ncu.edu.cn](mailto:ynni@ncu.edu.cn) (Y. Ni).

**Table 1**  
Chemical structures of the colorants (Part A) and their oxidation mechanism (Part B).

Part A: Chemical structure			
Compound	Molecular formula	Molecular weight	Structure
Amaranth	C <sub>20</sub> H <sub>11</sub> N <sub>2</sub> Na <sub>3</sub> O <sub>10</sub> S <sub>3</sub>	604.47	
Ponceau 4R	C <sub>20</sub> H <sub>11</sub> N <sub>2</sub> Na <sub>3</sub> O <sub>10</sub> S <sub>3</sub>	604.47	
Sunset Yellow	C <sub>16</sub> H <sub>10</sub> N <sub>2</sub> Na <sub>2</sub> O <sub>7</sub> S <sub>2</sub>	452.36	
Tartrazine	C <sub>16</sub> H <sub>9</sub> N <sub>4</sub> Na <sub>3</sub> O <sub>9</sub> S <sub>2</sub>	534.36	
Brilliant Blue	C <sub>37</sub> H <sub>34</sub> N <sub>2</sub> Na <sub>2</sub> O <sub>9</sub> S <sub>3</sub>	792.85	

Part B: Oxidation mechanism of the colorants by iron(III)–hexacyanoferrate(III) solution in sodium acetate/hydrochloric acid solution (pH 1.71)  
 Colorant + Iron(III) → Oxidation product + Iron(II) + H<sup>+</sup>  
 Iron(II) + hexacyanoferrate(III) → Prussian blue

cal precision and accuracy [16]. On the other hand, soft modelling with the use of chemometrics does not require the exact knowledge of reaction mechanisms and recently, kinetic spectrophotometric models have been reported for the simultaneous prediction of analytes in mixtures [17,18]. Typical multivariate calibrations were built with the aid of principal component regression (PCR), partial least squares (PLS) and artificial neural network (ANN) methods [19,20].

An analytical signal consists of the information from the analyte(s) plus residuals. To minimise the effect of the residuals data pre-treatment may be applied, and the wavelet transform (WT) method is one such useful approach. It is able to map the frequency content of a signal as a function of the original domain, offering the possibility of dual time–frequency localisation [21,22]. Wavelet packet transform (WPT) is an extension of the wavelet transform [23,24]. It retains time–frequency localisation capability from the corresponding wavelet functions, but provides more flexibility for representing different types of signal. In general, WPT has not been commonly applied in chemistry [25,26], and even less so in kinetic analysis [27].

In this paper, a simple differential spectrophotometric kinetic method was explored for the simultaneous determination of Amaranth, Ponceau 4R, Sunset Yellow, Tartrazine and Brilliant Blue food dyes in a mixture. It was based on the reduction of iron(III) by the dyes in sodium acetate/hydrochloric acid solution (pH 1.71) followed by a chromogenic reaction with potassium hexacyanoferrate(III) to form the Prussian blue species, which was detected

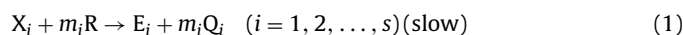
at  $\lambda_{\max} = 760$  nm. Different chemometrics methods, such as Iterative target transform factor analysis (ITTTFA), PCR, PLS, Principal component–radial basis function–artificial neural network (PC-RBF-ANN) with and without the WPT pre-treatment of the original kinetic data, were used for modelling, and these models were then verified with a separate set of mixtures. A set of real unknown samples containing the dye were analysed and the results were validated by comparative analysis with the use of a reference HPLC method.

## 2. Theoretical background and chemometrics

### 2.1. Differential kinetic method

Iron(III) and hexacyanoferrate(III) ions in acidic medium react with suitable organic substances such as drugs or dyes, and produce the strongly colored Prussian blue species. Rates of such reactions differ with different analytes, and this opens a pathway for simultaneous analysis of such organic molecules in a mixture. Kinetic mechanisms of such reactions involve consecutive steps [28,29]: (i) iron(III) is reduced by the organic reactant to the iron(II) intermediate, and (ii) iron(II) reacts with the hexacyanoferrate(III) ion to form the complex Prussian blue species (Table 1).

The steps can be represented as:





where  $X_i$ , R,  $E_i$ ,  $Q_i$ , S and  $P_i$  are the organic analyte, iron(III), iron(II), the oxidation product of  $X_i$ , hexacyanoferrate(III) ions and the Prussian blue product, respectively.  $m_i$  and  $n_i$  are the stoichiometric coefficients.

In the presence of a large excess of R and S, the two reactions may be considered in terms of pseudo-first-order kinetics [30]. Thus, the rate equations for a  $X_i$ ,  $E_i$  and  $P_i$  are:

$$\frac{dc_{X_i}}{dt} = -k_1 c_{X_i} \quad (3)$$

$$\frac{dc_{E_i}}{dt} = k_1 c_{X_i} - k_2 c_{E_i} \quad (4)$$

$$\frac{dc_{P_i}}{dt} = k_2 c_{E_i} \quad (5)$$

Integration of Eqs. (3)–(5) yields:

$$c_{X_i} = c_{X_0} \exp(-k_1 t) \quad (6)$$

$$c_{E_i} = k_1 c_{X_0} \frac{\exp(-k_1 t) - \exp(-k_2 t)}{k_2 - k_1} \quad (7)$$

$$c_{P_i} = c_{X_0} \left[ \frac{1 - k_2 \exp(-k_1 t) - k_1 \exp(-k_2 t)}{k_2 - k_1} \right] \quad (8)$$

where  $c_{X_0}$  is the initial concentration of the analyte,  $c_{X_i}$ ,  $c_{E_i}$ , and  $c_{P_i}$  are the concentrations of  $X_i$ ,  $E_i$  and  $P_i$  at time,  $t$ , respectively, and  $k_1$  and  $k_2$  are the pseudo-first-order rate constants for reactions (1) and (2), respectively.

Assuming that only  $P_i$  absorbs, and its absorbance,  $A_{X_i, \lambda}$ , obeys the Beer–Lambert law at any wavelength,  $\lambda$ , then for any time,  $t$ :

$$A_{X_i, \lambda} = \varepsilon_{X_i, \lambda} b c_{X_0} \left[ \frac{1 - k_2 \exp(-k_1 t) - k_1 \exp(-k_2 t)}{k_2 - k_1} \right] = K_{X_i, \lambda} \quad (9)$$

where  $K_{X_i, \lambda}$  represents the proportionality coefficient of  $X_i$ . If the responses from  $s$  analytes and the residuals are additive and follow similar kinetics, then the absorbance of the system may be represented as:

$$A_{\lambda, t} = A_b + \sum_{i=1}^s K_{X_i, \lambda}^i c_{X_i} \quad (10)$$

where  $A_{\lambda, t}$  and  $A_b$  represent the total absorbance of all the analytes and residuals.

Let  $c_{X_{(s+1)}} = 1$  and merge  $A_b$  into the main term, then Eq. (10) can be further simplified as:

$$A_{\lambda, t} = \sum_{i=1}^{s+1} K_{X_i, \lambda}^i c_{X_i} \quad (11)$$

If for  $j$  standard samples, the absorbance is monitored at  $k$  time points at a fixed wavelength, it then can be expressed in matrix form:

$$\mathbf{A}_{j \times k} = \mathbf{C}_{j \times (s+1)} \mathbf{K}_{(s+1) \times k} \quad (12)$$

where the first row in matrix  $\mathbf{K}$  represents the background vector. Thus, Eq. (12) allows one to resolve the kinetic system without the need to know the reaction mechanism in detail.

## 2.2. Iterative target transform factor analysis

Iterative target transform factor analysis (ITTFA) [31,32], is a member of the self-modelling curve resolution procedures. Such algorithms are able to calculate the underlying pure spectral and concentration profiles by making only very general assumptions about the model of these profiles. The ITTFA method is generally applicable for quantitative analysis of an analyte with unknown

interferences [33,34]. It also has been applied to resolve kinetic data [35], and for simultaneous analysis by multivariate calibrations [36].

The ITTFA method has two principal steps—(i) the kinetic data matrix, which is obtained from a set of reference samples and an unknown, is decomposed into three matrices by the singular value decomposition (SVD) method, and (ii) a projection matrix for concentrations, corresponding to the kinetic data in (i), is then obtained from the result of the SVD. Concentrations of unknowns are initialised with best guesses, and these are then refined by an iterative calculations of the target transform. Iteration is repeated until convergence. ITTFA is different from the classical factor analysis methods [37]; with this method, the kinetic data of the unknown as well as that of the reference samples are used for calibration.

## 2.3. Partial least squares and principal component regression

Partial least squares regression (PLS) and principal component regression (PCR) [38,39] are two well known prediction methods, which use statistically significant orthogonal factors to build regression models to determine the linear relationship between the dependent and independent variables. PCR is similar to PLS in that both are linear inverse least squares regression models. However, an important difference between the methods is that PCR [17] takes into account changes only in the independent variables whereas PLS, in addition, models the dependent variables. In general, PLS fits non-linear data somewhat better than PCR but neither method is designed for non-linear modelling.

## 2.4. Principal component-radial basis function-artificial neural network

In recent years, artificial neural network (ANN) modelling has been often applied to biological and pharmaceutical problems [40,41]. Some advantages of ANN methods include their denoising ability and their capacity to model non-linear data. Back propagation-artificial neural network (BP-ANN) [42,43] is a well known model but its modelling functions can be quite complex, and can encourage black box behaviour. Generally, Radial basis function-artificial neural network (RBF-ANN) are less commonly applied, although they have a simple structure, well-established theoretical basis and fast learning speed [44]. In this study, the classical architecture of the RBF model is based on previous work [45]. It has three different layers: (i) the input nodes; (ii) the hidden layer, which contains the kernel nodes with local functions dependent on their centre,  $c_j$ , and width,  $\sigma_j$ , and the outputs from the  $j$ th kernel neurons for input objects,  $x_i$ . This can be calculated by:

$$\text{output}_j = o_j(\mathbf{x}) = \exp \left( \frac{-|x_i - c_j|^2}{\sigma_j} \right) \quad (13)$$

where  $|x_i - c_j|$  is the Euclidean distance between  $x_i$ ; (iii) the output nodes, which compute the weighted sum of the hidden node outputs:

$$y_i = \sum_{j=1}^n \omega_{ji} o_j(x) \quad (14)$$

where  $\omega_{ji}$  represents the weights of the connections between the hidden layer,  $i$ , and output layer,  $j$ , and  $o_j(\mathbf{x})$  is obtained from Eq. (13).

Principal component analysis (PCA) is a well-known data display method, and compresses data into orthogonal PCs. In this work, the kinetic data matrix was compressed with the use of PCA e.g. [18], and the PC scores were used for further modelling with the RBF-ANN methods.

## 2.5. Wavelet packet transform

In general, wavelets are mathematical functions that divide data into frequency parts of different size, and then investigate each part separately using a resolution suitable for its scale. Typical applications include image compression and de-noising data, and in this paper, WPT has been applied for signal de-noising as a spectral pre-treatment. An important advantage of this methodology for this purpose is that it is carried out without signal smoothing. This produces a cleaned-up profile that has not lost important details [46]. Details associated with the WPT theory, modelling and applications may be found elsewhere. Here, we provide some background commencing with the generation of a wavelet packet,  $W_{jnk}$ , from a base function [47,48].

$$W_{jnk}(x) = 2^{(-j/2)}W_n(2^{-j}x - k) \quad (15)$$

where indices  $j$ ,  $n$  and  $k$  refer to the scale, oscillation and localisation parameters, respectively.  $j, k \in Z$ , where  $Z$  refers to a set of integers,  $n = 0, 1, 2, \dots, 2^j - 1$ . In WPT analysis, a signal,  $f(x)$ , is represented as the sum of orthogonal wavelet packet functions,  $W_{jnk}(x)$ , for different scales, oscillations and localities:

$$f(x) = \sum_j \sum_n \sum_k C_{jnk} W_{jnk}(x) \quad (16)$$

where  $C_{jnk}$  represents the wavelet packet coefficients, and is given by:

$$C_{jnk} = \int_{-\infty}^{\infty} f(x)W_{jnk}(x) dx \quad (17)$$

The whole orthonormal basis set is called the wavelet packet library, and every element of this library is determined by the function,  $W_{jnk}(x)$ . The Discrete wavelet transform (DWT) can be implemented with the use of Mallat's pyramid algorithm described elsewhere [49,50], and the WPT can be considered as an extension of DWT. Thus, a fast wavelet packet transform (FWPT) may be formulated as follows:

$$W_{j+1,2n} = HW_{jn} \quad (18)$$

$$W_{j+1,2n+1} = GW_{jn} \quad (19)$$

where  $W_{0,0}$  indicates the measured signal,  $f, H = \{h_l\}_{l \in Z}$  and  $G = \{g_l\}_{l \in Z}$  are the low- and high-pass matrix filters. The first and second indices of  $W$  indicate the level of decomposition and its position at that level. The reconstruction can be facilitated by:  $(20)W_{j,n} = H^*W_{j+1,2n} + G^*W_{j+1,2n+1}$  where  $H^*$  and  $G^*$  represent the conjugate matrices of  $H$  and  $G$ .

The wavelet packet de-noising procedure includes four steps: (i) WPT, (ii) estimation of the best basis function, (iii) thresholding of the wavelet packet (WP) coefficients, and (iv) reconstruction. A suitable basis function may be selected according to the entropy-based criterion described by Coifman and Wickerhauser [23]. This is followed by the thresholding of the WP coefficients. Only the coefficients whose absolute values are higher than a predefined threshold value are retained. This may be implemented by Donoho's SURE method [51], which is based on Stein's unbiased risk estimation [52], and the estimated WP coefficients can be defined in either hard or soft thresholding. Finally, by utilizing inverse WPT, the de-noised coefficients can be converted back to the original domain.

In this work, the original spectral data matrix representing the kinetic experiments was pre-treated by the WPT one-object-at-a-time, and then this matrix was submitted for analysis by the various mentioned chemometrics methods for the simultaneous prediction of the five colorants.

## 3. Experimental

### 3.1. Apparatus and software

Kinetic and spectral measurements were performed with the use of an Agilent 8453 diode array spectrophotometer equipped with a 10 mm thermostated cell compartment at 75 °C (temperature control accessory: Model ZC-10 (Ningbo Tianheng Instruments Factory, China)). The pH was measured with an SA-720 pH meter (Orion). The obtained data were processed by a Pentium computer with programs written in-house in MATLAB 6.5 (Mathworks).

HPLC measurements were made with an Agilent 1100 Series HPLC-DAD system, a vacuum degasser, quaternary pump, autosampler, injector with a 100  $\mu$ L loop, an Agilent ZORBAX Eclipse XDB-C18 column (4.6 mm  $\times$  250 mm, 5  $\mu$ m) together with an Agilent Zorbax high pressure reliance cartridge guard-column (C18, 12.5 mm  $\times$  4.6 mm, 5  $\mu$ m) and a variable wavelength UV visible detector.

### 3.2. Reagents

All reagents were of Analytical Reagent grade. Deionised distilled water (DW) was used throughout. Stock standard solutions (500 mg L<sup>-1</sup>) of Amaranth, Ponceau 4R, Sunset Yellow, Tartrazine and Brilliant Blue dyes (Source: Sixth Dye Chemical Factory of Shanghai) were prepared and stored at 4 °C in the dark. They were diluted with water (DW) as required. A 1.0 mol L<sup>-1</sup> sodium acetate–hydrochloric acid buffer (pH range: 0.65–4.19) was used to adjust the acidity of the reaction solution. A mixed solution containing the iron(III) (0.006 mol L<sup>-1</sup>) and hexacyanoferrate(III) ions (0.030 mol L<sup>-1</sup>) was prepared by dissolving 1.446 g of solid Fe<sub>2</sub>(SO<sub>4</sub>)<sub>3</sub>(NH<sub>4</sub>)<sub>2</sub>SO<sub>4</sub>·24H<sub>2</sub>O (The Second Reagent Factory of Shanghai) and 2.469 g of solid K<sub>3</sub>Fe(CN)<sub>6</sub> (The First Reagent Factory of Shanghai) in water (DW), and this was diluted to 250 mL.

### 3.3. Analytical procedure

Selected volumes of each standard dye solution—Amaranth, Ponceau 4R, Sunset Yellow, Tartrazine and Brilliant Blue (total dye solution volume:  $x$  mL), were micropipetted directly into the cell as required by the particular experiment. This was followed by 0.3 mL of 1.0 mol L<sup>-1</sup> sodium acetate–hydrochloric acid solution (pH 1.71) and (1.8 –  $x$ ) mL of water. After the mixture was thermostated at 75 °C for 2 min, 0.4 mL of the mixed solution containing the iron(III) and hexacyanoferrate(III) ions (in most of the experiments a volume of 0.4 mL was used) was added to give a total volume of 2.5 mL. The mixture was stirred throughout the reaction. The kinetic data were collected from 500 to 1000 nm, every 1 nm, at 2 s intervals during 600 s.

### 3.4. Procedure for the determination of the five analyte dyes

Apart from the synthetic dye working solutions noted above, the verified calibration models were applied for the determination of the dyes in various kinds of drink, e.g., fruit juices and tea, as well as in jellies. A drink sample (50 mL) was transferred to a 100 mL flask, boiled and stirred continuously to remove carbon dioxide. A jelly was mulled until it was broken up into small pieces, and then 5 g of this sample was placed in 50 mL of water (DW), and gently warmed until completely dissolved. The pH of a sample solution, drink or jelly, was adjusted to 4 with 20% citric acid. Subsequently, the solution of drink or jelly obtained above was warmed on a water-bath allowing the temperature to increase to 70 °C. 0.5 g of polyamide adsorbent powder (The Second Reagent Factory of Shanghai) was added, and the mixture was stirred vigorously until the solution was colorless (if color persisted, a small

amount of the polyamide powder adsorbent was added). The adsorbent was quantitatively filtered off and washed with 20 mL water (DW) three times at 70 °C. It was then washed several times with a solution of ethanol–ammonia (90:10) to desorb all the colorants. The dye solution collected was warmed on a water-bath to allow the ammonia to evaporate, and it was then transferred into a 50 mL volumetric flask. The pH was adjusted to 4 with suitable additions of 20% citric acid, and the solution was diluted to the mark with distilled water. The colorants in these solutions were then analysed according to the methods described above.

### 3.5. Chromatographic procedure

The determination of Amaranth, Ponceau 4R, Sunset Yellow, Tartrazine and Brilliant Blue dyes in commercial products was verified by HPLC at 252 nm (for the first four dyes) and 630 nm (Brilliant Blue) [53]. Two solutions were used for the mobile phase: (A) methanol and (B)  $2 \times 10^{-3}$  mol L<sup>-1</sup> ammonium acetate. Gradient was developed as follows: 10% (v/v) solution A was retained between 0 and 3 min, during 3–12 min the solution A (v/v) ratio was varied from 10% to 70%, and finally, between 12 and 15 min 70% (v/v) solution A was retained. The flow rate was kept at 0.15 mL min<sup>-1</sup> and under these conditions, the retention times were 3.0, 3.7, 4.5, 10.2 and 11.0 min for Tartrazine, Amaranth, Ponceau 4R, Sunset Yellow and Brilliant Blue, respectively. 20 µL of each sample solution was injected, and the concentrations were calculated on the basis of peak area ratios.

## 4. Results and discussion

### 4.1. Spectral and kinetic characteristics

The UV–visible absorption spectra of the individual samples of Amaranth, Ponceau 4R, Sunset Yellow, Tartrazine and Brilliant Blue (Fig. 1A) showed broad bands in the 300–700 nm range. These included the main information for each colorant, but the spectra overlapped significantly. When each of the five dye analytes was treated with iron(III) and the hexacyanoferrate(III) ions solutions, then each of the original dye spectra was replaced by that of the Prussian blue product (Fig. 1B). The profiles of these Prussian blue spectra occurred between 500 and 1000 nm ( $\lambda_{\max} = 760$  nm), but their intensities differed because of their different concentrations. The kinetic profiles of the five colorants were measured between 0 and 600 s at 760 nm (Fig. 2), and the kinetic pseudo-reaction rate constant for each dye i.e.,  $k_2$  in the reaction scheme (Section 2.1.) were extracted from these profiles by conventional procedures [54]. They were: Amaranth (0.0012 s<sup>-1</sup>), Ponceau 4R (0.0038 s<sup>-1</sup>), Sunset Yellow (0.0005 s<sup>-1</sup>), Tartrazine (0.0001 s<sup>-1</sup>), and Brilliant Blue (0.0036 s<sup>-1</sup>). The values of these constants vary by about a factor of 40 between the lowest for Tartrazine (0.0001) and the highest for Ponceau 4R (0.0038). These differences facilitate the application of the two-way chemometrics methods for the analysis of the five synthetic colorants.

### 4.2. Selection of experimental conditions

Spectral absorption of the kinetic system was influenced by the following experimental conditions: (i) concentration of the solution containing the iron(III) and hexacyanoferrate(III) ions, (ii) pH of the sodium acetate–hydrochloric acid solution, and (iii) temperature. All these factors were investigated one at a time.

The effect of the concentration of the mixed solution of iron(III) (0.006 mol L<sup>-1</sup>) and hexacyanoferrate(III) (0.03 mol L<sup>-1</sup>) on absorbance was studied in the range of 0.05–0.5 mL of above mixed solution, which was added to the cell as described in the Section

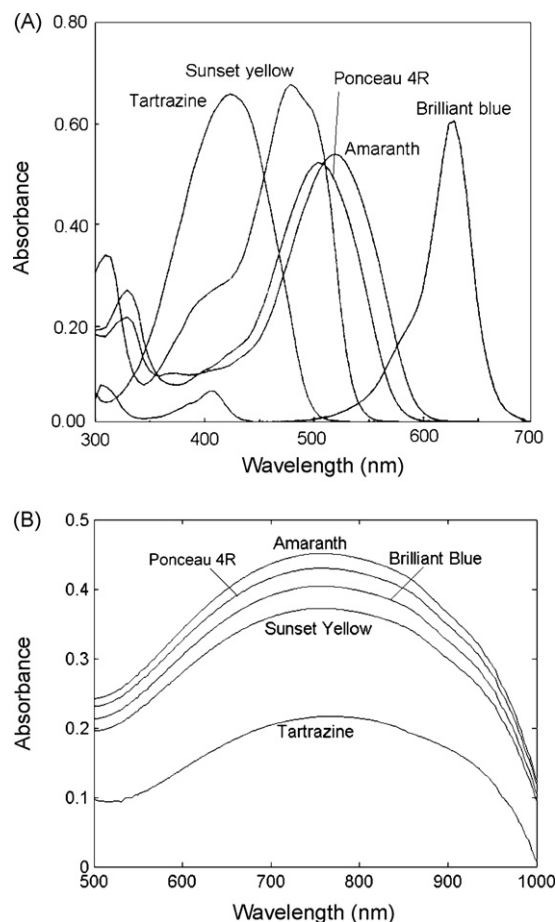


**Fig. 1.** (A) Absorption spectra of Amaranth (2.0 mg L<sup>-1</sup>), Ponceau 4R (3.0 mg L<sup>-1</sup>), Sunset Yellow (1.0 mg L<sup>-1</sup>), Tartrazine (4.0 mg L<sup>-1</sup>) and Brilliant Blue (0.8 mg L<sup>-1</sup>) in sodium acetate/hydrochloric acid solution (pH 1.71) at  $t = 600$  s. (B). Absorption spectra of the five analyte dyes after treatment with the iron(III) and hexacyanoferrate(III) ions. Other experimental conditions:  $T = 75$  °C,  $c_{\text{iron(III)}} = 9.6 \times 10^{-4}$  mol L<sup>-1</sup>,  $c_{\text{hexacyanoferrate(III)}} = 4.8 \times 10^{-3}$  mol L<sup>-1</sup>.

3.3. The results showed that the absorbance of these five synthetic colorants increased with the added amount of this mixed solution up to 0.4 mL. Hence, 0.4 mL of the mixed solution was added as the optimum amount (i.e. the concentrations of iron(III) and hexacyanoferrate(III) in the cell were 0.96 and 4.8 mmol L<sup>-1</sup>, respectively).

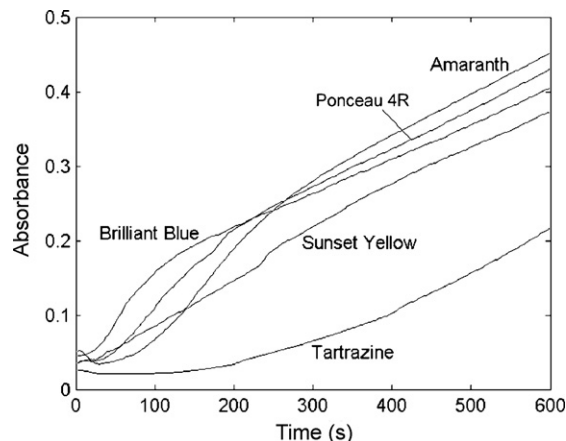


**Fig. 2.** Kinetic profiles for Amaranth, Ponceau 4R, Sunset Yellow, Tartrazine and Brilliant Blue dyes under the experimental conditions in Fig. 1.

The effect of the sodium acetate–hydrochloric acid medium (pH range: 0.65–5.20) was investigated on the above Prussian blue solution, and it was found that the absorbance ( $\lambda = 760$  nm) in the case of each colorant increased until pH 1.71, and then decreased for most colorants. Hence, pH 1.71 was selected for the experiments.

The effect of temperature (range: 55–85 °C) on the absorbance of the above Prussian blue solution was also studied. The results showed that the absorbance reached a steady value for each colorant at 75 °C. Therefore, this temperature was selected to facilitate the experimental work.

#### 4.3. Calibration models for single analytes

The absorbance of each colorant at different concentrations was measured at 760 nm as a function of time (Fig. 3). Linear calibration equations and their relative parameters (Table 2) were established at 600 s. The correlation coefficients for all calibration models (each based on 7 standards) were 0.9999. The linear ranges and the limits of detection (DL) were, respectively, as follows: Amaranth (0.2–8.0 mg L<sup>-1</sup>, 0.095 mg L<sup>-1</sup>), Ponceau 4R (0.5–6.0 mg L<sup>-1</sup>, 0.17 mg L<sup>-1</sup>), Sunset Yellow (0.5–18.0 mg L<sup>-1</sup>,

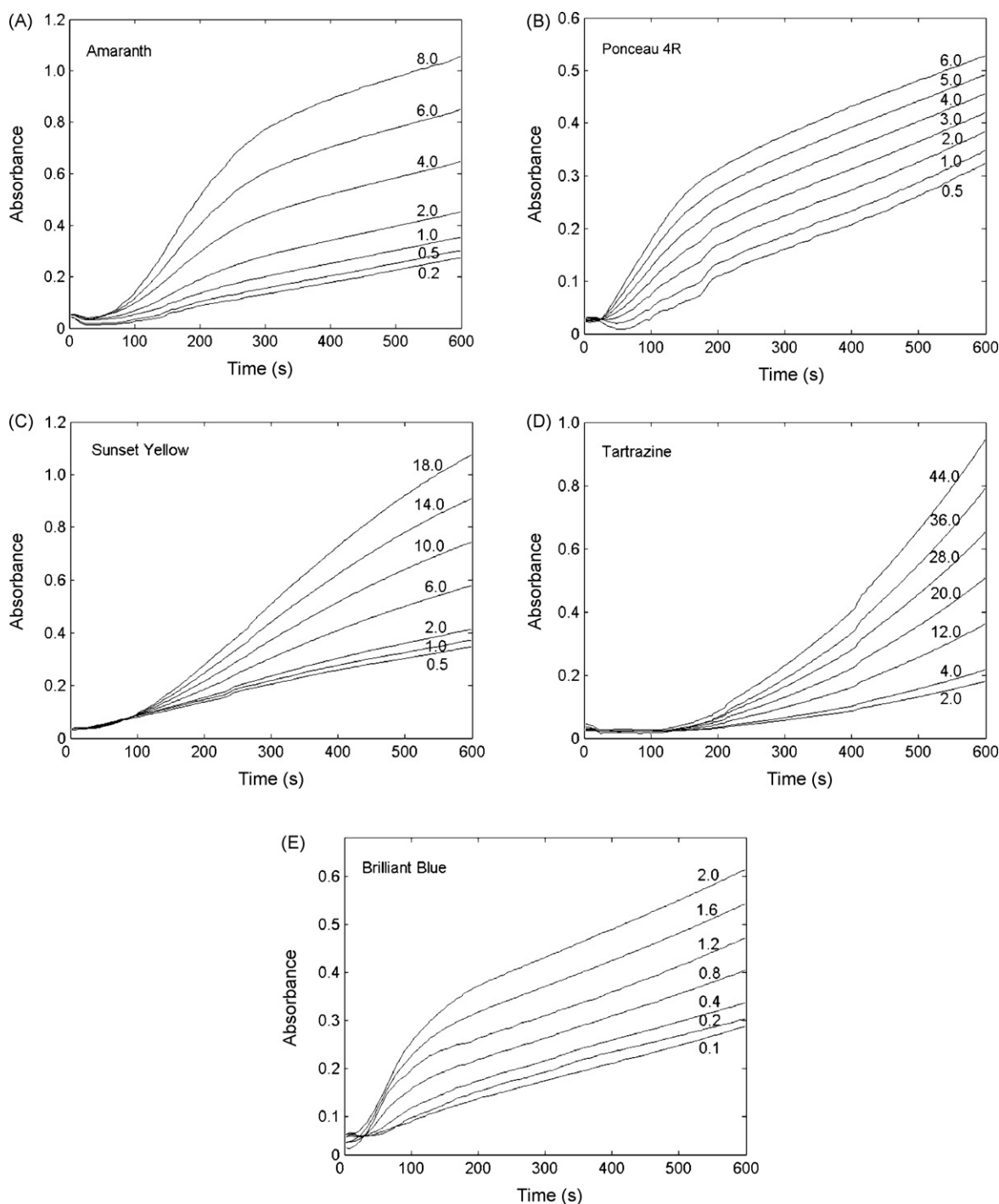


**Fig. 3.** Kinetic profiles for Amaranth, Ponceau 4R, Sunset Yellow, Tartrazine and Brilliant Blue dyes with different concentrations (mg L<sup>-1</sup>). Experimental conditions are as in Fig. 1.



**Table 2**  
Comparison of analytical figures of merit for the determination of Amaranth, Ponceau 4R, Sunset Yellow, Tartrazine and Brilliant Blue ( $t = 600$  s).

Parameter	Amaranth	Ponceau 4R	Sunset Yellow	Tartrazine	Brilliant Blue
Number of samples ( $n$ )	7	7	7	7	7
Linear range ( $\text{mg L}^{-1}$ )	0.2–8.0	0.5–6.0	0.5–18.0	2.0–44.0	0.1–2.0
Correlation coefficient	0.9999	0.9997	0.9999	0.9999	0.9999
Slope ( $\text{L mg}^{-1}$ )	0.095	0.037	0.042	0.018	0.17
Intercept	0.25	0.39	0.33	0.14	0.27
$s_R (\times 10^{-3})^a$	3.2	2.1	1.9	3.1	2.2
$s_S (\times 10^{-4})^a$	4.3	4.1	0.11	0.79	1.2
$s_I (\times 10^{-3})^a$	1.8	1.5	1.1	2.0	1.4
DL ( $\text{mg L}^{-1}$ ) <sup>a</sup>	0.095	0.17	0.14	0.51	0.038

<sup>a</sup>  $s_R$ ,  $s_S$ ,  $s_I$  and DL are the standard deviation of the regression, slope, and intercept as well as and the detection limits, respectively. They were calculated according to Miller's method [55].

0.14  $\text{mg L}^{-1}$ ), Tartrazine (2.0–44.0  $\text{mg L}^{-1}$ , 0.51  $\text{mg L}^{-1}\text{s}^{-1}$ ), and Brilliant Blue (0.1–2.0  $\text{mg L}^{-1}$ , 0.038  $\text{mg L}^{-1}$ ). These compare well or outperform results of similar previous studies [5–12] on the basis of the figures of merit. In our previous spectrophotometric work [11], the linear ranges were 2.0–18.0  $\text{mg L}^{-1}$  for Amaranth, Ponceau 4R and Tartrazine, 2.0–20.0 for Sunset Yellow, and 0.4–3.6  $\text{mg L}^{-1}$  for Brilliant Blue, the limit of quantitation, which is regarded as the lower limit for precise quantitative measurements [56], for each analyte, is much higher than for the present method. Chen et al. [5] reported a liquid chromatography method for analysis of eight synthetic colorants, and the DL values for Amaranth, Ponceau 4R, Sunset Yellow, Tartrazine and Brilliant Blue were 1.0, 0.5, 2.0, 0.5 and 0.03  $\text{mg L}^{-1}$ , respectively. Three of these values (Amaranth, Tartrazine and Brilliant Blue) were similar to our work, but two (Ponceau 4R, Sunset Yellow) were higher than our work. Thus, these results clearly show that the proposed method is a somewhat improved and appropriate procedure for the determination of the individual analytes. It was noted that the intercept values are rather high, ca. 0.3 absorbance units, which suggested that there were contributions from dye impurities to the chromogenic reaction, and this was reflected in the background.

#### 4.4. Multivariate calibration

##### 4.4.1. Composition of the calibration and the prediction sets

Calibration and prediction sets, each of 16 samples, were prepared and each sample included the five analyte dyes. These samples were made at four concentration levels, according to the orthogonal design, denoted by  $OA_{16}(4^5)$  [57]. The levels corresponded to values in the range of 0.5–4.0, 0.5–4.0, 0.5–8.0, 2.0–10.0

and 0.2–1.0  $\text{mg L}^{-1}$  for Amaranth, Ponceau 4R, Sunset Yellow, Tartrazine and Brilliant Blue, respectively. According to the analytical procedure described in Section 3.3, the measured kinetic data matrix,  $\mathbf{A}$  (16 objects and 301 wavelength variables), and the calibration concentration matrix,  $\mathbf{C}$  (dimensions;  $16 \times 5$ ), were constructed. These two matrices were used to establish calibration models with methods such as ITTFA, PCE, PLS, RBF-ANN and PC-RBF-ANN (see details, Table 3). These models were then used for prediction of unknown samples.

##### 4.4.2. Wavelet packet de-noising

As WPT is applied to one response-object-at-a-time, rather than to a set of responses, the mean kinetic profile of the calibration data matrix i.e. response,  $f$ , was selected and was submitted for processing by the FWPT method. Since the objective of the WPT procedure is to extract the cleaned-up signal from the original one (within the experimental error), it is important to have the optimum wavelet function for any given application because such functions are not transferable from one case to another. To find the optimum wavelet function as well as the wavelet decomposition level, Relative mean square difference (RMSD) between the original signal,  $f$ , and the reconstructed one were calculated:

$$\text{RMSD} = \frac{\text{norm}(f - a)}{\text{norm}(f)}$$

where 'norm' refers to the Euclidean norm:

$$\text{norm}(f) = \|f\| = \left( \sum_{j=1}^n |f_j|^2 \right)^{0.5} \quad (21)$$

**Table 3**  
Comparison of prediction results for synthetic samples obtained with the aid of different chemometrics methods.

Chemometrics methods	%RPE <sub>S</sub>					%RPE <sub>T</sub>
	Amaranth	Ponceau 4R	Sunset Yellow	Tartrazine	Brilliant Blue	
<i>Without wavelet packet transform pre-treatment</i>						
ITTFA	35.8 (118) <sup>a</sup>	35.6 (117)	47.7 (187)	34.8 (124)	30.4 (110)	38.6
PCR (7) <sup>b</sup>	9.3 (104)	11.1 (105)	11.1 (123)	9.5 (107)	9.1 (107)	10.0
PLS (6) <sup>b</sup>	9.4 (104)	12.0 (105)	10.7 (122)	9.4 (106)	8.7 (107)	9.9
RBF-ANN (9, 500) <sup>c</sup>	8.3 (103)	11.7 (106)	10.8 (118)	9.5 (107)	8.7 (107)	9.9
PC-RBF-ANN (6, 9, 2100) <sup>d</sup>	8.9 (105)	12.7 (108)	9.4 (119)	8.5 (106)	8.0 (106)	9.2
<i>With wavelet packet transform pre-treatment</i>						
ITTFA	35.6 (118)	35.7 (117.9)	41.7 (187)	34.8 (124)	30.4 (110)	38.0
PCR (6) <sup>b</sup>	8.1 (104)	11.4 (107)	8.9 (117)	9.2 (106)	8.4 (106)	9.2
PLS (6) <sup>b</sup>	7.8 (104)	10.9 (106)	8.9 (117)	9.2 (106)	8.5 (106)	9.1
RBF-ANN (8, 1800) <sup>c</sup>	8.2 (104)	12.6 (107)	9.3 (118)	9.6 (106)	8.5 (106)	9.7
PC-RBF-ANN (6, 7, 1450d) <sup>d</sup>	7.7 (104)	10.9 (107)	8.6 (117)	8.6 (106)	8.0 (106)	8.7

<sup>a</sup> Values in parentheses correspond to mean Recoveries (%).

<sup>b</sup> Values in parentheses correspond to number of factors used for PCR and PLS models.

<sup>c</sup> Values in parentheses correspond to nodes in the hidden layer and the spread coefficient (sc), respectively.

<sup>d</sup> Values in parentheses correspond to number of components used in PCA, nodes in the hidden layer and the spread coefficient (sc), respectively. PC scores were used as data for ANN training.

Clearly, the smallest RMSD indicates the optimum de-noising parameters. The wavelet functions tested were Daubechies 2, 6, ..., 20, Coiflet 1, 2, ..., 5, and Symmlet 2, 3, ..., 8, as well as the decomposition levels, 1–9. The RMSD values were distributed over a narrow range of  $(3.62\text{--}3.72) \times 10^{-4}$  and thus, the function with the lowest RMSD value, the Sym4 function ( $3.62 \times 10^{-4}$ ) was selected. However, the effect of the decomposition level was much more pronounced with the range being 3.62–790 in increasing order, and level 1 was chosen. In general it appears that the RMSD values strongly depended on the decomposition level.

Following the selection of the two key modelling parameters, each kinetic profile in the calibration set and the prediction set were processed individually, i.e. one row of the data matrix-at-time. Thus, each row vector of the calibration matrix and the predic-

tion one was decomposed and then reconstructed in the same way. The resulting WPT pretreated data matrix was then submitted to a variety of chemometrics methods, such as ITTFA, PCR, PLS, and PC-RBF-ANN.

#### 4.4.3. Prediction ability of the different calibration models

The performance of the different calibration models was assessed in terms of %RPE<sub>S</sub> and %Recovery (percent relative prediction error and mean recovery) for the individual compounds, and %RPE<sub>T</sub> for all compounds (total error) [15], with and without the WPT pre-treatment (Table 3, important parameters are in the footnotes).

An overview of the performance of the prediction models showed that the ITTFA method was significantly worse than all oth-

**Table 4**

Comparison of Amaranth, Ponceau 4R, Sunset Yellow, Tartrazine and Brilliant Blue concentrations in commercial products as determined by the proposed spectrophotometric method with that determined by the reference HPLC method. Wavelet Packet Transform data pre-treatment followed by PC-RBF-ANN calibration model.

Methods	PC-RBF-ANN ( $\mu\text{g g}^{-1}$ )	HPLC ( $\mu\text{g g}^{-1}$ )	RSE (%)
<i>1. Drink (Orange Flavour), Nanchang</i>			
Amaranth	0.92 ± 0.02 <sup>a</sup>	0.89 ± 0.01 <sup>a</sup>	3.4 <sup>b</sup>
Ponceau 4R	0.55 ± 0.01	0.57 ± 0.02	−3.5
Sunset Yellow	21.55 ± 0.04	21.41 ± 0.03	0.7
Tartrazine	5.76 ± 0.02	5.67 ± 0.02	1.6
Brilliant Blue	ND <sup>c</sup>	ND	− <sup>d</sup>
<i>2. Drink (Green Apple Flavour), Nanchang</i>			
Amaranth	4.76 ± 0.01	4.52 ± 0.02	5.3
Ponceau 4R	4.51 ± 0.02	4.57 ± 0.02	−1.3
Sunset Yellow	ND	ND	−
Tartrazine	ND	ND	−
Brilliant Blue	0.77 ± 0.02	0.72 ± 0.01	6.9
<i>3. Iced Tea, Wuhan</i>			
Amaranth	10.19 ± 0.03	10.09 ± 0.02	1.0
Ponceau 4R	2.29 ± 0.02	2.35 ± 0.02	−2.6
Sunset Yellow	ND	ND	−
Tartrazine	9.47 ± 0.02	9.55 ± 0.01 <sup>a</sup>	−1.0
Brilliant Blue	1.86 ± 0.01	1.82 ± 0.02	2.2
<i>4. Pineapple Beer, Zhaoqing</i>			
Amaranth	10.60 ± 0.02	10.32 ± 0.02	2.7
Ponceau 4R	16.20 ± 0.03	16.31 ± 0.01	−1.0
Sunset Yellow	ND	ND	−
Tartrazine	ND	ND	−
Brilliant Blue	0.59 ± 0.02	0.61 ± 0.01	−3.3
<i>5. Guoyuan Drink, Hangzhou</i>			
Amaranth	ND	ND	−
Ponceau 4R	ND	ND	−
Sunset Yellow	21.26 ± 0.02	21.13 ± 0.02	1.0
Tartrazine	5.75 ± 0.01	5.80 ± 0.01	−1.0
Brilliant Blue	ND	ND	−
<i>6. Fruit Jelly 1, Dongguan</i>			
Amaranth	2.43 ± 0.01	2.35 ± 0.02	3.4
Ponceau 4R	6.16 ± 0.01	6.21 ± 0.02	−1.0
Sunset Yellow	ND	ND	−
Tartrazine	ND	ND	−
Brilliant Blue	0.38 ± 0.01	0.40 ± 0.01	−5.0
<i>7. Fruit Jelly 2, Dongguan</i>			
Amaranth	3.92 ± 0.03	3.95 ± 0.01	−1.0
Ponceau 4R	7.65 ± 0.02	7.52 ± 0.03	1.7
Sunset Yellow	ND	ND	−
Tartrazine	ND	ND	−
Brilliant Blue	0.54 ± 0.02	0.51 ± 0.01	5.9
<i>8. Jelly, Shenzhen</i>			
Amaranth	0.53 ± 0.03	0.55 ± 0.017	−3.6
Ponceau 4R	5.75 ± 0.01	5.68 ± 0.01	1.2
Sunset Yellow	ND	ND	−
Tartrazine	ND	ND	−
Brilliant Blue	0.59 ± 0.021	0.62 ± 0.02	4.8

<sup>a</sup> Mean value of five determinations ± standard deviations.

<sup>b</sup> Relative standard error between the PC-RBF-ANN calibration and the reference HPLC method.

<sup>c</sup> ND means not present.

<sup>d</sup> The values between −0.04 and 0.04 mg L<sup>−1</sup>.

ers (%RPE<sub>T</sub> ~ 38%, %Recovery: mostly about 117% with over 180% for Sunset Yellow); thus, it will not be discussed further. With the other five methods, the %Recovery values were uniformly acceptable for Amaranth, Ponceau 4R, Sunset Yellow, Tartrazine and Brilliant Blue dyes (100–107%) and arguably borderline for Sunset Yellow analyte (115–123%). On the basis of the %RPE<sub>T</sub>, no particular prediction model with or without wavelet pre-treatment, performed significantly better than the others (%RPE<sub>T</sub> range 10–8.0%). Thus, on this basis no prediction model stands out clearly as the preferred method. A more detailed examination of the %RPE<sub>S</sub> information suggests that PC-RBF-ANN with WPT pre-treatment is a somewhat better performing model than the PCR and PLS ones. Also, this model performed well for the prediction of the five analytes with all %RPE<sub>S</sub> below 10%, and with the WPT pretreatment the results were arguably somewhat better. The PC-RBF-ANN model performed better than the RBF-ANN model with or without WPT pre-treatment. This is supported by the literature [58]. Thus, it could be concluded that the PC-RBF-ANN with the WPT pretreatment is a marginally better performing method.

#### 4.5. Interferences

To investigate the selectivity of the proposed method, the effect of various substances on the determination of a mixture contained 1.0 mg L<sup>-1</sup> of each of the five dyes was tested under optimum conditions, and the concentrations of the analyte dyes were predicted by the PC-RBF-ANN with the WPT pre-treatment model. Several representative potential interferents such as inorganic cations, anions and molecular species were investigated individually for their effect on the dye mixture and the subsequent spectra. The concentration of the tested interferent was increased until a RPE<sub>T</sub> of 10% on the determination of the mixture of Amaranth, Ponceau 4R, Sunset Yellow, Tartrazine and Brilliant Blue dyes. The maximum concentration of interfering species that could be tolerated was selected as that which produced RPE<sub>T</sub> just below 10% as defined above, and the tolerance levels were expressed as tolerance ratios (TL), i.e. mg of interferent per mg of dye. These were: 200–300—K<sup>+</sup>, Na<sup>+</sup>, Br<sup>-</sup>, Cl<sup>-</sup>, SO<sub>4</sub><sup>2-</sup>, C<sub>2</sub>O<sub>4</sub><sup>2-</sup>, CO<sub>3</sub><sup>2-</sup>; 50—tartrate, sorbate; ethyl p-hydroxyl benzoate, propyl p-hydroxyl benzoate; 30–10—Mg<sup>2+</sup>(II), Ca<sup>2+</sup>(II), Zn<sup>2+</sup>(II), Cr<sup>3+</sup>(III), Mn<sup>2+</sup>(II), Fe<sup>3+</sup>(III), starch; 5—ascorbic acid, glucose. The TL values suggest that common ions such as K<sup>+</sup>, Na<sup>+</sup>, SO<sub>4</sub><sup>2-</sup>, C<sub>2</sub>O<sub>4</sub><sup>2-</sup> were least intrusive (TL ~ 300), while ascorbic acid and glucose (TL ~ 5), were the most effective interferents. This indicates that for the analysis of the dyes in food, particular care should be taken with levels of common substances such as sugars and/or ascorbates.

#### 4.6. Application: simultaneous determination of the five analyte dyes in foodstuff samples

To illustrate the potential of the proposed method for application with real samples, simultaneous analysis for the five synthetic dyes was performed on several common food and drink items containing all or some of the five colorants. A selection of soft drinks and sweet food products was sampled (Table 4). To validate the performance of the new method, the sampled products were also analysed by HPLC as described earlier (Section 3.5).

Each of the eight different products was analysed for the five analyte dyes simultaneously. The number of dyes in different products varied from two to four, and of the forty determinations overall, 15 yielded a 'not detected' (ND) result. The overall dye concentration range was 0.38–21.55 μg g<sup>-1</sup> but the distribution of dye amounts varied considerably from sample to sample. Thus, for example, Sunset Yellow was present in just two products but in both it was in excess of 20 μg g<sup>-1</sup>, while Brilliant Blue was present in five products, and mostly, in amounts of less than 1 μg g<sup>-1</sup>.

Importantly, the comparison of the analytical results from the proposed method with those from the reference HPLC one indicated, in general, very good agreement on the basis of the relative standard error (RSE%), which reflected the difference between the prediction from the PC-RBF-ANN with WPT calibration model and that obtained from the reference HPLC analysis. The results were listed in Table 4. Twenty of the 25 recorded %RSE values were in the +3.4 to -3.6 range and the remaining five were in the 7–5% range with most of the samples belonging to the Brilliant Blue analyte, which as noted above was present in amounts of less than 1 μg g<sup>-1</sup> (This relatively low amount may have been partly responsible for the slightly higher %RSE values). Considering the 25 measurements together, there was no readily apparent bias on the basis of the %RSE values towards either the proposed spectrophotometric method or the reference HPLC one.

## 5. Conclusion

A new kinetic spectrophotometric method for the simultaneous analysis of five common food dyes has been successfully researched, developed and verified by a reference HPLC method.

- The proposed method was dependent on the reduction of iron(III) by the analyte dyes followed by the production of the Prussian blue species with the reaction of the iron(II) and the hexacyanoferrate(III) ion.
- The kinetics of this reaction were followed by spectrophotometry of the Prussian blue species, which facilitated the satisfactory prediction of the individual dye analytes.
- Simultaneous prediction models were constructed (ITFA, PCR, PLS, PC-RBF-ANN with and without the WPT pre-treatment). The ITFA model was found to be unsatisfactory, and the PC-RBF-ANN with WPT performed somewhat better than the remainder on the basis of %RPE<sub>T</sub> and %Recovery although the effect of the WPT pre-treatment was marginal (~0.5% RPE<sub>T</sub>). When this model was applied for the analysis of real foodstuff samples, the results produced were satisfactory, and were within 3–4% of those obtained with a reference HPLC method.
- These results indicate that the proposed method is satisfactory for the simultaneous determination of the five Amaranth, Ponceau 4R, Sunset Yellow, Tartrazine and Brilliant Blue dyes in food products.

## Acknowledgements

The authors gratefully acknowledge the financial support of this study by the Natural Science Foundation of China (NSFC-20562009), the State Key Laboratory of Food Science and Technology of Nanchang University (SKLF-TS-200819 and SKLF-MB-200807), the Jiangxi Province Natural Science Foundation (JXNSF0620041) and the program for Changjiang Scholars and Innovative Research Team in Universities (IRT0540).

## References

- [1] G. Otterstatter, Die Färbung von Lebensmitteln, Arzneimitteln, Kosmetika, second ed., Behr's Verlag, Hamburg, 1995.
- [2] J.J.B. Nevado, C.G. Cabanillas, A.M.C. Salcedo, Anal. Chim. Acta 378 (1999) 63–71.
- [3] J. Kirschbaum, C. Krause, S. Pfalzgraf, H. Brückner, Chromatographia 57 (suppl.) (2003) S115–S119.
- [4] V. Gianotti, S. Angioi, F. Gosetti, E. Marengo, M.C. Gennaro, J. Liq. Chromatogr. Relat. Technol. 28 (6) (2005) 923–937.
- [5] Q.C. Chen, S.F. Mou, X.P. Hou, J.M. Riviello, Z.M. Ni, J. Chromatogr. A 827 (1998) 73–81.
- [6] E.C. Vidotti, W.F. Costa, C.C. Oliveria, Talanta 68 (2006) 516–521.
- [7] M. Tripathi, S.K. Khanna, M. Das, J. AOAC Int. 87 (2004) 657–663.
- [8] M. Ma, X.B. Luo, B. Chen, S.P. Su, S.Z. Yao, J. Chromatogr. A 1103 (2006) 170–176.
- [9] E.C. Vidotti, J.C. Cancino, C.C. Oliveria, M.D.C. Rollemberg, Anal. Sci. 21 (2005) 149–153.

- [10] Y.N. Ni, M. Qi, S. Kokot, *Anal. Lett.* 34 (2001) 2585–2595.
- [11] Y.N. Ni, X.F. Gong, *Anal. Chim. Acta* 354 (1997) 163–171.
- [12] S. Sayar, Y. Ozdemir, *Food Chem.* 61 (1998) 367–372.
- [13] I.A. Darwish, *Anal. Chim. Acta* 551 (2005) 221–231.
- [14] N. Rahman, Y. Ahmad, S.N.H. Azmi, *Eur. J. Pharm. Biopharm.* 57 (2004) 359–367.
- [15] Y.N. Ni, Y. Wang, *Microchem. J.* 86 (2007) 216–226.
- [16] A. Afkhami, M. Bahram, *Talanta* 68 (2006) 1148–1155.
- [17] Y.N. Ni, Y. Wang, S. Kokot, *Anal. Lett.* 40 (2007) 1209–1226.
- [18] Y.N. Ni, C.F. Huang, S. Kokot, *Anal. Chim. Acta* 599 (2) (2007) 207–218.
- [19] T. Madrakian, A. Afkhami, R. Moein, M. Bahram, *Talanta* 72 (2007) 1847–1852.
- [20] M. Chamsaz, A. Safavi, J. Fadaee, *Anal. Chim. Acta* 603 (2007) 140–146.
- [21] L.M. Shao, X.Q. Lin, X.G. Shao, *Appl. Spectrosc. Rev.* 37 (2002) 429–450.
- [22] C.K. Chui, *An Introduction to Wavelets*, Academic Press, New York, 1993.
- [23] R.R. Coifman, M.V. Wickerhauser, *IEEE Trans. Inform. Theory* 38 (1992) 713–718.
- [24] B. Walczak, D.L. Massart, *Chemom. Intell. Lab. Syst.* 36 (1997) 81–94.
- [25] B. Walczak, D.L. Massart, *Chemom. Intell. Lab. Syst.* 36 (1997) 39–50.
- [26] E.R. Collantes, R. Duta, W.J. Welsh, W.L. Zielinski, J. Brower, *Anal. Chem.* 69 (1997) 1392–1397.
- [27] A.A. Ensafi, T. Khavamian, R. tabaraki, *Talanta* 71 (2007) 2021–2028.
- [28] N. Rahman, N. Anwar, M. Kashif, N. Hoda, *Acta Pharm.* 56 (2006) 347–357.
- [29] K. Basavaiah, U. Chandrashekar, H.C. Prameela, *IL Farmaco* 58 (2003) 141–148.
- [30] D. Harvey, *Modern Analytical Chemistry*, McGraw-Hill, New York, 2000.
- [31] P.J. Gemperline, *J. Chem. Inform. Comput. Sci.* 24 (1984) 206–212.
- [32] B.G.M. Vandeginste, W. Derks, G. Kateman, *Anal. Chim. Acta* 173 (1985) 253–264.
- [33] X. Liang, J.E. Andrews, J.A. de Haseth, *Anal. Chem.* 68 (1996) 378–385.
- [34] P.V. van Zomeren, H. Darwinkel, P.M.J. Coenegracht, G.J. de Jong, *Anal. Chim. Acta* 487 (2003) 155–170.
- [35] Z.L. Zhu, W.Z. Cheng, Y. Zhao, *Chemom. Intel. Lab. Syst.* 64 (2002) 157–167.
- [36] H. Abdollahi, M.R. Yafthian, S. Zeinali, *Anal. Chim. Acta* 531 (2005) 153–160.
- [37] E.R. Malinowski, D.G. Howery, *Factor Analysis in Chemistry*, Wiley, New York, 1980.
- [38] S. Wold, *SIAM J. Sci. Stat. Comput.* 5 (1984) 735–743.
- [39] H. Martens, T. Naes, *Multivariate Calibration*, Wiley, Chichester, 1989.
- [40] M. Cchastrette, D. Cretin, C. ElAidi, *J. Chem. Inform. Comput. Sci.* 36 (1996) 108–113.
- [41] A. Candolfi, D.L. Massart, *Appl. Spectrosc.* 54 (2000) 48–53.
- [42] T. Kohonen, *Neural Networks* 1 (1988) 3–16.
- [43] J. Zupan, J. Gasteiger, *Neural Network for Chemists, an Introduction*, VCH, Weinheim, 1993.
- [44] D. Broomhead, D. Lowe, *Complex Syst.* 2 (1988) 321–355.
- [45] J. Moody, C.J. Darken, *Neural Comput.* 12 (1989) 281–294.
- [46] F.T. Chau, Y.Z. Liang, J.B. Gao, X.G. Shao, *Chemometrics: From Basics to Wavelet Transform*, John Wiley & Sons, Hoboken, NJ, 2004.
- [47] M. Cocchi, R. Seeber, A. Ulrici, *Chemom. Intell. Lab. Syst.* 57 (2001) 97–119.
- [48] L.T. Mainardi, D. Origi, P. Lucia, G. Scotti, S. Cerutti, *Med. Eng. Phys.* 24 (2002) 201–208.
- [49] S. Mallat, W.L. Hwang, *IEEE Trans. Inform. Theory* 38 (1992) 617–643.
- [50] A.K.M. Leung, F.T. Chau, J.B. Gao, *Chemom. Intell. Lab. Syst.* 43 (1998) 165–184.
- [51] D.L. Donoho, *IEEE Trans. Inform. Theory* 41 (1995) 613–617.
- [52] C.M. Stein, *Ann. Stat.* 9 (1981) 1135–1151.
- [53] GB/T5009.35-1996, *Method for determination of synthetic colour in foods*, National Standard of the People's Republic of China, 1996.
- [54] N. Draper, H. Smith, *Applied Regression Analysis*, Wiley, New York, 1981.
- [55] J.N. Miller, *Analyst* 116 (1991) 3–14.
- [56] J.M. Miller, J.C. Miller, *Statistics and Chemometrics for Analytical Chemistry*, fourth ed., Prentice Hall, England, 2000, p. 122.
- [57] Y.N. Ni, *The Application of Chemometrics in Analytical Chemistry*, Chinese Science Press, Beijing, 2004.
- [58] H.S. Yang, P.R. Griffiths, J.D. Tate, *Anal. Chim. Acta* 489 (2003) 125–136.



# Speciation of mercury by ionic liquid-based single-drop microextraction combined with high-performance liquid chromatography-photodiode array detection

Francisco Pena-Pereira<sup>b</sup>, Isela Lavilla<sup>b</sup>, Carlos Bendicho<sup>b,\*</sup>, Lorena Vidal<sup>a</sup>, Antonio Canals<sup>a</sup>

<sup>a</sup> Departamento de Química Analítica, Nutrición y Bromatología, Universidad de Alicante, P.O. Box 99, E-03080 Alicante, Spain

<sup>b</sup> Departamento de Química Analítica y Alimentaria, Area de Química Analítica, Facultad de Química, Universidad de Vigo, Campus As Lagoas-Marcosende s/n, 36310 Vigo, Spain

## ARTICLE INFO

### Article history:

Received 4 September 2008

Received in revised form

24 November 2008

Accepted 2 December 2008

Available online 6 December 2008

### Keywords:

Mercury speciation

Ionic liquid

Single-drop microextraction

Liquid chromatography

## ABSTRACT

Room temperature ionic liquids can be considered as environmentally benign solvents with unique physicochemical properties. Ionic liquids can be used as extractant phases in SDME, being compatible with chromatographic systems. A single-drop microextraction method was developed for separation and preconcentration of mercury species (MeHg<sup>+</sup>, EtHg<sup>+</sup>, PhHg<sup>+</sup> and Hg<sup>2+</sup>), which relies on the formation of the corresponding dithizonates and microextraction of these neutral chelates onto a microdrop of an ionic liquid. Afterwards, the separation and determination were carried out by high-performance liquid chromatography with a photodiode array detector. Variables affecting the formation and extraction of mercury dithizonates were optimized. The optimum conditions found were: microextraction time, 20 min; stirring rate, 900 rpm; pH, 11; ionic liquid type, 1-hexyl-3-methylimidazolium hexafluorophosphate ([C<sub>6</sub>MIM][PF<sub>6</sub>]); drop volume, 4 μL; and no sodium chloride addition. Limits of detection were between 1.0 and 22.8 μg L<sup>-1</sup> for the four species of mercury, while the repeatability of the method, expressed as relative standard deviation, was between 3.7 and 11.6% (n=8). The method was finally applied to the determination of mercury species in different water samples.

© 2008 Elsevier B.V. All rights reserved.

## 1. Introduction

Mercury is considered a highly toxic element because of its accumulative and persistent character in the environment. It exists in a large number of different chemical and physical forms with a wide range of properties. Organometallic species of mercury are considerable more toxic than inorganic mercury, because of their high affinity to SH group of proteins and lipid tissues, which leads to accumulation of organomercury species in superior organisms [1]. Among these species, methylmercury is the most hazardous, being formed in the aquatic environment by biotic and/or abiotic processes [2]. Industrial use of inorganic and organometallic species in different activities, mainly pharmaceutical, paper, electrochemical and agriculture industries, accounts for the main anthropogenic sources [3].

Separation of mercury species before their determination is generally carried out by gas chromatography (GC) or high-performance liquid chromatography (HPLC). HPLC displays the possibility to separate a great variety of organomercury compounds (i.e. volatile and non-volatile). The detection systems used along with HPLC can be

broadly divided into three approaches: photometry, plasma techniques (ICP-MS, ICP-AES) and cold vapour atomic absorption and fluorescence spectrometry (CV-AAS, CV-AFS) [4]. Application of HPLC to speciation studies of Hg has been reviewed by Harrington [5].

Owing to the low levels of mercury species in environmental samples, a preconcentration technique is usually necessary before their determination. Single drop microextraction (SDME) [6] is a simple, low-cost, fast and environmentally friendly preconcentration technique based on a great reduction of the extractant phase-to-sample volume ratio. SDME can be operated in two different modes: headspace-single-drop microextraction (HS-SDME), when the extractant drop is exposed to the headspace of the sample, and Direct-single-drop microextraction (Direct-SDME), when analytes are extracted from the bulk aqueous phase onto a microdrop of extractant phase by immersion of the drop in a stirred aqueous sample solution. SDME is not an exhaustive technique, and only a small fraction of analytes is extracted/preconcentrated for analysis. One of the most important parameters that should be selected carefully when SDME is used is the extractant phase. The choice of extractant should be based on comparison of selectivity, extraction efficiency, incidence of drop loss, rate of drop dissolution and level of toxicity [7]. Moreover, the extractant phase should be compatible with the analytical technique ultimately employed. There are two

\* Corresponding author. Tel.: +34 986 812281; fax: +34 986 812556.  
E-mail address: [bendicho@uvigo.es](mailto:bendicho@uvigo.es) (C. Bendicho).

possibilities to select the extractant phase when the immersed-SDME mode is used: organic solvents and ionic liquids. Although organic solvents are mainly employed, the use of ionic liquids (ILs) is increasing because of their particular physicochemical properties, being environmentally friendly extractant phases [8]. 1-alkyl-3-methylimidazolium hexafluorophosphates ( $[C_n\text{MIM}][\text{PF}_6]$ ,  $n = 4, 6, 8$ ) have been used for SDME applications in both direct immersion and headspace modes for extraction. Analytes include of polycyclic aromatic hydrocarbons [9], chlorobenzenes [10,11], phenols [12,13], chloroanilines [14], trihalomethanes [15], BTEX (benzene, toluene, ethylbenzene, and xylene) [16], benzophenone-3 [17], formaldehyde [18] and 45 typical environmental pollutants [19] including BTEX, polycyclic aromatic hydrocarbons, phthalates, phenols, aromatic amines, herbicides, organotin and organomercury. As can be seen above, ILs have been used in SDME almost as a whole in the organic field.

Two papers have been published so far, where SDME is employed for extraction and preconcentration of mercury species. Gil et al. [20] employed Headspace-SDME in combination with ETAAS for determination of methylmercury after its derivatization with  $\text{NaBH}_4$  by using a microdrop of Pd(II) as both extractant and matrix modifier in the furnace. A 40-fold enrichment factor was achieved in only 2 min of microextraction. Liu et al. [19] studied the extractability of five organomercury compounds (methylmercury, ethylmercury, phenylmercury, dimethylmercury and diethylmercury) by SDME in its immersed mode combined with CV-AFS using two ILs, 1-alkyl-3-methylimidazolium hexafluorophosphate ( $[C_n\text{MIM}][\text{PF}_6]$ ,  $n = 4, 8$ ). Enrichment factors between 4 and 40 were achieved.

The aim of this study was to develop a new method for extraction and preconcentration of mercury species as dithizonates onto an ionic liquid microdrop using immersed-SDME in combination with HPLC with a photodiode array detector. Optimisation of variables such as type of ionic liquid, pH of the sample, microdrop volume, stirring rate, microextraction time and salt content in the sample were studied, and the optimized procedure was applied to determine mercury species in aqueous samples.

## 2. Experimental

### 2.1. Standard solutions and reagents

A stock standard solution of mercury (II) ( $1000 \text{ mg L}^{-1}$ ) was prepared by dissolving the corresponding amount of mercury (II) chloride from Fluka (Steinheim, Germany) in a 1%  $\text{HNO}_3$  solution. Stock standard solutions of methylmercury and ethylmercury ( $1000 \text{ mg L}^{-1}$  (as Hg)) were prepared by dissolving  $\text{CH}_3\text{HgCl}$  and  $\text{C}_2\text{H}_5\text{HgCl}$ , both from Riedel-de Haën (Seelze, Germany) in methanol. The stock standard solution of phenylmercury ( $1000 \text{ mg L}^{-1}$  (as Hg)) was prepared by dissolving  $\text{C}_6\text{H}_5\text{HgCl}$  (Riedel-de Haën, Seelze, Germany) in ethanol. Standard solutions were prepared daily by appropriate dilutions with methanol. All solutions were stored in the dark at  $4^\circ\text{C}$ .

Methanol, ethanol, acetonitrile and acetic acid were HPLC-grade, being obtained from Scharlau Chemie (Barcelona, Spain). HPLC-grade Tetrahydrofuran was purchased from Scharlau Chemie (Barcelona, Spain) and Sigma Aldrich (Steinheim, Germany).

De-ionized water (resistivity  $\geq 18 \text{ M}\Omega \text{ cm}$ ) obtained from a water purification system (Milli-Q Biocel A10) supplied by Millipore (Billerica, MA, USA) was used to prepare the mobile phase in the LC system.

Dithizone was obtained from Merck (Darmstadt, Germany) and used without further purification. The reagent solution was prepared weekly by dissolving 20.0 mg of dithizone in 100 mL of acetonitrile.

1-butyl-3-methylimidazolium hexafluorophosphate [ $\text{C}_4\text{MIM}][\text{PF}_6]$  and 1-octyl-3-methylimidazolium hexafluorophosphate [ $\text{C}_8\text{MIM}][\text{PF}_6]$  were purchased from Merck (Darmstadt, Germany), while 1-hexyl-3-methylimidazolium hexafluorophosphate [ $\text{C}_6\text{MIM}][\text{PF}_6]$  was obtained from Green Solutions (Vigo, Spain).

Sodium chloride from Merck (Darmstadt, Germany) was used to study the effect of ionic strength on the microextraction of mercury species. Analytical reagent-grade sodium acetate (99%) and ethylenediaminetetraacetic acid disodium salt (EDTA) were obtained from Aldrich (Steinheim, Germany) and Scharlau Chemie (Barcelona, Spain), respectively.

### 2.2. Water samples

Tap water from the main area water-supply network of San Vicente del Raspeig (Alicante, Spain), river water from Turia river (Valencia, Spain) and wastewater (Alicante, Spain) from a municipal wastewater treatment plant were used as water samples for recovery studies.

### 2.3. Apparatus

A Hamilton Gastight syringe (Model 1702 Hamilton Bonaduz AG, Bonaduz, Switzerland; length: 5.1 cm, i.d.: 0.015 cm) was used to suspend the drop of ionic liquid and inject it into the HPLC system.

A Waters LC system equipped with a Waters 600E high-pressure pump and a Waters 996 photodiode array detection (PDA) system set at 475 nm (Milford, MA, USA) was employed. A personal computer equipped with a Millennium 32 Waters program for LC system was used to process all chromatographic data.

A 7725i Rheodyne injector (Rohnert Park, CA, USA) and a Phenomenex C-18 ( $150 \times 4.60 \text{ mm}$  i.d.,  $3 \mu\text{m}$  particle size) column from Phenomenex (Torrance, CA, USA) were also used for injection and separation, respectively.

A Crison (Alella, Spain) micropH 2000 pH meter was used for pH measurements.

### 2.4. Procedure

A 12 mL aqueous sample solution containing  $\text{MeHg}^+$ ,  $\text{EtHg}^+$ ,  $\text{PhHg}^+$  and  $\text{Hg}^{2+}$  was added into a 20-mL amber vial, the pH value was adjusted to 11 with 1.5 mL of  $0.1 \text{ mol L}^{-1} \text{ HPO}_4^{2-}/\text{PO}_4^{3-}$  and a few drops of  $0.1 \text{ mol L}^{-1} \text{ NaOH}$ . Then, 1.5 mL of dithizone solution ( $20 \mu\text{g mL}^{-1}$  in acetonitrile) was added to the sample to form the corresponding dithizonates. The mixture was magnetically stirred for 3 min and degassed for 5 s before microextraction in order to remove the bubbles attached to the stirrer formed because of the mixture between the water sample and the acetonitrile, since bubbles can disturb the stability of the drop during the microextraction process. After that, the blunt tip of the needle of a 25- $\mu\text{L}$  Hamilton Gastight syringe was sheathed with a 3-mm long polytetrafluoroethylene (PTFE) tube (0.8 mm i.d. and 1.6 mm o.d.) to expose a 4  $\mu\text{L}$  drop of [ $\text{C}_6\text{MIM}][\text{PF}_6]$  to the sample. After stirred extraction at 900 rpm for 20 min, the remaining ionic liquid was withdrawn back into the microsyringe and then injected into the HPLC system for determination, where THF/MeOH/(0.1 M HAc/AcNa pH 4.0 + 50  $\mu\text{M}$  EDTA) (36/32/32%) at  $0.8 \text{ mL min}^{-1}$  flow rate was selected as mobile phase, based on a previous work [21]. EDTA was added to the mobile phase in order to eliminate the interference of other metal ions on Hg speciation [21].

### 3. Results and discussion

#### 3.1. Optimisation of SDME

##### 3.1.1. Selection of the ionic liquid

The selection of the most appropriate extractant phase is of major importance for the optimization of the SDME process. The optimal extractant must be selected by comparison of selectivity, extraction efficiency, incidence of drop loss, rate of drop dissolution and level of toxicity [7]. Moreover, it must be compatible with the analytical technique employed. In the last years, ionic liquids (ILs), especially 1-alkyl-3-methylimidazolium hexafluorophosphates ( $[C_nMIM][PF_6]$ ,  $n=4, 6, 8$ ), have been used as extractant phases in single-drop microextraction as an alternative to organic solvents because of their properties, being compatible with the mobile phase used in RP-HPLC. Three different ionic liquids, including  $[C_4MIM][PF_6]$ ,  $[C_6MIM][PF_6]$  and  $[C_8MIM][PF_6]$ , were tested as extractants of the corresponding mercurial dithizonates.

The experiments were performed by extraction, after derivatization with dithizone, of a fortified ultrapure water sample (12 mL at a level of  $50 \mu\text{g L}^{-1}$  (as Hg) of  $\text{MeHg}^+$ ,  $\text{EtHg}^+$  and  $\text{PhHg}^+$ , and  $100 \mu\text{g L}^{-1}$  of  $\text{Hg(II)}$ ) stirred at 900 rpm for 20 min (except for  $[C_4MIM][PF_6]$ , where 10 min were used because of the higher dissolution rate of the drop). The results showed that  $[C_6MIM][PF_6]$  exhibited the highest extraction efficiency for all the analytes when compared with the other ionic liquids. Moreover,  $[C_6MIM][PF_6]$  was the only IL with the ability to extract inorganic mercury under these conditions (Fig. 1). Therefore,  $[C_6MIM][PF_6]$  was selected as the best extractant.

##### 3.1.2. Effect of the pH

The pH of the aqueous sample can cause important effects in the extraction of mercury dithizonates since it can facilitate the corresponding derivatization reaction. The effect of the pH of the aqueous sample was studied in the range 3–11. Given that SDME is generally affected by the ionic strength of the sample, 1 mL of a  $0.1 \text{ mol L}^{-1}$   $\text{HPO}_4^{2-}/\text{PO}_4^{3-}$  solution was used in this optimisation to avoid the modification of the sample composition. After the microextraction process, the sample pH was checked and was observed that it maintained its original value. As can be observed in Fig. 2, an increase in the extraction efficiency of mercury dithizonates is achieved by increasing the sample pH from 7 to 11. Then, a pH value of 11 was used for all the subsequent extractions.

##### 3.1.3. Microdrop volume

Microdrop volumes of  $[C_6MIM][PF_6]$  were studied in the range 2–4  $\mu\text{L}$ . The effect of this variable was studied by exposing different drop volumes of the IL to 12 mL of an aqueous sample stirred at 900 rpm for 20 min. An almost linear increase on the analyti-

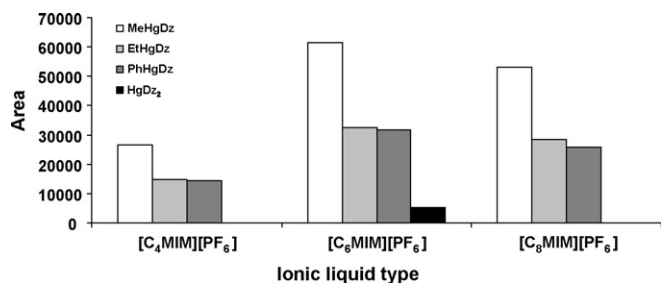


Fig. 1. Effect of the ionic liquid type. Conditions:  $50 \mu\text{g L}^{-1}$  (as Hg) of  $\text{MeHg}^+$ ,  $\text{EtHg}^+$ ,  $\text{PhHg}^+$ ,  $\text{Hg(II)}$ . 20 min of microextraction time (except for  $[C_4MIM][PF_6]$ , where 10 min were used because of the higher dissolution rate of the drop), 900 rpm, 4  $\mu\text{L}$  of drop volume, 12 mL of sample, 1  $\text{mg L}^{-1}$  of dithizone.

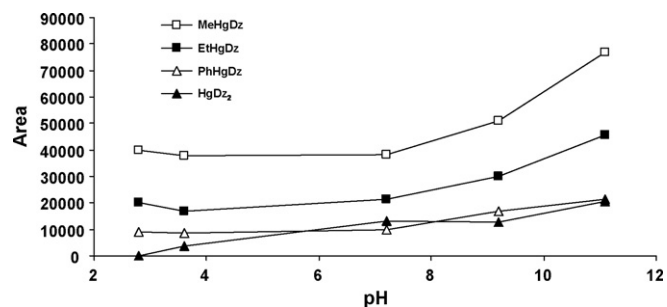


Fig. 2. Effect of the pH of the sample. Conditions:  $50 \mu\text{g L}^{-1}$  (as Hg) of  $\text{MeHg}^+$ ,  $\text{EtHg}^+$ ,  $\text{PhHg}^+$ , and  $100 \mu\text{g L}^{-1}$  of  $\text{Hg(II)}$ . 20 min of microextraction time, 900 rpm, 4  $\mu\text{L}$  of  $[C_6MIM][PF_6]$ , 12 mL of sample, 1  $\text{mg L}^{-1}$  of dithizone.

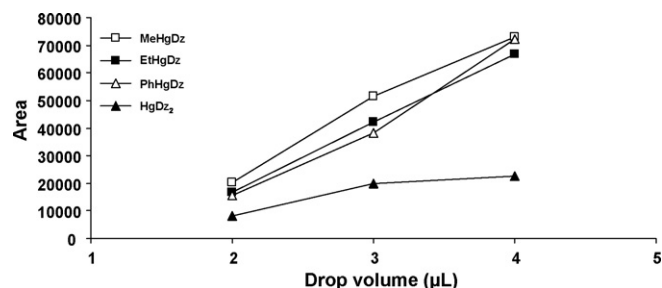


Fig. 3. Effect of the microdrop volume. Conditions:  $50 \mu\text{g L}^{-1}$  (as Hg) of  $\text{MeHg}^+$  and  $\text{EtHg}^+$ ,  $100 \mu\text{g L}^{-1}$  (as Hg) of  $\text{PhHg}^+$ , and  $200 \mu\text{g L}^{-1}$  (as Hg) of  $\text{Hg(II)}$ . 20 min of microextraction time  $[C_6MIM][PF_6]$ , 900 rpm, 12 mL of sample, pH 11, 1  $\text{mg L}^{-1}$  of dithizone.

cal signal of mercury dithizonates on increasing IL drop volume was observed in the studied range (Fig. 3.). Larger microdrop volumes easily fell off the needle of the microsyringe. Therefore, 4  $\mu\text{L}$  of  $[C_6MIM][PF_6]$  were used as the optimum drop volume.

##### 3.1.4. Stirring rate

An increase in the stirring rate of the aqueous sample causes an enhancement of the extraction efficiency in SDME, thereby reducing the necessary time to reach thermodynamic equilibrium. The film theory, valid for SDME [6], explains the positive effect of the higher stirring rates on the microextraction process since fast agitation of the aqueous phase involves a decrease in the thickness of the diffusion film corresponding to the aqueous phase. The study was carried out by varying the stirring rate in the range of 100–900 rpm. As can be seen in Fig. 4., the peak area of the corresponding signals increased in all the studied range. Faster stirring rates were avoided as they resulted in dislodgement of the ionic liquid drop from the needle tip. Thus, for all further experiments a stirring rate of 900 rpm was used.

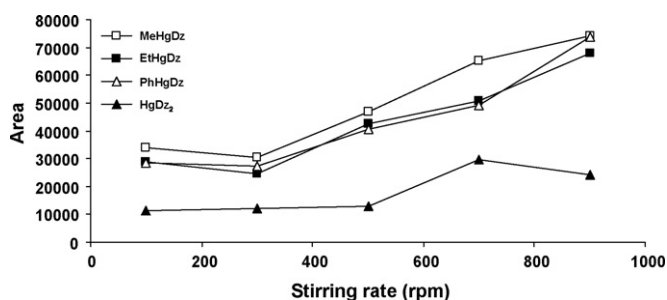
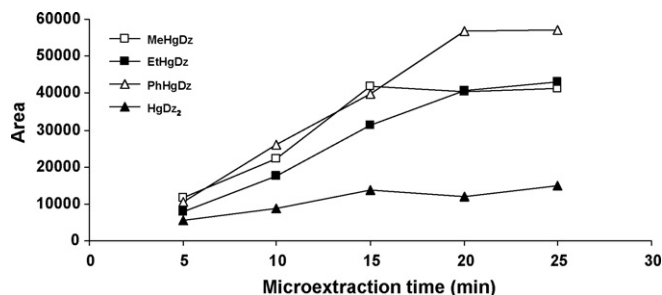


Fig. 4. Effect of the stirring rate. Conditions:  $50 \mu\text{g L}^{-1}$  (as Hg) of  $\text{MeHg}^+$  and  $\text{EtHg}^+$ ,  $100 \mu\text{g L}^{-1}$  (as Hg) of  $\text{PhHg}^+$ , and  $200 \mu\text{g L}^{-1}$  (as Hg) of  $\text{Hg(II)}$ . 20 min of microextraction time, 4  $\mu\text{L}$  of  $[C_6MIM][PF_6]$ , 12 mL of sample, pH 11, 1  $\text{mg L}^{-1}$  of dithizone.



**Fig. 5.** Effect of the microextraction time. Conditions:  $50 \mu\text{g L}^{-1}$  (as Hg) of  $\text{MeHg}^+$  and  $\text{EtHg}^+$ ,  $100 \mu\text{g L}^{-1}$  (as Hg) of  $\text{PhHg}^+$ , and  $200 \mu\text{g L}^{-1}$  (as Hg) of  $\text{Hg(II)}$ .  $4 \mu\text{L}$  of  $[\text{C}_6\text{MIM}][\text{PF}_6]$ , 900 rpm, 12 mL of sample, pH 11,  $1 \text{ mg L}^{-1}$  of dithizone.

### 3.1.5. Microextraction time

Microextraction time is one of the most important variables when SDME is used. The amount of analytes extracted at a given time depends on the mass transfer of analytes from the aqueous phase to the IL phase. The effect of time was studied in the range 5–25 min. As pointed out in Fig. 5., equilibrium is reached for methylmercury at 15 min, and at 20 min for the rest of analytes. 20 min was chosen as the extraction time because it is comparable to the duration of the chromatographic run allowing an increase on the sample throughput.

### 3.1.6. Ionic strength of the sample

Addition of salt to the aqueous sample is usually made to improve the extraction of several analytes when classical liquid–liquid extraction is used because the increase in ionic strength brings a reduction on the solubility of the hydrophobic analytes in the water solution. Nevertheless, in SDME the addition of salt to the sample can cause two opposed effects; on the one hand, a positive effect owing to the salting out effect and, on the other hand, a negative effect due to the modification of the nature of the Nernst diffusion film when the ionic strength of the aqueous phase is modified, reducing the diffusion rates of analytes into the microdrop, and consequently diminishing the analytical signals. The effect of the increase of the ionic strength was tested by addition of sodium chloride in the range 0–5% m/v. Higher salt contents caused the separation of phases between the aqueous phase and the acetonitrile used to dissolve dithizone and, therefore, were not studied. The obtained results are shown in Fig. 6. A decrease in the analytical signal of the four analytes with increasing sodium chloride content was observed. This negative effect is more pronounced for the most voluminous and hydrophobic complexes of mercury, i.e.,  $\text{PhHgDz}$  and  $\text{HgDz}_2$ . Based on the above consideration, salt addition was not used for further experiments.

## 3.2. Evaluation of the method performance

In order to evaluate the SDME performance, limits of detection (LOD) and quantification (LOQ), repeatability, enrichment factor, working range and linearity were assessed under the optimized conditions. Results are listed in Table 1.

**Table 1**  
Analytical figures of merit of the SDME optimized method.

	LOD ( $\mu\text{g L}^{-1}$ )	LOQ ( $\mu\text{g L}^{-1}$ )	Repeatability (R.S.D. %, $n = 8$ )	Enrichment factor	Working range ( $\mu\text{g L}^{-1}$ ) <sup>a</sup>	Correlation coefficient ( $r$ )
Methylmercury	1.0	3.4	5.3	27	5–120	0.9968
Ethylmercury	1.6	5.2	3.7	31	10–120	0.9987
Phenylmercury	7.1	23.8	9.4	11	40–240	0.9980
Mercury(II)	22.8	75.9	11.6	3	80–480	0.9962

<sup>a</sup> Number of calibration points,  $n = 5$ .

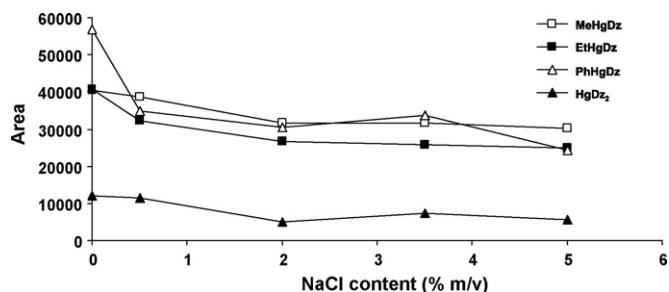


**Fig. 6.** Effect of the ionic strength of the sample. Conditions:  $50 \mu\text{g L}^{-1}$  (as Hg) of  $\text{MeHg}^+$  and  $\text{EtHg}^+$ ,  $100 \mu\text{g L}^{-1}$  (as Hg) of  $\text{PhHg}^+$ , and  $200 \mu\text{g L}^{-1}$  (as Hg) of  $\text{Hg(II)}$ . 20 min of microextraction time,  $4 \mu\text{L}$  of  $[\text{C}_6\text{MIM}][\text{PF}_6]$ , 900 rpm, 12 mL of sample, pH 11,  $1 \text{ mg L}^{-1}$  of dithizone.

The limit of detection (LOD) was estimated using a three signal-to-noise ratio criterium and the limit of quantification (LOQ) as 10 times the above-mentioned ratio. As can be seen from Table 1, lower limits of detection (LODs) were achieved for methylmercury and ethylmercury, in comparison with phenylmercury and, especially, mercury(II), probably owing to the larger solute diffusion coefficient of the smallest complexes of mercury into  $[\text{C}_6\text{MIM}][\text{PF}_6]$ , which has a large viscosity (560–586 mPa s) [8]. Lower LODs could be achieved by using a more sensitive Hg-specific detector.

The repeatability of the method was studied from eight replicate experiments. Relative standard deviations (R.S.D.s, %) were found between 3.7 and 11.6% for the four analytes.

The enrichment factor, defined as the ratio between the final analyte concentration in the extractant phase and the initial aqueous sample concentration, was calculated for mercury(II) and organomercurials. Enrichment factors between 3 and 31 were found. These values were calculated after interpolation of the peak area obtained by direct injection of an aqueous solution containing  $500 \mu\text{g L}^{-1}$  of each mercury species complexed with dithizone in the calibration graph obtained after SDME.

## 3.3. Analysis of water samples and recovery study

To assess the feasibility of the SDME procedure, the optimized method was examined for the extraction and determination of organomercurials and mercury(II) in tap water, river water and wastewater samples.

For the purpose of the present studies, five replicate analyses under the optimized experimental conditions were performed for each water sample.

The content of mercury species was below the corresponding LOD for all three water samples.

A recovery study was performed in order to check the matrix effects. Water samples were spiked with  $\text{MeHg}^+$  and  $\text{EtHg}^+$  at  $20 \mu\text{g L}^{-1}$  concentration,  $\text{PhHg}^+$  at  $40 \mu\text{g L}^{-1}$  concentration and  $\text{Hg(II)}$  at  $80 \mu\text{g L}^{-1}$  concentration. Fig. 7 shows a chromatogram of the wastewater sample and spiked wastewater sample with mercuric species after SDME. As could be seen in Table 2, recoveries for methylmercury, ethylmercury, phenylmercury and inorganic mercury were between 83 and 123% with an R.S.D. lower than 13%.



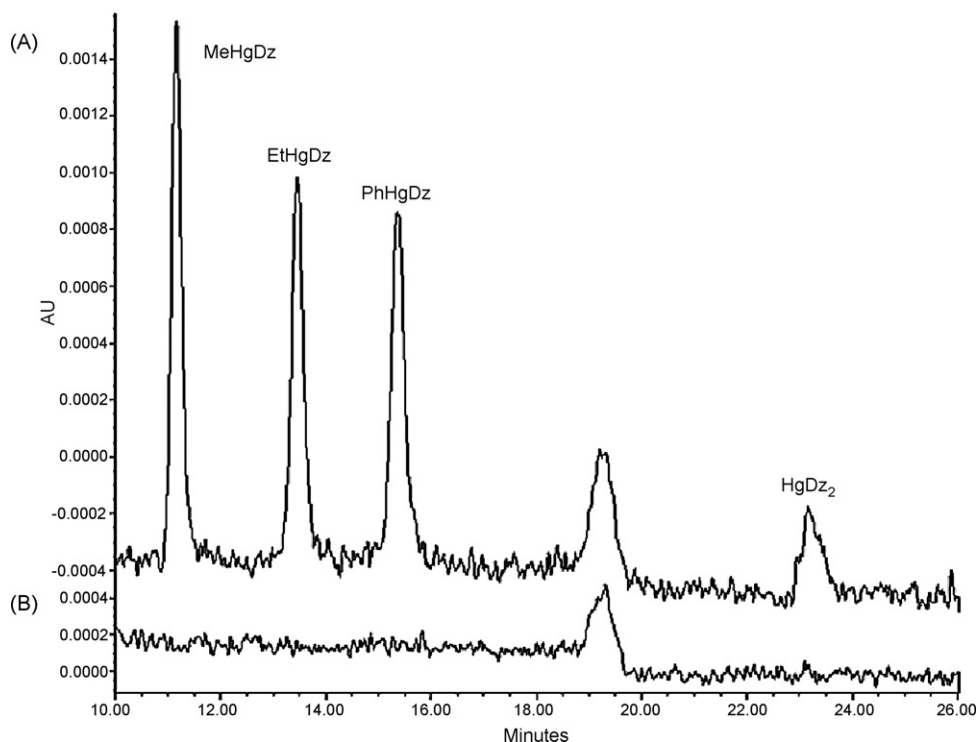


**Fig. 7.** Chromatograms of (A) a wastewater sample spiked with mercury species and (B) a wastewater sample. MeHgDz: Methylmercury dithizonate; EtHgDz: Ethylmercury dithizonate; PhHgDz: Phenylmercury dithizonate and HgDz<sub>2</sub>: Mercury(II) dithizonate. The peak that appears between PhHgDz and HgDz<sub>2</sub> is due to a non-reactive fraction of dithizone (decomposition fraction of dithizone) [22].

**Table 2**  
Analytical results for the determination of mercury species in spiked water samples.

Analytes	Added concentration ( $\mu\text{g L}^{-1}$ )	Relative recoveries (%) <sup>a</sup>		
		Tap water	River water	Wastewater
Methylmercury	20	115 ± 8	95 ± 11	96 ± 9
Ethylmercury	20	115 ± 11	89 ± 11	103 ± 13
Phenylmercury	40	98 ± 10	83 ± 11	91 ± 10
Mercury(II)	80	123 ± 2	98 ± 9	97 ± 4

<sup>a</sup> Average value ± standard deviation ( $n = 5$ ).

These results demonstrate that tap water, river water and wastewater matrices had little effect on SDME.

#### 4. Conclusions

This study demonstrates the suitability of ionic liquids for mercury speciation by combination of SDME with high-performance liquid chromatography. The proposed method allows the determination of inorganic and organomercury species in water samples, being easy to use, fast, economical and virtually extractant-free.

Dithizone, i.e. a sulphur containing complexing agent, was used for derivatisation of the four mercury species in the sample, prior to extraction of mercury dithizonates onto an ionic liquid drop. Lower detection limits were achieved for methylmercury and ethylmercury, in comparison with phenylmercury and mercury(II). The new method was applied to the determination of mercury species in different fortified water samples.

#### Acknowledgments

F.P.-P. thanks Xunta de Galicia for financial support as a researcher of the Maria Barbeito. F.P.-P also thanks Universidade de Vigo for a grant.

The authors gratefully acknowledge the financial support of the Spanish Government (project nos. PET2006-706-00, CTQ2005-09079-C03-01/BQU and CTQ2006-04111/BQU), the Regional Governments of Comunidad Valenciana and Galicia (project nos. ACOMP07/053, ARVIV/2007/062 and PGIDIT05PXIB31401PR) and the EU-COST Program (Action D32, working group WG/D32/005/04: “Microwave and ultrasound activation in chemical analysis”).

#### References

- [1] R. Pongratz, K.G. Heumann, *Chemosphere* 39 (1999) 89.
- [2] M. Logar, M. Horvat, I. Falnoga, V. Stibilj, Fresen. *J. Anal. Chem.* 366 (2000) 453.
- [3] J.E. Sánchez Uría, A. Sanz-Medel, *Talanta* 47 (1998) 509.
- [4] L.M.L. Nolllet (Ed.), *Chromatographic Analysis of the Environment*, 3rd ed., CRC/Taylor & Francis, Boca Raton, 2006.
- [5] C.F. Harrington, *Trends Anal. Chem.* 19 (2000) 167.
- [6] M.A. Jeannot, F.F. Cantwell, *Anal. Chem.* 69 (1997) 235.
- [7] E. Psillakis, N. Kalogerakis, *Trends Anal. Chem.* 21 (2002) 53.
- [8] J.F. Liu, J.A. Jonsson, G.B. Jiang, *Trends Anal. Chem.* 24 (2005) 20.
- [9] J.F. Liu, G.B. Jiang, Y.G. Chi, Y.Q. Cai, Q.X. Zhou, J.T. Hu, *Anal. Chem.* 75 (2003) 5870.
- [10] L. Vidal, E. Psillakis, C.E. Domini, N. Grané, F. Marken, A. Canals, *Anal. Chim. Acta* 584 (2007) 189.
- [11] L. Vidal, C.E. Domini, N. Grané, E. Psillakis, A. Canals, *Anal. Chim. Acta* 592 (2007) 9.
- [12] C. Ye, Q. Zhou, X. Wang, J. Xiao, *J. Sep. Sci.* 30 (2007) 42.
- [13] J.F. Liu, Y.G. Chi, G.B. Jiang, C. Tai, J.F. Peng, J.T. Hu, *J. Chromatogr. A* 1026 (2004) 143.
- [14] J.F. Peng, J.F. Liu, G.B. Jiang, C. Tai, M.J. Huang, *J. Chromatogr. A* 1072 (2005) 3.
- [15] E. Aguilera-Herrador, R. Lucena, S. Cárdenas, M. Valcárcel, *J. Chromatogr. A* 1209 (2008) 76.
- [16] E. Aguilera-Herrador, R. Lucena, S. Cárdenas, M. Valcárcel, *J. Chromatogr. A* 1201 (2008) 106.
- [17] L. Vidal, A. Chisvert, A. Canals, A. Salvador, *J. Chromatogr. A* 1174 (2007) 95.
- [18] J.F. Liu, J.F. Peng, Y.G. Chi, G.B. Jiang, *Talanta* 65 (2005) 705.
- [19] J.F. Liu, Y.G. Chi, G.B. Jiang, *J. Sep. Sci.* 28 (2005) 87.
- [20] S. Gil, S. Fragueiro, I. Lavilla, C. Bendicho, *Spectrochim. Acta: B* 60 (2005) 145.
- [21] X.D. Yao, J.C. Liu, J.K. Cheng, Y. Zeng, *Anal. Sci.* 8 (1992) 255.
- [22] W. Langseth, *Anal. Chim. Acta* 185 (1986) 249.



# Capillary electrophoresis-mass spectrometry using an in-line sol-gel concentrator for the determination of methionine enkephalin in cerebrospinal fluid

R. Ramautar<sup>a,\*</sup>, C.K. Ratnayake<sup>b</sup>, G.W. Somsen<sup>a</sup>, G.J. de Jong<sup>a</sup>

<sup>a</sup> Department of Biomedical Analysis, Utrecht University, P.O. Box 80082, 3508 TB Utrecht, The Netherlands

<sup>b</sup> Beckman Coulter, Inc., P.O. Box 3100, Fullerton, CA 92834-3100, USA

## ARTICLE INFO

### Article history:

Received 20 August 2008

Received in revised form 4 December 2008

Accepted 11 December 2008

Available online 24 December 2008

### Keywords:

Capillary electrophoresis-mass spectrometry

Sol-gel concentrator

Preconcentration

Cerebrospinal fluid

Methionine enkephalin

## ABSTRACT

In this study, a CE-MS method using a monolithic sol-gel concentrator for in-line solid-phase extraction (SPE) is evaluated for the analysis of methionine enkephalin in biological samples. Operational SPE parameters such as sample pH, loading volume, elution volume and composition have been studied. After optimization of the in-line preconcentration methodology, a 40-fold preconcentration was demonstrated for a methionine enkephalin test solution using a loading volume of 3200 nL. The method was linear in the range from 62.5 to 1000 ng/mL ( $R^2 > 0.99$ ). R.S.D. values for migration times and peak areas were 1.2% and 8.4%, respectively. Finally, the analysis of cerebrospinal fluid samples spiked with methionine enkephalin and deproteinized with perchloric acid (1:1, v/v) showed a detection limit ( $S/N = 3$ ) of approximately 1 ng/mL (ca. 5 nM). The recoveries of methionine enkephalin for three concentration levels (100, 10 and 1 ng/mL) were in the range of 74–91%, demonstrating the promising potential of the methodology for the analysis of biological samples.

© 2008 Elsevier B.V. All rights reserved.

## 1. Introduction

Capillary electrophoresis (CE) is an efficient separation technique for a wide variety of analytes. However, for the analysis of biological samples CE suffers from an inherent low concentration sensitivity due to the limited sample volume that can be loaded onto the capillary. Several strategies can be used to improve the concentration sensitivity in CE [1,2]. In general, analyte preconcentration via electrophoresis-based or chromatography-based methods is used to improve the concentration sensitivity in CE [3,4]. Chromatography-based methods can offer two to four orders of preconcentration [5–8], and therefore are attractive to improve the concentration-sensitivity in CE. Typically, chromatographic preconcentration is carried out either in an off-line, on-line, or in-line mode [9]. In the on-line mode, the precolumn is not part of the CE system and the coupling of the precolumn is performed via an interface [10]. In the in-line mode, the preconcentration column is an integrated part of the CE system. When using these chromatographic techniques, on-line or in-line methods are regarded as advantageous compared to the off-line approach as a result of their shorter total analysis times, minimum of sample handling and possibility of automation. The main advantage of the

in-line approach is that the entire preconcentrated amount of analyte can be transferred to the separation section of the CE capillary [9]. However, a disadvantage is that sample matrix components also pass through the separation capillary and may interfere with the CE analysis or they can adsorb onto the capillary wall, which can result in poor separations. Nevertheless, the in-line approach has the highest level of integration [9]. Various in-line SPE-CE approaches have been described such as an open-tubular capillary coated with a sorbent [11], a small (1–2 mm) packed section containing microsphere beads and retained by frits at the inlet of the capillary [12,13], and an immobilized particle-loaded membrane [14]. In the open-tubular configuration, the capacity is relatively low to load sufficient sample [15]. While packed SPE modules offer a relatively larger capacity, the introduction of a small packed section into the capillary can increase the back pressure, and rinsing the capillary using conventional CE instrumentation with low pressures can be problematic [15]. Moreover, the preparation of packed SPE modules in narrow bore capillaries can be difficult, especially with respect to the frit formation [15].

An alternative approach is the use of in situ formed monolithic materials [16]. By using UV-initiated polymerization, the monolithic SPE column can be made directly in the capillary. No frits are required as monolithic columns consist of a continuous piece of a highly porous microstructure. Monolithic columns can be used at high flow rates, thus minimizing sample loading time and backpres-

\* Corresponding author. Fax: +31 30 253 5180.

E-mail address: [R.Ramautar@uu.nl](mailto:R.Ramautar@uu.nl) (R. Ramautar).

sure. There are two types of monolithic columns, i.e. silica-based and polymer-based monoliths. Silica monoliths are prepared using sol–gel technology whereas polymer-based monoliths are made by in situ polymerization of monomers and cross-linkers [17]. Photopolymerized sol–gel monoliths have been used as a SPE sorbent and stationary phase in capillary electrochromatography for the preconcentration and separation of peptides [17–19]. However, sol–gel monoliths as preconcentration sorbents are still not used widely for in-line SPE-CE.

So far, a few papers have described the applicability of monolithic columns for in-line SPE-CE to preconcentrate compounds. For instance, an in-line SPE-CE method using a monolithic methacrylate polymer was used for the preconcentration of S-propranolol from aqueous solutions. A limit of detection (LOD) in the low nanomolar range was achieved for S-propranolol with this method [20]. In another study, a polymeric monolithic SPE column was prepared in situ within a fused silica capillary from butyl methacrylate-co-ethylene dimethacrylate [15]. Using a 1 cm SPE column placed at the inlet of the capillary, the compounds sertraline, fluoxetine and fluvoxamine were extracted from aqueous solutions by applying a pressure rinse. Enrichment factors of over 500 were achieved for the compounds of interest. A sulphopropyl methacrylate monolith was used to preconcentrate amino acids from standard solutions using in-line SPE-CE [21]. Monolithic columns have also been used for the preconcentration of inorganic anions using in-line SPE-CE [22]. A poly(butyl methacrylate-co-ethylene dimethacrylate-co-2-acrylamido-2-methyl-1-propanesulfonic acid) monolithic column with cation-exchange sites was used for that purpose. An in-line SPE-CE time-of-flight mass spectrometry (TOF-MS) method using a silica-based monolith was developed for the determination of escitalopram in human urine [23]. The limit of detection (LOD) for escitalopram was 10 pg/mL obtained with a loading volume of approximately 2.25  $\mu$ L. The intraday precision of the escitalopram peak area was less than 6.3%.

In the present paper the development and optimization of an in-line SPE-CE-MS method based on a silica-based monolithic sol–gel concentrator for the determination of methionine enkephalin in cerebrospinal fluid (CSF) is described. The main goal of this study was the evaluation of the feasibility of silica-based monolithic sol–gel capillaries for the analysis of CSF samples. The paper describes the systematic optimization of experimental parameters of the sol–gel concentrator, such as loading time, elution volume and composition of the elution solvent. Subsequently, repeatability of migration time and peak area, linearity and LODs have been determined. Finally, the potential of the in-line SPE-CE-ESI-MS method for CSF analysis is assessed.

## 2. Experimental

### 2.1. Chemicals

Ammonium acetate, sodium hydroxide, perchloric acid and acetonitrile (all analytical grade or higher) were purchased from Merck (Darmstadt, Germany) and Biosolve BV (Valkenswaard, The Netherlands), respectively. Acetic acid (analytical grade) and acetate salts of Leu-enkephalin (Tyr-Gly-Gly-Phe-Leu) and [Met<sup>5</sup>]-enkephalin (Tyr-Gly-Gly-Phe-Met) were obtained from Sigma–Aldrich (St. Louis, MO, USA). Human CSF was generously donated by the Utrecht Medical Centre (Utrecht, The Netherlands). Deionized water from a Milli-Q system (Millipore, Bedford, MA, USA) was used for all solutions. The background electrolyte (BGE) in all CE experiments was 5 mM ammonium acetate adjusted to pH 3.6 with acetic acid. The peptides were dissolved in BGE, unless otherwise stated.

### 2.2. Preparation of sol–gel capillaries

Sol–gel capillaries were obtained from Beckman Coulter (Fullerton, CA, USA). The monolithic sol–gel sorbent was prepared by mixing 500  $\mu$ L ethanol and 600  $\mu$ L tetraethoxysilane. Subsequently, 800  $\mu$ L of 1 M nitric acid was added to initiate hydrolysis and condensation. Then reversed phase silica particles (Beckman Coulter, Fullerton, CA, USA) were added to make a slurry. Bare fused silica capillaries were filled with this slurry to obtain an about 3–5 cm long plug which was heated to 120 °C for 48 h. Finally, the capillary was cut to obtain a monolithic sol–gel plug of 5 mm at the inlet of the capillary.

### 2.3. Instrumentation and procedures

CE-UV experiments were performed using a Beckman Coulter (Fullerton, CA, USA) PA 800 CE instrument equipped with a diode array detector (DAD). Capillaries with internal diameter (ID) of 50  $\mu$ m were from Composite Metal Services (The Chase, Hallow, UK). The sol–gel capillaries were flushed with acetonitrile (15 min) and 80% acetonitrile in BGE (10 min) prior to use. Sol–gel capillaries had a total length of 60 cm and effective length of 50 cm. Samples were injected for 5 min at 25 p.s.i. (injection volume of ca. 400 nL), unless otherwise stated, and the separation voltage was 30 kV. The capillary was thermostated at 20 °C and detection was carried out at 200 nm with a data acquisition rate of 16 Hz. CE-ESI-MS experiments were conducted using a PrinCE CE system from Prince Technologies B.V. (Emmen, The Netherlands) using 50  $\mu$ m ID sol–gel capillaries with a length of 90 cm. During sample injection, the nebulizer gas flow and the electrospray voltage of the CE-MS interface were turned off. CE was coupled to an Agilent Technologies 1100 Series LC/MSD SL IT mass spectrometer (Waldbronn, Germany) via a coaxial sheath-flow electrospray interface (Agilent). The CE capillary outlet was positioned at 0.2–0.5 mm from the tip of the interface. A sheath liquid of methanol–water–acetic acid (50:50:0.1, v/v/v) was supplied by a syringe pump at a flow rate of 10  $\mu$ L/min. The nebulizer-gas pressure was 10 p.s.i., and the flow and temperature of the drying gas were 4 L/min and 300 °C, respectively. The electrospray voltage was 4.5 kV. In the Agilent CE-MS set-up, the spray needle is grounded. MS detection was carried out in the positive ion mode and the scan range was 200–1200 *m/z*.

All sol–gel capillaries for in-line SPE-CE-MS were first conditioned by consecutive flushes of acetonitrile (10 min), 80% acetonitrile in BGE (10 min) and BGE (10 min) at 25 p.s.i. Dilute samples of methionine enkephalin in BGE were hydrodynamically injected at 25 p.s.i. for 40 min (unless otherwise stated). A washing rinse with the BGE at 25 p.s.i. for 20 min was applied before the elution of methionine enkephalin. Elution was performed by injecting a solution of 80:20 (v/v) acetonitrile–BGE (apparent pH 3.6) at 10 p.s.i. for 0.5 min (ca. 50 nL). Separation was carried out applying a voltage of 30 kV (normal polarity). Between runs, the capillary was rinsed for 5 min with a solution of 80:20 (v/v) acetonitrile–BGE and BGE, in order to avoid carry-over between consecutive analyses.

### 2.4. Sample preparation

The off-line pretreatment of blank and spiked CSF samples consisted of a protein precipitation step. This was carried out with 0.1 M perchloric acid in a ratio of 1:1 (v/v) (100  $\mu$ L CSF and 100  $\mu$ L perchloric acid). The supernatant was centrifuged (5 min at 9447  $\times$  g). Subsequently, the samples were hydrodynamically introduced at 25 p.s.i. for 40 min.

## 2.5. Evaluation of analytical parameters

The analytical parameters were calculated from data obtained by measuring the peak area and migration time from the extracted ion electropherogram of methionine enkephalin. The  $m/z$  of the molecular ion for leucine enkephalin was 556.0 and for methionine enkephalin 574.4. Repeatability studies ( $n=5$ ) were performed with methionine enkephalin dissolved in CSF at a concentration of 100 ng/mL. LOD ( $S/N=3$ ) for methionine enkephalin was obtained analyzing methionine enkephalin solutions of 10 ng/mL and 1 ng/mL. The linearity range was determined by injecting five concentrations in the range of 62.5–1000 ng/mL in BGE. Recoveries of methionine enkephalin spiked into CSF (at three concentration levels: 100, 10 and 1 ng/mL) were calculated using the calibration curve constructed for methionine enkephalin standards (62.5–1000 ng/mL range).

## 3. Results and discussion

### 3.1. SPE-CE optimization

A preliminary study was performed to find a suitable BGE for enkephalin analysis. For BGE optimization, two closely related peptides, i.e. leucine enkephalin and methionine enkephalin, were used. Ammonium acetate at four different pH values (2.5, 3.1, 3.6 and 4.0) was investigated as it is a volatile BGE. With a BGE of 5 mM ammonium acetate (pH 3.6), a baseline separation for the two peptides was obtained (Fig. 1). Additionally, this low-ionic-strength BGE is well compatible with ESI-MS. Therefore, for the in-line SPE-CE-MS experiments, 5 mM ammonium acetate (pH 3.6) was chosen as BGE. The optimum composition of the sheath liquid was determined by pressure-induced infusion of a solution of methionine enkephalin in BGE (1  $\mu\text{g}/\text{mL}$ ) using mixtures of methanol–water and acetonitrile–water containing 0.1% acetic acid. The optimum sheath liquid composition was methanol–water–acetic acid (50:50:0.1, v/v/v). The sheath liquid flow rate was optimized in the range from 2.5 to 12.5  $\mu\text{L}/\text{min}$  and the highest signal intensity for methionine enkephalin was obtained at a flow rate of 10  $\mu\text{L}/\text{min}$ .

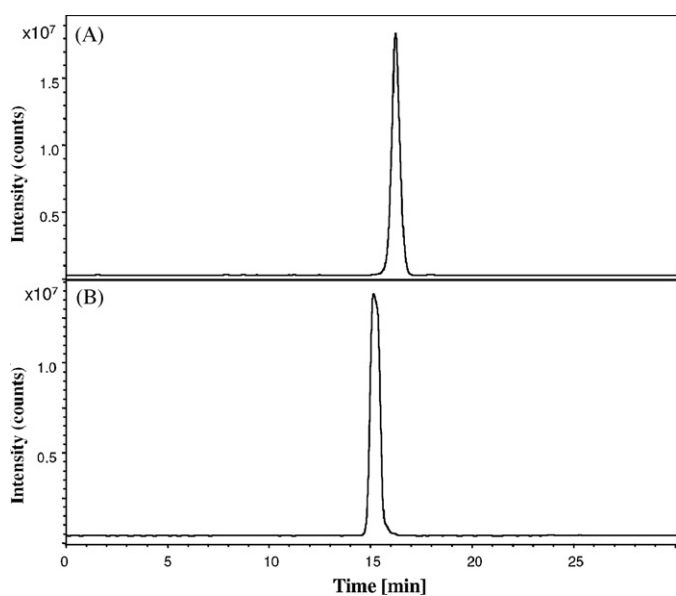


**Fig. 1.** Separation of leucine enkephalin from methionine enkephalin. (A) Extracted ion electropherogram of 100  $\mu\text{g}/\text{mL}$  methionine enkephalin. (B) Extracted ion electropherogram of 100  $\mu\text{g}/\text{mL}$  leucine enkephalin. BGE, 5 mM ammonium acetate (pH 3.6); capillary: 90 cm  $\times$  50  $\mu\text{m}$  i.d.; separation voltage, +30 kV; injection: 50 nL.

For optimization of the in-line SPE-CE-MS procedure, several parameters have to be considered in order to achieve optimum performance, i.e. the pH of the sample solution, the loading volume, elution volume and composition of the elution solvent. These parameters have been evaluated with methionine enkephalin as test compound. First, the pH of the injected sample solution was determined as this parameter will affect the retention of the analyte on the monolithic sol–gel concentrator. The pH of the injected sample solution was studied between pH 2.5 and 6.8 using 5 mM ammonium acetate. A loading volume of ca. 400 nL (loading time 5 min) and an elution volume of ca. 50 nL (80% acetonitrile in BGE) were used. The sample solution was introduced hydrodynamically into the in-line SPE-CE-MS system. In this way, the volume of sample introduced can be calculated, taking into account the flow-rate through the sol–gel capillary which can be determined via the mass loss of a buffer-filled vial at a certain pressure and time interval. Using pH values above 4.5 for sample loading resulted in high back pressures and also current drops upon voltage application. Similar peak areas for methionine enkephalin were obtained at pH values below 4.0. Therefore, a sample pH of 3.6 was selected as acetate has a good buffer capacity at this pH.

Next, the loading capacity of the sol–gel concentrator was evaluated using in-line SPE-CE-MS. The loading capacity of the monolithic sol–gel concentrator was determined by loading different volumes of a methionine enkephalin standard solution of 1000 ng/mL. In order to increase the speed of the analysis a loading pressure of 25 p.s.i. was chosen. Fig. 2A shows the effect of loading volume (i.e. loading time) on the peak area for methionine enkephalin. A linear relation of peak area versus loading volume could be observed up to a loading volume of ca. 3200 nL (40 min). The deviation from linearity above a loading volume of ca. 3200 nL indicated that the capacity of the sol–gel concentrator was exceeded after 40 min for methionine enkephalin. Therefore, for the preconcentration of methionine enkephalin, a loading volume of ca. 3200 nL was selected.

The influence of the composition of the elution solvent on the desorption of methionine enkephalin (1000 ng/mL) was studied by in-line SPE-CE-UV using a loading volume of 1000 nL and an elution volume of ca. 50 nL. The percentage of acetonitrile in the BGE was varied from 20 to 80%. The amount of methionine enkephalin desorption increased with a higher concentration of acetonitrile. A percentage of 80% acetonitrile in the BGE was required for complete desorption of methionine enkephalin. Subsequently, optimization of the elution volume (acetonitrile/BGE, 8/2, v/v) was determined by loading 1000 nL of 1000 ng/mL methionine enkephalin onto the monolithic sol–gel concentrator while increasing the elution volume (ca. 13, 25, 50 and 100 nL). Fig. 2B shows that the peak area of methionine enkephalin increased with the elution volume until ca. 50 nL. Above this volume the peak area remained constant. Therefore, an elution volume of ca. 50 nL was used for desorption.

On-line preconcentration using the sol–gel concentrator was evaluated with methionine enkephalin as test compound. When a 5000 ng/mL methionine enkephalin sample was loaded for 1 min (80 nL) a peak with an intensity of ca.  $4.2 \times 10^6$  counts was observed (Fig. 3A). When a 100 ng/mL methionine enkephalin sample was loaded for 40 min (3200 nL) a peak with an intensity of ca.  $3.4 \times 10^6$  counts was observed (Fig. 3B). The ratio of the peak intensities (1.23) corresponds well to the ratio of the amount of analyte loaded on the sol–gel concentrator (i.e., 0.40 ng/0.32 ng = 1.25). As a result, the 100 ng/mL methionine enkephalin sample was preconcentrated by a factor of 40.

Using methionine enkephalin concentrations in the range of 62.5–1000 ng/mL, peak area ( $y$ ) versus concentration ( $x$ ) regression line was calculated ( $n=5$ ). Linearity was observed over the range between 62.5–1000 ng/mL ( $R^2 > 0.995$ ) and the equation is  $y = 12,471x + 56,127$ . Using an injection volume of ca. 3200 nL, the

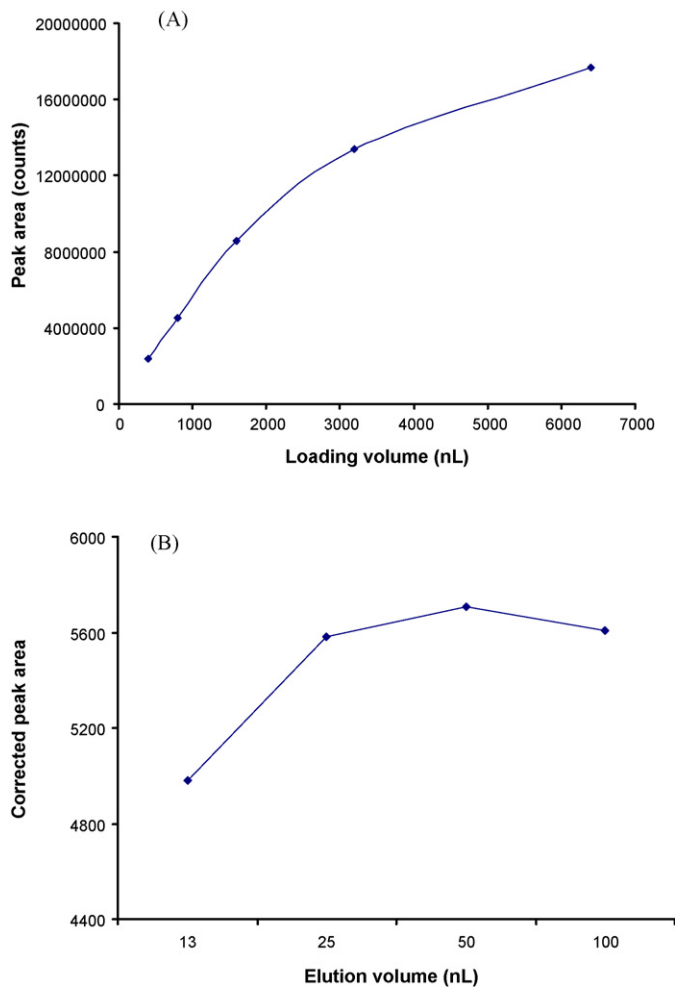


**Fig. 2.** (A) Effect of sample loading volume on peak area of methionine enkephalin (1000 ng/mL). A 5 mm monolithic sol-gel concentrator is employed. Capillary: 90 cm  $\times$  50  $\mu$ m i.d.; loading flow rate: 80 nL/min; elution: 50 nL acetonitrile-BGE (8:2, v/v). (B) Effect of elution volume on peak area of methionine enkephalin (1000 ng/mL) determined by CE-UV. A 5 mm monolithic sol-gel preconcentrator is employed. Capillary: 60 cm  $\times$  50  $\mu$ m i.d.; BGE, 5 mM ammonium acetate (pH 3.6); separation voltage, +30 kV (5 p.s.i. forward); injection: 25 p.s.i. for 5 min (ca. 400 nL); detection, UV at 214 nm.

limit of detection ( $S/N=3$ ) was approximately 1 ng/mL, which is comparable with the LOD value for methionine enkephalin obtained by in-line SPE-CE-MS method using microcartridges containing a C18 stationary phase [6]. A comparable LOD value for methionine enkephalin was also obtained by an on-line SPE-CE-MS method [7]. In this case, a sample injection of 100  $\mu$ L resulted in a LOD value of ca. 1 ng/mL for methionine enkephalin. For five replicate analyses of a standard solution of methionine enkephalin (100 ng/mL), the within-day R.S.D. for migration time was less than 1.2%. The within-day R.S.D. for peak area was less than 8.4%.

### 3.2. Applicability for CSF analysis

To demonstrate the feasibility of the SPE-CE-MS system for the analysis of biological samples, CSF spiked with methionine enkephalin was analyzed. Initially, the pH of the spiked CSF samples (10 ng/mL) were adjusted to pH 3.0 with acetic acid and then centrifuged (5 min at 13,200 rpm). When this sample was loaded onto the sol-gel concentrator, methionine enkephalin was not detected after elution and CE analysis. Probably the proteins in CSF compromised the sol-gel concentrator. Results using standard solutions of methionine enkephalin could not be repeated after this CSF

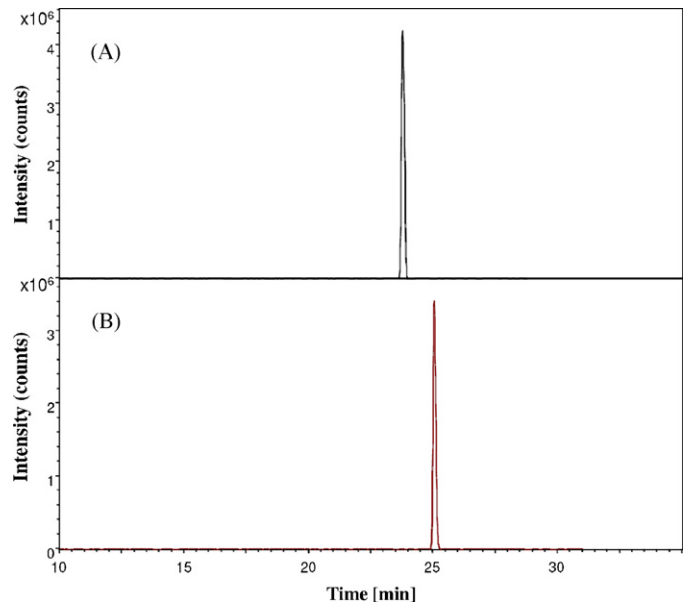


**Fig. 3.** On-line preconcentration of methionine enkephalin using the sol-gel concentrator. (A) Extracted ion electropherogram of an injection of 80 nL of 5000 ng/mL methionine enkephalin. (B) Extracted ion electropherogram of an injection of 3200 nL of 100 ng/mL methionine enkephalin. BGE, 5 mM ammonium acetate (pH 3.6); capillary: 90 cm  $\times$  50  $\mu$ m i.d.; separation voltage, +30 kV (5 p.s.i. forward); elution: 50 nL acetonitrile-BGE (8:2, v/v).

injection. Therefore, for deproteinization spiked CSF samples were diluted with 0.5 M acetic acid (pH 2.5) in a 1:1 ratio and then centrifuged. The supernatant was subsequently loaded onto the sol-gel concentrator. Fig. 4 shows a total ion electropherogram (TIE) of a spiked CSF sample and an extracted ion electropherogram of methionine enkephalin. The signal intensity of methionine enkephalin in CSF was approximately 30% lower compared to the signal intensity obtained for methionine enkephalin in BGE, how-

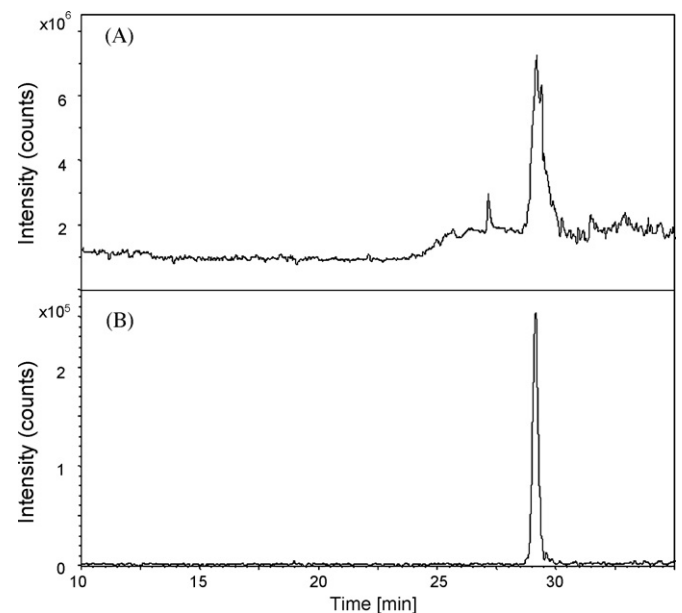


**Fig. 4.** Analysis of CSF sample spiked with 10 ng/mL methionine enkephalin using 0.5 M acetic acid for deproteinization. (A) Total ion electropherogram of the spiked CSF sample. (B) Extracted ion electropherogram of methionine enkephalin. BGE, 5 mM ammonium acetate (pH 3.6); capillary: 90 cm  $\times$  50  $\mu$ m i.d.; separation voltage, +30 kV (5 p.s.i. forward); injection: 3200 nL; elution: 50 nL acetonitrile-BGE (8:2, v/v).

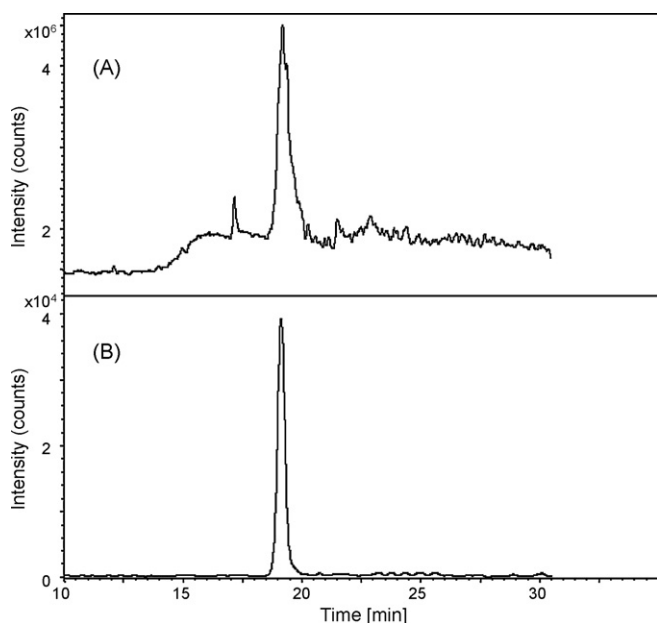


**Fig. 5.** Analysis of CSF sample spiked with 1 ng/mL methionine enkephalin using 0.1 M perchloric acid for deproteinization. (A) Total ion electropherogram of the spiked CSF sample. (B) Extracted ion electropherogram of methionine enkephalin. BGE, 5 mM ammonium acetate (pH 3.6). Capillary: 90 cm  $\times$  50  $\mu$ m i.d.; separation voltage, +30 kV (5 p.s.i. forward); injection: 3200 nL; elution: 50 nL acetonitrile–BGE (8:2, v/v).

ever, the peak areas were similar indicating that no analyte is lost. The high signal intensity between 28 and 30 min in the TIE indicates that also other compounds co-migrated with methionine enkephalin. Also the migration time of methionine enkephalin in CSF has been increased with approximately 5 min, which was probably due to adsorption of matrix components to the capillary wall. Moreover, the migration time of methionine enkephalin increased with ca. 10 min after a second injection of the spiked CSF sample on the same sol–gel capillary.

Therefore, 0.1 M perchloric acid was evaluated for deproteinization of CSF. Using 0.1 M perchloric acid for deproteinization, the signal intensities and peak areas for different concentration levels of methionine enkephalin in CSF was similar to the signal intensities and peak areas obtained in BGE. The migration time of methionine enkephalin did not increase; indeed it even slightly decreased. Fig. 5 shows a TIE of a spiked CSF sample pretreated with perchloric acid and an extracted ion electropherogram of methionine enkephalin (1 ng/mL). For methionine enkephalin, the LOD ( $S/N=3$ ) was approximately 1 ng/mL (ca. 5 nM) using extracted ion electropherograms. To further evaluate the performance of the in-line SPE–CE–MS system for the analysis of CSF samples using perchloric acid for sample pretreatment, untreated CSF was spiked at three concentration levels (100, 10 and 1 ng/mL) with methionine enkephalin. The recoveries were 91, 84 and 74%, respectively, which are acceptable values. Therefore, the in-line SPE–CE–MS

system shows good potential for the analysis of biological samples.

#### 4. Conclusions

A CE–MS method using an in-line sol–gel concentrator has been evaluated for the preconcentration and analysis of methionine enkephalin. After optimizing operational parameters for in-line SPE–CE–MS, preconcentration was demonstrated for methionine enkephalin solution using a loading volume of 3200 nL. A limit of detection ( $S/N=3$ ) below 1 ng/mL (<5 nM) was obtained using in-line preconcentration. Linearity was good over two orders of magnitude and R.S.D.s for migration times and peak areas were 1.2% and 8.4%, respectively.

The suitability of the method for the analysis of biological samples was tested with CSF samples spiked with methionine enkephalin. To allow the analysis of methionine enkephalin in CSF, pretreatment of spiked CSF samples with perchloric acid was necessary in order to precipitate the proteins. For the determination of endogenous enkephalins in CSF, which are present in the pg/mL to the low ng/mL range [24], sensitivity improvement is still required. In the near future, the system will also be used for the analysis of exogenous compounds, such as pharmaceuticals in urine and CSF. Increased sensitivity and selectivity may be achieved by the use of specialized monolithic sol–gel concentrators, e.g. with immobilized antibodies and metal-affinity materials.

#### References

- [1] P. Puig, F. Borrull, M. Calull, C. Aguilar, Trends Anal. Chem. 26 (2007) 664.
- [2] B.M. Simonet, A. Ríos, M. Valcárcel, Trends Anal. Chem. 22 (2003) 605.
- [3] S.L. Simpson Jr., J.P. Quirino, S. Terabe, J. Chromatogr. A 1184 (2008) 504.
- [4] F.W.A. Tempels, W.J.M. Underberg, G.W. Somsen, G.J. de Jong, Electrophoresis 29 (2008) 108.
- [5] S. Sentellas, L. Puignou, M.T. Galceran, J. Sep. Sci. 25 (2002) 975.
- [6] E. Hernández, F. Benavente, V. Sanz-Nebot, J. Barbosa, Electrophoresis 28 (2007) 3957.
- [7] F.W.A. Tempels, W.J.M. Underberg, G.W. Somsen, G.J. de Jong, Electrophoresis 28 (2007) 1319.
- [8] L.H. Zhang, C.J. Zhang, X. Chen, Y.Q. Feng, X.Z. Wu, Electrophoresis 27 (2006) 3224.
- [9] J.R. Veraart, H. Lingeman, U.A.Th. Brinkman, J. Chromatogr. A 856 (1999) 483.
- [10] F.W.A. Tempels, W.J.M. Underberg, G.W. Somsen, G.J. de Jong, Anal. Chem. 76 (2004) 4432.
- [11] M.C. Breadmore, A.S. Palmer, M. Curran, M. Macka, N. Avdalovic, P.R. Haddad, Anal. Chem. 74 (2002) 2112.
- [12] N.A. Guzman, S.S. Park, D. Schaufelberger, L. Hernandez, X. Paez, P. Rada, A.J. Tomlinson, S. Naylor, J. Chromatogr. B 697 (1997) 37.
- [13] F. Benavente, M.C. Vescina, E. Hernández, V. Sanz-Nebot, J. Barbosa, N.A. Guzman, J. Chromatogr. A 1140 (2007) 205.
- [14] Q. Yang, A.J. Tomlinson, S. Naylor, Anal. Chem. 71 (1999) 183A.
- [15] D. Schaller, E.F. Hilder, P.R. Haddad, Anal. Chim. Acta 556 (2006) 104.
- [16] E.F. Hilder, F. Svec, J.M.J. Fréchet, J. Chromatogr. A 1044 (2004) 3.
- [17] J.P. Quirino, M.T. Dulay, B.D. Bennett, R.N. Zare, Anal. Chem. 73 (2001) 3921.
- [18] J.P. Quirino, M.T. Dulay, B.D. Bennett, R.N. Zare, Anal. Chem. 73 (2001) 5539.
- [19] J.P. Quirino, M.T. Dulay, R.N. Zare, Anal. Chem. 73 (2001) 5557.
- [20] N.E. Barylá, N.P. Tótl, Analyst 128 (2003) 1009.
- [21] M.C. Breadmore, Anal. Chim. Acta 556 (2006) 121.
- [22] J.P. Hutchinson, P. Zakaria, A.R. Bowie, M. Macka, N. Avdalovic, P.R. Haddad, Anal. Chem. 77 (2005) 407.
- [23] N. Johannesson, J. Bergquist, J. Pharm. Biomed. Anal. 43 (2007) 1045.
- [24] M. Langemark, F.W. Bach, R. Ekman, J. Olesen, Pain 63 (1995) 103.



## Solid-phase molecularly imprinted pre-concentration and spectrophotometric determination of isoxicam in pharmaceuticals and human serum

B. Rezaei\*, S. Mallakpour, N. Majidi

Department of Chemistry, Isfahan University of Technology, Isfahan 84156-83111, Iran

### ARTICLE INFO

#### Article history:

Received 13 August 2008

Received in revised form

19 November 2008

Accepted 22 November 2008

Available online 3 December 2008

#### Keywords:

Molecularly imprinted polymer

Isoxicam

Spectrophotometry

Pharmaceutical and biological samples

### ABSTRACT

A selective molecularly imprinted polymer (MIP) has been synthesized for isoxicam pre-concentration, followed by its spectrophotometric determination based on hydrogen bonding interactions between examined drug and alizarin yellow GG. This method is able to evaluate isoxicam in range of  $1.0 \times 10^{-3}$  to  $20.0 \mu\text{g mL}^{-1}$ , with a limit of determination of  $1.0 \text{ ng mL}^{-1}$ . The retention capacity and pre-concentration factor of prepared sorbent are  $18.5 \text{ mg g}^{-1}$  and 200, respectively; and the prepared MIPs can be reused at least for five times. The MIP capability for isoxicam selection and extraction from the solution is higher than non-imprinted polymer (NIP). Under optimum conditions, this procedure can be successfully applied to assay trace amounts of isoxicam in pharmaceutical and biological samples.

© 2008 Elsevier B.V. All rights reserved.

### 1. Introduction

Non steroidal anti-inflammatory drugs (NSAIDs) are a well known class of anti-pyretic, analgesic and anti-inflammatory drugs [1]. Certain NSAID agents have been claimed as being able in decreasing the onset of tumors in patients to whom the drugs have been administrated for prolong period of time [2,3]. Recently, several other functions of this group of drugs have been identified which consist of chemoprevention [4–6], chemosuppression [7], UV-sensitization [8,9] and UV-protection [10]. Epidemiological studies have shown that long term use of NSAIDs reduces the risk of developing Alzheimer's disease and delays its onset [11–13].

Among NSAIDs those from the oxicam family have been extensively used all over the world in a variety of inflammatory and rheumatic disease in humans [14]. Isoxicam, 4-hydroxy-2-methyl-N-[5-methyl-3-isoxolyl-2H-1,2-benzothiazine-3-carboxamide-1,1-dioxide], is a potent, orally active, long life non steroidal anti-inflammatory drug. Side effects can occur with all medications, and the most important side effects that have been reported with isoxicam are hepatic toxicity and skin toxicity [15,16]. The importance of sensing isoxicam might benefit for elder home-care system especially Stevens-Johnson syndrome (SJS) or toxic epidermal necrolysis (TEN) [17,18].

A few numbers of techniques exist for the determination of isoxicam in biological fluids, including high performance liquid

chromatography [19,20] and liquid chromatography–tandem mass spectrometry [21], which are expensive, day to day maintenance is high and they have insufficient sensitivity owing to chromatographic interferences and also need the use of large biological fluid volumes and expensive and toxic solvents. So there is a considerable interest in developing a rapid and sensitive method with simple sample preparation steps for the determination of isoxicam in human plasma to evaluate pharmacokinetics in transdermal permeation studies. However, the availability of spectrophotometric apparatus and reagents and the simplicity of analytical procedure make the technique attractive for a wide range of determinations, but the procedure has low sensitivity.

Pre-treatment and enrichment processes are indispensable for trace analysis of target analytes in biological, pharmaceutical and environmental samples. Solid-phase extraction (SPE) is a well-established method for sample clean-up and pre-concentration for aqueous samples at trace levels. The main problem associated with SPE columns packed with ordinary stationary phases is low selectivity of the retention mechanism. Molecularly imprinted polymers (MIPs) capable of producing materials with “antibody-like” selectivity are extensively cross-linked polymers containing specific recognition sites with a predetermined selectivity for analytes of interest [22–27]. The chemical and physical robustness of the MIP, in combination with the polymer's stability, selectivity and sensitivity, has proven it to be a good sorbent for molecularly imprinted solid-phase extraction (MISPE) applications [28]. The combination of selective MIPs pre-concentration with spectrophotometric determination makes it possible to determine low concentrations of analyte.

\* Corresponding author. Tel.: +98 3113912351; fax: +98 3113912350.  
E-mail address: [rezaei@cc.iut.ac.ir](mailto:rezaei@cc.iut.ac.ir) (B. Rezaei).

In this work a selective MIP clean-up and pre-concentration approach is applied prior to spectrophotometric measurement of isoxicam to introduce a simple, rapid, economical and sensitive method for evaluation of isoxicam in complex matrixes. The proposed spectrophotometric determination is based on the molecular binding via hydrogen bonding interactions between the examined drug and alizarin yellow GG and the increase in the absorbance of the reagent, at  $\lambda_{\max} = 354$  nm, is proportional to the concentration of analyte. Various parameters have been evaluated and the developed procedure has been successfully employed for the evaluation of isoxicam in real samples with higher recoveries than other previous determination methods.

## 2. Experimental

### 2.1. Apparatus

A Diode Array UV–vis spectrophotometer (Lighthwave (Cambridge, WPA, England) was used for recording the absorption spectra. A Metrohm pH meter (Herisau, Switzerland) was applied to control the pH of the medium. A peristaltic pump (Ismatec (Zürich, MCP, Switzerland)) was used to adjust the flow rate and driving force. A polypropylene column (53.0 mm in length and 6.5 mm i.d.) was used in SPE procedure and Tygon rubber tubes with 0.76 mm i.d. were used for delivery of the solutions.

### 2.2. Reagents

A 100.0  $\mu\text{g mL}^{-1}$  standard solution of isoxicam was prepared by dissolving 0.0104 g of isoxicam (Sigma–Aldrich, Germany) in acetone and diluting it in a 100 mL volumetric flask. All working solutions of isoxicam were prepared by serial dilution of the stock solution with water. Because of the limited solubility of isoxicam, preparing its solution with higher concentrations was not possible.

An aqueous solution ( $2.0 \times 10^{-3}$  mol L<sup>-1</sup>) of alizarin yellow GG (Merck, Germany) was prepared by dissolving 0.0618 g of alizarin yellow GG in doubly distilled water and diluting it in a 100 mL volumetric flask.

Britton–Robinson Buffer solutions from 2.0 to 8.0 (phosphoric acid, acetic acid, and boric acid (0.04 mol L<sup>-1</sup>) with appropriate volumes of NaOH, 0.2 mol L<sup>-1</sup>), were prepared.

Dibucaine, piroxicam, hydrochlorothiazide and desipramine hydrochloride were Sigma–Aldrich products, Germany. Methacrylic acid (MAA), ethylene glycol dimethacrylate (EDMA), 2,2'-azobis(2-isobutyronitrile) (AIBN), dimethylformamide (DMF) and acetone were purchased from Fluka in extra pure grade. All solvents (methanol, acetic acid) were HPLC-grade from Merck, Germany. All other chemicals were analytical reagent grade, and deionized doubly distilled water was used for preparation of the solutions.

### 2.3. Real sample preparation

Three isoxicam capsules (containing: 100.0 mg Isoxicam, special 1,2-diacyl-glycero-3-phosphocoline, silica, calcium chloride) were weighed and powdered. An accurately weighed portion of the powder, equivalent to 5.0 mg of active ingredient, was dissolved in 5.0 mL of acetone. Using an ultrasonic bath, the powder was completely disintegrated and after centrifugation the solution was filtered. Before determination, the sample solution was diluted appropriately to ensure the concentrations were within the linear range.

To prepare human serum sample, 5.0 mL of blood sample (taken from the health center of Isfahan University of Technology) was kept at 37 °C for 5 min and after addition of 2.0 mL methanol, the mixture was centrifuged (5 min with 3000 rpm.). Then, the obtained deproteinized human serum was diluted to 20.0 mL by doubly distilled

water and an aliquot of 2.0 mL of this solution was used for each experiment.

### 2.4. Preparation of molecularly imprinted polymer

The synthesis of isoxicam-imprinted polymer was based on non-covalent interactions between the analyte and the functional monomer through the thermal radical copolymerization. In molecular imprinting process, a template molecule associates with monomer to form a complex. This complex is then polymerized with a matrix-forming monomer (cross-linker) to produce a resin. The experimental results and computational approaches (density functional theory method) determined that the most favorable monomer for preparing isoxicam-MIP was methacrylic acid and the preferred molar ratio of analyte:monomer:cross-linker was 1:5:25. Thus, isoxicam (0.78 mmol) was dissolved in the solvent (DMF, 8.5 mL) at 50 °C in a glass tube. Functional monomer (MAA, 3.9 mmol), cross-linker (EDMA, 19.5 mmol) and initiating agent (AIBN, 0.3 mmol) were added and the mixture was degassed with nitrogen for 10 min, and then was sealed. Then the glass tube was placed in a silicone oil bath to control the temperature (24 h at 60 °C). After polymerization, the glass tube was broken, and the polymer was mechanically grounded in a mortar. A steel sieve was used to select particles with sizes between ~50 and 70  $\mu\text{m}$ . Starting with 1.0 g of isoxicam, 15.0 g of MIPs will be synthesized.

Upon removal of the template species, cavity can then be used to selectively rebind the template from a mixture of chemical species. Essentially, the washing procedure should disrupt the polymer-template hydrogen bondings so that the template can be washed away, while at the same time leaving the polymeric architecture sculpted. To remove isoxicam, a soxhlet extraction system was used and the extraction with various ratios of methanol:acetic acid (9:1, 7:3, 5:5, 3:7 and 1:9) in different times, from 2 to 72 h, was followed by spectrophotometric determination to investigate the optimum rebinding conditions. Results (not shown here) indicated that the best ratio of extracting solvent (methanol:acetic acid) was 9:1 and the extraction time of 72 h was selected to be certain that all of the isoxicam has been removed from the polymer matrix. Then the prepared MIP particles were washed with a copious amount of pure water and kept in room temperature overnight. The overall time for preparation of MIPs was about five days.

As a control in polymerization, a non-imprinted polymer (NIP) was also synthesized in the same way but in the absence of the analyte (no template for trapping the analyte). To evaluate the imprinting effect and the nonspecific absorptions, the selectivity of NIP and MIP were also compared.

### 2.5. General procedure

#### 2.5.1. Spectrophotometric determination procedure

The comparison between absorption spectra obtained for isoxicam solution (pH 5.0) in the absence and presence of alizarin yellow GG showed an increase in the absorption value (354 nm) due to the isoxicam-alizarin yellow GG hydrogen bonding interactions (Fig. 1). The sensitivity coefficient, at 354 nm, was calculated to be  $6.12 \times 10^4$  L mol<sup>-1</sup> cm<sup>-1</sup>.

Specific amounts of buffer solution and acetone were transferred into a 10 mL calibrated flask to achieve suitable percent of acetone (v:v) in the final assay solution. Then an aliquot containing known amounts of isoxicam was added and in the final step, alizarin yellow GG was added to volumetric flask and completed the volume to 10.0 mL with water. The absorbance ( $A_s$ ) was measured for this system at 354 nm against the absorbance of blank solution prepared in the same way without addition of the examined drug ( $A_b$ ), and the signal was taken as the difference between two obtained absorptions ( $\Delta A = A_s - A_b$ ). In view of the fact that the results represented



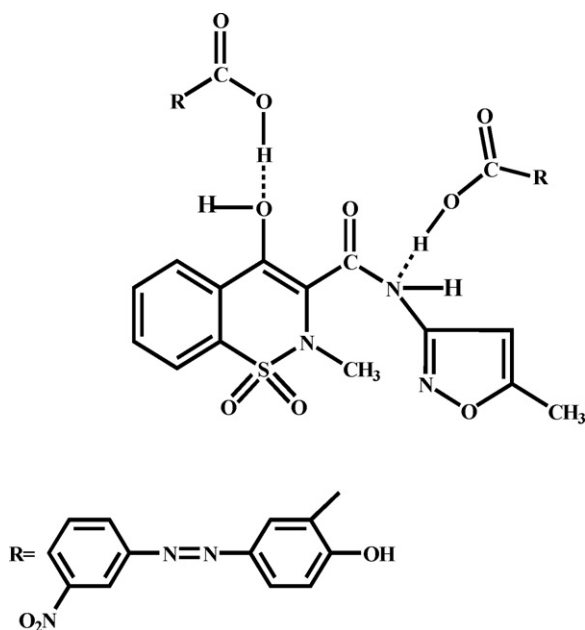


Fig. 1. The schematic structure of molecular coupling (hydrogen bonding interactions) between isoxicam and alizarin yellow GG.

low sensitivity, so a pre-treatment procedure is needed to pre-concentrate the sample from complex matrixes and improve the limit of determination. Under optimized conditions, spectrophotometric procedure outcomes (specially obtained calibration curve data) were used to evaluate the clean-up and pre-concentration results.

#### 2.5.2. The extraction and pre-concentration procedure

The cartridge was packed with 150 mg of prepared MIPs and he tygon tubes with i.d. 0.76 mm were applied to deliver solutions by means of a peristaltic pump at optimum flow rate. The absorbance of standard isoxicam solution was measured spectrophotometrically ( $A_1$ ) and then a specific volume of isoxicam, with the same concentration, was passed through column and its absorption was measured, too ( $A_2$ ). In order to investigate the binding affinity of column and SPE recoveries, the packed column was washed with 2.0 mL of extracting solvent (methanol, acetic acid mixture). After solvent evaporation and dissolving the remained solute in 2.0 mL of acetone, the concentration of eluted solution was determined spectrophotometrically (Fig. 2). By applying a suitable elution sol-

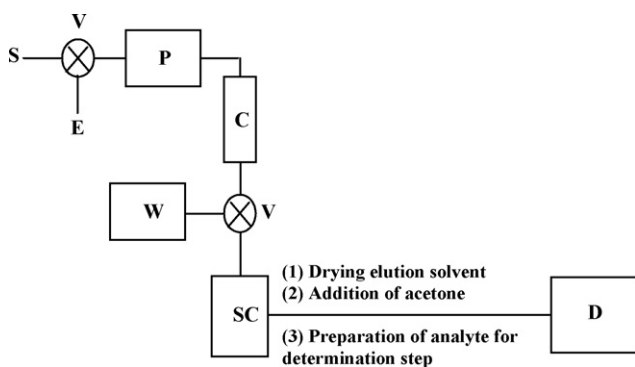


Fig. 2. Schematic diagram of extraction system applied for pre-concentration of isoxicam prior to its spectrophotometric determination. S: sample loop; E: eluting solvent loop; V: valve for directing sample or eluting solvent toward pump; P: peristaltic pump; C: MIPs packed column; SC: sample collector; D: determination system; W: waste.

vent, the nonspecific adsorption of analyte can be reduced and here the optimum mixture of acetic acid:methanol (1:9) was applied to wash isoxicam from polymers.

All of the process was repeated for NIP to control the selectivity of imprinted polymer and the obtained results demonstrated that NIP has no significant affinity to trap isoxicam and it will adsorb about 6.0% of isoxicam but the MIP will trap 95% of isoxicam, which is indicating that NIP has only nonspecific adsorption properties.

### 3. Results and discussion

#### 3.1. Determination step

##### 3.1.1. Effect of variables

By following general determination procedure with various amounts of acetone, the maximum and stable absorbance value was obtained with 30% of acetone (v:v). In low concentrations of acetone the solvation effect plays an important role. Although, increasing the amount of acetone to about 30% will amplify the molecular coupling, in higher concentrations, the polarity of solvent decreases the hydrogen bonding attraction in the system.

The general process was followed with different concentrations of reagent solution, and the maximum absorbance was obtained with  $4.0 \times 10^{-5}$  mol L<sup>-1</sup> of alizarin yellow GG. It can be due to the fact that by raising the alizarin concentration to  $4.0 \times 10^{-5}$  mol L<sup>-1</sup>, the molecular coupling increases; but in higher reagent concentrations the signal of blank solution dominates the changing signal of alizarin-isoxicam system.

The molar absorptivity of alizarin yellow GG is dependent on pH variations. The relation between analytical signal and pH has been shown in Fig. 3. As can be seen there are three distinctive peaks in this figure, two of them (pH 3.0 and pH 7.0) are related to the change of alizarin yellow GG molar absorptivity that has affected on the blank signal ( $A_b$ ). The maximum signal ( $\Delta A = A_s - A_b$ ), pH 5.0, would represent the effect of pH on hydrogen bonding formation. So, pH 5.0 was selected as optimum pH for determination procedure.

Moreover, the optimum volume of buffer solution, to achieve stable absorbance value, was also studied and found to be 4.0 mL (total of 10.0 mL of solution).

The most favorable sequence was 'buffer-acetone-drug-reagent' for achieving highest absorbance signal and other sequences needed longer time to obtain higher stability.

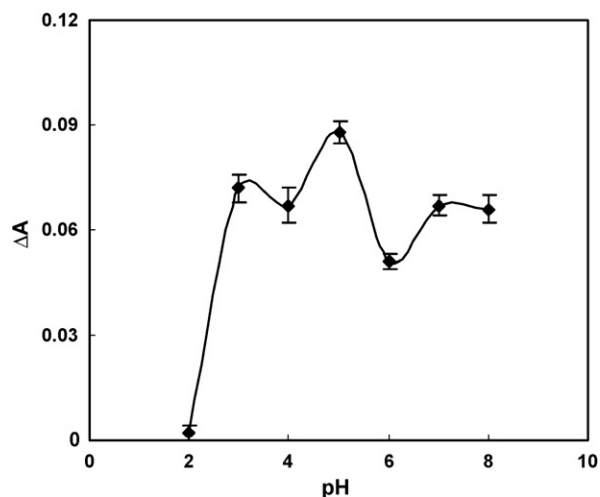


Fig. 3. Effect of pH on the determination of isoxicam. Conditions: isoxicam,  $2.0 \mu\text{g mL}^{-1}$ ; alizarin yellow GG,  $4.0 \times 10^{-5}$  mol L<sup>-1</sup>; acetone 30%.

**Table 1**  
Interferences effect on the determination of  $0.5 \mu\text{g mL}^{-1}$  isoxicam.

Species	Tolerance limit ( $W_{\text{int}}/W_{\text{isoxicam}}$ )
Citrate, Ascorbic acid, Glucose	1000
$\text{Mg}^{2+}$ , $\text{K}^{2+}$ , $\text{Na}^+$ , $\text{SCN}^-$ , $\text{NO}_3^-$ , Fructose, Sacarose	500
$\text{Cl}^-$	300
$\text{Ca}^{2+}$	100
Cysteine, $\text{Co}^{2+}$	50
$\text{Fe}^{2+}$ , $\text{Fe}^{3+}$	1

### 3.1.2. The stoichiometric relationship

The stoichiometric relationship between drug and alizarin system was investigated by applying the molar ratio method at the wavelength of maximum absorbance. The obtained results showed that the stoichiometric ratio of the molecular-association is 1:2 (isoxicam: alizarin yellow GG). In acidic media (pH 5.0), the carboxylic group of alizarin yellow GG can form hydrogen bonding with NH and OH groups of isoxicam (Fig. 1).

In strong ionic strengths, the intermolecular association (such as interaction of carboxylic group of alizarin with NH and OH groups of isoxicam) will overcome the intramolecular ones (such as interaction of hydroxyl bonding with carbonyl group in isoxicam and hydroxyl bonding with carbonyl group in alizarin). As a proof, the effect of ionic strength was investigated and the results indicated that the molecular coupling interaction increases by adding NaCl concentrations in the range  $0.05\text{--}0.4 \text{ mol L}^{-1}$ .

### 3.1.3. Influence of foreign matrix

The influence of contaminant species (present in various samples) on the determination of isoxicam was investigated. Synthetic mixtures of solution containing isoxicam ( $0.5 \mu\text{g mL}^{-1}$ ) and 1000-fold excess amounts of diverse ions were analyzed. Then, their signal was compared with the signal of isoxicam solution in the absence of contaminant species. If the presence of species caused a relative error more than 3.0%, the amount of contaminant species was decreased, and the procedure was followed as previous until a relative error less than 3.0% was achieved. The results are summarized in Table 1.

## 3.2. Pre-concentration step

### 3.2.1. Effect of variables

To evaluate the effective parameters, the extraction percent ( $E\%$ ) was calculated:

$$E\% = \frac{C_2}{C_1} \times 100\% \quad (1)$$

where  $C_2$  and  $C_1$  are the concentration of specific volume of isoxicam solution enriched by polymer (which can be obtained by recorded absorbance and calibration curve data) and the initial concentration of isoxicam with the same volume (before pre-concentration), respectively.

The effect of pH on the extraction of isoxicam was examined in range of 2.0–7.0, and the results depicted in Fig. 4. The maximum extraction percent (95.0%) was obtained at pH 5.0.

The influence of analyte retention time was investigated by passing 10.0 mL of isoxicam solution ( $3.0 \mu\text{g mL}^{-1}$ ) with pH 5.0 in different flow rates and the best flow rate was selected to be  $0.1 \text{ mL min}^{-1}$ . In higher flow rates, the analyte does not have enough residence time for effective interactions with sorbent.

### 3.2.2. Retention capacity of MIP

In this work a batch method was applied to determine the retention capacity of synthesized molecular imprinted polymer. 20.0 mL solutions of isoxicam ( $0\text{--}100.0 \mu\text{g mL}^{-1}$ , pH 5.0) were stirred with 0.050 g of MIP for 12 h. The amount of analyte adsorbed per unit

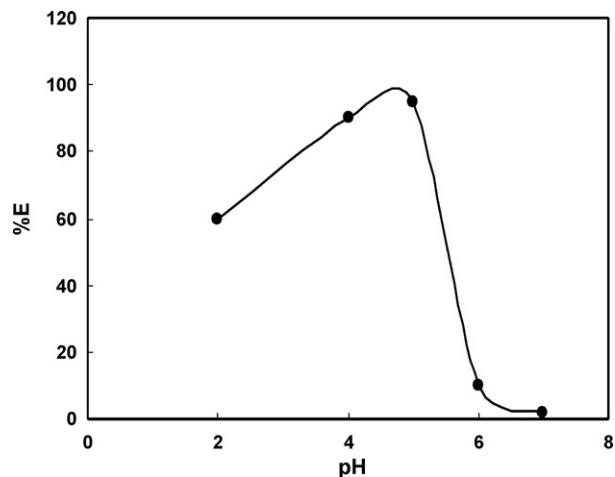


**Fig. 4.** Effect of pH on the pre-concentration and extraction of isoxicam solution with MIP. Conditions: isoxicam,  $3.0 \mu\text{g mL}^{-1}$ ; flow rate,  $0.125 \text{ mL min}^{-1}$ .

mass of the polymer increases with raising the initial concentration of isoxicam. The amount of bounded isoxicam was obtained using this equation:

$$Q = \frac{(C_i - C_f)V}{w} \quad (2)$$

where  $C_i$  and  $C_f$  are the concentration of isoxicam in the initial solution and after desorption, respectively;  $V$  is the solution volume and  $Q$  is the amount of analyte adsorbed on to the unit of the polymer ( $\text{mg g}^{-1}$ ). The maximum adsorption capacity ( $Q_{\text{max}}$ ) was found to be  $18.5 \text{ mg g}^{-1}$  of sorbent. The Langmuir model was applied to interpret adsorption of isoxicam on imprinted polymer. According to this model and the following expression:

$$Q = \frac{bCQ_{\text{max}}}{(1 + bC)} \quad (3)$$

there was a linear relationship between  $1/Q$  and  $1/C$  with a correlation coefficient of 0.9935. Where  $C$  is the equilibrium isoxicam concentration in solution and  $b$  is the Langmuir constant.

### 3.2.3. Breakthrough volume

The breakthrough volume is the volume at which the absorbance signal reaches 1% of its 100% value if the cartridge extracts no longer quantitative.

Different volumes of isoxicam solution ( $3.0 \mu\text{g mL}^{-1}$ ) from 10 to 500 mL were passed through the column and their recoveries were measured. After passing 400 mL of isoxicam solution, the column was saturated. The elution solvent volume (for removing trapped isoxicam) was 2.0 mL, and so a pre-concentration factor of 200 can be obtained by this MIP-SPE procedure.

### 3.2.4. Selectivity of MIP

To evaluate the interference effect, the isoxicam solution ( $3.0 \mu\text{g mL}^{-1}$ , pH 5.0) containing specific amount of interfering species was passed through the column. The column was washed with ultra pure water to remove physically adsorbed species, and then it was eluted by 2.0 mL of methanol:acetic acid (9:1), to remove isoxicam. After vaporization of eluting solvent, the residue was redissolved in acetone (2.0 mL) and the absorbance was recorded. The same process was repeated for isoxicam solution in the absence of interfering species. The tolerance limit was defined as the concentration of added species causing a relative error less than 3.0%. By molecularly imprinted solid-phase extraction, the interference of some ions such as  $\text{Fe}^{2+}$ ,  $\text{Fe}^{3+}$  and  $\text{Co}^{2+}$  (with spectral interference) would be completely removed which is important in analyzing of complex matrixes such as biological fluids.

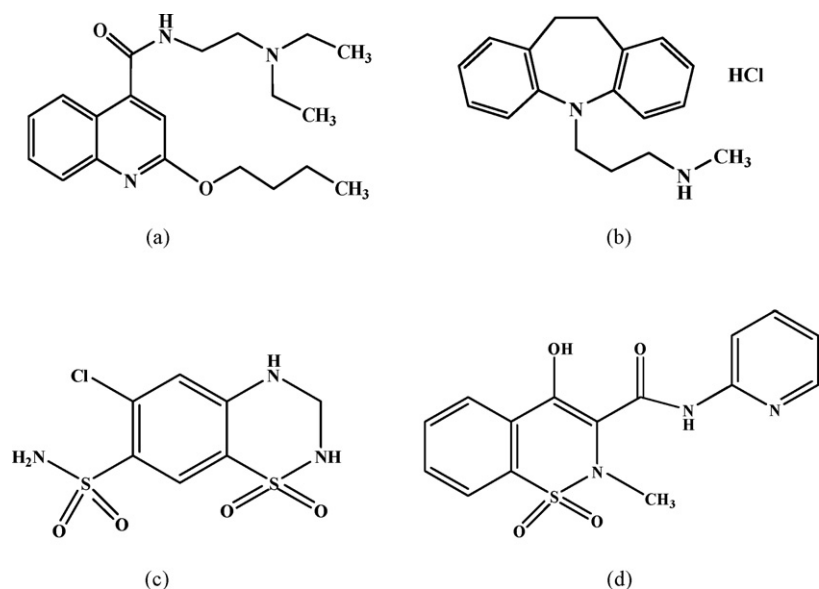


Fig. 5. The molecular structures of (a) dibucaine, (b) desipramine hydrochloride, (c) hydrochlorothiazide and (d) piroxicam.

The MIP-SPE and NIP-SPE procedures were repeated for some drugs (instead of isoxicam) which have functional groups like isoxicam that could also be involved in hydrogen bonding formation with the polymer ((Fig. 5a–d)). But the difference between MIP-SPE and NIP-SPE results was excessively negligible in comparison with the results for isoxicam solution (with the same volume). The results represented that the affinity and specificity of MIPs for isoxicam is more than other examined drugs. This fact can be attributed to the high selectivity of prepared MIP.

It is important to mention that in conventional SPE methods the separation is based on size, charge and functional groups and it is not dependent on the molecular shape and conformation. But, all of the mentioned factors above are important in molecularly imprinted polymer and the optimum monomers and conditions for preparing MIPs and NIPs would be different for each compound of interest which is dependent on these factors to augment the selectivity of sorbents.

### 3.2.5. Evaluation of sorbent reproducibility

For investigating the ability of molecularly imprinted polymer to adsorb isoxicam after sequential elution with 2.0 mL of eluting solvent (methanol: acetic acid, 9:1), the pre-concentration process was repeated several times with the imprinted particles. It was indicated that the recoveries were decreased from 95% to 94% after five repeated adsorption–desorption cycles.

### 3.3. Analytical features

Under mentioned optimized experimental conditions, a series of standard solutions of isoxicam were measured spectrophotometri-

cally before (1) and after using MIP-SPE procedure (2). All of the calibration results are summarized in Table 2.

There was a linear relationship (1) between absorbance and drug concentration in the range of 0.2–20.0  $\mu\text{g mL}^{-1}$  ( $A = 0.0356C + 0.0087$ ;  $r^2 = 0.9989$ ). The experimental limit of detection was 0.09  $\mu\text{g mL}^{-1}$  ( $3S_b/m = 3$ ;  $S_b$  was measured for ten replicate analysis of blank solution). For the concentrations of 0.7, 5.0 and 10.0  $\mu\text{g mL}^{-1}$  of isoxicam, the relative standard deviations (obtained by running ten replicate samples) were 4.8, 1.78 and 1.61%, respectively.

A calibration curve (2) from  $1.0 \times 10^{-3}$  to 20.0  $\mu\text{g mL}^{-1}$  was also plotted for isoxicam solution after passage through MIP column ( $A = 0.185C + 0.0147$ ;  $r^2 = 0.9980$ ) with a limit of determination of 1.0  $\text{ng mL}^{-1}$ .

For the concentrations of 0.7, 5.0 and 10.0  $\mu\text{g mL}^{-1}$  of isoxicam, the relative standard deviations (obtained by running ten replicate samples) were 4.8, 1.78 and 1.61%, respectively. The RSD of extraction percents obtained for solutions of isoxicam (four samples; 3.0  $\mu\text{g mL}^{-1}$ ) after passage through the column (one day) was 0.66%, and the inter-day assay of the method for three samples (3.0  $\mu\text{g mL}^{-1}$ ), measured in different days, was evaluated to be 1.81%.

### 3.4. Analytical application

The recommended method has been applied successfully for the extraction and determination of isoxicam in the pharmaceutical and biological samples. The analysis was performed on human serum and isoxicam capsule by using the standard addition technique. The results are summarized in the Table 3 (each analysis was

Table 2  
Calibration curve parameters.

Analyte	LOD <sup>a</sup> ( $\mu\text{g mL}^{-1}$ )	LOQ <sup>b</sup> ( $\mu\text{g mL}^{-1}$ )	Linear range ( $\mu\text{g mL}^{-1}$ )	$r^2$	$S_R^c$ ( $\times 10^{-3}$ )	$S_m^d$ ( $\times 10^{-5}$ )	$S_i^e$ ( $\times 10^{-4}$ )
Isoxicam (1)	0.09	0.2	0.2–20.0	0.9987	1.36	6.78	4.50
Isoxicam (2)	$1.0 \times 10^{-3}$	$1.0 \times 10^{-3}$	$1.0 \times 10^{-3}$ –20.0	0.9980	1.47	5.95	5.10

<sup>a</sup> LOD: Limit of detection.

<sup>b</sup> LOQ: Limit of quantitation.

<sup>c</sup>  $S_R$ : Regression coefficient error.

<sup>d</sup>  $S_m$ : Slope of the calibration curve.

<sup>e</sup>  $S_i$ : Intercept errors of the calibration curve.

**Table 3**  
Results of isoxicam determination in real samples.

Sample	Added ( $\mu\text{g mL}^{-1}$ )	Found ( $\mu\text{g mL}^{-1}$ )	Recovery (%)
Human serum	0.0	–	–
	3.0	$3.15 \pm 0.04^a$	$105.2 \pm 1.33$
	5.0	$5.34 \pm 0.04$	$106.7 \pm 0.80$
	7.0	$7.14 \pm 0.05$	$102.0 \pm 0.71$
	10.0	$9.70 \pm 0.03$	$97.0 \pm 0.30$
Isoxicam capsule	0.0	$0.94 \pm 0.06$	–
	3.0	$4.11 \pm 0.01$	$102.7 \pm 0.25$
	5.0	$5.99 \pm 0.05$	$99.8 \pm 0.83$
	7.0	$7.99 \pm 0.06$	$99.9 \pm 0.75$

<sup>a</sup> Standard deviation for three replicated measurements.

done three times) and good recoveries in all samples were obtained. In order to eliminate the interference of real sample ingredients, the column was washed with water after loading real samples on it and then it was eluted by elution solvent to measure isoxicam content (the same as described procedure). The linearity was ranged from 0.02 to 10.0  $\mu\text{g mL}^{-1}$  ( $r^2 = 0.9999$ ) and 0.01–10.0  $\mu\text{g mL}^{-1}$  ( $r^2 = 0.9996$ ) in human serum and isoxicam capsule analysis. The high percentage recoveries indicate no interferences from ingredients that might be found in different formulations, which evaluates the high efficiency of extraction procedure.

### 3.5. Response characteristics

As has been mentioned earlier there are a few proposed methods for evaluation of isoxicam. The RSD values for these methods were obtained from 2.6 to 10.0%, and between 3.3 and 9.0% for procedures explained in references 19 and 20, respectively. The recoveries (determination of isoxicam in plasma samples) for previous methods were from 94 to 96% [19]; and 102.5–105.4% (RSDs from 2.5 to 5.4%) [20]. Also the linearity in plasma ranged from 0.2 to 10.0  $\mu\text{g mL}^{-1}$  in both cases which are not as good as outcomes of proposed procedure. The recovery of isoxicam as internal standard for simultaneous determination of some oxamic drugs by LC–MS was 59.7% [21].

Bartesch et al. investigated the photo stability of isoxicam and also they applied some analytical methods for quantitation of this drug [29]. The analytical features of the applied procedure are as follows: for HPLC–densitometry, RSDs are from 1.98 to 3.33% ( $40 \text{ mg mL}^{-1}$  to  $2 \mu\text{g mL}^{-1}$ ) and the detection limit was  $5 \mu\text{g mL}^{-1}$ ; for HPLC, RSDs were between 1.5 and 2.57% ( $40 \text{ mg mL}^{-1}$  to  $2 \mu\text{g mL}^{-1}$ ) and the limit of detection was  $0.32 \mu\text{g mL}^{-1}$ ; and for Capillary electrophoresis, RSDs were from 1.42 to 3.47% ( $40 \text{ mg mL}^{-1}$  to  $2 \mu\text{g mL}^{-1}$ ) and the detection limit was  $1 \mu\text{g mL}^{-1}$ .

In comparison with these results, the precision of proposed method represented by RSD values in each step: determination (1.61–4.8%); pre-concentration (0.66%) and real sample analysis (human serum: 0.31–1.3%; isoxicam capsule: 0.24–0.83%) is better than the others. Also the determination limit and linear range in sample analysis and simple determination of isoxicam is improved in this procedure.

## 4. Conclusion

In view of the need for a selective and sensitive method to determine isoxicam in complex matrix samples, in this work a

non-covalently molecular imprinted polymer was synthesized and applied as sorbent in SPE to obtain a selective and safe enrichment of isoxicam with high recoveries. The extraction method is cost effective and does not consume large amounts of organic and toxic solvents. Also a simple spectrophotometric method was applied to determine isoxicam which was extracted from complex matrixes. However the preparation of sorbents is time consuming, but the amount of synthesized polymer is high and also each packed column can be used at least five times. The obtained results show that the proposed method can be used for pre-concentration and evaluation of trace amounts of isoxicam in real samples and the limit of determination, linear dynamic range, selectivity and precision is better than the other reported methods.

## Acknowledgments

The authors acknowledge the Isfahan University of Technology Council and Center of Excellency in Sensors and Green Chemistry Research for supporting this work.

## References

- [1] R. Banerjee, H. Chakraborty, M. Sarkar, Spectrochim. Acta: A 59 (2003) 1213.
- [2] N. Arber, C.J. Eagle, J. Spicak, I. Racz, P. Dite, J. Hajer, M. Zavoral, M.J. Lechuga, P. Gerletti, J. Tang, R.B. Rosenstein, K. Macdonald, P. Bhadra, R. Fowler, J. Wittes, A.G. Zauber, S.D. Solomon, B. Levin, N. Engl. J. Med. 355 (2006) 885.
- [3] Y.I. Cha, R.N. Dubois, Annu. Rev. Med. 58 (2007) 239.
- [4] M.B. Sporn, N. Suh, Carcinogenesis 21 (2000) 525.
- [5] S.A. Bingham, N.E. Day, R. Luben, P. Ferrari, N. Slimani, T. Norat, F. Clavel-Chapelon, E. Kesse, A. Nieters, H. Boeing, Lancet 361 (2003) 1496.
- [6] E.D. Courtney, D.M. Melville, R.J. Leicester, Aliment. Pharmacol. Ther. 19 (2004) 1.
- [7] E.M. Grossman, W.E. Longo, N. Panesar, J.E. Mazuski, D.L. Kaminski, Carcinogenesis 21 (2000) 1403.
- [8] D.E. Moore, Drug Saf. 25 (2002) 345.
- [9] G. Serrano, J.M. Fortea, J.M. Latasa, O. San Martin, J. Bonillo, M.A. Miranda, J. Am. Acad. Dermatol. 26 (1992) 545.
- [10] P. Mayer, U. Schäfer, H.J. Krämer, B. Irlinger, W. Steglich, Arch. Dermatol. Res. 294 (2002) 131.
- [11] K.P. Townsend, D. Praticó, FASEB J. 19 (2005) 1592.
- [12] B.A. In't Veld, A. Ruitenber, A. Hofman, L.J. Launer, C.M. van Duijn, Th. Stijnen, M.M.B. Breteier, B.H.C. Stricker, N. Engl. J. Med. 345 (2001) 1515.
- [13] C.A. Szekely, J.E. Thorne, P.P. Zandi, M. Ek, E. Messias, J.C.S. Breitter, S.N. Goodman, Neuroepidemiology 23 (2004) 159–169.
- [14] J. Steinmeyer, Y.T. Konttinen, Adv. Drug Deliver. Rev. 58 (2006) 168.
- [15] Ho. Ollagnon, B. Perpoint, H. Decousus, M. Ollagnier, Hepatogastroenterology 33 (1986) 109.
- [16] F. Von Bruchhausen, G. Dannhardt, S. Ebel, A.W. Frahm, E. Hackenthal, R. Hänsel, U. Holzgrabe, K. Keller, E. Nürnberg, H. Rimpler, G. Schneider, P. Surmann, H.U. Wolf, G. Wurm, Hagers Handbuch der Pharmazeutischen Praxis, 5th ed., Springer Verlag, Berlin, Heidelberg, 1993.
- [17] M. Mockenhaupt, J.P. Kelly, D. Kaufman, R.S. Stern, J. Rheumatol. 30 (2003) 2234.
- [18] L.H. Yueh, P.S. Ming, Singapore Gen. Hosp. Proc. 15 (2006) 114.
- [19] R.W. Bury, J. Chromatogr. B: Biomed. Sci. Appl. 337 (1985) 156.
- [20] A.C. Daftsios, E.L. Johnson, F.J. Keeley, C. Gryczko, V. Rawski, J. Chromatogr. B: Biomed. Sci. Appl. 305 (1984) 145.
- [21] H.Y. Ji, H.W. Lee, Y.H. Kim, D.W. Jeong, H.S. Lee, J. Chromatogr. B: Biomed. Sci. Appl. 826 (2005) 214.
- [22] L. Wang, Z. Zhang, Anal. Chim. Acta 592 (2007) 115.
- [23] C. Baggiani, L. Anfossi, C. Giovannoli, Anal. Chim. Acta 591 (2007) 29.
- [24] C. Baggiani, P. Baravalle, G. Giraudi, C. Tozzi, J. Chromatogr.: A 1141 (2007) 158.
- [25] J. Hantash, A. Bartlett, Ph. Oldfield, G. Denes, R. O'Rielly, D. Roudiere, S. Menduni, J. Chromatogr.: A 1125 (2006) 104.
- [26] L.D. Bolisay, J.N. Culver, P. Kofinas, Biomaterials 27 (2006) 4165.
- [27] G. D'Agostino, G. Alberti, R. Biesuz, M. Pesavento, Biosens. Bioelectron. 22 (2006) 145.
- [28] L.I. Andersson, J. Chromatogr.: B 739 (2000) 163.
- [29] H. Bartesch, A. Eiper, K. Habiger, H. Kopelent-Frank, J. Chromatogr.: A 846 (1999) 207.



## Use of near-infrared reflectance spectroscopy for shelf-life discrimination of green asparagus stored in a cool room under controlled atmosphere

María-Teresa Sánchez<sup>a,\*</sup>, Dolores Pérez-Marín<sup>b,\*</sup>, Katherine Flores-Rojas<sup>a</sup>, José-Emilio Guerrero<sup>b</sup>, Ana Garrido-Varo<sup>b</sup>

<sup>a</sup> Departamento de Bromatología y Tecnología de los Alimentos, Universidad de Córdoba, Edificio Charles Darwin, 14071 Córdoba, Spain

<sup>b</sup> Departamento de Producción Animal, Universidad de Córdoba, Campus Rabanales, 14071 Córdoba, Spain

### ARTICLE INFO

#### Article history:

Received 10 June 2008

Received in revised form

25 November 2008

Accepted 2 December 2008

Available online 6 December 2008

#### Keywords:

Green asparagus

NIR spectroscopy

Non-destructive analysis

Shelf-life

Post-harvest treatment

Discriminant analysis

PLS2

### ABSTRACT

This study sought to evaluate the ability of near-infrared reflectance spectroscopy (NIRS) to classify intact green asparagus, in refrigerated storage under controlled atmosphere, by storage time and post-harvest treatments applied. A total of 468 green asparagus (*Asparagus officinalis*, L., cultivar UC-157) were sampled after 7, 14, 21 and 28 days of refrigerated storage (2 °C, 95% R.H.) under three controlled atmosphere (CA) treatments: air (21 kPa O<sub>2</sub> + 0.3 kPa CO<sub>2</sub>), CA<sub>1</sub> (5 kPa O<sub>2</sub> + 5 kPa CO<sub>2</sub>) and CA<sub>2</sub> (10 kPa O<sub>2</sub> + 10 kPa CO<sub>2</sub>). Two commercially available spectrophotometers were evaluated for this purpose: a scanning monochromator (SM) of 400–2500 nm and a combination of diode array and scanning monochromator (DASM) of 350–2500 nm. Models developed using partial least squares 2-discriminant analysis (PLS2-DA) correctly classified between 81–100% of samples by post-harvest storage time, depending on the instrument used. Using similar models, the DASM instrument correctly classified 85% of samples by post-harvest treatment, compared with 72% using the SM. These results confirmed that NIR spectroscopy, coupled with the use of chemometric techniques, provides a reliable, accurate method of predicting the shelf-life of asparagus under different storage conditions and as a function of post-harvest treatment applied; the method can be readily applied at industrial level.

© 2008 Elsevier B.V. All rights reserved.

### 1. Introduction

Asparagus is a highly perishable vegetable, whose post-harvest metabolic activity prompts rapid and undesirable structural modifications [1]. Once cut, the spear undergoes a number of changes (e.g. hardening due to lignifications, loss of soluble carbohydrates, changes in protein content, loss of vitamins, tip lengthening) affecting texture and edibility, and thus shelf-life [2,3].

Asparagus fibrosity increases in the interval between harvest and product cooling, and is influenced both by the type and duration of post-harvest storage [1,4,5]. A negative correlation has been reported between heat accumulation and shelf-life [6,7], so that harvested spears should be cooled as quickly as possible, before they have been exposed to sunlight or adverse temperatures [8].

The requirements for asparagus storage are refrigeration at 0–4 °C and high relative humidity (90–95%) for a period of 2–10 days [1]. High relative humidity is essential, since asparagus dehydrates rapidly, leading to undesirable texture changes and weight

loss. Consumer demand has lately prompted a need for post-harvest storage techniques which not only extend the life of fruit and vegetables over a longer period, but also ensure that initial sensory quality is maintained [9]. Innovations in this field include the use of controlled atmospheres, which preserve product quality and allow the consumer to be presented with characteristics very similar to those of the fresh vegetable [10,11]. The storage of asparagus in a controlled atmosphere may prevent or lessen post-harvest changes in flavor, color and chemical composition [3,12,13]. However, the use of controlled atmospheres should be seen as complementary to the appropriate management of temperature and relative humidity during refrigerated storage [14].

The asparagus processing industry – using both fresh and minimally processed products – requires non-destructive measurement techniques that will allow asparagus to be classified in terms of quality and post-harvest treatment, as well as enabling shelf-life to be estimated. However, the estimation of shelf-life in fruit and vegetable products on the basis of single quality parameters is hindered by a number of constraints, since changes in quality may be due to a large number of factors [15]. In this respect, the information provided by the whole NIR spectrum, considered as the spectral fingerprint of the product analyzed, may be of great value in charting post-harvest asparagus quality and establishing shelf-life.

\* Corresponding authors. Tel.: +34 957 212576; fax: +34 957 212000.

E-mail addresses: [teresa.sanchez@uco.es](mailto:teresa.sanchez@uco.es) (M.-T. Sánchez), [pa2pemad@uco.es](mailto:pa2pemad@uco.es) (D. Pérez-Marín).

**Table 1**

Basic technical features of two spectrophotometers: scanning monochromator (SM) and diode array and scanning monochromator (DASM).

Properties	Instruments	
	SM: FNS-6500	DASM: LabSpec®Pro A108310
Detector type	Silicon, 400–1100 nm. Lead sulphide, 1100–2500 nm	Modular Silicon Array and 2 Peltier cooled InGaAs detectors
Wavelength range (nm)	400–2500	350–2500
Spectral bandpass	10 nm ± 1 nm in reflectance	3 nm at 700 nm. 10 nm at 1400–2100 nm
Spectral data rate	1.8 scans/s	0.1 s
Dispersion	Pre	Post
Light source	Full spectrum	Full spectrum
Analysis mode	Interactance–reflectance	Interactance–reflectance

Near-infrared reflectance spectroscopy (NIRS) shows considerable promise for the non-destructive analysis of food products, and is ideally suited to the requirements of the agrofood industry in terms of both quality control and traceability: it requires little or no sample preparation; it is both flexible and versatile (applicable to multiproduct and multicomponent analysis); it generates no waste, is less expensive to run than conventional methods, and can be built into the processing line, enabling large-scale individual analysis and real-time decision making [16,17]. Although a number of published studies have addressed the application of NIRS technology to prediction of quality parameters in fruit and vegetables [18,19], few papers have focused on its use in asparagus, and particularly in green asparagus. Research has covered neutral detergent and acid detergent fiber content [4], and the estimation of texture-related parameters [20] in dry ground asparagus. Models have been constructed to enable classification by variety [21], again in dry ground green asparagus, as well as by spear area and harvesting date in intact white asparagus [22]. However, no published studies have dealt with the application of NIR spectroscopy models for predicting shelf-life – a major commercial parameter – or the influence of post-harvest treatments on shelf-life.

Most published studies have used previously processed samples rather than intact asparagus [4,20,21], and have thus failed to exploit one of the main advantages of NIRS technology, its non-destructive nature. In recent years, NIRS equipment has undergone radical changes; new-generation instruments are much more versatile, more portable and better adapted to on-site, non-destructive measurement.

The use of PLS-discriminant analysis on spectral data for intact asparagus as a means of classifying the product by storage interval, as an estimator of the shelf-life of the product, and by type of post-harvest treatment was evaluated by comparing the performance of discrimination models with different instruments and different spectrum treatments; finally, the optimum wavelengths for classification purposes were determined.

## 2. Materials and methods

### 2.1. Samples

A total of 468 green asparagus spears (*Asparagus officinalis*, L., cultivar UC-157), grown in selected, controlled plots in Huétor-Tájar (Granada, Spain), were harvested by hand over one three-month crop season (April–June, 2007). Spears were placed under refrigeration (2 °C, 95% R.H.) and exposed to one of the three controlled atmosphere (CA) treatments: air (21 kPa O<sub>2</sub> + 0.3 kPa CO<sub>2</sub>), CA<sub>1</sub> (5 kPa O<sub>2</sub> + 5 kPa CO<sub>2</sub>) and CA<sub>2</sub> (10 kPa O<sub>2</sub> + 10 kPa CO<sub>2</sub>). The product was kept under these conditions throughout the trial period, with samples drawn for analysis at 7, 14, 21 and 28 days; fresh untreated samples (0 days) were used as control.

Fresh and stored asparagus spears were cut into three parts for analysis: tip (0–6 cm, measured from the apex of the spear), middle portion (6–12 cm) and base (12–18 cm); thus the total num-

ber of samples available for discrimination process was of 1404 samples.

### 2.2. Spectra collection

Spectra were collected from all samples in reflectance–interactance mode (Log 1/R) using two NIR-instruments: (1) FNS-6500 scanning monochromator (FOSS NIRSystems, Silver Spring, MD, USA); and (2) LabSpec®Pro A108310 Spectrometer (Analytical Spectral Device (ASD), Inc., Boulder, Colorado, USA). The main features of these instruments are listed in Table 1, the major difference between the two being the measuring principle involved.

The FNS-6500 scanning monochromator was interfaced to a remote reflectance fiber-optic probe (NR-6539-A) with a 50 mm × 6 mm window. Each spear portion to be analyzed was hand-placed in the probe so that the desired asparagus location was centred on, and in direct contact with, the probe. Two separate spectral measurements were made on each spear portion, rotating the sample through 180° after the first measurement. The optical absorption spectrum ranged from 400 nm to 2500 nm, in 2-nm steps. The signal was collected using WINISI v. 1.50 software package (Infrasoft International, Port Matilda, PA, USA).

The second instrument was a diode array scanning monochromator NIR spectrometer (LabSpec®Pro A108310) equipped with a fiber-optic contact probe (Ø 5 mm), working in reflectance–interactance mode in the spectral range 350–2500 nm (every 1 nm). The first measurement was made at the middle point of the spear portion to be analyzed, and the second after rotating the sample through 180°. The signal was collected using the Indico™ Pro software package (Analytical Spectral Device (ASD), Inc., Boulder, Colorado, USA) and pretreated using the Unscrambler v. 7.5 program (CAMO, ASA, Oslo, Norway).

In both cases, the averaged spectrum for each spear was used for data processing.

### 2.3. Definition of calibration and validation sets

The design of models to classify asparagus by post-harvest storage time with a view to estimating shelf-life was based on five classification groups: 0, 7, 14, 21 and 28 days' storage. Each group contained 108 samples for each of the three post-harvest treatments applied and for each NIRS instrument tested, except the 0 days group that only has 108 samples.

Models to classify asparagus by post-harvest treatment used three classification groups, one for each treatment tested: ambient air, controlled atmosphere 1 and controlled atmosphere 2. Each group comprised 108 samples for each storage interval tested: 7, 14, 21 and 28 days.

For structuring the calibration population, an initial principal component analysis (PCA) was performed to calculate the centre of the population and the distance of samples (spectra) from that centre in an *n*-dimensional space, using the Mahalanobis distance (GH); samples with a statistical value greater than 3 were consid-

**Table 2**  
Percentage of spears correctly classified by storage interval. PLS-DA. FNS-6500. Spectral range: 500–2200 nm.

Qualitative groups	Post-harvest treatments					
	21 kPa O <sub>2</sub> + 0.3 kPa CO <sub>2</sub>		5 kPa O <sub>2</sub> + 5 kPa CO <sub>2</sub>		10 kPa O <sub>2</sub> + 10 kPa CO <sub>2</sub>	
	A: 75% B: 0.32 C: 27 D: 1,10,5,1		A: 83% B: 0.29 C: 26 D: 1,10,5,1		A: 84% B: 0.29 C: 30 D: 1,10,5,1	
Storage time (days)	Training set	Validation set	Training set	Validation set	Training set	Validation set
Day 0	88%	95%	93%	95%	99%	100%
Day 7	79%	80%	80%	75%	83%	75%
Day 14	68%	80%	75%	80%	72%	95%
Day 21	61%	80%	85%	95%	82%	85%
Day 28	78%	65%	83%	90%	84%	100%

A, Percentage of correctly classified training samples after cross validation; B, Model SECV; C, number of factors; D, math treatment.

ered outliers or anomalous spectra [23]. After elimination of outlier spectra, samples to be used for calibration and external validation sets were selected solely on the basis of spectral data, following the method proposed by Shenk and Westerhaus [23], using the CENTER algorithm included in the WinISI II software package version 1.50 (Infrasoft International, Port Matilda, PA, USA). This algorithm performs a principal component analysis PCA, reducing the original spectral information (Log 1/R values) to a small number of linearly independent variables, thus facilitating the calculation of spectral distances. These new variables were used to calculate the centre of the spectral population and the distance (expressed as the Mahalanobis 'GH' distance) of each sample in the calibration set from that centre. Having ordered the sample set by spectral distances (from smallest to greatest distance to the centre), the 20 samples forming the external validation set for each discrimination group were selected, i.e. 1 out of every 5 samples in the overall set.

#### 2.4. Development of near-infrared classification models

Discriminant models were constructed to classify asparagus by storage time and post-harvest treatment, using PLS-discriminant analysis (PLS-DA) for supervised classification. Specifically, the PLS2 algorithm was applied, using the "Discriminant Equations" option in the WINISI v. 1.50 software package. The principles and procedures involved in NIRS discriminant analysis are essentially identical to those involved in quantitative analysis, the main difference between the two lying in the type of variables predicted: discriminant analysis uses discrete variables (membership or non-membership of a given group), rather than analyte concentrations or other continuous data [24]. Briefly, PLS discriminant analysis uses a training set to develop a qualitative prediction or calibration model which may subsequently be applied for the classification

**Table 3**  
Percentage of spears correctly classified by storage interval. PLS-DA. LabSpec® Pro A108310. Spectral range: 500–2200 nm.

Qualitative groups	Post-harvest treatments					
	21 kPa O <sub>2</sub> + 0.3 kPa CO <sub>2</sub>		5 kPa O <sub>2</sub> + 5 kPa CO <sub>2</sub>		10 kPa O <sub>2</sub> + 10 kPa CO <sub>2</sub>	
	A: 100% B: 0.14 C: 16 D: 2,5,5,1		A: 100% B: 0.14 C: 11 D: 2,5,5,1		A: 100% B: 0.15 C: 11 D: 2,5,5,1	
Storage time (days)	Training set	Validation set	Training set	Validation set	Training set	Validation set
Day 0	100%	100%	100%	100%	100%	100%
Day 7	100%	100%	100%	100%	100%	100%
Day 14	100%	100%	100%	100%	100%	100%
Day 21	100%	100%	100%	100%	100%	100%
Day 28	100%	100%	100%	100%	100%	100%

A, Percentage of correctly classified training samples after cross validation; B, Model SECV; C, number of factors; D, math treatment.

of new unknown samples. This model seeks to correlate spectral variations ( $X$ ) with defined classes ( $Y$ ), attempting to maximize the covariance between the two types of variables. In this type of approach, the  $Y$  variables used are not continuous, as they are in quantitative analysis, but rather categorical "dummy" variables created by assigning different values to the different classes to be distinguished.

All models were developed using four cross validation groups (i.e. the calibration set is partitioned into four groups; each group is then predicted using a calibration developed on the other samples), a spectral range from 500 to 2200 nm (every 2 nm), eliminating signal noise at the beginning and end of the spectral range, and combined SNV + Detrend treatment for scatter correction [25]. First- and second-derivative treatments were tested: 1,5,5,1; 1,10,5,1; 2,5,5,1 and 2,10,5,1, where the first digit is the number of the derivative, the second is the gap over which the derivative is calculated, the third is the number of data points in a running average or smoothing, and the fourth is the second smoothing [26].

The precision of the models obtained was evaluated using the standard error of cross validation (SECV) and the percentage of correctly classified samples, both for the global model and for each class.

### 3. Results and discussion

#### 3.1. Classification by storage time

Results for the best discriminant models, obtained by PLS2-DA, for predicting storage time and thus shelf-life in asparagus stored under refrigeration in a controlled atmosphere, using two analytical instruments and various training sets, are shown in Tables 2 and 3.

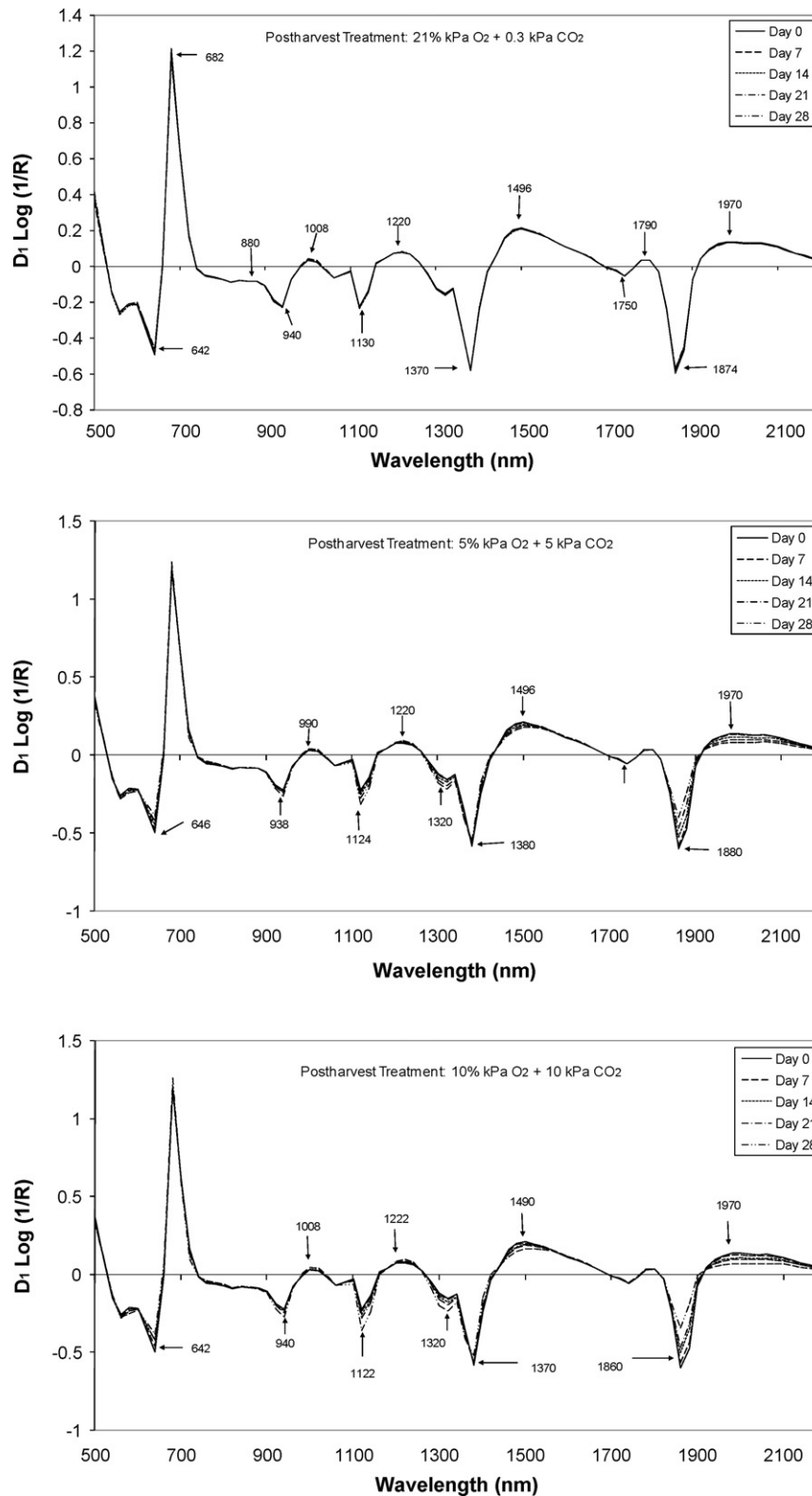


Fig. 1.  $D_1 \text{ Log}(1/R)$  for intact green asparagus for FNS-6500.

Generally speaking, the most accurate discriminant models were obtained using  $D_1 \text{ Log}(1/R)$  for the FNS-6500 and  $D_2 \text{ Log}(1/R)$  for the LabSpec®Pro A108310.

The LabSpec®Pro A108310 correctly classified 100% of samples in all three post-harvest treatment groups, while the shelf-life prediction models developed using the FNS-6500 correctly classified 75% of spears stored in ambient air and 83–84% of

samples stored in the two controlled atmospheres. A similar trend was recorded for partial or class-based discrimination data. SECV values for models to classify samples by post-harvest storage time were also lower with the LabSpec®Pro A108310 (0.14 in ambient air; 0.14 in CA<sub>1</sub>; 0.15 in CA<sub>2</sub>) than with the FNS-6500 (0.32 in ambient air; 0.29 in CA<sub>1</sub>; 0.29 in CA<sub>2</sub>).



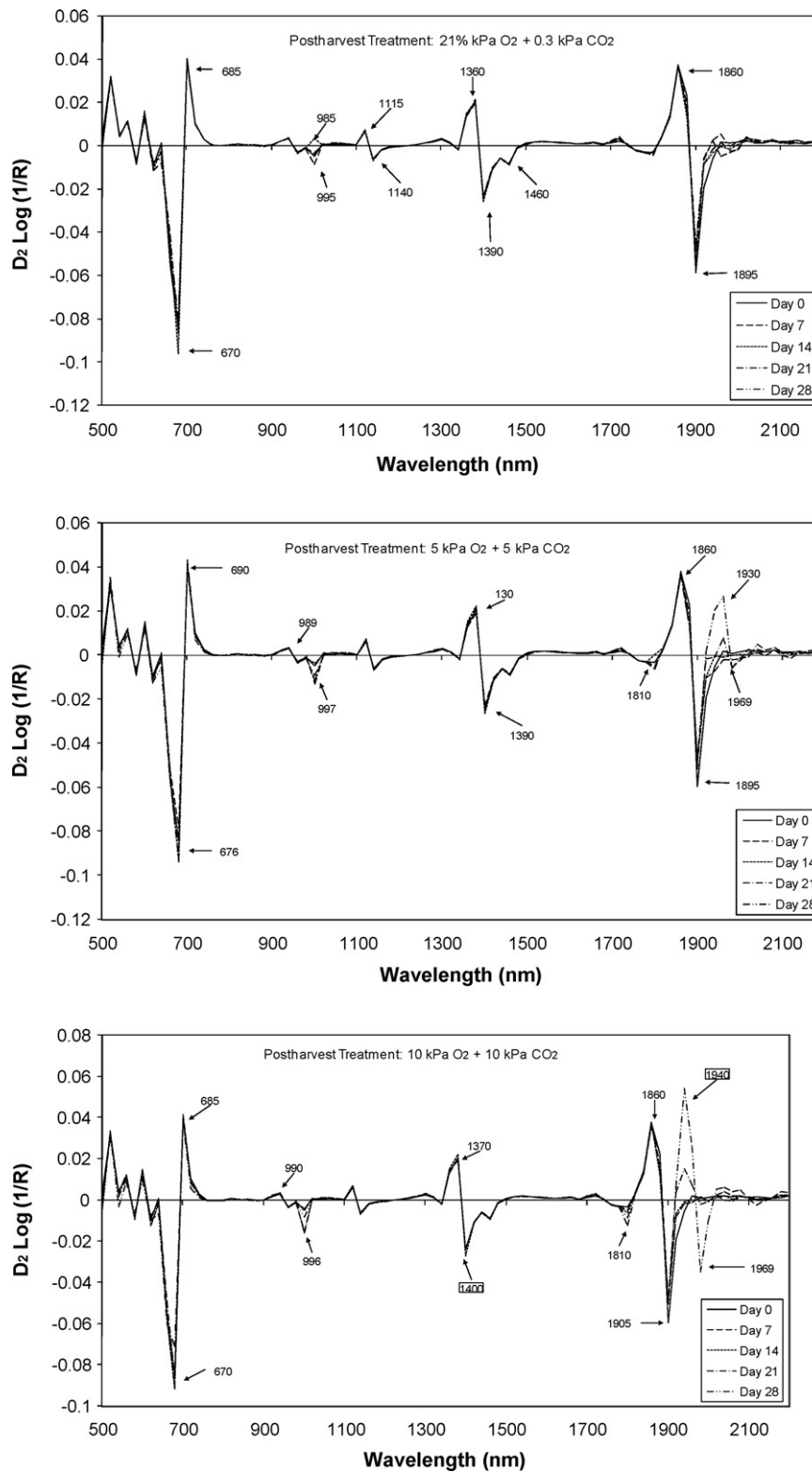


Fig. 2.  $D_2 \text{ Log}(1/R)$  for intact green asparagus for LabSpec® Pro A108310.

Figs. 1 and 2 show the mean spectra for each class (storage time), together with the spectral signal pretreatment that yielded the best result in each case, grouped by storage treatment and NIRS instrument used. For asparagus stored in ambient air and analyzed on the FNS-6500 – for which the lowest percentage of correctly classified samples was recorded (Table 2) – there was considerable overlap of mean spectra, which

hindered discrimination; absorption bands at around 642 nm, 682 nm and 1874 nm appeared to have the greatest classification weight. A higher percentage of correctly classified samples was obtained for asparagus in the two controlled atmosphere groups (Table 2). Mean spectra of these groups were more clearly differentiated (Fig. 1) considering absorption bands at around 642–646 nm, 938–940 nm, 990–1008 nm, 1122–1124 nm, 1320 nm,

**Table 4**

Percentage of spears correctly classified by post-harvest treatment. PLS-DA. FNS-6500. Spectral range: 500–2200 nm.

Qualitative groups	Storage time (days)							
	7 days		14 days		21 days		28 days	
	A: 74%		A: 69%		A: 72%		A: 74%	
	B: 0.40		B: 0.45		B: 0.48		B: 0.42	
	C: 14		C: 14		C: 29		C: 19	
	D: 1,10,5,1		D: 1,5,5,1		D: 1,10,5,1		D: 1,5,5,1	
Post-harvest treatments	Training set	Validation set	Training set	Validation set	Training set	Validation set	Training set	Validation set
21 kPa O <sub>2</sub> + 0.3 kPa CO <sub>2</sub>	92%	100%	85%	85%	87%	75%	94%	95%
5 kPa O <sub>2</sub> + 5 kPa CO <sub>2</sub>	66%	55%	49%	55%	64%	65%	65%	65%
10 kPa O <sub>2</sub> + 10 kPa CO <sub>2</sub>	65%	45%	73%	60%	65%	60%	65%	75%

A, Percentage of correctly classified training samples after cross validation; B, Model SECV; C, number of factors; D, math treatment.

**Table 5**Percentage of spears correctly classified by post-harvest treatment. PLS-DA. LabSpec<sup>®</sup>Pro A108310. Spectral range: 500–2200 nm.

Qualitative groups	Storage time (days)							
	7 days		14 days		21 days		28 days	
	A: 89%		A: 80%		A: 86%		A: 85%	
	B: 0.34		B: 0.44		B: 0.32		B: 0.34	
	C: 16		C: 26		C: 10		C: 11	
	D: 2,10,5,1		D: 2,10,5,1		D: 2,10,5,1		D: 2,5,5,1	
Post-harvest treatments	Training set	Validation set	Training set	Validation set	Training set	Validation set	Training set	Validation set
21 kPa O <sub>2</sub> + 0.3 kPa CO <sub>2</sub>	95%	100%	98%	90%	96%	100%	100%	95%
5 kPa O <sub>2</sub> + 5 kPa CO <sub>2</sub>	83%	95%	54%	50%	81%	80%	84%	75%
10 kPa O <sub>2</sub> + 10 kPa CO <sub>2</sub>	89%	85%	86%	75%	82%	80%	71%	75%

A, Percentage of correctly classified training samples after cross validation; B, Model SECV; C, number of factors; D, math treatment.

1370–1380 nm, 1490–1496 nm, 1860–1880 nm and 1970 nm. Using the LabSpec<sup>®</sup>Pro A108310 (Fig. 2), differentiation between classes was much clearer, suggesting that the models obtained provided excellent discriminant power. Generally speaking, discrimination of asparagus by shelf-life in the NIR region of the spectrum appears to be related to water content and O–H combinations, suggesting that differences caused by fiber profiles and water loss might contribute to the variations as a function of storage time. This confirms findings reported by Garrido et al. [4], who noted that NIR spectra were sensitive to chemical changes in neutral and acid detergent fiber over the storage period.

Models were validated using sample sets not included in model development: 100% of samples were correctly classified using the LabSpec<sup>®</sup>Pro A108310, while between 65% and 100% were correctly classified using the FNS-6500.

Generally speaking, while both instruments proved suitable for estimating shelf-life in green asparagus, better results were obtained with the LabSpec<sup>®</sup>Pro A108310, perhaps due to the measurement system used, i.e. the design of the sampler probe and the nature of the product–radiation interaction. The FNS-6500 performs a scan of the sample, while with the LabSpec<sup>®</sup>Pro A108310, the spectral measurement is made at a central point of each spear area to be analyzed, due to the small probe diameter. As a result, each spectrum captured by the FNS-6500 displays greater variability than its LabSpec<sup>®</sup>Pro A108310 counterpart, partly because spear deterioration is not wholly uniform. Moreover, the number of latent variables used with discriminant models, based on spectra obtained with the FNS-6500, was virtually twice that recommended for obtaining models using the LabSpec<sup>®</sup>Pro A108310 (Tables 2 and 3).

### 3.2. Classification by post-harvest treatment

The results obtained by the best discriminant models for classifying asparagus spears by post-harvest treatment, for the various

storage times tested and using the two analytical instruments, are shown in Tables 4 and 5.

Again, generally speaking, the best discriminant models were obtained  $D_1 \text{Log}(1/R)$  for FNS-6500 and  $D_2 \text{Log}(1/R)$  for LabSpec<sup>®</sup>Pro A108310.

The LabSpec<sup>®</sup>Pro A108310 yielded a higher overall percentage of correctly classified samples for the various storage periods analyzed: 7 days (89% vs. 74% for the FNS-6500), 14 days (80% vs. 69%), 21 days (86% vs. 72%) and 28 days (85% vs. 74%). The SECVs for the models obtained using the LabSpec<sup>®</sup>Pro A108310 were also lower than those recorded with the FNS-6500, although the difference was less marked than for discrimination by post-harvest storage interval.

Analysis of partial discrimination by classes within each model (Tables 4 and 5) showed that the lowest percentage of correctly classified samples was obtained after 14 days' storage using both instruments.

Models for classifying spears by post-harvest treatment were validated using new sample sets not included in model development: the percentage of correctly classified samples using the FNS-6500 ranged from 45% for asparagus stored in controlled atmosphere 2 for 7 days, and 100% for samples stored in ambient air for 7 days. Using the LabSpec<sup>®</sup>Pro A108310, the equivalent percentages ranged from 50% for asparagus stored for 14 days in controlled atmosphere 1 and 100% for samples stored in ambient air for 7 and 21 days. It should be noted that, in all cases, most misclassified samples belonged to one of the two controlled atmosphere sets; discrimination between the two was insufficient. By contrast, discrimination between samples stored in ambient air and those stored in either of the controlled atmospheres was sufficient.

### 4. Conclusions

These results suggest that NIRS technology enables classification of intact green asparagus stored in refrigeration under controlled

atmosphere, both by storage time and by post-harvest treatments applied, with an accuracy of up to 100%, using either of the two instruments tested. It should also be considered that the work here presented is a first step towards shelf-life prediction for asparagus, allowing increased sampling of each batch produced, and thus ensuring a more precise and accurate guarantee of specific quality.

### Acknowledgements

This research was funded by the Andalusian Regional Government under the Research Excellence Program (Project No. 3713 'Safety and Traceability in the Food Chain using NIRS') and the Research Program in Ecological Agriculture (Project No. 92162/3 'Postharvest Treatments for Increasing Asparagus Shelf-Life').

### References

- [1] C. Scheer, I. Schonhof, B. Brückner, M. Schreiner, D. Knorr, *J. Appl. Bot.* 77 (2003) 177.
- [2] P.K. Bhowmik, T. Matsui, K. Kawada, *Pak. J. Biol. Sci.* 3 (2000) 787.
- [3] M.J. McKenzie, L.A. Greer, J.A. Heyes, P.L. Hurst, *Postharvest Biol. Technol.* 32 (2004) 45.
- [4] A. Garrido, M.T. Sanchez, G. Cano, D. Perez, C. Lopez, *J. Food Qual.* 6 (2001) 539.
- [5] D. Albanese, L. Russo, L. Cinquanta, A. Brasiello, M. Di Matteo, *Food Chem.* 101 (2007) 274.
- [6] P.L. Hurst, G. Boulton, R.E. Lill, *Food Chem.* 61 (1998) 381.
- [7] D. Nei, T. Uchino, N. Sakai, S. Tanaka, *Postharvest Biol. Technol.* 37 (2005) 277.
- [8] A.A. Kader, *Postharvest Technology of Horticultural Crops*, vol. 3311, University of California, 1992.
- [9] F. Ramojaro, M. Zapata, P. Segura, *Nuevas Tecnologías de Conservación de Frutas y Hortalizas: Atmósferas Modificadas*, Mundi-Prensa, Madrid, España, 1996.
- [10] H. Izumi, A.E. Watada, W. Douglas, *J. Am. Soc. Hort. Sci.* 121 (1996) 127.
- [11] R.E. Lill, V.K. Corrigan, *Int. J. Food Sci. Technol.* 31 (1996) 117.
- [12] A.A. Kader, *Food Technol.* 40 (1986) 99.
- [13] J. An, M. Zhang, Q. Lu, Z. Zhang, *J. Food Eng.* 77 (2006) 951.
- [14] M.J. Villanueva, M.D. Tenorio, M. Sagardoy, A. Redondo, M.D. Saco, *Food Chem.* 91 (2005) 609.
- [15] C. Camps, P. Guillermin, J.C. Mauget, D. Bertrand, J. Near Infrared Spectrosc. 15 (2007) 169.
- [16] B.G. Osborne, T. Fearn, P.H. Hindle (Eds.), *Practical NIR Spectroscopy with Applications in Food and Beverage Analysis*, Longman, Essex, 1993, pp. 11–35.
- [17] J.S. Shenk, M.O. Westerhaus, *Analysis of Agriculture and Food Products by Near Infrared Reflectance Spectroscopy*, Monograph, NIRSystems, Inc., 12101 Tech Road, Silver Spring, MD 20904, USA, 1995.
- [18] D.C. Slaughter, J.A. Abbott, in: C.A. Roberts, J. Workman, J.B. Reeves III (Eds.), *Near-Infrared Spectroscopy in Agriculture*, ASA, CSSA and SSSA, Madison, Wisconsin, 2004, pp. 377–398.
- [19] S. Saranwong, S. Kawano, in: Y. Ozaki, W.F. McClure, A.A. Christy (Eds.), *Near-Infrared Spectroscopy in Food Science and Technology*, John Wiley & Sons, Inc., Hoboken, New Jersey, 2007, pp. 219–242.
- [20] D. Pérez, M.T. Sánchez, G. Cano, A. Garrido, *J. Food Qual.* 25 (2002) 277.
- [21] D.C. Perez, M.T. Sanchez, G. Cano, A. Garrido, *J. Food Sci.* 66 (2001) 323.
- [22] C. Jarén, S. Arazuri, M.J. García, P. Arnal, J.I. Arana, *Int. J. Infrared Milli* 27 (2006) 391.
- [23] J.S. Shenk, M.O. Westerhaus, *Crop Sci.* 31 (1991) 1548.
- [24] T. Naes, T. Isaksson, T. Fearn, A. Davies, *A User-friendly Guide to Multivariate Calibration and Classification*, NIR Publications, Chichester, UK, 2002.
- [25] ISI, *The Complete Software Solution Using a Single Screen for Routine Analysis, Robust Calibrations, and Networking*, Manual, FOSS NIRSystems/TECATOR, Infrasoft International, LLC, Sylver Spring MD, USA, 2000.
- [26] J.S. Shenk, M.O. Westerhaus, *Routine Operation, Calibration, Development and Network System Management Manual*, NIRSystem, Inc., 12101 Tech Road, Silver Spring, MD 20904, USA, 1995.



# Coupling ultra high-pressure liquid chromatography with single quadrupole mass spectrometry for the analysis of a complex drug mixture

Julie Schappler, Raul Nicoli, Dao Nguyen, Serge Rudaz, Jean-Luc Veuthey, Davy Guillarme\*

Laboratory of Pharmaceutical Analytical Chemistry, School of Pharmaceutical Sciences, University of Geneva, University of Lausanne, Boulevard d'Yvoy 20, 1211 Geneva 4, Switzerland

## ARTICLE INFO

### Article history:

Received 2 October 2008  
Received in revised form  
12 November 2008  
Accepted 20 November 2008  
Available online 27 November 2008

### Keywords:

Fast-LC  
Pharmaceutical  
UHPLC  
UPLC  
UHPLC–MS

## ABSTRACT

The coupling of ultra high-pressure liquid chromatography with a single quadrupole mass spectrometer was investigated for the analysis of several cytochromes P450 (CYP450) substrates and respective metabolites. The effect of numerous operating parameters (e.g. mobile phase pH, flow rate, gradient length, MS acquisition mode, dwell time, polarity switching, etc.) on selectivity, sensitivity and acquisition rate was studied. It was demonstrated that basic pH conditions provided the best compromise in terms of sensitivity and chromatographic selectivity with both acidic and basic compounds. The optimal mobile phase flow rate for UHPLC–MS experiments should be comprised between 300 and 600  $\mu\text{L}/\text{min}$  for 2.1 mm ID columns, while a higher flow rate generated up to 3-fold loss in sensitivity. It was also demonstrated that the fast polarity switching mode represented a valuable tool to improve throughput, maintaining acceptable performance. Finally, limits of detection were included in the range [1–50 ng/mL] in positive ionization mode and [50–250 ng/mL] in negative ionization mode, for investigated compounds.

© 2008 Elsevier B.V. All rights reserved.

## 1. Introduction

In the pharmaceutical industry, the drug development process represents a long and tedious task, which takes about 10–15 years from the screening of thousands of new chemical entities (NCEs) to the drug launching on the market [1]. Today, fast analytical procedures emerge to face with the increased number of NCEs [2] and numerous approaches have already been implemented to reduce the time necessary to complete the whole analytical process (including sample preparation, separation, detection and data treatment). Regarding the separation step, many improvements were brought to conventional gas chromatography (GC) [3,4], capillary electrophoresis (CE) [5–7], and liquid chromatography (LC).

In LC, several solutions have been proposed to speed up the separation such as the reduction of the column length and the simultaneous increase of mobile phase flow rates [8]. This strategy is easy to implement but generates limited efficiency and resolution [9]. Therefore, it could only be hyphenated with a MS detector, which provides supplementary selectivity for identification and confirmation of analytes in complex mixtures [10]. An alternative strategy uses monolithic supports [11–14]. Due to their bimodal structure (i.e., macropores and mesopores), they generate good performance (close to that of columns packed with 3–3.5  $\mu\text{m}$  particles)

with limited backpressure equivalent to that of a chromatographic column packed with 11  $\mu\text{m}$  particles [15]. However, there is a lack of silica-based column chemistries (e.g. only  $\text{C}_{18}$ ) and dimensions are not adapted to conventional MS sources [16]. Solutions were found in the literature and among them, (i) the use of a flow splitter [17], (ii) the use of atmospheric pressure chemical ionization (APCI) source instead of electrospray ionization (ESI), as the former is compatible with higher mobile phase flow rates [18,19], and (iii) the use of nano-monolithic columns with specific ESI emitter [20]. Another approach consists in increasing the mobile phase temperature, up to 200 °C, with adapted instrumentation and columns [21]. As example, separations 3–5 times faster can be achieved at 90 °C with equivalent efficiency and backpressure compared to ambient temperature [22,23]. In addition, high temperature liquid chromatography (HTLC) is fully compatible with all existing detection modes [24], particularly MS, where an improvement in sensitivity can be obtained, due to the easier compounds desolvation at high mobile phase temperature [25,26]. Nevertheless, even though manufacturers developed columns that withstand temperature of 90 °C [27] and suitable instrumentation for preheating the mobile phase [28], the thermal stability of the compounds can still be an issue, which must be deeply investigated [29]. The most recent strategy to reach good performance in terms of analysis time and efficiency uses chromatographic supports packed with sub-2  $\mu\text{m}$  particles in ultra high-pressure conditions (UHPLC technology). This strategy was originally developed by Jorgenson and coworkers who demonstrated the possibility to attain efficiencies as high as 300,000 plates at an extreme backpressure of 7000 bar [30]. It is now possible

\* Corresponding author. Tel.: +41 22 379 34 11; fax: +41 22 379 68 08.  
E-mail address: [davy.guillarme@unige.ch](mailto:davy.guillarme@unige.ch) (D. Guillarme).

to find commercial UHPLC systems that provide ultra-fast separations with the help of short columns packed with small particles and withstand elevated pressure (up to 1000 bar) [31]. Therefore, analysis time can be decreased by a factor of 10–20 compared to conventional LC, while maintaining excellent resolution [9].

The combination of UHPLC with MS looks promising for determining drugs at low concentration level within a short analysis time. However MS devices should be able to detect the very thin peaks generated by UHPLC (average peak width at baseline often lower or equal to 3 s), without compromising sensitivity [32]. To date, about 30% of the works published in UHPLC–MS were achieved with time-of-flight (TOF) or Q-TOF instruments. TOF analyzer is perfectly compatible with UHPLC due to its high acquisition rate over a broad mass range, necessary to properly define the chromatographic peak [33]. However, several providers have recently commercialized new quadrupole-based instruments with improved full scan acquisition rate (up to 10,000  $m/z/s$ ), reduced dwell time (as low as 5 ms) for selected ion monitoring (SIM) mode, and rapid (*ca.* 20 ms) polarity as well as ionization mode switching (for simultaneous ESI+/ESI–, APCI+/APCI–, ESI/APCI, and

APCI/APPI operations). Many publications appeared in UHPLC–MS and showed the benefits of UHPLC vs. HPLC [34,35]. The performance in terms of sensitivity was generally outlined but it must be noted that numerous studies compared chromatographic systems with detectors from different generations [36,37].

In this work, the performance of UHPLC coupled with a single quadrupole instrument was evaluated for the rapid analysis of a drug cocktail containing substrates and metabolites of the major cytochrome P450 (CYP450) isozymes [38]. The effect of several operating parameters (*e.g.* mobile phase flow rate, pH, gradient length, MS acquisition mode, dwell time, polarity switching, *etc.*) on selectivity, sensitivity and acquisition rate was investigated. Moreover, limits of detection (LOD) were determined in best conditions.

## 2. Experimental

### 2.1. Chemicals and reagents

Bupropion HCl, dextromethorphan HBr, dextroprphan tartras and acetaminophen were purchased from Sigma–Aldrich (Buchs,

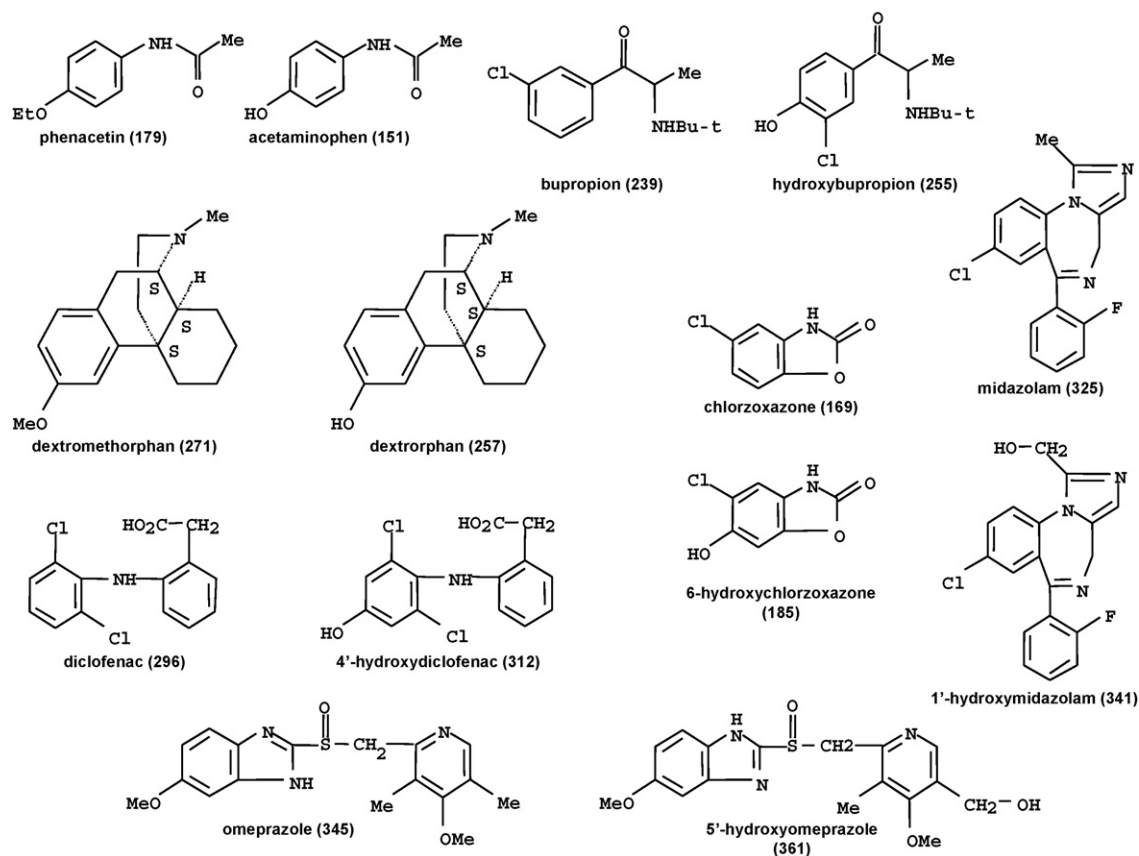


Fig. 1. Chemical structures (and molecular weights) of the 14 investigated CYP450 substrates and metabolites.

Table 1

Physico-chemical properties, concentrations and optimal cone voltages for investigated substrates and associated metabolites.  $pK_a$  values were estimated with ACD/Labs (Advanced Chemistry Development) software v8.14 for Solaris.

CYP450	Substrates	Conc. ( $\mu\text{g/mL}$ )	$m/z$	$pK_{ac}$	$pK_{ab}$	Metabolites	Conc. ( $\mu\text{g/mL}$ )	$m/z$	$pK_{ac}$	$pK_{ab}$	Cone voltage (V)
1A2	Phenacetin	1	+180	14.47	1.42	Acetaminophen	5	+152	9.86	1.72	30
2B6	Bupropion	1	+240	–	7.16	Hydroxybupropion	1	+256	6.15	7.31	12
2D6	Dextromethorphan	0.5	+272	–	9.13	Dextroprphan	0.5	+258	10.14	8.89	35
3A4	Midazolam	0.5	+326	–	5.56	1'-Hydroxymidazolam	0.5	+342	–	4.39	30
2E1	Chlorzoxazone	1	–168	8.46	–	6-Hydroxychlorzoxazone	2.5	–184	7.83	0.41	35
2C9	Diclofenac	10	–295	4.18	–	4'-Hydroxydiclofenac	10	–311	4.17	–	15
2C19	Omeprazole	1	–344	8.46	4.72	5'-Hydroxyomeprazole	1	–360	9.28	3.93	25

Switzerland), 1'-hydroxymidazolam and 6-hydroxychlorzoxazone were supplied by Cerilliant Corp. (TX, USA) and hydroxybupropion obtained from Lipomed AG (Arlesheim, Switzerland). Diclofenac, chlorzoxazone, midazolam, omeprazole, phenacetin, 4'-hydroxydiclofenac and 5'-hydroxyomeprazole were kindly offered by the Division of Clinical Pharmacology and Toxicology (Geneva University Hospitals, Switzerland). Chemical structures of the 14 investigated substrates and metabolites were reported in Fig. 1 while their physico-chemical properties, and considered concentrations summarized in Table 1. To reach suitable concentrations for MS detection, stock solutions at 1 mg/mL in MeOH were appropriately diluted with pure water.

Formic acid and acetonitrile (ACN) were of ULC/MS grade and purchased from Biosolve (Valkenswaard, Netherlands). Ammonium hydroxide was provided by Sigma–Fluka (Buchs, Switzerland). Water was obtained from a Milli-Q Water Purification System from Millipore (Bedford, MA, USA).

Formate buffer 10 mM was prepared with an adapted volume of formic acid and the pH adjusted to 3.0 with ammonium hydroxide. Acetate buffer 10 mM was prepared with an adapted volume of acetic acid and the pH adjusted to 5.0 with ammonium hydroxide. Ammoniac buffer 10 mM was prepared with an adapted volume of ammonium hydroxide and the pH adjusted to 9.0 with formic acid. pH was measured with a Metrohm pH meter (Herisau, Switzerland) and each prepared buffer had a buffer capacity higher than 5 mM/pH unit.

## 2.2. Instrumentation

Analyses were performed on a Waters ACQUITY UPLC system hyphenated with a single quadrupole SQD mass spectrometer operated at single mass resolution of  $m/z$  0.7 FWHM, which possesses an upper mass limit of  $m/z$  2045. UPLC included a binary solvent manager with a maximum delivery flow rate of 2 mL/min, a sample manager with an injection loop volume of 2  $\mu$ L (full loop injection), and a column oven set at 30 °C. The chromatographic column was a Waters ACQUITY UPLC BEH Shield RP<sub>18</sub> (50 mm  $\times$  2.1 mm ID, 1.7  $\mu$ m). Extra-column volume ( $V_{ext}$ ) of the UPLC–MS configuration was experimentally estimated at about 22  $\mu$ L and dwell volume ( $V_d$ ) at 100  $\mu$ L with the 2  $\mu$ L injection loop.

Ionization parameters and cone voltages were optimized by infusing each compound (1–10  $\mu$ g/mL) at pH 3 and 9 at various mobile phase flow rates. Optimal cone voltage values were summarized in Table 1. The capillary voltage and the source extractor voltage were set at  $\pm 3.5$  and  $\pm 2$  V, respectively. The source temperature was maintained at 140 °C, the desolvation gas temperature and flow at 450 °C and 700 L/h, respectively, and the cone gas flow at 50 L/h. For APCI operations, the corona discharge was set at 2  $\mu$ A.

MS detection was carried out in SIM and scan modes. Two ionization modes, ESI and APCI, were evaluated, as the ESCi<sup>®</sup> source allows separate or simultaneous ESI and APCI operations without requiring a physical change of the ionization source. Experiments were performed in negative, positive or negative/positive modes, depending on the nature of the compounds. The acquired  $m/z$  were summarized in Table 1 for each compound.

Data acquisition, data handling and instrument control were performed by Empower 2.0 Software (Waters, Milford, MA, USA).

## 2.3. Procedure

In this study, 270 experiments were conducted by UHPLC–MS to evaluate the influence of mobile phase pH, flow rate, gradient length, SIM dwell time and ionization mode on chromatographic selectivity, detector sensitivity and number of compounds that could be simultaneously detected. Investigated parameters and their respective ranges were summarized in Table 2. A system suitability experiment (SSE) was injected in the system every 20 runs to account for the change in MS ionization yield and chromatographic performance of the column during the sequence. A blank injection was performed before each SSE.

All experiments were performed in gradient mode to obtain the best compromise between resolution and analysis time. Three retention factors of solutes in the eluted mobile phase composition ( $k_e = 1, 3, 5$ ) were considered [39]. Gradient lengths were determined according to the mobile phase flow rate ( $F$ , mL/min), using the well-known definition of  $k_e$ :

$$k_e = \frac{t_{grad} \times F}{2.3 \times V_0 \times \Delta \Phi \times S} \quad (1)$$

where  $t_{grad}$  (min) is the gradient time,  $V_0$  (mL) is the column dead volume ( $V_0 = 120 \mu$ L considering column dimensions),  $\Delta \Phi = (\%B_{final} - \%B_{initial})/100$  is the relative change in ACN during the gradient, comprised between 0 and 1, and  $S$  is a constant term equal to 4 for small molecules.

The initial ACN composition was 5% while the final composition varied according to the gradient length: 70, 60 and 50% of ACN for  $k_e = 1, 3$  and 5, respectively. For  $k_e = 1$  to 5, gradient lengths were comprised between 1.86 and 9.30 min at 300  $\mu$ L/min, 0.93 and 4.65 min at 600  $\mu$ L/min, and 0.56–2.79 min at 1000  $\mu$ L/min. Finally, the re-equilibrating time was set to 4, 2 and 1.2 min at 300, 600 and 1000  $\mu$ L/min, respectively (ca.  $10t_0$ ).

Results were assessed in terms of signal-to-noise ratio (S/N) for each studied compound on respective extracted ion current (XIC). Because results were similar for all compounds, influence of each experimental parameter on S/N was only reported for a limited number of representative compounds and conditions.

## 3. Results and discussion

### 3.1. Optimization of chromatographic conditions

CYP450 represent the major oxidative drug-metabolizing enzymatic system in humans accounting for the biotransformation of many drugs [40]. For phenotyping studies, drug cocktails with different physico-chemical properties (Table 1) are often used in a single experiment for the determination of enzymatic activities [41,42]. In the present study, seven CYP450 probe substrates and their respective major metabolites were selected for their clinical relevance. A powerful UHPLC–MS method was developed to rapidly analyze this drug mixture.

**Table 2**  
Investigated experimental parameters.

	Mobile phase pH	Mobile phase flow rate ( $\mu$ L/min)	Gradient length ( $k_e$ )	Dwell time (ms)	Ionization mode
Min. value	3	300	1	5	ESI+ ESI–
Interm. value	5	600	3	10	ESI $\pm$ APCI $\pm$
Max. value	9	1000	5	20	ESCI <sup>®</sup> $\pm$

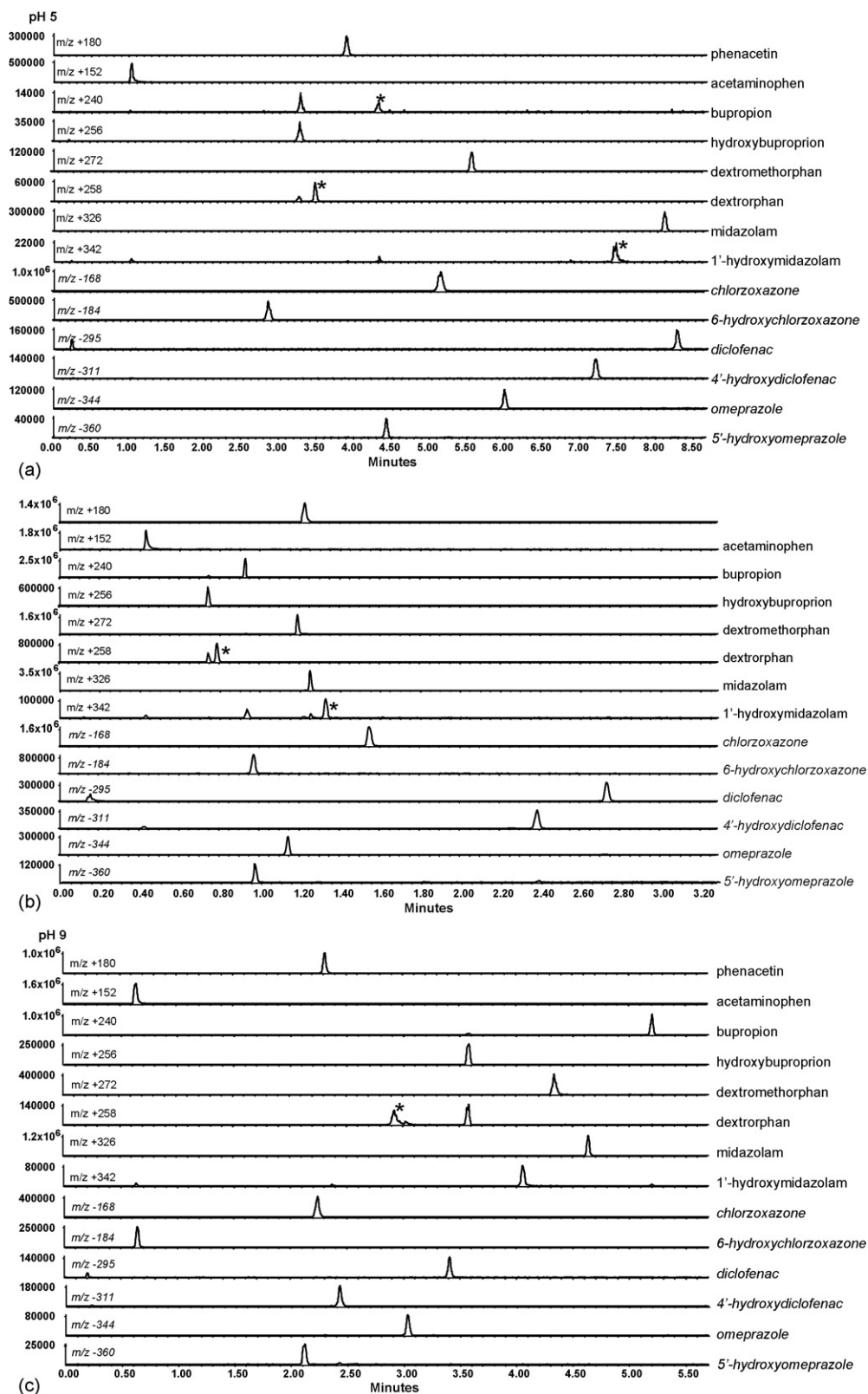


**Fig. 2.** Chromatograms of optimal separations obtained with ACQUITY BEH Shield RP18 50 mm  $\times$  2.1 mm ID, 1.7  $\mu$ m column at 30  $^{\circ}$ C and  $F=600 \mu$ L/min. (A) pH 5, with a linear gradient from 2.5 to 32.8% ACN in 7.97 min, then hold for 0.7 min. (B) pH 3, with a linear gradient from 2 to 56.5% ACN in 3.04 min, then hold for 0.7 min. (C) pH 9, with a linear gradient from 6.3 to 42.8% ACN in 5 min, then hold for 0.7 min. MS detection was performed in SIM mode, ESI $^{\pm}$  using source parameters described in Section 2. In presence of several peaks per chromatogram, peak that corresponded to  $[M+H]^+$  or  $[M-H]^-$  ion of the considered analyte was represented with \* symbol. Acidic compounds were emphasized with italic police.

### 3.1.1. Mobile phase pH

The determination of optimal pH conditions for the simultaneous LC–MS analysis of a mixture containing ionizable compounds, such as acidic and basic drugs, remains challenging. As ESI–MS is generally achieved with analytes under their ionized form, acidic conditions are commonly selected for basic compounds detected in the positive mode, while basic conditions are used for acidic compounds in the negative mode [33]. From a chromatographic point of view, these conditions might not be suitable because of (i) a lack of selectivity and retention for ionized species in RP–LC [43], and (ii) a poor peak shape for basic drugs, attributable to a significant tailing due to secondary interactions with residual silanol groups [44]. Plumb and co-workers [45,46] recently suggested that a good compromise on MS sensitivity, LC selectivity and peak shape could be reached at intermediate pH value (*i.e.*, pH 5).

**3.1.1.1. Effect on selectivity.** Since selected compounds possess a wide range of physico-chemical properties, three different buffers (*i.e.*, pH 3, 5 and 9) were initially investigated to obtain sufficient capacity (>5 mM/pH unit) and according to their volatility. The optimal chromatographic conditions at each pH were found thanks to HPLC modelling software (Osiris 4.1.1.2, Datalys, Grenoble, France) on the basis of two generic gradients that only differed in slope. At pH 3, the best separation was obtained with a linear gradient of ACN from 2 to 56.5% in 3.04 min, then hold for 0.7 min. At pH 5, the separation was performed with a linear gradient of ACN from 2.5 to 32.8% in 7.97 min, then hold for 0.7 min. At pH 9, the separation was achieved with a linear gradient of ACN from 6.3 to 42.8% in 5 min, then hold for 0.7 min. Fig. 2 shows the chromatograms considering the three pH values. All these chromatograms were obtained with a flow rate of 600  $\mu\text{L}/\text{min}$ .

The separation achieved at pH 5 (Fig. 2A) presented a high chromatographic selectivity, as all investigated compounds were baseline separated (*e.g.*  $m/z$  240, 256, 258). However, a significant sensitivity decrease was observed, comparing to other pH. Indeed, MS signals decreased by a factor of 2–20, depending on the considered analyte, and even 150-fold for bupropion, while background noise remained equivalent at each pH. Another limitation observed in Fig. 2A was the poor peak shape, attributable to possible secondary interactions of the compounds with the stationary phase at this pH. Chromatographic peaks were distorted and asymmetry became occasionally unacceptable (*e.g.*  $m/z$  152, 240, and 342). Due to these constraints, pH 5 was discarded of further investigation.

On the other hand, the chromatographic selectivity was limited at pH 3 (Fig. 2B) and most of the analytes were eluted within a short time window (0.8–1.6 min). This behavior was attributed to the lower retention and selectivity of basic analytes under acidic conditions, as expected. This could lead to interferences with unretained sample matrix components (*i.e.*, matrix effect) inducing ion suppression or enhancement [47]. Furthermore, the limited spectral resolution of the single quadrupole mass spectrometer ( $m/z$  0.7 FWHM) did not allow straightforward MS discrimination. In this study, this lack of selectivity was critical since: (i) isotopic abundance of  $\text{Cl}^{35}/\text{Cl}^{37}$  occurred in most investigated compounds, in conjunction with a small  $m/z$  difference for several analytes (*e.g.* hydroxybupropion,  $m/z$  256 vs. dextropran,  $m/z$  258), and (ii) in-source fragmentation produced fragmentation of metabolites (*e.g.* hydroxyl function loss of hydroxybupropion,  $m/z$  256), yielding two identical XIC peaks within the same SIM trace of the corresponding substrates (*e.g.* bupropion,  $m/z$  240). For these reasons, a selective UHPLC separation was mandatory prior to MS detection with a single quadrupole analyzer.

Finally, the separation was performed with a mobile phase at pH 9 (Fig. 2C). For successful operation in basic conditions, it is important to work with a column that withstands high pH. The column used in this study was a hybrid stationary phase with ethylene

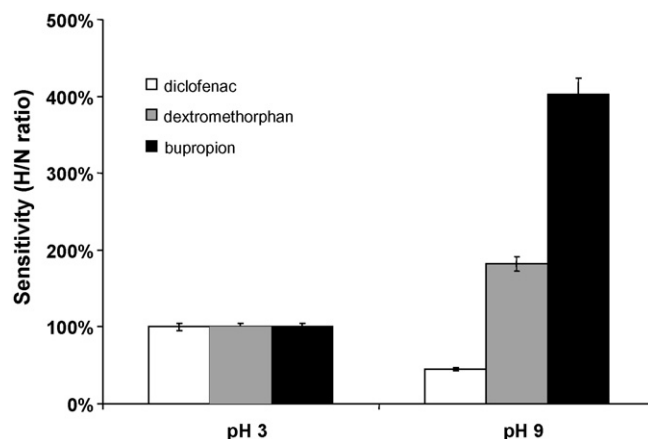


**Fig. 3.** Effect of pH value on ESI–MS sensitivity at  $F=600 \mu\text{L}/\text{min}$ . UHPLC–MS experiments of bupropion in ESI+, dextromethorphan in ESI+, and diclofenac in ESI–. MS detection was performed in SIM mode, ESI $\pm$  using source parameters described in Section 2. Results are presented in relative scale where values at pH 3 correspond to 100%.

bridges inside the silica matrix, ensuring high pH stability (up to pH 11). At pH 9, the column stability was excellent and the selectivity sufficient, as the separation was acceptable for almost all investigated compounds. Besides selectivity, the peak shapes of basic compounds were also improved as secondary interactions were strongly reduced with uncharged species. Finally, because basic compounds were more retained and eluted with more symmetrical peaks, the overall chromatographic resolution was increased.

**3.1.1.2. Effect on sensitivity.** The pH influence on MS response was investigated for the whole set of compounds. For clarity's sake, only results for three representative analytes were reported, namely diclofenac, bupropion and dextromethorphan, since results were similar for all studied analytes. Fig. 3 shows the MS sensitivity ( $S/N$ ) of these substrates at 600  $\mu\text{L}/\text{min}$  and two pH values (3 and 9). A distinct behavior was emphasized for acidic vs. basic compounds. For basic drugs, the MS response was clearly improved at pH 9 compared to pH 3. This increase was important with bupropion (factor 4) and less pronounced with dextromethorphan (factor 2). For acidic analytes, such as diclofenac, sensitivity decreased 2-fold under basic conditions. The increase in MS response with bases at pH 9 and acids at pH 3 is counter-intuitive but was already reported [48–50].

Several reasons may account for enhanced MS signal of basic drugs at pH 9. First, Enke suggested a mechanism to form pre-existing  $[\text{M}+\text{H}]^+$  ions in basic conditions [51]: a fixed amount of excess charge (*i.e.*, protons) is produced in ESI, depending on flow rate and capillary voltage, and basic analytes can be protonated even under alkaline conditions. Second, numerous works suggested that a proton-transfer reaction may occur between protonated amines, such as  $\text{NH}_4^+$  ions from buffer, and neutral bases in the gaseous phase [49,52,53]. It should also be stressed that the assessment of ionization degree of bases [48] could be biased since the nature and proportion of organic modifier affect the  $pK_a$  of buffer components and analytes [54]. Finally, pH of the droplets generated in ESI process may be significantly different from that of a bulk solution [33]. The ESI process also depends on desolvation, which is strongly influenced by chromatographic conditions. Indeed the mobile phase composition, its nature and the added modifiers affect the production of gas-phase analyte ions from the condensed phase and consequently alter the signal response [55]. Generally, the mobile phase parameters that affect ESI include its boiling point, surface tension and conductivity. It was demonstrated that the gas-phase ions generation is largely facilitated with volatile solvents



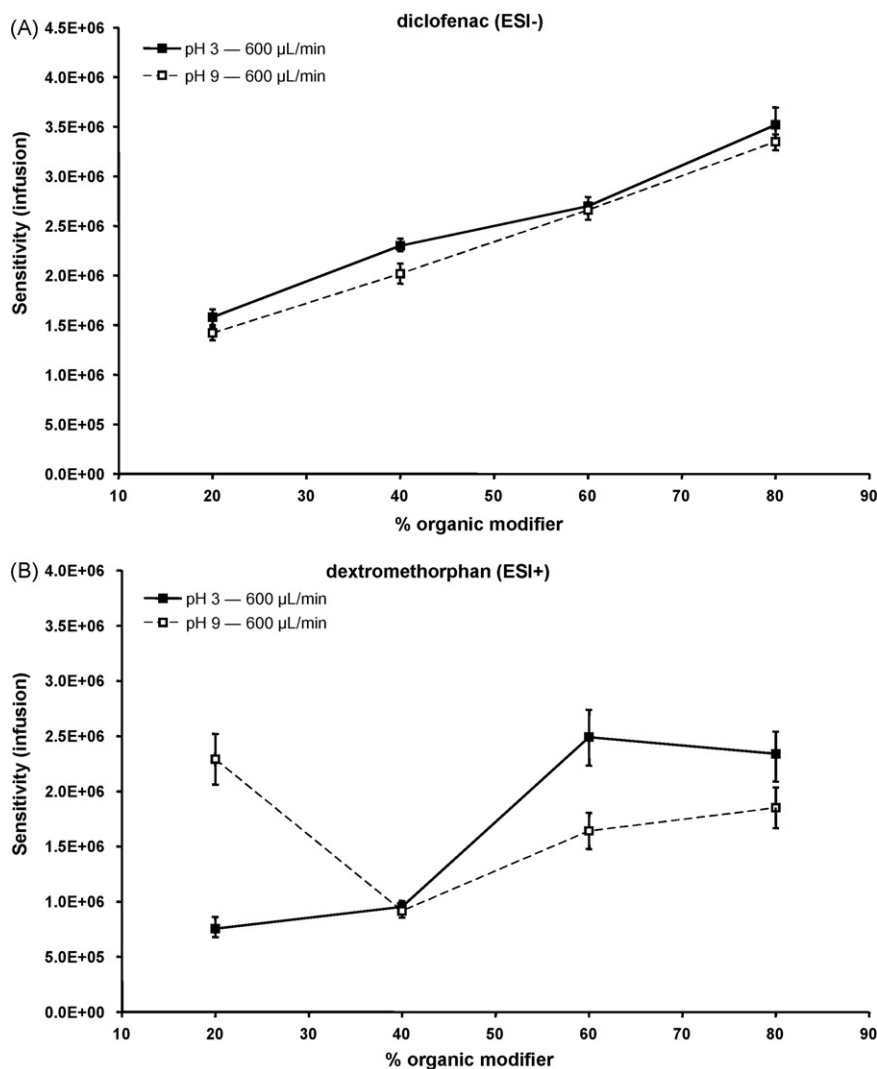


**Fig. 4.** Effect of mobile phase composition on ESI-MS sensitivity at two pH and  $F=600 \mu\text{L}/\text{min}$ . Infusion experiments of (A) diclofenac in ESI<sup>-</sup> and (B) dextromethorphan in ESI<sup>+</sup>. MS detection was performed in SIM mode, ESI<sup>±</sup> using source parameters described in Section 2.

[56]. Therefore, the high acetonitrile content used with acids at pH 3 and bases at pH 9 (higher retention) was beneficial for desolvation process and improved ESI spray stability by producing stable ion current [56,57].

Infusion experiments were carried out to determine if the intense signal observed for bases at pH 9 and acids at pH 3 arose from an improved ionization and/or a better desolvation. Hence, compounds were directly infused into MS at various pH (3 and 9) and mobile phase compositions (20, 40, 60 and 80% ACN). MS responses were monitored and reported in Fig. 4 for diclofenac and dextromethorphan.

For acidic compound (Fig. 4A), the impact of pH on absolute MS intensity at a given organic modifier proportion was quite limited. This behavior was counter-intuitive as diclofenac should be mostly on a neutral form at pH 3 and fully charged at pH 9 in solution. On the contrary, an ACN change from 20 to 80% generated a 2-fold sensitivity increase. Therefore, the signal improvement observed with diclofenac at pH 3 (Fig. 3A) could not be attributed to better ionization but mainly to enhanced desolvation.

For basic analyte (Fig. 4B), MS response was significantly different at pH 3 and 9. At pH 3, dextromethorphan was fully charged and similar curves to those reported for diclofenac were obtained, with a 2-fold increase in sensitivity from 20 to 80% of ACN. At pH 9, dextromethorphan was partially charged and relative contribution of

ionization vs. desolvation greatly differed depending on organic modifier proportion. The weak desolvation efficiency with highly aqueous solvent (20% ACN) was compensated by the significant quantity of ammonium ions in solution, leading to high MS sensitivity. At intermediate organic modifier percentage (40% ACN), the amount of  $\text{NH}_4^+$  ions was lower and the desolvation was not efficient as well, both contributions leading to a decrease in sensitivity. Finally, at high ACN%, the ionization yield was low but the desolvation process significantly improved, leading to an increase in sensitivity.

In order to summarize, numerous factors affected the production of gas-phase analyte ions from the condensed phase and accounted for observed sensitivity differences. On the one hand, the ionic character of analytes in solution (*i.e.*,  $\text{pK}_a$ , pH) and the ionization mechanism (*i.e.*, proton transfer from  $\text{NH}_4^+$  ions) determined ionization efficiency. On the other hand, the solvent composition and its surface tension were responsible for desolvation process. As the latter appeared critical for MS response, it could be interesting to work with methanol–water mixtures instead of acetonitrile–water to improve sensitivity, since methanol has lower boiling point than ACN [55] and is amphiprotic. However, the high viscosity of methanol–water mixtures significantly limits the use of fast or ultra-fast separations because of the high backpressures generated by columns packed with sub- $2 \mu\text{m}$  particles [22].

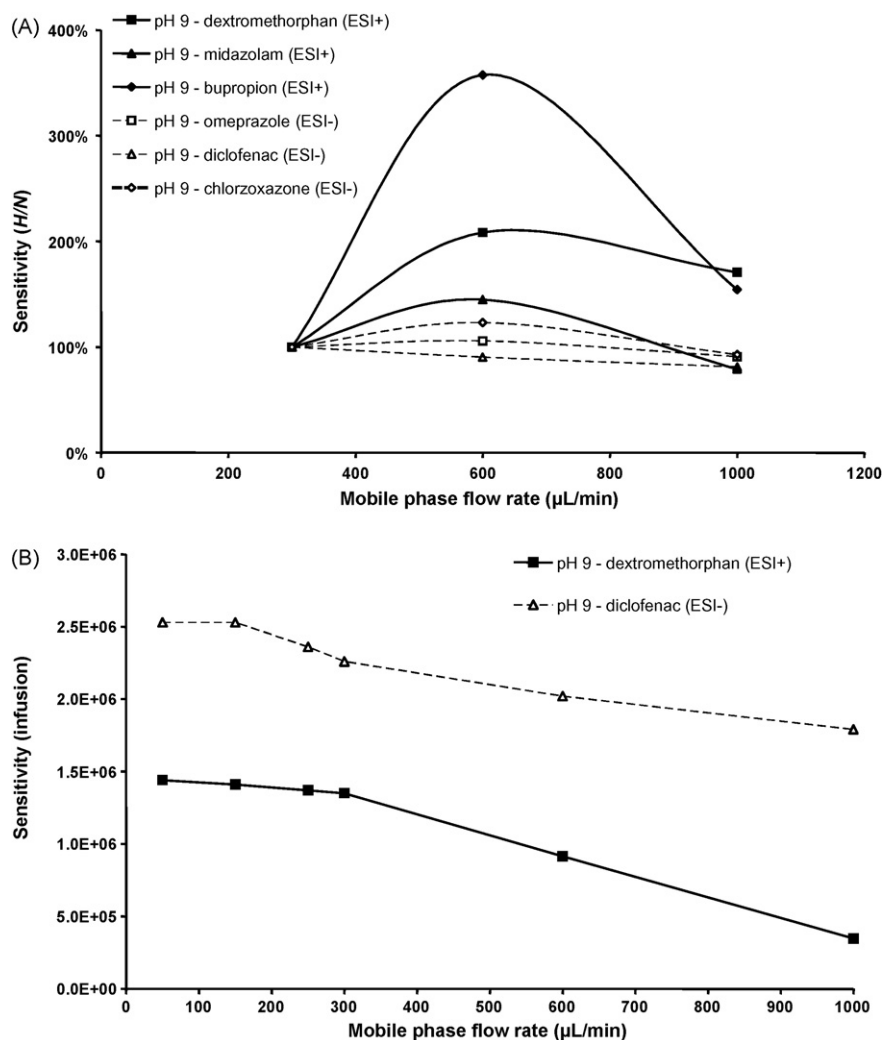


**Fig. 5.** Effect of mobile phase flow rate on ESI-MS sensitivity at pH 9. (A) UHPLC-MS experiments at  $F=300, 600$  and  $1000 \mu\text{L}/\text{min}$ . Results are presented in relative scale where values at  $F=300 \mu\text{L}/\text{min}$  correspond to 100%. (B) Infusion experiments at flow rates comprised between 50 and  $1000 \mu\text{L}/\text{min}$ . MS detection was performed in SIM mode, ESI $\pm$  using source parameters described in Section 2.

### 3.1.2. Mobile phase flow rate

The main advantage of UHPLC is to decrease the analysis time by using short columns packed with sub- $2 \mu\text{m}$  particles maintaining a good efficiency (*i.e.*,  $N=10,000$  for a 50 mm column packed with  $1.7 \mu\text{m}$ , equivalent to a 150 mm column packed with  $5 \mu\text{m}$ , but analysis time 9-fold lower). For instance, when  $1.7 \mu\text{m}$  particles are used instead of conventional  $5 \mu\text{m}$ , it is necessary to increase the mobile phase flow rate 3-fold to maintain the product  $u \cdot d_p$  constant [58,59]. Therefore, effect of mobile phase flow rate on MS response was investigated. Because the impact of mobile phase flow rate on sensitivity was similar for pH 3 and 9, only those obtained with a basic mobile phase were reported in Fig. 5. As shown in Fig. 5A, the effect of flow rate on MS response was different for acidic and basic compounds. A slight decrease in sensitivity was observed between 300 and  $1000 \mu\text{L}/\text{min}$  for acidic analytes (omeprazole, diclofenac and chlorzoxazone). This signal loss remained quite acceptable (*ca.* less than 15% at  $1000 \mu\text{L}/\text{min}$ ) and was attributed to a better compatibility of ESI-MS device with lower flow rates, as confirmed in Fig. 5B by infusion experiments. Regarding basic molecules, a different behavior occurred within the flow rate range, with a maximal sensitivity at  $600 \mu\text{L}/\text{min}$ . Two hypotheses could be suggested to explain this unexpected result. (i) A better ionization yield could be obtained at intermediate flow rate. However, data reported in Fig. 5B demonstrated a lower compatibility of MS

instrument at higher flow rate, since the MS sensitivity decreased continuously from 300 to  $1000 \mu\text{L}/\text{min}$ . (ii) A change in adduct distribution could occur according to the mobile phase flow rate [33]. Some additional experiments (data not shown) were carried out at three different flow rates (300, 600 and  $1000 \mu\text{L}/\text{min}$ ) and all frequent adducts observed in the positive mode were monitored (*e.g.*  $[\text{M}+\text{H}]^+$ ,  $[\text{M}+\text{NH}_4]^+$ ,  $[\text{M}+\text{Na}]^+$ ,  $[\text{M}+\text{CH}_3\text{OH}+\text{H}]^+$ ,  $[\text{M}+\text{K}]^+$ , and  $[\text{M}+\text{CH}_3\text{CN}+\text{H}]^+$ ). However, for each basic compound, adducts contribution represented less than 20% of the pre-existing  $[\text{M}+\text{H}]^+$  ion signal, whatever the flow rate. According to the results obtained in the infusion mode, it could be concluded that the better sensitivity obtained at intermediate flow rate (*i.e.*,  $600 \mu\text{L}/\text{min}$ ) was not related to ionization yield nor adducts distribution. Therefore, a third hypothesis was envisaged since the MS signal could also be significantly influenced by the chromatographic step. Peak width (Van Deemter curves [58]) and/or elution composition in gradient mode slightly differed depending on mobile phase flow rate, and could account for the observed parabolic curve shape.

Several suggestions were assessed to further improve productivity (*i.e.*, ultra-fast separations) maintaining sensitivity. (i) The use of 2.1 mm ID columns at  $1000 \mu\text{L}/\text{min}$  with a post-column flow split. However, an additional band broadening was observed in UHPLC as the peak volumes were very small and largely affected by the addition of a splitter, leading to a loss in resolution. (ii) The use

of 1 mm ID columns at a flow rate around 250  $\mu\text{L}/\text{min}$  (Fig. 5B). However, from a chromatographic point of view, performance of 1 mm ID columns was significantly reduced (lower efficiency and resolution) since the system was not fully adapted to this column dimension (larger peak widths from extra-column effect [9]).

In conclusion, this study demonstrated that the investigated ESI-MS apparatus was compatible with UHPLC for both acidic and basic compounds. Mobile phase flow rates up to 600  $\mu\text{L}/\text{min}$  could be used without compromising sensitivity. Moreover, no flow splitting device was required. For flow rates higher than 600  $\mu\text{L}/\text{min}$ , ultra-fast experiments could be performed to the detriment of sensitivity.

### 3.2. Comparison of ionization modes

The ionization source of the MS instrument used in this study permits simultaneous ESI/APCI operations (ESCI<sup>®</sup> multimode ionization source). This is accomplished by using a regular ESI probe with the APCI corona needle placed inside the ionization source [60]. As the ESCI<sup>®</sup> mode can also be implemented in conjunction with polarity switching feature, it is possible to simultaneously acquire ESI+, ESI-, APCI+ and APCI- data from a single run. Because peak widths could be very thin (e.g. down to 1 s in particular cases), the compatibility of all available ionization modes (i.e., ESI+, ESI-, ESI $\pm$ , APCI+, APCI-, APCI $\pm$  and ESCI<sup>®</sup> $\pm$ ) with UHPLC conditions was evaluated in terms of (i) sensitivity and (ii) data quality.

#### 3.2.1. Effect on sensitivity

ESI-MS responses obtained in the single polarity mode (i.e., one recorded SIM trace, ESI+ or ESI-) were compared with those obtained in ESI $\pm$  and ESCI<sup>®</sup> $\pm$ , where two (i.e., ESI+ and ESI-) and four (i.e., ESI+, ESI-, APCI+ and APCI-) SIM traces were recorded for each compound. For comparison purpose, only the highest signal was taken into account. The sensitivity was not altered by the polarity switching ( $\pm$ ) and remained equivalent between ESI in the single polarity mode and ESI $\pm$ . In fact, the observed MS signal reduction was never higher than 15%. When ESCI<sup>®</sup> was used instead of ESI in the single polarity mode, a significant decrease in MS response was observed. This reduction was comprised between 30 and 50% and up to 5-fold with bupropion, dextromethorphan and their respective metabolites. This loss in sensitivity was mainly attributed to the time necessary to perform ionization as well as polarity switching (ca. 20 ms each).

When APCI mode was selected instead of ESI mode, a MS signal reduction of 5–10-fold was observed (data not shown). This significant loss can be explained by the nature of the selected com-

pounds, preferentially ionized by ESI. Another explanation arose from the fact that APCI experiments were performed on the ESCI<sup>®</sup> multimode ionization source and not on a dedicated APCI source. Hence, results presented for APCI could be different with a dedicated probe. Furthermore, since APCI behaves as a mass-dependent device [61–63], analytes response was directly proportional to the mobile phase flow rate. In this context, APCI could be well adapted for UHPLC combined with high temperature conditions [23,64], which involves flow rates in the range 1–2 mL/min for 2.1 mm ID columns. Under such conditions, APCI could be the ionization source of choice, providing sensitivity remains satisfactory compared to ESI.

#### 3.2.2. Effect on data quality

In order to perform quantitative analyses, it is important to maintain at least 15 acquisition points *per* peak, which may be critical depending on the acquisition rate of the MS instrument and the peak width in gradient mode.

The MS acquisition rate with fast or ultra-fast LC is a crucial parameter that has to be evaluated when using multiple ionization stages. As an example, Fig. 6 presents the different steps of the MS process for a mixture of 4 compounds, when acquiring data in single ESI monitoring mode (e.g. ESI+), ESI $\pm$  and ESCI<sup>®</sup> $\pm$  with a dwell time of 20 ms. The cycle time varies from 105 ms in single ESI monitoring mode to 480 ms in ESCI<sup>®</sup> $\pm$ , involving respective acquisition rates comprised between 9.5 and 2.1 pts/s. Theoretical peak widths at baseline in time units ( $W_t$ ) were calculated for gradient modes lengthening from 1 to 5 min in UHPLC (with a 50 mm  $\times$  2.1 mm, 1.7  $\mu\text{m}$  column, at 600  $\mu\text{L}/\text{min}$ ), using the well-known equation proposed by Snyder and Dolan issued from the linear solvent strength (LSS) theory [65]:

$$W_t = \frac{4t_0}{\sqrt{N}} \cdot \left(1 + \frac{1}{2.3b}\right) \quad (2)$$

where  $t_0$  is equal to 0.2 min,  $N$  to 7000 plates, and  $b$  is the gradient steepness which can be expressed as

$$b = \frac{t_0 \cdot \Delta\Phi \cdot S}{t_{\text{grad}}} \quad (3)$$

Theoretical peak widths were equal to 1.2, 2.5 and 3.7 s, for a 1, 3 and 5 min gradient length, respectively. It should be noted that experimental peak widths at baseline were equal to 2.5, 3.8 and 5.1 s for similar gradients. These differences were evidently attributed to the numerous assumptions afforded by the LSS theory (e.g. lack

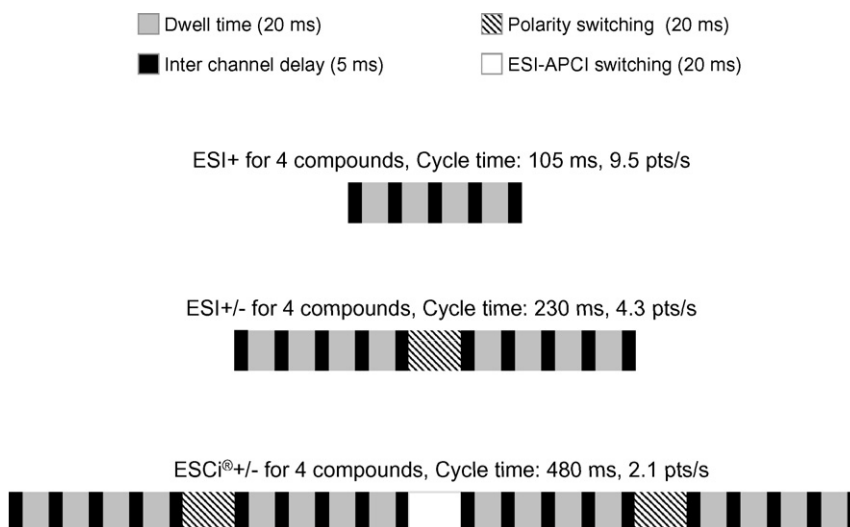


Fig. 6. Schematic representation of the different steps of the MS process for a mixture of 4 compounds, when acquiring data in ESI+, ESI $\pm$  and ESCI<sup>®</sup> $\pm$ .

**Table 3**

Number of data points across a peak for different set of conditions in single ESI monitoring mode, ESI± and ESCi®± modes. These values were based on the experimental estimation of peak width and on the acquisition rate of MS instrument (see Fig. 6).

	Number of data points across a peak				
	Number of compounds	Dwell time = 20 ms 1 min gradient run	Dwell time = 20 ms 3 min gradient run	Dwell time = 20 ms 5 min gradient run	Dwell time = 5 ms 1 min gradient run
Single ESI monitoring mode	2	50	76	102	125
	4	25	38	51	63
	6	17	25	34	42
	8	13	19	26	31
	10	10	15	20	25
	20	5	8	10	13
	50	2	3	4	5
ESI±	2	25	38	51	63
	4	13	19	26	31
	6	8	13	17	21
	8	6	10	13	16
	10	5	8	10	13
	20	3	4	5	6
	50	1	2	2	3
ESCi®±	2	13	19	26	31
	4	6	10	13	16
	6	4	6	9	10
	8	3	5	6	8
	10	3	4	5	6
	20	1	2	3	3
	50	1	1	1	1

of compressibility factor, inaccuracy of  $S$  parameter) and to the coupling with MS, which can significantly broaden the theoretical peaks. It was therefore difficult to evaluate *a priori* the peak width in gradient mode with MS detection, only on the basis of Eqs. (2) and (3). Therefore, average experimental peak widths were considered to calculate the number of data points across a peak for different conditions.

Results were reported for single ESI monitoring mode, ESI± and ESCi®± modes in Table 3. Regarding ionization mode, the ESI± and the multimode (ESCi®±) were only adapted for a couple of compounds (to maintain 15 points across the peak), even with the fast polarity switching of 20 ms, and should preferentially be dedicated to qualitative purpose. On the other hand, single ESI monitoring mode could be considered for simultaneous quantitation of a higher number of compounds. It is important to emphasize the strong influence of the peak width, attributable to the mobile phase flow rate, column geometry and gradient slope (directly related to  $k_e$ ) on the number of drugs that could be adequately quantified in the single ESI monitoring mode. Consequently, either a limited number of compounds could be monitored under ultra-fast conditions (*e.g.*

analysis time lower or equal to 1 min), or slower conditions should be preferred for quantifying a higher number of compounds. Finally, the SIM dwell time is a key parameter for acquisition rate. By selecting a dwell time of 5 ms instead of 20 ms, the number of data points across a peak could be drastically increased (Table 3), with a lower sensitivity.

### 3.3. Limits of detection (LOD)

After optimizing LC and MS parameters, LOD were determined for the different analytes in ESI± at pH 9, for two different flow rates and  $k_e$ . Table 4 summarized achievable LOD depending on acquisition mode (*i.e.*, SIM vs. scan). In SIM mode, two different conditions were tested, 300  $\mu\text{L}/\text{min}$  with  $k_e = 1$  and 600  $\mu\text{L}/\text{min}$  with  $k_e = 3$ , both with a dwell time of 20 ms and an equivalent analysis time of about 3 min. Sensitivities were similar and best conditions should be preferentially selected according to the quality of the chromatographic data. For instance, experiments at 600  $\mu\text{L}/\text{min}$  with  $k_e = 3$  were in general less sensitive but the chromatographic separation (in terms of peak width and selectivity) was improved compared to

**Table 4**

Achievable LOD (ng/mL) in optimal UHPLC–MS conditions at pH 9 with ESI± in three MS acquisition modes. Dwell time in SIM mode was 20 ms. SIM window conditions were: [0–1.55 min]:  $m/z$  152, 184, 311, 360; [1.56–1.81 min]:  $m/z$  168, 180, 295, 344; [1.82–2.09 min]:  $m/z$  256, 258, 342; [2.10–3.16 min]:  $m/z$  240, 272, 326. Scan rate was:  $m/z$  100–500 at 5000  $m/z/s$ .

	LOD (ng/mL)			
	SIM ( $F = 300 \mu\text{L}/\text{min}$ , $k_e = 1$ )	SIM ( $F = 600 \mu\text{L}/\text{min}$ , $k_e = 3$ )	SIM window ( $F = 300 \mu\text{L}/\text{min}$ , $k_e = 1$ )	Scan-XIC ( $F = 300 \mu\text{L}/\text{min}$ , $k_e = 1$ )
Phenacetin	50	50	50	1,000
Acetaminophen	50	100	50	5,000
Bupropion	3	20	2	1,000
Hydroxybupropion	2	20	2	1,000
Dextromethorphan	5	1	0.5	500
Dextrorphan	25	25	2.5	500
Midazolam	1	10	0.5	500
1'-Hydroxymidazolam	2.5	10	2.5	500
Chlorzoxazone	50	50	20	100
6-Hydroxychlorzoxazone	50	2500	25	250
Diclofenac	250	500	200	10,000
4'-Hydroxydiclofenac	200	200	100	10,000
Omeprazole	100	100	50	1,000
5'-Hydroxyomeprazole	70	50	50	1,000

that obtained at 300  $\mu\text{L}/\text{min}$  with  $k_e = 1$ . Best LODs were included in the range [1–50 ng/mL] in positive mode and [50–250 ng/mL] in negative mode. It has to be noted that LODs observed in ESI+ for basic compounds were generally 5–10-fold better than those measured in ESI– for acidic analytes, although the latter could also be ionized in positive mode with a similar or higher sensitivity. The lower sensitivity reached in negative mode is often observed in MS and could be even more critical at pH 9 as ionic current in the negative mode tends to be less stable [56]. The “SIM window” mode was also evaluated using a maximum of four ions detected during each time window, to maintain a sufficient number of data points across the peak for quantitation purpose (Table 3). In such conditions, the gain in sensitivity was about 2-fold for most compounds and 10-fold for dextromethorphan and its metabolite. Although this procedure was less generic, it can be useful for quantitative purpose of numerous compounds. Finally, the scan acquisition mode was performed from  $m/z$  100 to 500, with a scan rate of 5000  $m/z/s$ . LODs reported in Table 4 corresponded to the values obtained on extracted ion current. As expected, LODs were about 100 times higher than those obtained in SIM mode. The scan mode can thus be interesting only for qualitative purpose at high concentrations.

#### 4. Conclusion

In this study, experimental conditions were tuned to achieve the best compromise between a high MS sensitivity and sufficient chromatographic performance, for a mixture containing acidic and basic compounds.

Regarding chromatographic parameters, pH 9 was found favorable to achieve sufficient MS response in conjunction with an adequate selectivity and a mobile phase flow rate included within the range 300–600  $\mu\text{L}/\text{min}$ . The gradient slope was set according to the complexity of the separation. Concerning MS, the fast polarity switching ESI+/ESI– was a valuable tool to increase productivity, while the ESCi $^{\pm}$  mode was found of limited interest because it compromised sensitivity as well as the number of compounds, which could be simultaneously monitored. It was also emphasized that the SIM dwell time should be at least equal to 20 ms to limit loss in sensitivity. Finally, the scan mode appeared 100 times less sensitive and found its interest for qualitative purpose at high analytes concentration levels.

In optimized conditions, the UHPLC–MS coupling with single quadrupole analyzer for selected CYP450 substrates and metabolites provided good sensitivities, included within the range [1–50 ng/mL] in positive mode and [50–250 ng/mL] in negative mode, in conjunction with a significant analysis time reduction and excellent chromatographic resolution.

It is worth mentioning that optimal conditions of pH, flow rate, gradient slope, as well as source parameters could also be applied to achieve fast or ultra-fast separations of other drug mixtures analyzed by UHPLC–MS with a single quadrupole analyzer. Nevertheless, results presented in this study are instrument-dependent and conclusions could be different with another analyzer or interface geometry. As recently demonstrated by Delatour and Leclercq [66], some significant differences in analytes responses could be observed with two different mass spectrometers, although the same experimental conditions were used.

#### Acknowledgements

The authors wish to thank Waters for the loan of ACQUITY SQD instrument as well as Dr. D. Petit and Dr. A. Tei for helpful, stimulating discussions, and valuable comments. The authors also acknowledge Prof. P. Dayer and Dr. Y. Daali, from the Division of Clinical Pharmacology and Toxicology of the Geneva University Hospitals for providing several substrates and metabolites.

#### References

- [1] C. Prakash, C.L. Shaffer, A. Nedderman, *Mass Spectrom. Rev.* 26 (2007) 340.
- [2] S. Ahuja, in: S. Ahuja (Ed.), *Overview: Handbook of Pharmaceutical Analysis by HPLC*, Academic Press, San Diego, CA, 2005, p. 1.
- [3] L. Mondello, R. Shellie, A. Casilli, P.Q. Tranchida, P. Marriott, G. Dugo, *J. Sep. Sci.* 27 (2004) 699.
- [4] S. Bieri, O. Muñoz, J.L. Veuthey, P. Christen, *J. Sep. Sci.* 29 (2006) 96.
- [5] S. Rudaz, L. Geiser, S. Souverain, J. Prat, J.L. Veuthey, *Electrophoresis* 26 (2005) 3910.
- [6] S. Souverain, L. Geiser, S. Rudaz, J.L. Veuthey, *J. Pharm. Biomed. Anal.* 40 (2006) 235.
- [7] J. Kameoka, H.G. Craighead, H. Zhang, J. Henion, *Anal. Chem.* 73 (2001) 1935.
- [8] I.M. Mutton, *Chromatographia* 47 (1998) 291.
- [9] D. Guilleme, D. Nguyen, S. Rudaz, J.L. Veuthey, *Eur. J. Pharm. Biopharm.* 66 (2007) 475.
- [10] Y.F. Cheng, Z. Lu, U. Neue, *Rapid Commun. Mass Spectrom.* 15 (2001) 141.
- [11] F. Svec, J.M.J. Fréchet, *Anal. Chem.* 64 (1992) 820.
- [12] S. Hjertén, J.L. Liao, R. Zhang, *J. Chromatogr.* 473 (1989) 273.
- [13] H. Minakuchi, K. Nakanishi, N. Soga, N. Ishizuka, N. Tanaka, *Anal. Chem.* 68 (1996) 3498.
- [14] K.K. Unger, R. Skudas, M.M. Schulte, *J. Chromatogr. A* 1184 (2008) 393.
- [15] K. Cabrera, *J. Sep. Sci.* 27 (2004) 843.
- [16] D. Guilleme, D. Nguyen, S. Rudaz, J.L. Veuthey, *J. Chromatogr. A* 1149 (2007) 20.
- [17] M.Q. Huang, Y. Mao, M. Jemal, M. Arnold, *Rapid Commun. Mass Spectrom.* 20 (2006) 1709.
- [18] A. Bugey, S. Rudaz, C. Staub, *J. Chromatogr. B* 832 (2006) 249.
- [19] A. Bugey, C. Staub, *J. Sep. Sci.* 30 (2007) 2967.
- [20] S. Le Gac, J. Carlier, J.C. Camart, C. Cren-Olive, C. Rolando, *J. Chromatogr. B* 808 (2004) 3.
- [21] F.D. Antia, C. Horvath, *J. Chromatogr.* 435 (1988) 1.
- [22] D. Guilleme, S. Heinisch, J.L. Rocca, *J. Chromatogr. A* 1052 (2004) 39.
- [23] D. Guilleme, R. Russo, S. Rudaz, C. Bicchi, J.L. Veuthey, *Curr. Pharm. Anal.* 4 (2007) 221.
- [24] D. Guilleme, S. Heinisch, *Sep. Purif. Rev.* 34 (2005) 181.
- [25] M. Albert, G. Cretier, D. Guilleme, S. Heinisch, J.L. Rocca, *J. Sep. Sci.* 28 (2005) 1803.
- [26] L. Pereira, S. Aspey, H. Ritchie, *J. Sep. Sci.* 30 (2007) 1115.
- [27] D. Nguyen, D. Guilleme, S. Heinisch, M.-P. Barrioulet, J.L. Rocca, S. Rudaz, J.L. Veuthey, *J. Chromatogr. A* 1167 (2007) 76.
- [28] D. Cabooter, S. Heinisch, J.L. Rocca, D. Clicq, G. Desmet, *J. Chromatogr. A* 1143 (2007) 121.
- [29] J.D. Thompson, P.W. Carr, *Anal. Chem.* 74 (2002) 1017.
- [30] J.E. MacNair, K.C. Lewis, J.W. Jorgenson, *Anal. Chem.* 69 (1997) 983.
- [31] L. Novakova, L. Matysova, P. Solich, *Talanta* 68 (2006) 908.
- [32] P.D. Rainville, C.L. Stumpf, J.P. Shockcor, R.S. Plumb, J.K. Nicholson, *J. Proteome Res.* 6 (2007) 552.
- [33] R.B. Cole, in: R.B. Cole (Ed.), *Electrospray Ionization Mass Spectrometry: Fundamentals, Instrumentation and Applications*, Wiley, New York, NY, 1997, p. 577.
- [34] H. Sun, H. Lv, Y. Zhang, X. Wang, K. Bi, H. Cao, *J. Sep. Sci.* 30 (2007) 3202.
- [35] F. Qin, Y. Ma, Y. Wang, L. Chen, D. Wang, F. Li, *J. Pharm. Biomed. Anal.* 46 (2008) 557.
- [36] M. Farre, M. Kuster, R. Brix, F. Rubio, M.J. Lopez de Alda, D. Barcelo, *J. Chromatogr. A* 1160 (2007) 166.
- [37] J. Wang, D. Leung, *Rapid Commun. Mass Spectrom.* 21 (2007) 3213.
- [38] P. Baranczewski, A. Stanczak, K. Sundberg, R. Svensson, A. Wallin, J. Jansson, P. Garberg, H. Postlind, *Pharmacol. Rep.* 58 (2006) 453.
- [39] L.R. Snyder, J.W. Dolan, in: L.R. Snyder (Ed.), *High-Performance Gradient Elution: The Practical Application of the Linear-Solvent-Strength Model*, Wiley, Hoboken, NJ, 2007, p. 496.
- [40] R. Nicoli, M. Bartolini, S. Rudaz, V. Andrisano, J.L. Veuthey, *J. Chromatogr. A* 1206 (2008) 2.
- [41] U. Fuhr, A. Jetter, J. Kirchheiner, *Nature* 81 (2007) 270.
- [42] M.C. Jerdi, Y. Daali, M.K. Oestreich, S. Cherkaoui, P. Dayer, *J. Pharm. Biomed. Anal.* 35 (2004) 1203.
- [43] N.H. Davies, M.R. Euerby, D.V. McCalley, *J. Chromatogr. A* 1178 (2008) 71.
- [44] D.V. McCalley, *Adv. Chromatogr.* 46 (2008) 305.
- [45] K. Yu, L. Di, E. Kerns, S.Q. Li, P. Alden, R.S. Plumb, *Rapid Commun. Mass Spectrom.* 21 (2007) 893.
- [46] K. Yu, D. Little, R.S. Plumb, B. Smith, *Rapid Commun. Mass Spectrom.* 20 (2006) 544.
- [47] S. Souverain, S. Rudaz, J.L. Veuthey, *J. Chromatogr. A* 1058 (2004) 61.
- [48] R.D. Voyksner, in: R.B. Cole (Ed.), *Combining Liquid Chromatography with Electrospray Mass Spectrometry*, Wiley, New York, NY, 1977, p. 323.
- [49] L. Peng, T. Farkas, *J. Chromatogr. A* 1179 (2008) 131.
- [50] A.J. Tomlinson, R.M. Chic, *Rapid Commun. Mass Spectrom.* 17 (2003) 909.
- [51] C.G. Enke, *Anal. Chem.* 69 (1997) 4885.
- [52] R. Guevremont, K.W.M. Siu, J.C.Y. Leblanc, S.S. Berman, *J. Am. Soc. Mass Spectrom.* 3 (1992) 216.
- [53] R.G. Cooks, J.S. Patrick, S.A. Mcluckey, *Mass Spectrom. Rev.* 13 (1994) 287.
- [54] S. Espinosa, E. Bosch, M. Roses, *Anal. Chem.* 72 (2000) 5193.
- [55] Y.C. Cheng, Z. Lu, U.D. Neue, *Rapid Commun. Mass Spectrom.* 15 (2001) 141.
- [56] N.B. Cech, C.G. Enke, *Mass Spectrom. Rev.* 20 (2001) 362.
- [57] P.J. Kebarle, *J. Mass Spectrom.* 35 (2000) 804.

- [58] D. Nguyen, D. Guillarme, S. Rudaz, J.L. Veuthey, *J. Chromatogr. A* 1128 (2006) 105.
- [59] D. Nguyen, D. Guillarme, S. Rudaz, J.L. Veuthey, *J. Sep. Sci.* 29 (2006) 1836.
- [60] M. Balogh, A high speed combination multi-mode ionization source for mass spectrometers, *PCT Int. Appl.*, WO 2003102537 A2 20031211, 2003, 38 pp.
- [61] A. Asperger, J. Efer, T. Koal, W. Engewald, *J. Chromatogr. A* 937 (2001) 65.
- [62] G. Hopfgartner, K. Bean, J. Henion, R. Henry, *J. Chromatogr.* 647 (1993) 647.
- [63] R. Rosset, M. Caude, A. Jardy, *Chromatographies en Phase Liquide et Supercritique*, Masson, Paris, 1991, 919 pp.
- [64] R.S. Plumb, P. Rainville, B.W. Smith, K.A. Johnson, J. Castro-Perez, I.D. Wilson, J.K. Nicholson, *Anal. Chem.* 78 (2006) 7278.
- [65] L.R. Snyder, J.W. Dolan, *High Performance Gradient Elution*, Wiley-Interscience, New York, 2007.
- [66] C. Delatour, L. Leclercq, *Rapid Commun. Mass Spectrom.* 19 (2005) 1359.



# Triethanolamine-capped CdSe quantum dots as fluorescent sensors for reciprocal recognition of mercury (II) and iodide in aqueous solution

Zhuo Bin Shang<sup>a</sup>, Yu Wang<sup>a,\*</sup>, Wei Jun Jin<sup>a,b,\*\*</sup>

<sup>a</sup> School of Chemistry and Chemical Engineering, Shanxi University, Wucheng Road, Taiyuan 030006, PR China

<sup>b</sup> College of Chemistry, Beijing Normal University, Beijing 100875, PR China

## ARTICLE INFO

### Article history:

Received 15 September 2008

Received in revised form

18 November 2008

Accepted 19 November 2008

Available online 27 November 2008

### Keywords:

CdSe QDs

Triethanolamine

Mercury (II)

Iodide

Quenching

## ABSTRACT

Water-soluble luminescent CdSe quantum dots surface-modified with triethanolamine (TEA-CdSe-QDs) were prepared with high stability. The fluorescence of the TEA-CdSe-QDs was greatly quenched only when Hg<sup>2+</sup> and I<sup>-</sup> coexisted in the solution, whereas addition of either Hg<sup>2+</sup> or I<sup>-</sup> individually has no noticeable effect on the fluorescence emission. Such a unique quenching effect could be used for reciprocal recognition of mercury (II) ions and/or iodide anions in aqueous solution with rather high selectivity and sensitivity. The detection limits of Hg<sup>2+</sup> or I<sup>-</sup> ion were  $1.9 \times 10^{-7}$  mol L<sup>-1</sup> or  $2.8 \times 10^{-7}$  mol L<sup>-1</sup>, respectively. The adequate experiments showed that iodine (I) anions could bridge between TEA-CdSe-QDs and Hg<sup>2+</sup> to form a stable complex (QDs-I<sup>-</sup>-Hg<sup>2+</sup>) and the following effective electron transfer from the QDs to the Hg<sup>2+</sup> could be responsible for the fluorescence quenching of QDs.

© 2008 Elsevier B.V. All rights reserved.

## 1. Introduction

Owing to their unique optical properties such as broad excitation band, narrow emission spectrum, size- and composition-tunable emission wavelength and excellent anti-photobleaching [1–3], semiconductor quantum dots (QDs) have elicited considerable interest in the field of chemical sensing [4–6]. Via analyte-induced changes in photoluminescence [7–30], QDs have been reported over the past decade for optical sensing of various small molecules and ions, such as K<sup>+</sup> [12], Zn<sup>2+</sup> [13], Cu<sup>2+</sup> [13–18], Ag<sup>+</sup> [18–21], Cd<sup>2+</sup> [22], Pb<sup>2+</sup> [23], Hg<sup>2+</sup> [24,25], I<sup>-</sup> [26] and CN<sup>-</sup> [27,28]. Nearly all these studies involve the surface modification of QDs with appropriate ligand molecules to make QDs available for interactions with target analytes. These reports demonstrated that the surface-ligands of QDs have profound effects on fluorescence response of QDs to ions and therefore the selectivity and sensitivity for sensing target analytes can be altered by changing the capping layer on the quantum dots. By far, the mercapto-containing bifunctional ligands, including mercapto-alcohols [13,21,25,29], mercapto-acids [9–11,15,17,20,21,30], mercapto-ethers [12], mercapto-sulfonic acids [15,27], mercapto-amines [28] and mercapto-amino acids

[13,14,16–19,23,24] etc., have been extensively studied for QDs surface modification. In comparison with mercapto group, limited numbers of other functional groups have been explored as surface ligands. Hence, it can be expected that there would be a growing interest in the design of various QDs surface ligands for specific chemical sensing of analytes with high sensitivity.

Sharma et al. [31] reported that amine functional group could interact with CdSe QDs surface and influence their electronic and optical properties. Dannhauser et al. [32] also reported that binding of several ternary amines including N(Et)<sub>3</sub> led to enhanced luminescence of CdS or Cd<sub>3</sub>As<sub>2</sub> nanoparticles. In this context, we wish to examine the possibility of using water-soluble amino alcohols as the surface ligands of QDs. In the present work, we report a new and simple method for creating water soluble CdSe QDs by replacing the oleic acid chains on the CdSe QDs with highly water-soluble triethanolamine (TEA). Although it is a simple ligand, we show that TEA-CdSe-QDs are capable of selectively sensing Hg<sup>2+</sup> in the presence of I<sup>-</sup> and vice versa. To the best of our knowledge, this represents the first example of QDs that are able to detect ion pair.

## 2. Experimental

### 2.1. Reagents

Cadmium oxide (CdO, 99.99%), selenium (Se, powder, 100 mesh, 99.99%), Octadecane, triethanolamine (TEA), oleic acid (Ole),

\* Corresponding author. Tel.: +86 351 7010319; fax: +86 351 7011688.

\*\* Corresponding author at: College of Chemistry, Beijing Normal University, Beijing 100875, PR China. Tel.: +86 1 58802146; fax: +86 1 58802146.

E-mail addresses: [wangyu1168@sxu.edu.cn](mailto:wangyu1168@sxu.edu.cn) (Y. Wang), [wjjin@bnu.edu.cn](mailto:wjjin@bnu.edu.cn) (W.J. Jin).

anhydrous methanol and anhydrous chloroform were purchased from Aldrich (Milwaukee, WI, USA). The 4-(2-hydroxyethyl)-1-piperazine ethanesulfonic acid (HEPES) was obtained from Alfa Aesar (Karlsruhe, Germany). All the other chemical reagents were of analytical grade and used as received without further purification. Silver nitrate served as the source of  $\text{Ag}^+$  while all other metallic ions were supplied from their corresponding chlorides. Sodium salts with different anions including  $\text{F}^-$ ,  $\text{Cl}^-$ ,  $\text{Br}^-$ ,  $\text{I}^-$ ,  $\text{NO}_2^-$ ,  $\text{NO}_3^-$ ,  $\text{SO}_3^{2-}$ ,  $\text{SO}_4^{2-}$ ,  $\text{S}_2\text{O}_3^{2-}$ ,  $\text{PO}_4^{3-}$ ,  $\text{H}_2\text{PO}_4^-$ ,  $\text{CO}_3^{2-}$ ,  $\text{CH}_3\text{COO}^-$  were used for anions studies. All metal ion stock solutions were prepared by dissolving the appropriate amounts of metal salts with doubly distilled water.

## 2.2. Apparatus

Fluorescence spectra were taken on a LS-55 luminescence spectrometer (Perkin Elmer Inc.). Fluorescence decay measurements were carried out on a FL920 Fluorescence Lifetime Spectrometer (Edinburgh Instruments Ltd.) with the pulse width of 1 ns. Powder X-ray diffraction data were collected on a X'Pert PRO MPD (PANalytical, the Netherlands). TEM images were obtained with a JEM-2010 (JEOL, Japan) transmission electron microscope. The TEM specimens were prepared by placing a drop of hexane or water suspension of nanoparticles on a carbon-coated copper grid. The solvent was evaporated prior to the characterizations. Fourier transform infrared spectra (FTIR) were recorded with a SHIMADZU 8400S infrared spectrometer (Nicolet, Waltham, Japan). Samples for the IR measurements were prepared from the corresponding QDs solutions by centrifugation and then thoroughly washed with water. After being dried under vacuum at  $110^\circ\text{C}$  for 3 h, the nanoparticles were prepared as KBr pellets for the IR analysis. The surface charge of TEA–CdSe–QDs was determined with a DYY-8C electrophoresis apparatus (Beijing LiuYi Instrument Factory, Beijing, China) in Tris-acetate-EDTA (TAE) buffer ( $5\times$  TAE buffer: 2.0 M Tris-acetate and 50 mM EDTA, pH 8.0). Briefly, fill the electrophoresis tank with proper amount of  $1\times$  TAE buffer (pH 8.0), and then a suitable amount of TEA–QDs was added to the tank. After a 15 min run at 80 V, both the cathode and anode solutions were collected and their fluorescence spectra were measured separately.

## 2.3. Synthesis of TEA-capped CdSe QDs

The CdSe quantum dots stabilized by oleic acid were synthesized following the procedure described by Peng and Peng [33], using CdO as a precursor but introducing some slight modifications. Briefly, a mixture of CdO (116 mg, 0.9 mmol), Ole (5 mL) and octadecane (20 mL) was heated to  $300\text{--}310^\circ\text{C}$  for 15–20 min under  $\text{N}_2$  flow. After CdO was completely dissolved, a solution of Se (0.072 g, 0.9 mmol) dispersed in Ole (1 mL) was swiftly injected into this hot solution. After injection, a visual color change from colorless to red occurred. CdSe nanocrystals were left to grow for about 3–4 min at  $270\text{--}280^\circ\text{C}$ . After purification by methanol precipitation, centrifugation, and decantation, the CdSe QDs were redispersed in 10 mL of hexane.

Water-soluble TEA-capped CdSe QDs were prepared as follows: 5 mL CdSe QDs suspension dispersed in hexane was added into 1 mL of triethanolamine and then the mixture was stirred for 12 h until the top hexane layer became colorless. Afterwards, the hexane layer was discarded while the bottom TEA layer was collected and centrifuged. The liquid phase was carefully decanted and the solid phase was redispersed in doubly distilled water to obtain the stock solution of TEA–QDs. The resulting solution was stirred for another 12 h and stored at room temperature without any evidence of precipitation for at least 1 month.

## 2.4. General procedure

TEA–QDs working solution was prepared by diluting the stock solution of TEA–QDs (80  $\mu\text{L}$ ) with 10 mM HEPES buffer (pH 7.2). The spectrofluorimetric titrations were performed as follows: an aliquot of the TEA–QDs working solution was pipetted into a  $1\text{ cm} \times 1\text{ cm}$  quartz cell and varying volumes of ion stock solutions were added to the cell. The mixture was briefly shaken for a few seconds before making the fluorescence measurements. The total volume change after addition of ion solutions was less than 4%.

## 3. Results and discussion

### 3.1. Characterization of TEA-capped CdSe nanoparticles

The TEM images shows that the Ole–QDs are spherical and nearly monodispersed with an average diameter of 5 nm. After the TEA modification, the QDs exhibited no obvious change in shape or size.

The formation of oleic acid capped CdSe QDs (Ole–QDs) and TEA-capped CdSe QDs (TEA–QDs) was demonstrated by FTIR. As shown in Fig. 1, the characteristic absorption peak of carbonyl is shifted from  $1710\text{ cm}^{-1}$  (Fig. 1a) to  $1540\text{ cm}^{-1}$  (Fig. 1b), indicating that oleic acid was chemisorbed as a carboxylate on the surface of CdSe QDs and coordinated with the  $\text{Cd}^{2+}$  ions. The strong band at  $3392\text{ cm}^{-1}$  (O–H group vibration) plus those at  $1035$  and  $1074\text{ cm}^{-1}$  (C–O group vibration) in Fig. 1c clearly indicated the presence of TEA molecules that could not be removed from the solid nanoparticles by extensive washing with deionized water. However, the IR spectrum of TEA–QDs also shows the characteristic band associated with the carboxyl group, indicating that there still exist oleic acid ligands at the surface of the TEA–QDs. It is inferred from the present results that the nitrogen atom of TEA coordinate with  $\text{Cd}^{2+}$  ion on the QD surface, and the hydrophilic hydroxyl groups face outward and render QDs water-soluble. The final TEA–QDs at surface should be positively charged due to the replacement of the electronegative oleic acid by the neutral triethanolamine on the surface of CdSe QDs. After electrophoresis, only the cathode QDs solution displayed a strong fluorescence signal, confirming this speculation. It can be attributed to that coordination of a lone electron pair on the nitrogen atom of amine group of TEA with the  $\text{Cd}^{2+}$  of CdSe nanoparticles resulted in the positively charged amino-group.

### 3.2. Absorption and fluorescence characteristics of the TEA–QDs

The UV–vis absorption spectra (a, b) and fluorescence spectra (c, d) of the synthesized CdSe QDs are shown in Fig. 2. It can be seen that the absorption edges of CdSe were blue-shifted to higher energies and the fluorescence peak position of the QDs red-shifted

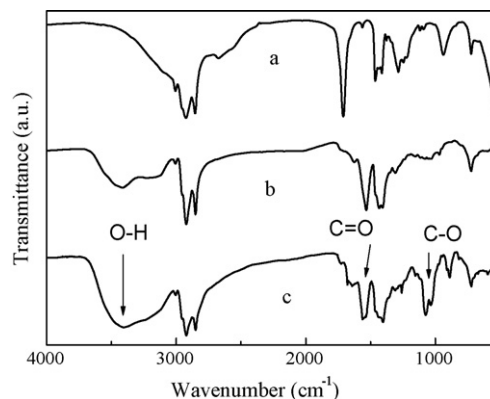
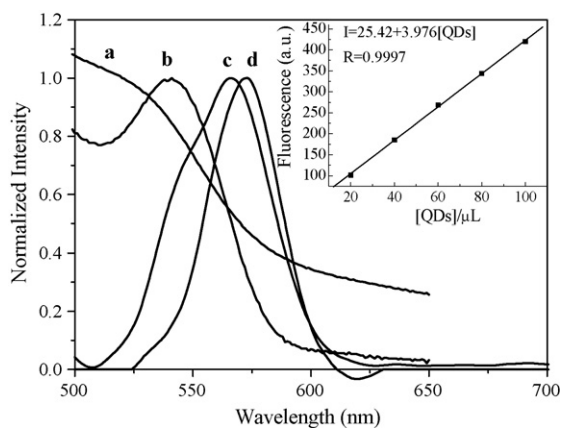


Fig. 1. FTIR spectra of (a) neat oleic acid (Ole), (b) Ole-capped CdSe QDs and (c) TEA modified CdSe QDs.





**Fig. 2.** UV-vis absorption and fluorescence spectra of the TEA-QDs (a and d) and the Ole-QDs (b and c). Inset: plot of peak fluorescence intensity vs. concentration of TEA-QDs in aqueous solution.

by about 5 nm after TEA modification, indicating the formation of the new complex structure [34,35]. The maximum emission peak of the TEA-CdSe solution appeared at 575 nm with the full width half maximum of about 30 nm, indicating a relative narrow size distribution [22]. Additionally, the plot of peak fluorescence intensity vs. the concentration of the TEA-QDs shows a good linear relationship in the range of 20–100  $\mu\text{L}$ , indicating that the functionalized QDs were still of monodisperse and uniform in aqueous solution over a large concentration range. Moreover, TEA-QDs were stable enough because QDs optical properties undergo no change over 1 month.

It is known that luminescence of QDs are pH sensitive. So the effect of pH on the fluorescence intensity of TEA-QDs was investigated using 0.01 M 4-(2-hydroxyethyl)-1-piperazine ethane-sulfonic acid (HEPES) buffer solutions (pH 3–10). The maximum change of fluorescence intensity appeared in the alkaline range of pH 8–10, in which the hydroxide ions may compete with TEA for the positively charged nanocrystal surface. The fluorescence intensity was relatively high and stable within the pH range of 3–7.6. Therefore, a physiological buffer condition of pH 7.2 was used in the following experiments.

### 3.3. Fluorescence detection for $\text{Hg}^{2+}$ and $\text{I}^-$ with TEA-CdSe-QDs

Interestingly, addition of either  $\text{Hg}^{2+}$  or  $\text{I}^-$  individually had no significant effect on the emission of the TEA-QDs. The fluorescence of the TEA-QDs, however, was greatly quenched with no spectral shift when  $\text{Hg}^{2+}$  and  $\text{I}^-$  coexisted in the solution, as shown in Fig. 3. Such a unique quenching pattern could be used to develop a method for the reciprocal recognition of  $\text{Hg}^{2+}$  and/or  $\text{I}^-$ . The plots of  $I_0/I$  vs. both  $\text{Hg}^{2+}$  and  $\text{I}^-$  concentration, however, did not fit a conventional linear Stern–Volmer relationship and steep upward curvatures were obtained, indicating that the quenching was neither purely static nor purely dynamic process [21,27,28,36]. For dynamic quenching, lifetime changes with quencher concentration whereas static quenching would not affect the lifetime. The fluorescence lifetime of the QDs was found to significantly decrease with increasing of  $\text{Hg}^{2+}$  in the presence of  $\text{I}^-$ , which suggested that the quenching observed here seems to be at least partially dynamic. When using a modified Stern–Volmer equation already proposed for the mechanisms where both dynamic and static quenching acts together [21,27,28], good linear relationships ( $R = 0.999$  and  $0.991$ ) were observed up to  $3.5 \times 10^{-5} \text{ mol L}^{-1}$   $\text{Hg}^{2+}$  and  $\text{I}^-$  ions. They are:  $\ln(I_0/I) = 0.1411[\text{Hg}^{2+}] - 0.03971$  and  $\ln(I_0/I) = 0.09378[\text{I}^-] - 0.2652$ ,  $[\text{Hg}^{2+}]$  and  $[\text{I}^-]$  being expressed in micromolarity per litre.

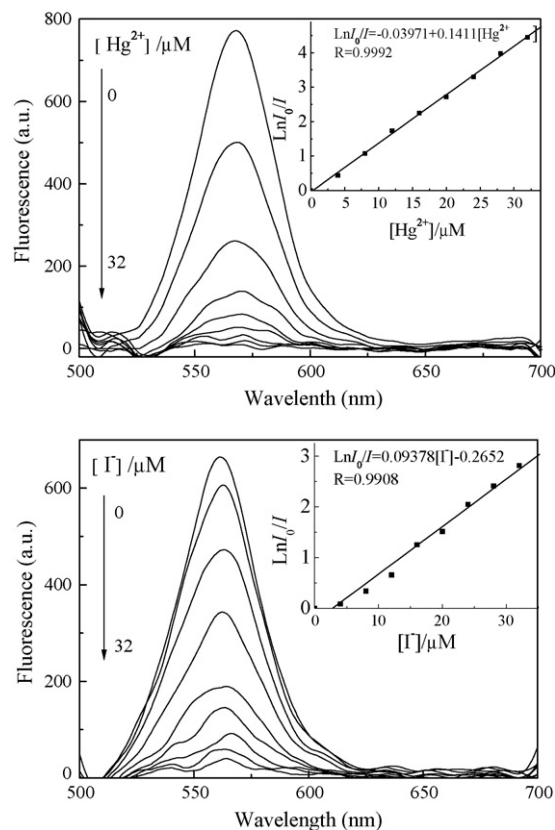


**Fig. 3.** Effect of  $\text{Hg}^{2+}$  and  $\text{I}^-$  concentrations on FL of the TEA modified CdSe QDs in HEPES buffer (pH 7.2). (A)  $[\text{I}^-] = 40 \mu\text{M}$ ; (B)  $[\text{Hg}^{2+}] = 40 \mu\text{M}$ .  $\lambda_{\text{ex}} = 480 \text{ nm}$ .

The detection limits, calculated following the  $3\sigma$  IUPAC criteria, were  $1.9 \times 10^{-7} \text{ mol L}^{-1}$  and  $2.8 \times 10^{-7} \text{ mol L}^{-1}$  for  $\text{Hg}^{2+}$  and  $\text{I}^-$ , respectively. The standard deviation for six replicate measurements of a solution containing  $4 \mu\text{M}$  ions is about 0.9%.

The fluorescence titrations of the TEA-QDs with various metal ions were conducted to evaluate the selectivity. As can be seen in Fig. 4A, the influence of other metal ions was very weak, i.e., TEA-QDs were rather selective towards mercury ion in the presence of  $\text{I}^-$ . Similarly, those relevant anionic species at the same concentrations as  $\text{I}^-$  do not produce any noticeable effect on the emission signal of TEA-QDs in the presence of  $\text{Hg}^{2+}$  (Fig. 4B). It is obvious that the proposed method exhibits high selectivity which makes it very attractive for the selective recognition of  $\text{Hg}^{2+}$  and/or  $\text{I}^-$ , although the detection limits of the method was not the lowest compared to the other reported methods [24,25,42–47].

### 3.4. Quenching pattern

Lakowicz et al. [26] reported that iodide could quench the fluorescence of CdS nanoparticles. However, a high concentration of the anion (0.2 M) was needed for the detection of QD luminescence changes. Our results clearly show that the quenching effect of  $\text{Hg}^{2+}$  on TEA-QDs fluorescence was much greater than that of  $\text{I}^-$ . Actually, the fluorescence of TEA-QDs was quenched by 13% upon addition of  $40 \mu\text{M}$   $\text{Hg}^{2+}$  alone, whereas a negligible quenching of only 0.4% was observed for the same concentration of  $\text{I}^-$ . Thus, the quenching of QDs fluorescence is suggested to be mainly due to the interaction between CdSe QDs and mercury ions.

It was reported [14,16,20] that heavy metal ions can reduce the fluorescence of QDs by displacing the Cd ions on the surface of nanoparticles. We therefore completed the powder X-ray diffraction experiments for TEA-QDs and the result reveals that the

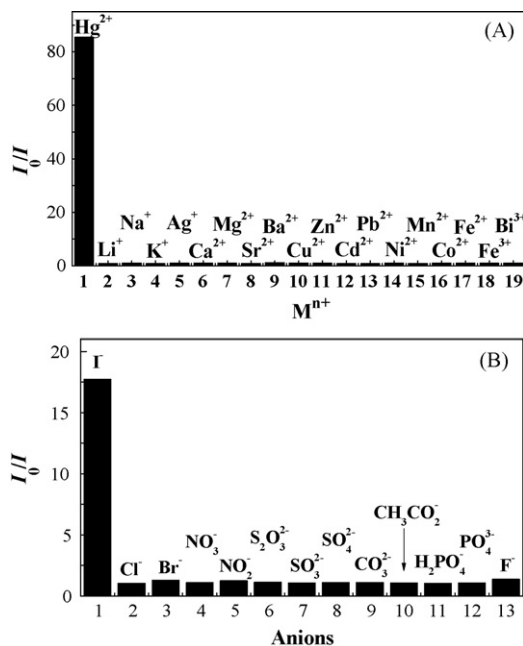


**Fig. 4.** Effect of different metal ions (A) and anions (B) on fluorescence of the TEA-QDs in HEPES buffer (pH 7.2). Conditions (A) [cations] =  $32 \times 10^{-6}$  M,  $[I^-] = 32 \times 10^{-6}$  mol L<sup>-1</sup> (B) [anions] =  $32 \times 10^{-6}$  M,  $[Hg^{2+}] = 32 \times 10^{-6}$  mol L<sup>-1</sup>.

diffraction patterns before and after addition of  $Hg^{2+}-I^-$  ion pair were identical. From the data we surely conclude that the added  $Hg^{2+}$  did not bind to Se on the surface of QDs to form  $HgSe$  particles, which is not similar to the case of  $HgS$  on  $CdS$  [37,38]. In addition, no spectral shift was noted in the absorption and emission spectra of the QDs upon addition of  $Hg^{2+}$ , further supporting that the metal ion displacement did not happen in our system.

In combination with the fluorescence decay time experimental results described above, we suggest that the fluorescence quenching in our case could be attributed to mercury ion binding with the surface-capping molecules of QDs, followed by an electron transfer process. The electron transfer from surface traps of QDs to  $Hg$  (II) facilitated nonradiative  $e^-/h^+$  recombination annihilation on the surface of QDs and resulted in the fluorescence quenching of QDs [24]. However, a sequent question is how the cation  $Hg^{2+}$  interacts with positively charged QDs.

The results above show that significant fluorescence quenching of TEA-QDs was observed only in the presence of both  $Hg^{2+}$  and

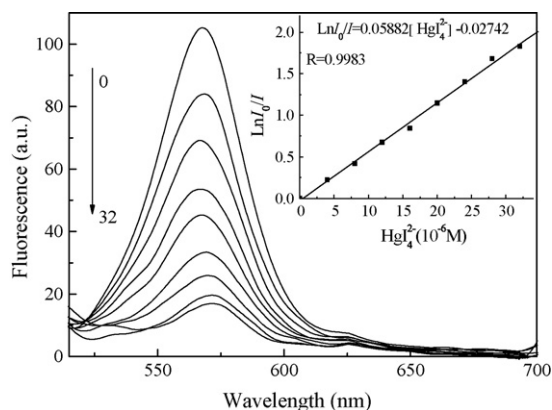
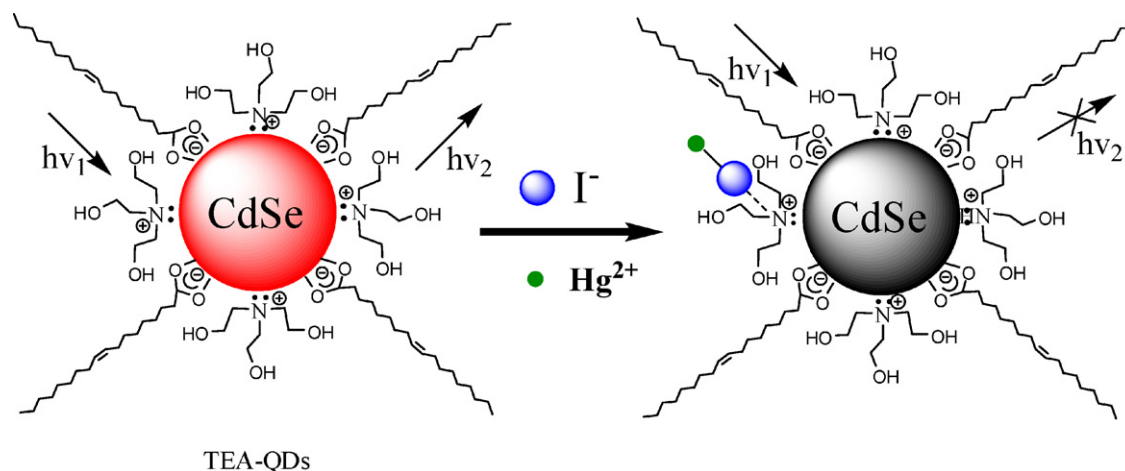


**Fig. 5.** Effect of  $HgI_4^{2-}$  concentration on fluorescence of the TEA-QDs in HEPES buffer (pH 7.2).  $\lambda_{ex} = 480$  nm. Inset: the modified Stern–Volmer plot.

$I^-$ . Apparently,  $I^-$  played a critical role in the selective response of TEA-QDs toward  $Hg^{2+}$ . It is well known that iodide and  $Hg^{2+}$  can form the soluble complex  $HgI_4^{2-}$  with a high stability constant of 29.79 [39]. Besides, iodine anions ( $I^-$ ) could interact with the positively charged nitrogen atom of TEA on the surface of TEA-QDs. It is thus reasonable to deduce that iodine anions could be a juncture that binds  $Hg^{2+}$  to the TEA-QDs, i.e.,  $I^-$  could bridge between  $Hg^{2+}$  and TEA-QDs to form a stable complex, most possibly in the form of QDs- $I^-$ - $Hg^{2+}$  structure as shown in Scheme 1. To confirm this hypothesis, we next examined the effect of the complex  $HgI_4^{2-}$  on the emission of TEA-QDs. As shown in Fig. 5, significant fluorescence quenching was also observed upon addition of  $HgI_4^{2-}$ . Moreover, the quenching process equally followed the modified Stern–Volmer model (Fig. 5 inset). These results suggested that the fluorescence quenching of TEA-QDs by  $Hg^{2+}-I^-$  ion pair was not induced by the direct binding of  $Hg^{2+}$  with the TEA-QDs surface, further supporting the proposed binding mode.

For many of the sensing systems based on the QDs, the concentration dependence of adduct-induced luminescence changes can be well fit by the Langmuir adsorption isotherm model, from which the binding constants between the analytes and the QDs surface could be estimated [13,19,22]. In our case, the fluorescence quenching effect of  $Hg^{2+}$  was observed only in the presence of  $I^-$  and vice versa, which is not similar to the previous reports. The quenching effect of ion on TEA-QDs luminescence in the presence of assistant ions can be effectively described by a diffusion double layer-type binding model. According to this model, a mass action law for ions



**Scheme 1.** Schematic illustration of the interactions between TEA-capped CdSe QDs and ion pair of  $Hg^{2+}I^-$ .

**Table 1**  
The factors of the diffusion double layer-type binding isotherm.

	$1 - \alpha$	$\ln K_{\text{Ions}}$	Measuring condition
A	2.40	12.03	Changing $[\text{Hg}^{2+}]$ at a fixed concentration of $40 \mu\text{M}$ $[\text{I}^-]$
B	2.45	11.43	Changing $[\text{I}^-]$ at a fixed concentration of $40 \mu\text{M}$ $[\text{Hg}^{2+}]$
C	1.49	11.34	Changing $[\text{HgI}_4^{2-}]$

adsorption is described by the following equation [40]:

$$\text{QDs} + \text{Ions} \leftrightarrow \text{QDs} - \text{Ions}, \quad K_{\text{Ions}} = \Theta_{\text{Ions}} \exp \frac{\{e\psi_0/kT\}}{a_{\text{Ions}}(1 - \Theta_{\text{Ions}})} \quad (1)$$

where  $K_{\text{Ions}}$  is the equilibrium constant,  $a_{\text{Ions}}$  is the activity of the ion in the bulk phase,  $\Theta_{\text{Ions}}$  is a measure of the concentration of free surface sites to which the ion can bind,  $1 - \Theta_{\text{Ions}}$  is a measure of the concentration of surface sites to which ions is bound,  $\psi_0$  is the electrostatic potential at the surface, the concentration of ions at the point where electrical potential is  $\psi_0$  is given by Boltzmann distribution  $a_{\text{surface}} = a_{\text{Ions}} \exp\{-e\psi_0/kT\}$  and  $e$ ,  $k$ , and  $T$  have their usual meaning [41].

Assume that the surface potential of QDs can be approximated by a quasi-Nernst equation:

$$\psi_0 = \frac{\alpha kT}{e} \ln(K_{\text{Ions}} a_{\text{Ions}}) \quad (2)$$

where  $\alpha$  is a parameter [41]. The Nernstian approach is based on the linear relationship between the surface potential and the ions activity, independent of the ionic strength. However, there was a discrepancy in the true values and the values of surface potentials, calculated by using the surface complexation model. This discrepancy is considered by the coefficient  $\alpha$  in Eq. (2).

Combining Eqs. (2) and (1) gives

$$\Theta_{\text{Ions}} = \frac{(K_{\text{Ions}} a_{\text{Ions}})^{(1-\alpha)}}{1 + (K_{\text{Ions}} a_{\text{Ions}})^{(1-\alpha)}} \quad (3)$$

The equation is analogous to the Langmuir isotherm used to analyze the adsorption behavior of uncharged species. Eq. (3) shows clearly that the function  $\Theta_{\text{Ions}}$  depends on  $(1 - \alpha)$  and  $\ln K$ , namely the electrostatic interaction and the equilibrium constant.

The fraction of occupied binding sites,  $\Theta_{\text{Ions}}$ , can be determined by Eq. (4):

$$\Theta_{\text{Ions}} = \frac{I_0 - I}{I_0} \quad (4)$$

where  $I_0$  is the maximum fluorescence intensity and  $I$  is the fluorescence intensity obtained at a given ion concentration. Substitution of Eq. (4) into Eq. (3) gives

$$\frac{I_0 - I}{I_0} = \frac{(K_{\text{Ions}} a_{\text{Ions}})^{(1-\alpha)}}{1 + (K_{\text{Ions}} a_{\text{Ions}})^{(1-\alpha)}} \quad (5)$$

Eq. (5) can be rewritten as the following linear equation:

$$\ln[(I_0 - I) - 1] = (1 - \alpha) \ln K_{\text{Ions}} + (1 - \alpha) \ln a_{\text{Ions}} \quad (6)$$

At very low ionic strength, the activity of ions in Eq. (6) can be replaced by the ion concentration  $C$  and thus Eq. (7) can be obtained.

$$\ln[(I_0/I) - 1] = (1 - \alpha) \ln K_{\text{Ions}} + (1 - \alpha) \ln C \quad (7)$$

Accordingly, if the diffusion double layer-type description of the binding of ions on the surface of the TEA-CdSe-QDs is correct, a plot of  $\ln[(I_0/I) - 1]$  as a function of  $\ln C$  should be linear. As shown in Fig. 6, the plots show a high linearity throughout the entire range of ions investigated. The correlation coefficients of the linear fits are higher than 0.990. Table 1 compares the diffusion double layer-type quenching factors  $(1 - \alpha)$  and  $\ln K$  of the TEA-QDs in the binding of various ions. It is clear that larger  $K$  values were obtained when the QDs solution was titrated with  $\text{Hg}^{2+}$  in the presence of  $\text{I}^-$  or vice

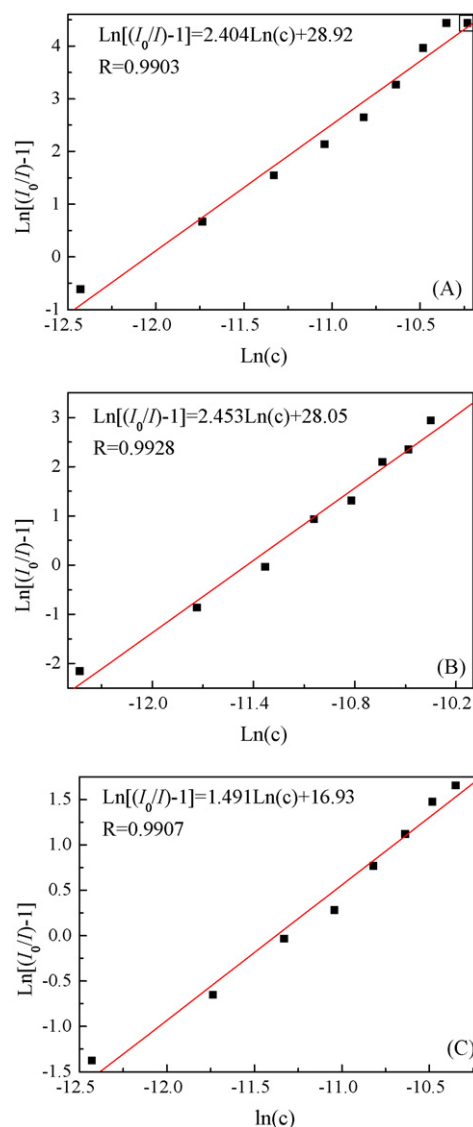


**Fig. 6.** The diffusion double layer-type binding isotherm description of the data. (A) effect of changing  $[\text{Hg}^{2+}]$  on  $\ln[(I_0/I) - 1]$  under fixed  $\text{I}^-$  concentration:  $40 \mu\text{M}$ . (B) effect of changing  $[\text{I}^-]$  on  $\ln[(I_0/I) - 1]$  under Fixed  $\text{Hg}^{2+}$  concentrations,  $40 \mu\text{M}$ . (C) Effect of changing  $[\text{HgI}_4^{2-}]$  on  $\ln[(I_0/I) - 1]$ .

versa. By comparison, a smaller value of  $K$  was obtained from  $\text{HgI}_4^{2-}$  titration data. This difference is probably due to the relative large size of  $\text{HgI}_4^{2-}$  which may hinder its adsorption onto the surface of QDs and decrease its electrostatic interaction with QDs.

Furthermore, the fluorescence titration results revealed that  $\text{Hg}^{2+}$  and  $\text{I}^-$  in a 1:1 ratio resulted in maximum fluorescence quenching, indicating that each  $\text{I}^-$  on the surface of TEA-QDs binds one  $\text{Hg}^{2+}$  ions. All these findings support our idea that iodine ( $\text{I}^-$ ) anions could bridge between TEA-QDs and  $\text{Hg}^{2+}$  to form a stable complex  $\text{QDs-I}^- - \text{Hg}^{2+}$ .

Based on the proposed binding model, the fluorescence response of TEA-QDs toward  $\text{Hg}^{2+} - \text{I}^-$  ion pair could be significantly influenced by pH because  $\text{H}^+$  could compete with  $\text{Hg}^{2+}$  to bind with  $\text{I}^-$  at lower pH while  $\text{OH}^-$  could partially replace  $\text{I}^-$  bound on the surface of QDs at higher pH. The fluorescence quenching experiment was performed at different pH values and the result is shown in Fig. 7. As expected, the degree of quenching is relatively much higher in neutral medium. This provides further support for the proposed binding model. It should be mentioned that the possibility of multicenter interaction between mercury ions and QDs still exists and

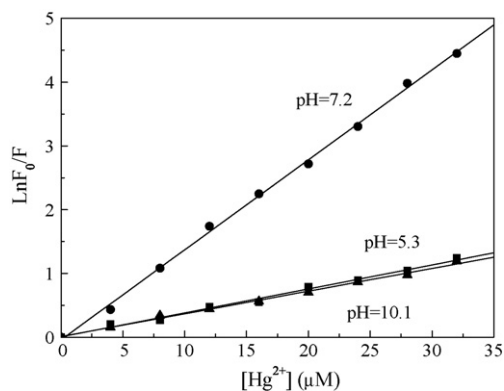


**Fig. 7.** The modified Stern–Volmer plots for the fluorescence quenching by  $\text{Hg}^{2+}$  ions in HEPES buffer solutions: (■) pH 5.3, (▲) pH 7.2, and (●) pH 10.1,  $[\text{I}^-] = 40 \mu\text{M}$ .

therefore additional research is still needed to determine the real binding model and the exact mechanism of quenching.

#### 4. Conclusions

We have successfully developed the novel water-soluble QDs modified with TEA. Based on the quenching of fluorescence signals of the functionalized CdSe QDs, a simple and specific method for the reciprocal recognition of mercury (II) ions and/or iodine (I) anions was proposed with wide linear range, low detection limits and good precision. Meanwhile, the results inspires that QDs system can be design as specific sensors for not only various ions but also ionic pairs if functionalized with appropriate ligands as that general organic receptors acted [48].

#### Acknowledgments

We thank the National Natural Science Foundation of China (No. 20475035), Natural Science Foundation of Shanxi Province (No. 2008011015-1) and the Undergraduate Foundation of Taiyuan City.

#### References

- [1] W.C.W. Chan, D.J. Maxwell, X.H. Gao, R.E. Bailey, M.Y. Han, S.M. Nie, *Curr. Opin. Biotechnol.* 13 (2002) 40.
- [2] M. Bruchez Jr., M. Moronne, P. Gin, S. Weiss, A.P. Alivisatos, *Science* 281 (1998) 2013.
- [3] W.C.W. Chan, S.M. Nie, *Science* 281 (1998) 2016.

- [4] F. Seker, K. Meeker, T.F. Kuech, A.B. Ellis, *Chem. Rev.* 100 (2000) 2505.
- [5] F.M. Raymo, I. Yildiz, *Phys. Chem. Chem. Phys.* 9 (2007) 2036.
- [6] J.M. Costa-Fernández, R. Pereiro, A. Sanz-Medel, *Trends Anal. Chem.* 25 (3) (2006) 207.
- [7] V. Maurel, M. Laferrrière, P. Billone, R. Godin, J.C. Scaiano, *J. Phys. Chem. B* 110 (2006) 16353.
- [8] J. Liang, S. Huang, D. Zeng, Z. He, X. Ji, X. Ai, H. Yang, *Talanta* 69 (2006) 126.
- [9] C.P. Huang, Y.K. Li, T.M. Chen, *Biosens. Bioelectron.* 22 (2007) 1835.
- [10] M. Tomasulo, I. Yildiz, F.M. Raymo, *J. Phys. Chem. B* 110 (2006) 3853.
- [11] J. Li, D. Bao, X. Hong, D. Li, J. Li, Y. Bai, T. Li, *Colloids Surf. A: Physicochem. Eng. Aspects* 257–258 (2005) 267.
- [12] C. Chen, C. Cheng, C. Lai, P. Wu, K. Wu, P. Chou, Y. Chou, H. Chiu, *Chem. Commun.* 3 (2006) 263.
- [13] Y. Chen, Z. Rosenzweig, *Anal. Chem.* 74 (2002) 5132.
- [14] H. Xie, J. Liang, Z. Zhang, Y. Liu, Z. He, D. Pang, *Spectrochim. Acta A* 60 (2004) 2527.
- [15] M.T. Fernandez-Argueelles, W.J. Jin, J.M. Costa-Fernández, R. Pereiro, A. Sanz-Medel, *Anal. Chim. Acta* 549 (2005) 20.
- [16] Y. Zhang, H. Zhang, X. Guo, H. Wang, *Microchem. J.* 89 (2008) 142.
- [17] B. Tang, J. Niu, C. Yu, L. Zhuo, J. Ge, *Chem. Commun.* 33 (2005) 4184.
- [18] K.M. Gatas-Asfura, R.M. Leblanc, *Chem. Commun.* 21 (2003) 2684.
- [19] J. Chen, C. Zhu, *Anal. Chim. Acta* 546 (2005) 147.
- [20] J. Liang, X. Ai, Z. He, D. Pang, *Analyst* 129 (2004) 619.
- [21] Y. Xia, C. Cao, C. Zhu, *J. Lumin.* 128 (2008) 166.
- [22] H. Li, Y. Zhang, X. Wang, *Sens. Actuat. B* 127 (2007) 593.
- [23] E.M. Ali, Y. Zheng, H. Yu, J.Y. Ying, *Anal. Chem.* 79 (2007) 9452.
- [24] J. Chen, Y. Gao, Z. Xu, G. Wu, Y. Chen, C. Zhu, *Anal. Chim. Acta* 577 (2006) 77.
- [25] H. Li, Y. Zhang, X. Wang, D. Xiong, Y. Bai, *Mater. Lett.* 61 (2007) 1474.
- [26] J.R. Lakowicz, I. Gryczynski, Z. Gryczynski, C.J. Murphy, *J. Phys. Chem. B* 103 (1999) 7613.
- [27] W.J. Jin, M.T. Fernandez-Argueelles, J.M. Costa-Fernández, R. Pereiro, A. Sanz-Medel, *Chem. Commun.* 7 (2005) 883.
- [28] W.J. Jin, J.M. Costa-Fernández, R. Pereiro, A. Sanz-Medel, *Anal. Chim. Acta* 522 (2004) 1.
- [29] A.Y. Nazzal, L. Qu, X. Peng, M. Xiao, *Nano Lett.* 3 (2003) 819.
- [30] X. Ji, J. Zheng, J. Xu, V.K. Rastogi, T. Cheng, J.J. DeFrank, R.M. Leblanc, *J. Phys. Chem. B* 109 (2005) 3793.
- [31] S.N. Sharma, Z.S. Pillai, P.V. Kamat, *J. Phys. Chem. B* 107 (2003) 10088.
- [32] T. Dannhauser, M. O'Neil, K. Johansson, D. Whitten, G. McLendon, *J. Phys. Chem.* 90 (1986) 6074.
- [33] Z.A. Peng, X. Peng, *J. Am. Chem. Soc.* 123 (2001) 183.
- [34] Y. Wang, J.F. Wong, X. Teng, X.Z. Lin, H. Yang, *Nano Lett.* 3 (2003) 1555.
- [35] J. Feng, S. Ding, M.P. Tucker, M.E. Himmela, Y. Kim, S.B. Zhang, B.M. Keyes, G. Rumbles, *Appl. Phys. Lett.* 86 (2005) 033108-1.
- [36] R.J. Hurtubise, A.H. Ackerman, B.W. Smith, *Appl. Spectrosc.* 55 (2001) 490.
- [37] A. Hasselbarth, A. Eychmuller, R. Eichberger, M. Giersig, A. Mews, H. Weller, *J. Phys. Chem.* 97 (1993) 5333.
- [38] A. Eychmuller, A. Hasselbarth, H. Weller, *J. Lumin.* 53 (1992) 113.
- [39] S.A. Wasay, P. Arnfalk, S. Tokunaga, *J. Hazard. Mater.* 44 (1995) 93.
- [40] J. Ståhlberg, *J. Chromatogr. A* 855 (1999) 3.
- [41] W. Piasecki, *Langmuir* 22 (2006) 6761.
- [42] M.S. Iandor, F. Geistmann, M. Schuster, *Anal. Chim. Acta* 388 (1999) 19.
- [43] A.G. Lista, M.E. Palomeque, B.S. Fernández Band, *Talanta* 50 (1999) 881.
- [44] B. Juskowiak, *Anal. Chim. Acta* 320 (1996) 115.
- [45] M.S. Hosseini, M.H. Hashemi, *Anal. Sci.* 20 (2004) 1449.
- [46] Z.X. Cai, H. Yang, Y. Zhang, X.P. Yan, *Anal. Chim. Acta* 559 (2006) 234.
- [47] C.Q. Zhu, L. Li, F. Fang, J.L. Chen, Y.Q. Wu, *Chem. Lett.* 34 (2005) 898.
- [48] H. Miyaji, D.S. Kim, B.Y. Chang, E. Park, S.M. Park, K.H. Ahn, *Chem. Commun.* 27 (2008) 753.



## Remote optical fibre microsensor for monitoring BTEX in confined industrial atmospheres

Lurdes I.B. Silva<sup>a,b,\*</sup>, Teresa A.P. Rocha-Santos<sup>b</sup>, A.C. Duarte<sup>a</sup>

<sup>a</sup> CESAM & Department of Chemistry, University of Aveiro, 3810-193 Aveiro, Portugal

<sup>b</sup> ISEIT/Viseu - Instituto Piaget, Estrada do Alto do Gaio, Galifonge, 3515-776 Lordosa, Viseu, Portugal

### ARTICLE INFO

#### Article history:

Received 28 May 2008

Received in revised form

26 November 2008

Accepted 2 December 2008

Available online 11 December 2008

#### Keywords:

BTEX detection

Optical fibre sensing

Confined atmospheres monitoring

Real-time analysis

### ABSTRACT

A portable optical fibre sensor has been developed for remote monitoring of benzene, toluene, ethylbenzene, p-xylene, m-xylene and o-xylene (BTEX). Firstly, the analyser was tested for calibration and its analytical performance for BTEX monitoring compared with a more classical analytical method, namely gas chromatography coupled to a flame ionization detector (GC-FID). The developed remote sensor shows several analytical advantages such as, high analytical sensitivity and accuracy, good linearity and stability of the analytical signal and short analytical time. Secondly, the optical fibre based sensor was applied to air monitoring for detection and quantification of BTEX in a confined industrial environment. The analytical signal measurement was performed by wireless at 20 m of distance from the local of analysis. Besides, the reported sensor showed a high degree of portability, compact design and high analytical performance for remote BTEX monitoring, *in situ* and in real-time.

© 2008 Elsevier B.V. All rights reserved.

### 1. Introduction

Volatile organic compounds (VOCs) are an important class of indoor air pollutants and even at a trace amounts, these compounds have a high potential hazard to human health due to their carcinogenic nature. In industrial environments, VOCs namely benzene, toluene, ethylbenzene, p-xylene, m-xylene and o-xylene (BTEX) could arise not only from industrial activities but also from outdoor sources (such as vehicle pollution) and from building materials (such as cleaning products, paints and adhesives/sealants). The level of exposure to VOCs in an industrial environment is substantially higher than in non-industrial environments. Human exposure to VOCs is a function of both time and concentration and symptoms of overexposure include fatigue, headache, nausea, dizziness, skin and eye irritation and central nervous system damage. The workplaces with low air quality could negatively affect worker's efficiency and productivity. Therefore, obtaining reliable monitoring data, *in situ* and in real-time, of VOCs in indoor industrial atmospheres to prevent exceeding safety levels and assuring an acceptable air quality becomes an important aim both in environmental sciences and in sensors technology.

Fibre optical sensors show very appropriate analytical characteristics and attractive advantages, especially when compared to the more classical analytical methods and chemical sensors, for pollutants monitoring. They show no electromagnetic interferences, high durability, small size, low maintenance cost, short analytical time and simple design [1]. Furthermore, optical fibre sensors provide the possibility for fast, accurate and safe detection of toxic compounds besides showing high potential for remote measurements in inaccessible and harsh environments, in a continuous mode operation. Many research groups [2–5] focused their attention on optical fibre sensors as a tool for monitoring the concentration of VOCs. Although some miniaturized devices have been reported for VOCs detection, such as for example, a microfluidic device mesoporous silicate adsorbent [6], they have not shown yet an adequate analytical selectivity or sensitivity.

This work aims at the development of a new and portable design for an optical fibre sensor for remote monitoring of BTEX in confined environments with both high selectivity and sensitivity besides a capability for transmission of data by wireless.

### 2. Experimental

#### 2.1. Optical fibre preparation

The sensor head consists on a monomode optical fibre (OF) pigtail coated with a nanometric fluorosiloxane polymer film. An optical coupler (OC) 50:50 was utilized with OF core and cladding diameters of 9/125  $\mu\text{m}$ , respectively. The OF was mechanically

\* Corresponding author at: ISEIT/Viseu - Instituto Piaget, Estrada do Alto do Gaio, Galifonge, 3515-776 Lordosa, Viseu, Portugal. Tel.: +351 232 910 100; fax: +351 232 910 183.

E-mail address: [lisilva@ua.pt](mailto:lisilva@ua.pt) (L.I.B. Silva).

uncladded and cleaved on a length of 20 mm with a Cleaver V6 (from Future Instrument) precision fibre cleaver. The sensitive film of poly[methyl(3,3,3-trifluoropropyl)siloxane] (PMTFPS) was deposited on the cleaved OF end by spray technique, using a coating solution of PMTFPS at 0.01% in dichloromethane. Finally the sensitized optical fibre section was cured at 70 °C overnight and then introduced through a Teflon plug inside the 7.2 cm long analytical tube (AT). The film thickness was estimated as 2 nm by Rutherford backscattering spectrometry (RBS).

## 2.2. Preparation of calibrants for BTEX determination

Aromatic volatiles standard mix solution of benzene, toluene, ethylbenzene, p-xylene, m-xylene and o-xylene, 100 µg/mL of each compound in methanol, was prepared from analytical grade reagents obtained from Supelco (Cat no. 47504).

## 2.3. Analytical details and experimental apparatus for calibration process

Fig. 1 shows the analytical apparatus and experimental lay out used for the calibration of the OF sensor. A standard mixture of BTEX was injected with a gastight micro-syringe (Hamilton) at the top of a glass cell (injection cell: IC). The temperature at the injection cell was controlled by a coiled tape heater (TH1) from Cole Parmer and kept at 150 °C. The aromatic compounds were injected as liquids, and after vapourization the aromatic vapours were carried by a continuous stream (25 mL min<sup>-1</sup>) of reagent grade air (Linde Minican, Linde Sogás), controlled with a flowmeter (R), from Sigma, to the glass tube (GT). The GT containing a fused silica fibre coated with a film of polydimethylsiloxane (PDMS) was surrounded by a second tape heater (TH2) and constitutes the adsorption/desorption system component. Three way valves (valve 1: V1 and valve 2: V2) were used to connect the three main components of the analytical system: injection/sampling, adsorption/desorption and detection. At the adsorption step the V1 is open for allowing the flow in the IC–GT direction, while V2 is closed for the GT–AT flow but open for air outflow; in this way during the adsorption phase a constant flow of air is introduced through the adsorption component but no air flows into the detection component.

The analyte molecules are thermally desorbed by increasing the temperature of the tape heater (TH2), which surrounds the glass tube, by means of a temperature program controlled by a software home-made. The tape heater starts at 25 °C with a program rate of 30 °C min<sup>-1</sup> until 75 °C and 10 °C min<sup>-1</sup> until 150 °C. At this desorption phase the V2 is open on GT–AT direction, allowing the flow of analyte to the detection component of the analytical device. The exposure of the fluorosiloxane polymer film to BTEX vapours inside the analytical tube leads to changes on the reflected light power,

which is measured with a photodiode as the analytical signal. The light source used was a laser diode (1 mW, λ = 1550 nm) set at CW (continuous waveform) regarding the operational mode frequency. The choice of a working wavelength of 1550 nm was based on a previous observed increase in the analytical signal when increasing the wavelength from 1310 nm to 1550 nm [8]. The laser and the photodetector were integrated in an electronic device home-made and data acquisition was performed by a computer with software also home-made.

## 2.4. Analytical methodology, including experimental apparatus for sampling at confined atmospheres

Sampling took place at a confined environment in a Portuguese solvent industry and the details of the analytical apparatus are shown in Fig. 2. The air sample is continuously vacuum pumped (VP) from the industrial atmosphere at a flow rate of 0.2 L min<sup>-1</sup> (during 25 min) controlled by a mass flowmeter (FM). A second flowmeter (R) was connected to the analytical tube in order to detect any gas leak. The aromatic compounds (sampling from the confined environment) are adsorbed onto the PDMS fibre placed inside the GT during the adsorption step.

The experimental lay out used for *in situ* BTEX monitoring was similar to the one used for the calibration, except for the injection system, which is absent in this analytical system, and for a new component which includes a vacuum pump for air sampling. During the gas sampling step, the valve V1 is open for allowing the air sample to contact the PDMS fibre enclosed in the glass tube, before exiting through V2 which is in position open for air outflow and closed for GT–AT flow.

During the desorption step, the analytes are thermal adsorbed by increasing the TH2 temperature, using the same temperature programme as for the sensor calibration. At this stage the position of valves V1 and V2 are changed: V1 is closed for air sampling and open to a flow of air (A) pure, while V2 is open in the direction of GT–AT flow; these changes in the position of the three way valves allow the desorption of the analytes from the PDMS fibre and the flow of the analytes into the OF detection system. The analytical tube was maintained at room temperature during both sampling and calibration processes. The light power guided through the OF is reflected when the analyte molecules are present at the fibre/fluorosiloxane film interface, thus causing a change in its refractive index leading to variations of the reflected optical power, which is monitored by a laptop with home-made software.

The sensor system elements excluding the air container, flowmeter, vacuum pump and laptop were appropriately located in a home-made box (height: 12.0 cm, width: 20.3 cm and length: 29.1 cm), providing the system with a very compact and portable design.

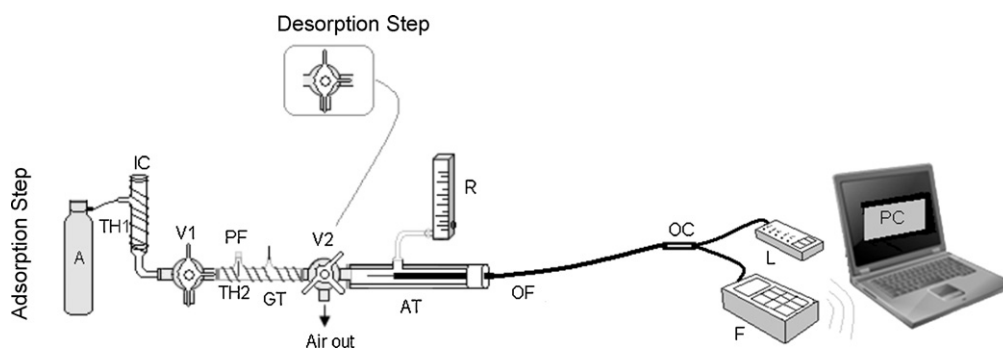
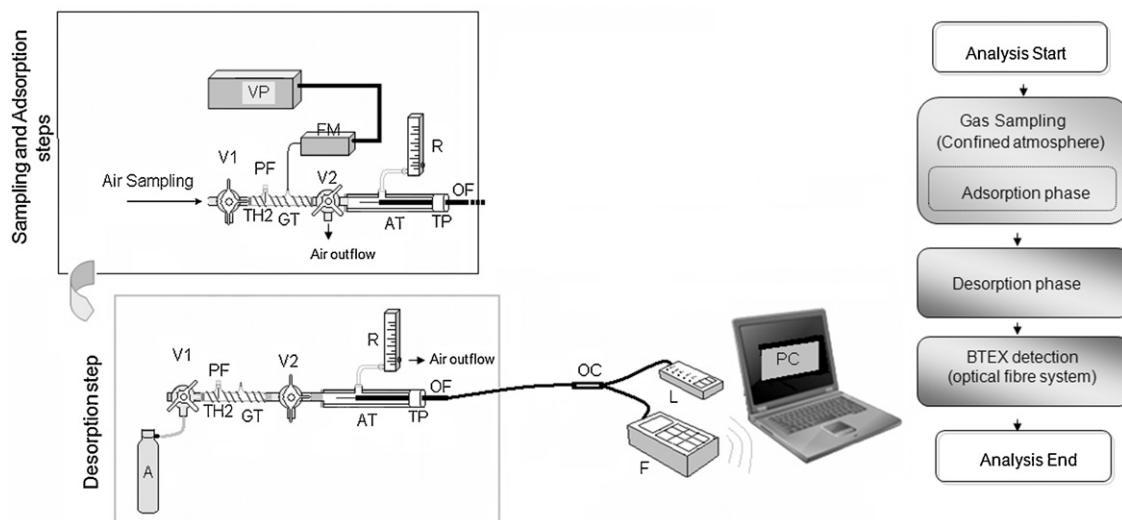


Fig. 1. Experimental apparatus used for the calibration (A: air, IC: injection cell, V1 and V2: three way valves, TH1 and TH2: tape heater, PF: PDMS fibre, GT: glass tube, AT: analytical tube, R: flowmeter, OF: optical fibre, OC: optical coupler, L: laser, F: photodetector, PC: laptop with home-made software).



**Fig. 2.** Schematic view of the analytical apparatus used for *in situ* BTEX monitoring at a confined environment (V1 and V2: three way valves, TH2: tape heater 2, PF: PDMS fibre, GT: glass tube, VP: vacuum pump, FM: mass flowmeter, AT: analytical tube, R: flowmeter, OF: optical fibre, OC: optical coupler, L: laser, F: photodetector, A: air, TP: Teflon plug, PC: laptop with home-made software).

The measurements of the analytical signals were performed by wireless at a distance of 20 m away from the confined area where sampling took place.

Additionally, air samples were also collected at the confined industrial environment for the GC-FID analysis according to the NIOSH method 1501 [7], in order to compare the analytical performance of the developed sensor to the classical analytical method concerning actual samples.

### 2.5. GC-FID methodology

The GC-FID methodology recommended in Method 1501 by NIOSH was implemented in a Gow-Mac Series 600 with a capillary column (fused silica-Supelcowax, 30 m × 0.32 mm ID × 1.0 μm, 100% PEG, Cat no. 24211, Supelco, Spain). The column temperature starts at 40 °C (10 min) and rises up to 230 °C with a program rate of 10 °C min<sup>-1</sup>. The temperature of the injector was kept at 250 °C during the analysis and the FID temperature was set at 300 °C; the carrier gas was helium at constant flow of 2.6 mL min<sup>-1</sup>.

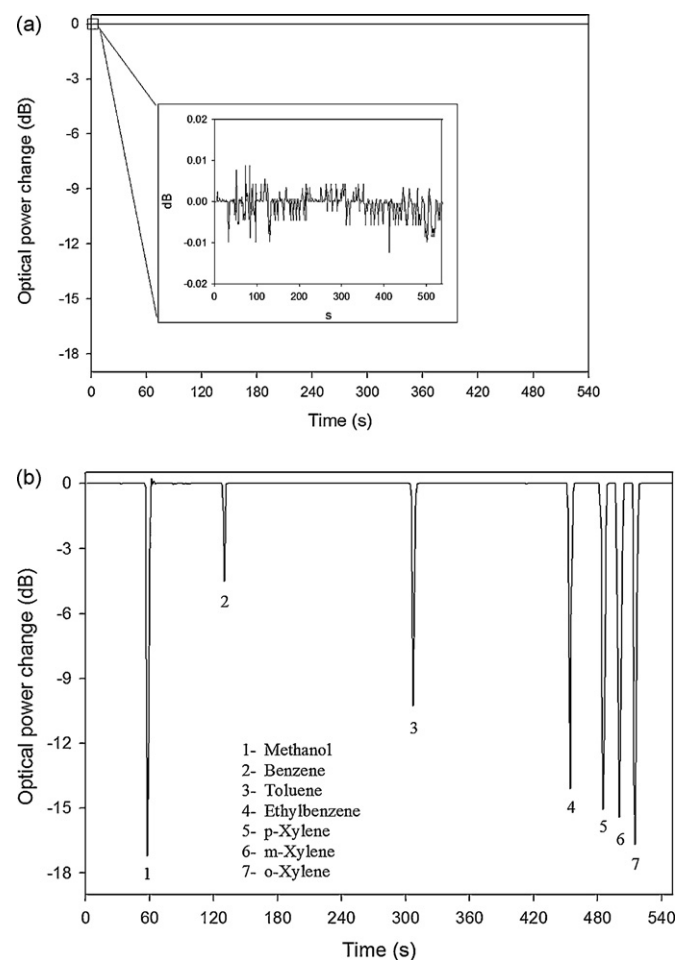
## 3. Results and discussion

Fig. 3a shows the baseline of the optical power signal monitored during 9 min, prior to the injection of BTEX and Fig. 3b shows the optical power decrease obtained with the OF sensor for a BTEX mixture containing 0.03 μg of each compound in methanol. The optical signal is very stable and no significant optical power changes were detected in the absence of aromatic hydrocarbons injections. In fact, the maximum signal variation when no injections of BTEX were performed was 0.012 dB, which represents 0.3% of the minimum value of the optical power variation (4.5 dB), observed for 0.03 μg of benzene. Changes up to 16 dB in the reflected optical power were detected during 0.03 μg of BTEX mixture analysis (Fig. 3b), indicating the suitability of the developed sensor for aromatic vapour detection.

The analytical response time for each aromatic hydrocarbon is very short, in the order of a few seconds and the total analytical time was found to be around 9 min for the 7 completely separated compounds detected as shown in Fig. 3b. The analytical signals measurements were performed at a distance of 20 m away from the sampling point which highlights the suitability of the developed analytical system for remote sensing at a very high safety level. Fur-

thermore, a distance of 60 m was found to be the maximum possible for collecting the analytical signal by wireless.

The regressions equations obtained were  $y = -15.8 + 679.0x$  ( $r^2 = 0.9993$ ;  $p < 7.82 \times 10^{-6}$ ) for benzene;  $y = -13.2 + 772.5x$



**Fig. 3.** Sensor response during BTEX analysis with the developed remote OF sensor ((a) baseline with inset showing the expansion of the baseline signal and (b) optical power decrease obtained for a BTEX mixture of 0.03 μg).

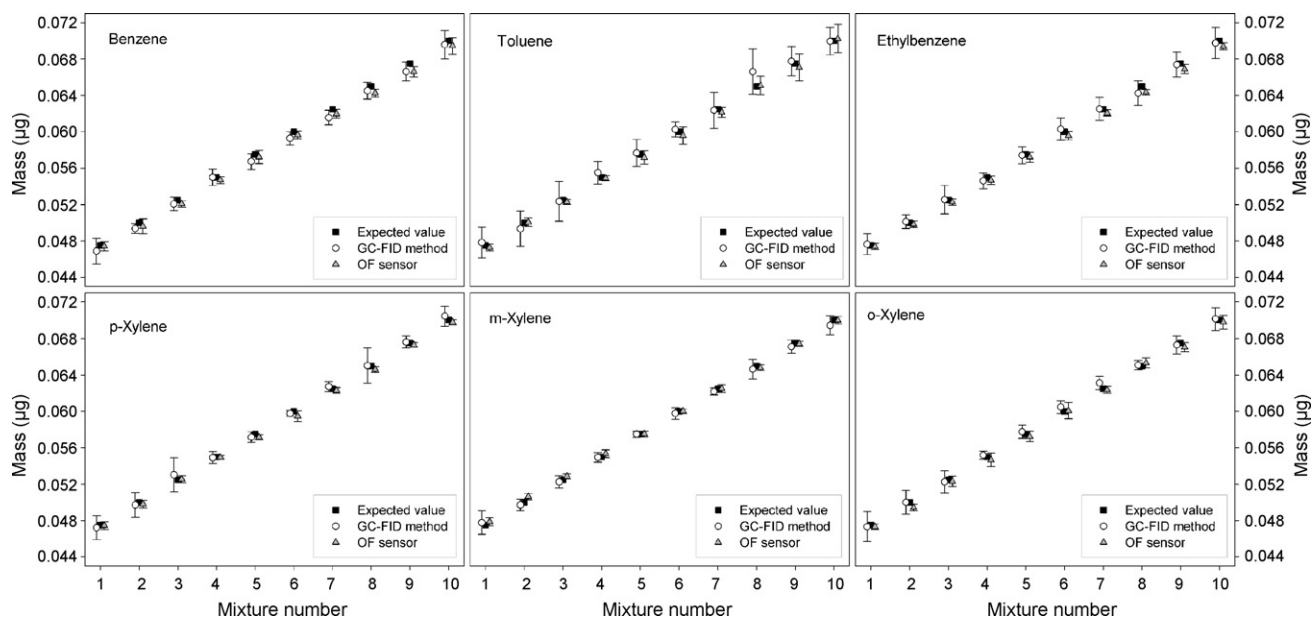


Fig. 4. Comparison of the BTEX determination (mean and standard deviation) obtained with the GC-FID method and the OF sensor.

( $r^2 = 0.9994$ ;  $p < 6.29 \times 10^{-6}$ ) for toluene;  $y = -11.2 + 831.3x$  ( $r^2 = 0.9997$ ;  $p < 2.23 \times 10^{-6}$ ) for ethylbenzene;  $y = -10.0 + 834.9x$  ( $r^2 = 0.9995$ ;  $p < 4.55 \times 10^{-6}$ ) for p-xylene;  $y = -9.8 + 842.5x$  ( $r^2 = 0.9997$ ;  $p < 2.14 \times 10^{-6}$ ) for m-xylene;  $y = -9.6 + 874.1x$  ( $r^2 = 0.9995$ ;  $p < 4.35 \times 10^{-6}$ ) for o-xylene.

The developed remote sensor shows different sensitivities (taken as the slope of the calibration curves) for the six aromatic hydrocarbons analysed, increasing in the following order: benzene < toluene < ethylbenzene < p-xylene < m-xylene < o-xylene. This increase follows the same order as the increase in terms of boiling temperature in °C (80.1 for benzene < 110.6 for toluene < 136.2 for ethylbenzene < 138.4 for p-xylene < 139.1 for m-xylene < 144.4 for o-xylene) and decrease of vapour pressure in mmHg at 25 °C (95.2 for benzene > 28.4 for toluene > 9.6 for ethylbenzene > 8.8 for p-xylene > 8.4 for m-xylene > 6.7 for o-xylene). This relationship between sensor sensitivity, boiling temperature and vapour pressures of the analytes has also been reported elsewhere [8,9] for the development of a non-remote optical fibre polymer based analysers for VOCs detection, at a laboratory scale.

The detection limits estimated for the six aromatic hydrocarbons analysed, based on 3 times the residual standard deviation [10] for

both GC-FID and OF sensor were, respectively, 1.6 and 1.4 ng for benzene, 1.5 and 1.3 ng for toluene, 1.2 and 1.0 ng for ethylbenzene, 1.3 and 1.2 ng for p-xylene, 1.7 and 0.9 ng for m-xylene and 2.0 and 1.2 ng for o-xylene. These values show that the detection limits for both methods were in the same order of magnitude.

In order to test and compare the performance of the OF sensor with the GC-FID methodology, ten different concentrations of a standard mixture of BTEX were determined with both the OF sensor and the GC-FID method. The expected values together with the results obtained by the GC-FID and the OF sensor are displayed in Fig. 4. The ANOVA of the results shows that there is no statistically significant difference ( $p = 0.568, 0.397, 0.058, 0.208, 0.056$  and  $0.235$  for benzene, toluene, ethylbenzene, p-xylene, m-xylene and o-xylene, respectively) for the effects of differences in the two methods. Although there is a statistical significance ( $p < 0.001$ ) for the effects of different levels of the expected value concentrations, the results obtained by the two methods do not depend ( $p = 0.931, 0.850, 0.994, 0.978, 0.918$  and  $0.939$ , for benzene, toluene, ethylbenzene, p-xylene, m-xylene and o-xylene, respectively) on what level the expected value concentration is present.

The analytical error, measured as the residual standard deviation of both methods, varied between  $6.5 \times 10^{-4}$  and  $1.3 \times 10^{-3}$  µg.

Table 1

Obtained results for five actual samples of air from a confined environment of a Portuguese solvent industry with both remote OF sensor and GC-FID method.

		Benzene ( $\mu\text{g L}^{-1}$ )	Toluene ( $\mu\text{g L}^{-1}$ )	Ethylbenzene ( $\mu\text{g L}^{-1}$ )	p-Xylene ( $\mu\text{g L}^{-1}$ )	m-Xylene ( $\mu\text{g L}^{-1}$ )	o-Xylene ( $\mu\text{g L}^{-1}$ )
Sample 1	OF sensor	$0.0075 \pm 0.0001$	$0.0085 \pm 0.0001$	$0.0035 \pm 0.0001$	$0.0029 \pm 0.0001$	$0.0046 \pm 0.0001$	$0.0038 \pm 0.0002$
	GC-FID	$0.0076 \pm 0.0005$	$0.0087 \pm 0.0005$	$0.0037 \pm 0.0002$	$0.0027 \pm 0.0001$	$0.0044 \pm 0.0002$	$0.0036 \pm 0.0002$
	Significant difference, $p$	0.59	0.47	0.23	0.14	0.07	0.15
Sample 2	OF sensor	$0.0075 \pm 0.0001$	$0.0086 \pm 0.0001$	$0.0031 \pm 0.0001$	$0.0028 \pm 0.0001$	$0.0046 \pm 0.0001$	$0.0037 \pm 0.0001$
	GC-FID	$0.0076 \pm 0.0003$	$0.0085 \pm 0.0005$	$0.0030 \pm 0.0002$	$0.0027 \pm 0.0002$	$0.0045 \pm 0.0002$	$0.0036 \pm 0.0002$
	Significant difference, $p$	0.52	0.57	0.19	0.96	0.52	0.38
Sample 3	OF sensor	$0.0073 \pm 0.0001$	$0.0083 \pm 0.0002$	$0.0035 \pm 0.0002$	$0.0029 \pm 0.0001$	$0.0045 \pm 0.0001$	$0.0037 \pm 0.0001$
	GC-FID	$0.0075 \pm 0.0004$	$0.0083 \pm 0.0004$	$0.0036 \pm 0.0002$	$0.0029 \pm 0.0002$	$0.0044 \pm 0.0002$	$0.0035 \pm 0.0002$
	Significant difference, $p$	0.39	0.77	0.38	0.87	0.28	0.11
Sample 4	OF sensor	$0.0074 \pm 0.0002$	$0.0084 \pm 0.0001$	$0.0033 \pm 0.0001$	$0.0028 \pm 0.0001$	$0.0045 \pm 0.0001$	$0.0038 \pm 0.0001$
	GC-FID	$0.0075 \pm 0.0005$	$0.0082 \pm 0.0003$	$0.0035 \pm 0.0002$	$0.0030 \pm 0.0002$	$0.0045 \pm 0.0003$	$0.0036 \pm 0.0002$
	Significant difference, $p$	0.67	0.13	0.12	0.06	0.06	0.10
Sample 5	OF sensor	$0.0074 \pm 0.0001$	$0.0085 \pm 0.0002$	$0.0034 \pm 0.0002$	$0.0027 \pm 0.0001$	$0.0047 \pm 0.0001$	$0.0038 \pm 0.0001$
	GC-FID	$0.0074 \pm 0.0004$	$0.0084 \pm 0.0004$	$0.0035 \pm 0.0002$	$0.0026 \pm 0.0002$	$0.0046 \pm 0.0002$	$0.0039 \pm 0.0002$
	Significant difference, $p$	0.81	0.51	0.10	0.44	0.30	0.28



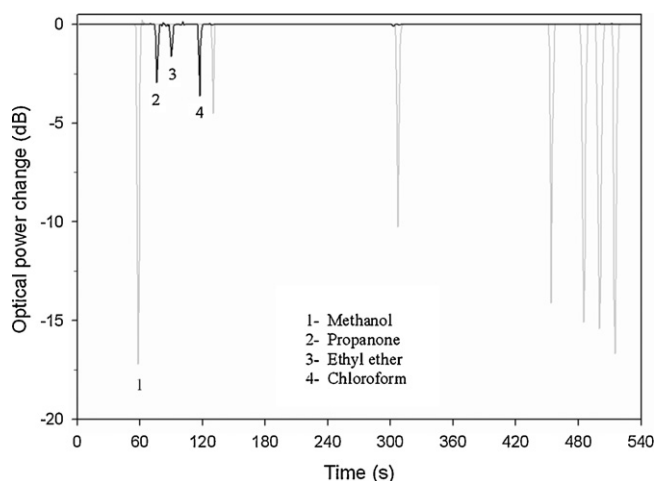


Fig. 5. Optical power decrease obtained for a mixture of 0.05  $\mu\text{g}$  of propanone, ethyl ether and chloroform regarding interferences study for remote OF sensor. The gray line represents the optical power decrease obtained during BTEX detection.

Although the analytical time achieved during BTEX detection with the remote OF sensor was 4 min lower than the one obtained with GC-FID (13 min), this was mainly due to the different instrumentation, namely different chromatographic components besides different temperatures program and flow rate.

After laboratorial calibration the developed sensor was also applied to air monitoring at a confined environment in a Portuguese solvent industry. The obtained results with both remote OF sensor and GC-FID method are displayed in Table 1 and they are around thousandth lower than the occupational exposure limits recommended for benzene ( $3.19 \text{ mg m}^{-3}$ ), toluene ( $3.77 \text{ mg m}^{-3}$ ), ethylbenzene ( $4.34 \text{ mg m}^{-3}$ ), p-xylene ( $4.34 \text{ mg m}^{-3}$ ), m-xylene ( $4.34 \text{ mg m}^{-3}$ ) and o-xylene ( $4.34 \text{ mg m}^{-3}$ ) by NIOSH [7].

In order to test the developed OF sensor for interferences that could be present in atmospheres of confined areas especially in industrial environments, the effect of propanone, ethyl ether and chloroform used as example of interferences compounds, on the analytical signal were also evaluated. In fact, each compound tested produces a peak, but in a different analytical time window of the compounds of interest as shown in Fig. 5 (black line). The obtained results allow to concluding that none of the above mentioned compounds exhibit any interference in the analytical signal and that the adjustment of the time window could be used for avoiding other potential interferences. As a consequence it is also possible to infer that the developed sensor could be also applied to monitoring of other class of VOCs.

#### 4. Conclusions

The developed OF sensor allows remote BTEX monitoring *in situ* with both high sensitivity and accuracy. The sensor system exhibit high analytical performance for BTEX detection, with high linearity of the analytical response and detection limits in the order of few nanograms. High portability, lower safety requirements and easiness of assemblage were also analytical features checked for this system.

One of the main advantages of the developed sensor system consists on the assessment of pollutants monitoring at a maximum distance of 60 m away from the sampling/analysis local. This sensor could be also advantageous for continuous measuring of BTEX compounds and used for setting warning and action limits in industrial environments besides general air control monitoring. Although this study is focused on BTEX monitoring at industrial confined atmospheres, the developed analytical system show a high potential for monitoring of organic vapours in any other environments and it could be also included in analytical networks for air quality assessment. The OF sensor compares more favourably with the GC-FID methodology, not only due to its lower total time of analysis and portability, but also regarding the lower cost of equipment.

#### Acknowledgments

This work has been developed under the scope of the FCT (Portugal) funded research project POCTI/CTA/44899/02: "Development of a new Optical Fiber Chemical Sensor for in-situ monitoring of VOCs (VOCSENSOR)" and a Ph.D. grant (SFRH/BD/17288/2004) awarded to Lurdes I.B. Silva is also gratefully acknowledged.

#### References

- [1] M. Campbell, *Sensor Systems for Environmental Monitoring*, vol. 1, Blackie Academic & Professional, London, 1997.
- [2] A. Abdelghani, N. Jaffrezic-Renault, *Sens. Actuators B* 74 (2001) 117–123.
- [3] F. Abdelmalek, J.M. Chevelon, M. Lacroix, N. Jaffrezic-Renault, V. Matejec, *Sens. Actuators B* 56 (1999) 234–242.
- [4] C. Bariáin, I. Matías, I. Romeo, J. Garrido, M. Laguna, *Sens. Actuators B* 76 (2001) 25–31.
- [5] C. Elosúa, C. Bariáin, I.R. Matías, F.J. Arregui, A. Luquin, M. Laguna, *Sens. Actuators B* 115 (2006) 444–449.
- [6] Y. Ueno, T. Horiuchi, O. Niwa, H.-S. Zhou, T. Yamada, I. Honma, *Sens. Actuators B* 95 (2003) 282–286.
- [7] *Hydrocarbons Aromatic: Method 1501*, NIOSH Manual of Analytical Methods (NMAM), 4th ed., DHHS (NIOSH) Publication, 2003.
- [8] L.I.B. Silva, T.A.P. Rocha-Santos, A.C. Duarte, *Sens. Actuators B* 132 (2008) 280–289.
- [9] L.I.B. Silva, T.A.P. Rocha-Santos, A.C. Duarte, *Talanta* 76 (2008) 395–399.
- [10] J.C. Miller, J.N. Miller, *Statistics for Analytical Chemistry*, 3th ed., Ellis Horwood and Prentice Hall, New York, 1993.



# Determination of $\text{Hg}^{2+}$ on poly(vinylferrocenium) ( $\text{PVF}^+$ )-modified platinum electrode

Mutlu Sönmez Çelebi, Haluk Özyörük, Attila Yıldız, Serdar Abacı\*

Hacettepe University, Faculty of Science, Department of Chemistry, 06532 Ankara, Turkey

## ARTICLE INFO

### Article history:

Received 16 April 2008

Received in revised form

16 November 2008

Accepted 20 November 2008

Available online 27 November 2008

### Keywords:

Mercury determination

$\text{PVF}^+$

Anodic stripping

Complexation

Interference

Aqueous solution

## ABSTRACT

A new surface based on poly(vinylferrocenium) ( $\text{PVF}^+$ )-modified platinum electrode was developed for determination of  $\text{Hg}^{2+}$  ions in aqueous solutions. The polymer was electrodeposited on platinum electrode by constant potential electrolysis as  $\text{PVF}^+\text{ClO}_4^-$ .  $\text{Cl}^-$  ions were then attached to the polymer matrix by anion exchange and the modified electrode was dipped into  $\text{Hg}^{2+}$  solution.  $\text{Hg}^{2+}$  was preconcentrated at the polymer matrix by adsorption and also complexation reaction with  $\text{Cl}^-$ . Detection of  $\text{Hg}^{2+}$  was carried out by differential pulse anodic stripping voltammetry (DPASV) after reduction of  $\text{Hg}^{2+}$ . Mercury ions as low as  $5 \times 10^{-10}$  M could be detected with the prepared electrode and the relative standard deviation was calculated as 6.35% at  $1 \times 10^{-6}$  M concentration ( $n=6$ ). Interferences of  $\text{Ag}^+$ ,  $\text{Pb}^{2+}$  and  $\text{Fe}^{3+}$  ions were also studied at two different concentration ratios with respect to  $\text{Hg}^{2+}$ . The developed electrode was applied to the determination of  $\text{Hg}^{2+}$  in water samples.

© 2008 Elsevier B.V. All rights reserved.

## 1. Introduction

Mercury is one of the most well known toxic metals. The growing awareness of environmental mercury pollution and toxicity makes the determination of very low concentrations very important. Mercury is one of the few metals which strongly bioconcentrates and biomagnifies, has only harmful effects with no useful physiological functions when present in living organisms and easily transformed from a less toxic inorganic form to a more toxic organic form especially in fish [1]. It is usually present at low concentrations in environmental samples therefore, preconcentration of the metal is usually necessary to carry out a successful determination.

Several methods can be used for mercury quantification such as cold vapor atomic absorption spectrometry (CV-AAS) [2], cold vapor atomic fluorescence spectrometry (CV-AFS) [3], inductively coupled plasma mass spectrometry (ICP-MS) [4] and, for relatively high concentrations, inductively coupled plasma atomic emission spectrometry (ICP-AES) [5]. All these techniques require expensive instrumentation and complicated sample preparation processes [6]. However, electrochemical methods are very good alternatives and provide easier and cheaper ways. Modification of the working electrode surfaces with an appropriate reagent offers analytical

methods with enhanced selectivity and sensitivity. Modification can be achieved by electrochemical, chemical or physical methods. Stripping electrochemical methods represent an interesting alternative for mercury determination owing to their sensitivity, versatility and low costs [7]. Ju and Leech accumulated mercury ions on a metallothionein-modified gold electrode at open circuit and determined trace  $\text{Hg}^{2+}$  by cathodic stripping differential pulse voltammetry [8]. Berchmans et al. preconcentrated  $\text{Hg}^{2+}$  chemically using 2-mercaptobenzimidazole-modified gold electrode and determined the mercury ions by stripping voltammetry after reduction of preconcentrated  $\text{Hg}^{2+}$  prior to determination by anodic stripping voltammetry [9]. Electrochemical preconcentration of mercury ions has been carried out by Ugo et al. at gold- and polymer-coated electrodes [10]. Preconcentration and voltammetric determination of mercury has also been studied using chemically modified carbon-paste electrodes [11,12], graphite electrodes [13,14], glassy carbon electrodes [15,16] and sol-gel electrodes [17,18].

Poly(vinylferrocene) (PVF), is a redox polymer, which has long been used as a fundamental conducting polymer system, with the advantages of simple electrochemistry (a reversible one-electron process), high stability (allowing multiple measurements to be made over extended time scale), and the ease of deposition of thin films using a variety of methods [19]. The polymer oxidizes from methylene chloride to give the less soluble ferrocenium form of the polymer, which precipitates onto the electrode surface to give a  $\text{PVF}^+$ -modified electrode.

\* Corresponding author. Tel.: +90 312 2976080; fax: +90 312 2992163.  
E-mail address: [sabaci@hacettepe.edu.tr](mailto:sabaci@hacettepe.edu.tr) (S. Abacı).

In the present study, the use of PVF<sup>+</sup>-modified Pt electrode for determination of Hg<sup>2+</sup> ions by differential pulse anodic stripping voltammetry was investigated in terms of the parameters that can affect the analytical response. Possible interferences and the repeatability of the method were determined.

## 2. Experimental

PVF was prepared by chemical polymerization of vinylferrocene (Alfa Product) at 70 °C for 24 h using 2,2'-azo-bis(2-methylpropionitrile) (AIBN) (Alfa Product) as the initiator [20]. Methylene chloride (Aldrich), which was used for preparing polymer solutions, was washed with concentrated H<sub>2</sub>SO<sub>4</sub> (Merck), triple distilled water, Na<sub>2</sub>CO<sub>3</sub> (Merck) (5%), and triple distilled water. Then it was distilled over P<sub>2</sub>O<sub>5</sub> (Merck) [21].

1 × 10<sup>-3</sup> M stock solution of Hg<sup>2+</sup> was prepared from HgCl<sub>2</sub> (BDH, Analar) using triple distilled water. NaCl solutions were prepared using triple distilled water with NaCl (Carlo Erba). Ag<sup>+</sup>, Fe<sup>3+</sup> and Pb<sup>2+</sup> solutions were prepared from AgNO<sub>3</sub> (BDH, 99.8% pure), FeNO<sub>3</sub> (Merck) and Pb(NO<sub>3</sub>)<sub>2</sub> (BDH, Analar) respectively.

Tetra-*n*-butyl ammonium perchlorate (TBAP) was used as the supporting electrolyte in the polymer solution. TBAP was obtained by the reaction of tetra-*n*-butyl ammonium hydroxide (40% aqueous solution, Merck) with perchloric acid (BDH) and recrystallised from the 1:9 mixture of water and ethyl alcohol by volume several times. It was then dried at 120 °C under vacuum for 12 h. This salt was always kept under nitrogen atmosphere.

NaCl (Carlo Erba) was used as the supporting electrolyte in the electrochemical experiments. The polymer solution and the NaCl solution that was used as the supporting electrolyte were deoxygenated by bubbling pure nitrogen gas (BOS).

In electrochemical studies, a platinum (Pt) disc electrode (*r* = 0.05 cm) or Pt foil electrode (1.2 cm × 0.8 cm) was used as the working electrode. Before each experiment, the working electrode was polished with slurry of Cr<sub>2</sub>O<sub>3</sub> with water, then rinsed with triple distilled water, cleaned in ultrasonic bath and dried. Finally, the electrode was washed with the solvent that was used for the experiment.

In the methylene chloride medium, a Ag/AgCl electrode was used as the reference electrode. The electrode was immersed in a separate compartment containing methylene chloride/0.1 M TBAP solution with a saturated amount of AgCl. In the electrochemical experiments that were carried out in methylene chloride medium, a Pt wire in separate compartment containing methylene chloride/0.1 M TBAP solution was used as the counter electrode. In aqueous medium, saturated calomel electrode (SCE) was used as the reference electrode and a Pt wire electrode with a surface area of 2 cm<sup>2</sup> in spiral form was used as the counter electrode.

The cyclic voltammetric and potential-controlled coulometric studies were carried out with PAR system, which consists of Model 175 Universal Programmer, Model 173 Potentiostat and Model 179 Digital Coulometer. The differential pulse anodic stripping voltammetric studies were performed with PAR Model 174A Polarographic Analyzer. Cyclic voltammograms and differential pulse anodic stripping voltammograms were recorded with EG&G PAR Model RE0150 X-Y recorder.

The PVF<sup>+</sup>ClO<sub>4</sub><sup>-</sup> film was electrodeposited on the electrode surface by the electrooxidation of 1.0 mg/mL PVF solution in methylene chloride containing 0.1 M TBAP at +0.7 V vs. Ag/AgCl. The uptake of ClO<sub>4</sub><sup>-</sup> as the counter anion to the polymer film was shown in a previous study by infrared spectroscopy [22].

The thicknesses of PVF<sup>+</sup>ClO<sub>4</sub><sup>-</sup> films were controlled by the charge passed during the electroprecipitation. This charge was considered as an indication of polymer film thickness. A charge of 1 × 10<sup>-3</sup> C corresponded to 1.32 × 10<sup>-6</sup> moles of the oxidized

PVF/cm<sup>2</sup> (dry thickness of ~300 μm [23], which corresponds to about 3 × 10<sup>5</sup> layers).

### 2.1. Procedure

The procedure of preconcentration and voltammetric determination of Hg<sup>2+</sup> ion on PVF<sup>+</sup>Cl<sup>-</sup>-modified electrode includes the following steps: (1) coating the Pt electrode with PVF<sup>+</sup>ClO<sub>4</sub><sup>-</sup> film; (2) immersion of the film in aqueous solution of Cl<sup>-</sup>; (3) immersion of PVF<sup>+</sup>Cl<sup>-</sup> film in aqueous solution of Hg<sup>2+</sup> at open circuit; (4) electrochemical reduction of Hg<sup>2+</sup> ions prior to determination; (5) determination of Hg<sup>2+</sup> ions by DPASV.

## 3. Results and discussion

The voltammetric behavior of PVF<sup>+</sup>ClO<sub>4</sub><sup>-</sup>-coated Pt electrode is shown in Fig. 1. No appreciable current and potential change for oxidative and reductive behaviors was recorded in this voltammogram with time and surface was determined as stable.

PVF<sup>+</sup>ClO<sub>4</sub><sup>-</sup>-coated Pt electrode was dipped into a solution which contained 1 × 10<sup>-4</sup> M Hg<sup>2+</sup> for 15 min, then, removed, washed and immersed into a blank solution (a solution only contained 0.1 M NaCl). A potential of -0.2 V vs. SCE electrode, which is beyond reduction potential of Hg<sup>2+</sup> to metallic Hg, was applied for 5 min for reducing presumably immobilized Hg<sup>2+</sup>. Then, differential pulse anodic stripping voltammogram (DPASV) in blank solution was recorded (Fig. 2b). As can be seen, immobilized mercury stripped around at -0.05 V vs. SCE. This result indicated that some of the Hg<sup>2+</sup> from the solution was adsorbed on PVF<sup>+</sup>ClO<sub>4</sub><sup>-</sup> matrix possibly due to electrostatic attraction. However, when PVF<sup>+</sup>ClO<sub>4</sub><sup>-</sup>-coated Pt electrode was initially immersed into 5 × 10<sup>-2</sup> M Cl<sup>-</sup> ion for 15 min before other processes described above was applied, stripping peak current considerably increased (Fig. 2c). Voltammogram of the PVF<sup>+</sup>ClO<sub>4</sub><sup>-</sup>-coated electrode was also recorded (Fig. 2a).

This result was explained as follows. PVF<sup>+</sup>ClO<sub>4</sub><sup>-</sup> matrix is sensitive to the anions present in the solution. Since the Cl<sup>-</sup> ions are negatively charged. The electrostatic immobilization of Cl<sup>-</sup> ions on PVF<sup>+</sup>ClO<sub>4</sub><sup>-</sup>-coated Pt electrode was accomplished via anion exchange. Complexation reaction occurred between Hg<sup>2+</sup> and Cl<sup>-</sup> ions, thus, deposited amount of Hg<sup>2+</sup> on electrode surface, therefore, stripping peak of mercury enhanced.

The immobilization and detection mechanism can be proposed as following:

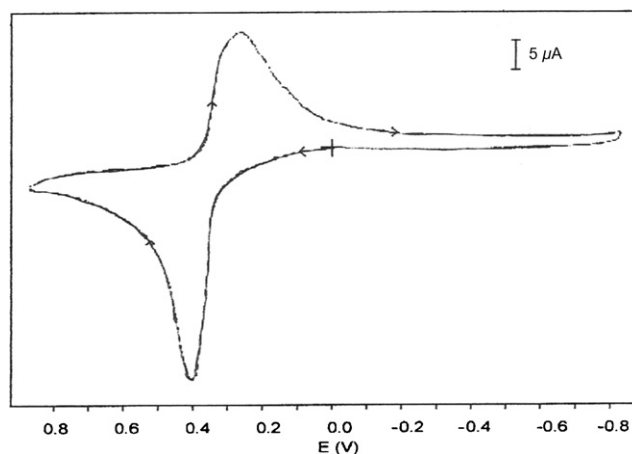
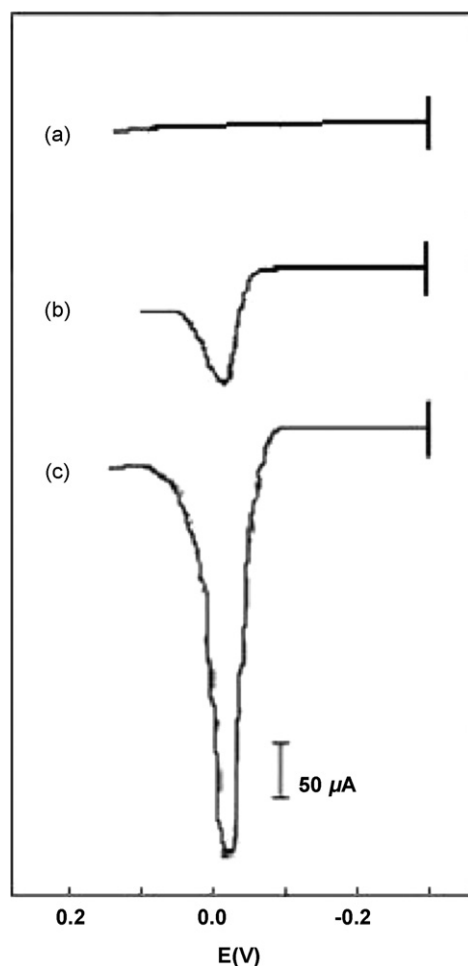
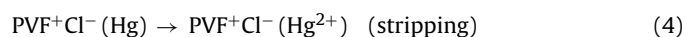
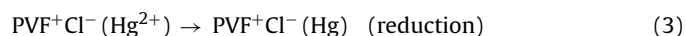
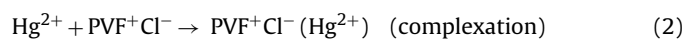


Fig. 1. Cyclic voltammetric behavior of PVF<sup>+</sup>ClO<sub>4</sub><sup>-</sup>-coated Pt disc electrode in 0.1 M NaCl solution. *v* = 100 mV/s; *A* = 7.85 × 10<sup>-3</sup> cm<sup>2</sup>.



**Fig. 2.** Differential pulse anodic stripping voltammogram of (a) PVF<sup>+</sup>ClO<sub>4</sub><sup>-</sup> film corresponding to 0.8 mC film thickness, (b) PVF<sup>+</sup>ClO<sub>4</sub><sup>-</sup> film immersed in 1 × 10<sup>-4</sup> M Hg<sup>2+</sup> solution for 15 min, (c) PVF<sup>+</sup>ClO<sub>4</sub><sup>-</sup> film immersed in 50 mM Cl<sup>-</sup> solution for 15 min, then in 1 × 10<sup>-4</sup> M Hg<sup>2+</sup> solution for 15 min, after 5 min cathodic electrolysis at -0.2 V vs. SCE.  $\nu = 5$  mV/s; mod. amp. = 100 mV;  $A = 7.85 \times 10^{-3}$  cm<sup>2</sup>.



These results and mechanism indicated that PVF<sup>+</sup>ClO<sub>4</sub><sup>-</sup>-coated Pt electrode can be used for Hg<sup>2+</sup> detection in aqueous solutions. However, several parameters had to be evaluated to get the optimum performance from this surface.

### 3.1. The effect of Cl<sup>-</sup> ion concentration

Fig. 3 shows the effect of Cl<sup>-</sup> ion concentration on the pre-concentration of Hg<sup>2+</sup> ions in the polymeric matrix. As can be seen, stripping peak current increased with the increase of Cl<sup>-</sup> ion concentration. This was an expected result according to proposed mechanism because increased concentration of Cl<sup>-</sup> leads to higher amounts of Hg<sup>2+</sup>-Cl<sup>-</sup> complex on the surface. However, when Cl<sup>-</sup> ion concentration exceeded 40 mM, stripping peak current started to decrease and the rupture of polymer films were visually observed when the concentration of Cl<sup>-</sup> ion was 80 mM. This was a clear indication of damaging effect of excess Cl<sup>-</sup> on the surface since it initiated pitting and that caused the rupture of the film.

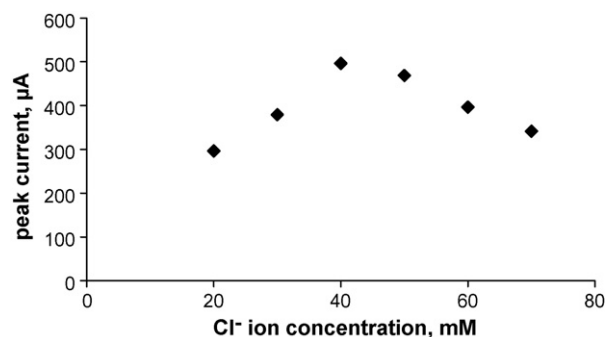


**Fig. 3.** The effect of Cl<sup>-</sup> ion concentration on the oxidation peak current for 1 × 10<sup>-4</sup> M Hg<sup>2+</sup> (1.0 mC film thickness, 15 min immersion time in Cl<sup>-</sup> ion solution, 15 min preconcentration time, -0.2 V electrolysis potential, 5 min electrolysis time).

### 3.2. The effect of immersion time in Cl<sup>-</sup> solution

The immersion time in Cl<sup>-</sup> ion solution was considered as an important parameter and its effect was studied. Fig. 4 shows the change of stripping peak currents with the immersion time of the modified electrode in Cl<sup>-</sup> solution. As can be seen, stripping peak currents showed an increase up to 15 min immersion time and decreased after this value. The result supported our claim about the damaging effect of excess Cl<sup>-</sup> ions deposited on the surface. Therefore, 15 min immersion time seemed the optimum immersion time.

### 3.3. The effect of polymeric film thickness

The effect of polymeric film thickness on the stripping peak current was investigated by varying the charge passed during the electrooxidation of PVF to PVF<sup>+</sup> and keeping the other variables constant (Fig. 5). When the thickness of PVF<sup>+</sup>ClO<sub>4</sub><sup>-</sup> or the amount of PVF<sup>+</sup> increased, accumulated amount of Cl<sup>-</sup> also increased and this caused stripping peak current to enhance due to higher amount of Hg<sup>2+</sup>-Cl<sup>-</sup> complex formation on the surface. However, after 0.8 mC film thicknesses, stripping peak current started to decrease with increase in film thickness due to excess Cl<sup>-</sup> accumulation. This is also another indication of damaging effect of excess Cl<sup>-</sup> which was described above. The decrease in the stripping peak current is also attributed to the change in the porosity of the polymer matrix at elevated film thicknesses.

### 3.4. The influence of preconcentration time

As can be determined from Fig. 6, the stripping peak current shows a steady increase up to 10 min preconcentration time and

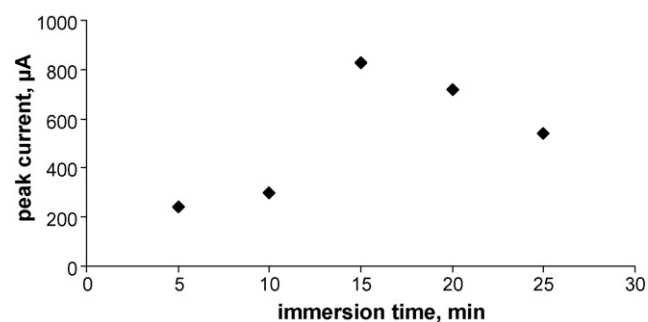


**Fig. 4.** The effect of immersion time in Cl<sup>-</sup> ion solution on the stripping peak current for 1 × 10<sup>-4</sup> M Hg<sup>2+</sup> (1.0 mC film thickness, 40 mM Cl<sup>-</sup> ion concentration, 15 min preconcentration time, -0.2 V electrolysis potential, 5 min electrolysis time).

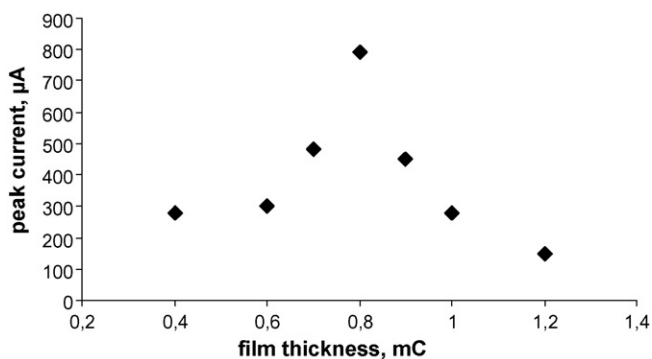


**Fig. 5.** The effect of polymeric film thickness on the stripping peak current for  $1 \times 10^{-4}$  M  $\text{Hg}^{2+}$  (50 mM  $\text{Cl}^-$  ion concentration, 15 min immersion time in  $\text{Cl}^-$  ion solution, 15 min preconcentration time,  $-0.2$  V electrolysis potential, 5 min electrolysis time).

remains constant after this time because of diffusion limitation. During evaluation of performance of the electrode, 5 min preconcentration time was used in order to assure that the electrode was not saturated with metal ions.

### 3.5. The influence of reduction potential

Various potentials were applied to for reduction of  $\text{Hg}^{2+}$  to Hg. The peak current showed a maximum at  $-0.3$  V vs. SCE and decreased after this potential. Two processes occur during the electrolysis of the modified electrode: (a) reduction of the metal ion in the polymer matrix and (b) reduction of PVF<sup>+</sup> to PVF. The latter is an undesirable process because, when the amount of PVF<sup>+</sup> in the polymer matrix decreases, the amount of the negatively charged complex species also decreases. It was thought that, up to  $-0.3$  V, as the reduction of the metal ion species is dominant, the stripping peak current increased. After this potential, because of the decrease at the stripping peak current, the second process was considered to be dominant. Therefore,  $-0.3$  V seemed to be the optimum electrolysis potential.

### 3.6. The influence of electrolysis time

The change in stripping peak current with electrolysis time was studied to obtain the optimum time needed for reduction of  $\text{Hg}^{2+}$  ions.  $-0.3$  V is the optimum electrolysis potential for the reduction of  $\text{Hg}^{2+}$  ions to Hg metal. Therefore, electrolytic reduction of the  $\text{Hg}^{2+}$  is the dominant process at this potential. Stripping peak current increased with increasing electrolysis time up to 4 min. However, when the electrolysis time exceeded

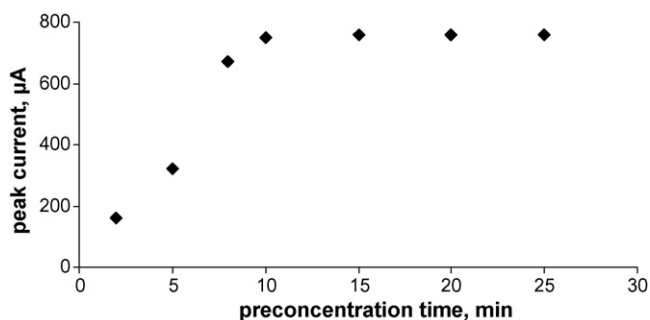


**Fig. 6.** The effect of preconcentration time on the stripping peak current for  $1 \times 10^{-4}$  M  $\text{Hg}^{2+}$  (0.8 mC film thickness, 40 mM  $\text{Cl}^-$  ion concentration, 15 min immersion time in  $\text{Cl}^-$  ion solution,  $-0.2$  V electrolysis potential, 5 min electrolysis time).

**Table 1**

Equation of calibration curves and  $R^2$  values for three concentration intervals.

Concentration range (M)	Equation of the calibration curve	$R^2$
$1 \times 10^{-3}$ to $5 \times 10^{-5}$	$y = 1884.1x + 8147$	0.9989
$1 \times 10^{-5}$ to $1 \times 10^{-6}$	$y = 3.7627x + 23.16$	0.9900
$1 \times 10^{-7}$ to $5 \times 10^{-10}$	$y = 0.1482x + 1.3908$	0.9832

**Table 2**

Interferences of some ions to the response of the electrode in 1:1 and 1:10 concentration ratios with respect to  $\text{Hg}^{2+}$ .

Interfering ion	% Interference	
	1:1	1:10
$\text{Ag}^+$	91.8	92.1
$\text{Fe}^{3+}$	52.2	92.3
$\text{Pb}^{2+}$	0.472	80.1

4 min, formed neutral mercury metal might have been released from the polymer matrix, consequently, stripping peak currents decreased. Thus, optimum electrolysis time was considered to be 4 min.

### 3.7. Repeatability, linearity and interferences

The performance of the method was evaluated with Pt foil electrode (1.2 cm  $\times$  0.8 cm) using the following conditions: 70 mC polymeric film thicknesses, 40 mM  $\text{Cl}^-$  ion concentration, 15 min immersion time in  $\text{Cl}^-$  solution, 5 min preconcentration time, 4 min electrolysis at  $-0.3$  V vs. SCE.

The repeatability was evaluated with  $1 \times 10^{-6}$  M  $\text{Hg}^{2+}$  solution for six observations. The relative standard deviation value was calculated as 6.35%.

Linearity of the electrode was investigated by starting with  $1 \times 10^{-3}$  M  $\text{Hg}^{2+}$  concentration in immobilization solution and gradually lowering the  $\text{Hg}^{2+}$  concentration and taking the stripping peak current of Hg as basis. Concentration of  $\text{Hg}^{2+}$  solutions was calculated by calibration curve method. There was linearity up to a concentration value of  $5 \times 10^{-5}$  M. After this value, slope of the curve changed and linearity was observed between  $1 \times 10^{-5}$  M and  $1 \times 10^{-6}$  M. After  $1 \times 10^{-6}$  M  $\text{Hg}^{2+}$  concentration, a greater sized platinum electrode was used to better detect the low amounts of mercury and linearity was obtained concentration interval  $1 \times 10^{-7}$  M and  $5 \times 10^{-10}$  M. Table 1 summarizes the equation of the calibration curve and  $R^2$  for three concentration intervals. No appreciable change in peak currents was observed for  $\text{Hg}^{2+}$  concentrations lower than  $5 \times 10^{-10}$  M.

Influences of interfering metal ions which are capable of forming chloride complexes on the response of the electrode were examined. The voltammogram of  $3 \times 10^{-3}$  M  $\text{Hg}^{2+}$  solution was recorded in the presence of  $\text{Ag}^+$ ,  $\text{Fe}^{3+}$  and  $\text{Pb}^{2+}$  ions in 1:1 and 1:10 con-

**Table 3**

Determination of  $\text{Hg}^{2+}$  ions in water samples.

Sample	$\text{Hg}^{2+}$ added (ng mL <sup>-1</sup> )	$\text{Hg}^{2+}$ found (ng mL <sup>-1</sup> )	% Recovery
Tap water	–	n.d.*	–
	40	$43.71 \pm 0.15^{**}$	109.3
Natural spring water	–	n.d.	–
	40	$40.60 \pm 0.18$	101.5

\* Not detected.

\*\* Mean value  $\pm$  standard deviation ( $n = 3$ ).

centration ratios with respect to  $\text{Hg}^{2+}$ . Interferences are given in Table 2.

### 3.8. Determination of mercury in water samples

The validity of the proposed method was tested in water samples by spiking known concentrations of mercury to water samples [24]. The results are summarized in Table 3.

## 4. Conclusions

PVF<sup>+</sup>-coated Pt surface has been shown to be a good choice for determining  $\text{Hg}^{2+}$  from aqueous solutions. The initial immersion of surface into  $\text{Cl}^-$  solution increased the accumulation of  $\text{Hg}^{2+}$  on the surface due to formation of  $\text{Hg}^{2+}\text{-Cl}^-$  complex. However, excess amounts of  $\text{Cl}^-$  on the surface caused pitting and rupture of the surface film. Detection mechanism was proposed. The reproducibility and sensitivity was satisfactory. Interferences from ions that might also form complexes with  $\text{Cl}^-$  were examined and reported. The validity of method was tested in water samples. It can be claimed that these surfaces are very good alternative to expensive analytical techniques such as atomic absorption spectrometry and ICP-MS. Another advantage of the method between electrochemical techniques is that, preparation of the surface and application of the method is simple and also cheaper than more costly materials such as gold.

## References

- [1] R.J. Irwin, M. VanMouwerik, L. Stevens, M.D. Seese, W. Basham, Environmental Contaminants Encyclopedia, National Park Service, Water Resources Division, Fort Collins, Colorado, 1997, p. 7.
- [2] S.C. Hight, J. Cheng, Food Chem. 91 (2005) 557.
- [3] M. Roulet, M. Lucotte, J.R.D. Guimaraes, I. Rheault, Sci. Total Environ. 261 (2000) 43.
- [4] P. Ugo, S. Zamperi, L.M. Moretto, D. Paolucci, Anal. Chim. Acta 434 (2001) 191.
- [5] A.C. Barbarosa, G.A. East, Ecol. Trace Element Res. 60 (1997) 153.
- [6] C.C. Huang, H.T. Chan, Anal. Chem. 78 (2006) 8332.
- [7] A. Giacomino, O. Abollino, M. Malandrino, E. Mentasti, Talanta 75 (2008) 266.
- [8] H. Ju, D.J. Leech, Electroanal. Chem. 484 (2000) 150.
- [9] S. Berchmans, S. Arivukkodi, V. Yegnaraman, Electrochem. Commun. 2 (2000) 226.
- [10] P. Ugo, S. Zampieri, L.M. Moretto, D. Paolucci, Anal. Chim. Acta 434 (2001) 291.
- [11] R. Agraz, M.T. Sevilla, L. Hernandez, J. Electroanal. Chem. 390 (1995) 47.
- [12] J. Wang, M. Bonakdar, Talanta 35 (1988) 277.
- [13] C. Faller, N.Y. Stojko, G. Henze, K.Z. Brainina, Anal. Chim. Acta 396 (1999) 195.
- [14] J. Labuda, V. Plaskon, Anal. Chim. Acta 228 (1990) 259.
- [15] P. Ugo, L.M. Moretto, G.A. Mazzocchin, Anal. Chim. Acta 305 (1995) 74.
- [16] J. Lu, X. He, X. Zeng, Q. Wan, Z. Zhang, Talanta 59 (2003) 553.
- [17] Y. Guo, A.R. Guadalupe, J. Pharmaceut. Biomed. 19 (1999) 175.
- [18] G. Cabello-Carramolino, M.D. Petit-Dominguez, Anal. Chim. Acta 614 (2008) 103.
- [19] L. Yu, M. Sathe, X. Zeng, J. Electrochem. Soc. 152 (2005) E357.
- [20] C. Aso, T. Kunitake, T. Nakashima, Macromol. Chem. 124 (1969) 232.
- [21] D.D. Perrin, W.L.F. Armarego, D.R. Perrin, Purification of Laboratory Chemicals, Pergamon Press, 1980.
- [22] H. Gülce, H. Özyörük, A. Yıldız, Electroanalysis 7 (1993) 178.
- [23] P.J. Pearce, A.J. Bard, J. Electroanal. Chem. 112 (1980) 97.
- [24] N. Rajesh, M.S. Hari, Spectrochim. Acta Part A 70 (2008) 1104.



# High-throughput quantification of a novel thiazolidinedione MCC-555 in rat plasma by ultra-fast liquid chromatography and its application in pharmacokinetic studies

Ning Sun<sup>a,b,c,1</sup>, Guocai Lu<sup>d,1</sup>, Mei Lin<sup>e</sup>, Guorong Fan<sup>a,b,c,\*</sup>, Yutian Wu<sup>a,b,c</sup>

<sup>a</sup> Department of Pharmaceutical Analysis, School of Pharmacy, Second Military Medical University, No. 325 Guohe Road, Shanghai 200433, PR China

<sup>b</sup> Shanghai Key Laboratory for Pharmaceutical Metabolite Research, No. 325 Guohe Road, Shanghai 200433, PR China

<sup>c</sup> Shanghai Research Centre for Drug (Chinese Materia Medica) Metabolism, No. 325 Guohe Road, Shanghai 200433, PR China

<sup>d</sup> Center for New Drug Evaluation, Institute of Basic Medical Science, Second Military Medical University, No. 800 XiangYin Road, Shanghai 200433, China

<sup>e</sup> Shanghai Institute for Drug Control, No. 615 Liuzhou Road, Shanghai 200233, PR China

## ARTICLE INFO

### Article history:

Received 4 August 2008

Received in revised form

26 November 2008

Accepted 29 November 2008

Available online 6 December 2008

### Keywords:

MCC-555

UFLC

HPLC

Rat plasma

Pharmacokinetics

## ABSTRACT

MCC-555 is a novel thiazolidinedione which reduces plasma glucose concentrations in Type 2 diabetes mellitus models due to enhancement of insulin sensitivity. A highly sensitive and selective quantitative method to accurately determine MCC-555 in rat plasma is crucial to the success of pharmacokinetic studies of MCC-555. To this purpose we have developed and validated a high-throughput method in a 96-well plate format using ultra-fast liquid chromatography (Shimadzu Prominence UFLC™ system) for the determination of MCC-555 in rat plasma. MCC-555 along with the internal standard resveratrol was extracted from 50  $\mu$ l of rat plasma by liquid–liquid extraction using ethyl acetate. Baseline separation of MCC-555 and resveratrol was achieved using UFLC technology on a C18 stationary-phase column with 2.2  $\mu$ m particle size. The influences of flow rate, column temperature and mobile phase pH on chromatographic performance were investigated. Comparing to the conventional HPLC method, UFLC showed many advantages including reduced run time, less solvent consumption and increased sensitivity. The UFLC method was sensitive with a lower limit of quantification of 0.002  $\mu$ g/ml, with good linearity ( $r > 0.999$ ) over the linear range of 0.002–2.0  $\mu$ g/ml. The intra- and inter-run precision was less than 8.6% and accuracy ranged from –6.4 to 8.2% for quality control samples. The extraction recovery from plasma was no less than 80%. The validation and sample analysis results show that the method is precise, accurate and well suited to support pharmacokinetic studies in rats involving three dose administrations.

© 2008 Elsevier B.V. All rights reserved.

## 1. Introduction

Thiazolidinediones (TZDs) represent a new class of oral anti-diabetic agents. Two of these, rosiglitazone and pioglitazone, are approved by the U.S. Food and Drug Administration for the treatment of non-insulin-dependent diabetes mellitus (NIDDM). Despite the clear clinical benefit of these drugs as a treatment for NIDDM, the use of the current generation of thiazolidinediones is

associated with side effects of clinical importance, such as weight gain, edema and anemia [1,2]. In addition, there is a growing concern about the reported deleterious effects of thiazolidinediones on bone cell function and the skeleton [3–6]. For these reasons, significant efforts are ongoing to develop novel thiazolidinediones, which retain their insulin sensitizing activity, but are devoid of activities that cause adverse effects.

MCC-555 (5-[[6-(2-fluorbenzyl)-oxy-2-naphyl] methyl]-2,4-thiazolidinedione) (Fig. 1) is a member of a new class of peroxisome proliferator-activated receptor gamma (PPAR- $\gamma$ ) ligands with distinct anti-diabetic [7]. MCC-555 has been reported to be over 50-fold more potent than rosiglitazone in decreasing blood glucose levels in rodent models of NIDDM, and 5- to 10-fold less effective than rosiglitazone in inducing adipogenesis in mouse preadipocytes [8,9]. These effects may be explained by the ability of MCC-555 to act as a PPAR- $\gamma$  agonist, partial agonist, or antagonist, depending on cell context, and can be attributed to its ability to recruit PPAR- $\gamma$  coactivators, distinct from those recruited by rosiglitazone [10].

**Abbreviations:** UFLC, ultra-fast liquid chromatography; HPLC, high-performance liquid chromatography; LC-MS, liquid chromatography tandem mass spectrometry; LLOQ, lower limit of quantification; TZDs, thiazolidinediones; NIDDM, non-insulin-dependent diabetes mellitus; PPAR- $\gamma$ , peroxisome proliferator-activated receptor gamma; IS, internal standard; QCs, quality control samples.

\* Corresponding author at: Second Military Medical University, School of Pharmacy, 325 Guohe Road, Shanghai 200433, China. Tel.: +86 21 2507 0388; fax: +86 21 2507 0388.

E-mail address: [Guorfan@yahoo.com.cn](mailto:Guorfan@yahoo.com.cn) (G. Fan).

<sup>1</sup> These two authors equally contributed to this work.

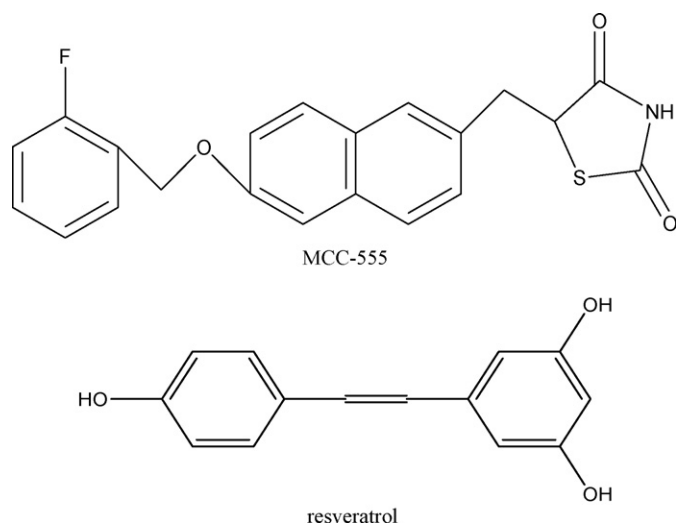


Fig. 1. Chemical structures of MCC-555 and resveratrol (IS).

Besides the pharmacodynamic evaluation, it is also important to determine the pharmacokinetic properties of MCC-555. Several methods have been reported for the extraction and detection of MCC-555 and TZDs drugs (rosiglitazone and pioglitazone) in biological fluids, drugs such as liquid chromatography (LC) with ultraviolet (UV) detection or fluorescence detection and liquid chromatography tandem mass spectrometry (LC-MS-MS) [11–14]. Among them, HPLC with fluorescence detection assay is well established and robust, but it is time-consuming (12 min at least) [14]. Therefore, we felt necessary to develop a rapid and reliable quality control method for rapid determination of MCC-555 in order to achieve high-throughput determination of considerable biological samples. Due to its inherent selectivity and sensitivity, ultra-fast LC offers higher sample throughput for pharmaceutical analysis as compared with the traditional HPLC methods. Therefore, the ultra-fast LC systems have become the instrument of choice for drug assays in the modern pharmaceutical industry. About ultra-fast LC there already have many types such as ultra-performance liquid chromatography (Waters Acquity UPLC™ system), rapid-resolution liquid chromatography (Agilent 1200 RRLC™ system) and ultra-fast liquid chromatography (Shimadzu Prominence UFLC™ system). A Waters Acquity UPLC™ system is performed on a Waters analytical column with 1.7  $\mu\text{m}$  particle size operated at high pressures and an Agilent 1200 RRLC™ system employs chromatographic separations based on a 1.8  $\mu\text{m}$  stationary phase operated at high pressures with the function of automatic delay volume reduction of automated sample injector. Recently, UFLC (Shimadzu Prominence UFLC™ system) has been introduced with increased separation performance compared to conventional HPLC. UFLC employs chromatographic separations based on a 2.2  $\mu\text{m}$  C18 stationary phase operated at normal pressure to give flow rates of 0.4–0.5 ml/min. One of the major advantages of this improvement in separation that UFLC affords is that chromatographic runtime can often be greatly reduced, giving a considerable saving in both instrument and analyst time; of value to those involved in high-throughput applications in drug discovery and development.

A number of approaches such as sample extraction in 96-well format plates [15], and fast chromatography [15–17] are integrated to increase sample throughput for the determination of small molecules in biological samples in our laboratory. In this paper, we describe a high-throughput UFLC method for the determination of MCC-555 from rat plasma by liquid–liquid extraction based on 96-well plates. UFLC system with C18 column (50 mm  $\times$  2.0 mm i.d.) packed with porous 2.2  $\mu\text{m}$  particles is powerful approach to dra-

matically improve peak resolution, sensitivity and speed of analysis. Results of the fully validation presented here demonstrate that the UFLC method is suitable for analyzing MCC-555 in rat plasma. It has been successfully applied to the pharmacokinetic study of MCC-555 in rats after three dose (2.5, 5.0, and 10.0 mg/kg) administrations. We also investigated the differences in system performance by conducting a comparison of UFLC with other method previously optimized for HPLC separation of MCC-555.

## 2. Material and methods

### 2.1. Reagents and chemicals

MCC-555 and the internal standard (IS) resveratrol (Fig. 1, purity of both  $\geq 99.7\%$ ) were obtained by Shanghai Jiahua Medicine Science, Co. Ltd. (Shanghai, China). Acetonitrile, methanol and ethyl acetate (all HPLC grades) were purchased from Merck Company (Darmstadt, Germany). All other reagents were of analytical grade. Double-distilled water was used and 0.45  $\mu\text{m}$  pore size filters (Millipore, MA) was used to filter the solutions.

### 2.2. Animals

Male and female Sprague–Dawley rats (weight, 200–300 g) were purchased from Shanghai SLAC Laboratory Animal Co. Ltd. The animals were acclimated for two weeks, and during this period, they were examined for any abnormalities suggestive of health problems; body weights were recorded. Environmental conditions were monitored and maintained at 19–25  $^{\circ}\text{C}$ , 55  $\pm$  15% relative humidity, and a 12-hr light/dark cycle of 150–300 lx, with water available *ad libitum*. All the animals used in this study in compliance with institutional animal care guidelines, and the animal use and care protocols were approved by the Local Institutional Committee of the Second Military Medical University.

### 2.3. Apparatus

HPLC analyses were performed on a Shimadzu-10A system equipped with a LC-10AD VP pump coupled with a RF-10A fluorescence detector operating at excitation and emission wavelengths of 232 nm and 352 nm, SIL-10AD VP automated sample injector, thermostatted column compartment CTO-10AS VP and N2000 workstation (Zhejiang University, Hangzhou, China).

A Shimadzu Prominence UFLC™ system, equipped with a LC-20AD VP pump, a SIL-20AD VP automated sample injector, a thermostatted column compartment CTO-20AC VP, a RF-10A fluorescence detector operating at excitation and emission wavelengths of 232 nm and 352 nm, was used for MCC-555 analysis under UFLC conditions. Data were processed with LCsolution software (Shimadzu, Japan).

### 2.4. Chromatographic conditions

#### 2.4.1. HPLC

The assay development including instrumental details was recently reported [14]. Briefly, separations were carried out on a Kromasil C18 reversed-phase column (5  $\mu\text{m}$ , 250 mm  $\times$  4.6 mm i.d.), protected by a Diamonsil™ ODS guard column; mobile phase consisted of solvent A, 10 mmol/l sodium phosphate buffer (pH 4.5), and solvent B, acetonitrile (35:65, v/v); flow rate, 1.0 ml/min; column temperature, 35  $^{\circ}\text{C}$ ; injection volume, 20  $\mu\text{l}$ ; analyses time, 12 min.

#### 2.4.2. UFLC

Samples were analyzed on a Shimadzu Prominence UFLC™ C18 column (2.2  $\mu\text{m}$ , 50 mm  $\times$  2.0 mm i.d.); mobile phase consisted of



solvent A, 10 mmol/l sodium phosphate buffer (pH 4.5), and solvent B, acetonitrile (40:60, v/v); flow rate, 0.5 ml/min; column temperature, 35 °C; injection volume, 5 µl; analysis time, 2 min.

### 2.5. Preparation of standards and quality control samples

The stock solution of MCC-555 (1.0 mg/ml) was prepared in methanol. Working standard solutions of MCC-555 were obtained in the concentrations of 0.1, 1.0, 10.0, and 100 µg/ml by further dilutions of the stock solution with methanol. Resveratrol was prepared at a concentration of 4 µg/ml in methanol. All the solutions were stored at –20 °C.

Calibration standards were prepared by spiking blank rat plasma with working standard solutions of MCC-555. The effective concentrations in standard plasma samples were 0.002, 0.005, 0.01, 0.02, 0.05, 0.1, 0.2, 0.5, 1.0 and 2.0 µg/ml. One calibration curve was constructed on each analysis day using freshly prepared calibration standards. The quality control samples (QCs) were prepared with blank plasma at low, middle and high concentrations of 0.04, 0.4 and 1.4 µg/ml and stored at –20 °C after preparations. The standards and quality controls were extracted on each analysis day with the same procedure for plasma samples as described below.

### 2.6. Sample preparation

Samples were prepared using liquid–liquid extraction in 96-well format plates. The liquid transfer steps were completed by eight-channel pipetting tools (Eppendorf Research®, Eppendorf AG, Hamburg, Germany) except when adding 1000 µl of extraction agent. Plasma samples (50 µl) were transferred to the 2-ml ArcticWhite 96-well polypropylene plate using 100-µl eight-channel pipetting tool. A 50 µl aliquot of 2 µg/ml internal standard solution and a 100 µl aliquot of 0.3 mol/l Na<sub>2</sub>HPO<sub>4</sub> solution were transferred to each well of the 96-well plate with the exception of the blanks, followed by capping and vortex mixing for 1 min. Following addition of 1000 µl of ethyl acetate, the wells were capped with the ArctiSeal mat; vortex mixed for 3 min, and centrifuged at 1047 × g for 10 min. The ethyl acetate layer was transferred to the respective positions of new 2-ml ArcticWhite 96-well plates. These sample extracts were evaporated at 45 °C under a stream of nitrogen, reconstituted with 50 µl of 60/40 acetonitrile/water, capped and vortex mixed before analysis.

### 2.7. Pharmacokinetic studies

Sprague–Dawley rats were divided into three groups (80 rats per group) and received 2.5, 5 and 10 mg/kg oral doses of MCC-555 in a suspension using 0.5% carboxy methyl cellulose via gastric gavage. All rats were fasted overnight with free water supply before experiments and had access to water and food 4 h after drug administration. Dose volumes were calculated based on the pretreatment body weights of the animals, rounded to the nearest 0.01 ml and measured carefully in calibrated syringe to minimize the variability of dosing.

Blood samples were collected by decapitation under slight ether anesthesia at different time points (0.25, 0.5, 0.75, 1, 1.5, 2, 3, 4, 6, 8, 10, 12, 24, 36, 48, and 72 h) after administration (5 rats/time point). Each collected blood sample was immediately transferred into a heparinized 1.5 ml microcentrifuge tube and centrifuged at 2992 × g for 6 min at room temperature. The resulting plasma samples were immediately frozen at –20 °C for further analysis. The plasma concentration–time data were analyzed and pharmacokinetic parameters were estimated by non-compartmental analysis. The merit of the non-compartmental analysis is to evaluate pharmacokinetic parameters without the restriction of the compartment model based on the test plasma concentrations. Because

some differences can be obtained using different mathematics methods or soft wares when pharmacokinetic parameters are estimated by the compartment model.

## 3. Results and discussion

High-performance liquid chromatography has been used for the analysis of MCC-555 biological samples. Recently, an improvement in chromatographic performance has been achieved by the introduction of UFLC. The van Deemter equation indicates that, when the particle size decreases to less than 2.5 µm there is a significant gain in efficiency and that efficiency does not diminish at increased flow rates or linear velocities. Thus, UFLC takes full advantage of chromatographic principles to run separations using columns packed with smaller particles (2.2 µm), with superior resolution and shorter analysis time. In our experiment, a 50 mm column submitted to an isocratic flow rate of 0.5 ml/min for 2 min was used to obtain the chromatograms. The very narrow chromatographic peaks generated by UPLC, resulted in an increase in the chromatographic efficiency and sensitivity.

As mentioned before, the aim of this study was to develop UFLC method for determination of MCC-555 in rat plasma. To purify complex sample matrix and concentrate MCC-555, a liquid–liquid extraction procedure was developed as a first step of this study. Sample extraction in 96-well format plates and fast chromatography are integrated to increase sample throughput for the determination of small molecules in biological samples in our laboratory. The second major point concerning with UFLC method development was to avoid co-elution of other compounds with MCC-555 and resveratrol, resulting in reasonable value of LLOQ. To solve this problem influence of column temperature, flow rate and mobile phase pH was studied. Developed procedures were further validated, and their applicability was verified on analysis of MCC-555.

### 3.1. Optimization of sample preparation

Low throughput on the currently available assays is generally due to labor-intensive sample preparation, while this limiting factor was significantly improved in this paper. In order to increase sample throughput, the liquid–liquid extraction in 96-well format plates was used, which resulted in shorter sample preparation time. Furthermore, it should be noted that only 50 µl of plasma was required for method development. To select a good organic solvent as the extract agent, a number of solvents have been tried including ethyl acetate, dichloromethane, acetone, diethyl ether or their mixtures; the only aim was to get a best extraction recovery and to remove the endogenous materials that might interfere with the peaks of MCC-555 and IS. The extraction efficiency of ethyl acetate was about 80%, and the chromatograms were free from any endogenous substances in peaks of MCC-555 and IS. So we selected ethyl acetate as the extraction agent. The extraction procedure without and with adding 10 mmol/l sodium phosphate buffer (100 µl) was also compared, and the latter gave a higher recovery.

### 3.2. UFLC method development

#### 3.2.1. Choice of internal standard

A synthetic intermediate of MCC-555 used to be the internal standard in reported paper [14]. However, owing to the difficulty to get the synthetic intermediate of MCC-555 by commercial purchase, we thought that it was necessary to find the new internal standard for pharmacokinetic studies. In the course of the selection of the internal standard telmisartan, naproxen, rosiglitazone and metoprolol had been tried. These compounds can be separated from MCC-555 with good resolution, but all failed partly for the

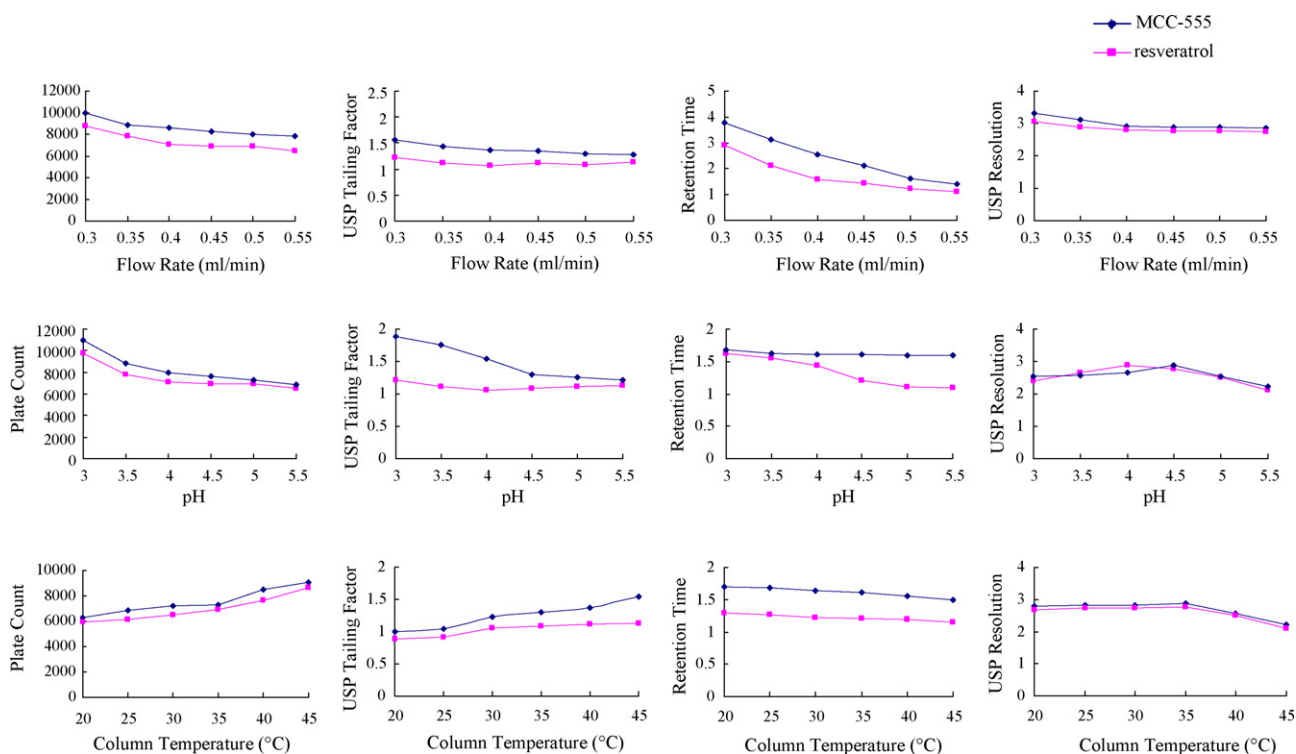


Fig. 2. Influence of flow rate, mobile phase pH and column temperature on UFLC chromatographic performance.

short retention time or being interfered by endogenous matrix. Resveratrol was selected as the internal standard, because it was also a fluorescent compound ( $\lambda_{\text{ex}} = 260 \text{ nm}$ ,  $\lambda_{\text{em}} = 364 \text{ nm}$ ) [18] and had a suitable retention time and a good resolution from MCC-555 under the chromatographic conditions in this study. There was no endogenous interferences in the regions where MCC-555 and IS eluted.

### 3.2.2. HPLC method development and transfer to UFLC

The basic chromatographic conditions like stationary phase, solvents and fluorescence detection, employed in HPLC were kept constant when developing the new UFLC method. Under these conditions the run time was around 1 min, but the separation between MCC-555 and resveratrol was not satisfactory. Attempts to improve the chromatographic separation were performed with varying the composition of mobile phase. Since no interferences with other compounds that originated from sample matrix were observed even with 60% of acetonitrile in mobile phase, this concentration was applied. To improve detector sensitivity and to achieve equivalent system performance compared with conventional HPLC at same sample concentration UFLC instrument manufacturer recommends using low injection volume.

Attempts to improve the chromatographic performance were made by altering the column temperature, flow rate and mobile phase pH. The results are shown in Fig. 2. The influence of flow rate was investigated with column temperature of  $35^\circ\text{C}$  and mobile phase pH 4.5; the flow rate was set at 0.5 ml/min and column temperature of  $35^\circ\text{C}$  when mobile phase pH was altered; the flow rate was set at 0.5 ml/min and mobile phase pH 4.5 when column temperature was altered.

The resolution, theoretical plates and tailing factor of MCC-555 and resveratrol showed unremarkable decline trend with flow rate increased, compared to noticeable declines of the retention time of MCC-555 and resveratrol. Considering system backpressure and running time, flow rate of 0.5 ml/min was preferred. Compared to

a noticeable decline of the retention time of resveratrol at pH 4.5, the retention time of MCC-555 showed unremarkable decline trend with mobile phase pH increased. And the resolutions of MCC-555 and resveratrol showed decline trend when mobile phase pH was over 4.5. The theoretical plates and tailing factor obtained for MCC-555 and resveratrol showed some improvements with the increase of column temperature. The resolution of MCC-555 and resveratrol showed a declining trend above  $35^\circ\text{C}$ . Hence, the column temperature of  $35^\circ\text{C}$  was preferred. At flow rate of 0.5 ml/min, mobile phase pH 4.5 and column temperature  $35^\circ\text{C}$ , a satisfactory and rapid separation was achieved in 2 min.

### 3.2.3. Comparison of UFLC and HPLC

UFLC system supports high-speed analysis through the following features: low volume tubing and flow cell decrease extra-column band spreading; 10 s ultra-fast injections with the Prominence SIL-20 Autosampler; temperature capability up to  $85^\circ\text{C}$ ; fast data acquisition allows for better signal tracing. These features, together with the use of a  $2.2 \mu\text{m}$  particle material column, can shorten analysis time 5- to 6-fold, giving a considerable saving in both instrument and analyst time; of value to those involved in high-throughput applications in drug discovery and development. Comparative data on chromatographic performance of UFLC and HPLC have been obtained by injecting extracted plasmas which were spiked with  $1 \mu\text{g/ml}$  of MCC-555 and  $2 \mu\text{g/ml}$  of the IS. Comparisons of UFLC and HPLC assay parameters and system performance are summarized in Table 1. Although validation parameters of both methods are almost equal, some differences between two studied methods could be seen. Major advantages of UFLC are mostly economical, i.e., low consumption of solvents and six times higher samples throughput of this method. The UFLC method showed comparatively better analysis efficiency than HPLC, though the theoretical plates obtained for MCC-555 in UFLC were somewhat poorer. Typical chromatograms HPLC and UFLC chromatograms are depicted in Fig. 3.

**Table 1**  
Comparison of UFLC and HPLC assay parameters and system performance.

	UFLC assay	HPLC assay
Column	Shimadzu C18 column (50 mm × 2.0 mm, 2.2 μm)	Kromasil C18 column (250 mm × 4.6 mm, 5 μm)
Flow rate (ml/min)	0.5	1.0
Injection volume (μl)	5	20
Total run time (min)	2	12
MCC-555 elution time (min)	1.62	10.72
Total solvent consumption	0.4 ml of water 0.6 ml of acetonitrile	4.2 ml of water 7.8 ml of acetonitrile
USP resolution	2.89	1.86
Tailing factor	1.30	1.42
USP plate count	5788	4856
LLOQ (μg/ml)	0.002	0.005

### 3.3. UFLC method validation

A full validation was performed to evaluate the performance of the method in accordance to the recommendations published by FDA [19]. Validation runs were conducted on three consecutive days. Each validation run consisted of a minimum of one set of calibration standards and six sets of QC plasma samples at three concentrations. The results from QC plasma samples in three runs were used to evaluate the precision and accuracy of the method developed. The peak area ratios of MCC-555/IS of unknown samples were then interpolated from the calibration curve to give the concentrations of MCC-555. During routine analysis, each analytical run included a set of calibration standards, a set of QC plasma samples in duplicate and plasma samples to be determined.

#### 3.3.1. Selectivity

Selectivity was studied by comparing chromatograms of six different batches of blank plasma obtained from six subjects with those of corresponding standard plasma samples spiked with MCC-555 and resveratrol and plasma sample after oral doses of MCC-555. Typical chromatograms obtained in rat plasma are shown in Fig. 4.

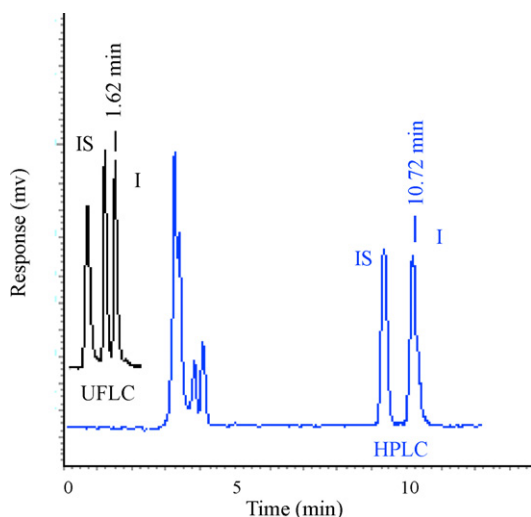


**Fig. 3.** The comparison of UFLC and HPLC chromatograms of test plasma (I: MCC-555, 1 μg/ml; IS: resveratrol, 2 μg/ml). UFLC: Shimadzu Prominence UFLC™ C18 column (2.2 μm, 50 mm × 2.0 mm i.d.); mobile phase consisted of solvent A, 10 mmol/l sodium phosphate buffer (pH 4.5), and solvent B, acetonitrile (40:60, v/v); flow rate, 0.5 ml/min; column temperature, 35 °C; injection volume, 5 μl; analysis time, 2 min. HPLC: Kromasil C18 reversed-phase column (5 μm, 250 mm × 4.6 mm i.d.), protected by a Diamonsil™ ODS guard column; mobile phase consisted of solvent A, 10 mmol/l sodium phosphate buffer (pH 4.5), and solvent B, acetonitrile (35:65, v/v); flow rate, 1.0 ml/min; column temperature, 35 °C; injection volume, 20 μl; analyses time, 12 min.

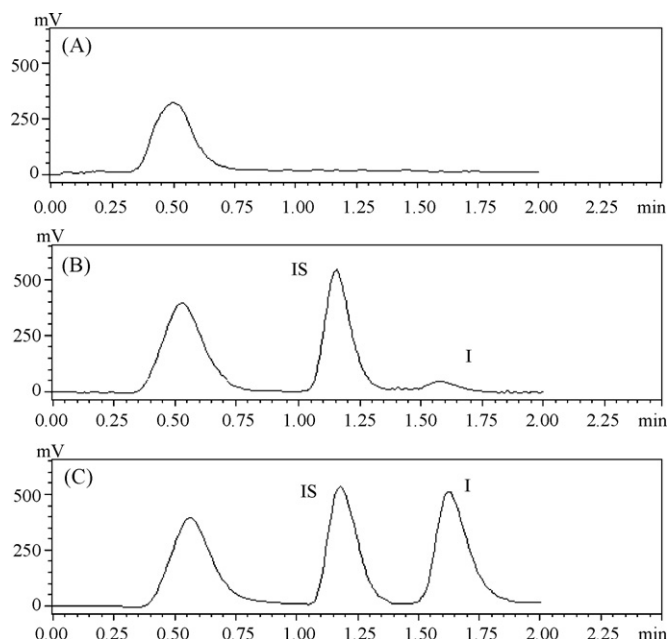


**Fig. 4.** Representative chromatograms for MCC-555 (I) and resveratrol (IS) from (A) a blank plasma sample; (B) a plasma sample with added MCC-555 at a LLOQ level (0.002 μg/ml) and resveratrol (2 μg/ml); (C) a plasma sample from a rat 1 h after the dose of 5 mg/kg (concentration 1.166 μg/ml). The retention times of MCC-555 and IS were 1.62 and 1.12 min, respectively.

As can be seen from these figures, no significant interfering peaks were observed at the retention times of MCC-555 and IS. The fast analysis speed with a total analysis time less than 2.0 min (1.62 min for MCC-555 and 1.12 min for IS) enabled high sample throughput to be achieved.

#### 3.3.2. Linearity and sensitivity

A weighted ( $1/x$ ) linear regression was used to perform standard calibration. The mean calibration equation was  $y = 8.4798$  (R.S.D. = 8.7%,  $n = 5$ ) $x - 0.0286$  (R.S.D. = 2.3%,  $n = 5$ ), where  $y$  represents the peak area ratios of the analyte to the IS and  $x$  represents the plasma concentration of analyte in μg/ml. Calibration curves showed an excellent linearity in the range of 0.002–2.0 μg/ml with the concentration coefficients consistently greater than 0.999.

The lower limit of quantitation (LLOQ) of the assay [20], defined as the lowest concentration on the standard curve that can be quantitated with accuracy within 15% of nominal and precision not exceeding 15%, was 0.002 μg/ml for MCC-555. The reproducibility of LLOQ was determined by examining five LLOQ samples independent from the standard curve. A typical chromatogram of an LLOQ sample is shown in Fig. 4.

#### 3.3.3. Precision and accuracy

Precision and accuracy were evaluated by analyzing the LLOQ, low, mid, and high concentration quality control samples (0.002, 0.004, 0.08 and 1.4 μg/ml). Precision was expressed as relative standard deviation (R.S.D. %) and accuracy expressed as percent relative error (R.E. %). Intra-run precision and accuracy were determined by repeated analysis of a set of standards on 1 day ( $n = 5$ ), while inter-run precision and accuracy by repeated analysis on three consecutive days ( $n = 5$  series per day). The R.S.D. and R.E. should be less than 15%, except at the LLOQ where it should not exceed 20% [21].

The data of intra-run and inter-run precision and accuracy for the method are listed in Table 2. The intra-run precision (R.S.D.) for LLOQ, low, mid and high QC levels of MCC-555 were 5.4%, 4.9%, 7.6% and 2.3%, respectively, with an accuracy (R.E.) within –4.8% to 7.4%, and that of inter-run analysis were 6.7%, 8.6%, 3.4%, 6.2%, respec-

**Table 2**

Precision and accuracy for the determination of MCC-555 in rat plasma (intra-run:  $n=5$ ; inter-run:  $n=5$  series per day, 3 days).

Concentration ( $\mu\text{g/ml}$ )		Precision R.S.D. (%)	Accuracy R.E. (%)
Spiked	Observed (mean $\pm$ S.D.)		
<b>Intra-run</b>			
0.002 (LLOQ)	0.002 $\pm$ 0.0003	5.4	6.6
0.04 (low)	0.004 $\pm$ 0.001	4.9	-4.8
0.8 (middle)	0.079 $\pm$ 0.007	7.6	7.4
1.4 (high)	1.38 $\pm$ 0.62	2.3	5.3
<b>Inter-run</b>			
0.002 (LLOQ)	0.002 $\pm$ 0.0005	6.7	8.2
0.04 (low)	0.004 $\pm$ 0.003	8.6	4.9
0.8 (middle)	0.082 $\pm$ 0.013	3.4	-6.4
1.4 (high)	1.41 $\pm$ 0.79	6.2	-3.8

tively, with an accuracy (R.E.) within -6.4% to 8.2%. The results of intra-run and inter-run analysis indicated that UFLC method were accurate, reliable and reproducible.

### 3.3.4. Extraction recovery

Extraction recovery of MCC-555 was determined by dividing the mean response obtained from blank plasma samples spiked with analyte before extraction with those from blank plasma samples to which analyte was added after extraction. This procedure was repeated in five replicates for the three QC concentrations.

The extraction recoveries of MCC-555 from rat plasma were  $83.4 \pm 5.0\%$ ,  $87.3 \pm 2.9\%$ , and  $85.9 \pm 4.5\%$  at concentration levels of 0.04, 0.4 and 1.4  $\mu\text{g/ml}$  and the mean extraction recovery of resveratrol was  $81.6 \pm 2.7\%$ .

### 3.3.5. Stability

Sample stability in plasma was investigated as follows using QC samples. Short-term stability was examined by analyzing samples at room temperature for 24 h. Long-term stability study was performed by analyzing samples stored for 2 months at  $-20^\circ\text{C}$ . For freeze-thaw stability study, the samples were left 1 h to thaw, and then refrozen for 24 h. This cycle was repeated three times and analysis was done after the third freeze-thaw cycle. The stability of MCC-555 in reconstituted extracts during runtime in the LC auto-injector was tested performing a second analysis of the same extracts left 8 h at room temperature. The criterion for an acceptable stability of compounds in plasma samples under different storage conditions is that the relative recovery of the drug should be at least 90% of the initial concentration [22].

MCC-555 was found to be stable in rat plasma samples for at least 24 h when stored at room temperature and for 2 months when stored at  $-20^\circ\text{C}$ . And the stock solutions of resveratrol were stable for at least 12 h when stored at room temperature and for 2 months when stored at  $-20^\circ\text{C}$ . Table 3 summarizes the results of all stability studies which all well met the criterion for stability measurements. The method is therefore proved to be applicable for routine analysis.

### 3.3.6. Sample dilution

The effect of diluting samples with MCC-555 concentrations above the standard curve range was examined. Plasma samples

**Table 3**

Stability of MCC-555 in rat plasma at three QC levels ( $n=5$ ).

Stability	Mean recovery (%)		
	0.04 ( $\mu\text{g/ml}$ )	0.4 ( $\mu\text{g/ml}$ )	1.4 ( $\mu\text{g/ml}$ )
Short-term stability	96.2 $\pm$ 4.1	99.7 $\pm$ 3.1	97.4 $\pm$ 2.2
Long-term stability	98.9 $\pm$ 2.4	100 $\pm$ 1.8	98.6 $\pm$ 2.5
Freeze-thaw stability	98.2 $\pm$ 4.8	99.6 $\pm$ 3.0	98.4 $\pm$ 1.8
Post-preparative stability	99.0 $\pm$ 2.8	99.3 $\pm$ 1.2	101 $\pm$ 1.3

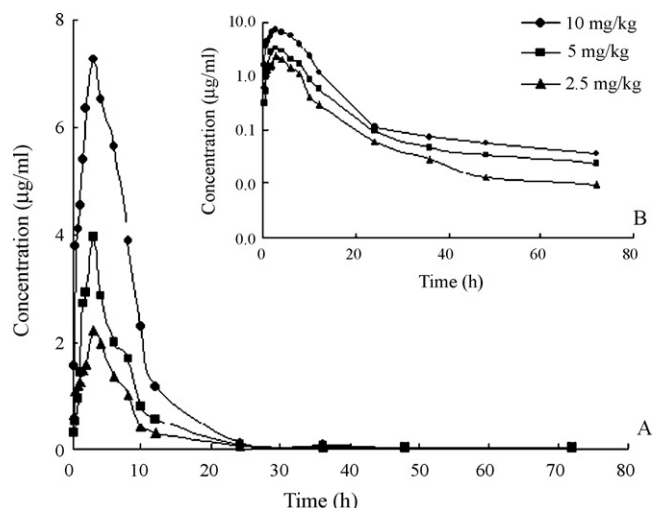


**Fig. 5.** Mean plasma concentration-time profiles of MCC-555 (A) and mean plasma concentration-time profiles (semilogarithm) of MCC-555 (B) after three doses to rats (2.5, 5 and 10 mg/kg). Symbols represented the observed data (mean  $\pm$  S.D., 5 rats/time point).

with MCC-555 concentrations up to 2  $\mu\text{g/ml}$  were diluted 5-fold with blank rat plasma and processed along with standards and QC samples. The precision (R.S.D. %) at each dilution ranged from 3.2 to 10.7  $c/o$  and accuracy (RE %) ranged from -5.6 to 8.2  $c/o$ . Plasma samples from the pharmacokinetics study of MCC-555 in rats that had MCC-555 concentrations above the quantification range were therefore diluted with blank plasma and then prepared and analyzed as described above.

### 3.4. Pharmacokinetics of MCC-555

Plasma concentrations of MCC-555 in rats following oral dosing at 2.5, 5, or 10 mg/kg were shown in Fig. 5, and corresponding mean pharmacokinetic parameters were listed in Table 4. Compartmental model analysis indicated that the MCC-555 pharmacokinetic profile after oral dosing fitted well to a two compartmental model. Based on the weighted regression analysis of the pooled data,  $C_{\text{max}}$  and  $\text{AUC}_{0-\infty}$  values increased as the dose increased in a linear manner ( $r^2 > 0.99$ ), with both being proportional to the administered dosages in rats. There were no significant differences between male and female rats for all pharmacokinetic characteristics studied. Following a single oral administration MCC-555 reached peak plasma concentration rapidly with a  $T_{\text{max}}$  of 3 h for all three doses. The pharmacokinetic properties of MCC-555 in rats obtained from the present study closely matched the reported in previous studies in dogs [14]. The elimination kinetics for MCC-555 in rats following three doses administration was not greatly different from our previous MCC-555 pharmacokinetic study in dogs conducted at the

**Table 4**

Pharmacokinetic parameters obtained after three doses administrations of MCC-555 in rats (mean  $\pm$  S.D., 5 rats/time point).

Parameter <sup>a</sup>	2.5 mg/kg	5 mg/kg	10 mg/kg
$t_{1/2}$ (h)	12.6 $\pm$ 4.2	13.7 $\pm$ 2.1	14.4 $\pm$ 3.8
$T_{\text{max}}$ (h)	3.0 $\pm$ 0.00	3.0 $\pm$ 0.00	3.0 $\pm$ 0.00
$C_{\text{max}}$ ( $\mu\text{g/ml}$ )	2.2 $\pm$ 0.7	3.7 $\pm$ 0.4	7.3 $\pm$ 1.2
$\text{AUC}_{0-72}$ ( $\mu\text{g h/ml}$ )	18.0 $\pm$ 3.8	32.8 $\pm$ 2.9	66.7 $\pm$ 4.1
$\text{AUC}_{0-\infty}$ ( $\mu\text{g h/ml}$ )	18.2 $\pm$ 2.9	33.5 $\pm$ 3.6	67.3 $\pm$ 3.7
MRT (h)	8.4 $\pm$ 0.7	9.8 $\pm$ 0.3	8.2 $\pm$ 0.5

<sup>a</sup>  $t_{1/2}$ : half-life of elimination;  $T_{\text{max}}$ : time to maximum concentration;  $C_{\text{max}}$ : maximum plasma concentration;  $\text{AUC}_{0-t}$ : area under the concentration-time curve from zero up to last quantifiable sample;  $\text{AUC}_{0-\infty}$ : area under the concentration-time curve from zero up to infinity; MRT: mean residence time.

same three doses (i.e.  $t_{1/2}$  = 12.6–14.4 h in rats vs.  $t_{1/2}$  = 12.5–16.4 h in dogs). However, Mean Residence Time (MRT) for MCC-555 was much shorter in rat at three doses (i.e. MRT = 8.2–9.8 h in rats vs. MRT = 15.7–19.1 h in dogs). The observed species difference in pharmacokinetics observed might be attributable to the intrinsic differences in the hepatic conjugation reactions involving the stereoselective disposition.

#### 4. Conclusion

A sensitive, selective and rapid UFLC method for the determination of MCC-555 in rat plasma is described for the first time. In this paper, we have demonstrated that the use of the reversed phase UFLC method resulted in improvements over the initial HPLC methods in terms of run time for MCC-555 than commonly used HPLC. The narrow peaks gained using the UFLC approach enable the detection of analytes at very low concentrations and with high resolution, making it appear preferable to HPLC. A sample preparation method employing liquid–liquid extraction based on 96-well format plates for the determination of MCC-555 concentrations in rat plasma was developed and validated over the range of 0.002–2 µg/ml. The UFLC method has been applied to the pharmacokinetic studies of MCC-555 in rats and proved to be reproducible and reliable for the high-throughput pharmacokinetic studies.

#### Acknowledgements

This work was supported by Shanghai Key Laboratory for Pharmaceutical Metabolites Research and Fundamental Research Key Project funded by Science & Technology department of Shanghai, P.R. China, Grant No. 03JC14005.

#### References

- [1] A.L. Werner, M.T. Travaglini, *Pharmacotherapy* 21 (2001) 1082.
- [2] P.S. Gillies, C.J. Dunn, *Drugs* 60 (2000) 333.
- [3] B. Lecka-Czernik, E.J. Moerman, D.F. Grant, J.M. Lehmann, S.C. Manolagas, R.L. Jilka, *Endocrinology* 143 (2002) 2376.
- [4] S.O. Rzonca, L.J. Suva, D. Gaddy, D.C. Montague, B. Lecka-Czernik, *Endocrinology* 145 (2004) 401.
- [5] M.A. Soroceanu, D. Miao, X.Y. Bai, H. Su, D. Goltzman, A.C. Karaplis, *J. Endocrinol.* 183 (2004) 203.
- [6] A.A. Ali, R.S. Weinstein, S.A. Stewart, A.M. Parfitt, S.C. Manolagas, R.L. Jilka, *Endocrinology* (2004) 1226.
- [7] O.P. Lazarenko, S.O. Rzonca, L.J. Suva, B. Lecka-Czernik, *Bone* 38 (2006) 74.
- [8] M.J. Reginato, S.T. Bailey, S.L. Krakow, C. Minami, S. Ishii, H. Tanaka, M.A. Lazar, *J. Biol. Chem.* 273 (1998) 32679.
- [9] L. Pickavance, P.S. Widdowson, P. King, S. Ishii, H. Tanaka, G. Williams, *Br. J. Pharmacol.* 125 (1998) 767.
- [10] R. Upton, P.S. Widdowson, S. Ishii, H. Tanaka, G. Williams, *Br. J. Pharmacol.* 125 (1998) 1708.
- [11] A.M. Muxlow, S. Fowles, P. Russell, *J. Chromatogr. B* 752 (2001) 77.
- [12] B.L. Kolte, B.B. Raut, A.A. Deo, M.A. Bagoor, D.B. Shinde, *J. Chromatogr. B* 788 (2003) 37.
- [13] J. He, Y.F. Hu, L.F. Duan, Z.R. Tan, L.S. Wang, D. Wang, W. Zhang, Z. Li, J. Liu, J.H. Tu, Y.M. Yao, Hong-Hao Zhou, *J. Pharm. Biomed. Anal.* 43 (2007) 580.
- [14] N. Sun, M. Lin, G.R. Fan, Z.Y. Hong, G.C. Lu, *J. Chromatogr. B* 835 (2006) 35.
- [15] J. Wen, Y.W. Wu, L.L. Zhang, Y.P. Qi, G.R. Fan, Y.T. Wu, Z. Li, *J. Chromatogr. B* 867 (2008) 153.
- [16] C. Wang, G.R. Fan, M. Lin, Y. Chen, W.Q. Zhao, Y.T. Wu, *J. Chromatogr. B* 854 (2007) 48.
- [17] Y. Chen, H.J. Miao, M. Lin, G.R. Fan, Z.Y. Hong, H.L. Wu, Y.T. Wu, *J. Chromatogr. B* 844 (2006) 268.
- [18] I. Durán-Merás, T. Galeano-Díaz, D. Airado-Rodríguez, *Food Chem.* 109 (2008) 825.
- [19] USFDA, 2001, <http://www.fda.gov/cder/guidance/4252fnl.htm>.
- [20] International Conference on Harmonization, Draft Guideline on Validation Procedures Definitions and Terminology, Federal Register, vol. 60, IFPMA, Switzerland, 1995, p. 11260.
- [21] S.M. Pathak, A.R. Kumar, P. Musmade, N. Udupa, *Talanta* 76 (2008) 338.
- [22] H.G. Gika, G.A. Theodoridis, I.D. Wilson, *J. Chromatogr. A* 1189 (2008) 314.



# Sandwich-type electrochemiluminescence immunosensor based on N-(aminobutyl)-N-ethylisoluminol labeling and gold nanoparticle amplification

Dayong Tian<sup>a</sup>, Chunfeng Duan<sup>a</sup>, Wei Wang<sup>a</sup>, Na Li<sup>a</sup>, Hao Zhang<sup>a</sup>, Hua Cui<sup>a,\*</sup>, Yingyu Lu<sup>b</sup>

<sup>a</sup> Department of Chemistry, University of Science and Technology of China, Hefei, Anhui 230026, People's Republic of China

<sup>b</sup> Department of The First Affiliated Hospital of Anhui Medical University, Hefei, Anhui 230026, People's Republic of China

## ARTICLE INFO

### Article history:

Received 5 September 2008

Received in revised form

19 November 2008

Accepted 20 November 2008

Available online 3 December 2008

### Keywords:

Electrochemiluminescence immunoassay

Human immunoglobulin G

N-(aminobutyl)-N-ethylisoluminol

Gold nanoparticles

## ABSTRACT

A novel electrochemiluminescence (ECL) sandwich-type immunosensor for human immunoglobulin G (hIgG) on a gold nanoparticle modified electrode was developed by using N-(aminobutyl)-N-ethylisoluminol (ABEI) labeling. The primary antibody, goat-anti-human IgG was first immobilized on a gold nanoparticle modified electrode, then the antigen (human IgG) and the ABEI-labeled second antibody was conjugated successively to form a sandwich-type immunocomplex. ECL was carried out with a double-step potential in carbonate buffer solution (CBS) containing 1.5 mM H<sub>2</sub>O<sub>2</sub>. The ECL intensity increased linearly with the concentration of hIgG over the range 5.0–100 ng/mL. The limit of detection was 1.68 ng/mL (S/N = 3). The relative standard deviation was 3.79% at 60 ng/mL (n = 9). The present immunosensor is simple and sensitive. It has been successfully applied to the detection of hIgG in human serums.

© 2008 Elsevier B.V. All rights reserved.

## 1. Introduction

Immunoassay has a wide range of applications in areas of clinical diagnostics [1,2], pharmaceutical studies [3], and environmental investigations [4]. Electrochemiluminescence immunoassay (ECLIA) has attracted much attention due to wide dynamic range, high sensitivity, low background, and simple formats of electrochemiluminescence (ECL) [5–11]. Sandwich-type is commonly used mode for ECLIA [9,11–14]. Ru-complex, for example, tris(2,2'-bipyridyl)ruthenium(II) (TBR), and tripropylamine (TPA) are the most widely used ECL label and coreactant, respectively [15–18]. In majority of the sandwich-type methods, polystyrene-type magnetic beads have been used as the immobilized support [9,11,12]. For many applications, for example, chip and disposable-type [19–22] biosensors are more convenient. Therefore, the electrode has also been used as the solid support for sandwich-type biosensor. However, only few papers have been published about the studies [13,14]. Bard and coworkers reported a method for the determination C reactive protein (CPR) on gold electrodes using TBR as ECL label. The CPR over the range 1–24 µg/mL could be detected [14]. Recently, Wang and coworkers utilized gold nanoparticle modified electrode as the immobilized support for the detection of albumin (BSA) and human immunoglobulin G (hIgG) via sandwich-type assay using 4-(dimethylamino) butyric acid (DMBA), an analogue of tripropyl-

amine, as ECL label. BSA and hIgG could be determined over the range 1–80 and 5–100 µg/mL, respectively. However, the sensitivity of the methods was limited [13].

N-(aminobutyl)-N-(ethylisoluminol) (ABEI), which is one kind of luminol derivatives, has been gradually used as an alternative ECL reagent. A promising property of this ECL reagent is relatively high ECL efficiency even when it was chemically attached to specific analytes. Therefore, ABEI as a labeling reagent has been used in homogenous immunoassay [23,24].

In our previous work, highly sensitive determination of luminol on a gold nanoparticle self-assembled electrode was achieved by virtue of the catalysis of gold nanoparticles [25]. However, the attachment of luminol to protein would lead to a decline in luminescence activity [26].

Therefore, in this work, ABEI labeling instead of luminol combined with gold nanoparticle amplification was used to develop a sensitive biosensor for the determination of hIgG. It was found that strong ECL intensity related to the concentration of hIgG was obtained under a double-step potential when ABEI-labeled anti-hIgG was immobilized on a gold nanoparticle modified electrode via sandwich mode. On this basis, an immunosensor for the detection of hIgG was proposed.

## 2. Experimental section

### 2.1. Chemicals and solutions

A HAuCl<sub>4</sub> stock solution (2% HAuCl<sub>4</sub>, w/w) was prepared by dissolving 1.0 g of HAuCl<sub>4</sub>·4H<sub>2</sub>O (Shanghai Reagent, China) in

\* Corresponding author. Tel.: +86 551 3606645; fax: +86 551 3600730.

E-mail address: [hcu@ustc.edu.cn](mailto:hcu@ustc.edu.cn) (H. Cui).

412 mL of purified water and stored at 4 °C. N-(aminobutyl)-N-(ethylisoluminol) (ABEI), N-hydroxysuccinimide (NHS), 1-ethyl-3-(3-dimethylaminopropyl) carbodiimide hydrochloride (EDC) and 1,3-propanedithiol were purchased from Sigma–Aldrich (USA). Bovine serum albumin (BSA), human immunoglobulin G (hIgG) and goat anti-human IgG were obtained from Solarbio (Beijing, China). A 2.0 mM stock solution of ABEI was prepared by dissolving 5.6 mg of ABEI in 10 mL of 0.10 mol/L phosphate buffer solution (PBS, pH 7.4) and was kept at 4 °C. All other reagents were of analytical grade. Ultrapure water was prepared by a Millipore Milli-Q system and used throughout.

## 2.2. Preparation of gold nanoparticle modified electrode

Gold nanoparticles with a diameter of 16 nm were prepared by reducing  $\text{AuCl}_4^-$  ions with 1% trisodium citrate [25] and stored at 4 °C. The bare gold electrode was polished to mirrorlike surface with chamois leather, rinsed with ethanol and ultrapure water, and then dried with filter paper. The electrode was then cleaned by cycling between 0 and 1.5 V versus SCE in  $\text{H}_2\text{SO}_4$  (0.5 mol/L) at a scan rate of 100 mV/s until reproducible cyclic voltammograms were obtained and was characterized by cycling between –0.2 and 0.6 V versus SCE in PBS (0.1 mol/L, pH 7.0) containing  $[\text{Fe}(\text{CN})_6]^{3-}$  and  $[\text{Fe}(\text{CN})_6]^{4-}$  (both 1 mM) at a scan rate of 100 mV/s until a well-shaped cyclic voltammogram with a peak-to-peak of 74 mV was observed. As-pretreated bare gold electrode was immersed in a 2 mM 1,3-propanedithiol–ethanol solution, and was incubated at room temperature for 20 h. The thiol self-assembled monolayer on the surface of the gold electrode was rinsed with ethanol and ultrapure water. After that, the thiol functionalized gold electrode was dipped into the gold colloid solution for 10 h at 4 °C. After rinsing with ultrapure water, the gold nanoparticle modified electrode was ready for further experiments.

Electrochemical impedance spectroscopy (EIS) experiment was used to monitor the modification procedures [27–31]. EIS was carried out on a CHI760B electrochemical workstation (Chenhua, China), PBS (0.1 mol/L, pH 7.0) containing  $[\text{Fe}(\text{CN})_6]^{3-}$  and  $[\text{Fe}(\text{CN})_6]^{4-}$  (both 1 mM) was used as working solution. The EIS results were recorded in the frequency range of 0.1 to 10 kHz at the formal potential of the corresponding redox couple and with a 5 mV amplitude of the alternating voltage. Gold nanoparticle

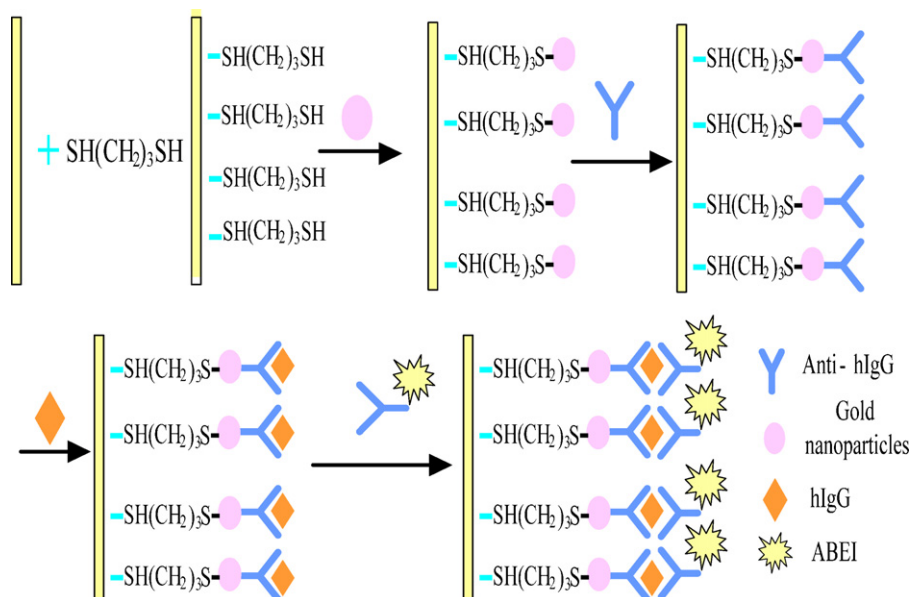
modified electrode was characterized by EIS (Figure S1 Supplementary Material). The results indicated that gold nanoparticles can not only be modified on a 1,3-propanedithiol modified electrode but also a favorable electron transfer property on the electrode can be obtained.

## 2.3. Preparation of ABEI-labeled anti-hIgG

Anti-hIgG labeled with ABEI was prepared as described in reference [32]. Anti-hIgG could be labeled with ABEI via amide reaction between  $-\text{NH}_2$  group in ABEI molecules and  $-\text{COOH}$  groups in anti-hIgG. EDC and NHS were used to catalyze the amide reaction. Briefly, 200  $\mu\text{L}$  containing 2 mM ABEI, 10 mg/mL NHS, and 20 mg/mL EDC was added to 1 mg anti-hIgG solution in 1 mL 0.10 mol/L PBS (pH 7.4) and incubated for 1 h at 37 °C. A model of PST-60 HL plus Thermo Shaker (Biosan, Latvia) was used to control the temperature of the reactions. The unreacted reagents were removed via dialysis for 2 days with 0.1 mol/L PBS (pH 7.4), and ABEI labeled anti-hIgG obtained. ABEI-labeled anti-hIgG was characterized by UV-vis spectroscopy (Figure S2 Supplementary Material). From Figure S2, it can be seen that the characteristic absorption peaks of ABEI-labeled anti-hIgG actually appeared at 278 nm and 318 nm, which corresponded to characteristic absorption peak of anti-hIgG antibody and ABEI, respectively. The results suggested that anti-hIgG could be labeled with ABEI.

## 2.4. Immobilization of hIgG via sandwich mode on a gold nanoparticle modified electrode

The gold nanoparticle modified electrode was further immersed in 0.1 mol/L PBS (pH 7.4) containing 0.1 g/L of the anti-hIgG and incubated over night at 4 °C. The modified electrode was subsequently rinsed thoroughly with 0.02 mol/L PBS (pH 7.4) to remove the weakly absorbed anti-hIgG. 1% (w/w) BSA in 0.01 mol/L PBS (pH 7.4) was used to saturate the possible bare gold nanoparticles for 30 min at 37 °C and rinsed by 0.02 mol/L PBS (pH 7.4). Then 40  $\mu\text{L}$  aliquots of different concentrations of hIgG in 0.01 mol/L PBS (pH 7.4) were dropped on with pipette modified electrode at 37 °C for 30 min, and rinsed with 0.02 mol/L PBS (pH 7.4) to remove unbound hIgG. Finally, 20  $\mu\text{L}$  aliquots of the ABEI-labeled anti-hIgG solution were dropped with pipette on the modified electrode



Scheme 1. Schematic illustration of the proposed ECLIA method.

at 37 °C for 30 min, and rinsed with 0.02 mol/L PBS (pH 7.4) to remove unbound ABEI-labeled anti-hIgG. The immobilization of hIgG onto the gold nanoparticle modified electrode and formation of sandwich-type (anti-hIgG)/hIgG/(ABEI-labeled anti-hIgG) are illustrated in Scheme 1.

### 2.5. ECL Measurements

ECL measurements were performed with a homemade ECL/Electrochemical cell system, including a model CHI760B electrochemical workstation (Chenhua, China), an H-type electrochemical cell (homemade), a model CR-105 photomultiplier tube (PMT) (Beijing, China) and a model REL-1 luminometer (Xi'an, china). A gold nanoparticle modified electrode immobilized by immunocomplex was used as the working electrode, a platinum wire as the counter electrode, and a silver wire as the quasi-reference electrode (AgQRE). Although the potential of the AgQRE was found to be essentially stable during an experiment, the measurements of  $\Delta E = E_{Ag/Ag^+} - E_{SCE}$  in different solution were taken for potential calibrations. A H<sub>2</sub>O<sub>2</sub> solution containing CBS (0.02 mol/L, pH 9.95) was used as working solution for the detection of hIgG. During measurements, a 3.0 mL portion of the working solution and blank solution without H<sub>2</sub>O<sub>2</sub> were added to the working compartment and the auxiliary compartment of the ECL cell, respectively. When a double-step potential (30 s pulse period, 0.25 s pulse time, 0.7 V pulse potential and 0 V initial pulse potential) was applied to the working electrode, an ECL signal was generated and recorded.

## 3. Results and discussion

### 3.1. ECL behavior

The ECL behavior of ABEI tagged on the immunocomplex was studied by cyclic voltammetry (CV) and double-step pulse potential. Figure 1 showed the ECL signals of the bare gold electrode, 1,3-propanedithiol modified electrode, gold nanoparticle modified electrode, and gold nanoparticle modified electrode immobilized with ABEI-labeled anti-hIgG via sandwich-type (100 ng/mL hIgG),

respectively. The results indicated that only the electrode immobilized with ABEI-labeled anti-hIgG could produce ECL signals. The ECL intensity generated by pulse potential was much stronger than that generated by cyclic voltammetry. This might be due to that more ABEIs were oxidized under pulse potential. Moreover, the ECL intensity generated by pulse potential was relatively stable in dozens of pulse potential in every experiment, whereas the ECL signals generated by cyclic voltammetry decreased with the increase of the cycling number (Figure 1A). This phenomenon was attributed to that the diffusion layer on the surface of electrode of ECL signals generated by cyclic voltammetry was difficult to recover in the next period. Therefore, the ECL signals generated by pulse potential were adopted in the following experiments.

The immobilization of antibody by gold nanoparticles has been well commented [13]. It has also been reported that the gold nanoparticles could catalyze the ABEI ECL [24]. The aim of the present work is to use the gold nanoparticles for the immobilization of the primary antibody and the amplification of the ABEI ECL. The result demonstrated that ABEI tagged on sandwich-type immunocomplex immobilized by gold nanoparticles exhibited excellent ECL property.

### 3.2. Optimization of the conditions for ECL

When a double-step potential was applied to the electrode, a pulse ECL signal was obtained. The pulse ECL intensity reached a stable value in second to ten periods in every experiment. The average intensity of three pulse ECL signal (three to five periods) in the stable area was used as an analytical signal for the detection of hIgG. To obtain the maximal ECL intensity, the effects of pH value, H<sub>2</sub>O<sub>2</sub> concentration, pulse period, pulse time, pulse potential, and initial potential on the ECL intensity were investigated.

#### 3.2.1. Effect of pH

It is well known that the ECL performance of luminol and its derivatives greatly depends on pH of the solution. The effect of pH in the range of 6.2–8.6 (PBS, 0.02 mol/L) and 8.6–11.3 (CBS, 0.02 mol/L) was examined. The maximal ECL intensity was obtained at pH 9.95

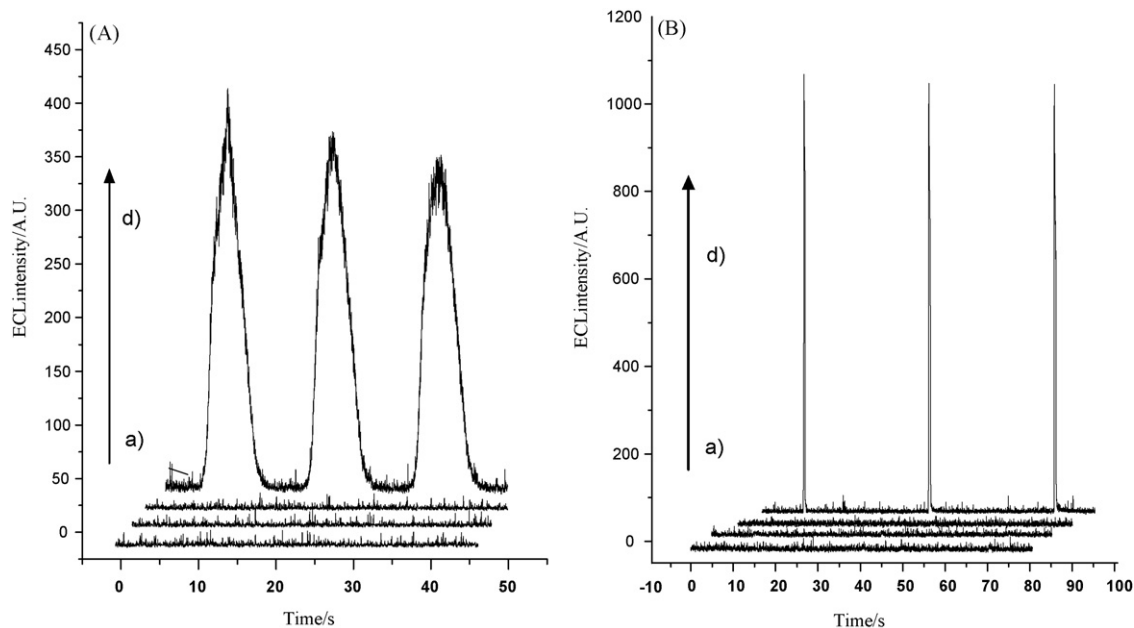


**Figure 1.** (A) ECL signals under cyclic voltammetry, from 0 to 0.7 V, scan rate of 100 mV/s. (B) ECL signals under pulse potential. Initial potential, 0 V; pulse period, 30 s; pulse time, 0.25 s; pulse potential, 0.7 V. ECL signals were obtained (a) on bare gold electrode, (b) on 1,3-propanedithiol modified electrode, (c) on gold nanoparticle modified electrode, and (d) on gold nanoparticle modified electrode combined with ABEI-labeled anti-hIgG via sandwich-type (100 ng/mL hIgG). All ECL signals were measured in 0.02 mM CBS (pH 9.95) solution containing 1.5 mM H<sub>2</sub>O<sub>2</sub>.



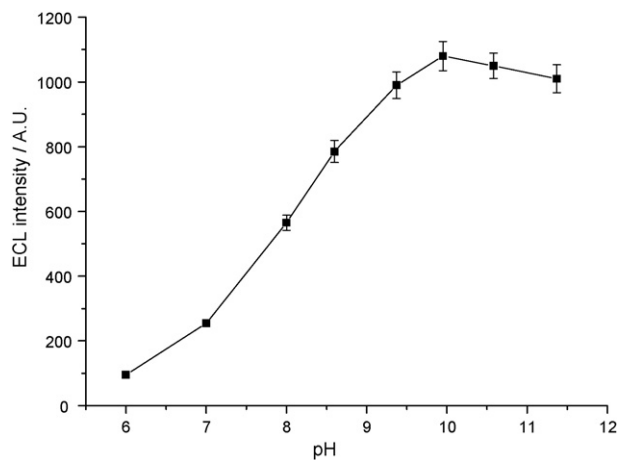


**Figure 2.** Effect of pH value on the ECL intensity. Initial potential, 0 V; pulse period, 30 s; pulse time, 0.25 s; pulse potential, 0.7 V;  $H_2O_2$ , 1.5 mM.

(Figure 2). Therefore, pH 9.95 was used in the following experiments.

### 3.2.2. Effect of $H_2O_2$ concentration

The change of ECL intensity with the concentration of  $H_2O_2$  is shown in Figure 3. From Figure 3, it can be seen that the ECL intensity markedly enhanced after the addition of  $H_2O_2$ . The ECL intensity increased with the increase of the concentration of  $H_2O_2$  and reached a maximum at 1.5 mM. This trend might be caused by of

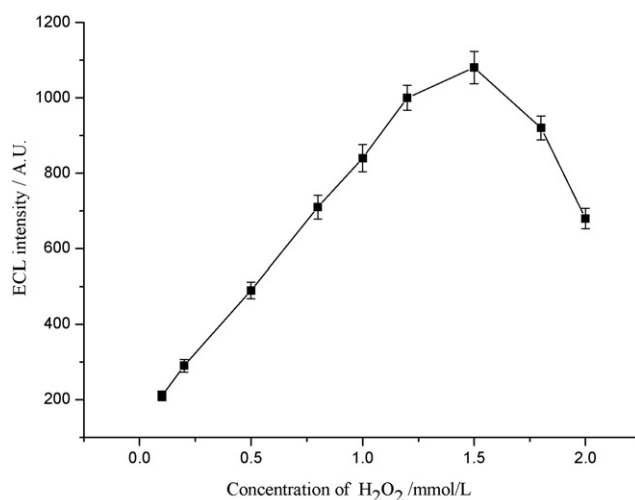


**Figure 3.** Effect of  $H_2O_2$  concentration on the ECL intensity. Initial potential, 0 V; pulse period, 30 s; pulse time, 0.25 s; pulse potential, 0.7 V; CBS, 0.02 mM (pH 9.95).

the co-oxidation function of  $H_2O_2$ . When the concentration of  $H_2O_2$  was higher than 1.5 mM, the ECL intensity decreased. Therefore, 1.5 mM  $H_2O_2$  was selected in the following experiments.

### 3.2.3. Effect of electrochemical parameters

The electrochemical parameters play very important roles due to that the ECL reaction is initiated by an electrochemical reaction

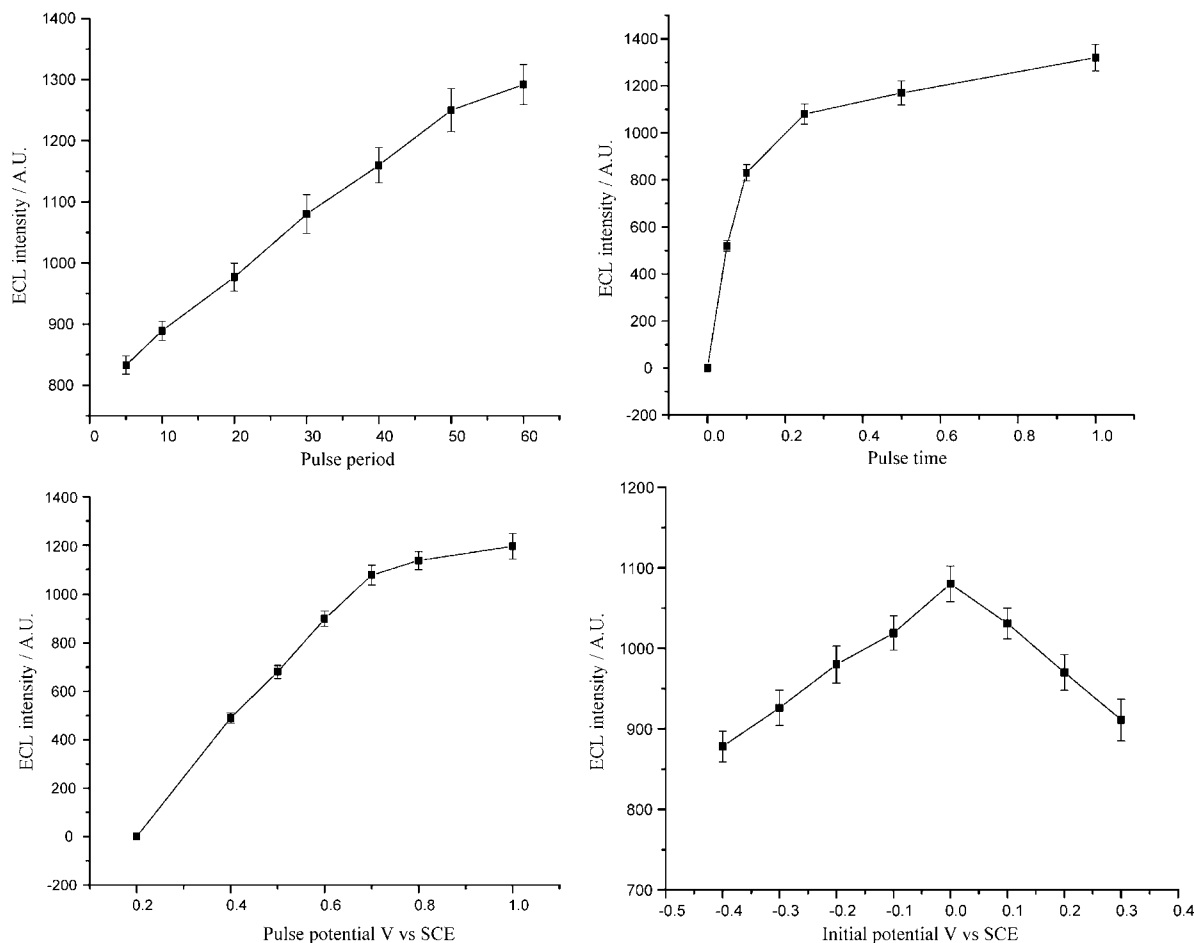


**Figure 4.** Effect of (A) pulse period, (B) pulse time, (C) pulse potential, and (D) initial pulse potential on ECL intensity.

at the electrode surface. Pulse wave was used as the work-waveform in the present work, because pulse wave probably produce more photons than the other waveforms in the same time [33].

The effect of the pulse period on the ECL intensity was investigated in the range of 5 – 60 s in CBS (0.02 mol/L) at pH 9.95 (Figure 4A). The ECL intensity showed a positive correlation with the pulse period. This phenomenon was attributed to more effective diffusion of H<sub>2</sub>O<sub>2</sub> in a longer pulse period. To obtain shorter analytical time and higher ECL intensity, a pulse period of 30 s was adopted in the following experiments.

The effect of the pulse time was examined in the range of 0–1 s (Figure 4B). The ECL intensity increased with the pulse time. However, when the pulse time was longer than 0.25 s, the ECL intensity decreased rapidly at the second period, and could not reach a stable ECL signal in the following period. This was due to that the diffusion layer on the surface of electrode became thicker in a relatively long pulse time, and was difficult to recover in the next pulse. Therefore, the pulse time of 0.25 s was chosen.

The effect of the pulse potential over the range 0.2–1.0 V (versus SCE) was studied (Figure 4C). Because the electro-oxidation of ABEI was much faster at higher electrode potential, a positive correlation between pulse potential and ECL intensity was also observed. However, if a high potential above 0.8 V was used, the stability and reproducibility of the modified electrode could be declined as shown in Figure S3. Wang and coworkers [13] proposed that Au-S bond between the 1,3-propanedithiol molecules and the gold electrode might be broken in high potential. Accordingly, the poor stability and reproducibility at higher potential may be due to the electro-oxidation of gold nanoparticles on the surface of electrode and the break of Au-S bond between the 1,3-propanedithiol molecules and the gold electrode. Thus, a pulse potential of 0.7 V was adopted.

The effect of the initial pulse potential in the range of –0.4 – 0.3 V was also investigated (Figure 4D). When the initial pulse potential was 0 V, a maximal ECL intensity was achieved. This is probably due to the initial pulse potential of 0 V has a better diffusion controlled reaction on the surface of the modified electrode. Therefore, this initial potential was used in the following experiments.

Finally, the optimized conditions for electrochemical parameters were optimized as follows: 30 s pulse period, 0.25 s pulse time, 0.7 V pulse potential and 0 V initial pulse potential.

### 3.3. Analytical performance

Under the optimized conditions, it was found that the ECL intensity increased linearly with the concentration of hIgG, indicating that it was feasible for the determination of hIgG via direct immobilization on gold nanoparticle modified electrode. The calibration curve for the determination of hIgG is shown in Figure 5. The regression equation was  $I = 37.85 + 9.61 C$  and the correlation coefficient was 0.9959, where  $I$  was ECL intensity and  $C$  was the concentration of hIgG (ng/mL). The linear range for the detection of hIgG was 5–100 ng/mL and the limit of detection was 1.68 ng/mL ( $S/N = 3$ ). The relative standard deviation of nine replicate determinations of 60 ng/mL hIgG was 3.79% ( $n = 9$ ). The results demonstrated that the proposed method could be used for the determination of hIgG. Moreover, the sensitivity of the present method has three orders of magnitude improvement over other sandwich-type methods based on the modified electrode as the immobilized support [13,14]. Therefore, the proposed method is sensitive compared with other sandwich-type biosensor based on the modified electrode as an immobilized support.

Control experiments were conducted to investigate the specificity of the ECL immunosensor protocol. When using BSA

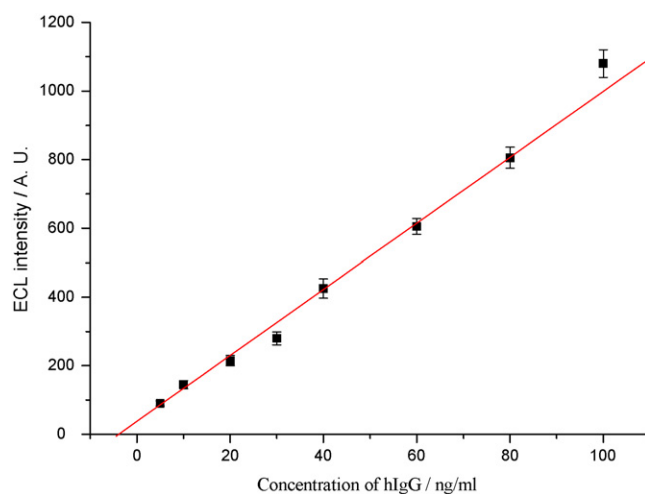


**Figure 5.** Calibration curve of ECL intensity versus concentration of hIgG. Initial potential, 0 V; pulse period, 30 s; pulse time, 0.25 s; pulse potential, 0.7 V; H<sub>2</sub>O<sub>2</sub>, 1.5 mM; CBS, 0.02 mM (pH 9.95).

(100 μg/mL) instead of hIgG for the ECL immunoassay, the ECL intensity was similar to the blank. It was also demonstrated that no ECL signal was observed from the system when omitting the antigen, hIgG. These results showed that the attachment of ABEI-labeled antibody to the surface of the gold nanoparticle modified electrode was essential to generate the enhanced ECL signals and the specificity of the present immunoassay protocol was good.

### 3.4. Application of the ECL immunosensor in human serum samples

The feasibility of the immunosensor for the clinical applications was investigated by analyzing several real samples, freshly obtained from University of Science and Technology of China Hospital. Before the test, the samples were diluted appropriately step by step to be in the linear range of the proposed method. The results of each corresponding serum sample obtained from Inspection Department of The First Affiliated Hospital of AnHui Medical University with turbidimetry method were used for a comparison. Table 1 showed that the values obtained by the proposed method were comparable with that by the clinic method (Relative deviation < 10%). Recovery experiments were also conducted (Table 2). It was found that the recoveries were in the range of 89.6–117.8%. Therefore, the developed immunosensor is applicable for the determination of hIgG in real samples, human serums.

**Table 1**

HlgG content in human serum samples measured by the proposed method and clinic method.

Sample	Clinic method (mg/mL)	The proposed method (mean ± SD $n = 5$ ) (mg/mL)	Relative deviation (%)
No. 1	10.53	9.81 ± 0.33	6.8
No. 2	13.79	12.52 ± 0.78	9.9
No. 3	13.14	12.34 ± 0.46	6.1
No. 4	12.35	12.90 ± 0.51	4.5
No. 5	9.28	10.02 ± 0.89	8.0
No. 6	11.65	11.04 ± 0.63	5.2
No. 7	9.87	9.21 ± 0.47	6.7
No. 8	12.22	13.02 ± 1.01	6.5
No. 9	11.82	11.27 ± 0.87	4.7

The serum sample was diluted appropriately.

Initial potential, 0 V; pulse period, 30 s; pulse time, 0.25 s; pulse potential, 0.7 V; H<sub>2</sub>O<sub>2</sub>, 1.5 mM; CBS, 0.02 mM (pH 9.95).

**Table 2**  
Recovery of hIgG in human serum samples.

Background content (ng/mL)	Add concentration (ng/mL)	Detected concentration (mean $\pm$ SD $n=5$ ) (ng/mL)	Recovery ratio (%)
9.81	5	14.29 $\pm$ 0.21	89.6
9.81	10	21.20 $\pm$ 0.57	113.9
9.81	20	33.37 $\pm$ 0.83	117.8
9.81	30	42.63 $\pm$ 1.02	109.4
9.81	50	64.91 $\pm$ 1.73	110.2

The serum sample was diluted appropriately.

Recovery ratio = (Detected concentration – Background content) / Add concentration  $\times$  100%.

Initial potential, 0V; pulse period, 30s; pulse time, 0.25s; pulse potential, 0.7V; H<sub>2</sub>O<sub>2</sub>, 1.5 mM; CBS, 0.02 mM (pH 9.95).

#### 4. Conclusion

A novel ECL immunosensor was developed by using ABEI labeling combined with gold nanoparticle amplification. Anti-hIgG can be effectively immobilized directly on a gold nanoparticle modified electrode, hIgG and anti-hIgG tagged with ABEI labels can be subsequently attached by conjugation. The formation of sandwich-type (anti-hIgG)/hIgG/(ABEI-labeled anti-hIgG) immunocomplex exhibited excellent ECL responses with a double-step potential in CBS containing 1.5 mM H<sub>2</sub>O<sub>2</sub>. HlgG in a range of 5.0–100 ng/mL could be detected by use of the ECL intensity. The sensitivity of the immunosensor has three orders of magnitude improvement over other sandwich-type methods based on the modified electrode as the immobilized support. Although the sensitivity of the present method is lower than that of homogeneous ECL immunoassay for hIgG using ABEI as a label at gold nanoparticles modified electrode [23,24], the practical applications of the homogeneous method in clinic diagnoses remain a challenge because the matrix of practical samples, for example, serum, may interfere with the determination of hIgG. It was reported that metal ions and organic compounds could enhance or inhibit the ECL intensity of luminol [34,35], leading to a change in ECL intensity. ABEI is a derivative of luminol. Metal ions and organic compounds in practical samples might influence the ECL intensity of ABEI, interfering with the determination of hIgG. Nevertheless, in the present method, the interferences in the matrix can be well separated from hIgG by simply washing the electrode, and thus the method has been successfully applied to the detection of hIgG in real samples, human serums. This work demonstrated that gold nanoparticles as the immobilized substrates could effectively amplify the ECL of sandwich-type immunocomplex labeled with ABEI, which is well suitable for developing a highly sensitive biosensor. In principle, the proposed technique should be applicable for the determination of other biological substances based on the immobilized DNA hybridizations and formation of antibody-antigen immunocomplex on a gold nanoparticle self-assembled electrode.

#### Acknowledgement

The support of this research by the National Natural Science Foundation of P.R. China (Grant Nos. 20625517 and 20573101), and the Overseas Outstanding Young Scientist Program of Chinese Academy of Sciences are gratefully acknowledged.

#### Appendix A. Supplementary data

Supplementary data associated with this article can be found at doi:10.1016/j.talanta.2008.11.037.

#### References

- [1] N. Christodoulides, M. Tran, P.N. Floriano, M. Rodriguez, A. Goodey, M. Ali, D. Neikirk, J.T. McDevitt, *Anal. Chem.* 74 (2004) 3030–3036.
- [2] K. Skogstrand, P. Thorsen, B. Nørgaard-Pedersen, D.E. Schendel, L.C. Sørensen, D.M. Hougaard, *Clin. Chem.* 51 (2005) 1854–1866.
- [3] A.P. Deng, M. Himmelsbich, Q.Z. Zhu, S. Frey, M. Sengl, W. Buchberger, R. Niessner, D. Knopp, *Environ. Sci. Technol.* 37 (2003) 3422–3429.
- [4] J.M. Van Emon, C. Gerlach, *J. Microbiol. Methods* 32 (1998) 121–131.
- [5] M.M. Richer, *Chem. Rev.* 104 (2004) 3003–3036.
- [6] Y. Li, H.L. Qi, Y.G. Peng, C.X. Zhang, *Electrochem. Commun.* 9 (2007) 2571–2575.
- [7] A.W. Kingt, *Trends. Anal. Chem.* 18 (1999) 47–62.
- [8] Y. Li, H.L. Qi, F. Fang, *Talanta* 72 (2007) 1704–1709.
- [9] W.J. Miao, A.J. Bard, *Anal. Chem.* 76 (2004) 5379–5386.
- [10] F. Li, Y.Q. Pang, X.Q. Lin, H. Cui, *Talanta* 59 (2003) 626–627.
- [11] W. Zhan, A.J. Bard, *Anal. Chem.* 79 (2007) 459–463.
- [12] Y. Namba, M. Usami, O. Suzuki, *Anal. Sci.* 15 (1999) 1087–1093.
- [13] X.B. Yin, B. Qi, X.P. Sun, X.R. Yang, E.K. Wang, *Anal. Chem.* 77 (2005) 3525–3530.
- [14] W.J. Miao, A.J. Bard, *Anal. Chem.* 75 (2003) 5825–5834.
- [15] H. Wei, J.F. Liu, L.L. Zhou, J. Li, X. Jiang, J.Z. Kang, X.R. Yang, S.J. Dong, E.K. Wang, *Chem. Eur. J.* 14 (2008) 3687–3693.
- [16] L.H. Shi, X.Q. Liu, H.J. Li, G.B. Xu, *Anal. Chem.* 78 (2006) 7330–7334.
- [17] H. Wei, Y. Du, J.Z. Kang, E.K. Wang, *Electrochem. Commun.* 9 (2007) 1474–1479.
- [18] J. Zhang, H.L. Qi, Y. Li, J. Yang, Q. Gao, C.X. Zhang, *Anal. Chem.* 80 (2008) 2888–2894.
- [19] L.J. Lucas, J.N. Chesler, J.-Y. Yoon, *Biosens. Bioelectron.* 23 (2007) 675–681.
- [20] R. Kurita, Y. Yokota, Y. Sato, F. Mizutani, O. Niwa, *Anal. Chem.* 78 (2006) 5525–5531.
- [21] J. Wang, B.M. Tian, *Anal. Chem.* 70 (1998) 1682–1685.
- [22] G.D. Liu, Y.-Y. Lin, J. Wang, H. Wu, C.M. Wai, Y.H. Lin, *Anal. Chem.* 79 (2007) 7644–7653.
- [23] K. Arai, K. Takahashi, F. Kusu, *Anal. Chem.* 71 (1999) 2237–2240.
- [24] H.L. Qi, Y. Zhang, Y.G. Peng, C.X. Zhang, *Talanta* 75 (2008) 684–690.
- [25] H. Cui, Y. Xu, Z.F. Zhang, *Anal. Chem.* 76 (2004) 4002–4010.
- [26] C. Dodeigne, L. Thunus, R. Lejune, *Talanta* 51 (2000) 415–439.
- [27] Y.Z. Fu, R. Yuan, D.P. Tang, Y.Q. Chai, L. Xu, *Colloids Surf. B40* (2005) 61–66.
- [28] S.L. Pan, L. Rothberg, *Langmuir* 21 (2005) 1022–1027.
- [29] J.J. Zhao, C.R. Bardbury, S. Huclova, I. Potapova, M. Carrara, D.J. Fermin, *J. Phys. Chem. B* 109 (2005) 22985–22994.
- [30] S.X. Zhang, N. Wang, H.J. Yu, Y.M. Niu, C.Q. Sun, *Bioelectrochemistry* 67 (2005) 15–22.
- [31] I. Szymanska, H. Radecka, J. Radecki, *Sens. Actuators B* 75 (2001) 95–100.
- [32] M.-L. Calvo-Munoz, A. Dupont-Filliard, M. Billon, S. Gillerez, G. Bidan, C. Marquette, L. Blum, *Bioelectrochemistry* 66 (2005) 139–143.
- [33] M. Yang, C.Z. Liu, K.J. Qian, P.G. He, Y.Z. Fang, *Analyst* 127 (2002) 1267–1271.
- [34] K.A. Fahnrich, M. Pravda, G.G. Guilbault, *Talanta* 54 (2001) 531–559.
- [35] M.J. Shi, H. Cui, *Acta Chim. Sinica* 65 (2007) 2555–2562.



# A molecularly imprinted polymer-coated nanocomposite of magnetic nanoparticles for estrone recognition

Xin Wang<sup>a</sup>, Lianyan Wang<sup>a</sup>, Xiwen He<sup>a</sup>, Yukui Zhang<sup>a,b</sup>, Langxing Chen<sup>a,\*</sup>

<sup>a</sup> Department of Chemistry, Nankai University, Tianjin 300071, PR China

<sup>b</sup> Dalian Institute of Chemical Physics, Chinese Academy of Sciences, Dalian 116011, PR China

## ARTICLE INFO

### Article history:

Received 1 August 2008

Received in revised form

12 November 2008

Accepted 13 November 2008

Available online 27 November 2008

### Keywords:

Fe<sub>3</sub>O<sub>4</sub> magnetic nanoparticles

Molecularly imprinted polymer

Estrone

Biochemical separation

## ABSTRACT

In this study, we synthesized Fe<sub>3</sub>O<sub>4</sub> magnetic nanoparticles coated estrone-imprinted polymer with controlled size using a semi-covalent imprinting strategy. In this protocol, the estrone–silica monomer complex (EstSi) was synthesized by the reaction 3-(triethoxysilyl)propyl isocyanate with estrone, where the template was linked to the silica coating on the iron oxide core *via* a thermally reversible bond. The removal of the template by a simple thermal reaction produced specific estrone recognition sites on the surface of silica shell. The resulting estrone-imprinted polymer coating Fe<sub>3</sub>O<sub>4</sub> magnetic hybrid nanoparticles exhibit a much higher specific recognition and saturation magnetization. The hybrid nanoparticles have been used for biochemical separation of estrone.

© 2008 Elsevier B.V. All rights reserved.

## 1. Introduction

In more recent years, magnetic nanoparticles (MNPs) have been studied for biomedical and biotechnological applications, including targeted drug delivery, MRI contrast enhancement, biosensor, rapid environmental and biological separation, and concentration of trace amounts of specific targets, such as bacteria or leukocytes and proteins [1–6]. For many of these applications, surface modification of MNPs is a key challenge. In general, surface modification can be accomplished by physical/chemical adsorption or surface coating of specific ligands, depending on the specific applications. When modified with a specific functional polymer, for example, the molecularly imprinted polymer (MIP), these magnetic nanoparticles coated MIP could be used to separate and concentrate chemicals more conveniently with the help of an external magnetic field. In this study, we focused on the development of a new methodology for preparing MNPs attached functional moieties of specific recognition with tailor-made properties through molecular imprinting technique.

The molecular imprinting technique is an attractive method for the generation of polymer-based molecular recognition elements tailor-made for a given target or group of target molecules [7,8]. The technique involves polymerization of functional monomers and a cross-linker around a template. Extraction of the template

leaves behind recognition sites of functional and shape complementarity to the template. MIP has been used in a variety of applications, such as separation media [9], mimicking antibody [10], chemical and biochemical sensing [11]. Therefore, by combining MNPs coated artificial receptor tailor-made with specific recognition and magnetic property can be an ideal candidate for the multifunctional nanomaterial toward bioseparation. The mechanical/chemical stability, low cost, ease of preparation of molecularly imprinted materials have attracted extensive research interest. However, they suffer from some drawbacks in certain applications, such as the heterogeneous distribution of the binding sites, low binding capacity and selectivity, poor site accessibility and slow binding kinetics. The development of molecular imprinting nanotechniques will provide a potential solution to overcome these problems [12–21]. Nanosized molecular imprinted materials (MIP nanoparticles [12–15], MIP nanocapsule [16], MIP nanowire [17–19], MIP nanotube [20,21]) having a small dimension with high surface-to-volume ratio are expected to improve the removal of template molecules, the binding capacity and fast binding kinetics over normal imprinting materials. By incorporating magnetic iron oxide, the superparamagnetic composite MIP beads with an average diameter of 13 μm were prepared by Ansell and Mosbach using suspension polymerization in perfluorocarbon liquid in the first time [22]. The magnetic MIP nanowires for theophylline using a nanopores alumina template was reported by Li et al. [23]. Tan recently reported bovine serum albumin surface-imprinted sub-micrometer particles (500–600 nm) with magnetic susceptibility through miniemulsion polymerization [24].

\* Corresponding author. Tel.: +86 22 23505091 fax: +86 22 23502358.

E-mail address: [lxchen@nankai.edu.cn](mailto:lxchen@nankai.edu.cn) (L. Chen).

In this work, we report the synthesis of the MIP-coated hybrid nanoparticles by “semi-covalent” imprinting technique [25] through a thermally reversible covalent bond and application for biochemical separation of estrone. Estrone is one of naturally estrogenic hormones, can be toxic and carcinogenic even at low levels. It has been reported that estrone influenced the normal development and maturation of female, and was suspected to induce cancer and has often been identified as the major contributor to the endocrine disrupting activity observed in environmental water samples [26,27]. In order to prevent these uncontrolled effects on human health and deleterious effects on the aquatic environment, it is of great significance to develop new adsorbents for the separation of estrone. Therefore estrone was selected as template molecule in this study. Chang et al. [28] reported the use of a thermally reversible covalent bond for imprinting estrone on silica spheres with diameter of 1.5–3  $\mu\text{m}$ . In this study, based on an approach modified from Chang, we bring together the  $\text{Fe}_3\text{O}_4$  magnetic core coated with molecularly imprinted silica films of nanosize. Compared to traditional MIPs nanoparticles, the molecular imprinted magnetic hybrid display several advantages: (i) the superparamagnetic iron oxide core enables the particles replace the centrifugation step with a magnetic separation, and facilitates the application of magnetic MIP in immunoassay and magnetically stabilized-fluidised-bed separation. (ii) The semi-covalent imprinting can be looked upon as a hybrid approach in which the imprinting is covalent, but the rebinding is noncovalent in nature. (iii) There are no randomly distributed functional groups and the binding sites are more uniform in nature [25]. (iv) The template removal by hydrolysis leaves the binding sites in the silica shell during the imprinting step, and the template molecules can reach the imprinting sites easily and quickly during the rebinding step.

## 2. Experimental

### 2.1. Materials

3-(Triethoxysilyl)propyl isocyanate, 3-aminopropyl triethoxysilane, tetraethoxysilane (TEOS), dibutyltin dilaurate (DBDU) were purchased from Alfa Aesar Chemical Company. Estrone and testosterone propionate were obtained from Sigma.  $\text{FeCl}_2 \cdot 4\text{H}_2\text{O}$ ,  $\text{FeCl}_3 \cdot 6\text{H}_2\text{O}$ , ammonium hydroxide (25%) were purchased from Tianjin Chemicals Ltd. THF and DMSO were used after

purification by standard methods. Other chemicals were used as received without further purification.

### 2.2. Preparation of $\text{Fe}_3\text{O}_4$ MNPs

$\text{FeCl}_2 \cdot 4\text{H}_2\text{O}$  (1.72 g) and  $\text{FeCl}_3 \cdot 6\text{H}_2\text{O}$  (4.72 g) was dissolved in 80 mL of deaerated highly purified water contained in a three neck flask with vigorous stirring (800 rpm) under nitrogen. As the temperature was elevated to 80 °C, 10 mL of ammonium hydroxide was added drop by drop, and the reaction was maintained for 30 min. The black product was separated by putting the vessel on a Nd–Fe–B permanent magnet and the supernatant was decanted. The black precipitate was washed for six times with highly purified water to remove the unreacted chemicals, then the black product  $\text{Fe}_3\text{O}_4$  was dried in the vacuum.

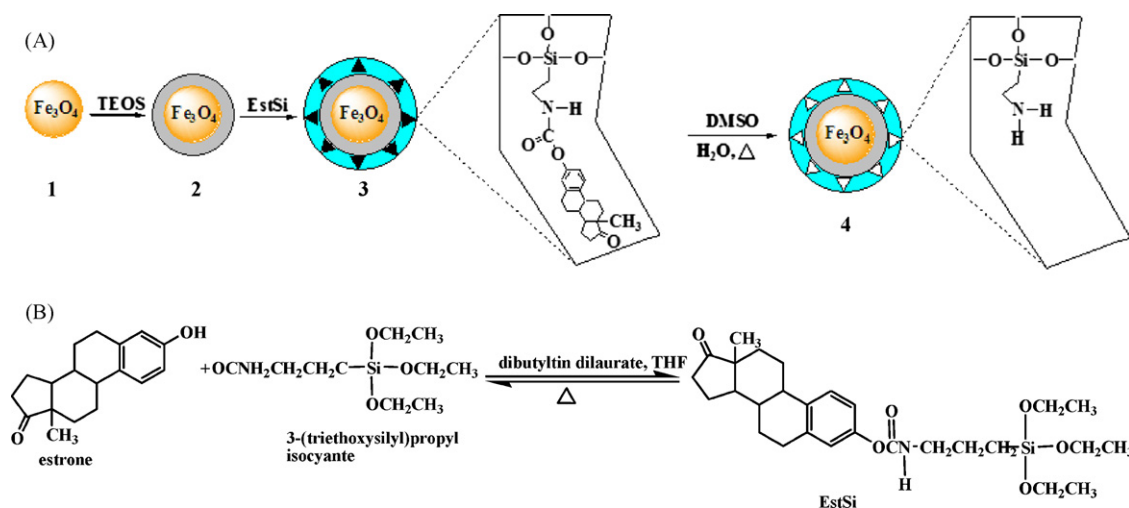
### 2.3. Synthesis of the $\text{Fe}_3\text{O}_4@/\text{SiO}_2$ MNPs

300 mg superparamagnetic magnetite nanoparticles were dissolved in 50 mL 2-propyl alcohol and 4 mL of highly purified water by sonication for 15 min, followed by the addition of 5 mL ammonium hydroxide and 2 mL TEOS sequentially. The mixture was reacted for 12 h at the room temperature under a continuous stirring. The resultant product was collected by an external magnetic field, and rinsed with highly purified water for six times thoroughly, and dry to powder in the vacuum.

### 2.4. Preparation of estrone-imprinted MNPs and a control silica-coated MNPs

EstSi (Scheme 1B) was synthesized according to the Chang et al.'s method [28]. The  $\text{Fe}_3\text{O}_4@/\text{SiO}_2$  MNPs (1 g) was dissolved into acetate buffer (0.1 mol L<sup>-1</sup>, pH 5.2), then EstSi (0.12 g) was added. The mixture was reacted for 12 h at room temperature with a mechanic stirring. The product was separated by the magnetic field and washed with acetone, then dried to powder. This imprinting MNPs (0.3 g) were added to a solution of DMSO (10 mL) and water (2 mL). The mixture was stirred for 3 h at 180 °C. Finally, estrone-imprinted MNPs with specific sites was separated by magnetic field and dried in vacuum oven at 25 °C for a week.

Control silica-coated MNPs were synthesized in the almost same manner for the preparation of estrone-imprinted MNPs except for 3-aminopropyl triethoxysilane was used in place of EstSi.



**Scheme 1.** (A) Multistep synthesis of estrone-imprinted MNPs.  $\text{Fe}_3\text{O}_4$  MNPs (1) were prepared by coprecipitation method and the MNPs surface was then transformed to silica shell by a sol-gel process using TEOS to give  $\text{Fe}_3\text{O}_4@/\text{SiO}_2$  MNPs (2). The  $\text{Fe}_3\text{O}_4@/\text{SiO}_2$  MNPs reacted with a template-silica monomer complex (EstSi) to produce silica surface functionalized with estrone-imprinted polymer (3). After remove the template estrone by simple thermal reaction, estrone-imprinted polymer coated MNPs (4) were obtained. (B) Synthesis of EstSi.

### 2.5. Binding experiment

Estrone-imprinted MNPs (20 mg) and control silica-coated MNPs (20 mg) were added to the solutions of estrone in chloroform (10 mL) at various concentrations respectively. After incubating for 24 h, the estrone-imprinted MNPs and control silica-coated MNPs were isolated by an external magnetic field, and rinsed with THF and chloroform. The filtrate was concentrated to dryness by evaporation of the solvent before HPLC analysis. The amount of estrone bound to the MNPs was determined by HPLC.

Reverse phase HPLC analysis was performed on a Shimadzu LC-20A system (Shimadzu, Kyoto, Japan) equipped with a ODS column and a UV–vis detector (set at 254 nm for all the compounds). The data were collected and analyzed using LCsolution software. The eluent is methanol at the flow rate of 1.0 mL min<sup>-1</sup>. For each analysis 20 μL of sample was injected.

### 2.6. Characterization

A Tecnai G<sup>2</sup> 20 S-TWIN microscope was used to obtain transmission electron microscope (TEM) images of Fe<sub>3</sub>O<sub>4</sub> MNP and estrone-imprinted MNPs. For TEM analyses, samples were prepared by placing one or two drops of nanoparticle solution onto the carbon-coated copper grid and drying it in air at room temperature.

Fourier transform infrared (FT-IR) spectra were recorded on a AVATAR 360 (Nicolet Corp., USA) and samples were dried at 80 °C in vacuo oven for at least 12 h prior to fabrication of the KBr pellet.

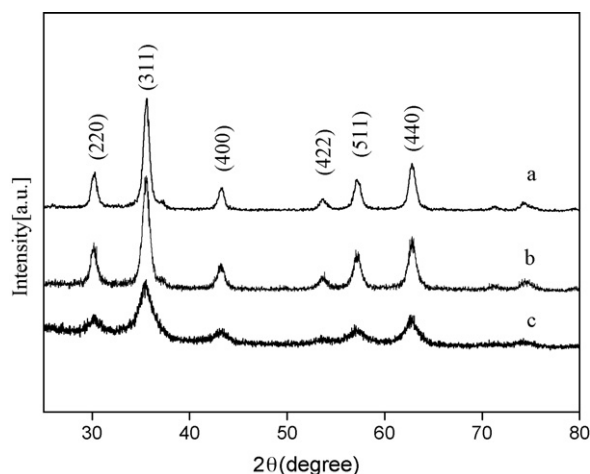


Fig. 1. XRD patterns of Fe<sub>3</sub>O<sub>4</sub> (a), Fe<sub>3</sub>O<sub>4</sub>@SiO<sub>2</sub> (b) and estrone-imprinted polymer coated MNPs (c).

In this context, 2 mg of each sample was thoroughly mixed and crushed with 100 mg of KBr, and the mixture was used for pellet fabrication. Fifty scans of the region between 400 and 4000 cm<sup>-1</sup> were collected for each FT-IR spectrum recorded.

<sup>1</sup>H NMR spectra of EstSi was investigated by Varian Mercury Vx-300.

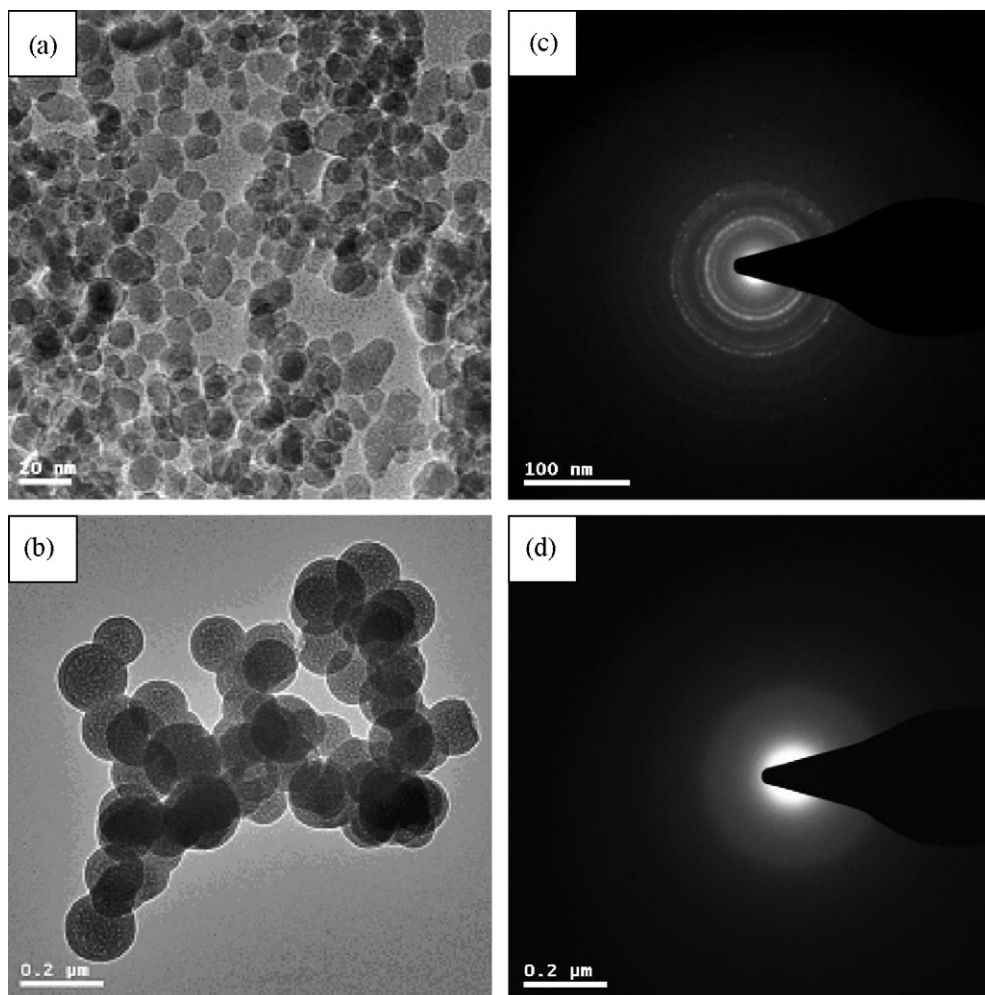


Fig. 2. TEM images of Fe<sub>3</sub>O<sub>4</sub> MNPs (a) and estrone-imprinted MNPs (b), and SAED of Fe<sub>3</sub>O<sub>4</sub> MNPs (c) and estrone-imprinted MNPs (d).

The identification of crystalline phase of the synthesized nanoparticles was performed by a Rigaku D/max/2500v/pc (Japan) X-ray diffractometer with Cu K $\alpha$  source. The  $2\theta$  angles probed were from  $10^\circ$  to  $80^\circ$  at a rate  $4^\circ/\text{min}$ .

The magnetic properties were analyzed with a vibrating sample magnetometer (VSM) (LDJ 9600-1, USA).

### 3. Results and discussion

#### 3.1. Preparation of imprinted magnetic nanoparticles

The synthesis of the MIP-coated MNPs via a multistep procedure is illustrated in Scheme 1A, which involves synthesis of  $\text{Fe}_3\text{O}_4$  MNPs, silica-shell deposition, MIP-functionalized onto the silica surface, and final extraction of estrone and generation of the recognition site.  $\text{Fe}_3\text{O}_4$  MNPs were synthesized by modifying the procedure as reported by Kang et al. [29]. The MNP surface was then transformed to silica shell by a sol-gel process [30,31] using tetraethoxysilane (TEOS) to give  $\text{Fe}_3\text{O}_4@\text{SiO}_2$ . Superparamagnetic nanoparticles having a silica shell provides good biocompatible, non-toxic coating as well as a hydrophilic surface. Furthermore, the silanol group on the silica coated can be easily modified to link bioconjugators by the sol-gel method with interesting biofunctionalities [32–34]. In this study, we used a thermally reversible bond for the preparation of template-silica monomer complex, which allowed us to remove the template by simple thermal reaction and simultaneously introduce functional groups into the cavity on the surface of MNPs. The silica coating MNPs  $\text{Fe}_3\text{O}_4@\text{SiO}_2$  reacted with EstSi to produce silica surface functionalized with MIPs.

EstSi (Scheme 1B) was synthesized by the 3-(triethoxysilyl)propyl isocyanate with estrone in the presence of dibutyltin dilaurate according to the Chang et al.'s method [28]. The reaction

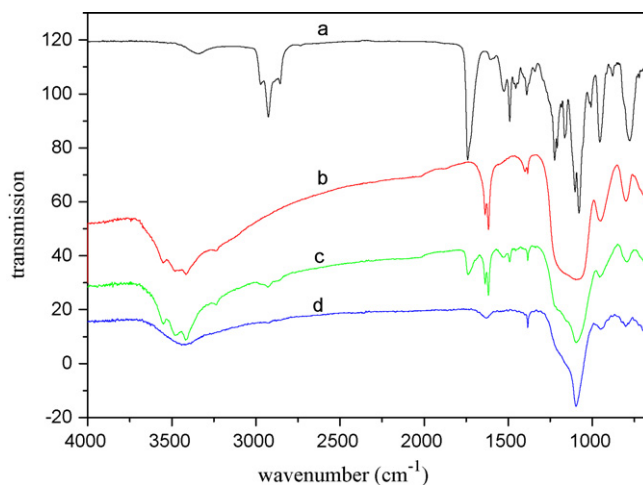


Fig. 3. FT-IR spectra of EstSi (a),  $\text{Fe}_3\text{O}_4@\text{SiO}_2$  (b), molecularly imprinted MNPs (c) before and (d) after extraction of estrone.

occurred between the isocyanate group of 3-(triethoxysilyl)propyl isocyanate and a phenol moiety of estrone, forming a thermally cleavable urethane bond.

The thermal cleavage of the urethane bond was investigated by  $^1\text{H}$  NMR. EstSi was dissolved in  $\text{DMSO}-d_6$  and its  $^1\text{H}$  NMR spectra at room temperature was investigated by Varian Mercury Vx-300. The aromatic ring proton peak appeared at 7.270, 6.835, 6.777 ppm, and the NH peak appeared at 7.675 showed the urethane is formed. The thermally cleavable urethane bond is stable at room temperature and undergoes reversible cleavage at elevated temperature and then the MIP coating was prepared by a sol-gel reaction of the EstSi.

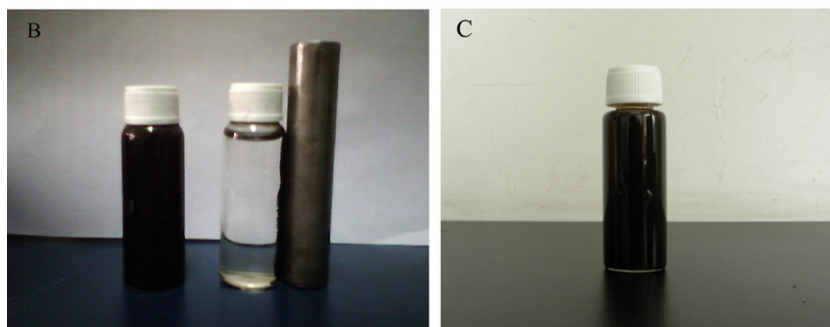
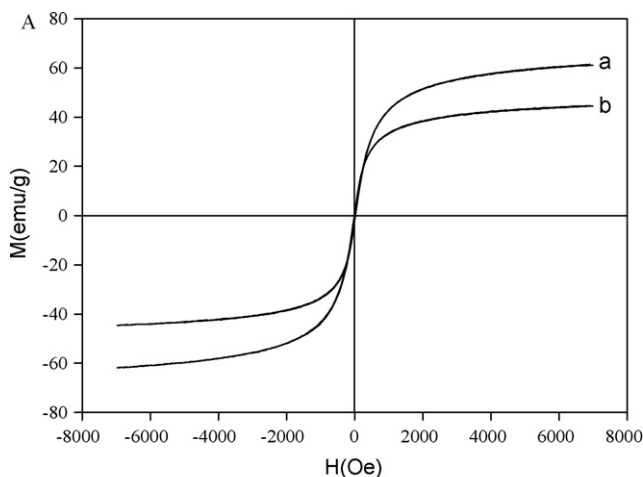


Fig. 4. (A) Magnetization curve at 298 K with (a)  $\text{Fe}_3\text{O}_4@\text{SiO}_2$  and (b) estrone-imprinted MNPs. (B) Separation of estrone-imprinted MNPs by a magnet. (C) Redispersion of estrone-imprinted MNPs after removing the magnet.

To extract the imprinted estrone molecules from the core-shell MNPs, the estrone-imprinted nanoparticles were heated at 180 °C in a mixture of DMSO and water, and the dissociated isocyanato group in silica shell was converted to an amino group by its reaction with H<sub>2</sub>O. The control MNPs were prepared with 3-aminopropyl triethoxysilane and TEOS in the absence of a template molecule.

### 3.2. Characterization of imprinted magnetic nanoparticles

The structural properties of synthesized MNPs were analyzed by X-ray power diffraction (XRD). As shown in Fig. 1, XRD patterns of the synthesized Fe<sub>3</sub>O<sub>4</sub>, Fe<sub>3</sub>O<sub>4</sub>@SiO<sub>2</sub> and estrone-imprinted polymer coated MNPs display several relatively strong reflection peaks in the 2θ region of 20–70°, which is quite similar to those of Fe<sub>3</sub>O<sub>4</sub> nanoparticles reported by other group. The discernible six diffraction peaks in Fig. 1 can be indexed to (220), (311), (400), (422), (511) and (440), which match well with the database of magnetite in JCPDS (JCPDS Card: 19-629) file. However, it is insufficient to exclude the possibility of γ-Fe<sub>2</sub>O<sub>3</sub>, there are probably two types of iron oxide particles in this dispersion: maghemite and magnetite [35]. The trace amounts of maghemite could be attributed to the oxidation of Fe<sub>3</sub>O<sub>4</sub> to γ-Fe<sub>2</sub>O<sub>3</sub> during the coprecipitation and silanization process [36–38]. Because they have similar magnetic properties, the identification is not important in the present study.

Transmission electron microscopy (TEM) revealed that the diameter of Fe<sub>3</sub>O<sub>4</sub> MNPs was in the range of 6–16 nm (Fig. 2a), while the average diameter of estrone-imprinted MNPs increased to about 150 nm (Fig. 2b) with a relatively narrow size distribution. The selected area electron diffraction (SAED) patterns are taken from Fe<sub>3</sub>O<sub>4</sub> MNPs and estrone-imprinted MNPs. It can be seen from SAED, the presence of the ring pattern indicated that Fe<sub>3</sub>O<sub>4</sub> MNPs are polycrystalline (Fig. 2c), but estrone-imprinted polymer coated MNPs are non-crystalline (Fig. 2d).

The extraction of the estrone and the presence of the molecule imprinted sites were confirmed by FT-IR spectroscopy measurements taken before and after removal of imprinted estrone (Fig. 3). The strong peaks at 1078 cm<sup>-1</sup> (Fig. 3a), 1099 cm<sup>-1</sup> (Fig. 3b), 1095 cm<sup>-1</sup> (Fig. 3c) and 1097 cm<sup>-1</sup> (Fig. 3d) are attributed to the stretch of Si–O–Si, indicating the formation of silica film. The peak was shifted from 1078 cm<sup>-1</sup> to 1097 cm<sup>-1</sup>. The typical peak of 1741 and 1737 cm<sup>-1</sup> represent the stretching vibration of carbonyl groups of the urethane bond and estrone respectively. These peaks disappeared after the extraction of the template molecules. The characteristic peak of –NH<sub>2</sub> at 3428 cm<sup>-1</sup> verified the successful introduction of the functional groups in the imprinted cavities.

Fig. 4A shows the plots of magnetization versus magnetic field (M–H loop) at 25 °C for the Fe<sub>3</sub>O<sub>4</sub>@SiO<sub>2</sub> and estrone-imprinted MNPs respectively. It is apparent that there is no hysteresis, both remanence and coercivity are zero, suggesting that the samples are superparamagnetic. The saturation magnetization (*M<sub>s</sub>*) values obtained at room temperature were 61.68 emu g<sup>-1</sup> and 44.63 emu g<sup>-1</sup> for Fe<sub>3</sub>O<sub>4</sub>@SiO<sub>2</sub> and estrone-imprinted MNPs respectively. The theoretical specific saturation magnetization of bulk magnetite is reported to be 92 emu g<sup>-1</sup> [39,40]. The decrease in magnetization value can be attributed to the small particle surface effect such as magnetically inactive layer containing spins that are not collinear with the magnetic field [41]. The saturation magnetization of estrone-imprinted MNPs was reduced to 44.63 emu g<sup>-1</sup> in comparison with the bulk Fe<sub>3</sub>O<sub>4</sub>, but remained strongly magnetic at room temperature and allowed for as effective magnetic separation carrier. Fig. 4B and C shows the separation and redispersion process of estrone-imprinted MNPs. In the absence of an external magnetic field, a dark homogeneous dispersion exists. When an external magnetic field was applied, the black particles were attracted to the wall of vial and the dispersion became clear and transparent. The superparamagnetism of estrone-imprinted MNPs

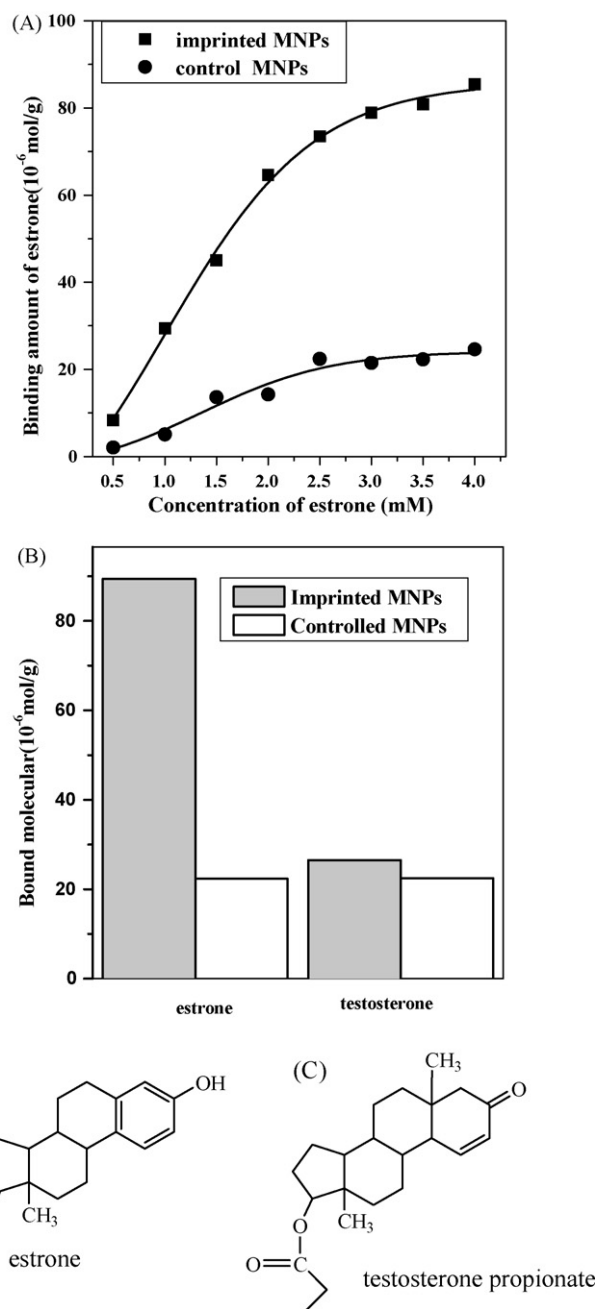


Fig. 5. (A) Amount of estrone bound by the estrone-imprinted MNPs (■) and control MNPs (●). (B) Amount of rebinding estrone and testosterone, filled bars represent estrone-imprinted MNPs, while empty bars correspond to control silica-coated MNPs. (C) The structures of estrone and testosterone propionate.

prevents MIP from aggregating and enables them to be redispersed rapidly after the magnetic field is removed (Fig. 4C).

### 3.3. Binding properties of imprinted magnetic nanoparticles

The recognition ability of the imprinted magnetic nanoparticles toward the template estrone was investigated. The estrone-imprinted MNPs (20 mg) were added into the solutions of estrone in chloroform (10 mL) at various concentrations. After incubating for 24 h, then the MNPs were collected by an external magnetic field instead of a complex centrifugal separation, the supernatant was concentrated to dryness by evaporation of the solvent. The amount of the estrone adsorbed by estrone-imprinted MNPs was measured by the residual estrone in the filtrate by HPLC, while the amount of



bound molecule of the control silica-coated MNPs was determined by the same manner. As shown in Fig. 5A, the estrone-imprinted MNPs had much higher recognition ability than the control MNPs at all concentration ranges.

The saturation binding data were further processed with Scatchard equation to estimate the binding properties of imprinted magnetic nanoparticles. The Scatchard equation was as follows:

$$\frac{Q}{C_e} = \frac{Q_{\max}}{K_d} - \frac{Q}{K_d}$$

where  $Q$  was the amount of estrone bound to estrone-imprinted MNPs at equilibrium,  $Q_{\max}$  was the apparent maximum number of binding sites,  $C_e$  was the free analytical concentration at equilibrium and  $K_d$  was the dissociation constant. The values of  $K_d$  and the  $Q_{\max}$  can be calculated from the slope and intercept of the linear line plotted in  $Q/C_e$  versus  $Q$ .

The Scatchard analysis for MIPs was performed. It was observed that the Scatchard plot was a single straight line, which indicated the binding sites of imprinted magnetic nanoparticles were identical. The “semi-covalent” imprinting technique [25] combines the advantages of both covalent and non-covalent imprinting techniques, which takes covalent imprinting technique to assemble sites that bind the target molecules in a non-covalent fashion.

The linear regression equation for the linear region is  $Q/C_e = 40.54 - 0.2210Q$  ( $R^2 = 0.9984$ ). From the slope and the intercept of the straight line obtained, the values of  $K_d$  and  $Q_{\max}$  were 4.525 mmol/L and 183.4  $\mu$ mol/g respectively.

We also investigated the specific recognition ability of estrone-imprinted MNPs for testosterone propionate which is structural analogue of estrone, under the same conditions. From the amounts of rebinding estrone and testosterone, estrone-imprinted polymer coated MNPs exhibited high selectivity for imprinting molecule estrone compared to the structural analogue testosterone propionate. The controlled MNPs showed low binding values for both estrone and testosterone (Fig. 5B). The adsorption of testosterone is due to unspecific adsorption. The results confirmed clearly the effectiveness of the molecular imprinting because the estrone-imprinted MNPs showed efficiently specific recognition ability to the template estrone in comparison with structural analogue testosterone propionate.

#### 4. Conclusions

In conclusion, we explored synthesis of estrone-imprinted polymer coated  $Fe_3O_4$  magnetic nanoparticles that exhibit a much higher specific recognition and saturation magnetization. This work provides a platform to prepare molecularly imprinted polymer modified magnetic nanoparticles with high affinity, selectivity and capacity to nearly any target molecules. We believe that the imprinted polymer coating magnetic nanoparticles can be one of the most promising candidates for various applications, including chemical and biochemical separation, cell sorting, recognition elements in biosensors and drug delivery.

#### Acknowledgements

This work was supported by National Basic Research Program of China (863 Program No. 2007AA10Z432, 973 Program No. 2007CB914100), the National Natural Science Foundation of China (20675040, 20875050), the Natural Science Foundation of Tianjin (07JCYBJC00500) and SRF for ROCS, SEM.

#### References

- [1] T. Neuberger, B. Schopf, H. Hofmann, M. Hofmann, B. von Rechenberg, J. Magn. Mater. 293 (2005) 483.
- [2] A.K. Gupta, M. Gupta, Biomaterials 26 (2005) 3995.
- [3] M.G. Harisinghani, J. Barentsz, P.F. Hahn, W.M. Deserno, S. Tabatabaei, C.H. van de kaa, J. de la Rosette, R.N. Weissleder, Engl. J. Med. 348 (2003) 2491.
- [4] I. Willner, E. Katz, Angew. Chem. Int. Ed. 42 (2003) 4576.
- [5] S. Bucak, D.A. Jones, P.E. Laibinis, T.A. Hatton, Biotechnol. Prog. 19 (2003) 477.
- [6] H. Gu, K. Xu, C. Xu, B. Xu, Chem. Commun. (2006) 941.
- [7] G. Wulff, Angew. Chem. Int. Ed. 34 (1995) 1812.
- [8] B. Sellergren, Molecularly Imprinted Polymers Man-made Mimics of Antibodies and their Application in Analytical Chemistry, Elsevier, New York, 2001.
- [9] H. Zhang, L. Ye, K. Mosbach, J. Mol. Recognit. 19 (2006) 248.
- [10] G. Wulff, Chem. Rev. 102 (2002) 1.
- [11] K. Haupt, K. Mosbach, Chem. Rev. 100 (2000) 2495.
- [12] S.R. Carter, S. Rimmer, Adv. Funct. Mater. 14 (2004) 553.
- [13] D. Silvestri, C. Borrelli, P. Giusti, C. Cristallini, G. Ciardelli, Anal. Chim. Acta 542 (2005) 3.
- [14] C.H. Lu, W.H. Zhou, B. Han, H.H. Yang, X. Chen, X.R. Wang, Anal. Chem. 79 (2007) 5457.
- [15] D. Gao, Z. Zhang, M. Wu, C. Xie, G. Guan, D. Wang, J. Am. Chem. Soc. 129 (2007) 7859.
- [16] C. Ki, J. Chang, Macromolecules 39 (2006) 3415.
- [17] H. Yang, S. Zhang, F. Tang, Z. Zhuang, X. Wang, J. Am. Chem. Soc. 127 (2005) 1378.
- [18] C. Xie, Z. Zhang, D. Wang, G. Guan, D. Gao, J. Liu, Anal. Chem. 78 (2006) 8339.
- [19] C. Xie, B. Liu, Z. Wang, D. Gao, G. Guan, Z. Zhang, Anal. Chem. 80 (2008) 437.
- [20] H. Yang, S. Zhang, W. Yang, X. Chen, Z. Zhuang, J. Xu, X. Wang, J. Am. Chem. Soc. 126 (2004) 4054.
- [21] H. Wang, W. Zhou, X. Yin, Z. Zhuang, H. Yang, X.R. Wang, J. Am. Chem. Soc. 128 (2006) 15954.
- [22] R.J. Ansell, K. Mosbach, Analyst 123 (1998) 1611.
- [23] Y. Li, X.F. Yin, F.R. Chen, H.H. Yang, Z.X. Zhang, X.R. Wang, Macromolecules 39 (2006) 4497.
- [24] C.J. Tan, H.G. Chua, K.H. Ker, Y.W. Tong, Anal. Chem. 80 (2008) 683.
- [25] N. Kirsch, M.J. Whitcombe, in: M. Yan, O. Ramström (Eds.), Molecularly Imprinted Materials Science and Technology, Marcel Dekker, 2005 (Chapter 5).
- [26] M.R. Tremblay, S.X. Lin, D. Poirier, Steroids 66 (2001) 821.
- [27] J.R. Pasqualini, J. Cortes-Prieto, G. Chetrite, M. Talbi, A. Ruiz, Int. J. Cancer 70 (1997) 639.
- [28] D.K. Chang, C. Oh, S.G. Oh, J.Y. Chang, J. Am. Chem. Soc. 124 (2002) 14838.
- [29] Y.S. Kang, S. Risbud, J.F. Rabolt, P. Stroeve, Chem. Mater. 8 (1996) 2209.
- [30] Z.Y. Ma, X.Q. Liu, Y.P. Guan, H.Z. Liu, Colloids Surf. A 275 (2006) 87.
- [31] M. Yamaura, R.L. Camilo, L.C. Sampaio, M.A. Macêdo, M. Nakamura, H.E. Toma, J. Magn. Mater. 279 (2004) 210.
- [32] C. Barbé, J. Bartlett, L. Kong, K. Finnie, H.Q. Lin, M. Larkin, S. Calleja, A. Bush, G. Calleja, Adv. Mater. 16 (2004) 1959.
- [33] T. Nann, P. Mulvaney, Angew. Chem. Int. Ed. 43 (2004) 5393.
- [34] T.J. Yoon, K.N. Yu, E. Kim, J.S. Kim, B.G. Kim, S.H. Yun, B.H. Sohn, M.H. Cho, J.K. Lee, S.B. Park, Small 2 (2006) 209.
- [35] Y. Lu, Y. Yin, B.T. Mayers, Y. Xia, Nanolett 2 (2002) 183.
- [36] R.E. Vandenberghe, R. Vandenberghe, E. De Grave, G. Robbrecht, J. Magn. Mater. 15 (1980) 1117.
- [37] T. Sato, T. Iijima, M. Seki, J. Inagaki, J. Magn. Mater. 65 (1987) 252.
- [38] E. Tronc, P. Belleville, J.P. Jolivet, J. Livage, Langmuir 8 (1992) 313.
- [39] J. Popplewell, L. Sakhnini, J. Magn. Mater. 142 (1995) 72.
- [40] V.S. Zaitsev, D.S. Filimonov, I.A. Presnyakov, R.J. Gambino, B. Chu, J. Colloid Interface Sci. 212 (1999) 49.
- [41] R.H. Kodama, A.E. Berkowitz Jr., E.J. McNiff, S. Foner, Phys. Rev. Lett. 77 (1996) 394.



# Sorption of heavy metal ions by silica gel-immobilized, proton-ionizable calix[4]arenes

Jing Wang, Dongmei Zhang, Thomas R. Lawson, Richard A. Bartsch\*

Department of Chemistry and Biochemistry, Texas Tech University, Lubbock, TX 79409-1061, United States

## ARTICLE INFO

### Article history:

Received 30 October 2008

Received in revised form

25 November 2008

Accepted 26 November 2008

Available online 3 December 2008

### Keywords:

Calix[4]arene

Heavy metal ions

Ion-exchange

Sorption

## ABSTRACT

Silica gel-immobilized, di-ionizable calix[4]arenes are employed as stationary phases in ion-exchange chromatography for selected heavy metal ions. Sorption efficiencies for  $\text{Pb}^{2+}$  are dependent on the structure of the calix[4]arene ligand and the linker that joins the ligand to the silica gel, as well as the acidity of the sample solution. Although the resins exhibit only poor sorption of  $\text{Cd}^{2+}$ , they are found to be scavengers for  $\text{Hg}^{2+}$ . Competitive sorption studies are conducted with selected resins.

© 2008 Elsevier B.V. All rights reserved.

## 1. Introduction

Heavy metals, such as lead, cadmium and mercury, are harmful to living organisms. Their accumulation in humans causes kidney failure, nervous system damage and bone softening, as well as other serious illness [1]. These metals can be released into the environment through several ways, of which wastewater discharge is a primary source. For example, the first cadmium poisoning in Japan was caused by release of the metal salts into rivers by mining companies [2]. Heavy metal ion removal from aqueous solutions has been achieved by chemical precipitation, oxidation/reduction, microbiological activity and ion exchange [3–5]. An advantage of ion exchange over other conventional methods is that the target metals can be selectively removed with subsequent regeneration of the operating system. Synthetic polymers have been successfully applied as ion-exchange resins for heavy metal removal [6–11].

Calixarenes, a class of cone-shaped macrocyclic molecules, have attracted attention as stationary phases in gas and liquid chromatography since 1993 [12]. They have been successfully applied to the separation of cations and molecules in liquid chromatography. For example, calix[4]arene-tetraacetamide covalently linked to silica gel was used for the separation of alkali and alkali earth

metal cations [13]. *p*-*tert*-Butylcalix[*n*]arenes with  $n = 4$  and 6 were immobilized on silica gel through long spacers. The immobilized calix[4]arenes were used to separate polycyclic aromatic hydrocarbons (PAHs), nucleosides and bases [14,15]. Calix[*n*]arenesulfonates with  $n = 4, 6$  and 8 non-covalently coated on an ion-exchange resin were employed for the separation of fullerenes [16]. However, the information on heavy metal cation separations using calixarenes as a chromatographic stationary phase is very limited [17–20]. Particularly, the effect of the structural changes of those calixarenes on their binding properties was rarely studied.

In previous research, we found that macrocyclic ligands of calix[4]arene with two pendant *N*-(*X*)sulfonyl carboxamide groups exhibited excellent solvent extraction selectivity for  $\text{Hg}^{2+}$  and good selectivity for  $\text{Pb}^{2+}$  over most alkali, alkaline earth and transition metal cations [21,22]. To employ such calixarenes in the column separation of metal cations, ligand immobilization on a polymeric support is required. Very recently, we developed synthetic strategies for immobilization of conformationally mobile di-ionizable calix[4]arenes on silica gel through single linkages of different lengths [23]. Structures of the functionalized resins are shown in Fig. 1. The immobilized ligands contain proton-ionizable *N*-(*X*)sulfonyl oxyacetamide groups [ $\text{OCH}_2\text{C}(\text{O})\text{NH}\text{SO}_2\text{X}$ ] for which the acidity may be varied by changing the electron-withdrawing abilities of *X*. In this report, the factors that may affect the heavy metal ion binding were investigated, which include structural changes in these calixarenes, acidity of the sample solutions and identity of the heavy metal ion species.

\* Corresponding author.

E-mail address: [richard.bartsch@ttu.edu](mailto:richard.bartsch@ttu.edu) (R.A. Bartsch).

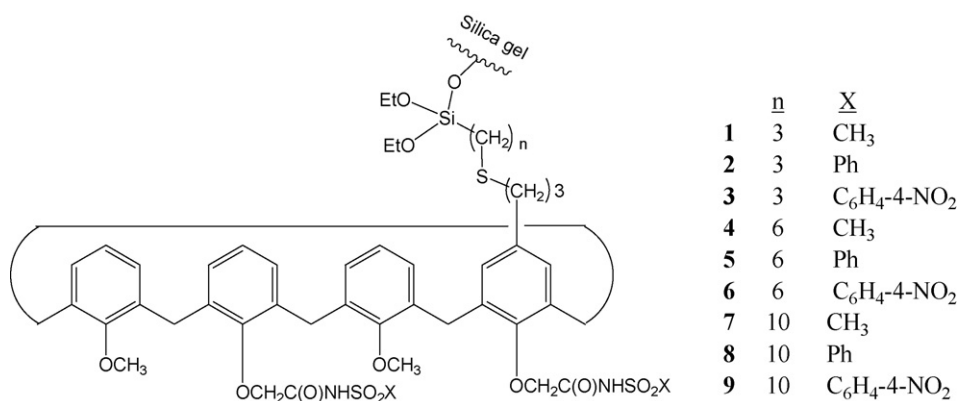


Fig. 1. Structures of silica gel-immobilized, di-ionizable calix[4]arenes 1–9.

## 2. Experimental

### 2.1. Reagents and instrumentation

All chemicals were analytical grade commercial products and were used as received. Silica gel 150 (60–200 mesh) SiliCAR<sup>®</sup> was purchased from Mallinckrodt. Deionized water was prepared by passing distilled water through three Barnstead D8922 combination cartridges in series.

A Shimadzu Model 6300 atomic absorption spectrophotometer with a Model 6100 autosampler was used to determine the concentrations of metal ions in aqueous solutions. The pH of the sample solutions was measured with a Fisher Accumet AR 25 meter and a combination electrode. To prevent metal contamination, all glassware was soaked in 5% HNO<sub>3</sub> for 24 h and rinsed with deionized water before use.

### 2.2. Apparatus

A related column assembly was reported earlier [24] and minor modifications were made for this research (Fig. 2.). A six-position switch transported eluent from three plastic reservoirs to a Milton Roy minipump (P/N 920148-03). Changing the pump settings varied the flow rate of the eluent. A Cole-Parmer pressure gauge (0–200 psi range) was employed and protected from acid solution by a gauge guard made of PVC/Teflon. The resin was dry packed into a 20-cm Dionex Tefzel column (0.42 cm i.d.) and supported by a 35- $\mu$ m filter. A Dionex air-actuated, four-way valve (P/N 35914) was used to transport the eluent either to the column or to waste. Activation of the valve was controlled by introducing 80 psi of nitrogen through a three-way switch. A plastic syringe was attached to the valve to supply air pressure to the column. The stripping solution was collected with a Bio-Rad Model 25 fraction collector. Teflon tubing (1/8 in.) was used to connect the reservoirs, the six-position switch and the pump; while the remainder of the assembly was connected with Tefzel tubing (1/16 in.) that could stand higher pressure.

### 2.3. Sample solution preparation

For non-competitive ion-exchange experiments, metal nitrate solutions were prepared such that the molar ratio of the metal ion species to calixarene units on the resin packing was 1:1. The metal nitrate was dissolved in deionized water to make 0.50 L of sample solution. The Pb(NO<sub>3</sub>)<sub>2</sub> sample solutions had a pH of 5.3. To examine the pH effect on Pb<sup>2+</sup> sorption, 0.10 M HNO<sub>3</sub> was added to the Pb(NO<sub>3</sub>)<sub>2</sub> sample solution to obtain varied pH values of 4.5, 4.0, 3.2 and 2.1. The Cd(NO<sub>3</sub>)<sub>2</sub> and NaNO<sub>3</sub> solutions had pH values

of 5.2–5.5 and 5.8, respectively. These sorption experiments were conducted only once.

For Pb<sup>2+</sup>/Cd<sup>2+</sup> competitive sorption experiments, the sample solution was prepared such that the molar ratio of Cd<sup>2+</sup>:Pb<sup>2+</sup>:calixarene units on the resin packing was 1:1:1. In Pb<sup>2+</sup>/Na<sup>+</sup> competitive sorption studies, the molar ratio of Na<sup>+</sup>:Pb<sup>2+</sup>:calixarene units was changed from 1:1:1 to 15:1:1 and then to 150:1:1. These sorption experiments were performed once.

### 2.4. Procedure

The column containing 1.00 g of resin was washed with 25 mL of 0.010 M HNO<sub>3</sub> and then with 100 mL of deionized water at a flow

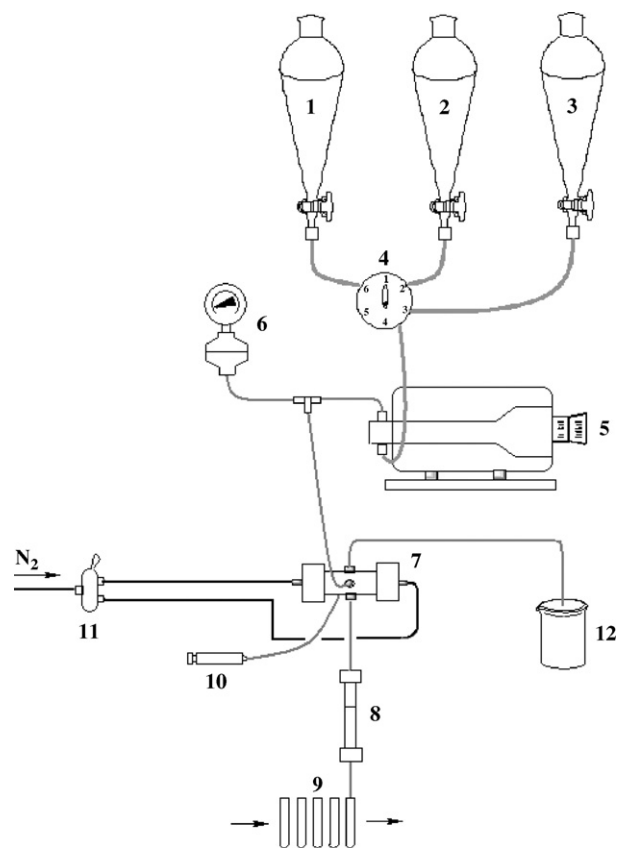


Fig. 2. Column assembly: (1) acid solution; (2) sample solution; (3) deionized water; (4) six-position switch; (5) pump; (6) pressure gauge with gauge guard; (7) four-way valve; (8) column; (9) fraction collector; (10) syringe; (11) three-way switch; (12) waste container.

**Table 1**  
Sorption of Pb<sup>2+</sup> by unfunctionalized silica gel (SG) and by resins 1–9.

Resin	Ion-exchange capacity (μmol calixarene/g resin)	Pb <sup>2+</sup> applied (μmol/g resin)	Pb <sup>2+</sup> recovered (μmol/g resin)	Pb <sup>2+</sup> sorption (%)
SG	–	77.4	1.8 ± 1.2	2.3 ± 1.6
1	78	77.4	15.4 ± 1.4	19.9 ± 1.8
2	118	116.3	24.2 ± 1.5	20.8 ± 1.3
3	54	52.7	13.1 ± 0.7	24.9 ± 1.3
4	61	59.8	7.8 ± 0.1	13.0 ± 0.1
5	132	130.3	22.0 ± 2.4	16.9 ± 1.8
6	96	95.1	12.5 ± 0.9	13.1 ± 0.9
7	189	186.6	25.0 ± 0.8	13.4 ± 0.4
8	128	126.8	26.0 ± 1.0	20.5 ± 0.8
9	221	218.6	23.7 ± 1.2	10.8 ± 0.5

rate of 3.0 mL/min. This pre-wash was performed to insure protonation of all binding sites on the ligands. Subsequently, the sample solution was prepared, from which a 2.0-mL portion was removed for metal ion analysis and a 5.0-mL portion for pH determination. The remainder of the solution was pumped through the column. A 2.0-mL portion of the loading effluent was collected for metal ion analysis. The column was then washed with 100 mL of deionized water to remove any unbound cations from the packing. Before elution was initiated, water remaining in the tubing was purged with 0.010 M HNO<sub>3</sub> through the waste line. The residual water in the column was removed by air pressurized with the plastic syringe. The sorbed cations were then stripped with 0.010 M HNO<sub>3</sub> at a flow rate of 0.3 mL/min. The stripping solution was collected in 0.25-mL fractions. Metal ion concentrations in the fractions, sample solution and loading effluent were analyzed by atomic absorption spectrophotometry after appropriate dilutions with deionized water.

### 3. Results and discussion

To investigate the affinities of the functionalized resins for selected heavy metal ions, the sorption experiments were first carried out in a non-competitive environment. Alkali metal cations, such as Na<sup>+</sup> and K<sup>+</sup>, are mostly encountered in our lives and they are the most possible interferences in heavy metal ion sorption during waste treatment processes. Therefore Na<sup>+</sup> sorption experiments were also performed with selected resins. To provide better information for potential practical metal ion separations, competitive ion exchange studies were also conducted with selected resins.

In the synthetic work, it was found that the nine calix[4]arene ligands exhibited different loading efficiencies on silica gel. Thus, the resins listed in Table 1 display a range of theoretical ion-exchange capacities from 54 to 221 μmol calixarene/g of resin. This ion-exchange capacity was calculated from the nitrogen percentage values obtained by combustion analyses of the resins.

#### 3.1. Sorption of Pb<sup>2+</sup>

Sorptions of Pb<sup>2+</sup> from source aqueous solutions at pH 5.3 were conducted with resins 1–9. To evaluate the sorption efficiencies of the calix[4]arene ligands in each resin, the percent of Pb<sup>2+</sup> sorption was calculated by the following equation and the resultant values

are presented in Table 1.

$$\text{sorption \%} = \frac{\text{number of moles of Pb}^{2+} \text{ recovered in all fractions}}{\text{number of moles of Pb}^{2+} \text{ applied to the column}} \quad (1)$$

The amounts of Pb<sup>2+</sup> recovered in the eluent fractions are listed in Table 1. The percent sorption data are averages from three independent experiments. For a single column, the amount of Pb<sup>2+</sup> recovered in all fractions satisfactorily matched the difference between the original sample and the loading effluent (experimental data not shown here). Thus 0.010 M HNO<sub>3</sub> was able to strip all of the bound Pb<sup>2+</sup> from the column and the amount of Pb<sup>2+</sup> recovered represents the amount that was sorbed by the resin.

As a conventional HPLC stationary phase, unfunctionalized silica gel can undergo cation exchange at as low as pH 2.0 in solution [25]. Divalent cations may have very high retention on silica gel [25]. To demonstrate that silica gel itself does not contribute appreciably to the binding of Pb<sup>2+</sup> in this research, sorption of Pb<sup>2+</sup> was also conducted with an unfunctionalized silica gel column (SG) using the same experimental conditions as those for resin 1. The sorption values for SG and resin 1 are compared in Table 1. The amount of Pb<sup>2+</sup> sorbed by SG was about one-eighth of that for resin 1. Therefore Pb<sup>2+</sup> retention was demonstrated to be due primarily to complexation with the calixarene ligands in the functionalized resin.

Resins 2, 5 and 7–9 gave sorption values in the range of 22.0–26.0 μmol/g resin, while the remainder of the polymers displayed sorption values of 7.8–15.4 μmol/g resin. The five polymers with higher theoretical ion-exchange capacities than the others sorbed larger amounts of Pb<sup>2+</sup> when amounts of Pb<sup>2+</sup> equivalent to their calixarene units were loaded onto the columns.

When the Pb<sup>2+</sup> sorption percentage values are compared, resin 3 with the lowest theoretical ion-exchange capacity exhibited the best sorption efficiency of 24.9%; while resin 9 with the highest theoretical ion-exchange capacity displayed the lowest sorption efficiency of 10.8%. Although resin 1 differs greatly from resins 2 and 8 in theoretical ion-exchange capacities, the three resins exhibit approximately the same sorption efficiency of 20% within experimental error. This shows that the calixarene ligands in the polymeric matrix possess different complexation abilities for Pb<sup>2+</sup>.

The effect of calix[4]arene structural variations on their Pb<sup>2+</sup> sorption capability was examined. The calix[4]arene units contain only one linker on the upper rim to provide flexibility after

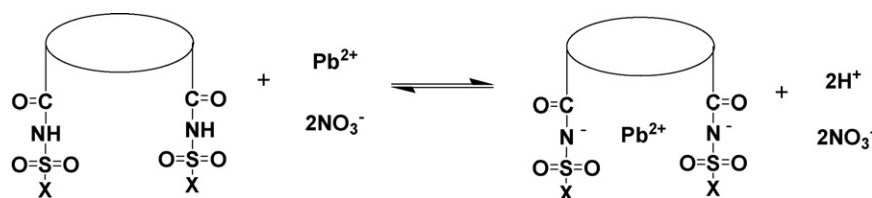


**Fig. 3.** Ion-exchange mechanism for complexation of Pb<sup>2+</sup> by di-ionizable calix[4]arenes.

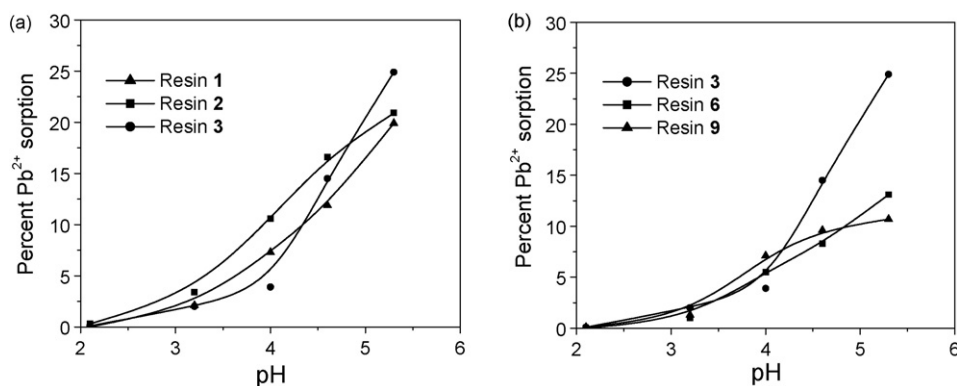


Fig. 4. Sample pH effects on Pb<sup>2+</sup> sorption as a function of (a) the X group and (b) the spacer length.

attachment to silica gel. The percent of Pb<sup>2+</sup> sorption values show that among the resins with the same X group, resins 1–3 with the shortest spacer length ( $n=3$ ) generally exhibited better sorption efficiencies than resins 4–9 with longer spacer lengths ( $n=6$  or 10). Apparently, having the calixarene ligands closer to the hydrophilic surface of the silica gel facilitates Pb<sup>2+</sup> sorption.

Variation of the X group also influenced the complexation behavior of the silica gel-bound calix[4]arenes. Among the resins with three-carbon spacers, resin 3 with X=4-nitrophenyl gave the best Pb<sup>2+</sup> sorption efficiency. On the other hand, among the resins with longer spacers ( $n=6$  or 10), the best sorption efficiency was observed from resins 5 and 8 with X=phenyl. Therefore, an electron-withdrawing substituent located close to the ionizable sites in the calix[4]arene ligand can help the binding of Pb<sup>2+</sup>. The ion-exchange mechanism for the result is shown in Fig. 3. Two acidic protons on the ionizable sites in one ligand molecule exchange with one divalent Pb<sup>2+</sup> to maintain the charge balance. Since it is an equilibrium interaction, the stronger the electron-withdrawing substituents attached to the ionizable sites, the more acidic are the protons and they are more easily exchanged with an incoming cation. It was anticipated that the electron-withdrawing ability order would be 4-nitrophenyl > phenyl  $\approx$  methyl. However, ligands bearing X=4-nitrophenyl are found to be less acidic than expected, because of the inter- or intra-molecular NH...ONC hydrogen bonding, or conformational peculiarities of the compound that hinder metal ion complexation [22].

Overall the percent Pb<sup>2+</sup> sorption values for these functionalized resins are in the range of 10.8–24.9%. To improve the sorption efficiency, increasing the sample concentration was attempted. In a run with a molar ratio of Pb<sup>2+</sup> to calixarene units is 4:1, the percent Pb<sup>2+</sup> sorption was found to be 3.7% for resin 1, which means that the amount of Pb<sup>2+</sup> bound on the resin remained the same. Incomplete deprotonation of the two ionizable sulfonyl oxyacetamide groups at pH 5.3 probably limits the binding capabilities of the ligands. Hence the ion exchange process might be improved further by anchoring calixarene ligands with more acidic ionizable groups on silica gel.

### 3.2. Effect of sample solution pH on Pb<sup>2+</sup> sorption by resins 1–3, 6 and 9

Pb<sup>2+</sup> sample solutions were prepared with pH values of 2.1, 3.2, 4.0 and 4.6 to augment the pH 5.3 solutions utilized earlier. The Pb<sup>2+</sup> sorption percentages for resins 1–3, 6 and 9 are shown in Fig. 4. As can be seen, uptake of Pb<sup>2+</sup> by all of these ion-exchange resins decreased markedly as the sample solution pH decreased. When the concentration of [H<sup>+</sup>] in solution becomes higher in the ion-exchange equilibrium system (Fig. 3), the reaction tends to shift back to the reactants side, which reduces the formation of the complexes. As a result, the sorption of Pb<sup>2+</sup> drops.

For pH 2.1, Pb<sup>2+</sup> uptake by the resins decreased to zero, which is even lower than the Pb<sup>2+</sup> sorption by unfunctionalized silica gel at pH 5.3. This is reasonable because the ion-exchange capacity of silica gel also falls off sharply as the pH approaches high acidity [25].

The pH effects as a function of the X group and as a function of the spacer length are revealed in Fig. 4a and b, respectively. Resins 1–3 contain the same three-carbon spacer, but different X groups. As shown in Fig. 4a, resin 3 with X=4-nitrophenyl exhibits a more pronounced pH effect on its percent Pb<sup>2+</sup> sorption than the other two resins. Its pH profile is steeper, especially in the pH range of 4.0–5.3. Resins 1 with X=methyl and 2 with X=phenyl show similar trends in their pH profiles. In Fig. 4b, the resins 3, 6 and 9 have the same 4-nitrophenyl X group, but different spacer lengths. Resin 3 with the shortest spacer exhibits a larger pH effect on the percent Pb<sup>2+</sup> sorption than resin 6 with the intermediate spacer ( $n=6$ ) and 9 with the longest spacer ( $n=10$ ). Although resins 6 and 9 do not display large differences in their pH profiles, the curves for resin 6 decrease more rapidly than that for 9.

The Pb<sup>2+</sup> sorbed on a resin undergoes a concentration process during the loading step. The enrichment effect is dependent on the sorption efficiencies of the resins and the experimental conditions. Such a technique can be utilized for lowering analytical detection limits, trace metal recoveries and multiple cation separations [26–29]. The column concentration capabilities for metal ions can be evaluated in terms of the concentration factor (CF):

$$CF = \frac{\text{concentration of Pb}^{2+} \text{ in the stripping solution}}{\text{initial concentration of Pb}^{2+} \text{ in the sample solution}} \quad (2)$$

By plotting the CF values against the elution volume (stripping solution volume), the Pb<sup>2+</sup> elution profiles for resins 1–3, 6 and 9 at various sample pHs were obtained (Fig. 5). A trend is observed for all of the profiles. At the beginning of the elution, the CF values for the first two or three fractions are quite small since most of the sorbed Pb<sup>2+</sup> ions are still tightly bound by the ligands. As the elution process proceeds, more and more of the Pb<sup>2+</sup> on the binding sites is replaced by H<sup>+</sup> from the stripping solution. As a result, the CF values for these fractions increase dramatically until a maximum value is reached. Subsequently, the CF values drop rapidly and become negligible when enough fractions have been collected.

Generally a resin with a higher Pb<sup>2+</sup> sorption efficiency exhibits a larger maximum CF value during the elution step. For example, the highest maximum CF value in Fig. 5 is 70 for resin 3 which has the highest Pb<sup>2+</sup> sorption efficiency. The sample solution pH also has a strong influence on the elution profile of the resins. The more acidic is the sample solution loaded on a single column, the less Pb<sup>2+</sup> is enriched on the packing and generally a smaller maximum CF value is observed. For instance, resin 1 has a maximum CF value of 55 at

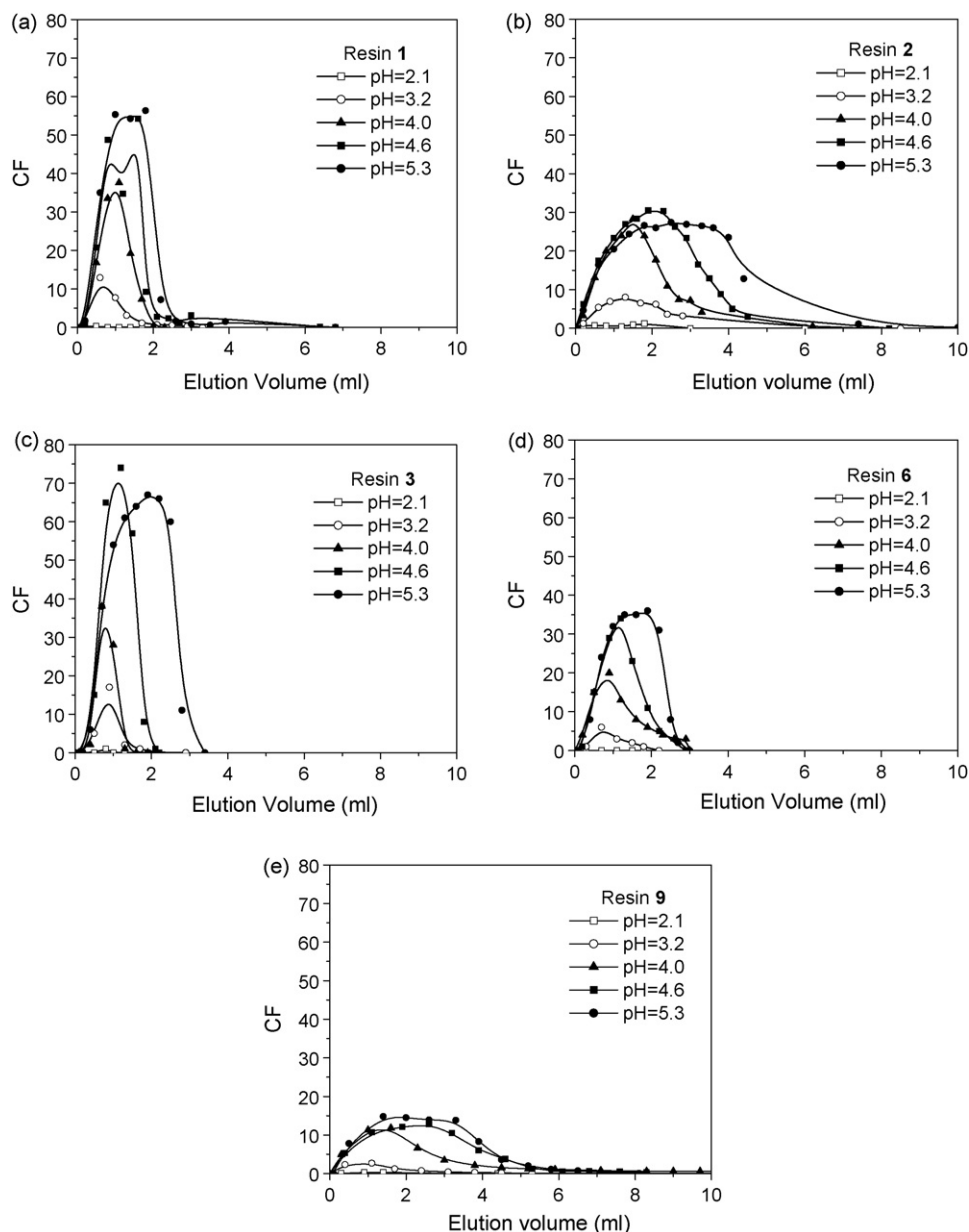


Fig. 5.  $Pb^{2+}$  elution profiles for functionalized resins (a) **1**, (b) **2**, (c) **3**, (d) **6** and (e) **9**.

pH 5.3. The CF value drops to 45, 35, 10 and 0.3 at pH values of 4.6, 4.0, 3.2 and 2.1, respectively (Fig. 4a). It was found that the  $Pb^{2+}$  desorption process is quite rapid. For elution with 0.010 M  $HNO_3$ , most of the bound  $Pb^{2+}$  ions on the resins were eluted in the first 4.0 mL of stripping solution at sample pH 5.3.

### 3.3. Sorption of $Cd^{2+}$ by resins 1–3

In view of their relatively high sorption efficiencies for  $Pb^{2+}$ , the sorption properties of resins 1–3 towards  $Cd^{2+}$  were studied

**Table 2**  
Sorption of  $Cd^{2+}$  by unfunctionalized silica gel (SG) and by resins 1–3.

Resin	$Cd^{2+}$ applied ( $\mu\text{mol/g resin}$ )	$Cd^{2+}$ recovered ( $\mu\text{mol/g resin}$ )	$Cd^{2+}$ sorption (%)
SG	77.5	1.9	2.4
<b>1</b>	77.6	4.3	5.5
<b>2</b>	116.1	6.2	5.3
<b>3</b>	52.8	6.0	11.4

(Table 2). It is observed that the calix[4]arene ligands in these resins are poorer hosts for this heavy metal ion. Although resin 3 with X = 4-nitrophenyl exhibits a stronger affinity for  $Cd^{2+}$  than did the other two polymers, the percent  $Cd^{2+}$  sorption is still much lower than that of  $Pb^{2+}$ . This result is in agreement with earlier research conducted with other polymeric ion-exchange resins [11,30,31].

### 3.4. $Pb^{2+}/Cd^{2+}$ competitive sorption by resin 3

Due to the coexistence of  $Pb^{2+}$  and  $Cd^{2+}$  in some wastewaters, a competitive sorption study for these two cations was undertaken.

**Table 3**  
Competitive sorption of  $Pb^{2+}$  and  $Cd^{2+}$  by resin 3.

Cation	Cation applied ( $\mu\text{mol/g resin}$ )	Cation recovered ( $\mu\text{mol/g resin}$ )	Cation sorption (%)
$Pb^{2+}$	52.9	7.9	15.0
$Cd^{2+}$	52.7	1.4	2.7

**Table 4**  
Competitive sorption of  $Pb^{2+}$  in the absence and presence of  $Na^+$  by resins **1** and **2**.

Resin	Molar ratio of $Na^+ : Pb^{2+} : calix[4]arene$	$Pb^{2+}$ recovered ( $\mu mol/g$ resin)	$Pb^{2+}$ sorption (%)
<b>1</b>	0:1:1	15.4	19.9
	1:1:1	13.9	18.0
	15:1:1	11.3	14.6
	150:1:1	6.1	7.9
<b>2</b>	0:1:1	23.6	20.3
	1:1:1	22.1	19.0
	15:1:1	18.0	15.5
	150:1:1	8.0	6.9

Resin **3** was chosen for the competitive sorption study due to its stronger affinity for both  $Pb^{2+}$  and  $Cd^{2+}$  than that of resins **1** and **2**. Concentrations of  $Pb^{2+}$  and  $Cd^{2+}$  in the collected fractions were measured. The results presented in Table 3 reveal that the competition of equivalent amounts of  $Cd^{2+}$  and  $Pb^{2+}$  for the limited binding sites in resin **3** leads to lower percent sorption values for both cations. The reason for the phenomenon can be explained as follows: the total number of ion-exchange sites on the resin is a constant, and the binding of  $Cd^{2+}$  is also an equilibrium reaction as shown in Fig. 3. Since there are two parallel reactions going on at the same time, the ion-exchange sites available for either reaction is definitely less than the total number of ion-exchange sites. As a result, there are fewer complexes formed for each reaction, compared to the individual sorption experiment with no interfering metal ions.

### 3.5. Sorption of $Hg^{2+}$ by resin **1**

Sorption of  $Hg^{2+}$  was investigated with resin **1** following the same experimental procedure as utilized for  $Pb^{2+}$  sorption. In the first run, no  $Hg^{2+}$  ions could be detected in the fractions or in the loading effluent. Therefore, all of the metal ions were still tightly bound on the resin and the 0.010 M  $HNO_3$  solution was not strong enough to strip  $Hg^{2+}$  from the column. To verify this assumption, the column used in the first run was utilized in a second run. It was found in the second run that the loading effluent had almost the same  $Hg^{2+}$  concentration as in the sample solution. This means that the  $Hg^{2+}$  in the first run occupied all of the possible binding sites of the calix[4]arene ligands and prevented further binding of  $Hg^{2+}$  from the second run. Presumably this strong sorption of  $Hg^{2+}$  arises from  $\pi$ -interaction with the aromatic rings of calixarenes. The extraordinary affinity for  $Hg^{2+}$  demonstrated here agrees with our solvent extraction results for mercury-selective calixarenes [21]. More acidic stripping solutions were also applied without suc-

cess. Although it might be argued that the sulfide donor group in the linker is at least partially responsible for the strong  $Hg^{2+}$  sorption, it should be noted that closely related, non-immobilized extractants devoid of sulfide linkages exhibit strong complexation of  $Hg^{2+}$  [22].

### 3.6. Sorption of $Na^+$ by resin **1**

The affinity of the polymers for  $Na^+$  was evaluated with resin **1**. The sorption result reveals that resin **1** has very poor capability for retaining  $Na^+$ . An equivalent amount of  $Na^+$  to the calixarene units in resin **1** was applied to the column and <1% of the cations was sorbed. When the sample solution containing one equivalent of  $Na^+$  and one equivalent of  $Pb^{2+}$  was loaded on the column, the recovery of  $Na^+$  was not changed.

In the monovalent cation exchange process, one of the two ionizable groups in calix[4]arene may undergo deprotonation to bind  $Na^+$ . However, this binding is not as strong as that for  $Pb^{2+}$  for two reasons: First, there is a stronger electrostatic interaction between the divalent  $Pb^{2+}$  and the two deprotonated ionizable groups. Second, the soft ionizable groups prefer to bind a softer cation like  $Pb^{2+}$  instead of a hard cation like  $Na^+$ .

### 3.7. $Pb^{2+}/Na^+$ competitive sorption by resins **1** and **2**

Sorption of  $Na^+$  in the presence of equivalent amount of  $Pb^{2+}$  was conducted with resin **1**. Since this resin showed extremely low affinity for  $Na^+$  under non-competitive conditions, it is not surprising to see the near zero retention of  $Na^+$  on the same column with the interference of  $Pb^{2+}$ .

Sorption of  $Pb^{2+}$  with interference of  $Na^+$  by resins **1** and **2** was also investigated. As expected, the percent  $Pb^{2+}$  sorption values for both resins were almost unaffected when equivalent amounts of  $Na^+$  and  $Pb^{2+}$  were present in the sample solutions (Table 4). When 15 equiv. of  $Na^+$  to  $Pb^{2+}$  were present in the sample solutions, the percent  $Pb^{2+}$  sorption values for both resins decreased, but not in a very large degree. However, when 150 equiv. of  $Na^+$  to  $Pb^{2+}$  were present as the interference, the  $Pb^{2+}$  sorption values dropped markedly.

Elution profiles for this competitive sorption study are shown in Fig. 6. For both resins **1** and **2**, the profiles for the samples with 1:1 and 15:1 molar ratios of  $Na^+$  to  $Pb^{2+}$  do not differ greatly from those for without  $Na^+$  interference. The areas enclosed by the 150:1 molar ratio elution profiles and the horizontal axis are obviously much smaller than those enclosed by the other molar ratio profiles and the horizontal axis.

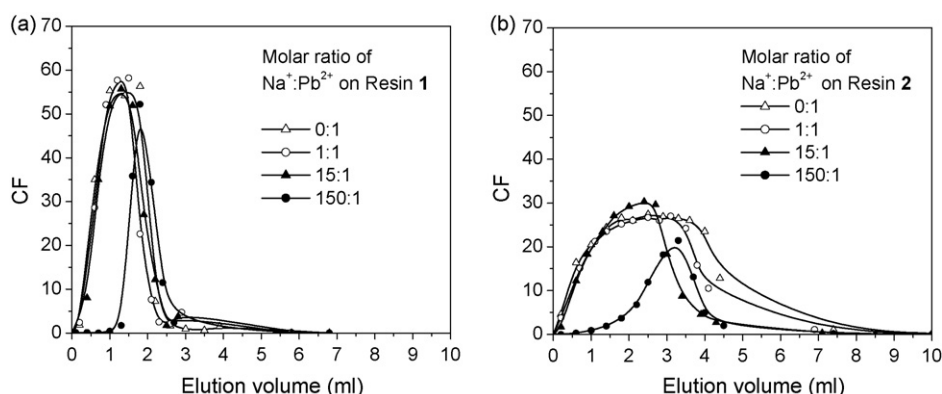


**Fig. 6.** Elution profiles for sorption of  $Pb^{2+}$  in the absence and presence of  $Na^+$  by resins (a) **1** and (b) **2**.

#### 4. Conclusions

We have examined the sorption properties of selected heavy metal ions by a series of silica gel-bound, di-ionizable calixarene-containing resins. Sorption reproducibility obtained in the three independent runs for a given resin and aqueous sample solution was good. No appreciable deterioration of sorption was observed after multiple runs with a single resin column.

For  $\text{Pb}^{2+}$  sorption by resins **1–9**, the sorption efficiencies are dependent on the structures of the calix[4]arene ligands and the acidity of the sample solutions. In competitive ion-exchange studies, the retention of  $\text{Pb}^{2+}$  on the selected resins was not dramatically influenced by the presence of up to 15 equiv. of  $\text{Na}^+$ , but was affected by the presence of large excesses of  $\text{Na}^+$  and an equivalent amount of competing  $\text{Cd}^{2+}$ . Stripping of sorbed  $\text{Hg}^{2+}$  from resin **1** could not be achieved due to the extremely high affinity of the resin for  $\text{Hg}^{2+}$ . In summary, these functionalized resins show the sorption selectivity order of  $\text{Hg}^{2+} \gg \text{Pb}^{2+} > \text{Cd}^{2+} > \text{Na}^+$ .

#### Acknowledgement

This research was supported by the Division of Chemical Sciences, Geosciences and Biosciences of the Office of Basic Energy Science of the U.S. Department of Energy (Grant DE-FG02-90ER14416).

#### References

- [1] D.R. Baldwin, W.J. Marshall, *Ann. Clin. Biochem.* 36 (1999) 267.
- [2] H. Horiguchi, H. Teranishi, K. Niiya, K. Aoshima, T. Katoh, N. Sakuragawa, M. Kasuya, *Arch. Toxicol.* 68 (1994) 632.
- [3] S.V. Matagi, D. Swai, R. Mugabe, *Afr. J. Trop. Hydrobiol. Fish* 8 (1998) 23.
- [4] R. Gupta, P. Ahuja, S. Khan, R.K. Saxena, H. Mohapatra, *Curr. Sci.* 78 (2000) 967.
- [5] D. Feng, C. Aldrich, H. Tan, *Miner. Eng.* 13 (2000) 623.
- [6] W.M. Landing, C. Haraldsson, N. Paxgus, *Anal. Chem.* 58 (1986) 3031.
- [7] B.L. Rivas, H.A. Maturana, I.M. Perić, *Angew. Makromol. Chem.* 211 (1993) 103.
- [8] I.M.M. Kenawy, M.A.H. Hafez, M.A. Akl, R.R. Lashein, *Anal. Sci.* 16 (2000) 493.
- [9] W. Trochimczuk, B.N. Kolarz, D. Jermakowicz-Bartkowiak, *Eur. Polym. J.* 37 (2001) 559.
- [10] C.C. Wang, C.Y. Chang, C.Y. Chen, *Macromol. Chem. Phys.* 202 (2001) 882.
- [11] E. Pehlivan, T. Altun, *J. Hazard. Mater. B* 134 (2006) 149.
- [12] J.D. Glennon, K. O'Connor, S. Srijaranai, K. Manley, S.J. Harris, M.A. Mc Kervey, *Anal. Lett.* 26 (1993) 153.
- [13] J.D. Glennon, E. Horne, K. Hall, D. Cocker, A. Kuhn, S.J. Harris, M.A. Mc Kervey, *J. Chromatogr. A* 731 (1996) 47.
- [14] W. Xu, J.S. Li, Y.Q. Feng, S.L. Da, Y. Zhang, *Chromatographia* 48 (1998) 245.
- [15] X.Z. Xiao, Y.Q. Feng, S.L. Da, Y. Zhang, *Chromatographia* 49 (1999) 643.
- [16] T. Takeuchi, J. Chu, T. Miwa, *Analysis* 24 (1996) 271.
- [17] M.P. O'-Connell, J. Treacy, C. Merly, C.M.M. Smith, J.D. Glennon, *Anal. Lett.* 32 (1999) 185.
- [18] K. Ohto, Y. Tanaka, K. Inoue, *Chem. Lett.* 7 (1997) 647.
- [19] K. Ohto, Y. Tanaka, M. Yano, T. Shinohara, E. Murakami, K. Inoue, *Solvent Extr. Ion Exch.* 19 (2001) 725.
- [20] K. Ohto, S. Inoue, N. Eguchi, T. Shinohara, K. Inoue, *Sep. Sci. Technol.* 37 (2002) 1943.
- [21] G.G. Talanova, H.S. Hwang, V.S. Talanov, R.A. Bartsch, *J. Chem. Soc., Chem. Commun.* 13 (1998) 1329.
- [22] G.G. Talanova, H.S. Hwang, V.S. Talanov, R.A. Bartsch, *J. Chem. Soc., Chem. Commun.* 3 (1998) 419.
- [23] D.M. Zhang, J. Wang, T.R. Lawson, R.A. Bartsch, *Tetrahedron* 63 (2007) 5076.
- [24] M.G. Hankins, T. Hayashita, S.P. Kasprzyk, R.A. Bartsch, *Anal. Chem.* 68 (1996) 2811.
- [25] R.L. Smith, D.J. Pietrzyk, *Anal. Chem.* 56 (1984) 610.
- [26] T. Hayashita, R.A. Bartsch, *Anal. Chem.* 63 (1991) 1847.
- [27] T. Hayashita, M.J. Goo, J.C. Lee, J.S. Kim, J. Krzykawski, R.A. Bartsch, *Anal. Chem.* 62 (1990) 2283.
- [28] T. Hayashita, J.H. Lee, S. Chen, R.A. Bartsch, *Anal. Chem.* 63 (1991) 1844.
- [29] T. Hayashita, J.H. Lee, M.G. Hankins, J.C. Lee, J.S. Kim, J.M. Knobeloch, R.A. Bartsch, *Anal. Chem.* 64 (1992) 815.
- [30] N. Ünlü, M. Ersoz, *J. Hazard. Mater. B* 136 (2006) 272.
- [31] A. Demirbas, E. Pehlivan, F. Gode, T. Altun, G. Arslan, *J. Colloid Interf. Sci.* 282 (2005) 20.





## Studies on the origin of the voltammetric response of the PC-3 cell suspension

Dong-Mei Wu<sup>a,b</sup>, Guang-Lei Fu<sup>b</sup>, Hong-Zhuang Fang<sup>b</sup>, Ling Hu<sup>b</sup>, Jin-Lian Li<sup>b</sup>,  
Xing Yuan<sup>a,\*</sup>, Zhuo-Yong Zhang<sup>a,c,\*</sup>

<sup>a</sup> College of Urban and Environmental Science, Northeast Normal University, Changchun 130024, China

<sup>b</sup> College of Chemistry and Pharmacy, Jiamusi University, Jiamusi 154007, China

<sup>c</sup> Department of Chemistry, Capital Normal University, Beijing 100037, China

### ARTICLE INFO

#### Article history:

Received 15 September 2008

Received in revised form

29 November 2008

Accepted 7 December 2008

Available online 13 December 2008

#### Keywords:

Electrochemistry

PC-3 cell

Guanine

Xanthine

### ABSTRACT

A novel experimental method was developed to study the origin of the voltammetric response of human prostate cancer (PC-3) cell suspension as a model in consideration of the biological characters of living cells. The presence of guanine and xanthine in the cell eluent secreted by the living cells was verified by HPLC assay with a DAD system and chemometric method. Comparative studies of voltammetric behaviors of the PC-3 cell suspension, the PC-3 cell eluent, and the PC-3 cell sediment re-suspension showed that the voltammetric response of the PC-3 cells was given by xanthine and guanine bases in the PC-3 cell eluent, not by the cells. Linear relationship between the peak currents of guanine and xanthine in the cell eluent and the cell concentrations was found. Other factors, such as the cell secretion time and the immersion time of the multiwalled carbon nanotubes modified glassy carbon electrode (MWCNTs-modified GCE) in the cell eluent, also influenced the intensity of the peak currents. The biochemical mechanisms of the voltammetric behavior for the cell suspension were proposed.

Crown Copyright © 2008 Published by Elsevier B.V. All rights reserved.

### 1. Introduction

Cell viability is traditionally evaluated by morphological observation including spectrophotometric methods, fluorescent microscopy, flow cytometry, and specialized fluorescence instruments such as plate readers [1]. In recent years, particular interest has been focused on the investigation of electrochemical behavior of tumor cells. Electrochemical methods, such as electrochemical impedance spectroscopy [2–5], scanning electrochemical microscopy [6,7], electric cell-substrate impedance sensing [8–11], open circuit potential at the cell/sensor interface [12], and electron transfer at electroactive centers in cells [13], have been approved to be effective to provide nonmorphological observation for following cell health state and establishing effective in vitro antitumor drug sensitivity tests [14]. Electrochemical methods are much more rapid, highly sensitive and inexpensive compared with conventional morphological methods. Efforts launched in this area have been focused mostly on constructing nano-material modified electrodes and building toolboxes for the investigation of immobilized whole tumor cells to obtain better electrochemical responses.

Carbon nanotubes (CNTs) modified electrodes exhibited excellent performance in monitoring the electrochemical behavior of tumor cells [14–16], and in evaluating the cytotoxicity of different drugs. Gold nanoparticles modified electrodes [17–19] were designed for immobilization of living tumor cells and monitoring adhesion, proliferation, and apoptosis of cells.

Despite of great efforts launched in this area, the mechanism of the electrochemical behavior of living cells is relatively poorly understood. Two possible mechanisms in previous reports were proposed as followed: (1) the voltammetric responses of the cells had relation with some enzymes [20–22], and (2) the electrochemical behavior of the living cells was attributed to the redox system of the living cells, which were derived from the redox centers in living cells or the species in cell cytoplasm, passing cell membrane rapidly, such as ions, proteins, nucleotide and metabolic products [23,24]. However, it seems that more information was needed to confirm the mechanism. There were few experiments had been performed to verify the presumptive voltammetric mechanism of living tumor cells mentioned above until Ju and his coworkers reported a significant discovery in 2005 [16,18]. They proposed that the voltammetric response was possibly related to the oxidation of guanine in cytoplasm by applying HPLC and LC-MS to verify the presence of guanine in cytoplasm and by using cyclic voltammetry to exhibit the similarity of voltammetric behavior between the living cells and guanine. Furthermore, due to some biological metabolism processes, transport process and cell death, an important fact that living cells constructed a dynamic living system

\* Corresponding authors: College of Urban and Environmental Science, North east Normal University, Changchun 130024, China. Tel.: +86 431 58099169; fax: +86 454 8793689.

E-mail addresses: [yuanx@nenu.edu.cn](mailto:yuanx@nenu.edu.cn) (X. Yuan), [gusto2008@vip.sina.com](mailto:gusto2008@vip.sina.com) (Z.-Y. Zhang).

rather than an unchangeable system, was neglected in the previous electrochemical measurements [25–28]. J. H. Chen presumed that the electroactive species existed not only on cell membrane but also intracellularly and extracellularly, due to the change of the cell permeability [15]. However, no further investigation was performed on the mechanism. Due to the shortage of information about the voltammetric mechanism of the living cells, applications of electrochemistry in the investigation of cell adhesion, proliferation, and apoptosis developed slowly. The mechanism of the electrochemical behaviors of the living cells is a challenging task and is of vital importance to promote the development of the cell electrochemistry.

Enlightened by the previous works of Ju and Chen mentioned above, accompanying with the consideration of the biological character of the living cells, the voltammetric mechanism of living human prostate cancer cells (PC-3) as a model was discussed and verified with a novel experimental method in this paper. The voltammetric response of living PC-3 cells was given by the oxidation of guanine and xanthine in the PC-3 cell secretion, which were related to the nucleotide catabolism in the living cells, not by the cells. The presence of uric acid was discovered and discussed. The peak currents of guanine and xanthine in the cell secretion were found having linear relationship with the cell concentration, and were also affected by the exogenous factors, including the cell secretion time and the immersion time of the multiwalled carbon nanotubes modified glassy carbon electrode (MWCNTs-modified GCE) in the cell eluent. Biochemical mechanisms of the voltammetric behavior for the cell suspension were proposed.

## 2. Experimental

### 2.1. Chemicals

Xanthine (Sigma, USA), xanthine oxidase (XOD, from cow buttermilk, Sigma, USA), guanine (National Institute for Control of Pharmaceutical and Biological Products, China) were obtained from the sources indicated. Xanthine, guanine and xanthine oxidase solutions were made up with phosphate buffer saline (PBS, pH 7.4) containing 136.7 mM NaCl, 2.7 mM KCl, 9.7 mM  $\text{Na}_2\text{HPO}_4 \cdot 12\text{H}_2\text{O}$ , 1.5 mM  $\text{KH}_2\text{PO}_4$ . Prior to use, high purity multiwalled carbon nanotubes modified (MWCNTs, 10–20 nm in diameter, Shenzhen Nanotech Port Co., China) were purified by refluxing in 30% nitric acid at 100 °C for 24 h. After separation from the mixture, the sediment was washed with double-distilled water until the pH reached 7.0, and then followed by filtering, rinsing with double-distilled water and drying. Finally, a 1.0 mg mL<sup>-1</sup> MWCNTs suspension was obtained. All other chemicals were of analytical grade and used as received.

### 2.2. Cell culture and collection

PC-3 cells were obtained as a gift from Institute of Biochemistry, Northeast Forestry University (Haerbin, China). The cells were cultured in RPMI 1640 medium (Gibco) containing 10% fetal calf serum, 100 µg mL<sup>-1</sup> penicillin (Gibco) and 100 µg mL<sup>-1</sup> streptomycin (Gibco) in an incubator (5% CO<sub>2</sub>, 37 °C). After a growth stage of 2 days, several flasks of obtained cells were digested with 0.25% trypsinase, separated from the medium by centrifugation at 1000 × g for 10 min, the obtained cell sediment was then washed with the sterile pH 7.4 PBS for three times, finally, the sediment was suspended in the sterile pH 7.4 PBS to obtain the PC-3 cell suspension with a certain cell concentration. Cell concentration was determined by using a CBC DRM-700 cell counting plate (China).

### 2.3. Production of the MWCNTs-modified GCE

Glassy carbon electrodes (GCE, 3 mm in diameter) were polished successively with 1.0, 0.3 and 0.05 µm alumina slurry, followed by rinsing thoroughly with double-distilled water. After sonicated in double-distilled water and alcohol successively, the electrodes were then dried at room temperature in a desiccator. After the MWCNTs suspension were fully dispersed by sonication, 10 µL of 1.0 mg mL<sup>-1</sup> MWCNTs suspension obtained was cast onto the surface of the GCE, and the electrodes were allowed to dry under an infrared lamp to give the MWCNTs-modified GCEs. Prior to the cyclic voltammetric measurement, the obtained MWCNTs-modified GCEs were electrochemically treated by performing several cycles between 0.0 and +0.8 V in pH 7.4 PBS until stable background lines were obtained. The MWCNTs-modified GCE remained about 87% of the initial current response of guanine in pH 7.4 PBS after being continuously processed for 30 times, which was scanned in pH 7.4 PBS containing guanine for one cycle and in pH 7.4 PBS for three cycles between 0.0 and +0.8 V.

### 2.4. Electrochemical measurements

Electrochemical measurements were performed on a LK2005 electrochemical analyzer (Tianjin Lanlike Instruments Co., China) with a conventional three-electrode system comprising a platinum wire as auxiliary, a Ag/AgCl (saturated KCl) electrode as reference, and a MWCNTs-modified GCE as the working electrode. The electrochemical behavior of PC-3 cells was studied using cyclic voltammetry in the potential range from 0.0 to +0.8 V with a scan rate of 50 mV s<sup>-1</sup> at 37 ± 0.5 °C. After each measurement, the MWCNTs-modified GCEs were scanned for five cycles between 0.0 and +0.8 V in pH 7.4 PBS, and rinsed thoroughly with double-distilled water, the obtained electrodes showed not only very similar shape but also very similar height in the same sample solution by cyclic scan, indicating that the used MWCNTs-modified GCEs were well renewed based on their maintenance of stability. All voltammetric measurements except indicated specially in the text were immediately performed after the MWCNTs-modified GCE was immersed into sample solutions.

### 2.5. HPLC measurements

6.2 × 10<sup>6</sup> cells mL<sup>-1</sup> PC-3 cell suspension secreted for 35 min at 37 °C was centrifuged at 1000 × g for 10 min, and the obtained eluent was stored at 50 °C for 30 min to remove the protein. After a further centrifugation at 14000 × g for 50 min, the obtained cell eluent was filtrated through a 0.22 µm filter. The voltammetric behavior of the cell eluent obtained above consisted with that of the cell eluent obtained by centrifuged at 1000 × g for 10 min, which was used in electrochemical measurements (not shown data). This result indicated that both of the cell eluents contained the same electroactive species. The former was subjected to HPLC analysis. HPLC detections at 270 nm were performed on an Angilent 1100 separation module comprising an Angilent XDB-C18 column (4.6 mm × 250 mm) at 25 °C equipped with a DAD system. The mobile phase, consisting of 897 mL H<sub>2</sub>O, 100 mL CH<sub>3</sub>OH, 1.5 mL CH<sub>3</sub>COOH, and 1.5 mL C<sub>16</sub>H<sub>37</sub>NO (40%), was run at 1.0 mL min<sup>-1</sup>. 20 µL of each sample was injected into the HPLC system for analysis.

### 2.6. Component identification

Spectra of guanine and xanthine standards and sample solution were recorded by DAD at 200–360 nm. Then cosine values between spectral vectors of suspected components and guanine and xanthine standards were calculated, respectively. If the cosine value between the spectral vectors of suspected component and

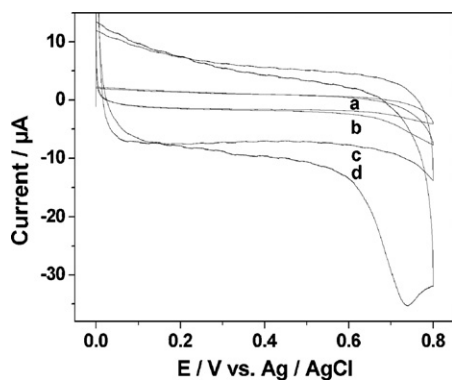


**Fig. 1.** Cyclic voltammograms of (a) the bare GCE in pH 7.4 PBS, (b) the bare GCE in the PC-3 cell suspension, (c) the MWCNTs-modified GCE in pH 7.4 PBS, (d) the MWCNTs-modified GCE in the PC-3 cell suspension. Cell concentration,  $2.5 \times 10^6$  cells  $\text{mL}^{-1}$ ; immersion time of the electrodes, 30 min; the PC-3 cell suspension time in pH 7.4 PBS, 35 min.

standard is close to 1.000, the suspected component can be considered as the same as the standard.

### 3. Results and discussion

#### 3.1. Voltammetric behavior of PC-3 cells

The freshly collected PC-3 cells were suspended in pH 7.4 PBS at  $37^\circ\text{C}$  for 35 min, then the cyclic voltammograms of PC-3 cells were measured after the bare or the MWCNTs-modified GCE was immersed in the above PC-3 cell suspension for 30 min as shown in Fig. 1. No peak was observed at the bare GCE in pH 7.4 PBS (Fig. 1a), the MWCNTs-modified GCE in pH 7.4 PBS (Fig. 1c), and the bare GCE in the PC-3 cell suspension (Fig. 1b). The background current of the MWCNTs-modified GCE was greater than that of the bare GCE, which was due to the enhanced effective surface area of the modified electrode. At the MWCNTs-modified GCE, the PC-3 cell suspension showed a well-defined anodic peak at  $+0.738\text{ V}$  (Fig. 1d) in the first scan, implying that MWCNTs showed electrocatalytic property to the electrochemical oxidation of electroactive species in the PC-3 cell suspension. No corresponding reduction peak appeared in the inverse scan, which was characteristic of an irreversible electrode process. The peak current decreased greatly or disappeared in the second scan (not shown in Fig. 1) attributed to possible products of oxidation reaction that blocked the electrode surface.

The conventional experiments of measuring voltammetric response of tumor cells were usually carried out in the tumor

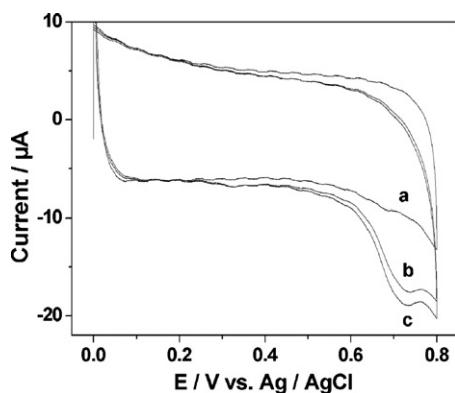


**Fig. 2.** Cyclic voltammograms of (a) the PC-3 cell sediment re-suspension, (b) the PC-3 cell eluent, (c) the PC-3 cell suspension uncentrifuged. Cell concentration,  $4.5 \times 10^6$  cells  $\text{mL}^{-1}$ ; cell suspension time, 35 min.

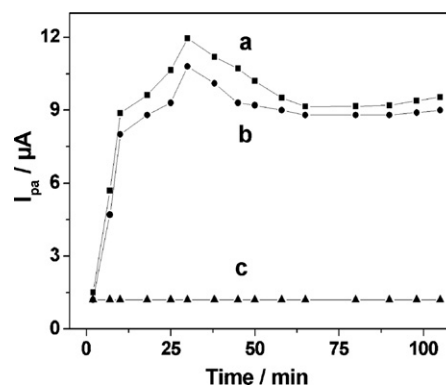


**Fig. 3.** Effect of secretion time of PC-3 cells on the peak current of (a) the PC-3 cell suspension, (b) the PC-3 cell eluent, (c) the PC-3 cell sediment re-suspension. Cell concentration,  $1.2 \times 10^6$  cells  $\text{mL}^{-1}$ .

cell suspension, which contained both living cells and secretion released by the living cells, in fact. To study the sources of the voltammetric response of PC-3 cells, the PC-3 cell suspension obtained in pH 7.4 PBS for 35 min at  $37^\circ\text{C}$ , was partly separated into two parts by centrifugation at  $1000 \times g$  for 10 min. One was the cell eluent and the other was the cell sediment, the latter was then re-suspended with pH 7.4 PBS of the same volume to that of the PC-3 cell eluent. The voltammetric measurement was immediately performed when the MWCNTs-modified GCE was immersed into the PC-3 cell suspension, the PC-3 cell eluent and the cell sediment re-suspension, respectively. An interesting phenomenon was observed as shown in Fig. 2. Voltammetric response of the PC-3 cell eluent (Fig. 2b) approximated sufficiently to that of the PC-3 cell suspension uncentrifuged (Fig. 2c), whereas the cell sediment re-suspension (Fig. 2a) showed an obvious weak response. The result implied that the voltammetric response of the PC-3 cell was produced mostly from the extracellular species secreted by PC-3 cells, but rarely from the membrane or the interior of PC-3 cells. However, the previous reports speculated mostly that the voltammetric response of living cells suspension should be produced from cell cytoplasm or cell membrane [16,18,19,23,24].

Fig. 3 showed the effect of secretion time of PC-3 cells on the peak currents of the PC-3 cell suspension, the PC-3 cell eluent and the PC-3 cell sediment re-suspension. As the secretion time increased, the peak currents of the cell eluent and the cell suspension increased until 30 min. The influence of secretion time on the peak current of the cell eluent corresponded well with that of the cell suspension. However, the peak currents of the cell suspension were higher than that of the cell eluent. But the peak currents of the cell sediment re-suspension were almost independent on the secretion time. These phenomena implied that with the increase of secretion time, the concentration of the electroactive species increased in the eluent and constant on the cell membrane. In measuring process, the concentrations of the electroactive species in the cell suspension changed with the measuring times, whereas, these in the cell eluent, which was separated from the cell suspension, did not change with the measuring times and possessed the similar intensity of the peak currents. Thus, measuring voltammetric response of the cell eluent is more significant than that of the cell suspension. However, it was difficult to interpret the decrease of the peak currents of both the cell eluent and the cell suspension after 30 min, which needed further investigation.

#### 3.2. HPLC and chemometric confirmation of xanthine and guanine in PC-3 cell eluent

The typical chromatogram of the mixture of  $32.47\ \mu\text{g mL}^{-1}$  guanine and  $3.83\ \mu\text{g mL}^{-1}$  xanthine detected at 270 nm was shown

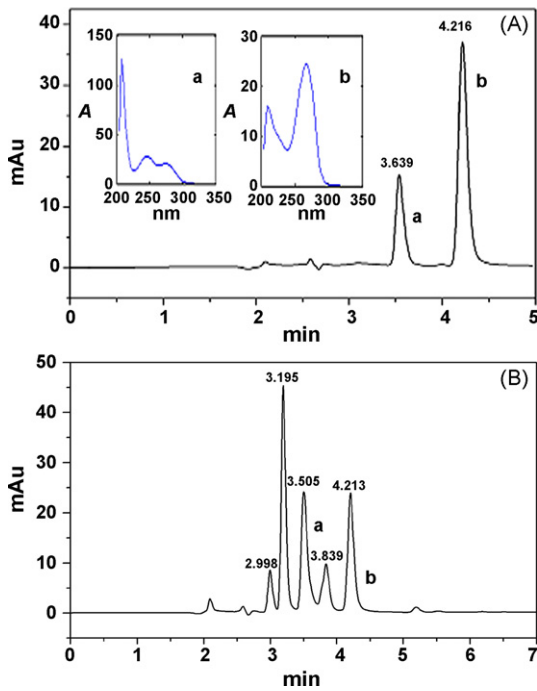


Fig. 4. Chromatograms of (A) the mixture of  $32.47 \mu\text{g mL}^{-1}$  guanine (a) and  $3.83 \mu\text{g mL}^{-1}$  xanthine (b), (B) the PC-3 cell eluent ( $6.2 \times 10^6$  cells  $\text{mL}^{-1}$ ) secreted for 35 min. Inset: UV spectrum of (a) guanine, (b) xanthine.

in Fig. 4A. The inserted subfigures (a) and (b) gave the UV spectra at the peaks in the chromatogram. Guanine and xanthine showed a retention time of 3.539 and 4.216 min, respectively. The peak areas were proportional to guanine and xanthine concentration in the range of  $1.00\text{--}100.00 \mu\text{g mL}^{-1}$  and  $0.10\text{--}10.00 \mu\text{g mL}^{-1}$  with a detection limit of  $0.01 \mu\text{g mL}^{-1}$ , respectively. The regression equations with the same correlation coefficient of 0.9999 were  $S_{\text{guanine}} = 2.82C_{\text{guanine}} (\mu\text{g mL}^{-1}) - 1.24$  and  $S_{\text{xanthine}} = 66.59C_{\text{xanthine}} (\mu\text{g mL}^{-1}) - 4.95$ , respectively. The chromatogram of the PC-3 cell eluent, in which the PC-3 cells had secreted for 35 min, displayed five chromatographic peaks at 2.998, 3.195, 3.505, 3.839 and 4.213 min (Fig. 4B), respectively. Two chromatographic peaks at 3.505 and 4.213 min of the PC-3 cell eluent were in good agreement with that of the mixture of guanine and xanthine, indicating the probable existence of guanine and xanthine in the PC-3 cell eluent. Similarities were calculated for the obtained spectra with guanine and xanthine, respectively. The cosine value between the spectral vector of PC-3 cell eluent at 3.505 min and that of guanine is 0.9980, and the cosine value between the spectral vector of PC-3 cell eluent at 4.213 min and that of xanthine is 0.9960. It can be concluded that the components in the PC-3 cell eluent at 3.505 and 4.213 min are guanine and xanthine, respectively. However, there were another three unknown chromatographic peaks in the cell eluent as observed, which needed further investigation. From the peak areas of guanine and xanthine in the PC-3 cell eluent and the regression equations, the concentration of guanine and xanthine in the PC-3 cell eluent ( $6.2 \times 10^6$  cells  $\text{mL}^{-1}$ ) secreted for 35 min were detected to be  $63.78$  and  $2.56 \mu\text{g mL}^{-1}$ , respectively.

### 3.3. Voltammetric comparison among guanine, xanthine, and the PC-3 cell eluent

Oxidation peak potentials ( $E_{\text{pa}}$ ) of both xanthine and guanine were linearly dependent on the pH value of solutions as shown in Fig. 5. The linear equation of xanthine and guanine in pH range of 6.4–8.0 were  $E_{\text{pa}} = 1.18 - 0.0647\text{pH}$  ( $R = 0.99524$ ),  $E_{\text{pa}} = 1.19 - 0.0644\text{pH}$  ( $R = 0.99815$ ), respectively. The slope of xan-

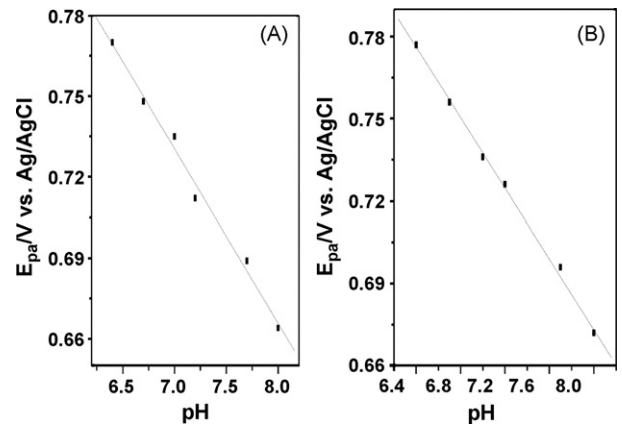


Fig. 5. Influence of pH on the oxidation peak potential of (A) xanthine, (B) guanine.

thine and guanine were  $64.7$  and  $64.4 \text{ mV/pH}$ , respectively, which were close to the theoretical value of  $58.6 \text{ mV/pH}$ , indicating that there were two protons involved per transfer of two electrons during the oxidation of both xanthine and guanine [18,29]. As the pH value increased,  $E_{\text{pa}}$  of both xanthine and guanine shifted to the negative direction.

In Fig. 6, the peak potentials of guanine (Fig. 6b) and xanthine (Fig. 6c) were  $+0.709$  and  $+0.702 \text{ V}$ , respectively, which were similar to that of the PC-3 cell eluent ( $+0.673 \text{ V}$ , Fig. 6a). A negligible difference in peak potentials between the cell eluent and guanine and xanthine in pH 7.4 PBS was possibly attributed to the weak pH increase resulted by secreting guanine base and xanthine base into the cell eluent of PC-3 cells. The result indicated that the irreversible anodic peak of the PC-3 cell eluent was attributed to the oxidation of guanine and xanthine secreted in the cell eluent by PC-3 cells.

### 3.4. Catalytic action of xanthine oxidase on the PC-3 cell eluent

XOD is a metalflavoprotein that plays an important role in the metabolism of nucleotides. It catalyzes the oxidation of hypoxanthine to xanthine and xanthine to uric acid. XOD is present in large amounts in liver and intestinal mucosa and in traces in other tissues [30]. Fig. 7 showed the catalytic action of XOD on the cell eluent. The cyclic voltammogram of XOD in pH 7.4 PBS (Fig. 7e) showed no peak. The anodic peak current of xanthine in pH 7.4 PBS (Fig. 7c) decreased dramatically after incubated with XOD (Fig. 7d), an obvious irreversible anodic peak of uric acid appeared at about  $+0.300 \text{ V}$ , indicating the highly catalyzing of xanthine to uric acid by XOD. Significantly, there was a similar phenomenon after XOD was added to

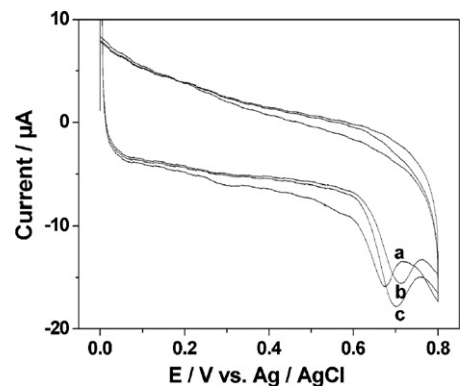
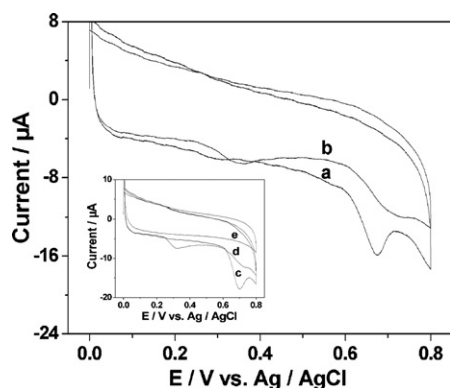


Fig. 6. Cyclic voltammograms of (a) the PC-3 cell eluent, (b)  $10 \mu\text{g mL}^{-1}$  guanine in pH 7.4 PBS, (c)  $10 \mu\text{g mL}^{-1}$  xanthine in pH 7.4 PBS. Cell concentration,  $4.5 \times 10^6$  cells  $\text{mL}^{-1}$ ; secretion time, 10 min.

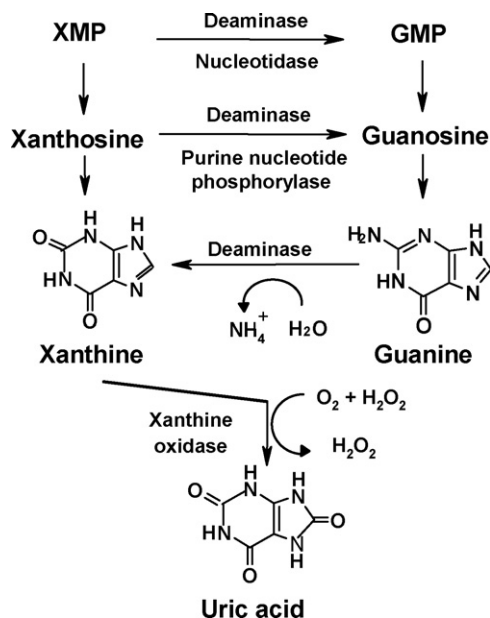


**Fig. 7.** Cyclic voltammograms of (a) the PC-3 cell eluent, (b) the PC-3 cell eluent after incubated with  $5 \times 10^{-5}$  M xanthine oxidase for 30 min at  $37^\circ\text{C}$ , (c)  $10 \mu\text{g mL}^{-1}$  xanthine in pH 7.4 PBS, (d)  $10 \mu\text{g mL}^{-1}$  xanthine in pH 7.4 PBS after incubated with  $5 \times 10^{-5}$  M xanthine oxidase for 30 min at  $37^\circ\text{C}$ , (e)  $5 \times 10^{-5}$  M xanthine oxidase in pH 7.4 PBS.

both xanthine and the PC-3 cell eluent (Fig. 7), indicating that xanthine is one of the important sources of the voltammetric response of the PC-3 cell eluent, despite the concentration of xanthine in the PC-3 cell eluent was lower than that of guanine. The same anodic peak of uric acid appeared in both the cell suspension and the eluent when the cells secreted for longer time without XOD.

In addition to their well known intracellular functions related to the nucleotide metabolism, purines intracellular including guanine, xanthine, adenine and hypoxanthine, are able to be secreted into the extracellular space, where they act as intracellular signalling molecules stimulated by exogenous conditions [31]. Guanine and xanthine intracellular could be related to the catabolism of guanine nucleotide (GMP) and xanthine nucleotide (XMP) in living cells as illustrated in Scheme 1.

Guanine and xanthine were catabolic intermediates of the catabolic process, and uric acid is the end product whose extracellular concentration depends on the content of xanthine oxidase in living cells as illustrated. Guanine and xanthine were then secreted into the cell eluent by transport process, and the electrochemical response was given by xanthine and guanine bases, not by the cells. Thus, the electrochemical measurement of guanine and xanthine



**Scheme 1.** Catabolism of guanine and xanthine nucleotides intracellular.

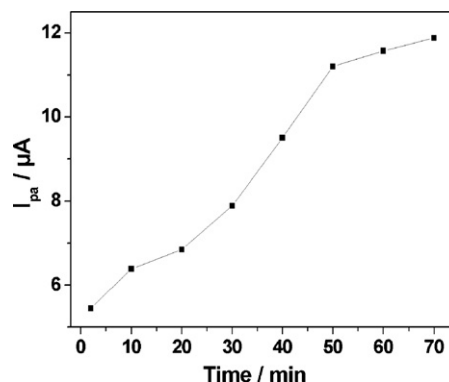


**Fig. 8.** Influence of immersion time of the MWCNTs-modified GCE in the PC-3 cell eluent on the peak current. Cell concentration,  $1.5 \times 10^6$  cells  $\text{mL}^{-1}$ ; secretion time, 35 min.

extracellular could provide important information on intracellular nucleotides which have intimate relation with the cell viability. There is no doubt that knowledge on nucleotide metabolism in normal and tumor cells would be important for identifying the main changes between normal and tumor cells [32–34]. So, the proposed biochemical mechanism of the voltammetric behavior of the cells was beneficial for the further application of the electrochemical method in cell bioanalysis. For example, based on the mechanism, the simple electrochemical method could be used to continuously monitor guanine and xanthine secreted by the living cells to obtain the information on nucleotide metabolism, which could evaluate cell health state and antitumor drug sensitivity. The mechanism could also guide constructing the modified electrode as a cellular biosensor to obtain strong voltammetric response of the cells.

### 3.5. Influence of immersion time of the electrode in the cell eluent on the peak current

With the increasing immersion time of the MWCNTs-modified GCE in the cell eluent, the peak current increased obviously until 50 min as shown in Fig. 8, and longer immersion time did not increase the current response positively. The result exhibited a distinct character of adsorptive electrode process of electroactive species, such as xanthine and guanine secreted in the cell eluent by PC-3 cells. The similar phenomenon was found in measuring the voltammetric response of the PC-3 cell suspension, the PC-3 cell sediment re-suspension, guanine and xanthine (not shown data).

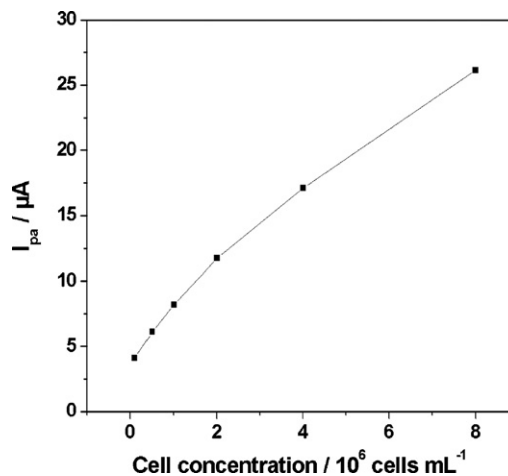


**Fig. 9.** Relationship between the peak current of the PC-3 cell eluent and the cell concentration. Immersion time of the electrode, 30 min; secretion time, 35 min.

### 3.6. Relationship between the peak current of the PC-3 cell eluent and the cell concentration

Cyclic voltammograms of PC-3 cell eluents with different cell concentrations were measured. As previously reported, there was a linear relationship between the peak currents of living cells cultured in the same condition and the cell concentrations [25], however, in this paper, a nonlinear relationship between the peak currents of the cell eluent and the cell concentrations from  $10^5$  to  $8 \times 10^6$  cells mL<sup>-1</sup> was found as shown in Fig. 9.

### 4. Conclusions

The first insight into the mechanism of the voltammetric behavior of the PC-3 cells as a model was provided by a novel experimental method. Electrochemical response of living cells was given by xanthine and guanine bases in the PC-3 cell eluent, not by the cells. The existence of uric acid was discovered and discussed. Guanine, xanthine and uric acid were related to the catabolism of guanine nucleotide and xanthine nucleotide. With the increasing of the cell secretion time, peak currents of guanine and xanthine in the cell eluent increased until 35 min, while peak currents of the cell membrane or interior were constant. Peak currents of guanine and xanthine in the cell eluent were found having linear relationship with the cell concentration, and were affected by the immersion time of the electrode in the cell eluent. Biochemical mechanisms of the voltammetric behavior for the cells were proposed, which were beneficial for the further application of the electrochemical method in cell bioanalysis.

### Acknowledgements

We gratefully acknowledge the financial support of the National Natural Science Foundation of China (20875065), the Nature Science Foundation of Heilongjiang province (B200609) and Zhejiang (Y205706), Science Foundation of Heilongjiang province Ministry of Education (10541221) and the Foundation of Jiamusi University (L2007-90).

### References

- [1] S. Andreescu, O.A. Sadik, D.W. McGee, *Anal. Chem.* 76 (2004) 2321.
- [2] L. Yang, Y. Li, C.L. Griffis, M.G. Johnson, *Biosens. Bioelectron.* 19 (2004) 1139.
- [3] A. Dheilly, I. Linossier, A. Darchen, D. Hadjiev, C. Corbel, V. Alonso, *Appl. Microbiol. Biotechnol.* 79 (2008) 157.
- [4] L.J. Yang, Y.B. Li, G.F. Erf, *Anal. Chem.* 76 (2004) 1107.
- [5] H. Chen, C.K. Heng, P.D. Puiui, X.D. Zhou, A.C. Lee, T.M. Lim, S.N. Tan, *Anal. Chim. Acta* 554 (2005) 52.
- [6] Y. Torisawa, T. Kaya, Y. Takii, D. Oyamatsu, M. Nishizawa, T. Matsue, *Anal. Chem.* 75 (2003) 2154.
- [7] P.M. Diakowski, Z.F. Ding, *Phys. Chem. Chem. Phys.* 9 (2007) 5966.
- [8] C. Xiao, B. Lachance, G. Sunahara, J.H.T. Luong, *Anal. Chem.* 74 (2002) 5748.
- [9] L. Ding, D. Du, J. Wu, H.X. Ju, *Electrochem. Commun.* 9 (2007) 953.
- [10] C. Xiao, J.H.T. Luong, *Toxicol. Appl. Pharm.* 206 (2005) 102.
- [11] S. Arndt, J. Seebach, K. Psathaki, H.J. Galla, J. Wegener, *Biosens. Bioelectron.* 19 (2004) 583.
- [12] D.E. Woolley, L.C. Tetlow, D.J. Adlam, D. Gearey, R.D. Eden, T.H. Ward, T.D. Allen, *Exp. Cell Res.* 273 (2002) 65.
- [13] H.N. Li, Y.X. Ci, J. Feng, K. Cheng, S. Fu, D.B. Wang, *Bioelectrochem. Bioenerg.* 48 (1999) 171.
- [14] K. Chen, J.H. Chen, M.L. Guo, Z.F. Li, S.Z. Yao, *Electroanalysis* 18 (2006) 1179.
- [15] W. Cheng, L. Ding, J.P. Lei, S.J. Ding, H.X. Ju, *Anal. Chem.* 80 (2008) 3867.
- [16] J. Chen, D. Du, F. Yan, H.X. Ju, H.Z. Lian, *Chem. Eur. J.* 11 (2005) 1467.
- [17] F. Yan, J. Chen, H.X. Ju, *Electrochem. Commun.* 9 (2007) 293.
- [18] D. Dua, S.L. Liu, J. Chen, H.X. Ju, H.Z. Lian, J.X. Lia, *Biomaterials* 26 (2005) 6487.
- [19] L. Ding, C. Hao, Y.D. Xue, H.X. Ju, *Biomacromolecules* 8 (2007) 1341.
- [20] J. Feng, G.A. Luo, H.Y. Jian, R.G. Wang, C.C. An, *Electroanalysis* 12 (2000) 513.
- [21] J. Li, X. Liu, M. Guo, Y. Liu, S. Liu, S. Yao, *Anal. Sci.* 21 (2005) 561.
- [22] A. Sucheta, B.A.C. Ackrell, B. Cochran, F.A. Armstrong, *Nature* 356 (1992) 361.
- [23] D.E. Woolley, L.C. Tetlow, D.J. Adlam, D. Gearey, R.D. Eden, T.H. Ward, T.D. Allen, *Exp. Cell Res.* 273 (2002) 65.
- [24] W. Nonner, B. Eisenberg, *J. Mol. Liq.* 87 (2000) 149.
- [25] Y.X. Ci, Q. Zhai, S. Wang, W.B. Chang, C.Y. Zhang, H. Ma, D.Y. Chen, M.Z. Zhao, S.W. Hu, *Talanta* 55 (2001) 693.
- [26] J. Feng, Y.X. Ci, J.L. Lou, X.Q. Zhang, *Bioelectrochem. Bioenerg.* 48 (1999) 217.
- [27] H.N. Li, Y.X. Ci, J. Feng, K. Cheng, S. Fu, D.B. Wang, *Bioelectrochem. Bioenerg.* 48 (1999) 171.
- [28] Y.X. Ci, Z.J. Feng, W. Jiang, D.Z. Luo, *Bioelectrochem. Bioenerg.* 43 (1997) 293.
- [29] P.V. Bernhardt, M.J. Honeychurch, A.G. McEwan, *Electrochem. Commun.* 8 (2006) 257.
- [30] R. Harrison, *Free Rad. Biol. Med.* 33 (2002) 774.
- [31] F. Xiao, C.P. Ruan, J.G. Li, L.H. Lin, *Electroanalysis* 20 (2008) 361.
- [32] P. Di Iorio, P. Ballerini, F. Caciagli, L. Ciccarelli, *Pharmacol. Res.* 37 (1998) 169.
- [33] I. Baranowska-Bosiacka, B. Machalinski, J. Tarasiuk, *Cell. Mol. Biol. Lett.* 10 (2005) 217.
- [34] M.J. Clark, S.M. Richards, M. Hettiarachchi, J.M. Ye, G.J. Appleby, S. Rattigan, E.Q. Colquhoun, *Biochem. J.* 266 (1990) 765.



# Automated sampling system for the analysis of amino acids using microfluidic capillary electrophoresis

Zhang-Run Xu\*, Yue Lan, Xiao-Feng Fan, Qi Li

Research Center for Analytical Sciences, Northeastern University, Shenyang 110004, China

## ARTICLE INFO

### Article history:

Received 14 September 2008

Received in revised form

23 November 2008

Accepted 24 November 2008

Available online 3 December 2008

### Keywords:

Automated sampling

Microfluidics

Capillary electrophoresis

Liquid-core waveguide

Laser-induced fluorescence

Amino acids

## ABSTRACT

An improved automated continuous sample introduction system for microfluidic capillary electrophoresis (CE) is described. A sample plate was designed into gear-shaped and was fixed onto the shaft of a step motor. Twenty slotted reservoirs for containing samples and working electrolytes were fabricated on the “gear tooth” of the plate. A single 7.5-cm long Teflon AF-coated silica capillary serves as separation channel, sampling probe, as well as liquid-core waveguide (LCW) for light transmission. Platinum layer deposited on the capillary tip serves as the electrode. Automated continuous sample introduction was achieved by scanning the capillary tip through the slots of reservoirs. The sample was introduced into capillary and separated immediately in the capillary with only about 2-nL gross sample consumption. The laser-induced fluorescence (LIF) method with LCW technique was used for detecting fluorescein isothiocyanate (FITC)-labeled amino acids. With electric-field strength of 320 V/cm for injection and separation, and 1.0-s sample injection time, a mixture of FITC-labeled arginine and leucine was separated with a throughput of 60/h and a carryover of 2.7%.

© 2008 Elsevier B.V. All rights reserved.

## 1. Introduction

Amino acids are basic protein constituents and are important biological compounds with special physiological functions in antibodies as a necessary nutritional ingredient. The analysis of amino acids is a field which has been much concerned and full of challenge. High-performance liquid chromatography (HPLC) is often used for the analysis of amino acids; nevertheless it sometimes leads to long separation time and large dissolvent consumption. CE has come to be a powerful separation technique for amino acid analysis in years past due to its high separation efficiency, short analysis time and small sample consumption [1,2]. These advantages are better displayed in microfluidic CE systems [3–5]. Despite all that, sample introduction is still the bottleneck in microfluidic CE systems. The troublesome and time-consuming sample changing greatly affects the overall throughput in most microfluidic CE systems.

Some automated sample introduction methods were proposed to solve the world-to-chip interface problem in microfluidic devices [6,7]. Unfortunately, only a few methods were related to amino acid analysis with microfluidic CE. Fang's group reported flow/sequential injection coupled to the miniaturized CE systems through split-flow sampling interfaces for achieving continuous

sample introduction [8–12]. The maximum throughputs of 48/h [8], 144/h [9] and 80/h [10] were achieved with sample consumptions of 3.3, 30 and 80  $\mu$ L, respectively for amino acids analysis. Harrison's group [13] reported a split-flow sampling interface for automating sample introduction into electrokinetic microchip without perturbing the liquids within the microfluidic device. A house vacuum and a three-way valve were used in the system, and the sample consumption was 6  $\mu$ L. Lin et al. [14] reported an interface that coupled electrophoretic microchip with flow-through analyzer for uninterrupted sampling. A syringe pump was utilized to transport the external sample. Using split-flow sampling interfaces, automated high-throughput sampling was achieved in these systems. Although only pL–nL level samples were injected into the separation channels, the sample consumption usually exceeded 10  $\mu$ L for sample changing and introduction.

The sample consumption would be decreased by using a capillary as sampling probe. Fang's group [15] reported an efficient world-to-chip interface for chip-based CE separation of amino acids. A platinum electrode was fixed on the tip of a fused-silica capillary connecting with the sample-loading channel of a crossed-channel chip. Scanning the capillary probe through the slots of the vials, samples were continuously introduced electrokinetically into the sample-loading channel. A throughput of 36/h was achieved with 240-nL net sample consumption. Recently, a monolithic sampling probe on glass chip was used for substituting the capillary, and a much lower sample consumption of 30 nL was obtained [16]. In above-mentioned systems, the sample was introduced into a

\* Corresponding author. Tel.: +86 24 83687659; fax: +86 24 83676698.

E-mail address: [xuzr@mail.neu.edu.cn](mailto:xuzr@mail.neu.edu.cn) (Z.-R. Xu).

loading channel via the capillary, and then the sample was injected into the separation channel by a cross-channel injector on microchip. A simpler sample introduction interface was reported by Wang's group [17]. The sample was introduced directly into the separation channel through a sharp inlet tip placed in the sample vial. The inlet terminal of the separation channel was sharpened with a diamond saw, and a Pt wire attached to the sharp inlet served as contact to the high-voltage power supply. Fang's group [18] also reported a simple sample introduction system for miniaturized CE system. Automated continuous sample introduction and separation were achieved with a short capillary and a sample introduction system based on slotted micro-vial array. The system was applied in separation of sulphamethoxazole and trimethoprim in sulphatrim tablets, and a high-throughput of 72/h and a low carryover of 1.4% were achieved.

In our earlier report [19], a slotted-vial array sample introduction system was combined with miniaturized capillary electrophoresis for DNA analysis. The homemade slotted-vials and circular sample plate were used for sample presentation. In this work, a modified continuous sample introduction system was combined with a short Teflon AF-coated silica capillary to form an automated microfluidic CE system. The automated sampling system was composed of a monolithic plastic sample plate with reservoirs and a step motor controlled by personal computer. The performances of the system were demonstrated by the separation and determination of FITC-labeled amino acids with liquid-core waveguide (LCW)-based laser-induced fluorescence (LIF) detection.

## 2. Experimental

### 2.1. Chemicals

All reagents used were of analytical reagent grade, and deionized water was used throughout. Working electrolyte for CE separation was 10 mmol/L sodium tetraborate buffer by adjustment with 1 mol/L NaOH solution to pH 9.2. A 0.1 mol/L NaOH was used as capillary washing solution. Stock solutions of 10 mmol/L arginine and leucine (Kangda Amino Acid Works, Shanghai, China) were prepared in water. Forty millimole per liter FITC (Sigma, St. Louis, MO, USA) labeling reagent was prepared in acetone (containing 1%, v/v pyridine) fresh before use. FITC-labeled amino acid stock solutions containing each amino acid at 3.5 mmol/L were prepared by mixing 350  $\mu$ L of each amino acid stock solution with 550  $\mu$ L of sodium tetraborate buffer and 100  $\mu$ L of FITC solution, and allowed reaction overnight in the dark. Working sample solutions were prepared by diluting FITC-labeled amino stock solutions with 10 mmol/L borate buffer.

### 2.2. Apparatus

The experimental setup was shown in Fig. 1. The automated sampling system was composed of a plastic sample plate with reservoirs (7-mm depth and 3.5-mm diameter), and a step motor which was used to drive the plate. The diameter of sample plate was only 7 cm. Twenty reservoirs with slot for containing samples and working electrolytes distributed proportionally on the edge of the plate. A home-built high-voltage power supply (variable range 0–3000 V) controlled by a personal computer was used for sample introduction and CE separation. A diode laser with 473 nm (MBL-I, 10 mW, Changchun New Industries Optoelectronics Tech. Co., Ltd., Changchun, China) was used as excitation light source. The laser beam illuminating the excitation point was restricted using a pin-hole of 200- $\mu$ m diameter fixed close to the capillary. A 7.5-cm long fused-silica capillary coated by Teflon AF-1600 (50  $\mu$ m i.d., 363  $\mu$ m o.d., TSU050375, Polymicro Technologies, Phoenix, AZ, USA) served

as the separation channel and LCW for transmitting emission light. The inlet terminal of the capillary was deposited with titanium film by sputtering, and then a platinum layer, served as electrode, was deposited onto the titanium film. The capillary outlet was in a reservoir which had a 0.2-mm-thick glass window allowing the emission light to pass. A photomultiplier tube (PMT, Model H5784, Hamamatsu, Shizuoka-Ken, Japan) faced the glass window, and a long-wave pass filter (510 nm cutoff filter, HB Optical, Shenyang, China) was between them. The signal output from the PMT was recorded using a chromatography workstation (Model HW-2000, Qianpu Software Co., Shanghai, China). The entire detection system was enclosed in a black box. The sampling system and high-voltage power supply were controlled by a computer program written in Visual Basic.

### 2.3. Procedures

Before use, the capillary was sequentially washed with 0.1 mol/L NaOH, water, and 10 mmol/L sodium tetraborate buffer, each for 2 min for refreshing the capillary wall. A platinum electrode was immersed into the buffer solution in the outlet reservoir. The reservoirs of the sample plate were filled alternately with 40  $\mu$ L samples and 40  $\mu$ L buffer. The capillary inlet terminal deposited with platinum layer was immersed in the buffer by rotating the sample plate. Then, voltages of 2400 and 0 V were applied to the inlet electrode and outlet electrode, respectively. The automated electrokinetic continuous sampling process was achieved by sweeping the capillary tip through slots of the reservoirs.

## 3. Results and discussion

### 3.1. Considerations in the automated sampling system design

In the slotted-vial array sample introduction system, free passage of the capillary sampling probe through all the vial slots is the key to achieving automated continuous sample introduction. In previous reports [15,16,18–20], the slotted-vials were manually produced from 0.2-mL microtube by fabricating 1.5-mm-wide or 1-mm-wide, 2-mm-deep slots on the bottom of the tubes for pass-through of the sampling probe. Even though the slots were fabricated carefully, it is still difficult to ensure unification of the slots in shape and dimension. The slotted-vials were horizontally fixed on a platform in an array. The positions (such as right and left, up and down, back and forth, etc.) of the vials need adjusting carefully. In those work, good results have been obtained, however, scanning of the probe through all the slots was still not easy to achieve, which would greatly affect the reliability of the systems.

To ensure the reliability of the automated sampling, a monolithic plastic sample plate was designed in this work. In our earlier work, the sample plate was designed into a circular shape, and a slot was fabricated along the profile edge of the plate. For holding the same number of vials, circular array is three times shorter than linear array. And also movement of linear array requires about twice dimensional space. Compared with the linear slotted-vial array, the circular array facilitates miniaturization of the system. Unfortunately, severe cross-contamination is likely to occur due to the sample carried by the probe passing between the neighboring reservoirs. In our following work, the design of a gear-shaped sample plate was adopted. Slotted reservoir was fabricated on each "gear tooth". The sample was not remarkably carried by the passing probe, and cross-contamination was reduced effectively. A magnified diagram of the slot is shown in Fig. 1. The slots with width of 0.8, 1.0, 1.2, 1.5 and 2.0 mm were investigated at an angular velocity of 2.5 rad/s of the sample plate.



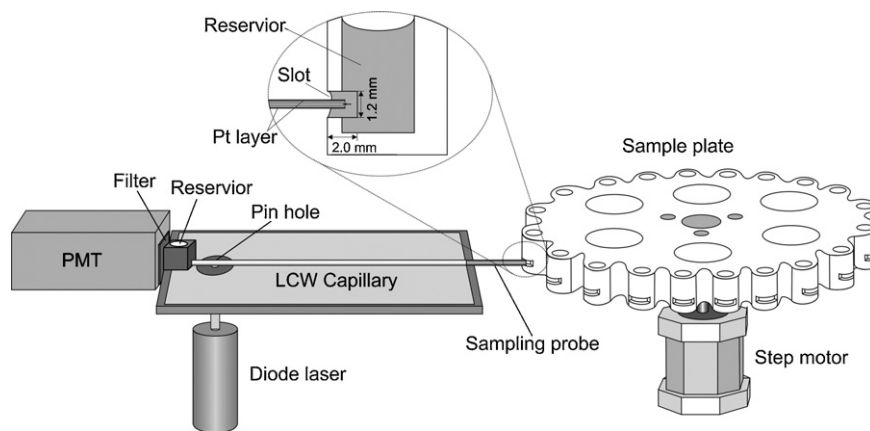


Fig. 1. Schematic diagram of the miniaturized CE system with the improved automated continuous sample introduction system.

Wider slots facilitated free passage of the probe, but the solutions in the slots were likely to leak out owing to centrifugal force. The slots with width of 1.2 and 1.5 mm were all applicable. In this work, 1.2-mm-wide and 2.0-mm-deep slots were fabricated, which allow easy pass-through of the sampling probe. With the step motor rotating at an angular velocity of 2.5 rad/s (corresponding to the time for a step movement of 0.13 s), aqueous sample/buffer solutions were retained in the reservoirs without any leakage owing to the surface tension. To prevent evaporation of solutions, a silicon rubber slab was used for covering the reservoirs.

In the electrokinetic sampling system [15–18], it is required that a platinum wire electrode was tightly bound to the capillary sampling probe or glued to the sharp inlet of the chip, which however increased thickness of the sampling probe. The thicker sampling probe inevitably rubs walls of the slots, which would disturb the sample introduction and separation. In this work, the platinum layer was deposited on the surface of the capillary tip, to replace the bound platinum wire. To improve the adhesion between platinum and Teflon coat of capillary surface, a titanium film was firstly sputtered on the surface. The depth of the metal layers was *ca.* 1  $\mu\text{m}$ , which did not affect the thickness of the sampling probe (see Fig. 2). The probe could easily scan through all slots of the sample plate without rubbing. Uniform shape of the reservoirs and the thinner sampling probe ensured continuous sample introduction and changing.

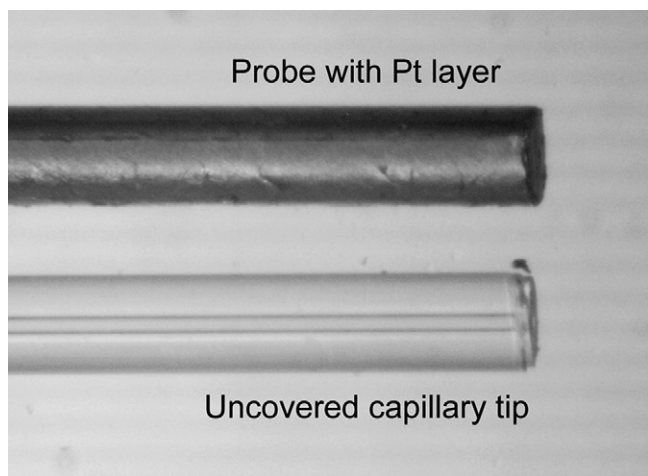


Fig. 2. Photo of the capillary probe with deposited platinum layer and an uncovered capillary tip.

### 3.2. Effects of injection voltage and injection time

In continuous sample introduction system of CE, to improve sample throughput, the next sample is usually introduced while the previous sample is being separated. In the present system, the introduced sample was electrokinetically injected into the separation capillary. The difference between voltages applied to injection and separation would affect the separation efficiency and reproducibility. In addition, the voltage switch and slot shift should be strictly synchronous, which makes control system sophisticated. Thus the same voltage for injection and separation was adopted in this work. During the process of sample changing, the sampling probe had to experience a period outside the vials (less than 0.2 s) while the voltage was not switched off. Nevertheless, the current was not interrupted, probably owing to the slight amount of solution remaining at the sampling probe tip, and thus the separation was not perturbed.

The effects of the injection time were studied in the range 0.2–2.0 s with the field strength of 320 V/cm (Fig. 3). As may be expected, the peak height increased gradually with the increase in injection time. While on the other hand, a significant increase in the plate height was observed within the range 1.0–1.5 s, possibly because length of the introduced sample plug contributed to plate height. Then almost constant plate heights were observed

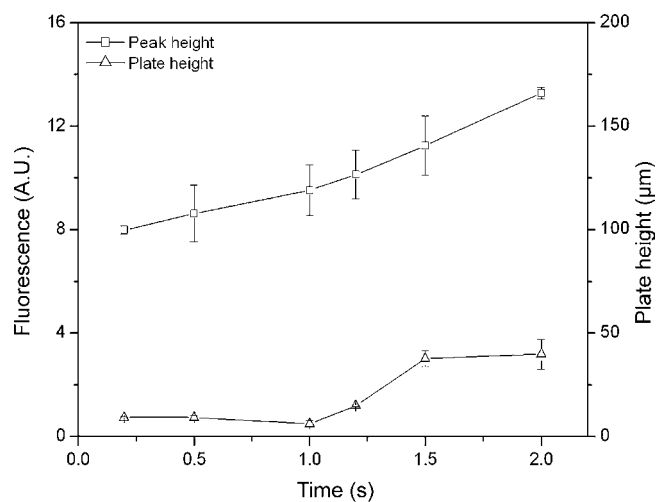
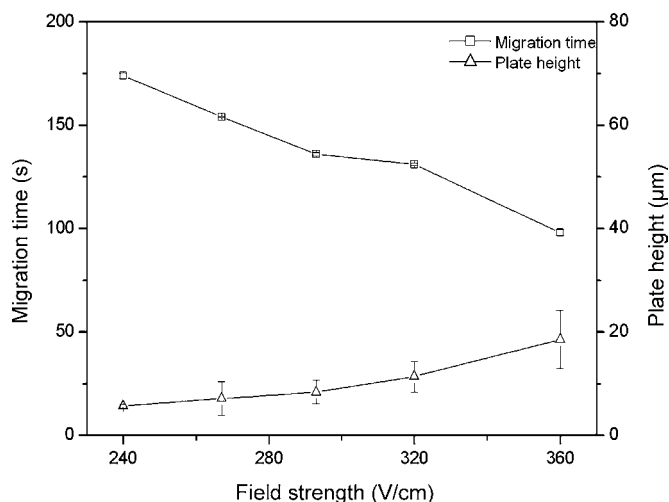


Fig. 3. Effects of sampling time on plate height and fluorescence signal. Samples, 0.7  $\mu\text{mol/L}$  FITC-arginine; effective separation length, 6.0 cm; working electrolyte, 10 mmol/L sodium tetraborate buffer (pH 9.2); applied field strength for both injection and separation, 320 V/cm.



**Fig. 4.** Effects of field strength on plate height and migration time. Injection time 1.0 s other conditions as in Fig. 3.

within the range 0.2–1.0 s. An injection time of 1.0 s was chosen as a compromise between separation efficiency and sensitivity.

### 3.3. Effects of separation field strength

The effects of the separation field strength were studied in the range 240–360 V/cm with the same voltage for sampling (Fig. 4). As expected, the migration time of analyte continuously decreased with the increases in separation field strength within the range studied. For arginine, increasing the field strength from 240 to 360 V/cm resulted in over 1 min reduction of the migration time, which markedly affected the sample throughput. However,

the increases in plate height were observed within the range 240–360 V/cm due to contributions to plate height from Joule heating and the longer sample plug introduced in higher field strength. With concurrent considerations in throughput and separation efficiency, field strength of 320 V/cm was adopted in further studies.

### 3.4. Analytical performance of the system

The performance of the system was demonstrated by the separation and determination of FITC-labeled arginine and leucine under the optimized conditions. The reproducibility of the system was demonstrated by repeatedly injecting a mixture of FITC-labeled arginine and leucine (Fig. 5A). The peak heights R.S.D. were 5.3%, 5.7% and 4.5% ( $n=7$ ) for arginine, leucine and FITC, respectively. The best plate height obtained was 3.1 μm for arginine and 2.3 μm for leucine. Fig. 5B illustrates alternate injections of three sample solutions in a 1:2:4 concentration ratio (0.1, 0.2, and 0.4 μmol/L, respectively). With a throughput of 60/h, the average carryover was 2.7%. The limit of detection ( $S/N=3$ ) was about 3.0 nmol/L for arginine and 14.0 nmol/L for leucine, corresponding to 6 and 28 amol, respectively. The gross sample consumption was only about 2 nL for each assay, which is one to two orders magnitude lower than what was previously reported [15,16]. The remaining sample could be recovered for further use as less cross-contamination occurred in the sample introduction process.

## 4. Conclusion

In the present work, an automated continuous sample introduction system with a monolithic sample plate and a capillary sampling probe deposited with platinum layer was developed, achieving the rapid separation and detection of amino acids using microfluidic CE and LIF detector with LCW technique. In this work, the 7-cm diameter sample plate holds 20 reservoirs. To meet the requirement of high-throughput analysis, a sample plate only 3-cm larger in diameter holding 40 reservoirs is being fabricated. The auto-sampling system developed in this work demonstrates future potentials in being commercialized for automated sample introduction of microfluidic CE system or flow analysis system.

## Acknowledgements

We gratefully acknowledge support from National Natural Science Foundations of China (20675012 and 20527003), and National Basic Research Program of China (2007CB714503). The authors thank Beijing Titan Instruments Co., Ltd. for their help in designing and fabricating the sample plate, and also thank Dr Yan-Xia Guan for her help in depositing the platinum layer on capillary.

## References

- [1] V. Poinso, M. Lacroix, D. Maury, G. Chataigne, B. Feurer, F. Couderc, *Electrophoresis* 27 (2006) 176.
- [2] M.M. Hsieh, S.M. Chen, *Talanta* 73 (2007) 326.
- [3] M. Pumera, *Electrophoresis* 28 (2007) 2113.
- [4] Y. Xiao, X.D. Yu, K. Wang, J.J. Xu, J. Huang, H.Y. Chen, *Talanta* 71 (2007) 2048.
- [5] H.L. Zeng, H.F. Li, X. Wang, J.M. Lin, *Talanta* 69 (2006) 226.
- [6] Q.H. He, Q. Fang, Z.L. Fang, *Chin. J. Anal. Chem.* 34 (2006) 729.
- [7] Y.H. Kim, I. Yang, S.R. Park, *Anal. Chem.* 79 (2007) 9205.
- [8] Q. Fang, F.R. Wang, S.L. Wang, S.S. Liu, S.K. Xu, Z.L. Fang, *Anal. Chim. Acta* 390 (1999) 27.
- [9] S.L. Wang, X.J. Huang, Z.L. Fang, *Anal. Chem.* 73 (2001) 4545.
- [10] Q. Fang, G.M. Xu, Z.L. Fang, *Anal. Chem.* 74 (2002) 1223.
- [11] C.G. Fu, Z.L. Fang, *Anal. Chim. Acta* 422 (2000) 71.

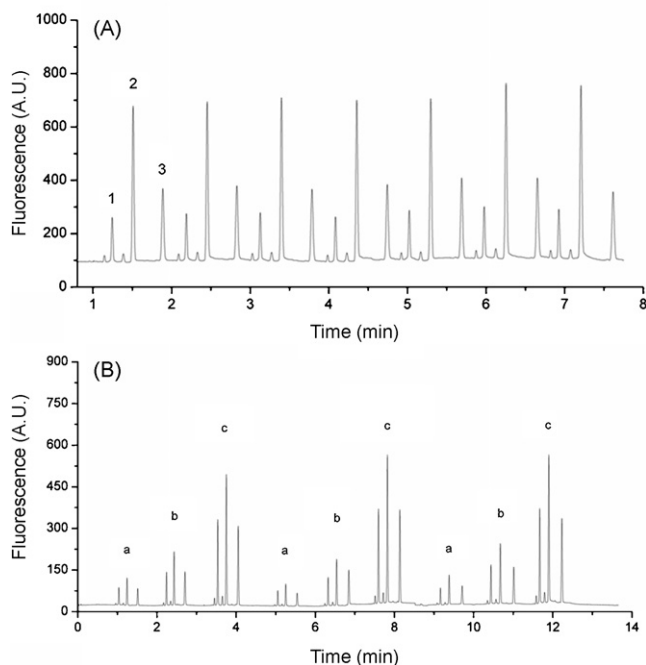


**Fig. 5.** (A) Electropherogram of repetitively introducing a mixture of FITC-labeled arginine and leucine for seven times: (1) FITC-arginine (0.4 μmol/L); (2) FITC; (3) FITC-leucine (0.8 μmol/L) and (B) electropherogram of alternately introducing samples of different concentrations for three cycles: (a) Mixture of 0.1 μmol/L FITC-arginine and 0.2 μmol/L FITC-leucine; (b) mixture of 0.2 μmol/L FITC-arginine and 0.4 μmol/L FITC-leucine; (c) mixture of 0.4 μmol/L FITC-arginine and 0.8 μmol/L FITC-leucine. Injection time 1.0 s other conditions as in Fig. 3.

- [12] Z.R. Xu, S.L. Wang, X.F. Fan, F.R. Wang, Z.L. Fang, *Chin. J. Anal. Chem.* 31 (2003) 1527.
- [13] S. Attiya, A.B. Jemere, T. Tang, G. Fitzpatrick, K. Seiler, N. Chiem, D.J. Harrison, *Electrophoresis* 22 (2001) 318.
- [14] Y.H. Lin, G.B. Lee, C.W. Li, G.R. Huang, S.H. Chen, *J Chromatogr. A* 937 (2001) 115.
- [15] Q.H. He, Q. Fang, W.B. Du, Y.Z. Huang, Z.L. Fang, *Analyst* 130 (2005) 1052.
- [16] Q.H. He, Q. Fang, W.B. Du, Z.L. Fang, *Electrophoresis* 28 (2007) 2912.
- [17] G. Chen, J. Wang, *Analyst* 129 (2004) 507.
- [18] J. Liu, Q. Fang, W.B. Du, *Chin. J. Anal. Chem.* 33 (2005) 1799.
- [19] X.F. Fan, Q. Li, S.L. Wang, Z.R. Xu, W.B. Du, Q. Fang, Z.L. Fang, *Electrophoresis* 29 (2008) 4733.
- [20] W.B. Du, Q. Fang, Q.H. He, Z.L. Fang, *Anal. Chem.* 77 (2005) 1330.



## Green synthesis of nanowire-like Pt nanostructures and their catalytic properties

Wen Yang<sup>a,b</sup>, Cheng Yang<sup>a,b</sup>, Ming Sun<sup>a,b</sup>, Fan Yang<sup>a</sup>, Ying Ma<sup>a</sup>,  
Zhanxia Zhang<sup>a,b</sup>, Xiurong Yang<sup>a,\*</sup>

<sup>a</sup> State Key Laboratory of Electroanalytical Chemistry, Changchun Institute of Applied Chemistry, Chinese Academy of Sciences, 5625 # Renmin Street, Changchun, Jilin, 130022, China

<sup>b</sup> Graduate School of the Chinese Academy of Sciences, Beijing, 100039, China

### ARTICLE INFO

#### Article history:

Received 21 July 2008

Received in revised form 2 December 2008

Accepted 2 December 2008

Available online 11 December 2008

#### Keywords:

Green synthesis

Dextran

Nanowire-like Pt nanostructures

Electrocatalysis

Reduction of oxygen

Oxidation of NADH

### ABSTRACT

We reported a simple and effective green chemistry route for facile synthesis of nanowire-like Pt nanostructures at one step. In the reaction, dextran acted as a reductive agent as well as a protective agent for the synthesis of Pt nanostructures. Simple mixing of precursor aqueous solutions of dextran and  $K_2PtCl_4$  at  $80^\circ C$  could result in spontaneous formation of the Pt nanostructures. Optimization of the experiment condition could yield nanowire-like Pt nanostructures at 23:1 molar ratio of the dextran repeat unit to  $K_2PtCl_4$ . Transmission electron microscopy results revealed that as-prepared nanowire-like Pt nanostructures consisted of individual Pt nanoparticles with the size range from 1.7 to 2.5 nm. Dynamic light scattering analysis indicated that as-prepared nanowire-like nanostructures have already formed in solution. The as-prepared nanowire-like Pt nanostructures were further characterized by UV–vis spectroscopy, X-ray photoelectron spectroscopy and Fourier transform infrared spectroscopy. In addition, the ratio dependence and temperature dependence of this reaction have also been investigated. The as-prepared nanowire-like Pt nanostructures can be immobilized on glassy carbon electrodes using an electrochemical coupling strategy, and the resulting nanowire-like Pt nanostructures modified film exhibited an excellent electrocatalytic activity for the reduction of oxygen and the oxidation of NADH.

© 2008 Elsevier B.V. All rights reserved.

### 1. Introduction

In recent years, the concept of green chemistry has attracted considerable attention [1,2]. The aim of green chemistry is to explore chemistry techniques and methodologies that reduce or eliminate the use or generation of feedstock, products, byproducts, solvents, reagents, etc., that are hazardous to human health or the environment. Nowadays, green chemistry is becoming one of the main goals of designing new processes and reactions in the emerging areas of nanoscience and nanotechnology [1,2]. The 12 principles of green chemistry have provided a framework for the designing of new materials, products, processes, and systems in nanoscience and nanotechnology [1,2]. Employing the concept of green chemistry toward nanoscience will facilitate not only the production and processing of safer nanomaterials and nanodevices, but also nanoscience and nanotechnology as a mature technology for commercialization [1,2].

It is well known that biomolecules have the ability of self-assembling into supermolecules [2]. Utilizing the intrinsic

properties of bimolecular to synthesize different kinds of nanoparticles will be very attractive, and novel nanostructures with special function could be developed [2]. Moreover, harnessing biomolecules to control over the shape of nanoparticles with minimized environmental effects also embodies most of the twelve principles of green chemistry. We may synthesize shape-controlled nanoparticles in the presence of biomolecules at ambient condition. Thus, the use of biomolecules for the synthesis of new kinds of Pt NSs could be very attractive [2]. Nowadays, many different nanostructures have been synthesized via green chemistry, such as Ag [1], and Au nanoparticles [3], superparamagnetic nanoparticles [4], and semiconductor nanocrystals (CdS) etc. [5]. However, there are a few reports on green synthesis of Pt nanostructures (Pt NSs) [6,7].

Owing to both its fundamental and technological interest and importance, Pt has been the major focus of interest. Platinum plays a major role in many applications, such as, a catalyst in polymer electrolyte fuel cells and direct methanol fuel cells [8,9], bioanalysis [10], catalysis [7,11], and surface-enhanced Raman scattering (SERS) substrates, etc. [12]. All of these applications require the use of Pt NSs, not only because of the limited supply and high cost of Pt, but also the peculiar surface properties of Pt NSs, which are different from bulk materials. As a result, growing attention has been devoted to fabrication of Pt NSs, and many kinds of Pt NSs have been

\* Corresponding author. Tel.: +86 431 85262056; fax: +86 431 85689278.  
E-mail address: [xryang@ciac.jl.cn](mailto:xryang@ciac.jl.cn) (X. Yang).

synthesized, including spherical nanoparticles [7,13], nanocubes [8,11], nanorods [14], nanotubes [15], hollow nanospheres [16], nanowires [17] and dendrite nanoparticles [18], etc. It is well known that the morphology (including dimensionality and shape) of Pt NSs can effectively influence their electronic, magnetic and catalytic properties [8,11]. Therefore, the synthesis of shape-controlled Pt nanostructures is a highly desired objective [11,14].

There are plenty of papers concerned with the synthesis of shape-controlled Pt NSs. However, using dextran to synthesize nanowire-like Pt NSs, which consist of individual Pt nanoparticles in the size range from 1.7 to 2.5 nm, has not been reported. Moreover, the catalytic and electrochemical properties of nanowire-like Pt NSs are still unknown. In the present work, we present a green approach toward the synthesis and stabilization of nanowire-like Pt NSs at one step. Dextran was used as a reducing agent as well as a protecting agent. Our results indicated that the quantity of dextran was the key to yielding the nanowire-like Pt NSs. Only at a molar ratio of [the repeating units of dextran]/[Pt<sup>2+</sup>]=23 could produce nanowire-like Pt NSs. Those dextran protected Pt NSs were immobilized onto the surface of glassy carbon electrode (GCE) in an aqueous solution containing 0.1 M LiClO<sub>4</sub> by an electrochemical coupling strategy. Electrode modified with these dextran coated Pt NSs possessed good catalytic activity toward the reduction of O<sub>2</sub> and the oxidation of NADH.

## 2. Experimental

### 2.1. Reagents and chemicals

Potassium tetrachloroplatinate was purchased from Alfa Aesar (USA). Dextran (Mw 10,000) was obtained from Herbon Polysaccharide Biotech. Ltd. (Shenzhen, China). Aminodextran was prepared according to our previous report [7]. Reduced β-dihyronicotinamide adenine dinucleotide (NADH) was obtained from Genview (USA). Lithium perchlorate was purchased from ACROS (USA). Sulfuric acid was purchased from Beijing Beihua Fine Chemicals Co. Ltd (Beijing, China). All those reagents were used without further purification. 0.2 M phosphate buffer (pH 6.9) was prepared by mixing the stock solution of potassium dihydrophosphate and sodium hydroxide. All glassware used in the following procedures was cleaned in a bath of freshly prepared 3:1 HCl/HNO<sub>3</sub>, and rinsed thoroughly with double distilled water prior to use.

### 2.2. Preparation of dextran protected nanowire-like Pt NSs

The nanowire-like Pt NSs were prepared according to the following procedure (sample 1): In each synthesis, dextran was dissolved in 20 mL water hosted in a 50 mL two-neck flask (equipped with a reflux condenser and a stirring bar), and the solution was heated to 80 °C under magnetic stirring. Then, an aqueous solution containing K<sub>2</sub>PtCl<sub>4</sub> prepared freshly (within 5 min) was added to 11.5 mM dextran solution (calculated in terms of the repeating unit, 2 mg mL<sup>-1</sup>). The final molar ratio of dextran-to-Pt was fixed at 23:1, and the final concentration of potassium tetrachloroplatinate was 0.5 mM in the solution. At last, the mixture was kept at 80 °C for 2 h.

To investigate the influence of the molar ratio of dextran to K<sub>2</sub>PtCl<sub>4</sub> on the nanowire-like Pt NSs thus formed, the amount of dextran used was investigated. We conducted a series of experiments by varying the molar ratio of dextran to K<sub>2</sub>PtCl<sub>4</sub>. The procedure of synthesis was identical to those used for preparing sample 1 except that the final dextran-to-Pt was varied to 5.8:1 or 115:1.

The influence of temperatures on the nanowire-like Pt NSs thus formed was studied as follows: in a typical synthesis route, 11.5 mM dextran and 0.5 mM K<sub>2</sub>PtCl<sub>4</sub> were added into 20 mL water under

constant strong stirring. After stirring for 10 min, the solution was transferred into a 35 mL Teflon lined stainless steel autoclave. The autoclave was heated at 180 °C for different periods, cooled to room temperature naturally. The black precipitates were collected, centrifuged, and washed with distilled water for several times. Then, the black precipitates were dried at room temperature.

The synthesis procedure of aminodextran protected Pt nanoparticle was similar to dextran protected Pt NSs, except that 20 mL of 2 mg mL<sup>-1</sup> aminodextran solution was used [7].

### 2.3. Electrochemical experiments

The immobilization of nanowire-like Pt NSs on GCE (3 mm in diameter) was prepared using a procedure similar to that reported by Crooks for the modification of dendrimer-encapsulated Pt nanoparticles [9]. GCE was polished with 0.3 μm alumina slurry and then washed ultrasonically in water for a few minutes. The cleaned GCE electrode was dried with high-purity nitrogen steam for the next modification. The freshly polished GCE was placed in 10 mL as-prepared nanowire-like Pt NSs solution containing 0.1 M LiClO<sub>4</sub>, and then the potential was scanned three times between 0 and 1.0 V with the scan rate of 10 mV s<sup>-1</sup>. The modified electrodes were rinsed with distilled water to remove the loosely bounded nanowire-like Pt NSs, and then immersed in 0.5 M H<sub>2</sub>SO<sub>4</sub> solution for electrochemical measurement.

Electrochemical measurements were performed with CHI 660B electrochemical workstation (USA). Conventional three-electrode electrochemical cell with the modified GCE as the working electrode, a large platinum foil as the auxiliary electrode and an Ag/AgCl (saturated KCl) electrode as the reference electrode.

### 2.4. Instrumentations

UV–vis detection was carried out on a Cary 50 UV–vis spectrophotometer (Varian, USA). The TEM measurement was performed on a JEOL 2010 transmission electron microscopy operated at an accelerating voltage of 200 kV. Samples for TEM were prepared by placing a drop of as-prepared nanowire-like Pt NSs solution onto a carbon-coated copper grid and dried at room temperature. The dynamic light scattering experiment (DLS) was conducted with a vertically polarized HeNe laser (DAWNEOS, Wyatt Technology) at a fixed scattering angle of 90° and at a constant temperature of 25 °C. X-ray photoelectron spectroscopy (XPS) measurement was conducted with an ESCALAB MK II spectrometer (VG Co., U.K.). Fourier transform infrared spectroscopy (FT-IR) was acquired on a BRUKER vertex 70 FTIR (German). Samples for FT-IR were prepared by forming thin transparent KBr pellet.

## 3. Results and discussion

### 3.1. Formation of nanowire-like Pt NSs

Formation of Pt NSs was confirmed by TEM. Fig. 1A depicts a typical TEM image of the as-prepared nanowire-like Pt NSs with a molar ratio of the dextran repeat unit to K<sub>2</sub>PtCl<sub>4</sub> of 23:1. The interesting features of the morphology of nanowire-like Pt NSs are twofold; first, the Pt nanoparticles interconnected with each other to form nanowire-like NSs; second, the nanowire-like structures were several nanoparticles wide and comprised bifurcated junction with outgrowth that often interconnected to produce a branched structure. High-resolution TEM image that is shown in Fig. 1B reveals that the nanowire-like NSs are constituted of individual Pt nanoparticles in the size range 1.7–2.5 nm. The inset of Fig. 1 shows selected-area electron diffraction patterns of as-prepared nanowire-like Pt nanostructures, revealing some bright concentric rings, attributed to the (1 1 1), (2 0 0), (2 2 0), and (3 1 1) diffractions of the Pt fcc

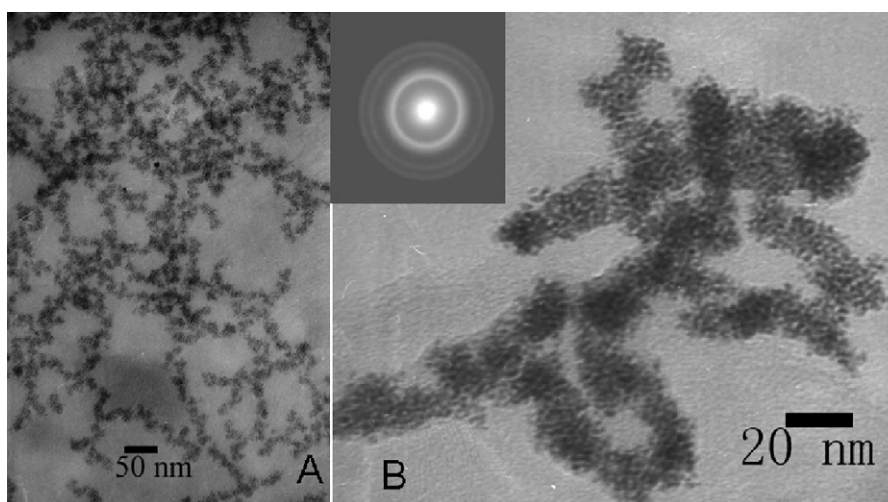


**Fig. 1.** Typical TEM and higher magnification TEM images of as-prepared nanowire-like Pt NSs where the molar ratio of dextran to  $K_2PtCl_4$  was 23:1 (A and B).

crystal structure. This confirms that the nanowire-like Pt NSs, prepared by this method, crystallize in a phase similar to bulk Pt. A corresponding particle size distribution histogram (Fig. S-1) was determined over 200 nanoparticles from the grid, indicated that the mean particle diameter is 2.2 nm with monodisperse size.

In order to confirm the formation of nanowire-like NSs in solution, as-prepared nanowire-like Pt NSs were also studied by DLS (Fig. 2). The hydrodynamic diameter of the as-prepared nanowire-like Pt NSs (Fig. 2A) shows two separate distributions. The first one indicates that the mean diameter of Pt nanoparticles is 3.4 nm (Fig. 2B), which is 1.2 nm larger than the result of TEM (Fig. 1). It is possible that the TEM results are obtained from the dry state of the as-prepared Pt nanoparticles, while DLS results are obtained from the hydrated state of dextran, which coated on Pt nanoparticles. The second one shows a larger hydrodynamic diameter than as-

prepared Pt nanoparticles at the size range of 65.8–390 nm (Fig. 2A). The second one distribution indicates that nanowire-like Pt NSs indeed form in solution. The DLS data match the results of TEM shown in Fig. 1.

### 3.2. Characterization of nanowire-like Pt NSs

For further characterization of the as-prepared nanowire-like Pt NSs, UV-vis spectrum, XPS spectrum, and FT-IR spectrum analysis were carried out. The formation of nanowire-like Pt NSs was confirmed by UV-vis spectrum. As shown in Fig. 3a, the absorption peak of  $K_2PtCl_4$  at about 215 nm, due to the ligand-to-metal charge transfer transition of the  $PtCl_4^{2-}$  [7]. With refluxing time increased, the color of the solution gradually changed from yellow brown to dark brown. The peak at 215 nm finally disappeared after the reaction,

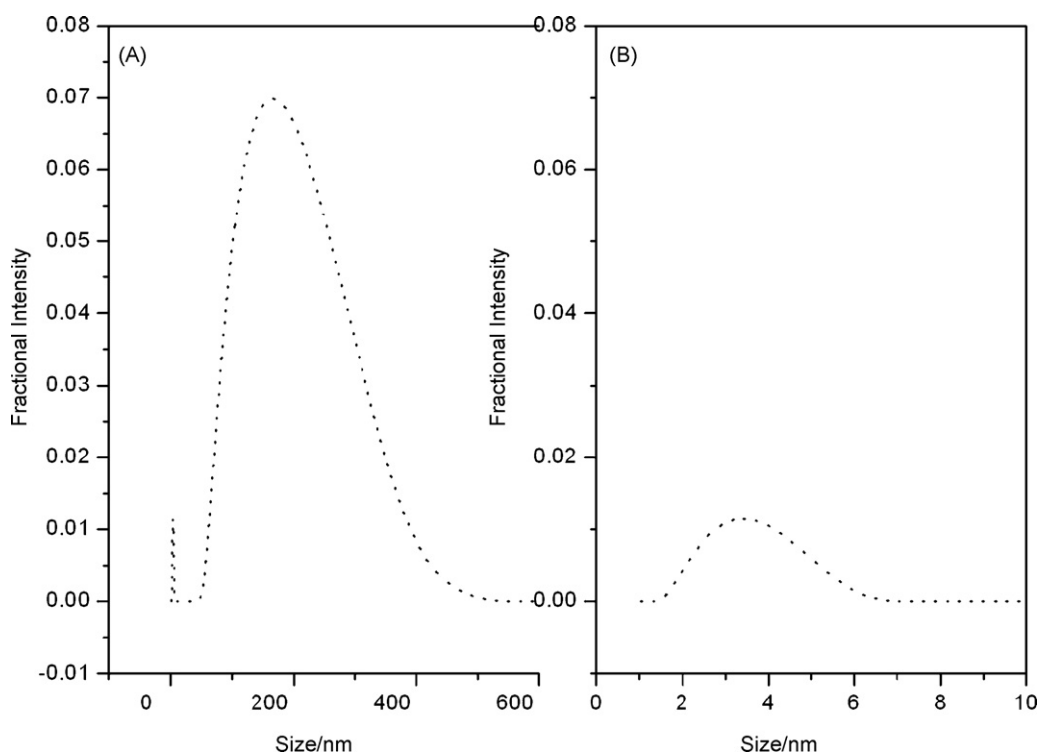


**Fig. 2.** DLS data of dextran-protected nanowire-like Pt NSs, whole size distribution of nanowire-like Pt NSs (A), and the first size distribution of Pt NSs (B).

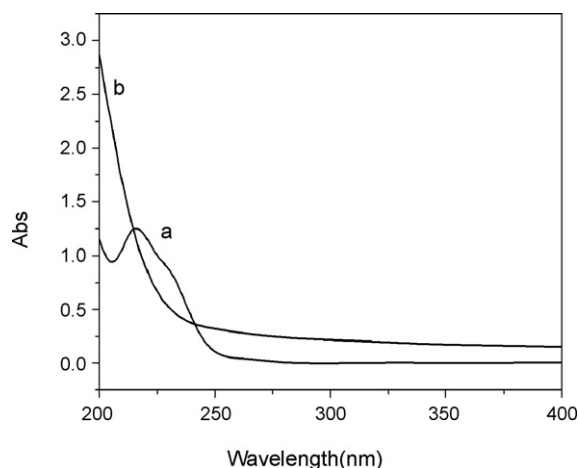


Fig. 3. UV-vis absorption of K<sub>2</sub>PtCl<sub>4</sub> (a), dextran protected nanowire-like Pt NSs (b).

indicating that the PtCl<sub>4</sub><sup>2-</sup> ions were completely reduced [7]. The as-prepared Pt NSs have absorption in all ranges of the UV-vis spectrum and the absorption increases with the decrease of wavelength, as shown in Fig. 3b. The as-prepared nanowire-like Pt NSs are stable for more than one month without any observable aggregation under air conditions.

XPS data were collected to examine the change in the oxide states for Pt after the reduction reaction occurred. Fig. 4 shows clear signature of neutral Pt formed in solution. In our previous report, the Pt (4f<sub>7/2</sub>) and Pt (4f<sub>5/2</sub>) peaks of K<sub>2</sub>PtCl<sub>4</sub> presented at 73.5 and 76.8 eV, respectively [7]. The XPS spectrum of the as-prepared nanowire-like Pt NSs shows the Pt 4f<sub>7/2</sub> and 4f<sub>5/2</sub> doublet with the binding energies of 71.4 and 74.8 eV (Fig. 4), respectively. These are typical values for Pt<sup>0</sup>, indicating the formation of Pt NSs [7].

To investigate the protecting mechanism of dextran, FT-IR exploration was carried out. Both the FT-IR spectrum of pure dextran and dextran protected nanowire-like Pt NSs were recorded (shown in Fig. 5a and b, respectively). Most of IR spectrum of the nanowire-like Pt NSs is similar to that of dextran except for some differences [19,20]. The spectrum of dextran coated on nanowire-like Pt NSs exhibits the polysaccharides characteristic absorption bands [19,20]. It is well known that the -OH stretching mode absorption can be used as an indicator of the intermolecular of hydrogen bonding and lower energies of stretching vibration correspond to the increase in the strength of intermolecular of hydrogen bonding [6,21]. The stretching vibration of -OH experiences a shift from 3430 to 3422 cm<sup>-1</sup> with the nanowire-like

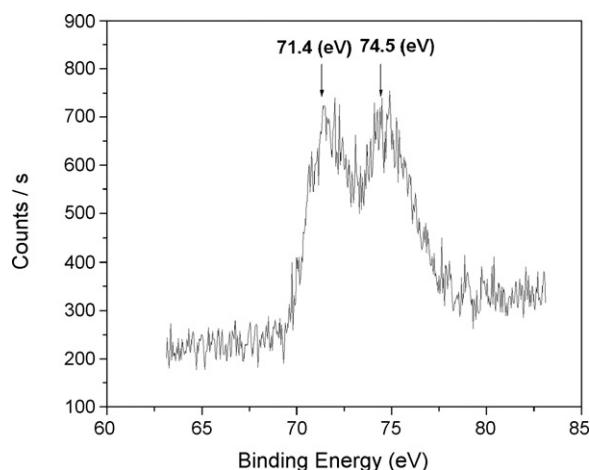


Fig. 4. XPS spectrum of dextran protected nanowire-like Pt NSs.

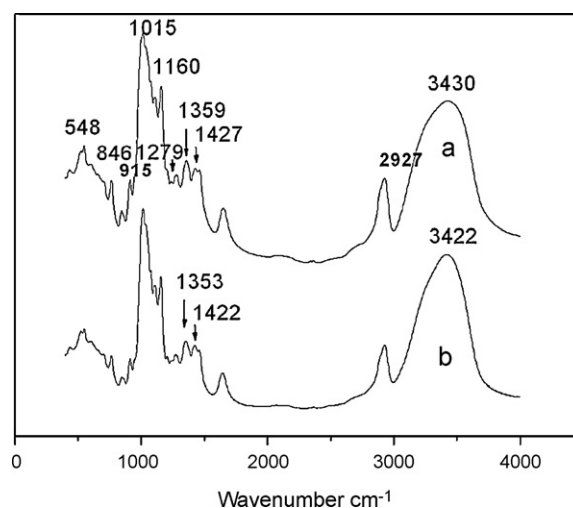


Fig. 5. FT-IR spectra of pure dextran (a) and the nanowire-like Pt NSs (freeze-dried) (b).

Pt NSs, suggesting the existence of a hydrogen bonding interaction between the dextran molecules and the nanowire-like Pt NSs surface [6,21].

In the low-frequency region, the peaks of pure dextran at 1427, 1359, and 1279 cm<sup>-1</sup> can be assigned to the H-C-OH deformation vibration mode [19,20]. Many of those peak positions in the nanowire-like Pt NSs samples are red shift 2–7 cm<sup>-1</sup>, supporting the notion that dextran adsorbed on the surface of Pt nanoparticles [6,20–25]. The band at about 1160 cm<sup>-1</sup> for pure dextran is assigned to asymmetrical stretching vibration of the C-O-C bond and glycoside bridge, however, the peak position slightly shifts to lower frequency (3 cm<sup>-1</sup>) in the case of surface bound molecules [19,22,25]. The peak at 1108 cm<sup>-1</sup> arises from the vibration of the C-O bond at the C-4 position of a glucose residue. The peak at 1015 cm<sup>-1</sup> for pure dextran corresponds to the crystalline and amorphous phase of dextran [22]. The band of 1015 cm<sup>-1</sup> is much weaker in the dextran coated nanowire-like Pt NSs (Fig. 6b), indicates that the dextran adsorbed onto the surface of Pt nanoparticles is amorphous and less ordered than pure dextran itself [19,22]. The peaks at 915, 846, and 548 cm<sup>-1</sup> for pure dextran and dextran coated nanowire-like Pt NSs are due to α-glucopyranose ring deformation modes [19,22,24,25]. Our FT-IR results confirmed that dextran could adsorb onto the surface of Pt nanoparticles via hydroxyl group [6,21–24,26,27].

### 3.3. Ratio dependence and temperature dependence

To further investigate the role of dextran in the formation of nanowire-like Pt NSs, the influence of molar ratio of the reactants (here the dextran repeat unit and K<sub>2</sub>PtCl<sub>4</sub>, respectively) was studied in detail. At a 5.8:1 molar ratio of the dextran repeat unit to K<sub>2</sub>PtCl<sub>4</sub>, spherical Pt NSs are obtained (Fig. 6A). DLS data of the result of Fig. 6A exhibited only one size distribution in size range of 39–72.2 nm. It may be the result of aggregation of small Pt nanoparticles (Fig. S-2). As for 115:1 molar ratio of the dextran repeat unit to K<sub>2</sub>PtCl<sub>4</sub>, we also obtain nanowire-like Pt NSs (Fig. 6B), however, the nanowires are more loosely compared with the product of Fig. 1. Interestingly, the size of these Pt nanoparticles at a 5.8:1 and 115:1 molar ratio of the dextran repeat unit to K<sub>2</sub>PtCl<sub>4</sub> approximates to the size of Pt nanoparticles obtained at 23:1 molar ratio of the dextran repeat unit to K<sub>2</sub>PtCl<sub>4</sub>. The state of products of Fig. 6B nanostructures in solution was also studied by DLS (Fig. S-3), and the results were closed to the situation described in Fig. 2.

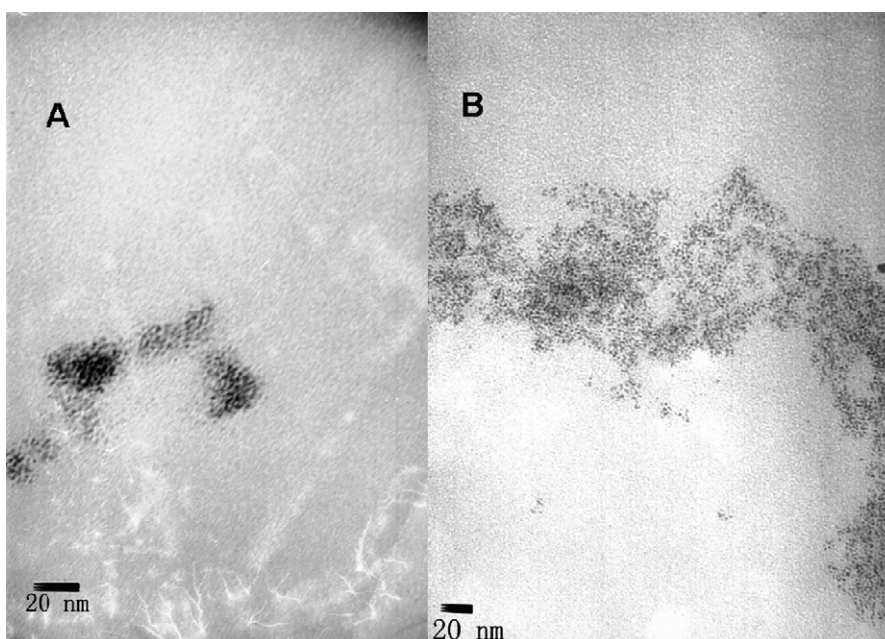


**Fig. 6.** Typical TEM images of as-prepared Pt NSs, the molar ratio of dextran to  $K_2PtCl_4$  was 5.8:1 (A), and the molar ratio of dextran to  $K_2PtCl_4$  was 115:1 (B).

To further identify the controlling factors that lead to the formation of nanowire-like Pt NSs, temperature dependence experiments were performed. Fig. 7A shows the TEM image of the result of reaction at  $180^\circ C$  for 2 h under hydrothermal condition, the molar ratio of dextran to  $K_2PtCl_4$  was 23:1. From the TEM image, we can see that Pt nanowires were obtained, while this reaction lasted for 24 h, the same Pt nanowires were obtained, as shown in the Fig. 7B. Fig. 7C shows the TEM image of the results of reaction at  $180^\circ C$  for 24 h where the molar ratio of the dextran repeat unit to  $K_2PtCl_4$  was 5.8:1, we also obtained Pt nanowires, however, the length of as prepared Pt nanowires (Fig. 7C) is much shorter. As for 115:1 molar ratio of dextran to  $K_2PtCl_4$ , Fig. 7D shows the result of its reaction at  $180^\circ C$  for 24 h, Pt nanowires with much longer length are obtained in the reaction, and a carbon membrane enwraps on the surface of Pt nanowires. All those results indicate that dextran may act as a template for the formation of Pt nanowire [23], and have great influence on the length of Pt nanowires.

#### 3.4. Mechanism

The mechanism of reaction on the formation of nanowire-like Pt NSs was an interesting topic of the current study. Dextran is composed of D-glucose with a predominance of alpha-1,6-linkages [23]. Recently, dextran has been chosen as a soft template for the synthesis of metallic and metal oxide sponges [23], Ag microcrystals [28], hydroxyapatite [29], and high order zeolite etc. [30]. Taking together all our results, we think the formation of nanowire-like Pt NSs was proceeded through a three-stage process [6,31]; first,  $K_2PtCl_4$  was facilitated into the molecular matrix of dextran by the extensive number of hydroxyl groups present in dextran in our systems [23]; second,  $PtCl_4^{2-}$  was reduced by dextran to form Pt nanoparticles [23]; third, the Pt nanoparticles could self-assemble to form nanowire-like aggregates [6,23,31].

Dextran used here acted as a reducing agent as well as a stabilizer [23,26]. However, dextran can only protect nanowire-like Pt NSs by hydroxyl group and the steric bulk of dextran framework. The binding interaction between hydroxyl and metal is relatively weak as compared with the interaction between metal and typical protect-

ing groups, such as -SH,  $-NH_3$  and  $-COOH$  etc. Because it is believed that -SH,  $-NH_3$  and  $-COOH$  groups could form covalent and electrostatic interaction with metal [6,26,27]. For conformation of this result, a control experiment of introducing aminodextran instead of dextran in the synthesis of Pt nanoparticles was performed. Fig. 8 shows TEM image of the aminodextran protected Pt nanoparticles. The characteristic spherical Pt nanoparticles are observed in Fig. 8 with a relatively narrow particle size distribution (1.5–3 nm range). The TEM image of aminodextran protected Pt nanoparticles is consistent with our previous work [7]. The morphology of aminodextran protected Pt nanoparticles is totally different with dextran-protected nanowire-like Pt NSs. Aminodextran can stabilize Pt nanoparticles via amino functional group [7]. Therefore, nanowire-like Pt NSs were obtained due to the limited protecting ability of dextran. When the ratio of the dextran to  $K_2PtCl_4$  was high up to 115:1 (Fig. 6B), dextran still could not encapsulate the whole surface of Pt nanoparticles, a loosely nanowire-like Pt NSs was obtained [6]. By decreasing the ratio of the dextran to  $K_2PtCl_4$  to 23:1 (Fig. 2), breadth of the nanoparticle chains became slimmer, while the length of the nanoparticle chains became longer. When the ratio of the dextran to  $K_2PtCl_4$  was decreased to 5.8:1 (Fig. 6A), only spherical aggregates were obtained.

In summary, those phenomena were consistent with the aggregation mechanism based on the non-uniform distribution of stabilizers [6,31]. Dextran molecules preferentially adsorbed onto only a small fraction of the Pt nanoparticles' surface due to the different structure of various crystallographic facets [6,31]. The bare surfaces of Pt nanoparticles that were not protected by the dextran oriented against each other to form the nanowire-like Pt nanostructures. Increasing the dextran concentration meant that dextran molecules might start to be adsorbed on less preferred crystal surface of Pt nanoparticles, and the contact opportunity for Pt nanoparticles with each other decreases, which leads to the formation of a loosely nanowire-like Pt nanostructures [6,31]. In addition, the long-range order dipole-dipole between Pt nanoparticles, which originated from non-uniform distribution of the stabilizer of the surface of Pt nanoparticles, may also play an important role in the formation of nanowire-like Pt nanostructures [32].



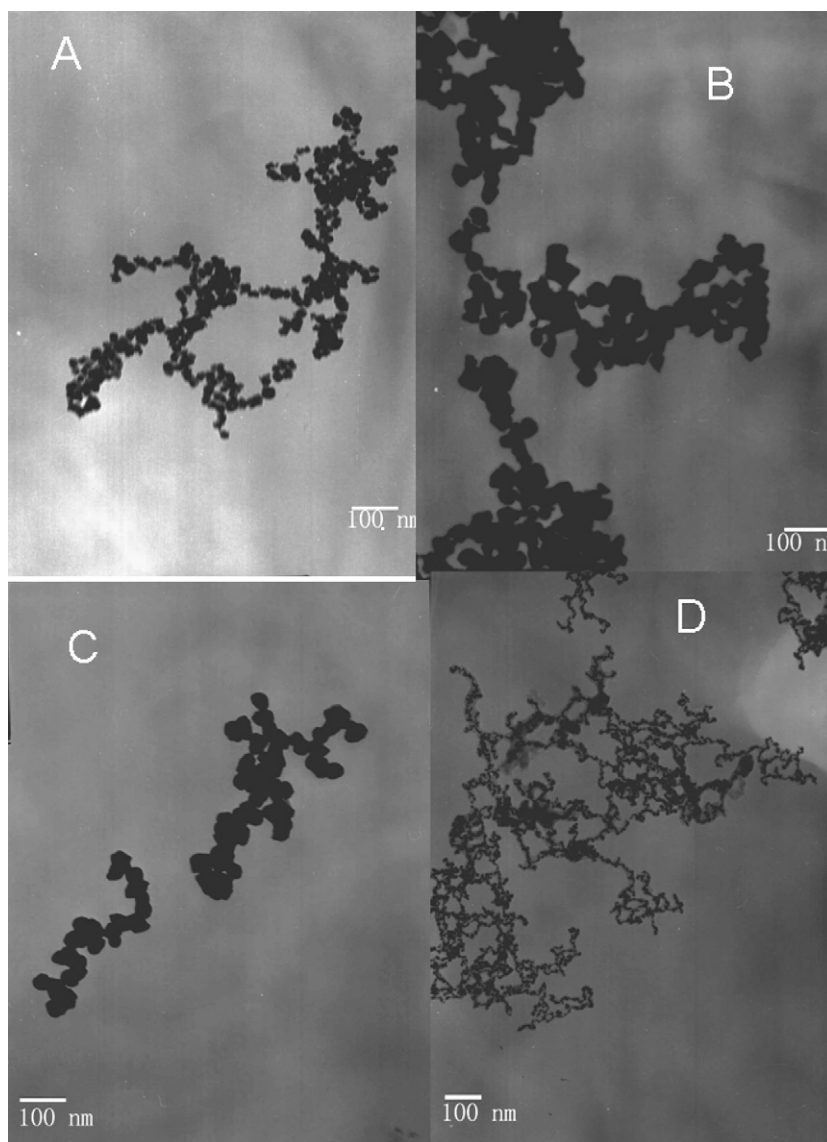


**Fig. 7.** Typical TEM images of as-prepared Pt NSs, the result of reaction at 180 °C for 2 h where the molar ratio of dextran to  $K_2PtCl_4$  was 23:1 (A), the result of reaction at 180 °C for 24 h where the molar ratio of dextran to  $K_2PtCl_4$  was 23:1 (B), the result of reaction at 180 °C for 24 h where the molar ratio of dextran to  $K_2PtCl_4$  was 5.8:1 (C), the result of reaction at 180 °C for 24 h where the molar ratio of dextran to  $K_2PtCl_4$  was 115:1 (D).

### 3.5. Electrochemical properties and electrocatalytic activity of the as-prepared nanowire-like Pt NSs

It is well known that Pt nanostructures exhibit high catalytic properties for many reactions. These unique catalytic properties make Pt NSs to be a promising candidate in the fields of fuel cell and electrocatalysis. Here, we studied the as-prepared PNSs for oxygen and NADH. The oxygen reduction is very important for polymer electrolyte fuel cells (PEFCs), batteries, and many other electrode applications [8,9]. Nanowire-like Pt NSs exhibited excellent electrocatalytic activity toward the reduction of  $O_2$ . Prior to measuring their catalytic activities, nanowire-like Pt NSs were deposited onto GCE surfaces using an immobilization method developed by Crooks et al. [9,33–36]. Crooks, et al have used this method to directly immobilize G4-OH encapsulated Pt nanoparticles onto GCE, the as-prepared films were electrocatalytically active for  $O_2$  reduction, and they were remarkable stable [9]. It was well known that dextran also had multiple hydroxyl groups in its structures. Therefore, we use this method to immobilize dextran (Fig. S-4) and dextran coated nanowire-like Pt nanostructures [9,33–36]. A freshly polished GCE

was placed in 10 mL as-prepared nanowire-like Pt NSs solution containing 0.1 M  $LiClO_4$ , and then the potential was scanned three times between 0 and 1.0 with the scan rate of  $10\text{ mV s}^{-1}$  (Fig. S-5). However, aminodextran protected Pt nanoparticles could not be deposited onto the surface of GCE using Crook's method, and the exact reason was still not known.

Cyclic voltammogram (CV) measurements confirmed the immobilization of as-prepared nanowire-like Pt NSs. Fig. 9 shows the cyclic voltammogram of GCE modified with nanowire-like Pt NSs in 0.5 M  $H_2SO_4$  saturated with nitrogen at a scan rate of  $50\text{ mV s}^{-1}$  from  $-0.2$  to 1.5 V. It can be seen that GCE modified with nanowire-like Pt NSs produced high specific current in the hydrogen region from  $-0.2$  to 0.15 V. The platinum oxide was reduced at about 0.33 V. The electrochemical properties of as-prepared nanowire-like Pt NSs were consistent with those of bare platinum electrode, indicating the as-prepared nanowire-like Pt NSs had an active surface [8,9].

The electrocatalysis of the as-prepared nanowire-like Pt NSs toward oxygen reduction was also investigated [8,9]. Fig. 10 shows the typical cyclic voltammograms of the oxygen reduction at the nanowire-like Pt NSs modified GCE in a 0.5 M  $H_2SO_4$ . Curves a and

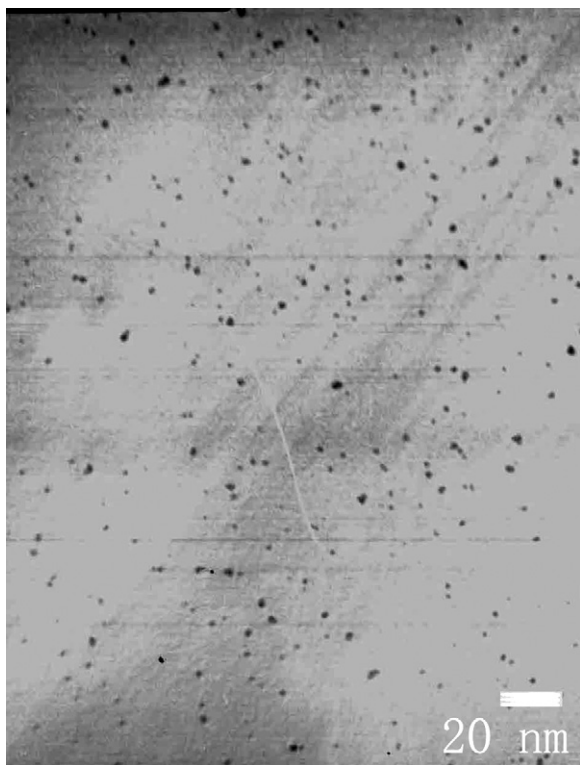


Fig. 8. Typical TEM image of aminodextran protected Pt nanoparticles.

b correspond to the CV of the modified electrode in  $N_2$ -saturated  $0.5\text{ M H}_2\text{SO}_4$  and in air-saturated  $0.5\text{ M H}_2\text{SO}_4$ . In the presence of oxygen (Fig. 10c), the nanowire-like Pt NSs exhibited high electrocatalytic activity toward oxygen, and the reduction peak at about  $0.25\text{ V}$  in  $0.5\text{ M H}_2\text{SO}_4$  saturated with oxygen.

The electrocatalysis of the as-prepared nanowire-like Pt nanostructures toward the oxidation NADH was also investigated [37,38]. For further electrochemical measurements, the electrode was then transferred into the phosphate buffer with or without NADH. Fig. 11 shows typical voltammograms demonstrating the electrocatalytic activity of GCE modified with nanowire-like Pt NSs for the oxidation of NADH. Voltammogram a observed in the absence of NADH that there was a tail-like response without any well defined peak for GCE modified with nanowire-like Pt NSs. However, voltammogram

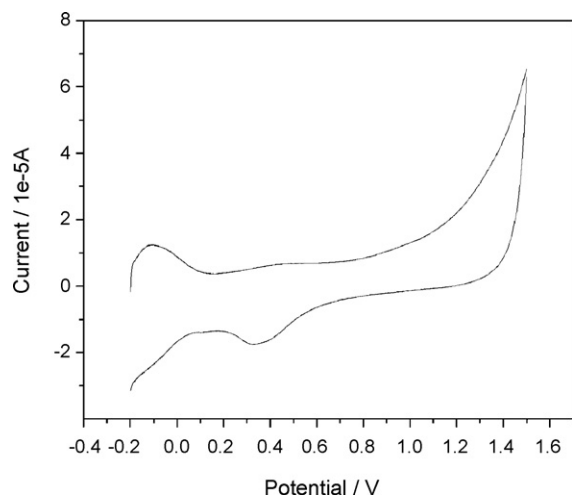


Fig. 9. Cyclic voltammogram of GCE modified with nanowire-like Pt NSs in  $0.5\text{ M H}_2\text{SO}_4$  saturated with nitrogen. Scan rate:  $50\text{ mV s}^{-1}$ .

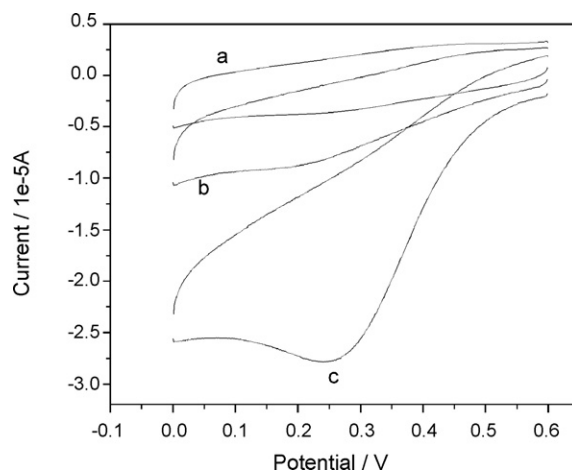


Fig. 10. Typical cyclic voltammograms of the oxygen reduction at as-prepared nanowire-like Pt NSs modified GCE in a  $N_2$ -saturated  $0.5\text{ M H}_2\text{SO}_4$  (a), air-saturated  $0.5\text{ M H}_2\text{SO}_4$  (b), and oxygen-saturated  $0.5\text{ M H}_2\text{SO}_4$ . Scan rate:  $50\text{ mV s}^{-1}$ .

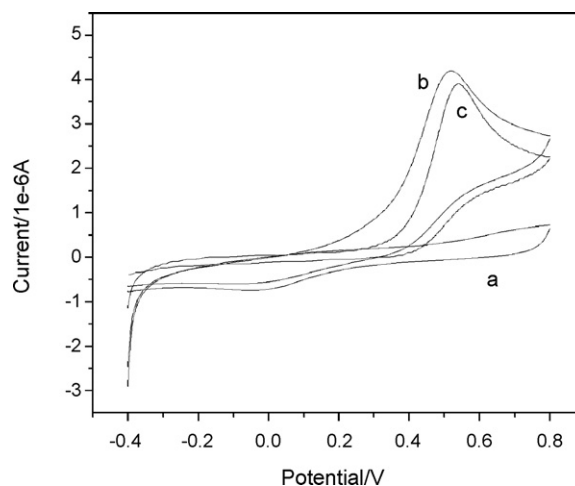


Fig. 11. Cyclic voltammograms of (a and b) nanowire-like Pt NSs modified GCE electrode in the absence (a) and the presence (b and c) of  $1\text{ mM NADH}$ . Voltammogram (c) was obtained at a bare GCE. Scan rate:  $10\text{ mV s}^{-1}$ .

b observed in the presence of NADH showed an enhanced oxidation current and a large negative shift in the anodic peak potential of about  $50\text{ mV}$ , compared with that obtained at the bare GCE as shown in voltammogram c [38]. We also have done a control experiment. Fig. S-6 depicts a cyclic voltammogram for NADH at a Pt electrode. The irreversible oxidation of NADH at the Pt electrode surface requires a high overpotential [37]. These results demonstrated the electrocatalytic oxidation of NADH by nanowire-like Pt NSs.

#### 4. Conclusion

We have reported a green chemical strategy for the one-step preparation of nanowire-like Pt NSs using dextran. Dextran acted as the reducing agent, protective agent, and template in the reaction. The as-prepared nanowire-like Pt NSs were very stable. TEM images indicated that those nanowire-like Pt NSs were constituted of individual Pt nanoparticles in the size range  $1.7\text{--}2.5\text{ nm}$ . It was also found that the molar ratio of dextran to  $K_2PtCl_4$  played an important role in the formation of well-defined nanowire-like Pt NSs. Only the dextran repeat units molar ratio to  $K_2PtCl_4$  being controlled at proper ratio (23:1), well-defined nanowire-like Pt NSs could be obtained. Our work here may open up a new possibility for the

preparation of Pt NSs by use of polysaccharide as template. Moreover, thus formed nanowire-like Pt NSs can be immobilized onto the surface of GCE using an electrochemical attachment method via –OH of dextran. The resulting film exhibited good catalytic activities for the reduction of oxygen and the oxidation of NADH. Therefore, they hold great promise for catalytic and bioanalytical applications.

### Acknowledgment

This work was supported by the National Natural Science Foundation of China (No. 90713022), the National Key Basic Research Development Project of China (No. 2007CB714500) and the Project of Chinese Academy of Sciences (No. KJ CX2. YW. H09). Insightful suggestions by Ms. Zhijuan Wang, Mr. Hui Wei, and Mr. Zhonghua Zhang during the development of this work are greatly appreciated.

### Appendix A. Supplementary data

Supplementary data associated with this article can be found, in the online version, at [doi:10.1016/j.talanta.2008.12.009](https://doi.org/10.1016/j.talanta.2008.12.009).

### References

- [1] P. Raveendran, J. Fu, S.L. Wallen, *J. Am. Chem. Soc.* 125 (2003) 13940.
- [2] J.A. Dahl, B.L.S. Maddux, J.E. Hutchison, *Chem. Rev.* 107 (2007) 2228.
- [3] Y. Ma, N. Li, C. Yang, X.R. Yang, *Anal. Bioanal. Chem.* 382 (2005) 1044.
- [4] K.G. Paul, T.B. Frigo, J.Y. Groman, E.V. Groman, *Bioconjug. Chem.* 15 (2004) 394.
- [5] I. Sondi, O. Siiman, S. Koester, E. Matijevic, *Langmuir* 16 (2000) 3107.
- [6] J.C. Liu, P. Raveendran, G.W. Qin, Y. Ikushima, *Chem. Commun.* (2005) 2972.
- [7] W. Yang, Y. Ma, J. Tang, X.R. Yang, *Colloid. Surface A* 302 (2007) 628.
- [8] W. Yang, X. Wang, F. Yang, C. Yang, X. Yang, *Adv. Mater.* 20 (2008) 2579.
- [9] H.C. Ye, R.M. Crooks, *J. Am. Chem. Soc.* 127 (2005) 4930.
- [10] E.B. Bustos, M.G.G. Jimenez, B.R. Diaz-Sanchez, E. Juaristi, T.W. Chapman, A. Luis, *Godinez, Talanta* 72 (2007) 1586.
- [11] H. Lee, S.E. Habas, S. Kweskin, D. Butcher, G.A. Somorjai, P.D. Yang, *Angew. Chem. Int. Ed.* 45 (2006) 7824.
- [12] Z.Q. Tian, Z.L. Yang, B. Ren, J.F. Li, Y. Zhang, X.F. Lin, J.W. Hu, D.Y. Wu, *Faraday Discuss.* 132 (2006) 159.
- [13] T. Teranishi, M. Hosoe, T. Tanaka, M. Miyake, *J. Phys. Chem. B* 103 (1999) 3818.
- [14] J.Y. Chen, T. Herricks, M. Geissler, Y.N. Xia, *J. Am. Chem. Soc.* 126 (2004) 10854.
- [15] T. Kijima, T. Yoshimura, M. Uota, T. Ikeda, D. Fujikawa, S. Mouri, S. Uoyama, *Angew. Chem. Int. Ed.* 43 (2004) 228.
- [16] H.P. Liang, H.M. Zhang, J.S. Hu, Y.G. Guo, L.J. Wan, C.L. Bai, *Angew. Chem. Int. Ed.* 43 (2004) 1540.
- [17] Z. Shen, M. Yamada, M. Miyake, *Chem. Commun.* (2007) 245.
- [18] Y.J. Song, Y. Yang, C.J. Medforth, E. Pereira, A.K. Singh, H.F. Xu, Y.B. Jiang, C.J. Brinker, F.V. Swol, J.A. Shelnutz, *J. Am. Chem. Soc.* 126 (2004) 635.
- [19] K.I. Shingel, *Carbohydr. Res.* 337 (2002) 1445.
- [20] H.X. Niu, Q. Yang, K.B. Tang, Y. Yie, *Scripta. Mater.* 54 (2006) 1791.
- [21] J.P. Sylvestre, A.V. Kabashin, E. Sacher, M. Meunier, J.H.T. Luong, *J. Am. Chem. Soc.* 126 (2004) 7176.
- [22] X.Q. Xu, H. Shen, J.R. Xu, J. Xu, X.J. Li, X.M. Xiong, *Appl. Surf. Sci.* 252 (2005) 494.
- [23] D. Walsh, L. Arcelli, T. Ikoma, J. Tanaka, S. Mann, *Nat. Mater.* 2 (2003) 386.
- [24] M.C. Bautista, O. Bomati-Miguel, M.D. Morales, C.J. Serna, S. Veintemillas-Verdaguer, *J. Magn. Mater.* 293 (2005) 20.
- [25] M.C. Bautista, O. Bomati-Miguel, X. Zhao, M.P. Morales, T. Gonzalez-Carreno, R.P. de Alejo, J. Ruiz-Cabello, S. Veintemillas-Verdaguer, *Nanotechnology* 15 (2004) S154.
- [26] Y.J. Huang, L. Di, J.H. Li, *Chem. Phys. Lett.* 389 (2004) 14.
- [27] Y.L. Liu, K.B. Male, P. Bouvrette, J.H.T. Luong, *Chem. Mater.* 15 (2003) 4172.
- [28] J.H. Yang, L.M. Qi, D.B. Zhang, J.M. Ma, H.M. Cheng, *Cryst. Growth. Des.* 4 (2004) 1371.
- [29] R. Gonzalez-McQuire, D. Green, D. Walsh, S. Hall, J.Y. Chane-Ching, R.O.C. Oreffo, S. Mann, *Biomaterials* 26 (2005) 6652.
- [30] D. Walsh, A. Kulak, K. Aoki, T. Ikoma, J. Tanaka, S. Mann, *Angew. Chem. Int. Ed.* 43 (2004) 6691.
- [31] L. Wu, C. Shi, L. Tian, J.J. Zhu, *J. Phys. Chem. C* 112 (2008) 319.
- [32] Z.Y. Tang, N.A. Kotov, M. Giersig, *Science* 297 (2002) 237.
- [33] H. Maeda, M. Itami, Y. Yamauchi, H. Ohmori, *Chem. Pharm. Bull.* 44 (1996) 2294.
- [34] H. Maeda, Y. Yamauchi, M. Hosoe, T. Li, E. Yamaguchi, M. Kasammatsu, H. Ohmori, *Chem. Pharm. Bull.* 42 (1994) 1870.
- [35] H. Maeda, K. Katayama, R. Matsui, Y. Yamauchi, H. Ohmori, *Anal. Lett.* 16 (2000) 293.
- [36] Y. Li, X. Lin, *Sens. and Actuators B* 115 (2006) 134.
- [37] C. Laua, G. Flechsig, P. Grundler, J. Wang, *Anal. Chim. Acta* 554 (2005) 499.
- [38] Q. Gao, X. Cui, F. Yang, Y. Ma, Y. Yang, *Biosens. Bioelectron.* 19 (2003) 277.



# Porous redox-active Cu<sub>2</sub>O–SiO<sub>2</sub> nanostructured film: Preparation, characterization and application for a label-free amperometric ferritin immunosensor

Xia Yang, Ruo Yuan\*, Yaqin Chai, Ying Zhuo, Chenglin Hong, Zhongyuan Liu, Huilan Su

Key Laboratory on Luminescence and Real-Time Analysis, Ministry of Education, College of Chemistry and Chemical Engineering, Southwest University, Chongqing 400715, PR China

## ARTICLE INFO

### Article history:

Received 5 September 2008

Received in revised form 2 December 2008

Accepted 7 December 2008

Available online 13 December 2008

### Keywords:

Cu<sub>2</sub>O–SiO<sub>2</sub>

Nanostructure

Redox activity

Ferritin

Amperometric immunosensor

## ABSTRACT

A novel Cu<sub>2</sub>O–SiO<sub>2</sub> nanostructured particle was synthesized by a solution-phase method and was adopted for construction of a label-free amperometric immunosensor. The porous Cu<sub>2</sub>O–SiO<sub>2</sub> nanoparticles had good redox electrochemical activity, large surface-to-volume ratio, film-forming ability and high stability. The physical morphology and structure of Cu<sub>2</sub>O–SiO<sub>2</sub> nanoparticles were examined by scanning electron microscope (SEM) and transmission electron microscopy (TEM). The chemical component of Cu<sub>2</sub>O–SiO<sub>2</sub> was confirmed by X-ray photoelectron spectroscopy (XPS) and auger electron spectra (AES). The electrode modification process was probed by cyclic voltammetry (CV) and the performance of the immunosensor was studied by differential pulse voltammetry (DPV) measurements. To improve the analytical characteristics of the immunosensor, the experimental conditions were optimized. The immunosensor exhibited a good response to ferritin in ranges from 1.0 to 5.0 and 5.0 to 120.0 ng mL<sup>-1</sup> with a detection limit of 0.4 ng mL<sup>-1</sup>. The fabricated immunosensor could make a low-cost, sensitive, quantitative detection of ferritin, and would have a potential application in clinical immunoassays.

© 2008 Elsevier B.V. All rights reserved.

## 1. Introduction

Ferritin, as an iron storage protein, which distributes in body's liver, spleen and marrow, has drawn much attention for its biological properties [1]. It is a tumor marker which plays an important part in iron metabolism in organisms [2]. Normal value of ferritin in a healthy adult serum is less than 200 ng mL<sup>-1</sup> for men and 90 ng mL<sup>-1</sup> for women [3].

Nowadays, immunoassay has been applied widely in many fields such as clinical chemistry, food industry and environment analysis. Electrochemical immunosensor is a device based on the specific immunoreaction of antibody and antigen. Along with the progress of biosensors, many kinds of special materials were employed to fabricate biosensors, such as sol–gel materials, polymers and nanomaterials. Sol–gel materials such as organic–inorganic chitosan composite film were often utilized to entrap proteins owing to their excellent film-forming ability, physical rigidity, chemical inertness and thermal stability [4,5]. A molecularly imprinted biocompatible polymer was still used for biosensor modification materials because of its lock–key structure [6]. More importantly, as is known to all, the development of nanomaterials have revolution-

ized the fields of biosensors. Various nanoparticles were adopted for construction process of biosensors like gold [7], silver [8], and platinum metals [9] for their high surface area, strong adsorption ability, good biocompatibility, and a heterogeneous electron transfer catalyzing ability [10]. Recently, hybrid nanomaterials have drawn much attention by biosensor researchers because they not only show their unexpected combined properties of the original components but also cause changes in optical, chemical or other performances compared with those of the individual components. For example, nanocomposites with carbon nanotubes [11], core–shell nanoparticles [12] were applied to fabricate biosensors. These hybrid nanomaterials show good stability and bioactivity for protein immobilization, but few of them have redox electrochemical activity, which are important and deserve attentions. In present work, the porous Cu<sub>2</sub>O–SiO<sub>2</sub> nanoparticles were prepared and they showed the particular performance of good redox electrochemical activity, large surface-to-volume ratio and high stability.

Cu<sub>2</sub>O is a brick-red p-type semiconductor with a band gap of about 2.17 eV. It attracts considerable interest as it has latent applications in gas sensors, solar energy conversion, electronics, magnetic storage, catalysis, lithium ion batteries and other fields [13,14]. Different morphology of Cu<sub>2</sub>O has been obtained by many methods: electrolysis [13], electrodeposition onto single-crystalline silicon [15], deposition without any template or surfactant [14], reduction of cupric salts [16]. However, it rarely

\* Corresponding author. Tel.: +86 23 68252277; fax: +86 23 68252277.  
E-mail address: [yuanruo@swu.edu.cn](mailto:yuanruo@swu.edu.cn) (R. Yuan).

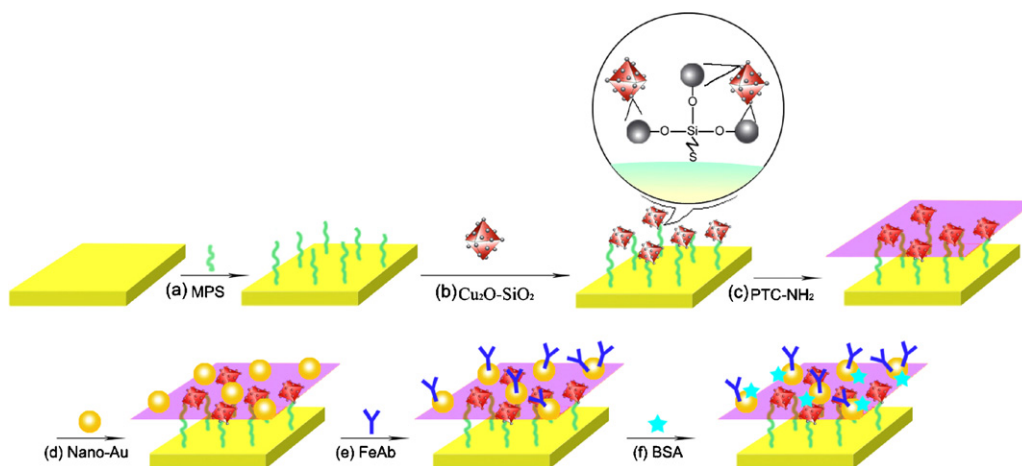


Fig. 1. Schematic illustration of fabrication of the immunosensor.

applies in immunoassays because nano-Cu<sub>2</sub>O inclines to aggregate and is hard to be coated on the electrode directly. Nano-SiO<sub>2</sub> is a porous and hydrophilic material which has surface -OH groups [17]. It is often used as a substrate or template for preparation of materials [18]. Some core-shell structured sphere like SiO<sub>2</sub>/ZnS and SiO<sub>2</sub>/Au had been studied in many literatures [19,20]. In previous work, we have synthesized many types of hybrid nanomaterials such as CoFe<sub>2</sub>O<sub>4</sub>/SiO<sub>2</sub> composite nanoparticles, thionine (TH)-doped magnetic gold nanospheres and so on [21,22]. In this study, a new kind of hybrid nanomaterials, comprised of Cu<sub>2</sub>O and SiO<sub>2</sub>, was obtained by solution-phase method. The Cu<sub>2</sub>O-SiO<sub>2</sub> nanoparticles containing -OH groups were a porous material. Significantly, it exhibited good conductivity and efficient redox activity resulted from the Cu(I) and Cu(II) [23]. Thus, the Cu<sub>2</sub>O-SiO<sub>2</sub> nanoparticles with film-forming ability and good biocompatibility would have a potential application in immunoassays.

In present work, a new immunosensor was proposed using anti-ferritin and ferritin as a model system. Firstly, a monolayer of (3-mercaptopropyl) trimethoxysilane (MPS) which had thiol headgroup was formed on the Au electrode by S-Au bond [24]. Subsequently, Cu<sub>2</sub>O-SiO<sub>2</sub> can be adsorbed onto the electrode surface to obtain a porous nanostructured film via the covalent bond formed by the methoxysilane groups of MPS pointing outward and the surface -OH groups of SiO<sub>2</sub> [25]. Then one kind of organic compound (PTC-NH<sub>2</sub>) was employed to drop on the Cu<sub>2</sub>O-SiO<sub>2</sub>/MPS/Au electrode, synthesized by ammonolysis of 3,4,9,10-perylenetetracarboxylic dianhydride (PTCDA). PTCDA is a kind of  $\pi$ -stacking organic molecules which has the desirable organic electronic properties and interspaces on the surface

[26]. Later, nano-Au was adsorbed on the surface of the PTC-NH<sub>2</sub> film through Au-NH<sub>2</sub> bond. Then the amperometric biosensor for detection of ferritin was constructed by adsorption of anti-ferritin onto the nano-Au monolayer. Lastly, BSA was used to block possible remaining active sites. The Cu<sub>2</sub>O-SiO<sub>2</sub> nanoparticles were characterized by scanning electron microscope (SEM), transmission electron microscopy (TEM), X-ray photoelectron spectroscopy (XPS) and auger electron spectra (AES). The electrode modification process was probed by cyclic voltammetry (CV), the optimization of the experimental conditions and the performance of the ferritin immunosensor were studied by differential pulse voltammetry (DPV).

## 2. Experimental

### 2.1. Reagents and materials

Anti-ferritin and ferritin were purchased from ABBOMAX Co. (USA). MPS was obtained from J&K Chemical Co. Ltd. (Beijing, China). PTCDA was purchased from Lian Gang Dyestuff Chemical Industry Co. Ltd. (Liaoning, China). Bovine serum albumin (BSA) (96–99%), gold chloride (HAuCl<sub>4</sub>) and sodium citrate were obtained from Sigma Chemical Co. (St. Louis, MO, USA). Copper sulfate, hydrazine hydrate, ethylenediamine, cetyl trimethylammonium bromide (CTAB), tetraethyl silicate (TEOS) and other chemicals were of analytical grade and purchased from regular company.

Quantities of PTCDA were dissolved in acetone under stirring, and then excessive ethylenediamine was added drop by drop. After the reaction ended, wash the precipitate with acetone and ethanol.

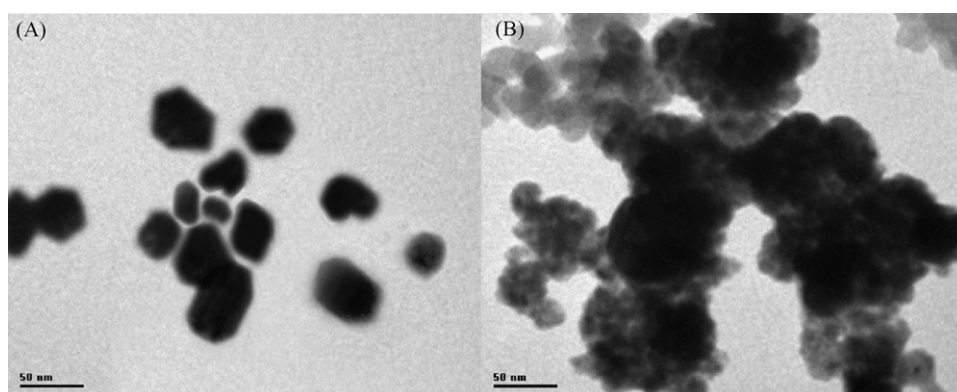


Fig. 2. TEM of pure Cu<sub>2</sub>O (A) and Cu<sub>2</sub>O-SiO<sub>2</sub> nanoparticles (B).

PTC-NH<sub>2</sub> was dispersed homogeneously in the ethanol solution.

SiO<sub>2</sub> was prepared according to Ref. [27].

Au colloid was obtained according to Ref. [28].

## 2.2. Apparatus

Cyclic voltammetric and differential pulse voltammetry measurements were carried out with a CHI 610A electrochemistry workstation (Shanghai CH Instruments, China). A three-compartment electrochemical cell contained a platinum wire auxiliary electrode, a saturated calomel reference electrode (SCE) and the modified gold electrode ( $\Phi=4$  mm) as working electrode. The structure of Cu<sub>2</sub>O–SiO<sub>2</sub> was estimated by TEM (H600, Hitachi Instrument, Japan). The electrode modification was characterized by SEM (S-4800, Hitachi, Tokyo, Japan). XPS and AES spectrometer (ESCALAB250, Thermoelectricity Instruments, USA) were used to analyze the component of the Cu<sub>2</sub>O–SiO<sub>2</sub> nanoparticles. The pH measurements were made with a pH meter (MP 230, Mettler-Toledo, Switzerland) and a digital ion analyzer (Model PHS-3C, Dazhong Instruments, Shanghai, China).

## 2.3. Preparation of Cu<sub>2</sub>O–SiO<sub>2</sub> nanoparticles

Cu<sub>2</sub>O–SiO<sub>2</sub> nanoparticles were prepared according to the following steps: 2.5 g CuSO<sub>4</sub>·5H<sub>2</sub>O and 5.0 g NaOH were dissolved into 100 mL distilled water. Then the suspension was centrifuged till the pH was near to 7.0. Later, the precipitate was dispersed in 30 mL water and then 30 mg surfactant of CTAB was added. After magnetically stirring for 30 min, 10 mL suspension of SiO<sub>2</sub> was mixed. Finally, 4.5 mL hydrazine hydrate (1 mol/L) was dropped slowly under vigorous stirring. The mixture was centrifuged, washed, and dispersed in distilled water. Pure Cu<sub>2</sub>O, which was for contrast, was obtained from Ref. [16] with slight modification.

## 2.4. Modification of the immunosensor

The schematic graph of the fabrication process was shown in Fig. 1. Firstly, the gold electrode was pretreated according to literature [29]. Then the Au electrode was dipped into MPS solution (5 mmol L<sup>-1</sup>) for 30 min to obtain a MPS monolayer (Fig. 1a). Subsequently, 10  $\mu$ L Cu<sub>2</sub>O–SiO<sub>2</sub> was coated on the electrode and dried in the air (Fig. 1b). Later, 10  $\mu$ L PTC-NH<sub>2</sub> suspension was dropped (Fig. 1c) and then the electrode was immersed into Au colloid for 8 h at 4 °C (Fig. 1d). In succession, anti-ferritin (FeAb) was adsorbed by

incubating into FeAb solution for 12 h (Fig. 1e). At last, BSA solution (0.25%) was used for blocking non-specific adsorption (Fig. 1f). The fabricated immunosensor was stored at 4 °C when not in use.

## 3. Result and discussion

### 3.1. Transmission electron microscopy, X-ray photoelectron spectroscopy and auger electron spectra measurement of Cu<sub>2</sub>O–SiO<sub>2</sub> nanoparticles

TEM was used to confirm the configuration of the Cu<sub>2</sub>O–SiO<sub>2</sub> nanoparticles. In Fig. 2, the micrographs of pure Cu<sub>2</sub>O (A) and Cu<sub>2</sub>O–SiO<sub>2</sub> (B) were shown for contrast. Cu<sub>2</sub>O crystals with an average size of 50 nm were obtained from Fig. 2(A). They had polyhedron structures because some hexagons could be clearly seen in the image. From Fig. 2(B) we can judge that there were two kinds of particles with different colors. The darker particles about 50 nm was Cu<sub>2</sub>O while the lighter one outside was SiO<sub>2</sub>, indicating that the porous SiO<sub>2</sub> was on the surface of Cu<sub>2</sub>O. It can be concluded that the Cu<sub>2</sub>O–SiO<sub>2</sub> film was porous, had surface –OH groups and large specific surface area due to SiO<sub>2</sub>.

XPS is a surface technique which has been extensively used in the chemical analysis of copper oxides to judge its oxidation state. XPS of Cu<sub>2</sub>O–SiO<sub>2</sub> had been detected in comparison with pure Cu<sub>2</sub>O and SiO<sub>2</sub>. In Fig. 3(A), pure Cu<sub>2</sub>O (curve a) and Cu<sub>2</sub>O–SiO<sub>2</sub> (curve c) had the peak at 932.24 eV and it was in agreement with that of Cu<sub>2</sub>O reported in other works [30,31]. Similarly, Cu<sub>2</sub>O–SiO<sub>2</sub> had the peak of SiO<sub>2</sub> at 102.47 eV that correspond to the pure SiO<sub>2</sub> (curve b). Fig. 3(B) shows the XPS analysis of Cu<sub>2</sub>O–SiO<sub>2</sub> and pure Cu<sub>2</sub>O from 960 to 930 eV by the step of 0.1 eV, from which we can see Cu 2p level was split into two sublevels: 2p<sub>3/2</sub> and 2p<sub>1/2</sub>. From curve b of Fig. 3(B), it was obviously seen that two peaks of the photoelectron spectrum of Cu 2p core level of Cu<sub>2</sub>O–SiO<sub>2</sub>, which are same to pure Cu<sub>2</sub>O (curve a) [32].

AES is also useful in distinguishing oxidation states between Cu(I) and Cu(II). Thus AES was employed to confirm the component of Cu<sub>2</sub>O–SiO<sub>2</sub> combining with XPS. Fig. 3(C) shows AES measurement of pure Cu<sub>2</sub>O (curve a), Cu<sub>2</sub>O–SiO<sub>2</sub> nanoparticles (curve b). According to the report, the position of the kinetic energy (KE) of Cu<sub>2</sub>O–SiO<sub>2</sub> at 917.13 eV is for Cu<sub>2</sub>O [33]. The results were consistent with above XPS results, showing firmly the chemical component of Cu<sub>2</sub>O–SiO<sub>2</sub> nanoparticles.

Concerning the fabrication of the Cu<sub>2</sub>O–SiO<sub>2</sub> nanoparticles, this mechanism assumes that the cupric hydroxide colloid, obtained

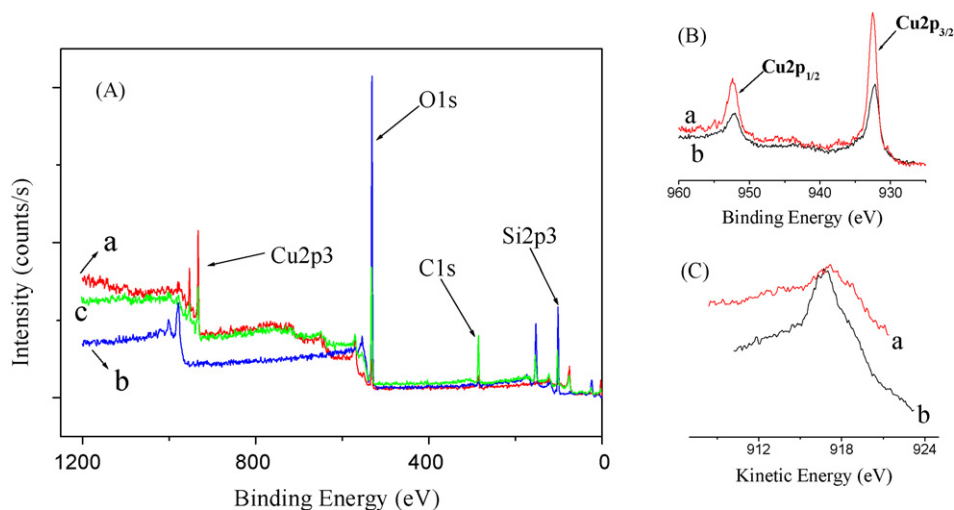
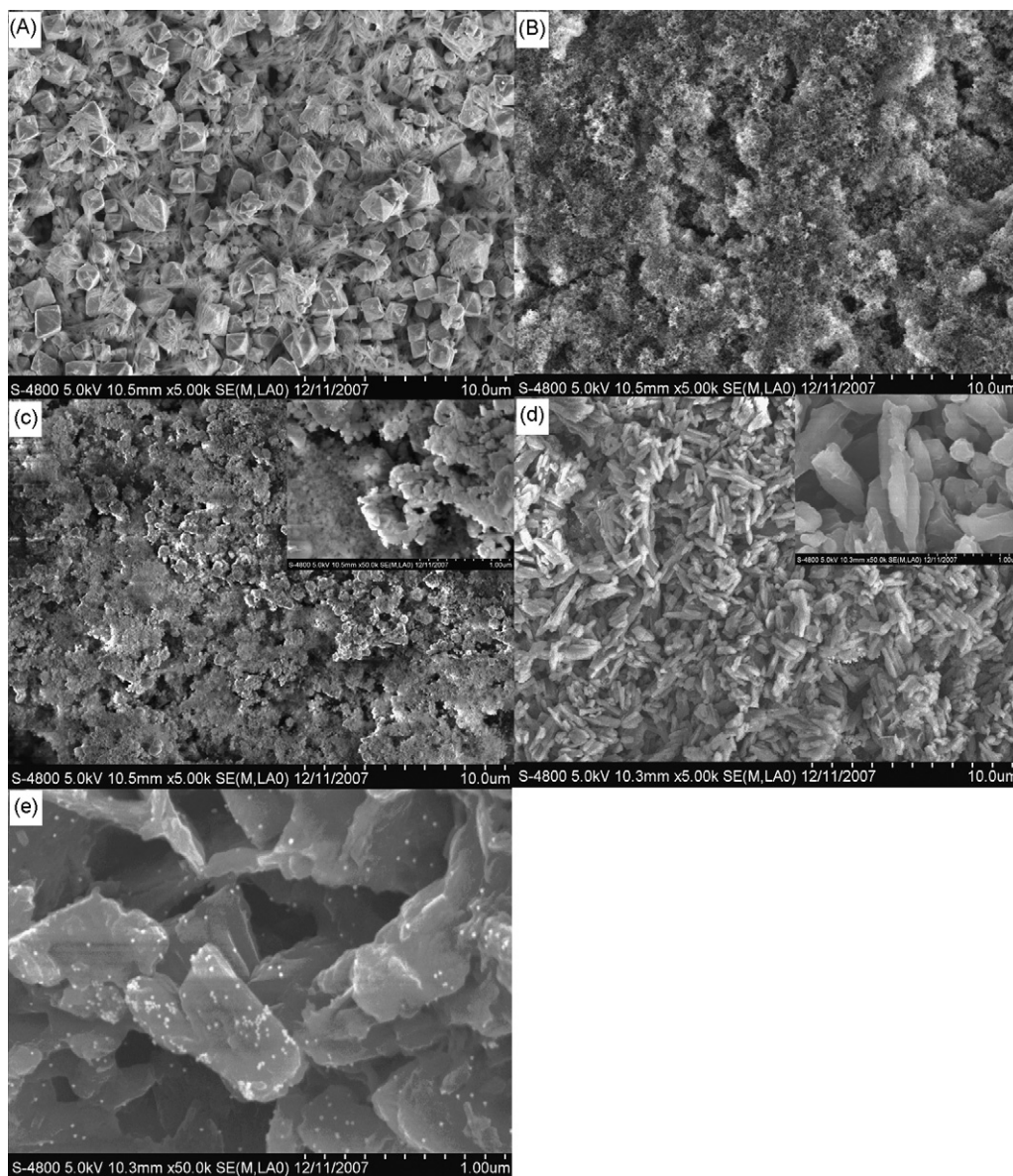
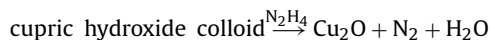


Fig. 3. XPS spectrum (image A) obtained for different coverages of pure Cu<sub>2</sub>O (a), pure SiO<sub>2</sub> (b), Cu<sub>2</sub>O–SiO<sub>2</sub> nanoparticles (c). XPS spectrum (image B) in the Cu 2p core level region of pure Cu<sub>2</sub>O (a) and Cu<sub>2</sub>O–SiO<sub>2</sub> nanoparticles (b). AES (image C) of pure Cu<sub>2</sub>O (a) and Cu<sub>2</sub>O–SiO<sub>2</sub> nanoparticles (b).



**Fig. 4.** SEM of pure  $\text{Cu}_2\text{O}$  (A), pure  $\text{SiO}_2$  (B),  $\text{Cu}_2\text{O-SiO}_2$  nanoparticles modified surface (C), PTC- $\text{NH}_2/\text{Cu}_2\text{O-SiO}_2$  modified surface (D) and nano-Au/PTC- $\text{NH}_2/\text{Cu}_2\text{O-SiO}_2$  modified surface (E).

from reaction of  $\text{CuSO}_4 \cdot 5\text{H}_2\text{O}$  and  $\text{NaOH}$ , had adsorbed sodium ions in the solution, so charged positively. When  $\text{SiO}_2$  was added, it was adsorbed onto the surface of cupric hydroxide colloid because  $\text{SiO}_2$  charged negatively [34]. As we know, the surface of  $\text{SiO}_2$  was porous, so when the reductant  $\text{N}_2\text{H}_4$  was added,  $\text{N}_2\text{H}_4$  came into the inside through the small fenestra of  $\text{SiO}_2$ . Therefore, cupric hydroxide colloid was deoxidized to  $\text{Cu}_2\text{O}$  under the surrounding of  $\text{SiO}_2$ . The overall reaction of the system was thought to be as follows:



### 3.2. Scanning electron microscope of the modification process of immunosensor

SEM was used to characterize the stepwise fabrication process of immunosensor. Many octahedral single crystals of pure  $\text{Cu}_2\text{O}$  can be found in Fig. 4(A), the same configuration of  $\text{Cu}_2\text{O}$  was also obtained in other literatures [14,35]. It corresponded with the result

of TEM image. From Fig. 4(B), we can see the surface of pure  $\text{SiO}_2$  was porous and had a lot of small fenestra. Fig. 4(C) shows the image of  $\text{Cu}_2\text{O-SiO}_2$  film, from which the morphology of  $\text{Cu}_2\text{O-SiO}_2$  nanoparticles can be seen, exhibiting  $\text{SiO}_2$  had covered with  $\text{Cu}_2\text{O}$  because there were many porous particles in sight. It can be concluded that  $\text{SiO}_2$  was on the surface of  $\text{Cu}_2\text{O}$ . Fig. 4(D) shows the image of PTC- $\text{NH}_2/\text{Cu}_2\text{O-SiO}_2$  modified surface, the size of PTC- $\text{NH}_2$  was about 500 nm. There were many interspaces on the surface which can integrate with  $\text{Cu}_2\text{O-SiO}_2$ . As shown in Fig. 4(E), many small bright particles can be observed on the PTC- $\text{NH}_2$  film, indicating that nano-Au had been adsorbed successfully because of the strong bond between  $-\text{NH}_2$  and nano-Au.

### 3.3. Cyclic voltammetric behavior of modified electrode

CV has been proved that it is a useful technology to probe the process of electrode modification. As shown in Fig. 5, the CVs of differently modified electrodes were given in the potential range of  $-0.4$  to  $0.4\text{V}$  in 6.0 BR buffer with a scan rate of

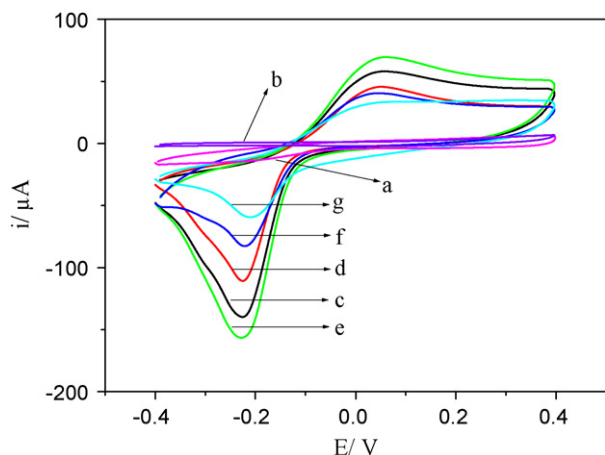


**Fig. 5.** CVs of the electrodes in 6.0 BR buffer solution: bare gold electrode (a), MPS modified electrode (b),  $\text{Cu}_2\text{O-SiO}_2/\text{MPS}$  modified electrode (c),  $\text{PTC-NH}_2/\text{Cu}_2\text{O-SiO}_2/\text{MPS}$  modified electrode (d),  $\text{nano-Au/PTC-NH}_2/\text{Cu}_2\text{O-SiO}_2/\text{MPS}$  modified electrode (e),  $\text{FeAb/nano-Au/PTC-NH}_2/\text{Cu}_2\text{O-SiO}_2/\text{MPS}$  modified electrode (f),  $\text{ferritin/BSA/FeAb/nanoAu/PTC-NH}_2/\text{Cu}_2\text{O-SiO}_2/\text{MPS}$  modified electrode (g).

$100 \text{ mV s}^{-1}$ . The image showed the CVs of bare gold electrode (Fig. 5a) and MPS (Fig. 5b) modified electrode, in which no peak was observed as a result of lack of redox-active material. When the electrode was coated with  $\text{Cu}_2\text{O-SiO}_2$  nanoparticles (Fig. 5c), there was a good pair of redox peak. It was the reason that  $\text{Cu}_2\text{O-SiO}_2$  was an excellent redox-active material attributed to the redox reaction of  $\text{Cu(I)}$  and  $\text{Cu(II)}$ . After  $\text{PTC-NH}_2$  (Fig. 5d) was coated, the peak current decreased because  $\text{PTC-NH}_2$  would hinder the transfer of electrons. The anodic and cathodic peaks increased when Au colloid was adsorbed onto the surface of the  $\text{PTC-NH}_2/\text{Cu}_2\text{O-SiO}_2/\text{MPS}$  modified electrode (Fig. 5e), because nano-Au could accelerate the reaction of  $\text{Cu(I)}/\text{Cu(II)}$ . Fig. 5f shows an obvious peak decrease for the adsorption of FeAb onto the surface of the electrode. It was due to that antibody was a kind of protein which would block the electron diffusion toward the electrode surface. After the fabricated immunosensor was incubated with  $20 \text{ ng mL}^{-1}$  ferritin (Fig. 5g), a decline could be seen, for antigen-antibody complex acted as the inert electron and mass transfer blocking layer. CV responses of the immunosensor at different scan rates were recorded. The result showed that the peak current increased with the scan rates in the range of  $25\text{--}250 \text{ mV s}^{-1}$ . Square root of scan rate showed a linear relation with peak current, indicating a diffusion-controlled behavior of the immunosensor.

#### 3.4. Optimization of the experimental conditions

DPV technology was used to optimize the experimental conditions of the immunosensor. It was carried out in the potential range of  $-0.3$  to  $0.2 \text{ V}$  in BR buffer solution.

##### 3.4.1. Influence of pH value

The performance of the immunosensor was related to the pH value of the detection solution. The effect of pH on the DPV peak current was tested over a pH range from 4.0 to 8.5. From Fig. 6, we can see the peak current reach the highest at the value of 6.0. It was presumed that  $\text{Cu}_2\text{O}$  may dissolve under strong acidic condition, while  $\text{SiO}_2$  may react with  $\text{OH}^-$  under alkali condition. So we use pH 6.0 as experimental condition.

##### 3.4.2. Influence of incubation temperature

Incubation temperature would also affect the performance of the immunosensor. The immunosensor was incubated with  $20 \text{ ng mL}^{-1}$  ferritin (pH 6.0) under a range of temperature from 15 to  $50^\circ\text{C}$ . Fig. 6(B) exhibited a rapid decline of peak current before  $35^\circ\text{C}$  and there was a little change from 35 to  $50^\circ\text{C}$ . It was due to that ferritin and FeAb had combined gradually. On the other hand, protein may lose bioactivity at high temperature, so  $35^\circ\text{C}$  was selected to be the incubation temperature.

##### 3.4.3. Influence of incubation time

Incubation time was an important effect factor of the immunosensor. The immunosensor was incubated with the same concentration of ferritin (pH 6.0) at  $35^\circ\text{C}$  for 5, 10, 15, 20, 25, 30, 35, 40 min. It was found that the peak current decrease with the increasing incubation time in Fig. 6(C). But after 30 min, the current response was stable because ferritin and FeAb had combined entirely. So we choose 30 min as incubation time.

#### 3.5. The performance of the immunosensor

##### 3.5.1. The response of the immunosensor to ferritin

DPV technology had been used to check the response of the immunosensor to different concentration of ferritin. As seen in Fig. 7, the current peak decreased with the increasing concentration and it was proportional to the ferritin concentration in two ranges (inset):  $1.0\text{--}5.0 \text{ ng mL}^{-1}$  (Fig. 7A) and  $5.0\text{--}120.0 \text{ ng mL}^{-1}$  (Fig. 7B). The linear regression equation was  $I = -39.1 + 1.7C_{\text{ferritin}}$  and  $I = -30.1 + 0.1C_{\text{ferritin}}$ , with a correlation coefficient of 0.9938 and 0.9951, respectively. The limit of detection was estimated at  $0.4 \text{ ng mL}^{-1}$  by three times of the standard deviation of the blank.

##### 3.5.2. Stability and repeatability of the immunosensor

The immunosensor was estimated by performing three cycles per day. The data was collected 15 days. It showed that the last DPV peak current retained 87.6% of its initial current, which proved the fabricated immunosensor had good stability.

In order to know the repeatability of the sensor, 100 continuous cycle scan was carried out in the potential range from  $-0.3$  to  $0.2 \text{ V}$  with a scan rate of  $100 \text{ mV s}^{-1}$ . A decrease of about 8.4% of the initial DPV response signal was observed. The result of repeatability in my experiment was acceptable.

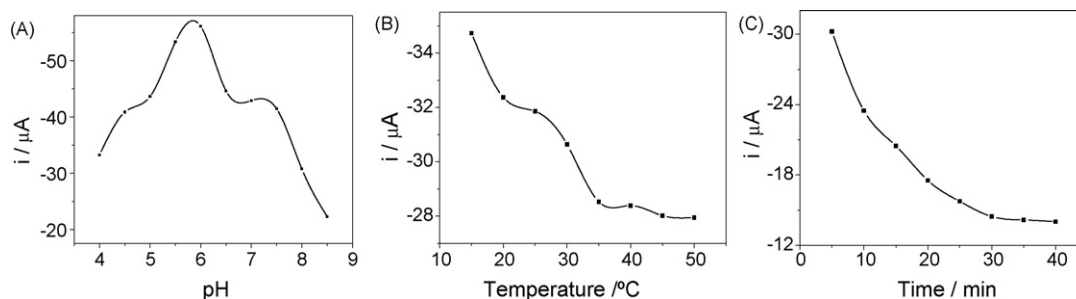


**Fig. 6.** Effect of pH (A), temperature (B), incubation time (C) on the immunosensor current response.



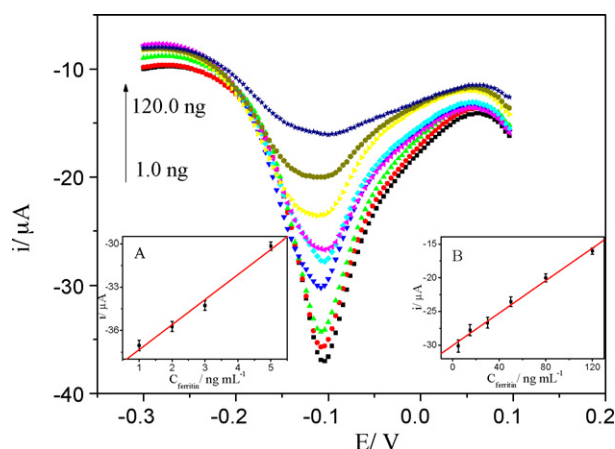


**Fig. 7.** DPVs of the immunosensor at different ferritin solutions with concentrations of 1.0, 2.0, 3.0, 5.0, 15.0, 30.0, 50.0, 80.0, 120.0 ng mL<sup>-1</sup> under optimal conditions. The inset shows linear relationship between the current response and ferritin concentration in ranges of 1.0–5.0 ng mL<sup>-1</sup> (A) and 5.0–120.0 ng mL<sup>-1</sup> (B).

**Table 1**  
Experimental results of different methods obtained in serum samples.

Serum samples	1	2	3	4	5	6
ELISA (ng/mL)	3.52	41.87	72.26	26.35	96.73	107.64
This method (ng/mL)	3.41	44.38	75.85	24.92	94.59	112.06
Relative deviation (%)	-3.13	+5.99	+4.97	-5.43	-2.21	+4.11

### 3.5.3. The preliminary application of the immunosensor

To investigate the performance of the immunosensor for detection of ferritin, three blank human serum samples, adding different concentration of ferritin were assayed. The value of ferritin obtained by the proposed immunosensor were 23.2, 57.8, 102.6 ng mL<sup>-1</sup>, while the standard concentration were 25.0, 60.0, 100.0 ng mL<sup>-1</sup>. The recovery rate was in the range of 92.8–102.6%.

To further demonstrate the clinical applications of the developed immunosensor, six serum samples from the Ninth People's Hospital of Chongqing, China, were analyzed by this method to compare with ELISA method. These serum samples were diluted to different concentrations with a PBS of pH 7.5. Table 1 shows the comparison results between the two methods. The relative error was from -2.21 to 5.99%, suggesting an acceptable agreement. Thus, the presented immunosensor could be satisfactorily applied to the clinical determination of ferritin in human serum.

## 4. Conclusions

In the study, we have presented a strategy for preparing porous Cu<sub>2</sub>O–SiO<sub>2</sub> nanostructured film with large specific surface area and redox electrochemical activity. The resulting Cu<sub>2</sub>O–SiO<sub>2</sub> nanoparticles were used for construction of a novel immunosensor. The fabricated amperometric immunosensor exhibited direct

quantification and high sensitive detection of ferritin without a labeling step, which demonstrated the application prospect of the Cu<sub>2</sub>O–SiO<sub>2</sub> nanoparticles. It is expected that this technique of immunosensor fabrication will be useful for immunoassays.

## Acknowledgements

This work was supported by the NNSF of China (20675064), the Natural Science Foundation of Chongqing City (CSTC-2004BB4149, 2005BB4100), High Technology Project Foundation of Southwest University (XSGX02), China, Chongqing Science & technology commission (2008AB5081).

## References

- [1] S. Allen, X.Y. Chen, J. Davies, M.C. Davies, A.C. Dawkes, J.C. Edwards, C.J. Roberts, J. Sefton, S.J.B. Tendler, P.M. Williams, *Biochemistry* 36 (1997) 7457.
- [2] M.S. Wilson, W.Y. Nie, *Anal. Chem.* 78 (2006) 6476.
- [3] S.F. Chou, W.L. Hsu, J.M. Hwang, C.Y. Chen, *Anal. Chim. Acta* 453 (2002) 181.
- [4] E. Han, D. Shan, H.G. Xue, S. Cosnier, *Biomacromolecules* 8 (2007) 971.
- [5] G.H. Wang, L.M. Zhang, *J. Phys. Chem. B* 110 (2006) 24864.
- [6] R. Jacob, M. Tate, Y. Banti, C. Rix, D.E. Mainwaring, *J. Phys. Chem. A* 112 (2008) 322.
- [7] M. Dequaire, C. Degrand, B. Limoges, *Anal. Chem.* 72 (2000) 5521.
- [8] D.A. Gish, F. Nsiah, M.T. McDermott, M.J. Brett, *Anal. Chem.* 79 (2007) 4228.
- [9] S. Hrapovic, Y.L. Liu, K.B. Male, J.H.T. Luong, *Anal. Chem.* 76 (2004) 1083.
- [10] I. Streeter, R. Baron, R.G. Compton, *J. Phys. Chem. C* 111 (2007) 17008.
- [11] (a) Y.F. Ma, S.R. Ali, A.S. Dodoo, H.X. He, *J. Phys. Chem. B* 110 (2006) 16359; (b) Q. Zhang, L. Zhang, J.H. Li, *J. Phys. Chem. C* 111 (2007) 8655; (c) J. Wang, M. Musameh, *Anal. Chem.* 75 (2003) 2075.
- [12] W. Yan, X.J. Chen, X.H. Li, X.M. Feng, J.J. Zhu, *J. Phys. Chem. B* 112 (2008) 1275.
- [13] D.P. Singh, N.R. Neti, A.S.K. Sinha, O.N. Srivastava, *J. Phys. Chem. C* 111 (2007) 1638.
- [14] S.J. Guo, Y.X. Fang, S.J. Dong, E.K. Wang, *Inorg. Chem.* 46 (2007) 9537.
- [15] J.A. Switzer, R. Liu, E.W. Bohannon, F. Ernst, *J. Phys. Chem. B* 106 (2002) 12369.
- [16] Y.J. Dong, Y.D. Li, C. Wang, A.L. Cui, Z.X. Deng, *J. Colloid Interface Sci.* 243 (2001) 85.
- [17] D.B. Asay, S.H. Kim, *J. Phys. Chem. B* 109 (2005) 16760.
- [18] R. Garcia, M. Tello, *Nano Lett.* 4 (2004) 1115.
- [19] K.P. Velikov, A. Moroz, A. Van Blaaderen, *Appl. Phys. Lett.* 80 (2002) 49.
- [20] B. Sadtler, A. Wei, *Chem. Commun.* (2002) 1604.
- [21] D.P. Tang, R. Yuan, Y.Q. Chai, H.Z. An, *Adv. Funct. Mater.* 17 (2007) 976.
- [22] D.P. Tang, R. Yuan, Y.Q. Chai, *Anal. Chem.* 80 (2008) 1582.
- [23] T.Y. You, O. Niwa, M. Tomita, H. Ando, M. Suzuki, S. Hirono, *Electrochem. Commun.* 4 (2002) 468.
- [24] J.B. Jia, B.Q. Wang, A.G. Wu, G.J. Cheng, Z. Li, S.J. Dong, *Anal. Chem.* 74 (2002) 2217.
- [25] P.A. Buining, B.M. Humbel, A.P. Philipse, A.J. Verkleij, *Langmuir* 13 (1997) 3921.
- [26] Y. Zhuo, P.X. Yuan, R. Yuan, Y.Q. Chai, C.L. Hong, *Biomaterials* 29 (2008) 1501.
- [27] K. Han, Z. Xiang, Z. Wang, C.L. Wang, M.J. Li, J.H. Zhang, B. Yang, *Chem. Res. Chin. U* 22 (2006) 76.
- [28] G. Frens, *Nat. Phys. Sci.* 241 (1973) 20.
- [29] H.Z. An, R. Yuan, D.P. Tang, Y.Q. Chai, N. Li, *Electroanalysis* 19 (2007) 479.
- [30] Y.H. Lee, I.C. Leu, S.T. Changa, C.L. Liao, K.Z. Fung, *Electrochim. Acta* 50 (2004) 553.
- [31] M.F. Al-Kuhaili, *Vacuum* 82 (2008) 623.
- [32] J.B. Reitz, E.I. Solomon, *J. Am. Chem. Soc.* 120 (1998) 11467.
- [33] J.J. Teo, Y. Chang, H.C. Zeng, *Langmuir* 22 (2006) 7369.
- [34] Z.H. Guo, Y. Shen, M.K. Wang, F. Zhao, S.J. Dong, *Anal. Chem.* 76 (2004) 184.
- [35] (a) M.J. Siegfried, K.S. Choi, *Adv. Mater.* 16 (2004) 1743; (b) M.J. Siegfried, K.S. Choi, *Angew. Chem. Int. Ed.* 44 (2005) 3218; (c) H. Xu, W. Wang, W. Zhu, *J. Phys. Chem. B* 110 (2006) 13829.



## Speciation analysis of arsenic in *Mya arenaria* Linnaeus and *Shrimp* with capillary electrophoresis-inductively coupled plasma mass spectrometry

GuiDi Yang<sup>a,b</sup>, JinHua Xu<sup>a</sup>, JinPing Zheng<sup>a</sup>, XueQin Xu<sup>a</sup>, Wei Wang<sup>a</sup>,  
LiangJun Xu<sup>a</sup>, GuoNan Chen<sup>a</sup>, FengFu Fu<sup>a,\*</sup>

<sup>a</sup> Key Laboratory of Analysis and Detection Technology for Food Safety of Ministry of Education and Department of Chemistry, Fuzhou University, Fuzhou, Fujian 350108, China

<sup>b</sup> College of Life Sciences, Fujian Agriculture and Forestry University, Fuzhou 350002, China

### ARTICLE INFO

#### Article history:

Received 18 September 2008

Received in revised form

25 November 2008

Accepted 26 November 2008

Available online 3 December 2008

#### Keywords:

Speciation analysis

Arsenic

CE-ICP-MS

*Mya arenaria* Linnaeus

Shrimps

### ABSTRACT

An improved sheath-flow interface used to couple capillary electrophoresis (CE) with inductively coupled plasma mass spectrometry (ICP-MS) and a microwave-assisted extraction used to extract each arsenic species in seafood were developed in this work. The improved sheath-flow interface completely avoids laminar flow in CE capillary caused by the suction from ICP-MS, makes electric supply more stable in CE, and transports analyte solution to ICP-MS easily and more efficiently. CE-ICP-MS coupled with our interface have two quantitative analysis modes: continuous sample-introduction mode and collective sample-introduction mode. The collective sample-introduction technique greatly reduced the dead volume of interface to approximately zero, obviously avoided the excessive dilution of analyte, and eventually led to a much lower detection limit and a much better electrophoretic resolution. This was demonstrated by the better symmetry and narrow peak widths (10–12 s) and much lower detection limits (0.030–0.042  $\mu\text{g/L}$ ) of four species of arsenic determined with collective sample-introduction mode.

With the help of this improved sheath-flow interface and the microwave-assisted extraction, we have successfully separated and determined four arsenic species, As(III), As(V), monomethylarsonic acid (MMA) and dimethylarsinic acid (DMA) in dried *Mya arenaria* Linnaeus and *Shrimp* samples using CE-ICP-MS within 10 min with a relative standard deviation of 2–4% (peak areas,  $n=6$ ) and a recovery of 96–105%.

© 2008 Elsevier B.V. All rights reserved.

### 1. Introduction

Many researches have reported that the toxicity and bio-availability of an element are rather dependent on its speciation [1–5]. For example, different species of arsenic has quite different toxicity and accumulative capability in the environment and biologic tissues [6–10]. Especially, arsenic is abundant in seafood at concentrations as high as several hundred micrograms per gram [11], therefore, it is very important to analyze the concentrations of individual arsenic species in seafood in order to evaluate the level of toxicity.

So far, the main techniques employed to the speciation analysis of arsenic are based on the combination of separation techniques such as liquid chromatography (LC) or gas chromatography (GC) and element-selective detectors such as inductively coupled plasma mass spectrometry (ICP-MS), inductively coupled plasma emission spectrometry (ICP-ES), molecular UV-spectrometry, atomic absorp-

tion spectrometry (AAS) and so on [12–23]. However, currently available techniques for speciation analysis of arsenic often suffer from one or more of the following deficiencies: long analytical time, lower separation efficiency, inadequate stability, amenable to a limited range of sample types and inadequate detection limits [24].

Compared to LC and GC, capillary electrophoresis (CE) offers higher separation efficiency, a relatively rapid separation and requires much smaller volume of sample [25]. Therefore, the coupling of CE with ICP-MS promises a powerful analytical technique for the speciation analysis of arsenic [24,26,27]. The coupling of CE with ICP-MS usually requires an interface that should maintain a stable electrical connection to CE, efficiently introduces trace analyte solution into ICP-MS, not degrades the resolution of CE and not dilutes analyte excessively [28]. Up to now, there are three kinds of interface used to couple CE with ICP-MS on-line or off-line: no-sheath-flow interface, sheath-flow interface and hydride generation interface [29–35]. Among the above three interfaces, sheath-flow interface received more attention because it transports analyte solution easily and makes the electrical connection to CE more stable. However, sheath-flow interface reported previ-

\* Corresponding author. Tel.: +86 591 28306608; fax: +86 591 28306608.  
E-mail address: [fengfu@fzu.edu.cn](mailto:fengfu@fzu.edu.cn) (F. Fu).

ously cannot completely avoid laminar flow in CE capillary caused by the suction from ICP-MS, and finally results in the degradation of electrophoretic resolution, although makeup solution was introduced to minimize the suction effect. In addition, the introduction of makeup solution excessively diluted the analyte and finally led to a relatively lower sensitivity since the flow rate of CE is much smaller than that of ICP-MS.

To perform the speciation analysis of arsenic in seafood, the extraction of each arsenic species is another key point. The extraction method must be capable of quantitatively extracting each arsenic species from samples without altering the individual arsenic species during extraction process [36]. So far, solvent extraction together with agitation, sonication, microwave heating and so on has been tried to extract organic arsenic species from fish tissues. In this work, we developed an improved sheath-flow interface used to couple CE with ICP-MS and a microwave-assisted extraction used to extract each arsenic species from seafood, in order to determine the concentrations of individual arsenic species in *Mya arenaria* Linnaeus and *Shrimp*. The improved sheath-flow interface completely avoids laminar flow in CE capillary caused by the suction from ICP-MS and transports analyte solution to ICP-MS with two modes: continuous sample-introduction mode and collective sample-introduction mode. With the help of this improved sheath-flow interface and microwave-assisted extraction method, we have successfully coupled CE with ICP-MS and determined four species of arsenic including As(III), As(V), dimethylarsinic acid (DMA) and monomethylarsonic acid (MMA) in *Mya arenaria* Linnaeus and *Shrimp*.

## 2. Materials and methods

### 2.1. Reagents

The analytical grade of four species of arsenic including As<sub>2</sub>O<sub>3</sub>, DMA, MMA sesquihydrate and Na<sub>2</sub>HAsO<sub>4</sub> were purchased from Shenzhen Meryer Chemical Technology Co., Ltd. (Shenzhen, China). The 1000 µg/mL stock standard solution of As(III) was prepared by dissolving the above As<sub>2</sub>O<sub>3</sub> in 0.2% NaOH solution, and the 1000 µg/mL stock standard solutions of DMA, MMA and As(V) were prepared by dissolving the above standard matters in Milli-Q water. All the stock standard solutions were stored at 4 °C, and the running standard solutions were prepared by diluted stock standard solutions to the desired concentration with running buffer solution. The running buffer solution of 20 mmol/L of NaH<sub>2</sub>PO<sub>4</sub>–5.00 mmol/L of Na<sub>2</sub>B<sub>4</sub>O<sub>7</sub> (pH 6.50) was prepared by dissolving analytical grade sodium dihydrogenphosphate (NaH<sub>2</sub>PO<sub>4</sub>·2H<sub>2</sub>O) and sodium tetraborate (Na<sub>2</sub>B<sub>4</sub>O<sub>7</sub>·10 H<sub>2</sub>O), which were purchased from Shanghai Reagents Co., Ltd. (Shanghai, China), in Milli-Q water. All solutions were treated by ultrasonic agitation and filtered through a 0.22 µm membrane filter before use. All experiments were performed at room temperature in which the temperature was regulated in 25–27 °C by an air conditioner, and water used in this experiment is Milli-Q water (18.2 MΩ) prepared by a Milli-Q equipment (Millipore, Bedford, USA), the super-pure grade of HNO<sub>3</sub>, CH<sub>3</sub>OH and NaOH were purchased from Shanghai Reagents Co., Ltd. (Shanghai, China).

### 2.2. CE-ICP-MS system

The CE-ICP-MS system consists of an home-made CE system and an Agilent 7500ce ICP-MS (Agilent Technologies, USA) which is equipped with a microconcentric nebulizer (MCN, Agilent Technologies, USA, optimum flow is 50–200 µL/min). The CE system was fabricated with a 60 cm length × 75 µm i.d. × 375 µm o.d. fused-silica capillary (Hebei Yongnian Optic Fiber Factory, Hebei, China)

and a high-voltage power supply, which can be operated in a voltage range of –30 to +30kV (Shanghai Institute of Atomic Nuclear Science Research, Chinese Academy of Science, Shanghai, China). A home-made improved sheath-flow interface (see Fig. 1) was used to couple CE with ICP-MS.

### 2.3. The improved sheath-flow interface

The interface used in this study was fabricated on the basis of our previous work [35] and its schematic diagram was shown in Fig. 1. As shown in Fig. 1, the interface was composed of a stainless steel capillary (1.5 cm length × 600 µm i.d. × 800 µm o.d.), some tygon tubes, two peristaltic pumps, a pulse controller and a three-way PEEK union. As shown in Fig. 1, two tygon tubes with an inner diameter of 190 µm were inserted into two sides of stainless steel capillary and the outlet end of the CE capillary was directly inserted into stainless steel capillary through tygon tube, another side of stainless steel capillary connected to peristaltic pump 1 through tygon tube. The cathode of CE power supply was directly connected to stainless steel capillary. The pulse controller was used to control the driving of peristaltic pump 1 and peristaltic pump 2. Unlike our previous interface [35], a tiny sheath-flow was introduced into the outlet of CE capillary by pump 1 in order to make the electrical connection to CE easier and more stable, and as well as transports CE eluent to ICP-MS more smoothly and efficiently.

Compared with other sheath-flow interface reported previously, the main difference of our interface is that two peristaltic pumps, pump 1 and 2, were used. The pump 1 was designed to segregate suction from ICP-MS, control the flow rate of sheath-flow and transport the eluent from the CE to three-way PEEK union, whereas, pump 2 was designed to finally send eluent from three-way PEEK union to ICP-MS for the determination and introduce a makeup solution in order to get a stable atomization and ionization efficiency. For the above features, our improved sheath-flow interface near the completely avoided suction caused from ICP-MS, transported eluent of CE to ICP-MS more smoothly and efficiently, made electric supply in CE much easier and more stable, and finally made CE-ICP-MS keeps the intrinsic separation-efficiency and resolution of CE and has much higher sensitivity or much lower detection limit.

### 2.4. Measuring procedure

The CE capillary was conditioned daily by purging with Milli-Q water for 10 min, 0.1 mol/L NaOH solution for 10 min, Milli-Q water for 10 min and running buffer solution for 10 min. Between each run, the CE capillary was flushed with Milli-Q water and running buffer solution for 2 min, respectively. The sample was injected into the CE capillary for determination by electro-migration injection.

As we mentioned above, one of the advantages of our interface is that CE-ICP-MS coupled with our interface have two quantitative analysis modes:

- Continuous sample-introduction mode*: In this mode, our interface works as normal sheath-flow interface reported previously, standard solution and sample were measured by CE-ICP-MS under the continuous driving of both peristaltic pumps 1 and 2. The CE eluent was continuously transported into ICP-MS for determination.
- Collective sample-introduction mode*: In this mode, the standard solution or sample was injected into CE for separation under the stop of peristaltic pump 1 and the driving of peristaltic pump 2 in order to completely avoid the suction effect caused by ICP-MS. When one analyte was completely separated and eluted out of the CE capillary (according to the migration time obtained with continuous sample-introduction mode), then, the pump 1 was driven to transport the analyte solution to ICP-MS for

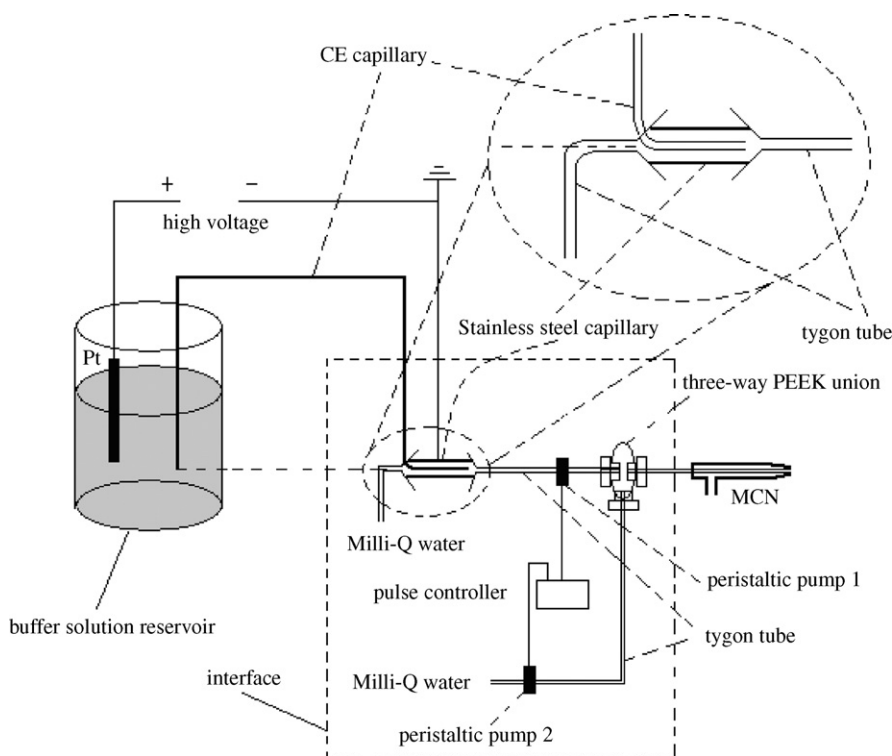


Fig. 1. Schematic diagram of the improved sheath-flow interface.

determination. After the first analyte was transported to ICP-MS, the peristaltic pump 1 was stopped again until the second analyte was completely separated and eluted out of the CE capillary according to the migration time obtained with continuous sample-introduction mode, and then the pump 1 was driven to transport the solution of second analyte to ICP-MS again. The above process was repeated until all analytes were determined. The collective sample-introduction mode completely avoided the suction from ICP-MS, greatly reduced the liquid dead volume of interface, obviously avoided the excessive dilution of analyte, and eventually led to a much lower detection limit and a much better electrophoretic resolution.

### 3. Results and discussion

#### 3.1. Optimization of CE-ICP-MS conditions for the analysis of MMA, DMA, As(III) and As(V)

Buffer solution including its chemical components, pH and concentration greatly affects the separation of analytes by affecting the migration time of each analyte. In order to obtain a better electrophoretic resolution, we optimized buffer solution under continuous sample-introduction mode with the similar manner reported in our previous paper [35]. The experimental results showed that the mixture of phosphate and borate (phosphate:borate = 4:1, mole concentration) gave the most acceptable separation efficiency and reproducibility, therefore, the mixed solution of phosphate and borate (4:1, mole concentration) was chosen as running buffer solution.

The relationship between migration times/resolution and pH was studied in detail with a phosphate–borate buffer solution in the pH range of 5.50–6.75, we found that pH 6.50 was the optimum pH value for the separation of As(III), DMA, MMA and As(V).

The effect of concentration of running buffer solution on the separation was also studied by using different concentration of phosphate–borate buffer solution (phosphate:borate = 10:2.50,

15:3.75, 20:5.00, 25:6.25 and 30:7.50 mmol/L) at pH 6.50. The results showed that the peak shapes of all four arsenic species were improved and the migration times became longer with the increase of the concentration of running buffer solution. Considering the analytical time and electrophoretic resolution, 20 mmol/L of  $\text{NaH}_2\text{PO}_4$ –5.00 mmol/L of  $\text{Na}_2\text{B}_4\text{O}_7$  (pH 6.50) was selected as the running buffer solution.

Different from the interface reported in our previous paper [35], in this study, pump 1 was designed not only to transport the analyte solution eluted out of the CE capillary to three-way PEEK union but also to introduce a tiny sheath-flow into the outlet of CE capillary, the flow rate of pump 1 will greatly influence the stability, the peak shapes and the sensitivity. By changing the rate of pump 1 from 1.5 rpm ( $3 \mu\text{L}/\text{min}$ ) to 7.5 rpm ( $15 \mu\text{L}/\text{min}$ ), we found that the flow rate of 6.0 rpm ( $12 \mu\text{L}/\text{min}$ ) provides a better peak shapes and sensitivity. Like our previous interface [35], the peristaltic pump 2 was used to further transport analyte solution from three-way PEEK union to ICP-MS and pump Milli-Q water to ICP-MS nebulizer in order to achieve stable atomization and ionization efficiency too. The higher flow rate of pump 2 will excessively dilute the analyte and results in the degradation of sensitivity, whereas the lower flow rate of pump 2 will influence the atomization efficiency of analyte and results in the degradation of sensitivity too. The optimum rate of pump 2 was selected by changing the rate from 0 rpm ( $0 \mu\text{L}/\text{min}$ ) to 10.0 rpm ( $400 \mu\text{L}/\text{min}$ ), and the results showed that the flow rate of pump 2 = 3.0 rpm ( $120 \mu\text{L}/\text{min}$ ) is a best choice. Compared to our previous interface [35], the optimum flow rates of both pump 1 and pump 2 are relative small, and this feature is favorable to promise a higher sensitivity. This will be demonstrated by the detection limits of both continuous sample-introduction mode and collective sample-introduction mode shown below.

The effect of the separation voltage on the migration time and electrophoretic resolution was investigated in the range of 8–18 kV. The results showed that higher voltage was favorable to shorten migration time, however, high voltage led to the broadening of peak due to Joule heating effect. Considering the reproducibility, analyt-

**Table 1**  
Running parameters of CE-ICP-MS.

Parameter	Value
CE voltage	12 kV
Sampling time	10 s
CE capillary	i.d. 75 $\mu$ m; o.d. 365 $\mu$ m; 60 cm long
Room temperature	25–27 °C
Running buffer solution	20 mmol/L NaH <sub>2</sub> PO <sub>4</sub> –5 mmol/L Na <sub>2</sub> B <sub>4</sub> O <sub>7</sub> , pH 6.50
Flow rate of pump 1	12 $\mu$ L/min
Flow rate of pump 2	120 $\mu$ L/min
RF power	1300 W
Outer plasma gas	13 L/min
Intermediate plasma gas	1.0 L/min
Carrier gas	0.75 L/min
Monitored isotope ( <i>m/z</i> )	75 (As <sup>+</sup> )
Nebulizer type	MCN (optimum flow is 50–200 $\mu$ L/min)

ical time and peak shapes, +12 kV was selected as the separation voltage.

Different sample-injection times (5, 10, 15, 20 and 25 s) were tested in this experiment, and results showed that the signal of ICP-MS becomes higher with the increase of injection time. However, longer injection time will degrade electrophoretic resolution. Considering both of sensitivity and separation efficiency, we selected 10 s as sample's injection time.

At above optimum conditions (see Table 1), four species of arsenic were base line separated within 10 min under continuous sample-introduction mode (see Fig. 2a). The same experiment was repeated for six times, and the R.S.D. (relative standard deviation,  $n=6$ ) of migration times was calculated to be 2, 2, 3 and 3% for As(III), DMA, MMA and As(V), respectively, and that of peak areas is 5, 5, 4 and 4% for As(III), DMA, MMA and As(V), respectively. The detection limit ( $3\sigma/S$ , the concentration necessary to yield a net signal equal to three times the standard deviation of the background) calculated with counts is 0.10, 0.18, 0.19 and 0.10  $\mu$ g/L for As(III), DMA, MMA and As(V), respectively under continuous sample-introduction mode. Compared to our previous interface [35], the present one provides much better R.S.D., much higher sensitivity and much lower detection limits under continuous sample-introduction mode, and finally makes continuous sample-introduction mode suitable for quantitative analysis, whereas the continuous sample-introduction mode of our previous interface is not suitable for quantitative analysis due to bad reproducibility, lower sensitivity and poor peak shape [35].

### 3.2. Determination of MMA, DMA, As(III) and As(V) with collective sample-introduction mode

Fig. 2a shows the electrograms of MMA, DMA, As(III) and As(V) obtained with continuous sample-introduction mode. From Fig. 2a, we found that the migration time of As(III), DMA, MMA and As(V) was 366–389, 433–460, 485–509 and 532–559 s, respectively.

Under collective sample-introduction mode, standard solutions were injected into CE-ICP-MS for determination with the stop of pump 1 and the driving of pump 2. The pulse controller was set to control pump 1 drive at 389 s (the time when As(III) was completely separated and flowed out of CE), 460 s (DMA), 509 s (MMA) and 559 s (As(V)) for 10 s, respectively to transport the CE eluent of each arsenic species to three-way PEEK union and further transport it to ICP-MS for determination by pump 2. The real electrograms of four arsenic species determined with collective sample-introduction mode were shown in Fig. 2b. Comparing Fig. 2b with Fig. 2a, we clearly observed that the peak shapes and the sensitivity of four arsenic species were obviously improved under collective sample-introduction mode. The peak widths and detection limits of four arsenic species are 10–12 s and 0.030–0.042  $\mu$ g/L, respectively under collective sample-introduction mode, much

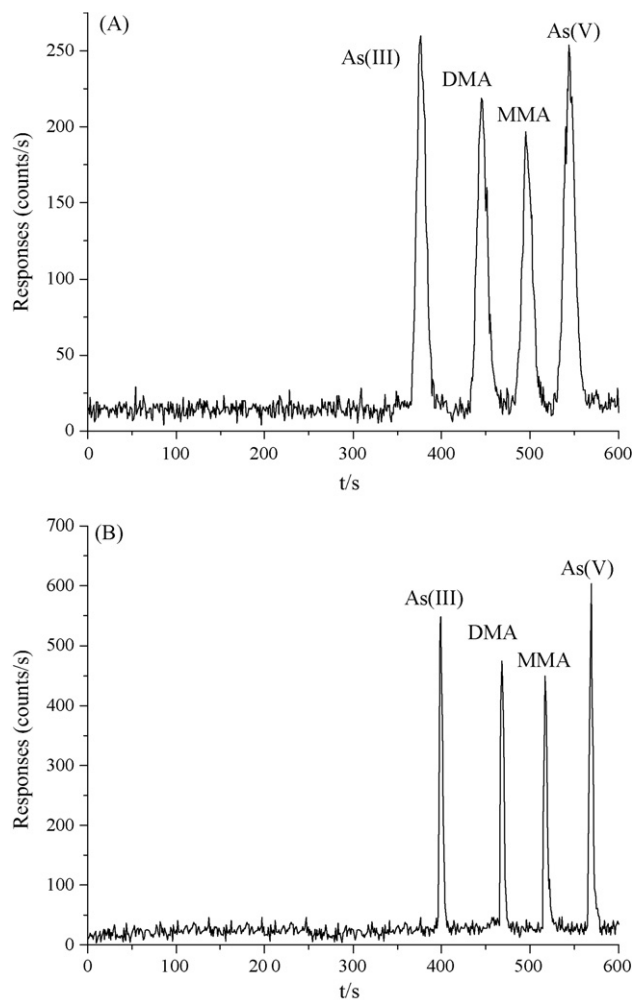


**Fig. 2.** The electrograms of As(III), DMA, MMA and As(V) under continuous sample-introduction mode (a) and collective sample-introduction mode (b). The data was obtained by determining a 25  $\mu$ g/L mixed standard solution of four arsenic species with CE-ICP-MS under conditions of Table 1.

smaller than 23–27 s and 0.10–0.19  $\mu$ g/L obtained with continuous sample-introduction mode and 14–28 s and 0.3–0.5  $\mu$ g/L reported previously for other sheath-flow interfaces [37]. The detection limits of 0.030–0.042  $\mu$ g/L are also smaller than 0.046–0.075  $\mu$ g/L obtained with our previous interface, although the peak widths of 10–12 s are slightly wider than 7–10 s [35]. Our results showed that the collective sample-introduction mode is suitable for the determination of samples in which contained much lower arsenic.

### 3.3. Determination of As(III), DMA, MMA and As(V) in dried *Mya arenaria* Linnaeus and Shrimp samples

The applicability of our method to real samples was demonstrated by the analysis of dried *Mya arenaria* Linnaeus and Shrimp samples purchased from the local market. About 0.5 g of sample was used for the speciation analysis of arsenic. Firstly, about 0.5 g of dried *Mya arenaria* Linnaeus or Shrimps was accurately weighed and was put into a 15 mL polyethylene centrifuge tube, and 5.0 mL of CH<sub>3</sub>OH–H<sub>2</sub>O solution (1:1, v/v) was added. Then, the tube was put into microwave digester (Sineo Microwave Chemical Technology Co., Ltd., Shanghai, China) and the microwave digester was programmed to heat the whole at 60 °C for 3 min. After the whole was cooled to room temperature, the extract solution was separated by filtering it through a 0.22  $\mu$ m membrane filter and was diluted to desired volume with milli-Q water (according to the arsenic con-

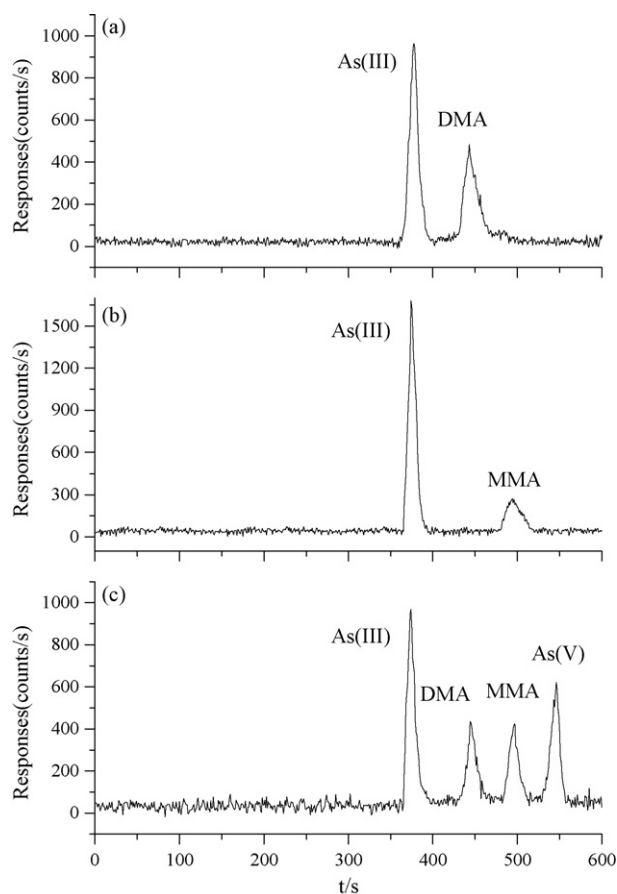


**Fig. 3.** The electropherograms of As(III), DMA, MMA and As(V) obtained with continuous sample-introduction mode and conditions of Table 1. (a) *Mya arenaria* Linnaeus; (b) *Shrimps*; (c) dried *Shrimps* spiked with 8 µg/g of As(III), DMA, MMA and As(V), the mass of dried *Shrimp* sample in (c) was a quarter of that in (b).

tent in the sample), and the final solution was used for CE-ICP-MS determination.

In this study, the concentrations of As(III), DMA, MMA and As(V) in dried *Mya arenaria* Linnaeus and *Shrimp* were determined with continuous sample-introduction mode. The analytical results were shown in Table 2, and their electropherograms were shown in Fig. 3.

It was well known, if all arsenics in samples were completely extracted and if each arsenic species keep no change during extraction process are two key points to the speciation analysis of arsenic. From results shown in Table 2, we found that the sum of the concentrations of each arsenic species is consistent well with the total concentrations of arsenic, indicated that all arsenic had been completely extracted using our method. The approximate 100% recovery for all As(III), DMA, MMA and As(V) (see Table 2) obviously indicated that each arsenic species kept no change during extracting and analytical process, since the recovery of at least one species of arsenic should excessively deviated 100% if any arsenic species was changed during extracting and analytical process. The detection limits of each arsenic species in sample can be calculated according to the detection limits of instrument and the preconcentration times of sample. In the case of dried *Mya arenaria* Linnaeus and *Shrimp*, 5 mL extract solution of 0.5 g sample can be directly analyzed by CE-ICP-MS, therefore the detection limits of each arsenic species in dried *Mya arenaria* Linnaeus and *Shrimp* were calculated to be 1.0, 1.8, 1.9 and 1.0 µg/L for As(III), DMA, MMA and As(V), respectively under continuous sample-introduction mode, and 0.30–0.42 µg/L under collective sample-introduction mode.

From the electropherograms shown in Fig. 3, it was clearly found that As(III) and DMA were detected in dried *Mya arenaria* Linnaeus,

**Table 2**  
Analytical results of each arsenic species in dried *Mya arenaria* Linnaeus and *Shrimp* purchased from local market.

Total concentration <sup>a</sup>	Dried <i>Mya arenaria</i> Linnaeus				Dried <i>Shrimp</i>			
	DL <sup>b</sup>	Added concentration <sup>c</sup>	Detected concentration <sup>c</sup>	Rec. (%)	DL <sup>b</sup>	Added concentration <sup>c</sup>	Detected concentration <sup>c</sup>	Rec. (%)
As(III)	1.0	0	4.4	4	1.0	0	6.1	103
		8.0	12.2	2		8.0	14.3	
DMA	1.8	0	2.6	4	1.8	0	<DL	105
		8.0	10.8	2		8.0	8.4	
MMA	1.9	0	<DL	3	1.9	0	1.1	96
		8.0	8.3			8.0	8.8	
As(V)	1.0	0	<DL	4	1.0	0	<DL	98
		8.0	7.8			8.0	7.8	
Total concentration <sup>a</sup>		6.9 ± 0.3			7.4 ± 0.2			
			RSD (%) <sup>d</sup>				RSD (%) <sup>d</sup>	

<sup>a</sup> The concentrations determined with ICP-MS after samples were completely decomposed with 7 mol/L HNO<sub>3</sub>, unit is µg As/g.

<sup>b</sup> The detection limits of each arsenic species in samples, unit is ng As/g.

<sup>c</sup> Unit is µg As/g.

<sup>d</sup> *n* = 6.

and As(III) and MMA were detected in dried *Shrimps*. So far, a lot of researches reported that organoarsenicals were the major species of arsenic in marine animals [37,38], only a few report detected inorganic arsenic in marine animals [39]. As shown in Table 2, *Mya arenaria* Linnaeus and *Shrimps* contained much more As(III) than organoarsenicals such as MMA and DMA. The As(III) concentrations were detected to be 4.4 and 6.1  $\mu\text{g/g}$  in dried *Mya arenaria* Linnaeus and *Shrimps*, respectively, much higher than that in other sea foods reported previously [40], the reasons for the higher As(III) in *Mya arenaria* Linnaeus and dried *Shrimps* should be further investigated.

#### 4. Conclusion

An improved sheath-flow interface used to couple CE with ICP-MS and a microwave-assisted extraction used to extract each arsenic species from seafood were developed in this study. The improved sheath-flow interface completely avoids the suction from ICP-MS, makes electric supply easier and more stable in CE, transports analyte solution to ICP-MS easily and more efficiently. CE-ICP-MS coupled with the interface provides two quantitative analysis modes: continuous sample-introduction mode and collective sample-introduction mode. The continuous sample-introduction mode works as normal sheath-flow interface reported previously and is suitable for the quantitative analysis of sample in which contained relative higher analytes. The collective sample-introduction technique greatly reduced the liquid dead volume of interface to approximately zero, obviously avoided the excessive dilution of analyte, and eventually led to a much lower detection limit and a much better electrophoretic resolution. The peak widths and detection limits of four arsenic species obtained with collective sample-introduction mode are 10–12 s (see Fig. 2) and 0.030–0.042  $\mu\text{g/L}$ , respectively, much smaller than 23–27 s and 0.10–0.19  $\mu\text{g/L}$  obtained with continuous sample-introduction mode, indicated that collective sample-introduction mode can be directly used to analyze the samples contained much lower analyte.

With the help of the improved sheath-flow interface and the microwave-assisted extraction, we have successfully determined As(III), DMA, MMA and As(V) in dried *Mya arenaria* Linnaeus and *Shrimp* with a R.S.D. ( $n=6$ ) of 2–3% (migration times) and 2–4% (peak areas) and a recovery of 96–105%. All the above features of the improved sheath-flow interface suggest a good potential to routinely use the interface in coupling CE with ICP-MS for real sample speciation analysis.

#### Acknowledgments

This work was supported by Fujian Provincial Department of Science and Technology (2005HZ1009, 2008Y0034) and National Nature Sciences Funding of China (NSFC, 20735002).

#### References

- [1] C.S. Jang, C.W. Liu, K.H. Lin, F.M. Huang, S.W. Wang, Environ. Sci. Technol. 40 (2006) 1707.
- [2] X.C. Le, X.F. Lu, M.S. Ma, W.R. Cullen, H.V. Aposhian, B.S. Zheng, Anal. Chem. 72 (2000) 5172.
- [3] A.R. Keimowitz, Y. Zheng, S.N. Chillrud, B. Mailloux, H.B. Jung, M. Stute, H.J. Simpson, Environ. Sci. Technol. 39 (2005) 8606.
- [4] A. Kot, J. Namiesnik, Trends Anal. Chem. 19 (2000) 69.
- [5] J.A. Caruso, B. Klaue, B. Michalke, D.M. Rocke, Ecotoxicol. Environ. Safe. 56 (2003) 32.
- [6] M. Bissen, F.H. Frimmel, Acta Hydrochim. Hydrobiol. 31 (2003) 9.
- [7] M. Leermakers, W. Baeyens, M.D. Gieter, B. Smedts, C. Meert, H.C.D. Bisschop, R. Morabito, P. Quevauviller, Trends Anal. Chem. 25 (2006) 1.
- [8] J.K. Yang, M.O. Barnett, J. Zhuang, S.E. Fendorf, P.M. Jardine, Environ. Sci. Technol. 39 (2005) 7102.
- [9] I. Pizarro, M. Gómez, C. Cámara, M.A. Palacios, Anal. Chim. Acta 495 (2003) 85.
- [10] P. Andrewes, D.M. DeMarini, K. Funasaka, K. Wallace, V.W.M. Lai, H. Sun, W.R. Cullen, K.T. Kitchin, Environ. Sci. Technol. 38 (2004) 4140.
- [11] X.-C. Le, X. Lu, X.-F. Li, Anal. Chem. 76 (2004) 27A.
- [12] U. Kohlmeier, E. Jantzen, J. Kuballa, S. Jakubik, Anal. Bioanal. Chem. 377 (2003) 6.
- [13] G.F. Pearson, G.M. Greenway, E.I. Brima, P.I. Haris, J. Anal. Atom. Spectrom. 22 (2007) 361.
- [14] P. Pinel-Raffaitin, I.L. Hecho, D. Amouroux, M. Potin-Gautier, Environ. Sci. Technol. 41 (2007) 4536.
- [15] E. Schmeisser, W. Goessler, N. Kienzl, K.A. Francesconi, Anal. Chem. 76 (2004) 418.
- [16] E. Sanz, R. Muñoz-Olivas, C. Cámara, J. Chromatogr. A 1097 (2005) 1.
- [17] J.J. Sloth, E.H. Larsen, K. Julshamn, J. Anal. Atom. Spectrom. 18 (2003) 452.
- [18] M. Monperrus, P.R. Gonzalez, D. Amouroux, J.I.G. Alonso, O.F.X. Donard, Anal. Bioanal. Chem. 390 (2008) 655.
- [19] H. Tao, C.R. Quétel, T. Nakazeto, M. Tominaga, A. Miyazaki, R.B. Rajendran, Anal. Chem. 71 (1999) 4208.
- [20] J. Mejía, M. Montes-Bayon, D.D.L. Le, N. Terry, J.A. Caruso, Anal. Chem. 74 (2002) 5837.
- [21] P. Kubáň, R. Guchardi, P.C. Hauser, Trends Anal. Chem. 24 (2005) 192.
- [22] P. Krystek, R. Ritsema, Anal. Bioanal. Chem. 381 (2005) 354.
- [23] J. Heilmann, K.G. Heumann, Anal. Chem. 80 (2008) 1952.
- [24] G. Alvarez-Llamas, F. Lacampa, A. Sanz-Medel, Trends Anal. Chem. 24 (2005) 28.
- [25] J. Li, T. Umemura, T. Odake, K.I. Tsunoda, Anal. Chem. 73 (2001) 5992.
- [26] S.S. Kannamkumarath, K. Wrobel, K. Wrobel, C. B'Hymer, J. Chromatogr. A 975 (2002) 245.
- [27] A.R. Timerbaev, Talanta 52 (2000) 573.
- [28] B. Michalke, Electrophoresis 26 (2005) 1584.
- [29] J.W. Olesik, J.A. Kinzer, S.V. Olesik, Anal. Chem. 67 (1995) 1.
- [30] D.D. Richardson, S.S. Kannamkumarath, R.G. Wuilloud, J.A. Caruso, Anal. Chem. 76 (2004) 7137.
- [31] Y. Liu, V. Lopez-Avila, J.J. Zhu, D.R. Wiedner, W.F. Beckert, Anal. Chem. 67 (1995) 2020.
- [32] Q. Lu, S.M. Bird, R.M. Barnes, Anal. Chem. 67 (1995) 2949.
- [33] A. Tangen, W. Lund, B. Josefsson, H. Borg, J. Chromatogr. A 826 (1998) 87.
- [34] D. Schaumlöffel, A. Prange, Fresenius J. Anal. Chem. 364 (1999) 452.
- [35] G.-D. Yang, X.-Q. Xu, W. Wang, L.J. Xu, G.-N. Chen, F.-F. Fu, Electrophoresis 29 (2008) 2862.
- [36] F. Simon, M. William, K. Frank, A. Simon, Talanta 71 (2007) 537.
- [37] C.F. Yeh, S.J. Jiang, Electrophoresis 26 (2005) 1615.
- [38] S.X.C. Le, W.R. Cullen, K.J. Reimer, Environ. Sci. Technol. 28 (1994) 1598.
- [39] J.J. Sloth, K.J. Julshamn, J. Agric. Food Chem. 56 (2008) 1269.
- [40] S.D. Rosemond, Q. Xie, K. Liber, Environ. Monit. Assess. (online available).



# Uranium enrichment measurements using the intensity ratios of self-fluorescence X-rays to 92<sup>\*</sup> keV gamma ray in UXK<sub>α</sub> spectral region

H. Yücel<sup>a,\*</sup>, H. Dikmen<sup>b</sup>

<sup>a</sup> Turkish Atomic Energy Authority (TAEA), Besevler Yerleskesi, TR-06100 Tandogan, Ankara, Turkey

<sup>b</sup> TAEA-Sarayköy Nuclear Research and Training Center (SNRTC), Atom Cad. No. 27, TR-06983 Sarayköy, Ankara, Turkey

## ARTICLE INFO

### Article history:

Received 3 June 2008

Received in revised form 6 November 2008

Accepted 20 November 2008

Available online 27 November 2008

### Keywords:

Uranium  
Enrichment measurements  
γ-Ray spectrometry  
X-ray fluorescence  
MGAU  
Nuclear safeguards

## ABSTRACT

In this paper, the known multigroup γ-ray analysis method for uranium (MGAU) as one of the non-destructive γ-ray spectrometry methods has been applied to certified reference nuclear materials (depleted, natural and enriched uranium) containing <sup>235</sup>U isotope in the range of 0.32–4.51% atom <sup>235</sup>U. Its analysis gives incorrect results for the low component <sup>235</sup>U in depleted and natural uranium samples where the build-up of the decay products begins to interfere with the analysis. The results reveal that the build-up of decay products seems to be significant and thus the algorithms for the presence of decay products should be improved to resulting in the correct enrichment value. For instance, for the case of <sup>235</sup>U analysis in depleted uranium or natural ore samples, self-induced X-rays such as 94.6 keV and 98.4 keV lying in UXK<sub>α</sub> spectral region used by MGAU can be excluded from the calculation. Because the significant increases have been observed in the intensities of uranium self-induced X-rays due to γ-ray emissions with above 100 keV energy arising from decay products of <sup>238</sup>U and <sup>235</sup>U and these parents. Instead, the use of calibration curve to be made between the intensity ratios of self-fluorescence X-rays to 92<sup>\*</sup> keV γ-ray and the certified <sup>235</sup>U abundances is suggested for the determination of <sup>235</sup>U when higher amounts of decay products are detected in the γ-ray spectrum acquired for the MGAU analysis.

© 2008 Elsevier B.V. All rights reserved.

## 1. Introduction

The determination of uranium enrichment in samples is a key measurement for product and process control in enrichment and fuel fabrication plants, technological process measurements, waste characterization, tracking of nuclear materials issued in illicit trafficking, and homeland security activities against terrorist threats and attacks, and it is also very important in internationally nuclear safeguards inspections to verify that uranium stock is being used for peaceful purposes. To carry out these inspections, the authorities are looking for rapid and more easy methods. These inspections must, of course, be, as far as possible, non-destructive, which favors γ-ray spectrometry over other methods like mass spectrometry. Moreover, it is desirable to get the accurate information in a short time of period without destroying the material in many nuclear applications [1]. Therefore, this aim requires a non-destructive detection and measurement technique such as γ-ray spectrometry. This technique also allows analysts or first responders in situ to measure, identify and find the location of the radiation sources and

radioactive materials. Among the different methods developed in the γ-ray spectrometry, the most widely employed and oldest one is that “uranium enrichment meter” principle which makes use of the 185.7 keV (57.7%) of <sup>235</sup>U full energy peak recorded either with NaI scintillation detector or with HPGe detectors [2–3]. This principle requires calibration of instrumentation with use of reference standard materials having at least two different enrichments by fixing the measurement conditions, and provided that the measured sample is identical to the standard materials [4]. Hence in routine field measurements the necessary calibrations are not always appropriate because of changes in geometry or container wall thickness. Therefore, the determination of relative abundances of uranium isotopes has recently been widely performed by γ-ray spectrometry utilizing either a set of uranium isotopic reference materials (SRMs) or a calibrated γ-ray detector using a set of radionuclide standards, or intrinsically calibrated Ge detector without use of any standards [5–8]. To overcome these difficulties and avoid the use of external standards, other methods based on self-calibration have been proposed [9]. More particularly X- and γ-ray spectrometry have been developed or are in progress for uranium enrichment measurements [10]. Especially, the introduction of MGAU method for non-destructive analysis of <sup>235</sup>U isotope characterization in depleted, natural or enriched uranium materials demonstrated the usefulness of intrinsically calibrated measurements for safeguards inspections. Additionally, MGAU method provides a very rapid

\* Corresponding author. Present address: Institute of Nuclear Sciences, Ankara University, Besevler Yerleskesi, TR-06100 Tandogan, Ankara, Turkey.  
Tel.: +90 312 212 85 77/160; fax: +90 312 215 33 07.

E-mail address: [haluk.yucel@taek.gov.tr](mailto:haluk.yucel@taek.gov.tr) (H. Yücel).



assay (30–60 min in routine basis) results for isotopic abundances when used a suitable planar/coaxial Ge or a CdZnTe semiconductor detector. Because it is more practical to determine from the same spectrum both isotopic ratios and abundances of U and/or Pu bearing samples by using a portable multichannel analyzer (MCA) system equipped with a special high resolution Low Energy Ge (e.g., Canberra LEGe) detector or Safeguards Coaxial Ge detector (e.g., Ortec SGD-GEM). Such systems can give the analysts more accurate results from the lower part of a  $\gamma$ -ray spectrum (below 300 keV) utilizing multigroup analysis methodology (MGA) for determining U or Pu isotopic abundances. MGAU method was first formulated and established in 1994 [11], and since that time, a number of MGAU commercial program versions were released (V.1.0, V.2.2, 3.0, V.4.0) or as a MGA++ code suite and it has found a wide application in numerous fields as mentioned above. It is reported that MGAU method can be used to determine uranium enrichments of depleted to several tens of percent  $^{235}\text{U}$  atoms in samples, with both accuracies and precisions of 1–2% [7]. After testing the performance of MGAU method in different measurement conditions and with reference uranium samples having different physical and chemical forms, isotopic conditions, the adequacy of MGAU method was confirmed, however, the tests revealed also a number of major and minor deficiencies described in detail [12]. At the same time, the applicability of MGA method for depleted and natural uranium isotopic analysis in presence of some actinides in the samples was investigated, and it has been pointed out the remarkable contributions from the actinides to the uranium analytical peaks, thus leading to erroneous results being 6–25 times higher than their declared abundances for uranium isotopic analysis [13].

Since self-induced fluorescence X-rays such as 94.6 keV  $\text{UK}\alpha_2$  and 98.4 keV  $\text{UK}\alpha_1$  are used in URADOS and MGAU methods for the determination of uranium enrichment values, it is required to take into account the treatment of a very limited and complex  $\text{UXK}\alpha$  region [7,9,11]. Therefore, the aim of the present study is to investigate the effect of changes in the intensity ratios of self-induced fluorescence X-rays lying in  $\text{UXK}\alpha$  spectral region on uranium enrichment results obtained by MGAU. As pointed out in Ref. [7], a relation can be established between the known certified  $^{235}\text{U}$  enrichment values and both the intensity ratios of 94.6 keV  $\text{UK}\alpha_2$  fluorescence X-ray to the 92\* keV  $\gamma$ -ray and of the 98.4 keV  $\text{UK}\alpha_1$  fluorescence X-ray to the 92\* keV  $\gamma$ -ray from decay product  $^{234}\text{Th}$  of  $^{238}\text{U}$  parent, where the symbol (\*) denotes almost a real doublet (92.38 + 92.80 keV) peak with an average energy of  $\sim 92.6$  keV. To do this, a spectrum de-convolution process of the superimposed peaks lying in the  $\text{UXK}\alpha$  region is treated delicately by non-linear least squares fitting method employing a Gaussian function for  $\gamma$ -ray peaks and a pseudo-Voigt function for X-ray peaks.

## 2. Experimental

### 2.1. Materials and equipment

In this study, five uranium reference materials SRM series 969 consisting of nominal abundances of 0.32%, 0.72%, 1.96%, 2.98% and 4.51% atom  $^{235}\text{U}$ , and additionally two certified natural uranium ore materials containing 7.09 wt% uranium (BL-5) and 75.42 wt% uranium (CUP-2) with nominal  $^{235}\text{U}$  abundances of 0.72% atom  $^{235}\text{U}$  were used, as given in Table 1. Each of the SRM 969 samples contained  $200.1 \pm 0.2$  g of  $\text{U}_3\text{O}_8$  powder (density:  $2.5 \text{ g cm}^{-3}$ ) encased in Al cylinder containers with internal dimensions of 70 mm diameter  $\times$  20.8 mm height. The powdered-natural ore materials of  $100 \pm 0.1$  g for BL-5 and  $25 \pm 0.1$  g for CUP-2 were filled in plastic bottles (40 mm diameter) with a 1.5 mm thickness. Then, they were sealed tightly to ensure radioactive equilibrium attain between  $^{238}\text{U}$  and its decay products.

A portable  $\gamma$ -ray spectrometry (Canberra U-Pu Inspector 2000), based on digital signal processing MCA analyzer with a LEGe detector (Canberra GL0515R) was used. The detector has a planar Ge crystal with a  $500 \text{ mm}^2$  active surface and a 15 mm thickness and its Al window is 0.5 mm in thickness. The detector has a measured resolution of 597 eV at 122 keV ( $^{57}\text{Co}$ ). It was calibrated to collect 4096 channel spectra with a gain of 0.07521 keV/channel, thus covering up to 308 keV energy. The data acquisition was carried out a commercially available gamma spectroscopy software (Canberra Genie 2000) and then analyzed with a MGAU software for uranium isotopic analysis. The measurements were performed with and without use of a 5 cm thick Pb shield against background radiations, especially for the reduction of  $\gamma$ -rays with low energies below 300 keV. In order to ensure good shapes of full energy peaks and to minimize peak count losses due to true coincidence summing effects, the measurements were performed at a distance of at least 10 cm between sample and detector window. The system dead time over all measurements were kept below 2.5% to avoid random coincidence corrections. The measurement periods were chosen as 10 min, 1 h, 14 h and 24 h to get better counting statistics of the  $\gamma$ -ray spectrum counts.

### 2.2. Multigroup $\gamma$ -ray analysis method

The multigroup  $\gamma$ -ray analysis method for uranium (MGAU) employs generally X- and  $\gamma$ -rays in the 80–130 keV region of a  $\gamma$ -ray spectrum taken from uranium without use of radionuclide standard sources or nuclear material standards. The descriptions of peak shapes, efficiencies, geometry, absorbing material effect and background subtraction considerations of the MGA methodology is described in detail [6,8]. In the principle of the MGA method, normalized “response functions” are constructed for each individual isotope based on available a priori information about energies and intensities of their X- and  $\gamma$ -rays. The method for the determination of the isotopic ratio is to measure basically the intensity of two or more peaks from  $\gamma$ -rays of similar energy (nearest energies) but arising from different isotopes. Since the  $\gamma$ -ray emission probabilities and half-lives of the isotopes are known, the isotopic ratios of two different atoms can be calculated if relative detection efficiencies for the peaks of interest can be estimated by the following relation:

$$\frac{N_1}{N_2} = \frac{I_1(E_1^i)\lambda_2 P_{\gamma_2}^j(E_2^j)\varepsilon_2(E_2^j)T_2(E_2^j)\Delta\Omega_2(E_2^j)}{I_2(E_2^j)\lambda_1 P_{\gamma_1}^i(E_1^i)\varepsilon_1(E_1^i)T_1(E_1^i)\Delta\Omega_1(E_1^i)} \quad (1)$$

where  $I_1$  and  $I_2$ : the measured peak intensity of isotope one and two (in cps),  $\lambda_1$  and  $\lambda_2$ : decay constant of isotope one and two ( $=0.693/\text{half-life}$ , in  $\text{s}^{-1}$ ),  $N_1$  and  $N_2$ : the number atoms of isotope one and two,  $P_{\gamma_1}$ : emission probability of  $\gamma$ -ray  $i$  from isotope one and  $P_{\gamma_2}$ : emission probability of  $\gamma$ -ray  $j$  from isotope two,  $\varepsilon_1$ : relative counting efficiency for  $\gamma$ -ray peak  $i$  with the energy  $E_1^i$  of isotope one,  $\varepsilon_2$ : relative counting efficiency for the  $\gamma$ -ray peak  $j$  with the energy  $E_2^j$  of isotope two,  $T_1$  and  $T_2$ :  $\gamma$ -rays  $i$  and  $j$  transmission factor to the detector,  $\Delta\Omega_1$  and  $\Delta\Omega_2$ : fractional solid angle of the detector  $[(1/4\pi)\Omega]$ , solid angle in steradians, in which the symbols represent the isotope one as subscript (1) and the isotope two as subscript (2), respectively. Since the counting geometry or the counting efficiency is not reproducible, and the  $\gamma$ -ray attenuation by sample matrix effect or other absorbing materials such as container materials is not known for various samples, the MGA method provides a great advantage as a *standardless* analysis over other laborious spectroscopic methods. Because it practically makes use of the efficiency ratios that remove the need for reproducible geometry. Thus this property makes this method applicable to the samples in any arbitrary size, shape and composition. In order to obtain the isotopic ratio from Eq. (1), the MGA software uses

**Table 1**  
Certified isotopic compositions of standard reference materials.

Reference sample code <sup>a,b,c</sup>	Uranium amount (wt%)	Isotopic composition			
		atom%		mass%	
		<sup>235</sup> U/U	<sup>238</sup> U/U	<sup>235</sup> U/U	<sup>238</sup> U/U
SRM969-031	84.5 ± 0.3	0.3206 ± 0.0002	99.6627 ± 0.0004	0.3166 ± 0.0002	99.6668 ± 0.0004
BL-5	7.09 ± 0.03	0.7209 ± 0.0006	99.2738 ± 0.0010	0.7119 ± 0.0006 <sup>d</sup>	99.2828 ± 0.0010 <sup>d</sup>
CUP-2	75.42 ± 0.17	0.7209 ± 0.0006	99.2738 ± 0.0010	0.7119 ± 0.0006 <sup>d</sup>	99.2828 ± 0.0010 <sup>d</sup>
SRM969-071	84.5 ± 0.3	0.7209 ± 0.0005	99.2738 ± 0.0002	0.7119 ± 0.0005	99.2828 ± 0.0002
SRM969-194	84.5 ± 0.3	1.9664 ± 0.0014	98.0159 ± 0.0009	1.9420 ± 0.0014	98.0406 ± 0.0009
SRM969-295	84.5 ± 0.3	2.9857 ± 0.0021	96.9826 ± 0.0015	2.9492 ± 0.0021	97.0196 ± 0.0015
SRM969-446	84.5 ± 0.3	4.5168 ± 0.0032	95.4398 ± 0.0016	4.4623 ± 0.0032	95.4950 ± 0.0016

<sup>a</sup> Canadian Certified Reference Materials (CRM) were obtained from CANMET-Mining and Mineral Sciences, Canada.

<sup>b</sup> Standard Reference Materials (SRM 969) were obtained from New Brunswick Laboratory, Argonne, USA. The abundances <sup>234</sup>U/U and <sup>236</sup>U/U in SRM 969 are not given in this table since they are out of the scope of this study.

<sup>c</sup> The uncertainties quoted here are at 95% confidence level.

<sup>d</sup> The percentage values in mass were calculated approximately by multiplying a factor from the isotope content in atom% × (235/238).

the local intragroup relative efficiencies that can be determined by delineating intergroup efficiency known as intrinsic efficiency curve, which is determined by fitting observed peak intensities (divided by  $\gamma$ -ray emission probability) to a function in the form:  $\varepsilon(E_k^m) \propto I(E_k^m)/P_{\gamma,k}^m(E_k^m)$ , where  $m$  corresponds to the  $\gamma$ -ray  $i$  or the  $\gamma$ -ray  $j$ , and  $k=1, 2$  corresponds to isotope one (<sup>235</sup>U) and isotope two (<sup>238</sup>U), if the isotope <sup>234</sup>U with very low content is ignored for the simplicity. The X- and  $\gamma$ -ray peaks are very close in energy, e.g., in the 80–100 keV and 100–120 keV energy regions. Additionally, when the energies are nearly equal, the efficiency and  $\gamma$ -ray transmission or attenuation differences are also small. Therefore, a special iterative procedure in MGA method to separate contributions of <sup>235</sup>U and <sup>238</sup>U to the spectrum region of interest. In general,

the MGA method is greatly simplified by considering the following observations: (a) if two  $\gamma$ -rays energies in the same spectrum are close, then  $[\varepsilon_2 T_2]/[\varepsilon_1 T_1] \cong 1$ , (b) the fractional solid angle of detector is the same for both  $\gamma$ -rays originated from the isotopes,  $\Delta\Omega_1 = \Delta\Omega_2$ . Then, if the measured peak intensities can be determined extremely accurately, the isotopic ratio expressed in Eq. (1) can be obtained more precisely [14]. However, it is worth noting that the calculation methods for U and Pu isotopic analysis used in commercially available MGA codes differ from each other in at least some ways, e.g. (i) the technique for delineating the “intrinsic” efficiency curve and (ii) the use of most intense peaks in a  $\gamma$ -ray spectrum depending on U or Pu analysis procedures. For example, while the MGA software for Pu isotopic analysis uses the  $\gamma$ - and X-rays below 210 keV, the MGAU software for U isotopic analysis

**Table 2**  
The results for <sup>235</sup>U and <sup>238</sup>U abundances in depleted, natural and enriched uranium samples obtained by MGAU method.

Reference sample code	Sample type	Counting time	Isotopic abundance <sup>a</sup>			
			Isotope <sup>235</sup> U		Isotope <sup>238</sup> U	
			MGAU measured ± unc. (%)	(%) [relative difference] <sup>b</sup>	MGAU measured ± unc. (%)	(%) [relative difference] <sup>b</sup>
SRM969-031	Depleted uranium	10 min	0.379 ± 0.153	18.22	99.618 ± 0.154	−0.04
		1 h	0.267 ± 0.069	−16.72	99.733 ± 0.070	0.07
		14 h	0.314 ± 0.018	−2.06	99.684 ± 0.018	0.02
		24 h	0.326 ± 0.014	1.68	99.672 ± 0.014	0.01
BL-5	Depleted uranium	10 min	0.942 ± 0.114	31.08	99.132 ± 0.133	−0.14
		1 h	0.921 ± 0.029	27.76	99.070 ± 0.030	−0.21
		14 h	0.912 ± 0.009	26.51	99.088 ± 0.095	−0.19
		24 h	0.911 ± 0.007	26.46	99.084 ± 0.072	−0.19
CUP-2	Natural uranium	10 min	0.770 ± 0.052	6.81	99.226 ± 0.052	−0.05
		1 h	0.751 ± 0.012	4.18	99.242 ± 0.013	−0.03
		14 h	0.752 ± 0.004	4.31	99.244 ± 0.004	−0.03
		24 h	0.762 ± 0.003	5.70	99.234 ± 0.003	−0.04
SRM969-071	Natural uranium	10 min	0.821 ± 0.124	13.89	99.179 ± 0.125	−0.10
		1 h	0.741 ± 0.051	2.79	99.252 ± 0.052	−0.02
		14 h	0.724 ± 0.015	0.43	99.272 ± 0.015	0.00
		24 h	0.707 ± 0.012	−1.93	99.289 ± 0.012	0.02
SRM969-194	Natural uranium	10 min	1.956 ± 0.116	−0.53	98.031 ± 0.118	0.02
		1 h	1.967 ± 0.048	0.03	98.021 ± 0.049	0.01
		14 h	1.954 ± 0.017	−0.63	98.032 ± 0.017	0.02
		24 h	1.961 ± 0.015	−0.27	98.026 ± 0.015	0.01
SRM969-295	Enriched uranium	10 min	2.779 ± 0.129	−6.92	97.195 ± 0.131	0.22
		1 h	2.950 ± 0.056	−1.20	97.031 ± 0.057	0.05
		14 h	2.980 ± 0.023	−0.19	96.999 ± 0.023	0.02
		24 h	2.983 ± 0.020	−0.09	96.996 ± 0.021	0.01
SRM969-446	Enriched uranium	10 min	4.473 ± 0.158	−0.97	95.506 ± 0.160	0.07
		1 h	4.431 ± 0.068	−1.90	95.540 ± 0.069	0.10
		14 h	4.468 ± 0.031	−1.08	95.507 ± 0.031	0.07
		24 h	4.507 ± 0.029	−0.22	95.466 ± 0.029	0.03

unc.: uncertainties are based on  $\pm 1\sigma$  confidence interval.

<sup>a</sup> The certified abundances for <sup>235</sup>U and <sup>238</sup>U are given in Table 1.

<sup>b</sup> The percentage relative bias (relative difference %) =  $100 \times (\text{measured}_{\text{MGAU}} - \text{certified})/\text{certified}$ .

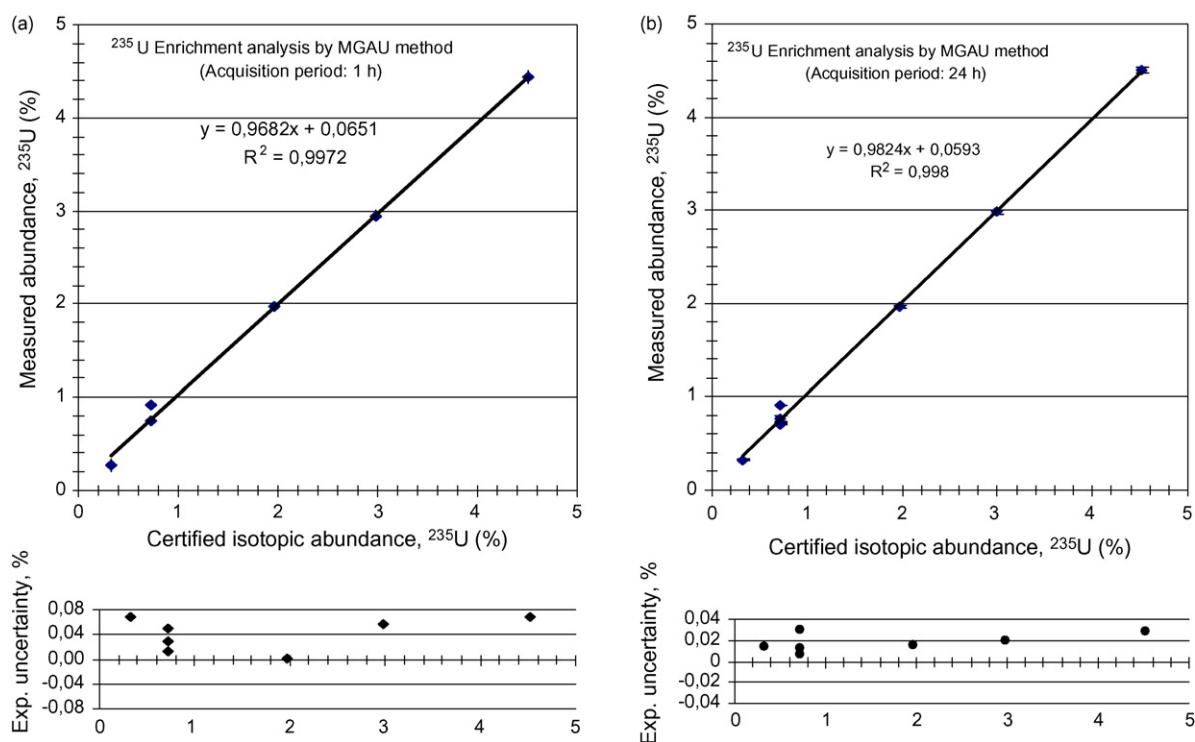


Fig. 1. Results for  $^{235}\text{U}$  abundance analysis by MGAU for certified uranium materials. (a) for 1 h counting period, (b) for 24 h counting period.

uses the energy region of 80–130 keV in the “intrinsic calibration” method.

### 3. Results and discussion

The results for  $^{238}\text{U}$  abundances in certified samples of depleted, natural and enriched uranium are given in Table 2, together with percentage relative biases from the certified values. The results for  $^{238}\text{U}$  abundance in the samples determined by MGAU are within uncertainty limits for a confidence interval of  $\pm 1\sigma$ . It has not been observed any remarkable difference between measured and certified isotopic abundance of  $^{238}\text{U}$ . That is, the measured abundances of  $^{238}\text{U}$  in all uranium samples are within 0.01–0.22% of those certified values and their precisions are also very high.

The results for  $^{235}\text{U}$  abundance obtained by MGAU are also given in Table 2. If the longer measurement period, say, more than 1 h up to 24 h employs for the data acquisition, it is evident that the measured abundances of  $^{235}\text{U}$  agree well only within 5% of the certified ones, except for depleted and natural uranium samples. When this measurement period compared to acceptable routinely safeguard verification analysis period of 30 min to 1 h employs, it is quite longer and the measured abundances of  $^{235}\text{U}$  in depleted and natural uranium are still inconsistent with those certified values. However, the experimental uncertainties in the determination of  $^{235}\text{U}$  are very low in which they are generally within the range of  $\pm(0.04\text{--}0.08\%)$  of the measured abundances in the certified materials ranging from 0.72% to 4.51% atom  $^{235}\text{U}$ , shown in Fig. 1(a) and (b) for the examples of 1 h and 24 h measurement periods, respectively. This indicates that the sufficient counting statistics for the uranium  $\gamma$ -ray spectra is accomplished for a measurement time being longer than 1 h.

On the other hand, the percentage relative biases between the measured and certified values of  $^{235}\text{U}$  isotope for enriched uranium materials remained below 2% of their certified values, thus MGAU method shows a good performance for enriched uranium materials

with higher measured precisions. In contrary, it is clearly seen in the examples in Fig. 2(a) and (b) that the percentage relative biases for the  $^{235}\text{U}$  contained in both depleted and natural uranium materials are higher than their certified isotopic abundances by 26.46% even if a relatively long measurement period, e.g., 24 h is chosen for testing.

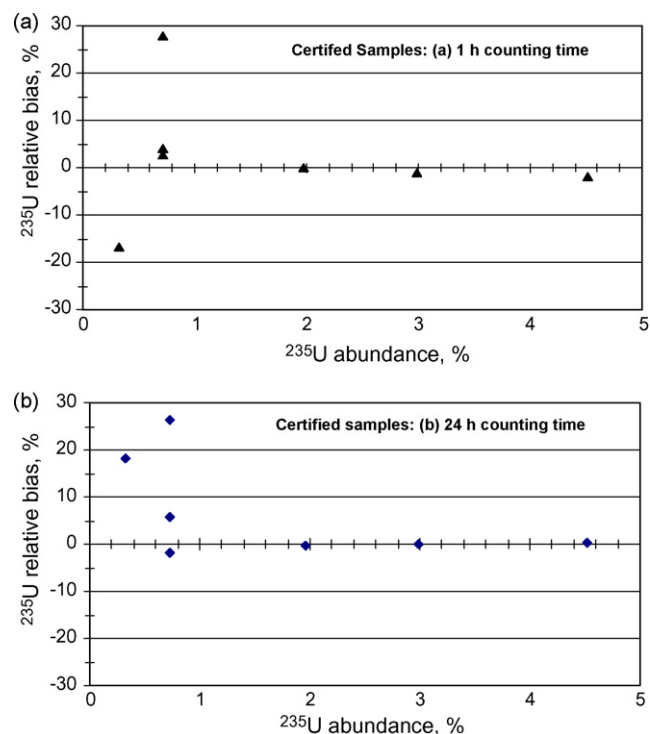


Fig. 2. Percentage relative biases on the determination of  $^{235}\text{U}$  in certified uranium materials containing from 0.32% to 4.51% atom  $^{235}\text{U}$ .

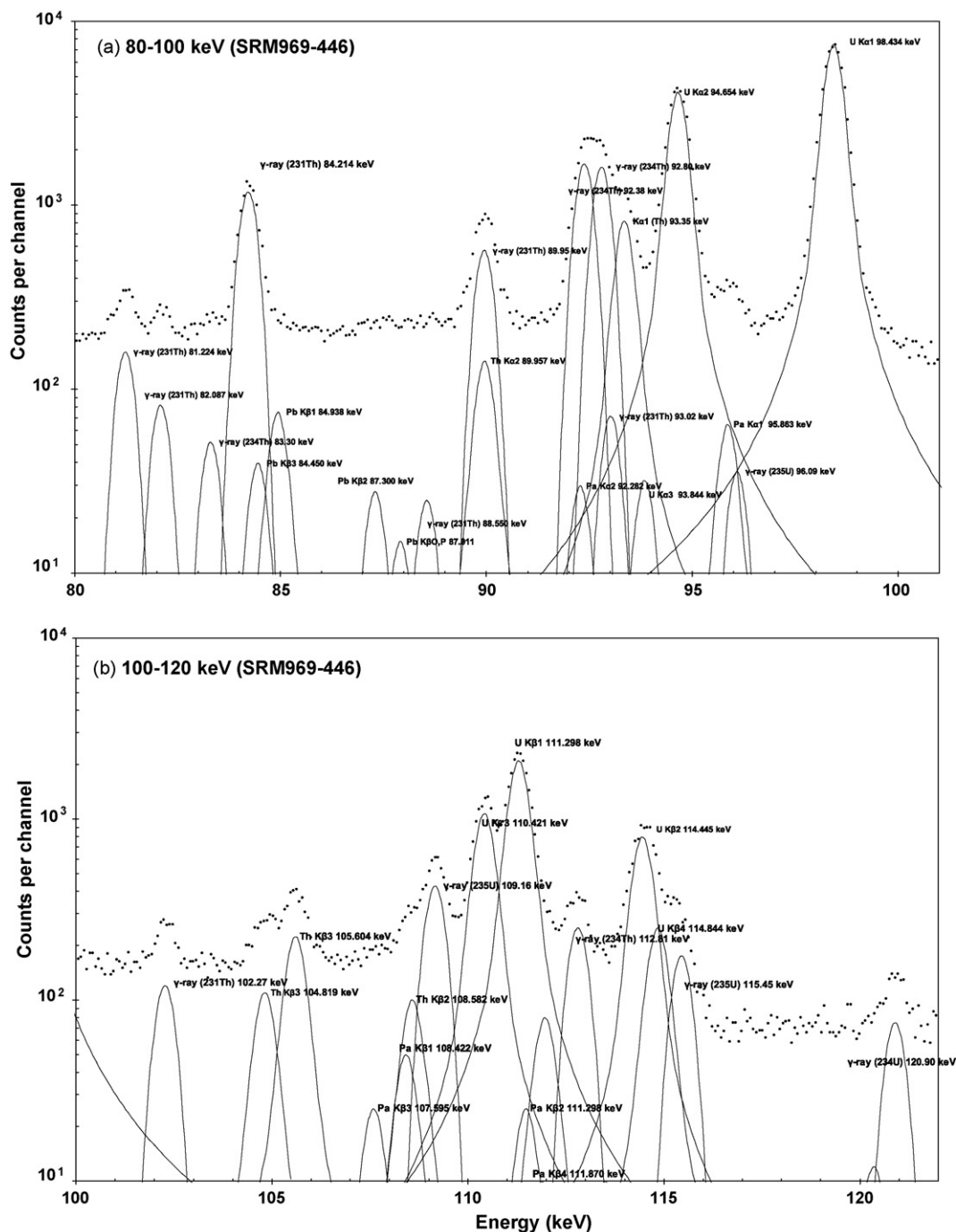


Fig. 3. (a and b) A typical fitting of the X- and  $\gamma$ -ray peaks in  $UXK_{\alpha}$  and  $UXK_{\beta}$  region of enriched uranium spectrum.

This limitation for depleted and natural uranium is mainly due to the low  $^{235}\text{U}$  component, in relation to those of  $^{238}\text{U}$  and uranium self-induced X-ray fluorescence, in the analyzed spectrum [15]. Particularly, the results obtained from depleted and natural uranium imply that the self-fluorescence X-ray peaks lying in spectral regions of  $UXK_{\alpha}$  and  $UXK_{\beta}$  of an uranium spectrum analyzed by MGAU can seriously be affected due to the contributions of emissions with the energy of above 100 keV from decay products of  $^{235}\text{U}$  and  $^{238}\text{U}$ . To demonstrate this, the increases in the intensities of self-induced X-rays such as 94.6 keV (28.3%) and 98.4 keV (45.8%) of uranium have been determined. For this, a non-linear least squares fitting procedure has been applied to fit the observed counts in the 80–100 keV  $UXK_{\alpha}$  region shown in Fig. 3(a) and those

in the 100–120 keV  $UXK_{\beta}$  region shown in Fig. 3(b) of the measured uranium  $\gamma$ -ray spectrum by adjusting the fit parameters.

As previously described in Ref. [13], the measured data were used to describe the peak line shapes in the de-convolution treatment of the X-rays and  $\gamma$ -ray peaks in the energy regions chosen in each spectrum, with a Gaussian function,  $G(E)$  for  $\gamma$ -ray peak and a pseudo-Voigt function for X-rays,  $V_p(E)$  consisting of an overall function, which is a weighted sum of Gaussian function,  $G(E)$  and Lorentzian function,  $L(E)$ . Then, a linear background  $B(E)$  function was added to both them as follows:

$$V_p = kG(E) + (1 - k)L(E) + B(E) \quad (2)$$

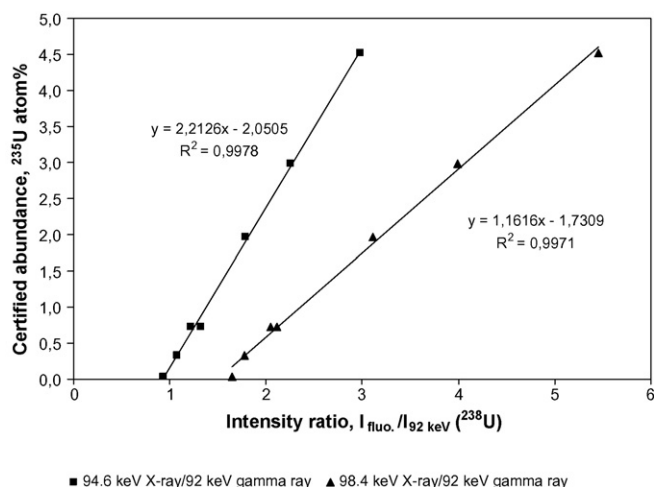


Fig. 4. Intensity ratios of the 94.6 keV X-ray to 92<sup>+</sup> keV  $\gamma$ -ray and the 98.4 keV X-ray to 92<sup>+</sup> keV  $\gamma$ -ray plotted versus certified <sup>235</sup>U abundance.

where  $k$  is a weighting factor, taken as 0.57 in a pseudo-Voigt function [16,17]. The same full-width at half maximum,  $\sigma = \text{FWHM}$  is chosen for both  $G(E)$  and  $L(E)$  functions:

$$G(E) = I_{\max} \left[ -\ln 2 \left( \frac{E - E_0}{\sigma/2} \right)^2 \right] \quad (3)$$

$$L(E) = \frac{I_{\max}}{1 + [(E - E_0)/(\sigma/2)]^2} \quad (4)$$

where  $I_{\max}$  is the height of the peak and  $E_0$  is the centroid energy of the peak. In the fitting procedure, while the Gaussian function  $G(E)$  fits the top of the peak, the Lorentzian function  $L(E)$  fits the tail of the peak described by a pseudo-Voigt function. No additional terms such as short and long tailing and/or a step-wise function for background were added to the fitting functions to characterize the line shapes of individual peaks. This choice of functions allowed to reduce the number of fit parameters as much as possible.

After the fitting process, the peak intensity of 92<sup>+</sup> keV  $\gamma$ -ray for <sup>238</sup>U from both the 92.4 keV and 92.8 keV  $\gamma$ -rays of <sup>234</sup>Th (<sup>238</sup>U) is determined more accurately by using a simple weighted average employing the four data sets [18–21], given in Table 3.

In order to obtain the mean intensity of the 92<sup>+</sup> keV  $\gamma$ -ray, the following equation was used:

$$I_{92^+ \text{ keV}}(i) = \frac{P_{\gamma 1} I_1 + P_{\gamma 2} I_2}{P_{\gamma 1} + P_{\gamma 2}} \quad (5)$$

where  $i = 1, 2, 3, 4$  denotes individual data set for different emission probabilities,  $I_1$  is the peak intensity for the 92.4 keV  $\gamma$ -ray and  $I_2$  is the peak intensity for the 92.8 keV  $\gamma$ -ray, obtained after fitting procedure.

The final intensity for the 92<sup>+</sup> keV  $\gamma$ -ray peak,  $I(^{238}\text{U})$  is calculated from arithmetic mean of these four weighted values,  $I_{92^+ \text{ keV}}(i)$  and they are given in Table 4 for each kind of uranium.

Subsequently, the intensity ratios of 94.6 keV self-fluorescence X-ray to 92<sup>+</sup> keV  $\gamma$ -ray, and of 98.4 keV self-fluorescence X-ray to 92<sup>+</sup> keV  $\gamma$ -ray are determined from the fitted net counts for each peak. The intensity ratios of 94.6 keV fluorescence X-ray to 92<sup>+</sup> keV  $\gamma$ -ray and of 98.4 keV fluorescence X-ray to 92<sup>+</sup> keV  $\gamma$ -ray are plotted to those <sup>235</sup>U certified abundances of the reference materials as shown in Fig. 4.

These plots show the good linear relations between the increasing intensity ratios of the uranium self-fluorescence X-rays versus the <sup>235</sup>U abundance in uranium materials with regression coefficients,  $R^2 \geq 0.99$ . This linear relation seen in Fig. 4 implies that if a calibration curve is made for these self-fluorescence X-rays using

Table 3  
Nuclear data sets for the 92<sup>+</sup> keV  $\gamma$ -rays and self-fluorescence X-rays lying in UXK<sub>α</sub> energy region of uranium spectrum.

Origin	Energy (keV)	Data set no. 1, Ref. [9]		Data set no. 2, Ref. [19]		Data set no. 3, Ref. [20]		Data set no. 4, Ref. [21]	
		Energy (keV)	$\gamma$ -Ray emission probability (%)	Energy (keV)	$\gamma$ -Ray emission probability <sup>a</sup> (%)	Energy (keV)	$\gamma$ -Ray emission probability (%)	Energy (keV)	$\gamma$ -Ray emission probability (%)
$\gamma$ -Ray ( <sup>238</sup> U/ <sup>234</sup> Th)	92.4	92.367	2.52 ± 0.06	92.359	2.621	92.38	2.81 ± 0.15	92.38	2.81 ± 0.24
$\gamma$ -Ray ( <sup>238</sup> U/ <sup>234</sup> Th)	92.8	92.793	2.50 ± 0.06	92.784	2.648	92.80	2.77 ± 0.15	92.80	2.77 ± 0.24
Self-fluo. X-ray K $\alpha_2$	94.6	94.654	61.2 ± 0.2 <sup>b</sup>	94.652	62.5 <sup>b</sup>	94.654	28.3 ± 0.6	94.654	28.2 ± 0.6
Self-fluo. X-ray U K $\alpha_1$	98.4	98.435	100 <sup>b</sup>	98.434	100 <sup>b</sup>	98.434	45.8 ± 0.9	98.434	45.1 ± 0.9

<sup>a</sup> No uncertainties quoted.

<sup>b</sup> Self-fluorescence % relative intensity.

**Table 4**  
The fitted peak intensities of uranium self-fluorescence X-rays and 92<sup>+</sup> keV  $\gamma$ -rays of <sup>234</sup>Th and their intensity ratios.

Reference sample code	Sample type	$\gamma$ -Ray intensity (cps)		Self-fluorescence X-ray intensity (cps)		Ratio of peak intensities <sup>a</sup>	
		92.4 keV $\gamma$ -ray <sup>234</sup> Th( <sup>238</sup> U) $I_1$	92.8 keV $\gamma$ -ray <sup>234</sup> Th( <sup>238</sup> U) $I_2$	94.6 keV UK $\alpha_2$ $I_{\text{flu}}$	98.4 keV UK $\alpha_1$ $I_{\text{flu}}$	94.6 keV/92 <sup>+</sup> keV $I_{\text{flu}}/I(^{238}\text{U})$	98.4 keV/92 <sup>+</sup> keV $I_{\text{flu}}/I(^{238}\text{U})$
SRM969-031	Depleted uranium	0.2957	0.2905	0.3172	0.5204	1.0798	1.7716
BL-5		0.6654	0.6866	0.8882	1.4216	1.3191	2.1113
CUP-2	Natural uranium	1.7111	1.6900	1.5860	2.7924	0.9312	1.6395
SRM969-071		0.2852	0.2852	0.3489	0.5839	1.2234	2.0473
SRM969-194		0.2588	0.2324	0.4441	0.7743	1.7842	3.1108
SRM969-295	Enriched uranium	0.2509	0.2350	0.5519	0.9773	2.2532	3.9899
SRM969-446		0.2482	0.2377	0.7296	1.3327	2.9869	5.4559

The symbol (\*) means that this energy is a doublet: (92.4 + 92.8 keV).

<sup>a</sup> The mean intensities calculated from the weighted intensities of  $I_1$  (92.4 keV) and  $I_2$  (92.8 keV) by using Eq. (5) for the  $\gamma$ -ray emission probabilities  $P_{\gamma 1}$  and  $P_{\gamma 2}$  taken from Data Sets No. 1–4 given in Table 3.

the intensity ratios of the 94.6 keV X-ray to 92<sup>+</sup> keV  $\gamma$ -ray and the 98.4 keV X-ray to 92<sup>+</sup> keV  $\gamma$ -ray plotted versus certified <sup>235</sup>U abundance, then the unknown enrichment value can easily be estimated. Such a calibration curve taken into account the fluorescence X-rays can be useful to determine the <sup>235</sup>U abundance especially when the samples have higher amounts of decay products for case of natural uranium ore materials. It is clearly seen in Fig. 4 that the intensities of uranium self-induced X-rays for both the 94.6 keV and 98.4 keV have been increased substantially due to the contributions from X- and  $\gamma$ -rays with energy above 100 keV arising from the decay products of <sup>235</sup>U and <sup>238</sup>U, and themselves. However, the increases in the intensity ratios of the uranium fluorescence X-rays to 92<sup>+</sup> keV  $\gamma$ -ray are higher than those expected in natural uranium ore samples such as BL-5 and CUP-2. This is the reason that they have higher amounts of the decay products in the ore materials than those of the processed uranium such as U<sub>3</sub>O<sub>8</sub>. Hence the MGAU analysis program gives incorrect results for <sup>235</sup>U abundance in uranium ore samples such as BL-5 and CUP-2 as is seen in Table 2, where the build-up of the decay products begins to interfere with the analysis. On the other hand, it might be expected the variations in the self-fluorescence X-ray peak intensities which may also depend on sample matrix and matrix form (liquid, powder), density, size, chemical composition of sample and its container, etc. But these probable effects of the material characteristics on the self-induced X-rays have not been investigated in this study due to out of the scope and lack of varieties of uranium samples in a different forms.

#### 4. Conclusion

In case of <sup>235</sup>U isotopic analysis in depleted or natural uranium samples, the build-up of decay products seems to be significant and the algorithms for analysis such as MGAU and URADOS for the presence of decay products should be improved to resulting in a correct enrichment value. For instance, self-induced X-rays such as 94.6 keV and 98.4 keV lying in UXK $\alpha$  spectral region used by MGAU program can be excluded either from the calculation procedure or from the increases in the peak areas of self-fluorescence X-rays can be compared with the results for <sup>235</sup>U enrichment determination by means of a known calibration curve of using self-fluorescence X-rays. When depleted or natural uranium samples are measured, the significant increases have been observed in the intensities of uranium self-induced X-rays due to  $\gamma$ -ray emissions with above 100 keV energy arising from decay products of <sup>238</sup>U and <sup>235</sup>U and themselves, thus resulting in erroneous abundances for <sup>235</sup>U. In case higher amounts of decay products are detected in the  $\gamma$ -ray spectrum acquired for the MGAU analysis, it is suggested that a calibration curve be made between the intensity ratios of self-fluorescence X-rays to 92<sup>+</sup> keV  $\gamma$ -ray and certified <sup>235</sup>U abundances for the determination of <sup>235</sup>U enrichment.

#### Acknowledgements

The measurements were performed at TAEA-SNRTC in 2006. Authors are thankful to Mr. E. Yeltepe and Mr. M. Vural who are the staff at SNRTC for their valuable assistance.

#### References

- [1] S. Anilkumar, A.K. Deepa, K. Narayani, A.K. Rekha, P.V. Achuthan, G. Krishnamachari, D.N. Sharma, J. Radioanal. Nucl. Chem. 274 (1) (2007) 161.
- [2] T.D. Reilly, E.R. Martin, J.L. Parker, L.G. Speir, R.B. Walton, Nucl. Technol. 23 (1974) 318.
- [3] P. Mattussek, Accurate determination of the <sup>235</sup>U isotope abundance by gamma spectrometry. A user's manual for the Certified Reference Material EC-NRM-171/NBS-SRM-969, Institut für Kernphysik, Report KfK 3752, Kernforschungszentrum Karlsruhe GmbH, Karlsruhe, Germany, 1985.
- [4] P. Mortreau, R. Berndt, Nucl. Instrum. Methods A 530 (2004) 559.
- [5] T. Dragnev, Appl. Radiat. Isot. 44 (3) (1993) 613.

- [6] R. Gunnink, MGA: a gamma-ray spectrum analysis for determining plutonium isotopic abundances, Lawrence Livermore National Laboratory Report Vol. 1, UCRL-LR-103220, Livermore, California, 1990.
- [7] S. Abousahl, M. Michiels, M. Bickel, R. Gunnink, J. Verplancke, Nucl. Instrum. Methods A 368 (1996) 443.
- [8] D. Clark, U235: a gamma-ray spectrum analysis code for uranium isotopic determination, Lawrence Livermore National Laboratory Report, UCRL-ID-125727, 1996.
- [9] J. Morel, M. Etcheverry, G. Riazuelo, Appl. Radiat. Isot. 49 (9–11) (1998) 1251.
- [10] J. Morel, C. Hill, M. Bickel, A. Alonso-Munoz, S. Napier, B. Thauereil, Appl. Radiat. Isot. 52 (2000) 509.
- [11] R. Gunnink, W.D. Ruhter, P. Miller, J. Goerten, M. Swinhoe, H. Wagner, J. Verplancke, M. Bickel, S. Abousahl, M. IAEA Symposium on International Safeguards, Vienna, Austria, March 8–14, 1994, Lawrence Livermore National Laboratory Report UCRL-JC-114713, Livermore, California, 1994.
- [12] A.N. Berlizov, R. Gunnink, J. Zsigrai, C.T. Nguyen, V.V. Tryshyn, Nucl. Instrum. Methods A 575 (2007) 498.
- [13] H. Yücel, Appl. Radiat. Isot. 65 (2007) 1269.
- [14] W.E. Parker, T.F. Wang, D. Clark, N.M. Buckley, W. Romine, W.D. Ruhter, 6th International Meeting on Facilities Operations-Safeguards Interface, Jackson Hole, WY, September 20–24, 1999, Lawrence Livermore National Laboratory Report UCRL-JC-L 133130, 1999.
- [15] K. Abbas, J. Morel, M. Etcheverry, G. Nicolaou, Nucl. Instrum. Methods A 405 (1998) 153.
- [16] C. Fournier, C. Merlet, O. Dugne, M. Fialin, J. Anal. Atom. Spectrom. 14 (1999) 381.
- [17] T. Ida, M. Ando, F. Toray, J. Appl. Crystallogr. 33 (2000) 1311.
- [18] R.R. Kinsey, The NuDat program for nuclear data on the web page: <http://www.nndc.bnl.gov/nndc/nudat>, Ver.2.5, NNDC, BNL, New York, 1996.
- [19] J. Morel, L. De, Clark, Appl. Radiat. Isot. 56 (2002) 85.
- [20] S.Y.F. Chu, L.P. Ekström, R.B. Firestone, The Lund/LBNL nuclear data search Ver.2.0, February 1999: www table of radioactive isotopes, <http://nucleardata.nuclear.lu.se/nucleardata/toi/>.
- [21] R.B. Firestone, V.S. Shirley (Eds.), Table of Isotopes, CD ROM edition, Ver.1.0, 1996.



# Determination of butyl- and phenyltin compounds in human urine by HS-SPME after derivatization with tetraethylborate and subsequent determination by capillary GC with microwave-induced plasma atomic emission and mass spectrometric detection

G.A. Zachariadis<sup>a,b,\*</sup>, E. Rosenberg<sup>b</sup>

<sup>a</sup> Laboratory of Analytical Chemistry, Dept. of Chemistry, Aristotle University, University Campus, 54124 Thessaloniki, Greece

<sup>b</sup> Institute of Chemical Technologies and Analytics, Vienna University of Technology, Getreidemarkt 9/164 AC, 1060 Vienna, Austria

## ARTICLE INFO

### Article history:

Received 15 October 2008

Received in revised form

25 November 2008

Accepted 2 December 2008

Available online 11 December 2008

### Keywords:

Organotin compounds

Headspace solid-phase micro-extraction

Urine

Gas chromatography

Microwave-induced plasma atomic

emission detector

Mass spectrometry

## ABSTRACT

A headspace solid-phase micro-extraction (HS-SPME) method was developed and optimized for gas chromatographic separation and determination of commonly found organotin compounds in human urine after potential exposure. Butyl- and phenyltin compounds were in situ derivatized to ethylated derivatives by sodium tetraethylborate (NaBEt<sub>4</sub>) directly in the urine matrix. The relevant parameters affecting the yield of the SPME procedure were examined using tetrabutyltin as internal standard. The method was optimized for direct use in the analysis of undiluted human urine samples and mono-, di- and tri-substituted butyl- and phenyltin compounds could be determined after a 15-min headspace extraction time at room temperature. The selectivity of the microwave-induced plasma atomic emission detector (MIP-AED) as an element specific detector in combination with the relatively selective sample preparation technique of HS-SPME allowed the interference-free detection of the organotin compounds in all cases. A quadrupole mass spectrometer was used in parallel experiments as a detector for the confirmation of the identity molecular structure of the eluted compounds. The performance characteristics of the developed method are given for the determination of mixtures of these compounds. Finally the proposed method was applied to the analysis of several human urine samples.

© 2008 Elsevier B.V. All rights reserved.

## 1. Introduction

Tin compounds have been used – and still are in use – in large quantities as stabilizers for polymers and also as agricultural biocides [1,2]. Organotin compounds like tributyltin, have been extensively used as antifouling coatings for marine vessels, and are still detected in aquatic environments, although their use has been banned by many international regulations and directives [3]. Biological and physico-chemical processes are usually responsible for various transformations of tin compounds, when they are released into the aquatic ecosystems. Biodegradation like that of tributyltin to mono- and dibutyl-derivatives [4], or biomethylation of inorganic tin due to the action of anaerobic bacteria in sediments and soils are mechanisms observed to occur in the environment [5]. Finally, there is evidence for the metabolization of organotin and other organometallic compounds in the human body, and the produced metabolites are usually excreted in the urine [2], making this

an attractive sample to monitor the contamination and exposure of the individuals [6,7].

Most organotin compounds exhibit a wide range of toxic effects for humans and living organisms, and the level of toxicity is strongly depending on the different structure of each compound. Consequently, environmental pollution and occupational exposure to these compounds has become a serious problem, and the development of analytical methods suitable for the speciation of such compounds in biological samples, and especially in human body fluids, is very important.

There are several reports in the literature concerning organotin analyses in environmental samples [8,9] and biological samples but those referring to the analysis of organotin compounds in body fluids and particularly urine are rather scarce, as it is revealed in a review by Pereiro and Diaz [10].

The majority of the OT speciation methods refer to the employment of GC-MS technique [11,12], but there are also other very convenient types of detectors to be used [13,14]. Among the large number of hyphenated techniques based on liquid or gas chromatographic separation for the determination of organotin compounds, capillary gas chromatographic techniques offer better resolution of the separated peaks and highly sensitive and selective detectors.

\* Corresponding author at: Laboratory of Analytical Chemistry, Dept. of Chemistry, Aristotle University, University Campus, 54124 Thessaloniki, Greece.

E-mail address: [zacharia@chem.auth.gr](mailto:zacharia@chem.auth.gr) (G.A. Zachariadis).



Consequently, GC separation coupled with various detectors, like GC–MS [12,13], GC–FPD [2], and GC–MIP–AED [4,14–16] and more recently, GC–ICP–MS [17–19] is frequently applied for organotin analysis in environmental and biological samples.

Gas chromatographic analysis of organotin compounds in biological or environmental samples typically requires a sample preparation procedure that includes at least the two steps extraction and derivatization. The former step is required to transfer the analytes from aqueous to organic phase, to preconcentrate them in a GC-compatible organic medium like hexane, or iso-octane [15,20] and to remove possible matrix interferences. Alternatively to solvent extraction, the SPME (solid-phase micro-extraction) technique can be employed which makes use of a polymeric fibre for the solventless extraction of the analytes either directly from the aqueous solution or from the headspace over the solution. Characteristics of both extraction modes and an overview of relevant applications in speciation analysis can be found in reviews like that by Mester et al. [21] and Dietz et al. [22].

The extraction of analytes from urine samples to an organic phase is a significant problem because of the formation of gels or foams which prevents the easy separation of the two phases [6]. As the analysis of organotin compounds in human urine samples is relevant for monitoring occupational exposure, and since only few reports have addressed this problem [23–25], we have developed in this work a method for in situ derivatization and extraction of the most commonly found organotin compounds, based on in situ ethylation by sodium tetraethylborate and simultaneous headspace solid-phase micro-extraction which avoids the difficulties of liquid–liquid phase separation, and on the other hand offers the advantages of requiring only small sample amounts, minimizing interferences due to headspace sampling, and completely avoiding the use of organic solvents. For the conversion of the ionic organotin compounds into volatile compounds that can be extracted into a hydrophobic phase such as the SPME fibre coating there are various derivatization chemistries – typically alkylations – and reagents available [10,15].

The derivatization of ionic organotin compounds can be performed either using a Grignard reagent for alkylation in an aprotic solvent environment or more conveniently using tetralkylborate reagents for alkylation directly in the aqueous sample. Since it is not known if or how the presence of various urine constituents like urea, creatinine, proteins, metabolites, or salts could potentially affect the alkylation yield, this was tested as part of the optimization of experimental parameters.

Therefore, in order to develop a convenient method for urine analysis while minimizing sample preparation, we report here the optimization and use of headspace SPME after in situ derivatization with NaBEt<sub>4</sub> for the simultaneous determination of butyl-

and phenyltin species by gas chromatography coupled with atomic emission detection. The proposed speciation method includes six organotin species, namely monobutyltin (MBT, BuSn<sup>3+</sup>), dibutyltin (DBT, Bu<sub>2</sub>Sn<sup>2+</sup>), tributyltin (TBT, Bu<sub>3</sub>Sn<sup>+</sup>), tetrabutyltin (TeBT, Bu<sub>4</sub>Sn), monophenyltin (MPHT, PhSn<sup>3+</sup>) and diphenyltin (DPHT, Ph<sub>2</sub>Sn<sup>2+</sup>). TeBT was included in the speciation scheme although ethylation is not required for this compound. Attempts to include triphenyltin species in this speciation scheme were not successful, most likely due to its very low volatility. The overall efficiency of the NaBEt<sub>4</sub> ethylation and the HS–SPME procedure was estimated for the analysis of undiluted urine matrices. The GC–AED technique was applied as quantitative method, because it offers significant specificity and excellent sensitivity for tin measurements, while the GC–MS technique was employed in some parallel measurements, in order to confirm the structure of the derivatized compounds.

## 2. Experimental

### 2.1. Instrumentation

A HP 5890 II gas chromatograph equipped with a split/splitless injection port and interfaced with a HP 5921A microwave-induced plasma atomic emission detector (Hewlett Packard, now Agilent Technologies, Palo Alto, CA, USA) was employed for the GC–MIP–AED measurements. A HP 5989A Mass Spectrometer with a quadrupole mass filter was used in the scan mode for the GC–MS measurements. Electron impact mass spectra were acquired applying 70 eV ionisation potential. The injection, separation, atomization and detection parameters of GC–MIP–AED and those of the GC–MS systems are given in Table 1. For the injection of hexane standards, a HP 7673 autosampler was used, which is controlled by the GC software (Chemstation software of different versions, Hewlett Packard, now Agilent Technologies, Palo Alto, CA, USA).

The SPME procedure was carried out manually using the appropriate SPME device (Supelco, Bellefonte, PA, USA) with a fused silica fibre with a film of polydimethylsiloxane (PDMS) with 100 μm thickness. The fibres could be used up to 120 extractions without any loss in reproducibility.

### 2.2. Reagents and solutions

All solvents and reagents used were of analytical-reagent grade and deionised water prepared with a Milli-Q apparatus (Millipore, Molsheim, France) was used for the preparation of all aqueous solutions. For buffer preparation (pH 4–6), sodium acetate trihydrate (NaAc) and acetic acid (HAc, 100%) were purchased from Merck (Darmstadt, Germany) and methanol (MeOH) and hexane from Riedel-de Haen (Seelze, Germany).

**Table 1**

Instrumental parameters applied for the GC–MIP–AED and GC–MS systems for organotin speciation in urine.

Gas chromatography		Detectors	
<i>HP 5890 Series II Gas Chromatograph</i>		<i>HP 5921A Atomic Emission Detector</i>	
Injection port liner	4 mm id., silanised	Transfer line temperature	250 °C (optimized)
Injection technique	Splitless	Detection wavelength	303.419 nm
Purge delay time	3 min	Hydrogen pressure	480 kPa (optimized)
Inlet temperature	250 °C	Oxygen pressure	180 kPa (optimized)
Capillary column (AED)	HP-1	Cavity pressure	12 kPa
100% polydimethylsiloxane (PDMS)		He-total flow	150 mL min <sup>-1</sup> (opt.)
Length/i.d./film	25 m × 0.32 mm × 0.17 μm	Spectrometer purge (N <sub>2</sub> )	2.0 L min <sup>-1</sup>
Capillary column (MS)	DB-5	Cavity temperature	250 °C
95%PDMS/5% polydiphenylsiloxane		<i>HP 5989A Mass spectrometric Detector</i>	
Length/i.d./film	30 m × 0.25 mm × 0.10 μm	Mass filter	Quadrupole
Column head pressure	15 kPa at 50 °C	Ion source, voltage	EI, 70 eV
Column helium flowrate	4.20 mL min <sup>-1</sup> , 50 °C	MS Quadrupole temp.	100 °C
Carrier gas: helium	Purity 99.9996%	MS Source temperature	200 °C
Oven program: 50 °C (3 min), rate 30 °C min <sup>-1</sup> to 250 °C		Scan range (m/z)	50–500

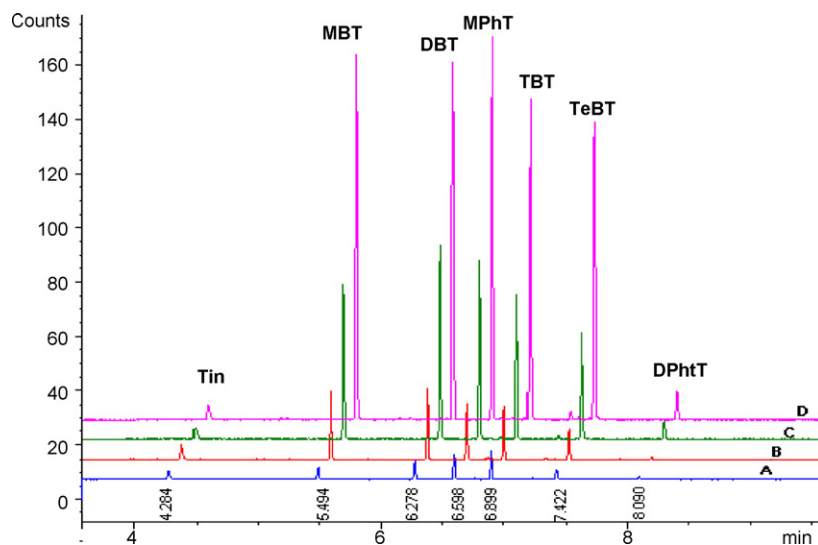


**Fig. 1.** GC-MIP-AED chromatogram of a mixture of butyl- and phenyltin compounds spiked to a blank urine matrix in increasing concentrations, obtained by HS-SPME GC-AED. Approximate concentration level of standards: (A)  $0.100 \mu\text{g L}^{-1}$ ; (B)  $0.400 \mu\text{g L}^{-1}$ ; (C)  $2.00 \mu\text{g L}^{-1}$ ; (D)  $8.00 \mu\text{g L}^{-1}$ .

For the preparation of stock and working standards, the following substances were used: monobutyltin trichloride (MBT,  $\text{BuSnCl}_3$ ), dibutyltin dichloride (DBT,  $\text{Bu}_2\text{SnCl}_2$ ), tributyltin chloride (TBT,  $\text{Bu}_3\text{SnCl}$ ), monophenyltin trichloride (MPhT,  $\text{PhSnCl}_3$ ), diphenyltin dichloride (DPhtT,  $\text{Ph}_2\text{SnCl}_2$ ) (>98% (w/w), obtained in the frame of an earlier intercalibration exercise from the Institute for Environmental Studies, Free University Amsterdam, The Netherlands). Tetrabutyltin (TeBT,  $\text{Bu}_4\text{Sn}$ , >98% (w/w), Fluka, Switzerland) was used as internal standard. For the optimization of the MIP-AED performance, a separate solution of tetrabutyltin was prepared in hexane.

All the compounds and the primary stock solutions of the individual compounds in methanol were stored in the dark at  $-20^\circ\text{C}$ , while the secondary dilutions containing tin concentrations of 10 and  $1 \text{ mg L}^{-1}$  were prepared in methanol and stored in the refrigerator at  $2-4^\circ\text{C}$ . All individual primary stock solutions were prepared monthly, while the secondary dilutions of individual compounds were prepared every week. The final diluted working standards were freshly prepared just before use. The butyl- and phenyltin chlorides were not combined in one solution, in order to avoid any rearrangement reactions.

Sodium tetraethylborate ( $\text{NaBEt}_4$ , purity >98% (w/w), Fluka, Switzerland) and tetrahydrofuran (THF, HPLC grade without stabilizer, Aldrich, Germany) were used for the ethylation reagent: sodium tetraethylborate is commercially available in septum cap bottles of 1 g thus a 20% (w/v) solution was prepared by dissolving the entire contents of a 1 g bottle of the reagent in 5 mL of THF directly. From this solution a 1:2 working dilution (i.e. 10% (w/v)) in THF was made in order to be used. When stored air-tight in septum cap vials in  $4^\circ\text{C}$  the reagent solution is stable for several weeks.

### 2.3. Headspace SPME procedure

25 mL of urine sample or aqueous buffer solution were transferred into 40 mL vials with Mininert valves (Supelco, Bellefonte, PA, USA) and spiked with the appropriate amounts of individual or mixed standards. A volume of  $50 \mu\text{L}$  of the ethylation reagent was also added, and the mixture was stirred magnetically at 900 rpm for 15 min. To examine the effect of the extraction temperature the vial was thermostatted in a water bath. After extraction of the analytes by exposing the SPME fibre to the headspace of the solution, the fibre was immediately transferred to the GC injection port for desorption of the analytes. All steps should be followed precisely, as the

overall reproducibility of the SPME procedure is critically depending on equilibration conditions and time [21]. Thorough cleaning of all glassware used and the Teflon-coated stir-bar is critical, because of their capability to retain traces of the ethylated organotin compounds. This is also possible for the Teflon material of the Mininert valves, which bear the possibility of retaining traces of volatiles in some parts of the housing.

## 3. Results and discussion

### 3.1. Gas chromatographic separation

$1 \mu\text{L}$  of a hexane solution of TeBT and of the alkylated organotin compounds, respectively, was automatically injected in order to optimize the chromatographic separation and the signal intensity, for various gas chromatographic conditions. The following oven program was finally adopted:  $50^\circ\text{C}$  initial temperature (hold 3 min), ramp with  $30^\circ\text{C min}^{-1}$  to  $250^\circ\text{C}$ , which allowed a measurement to be completed in 10 min.

### 3.2. GC-MIP-AED detection

With the above GC conditions, peaks are obtained at 5.494, 6.278, 6.598, 6.899, 7.422 and 8.090 min for the ethylated MBT, DBT, MPhT, TBT, TeBT and DPhtT compounds, respectively. A typical chromatogram of a mixture of the examined organotins is presented in Fig. 1. The peaks of six compounds are well resolved without tailing and can easily be assigned. The signal of DPhtT is the lowest both using AED and MS detectors which we attributed to the lower rate of derivatization and extraction of this species. Reasoning a similar way, the detection of triphenyltin species could not be achieved under these conditions with acceptable sensitivity due to its lower efficiency of extraction from the headspace. It has to be mentioned that the peak at 4.284 min is produced from inorganic tin species after tetraethylation, however this reaction is not quantitative.

### 3.3. GC-MS detection

Using the same oven program and gas chromatographic instrumentation as for the GC-AED measurements, however with a chromatographic column with 95% polydimethylsiloxane/5% polydiphenylsiloxane as stationary phase with slightly different column dimensions (see Table 1), all peaks of the derivatized organotin

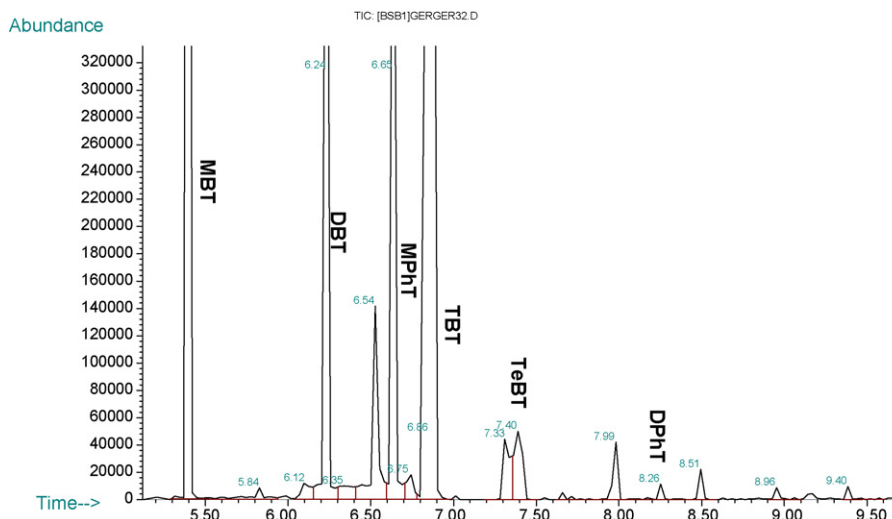


**Fig. 2.** GC-MS chromatogram of a mixture of butyl- and phenyltin compounds using HS-SPME, obtained from spiked urine sample with organotin compounds (tin concentration  $10 \mu\text{g L}^{-1}$ ).

compounds could be detected and identified in spiked urine samples in scan mode. A typical GC/MS chromatogram for the detection of organotin compounds in a spiked urine sample is given in Fig. 2. The lower selectivity of this detector in comparison with the AED becomes evident.

The matching of the retention times of the organotin compounds between the GC-AED- and the GC-MS systems was very good, with only slight deviations due to different geometry of the column used in either case. The peaks at 5.396, 6.231, 6.635, 6.878, 8.261 and 7.390 min were confirmed as ethylated MBT, DBT, MPhT, TBT, and DPhT species and TeBT, respectively, according to the characteristic mass spectra produced by electron ionisation. The following ions were considered characteristic in the mass spectra of the individual organotin compounds:  $m/z$  149–179–235 for MBT,  $m/z$  207–235–263 for DBT,  $m/z$  235–263–291 for TBT,  $m/z$  197–227–255 for MPhT, and  $m/z$  197–274–302 for DPhT, respectively. In addition, the peak at 4.075 min, corresponding to that of 4.284 min with the GC-MIP-AED, was clearly identified as tetraethyl tin (TeET), and this confirmed the presence of traces of inorganic tin in urine samples. Some other peaks are produced by the reagents used, especially from sodium tetraethylborate (e.g., boroxine).

### 3.4. Optimization of MIP-AED parameters

Tin can be quantitated by using either of its characteristic emission lines at 270.651, 283.996, 303.419 or 326.230 nm. The lines at 270.651 and 303.419 nm have similar sensitivity, as was observed by other groups [1]. Thus, the 303.419 nm line was selected for these experiments. Other sensitive wavelengths for tin determination like the one at 326.230 nm were also used by other researchers [26], while the sensitive line at 283.996 nm is not extensively used, because it is superimposed by molecular bands, mainly of CO formation [15]. The temperature of the plasma cavity is also an important factor for the overall performance of the atomization, which was examined in the range of 220, 250 and 280 °C. The highest signal was observed at 250 °C, thus this temperature was maintained throughout the study.

The performance of microwave-induced plasma atomic emission detection of tin was assessed by using a hexane standard solution of TeBT.  $1 \mu\text{L}$  of this solution (corresponding to 2 ng TeBT as Sn) was injected by an autosampler in order to monitor the signal intensity obtained, under various helium (plasma gas) makeup flow rates and hydrogen and oxygen (reagent gas) pressures. The

results of this study are given in Fig. 3, for both, the peak area and peak height.

The optimum helium makeup flow rate was found to be at  $150 \text{ mL min}^{-1}$ , although in the literature several different flow rates have been suggested, even when using the same equipment [27]. The diverse makeup gas flow rates may be a result of the different tin compounds or different wavelengths used [4,10,15] or may even be due to inconsistencies in reporting these settings (e.g., when including the reagent gas flows or not). Increasing the helium flow

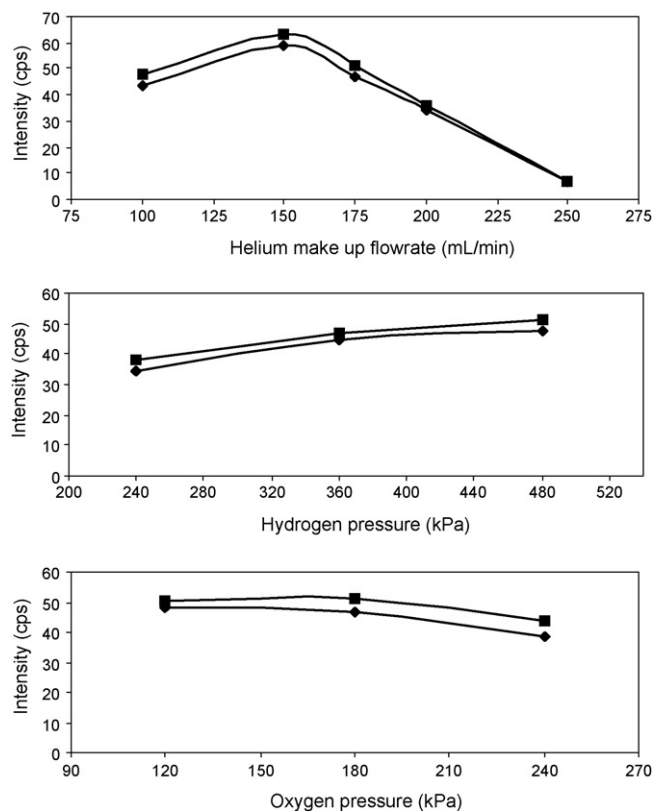


**Fig. 3.** Effect of critical MIP-AED parameters on the signal intensity of  $1 \mu\text{L}$  hexane standard solution containing 2 ng TeBT injected in split mode (1:10). Peak area (◆) and peak height (■) are plotted for each factor/parameter, respectively. Other settings as listed in Table 1.

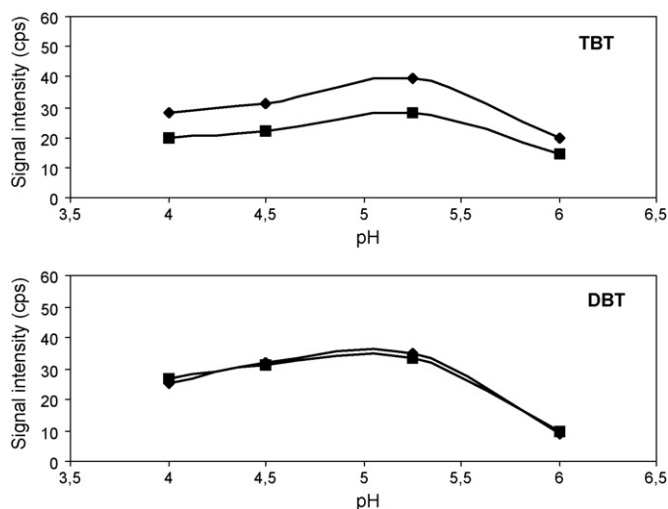


**Fig. 4.** Effect of sample pH on signal intensity of TBT and DBT in urine matrix spiked with individual species in amounts equivalent to  $1 \mu\text{g L}^{-1}$  Sn, 15 min HS-SPME at  $20^\circ\text{C}$ . Peak area ( $\blacklozenge$ ) and peak height ( $\blacksquare$ ).

rate to more than  $250 \text{ mL min}^{-1}$  may result in shortening the available time for atomization of tin in the plasma, as well as cooling of plasma and of course some degradation of the analyte signal because of dilution [4].

The addition of hydrogen to the plasma is known to have an auxiliary positive effect for tin atomization, and various mechanisms to explain the exact reason for this have been proposed in the literature [9]. The pressure set at the hydrogen gas supply cylinder was used as the optimization variable, and it was shown that this should be at the highest practical level. So it was set at 480 kPa for the rest of the study. Finally, increasing the oxygen inlet pressure, a slightly negative effective is observed due to the well-known tendency of tin to form stable oxides during atomization in the low-power microwave plasma, so 180 kPa was chosen as working value in order to prevent the formation of carbon deposits on the discharge tube walls.

### 3.5. Optimization of HS-SPME parameters

The optimum pH for the in situ-derivatization and extraction procedure by HS-SPME is mainly depending on the alkylation reaction. Ethylation of organotin compounds with  $\text{NaBeEt}_4$  is more favourable at a pH range 4–6 although, according to various reports, there are some discrepancies about the exact optimum. Various pH values like 5.3 [11] or 5.0 [14] or even 4.8 [16] are reported in the literature, which are mainly due to the fact that all SPME variables are usually optimized by a univariate process, although a multivariable process could reveal some interactions between variables. Also, the increments used during optimization affect the final optimum value. Accordingly, the effect of sample acidity was examined in the above-mentioned range (Fig. 4). In this study a pH 5.25 was considered as optimum for the derivatization, and this fits quite well with the fact that urine samples are normally slightly acidic, with a pH 5.2–5.6, thus little or no pH adjustment is needed with the proposed method. However, because at higher pH the signal is significantly lowered, the samples should always be checked for their acidity and if it is required they should be adjusted using acetate buffer.

The results of the investigation of temperature effect on the recovery of DBT and TBT showed that at temperatures up to  $40^\circ\text{C}$  (DBT) or  $60^\circ\text{C}$  (TBT) a 10–30% increase of the signal is observed, which is the case for the other species also. At higher temperatures, the rate of analyte derivatization and subsequent volatilisation is

higher however the efficiency of extraction onto the fibre coating is decreased, because analyte absorption onto the polymeric material is an exothermic process. Moreover, derivatization and extraction of the organotin compounds may occur to different degrees, depending on, e.g., the volatility of each compound. Accordingly, the repeatability of the extraction is questionable at high temperatures. Thus, to simplify the whole procedure,  $20^\circ\text{C}$  (room temperature) was chosen as derivatization/extraction temperature.

By increasing the extraction time up to 50 min, a slight increase of the signal occurs, as derivatization (ethylation) and extraction of organotin compounds is only slowly reaching equilibrium. As it was shown in previous works [14], a significant fraction of the alkylated tin species is extracted after 20 min or less, depending on the molecular weight and the organic moiety of the molecule. Consequently, a 15-min extraction time was selected for the rest of the study, as a compromise between sample throughput and sensitivity.

### 3.6. Analytical performance of organotin determination by GC-MIP-AED

Analytical figures of merit for the quantitative determination of organotin compounds by in situ ethylation and simultaneous headspace solid-phase micro-extraction followed by GC-MIP-AED were derived from the calibration with external standards, using spiked solutions of an analyte-free pooled urine sample matrix. For TeBT, which does not require ethylation, exactly the same procedure was followed, to ensure comparable conditions. The calibration results obtained by linear regression on peak area signals are listed in Table 2, for each individual organotin compound while chromatograms of a typical standard addition procedure are presented in Fig. 1.

The sensitivity and other calibration parameters were estimated in a two-step approach. In the first step of this procedure, a series of urine sub-samples was spiked by single compound solutions, at increasing organotin concentrations. This procedure allowed to estimate the sensitivity of the method for each specific compound, and also to monitor possible rearrangement reactions, in the presence of the urine matrix. To some extent, such a behavior was observed for TBT and DPhT, but a slight degradation was not considered to be an important problem for quantitative analysis.

In the second step of this procedure, a series of urine sub-samples was spiked with all six compounds, at increasing concentrations. In all cases, a small peak at 4.285 min was also recorded, with almost constant peak area/height. This was again attributed to the formation of tetraethyltin, from traces of inorganic tin ions, either produced by a limited hydrolysis during the 15 min

**Table 2**

Analytical characteristics for the quantitative determination of butyl- and phenyltin compounds in urine matrix by HS-SPME derivatization and extraction followed by GC-MIP-AED. All concentrations of organotin species refer to tin.

Analyte species	Slope, $S$ ( $\mu\text{g L}^{-1}$ ) $^{-1}$	Correlation coefficient, $r$	R.S.D. (%)	Detection limit ( $\text{ng L}^{-1}$ )
Single-compound spiking				
MBT	24.60	0.9837	8.5	13
DBT	34.00	0.9856	7.0	9
TBT	33.29	0.9834	3.2	9
TeBT	17.49	0.9945	3.9	15
MPhT	28.24	0.9909	3.5	15
DPhT	2.37	0.9958	4.7	57
Multi-compound spiking				
MBT	27.42	0.9909	6.3	13
DBT	34.42	0.9923	3.7	10
TBT	25.21	0.9901	8.0	12
TeBT	19.06	0.9974	11.4	15
MPhT	31.31	0.9926	10.5	17
DPhT	3.55	0.9949	7.7	50

**Table 3**

Organotin analysis performed in different human urine samples. Mean concentrations ( $\text{ng L}^{-1}$  Sn) after  $n = 5$  replicate analyses and 95% confidence interval.

Tin species	Urine samples			
	HU1	HU2	HU3	HU4
MBT	n.d.	n.d.	$34 \pm 4$	n.d.
DBT	n.d.	n.d.	n.d.	n.d.
TBT	n.d.	$25 \pm 4$	$49 \pm 6$	n.d.
TeBT	n.d.	n.d.	n.d.	n.d.
MPhT	n.d.	n.d.	n.d.	n.d.
DPhT	n.d.	n.d.	n.d.	n.d.
Inorganic Sn	–	+	+	+

n.d.: lower than detection limit; +/–: species detected but not quantitated.

ethylation reaction or existing in the urine sample solutions at background levels. Mean levels up to  $6.3 \mu\text{g L}^{-1}$  in urine or equivalent to  $5.0 \mu\text{g g}^{-1}$  creatinine levels are reported to exist in the average population [7].

According to the results listed in Table 2 which compares the results of single-compound standard addition vs. multi-compound standard addition, very similar slopes were obtained for all determined OT species, indicating that in the investigated concentration range there is no competitive interaction of organotin compounds when partitioning in the SPME fibre coating. The slopes obtained with this method are relatively uniform for MBT, DBT, TBT, and MPhT species, and are significantly lower for TeBT. Certainly, the relative sensitivity of detection reflects in part the relative volatility of organotin compounds, and TeBT is the least volatile one of the four (ethylated) butyltin compounds, but the magnitude of the effect is surprising. Even lower sensitivity was obtained for DPhT, for which the simultaneous derivatization and extraction produces a much lower overall yield under the applied conditions. However, this species was also included in the speciation scheme, because under the above conditions its determination is accurate and precise, with somewhat higher detection limit. As it was mentioned above, TePhT could not be included in the proposed speciation scheme.

The precision of the method was tested by analyzing a series of urine sub-samples spiked with the same amount of multi-compound and was found highly satisfactory for all species as can be seen in Table 2. The relative standard deviation varied in the range 3–11% for the individual species. The limits of detection under the given conditions are in the low  $\text{ng L}^{-1}$  range (reported as Sn, Table 2), with the exception of DPhT, and allow the speciation of organotin compounds in urine samples at relevant concentration levels. The limit of detection of each species was calculated using the 3s criterion, based on the standard deviation of 10 blank measurements and refers to the entire procedure. This value is currently limited by the sensitivity of the instrument. Only for DBT and TBT very small signals were detected in the procedural blanks. These were caused by carry-over by the caps with Mininert valves and the magnetic stir-bars during their extensive use in the optimization process, indicating that particularly for these two analytes a more rigid cleaning procedure is required.

### 3.7. Applications to human urine samples

To demonstrate the applicability of the proposed method for human biomonitoring studies, four human urine samples were collected during a period of 24 h from male volunteers (age 24–45 years), and were directly analyzed using the proposed method. All the examined samples were slightly acidic, with a pH range between 5.2 and 5.5. The results are listed in Table 3. Due to the excellent selectivity of the atomic emission detector, the chromatographic baseline was very stable, allowing the detection of organotin species at the low  $\text{ng L}^{-1}$  level. Only some traces of MBT

and TBT were observed in two of the samples, while in the rest of the samples no organotin species were detected. In some of the examined urine samples the peak at 4.28 min was observed, which is due to the presence of inorganic tin that is ethylated to give TeET. Paschal et al. [7] reported that traces of inorganic tin are usually found in background levels in a significant fraction (almost 89%) of the normal population. As it was mentioned above, the peak of tetraethylated inorganic tin was not quantitated, although it may be possible to include this specie as well in the proposed speciation scheme.

## 4. Conclusions

Urine samples are commonly used for monitoring environmental, nutritional and occupational exposure to organic and inorganic hazards, however, they have only been used to a limited extent so far for the biomonitoring of organometallic compounds. A speciation method has thus been developed and is reported here which, to the best of our knowledge, combines for the first time the in situ derivatization and extraction of organotin species by HS-SPME in human urine samples with gas chromatography with microwave-induced plasma atomic emission detection. Sample preparation for undiluted urine matrices is significantly facilitated with the employment of headspace solid-phase micro-extraction with in situ ethylation of the ionic organometallic compounds. Ethylation using sodium tetraethylborate allows the derivatization directly in the aqueous phase, which is a clear advantage over using Grignard reagents. A key element for the success of this method is the selectivity of atomic emission detection which allows the determination of six biologically relevant organotin compounds in human urine samples, unaffected by matrix effects and with minimum sample preparation. Detection limits in the low  $\text{ng L}^{-1}$  range are achieved which makes the technique suitable for sensitive routine analysis of human urine samples.

## References

- [1] M. Hoch, Appl. Geochem. 16 (2001) 719.
- [2] E. Rosenberg, in: R. Cornelis, J. Caruso, H. Crews, K. Heumann (Eds.), Handbook of Environmental Speciation, vol. 2, Wiley, Chichester, 2005, (Chapter 2.22: Speciation of Tin).
- [3] M.A. Champ, Sci. Total Environ. 258 (2000) 21.
- [4] A.S. Stasinakis, N.S. Thomaidis, A. Nikolaou, A. Kantifis, Environ. Pollut. 134 (2005) 431.
- [5] WHO, Tributyltin compounds, Environmental Health Criteria No. 116, Geneva, Switzerland, 1990; WHO, Mono- and disubstituted methyltin, butyltin, and octyltin compounds, Concise International Chemical Assessment Document No. 73, Geneva, Switzerland, 2006.
- [6] B. Pons, A. Carrera, C. Nerin, J. Chromatogr. B 716 (1998) 139.
- [7] D.C. Paschal, B.G. Ting, J.C. Morrow, J.L. Pirkle, R.J. Jackson, E.J. Sampson, D.T. Miller, K.L. Caldwell, Environ. Res. A 76 (1998) 53.
- [8] C. Alzieu, Ocean Coast. Manage. 40 (1998) 23.
- [9] S. Diez, S. Lacorte, P. Viana, D. Barcelo, J.M. Bayona, Environ. Pollut. 136 (2005) 525.
- [10] R.I. Pereiro, C.A. Diaz, Anal. Bioanal. Chem. 372 (2002) 74.
- [11] L. Dunemann, H. Hajimiragha, J. Begerow, Fresenius J. Anal. Chem. 363 (1999) 466.
- [12] V. Colombini, C. Bancon-Montigny, L. Yang, P. Maxwell, R.E. Sturgeon, R.E. Mester, Talanta 63 (2004) 555.
- [13] C.C. Chou, M.R. Lee, J. Chromatogr. A 1064 (2005) 1.
- [14] M. Crnoja, C. Haberhauer-Troyer, E. Rosenberg, M. Grasserbauer, J. Anal. Atom. Spectrom. 16 (2001) 1160.
- [15] S. Tutschku, S. Mothes, K. Ditttrich, J. Chromatogr. B 683 (1994) 269.
- [16] N. Campillo, N. Aguinaga, P. Vinas, I. Lopez-Garcia, M. Hernandez-Cordoba, Anal. Chim. Acta 525 (2004) 273.
- [17] D. Point, W. Clay Davis, S.J. Christopher, M.B. Ellisor, R.S. Pugh, P.R. Becker, O.F.X. Donard, B.J. Porter, S.A. Wise, Anal. Bioanal. Chem. 387 (2007) 2343.
- [18] K. Inagaki, A. Takatsu, T. Watanabe, T. Kuroiwa, Y. Aoyagi, K. Okamoto, Anal. Bioanal. Chem. 378 (2004) 1265.
- [19] I.J. Alonso, J. Encinar, P. González, A. Sanz-Medel, Anal. Bioanal. Chem. 373 (2002) 432.
- [20] S. Gironi, E. Rosenberg, A. Voulgaropoulos, M. Grasserbauer, J. Fresenius, Anal. Chem. 358 (1997) 828.
- [21] Z. Mester, R. Sturgeon, J. Pawliszyn, Spectrochim. Acta B 56 (2001) 233.

- [22] C. Dietz, J. Sanz, E. Sanz, R. Munoz-Olivas, C. Camara, J. Chromatogr. A 1153 (2007) 114.
- [23] J. Gui-Bin, Z. Qun-Fang, H. Bin, Bull. Environ. Contam. Toxicol. 65 (2000) 277.
- [24] G.J. Olson, F.E. Brinckman, J.A. Jackson, Int. J. Environ. Anal. Chem. 15 (1983) 249.
- [25] C.I. Yoo, Y. Kim, K.S. Jeong, C.S. Sim, N. Choy, J. Kim, J.B. Eum, Y. Nakajima, Y. Endo, Y.J. Kim, J. Occup. Health 49 (2007) 305.
- [26] A. Sadiki, D. Williams, Chemosphere 32 (1996) 1983.
- [27] G. Becker, A. Colmsjo, K. Janak, U. Nilsson, C. Ostman, J. Microcolumn Sep. 8 (1996) 345.



# Selective determination of penicillamine by on-line vapor-phase generation combined with Fourier transform infrared spectrometry

Mohsen Zeeb<sup>a</sup>, Mohammad Reza Ganjali<sup>a,\*</sup>, Parviz Norouzi<sup>a</sup>, Seyyed Rezvan Moeinossadat<sup>b</sup>

<sup>a</sup> Center of Excellence in Electrochemistry, Faculty of Chemistry, University of Tehran, P.O. Box 14155-6455, Tehran, Iran

<sup>b</sup> Mehravar Ab Iranian, Tehran, Iran

## ARTICLE INFO

### Article history:

Received 14 October 2008

Received in revised form 4 December 2008

Accepted 5 December 2008

Available online 13 December 2008

### Keywords:

Vapor-phase generation

FTIR

Penicillamine

Pharmaceutical formulations

## ABSTRACT

In this work, an on-line system with vapor-phase generation (VPG) and Fourier transform infrared (FTIR) spectrometric detection has been developed as a direct and highly selective analytical technique for the assay of penicillamine (PA). Potassium iodate solution was injected into a reactor, heated at 75 °C, containing PA. The CO generated under these conditions was transported by means of N<sub>2</sub> gas carrier stream to an infrared gas cell and corresponding FTIR spectra were acquired in a continuous mode. The maximum absorbance of CO band at 2170 cm<sup>-1</sup>, corrected by a baseline established between 2240 and 2000 cm<sup>-1</sup> at a nominal resolution of 2 cm<sup>-1</sup>, was selected as a measurement criterion. Initially, the effect of different chemical, physical and spectroscopic parameters, such as concentration and volume of oxidant, pH, equilibrium time, reactor temperature, reactor volume, N<sub>2</sub> carrier flow rate and number of scans on the analytical signals were evaluated by using a short path length (10 cm) IR gas cell. At optimum experimental conditions, the method provided a relatively broad linear dynamic range of 4–380 mg L<sup>-1</sup>, a limit of detection of 0.5 mg L<sup>-1</sup>, a sampling frequency of 15 h<sup>-1</sup> and a relative standard deviation (R.S.D.) of 1.6%. Further, the method was successfully applied to the determination of PA in pharmaceutical formulations and results compared well with those obtained by a reference colorimetric method.

© 2008 Elsevier B.V. All rights reserved.

## 1. Introduction

Penicillamine (PA) is a thiol amino acid that is naturally occurring and has many therapeutic applications. This compound is a strong chelating agent and can react with the majority of heavy metal ions. The outstanding metal-binding capability is reflected in the pharmaceutical importance of PA [1]. Thus, PA is the drug of choice in the treatment of hepatolenticular degeneration (Wilson's disease) and is also effective for the treatment of several disorders including rheumatoid arthritis, primary biliary cirrhosis, scleroderma, fibrotic lung diseases, cystinuria, heavy element poisoning and progressive systemic sclerosis [2–6]. PA can exist in D and L enantiomeric forms that show different biological and toxicological properties. However, only D type is clinically useful due to excessive toxicity of the L type [7].

Various analytical methods have been reported for the determination of PA in both pharmaceutical preparations and biological samples. These methods include high performance liquid chromatography (HPLC) [8–10], fluorimetry [11,12], colorimetry [13,14], spectrophotometry [15,16], chemiluminescence [17,18], flow injection analysis [19,20], capillary electrophoresis [21–23]

and electrochemistry [24,25]. One of the important limitations of LC techniques is the fact that this thiol compound lacks sufficient UV absorption so a pre- or post-column derivatization procedure is normally required [26]. Due to the shortage of chromophore and/or auxochrome in PA molecule, direct spectrometry cannot be used for its analysis. Most of the reported colorimetric methods are time consuming or lacking selectivity owing to the problem of interference with degradation product of coloring agents [27]. In electrochemical methods, mercury and mercury amalgam [28] have been extensively used for thiol compounds determination. However, mercury has limitations because of its toxicity and the rapid deterioration of electrode response [29]. Thus, there has been an increasing need in the development of new, direct and selective methods for the determination of PA in both pharmaceutical formulations and biological samples.

The literature relates interesting contributions of Fourier transform infrared (FTIR) spectrometry applied to liquid and solid samples analysis based on the on-line generation of vapor phase by means of the simple sample volatilization or a chemical reaction. Main applications involve determination of carbonates in liquid and solid samples [30,31], alcohols in different matrices [32,33], L-cysteine and L-cystine in pharmaceutical and urine samples [34], seafood freshness [35], nitrite [36], and nitrogen in hydrolyzed protein formulation [37]. Recently, a complete review about on-line vapor-phase generation combined with Fourier transform infrared

\* Corresponding author. Tel.: +98 21 61112788; fax: +98 21 66405141.  
E-mail address: [ganjali@khayam.ut.ac.ir](mailto:ganjali@khayam.ut.ac.ir) (M.R. Ganjali).

spectrometry has been published by Armenta et al. [38]. In this review, they tried to demonstrate the analytical potential of the aforementioned method in vibrational spectrometry in order to improve the selectivity and the sensitivity of the measurement step and also to make environmentally friendly procedures available for problem solving in the analytical laboratory.

FTIR spectrometry is very useful for carrying out determinations in gaseous or vapor samples, owing to the high transparency of gases (e.g., N<sub>2</sub>), the low background values obtained for cells filled with inert gases (e.g., N<sub>2</sub>, He or Ar), and the possibilities offered by cells long enough to allow many passes and increase the analytical sensitivity [39]. To our knowledge, no study on the mechanism of oxidation of PA with potassium iodate, and the gaseous species produced in this reaction has been reported. Thus, in this paper, we present and discuss for the first time a rapid, direct and highly selective technique for the determination of PA based on vapor-phase generation FTIR through the reaction of PA with potassium iodate and continuous measurement of CO gas liberated.

## 2. Experimental

### 2.1. Instrumentation

A Vector 22 FTIR spectrometer from Bruker (Ettlingen, Germany), equipped with a DTGS mid-range detector, a KBr Ge/Sb<sub>2</sub>S<sub>3</sub>-coated beamsplitter and a Globar source was employed to carry out the IR measurements, using a low cost home made IR gas cell with a path length of 10 cm and an internal diameter of 0.9 cm, equipped with circular ZnSe windows. The spectrum Opus software, developed by Bruker, was used to control the instrument, for data acquisition and also for processing the analytical results.

The manifold employed for vapor-phase generation FTIR measurements (Fig. 1) was a single-channel manifold with a nitrogen carrier flow, which included a laboratory-made removable glass sample vessel of 20 mL internal volume with a gas inlet, a gas outlet and a septum. Sample vessel (reactor) was introduced inside a hot water-bath, the temperature of which was controlled by means of a thermocouple and operated using laboratory-made electrically controlled heater. To avoid the presence of water drops inside the measurement cell, at the exit of the glass reactor a small stainless steel u-form tube was introduced inside an ice-bath to act as a water trap in which the excess water vapor condensed before passing through the gas cell. Other tubes employed in the manifold were made of PTFE.

### 2.2. Reagents and materials

D-Penicillamine (D-PA, 3,3-dimethyl cysteine) was obtained from Fluka (Buchs, Switzerland). PA capsules were purchased from commercial sources. All other chemicals used in this work were of analytical grade. PA standard solution (2000 mg L<sup>-1</sup>) was prepared

by dissolving 0.3 g of PA in de-ionized water and diluting with citric acid buffer to a final volume of 150 mL. This standard solution was kept in refrigerator for preservation, and can be stored for at least 2 months. Working standard solutions were daily prepared by diluting the stock solutions in citric acid buffer. To prepare citric acid buffer with a pH 3, 1.7963 g citric acid monohydrate and 0.4265 g tri-sodium citrate dehydrate were dissolved in de-ionized water, and diluted to 1 L. Nitrogen of 99.95% purity was employed as the carrier gas and de-ionized water was used throughout.

### 2.3. General procedure

Ten milliliters of PA standard solutions of drugs in the working concentration range (4–380 mg L<sup>-1</sup>) were transported into the glass vessels (reactors), incorporated in the manifold depicted in Fig. 1, and then heated at 75 °C. The FTIR background was obtained by passing N<sub>2</sub> through the gas measurement cell. Two milliliters of 4.5% m/v potassium iodate (KIO<sub>3</sub>) solution were injected inside the sample vessel. The CO vapor generated under these conditions was carried into the gas cell of the FTIR spectrometer using a nitrogen flow rate of 5 mL min<sup>-1</sup>, without the need for an equilibrium time before measurement. FTIR spectra, between 2240 and 2000 cm<sup>-1</sup>, were continuously recorded as a function of time, by accumulating 15 scans per spectrum at 2 cm<sup>-1</sup> nominal resolution. Analytical measurements for PA were carried out in the aforementioned spectral range. The peak absorbance of the CO band at 2170 cm<sup>-1</sup> with maximum signal, corrected by a baseline established between 2240 and 2000 cm<sup>-1</sup>, was selected as a measurement criterion.

### 2.4. Assay procedure for capsules

The contents of ten PA capsules were accurately weighed and the mean value of weight of one capsule was calculated. An amount of the powder equivalent to about 22.5 mg of PA was accurately weighed and transferred into 150 mL volumetric flask. About 100 mL of citric acid buffer was added and the solution was shaken for 4 min and completed to the volume with citric acid buffer to give a final concentration of 150 mg L<sup>-1</sup>.

### 2.5. Reference colorimetric procedure

A simple and selective colorimetric procedure based on oxidation of PA with potassium iodate in 30% sulphuric acid medium at room temperature and measurement of the liberated iodine at 520 nm after extraction with tetrachloride, was applied as the reference method [40].

## 3. Results and discussion

### 3.1. Gaseous FTIR spectrum of CO

Fig. 2 shows the absorption of FTIR spectrum of the gaseous monoxide carbon (CO (g)) obtained in the proposed system. The spectrum is characterized by a sensitive double band between 2240 and 2000 cm<sup>-1</sup>, with maximum absorbance at 2170 cm<sup>-1</sup>. In this spectral range, water shows a very low absorption and hence the use of vapor-phase generation of CO from PA provides a simple and sensitive approach for the determination of PA in real samples.

### 3.2. Selection of oxidant

PA is an un-physiological sulfur-containing amino acid that belongs to the amino thiols family with both hydrogen atoms in the beta-carbon of cysteine replaced by methyl groups. The structure of PA is very similar to L-cysteine; therefore it can be oxidized by potassium iodate to generate CO and CO<sub>2</sub> gases [34]. This fact

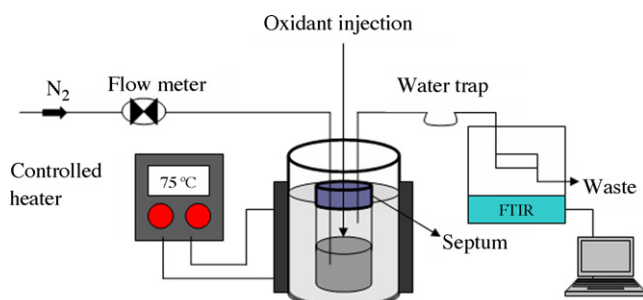


Fig. 1. Manifold employed for vapor-phase generation FTIR determination of penicillamine.



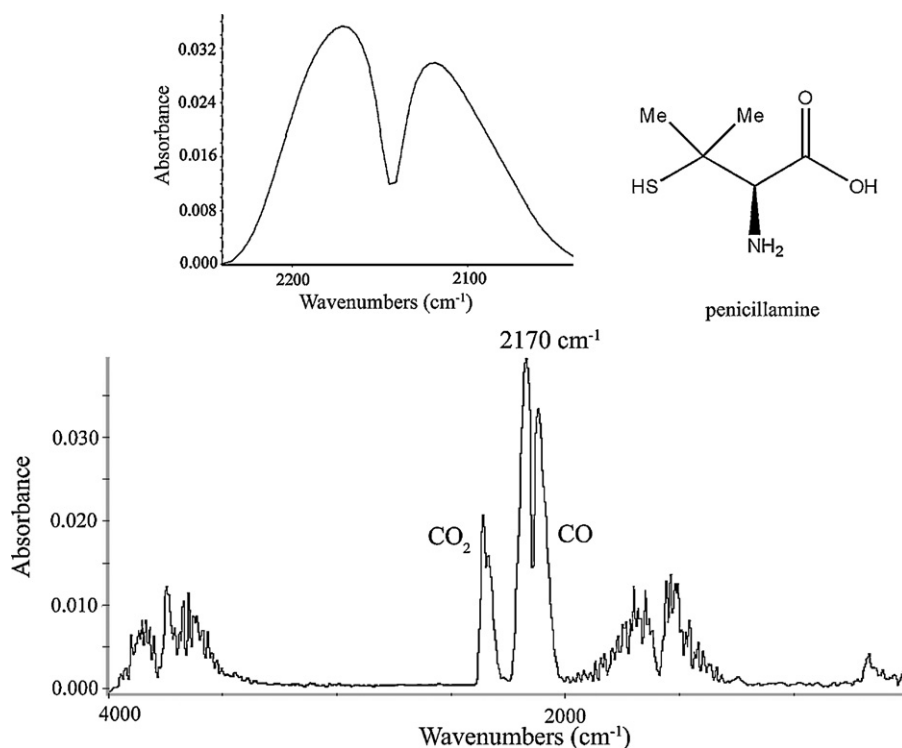


Fig. 2. Vapor phase FTIR spectrum of the gaseous species generated in the reaction between PA and iodate. Inset: detailed spectrum in the selected measurement region.

was confirmed by recording the FTIR spectra of all gaseous species produced in the reaction between PA and iodate (see Fig. 2).

Some other oxidants, such as sodium metaperiodate, potassium permanganate and N-bromosuccinimide are very forceful and can oxidize a wide range of compounds, which are usually present in pharmaceutical formulations to generate CO<sub>2</sub> or other gases. Therefore, they are not selective for vapor phase Fourier transform infrared spectrometric measurements. In contrast, scarce compounds can generate CO or CO<sub>2</sub> gases during the reaction with potassium iodate due to the weak oxidizing capability of this reagent. However, potassium iodate was selected for all further studies to achieve selective and precise analytical consequences. As can be seen in Fig. 2, the height of the CO absorbance signal is about twice of that the CO<sub>2</sub> signal in using potassium iodate as an oxidizing agent. Hence, by selecting CO instead of CO<sub>2</sub> as a final analyte, more precise and sensitive results were obtained in the proposed system.

### 3.3. Influence of chemical, physical and spectroscopic parameters

The on-line VPG-FTIR system proposed in this work involves four steps: (i) the oxidation of PA, (ii) the generation of CO, (iii) the stripping of CO and its transport to the IR gas cell, and (iv) the acquisition of the corresponding FTIR spectrum. Different chemical, physical and spectroscopic parameters were selected by the univariate study to introduce the highest and most reproducible amount of CO into the IR gas cell. However, the validity of the previously selected parameters was verified. In this process, a 150 mg L<sup>-1</sup> PA standard solution was used through the rest of the work.

#### 3.3.1. Influence of potassium iodate concentration on CO generation

Potassium iodate is required to oxidize PA in order to generate CO. The concentration and volume of the oxidant necessary for complete generation of CO from PA were evaluated. Studies carried

out on the oxidation of PA standard solutions evidenced that 2 mL of potassium iodate solution, with excess concentration (4.5%, m/v) was sufficient to provide the total generation of CO and repeatability of FTIR measurements.

#### 3.3.2. Influence of pH

The solution pH of the sample is an important factor, which may affect the chemical behavior of potassium iodate as an oxidizing agent. The effect of pH on the oxidation of PA with potassium iodate, and the generation of CO was investigated within the range of 0.5–5 by using appropriate buffer. The results illustrated in Fig. 3 reveal that analytical signals, obtained for the CO generated from PA, depend on pH. As can be seen, signal intensity increases as pH increases from 0.5 to 3.5, and then decreases. In order to obtain a compromise between oxidation efficiency and reproducibility of the analytical signals a pH 3 (using citric acid buffer) was chosen for further experiments.

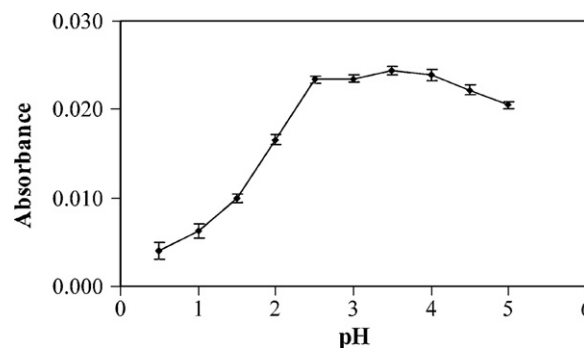


Fig. 3. Influence of pH on the determination of PA by vapor phase FTIR. Experimental conditions: PA concentration 150 mg L<sup>-1</sup>; KIO<sub>3</sub> concentration 4.5% (m/v); KIO<sub>3</sub> volume 2 mL; reactor volume 20 mL; sample volume 10 mL; N<sub>2</sub> carrier flow rate 5 mL min<sup>-1</sup>; reactor temperature 75 °C; number of scans 15. Peak absorbance values indicated are the average of three independent measurements and error bars correspond to their standard deviations.

**Table 1**  
Influence of N<sub>2</sub> carrier flow rate on vapor-phase generation FTIR measurement of PA.

N <sub>2</sub> flow rate (mL min <sup>-1</sup> )	Absorbance ± s <sub>n-1</sub>	Sampling frequency (h <sup>-1</sup> )
2.5	0.0296 ± 0.0005	12
5	0.0237 ± 0.0004	15
7.5	0.0189 ± 0.0004	18
10	0.0151 ± 0.0006	22
12.5	0.0128 ± 0.0005	25
15	0.0092 ± 0.0006	30

Experimental conditions: PA concentration 150 mg L<sup>-1</sup>; KIO<sub>3</sub> concentration 4.5% (m/v); KIO<sub>3</sub> volume 2 mL; pH 3; reactor volume 20 mL; sample volume 10 mL; reactor temperature 75 °C; number of scans 15. The standard deviation values correspond to three independent measurements.

### 3.3.3. Influence of reactor volume

The effect of reactor volume on the analytical signals, obtained for the CO produced from PA, was evaluated from 14 to 40 mL. Comparable values were achieved for the whole range of reactor volumes studied. An increase in the sample vessel volume, which increases the CO dispersion by increasing the total volume of the system, has very small influence on the analytical signals obtained from the CO absorption band. A reactor volume of 20 mL, which corresponds to the standard size, was selected for further studies.

### 3.3.4. Influence of N<sub>2</sub> carrier flow rate

It is well established that carrier gas flow rate meaningfully affects the analytical response in both hydride generation [41,42] and gaseous FTIR spectrometric systems [43,44]. The functions of the gas carrier in the proposed VG-FTIR systems are: (i) the stripping of the CO from the solution, and (ii) its transport to the IR gas cell. The gas carrier drastically influences the analytical sensitivity and the sampling frequency. The effect of the N<sub>2</sub> carrier gas flow rate was evaluated from 2.5 to 15 mL min<sup>-1</sup> (see Table 1). As can be ascertained, an increase in the carrier flow rate causes a decrease in sensitivity, but increases the sampling frequency. Hence, a nitrogen flow rate of 5 mL min<sup>-1</sup>, which allows a 15 h<sup>-1</sup> sampling frequency was selected in order to achieve a compromise between analytical sensitivity and sample throughput.

### 3.3.5. Influence of temperature

The study of the temperature effect on CO generation revealed that it is a decisive factor. In addition, the temperature affects the kinetic of the reaction between PA and potassium iodate, and the liberation of CO from the PA solution. Results obtained in the range 25–95 °C are presented in Fig. 4. As can be seen, the absorbance of the peaks increases, as the reactor temperature increases. However, from an experimental point of view fast measurement of CO creates problems with respect to monitoring absorption spectra. There-

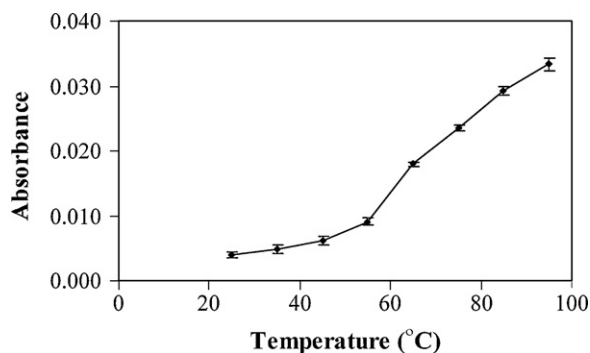


**Fig. 4.** Influence of temperature on the vapor-phase generation FTIR determination of PA. Experimental conditions: as indicated in Fig. 3 with a pH 3. Error bars correspond to three independent measurements.

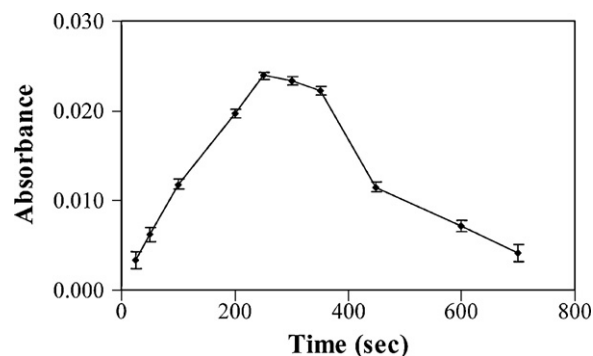


**Fig. 5.** Influence of equilibrium time on the determination of PA by vapor phase FTIR. Experimental conditions: as indicated in Fig. 4 with a reactor temperature of 75 °C. Peak absorbance values indicated are the average of three independent measurements and error bars correspond to their standard deviations.

**Table 2**  
The VPG-FTIR conditions for PA determination.

Component	Parameter	Value
FTIR	Number of scans accumulated for background/spectrum	15
	Nominal resolution	2 cm <sup>-1</sup>
VPG	KIO <sub>3</sub> concentration	4.5% m/v
	KIO <sub>3</sub> volume	2 mL
	pH	3
	Reactor volume	20 mL
	Temperature	75 °C
	N <sub>2</sub> gas carrier flow rate	5 mL min <sup>-1</sup>

**Table 3**  
Recoveries obtained for PA in pharmaceutical samples by vapor phase FTIR spectrometry.

Sample	Endogenous value <sup>a</sup> (mg L <sup>-1</sup> )	PA added (mg L <sup>-1</sup> )	PA found <sup>b</sup> (mg L <sup>-1</sup> )	Recovery (%)
PA capsule 1 <sup>c</sup>	75.0	0	75.3 ± 0.8	–
		20	96.2 ± 0.9	106.1
		50	125 ± 1	100.2
		75	147 ± 2	95.9
		100	176 ± 1	101.1
PA capsule 2 <sup>c</sup>	37.5	0	38 ± 2	–
		20	56.0 ± 0.6	92.6
		50	90 ± 1	104.2
		75	112.3 ± 0.8	99.8
		100	139 ± 1	101.7

<sup>a</sup> Correspond to a dilution of the sample solution.

<sup>b</sup> The standard deviation values correspond to three independent measurements.

<sup>c</sup> PA capsules 1 and 2: sample solutions with different dilutions.

fore, a temperature of 75 °C was selected in order to decrease water vapor transfer to a minimum and to obtain a compromise between speed, sensitivity, simplicity and reproducibility of the analytical signals.

**Table 4**  
Effect of the presence of foreign compounds on the determination of 150 mg L<sup>-1</sup> PA.

Interference	Concentration (mg L <sup>-1</sup> )	Error (%) <sup>a</sup>
Ascorbic acid	1000	-3.33
Calvulanic acid	1200	+1.23
Benzylpenicillin	1200	-2.10
Phenylmethylpenicillin	1200	-1.86
Glucose	1500	+1.12
Lactose	1500	+1.75
Sucrose	1500	-1.31
Fructose	1500	-2.24
Saccharin	1500	+1.51

<sup>a</sup> Error (%) = [signal (PA + interference) – signal (PA)] × 100/signal (PA).

**Table 5**  
Results of analysis of PA capsules by vapor phase FTIR and by a reference method [40].

Experiment number	Labeled value (mg/capsule)	Proposed method (mg) <sup>a</sup>	Reference method (mg) <sup>a</sup>	Error (%) <sup>b</sup>	Error (%) <sup>c</sup>
1	150.0	152.2 (±1.3)	154.3 (±1.0)	+1.5	−1.4
2	250.0	246.6 (±0.6)	256.2 (±0.9)	−1.3	−3.7

<sup>a</sup> Values in parenthesis give the standard deviation based on three replicates.

<sup>b</sup> Error against the declared value.

<sup>c</sup> Error against the reference method.

### 3.3.6. Influence of equilibrium time

A series of supplemental experiments were carried out by isolating the reactor from the N<sub>2</sub> carrier flow during the addition of potassium iodate solution, for different periods of time. In fact in this mode of experiments, the oxidant was injected and after a fixed reaction time the CO evolved under these conditions was introduced into the measurement cell by means of carrier gas. This allows the oxidation reaction and CO release to reach an equilibrium state before measurement.

Times between 50 and 700 s were tested as equilibrium times before measurement and, as can be seen in Fig. 5, a growth in the equilibrium time up to 250 s leads to an increase in the analytical signal and then to a decrease. Maximum obtainable sensitivity in 250 s fixed reaction time shows no improvement compared with sensitivity obtained by continuous flow mode. So, it is recommended to work in the continuous flow mode after injection of potassium iodate using a constant flow rate of N<sub>2</sub> to introduce the generated CO continuously into the IR gas cell.

### 3.3.7. Influence of the number of scans

The effect of the number of scans employed to establish the background and to obtain each spectrum was studied from 5 to 35. 15 scans are enough to obtain a stable background and appropriate signal-to-noise ratio. So, this number of scans was selected for further studies. Higher values than 15 do not improve significantly the quality of the analytical signals, and deteriorated the sample throughput. Table 2 summarized both instrumental and experimental conditions selected in the proposed system.

## 4. Applications

### 4.1. Analytical characteristics

Under the optimum experimental conditions, the relationship between the analytical signal and concentration was studied over the range 2–750 mg L<sup>−1</sup> and found to be linear from 4 to 380 mg L<sup>−1</sup>. The corresponding fitted equation was  $A = 0.0002273 + 0.0001521C$  with  $r^2 = 0.9995$ , where  $A$  is the absorbance at 2170 cm<sup>−1</sup>, corrected by means of a baseline established between 2240 and 2000 cm<sup>−1</sup>, and  $C$  is the penicillamine concentration in mg L<sup>−1</sup>. The limit of detection was determined by using the criterion,  $LOD = ks_{bl}/m$ , where  $k$  is a factor (=3),  $s_{bl}$  is the standard deviation of the blank measurements and  $m$  is the calibration slope. The value thus found was 0.5 mg L<sup>−1</sup>. The repeatability of the system was determined from seven consecutive insertions of a 150 mg L<sup>−1</sup> standard solution of penicillamine; the relative standard deviation (R.S.D.) thus obtained was 1.6%. The calculated throughput for this experimental series was 15 samples h<sup>−1</sup>.

Initially, the accuracy of the proposed method was evaluated by means of recovery experiences. For this purpose, different amounts of authentic PA were added to the diluted sample solutions, obtained from PA capsules, and subsequently assayed by the developed procedure. The results of this recovery study are shown in Table 3. As can be ascertained, in all cases, the quantitative recoveries (92.6–106.1%) were obtained.

### 4.2. Study of interferences

The potential interferences studied included various excipients present in commercially available PA formulations. Solutions containing the analyte at a 150 mg L<sup>−1</sup> concentration and the interferences at levels above those typically found in the formulations were used for this purpose. A compound was deemed an interference when the error in the signal for a 150 mg L<sup>−1</sup> standard of PA exceeded 4%, in which case the concentration of the compound concerned was lowered until no interferences was observed. Table 4 shows the results obtained.

### 4.3. Analysis of real samples

Finally, the developed procedure was applied to the determination of PA in the commercial pharmaceutical preparations. The sample solutions, obtained from PA capsules, were treated as mentioned in the general procedure to calculate the amounts of PA in the samples using simple calibration line. Table 5 presents results obtained by applying the vapor phase FTIR approach and those obtained by the reference colorimetric method [40]. These results indicate the accuracy of the proposed method, and its viability for the analysis of PA in this type of samples.

## 5. Conclusion

The on-line vapor phase FTIR procedure developed in this work permits the fast, precise and accurate determination of PA in commercial pharmaceutical preparations. In contrast to some fluorimetric, spectrometric and electrochemical methods, proposed previously for the determination of PA, the present methodology does not have matrix interferences, nor does it require any sample preparation step. Additional advantages are the relatively inexpensive set-up and the low consumption of reagents and the absence of use of toxic organic reagents, which is a common practice in the FTIR analysis.

## Acknowledgment

Support of this investigation by the Research Council of University of Tehran through Grant is gratefully acknowledged.

## References

- [1] M. Bieri, T. Burgi, *Langmuir* 22 (2006) 8379.
- [2] E.C. LeRoy, M. Trojanowska, E.A. Smith, *Clin. Exp. Rheumatol.* 9 (1991) 173.
- [3] B. Sarkar, *Chem. Rev.* 99 (1999) 2535.
- [4] I.L. Bonta, M.J. Parnhman, L.E. Vincent, P.C. Bragt, *Prog. Med. Chem.* 17 (1980) 203.
- [5] C.R. Chong, D.S. Auld, *Biochemistry* 39 (2000) 7580.
- [6] V.R. Preedy, W.S. Wassif, D. Baldwin, J. Jones, G. Falkous, J.S. Marway, D. Mantle, D.L. Scott, *Int. J. Biochem. Cell B* 33 (2001) 1026.
- [7] R. Munro, H.A. Capell, *Br. J. Rheumatol.* 36 (1997) 104.
- [8] S. Biffar, V. Greely, D. Tibbetts, *J. Chromatogr.* 318 (1985) 404.
- [9] R. Saetre, D.L. Rabenstein, *Anal. Chem.* 50 (1987) 276.
- [10] G.T. Yamashita, D.L. Rabenstein, *J. Chromatogr.* 491 (1989) 341.
- [11] V. Cavrini, R. Gatti, P. Roveri, M.R. Cesaroni, *Analyst* 113 (1988) 1447.
- [12] R. Segarra-Guerrero, S. Sagrado-Vives, J. Martinez-Calatayud, *Microchem. J.* 43 (1991) 176.
- [13] A. Besada, N.B. Tadros, Y.A. Gawargious, *Anal. Lett.* 20 (1987) 809.

- [14] A. Besada, *Anal. Lett.* 21 (1988) 435.
- [15] A.A. Al-Majed, *J. Pharm. Biomed. Anal.* 21 (1999) 827.
- [16] F.E.O. Suliman, H.A.J. Al-Lawati, S.M.Z. Al-Kindy, I.E.M. Nour, S.B. Salama, *Talanta* 61 (2003) 221.
- [17] P. Vinas, I. Lopez-Garcia, J.A. Martinez-Gil, *J. Pharm. Biomed. Anal.* 11 (1993) 15.
- [18] Z.D. Zhang, W.R.G. Baeyens, X.R. Zhang, G.V.D. Weken, *Analyst* 121 (1996) 1569.
- [19] P. Vinas, J.A. Sanchez-Prieto, M. Hernandez-Cordoba, *Microchem. J.* 41 (1990) 2.
- [20] M.C. Icardo, O.A. Estrela, M. Sajewicz, J.V.G. Mateo, J.M. Calatayud, *Anal. Chim. Acta* 438 (2001) 281.
- [21] M. Wronski, *J. Chromatogr. B* 676 (1996) 29.
- [22] A. Zinellu, C. Carru, S. Sotiga, L. Deiana, *J. Chromatogr. B* 803 (2004) 299.
- [23] X. Yang, H. Yuan, C. Wang, X. Su, L. Hu, D. Xiao, *J. Pharm. Biomed. Anal.* 45 (2007) 362.
- [24] S. Shahrokhian, S. Bozorgzadeh, *Electrochim. Acta* 51 (2006) 4271.
- [25] A.A.J. Torriero, H.D. Piola, N.A. Martinez, N.V. Panini, J. Raba, J.J. Silber, *Talanta* 71 (2007) 1198.
- [26] V. Amarnath, K. Amarnath, *Talanta* 56 (2002) 745.
- [27] N. Buyuktimkin, S. Buyuktimkin, *Pharmazie* 40 (1985) 581.
- [28] D.L. Rabenstein, G.T. Yamashita, *Anal. Biochem.* 180 (1989) 259.
- [29] S. Zhang, W. Sun, W. Zhang, W. Oi, L. Jin, K. Yamamoto, S. Tao, J. Jin, *Anal. Chim. Acta* 386 (1999) 21.
- [30] A. Perez-Ponce, J.M. Garrigues, S. Garrigues, M. de la Guardia, *Analyst* 123 (1998) 1817.
- [31] A. Perez-Ponce, S. Garrigues, M. de la Guardia, *Vib. Spectrosc.* 16 (1998) 61.
- [32] A. Perez Ponce, F.J. Rambla, J.M. Garrigues, S. Garrigues, M. de la Guardia, *Analyst* 123 (1998) 1253.
- [33] S. Armenta, F.A. Esteve-Turrillas, G. Quintas, S. Garrigues, A. Pastor, M. de la Guardia, *Anal. Chim. Acta* 569 (2006) 238.
- [34] K. Kargosha, S.H. Ahmadi, M. Zeeb, S.R. Moeinossadat, *Talanta* 74 (2008) 753.
- [35] S. Armenta, N.M.M. Coelho, R. Roda, S. Garrigues, M. de la Guardia, *Anal. Chim. Acta* 580 (2006) 216.
- [36] M. Gallignani, M. Valero, C. Ayala, M.R. Brunetto, A. Sanchez, J.L. Burguera, M. Burguera, *Talanta* 64 (2004) 1290.
- [37] N.M.M. Coelho, S. Garrigues, M. de la Guardia, *Talanta* 68 (2006) 836.
- [38] S. Armenta, S. Garrigues, M. de la Guardia, *Trends Anal. Chem.* 27 (2008) 15.
- [39] P.L. Hanst, *Fresen. J. Anal. Chem.* 324 (1986) 579.
- [40] A. Besada, N.B. Tadros, *Microchim. Acta* 2 (1987) 225.
- [41] J.L. Burguera, M. Burguera, C. Rivas, *Quím. Anal.* 16 (1997) 165.
- [42] M. Gallignani, C. Ayala, M.R. Brunetto, M. Burguera, J.L. Burguera, *Talanta* 59 (2002) 923.
- [43] K. Kargosha, M. Khanmohammadi, M. Ghadiri, *Analyst* 126 (2001) 1432.
- [44] A.R. Cassella, S. Garrigues, R.C. de Campos, M. de la Guardia, *Talanta* 54 (2001) 1087.



# Systematic screening and characterization of tertiary and quaternary alkaloids from *corydalis yanhusuo* W.T. Wang using ultra-performance liquid chromatography–quadrupole–time-of-flight mass spectrometry

Jing Zhang<sup>a</sup>, Yu Jin<sup>b</sup>, Jun Dong<sup>a</sup>, Yuansheng Xiao<sup>a</sup>, Jiatao Feng<sup>a</sup>, Xingya Xue<sup>a</sup>, Xiuli Zhang<sup>a,\*</sup>, Xinmiao Liang<sup>a,b,\*</sup>

<sup>a</sup> Key Laboratory of Separation Science for Analytical Chemistry, Dalian Institute of Chemical Physics, Chinese Academy of Sciences, Dalian 116023, China

<sup>b</sup> School of Pharmacy, East China University of Science and Technology, Shanghai 200237, PR China

## ARTICLE INFO

### Article history:

Received 19 September 2008  
Received in revised form 1 December 2008  
Accepted 1 December 2008  
Available online 6 December 2008

### Keywords:

UPLC/Q-TOF  
MS/MS  
Screening  
Alkaloids  
*Corydalis yanhusuo* W.T. Wang

## ABSTRACT

Ultra-performance liquid chromatography–quadrupole–time-of-flight mass spectrometry (UPLC–Q-TOF–MS) is an effective technique for analysis of complex samples with offering rapid, efficient separation in combination with accurate mass measurement and tandem mass spectrometry (MS/MS). This paper exploits this technique to identify the alkaloids in *corydalis yanhusuo*, an important analgesic Traditional Chinese Medicine (TCM). The mass spectral fragmentation behavior of one tertiary alkaloid and two quaternary alkaloids was studied in detail. Low-abundance product ions of tertiary and quaternary alkaloids were investigated and compared between each other. Sixteen alkaloids were screened out by using a systematic screening method developed in our laboratory; structures of eight therein were identified by characteristic UV absorption spectrum and positive ion mode of Q-TOF-MS/MS; and two of them were discovered for the first time in *corydalis yanhusuo* to our knowledge. This research demonstrates the potential of UPLC–Q-TOF–MS in structural characterization and identification of components in traditional Chinese herbal medicines.

© 2008 Elsevier B.V. All rights reserved.

## 1. Introduction

The traditional Chinese medicine (TCM) is a kind of natural therapeutic agent used under the guidance of the theory of traditional Chinese medical sciences which has been used for over thousands of years in China. Analysis of the chemical constituents of TCM is a considerable challenge to the researchers since it always contains hundreds and thousands of compounds in macro, micro, and even trace concentrations. Under many practical circumstances, chemical components bearing therapeutic effects are still unclear. Development of simple, effective and sensitive methods for qualification, and even quantification, of components in TCM, thus, poses a crucial role in the development of TCM science.

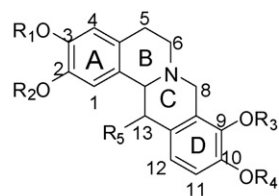
Up to now, several methods have been reported for the determination and analysis of compounds in TCM, including high-performance liquid chromatography (HPLC) [1–3], high-performance liquid chromatography–mass spectrometry (HPLC–MS) [4–7], capillary electrophoresis (CE) [8–10] and cap-

illary electrophoresis/mass spectrometry (CE/MS) [9]. It has been demonstrated that HPLC–MS is a useful tool for the identification and elucidation of compounds in complex TCM samples [11,12]. Among various types of LCs, ultra-performance liquid chromatography (UPLC), using sub-2 mm particles, has especially high resolution, sensitivity and speed when performing TCM analysis. In addition, UPLC could detect more components than HPLC. A number of mass analyzers can be used for TCM analysis, such as, triple quadrupoles [11] and ion traps [13,14]. While the former provides well established know-how such as neutral loss and product ion scanning, the latter allows MS<sup>n</sup> for structural elucidation. Both analyzers provide nominal mass accuracy. Time-of-flight mass spectrometry (TOF-MS) is another type of mass analyzers that allows the generation of mass information with enhanced accuracy and precision. These accurately measured mass values can then be used to produce candidate empirical formulae which significantly reduce the number of possible structures of target compounds [15–18].

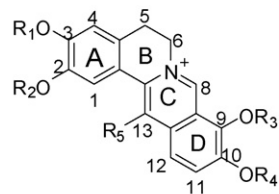
*Corydalis yanhusuo* W.T. Wang is an important kind of TCM with antibacterial, antiviral, and anticancer activities [2]. It has gained ever-increasing popularity in today's world because of its therapeutic effects on promoting blood circulation, reinforcing vital energy, and alleviating pain such as headache, chest pain, epigastric pain, abdominal pain, backache, arthralgia or trauma

\* Corresponding author. Tel.: +86 411 8437 9519; fax: +86 411 8437 9539.

E-mail addresses: [zhangxiuli@dicp.ac.cn](mailto:zhangxiuli@dicp.ac.cn) (X. Zhang), [liangxm@dicp.ac.cn](mailto:liangxm@dicp.ac.cn) (X. Liang).



Tertiary alkaloids	R <sub>1</sub>	R <sub>2</sub>	R <sub>3</sub>	R <sub>4</sub>	R <sub>5</sub>
Corydaline	CH <sub>3</sub>	CH <sub>3</sub>	CH <sub>3</sub>	CH <sub>3</sub>	CH <sub>3</sub>
Tetrahydropalmation	CH <sub>3</sub>	CH <sub>3</sub>	CH <sub>3</sub>	CH <sub>3</sub>	H
Tetrahydrocoptision	-CH <sub>2</sub> -		-CH <sub>2</sub> -		H
Canadine	-CH <sub>2</sub> -		CH <sub>3</sub>	CH <sub>3</sub>	H



Quaternary alkaloids	R <sub>1</sub>	R <sub>2</sub>	R <sub>3</sub>	R <sub>4</sub>	R <sub>5</sub>
Palmation	CH <sub>3</sub>	CH <sub>3</sub>	CH <sub>3</sub>	CH <sub>3</sub>	H
Berberine	-CH <sub>2</sub> -		CH <sub>3</sub>	CH <sub>3</sub>	H
Dehydrocorydaline	CH <sub>3</sub>	CH <sub>3</sub>	CH <sub>3</sub>	CH <sub>3</sub>	CH <sub>3</sub>
Coptision	-CH <sub>2</sub> -		-CH <sub>2</sub> -		H
Columbimine	H	CH <sub>3</sub>	CH <sub>3</sub>	CH <sub>3</sub>	H

Fig. 1. The structure of tertiary and quaternary alkaloids.

[5,19]. *Corydalis yanhusuo* is traditionally and mainly cultivated in Zhejiang province of China as an annual crop using tubers [20]. The tuber contains many tertiary and quaternary alkaloids that are the main bioactive components. The structures of some alkaloids are shown in Fig. 1. However, there are still a lot of alkaloids in the tubers that remain uninvestigated, especially those in the micro, or even trace concentrations, which cannot be easily separated and identified by traditional phytochemistry methods.

A variety of methods have been reported for the determination of tertiary and quaternary alkaloids, HPLC [2], HPLC–MS [11,14,21], etc. Among these techniques, HPLC–MS, especially when coupled with soft ionization source, has become a very powerful tool in the analysis of alkaloids. The mass spectrometric fragmentation behavior of five quaternary alkaloids was investigated by ion trap MS in detail [14]. In a recent work, ten alkaloids from *corydalis yanhusuo* including seven tertiary alkaloids and three quaternary alkaloids were studied and a proposed fragmentation rule has been obtained to facilitate the identification alkaloids in *corydalis yanhusuo* [11].

Ultra-performance liquid chromatography–quadrupole-time-of-flight mass spectrometry (UPLC–Q-TOF-MS) with high sensitivity and resolution has been widely used in the analysis of peptides and proteomic. Its usage in the analysis of compounds in TCMs is still in its early stage [15,22]. This paper exploits high-resolution-and-sensitivity UPLC–Q-TOF to analyze the alkaloids in *corydalis yanhusuo* and attempts to reveal more useful information of this important analgesic TCM. In this work, three standards including one tertiary alkaloid and two quaternary alkaloids were used to establish the mass spectrometry method. This method included protocols to analyze low abundance product ions, characterize the structures of alkaloids in *corydalis yanhusuo*, and identify the accurate structures of the target compounds. Two new alkaloids in *corydalis yanhusuo* were found.

## 2. Experimental

### 2.1. Materials and chemicals

Acetonitrile (HPLC grade) was purchased from Merck (Germany); Formic acid was purchased from J&K CHEMICA (USA); water was purified by a Milli-Q system (Millipore, Billerica, MA, USA). Other solvents and chemicals were purchased from Shenyang Chemical Engineering Factory (Shenyang, China). The standards of tetrahydropalmatine, berberine and palmatine were purchased from the National Institute for the Control of Pharmaceutical and Biological Products (Beijing, China).

### 2.2. Instruments and methods

UPLC/Q-TOF-MS analysis was performed with a Waters Acquity UPLC coupled with a Q-TOF Premier, a quadrupole and orthogonal acceleration time-of-flight tandem MS (Waters Co., UK), which was equipped with the LockSpray and ESI interface. This system was operated under MassLynx 4.1 software (Waters Co., USA).

Chromatography was performed using a Waters ACQUITY UPLC system, equipped with a binary solvent delivery system, an autosampler, and a tunable UV detector. The chromatographic column used was Waters ACQUITY BEH C18 (100 mm × 2.1 mm i.d., 1.7 μm). Chromatography was carried out in gradient mode. The elution system consisted of acetonitrile (A) and 0.5% formic acid aqueous solution (B). The gradient was: 0–10 min, 20%A–30%A.

The mass spectrometry was performed on a Q-TOF system (Waters Co., UK). The Q-TOF instrument was operated in V mode, for MS experiments, with the TOF data being collected between *m/z* 100 and 1000. The optimized conditions were desolvation gas 800 L/h at a temperature of 350 °C, cone gas 50 L/h, and source temperature 120 °C, capillary and cone voltages 3 kV and 40 V, respectively. The TOF mass spectrometer was calibrated routinely in

the positive electrospray ionization (ESI<sup>+</sup>) mode using the solution of Fibrinopeptide B. Data were centralized during acquisition using independent reference lock-mass ions via the Lock Spray interface to ensure mass accuracy and reproducibility. The solution of Leucine enkephalin (Sigma Chemical Co.) was used as lock-mass, with an [M+H]<sup>+</sup> ion of *m/z* 556.2771. The MS/MS experiments were performed using a variable collision energy (10–30 eV), which was optimized for each individual compound. The LockSpray frequency was set at 15 s. The accurate mass and composition for the precursor and fragment ions were calculated using the MassLynx 4.1 software incorporated in the instrument.

### 2.3. Plant material and sample preparation

*Corydalis yanhusuo* was collected from Dongyang County (Zhejiang, China). The herb was authenticated by Institute of Medication, Xiyuan Hospital of China Academy of Traditional Chinese Medicine. The extraction was performed by Mai-DiHai Pharmacy (China). The procedure was as follows: 10 kg herb was grounded into powder and decocted in 100 L of water at 100 °C for 120 min. Then the residue was collected and re-decocted in 100 L of water at 100 °C for 90 min. The decoctions were collected at both times and dried by spray drying. Then, 0.15 kg of extract was dissolved in 1.5 L of water/ethanol 30:70 (v/v) and the solution was extracted in 0.75 L of ethyl acetate for three times. Residual was extracted in 0.75 L of *n*-butanol. Repeating the extracted process again, the fraction of *n*-butanol was collected and dried with a rotary evaporator at 60 °C. An aliquot of *n*-butanol fraction was dissolved in methanol and filtered through 0.22 μm membranes for analysis.

## 3. Results and discussion

### 3.1. Finding potential alkaloids by UPLC-Q-TOF with screening table

The major problem with the analysis of alkaloids is that the interaction of basic alkaloids with anionic silanol functional groups results in strong peak tailing. Several strategies were commonly applied to solve the problem. For example, buffer solution and ion

pair reagents were possible ways to avoid these interactions [23]. But these methods were complex, expensive, and unable to be combined with mass spectrometry directly. In this study, the usage of ACQUITY BEH C18, porous hybrid organic–inorganic silicon-based particles with a narrow size distribution around 1.7 μm, was observed to be able to avoid the interaction mentioned above and thus without the addition of salts or ion pair reagents, the alkaloids got good separation on ACQUITY BEH C18 column as shown in Fig. 2, in which every peak width is less than 0.2 min. In addition, the mobile phase shown in experiments make this UPLC analysis method can easily coupled with MS.

In order to systematically characterize the alkaloids in *corydalis yanhusuo*, a screening table was designed. In *corydalis yanhusuo*, the main alkaloids are tertiary and quaternary alkaloids. The basic skeleton of tertiary and quaternary alkaloids was used to construct the screening table for alkaloids by adding the substitute groups. The basic skeleton of tertiary and quaternary alkaloids has two molecular weights 235 and 232 which are shown in Fig. 1. According to the literature, the main substitute groups were methylenedioxy, hydroxyl, methoxyl and methyl. The number of substitute group was limited to 2, 1, 4 and 1, respectively. The substitution sites were 2, 3, 9, 10, 5 and 13. For the methylenedioxy group needs two neighbor substitute sites, the substitute sites were 2 and 3 or 9 and 10. According to the characteristic of the alkaloids in *corydalis yanhusuo*, the methylenedioxy and methoxyl groups were never connected to the position 5 or 13 as well as we have known. On the basis of this condition, the screening table was finished (Table 1). In this table, the first, second, and third columns were designed for the tertiary alkaloids while the ninth, tenth, and eleventh were for the quaternary alkaloids. According to the literature, the substitute group in the position 5 is hydroxyl, methyl, or nothing. We can suppose the substitute group one by one in the design of the screening table. If position 5 did not have any substitute group, then the third and ninth columns would be designed for the tertiary and quaternary alkaloids by arranging the substitute groups at five substitution sites of two basic skeletons, respectively. Similarly, if the methyl or hydroxyl was connected to position 5, then the first and second columns would be designed for the tertiary alkaloids, respectively, and the ninth and tenth columns would be

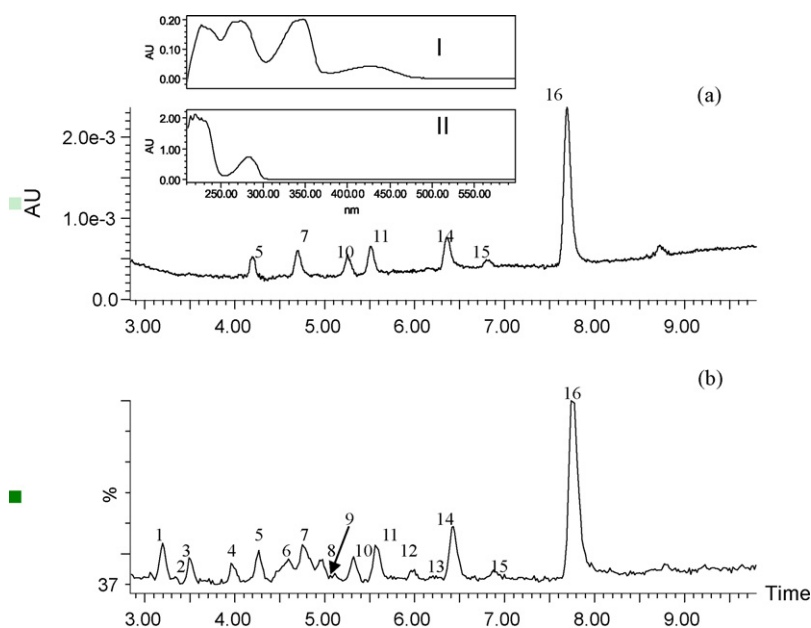


**Fig. 2.** The UPLC–Q-TOF–MS analysis chromatogram. (a) The UPLC analysis chromatogram (I) the characteristic spectrum of quaternary alkaloids (II) the characteristic spectrum of tertiary alkaloids. (b) The total ion chromatogram; conditions: ACQUITY UPLCTM BEH C18 (1.7 μm, 100 mm × 2.1 mm i.d.); mobile phase: A acetonitrile; B water with 0.5% formic acid; gradient: from 20%A to 30%A in 10 min.

**Table 1**  
The screening table of tertiary and quaternary alkaloids.

Tertiary alkaloids			CH <sub>2</sub> O <sub>2</sub> (+44) <sup>b</sup>	–OCH <sub>3</sub> (+30) <sup>c</sup>	–OH (+16) <sup>c</sup>	–CH <sub>3</sub> (+14) <sup>c</sup>	H (+0)	Quaternary alkaloids		
[M+H] <sup>+</sup> (5-CH <sub>3</sub> ) 249 <sup>a</sup>	[M+H] <sup>+</sup> (5-OH) 251 <sup>a</sup>	[M+H] <sup>+</sup> (5-H) 235 <sup>a</sup>						[M] <sup>+</sup> (5-CH <sub>3</sub> ) 246 <sup>a</sup>	[M] <sup>+</sup> (5-OH) 248 <sup>a</sup>	[M] <sup>+</sup> (5-H) 232 <sup>a</sup>
(370)	372	356	1	2	1	0	0	(366)	368	352
–	370	354	1	2	0	1	0	–	366	350
(354)	356	340	1	2	0	0	1	(350)	352	336
354	356	340	2	0	1	0	0	350	352	336
–	354	(338)	2	0	0	1	0	–	350	334
–	340	324	2	0	0	0	1	(334)	336	320
–	342	326	1	0	2	1	0	–	338	322
(326)	(328)	312	1	0	2	0	1	(322)	324	308
–	326	310	1	0	1	1	1	–	322	306
(310)	312	(296)	1	0	1	0	2	(306)	308	(292)
–	310	(294)	1	0	0	1	2	–	306	(290)
(356)	(358)	342	1	1	2	0	0	(352)	354	338
–	356	340	1	1	1	1	0	–	352	336
(340)	342	326	1	1	1	0	1	(336)	338	322
–	340	324	1	1	0	1	1	–	336	320
(324)	326	310	1	1	0	0	2	(320)	322	306
(386)	(388)	372	0	4	1	0	0	(382)	(384)	368
–	386	370	0	4	0	1	0	–	382	366
–	372	356	0	4	0	0	1	366	368	352
(372)	(374)	(358)	0	3	2	0	0	(368)	370	354
–	372	356	0	3	1	1	0	–	368	352
356	358	342	0	3	1	0	1	(352)	354	338
–	356	340	0	3	0	1	1	–	352	336
340	342	326	0	3	0	0	2	336	338	322
–	358	342	0	2	2	1	0	–	354	338
(342)	(344)	328	0	2	2	0	1	338	340	324
–	342	326	0	2	1	1	1	–	338	322
(326)	328	312	0	2	1	0	2	322	324	308
–	328	312	0	1	2	1	1	–	324	308
(312)	(314)	298	0	1	2	0	2	(308)	310	294
–	312	296	0	1	1	1	2	–	308	292
–	(298)	(282)	0	0	2	1	2	–	294	(278)

The molecular weight in brackets is the repeated ones in the table.

<sup>a</sup> 235, 232 is the *m/z* value of tertiary alkaloids and quaternary alkaloids without any substitute group, respectively. 249, 251 is the *m/z* of tertiary alkaloids with the methyl, hydroxyl connecting to the substitute site 5, respectively. 246, 248 is the *m/z* of quaternary alkaloids with the methyl, hydroxyl connecting to the substitute site 5, respectively.

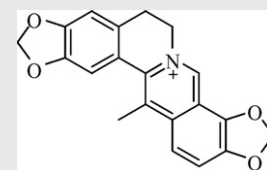
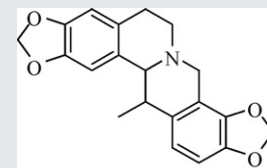
<sup>b</sup> (+44) is the molecular weight of methylenedioxy subtract the molecular weight of two hydrogens for the two substitute sites in the basic skeleton.

<sup>c</sup> (+30), (+16), (+14) is the molecular weight of methoxy, hydroxyl and methyl subtract the molecular weight of one hydrogen for the one substitute site in the basic skeleton, respectively.



**Table 2**  
retention time(RT), MS data, UV  $\lambda_{\max}$  and elemental composition of the target compounds screened out by the screening table.

Peak number	RT (min)	[M+H] <sup>+</sup> (m/z)	Empirical formula	UV $\lambda_{\max}$ (nm)	ESI-MS/MS (m/z)	Identification
1	3.2	356.184	C <sub>21</sub> H <sub>26</sub> NO <sub>4</sub>	232	192.1028	Tertiary alkaloid
2	3.52	356.1854	C <sub>21</sub> H <sub>26</sub> NO <sub>4</sub>	283	177.0784	Tertiary alkaloid
3	3.35	356.1852	C <sub>21</sub> H <sub>26</sub> NO <sub>4</sub>	231	192.1028	Tertiary alkaloid
4	3.97	354.1326	C <sub>20</sub> H <sub>20</sub> NO <sub>5</sub>	280	177.0784	Tertiary alkaloid
5	4.27	338.1372	C <sub>20</sub> H <sub>20</sub> NO <sub>4</sub>	231	192.1034 (RDA-tetrahydroisowuinolin)	Tetrahydropalmatine
6	4.58	370.1664	C <sub>21</sub> H <sub>24</sub> NO <sub>5</sub>	286	177.0789 (RDA-benzene-ring)	Tertiary alkaloid
7	4.75	320.0916	C <sub>19</sub> H <sub>14</sub> NO <sub>4</sub>	231	188.0713, 149.0594	Tertiary alkaloid
8	4.84	370.2005	C <sub>22</sub> H <sub>28</sub> NO <sub>4</sub>	234	322.1089, 323.1152, 320.0909, 308.0936, 294.1134	Quaternary alkaloid
9	5.12	338.139	C <sub>21</sub> H <sub>24</sub> NO <sub>5</sub>	276	322.1063, 308.0950	Quaternary alkaloid
10	5.32	352.1538	C <sub>21</sub> H <sub>22</sub> NO <sub>4</sub>	267	294.1149, 279.0907	Quaternary alkaloid
11	5.56	352.1537	C <sub>21</sub> H <sub>22</sub> NO <sub>4</sub>	352	318.0760 [M-2H] <sup>+</sup>	Coptisine
12	5.96	354.1707	C <sub>21</sub> H <sub>24</sub> NO <sub>4</sub>	455	292.0951 [M-CO] <sup>+</sup>	Coptisine
13	6.20	334.1075	C <sub>20</sub> H <sub>16</sub> NO <sub>4</sub>	267	290.0818 [M-2H-CO] <sup>+</sup>	Corydaline
14	6.4	352.1534	C <sub>21</sub> H <sub>22</sub> NO <sub>4</sub>	232	262.0864 [M-2H-2CO] <sup>+</sup>	Corydaline
15	6.88	336.123	C <sub>20</sub> H <sub>18</sub> NO <sub>4</sub>	280	207.1200 (RDA-tetrahydroisowuinolin)	Corydaline
16	7.74	366.1675	C <sub>22</sub> H <sub>24</sub> NO <sub>4</sub>	234	191.0955 (RDA-benzene-ring)	Corydaline
17				234	190.0841 (RDA-tetrahydroisowuinolin)	
18				268	149.0612 (RDA-benzene-ring)	
19				234	337.1306	Quaternary alkaloid
20				263	336.1220	Quaternary alkaloid
21				340	322.1085	Quaternary alkaloid
22				437	308.1253	Quaternary alkaloid
23				234	336.1225	Quaternary alkaloid
24				268	337.1286	Quaternary alkaloid
25				342	322.1084	Quaternary alkaloid
26				440	308.1295	Quaternary alkaloid
27				234	190.0863, 188.0733	Tertiary alkaloid
28				278		Tertiary alkaloid
29				234	332.0651 [M-2H] <sup>+</sup>	
30				274	306.0962 [M-CO] <sup>+</sup>	
31				346	304.0816 [M-2H-CO] <sup>+</sup>	
32				427	276.0861 [M-2H-2CO] <sup>+</sup>	
33				234	336.1233 [M-CH <sub>3</sub> -H] <sup>+</sup>	
34				274	337.1286 [M-CH <sub>3</sub> ] <sup>+</sup>	
35				346	322.1086 [M-2CH <sub>3</sub> ] <sup>+</sup>	
36				427	320.1259 [M-2CH <sub>3</sub> -2H] <sup>+</sup>	
37					308.1293 [M-CH <sub>3</sub> -H-CO] <sup>+</sup>	
38					294.1135 [M-2CH <sub>3</sub> -CO] <sup>+</sup>	
39				234	321.0995 [M-CH <sub>3</sub> ] <sup>+</sup>	
40				264	320.0958 [M-CH <sub>3</sub> -H] <sup>+</sup>	
41				347	306.0749 [M-2CH <sub>3</sub> ] <sup>+</sup>	
42				427	292.0967 [M-CH <sub>3</sub> -H-CO] <sup>+</sup>	
43					278.0699 [M-2CH <sub>3</sub> -CO] <sup>+</sup>	
44				231	351.1452 [M-CH <sub>3</sub> ] <sup>+</sup>	
45				264	350.1381 [M-CH <sub>3</sub> -H] <sup>+</sup>	
46				337	336.1241 [M-2CH <sub>3</sub> ] <sup>+</sup>	
47				418	334.1442 [M-2CH <sub>3</sub> -2H] <sup>+</sup>	
48					322.1432 [M-CH <sub>3</sub> -H-CO] <sup>+</sup>	
49					308.1299 [M-2CH <sub>3</sub> -CO] <sup>+</sup>	



designed for the quaternary alkaloids, respectively. In the screening table, the blank means the designed structures were repeated. The molecular weights in brackets represent this molecular weight was repeated in the table. Finally, there were 160 compound structures

with 40 molecular weights in this screening table. On the basis of the MS data and the screening table, 16 alkaloids were selected out (Table 2). Eight of them were quaternary alkaloids while the other eight were tertiary alkaloids.

Before being distinguished by MS, quaternary and tertiary alkaloids can firstly be classified by UV spectrum. As shown in Fig. 2, the alkaloids have two different UV absorption spectrum types. One type has four maximum wavelengths and the other has two which response to quaternary and tertiary alkaloid by comparing with the standards, respectively. Moreover, it is interesting to note that several compounds have the same molecular weight but different retention time. Namely, many isomeric compounds exist in *corydalis yanhusuo*. For example, peaks 10, 11, and 14 own the same  $m/z$  value (352) but varied retention time (5.32, 5.56, and 6.40, respectively). From the UV absorption spectrum, peaks 11 and 14 were categorized to quaternary alkaloids while peak 10 to tertiary alkaloids. Although the basic skeleton can be determined according to the UV absorption spectrum, it is difficult to characterize the accurate structure when it is only based on the full scan MS data. A further Q-TOF-MS/MS analysis should be taken for the structure analysis of these compounds.

### 3.2. Structure characterization of the alkaloids by Q-TOF

In this work, three standards were used to study the MS fragmentation mechanism. Tetrahydropalmatine is a tertiary alkaloid while berberine and palmatine belong to quaternary alkaloids. The ESI-MS/MS spectrums of these three compounds were shown in Fig. 3.

In MS/MS of tetrahydropalmatine (Fig. 3a), the predominant ion appeared at  $m/z$  192.1007, which corresponds to the Retro-Diels-Alder (RDA) fragmentation reaction of c-ring opening. Two fragment ions were obtained from the part of tetrahydroisowuinolin and benzene-ring at  $m/z$  192.1007 and 165.0915, respectively, which is in agreement with the literature [11]. It is also the characteristic fragmentation pathway for the tertiary alkaloids. Furthermore, the interesting fragment ions observed at  $m/z$  150.0685 and 177.0797 correspond to the elimination of the methyl radical of the benzene-ring and tetrahydroisowuinolin, respec-

tively. The fragmentation pathway was shown in dashed line frame in Fig. 4.

In MS/MS of berberine and palmatine (Fig. 3b and c), the mass spectrum pattern is quite different from the tertiary alkaloids. It is difficult to open the ring for the conjugate plane structure of quaternary alkaloids, thus there is no RDA fragmentation reaction. The fragment ion was produced by the loss of small groups from the compounds as shown in Fig. 5. The predominant ion appeared at  $m/z$  336.1232 for palmatine, which corresponds to the loss of methyl and H radicals. The ion at  $m/z$  337.1301 was determined as the neutral loss of the methyl radical group. In addition, the ion at  $m/z$  322.1084 was observed for the loss of two methyl radicals from the ion at  $m/z$  337.1301. Then, the ion at  $m/z$  308.1294 and  $m/z$  294.1105 was formed by the neutral elimination of CO fragment from the ion at  $m/z$  336.1232 and 322.1084, respectively. The fragmentation pathway of berberine is similar to that of palmatine, all of them are in agreement with the literature [14]. It is the characteristic MS/MS spectrum pattern for quaternary alkaloids.

In this study, low abundance product ions of alkaloids, which were always neglected in the previous study, were firstly paid much attention. Compared the magnified MS/MS spectrum of tetrahydropalmatine with that of palmatine in Fig. 3, it is interesting to note that some fragment ions occurred in both spectrums, such as  $m/z$  308.1342, 322.1434. This indicated that tetrahydropalmatine may have two fragment pathways: RDA reaction and the similar way as palmatine. According to the  $m/z$  value of fragment, the fragment pathway of tetrahydropalmatine was deduced as shown in Fig. 4. In the magnified MS/MS spectrum of tetrahydropalmatine, the ion at  $m/z$  341.1615 was observed by the loss of methyl radical. Then, the ion at  $m/z$  326.1399 and  $m/z$  340.1551 were formed by the neutral elimination of CO fragment and H radical from the ion at  $m/z$  341.1615, respectively. Also the ion at  $m/z$  312.1544 was formed by the neutral elimination of CO fragment from the ion at  $m/z$  340.1551. This fragmentation pathway is similar to palmatine. In the process of forming the fragments, the whole molecular structure tends to turn into a more stable state. For example, the ion at

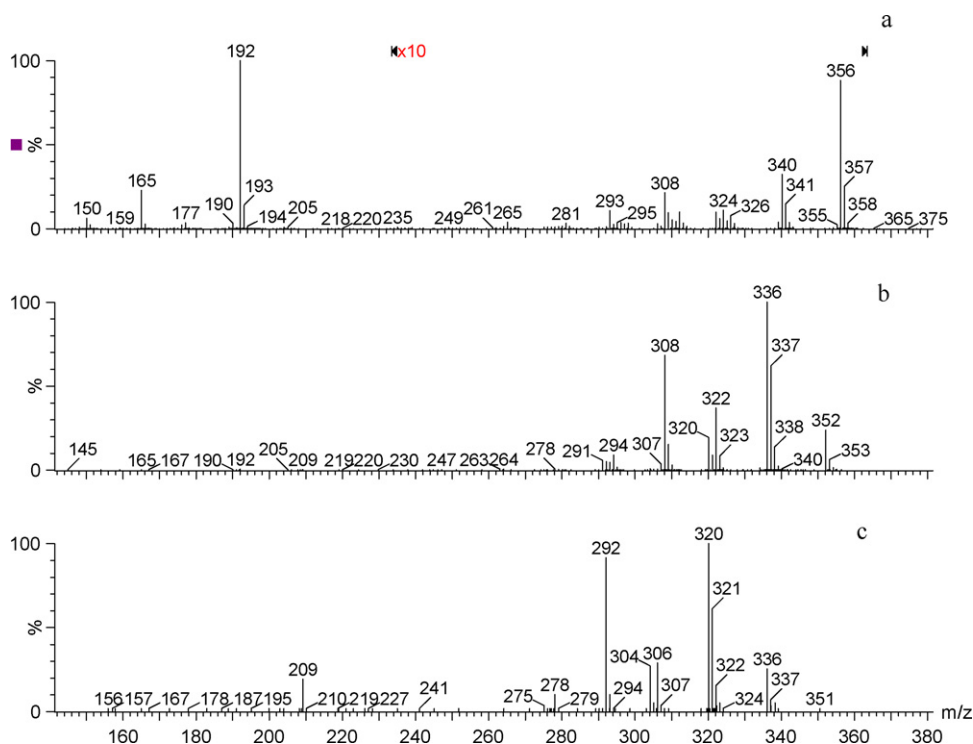


Fig. 3. ESI-MS/MS spectrums of (a) tetrahydropalmatine, (b) palmatine and (c) berberine.

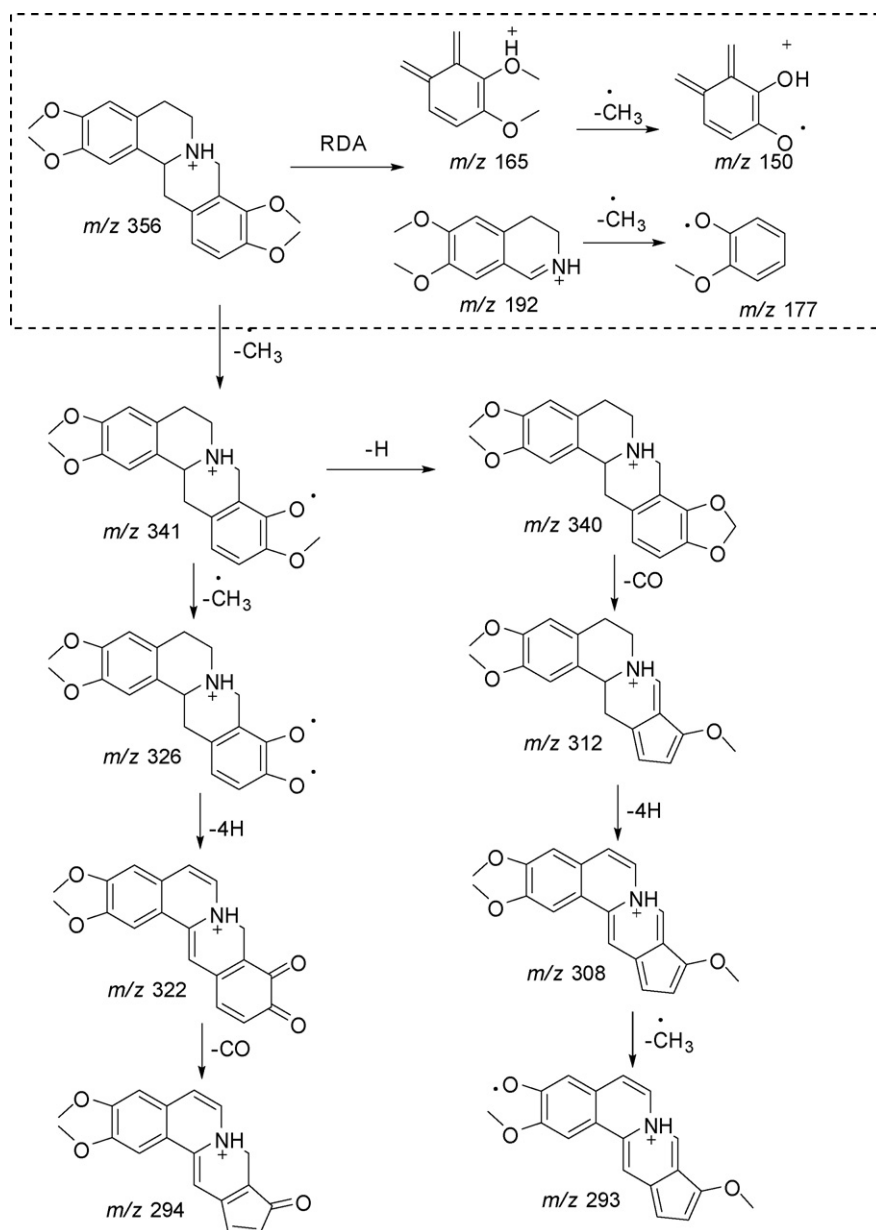


Fig. 4. Fragmentation pathway of tetrahydropalmatine.

$m/z$  322.1434 was formed by means of the loss of four hydrogens from the ion at  $m/z$  326.1399 to reach a more stable state of a conjugated structure. Similarly, the ion at  $m/z$  308.1342 corresponds to the loss of four hydrogens from the ion at  $m/z$  312.1544. These two fragment ions were exactly the same as the fragments of palmatine. Then, the ion at  $m/z$  294.1105 was formed by the neutral elimination of CO fragment from the ion at  $m/z$  322.1434, which was also included in the fragments of palmatine. All information showed that a tertiary alkaloid had the similar fragmentation behavior as its corresponding quaternary alkaloids, which helps to identify the accurate structure of the alkaloids.

In the extract sample of *corydalis yanhusuo*, sixteen target compounds were obtained by the screening study using the full scan mode (Table 2). The characterization of the target compounds was performed by Q-TOF using the CID mode. From the MS/MS spectrum, there were two different patterns. One is similar to tetrahydropalmatine, which has RDA fragmentation reaction, and the other is similar to berberine and palmatine, which the predominant ion is in the relatively high  $m/z$  value section. This result is

in agreement with the UV characterization. Although the structural framework and substitute groups can be decided, the accurate structure of the alkaloids is difficult to determine because of the uncertain connecting position. However, based on the screening results, empirical formula, fragmentation pathway and literature data, the structures of 8 compounds were finally identified. The rest needed to be further investigated.

In order to determine the structure of each compound, the UV absorption spectrum pattern and ESI-MS/MS spectrum pattern were taken to decide which kind of alkaloids the compounds belonged to. Then the MS/MS data was used for further investigation. Take peak 7 for example, the UV absorption and MS/MS spectrums were similar to the quaternary alkaloids. The predominant ion appeared at  $m/z$  292.0951, which corresponds to the loss of a neutral CO fragment. The ion at  $m/z$  318.0760 was found in this experiment corresponding to the loss of two hydrogens for the stable state of a conjugated structure. Then, the ion at  $m/z$  290.0818 was formed by the subsequent neutral loss of CO fragment from the ion at  $m/z$  318.0760. And a further ion at  $m/z$  262.0864 was formed

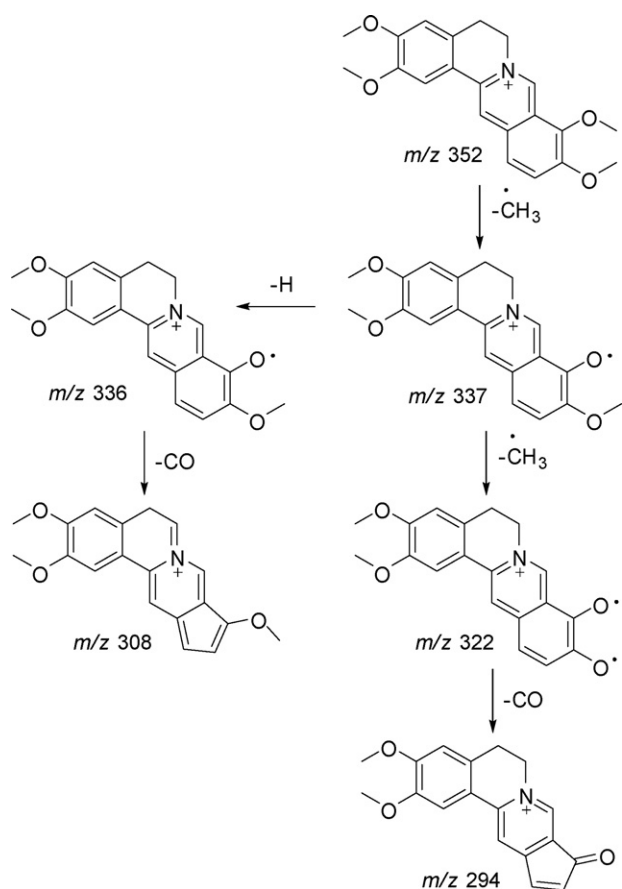


Fig. 5. Fragmentation pathway of palmatine.

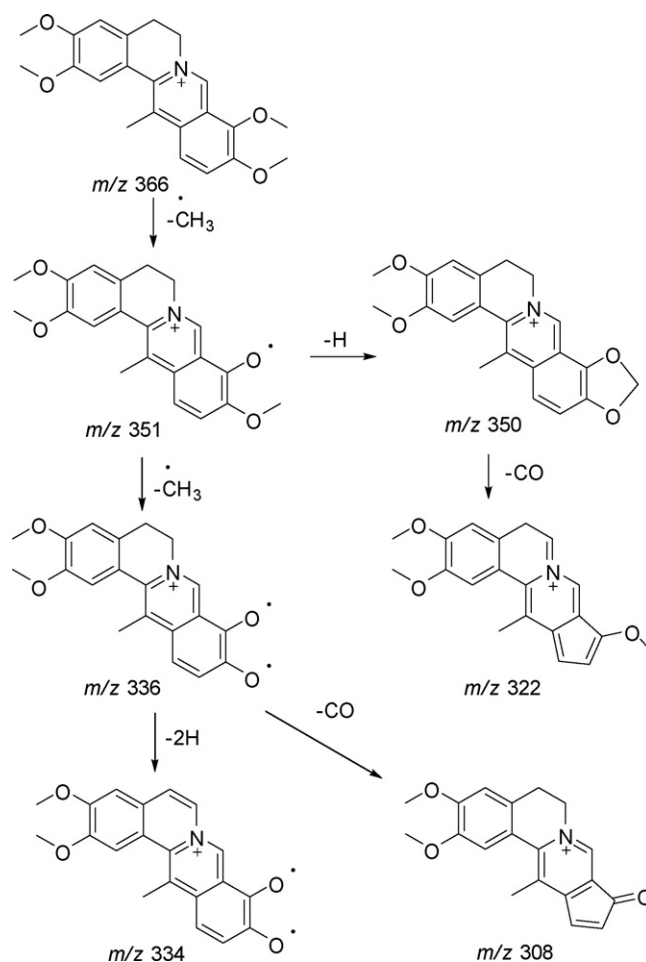


Fig. 7. Fragmentation pathway of peak 16.

by another neutral loss of CO fragment from the ion at  $m/z$  290.0818. Compared to the literature [14], this compound was identified as coptisine.

The accurate molecular weight afforded by the Q-TOF is valuable information for the accurate structure determination. For example,  $m/z$  366 of peak 16 have four different positions in screening table, including M-5-CH<sub>3</sub> (line 1), M-5-OH (line 2), M-5-H (line 18), M-5-CH<sub>3</sub> (line 19), which meant that it will be very difficult to determine the structure of peak 16th with  $m/z$  366 only depending on the screening table. Basing on the accurate molecular weight afforded

by TOF, the empirical formula of peak 16th was C<sub>22</sub>H<sub>24</sub>NO<sub>4</sub>, in which the number of oxygen molecular in the compound was four. So, there were two possible structures left for the further investigation. Then we investigate the MS/MS fragments of peak 16th by Q-TOF. In the MS/MS data (Fig. 6b), the ion at  $m/z$  351.1452 corresponds to the loss of methyl radical and the ion at  $m/z$  350.1381 formed by the loss of methyl and H radicals. In addition, the ion at  $m/z$  336.1241 was also observed for the elimination of two methyl

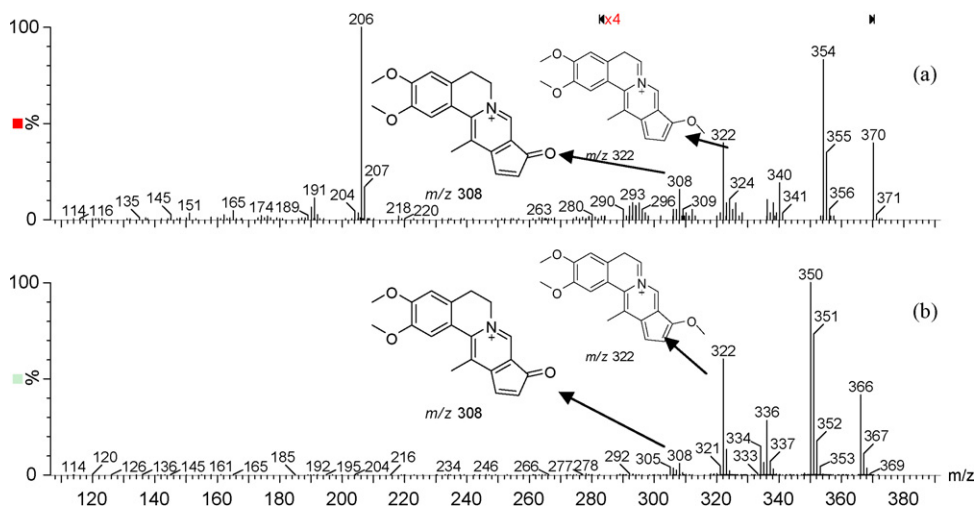


Fig. 6. ESI-MS/MS spectrums of peak 8 (a) and peak 16 (b).

radicals. Furthermore, the ions at  $m/z$  336.1241 and  $m/z$  350.1381 undergo subsequent neutral loss of CO fragment to form the ions at  $m/z$  308.1299 and  $m/z$  322.1432, respectively. The fragmentation pathway as shown in Fig. 7 is similar to palmatine. It is noted that the difference  $m/z$  value of the corresponding fragments of these two compounds was 15 Da. Therefore, it can be deduced that the H in palmatine was replaced by methyl to form the compound structure of peak 16. If the methyl group was connected to C-5, the methyl group would be easily eliminated for the more stable state of a conjugated structure, so the ion at  $m/z$  350.1381 would not be found [14]. So, the methyl group was connected to C-13, this compound was identified as dehydrocorydaline.

The fragment behavior similarity of tertiary alkaloids and its corresponding quaternary alkaloids in the relatively high  $m/z$  value section was useful in the structure identification. For example, peak 8 was a tertiary alkaloid according to the characteristic UV absorption spectrum and the characteristic MS/MS spectrum type. In screening table, there were three different positions, including M+H-5-CH<sub>3</sub> (line 1), M+H-5-OH (line 2), M+H-5-H (line 18). The

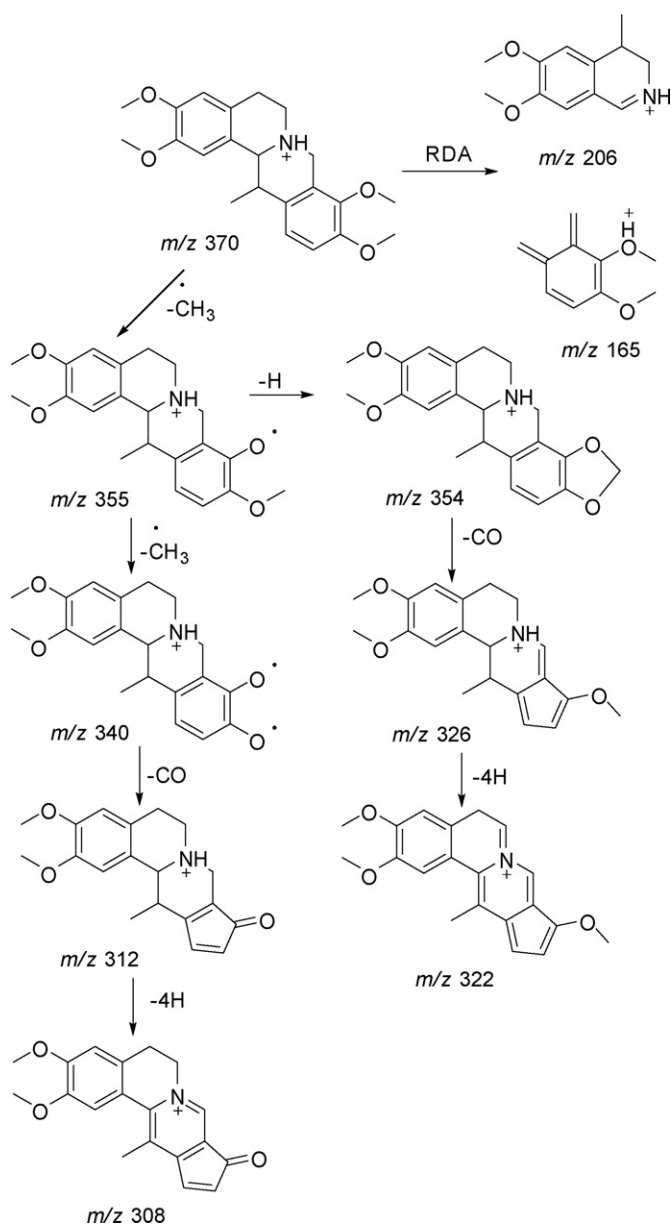


Fig. 8. Fragmentation pathway of peak 8.

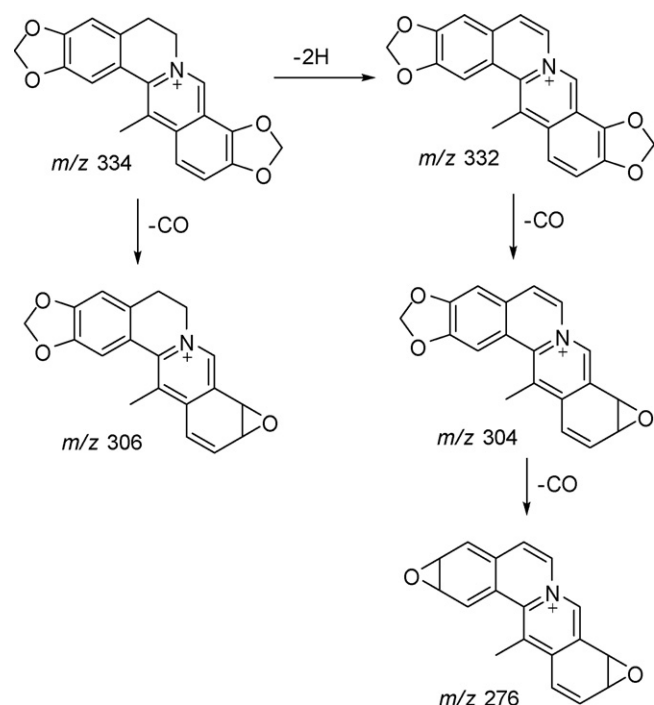


Fig. 9. Fragmentation pathway of peak 13.

empirical formula of peak 8th was C<sub>22</sub>H<sub>28</sub>NO<sub>4</sub>, in which the number of oxygen molecular in the compound was four. So this compound could be identified as corydaline. Corydaline was the corresponding tertiary alkaloids of dehydrocorydaline. Then, take a close look at the MS/MS data from  $m/z$  280 to 370 of peaks 8 and 16 (Fig. 6), it was noted that some fragment ions occurred in both spectrometry, such as  $m/z$  308.1280, 322.1434. This displayed the fragment behavior similarity between corydaline and dehydrocorydaline which was similar to that of the tetrahydropalmatine and palmatine we have investigated above. And it got fine mutual verification. The fragmentation pathway was shown in Figs. 7 and 8 for peaks 16 and 8.

Because of the screening methods, some minor peaks were also identified in this work. For example, peaks 9 and 13 were two minor peaks no matter from the UV spectrum or MS spectrum (Fig. 2). The basic skeleton of these two compounds can be easily determined according to the characteristic UV absorption spectrum and the characteristic MS/MS spectrum type. Peak 9 was a kind of tertiary alkaloid with  $m/z$  338 and peak 13 was a quaternary alkaloid with  $m/z$  334 (Table 2). From the screening table, there were two methylenedioxy groups and one methyl in these two structures. The two methylenedioxy groups were connected to the position 2, 3 and 9, 10. The methyl group might be connected to position 5 or 11. For peak 9, the basic skeleton was a symmetrical structure. Moreover, in the MS/MS data, the ion at  $m/z$  190.0841 corresponds to the RDA fragmentation reaction of the c-ring opening which was the characteristic fragment of tertiary alkaloid. So, the structure of this compound was easily identified as shown in Table 2. For peak 13, it was not a symmetrical structure. The methyl group could be connected to C-5 or C-13, which meet two different compounds. However, if the methyl group was connected to C-5, the ion at  $m/z$  332.0651 would not be found for the formation of the more stable state of a conjugated structure. So, the methyl group in peak 13 was connected to C13 and the structure of peak 13 was identified as shown in Table 2. The fragmentation pathway was shown in Fig. 9 for peak 13. These two compounds were found in *corydalis yanhusuo* for the first time.

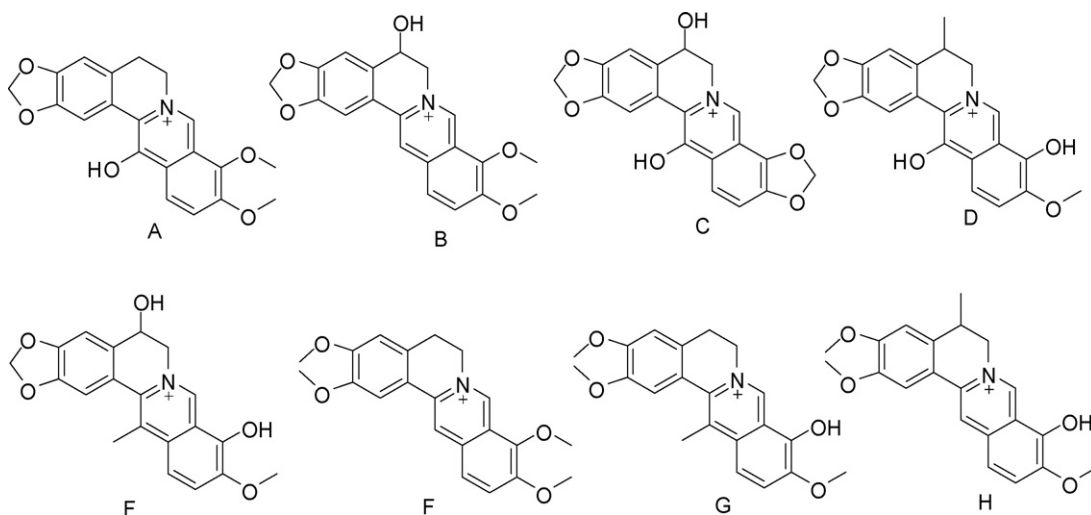


Fig. 10. Eight compounds which has the  $m/z$  value of 352, were screened out by the screening table.

Although sometimes it is difficult to obtain the accurate structure only based on the MS data in the process to determine the structure, a possible structure can be obtained using this method. Take  $m/z$  352 for example, there were eight possible compounds with different number of substitutes and different substitute sites (Fig. 10) based on the screening table. The experiments data showed that the empirical formula was  $C_{21}H_{22}NO_4$  which mean the number of oxygen molecular in the compounds was four. So, the compounds of F, G and H were left for further investigation. Compared to the standard, the  $m/z$  352 eluting at 6.43 min was identified as palmatine. As to the other two compounds, the substitute site of methyl can be determined by the MS/MS data which is similar to peak 16. For the changeable of the substitute site of the hydroxyl, it is difficult to identify the accurate structure solely on MS data.

In this method, UPLC–Q–TOF–MS/MS is used for the better resolution and valuable information (MS/MS data, accurate mass, empirical formula). Taking full use of the literature data and combining the characteristic of each compound, this method is effective for the identification of compounds, especially for complex samples.

#### 4. Conclusion

UPLC–Q–TOF–MS proved to be an effective method for the structure characterization and identification of alkaloids in *corydalis yanhusuo*. The fragmentation mechanism of tetrahydropalmatine, berberine and palmatine was investigated in this work. The considerable fragmentation information obtained by MS/MS is very useful for the structure elucidation. The low abundance product ions obtained before RDA reaction of tetrahydropalmatine were studied and compared with palmatine. The results showed the fragmentation behavior similarity between tertiary alkaloids and its corresponding quaternary alkaloids. It will be very useful in the structure identification of alkaloids. According to the screening table, 16 alkaloids were screened out finally. The characteristic UV absorption and tandem mass spectrum were combined to identify the accurate structure of the target compounds. Moreover,

TOF–MS is able to give useful information for the accurate structure determination like accurate molecular weight, empirical formula. Finally, eight compounds were identified in this work.

#### Acknowledgement

This work was supported by “Project of International Cooperation Plan from Ministry of Science and Technology of China (20071816)”.

#### References

- [1] Z.D. Zhai, Y.P. Shi, X.M. Wu, X.P. Luo, *Anal. Bioanal. Chem.* 384 (2006) 939.
- [2] J.J. Ou, L. Kong, C.S. Pan, X.Y. Su, X.Y. Lei, H.F. Zou, *J. Chromatogr. A* 1117 (2006) 163.
- [3] L. Dhooghe, K. Mesia, E. Kohtala, L. Tona, L. Pieters, A.J. Vlietinck, S. Apers, *Talanta* 76 (2008) 462.
- [4] Z.H. Cheng, T.L. Guo, H.Y. Wang, G.Q. Chen, *J. Nat. Med.* 2 (2004) 99.
- [5] Z.H. Cheng, Y.L. Guo, H.Y. Wang, G.Q. Chen, *Anal. Chim. Acta* 555 (2006) 269.
- [6] J.J. Liu, B. Chen, S.Z. Yao, *Talanta* 71 (2007) 668.
- [7] L.L. Ren, X.Y. Xue, F.F. Zhang, Q. Xu, X.M. Liang, *J. Sep. Sci.* 30 (2007) 833.
- [8] Y. Bitar, U. Holzgrabe, *Electrophoresis* 28 (2007) 2693.
- [9] C.W. Chiu, H.H. Liang, H.Y. Huang, *Electrophoresis* 28 (2007) 4220.
- [10] M. Humam, S. Bieri, L. Geiser, O. Munoz, J.L. Veuthey, P. Christen, *Phytochem. Anal.* 16 (2005) 349.
- [11] B. Ding, T.T. Zhou, G.R. Fan, Z.Y. Hong, Y.T. Wu, *J. Pharm. Biomed. Anal.* 45 (2007) 219.
- [12] T. Mroczek, K. Ndjoko, K. Glowinski, K. Hostettmann, *J. Chromatogr. A* 1056 (2004) 91.
- [13] Y. Jin, Y.S. Xiao, F.F. Zhang, X.Y. Xue, Q. Xu, X.M. Liang, *J. Pharm. Biomed. Anal.* 46 (2008) 418.
- [14] D.W. Wang, Z.Q. Liu, M.Q. Guo, S.Y. Liu, *J. Mass. Spectrom.* 39 (2004) 1356.
- [15] E.C.Y. Chan, S.L. Yap, A.J. Lau, P.C. Leow, D.F. Toh, H.L. Koh, *Rapid Commun. Mass Spectrom.* 21 (2007) 519.
- [16] H. Kawanishi, T. Toyooka, K. Ito, M. Maeda, T.I. Hamada, T. Fukushima, M. Kato, S. Inagaki, *J. Chromatogr. A* 1132 (2006) 148.
- [17] Y. Pico, M.L. Farre, C. Soler, D. Barcelo, *J. Chromatogr. A* 1176 (2007) 123.
- [18] R. Plumb, J. Castro-Perez, J. Granger, I. Beattie, K. Joncour, A. Wright, *Rapid Commun. Mass Spectrom.* 18 (2004) 2331.
- [19] H.L. Li, W.D. Zhang, R.H. Liu, C. Zhang, T. Han, X.W. Wang, X.L. Wang, J.B. Zhu, C.L. Chen, *J. Chromatogr. B* 831 (2006) 140.
- [20] H.Y. Ling, L.M. Wu, L. Li, *Phytother. Res.* 20 (2006) 448.
- [21] X.B. Luo, B. Chen, S.Z. Yao, *Talanta* 66 (2005) 103.
- [22] C.M. Li, X.Y. Xue, F.F. Zhang, Q. Xu, X.M. Liang, *Rapid Commun. Mass Spectrom.* 22 (2008) 1941.
- [23] M. Ganzera, C. Lanser, H. Stuppner, *Talanta* 66 (2005) 889.



# Combination of $\beta$ -elimination and liquid chromatography/quadrupole time-of-flight mass spectrometry for the determination of O-glycosylation sites

Yufang Zheng<sup>a</sup>, Zhihong Guo<sup>b</sup>, Zongwei Cai<sup>a,\*</sup>

<sup>a</sup> Department of Chemistry, Hong Kong Baptist University, Kowloon Tong, Kowloon, Hong Kong SAR, PR China

<sup>b</sup> Department of Chemistry, The Hong Kong University of Science and Technology, Clear Water Bay, Kowloon, Hong Kong SAR, PR China

## ARTICLE INFO

### Article history:

Received 30 June 2008

Received in revised form

18 November 2008

Accepted 19 November 2008

Available online 27 November 2008

### Keywords:

O-glycosylation site

Glycopeptide

$\beta$ -Elimination/addition

LC/Q-TOF MS

## ABSTRACT

Determination of O-glycosylation sites in glycopeptides was developed by using two model compounds designed from mucin2 tandem repeat motif and erythropoietin.  $\beta$ -Elimination/addition reaction using dimethylamine on glycosylated site through a Michael-type condensation produced efficient deglycosylation with appropriate chemical modification. The use of dimethylamine was efficient to release the O-linked glycan in a reaction time period of 2–6 h at 55 °C. Peptide sequencing was then performed using the liquid chromatography/quadrupole time-of-flight mass spectrometry and MS–MS experiments. Interpretation of fragmentation pathways of the  $\beta$ -elimination/addition products enabled straightforward recognition of glycosylation site. Compared to the fragmentation of corresponding native peptides, mass shift of –18 Da or +27 Da was clearly observed for the two kinds of  $\beta$ -elimination/addition products of the glycosylated threonine. Dimethylamine was found to provide higher efficiency of  $\beta$ -elimination/addition than methylamine and ammonia.

© 2008 Elsevier B.V. All rights reserved.

## 1. Introduction

Characterization of O-glycosylation in terms of structure and site location is likely to be one of the most difficult features to study for post-translational modifications of proteins. The O-glycosylation process involves linkage of N-acetyl-D-galactosamine (GalNAc) or N-acetyl-D-glucosamine (GlcNAc) residues through the oxygen in the hydroxyl group of Ser (serine) or Thr (threonine) residues [1–4].

The mapping of O-glycosylated protein and peptides has been performed by enzymatically tagging proteins and peptides with radio labeled galactose in the past [5], but the process was very lengthy and tedious. In recent years, lectin affinity selection technology [6,7] is being used increasingly in glycoproteomics, especially in the case of O-glycoproteins. Mass spectrometry is also widely used in the analysis of glycopeptides, but the conventional collision-activated dissociation (CAD) [8–10] and post-source decay (PSD) mass spectrometry techniques [4,11] often fails O-glycosylation site identification due to the liability of the glycan–peptide bond. Only the new MS/MS methods of electron-capture detection [12–14] and electron-transfer dissociation [15] can generate in high yield the glycosylated fragment ions of the c and z series for site-specific determination of O-glycosylation. However, such instrument is not commonly available in biological laboratories.

\* Corresponding author. Tel.: +852 34117070; fax: +852 34117348.

E-mail address: [zwcai@hkbu.edu.hk](mailto:zwcai@hkbu.edu.hk) (Z. Cai).

Different chemical approaches have been developed to overcome instrumental limitations on O-glycopeptides determination. Deglycosylation with hydrazinolysis is useful but is associated with degradation of the polypeptide backbone [16,17].  $\beta$ -Elimination with NaOH is a common deglycosylation procedure for O-linked glycans, which can normally convert the glycosylated Ser and Thr residues into dehydroalanine and dehydrobutyric acid, respectively [18–20]. Rademaker et al. [21] have demonstrated that ammonia is preferred compared to the NaOH treatment. However, the difference of only one mass between –OH and –NH<sub>2</sub> groups renders the structural elucidation using MS techniques at low resolution such as CAD with triple quadrupoles or MALDI/PSD difficult. Hanisch et al. [22] and Mirgorodskaya et al. [23] reported  $\beta$ -elimination with methylamine followed by MALDI-TOF/ion trap MS mapping for locating O-glycosylation sites. Calet et al. [24] and Czeszak et al. [25] have described  $\beta$ -elimination with dimethylamine and ethanethiol for recognizing O-glycosylation sites. In other approaches, the partial acid hydrolysis combined with MALDI–MS was explored for the determination of glycosylation sites in mucin-type glycopeptides [23,26]. Czeszak et al. [27] demonstrated that MALDI/PSD analysis of the molecular cation of glycopeptides derivatized at their amino terminus with a phosphonium group enabled localization of O-glycans on the peptide chain. Recently our group also presented a chip-based capillary electrophoresis coupled to mass spectrometry (CE–MS) method [28] for the separation of a O-glycosylated peptide based on ammonia and dimethylamine, but further study is still needed to investigate its practical application.

In this report we describe a method for the assignment of O-glycosylation sites in the glycopeptides designed from mucin2 tandem repeat motif and erythropoietin using  $\beta$ -elimination with dimethylamine, followed by liquid chromatography/electrospray quadrupole time-of-flight mass spectrometry (LC/ESI-Q-TOF) mapping. Deglycosylation was achieved in 2–6 h at 55 °C. It transformed O-glycosylated Thr residue into the  $\beta$ -elimination/addition derivatives with a mass shift of –18 Da or +27 Da compared to the non-glycosylated Thr. The derivatives were stable under LC-ESI-MS/MS conditions and interpretation of the resulting spectra was achieved.

## 2. Experimental

### 2.1. Chemicals

Acetonitrile and formic acid were HPLC-grade purchased from Tedia (Fairfield, OH, USA). Water was collected from Milli-Q Ultra-pure water system (Millipore, Bedford, MA, USA). Dimethylamine solution (26% in water) and methylamine solution (40% in water) were purchased from Sigma (St. Louis, MO, USA). Ammonia solution (28% in water) was from Merck (Darmstadt, Germany). Two glycosylated peptides were immunograde purchased from Neosystem (Strasbourg, France). The structures of the glycopeptides used in the present work are depicted in Fig. 1. The corresponding non-modified peptides were synthesized by Hong Kong University of Science and Technology without further purification.

### 2.2. $\beta$ -Elimination/addition reaction

10  $\mu$ l of glycopeptide solution (5–500 pmol) in a 4-ml glass vial (AllTech, Los Alamitos, CA, USA), 300  $\mu$ l of different amines (26% dimethylamine, 40% methylamine or 28% ammonia solution) were added. After stirring, the reaction was carried out at 37 °C, 45 °C, 55 °C or 70 °C for 0–16 h, and subsequently stopped by removing the reagent under vacuum. The residue was dissolved in 150  $\mu$ l Milli-Q water and stored at –20 °C prior to analysis.

### 2.3. LC-ESI-MS and MS-MS analysis

HPLC experiments were conducted on a HP1100 capillary system equipped with an autosampler and two micro-mode pumps (Agilent Technologies, San Francisco, CA, USA). A reverse-phase column (Waters Symmetry C<sub>18</sub>, 2.1 mm  $\times$  100 mm, 3.5  $\mu$ m) was used to separate  $\beta$ -elimination/addition products of glycopeptides. Injection volume was 10  $\mu$ l. The mobile phase consisted of two components, with component I (A) being 0.1% formic acid in H<sub>2</sub>O and component II (B) being 0.1% formic acid in acetonitrile. The solvent gradient was

started from 15% B and held for 2 min, then programmed to 25% B in 15 min, followed by a linear gradient of 25–65% B over the next 5 min, all at a flow rate 200  $\mu$ l/min.

ESI-MS and MS-MS analyses were conducted on a Q-TOF tandem mass spectrometer (API Q-STAR Pulsar i; Applied Biosystems, Foster City, CA, USA). Turboionspray parameters for positive ion mode ESI-MS were optimized for glycopeptides as follows: ionspray voltage 5000 V, declustering potential I 30 V, focusing potential 140 V and declustering potential II 10 V. The ion source gas I, gas II, curtain gas, collision gas and the temperature of gas II were 30 °C, 15 °C, 30 °C, 3 °C and 375 °C, respectively. The mass range was from  $m/z$  400 to 1400. The collision energy for product ion scans of glycopeptides and their  $\beta$ -elimination/addition products varied from 23 eV to 28 eV for the MS/MS experiment.

### 2.4. Calculation of the percentage conversion of glycopeptides after $\beta$ -elimination/addition and LC-ESI-MS analysis

The peak areas of specific extracted ion chromatograms from each LC-ESI-MS profile were used to calculate the percentage conversion of the glycopeptides to the  $\beta$ -elimination/addition forms. The extracted ion chromatogram at  $m/z$  638.30 was used for the glycopeptide 1. The extracted ion chromatograms at  $m/z$  550.30, 543.30 and 536.30 were used as the corresponding  $\beta$ -elimination/addition products of the glycopeptide treated with dimethylamine, methylamine and ammonia, respectively. The percentage conversion of the glycopeptide and its  $\beta$ -elimination/addition forms were calculated as the corresponding peak areas at each time point relative to the  $m/z$  638.3 peak area at time 0. The same calculation procedure was applied to glycopeptide 2 and its elimination/addition products.

## 3. Results and discussions

### 3.1. Analysis of glycopeptides and native peptides by LC-ESI-MS and MS-MS

The two glycopeptides were chosen for the determination of glycosylation site because they present naturally occurring sites of O-GalNAc attachment in mucin2 tandem repeat motif and erythropoietin. Total ion chromatogram and mass spectra for glycopeptide 1 and native peptide are presented in Fig. 2. The LC-ESI-MS results were consistent with the expected major doubly charged ion peaks at  $m/z$  638.31 and 536.78, respectively. Fig. 3 shows LC-MS/MS spectra of glycopeptide 1 and native peptide. It shows that b and y ions of the glycopeptide were similar to those for the native peptide except for the mass ion at 204.09 from the neutral loss of GalNAc. Glycopeptide 2 also showed a similar fragmentation pattern (data not shown). Thus, a  $\beta$ -elimination approach was used in order to acquire valuable MS/MS fragment information.

### 3.2. Comparison of $\beta$ -elimination/addition reaction with ammonia, methylamine and dimethylamine

Glycopeptide 1 was incubated with ammonia, methylamine and dimethylamine at 55 °C for 6 h. The reactions were monitored using LC-ESI-MS, which showed that the O-glycosylated Thr residue was converted into its stable derivatives under the  $\beta$ -elimination with different amine (Figs. 4 and 5), which aids identification of the glycosylation site.  $\beta$ -Elimination with dimethylamine and methylamine resulted in the conversion of the glycopeptide to 69.2% dimethylamine derivative at  $m/z$  550.32 and 61.5% methylamine derivative at  $m/z$  543.33, respectively (Fig. 6). However, the incubation of the glycopeptide in ammonia only resulted in 8% production at  $m/z$  536.28. Regarding the  $\beta$ -elimination result of glycopeptide

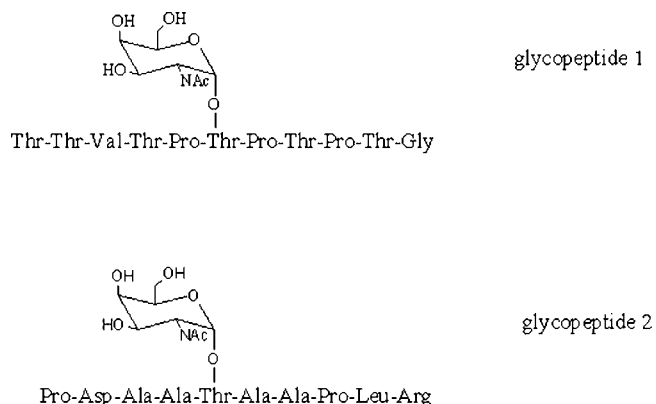
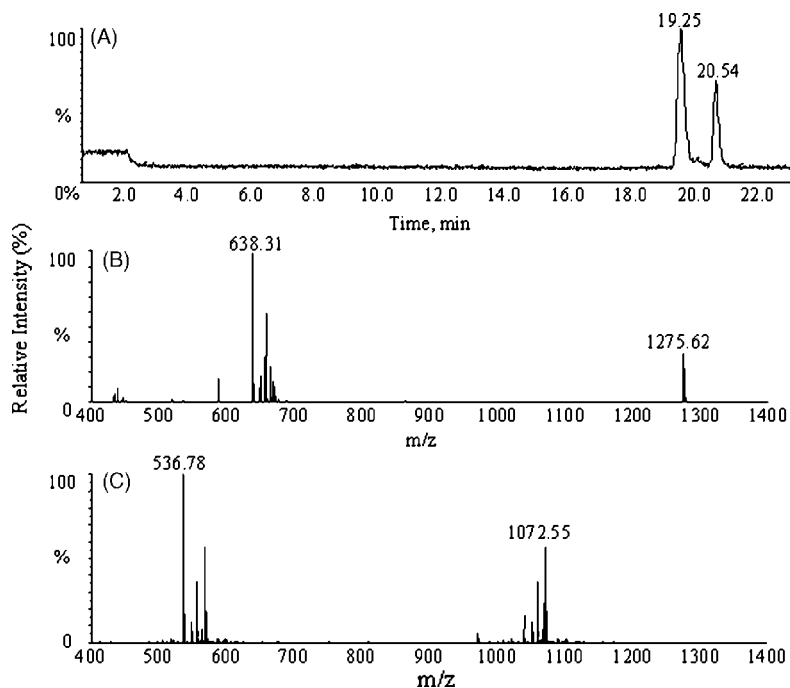


Fig. 1. Structures of the glycopeptides.





**Fig. 2.** Total ion LC/MS chromatogram of the mixture of glycopeptide 1 and its non-modified peptide (A); mass spectrum corresponding to the glycopeptide 1 with the retention time of 19.25 min (B); the mass spectrum corresponding to the non-modified peptide with the retention time of 20.54 min (C).

2, the data showed that 71.2% and 55.0% products were obtained under the condition of dimethylamine and ammonia. However, the glycopeptide treated with methylamine was only converted 35.7% to the  $\beta$ -elimination product. The result was not in agreement with the previous study that  $\beta$ -elimination with methylamine resulted in the complete deglycosylation of glycopeptide [23]. The obtained results indicated that  $\beta$ -elimination with dimethylamine

was more efficient to release the O-linked glycan from the glycopeptides.

$\beta$ -Elimination/addition reaction would be affected by glycopeptides structures. Under the condition of different amines, glycopeptide 2 was converted to four kinds of  $\beta$ -elimination products (Fig. 7). In addition to the three kinds of  $\beta$ -elimination/addition products mentioned above, the product from the sole elimina-

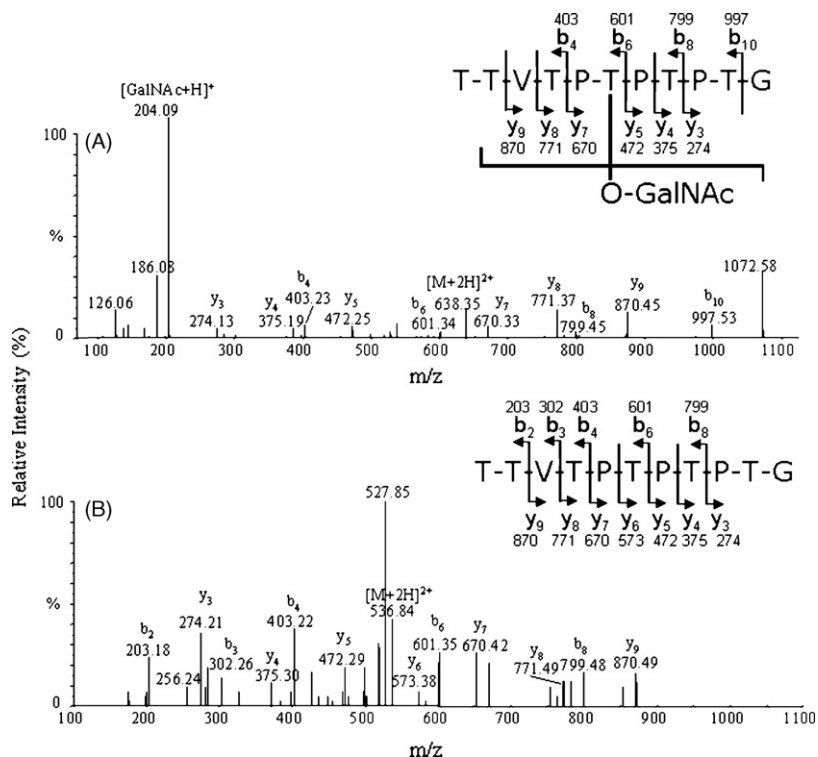


**Fig. 3.** LC-MS/MS spectra of the doubly charged ion of glycopeptide 1 at  $m/z$  638.31 (A) and of its non-modified peptide at  $m/z$  536.78 (B).

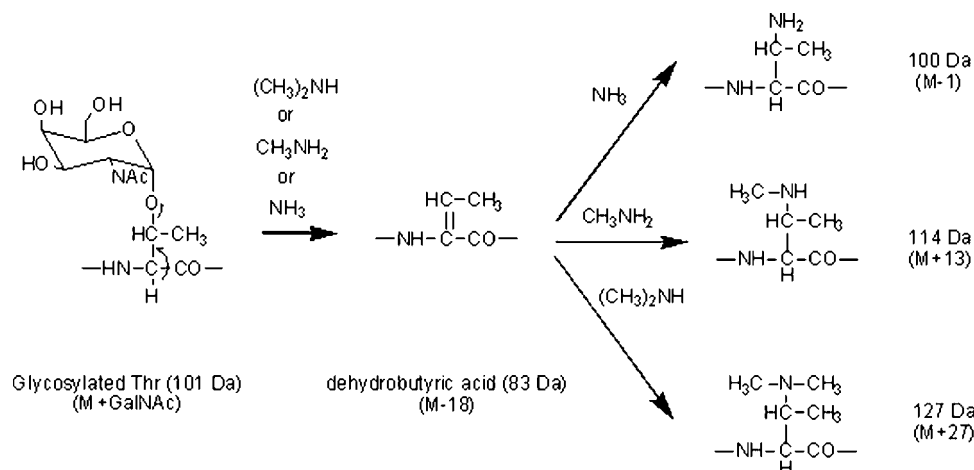


**Fig. 4.** Proposed mechanism of the β-elimination/addition reactions of O-linked glycopeptide with ammonia, methylamine and dimethylamine. The resulted stable amino acid derivatives have a mass difference of −1 Da (addition of ammonia), +13 Da (addition of methylamine) and +27 Da (addition of dimethylamine) compared to the native peptide (*M* is the molecular weight of the native peptide).

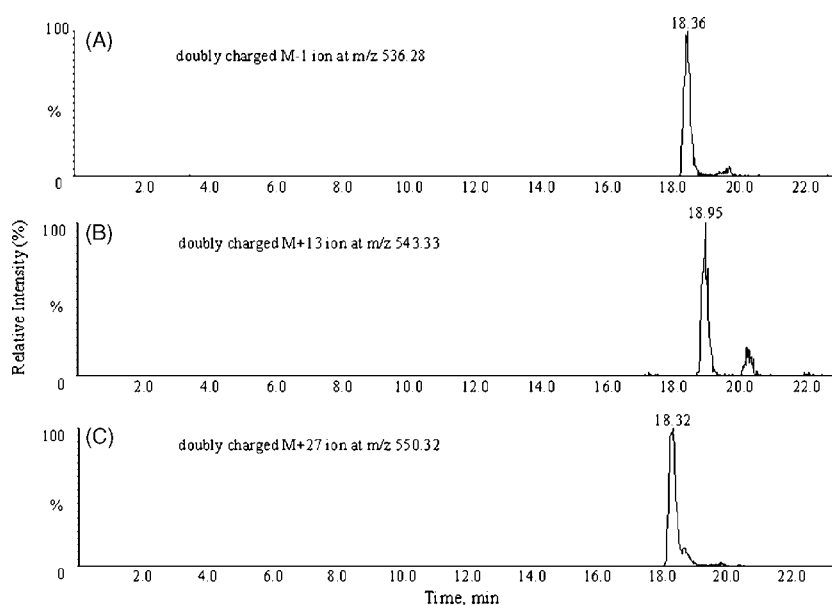


**Fig. 5.** Extracted ion chromatograms of the β-elimination/addition products of glycopeptide 1 treated with ammonia at *m/z* 536.28 (A), with methylamine at *m/z* 543.33 (B), and with dimethylamine at *m/z* 550.32 (C) for 6 h at 55 °C. Peaks are labeled according to Fig. 4.

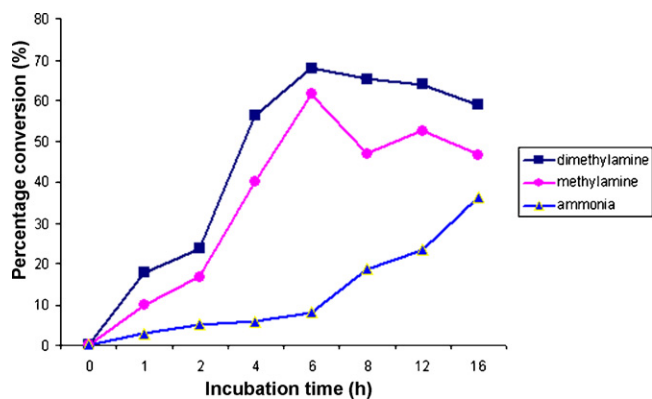


**Fig. 6.** Time-dependent β-elimination of glycopeptide 1 (50 pmol) treated with dimethylamine, methylamine and ammonia at 55 °C. At the indicated times the reaction was terminated and analyzed by LC–MS. See Section 2 for the details concerning the calculations of the percentage conversion.

tion (i.e., without the subsequent addition) was also produced. The result also showed that β-elimination for glycopeptide 2 was significantly faster than that of glycopeptide 1. Glycopeptide 2 resulted in the maximum yield of the released peptide for 2 h, while glycopeptide 1 was optimally released for 6 h by using dimethylamine at 55 °C. Thr6 (from the C-terminus) of glycopeptide 1 might be sterically hindered due to the two adjacent prolines, which might lead to less susceptible to β-elimination. The similar phenomena were also reported in β-elimination with ammonia [21,29].

The efficiency of β-elimination/addition reaction also strongly depended on the reaction temperature. It was found that the incubation of glycopeptide 1 with dimethylamine at 37 °C and 45 °C for 6 h, only resulted in 25.3% and 42.3% yields. At higher temperatures, the yields of dimethylamine derivative were 69.2% (55 °C) and 75.1% (70 °C) for 6 h, respectively. However, at the temperature of above 55 °C the reaction led to undesirable side reactions, such as polypeptide chain cleavages and dimethylamidation of the C-termini.

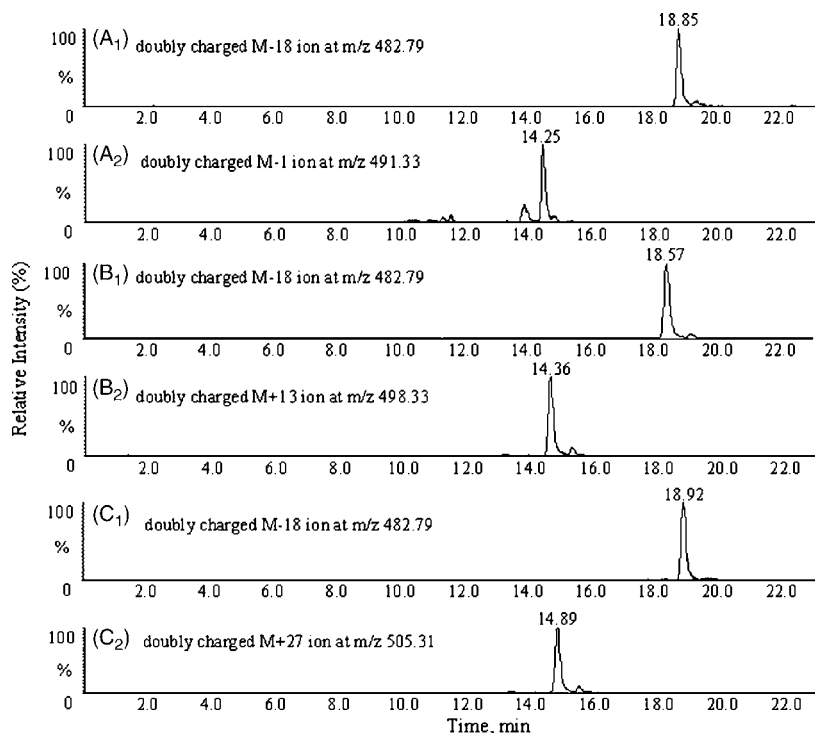


**Fig. 7.** Extracted ion chromatograms of the products of glycopeptide 2 after the  $\beta$ -elimination/addition reactions for 2 h at 55 °C with ammonia at  $m/z$  482.79 ( $A_1$ ) and  $m/z$  491.33 ( $A_2$ ); with methylamine at  $m/z$  482.79 ( $B_1$ ) and  $m/z$  498.33 ( $B_2$ ); with dimethylamine at  $m/z$  482.79 ( $C_1$ ) and  $m/z$  505.31 ( $C_2$ ). The peaks are labeled according to Fig. 4.

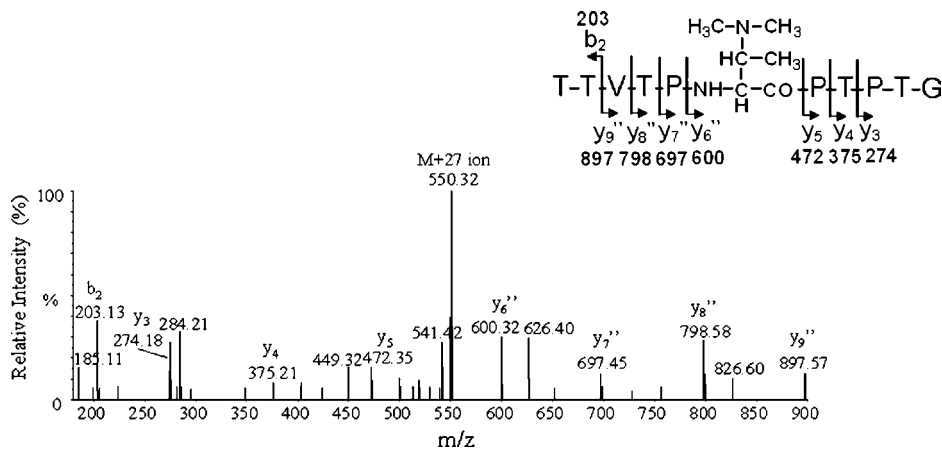


**Fig. 8.** Product ion spectrum of the doubly charged M+27 ion at  $m/z$  550.32 from the LC-MS/MS analysis of the  $\beta$ -elimination/addition product of glycopeptide 1 treated with dimethylamine. The parent ion is labeled according to Fig. 4.

### 3.3. Identification of the glycosylation site of glycopeptides treated with dimethylamine

After optimizing reaction conditions for the  $\beta$ -elimination/addition product of glycopeptide 1, identification of the glycosylation site was achieved by LC-ESI-MS/MS of the doubly charged M+27 ions ( $m/z$  550.32). The data in Fig. 8 showed the mass difference of +27 Da for  $y_6''$ ,  $y_7''$ ,  $y_8''$  and  $y_9''$  ions compared to those of the native peptide, which clearly indicated that Thr6 (from the C-terminus) was the site of glycosylation. The interpretation of series of  $y''$  ions allowed the site of glycosylation to be identified without ambiguity. Good results were also obtained for the  $\beta$ -elimination/addition products of glycopeptide 2. The intensive fragmentation from the doubly charged M-18 ion ( $m/z$  482.79) and M+27 ion ( $m/z$  505.31) were similar to those obtained from the chip-based CE-MS/MS analysis for the identification the glycopeptide [28], demonstrating that the glycan was released from Thr by

the  $\beta$ -elimination to yield dehydrobutyric acid and the amines were subsequently added to the double bond via a Michael-type addition reaction.

To obtain an indication of the sensitivity of the method, the whole procedure was performed using different amounts of glycopeptide 2. At the low level of 5 pmol of glycopeptide treated with dimethylamine at 2 h for 55 °C, the MS/MS spectrum yielded by M-18 ion ( $m/z$  482.79) clearly contained all those fragment ions needed for the determination of the glycosylation site.

## 4. Conclusion

An effective method for the determination of O-glycosylation sites of the glycopeptides by combining  $\beta$ -elimination/addition reaction with dimethylamine and LC-ESI-MS/MS analysis was demonstrated.  $\beta$ -Elimination with dimethylamine gave the higher reaction efficiency than methylamine and ammonia with 2–6 h at

55 °C. The use of dimethylamine converted Thr residue of the glycopeptides into its  $\beta$ -elimination/addition derivatives, resulting in a readily detectable mass difference of  $-18$  Da or  $+27$  Da. Further work is in progress to apply the methodology to glycoproteins containing complex carbohydrate moieties.

### Acknowledgement

The financial support from the Faculty Research Grant of Hong Kong Baptist University (FRG/07-08/II-21) is acknowledged.

### References

- [1] B.C. O'Connell, F.K. Hagen, L.A. Tabak, *J. Biol. Chem.* 267 (1992) 25010.
- [2] H. Clausen, E.P. Bennett, *Glycobiology* 6 (1996) 635.
- [3] J.D. Marth, *Glycobiology* 6 (1996) 701.
- [4] S. Müller, S. Goletz, N. Packer, A. Gooley, M. Lawson, F.G. Hanisch, *J. Biol. Chem.* 272 (1997) 24780.
- [5] E. Roquemore, T. Chou, G. Hart, *Methods Enzymol.* 230 (1994) 443.
- [6] R. Rosenfeld, H. Bangio, G.J. Gerwig, R. Rosenberg, R. Aloni, Y. Cohen, Y. Amor, I. Plaschkes, J.P. Kamerling, R. Ben-Yakar, Maya, *J. Biochem. Biophys. Methods* 70 (2007) 415.
- [7] M. Durham, F.E. Regnier, *J. Chromatogr. A* 1132 (2006) 165.
- [8] F.G. Hanisch, B.N. Green, R. Bateman, J. Peter-Katalinic, *J. Mass Spectrom.* 33 (1998) 358.
- [9] K. Alving, R. Körner, H. Paulsen, J. Peter-Katalinic, *J. Mass Spectrom.* 33 (1998) 1124.
- [10] K. Alving, H. Paulsen, J. Peter-Katalinic, *J. Mass Spectrom.* 34 (1999) 395.
- [11] S. Goletz, M. Leuck, P. Franke, U. Karsten, *Rapid Commun. Mass Spectrom.* 11 (1997) 1387.
- [12] E. Mirgorodskaya, P. Roepstorff, R.A. Zubarev, *Anal. Chem.* 71 (1999) 4431.
- [13] M. Mormann, H. Paulsen, J. Peter-Katalinic, *Eur. J. Mass Spectrom.* 11 (2005) 497.
- [14] B.H. Clowers, E.D. Dodds, R.R. Seipert, C.B. Lebrilla, *J. Proteome Res.* 6 (2007) 4032.
- [15] L.M. Mikesch, B. Ueberheide, A. Chi, J.J. Coon, J.E.P. Syka, J. Shabanowitz, D.F. Hunt, *Biochim. Biophys. Acta* 1764 (2006) 1811.
- [16] T. Gerken, R. Gupta, N. Jentoft, *Biochemistry* 31 (1992) 639.
- [17] K. Greis, B. Hayes, F. Comer, M. Kirk, S. Barnes, T. Lowary, G. Hart, *Anal. Biochem.* 234 (1996) 38.
- [18] G.J. Rademaker, J. Haverkamp, J. Thomas-Oates, *Org. Mass Spectrom.* 28 (1993) 1536.
- [19] K.D. Greis, B.K. Hayes, F.I. Comer, M.K. Kirk, S. Barnes, T.L. Lowary, G.W. Hart, *Anal. Biochem.* 234 (1996) 38.
- [20] A. Nita-Lazar, R.S. Haltiwanger, *Methods Enzymol.* 417 (2006) 93.
- [21] G.J. Rademaker, S.A. Pergantis, L. Blok-Tip, J.I. Langridge, A. Kleen, J. Thomas-Oates, *Anal. Biochem.* 257 (1998) 149.
- [22] F.-G. Hanisch, M. Jovanovic, J. Peter-Katalinic, *Anal. Biochem.* 290 (2001) 47.
- [23] E. Mirgorodskaya, H. Hassan, H. Clausen, P. Roepstorff, *Anal. Chem.* 73 (2001) 1263.
- [24] G. Cauet, J.-M. Strub, E. Leize, E. Wagner, A.V. Dorsselaer, M. Lusky, *Biochemistry* 44 (2005) 5453.
- [25] X. Czeszak, G. Ricart, D. Tetaert, J.C. Michalski, J. Lemoine, *Rapid Commun. Mass Spectrom.* 16 (2002) 27.
- [26] E. Mirgorodskaya, H. Hassan, H.H. Wandall, H. Clausen, P. Roepstorff, *Anal. Biochem.* 269 (1999) 54.
- [27] X. Czeszak, W. Morelle, G. Ricart, D. Tetaert, J. Lemoine, *Anal. Chem.* 76 (2004) 4320.
- [28] Y. Zheng, H. Li, Z. Guo, J.M. Lin, Z. Cai, *Electrophoresis* 28 (2007) 1305.
- [29] E. Tarelli, *Carbohydr. Res.* 342 (2007) 2322.



# $\beta$ -Cyclodextrin-cross-linked polymer as solid phase extraction material coupled with inductively coupled plasma mass spectrometry for the analysis of trace Co(II)

Xiashi Zhu\*, Min Wu, Ying Gu

Department of Chemistry, Yangzhou University, Yangzhou 225002, PR China

## ARTICLE INFO

### Article history:

Received 2 September 2008

Received in revised form 2 December 2008

Accepted 2 December 2008

Available online 11 December 2008

### Keywords:

Cobalt

$\beta$ -Cyclodextrin cross-linked polymer

Solid phase extraction

Inductively coupled plasma mass spectrometry

## ABSTRACT

A sensitive method for the separation/analysis of Co(II) was described. The  $\beta$ -cyclodextrin cross-linked polymer ( $\beta$ -CDCP) was synthesized and used as solid phase extraction material (SPE) to separate/pre-concentrate trace cobalt coupled with inductively coupled plasma mass spectrometry (ICP-MS) for the analysis of Co(II). The method was based on  $\alpha$ -pyridylazo- $\beta$ -naphthol (PAN) as the complexing agent for Co(II)-PAN at neutral condition and the adsorption behavior of Co(II)-PAN on  $\beta$ -CDCP was studied. Further, *p*-octylpolyethylene-glycolphenyl ether (Triton X-100) as environment-friendly eluant was used. The linear range, detection limit (DL) and the relative standard deviation (R.S.D.) was 5.0–160.0 ng/mL, 5.84 ng/L and 2.27% ( $n=3$ ,  $c=30.0$  ng/mL) respectively. The enhancement factor was 10. Moreover, the  $\beta$ -CDCP could be used repeatedly and offered better recovery and estimation of standard samples.

© 2009 Published by Elsevier B.V.

## 1. Introduction

The detrimental effects of toxic heavy metals are quite pronounced, even at very low concentrations, it often requires methods capable of quantitatively monitoring its presence at trace levels. However, the determination of trace elements in real samples is particularly difficult because of the complexity of matrix and the usual low concentration, so sensitive instrumental techniques and a preconcentration step are required. There are many preconcentration methods for trace metal elements, such as coprecipitation [1], solvent extraction [2], electrochemical deposition [3], membrane extraction [4], and solid-phase extraction (SPE) (adsorbing material such as activated carbon [5], modified silica [6,7], biological cell-sorption [8] chelating resin [9], poly(vinyl chloride) [10], carbon nanofibers microcolumn [11–13], cellulose [14] and  $\beta$ -cyclodextrin polymer, etc.). The applications of  $\beta$ -CD polymers as solid-phase extraction material are listed in Table 1.

Cobalt is known to be essential at trace levels to animals and plants for metabolic processes [20]. It is necessary in human dietary intake, possessing anti-anemic properties and acting as the central atom of vitamin-B<sub>12</sub> (cyanocobalamin), which is widely responsible for the production of red blood cells. Due to that, trace and ultra-

trace determinations of Co in environmental and biological samples have become of increasing interest.

Various techniques (UV-vis spectral [21], AAS [22], ICP-AES [23], ICP-MS [24], electrochemistry [25], etc.) have been applied to quantitatively monitoring cobalt at trace levels in samples. However, the direct determination with various instrumental methods is difficult owing to matrix effects and low concentration of cobalt in samples. Therefore, the necessity of separation/pre-concentration procedure of cobalt is significant. Several separation/pre-concentration methods have been reported in former references (such as co-precipitation [26], cathodic stripping voltammetry [27], solid phase extraction [28–30]), but  $\beta$ -cyclodextrin cross-linked polymer ( $\beta$ -CDCP) used as SPE material to separation/pre-concentration cobalt seem to be lacking.

$\beta$ -CDCP by polymerizing cyclodextrin with epichlorohydrine was a spherical or grainy solid subject and insoluble in water, which still retained the inclusion property of  $\beta$ -CD, was synthesized by the reaction of  $\beta$ -CD and cross-linked agent.  $\beta$ -CDCP as a solid phase extraction material had been applied to separation/pre-concentration the trace metal element [15].

The aim of this work was to use  $\beta$ -CDCP as solid phase extraction (SPE) material coupled with ICP-MS for separation/analysis Co(II). It exhibited satisfactory adsorption ability towards Co(II) in soybean standard sample (GBW10013), water standard sample (GSB50030-94) and tea standard sample (GBW08513). The proposed method had been successfully applied to the determination of Co(II) in

\* Corresponding author. Tel.: +86 514 7975244; fax: +86 514 7975244.  
E-mail addresses: [xszhu@yzu.edu.cn](mailto:xszhu@yzu.edu.cn), [zhuxiashi@sina.com](mailto:zhuxiashi@sina.com) (X. Zhu).

**Table 1**  
Application of  $\beta$ -CD polymers in solid-phase extraction.

SPE sorbents	Samples	Techniques	Refs.
$\beta$ -CDPCP	Cu(II)	GFAAS	[15]
$\beta$ -CD polymers inclusion membrane	Cu(II), Co(II), Ni(II) and Zn(II)	CE-UV	[16]
$\beta$ -CD entrapped polymer	Hydrolyzed urine	GC-MS/LC-MS	[17]
$\beta$ -CD polymer	Urinary cannabinoids	GC-MS	[18]
$\beta$ -CD-polyurethane polymer	Aromatic amines	HPLC	[19]

real water sample and VB<sub>12</sub> (injections and tablets) indirectly with quantitative recovery.

## 2. Experimental

### 2.1. Apparatus and reagents

Centrifuge (Anke Scientific Instrument Factory, Shanghai), timing multifunctional oscillator (Guohua Limited Company, China), digital constanttemperature water-bath (Guohua Limited Company, China), and ICP-MS (DRC-e, PE Company, USA) were used. The operating conditions for ICP-MS are listed in Table 2.

Soybean Standard Sample GBW10013 (National reference materials (China)), tea standard sample GBW08513 (National reference materials (China)), water standard sample GSBZ50030-94 (National reference materials (China)), VB<sub>12</sub> injection (Xuzhou Ryen Pharma. Co., Ltd.), VB<sub>12</sub> tablets (Shanghai Fuderui Pharma. Co., Ltd.),  $\beta$ -CD (Shanghai Chemical Reagent Corporation, China), Triton X-100 (Sigma–Aldrich, USA), Sodium dodecyl sulfate (SDS, Sangon Biological Engineering Technology Co. Ltd., China), cetyltrimethyl ammonium bromide (CTAB; Shanghai Chemical Reagent Factory, China), Bromopyrogallol Red ((BPR) State-private Ownership Xin Zhong Chemical Reagent Factory, China), (phenylfluoronl (PF) Sinopharm Chemical Reagent Co. Ltd., China), xylenal orange ((XO) Shang Hai SSS Chemical Reagent Co. Ltd., China), 4-(2-Pyridylazo) resorcinol ((PAR) Sinopharm Chemical Reagent Co. Ltd.), 2 [(5-bromo-2-pyridyl)-zao]-5-(diethyl-amino) phenol ((5-Br-PADAP) Beijing Chemical Reagent Corporation, China), 1-(2-pyridylazo)-2-naphthol ((PAN) Shanghai Chemical Reagent Corporation, China).  $\beta$ -CDPCP was prepared as Ref. [15].

### 2.2. Experimental procedure

#### 2.2.1. Static adsorption of Co(II)-PAN complex

At room temperature, the amount of Co(II) (1.5 mL, 100.0 ng/mL), 0.050 mL PAN (0.1%w/v, ethanol) and 0.050 g  $\beta$ -CDPCP was mixed, controlling the appropriate acidity. The mixture (15 mL) was shaken on the timing multifunctional oscillator for 10 min and then centrifugal.

**Table 2**  
Operating conditions for ICP-MS.<sup>a</sup>

Parameter	Value
ICP–RF–Power (W)	1350
Plasma argon flow rate (L/min)	14.5
Auxiliary argon flow rate (L/min)	1.5
Nebulizer argon flow rate (L/min)	0.94
Sample orifice (mm)	1.1
Skimmer orifice (mm)	0.9
Scan mode	Peak hopping
Number of sweep	20
Dwell time (ms)	50
Replicates	3
Isotopes	<sup>59</sup> Co

<sup>a</sup> The concentration of ethanol has a great effect on signal intensity of ICP-MS. So ethanol was strictly excluded in this experiment [31].

#### 2.2.2. Elution of Co(II)-PAN complex

The  $\beta$ -CDPCP was eluted by 1.5 mL Triton X-100 (10%w/v) solution. Co(II)-PAN in effluent solution was detected by ICP-MS. The preconcentration factor was 10 (the quotient of volume before absorption and after elution).

#### 2.2.3. Sample preparation

2.000 g of the soybean standard sample (GBW10013) was accurately weighed into the beaker, 10.0 mL concentrated HNO<sub>3</sub> and 5.0 mL of 30%(w/v) H<sub>2</sub>O<sub>2</sub> were added. The mixture was digested on electrical-heat panel, and then it was filtered and adjusted pH to neutral with NaOH (1.0 mol/L) solution. Finally the solution was transferred into a 10 mL of flask, fixed with distilled water and stored for determination. The solution was diluted before determination.

4.000 g standard tea sample (GBW08513) was actually weighed into a breaker, 12.0 mL concentrated HNO<sub>3</sub> and 10.0 mL HClO<sub>4</sub> were added. The mixture was digested on electrical-heat panel at low temperature and then 16.0 mL 1.0 mol/L HCl was added in order to dissolve the salt in the residue. The mixture was filtered and transferred into 50 mL flask, then fixed with distilled water and stored for determination. The solution was diluted before determination.

0.50 mL VB<sub>12</sub> injection (ten VB<sub>12</sub> tablets was weight and ground, the powder was dissolved with distilled water) and 5.0 mL 8.0 mol/L HNO<sub>3</sub> was added to 50.0 mL beaker to digest on electrical-heat panel, then two drops of 30%(w/v) H<sub>2</sub>O<sub>2</sub> were added and evaporated. 3.0 mL HCl (1:1) was added to dissolve the soluble salt which was residual in breaker, adjusted pH to neutral with NaOH (1 mol/L) solution, then fixed to 50.0 mL flask with distilled water. The solution was diluted before determination.

#### 2.2.4. Reproduction of $\beta$ -CDPCP

The adduct of the  $\beta$ -CDPCP and Co(II)-PAN was dipped in TritonX-100(10.0%w/v) for 1 h and then washed with distilled water,  $\beta$ -CDPCP was treated with HNO<sub>3</sub> (5.0 mol/L) and washed with distilled water again to neutral condition then centrifugal and dried.

## 3. Results and discussion

### 3.1. Optimization of static adsorption conditions

#### 3.1.1. Select the chelating agent

The adsorption behavior of cobalt complex (CoL<sub>n</sub>) on  $\beta$ -CDPCP was investigated. The results showed that the adsorption behavior was greatly affected by complex agents phenylfluoronl (PF), bromopyrogallol red (BPR), xylenal orange (XO), 4-(2-Pyridylazo) resorcinol (PAR), 2 [(5-bromo-2-pyridyl)-zao]-5-(diethyl-amino) phenol (5-Br-PADAP) and 1-(2-pyridylazo)-2-naphthol (PAN). The retention efficiency of complex was shown in Fig. 1, it could be seen that the retention efficiency of the complexes increased orderly and the Co(II)-PAN was the best. The adsorption behavior of cobalt complex (CoL<sub>n</sub>) on  $\beta$ -CDPCP relate to the stability of complex and the hydrophobicity of complexant (such as Co(II)-XO(<sup>+</sup>lgK' = 6.78) < Co(II)-BPR(lgK' = 9.31) < Co(II)-PAR(lgK' = 10.0) < Co(II)-PAN (lgK' > 12.0), lgK' is the stability constant for the complex CoL<sub>n</sub> [32]). The order of hydrophobicity of complexant was XO ~ BPR ~ PF < PAR < 5-Br-PADAP < PAN, which was the same with the order of hydrophobicity of complexes [32]). PAN was chosen as the complex agent.

#### 3.1.2. Effect of pH

The formation and stability of the complex Co(II)-PAN were infected by the system acidity, the retention efficiency of the complex on  $\beta$ -CDPCP was varied with the pH (Fig. 2). When pH was lower than 5.0, the retention efficiency was relatively low, in the range

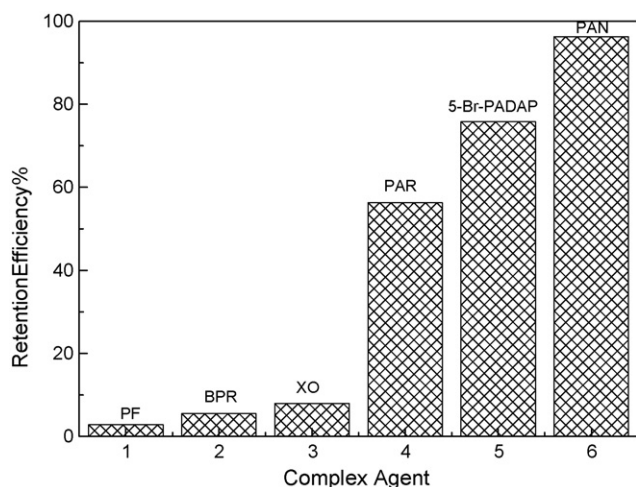


Fig. 1. Effect of different complex agent on retention efficiency ( $c_{Co} = 30.0$  ng/mL).

pH 5.0–8.0, the retention efficiency was much higher, it was even above 95.5% at neutral condition. It was in accordance with the stabilities of the complexes at different pH. When pH was 5.0–8.0, the form of existence of PAN was neutral molecule ( $pK_{a1} = 2.9$  ( $H_2^+L$ ),  $pK_{a2} = 11.6$  (HL)) [32], which was favorable for the formation of Co(II)-PAN. So, neutral condition was chosen.

### 3.1.3. Effect of temperature

In this experiment, the retention efficiency of Co(II)-PAN on  $\beta$ -CD/CP at different temperatures (2.0–50.0 °C) was studied. The retention efficiency was scarcely any variation with temperature raised. The experiment was conducted at room temperature.

### 3.1.4. Effect of the sample volume

The amount of Co(II) was fixed at 150.0 ng and the volume of the sample solution increased from 2.0 mL to 45.0 mL. The results were shown in Fig. 3. It could be seen from Fig. 3 that the retention efficiency was greater than 95% in the volume of sample 2.0–15 mL, when the volume of sample was larger than 25.0 mL, the retention efficiency is lesser than 90%. In this work, the sample volume of 15.0 mL was adopted.

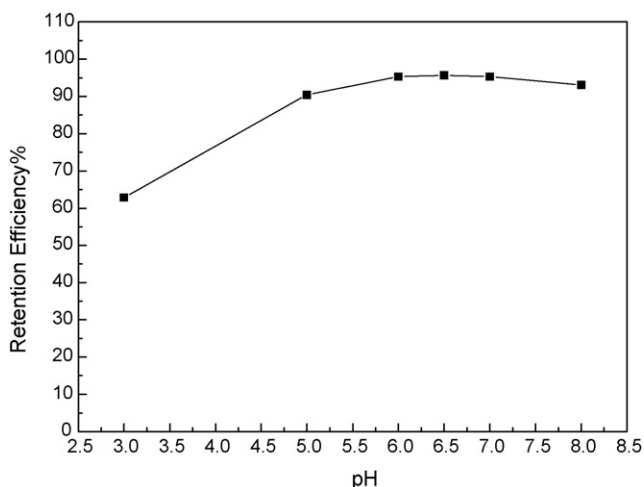


Fig. 2. Effect of pH on the retention efficiency ( $c_{Co} = 30.0$  ng/mL).

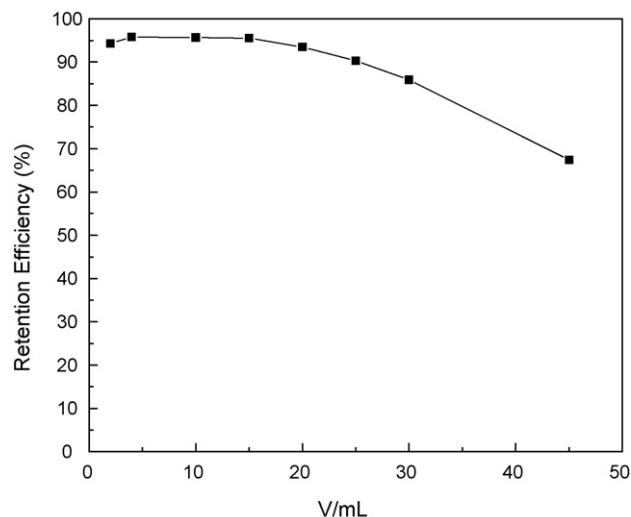


Fig. 3. Effect of sample volume on the retention efficiency ( $c_{Co} = 30.0$  ng/mL).

### 3.1.5. Effect of $\beta$ -CD

The retention efficiency did not change with the increasing concentration of  $\beta$ -CD in the system. It was possible that  $\beta$ -CD/CP has more clathration than  $\beta$ -CD due to the hydrophobic network [15], Co(II)-PAN was prefer to bind on  $\beta$ -CD/CP and the retention efficiency did not change.

### 3.1.6. Effect of surfactant

The effect of surfactants (Triton X-100, CTAB and SDS) on the retention efficiency was investigated. As the results shown in Fig. 4. With the increase of the concentration of surfactant, the retention efficiency of Co(II)-PAN on  $\beta$ -CD/CP decreased dramatically, and the order were Triton X-100 > CTAB > SDS. The effect of the surfactants on the retention efficiency rested with its solubilization. The solubilization was highly dependent on the charge types of the surfactant and the volume fraction of the organic component. The distribution coefficient ( $K_D$ ) reflects the solubilization and enrichment ability of solute in surfactants,  $K_{D(TritonX-100-PAN)}$  and  $K_{D(CTAB-PAN)}$  were higher than  $K_{D(SDS-PAN)}$  [33]. The UV-vis spectra shown that the  $\lambda_{max}$  of complex (Co(II)-PAN) in Triton X-100 (428–595 nm) and CTAB (428–587 nm) was bathochromic shift and the intensity were largely enhanced, while the  $\lambda_{max}$  in SDS (428–410 nm) was blue shift, the intensity declined dramatically, it indicated that the

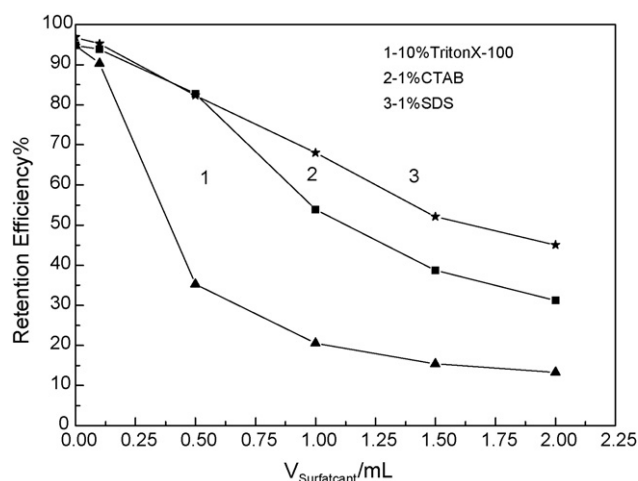


Fig. 4. Effect of different surfactants on the retention efficiency ( $c_{Co} = 30.0$  ng/mL).

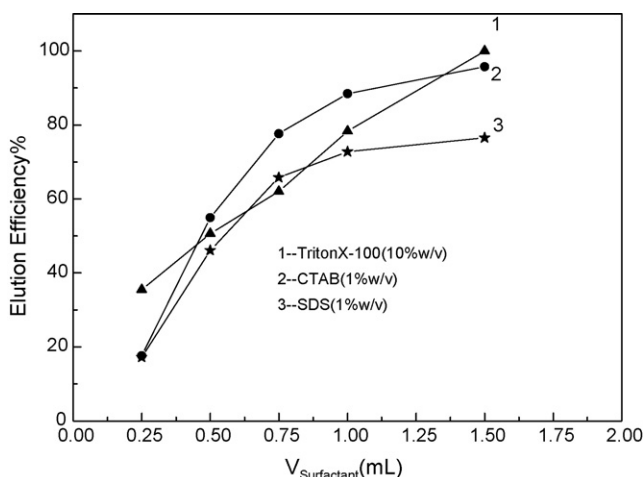


Fig. 5. Effect of different surfactants on the elution efficiency ( $c_{Co} = 30.0 \text{ ng/mL}$ ).

solubilization of Triton X-100 was higher due to formation of the complexes (Co(II)-PAN-Triton X-100,  $K = 50,000$  [34]).

### 3.2. Adsorption kinetics of $\beta$ -CDCP

The adsorption kinetic process of  $\beta$ -CDCP at room temperature with pH 6.5 was investigated. With the increase of adsorption time (5.0–60.0 min), The adsorption process was completed within 5.0 min, and the retention efficiency was not changed in 1 h, the adsorption efficiency almost kept stable (all above 95.0%). It may be the reason that the polymer network formed with  $\beta$ -CD as monomer has good permeability due to special hollow structure. 10.0 min was adopted as the adsorption time for Co(II)-PAN.

### 3.3. Retention capacity

To determine the retention capacity (or sorption capacity) of the  $\beta$ -CDCP (maximum amount of Co(II) retained from 1 g of  $\beta$ -CDCP), 0.050 g  $\beta$ -CDCP was equilibrated with 10 mL solution in the range of concentration of Co(II) (10–200 ng/mL), and measuring the Co(II) content in the eluates by ICP-MS. When the concentration of Co(II) reached 160 ng/mL, the retention capacity arrived at its maximum value. A retention capacity of the polymer was calculated to be 28.0  $\mu\text{g/g}$ .

### 3.4. Optimization of elution conditions

#### 3.4.1. Select the eluants

The  $\beta$ -CDCP could be reproduced by eluants. Different eluants were investigated. The order of elution efficiency was HCl (36.2%) < EDTA (63.8%) < SDS (76.6%) < HNO<sub>3</sub> (85.1%) < CTAB (95.7%) < Triton X-100 (100.0%), it indicated that Co(II)-PAN could not be quantitatively eluted by HCl, HNO<sub>3</sub>, EDTA and SDS, while surfactants (CTAB and Triton X-100) behaved excellent eluting ability, further, the surfactant was environment-friendly eluant. Fig. 5 showed that the elution efficiency was increased with the concentration of surfactants. When 1.5 mL surfactant was added, the elution efficiency for Triton X-100 and CTAB reached 100%, 95.7% respectively, but SDS was just 76.6%. This result was consistent with 3.1.6 (Fig. 4). So Triton X-100 was investigated as eluent.

#### 3.4.2. Effect of Triton X-100 (10.0%w/v) volume

The elution efficiency of Co(II)-PAN with 1.5–8.0 mL of Triton X-100 was investigated. The elution efficiency of Co(II)-PAN kept all

Table 3

Determination results of samples (mean  $\pm$  S.D.,  $n = 3$ ).

Sample	Certified value	Determination value	Recovery (%)
GBW10013 <sup>a</sup> (Soybean)	0.125 $\pm$ 0.012 ( $\mu\text{g/g}$ )	0.126 $\pm$ 0.005 ( $\mu\text{g/g}$ )	100.8
GSBZ50030-94 <sup>a,b</sup> (water)	1.15 $\pm$ 0.08 ( $\mu\text{g/mL}$ )	1.16 $\pm$ 0.02 ( $\mu\text{g/mL}$ )	100.9
GBW08513 <sup>a</sup> (tea)	(0.18) ( $\mu\text{g/g}$ )	0.169 $\pm$ 0.048 ( $\mu\text{g/g}$ )	93.9
VB <sub>12</sub> injection <sup>b</sup>	0.500 (mg/mL)	0.491 $\pm$ 0.005 (mg/mL)	98.2
VB <sub>12</sub> tablets <sup>b</sup>	0.156 (mg/g)	0.150 $\pm$ 0.004 (mg/g)	96.2
Tap-water	ND	ND	ND
	11.5 (ng/mL)	11.58 $\pm$ 0.034	100.7
	23.0 (ng/mL)	23.07 $\pm$ 0.013	100.3
	34.5 (ng/mL)	34.36 $\pm$ 0.084	99.6

ND, non-detected.

<sup>a</sup> National reference materials (China).

<sup>b</sup> The sample was diluted before determination.

above 99.8%. So optimum volume of Triton X-100 (10.0%w/v) solution chosen for this work was 1.5 mL. The preconcentration factor was 10 (the quotient of volume before absorption and after elution).

### 3.5. Reversibility and reproducibility of $\beta$ -CDCP

$\beta$ -CDCP was reproduced 6 times as 2.2.3 and its retention efficiency for Co(II)-PAN kept stable (above 95.0%). It demonstrated that  $\beta$ -CDCP exhibited good reversibility and reproducibility, which was associated with the fact that the inclusion interaction between  $\beta$ -CDCP and Co(II)-PAN was a reversible process.

### 3.6. Interferences

Determination of Co(II) 30.0 ng/mL in the presence of foreign substances was investigated. With a relative error of less than  $\pm 5\%$ , the tolerance limit for various foreign substances was as follows (tolerance ratio in mass): Na<sup>+</sup>, K<sup>+</sup>, Ca<sup>2+</sup>, Mg<sup>2+</sup>, Cl<sup>-</sup>, NO<sub>3</sub><sup>-</sup> (1000); Fe(II), Fe(III), Cr(VI), Cu(II) (10); Mn(II), Pt(IV), Cd(II), W(VI), Mo(VI), Cr(III) (5).

### 3.7. Analytical parameters

The calibration graph for the ICP-MS determination of Co(II) was linear 5.0–160.0 ng/mL. The linear equation was  $I = 8392.75 + 9454.38C$  (ng/mL), the corresponding coefficient of correlation was 0.9991. The relative standard deviation was 2.27% ( $n = 3$ ,  $c = 30.0 \text{ ng/mL}$ ). The limit of detection by the described procedure was 5.84 ng/L. The preconcentration factor was 10.

### 3.8. Sample analysis

Soybean Standard Sample (GBW10013), standard water sample (GSBZ50030-94) and standard tea sample (GBW08513), tap-water, VB<sub>12</sub> injection and VB<sub>12</sub> tablets samples were determined under the optimal conditions by standard curve method and standard adding method respectively. Results were listed in Table 3. The contents of Co(II) in the national reference materials were in agreement with the certified value. This method has been successfully applied to the analysis of real samples with satisfactory results.

## 4. Conclusion

A new method of  $\beta$ -CDCP used as solid phase extraction material (SPE) to pre-concentrate/separate trace cobalt coupled with inductively coupled plasma mass spectrometry for the analysis of cobalt was established. The proposed SPE is an easy, safe and inexpensive methodology for the separation and determination of trace



amounts of Co(II). The analytical results obtained lead to the conclusion that the method developed can be successfully adopted for the separation/analysis of Co(II) with high sensitivity and selectivity

### Acknowledgements

The authors acknowledge the financial support from the National Natural Science Foundation of China (20875082) and the Foundation of the Educational Committee of Jiangsu Provincial Universities Excellence Science and Technology Invention Team in Yangzhou University.

### References

- [1] M. Soylak, B. Kaya, M. Tuzen, J. Hazard. Mater. 147 (2007) 832.
- [2] B. Ramachandra Reddy, D. Neela Priya, J. Power Sources 161 (2006) 1428.
- [3] Y.R. Kang, J.L. Zhao, J.L. Tao, X.X. Wang, Y.X. Li, Appl. Surf. Sci. 254 (2008) 3935.
- [4] B. Swain, J.K. Jeong, J.C. Lee, G.H. Lee, J. Membr. Sci. 297 (2007) 253.
- [5] K. Kiran, K. Suresh Kumar, K. Suvaradhan, K. Janardhanam, P. Chiranjeevi, J. Hazard. Mater. 147 (1/2) (2007) 15.
- [6] W. Ngeontae, W. Aeungmaitrepirom, T. Tuntulani, Talanta 71 (2007) 1075.
- [7] G.Z. Fang, J. Tan, X.P. Yan, Anal. Chem. 77 (2005) 1734.
- [8] A.M. Zou, M.L. Chen, Y. Shu, M. Yang, J.H. Wang, J. Anal. At. Spectrom. 22 (2007) 392.
- [9] I. Narin, Y. Surme, E. Bercin, M. Soylak, J. Hazard. Mater. 145 (2007) 113.
- [10] H.B. Alexandra, P. Rohani, W.C. Robert, D.K. Spas, Talanta 71 (2007) 419.
- [11] S.Z. Chen, M.F. Xiao, D.B. Lu, Z. Wang, Spectrochim. Acta B 62 (2007) 1216.
- [12] Y. Wang, J.H. Wang, Z.L. Fang, Anal. Chem. 77 (2005) 5396.
- [13] Y. Wang, M.L. Chen, J.H. Wang, J. Anal. At. Spectrom. 21 (2006) 535.
- [14] M.L. Chen, Y. Tian, J.H. Wang, J. Anal. At. Spectrom. 23 (2008) 876.
- [15] X.S. Zhu, M. Wu, J. Sun, X.F. Zhang, Anal. Lett. 41 (2008) 2186.
- [16] C.A. Kozlowski, T. Girek, W. Walkowiak, J.J. Koziol, Sep. Purif. Technol. 46 (2005) 136.
- [17] J.Y. Moon, H.J. Jung, M.H. Moon, B.C. Chung, M.H. Choi, Steroids 73 (2008) 1090.
- [18] J.Y. Moon, J.Y. Kim, M.H. Moon, B.C. Chung, M.K. In, M.H. Choi, J. Chromatogr. A 1204 (2008) 87.
- [19] M. Bhaskar, P. Aruna, R. Jeevan, G. Jeevan, G. Radhakrishnan, Anal. Chim. Acta 509 (2004) 395.
- [20] E.J. Underwood, Trace Elements in Human and Nutrition, fourth ed, Academic Press, New York, 1977.
- [21] The Committee of China Official Pharmacopoeia, The official pharmacopoeia of People's Republics of China, Chemical Engineering Press, Beijing, 2005, p. 668.
- [22] C.G. Bruhn, F.E. Ambiado, H.J. Cid, R. Woerner, J. Tapia, R. Garcia, Anal. Chim. Acta 306 (1995) 183.
- [23] D.M. Hopkins, J. Geochem. Explor. 41 (1991) 349.
- [24] M.I. Chicarelli, C.B. Eckardt, C.R. Owen, J.R. Maxwell, G. Eglinton, R.C. Hutton, A.N. Eaton, Org. Geochem. 15 (1990) 267.
- [25] A. Bobrowski, Anal. Lett. 23 (1990) 1487.
- [26] Q.B. Zhang, H. Minami, S. Inoue, I. Atsuya, Anal. Chim. Acta 407 (2000) 147.
- [27] M. Ghaedi, F. Ahmadi, M. Soylak, J. Hazard. Mater. 147 (2007) 226.
- [28] M. Vega, C.M.G. van den Berg, Anal. Chem. 69 (1997) 874.
- [29] M. Tuzen, M. Soylak, L. Elci, Anal. Chim. Acta 548 (2005) 101.
- [30] M. Shibukawa, A. Unno, T. Miura, A. Nagoya, K. Oguma, Anal. Chem. 75 (2003) 2775.
- [31] J.Z. Kang, T.C. Duan, P.R. Guo, C. Wang, H.T. Chen, X.J. Zeng, Chem. J. Chin. Univ. 25 (2004) 252.
- [32] Y.E. Zeng, H.S. Zhang, Z.H. Chen, Current Chemical Reagent Manual, 4th Manual, Inorganic Ion Chelating Agent, Chemical Engineering Press, Beijing, 1989.
- [33] X.S. Zhu, R. Guo, W.B. Qie, Chin. J. Anal. Chem. 23 (9) (1995) 989.
- [34] X.S. Zhu, R. Guo, W.B. Qie, Chin. J. Anal. Chem. 25 (7) (1997) 860.



# Development of a new analytical method for online simultaneous qualitative determination of aluminium (free aluminium ion, aluminium-fluoride complexes) by HPLC-FAAS

Anetta Ziola-Frankowska, Marcin Frankowski\*, Jerzy Siepak

Department of Water and Soil Analysis, Adam Mickiewicz University, Drzymały 24, 60-613 Poznań, Poland

## ARTICLE INFO

### Article history:

Received 16 July 2008

Received in revised form 8 December 2008

Accepted 11 December 2008

Available online 24 December 2008

### Keywords:

Aluminium

Aluminium fluoride complexes

Hyphenated technique

HPLC-FAAS

## ABSTRACT

The paper presents a novel method for simultaneous online examination of inorganic forms of aluminium:  $\text{AlF}_2^+$ ,  $\text{AlF}^{2+}$ , and  $\text{Al}^{3+}$  by means of the high performance liquid chromatography hyphenated with a detection by the atomic absorption spectrometry with flame atomization (HPLC-FAAS) without post-column reaction. The application of optimization procedure conditions of chromatographic separation of inorganic forms of aluminium was achieved by the analytical column IonPac CS5A (Dionex) with guard column IonPac CG5A (Dionex) and an aqueous ammonium chloride mobile phase, at pH about 3 with gradient elution. The separation of Al forms with nominal charge of 1+, 2+, 3+ required a run time of less than 8 min during a single analysis. The proposed method has been successfully used for the examination of aluminium forms formation  $\text{AlF}_n^{(3-n)+}$  in environmental samples.

© 2008 Elsevier B.V. All rights reserved.

## 1. Introduction

Aluminium as an element commonly found in the earth's crust (8% wt.), characterised by strong amphoteric nature [1,2]. It can create numerous species complexes [3–5]. The type of these aluminium complexes depends on the following factors: pH, temperature, concentration of inorganic and organic ligands occurrence in water [6,7]. The total aluminium found in surface water can be divided into three fractions: acid-soluble aluminium, containing bonds in the form of polymers, colloids, and stable organic and hydroxy organic complexes. The second fraction is non labile monomeric (organic) aluminium containing chelated organic aluminium forms. The last fraction, called labile monomeric aluminium (inorganic), consists of a free  $\text{Al}^{3+}$  ion and inorganic-fluoride, -hydroxy and -sulfate aluminium complexes [8]. The form in which aluminium occurs in the environment affects its mobility, bioavailability and toxic influence on living organisms and vegetation [9–12]. Aluminium toxicity is mainly connected with the occurrence of a free  $\text{Al}^{3+}$  ion, hydroxy forms (including  $\text{Al}(\text{OH})_2^+$ ,  $\text{Al}(\text{OH})_2^+$ ) and inorganic form of complexes [12–14]. Among inorganic forms the aluminium fluoride complexes are dominating [3,4,8,9,15]. They are characterised by high values of stability constant ( $\text{AlF}_2^+$ ,  $\log K = 12.600$ ;  $\text{AlF}^{2+}$ ,  $\log K = 7.000$ ) (data obtained from a chemical equilibrium modeling system Mineql+

ver. 4.5). The forms of aluminium fluoride complexes ( $\text{AlF}_2^+$ ,  $\text{AlF}^{2+}$ ,  $\text{AlF}_3$ ,  $\text{AlF}_4^-$ ,  $\text{AlF}_5^{2-}$ ,  $\text{AlF}_6^{3-}$ ) and their occurrence depend on pH and  $\text{F}^-$  concentration in water [16,17]. The complexity of aluminium speciation forms determination is conditioned by the necessity to determine them both in water and soil [2]. It should be emphasised that determination of only total concentration of aluminium does not provide full data concerning the processes the element undergoes in the natural environment and, in consequence, does not provide information on migration, actual toxicity, bioavailability and cumulation in particular components of the environment [18]. The subject of aluminium speciation analysis has evoked wide interest among researchers. One of the best known and most commonly applied procedures of speciation analysis is the Driscoll's method, which enables isolating a fraction of labile monomeric inorganic aluminium containing an  $\text{Al}^{3+}$  ion and bonds with inorganic fluoride and sulfate ligands [4,19,20]. However, the above method does not enable direct determination of particular speciation forms of aluminium, including fluoride complexes and  $\text{Al}^{3+}$ ,  $\text{Al}(\text{OH})_2^+$ ,  $\text{Al}(\text{OH})_2^+$  species [20,21]. The use of liquid chromatography provides a lot of possibilities to separate particular forms of aluminium, both cation and anion ones [12,13,20,22]. The use of liquid chromatography for determination of aluminium fluoride complexes enables the separation and identification of anion and cation bonds of aluminium with fluoride [9]. Bertsh and Anderson [23] were among the first researchers who suggested the separation of aluminium fluoride complexes using the ion chromatography. They used  $\text{NH}_4\text{Cl}$  (0.7 M) solution as the eluent with UV detection and post-column reaction with Tiron (4,5-dihydroxy-m-benzenedisulfonic acid) as well as the

\* Corresponding author. Tel.: +48 61 829 3443; fax: +48 61 829 3448.  
E-mail address: [Marcin.Frankowski@amu.edu.pl](mailto:Marcin.Frankowski@amu.edu.pl) (M. Frankowski).

separation in CS3 (Dionex) cation column in order to determine stable  $AlF_x$  complexes. The conditions for determinations were used in the analysis of standard solutions in order to isolate  $Al^{3+}$  from fluoride, citrate and oxalate complexes. Retention times obtained did not differ significantly for citrate, oxalate aluminium complexes and fluoride  $AlF_2^+$  complexes. The  $AlF_2^+$  and  $Al^{3+}$  forms were separated. The above method was not used in environmental samples determination. Also Willet [25], who used  $K_2SO_4$  at pH 3.0 as the eluent and CG2 (Dionex) guard column and post-column reaction with mixture of PCV (Pyrocatechol Violet) and 1,10-phenanthroline, hydroxylamine (in order to mask the influence of  $< \mu mol L^{-1} Fe^{3+}$ ) did not obtain a good separation of  $AlF_2^+$  and  $AlF_2^+$  forms, despite the quick separation (4 min per sample). Similar to Willet [25], Jones [26] used the CG2 (Dionex) guard column additionally stabilized in the temperature of  $50^\circ C$  and fluorometric detection with post-column reaction in order to directly determine monomeric aluminium hydroxy forms. Jones [26] used  $K_2SO_4$  (0.06–0.1 M) at pH 3.0 as the eluent and HQS (8-Hydroxyquinoline-5-sulfonic acid) as the post-column reagent. Neither Willet [25] nor Jones [26] managed to separate the  $AlF_2^+$  and  $AlF_2^+$  forms, they were eluted in a non resolved peak close to the solvent front and also they were not quite resolved. Motellier and Pitsch [27], who used CS2 (Dionex) cation column connected with CG2 (Dionex) guard column and  $NH_4Cl$  (0.5 M) as the eluent acidified by the solution of HCl (0.01 M), and post-column reaction with Tiron in ammonium acetate followed by UV spectrophotometry, did not obtain the full resolution for the first two peaks  $AlF_2^+$  and  $AlF_2^+$ . To date, the research on  $AlF_x$  complexes speciation using ion chromatography has been based on isocratic elution. Firstly Bormann and Seubert [28] used perchloric acid ( $10^{-3} M$ , pH3.0) and ethylenediamine perchlorate (0.4 M, pH3.0) for speciation of Al and its fluoro, oxalate and citrate complexes. These forms were determined by post-column reaction with Tiron (4,5-dihydroxy-m-benzenedisulfonic acid) followed by UV spectrophotometry and atomic spectrometry ICP-AES as well (for Al-citrate-oxalate complexes). Depending on the proportion of ligands in standard solutions, in the case of Al-F complexes in the amount of 1:1 (Al:F). The obtained signals were assigned to the following forms:  $AlF_2^+$ ,  $AlF_2^+$  and  $Al^{3+}$  (by post-column reaction with Tiron followed by UV spectrophotometry). It also seems noteworthy that the separation of aluminium fluoride species obtained by Bormann and Seubert [28] was affected by the use of post-column reaction followed by UV detection.

To date, the combination of HPLC with ICP: mass spectrometry and atomic emission spectrometry (ICP-MS, ICP-AES) in the online [6,7,22,27–31] as well as offline system [13,32] have been used. The researchers have also applied atomic absorption spectrometry with electrothermal atomization in the offline system [10,33].

The determination conditions suggested by the above researchers did not always result in full separation of particular aluminium fluoride complexes nor provided the possibility of their qualitative and quantitative determination. Moreover, they were not used in environmental analyses. The main aims of this study were: (1) development of a new analytical method and optimization, (2) examination of the formation of aluminium-fluoride complexes in model system and (3) examination of a new analytical method in environmental samples.

## 2. Experimental

### 2.1. Instrumentation and chromatographic separation

The chromatographic separation was performed by liquid chromatography system consisting of: Shimadzu solvent delivery module LC-10 ADVP liquid chromatograph (Shimadzu Corporation, Japan) and low pressure gradient flow control valve Shimadzu

**Table 1**

Time schedule for the separation inorganic forms of aluminium by liquid chromatography (in HPLC-FAAS analytical system) with gradient elution (eluent A,  $H_2O$ ; eluent B, 1.8 M ammonium chloride).

Time (min)	Eluent A (%)	Eluent B (%)	Injection valve	Comments
0.00	100	0	Load	Start conditions
2.00	100	0	Injection	Sample injection
3.99	100	0	Injection	Start linear gradient
4.15	0	100	Injection	Increase in eluent strength
5.15	0	100	Injection	Start data collection <sup>a</sup>
6.15	0	100	Injection	Stop data collection
6.16	100	0	Injection	Return to initial conditions
8.00	100	0	Load	Stop data collection

<sup>a</sup> Time of calculating the analytical signal from 5.15 at the time of gradient start 4.15–5.15 the sample runs through chromatographic system to nebulizer system. The sample is passed through analytical column to nebulizer system. For the FAAS detection the effluent leaving the column was connected directly to the nebulizer.

FCV-10 ALVP (Shimadzu Corporation, Japan) with Rheodyne Model 7725i Injection Valve (Rheodyne LLC, USA). The liquid chromatography system was coupled to ion-exchange column–Dionex IonPac CS5A (analytical column, 250 mm, 4.0 mm i.d., particle size  $9.0 \mu m$ , containing mixed anion and cation beds with sulfonic acid and alkanol quaternary ammonium functional groups) (Dionex, USA) and IonPac CG5A (guard column, 50 mm, 4 mm i.d., particle size  $9.0 \mu m$ ) (Dionex, USA). The chromatographic run was gradient at  $2 mL min^{-1}$  with an injection volume of  $500 \mu L$ . The gradient elution program is shown in Table 1. The species of aluminium were determined by the technique of atomic absorption spectrometry with acetylene-nitrous oxide flame atomisation (F-AAS) with the use of a double-beam PerkinElmer apparatus, AAnalyst 300 model (PerkinElmer, Norwalk, CT, USA). The hollow cathode lamp (HCL) Al Lumina used was also purchased from the same firm (PerkinElmer, Norwalk, CT, USA). Data capturing and peak analysis were performed with the use of AAWinLab32 software (PerkinElmer, Norwalk, CT, USA).

The analytical chromatographic column was directly connected to the nebulizer system simultaneously working type of atomic absorption spectrometer.

### 2.2. Reagents

All chemicals used were of high-purity grade. Deionised water from Milli-Q RG water unit (Millipore, France) was used for dilution of stock solutions as well as for any reagent preparation. All stock solutions of aluminium were obtained by dissolving standard solution  $1000 mg L^{-1}$  from Merck (Dramstadt, Germany). Stock standard solutions of fluorine  $1000 mg L^{-1}$  were prepared from Merck (Dramstadt, Germany). Working solutions were prepared daily just before measurements by appropriate dilution. The eluent used for gradient elution consisted of A: deionised water, B: ammonium chloride (1.8 M pH about 3). The eluent was made by dissolving a weighted portion of  $NH_4Cl$  (Merck, Dramstadt, Germany) in deionised water and finally diluted to 1000 mL by deionised water. The solution of  $NH_4Cl$  was acidified by 1 mM hydrochloric acid (Merck, Dramstadt, Germany) to pH about 3 in a volumetric flask. A series of standards mixtures of Al-F were prepared by the appropriate dilution of solutions containing aluminium and fluoride ions in various concentrations.

### 2.3. Samples

The environmental samples were taken in the area of Chemical Plants situated in Luboń (Poland). The ground water samples were collected from the piezometers located in the area of Chemical Plants using a pump for ground water sampling. Then, samples were collected into high density polyethylene containers. The containers

were filled up to the brim with the samples to avoid any air space and then transported to the laboratory without any additives. The qualitative analysis of the inorganic aluminium species (aluminium fluoride complexes) present was carried out using hyphenated technique by HPLC-FAAS as soon as possible return to the laboratory. Moreover the groundwater samples were mixed manually and then filtered through a filter-membrane (0.45  $\mu\text{m}$ ) before injection into the analytical column to prevent fouling problems.

### 3. Results and discussion

One of the main aim of the study was creating the conditions for chromatographic determination which would enable full separation of three inorganic forms of aluminium:  $\text{AlF}_2^+$ ,  $\text{AlF}^{2+}$  and  $\text{Al}^{3+}$  and their online detection using flame atomic absorption spectrometry (HPLC-FAAS). The research involved: selecting the proper analytical column and type of eluent in terms of defining the column type and the type and concentration of the mobile phase in the number of separated aluminium forms in the investigated model solutions. Two analytical columns were used in the research: IonPac CS5A (Dionex, USA) and Supelcosil<sup>TM</sup> LC-SCX (Supelco, USA), as well as the mobile phases previously used by other researchers:  $\text{K}_2\text{SO}_4$  (0.1 M) [22,24,25,28,34],  $\text{Na}_2\text{SO}_4$  (0.1 M) [35–38],  $\text{NH}_4\text{NO}_3$  (2.0 M) [10,13],  $\text{NH}_4\text{Cl}$  (0.8 M) [23]. Separation of three aluminium forms was obtained only using the IonPac CS5A column. Investigations defining the influence of type and concentration of eluents on the separation degree in the IonPac CS5A column enabled the separation of three forms only using  $\text{NH}_4\text{Cl}$ . Further optimization work was done in the mobile phase of  $\text{NH}_4\text{Cl}$  solution using the solution concentrations of 0.5 M, 0.8 M, 1.0 M, 1.2 M, 1.5 M, 1.8 M. The best separation was obtained for  $\text{NH}_4\text{Cl}$  concentration 1.8 M, while for the remaining concentrations the asymmetry of peaks and peak distortion for the forms subject to elution at the beginning and end of the process were observed.

The use of optimized analytical conditions for  $\text{AlF}_x$  complexes determination enabled obtaining full separation of the following forms:  $\text{AlF}_2^+$ ,  $\text{AlF}^{2+}$  and  $\text{Al}^{3+}$  during a single analysis lasting 8 min. Furthermore, depending on Al and  $\text{F}^-$  concentration, different forms and shapes of particular  $\text{AlF}_x$  forms were obtained. Based on the literature data [24,27,35–40] and the property of the mixture components separation according to increasing charge of these forms, it was assumed that the first component (aluminium form) subject to elution was form  $\text{AlF}_2^+$ , then  $\text{AlF}^{2+}$  and finally  $\text{Al}^{3+}$ . The occurrence of a given form in the investigated model solutions at the constant aluminium concentration was dependent on the changing concentration of  $\text{F}^-$  ions. That is why a number of solutions were analysed in order to present the influence of aluminium and fluoride concentration on the type of fluoride and aluminium fluoride species formed in standard solutions. (Figs. 1–5).

#### 3.1. Examination of the formation of $\text{AlF}_x$ complexes in model solutions containing different quantities of aluminium and fluoride

##### 3.1.1. Standard solutions containing (Al:F)

(a) Al: 100  $\text{mg L}^{-1}$ ,  $\text{F}^-$ : 5  $\text{mg L}^{-1}$ ; (b) Al: 100  $\text{mg L}^{-1}$ ,  $\text{F}^-$ : 25  $\text{mg L}^{-1}$ ; (c) Al: 100  $\text{mg L}^{-1}$ ,  $\text{F}^-$ : 50  $\text{mg L}^{-1}$ ; (d) Al: 100  $\text{mg L}^{-1}$ ,  $\text{F}^-$ : 75  $\text{mg L}^{-1}$ ; (e) Al: 100  $\text{mg L}^{-1}$ ,  $\text{F}^-$ : 100  $\text{mg L}^{-1}$ .

In all standard solutions (a–e), full separation of three  $\text{AlF}_2^+$ ,  $\text{AlF}^{2+}$  and  $\text{Al}^{3+}$  forms were obtained. It was observed that, along with the increase of  $\text{F}^-$  concentration,  $\text{AlF}^{2+}$  was the dominating form (for solutions d and e) (Fig. 1d and e). For the remaining solutions (a–b),  $\text{Al}^{3+}$  showed the largest participation (Fig. 1a and b) and for solution (c) similar participation between  $\text{AlF}^{2+}$  and  $\text{Al}^{3+}$  forms was observed (Fig. 1c). Smaller concentration of  $\text{F}^-$  in solutions was

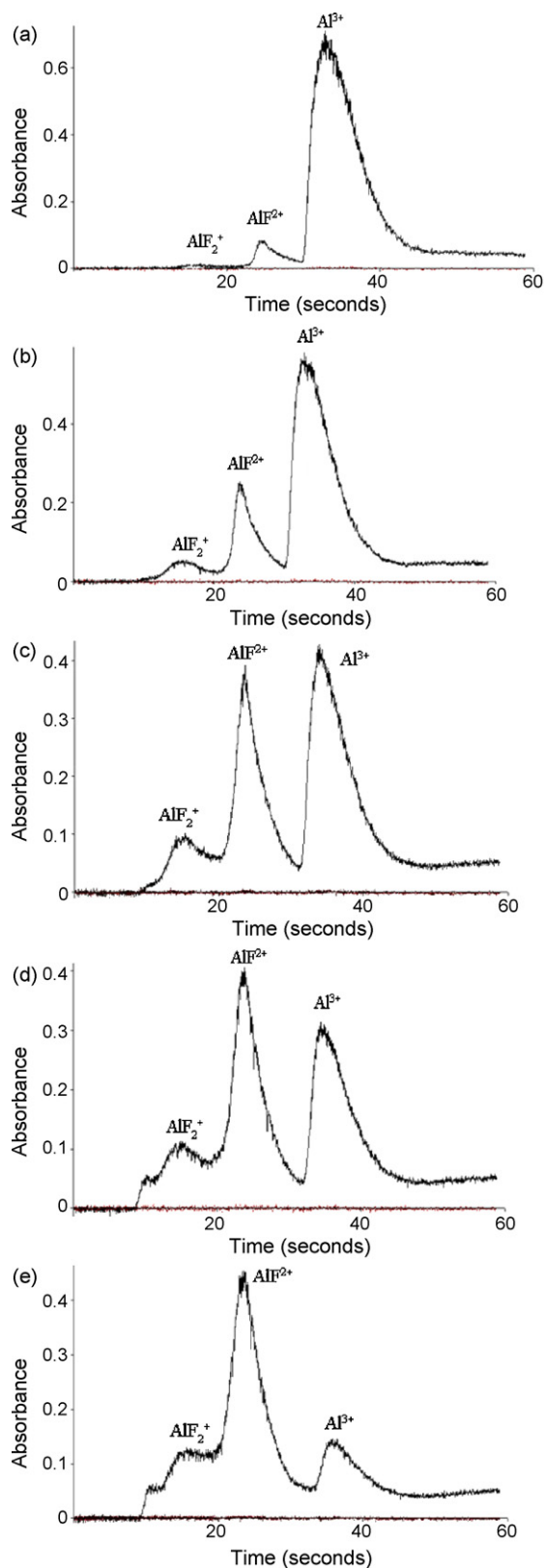
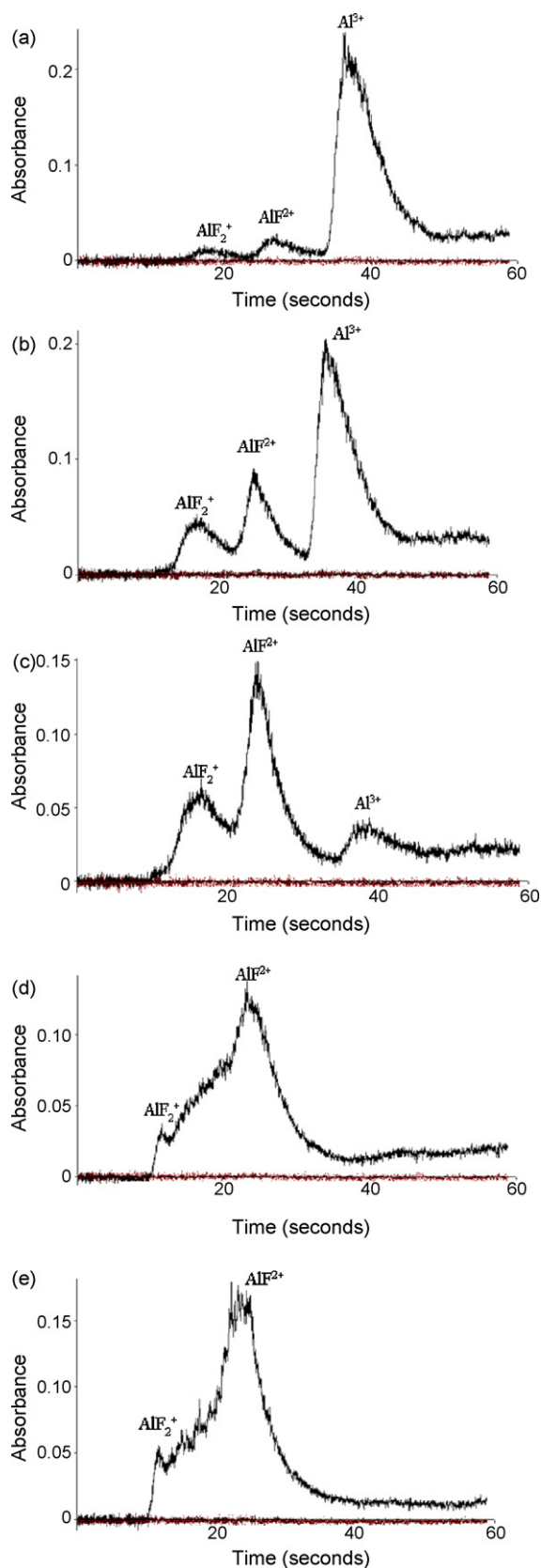
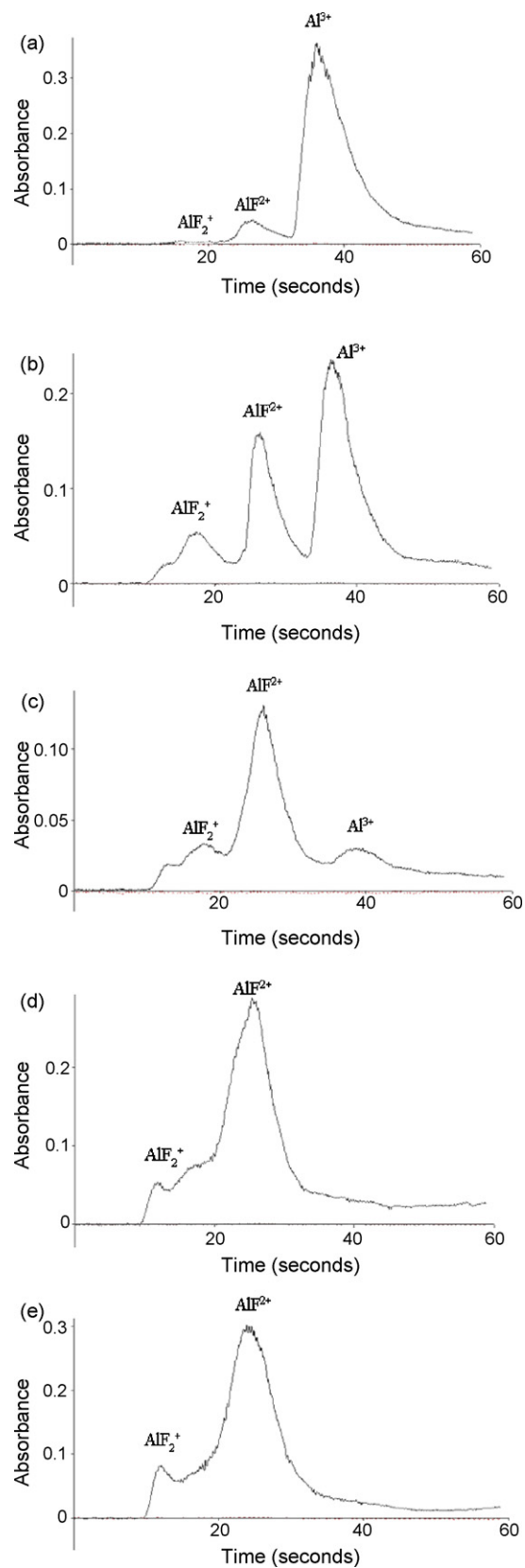


Fig. 1. Chromatograms obtained for: (a) Al: 100  $\text{mg L}^{-1}$ ,  $\text{F}^-$ : 5  $\text{mg L}^{-1}$ ; (b) Al: 100  $\text{mg L}^{-1}$ ,  $\text{F}^-$ : 25  $\text{mg L}^{-1}$ ; (c) Al: 100  $\text{mg L}^{-1}$  and  $\text{F}^-$ : 50  $\text{mg L}^{-1}$ ; (d) Al: 100  $\text{mg L}^{-1}$  and  $\text{F}^-$ : 75  $\text{mg L}^{-1}$ ; (e) Al: 100  $\text{mg L}^{-1}$  and  $\text{F}^-$ : 100  $\text{mg L}^{-1}$  using FAAS detection.



**Fig. 2.** Chromatograms obtained for: (a) Al:  $75 \text{ mg L}^{-1}$ ,  $\text{F}^-$ :  $5 \text{ mg L}^{-1}$ ; (b) Al:  $75 \text{ mg L}^{-1}$ ,  $\text{F}^-$ :  $25 \text{ mg L}^{-1}$ ; (c)  $75 \text{ Al mg L}^{-1}$ ,  $\text{F}^-$ :  $50 \text{ mg L}^{-1}$ ; (d) Al:  $75 \text{ mg L}^{-1}$ ,  $\text{F}^-$ :  $75 \text{ mg L}^{-1}$ ; (e) Al:  $75 \text{ mg L}^{-1}$ ,  $\text{F}^-$ :  $100 \text{ mg L}^{-1}$  using FAAS detection.



**Fig. 3.** Chromatograms obtained for: (a) Al:  $50 \text{ mg L}^{-1}$ ,  $\text{F}^-$ :  $5 \text{ mg L}^{-1}$ ; (b) Al:  $50 \text{ mg L}^{-1}$ ,  $\text{F}^-$ :  $25 \text{ mg L}^{-1}$ ; (c) Al:  $50 \text{ mg L}^{-1}$ ,  $\text{F}^-$ :  $50 \text{ mg L}^{-1}$ ; (d) Al:  $50 \text{ mg L}^{-1}$ ,  $\text{F}^-$ :  $75 \text{ mg L}^{-1}$ ; (e) Al:  $50 \text{ mg L}^{-1}$ ,  $\text{F}^-$ :  $100 \text{ mg L}^{-1}$  using FAAS detection.

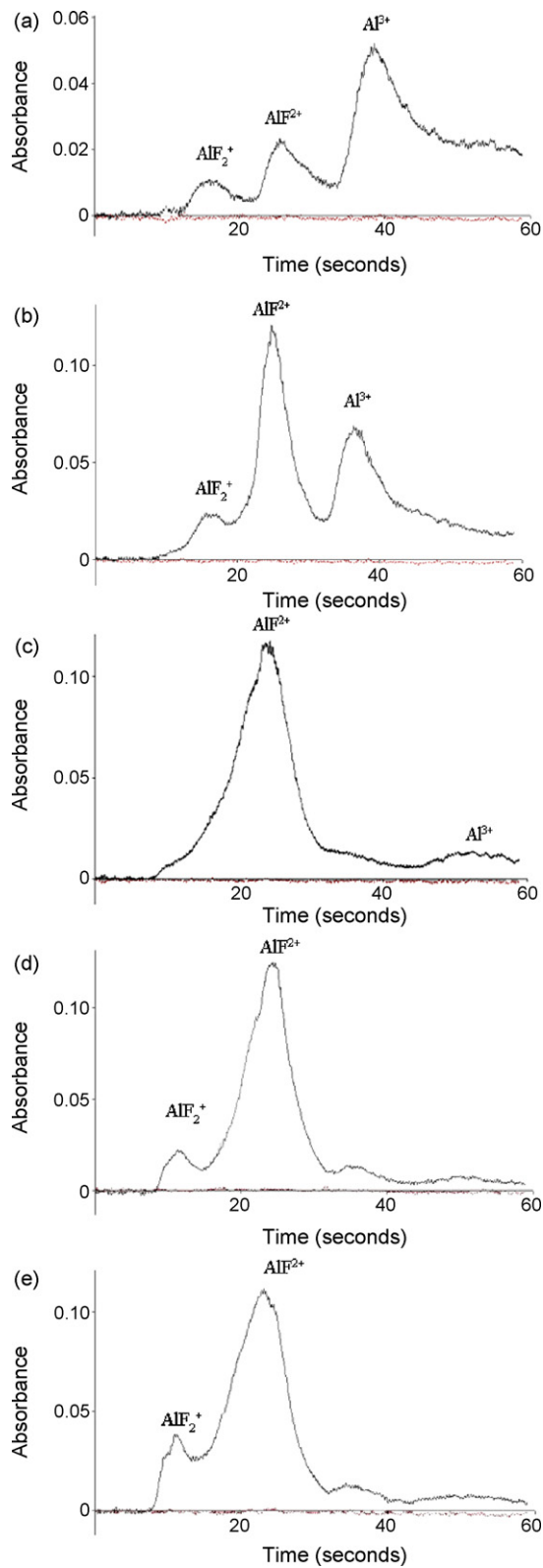


**Fig. 4.** Chromatograms obtained for: (a) Al: 25 mg L<sup>-1</sup>, F<sup>-</sup>: 5 mg L<sup>-1</sup>; (b) Al: 25 mg L<sup>-1</sup>, F<sup>-</sup>: 25 mg L<sup>-1</sup>; (c) Al: 25 mg L<sup>-1</sup>, F<sup>-</sup>: 50 mg L<sup>-1</sup>; (d) Al: 25 mg L<sup>-1</sup>, F<sup>-</sup>: 75 mg L<sup>-1</sup>; (e) Al: 25 mg L<sup>-1</sup>, F<sup>-</sup>: 100 mg L<sup>-1</sup> using FAAS detection.

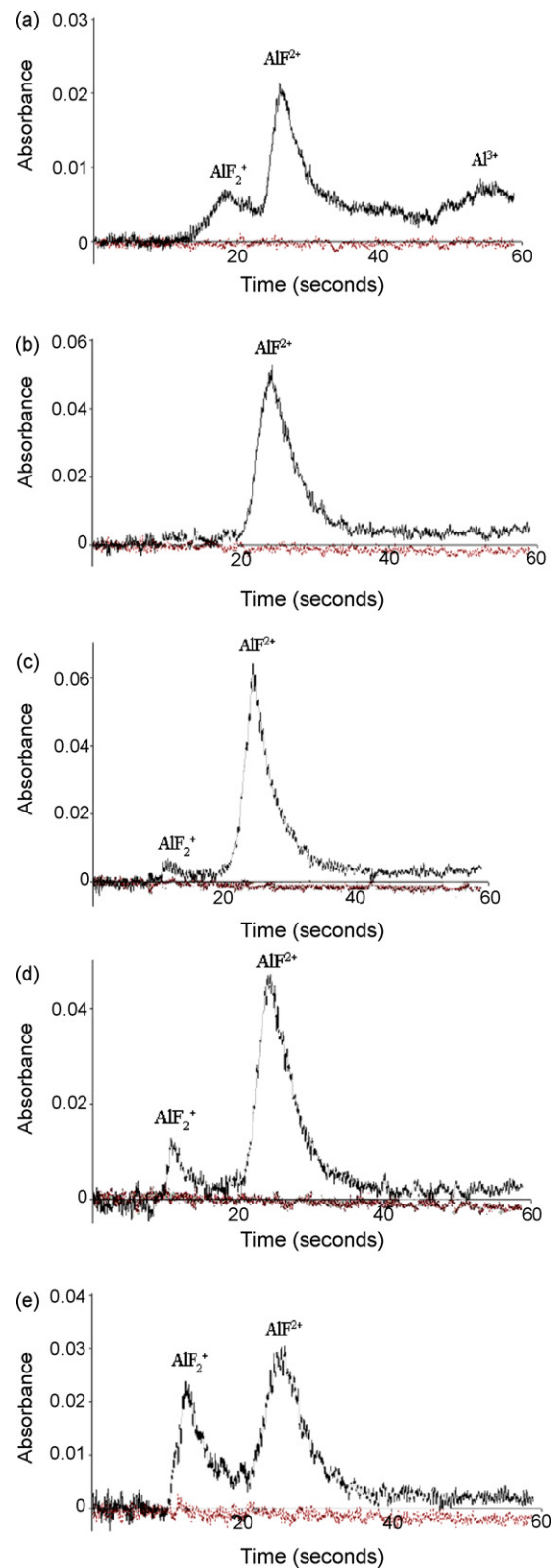


**Fig. 5.** Chromatograms obtained for: (a) Al: 5 mg L<sup>-1</sup>, F<sup>-</sup>: 5 mg L<sup>-1</sup>; (b) Al: 5 mg L<sup>-1</sup>, F<sup>-</sup>: 25 mg L<sup>-1</sup>; (c) Al: 5 mg L<sup>-1</sup>, F<sup>-</sup>: 50 mg L<sup>-1</sup>; (d) Al: 5 mg L<sup>-1</sup>, F<sup>-</sup>: 75 mg L<sup>-1</sup>; (e) Al: 5 mg L<sup>-1</sup>, F<sup>-</sup>: 100 mg L<sup>-1</sup> using FAAS detection.

accompanied by much smaller participation of  $\text{AlF}_2^+$ ,  $\text{AlF}^{2+}$  forms compared with  $\text{Al}^{3+}$ , especially for solution a (Fig. 1a).

### 3.1.2. Standard solutions containing (Al:F)

(a) Al:  $75 \text{ mg L}^{-1}$ ,  $\text{F}^-$ :  $5 \text{ mg L}^{-1}$ ; (b) Al:  $75 \text{ mg L}^{-1}$ ,  $\text{F}^-$ :  $25 \text{ mg L}^{-1}$ ;  
(c) Al:  $75 \text{ mg L}^{-1}$ ,  $\text{F}^-$ :  $50 \text{ mg L}^{-1}$ ; (d) Al:  $75 \text{ mg L}^{-1}$ ,  $\text{F}^-$ :  $75 \text{ mg L}^{-1}$ ;  
(e) Al:  $75 \text{ mg L}^{-1}$ ,  $\text{F}^-$ :  $100 \text{ mg L}^{-1}$ .

In the case of the analysed solutions, three forms were obtained ( $\text{AlF}_2^+$ ,  $\text{AlF}^{2+}$  and  $\text{Al}^{3+}$ ) for a and b, with  $\text{Al}^{3+}$  dominating (Fig. 2a and b), and for c in which case  $\text{AlF}^{2+}$  form showed the largest participation (Fig. 2c). In the case of solutions (Fig. 2d and e), the full separation of  $\text{AlF}_2^+$  and  $\text{AlF}^{2+}$  was not obtained (Fig. 2d and e). Formation of form  $\text{Al}^{3+}$  was not observed either.

### 3.1.3. Standard solutions containing (Al:F)

(a) Al:  $50 \text{ mg L}^{-1}$ ,  $\text{F}^-$ :  $5 \text{ mg L}^{-1}$ ; (b) Al:  $50 \text{ mg L}^{-1}$ ,  $\text{F}^-$ :  $25 \text{ mg L}^{-1}$ ;  
(c) Al:  $50 \text{ mg L}^{-1}$ ,  $\text{F}^-$ :  $50 \text{ mg L}^{-1}$ ; (d) Al:  $50 \text{ mg L}^{-1}$ ,  $\text{F}^-$ :  $75 \text{ mg L}^{-1}$ ;  
(e) Al:  $50 \text{ mg L}^{-1}$ ,  $\text{F}^-$ :  $100 \text{ mg L}^{-1}$ .

For solutions containing  $50 \text{ mg L}^{-1}$  of Al, three forms were separated ( $\text{AlF}_2^+$ ,  $\text{AlF}^{2+}$  and  $\text{Al}^{3+}$ ) for solution a and b, with form  $\text{Al}^{3+}$  dominating (Fig. 3a and b), and for solutions c, with form  $\text{AlF}^{2+}$  dominating (Fig. 3c). In solutions d and e, two forms  $\text{AlF}_2^+$ ,  $\text{AlF}^{2+}$  were obtained with the largest participation of monofluoroaluminium (II) form (Fig. 3d and e).

### 3.1.4. Standard solutions containing (Al:F)

(a) Al:  $25 \text{ mg L}^{-1}$ ,  $\text{F}^-$ :  $5 \text{ mg L}^{-1}$ ; (b) Al:  $25 \text{ mg L}^{-1}$ ,  $\text{F}^-$ :  $25 \text{ mg L}^{-1}$ ;  
(c) Al:  $25 \text{ mg L}^{-1}$ ,  $\text{F}^-$ :  $50 \text{ mg L}^{-1}$ ; (d) Al:  $25 \text{ mg L}^{-1}$ ,  $\text{F}^-$ :  $75 \text{ mg L}^{-1}$ ;  
(e) Al:  $25 \text{ mg L}^{-1}$ ,  $\text{F}^-$ :  $100 \text{ mg L}^{-1}$ .

In this case three forms ( $\text{AlF}_2^+$ ,  $\text{AlF}^{2+}$  and  $\text{Al}^{3+}$ ) were separated in solution a, with form  $\text{Al}^{3+}$  dominating (Fig. 4a), and solution b, with form  $\text{AlF}^{2+}$  dominating (Fig. 4b). For solution c, the separation of  $\text{AlF}^{2+}$  and  $\text{Al}^{3+}$  forms were obtained, with the largest participation of monofluoroaluminium (II) (Fig. 4c). For the remaining d and e solutions  $\text{AlF}_2^+$  and  $\text{AlF}^{2+}$  signals were obtained (with form  $\text{AlF}^{2+}$  dominating) without  $\text{Al}^{3+}$  form which was not observed (Fig. 4d and e).

### 3.1.5. Standard solutions containing (Al:F)

(a) Al:  $5 \text{ mg L}^{-1}$ ,  $\text{F}^-$ :  $5 \text{ mg L}^{-1}$ ; (b) Al:  $5 \text{ mg L}^{-1}$ ,  $\text{F}^-$ :  $25 \text{ mg L}^{-1}$ ; (c) Al:  $5 \text{ mg L}^{-1}$ ,  $\text{F}^-$ :  $50 \text{ mg L}^{-1}$ ; (d) Al:  $5 \text{ mg L}^{-1}$ ,  $\text{F}^-$ :  $75 \text{ mg L}^{-1}$ ; (e) Al:  $5 \text{ mg L}^{-1}$ ,  $\text{F}^-$ :  $100 \text{ mg L}^{-1}$ .

For solution a, the separation of three forms ( $\text{AlF}_2^+$ ,  $\text{AlF}^{2+}$  and  $\text{Al}^{3+}$ ) were obtained, with the domination of form  $\text{AlF}^{2+}$  (Fig. 5a) while for solution b only one form ( $\text{AlF}^{2+}$ ) was obtained (Fig. 5b). For solutions c, d and e,  $\text{AlF}_2^+$ ,  $\text{AlF}^{2+}$  forms were separated, with form  $\text{AlF}^{2+}$  dominating (Fig. 5c and d), and with similar scale for solution e (Fig. 5e).

## 3.2. Qualitative analysis of aluminium fluoride complexes in ground water samples

The developed method of the simultaneous determination of aluminium fluoride complexes ( $\text{AlF}_2^+$ ,  $\text{AlF}^{2+}$  and  $\text{Al}^{3+}$  forms) within a single analysis was used in the analysis of ground water samples, originated from the piezometers located in the proximity of Chemical Plants (Luboń, Poland). The investigated ground water samples were characterised by high concentrations of fluoride ions ( $0.49\text{--}1650 \text{ mg L}^{-1}$ ),  $\text{Al}_{\text{tot}}$  ( $0.21\text{--}1047 \text{ mg L}^{-1}$ ) and pH values ( $1.81\text{--}7.75$ ). Such conditions, as the research on model solutions shows, created high affinity of fluoride ions to form aluminium fluoride complexes.

In all presented samples of ground water full separation of  $\text{AlF}_2^+$ ,  $\text{AlF}^{2+}$  and  $\text{Al}^{3+}$  forms were obtained (Fig. 6a–c). Based on chromatogram (Fig. 6a) three forms of aluminium fluoride complexes were obtained with difluoroaluminium (I) dominating

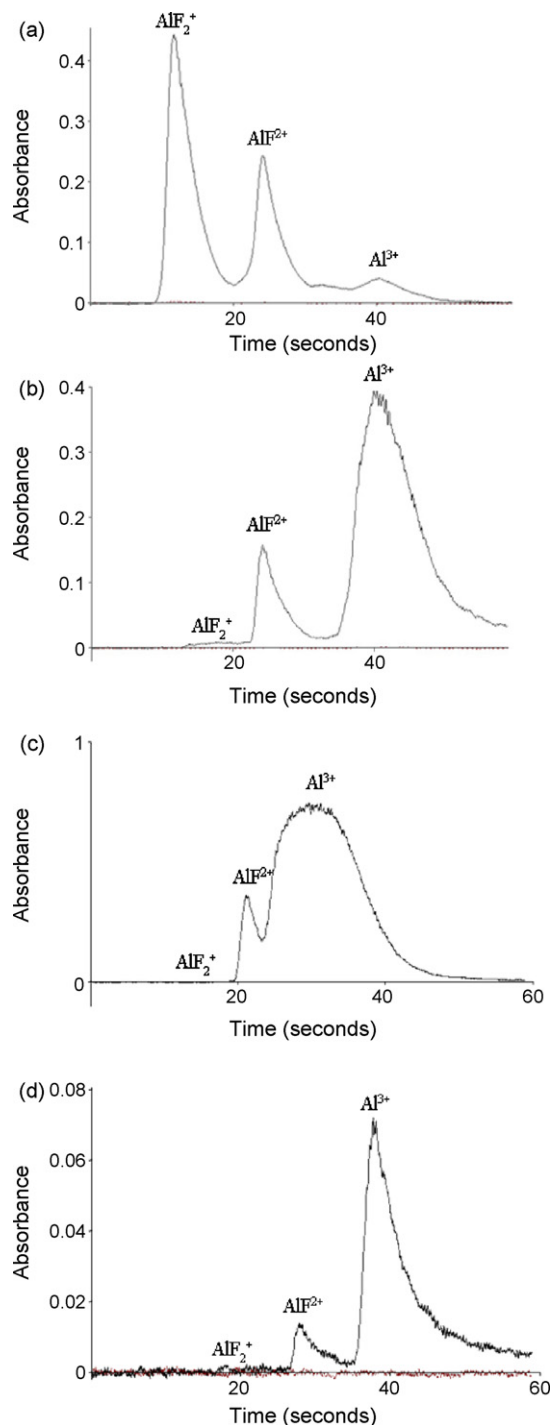
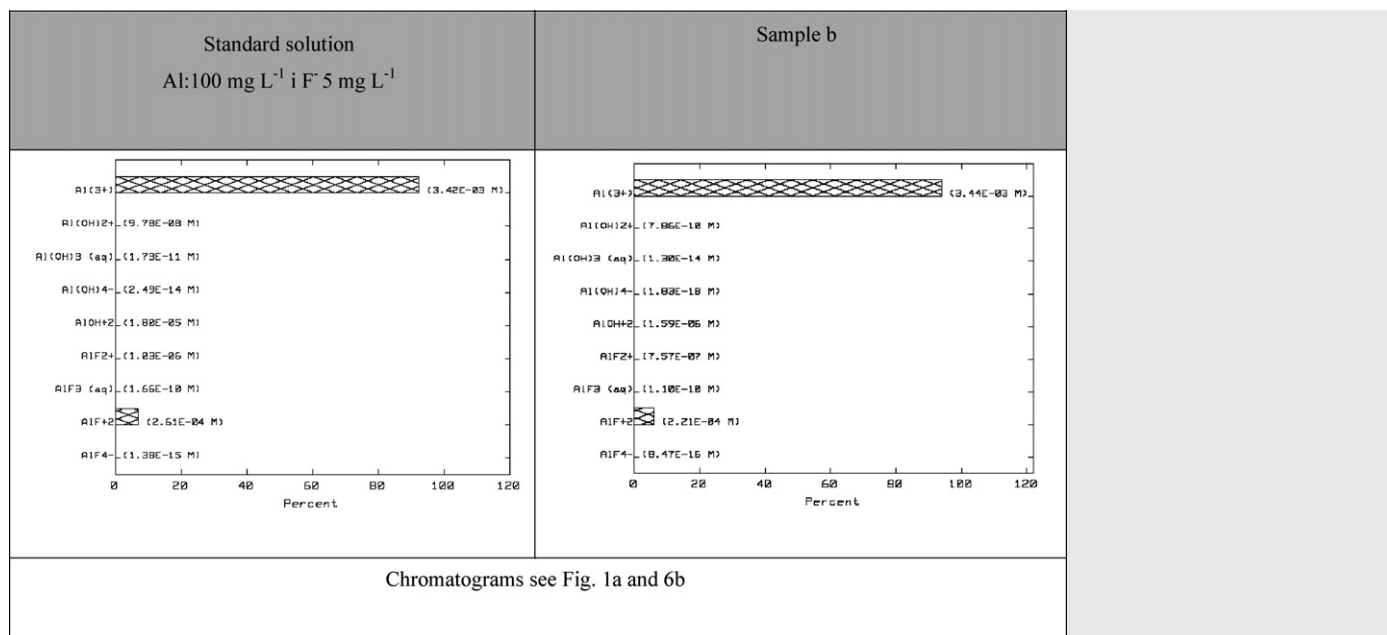


Fig. 6. Chromatograms obtained for ground water samples: a–d (sample d: dilution 1:20 by deionised water of sample c) collected from Chemical Plants (Luboń, Poland).

which is rarely present. Moreover it should also be emphasized that dominance of the  $\text{AlF}_2^+$ ,  $\text{AlF}^{2+}$  forms contributed to increase participation of toxic form of aluminium ( $\text{Al}^{3+}$ ) ( $\text{F}^-$ :  $162 \text{ mg L}^{-1}$ ,  $\text{Al}_{\text{tot}}$ :  $296 \text{ mg L}^{-1}$ ) For sample b and c we observed reverse situation which can be connected with lowest concentration of fluoride ions in analysed samples (for b,  $\text{F}^-$ :  $4.23 \text{ mg L}^{-1}$ ,  $\text{Al}_{\text{tot}}$ :  $98.9 \text{ mg L}^{-1}$ ; for c,  $\text{F}^-$ :  $5.16 \text{ mg L}^{-1}$ ,  $\text{Al}_{\text{tot}}$ :  $374 \text{ mg L}^{-1}$ ). For samples c (undiluted sample) and d (dilution 1:20 by deionised water of sample c) (Fig. 6c and d) it was found that dilution of sample did not change distribution of aluminium fluoride forms, but on the other hand the dilution allowed to improve

**Table 2**

Comparison of aluminium fluoride complexes distribution determined by HPLC-FAAS system and by calculation using chemical equilibrium modeling system Mineql 4.5+.



the separation of three forms of aluminium fluoride complex.

### 3.3. Comparison between obtained results from standard solution and environmental sample with data from Chemical Equilibrium Modeling System Mineql 4.5+

Standard solution containing Al: 100 mg L<sup>-1</sup> and F<sup>-</sup>: 5 mg L<sup>-1</sup> and ground water containing Al: 98.9 mg L<sup>-1</sup> and F<sup>-</sup>: 4.3 mg L<sup>-1</sup> were used to check the correctness of the performed analyses using the Chemical Equilibrium Modeling System, Mineql 4.5+ program. A comparison of experimentally determined species distributions versus calculated distributions is shown in Table 2. The simulation performed with the use of the simulation program Mineql 4.5+ revealed that, in both solutions, Al<sup>3+</sup> was the dominating form. The total concentration of aluminium in the model solution amounted to Al: 100 mg L<sup>-1</sup> and F<sup>-</sup>: 5 mg L<sup>-1</sup>. For the sample "b" it amounted to 98.9 mg L<sup>-1</sup> Al and 4.3 mg L<sup>-1</sup> F<sup>-</sup>. The concentration calculated by the Mineql 4.5+ program for Al<sup>3+</sup> amounted to 92.3 mg L<sup>-1</sup> for the model solution and 92.7 mg L<sup>-1</sup> for sample "b". The other form was AlF<sup>2+</sup> with the concentration of 4.96 mg L<sup>-1</sup> and 4.2 mg L<sup>-1</sup> for the actual sample. In the case of the third form AlF<sub>2</sub><sup>+</sup>, the concentration in both samples was very low and amounted to 0.012 mg L<sup>-1</sup> for the model solution and 0.014 mg L<sup>-1</sup> for the sample. Comparing the obtained results presented in chromatograms (Figs. 1a and 6b) with the results calculated using the Mineql+ 4.5 program, the agreement in the participation degree of forms AlF<sub>2</sub><sup>+</sup>, AlF<sup>2+</sup> and Al<sup>3+</sup> in the sample was obtained. Theoretical distributions confirmed the assumption made on the basis of visual analysis of model solutions chromatograms that the high concentration of aluminium in a sample with low concentrations of fluorides is accompanied by the dominating Al<sup>3+</sup> form in relation to much lower participation of aluminium fluoride forms, especially AlF<sub>2</sub><sup>+</sup>.

## 4. Conclusions

The suggested method for qualitative determination of inorganic aluminium forms in a combined online hyphenated technique system of high-performance liquid chromatography and atomic

absorption spectrometry with flame atomization (HPLC-FAAS) is a novel solution which has not been applied in analytical chemistry to date. Optimized determination conditions for the HPLC-FAAS system using the IonPac CS5A (Dionex) analytical column and NH<sub>4</sub>Cl (1.8 M) as an eluent enabled to obtain full separation of three forms AlF<sub>2</sub><sup>+</sup>, AlF<sup>2+</sup> and Al<sup>3+</sup> during one analysis, which has not been achieved by other research centers before. It should also be emphasized that identification of particular AlF<sub>x</sub> forms (AlF<sub>2</sub><sup>+</sup>, AlF<sup>2+</sup> and Al<sup>3+</sup>) was performed without applying the reaction of derivatization. The presented method enables to define toxic form of aluminium present as "free" ion Al<sup>3+</sup> in a sample and to separate the remaining forms included in labile inorganic aluminium. The Driscoll's method, used to date, enabled determination of the sum of inorganic aluminium forms, such as aluminium fluoride complexes, but it did not provide the possibility to determine a single Al<sup>3+</sup> ion form. Furthermore, the study presents the influence of fluoride ions concentration on the type of aluminium fluoride complexes. Different stoichiometry of aluminium and fluorides concentration in model solutions was strictly related to the type of aluminium fluoride forms present in the sample. The analysis of numerous standard solutions showed that, along with the increase of F<sup>-</sup> ions concentration in the analysed solutions, AlF<sub>2</sub><sup>+</sup>, AlF<sup>2+</sup> forms (especially monofluoroaluminium (II)) were dominating, while the Al<sup>3+</sup> ion aluminium form showed a smaller participation. Parallel smaller numbers of F<sup>-</sup> ions compared with the domination in aluminium solution caused their smaller participation in forming aluminium fluoride complexes, with the domination of Al<sup>3+</sup> form. The presented method may be the application for qualitative analysis of inorganic aluminium forms, including AlF<sub>2</sub><sup>+</sup>, AlF<sup>2+</sup> and Al<sup>3+</sup> toxic form in environmental samples with the use of the combined online hyphenated technique HPLC-FAAS. The proposed method has been demonstrated to be applicable for analysis of aluminium fluoride complexes in groundwater samples. The results obtained by the method HPLC-FAAS showed considerable participation of toxic form Al<sup>3+</sup>. Besides the experimental results were compared with theoretical calculations. The comparison of aluminium fluoride complexes forms distributions obtained by HPLC-FAAS analytical system and by Mineql+ver. 4.5 Chemical Equilibrium Modeling System has shown good agreement.



## Acknowledgement

The research was supported by the Polish Ministry of Science and Higher Education through research grants No. N 305 362833 and N 305 101235.

## References

- [1] A. Kabata-Pendias, H. Pendias, PWN Warsaw, 1999, p. 192 (in Polish).
- [2] M.J. Shaw, P.R. Haddad, *Environ. Int.* 30 (2004) 403.
- [3] M. Busch, A. Seubert, *Anal. Chim. Acta* 399 (1999) 223.
- [4] N. Clarke, L.G. Danielsson, A. Sparén, *Pure Appl. Chem.* 68 (8) (1996) 1597.
- [5] V. Arancibia, C. Muñoz, *Talanta* 73 (2007) 546.
- [6] O. Happel, A. Seubert, *J. Chromatogr. A* 1108 (2006) 68.
- [7] J. Tria, E.C.V. Butler, P.R. Haddad, A.R. Bowie, *Anal. Chim. Acta* 588 (2007) 153.
- [8] N. Radić, M. Bralić, *Sci. Total Environ.* 172 (1995) 237.
- [9] M. Busch, A. Seubert, *Fresenius J. Anal. Chem.* 366 (2000) 351.
- [10] B. Mitrović, R. Milačić, B. Pihlar, P. Simončić, *Analisis* 26 (1998) 381.
- [11] B. Platt, A.J. Drysdale, C. Nday, E. Linstow Roloff, B.D. Drever, A. Salifoglou, *Neurotoxicology* 28 (2007) 576.
- [12] S. Bi, X. Yang, F. Zhang, X. Wang, G. Zou, *Fresenius J. Anal. Chem.* 370 (2001) 984.
- [13] B. Mitrović, R. Milačić, *Sci. Total Environ.* 258 (2000) 183.
- [14] A. Ruzczyńska, K. Pyrzyńska, E. Bulska, *Chem. Anal.* 49 (19) (2004) 20.
- [15] C.T. Driscoll, K.M. Postek, *Environ. Chem. Aluminium* (1996) 364 (Chapter 9).
- [16] A. Strunecká, O. Strunecký, J. Potočka, *Physiol. Res.* 51 (2002) 557.
- [17] M. Suwalsky, B. Norris, F. Villena, F. Cuevas, P. Sotomayor, P. Zatta, *Food Chem. Toxicol.* 42 (2004) 925.
- [18] A. Ziola, T. Sobczyński, *Pol. J. Environ. Stud.* 14 (2005) 101.
- [19] C.T. Driscoll, *Int. J. Environ. Anal. Chem.* 16 (1984) 267.
- [20] H. Lian, Y. Kang, S. Bi, A. Yasin, D. Shao, D. Li, Y. Chen, L. Dai, N. Gan, L. Tian, *Talanta* 62 (2004) 43.
- [21] H. Lian, Y. Kang, S. Bi, A. Yasin, D. Shao, D. Li, Y. Chen, L. Dai, L. Tian, *Anal. Bioanal. Chem.* 376 (2003) 542.
- [22] A. Fairman, A. Sanz-Medel, P. Jones, E. Hywel Evans, *Analyst* 123 (1998) 699.
- [23] P.M. Bertsch, M.A. Anderson, *Anal. Chem.* 61 (6) (1989) 535.
- [24] M. Montes Bayón, A. Rodríguez García, J.I. García Alonso, A. Sanz-Medel, *Analyst* 124 (1999) 27.
- [25] I.R. Willet, *Soil Sci. Am. J.* 53 (1989) 1385.
- [26] P. Jones, *Int. J. Environ. Anal. Chem.* 44 (1991) 1.
- [27] S. Motellier, H. Pitsch, *J. Chromatogr. A* 660 (1994) 21.
- [28] G. Borrmann, A. Seubert, *Anal. Chim. Acta* 332 (1996) 233.
- [29] H. Hara, H. Kobayashi, M. Maeda, A. Ueno, Y. Kobayashi, *Anal. Chem.* 73 (2001) 5590.
- [30] G. Borrmann, A. Seubert, *Anal. Chim. Acta* 386 (1999) 77.
- [31] H. Hils, M. Grote, E. Janßen, J. Eichhorn, *Fresenius J. Anal. Chem.* 364 (1999) 457.
- [32] T. Bantan-Polak, B. Mitrović, R. Milačić, *Anal. Chim. Acta* 540 (2005) 83.
- [33] T. Bantan-Polak, B. Mitrović, R. Milačić, *Talanta* 47 (1998) 929.
- [34] T. Umemura, Y. Usami, S. Aizawa, K. Tsunoda, K. Satake, *Sci. Total Environ.* 317 (2003) 149.
- [35] O. Drábek, L. Boruvka, L. Mládková, M. Kocarek, *J. Inorg. Biochem.* 97 (2003) 8.
- [36] O. Drábek, L. Mladkova, L. Boruvka, J. Száková, A. Nikodem, K. Nemecek, *J. Inorg. Biochem.* 99 (2005) 1788.
- [37] O. Drábek, L. Boruvka, L. Pavlu, A. Nikodem, I. Pírková, O. Vacek, *J. Inorg. Biochem.* 101 (2007) 1224.
- [38] R. Street, O. Drábek, J. Száková, L. Mládková, *Ford Chem.* 104 (2007) 1662.
- [39] M.G. Whitten, G.S.P. Ritchie, I.R. Willet, *J. Soil Sci.* 43 (1992) 283.
- [40] K. Tsunoda, T. Umemura, K. Ohshima, S. Lizawa, E. Yoshimura, K. Satake, *Water Air Soil Pollut.* 130 (2001) 1589.